Journal of Function Spaces

Numerical Methods for Differential and Integral Equations

Lead Guest Editor: Youssri H. Youssri
Guest Editors: Anna Napoli and Behrouz Parsa Moghaddam

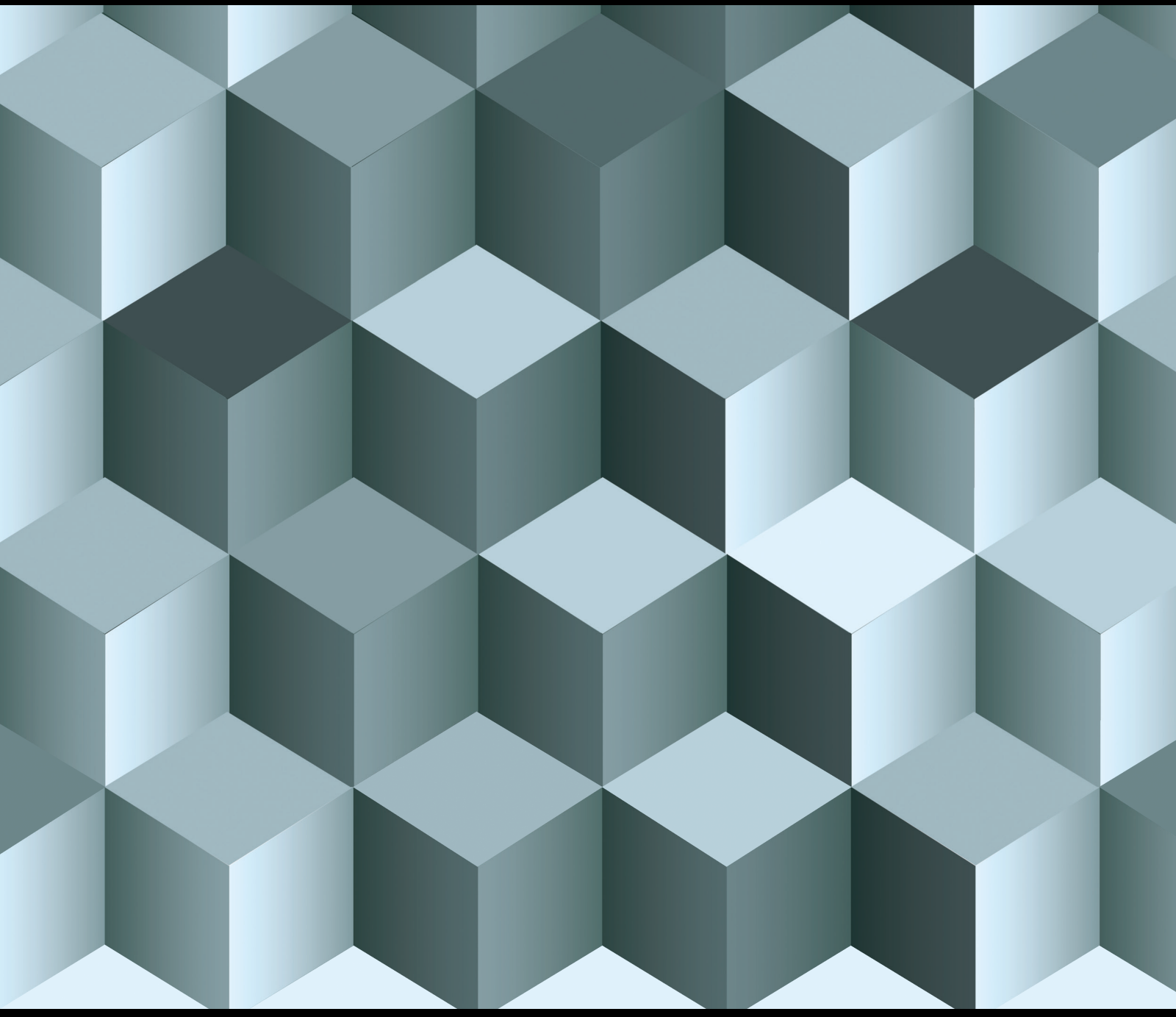

Numerical Methods for Differential and Integral Equations

Journal of Function Spaces

Numerical Methods for Differential and Integral Equations

Lead Guest Editor: Youssri H. Youssri
Guest Editors: Anna Napoli and Behrouz Parsa Moghaddam

Contents

Contents

Hindawi
Journal of Function Spaces
Volume 2023, Article ID 6833404, 16 pages
https://doi.org/10.1155/2023/6833404

Research Article

Newfangled Linearization Formula of Certain Nonsymmetric Jacobi Polynomials: Numerical Treatment of Nonlinear Fisher's Equation

W. M. Abd-Elhameed,[1] **Afnan Ali**,[2] **and Y. H. Youssri**[1,3]

[1]*Department of Mathematics, Faculty of Science, Cairo University, Giza 12613, Egypt*
[2]*Department of Mathematics, Faculty of Science, University of Jeddah, Jeddah, Saudi Arabia*
[3]*Faculty of Engineering, Egypt University of Informatics, New Administrative Capital, Egypt*

Correspondence should be addressed to W. M. Abd-Elhameed; waleed@cu.edu.eg and Y. H. Youssri; youssri@aucegypt.edu

Received 18 January 2022; Revised 9 April 2022; Accepted 13 April 2022; Published 21 August 2023

Academic Editor: Richard I. Avery

This article is devoted to deriving a new linearization formula of a class for Jacobi polynomials that generalizes the third-kind Chebyshev polynomials class. In fact, this new linearization formula generalizes some existing ones in the literature. The derivation of this formula is based on employing a new moment formula of this class of polynomials and after that using suitable symbolic computation to reduce the resulting linearization coefficients into simplified forms that do not contain any hypergeometric functions or sums. The new formula is employed along with some other formulas and with the utilization of the spectral tau method to obtain numerical solutions to the nonlinear Fisher equation. The presented method is used to convert the equation governed by its underlying conditions into a nonlinear system of equations. The solution of the resulting system can be obtained through any suitable standard numerical scheme. To demonstrate the efficiency and usefulness of the proposed algorithm, some examples are shown, including comparisons with some existing techniques in the literature.

1. Introduction

The study and the utilization of special functions in general and of orthogonal polynomials, in particular, is a very old and important branch of mathematics. Orthogonal polynomials are fruitfully used for obtaining numerical solutions to all types of differential equations. Among the important polynomials are the classical Jacobi polynomials. These polynomials have important parts in different disciplines. Some applications of Jacobi polynomials in some areas of science and engineering such as integral equations and food engineering can be found in [1–4]. In fact, the class of Jacobi polynomials involves six well-known polynomials. They are the Legendre, Gegenbauer, and the four kinds of Chebyshev polynomials. The existence of four different kinds of Chebyshev polynomials leads to a wide range of outcomes in a variety of fields, such as approximation, interpolation, series expansions, and quadrature and integral equations (see, for example, [5, 6]). These kinds of Chebyshev polynomials have been thoroughly investigated theoretically and numerically. For example, Oloniiju et al. in [7] used the first-kind Chebyshev polynomials to find a pseudospectral solution to a certain multidimensional fractional problem. The authors in [8] established new expressions of the high-order derivatives of Chebyshev polynomials of the third and fourth kinds. In addition, they utilized these formulas to treat numerically specific types of differential equations.

Deriving formulas that are concerned with different special functions and orthogonal polynomials is of interest. In fact, there are many formulas that serve in the numerical treatment of different types of differential equations. Obtaining

expressions for the high-order derivatives of orthogonal polynomials in terms of their original ones is very useful in treating numerically the differential equations of different types if the spectral methods are applied. For example, the authors in [9] established new expressions for the high-order derivatives of the fifth-kind Chebyshev polynomials in terms of their original polynomials. These expressions include terminating hypergeometric functions of the type ${}_4F_3(1)$. Moreover, these formulas are employed to treat numerically the convection-diffusion equation. Also, among the important formulas of orthogonal polynomials are the linearization formulas of these polynomials. Because of their importance, linearization problems have attracted the attention of many authors. For example, some articles were devoted to solving the linearization problems of Jacobi polynomials and their special classes. There are different approaches in order to developing these linearization formulas. One can be referred for example to Rahman [10], Chaggara and Koepf [11]. As an application to the linearization formulas, recently, Abd-Elhameed in [12] developed linearization formulas for specific classes of Jacobi polynomials. Furthermore, a certain linearization formula along with the tau spectral method was employed to handle a type of nonlinear Riccati differential equation.

Spectral methods are a class of important methods that treat numerically different types of differential equations. The numerical solution is expressed as a suitable combination of specific polynomials, which is the basic assumption underpinning the implementation of spectral methods. Because of its importance in the area of numerical solutions of differential and integral equations, many types of spectral methods have received a lot of attention. For further information on the numerous applications of spectral approaches in various areas, see [13–15]. Spectral approaches include the Galerkin, tau, and collocation methods. The Galerkin method can be fruitfully utilized for treating several forms of differential equations (see, for instance, [16–20]). Unlike the Galerkin technique, the tau method is more flexible in its application because it does not require selecting basis functions that meet the underlying initial/boundary conditions (see, for example, [21–24]). The collocation method is the most popular method. It may be used to solve any differential equation. The authors in [25–27] used the collocation method to obtain numerical solutions to many types of differential equations.

Fisher's equation arises in various applications like tissue engineering, chemical reactions, and neurophysiology (see [28, 29]). This equation has been treated by both analytic and numerical techniques. For example, Wazwaz and Gorguis in [30] studied analytically the nonlinear Fisher equation by using the Adomian decomposition method. Chandraker et al. in [31] developed implicit numerical techniques for treating Fisher's equation. From a numerical point of view, Haar wavelet's method is applied for solving Fisher's equation in [32]. For some other articles that deal with Fisher's equation and its generalizations and modifications, one can consult [33–36].

Recently, Abd-Elhameed and Alkenedri in [37] investigated two generalized classes of the third- and fourth-kind Chebyshev polynomials. They developed new high-order derivative expressions of these polynomials. In addition and based on these formulas, they obtained spectral solutions to the high-even-order linear and nonlinear boundary value problems. In this article, we are interested in developing some theoretical results concerned with certain generalized third-kind Chebyshev polynomials and after that employing such polynomials to treat numerically the nonlinear Fisher equation.

The five main goals of the current paper can be listed as follows:

(i) Derivation of a new moment formula of the generalized third-kind Jacobi polynomials

(ii) Establishing a new linearization formula of the generalized third-kind Jacobi polynomials

(iii) Deducing some existing moment and linearization formulas in the literature as special cases of our new moment and linearization formulas

(iv) Employing the derived linearization formula in conjunction with the high-order derivative expression of the generalized polynomials to numerically solve the nonlinear Fisher equation using the spectral tau approach

(v) Testing the efficiency and applicability of our proposed algorithm by presenting some examples accompanied by comparisons with some other methods in the literature

The rest of the paper is as follows. In Section 2, some interesting properties concerned with the classical Jacobi polynomials and their shifted ones are presented. Section 3 is devoted to developing new moment formula of the generalized third-kind Chebyshev polynomials. Some specific moment formulas are also deduced by reducing the corresponding moment coefficients via the utilization of Zeilberger's algorithm. Section 4 establishes the main formula in this paper in which we give with proof a new linearization formula of the generalized third-kind Chebyshev polynomials. Section 5 concentrates on proposing a numerical algorithm for solving spectrally the nonlinear Fisher equation. In Section 6, some numerical examples accompanied by comparisons with some other techniques in the literature are displayed. We end the paper with some concluding remarks in Section 7.

2. Some Interesting Properties and Formulas of Jacobi Polynomials

The standard Jacobi polynomial $P_j^{(\lambda,\mu)}(x)$ of degree j can be defined in hypergeometric form as (see, for example, Andrews et al. [38])

$$P_j^{(\lambda,\mu)}(x) = \frac{(\lambda+1)_j}{j!}\,{}_2F_1\left(\begin{matrix}-j, j+\lambda+\mu+1\\ \lambda+1\end{matrix}\middle|\frac{1-x}{2}\right). \tag{1}$$

The Jacobi polynomials can be normalized (see [12]); that is, we can define $R_j^{(\lambda,\mu)}(x)$ such that

$$R_j^{(\lambda,\mu)}(x) = 1, \quad \forall j \geq 0, \tag{2}$$

and therefore,

$$R_j^{(\lambda,\mu)}(x) = \frac{P_j^{(\lambda,\mu)}(x)}{P_j^{(\lambda,\mu)}(1)} = \frac{j!}{(\lambda+1)_j} P_j^{(\lambda,\mu)}(x) = {}_2F_1\left(\begin{matrix} -j, j+\lambda+\mu+1 \\ \lambda+1 \end{matrix} \middle| \frac{1-x}{2}\right). \tag{3}$$

The orthogonality property of $R_j^{(\lambda,\mu)}(x)$ on $[-1, 1]$ is

$$\int_{-1}^{1} (1-x)^{\lambda}(1+x)^{\mu} R_i^{(\lambda,\mu)}(x) R_j^{(\lambda,\mu)}(x)\, dx = \begin{cases} 0, & j \neq i, \\ h_i^{(\lambda,\mu)}, & j = i, \end{cases} \tag{4}$$

where

$$h_i^{(\lambda,\mu)} = \frac{2^{\lambda+\mu+1}\, i!\Gamma(i+\mu+1)\,[\Gamma(\lambda+1)]^2}{(2i+\lambda+\mu+1)\,\Gamma(i+\lambda+\mu+1)\,\Gamma(i+\lambda+1)}. \tag{5}$$

One comments here that the following six special classes of polynomials can be extracted from $R_j^{(\lambda,\mu)}(x)$ with suitable choices of λ and μ. We have

$$\begin{aligned} &C_i^{(\alpha)}(x) = R_i^{(\alpha-(1/2),\alpha-(1/2))}(x),\ T_i(x) = R_i^{(-(1/2),-(1/2))}(x), \\ &U_i(x) = (i+1)\, R_i^{(1/2,1/2)}(x),\ V_i(x) = R_i^{(-(1/2),1/2)}(x), \\ &W_i(x) = (2i+1)\, R_i^{(1/2,-(1/2))}(x),\ P_i(x) = R_i^{(0,0)}(x), \end{aligned} \tag{6}$$

where $C_i^{(\alpha)}(x)$, $T_i(x)$, $U_i(x)$, $V_i(x)$, $W_i(x)$, and $P_i(x)$ are the ultraspherical, first-, second-, third-, and fourth kinds of Chebyshev polynomials and Legendre polynomials, respectively.

Also, the following relation is noted:

$$R_i^{(\lambda,\mu)}(-x) = \frac{(-1)^i\,\Gamma(\lambda+1)\,\Gamma(i+\mu+1)}{\Gamma(\mu+1)\,\Gamma(i+\lambda+1)} R_i^{(\mu,\lambda)}(x). \tag{7}$$

Now, consider the special class of Jacobi polynomials $R_i^{(\alpha,\alpha+1)}(x)$. It is clear that this class reduces to the class of third-kind Chebyshev polynomials for the case corresponding to $\alpha = -(1/2)$.

Now, define the shifted Jacobi polynomials class on $[0, 1]$ as

$$J_i^{(\alpha)}(z) = R_i^{(\alpha,\alpha+1)}(2z-1). \tag{8}$$

The orthogonality relation of $J_i^{(\alpha)}(z)$ on $[0, 1]$ is given by

$$\int_0^1 w_1(z) J_i^{(\alpha)}(z)\, J_j^{(\alpha)}(z) dz = h_i \delta_{i,j}, \tag{9}$$

where $w_1(z) = (1-z)^{\alpha} z^{\alpha+1}$, δ_{ij} is the well-known Kronecker delta function, and h_i is given by

$$h_i = \frac{i!\Gamma(\alpha+1)]^2}{2\,\Gamma(i+2\alpha+2)}. \tag{10}$$

The classical Jacobi polynomials and their special ones are investigated in a variety of books (see, for example, Andrews et al. [38] and Mason and Handscomb [6]).

The following three lemmas are of fundamental importance to derive our proposed results in the upcoming sections.

Lemma 1 (see [37]). *Let j be a nonnegative integer. The polynomials $R_j^{(\alpha,\alpha+1)}(x)$ have the following power form representation:*

$$R_j^{(\alpha,\alpha+1)}(x) = \sum_{r=0}^{\lfloor j/2 \rfloor} A_{r,j} x^{j-2r} + \sum_{r=0}^{\lfloor (j-1)/2 \rfloor} B_{r,j} x^{j-2r-1}, \tag{11}$$

where

$$\begin{aligned} A_{r,j} &= \frac{(-1)^r\, 2^{1+j-2r+2\alpha} j!\Gamma(1+\alpha)\,\Gamma((3/2)+j-r+\alpha)}{\sqrt{\pi}\, r!(j-2r)!\Gamma(2+j+2\alpha)}, \\ B_{r,j} &= \frac{(-1)^{1+r}\, j! 2^{j-2r+2\alpha}\,\Gamma(1+\alpha)\,\Gamma((1/2)+j-r+\alpha)}{\sqrt{\pi}\, r!(j-2r-1)!\Gamma(2+j+2\alpha)}, \end{aligned} \tag{12}$$

where $\lfloor z \rfloor$ denotes the well-known floor function.

Lemma 2 (see [37]). *For every nonnegative integer j, the following inversion formula for the polynomials $R_j^{(\alpha,\alpha+1)}(x)$ holds:*

$$x^j = \sum_{i=0}^{\lfloor j/2 \rfloor} Q_{i,j} R_{j-2i}^{(\alpha,\alpha+1)}(x) + \sum_{i=0}^{\lfloor (j-1)/2 \rfloor} \bar{Q}_{i,j} R_{j-2i-1}^{(\alpha,\alpha+1)}(x), \tag{13}$$

where

$$\begin{aligned} Q_{i,j} &= \frac{2^{-1-j-2\alpha}\sqrt{\pi}\, j!\Gamma(2-2i+j+2\alpha)}{i!(j-2i)!\Gamma(1+\alpha)\,\Gamma((3/2)-i+j+\alpha)}, \\ \bar{Q}_{i,j} &= \frac{2^{-1-j-2\alpha}\sqrt{\pi}\, j!\Gamma(1-2i+j+2\alpha)}{i!(j-2i-1)!\Gamma(1+\alpha)\,\Gamma((3/2)-i+j+\alpha)}. \end{aligned} \tag{14}$$

Lemma 3 (see [37]). *The qth derivative of the shifted Jacobi polynomial $J_i^{(\alpha)}(z)$ is linked by their original ones by the relation*

$$D^q J_i^{(\alpha)}(z) = \sum_{j=0}^{i-q} d_{j,i,q} J_j^{(\alpha)}(z), \tag{15}$$

where the coefficients $d_{j,i,q}$ are given by

$$d_{j,i,q} = \frac{2^{2q}\, i!\Gamma(j+2\alpha+2)}{j!(q-1)!\,\Gamma(i+2\alpha+2)} \begin{cases} \dfrac{((i-j+q-2)/2)!\,\Gamma((i+j+q+2\alpha+3)/2)}{((i-j-q)/2)!\,\Gamma((i+j-q+2\alpha+3)/2)}, & (i+j+q)\text{ even}, \\ \dfrac{((i-j+q-1)/2)!\,\Gamma((i+j+q+2\alpha+2)/2)}{((i-j-q-1)/2)!\,\Gamma((i+j-q+2\alpha+4)/2)}, & (i+j+q)\text{ odd}. \end{cases} \tag{16}$$

3. New Moment Formula of the Jacobi Polynomials $R_i^{(\alpha,\alpha+1)}(x)$

This section is devoted to the implementation of a new moment formula of the Jacobi polynomials $R_j^{(\alpha,\alpha+1)}(x)$. The derivation of this formula is based on the power-form representation of these polynomials along with their inversion formula.

Theorem 4. *Let m an n be positive integers. One has*

$$x^m R_j^{(\alpha,\alpha+1)}(x) = \sum_{p=0}^{\lfloor (j+m)/2 \rfloor} U_{p,j,m} R_{j+m-2p}^{(\alpha,\alpha+1)}(x) + \sum_{p=0}^{\lfloor (1/2)(j+m-1) \rfloor} \bar{U}_{p,j,m} R_{j+m-2p-1}^{(\alpha,\alpha+1)}(x), \tag{17}$$

where

$$U_{p,j,m} = \frac{j!\Gamma(2+j+m-2p+2\alpha)}{2^m\,(j+m-2p)!\Gamma(2+j+2\alpha)} \times \sum_{\ell=0}^{p} \frac{(-1)^\ell (j-2\ell+m-1)!\Gamma((1/2)+j-\ell+\alpha)}{\ell!(j-2\ell)!(p-\ell)!\Gamma((3/2)+j-\ell+m-p+\alpha)} \times \left((j-2\ell)(\ell-p)+\frac{1}{2}(j-2\ell+m)(1+2j-2\ell+2\alpha)\right), \tag{18}$$

$$\bar{U}_{p,j,m} = \frac{j!\Gamma(1+j+m-2p+2\alpha)}{2^{m+1}\,(j+m-2p-1)!\Gamma(2+j+2\alpha)} \times \sum_{\ell=0}^{p} \frac{(-1)^\ell\,(m+2\ell m+2jp-4\ell p+2m\alpha)\,(j-2\ell+m-1)!\Gamma((1/2)+j-\ell+\alpha)}{\ell!(j-2\ell)!(p-\ell)!\Gamma((3/2)+j-\ell+m-p+\alpha)}. \tag{19}$$

Proof. The analytic formula of $R_j^{(\alpha,\alpha+1)}(x)$ enables one to write

$$x^m R_j^{(\alpha,\alpha+1)}(x) = \frac{j!\Gamma(1+\alpha)}{\sqrt{\pi}\,\Gamma(2+j+2\alpha)} \cdot \left(\sum_{r=0}^{\lfloor (j/2) \rfloor} \frac{(-1)^r\, 2^{1+j-2r+2\alpha}\,\Gamma((3/2)+j-r+\alpha)}{r!(j-2r)!} x^{j+m-2r} + \sum_{r=0}^{\lfloor (j-1)/2 \rfloor} \frac{(-1)^{1+r}\, 2^{j-2r+2\alpha}\,\Gamma((1/2)+j-r+\alpha)}{r!(j-2r-1)!} x^{j+m-2r-1} \right). \tag{20}$$

In virtue of (13) and after doing some lengthy manipulations, we can write

$$x^m R_j^{(\alpha)}(x) = \sum_{p=0}^{\lfloor (j+m)/2 \rfloor} U_{p,j,m} R_{j+m-2p}^{(\alpha,\alpha+1)}(x) + \sum_{p=0}^{\lfloor (1/2)(j+m-1) \rfloor} \bar{U}_{p,j,m} R_{j+m-2p-1}^{(\alpha,\alpha+1)}(x), \tag{21}$$

where $U_{p,j,m}$ and $\bar{U}_{p,j,m}$ are as given in (18) and (19). This ends the proof. □

Corollary 5. *The moment formula of Chebyshev polynomials of the third kind is given explicitly as*

$$x^m V_j(x) = \frac{1}{2^m} \sum_{p=0}^{m} \binom{m}{p} V_{j+m-2p}(x). \tag{22}$$

Proof. Setting $\alpha = -(1/2)$ in (17) gives the following formula:

$$x^m V_j(x) = \frac{1}{2^m} \left(\sum_{p=0}^{\lfloor (j+m)/2 \rfloor} H_{p,j,m} R_{j+m-2p}^{(\alpha,\alpha+1)}(x) + \sum_{p=0}^{\lfloor (1/2)(j+m-1) \rfloor} \bar{H}_{p,j,m} R_{j+m-2p-1}^{(\alpha,\alpha+1)}(x) \right), \tag{23}$$

where

$$H_{p,j,m} = \sum_{\ell=0}^{p} \frac{(-1)^{1+\ell}\left(-j^2 + \ell(m-2p) + j(2\ell - m + p)\right)(j-\ell-1)!(j-2\ell+m-1)!}{\ell!(j-2\ell)!(p-\ell)!(j-\ell+m-p)!}, \tag{24}$$

$$\bar{H}_{p,j,m} = \sum_{\ell=0}^{p} \frac{(-1)^{\ell}\left(\ell(m-2p) + jp\right)(j-\ell-1)!(j-2\ell+m-1)!}{(j-2\ell)!\ell!(p-\ell)!(j-\ell+m-p)!}. \tag{25}$$

Regarding the sum in (24), the utilization of Zeilberger's algorithm (see [39]) enables one to obtain the following recurrence relation for $H_{p,j,m}$:

$$(p+1)H_{p+1,j,m} - (m-p)\,H_{p,j,m}, H_{0,j,m} = 1, \tag{26}$$

which can be handled quickly to provide

$$H_{p,j,m} = \binom{m}{p}. \tag{27}$$

In addition, it is easy to demonstrate the following formula:

$$\bar{H}_{p,j,m} = 0. \tag{28}$$

Now, the two sums in (27) and (28) along with formula (23) lead to the following simplified moment formula:

$$x^m\, V_j(x) = \frac{1}{2^m}\sum_{p=0}^{m}\binom{m}{p} V_{j+m-2p}(x). \tag{29}$$

□

Remark 6. It is worth mentioning here that the moment formula (22) is similar to that obtained in Ref. [40].

Corollary 7. *For the case corresponds to $\alpha = 1/2$, the following moment formula holds for all nonnegative integers m and j:*

$$\begin{aligned} x^m R_j^{(1/2,3/2)}(x) = {} & \frac{1}{2^m(j+1)(j+2)} \\ & \cdot \left(\sum_{p=0}^{\lfloor (j+m)/2\rfloor}\binom{m}{p}(2+m+j(3+j+m-2p)-3p)\right. \\ & \left.\cdot R_{j+m-2p}^{(1/2,3/2)}(x) + \sum_{p=0}^{\lfloor (1/2)(j+m-1)\rfloor}\binom{m}{p}(m-p)R_{j+m-2p+1}^{(1/2,3/2)}(x)\right). \end{aligned} \tag{30}$$

Proof. Setting $\alpha = 1/2$ in the moment formula (17) gives the following formula:

$$x^m R_j^{(1/2,3/2)}(x) = \left(\sum_{p=0}^{\lfloor (j+m)/2\rfloor} M_{p,j,m} R_{j+m-2p}^{(1/2,3/2)}(x) + \sum_{p=0}^{\lfloor 1/2(j+m-1)\rfloor} \bar{M}_{p,j,m} R_{j+m-2p-1}^{(1/2,3/2)}(x)\right), \tag{31}$$

where

$$M_{p,j,m} = \frac{(1+j+m-2p)(2+j+m-2p)}{2^m(j+1)(j+2)} \times \sum_{\ell=0}^{p}\frac{(-1)^{\ell}\left(j^2+m-\ell(2+m-2p)+j(1-2\ell+m-p)\right)(j-\ell)!(j-2\ell+m-1)!}{\ell!(p-\ell)!(j-2\ell)!(j-\ell+m-p+1)!}, \tag{32}$$

$$\bar{M}_{p,j,m} = \frac{(j+m-2p)(1+j+m-2p)}{2^m(j+1)(j+2)} \times \sum_{\ell=0}^{p}\frac{(-1)^{\ell}(m+\ell m+jp-2\ell p)(j-\ell)!(j-2\ell+m-1)!}{\ell!(j-2\ell)!(p-\ell)!(j-\ell+m-p+1)!}. \tag{33}$$

Regarding the two summations that appear in equations (32) and (33), set

$$\begin{aligned} S_{p,j,m} &= \sum_{\ell=0}^{p}\frac{(-1)^{\ell}\left(j^2+m-\ell(2+m-2p)+j(1-2\ell+m-p)\right)(j-\ell)!(j-2\ell+m-1)!}{(j-2\ell)!\ell!(p-\ell)!(j-\ell+m-p+1)!}, \\ \bar{S}_{p,j,m} &= \sum_{\ell=0}^{p}\frac{(-1)^{\ell}(m+\ell m+jp-2\ell p)(j-\ell)!(j-2\ell+m-1)!}{(j-2\ell)!\ell!(p-\ell)!(j-\ell+m-p+1)!} \end{aligned} \tag{34}$$

and utilize Zeilberger's algorithm ([39]) to show that the following two recurrence relations are, respectively, satisfied by $S_{p,j,m}$ and $\bar{S}_{p,j,m}$:

$$\begin{aligned}&(p+1)(-2p+j+m-1)(-2p+j+m)\\&\quad\cdot(-3p+m+j(-2p+j+m+3)+2)\\&\quad\cdot S_{p+1,j,m}+(p-m)(-2p+j+m+1)\\&\quad\cdot(-2p+j+m+2)(-3p+m+j(-2p+j+m+1)-1)\\&\quad\cdot S_{p,j,m}=0,\end{aligned}\tag{35}$$

with the following initial condition:

$$\begin{aligned}&S_{0,j,m}=\frac{j+1}{m+j+1},\\&(p+1)(-2p+j+m-2)(-2p+j+m-1)\\&\quad\cdot\bar{S}_{p+1,j,m}-(-p+m-1)(-2p+j+m)\\&\quad\times(-2p+j+m+1)\bar{S}_{p,j,m}=0,\end{aligned}\tag{36}$$

with the following initial condition:

$$\bar{S}_{0,j,m}=\frac{m}{(m+j)(m+j+1)}.\tag{37}$$

The above two recurrence relations can be directly solved to give

$$\begin{aligned}S_{p,j,m}&=\frac{(m-p+1)_p\,(-3p+m+j(-2p+j+m+3)+2)}{p!(-2p+j+m+1)\,(-2p+j+m+2)},\\\bar{S}_{p,j,m}&=\frac{(m-p)_{p+1}}{p!(-2p+j+m+1)\,(-2p+j+m)},\end{aligned}\tag{38}$$

and consequently, the linearization coefficients $M_{p,j,m}$ and $\bar{M}_{p,j,m}$ reduce to the following expressions:

$$\begin{aligned}M_{p,j,m}&=\frac{(2+m+j(3+j+m-2p)-3p)(1+m-p)_p}{2^m\,(j+1)\,(j+2)\,p!},\\\bar{M}_{p,j,m}&=\frac{(m-p)_{p+1}}{2^m\,(j+1)\,(j+2)\,p!},\end{aligned}\tag{39}$$

and therefore, the linearization formula (30) can be obtained. □

4. Linearization Formula of $R_i^{(\alpha,\alpha+1)}(x)$

In this section and based on the moment formula that was derived in the previous section, we present and prove a new linearization formula of the generalized third-kind Chebyshev polynomials $R_i^{(\alpha,\alpha+1)}(x)$.

Theorem 8. *For all nonnegative integers i and j, the following linearization formula is valid:*

$$R_i^{(\alpha,\alpha+1)}R_j^{(\alpha,\alpha+1)}=\sum_{p=0}^{2\min(i,j)}H_{p,i,j}R_{i+j-p}^{(\alpha,\alpha+1)}(x),\tag{40}$$

where

$$\begin{aligned}H_{p,i,j}=&\frac{2^{2\alpha+1}\,i!j!\Gamma(\alpha+1)}{\sqrt{\pi}\,\Gamma(2+i+2\alpha)\,\Gamma(2+j+2\alpha)\,\Gamma((3/2)+\alpha)}\\&\times\begin{cases}\dfrac{\Gamma((3/2)+i-(p/2)+\alpha)\Gamma((3/2)+j-(p/2)+\alpha)\Gamma((3+p)/2+\alpha)\Gamma(2+i+j-(p/2)+2\alpha)}{(i-(p/2))!(j-(p/2))!(p/2)!\Gamma((3/2)+i+j-(p/2)+\alpha)}, & p\text{ even},\\[2ex] -\dfrac{\Gamma(1+i-(p/2)+\alpha)\Gamma(1+j-(p/2)+\alpha)\Gamma(1+(p/2)+\alpha)\Gamma((5/2)+i+j-(p/2)+2\alpha)}{(i-(p+1/2))!(j-(p+1/2))!((p-1)/2)!\,\Gamma(2+i+j-(p/2)+\alpha)}, & p\text{ odd}.\end{cases}\end{aligned}\tag{41}$$

Proof. Starting with the power form representation of $R_i^{(\alpha,\alpha+1)}(x)$ yields

$$R_i^{(\alpha,\alpha+1)}(x)\,R_j^{(\alpha,\alpha+1)}(x)=\sum_{r=0}^{\lfloor j/2\rfloor}A_{r,j}\,x^{j-2r}\,R_i^{(\alpha,\alpha+1)}(x)+\sum_{r=0}^{\lfloor (j-1)/2\rfloor}B_{r,j}\,x^{j-2r-1}R_i^{(\alpha,\alpha+1)}(x).\tag{42}$$

Based on the moment formula in (17), the last relation turns into

$$\begin{aligned} R_i^{(\alpha,\alpha+1)}(x)R_j^{(\alpha,\alpha+1)}(x) = \sum_{r=0}^{\lfloor j/2\rfloor} A_{r,j}\Bigg(&\sum_{p=0}^{\lfloor (1/2)(i+j)\rfloor - r} U_{p,i,j-2r}R_{i+j-2r-2p}^{(\alpha,\alpha+1)}(x) \\ &+ \sum_{p=0}^{\lfloor (1/2)(i+j-1)\rfloor - r} \bar{U}_{p,i,j-2r}\, R_{i+j-2r-2p-1}^{(\alpha,\alpha+1)}(x)\Big) \\ &+ \sum_{r=0}^{\lfloor (j-1)/2\rfloor} B_{r,j}\Bigg(\sum_{p=0}^{\lfloor (1/2)(i+j-1)\rfloor - r} U_{p,i,j-2r-1}R_{i+j-2r-2p-1}^{(\alpha,\alpha+1)}(x) \\ &+ \sum_{p=0}^{\lfloor (1/2)(i+j)\rfloor - r-1} \bar{U}_{p,i,j-2r-1}R_{i+j-2r-2p-2}^{(\alpha,\alpha+1)}(x)\Bigg). \end{aligned} \tag{43}$$

After some algebraic computations, equation (43) can be rewritten in the following form:

$$R_i^{(\alpha,\alpha+1)}(x)R_j^{(\alpha,\alpha+1)}(x) = \sum_1 + \sum_2, \tag{44}$$

where

$$\begin{aligned} \sum_1 = &\sum_{r=0}^{\lfloor j/2\rfloor} A_{r,j} \sum_{p=0}^{\lfloor (1/2)(i+j)\rfloor - r} U_{p,i,j-2r}R_{i+j-2r-2p}^{(\alpha,\alpha+1)}(x) \\ &+ \sum_{r=0}^{\lfloor (j-1)/2\rfloor} B_{r,j} \sum_{p=0}^{\lfloor (1/2)(i+j)\rfloor - r-1} \bar{U}_{p,i,j-2r-1}R_{i+j-2r-2p-2}^{(\alpha,\alpha+1)}(x), \end{aligned} \tag{45}$$

and

$$\begin{aligned} \sum_2 = &\sum_{r=0}^{\lfloor j/2\rfloor} A_{r,j} \sum_{p=0}^{\lfloor 1/2(i+j-1)\rfloor - r} U_{p,i,j-2r}R_{i+j-2r-2p-1}^{(\alpha,\alpha+1)}(x) \\ &+ \sum_{r=0}^{\lfloor (j-1)/2\rfloor} B_{r,j} \sum_{p=0}^{\lfloor (1/2)(i+j-1)\rfloor - r} U_{p,i,j-2r-1}R_{i+j-2r-2p-1}^{(\alpha,\alpha+1)}(x). \end{aligned} \tag{46}$$

After expanding and rearranging the terms in (45) and (46), they can be written in the following expressions:

$$\begin{aligned} \sum_1 &= \sum_{p=0}^{\lfloor (i+j)/2\rfloor} \left\{\sum_{\ell=0}^{p}\left(A_{\ell,j}U_{p-\ell,i,j-2\ell} + B_{\ell,j}\bar{U}_{p-\ell-1,i,j-2\ell-1}\right)\right\} R_{i+j-2p}^{(\alpha,\alpha+1)}(x), \\ \sum_2 &= \sum_{p=0}^{\lfloor (1/2)(i+j-1)\rfloor} \left\{\sum_{\ell=0}^{p}\left(A_{\ell,j}\bar{U}_{p-\ell,i,j-2\ell} + B_{\ell,j}U_{p-\ell,i,j-2\ell-1}\right)\right\} R_{i+j-2p-1}^{(\alpha,\alpha+1)}(x). \end{aligned} \tag{47}$$

Now and in order to obtain the linearization coefficients of the linearization formula of $R_i^{(\alpha,\alpha+1)}(x)$ in a reduced formula that is free of any sums, we employ symbolic computation. For such purpose, set

$$\begin{aligned} M_{p,i,j} &= \sum_{\ell=0}^{p}\left(A_{\ell,j}U_{p-\ell,i,j-2\ell} + B_{\ell,j}\bar{U}_{p-\ell-1,i,j-2\ell-1}\right), \\ \bar{M}_{p,i,j} &= \sum_{\ell=0}^{p}\left(A_{\ell,j}\bar{U}_{p-\ell,i,j-2\ell} + B_{\ell,j}U_{p-\ell,i,j-2\ell-1}\right). \end{aligned} \tag{48}$$

It can be shown by symbolic computation and, in particular, Zeilberger's algorithm that the following two recurrence relations, each of order one, are satisfied, respectively, by $M_{p,i,j}$ and $\bar{M}_{p,i,j}$:

$$\begin{aligned} &(p+1)(-2p+2i+2\alpha+1)(-p+i+j+2\alpha+1) \\ &\quad\cdot(-2p+2j+2\alpha+1)M_{p+1,i,j} - (i-p)(j-p) \\ &\quad\cdot(2p+2\alpha+3)(-2p+2i+2j+2\alpha+1)M_{p,i,j} = 0, \end{aligned} \tag{49}$$

with the following initial value:

$$\begin{aligned} M_{0,i,j} &= \frac{2^{1+2\alpha}\Gamma(1+\alpha)\Gamma((3/2)+i+\alpha)\Gamma((3/2)+j+\alpha)\Gamma(2+i+j+2\alpha)}{\sqrt{\pi}\,\Gamma((3/2)+i+j+\alpha)\Gamma(2+i+2\alpha)\Gamma(2+j+2\alpha)}, \\ &(p+1)(-2p+2i+2\alpha-1)(-p+i+j+2\alpha+1) \\ &\quad\cdot(-2p+2j+2\alpha-1)\bar{M}_{p+1,i,j} - (i-p-1)(j-p-1) \\ &\quad\cdot(2p+2\alpha+3)(-2p+2i+2j+2\alpha+1)\bar{M}_{p,i,j} = 0, \end{aligned} \tag{50}$$

with the following initial value:

$$\bar{M}_{0,i,j} = \frac{-2^{1+2\alpha}\, i\, j\,\Gamma(1+\alpha)\Gamma((1/2)+i+\alpha)\Gamma((1/2)+j+\alpha)\Gamma(2+i+j+2\alpha)}{\sqrt{\pi}\,\Gamma((3/2)+i+j+\alpha)\Gamma(2+i+2\alpha)\Gamma(2+j+2\alpha)}. \tag{51}$$

The above two recurrence relations can be directly solved to give

$$M_{p,i,j} = \frac{-2^{1+2\alpha}\, i!j!\Gamma(1+\alpha)\Gamma((3/2)+i-p+\alpha)\Gamma((3/2)+j-p+\alpha)\Gamma((3/2)+p+\alpha)\Gamma(2+i+j-p+2\alpha)}{\sqrt{\pi}\,p!(i-p)!(j-p)!\Gamma((3/2)+\alpha)\Gamma((3/2)+i+j-p+\alpha)\Gamma(2+i+2\alpha)\Gamma(2+j+2\alpha)}, \tag{52}$$

$$\bar{M}_{p,i,j} = \frac{-2^{1+2\alpha} i!j!\Gamma(\alpha+1)\Gamma((1/2)+i-p+\alpha)\Gamma((1/2)+j-p+\alpha)\Gamma((3/2)+p+\alpha)\Gamma(2+i+j-p+2\alpha)}{\sqrt{\pi}p!(i-p-1)!(j-p-1)!\Gamma((3/2)+\alpha)\Gamma((3/2)+i+j-p+\alpha)\Gamma(2+i+2\alpha)\Gamma(2+j+2\alpha)}. \tag{53}$$

Therefore, the following linearization formula is obtained:

$$R_i^{(\alpha,\alpha+1)} R_j^{(\alpha,\alpha+1)} = \sum_{p=0}^{\lfloor (i+j)/2 \rfloor} M_{p,i,j} R_{i+j-2p}^{(\alpha,\alpha+1)} + \sum_{p=0}^{\lfloor (1/2)(i+j-1) \rfloor} \bar{M}_{p,i,j} R_{i+j-2p-1}^{(\alpha,\alpha+1)}(x), \tag{54}$$

here the linearization coefficients $M_{p,i,j}$ and $\bar{M}_{p,i,j}$ are, respectively, given by (52) and (53). Formula (54) can be written alternatively as

$$R_i^{(\alpha,\alpha+1)} R_j^{(\alpha,\alpha+1)} = \sum_{p=0}^{2 \min (i,j)} H_{p,i,j} R_{i+j-p}^{(\alpha,\alpha+1)}(x), \tag{55}$$

with the following linearization coefficients $H_{p,i,j}$:

$$H_{p,i,j} = \frac{2^{1+2\alpha}\, i!j!\Gamma(1+\alpha)}{\sqrt{\pi}\,\Gamma(2+i+2\alpha)\,\Gamma(2+j+2\alpha)\,\Gamma((3/2)+\alpha)} \times \begin{cases} \dfrac{\Gamma((3/2)+i-(p/2)+\alpha)\Gamma((3/2)+j-(p/2)+\alpha)\Gamma((3+p)/2+\alpha)\Gamma(2+i+j-(p/2)+2\alpha)}{(i-(p/2))!(j-(p/2))!((p/2))!\Gamma((3/2)+i+j-(p/2)+\alpha)}, & p \text{ even}, \\ -\dfrac{\Gamma(1+i-(p/2)+\alpha)\Gamma(1+j-(p/2)+\alpha)\Gamma(1+(p/2)+\alpha)\Gamma((5/2)+i+j-(p/2)+2\alpha)}{(i-(p+1/2))!(j-(p+1/2))!((p-1)/2)!\,\Gamma(2+i+j-(p/2)+\alpha)}, & p \text{ odd}. \end{cases} \tag{56}$$

This completes the proof of Theorem 8. □

In the following two corollaries, we give two specific linearization formulas of the linearization formula (40).

Corollary 9. *Setting $\alpha = -(1/2)$ in (40) leads to the following linearization formula:*

$$V_i(x)\, V_j(x) = \sum_{p=0}^{2 \min (i,j)} (-1)^p\, V_{i+j-p}(x). \tag{57}$$

Remark 10. The linearization formula (57) was previously obtained in [41], but here, it is derived in an alternative approach.

Corollary 11. *Setting $\alpha = 1/2$ in (40) leads to the following linearization formula:*

$$R_i^{(1/2,3/2)} R_j^{(1/2,3/2)} = \sum_{p=0}^{2 \min (i,j)} H_{p,i,j}\, R_{i+j-p}^{(1/2,3/2)}(x), \tag{58}$$

with

$$H_{p,i,j} = (1/8(i+1)(i+2)(j+1)(j+2)) \times \begin{cases} (2+2i-p)(2+2j-p)(4+2i+2j-p)(2+p), & p \text{ even}, \\ -(1+2i-p)(1+2j-p)(5+2i+2j-p)(p+1), & p \text{ odd}. \end{cases} \tag{59}$$

Remark 12. The linearization formula (57) was previously obtained in [42].

Remark 13. The basic linearization formula (40) in Theorem8holds for the shifted Jacobi polynomials $J_i^{(\alpha)}(x)$, only if x is replaced by $(2x-1)$. The following theorem exhibits this formula in an appropriate form.

Theorem 14. *For all nonnegative integers i and j, the following linearization formula is valid:*

$$J_i^{(\alpha)}(x)\, J_j^{(\alpha)}(x) = \sum_{p=|i-j|}^{i+j} G_{p,i,j}\, J_p^{(\alpha)}(x), \tag{60}$$

with the following linearization coefficients $G_{p,i,j}$:

$$G_{p,i,j} = \frac{2^{2\alpha+1}\, i!j!\Gamma(\alpha+1)}{\sqrt{\pi}\,\Gamma((3/2)+\alpha)\,\Gamma(i+2\alpha+2)\,\Gamma(j+2\alpha+2)} \times \begin{cases} \dfrac{\Gamma((1/2)(i+j-p+3)+\alpha)\,\Gamma((1/2)(i-j+p+3)+\alpha)}{((1/2)(i+j-p))!\,((1/2)(i-j+p))!\,((1/2)(-i+j+p))!} \times \\ \dfrac{\Gamma((1/2)(-i+j+p+3)+\alpha)\,\Gamma((1/2)(i+j+p+4\alpha+4))}{\Gamma((1/2)(i+j+p+3)+\alpha)}, & (i+j-p) \text{ even}, \\ \dfrac{-\Gamma(1+(1/2)(i+j-p)+\alpha)\,\Gamma((1/2)(i-j+p+2)+\alpha)}{\Gamma((1/2)(i+j-p+1))\Gamma((1/2)(i-j+p+1))} \times \\ \dfrac{\Gamma((1/2)(2-i+j+p)+\alpha)\Gamma((1/2)(i+j+p+4\alpha+5))}{\Gamma((1/2)(-i+j+p+1))\Gamma((1/2)(i+j+p+4)+\alpha)}, & (i+j-p) \text{ odd}. \end{cases} \tag{61}$$

Input Given κ, M, η, ξ_0 and ξ_1.
Step 1. Evaluate the derivatives coefficients $d_{j,r,1}, d_{j,s,2}$ from relation (16), and the linearization. coefficients $G_{\bar{v},\bar{s},s}, G_{v,\bar{r},r}$ from relation (61).
Step 2. Assume an approximate solution in the form: $\mathscr{V}_M = \sum_{r=0}^{M}\sum_{s=0}^{M} v_{rs} J_s^{(\alpha)}(x) J_r^{(\alpha)}(t)$.
Step 3. Compute the residuals: $RE(x,t), RI(x), RB_0(t), RB_1(t)$ via Eqs. (69-72z).
Step 4. Apply the tau method to obtain the system in ((74)-(77)).
Step 5. Employ Newtons' iterative method -*FindRoot*- to obtain the coefficients v_{rs}.
Step 6. Find the double expansion: $\sum_{r=0}^{M}\sum_{s=0}^{M} v_{rs} J_s^{(\alpha)}(x) J_r^{(\alpha)}(t)$.
Output the approximate solution: $\mathscr{V}_M$.

Algorithm 1: Coding algorithm for the proposed scheme.

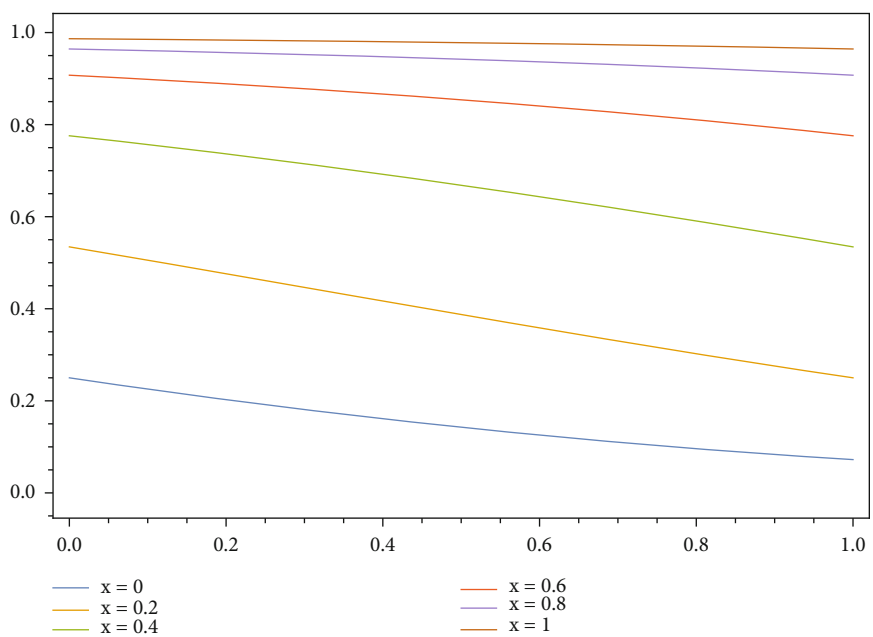

Figure 1: Solution of Example 1 at different values of x.

5. The Proposed Algorithm for the Numerical Treatment of the Nonlinear Fisher Equation

In this section, we are interested in obtaining a numerical algorithm for solving the nonlinear Fisher equation. More precisely, we will employ the established linearization formula along with the derivatives formula of the shifted polynomials $J_i^{(\alpha)}(x)$ to obtain a numerical solution based on applying the tau method. We denote our algorithm by the nonsymmetric Jacobi Tau Method (NJTM).

Now, consider the Fisher differential equation [32]:

$$\frac{\partial \mathscr{V}}{\partial t} = \frac{\partial^2 \mathscr{V}}{\partial x^2} + \kappa \mathscr{V}(1-\mathscr{V}), \quad (x,t) \in \Omega = (0,1)\times(0,1), \tag{62}$$

governed by the following initial and boundary conditions:

$$\mathscr{V}(x,0) = \eta(x), \quad x \in (0,1), \tag{63}$$

$$\begin{aligned} \mathscr{V}(0,t) &= \xi_0(t), \\ \mathscr{V}(1,t) &= \xi_1(t), \quad t \in (0,1), \end{aligned} \tag{64}$$

where κ is the positive coefficient of kinematic viscosity and η, ξ_0 and ξ_1 are prescribed known continuous functions. Now, for solving (62) governed by the conditions (63) and (64), we utilize the spectral tau method.

Now, assume that $\mathscr{V}(x,y) = \mathscr{V} \in L^2(\Omega)$ and let it have the following double series expansion:

$$\mathscr{V} = \sum_{r=0}^{\infty}\sum_{s=0}^{\infty} v_{rs} J_s^{(\alpha)}(x) J_r^{(\alpha)}(t). \tag{65}$$

Furthermore, assume an approximate solution to (62) in the form

$$\mathscr{V} \simeq \mathscr{V}_M = \sum_{r=0}^{M}\sum_{s=0}^{M} v_{rs} J_s^{(\alpha)}(x) J_r^{(\alpha)}(t). \tag{66}$$

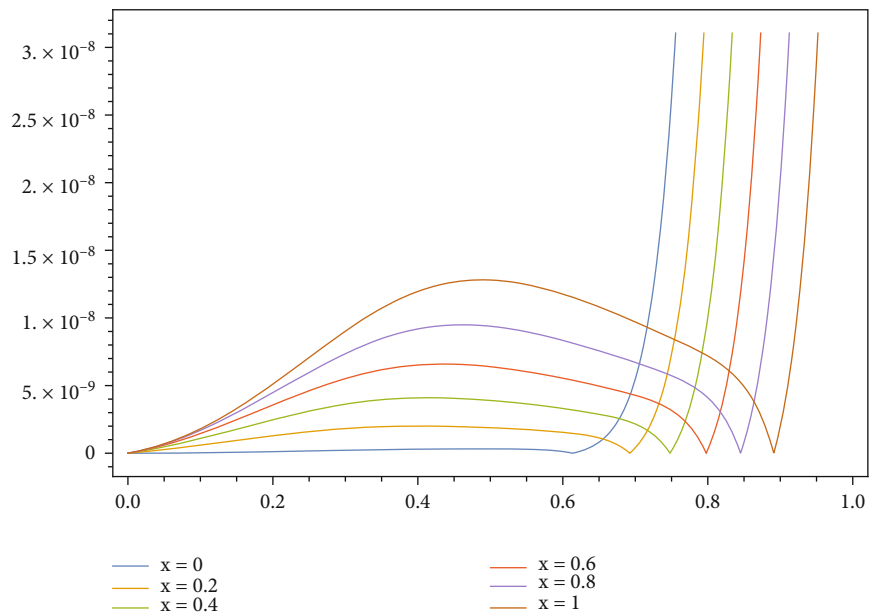

Figure 2: Absolute error of Example 1 at different values of x.

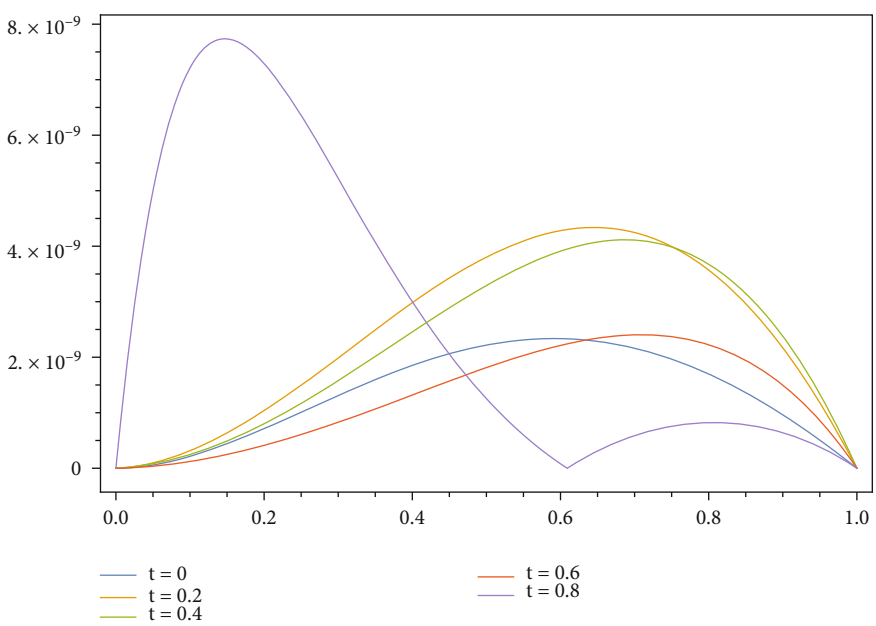

Figure 3: Absolute error of Example 1 at different values of t.

In virtue of formula (15), it can be shown that $\partial \mathscr{V}_M/\partial t$ and $\partial^2 \mathscr{V}_M/\partial x^2$ can be represented as follows:

$$\begin{aligned} \frac{\partial \mathscr{V}_M}{\partial t} &= \sum_{r=1}^{M}\sum_{s=0}^{M}\sum_{j=0}^{r-1} d_{j,r,1}\, v_{rs} J_s^{(\alpha)}(x) J_j^{(\alpha)}(t), \\ \frac{\partial^2 \mathscr{V}_M}{\partial x^2} &= \sum_{r=0}^{M}\sum_{s=2}^{M}\sum_{j=0}^{s-2} d_{j,s,2}\, v_{rs} J_j^{(\alpha)}(x) J_r^{(\alpha)}(t). \end{aligned} \tag{67}$$

Table 1: MAE for Example 1.

M	$\alpha = 0$	$\alpha = 1/2$	$\alpha = 1$
4	2.35×10^{-2}	3.48×10^{-2}	5.61×10^{-2}
6	3.41×10^{-6}	5.47×10^{-6}	8.35×10^{-6}
8	4.73×10^{-8}	5.27×10^{-8}	9.37×10^{-8}

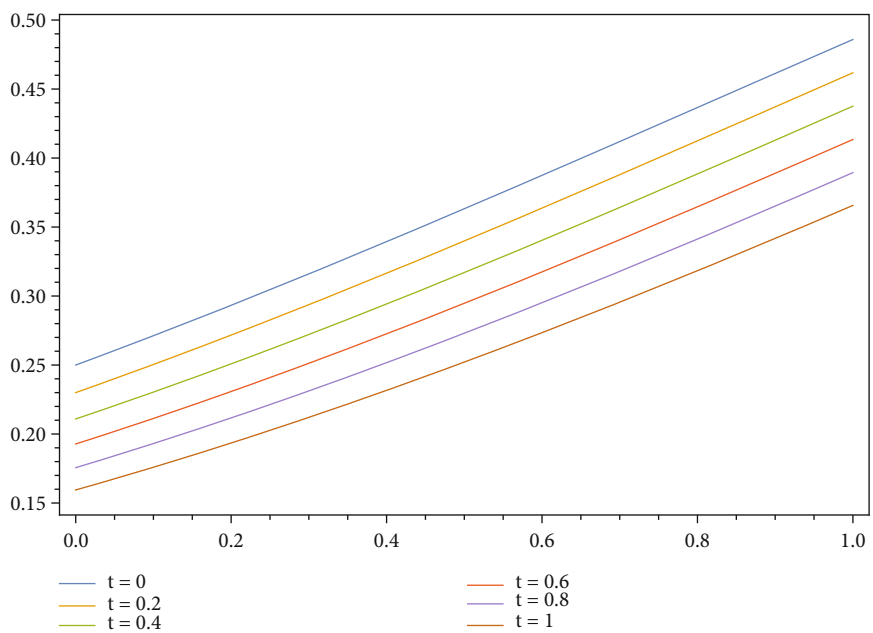

Figure 4: Solution of Example 2 at different values of t.

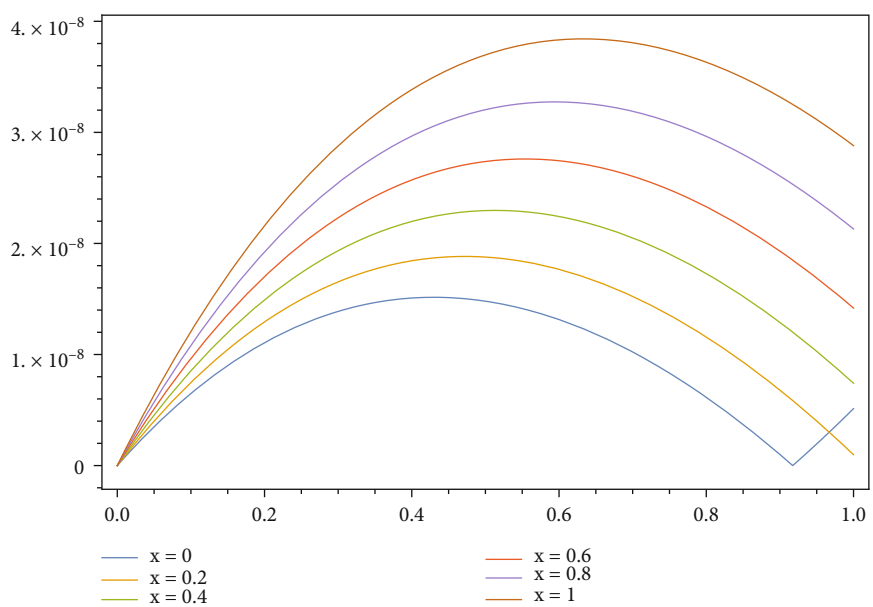

Figure 5: Absolute error of Example 2 at different values of x.

Based on the linearization formula (60), the nonlinear term $(\mathscr{V}_M)^2$ can be written in the following form:

$$(\mathscr{V}_M)^2 = \sum_{\bar{r}=0}^{M}\sum_{\bar{s}=0}^{M}\sum_{r=0}^{M}\sum_{s=0}^{M}\sum_{\bar{\nu}=|\bar{s}-s|}^{\bar{s}+s}\sum_{\nu=|\bar{r}-r|}^{\bar{r}+r} G_{\bar{\nu},\bar{s},s}\, G_{\nu,\bar{r},r}\, \nu_{\bar{s}\bar{r}}\, \nu_{rs} J_{\bar{\nu}}^{(\alpha)}(x)\, J_{\nu}^{(\alpha)}(t). \tag{68}$$

Now, to apply the tau method to (62) governed by the conditions (63) and (64), we first compute the residual $RE(x,t)$ of the differential equation (62). It is given explicitly as

$$\begin{aligned} RE(x,t) = \frac{\partial \mathscr{V}_M}{\partial t} - \frac{\partial^2 \mathscr{V}_M}{\partial x^2} - \kappa \mathscr{V}_M + \kappa (\mathscr{V}_M)^2 &= \sum_{r=1}^{M}\sum_{s=0}^{M}\sum_{j=0}^{r-1} d_{j,r,1}\, \nu_{rs} J_s^{(\alpha)}(x) J_j^{(\alpha)}(t) \\ &- \sum_{r=0}^{M}\sum_{s=2}^{M}\sum_{j=0}^{s-2} d_{j,s,2}\, \nu_{rs} J_j^{(\alpha)}(x) J_r^{(\alpha)}(t) - \kappa \sum_{r=0}^{M}\sum_{s=0}^{M} \nu_{rs} J_s^{(\alpha)}(x) J_r^{(\alpha)}(t) \\ &+ \kappa \sum_{\bar{r}=0}^{M}\sum_{\bar{s}=0}^{M}\sum_{r=0}^{M}\sum_{s=0}^{M}\sum_{\bar{\nu}=|\bar{s}-s|}^{\bar{s}+s}\sum_{\nu=|\bar{r}-r|}^{\bar{r}+r} G_{\bar{\nu},\bar{s},s}\, G_{\nu,\bar{r},r}\, \nu_{\bar{s}\bar{r}}\, \nu_{rs} J_{\bar{\nu}}^{(\alpha)}(x)\, J_{\nu}^{(\alpha)}(t). \end{aligned} \tag{69}$$

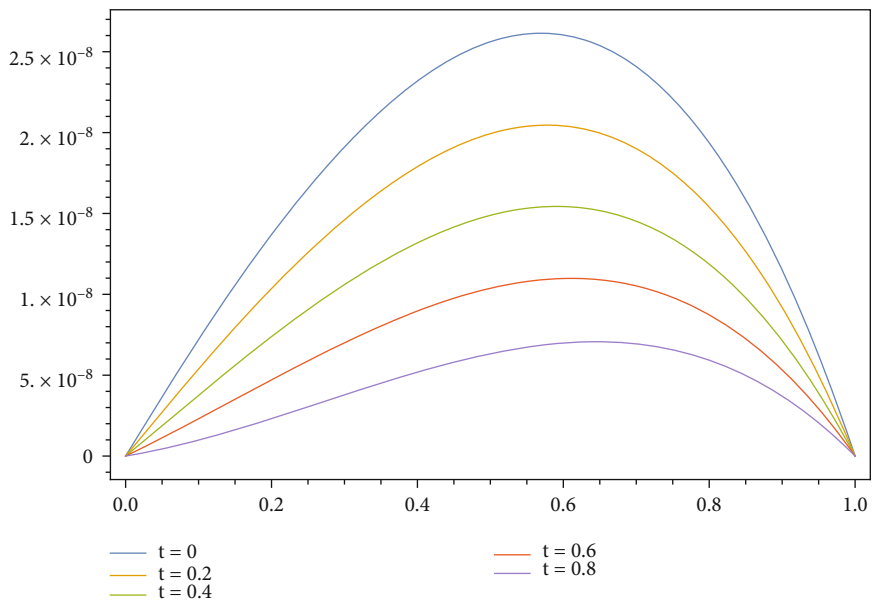

Figure 6: Absolute error of Example 2 at different values of t.

On the other hand, the residual of (63) ($RI(x)$) can be written:

$$RI(x) = \mathscr{V}_M(x,0) - \eta(x) = \sum_{r=0}^{M}\sum_{s=0}^{M} v_{rs} J_s^{(\alpha)}(x) J_r^{(\alpha)}(0) - \eta(x). \tag{70}$$

Moreover, the two residuals of the boundary conditions (64) ($RB_0(t)$ and $RB_1(t)$) are given by

$$RB_0(t) = \mathscr{V}_M(0,t) - \xi_0(t) = \sum_{r=0}^{M}\sum_{s=0}^{M} v_{rs} J_s^{(\alpha)}(0) J_r^{(\alpha)}(t) - \xi_0(t), \tag{71}$$

$$RB_1(t) = \mathscr{V}_M(1,t) - \xi_1(t) = \sum_{r=0}^{M}\sum_{s=0}^{M} v_{rs} J_s^{(\alpha)}(1) J_r^{(\alpha)}(t) - \xi_1(t). \tag{72}$$

Now, the application of the tau method leads to the following equations:

$$\begin{aligned}
&\int_0^1\int_0^1 RE(x,t)\, J_r^{(\alpha)}(x) J_s^{(\alpha)}(t) w_1(x) w_1(t)\, dx dt = 0, \quad 0 \le r \le M-1, 0 \le s \le M-1,\\
&\int_0^1 RI(x)\, J_0^{(\alpha)}(x) w_1(x)\, dx = 0,\\
&\int_0^1 RB_0(t)\, J_r^{(\alpha)}(t) w_1(t)\, dt = 0, \quad 0 \le r \le M-1,\\
&\int_0^1 RB_1(t)\, J_r^{(\alpha)}(t) w_1(t)\, dt = 0, \quad 0 \le r \le M-1.
\end{aligned} \tag{73}$$

The substitution by the four residuals in equations (69), (70), (71), and (72) yields, respectively, the following equations:

Table 2: MAE for Example 2.

M	$\alpha = 0$	$\alpha = 1/2$	$\alpha = 1$
3	4.24×10^{-3}	8.27×10^{-3}	2.16×10^{-2}
5	5.37×10^{-6}	5.69×10^{-6}	4.88×10^{-5}
7	2.66×10^{-8}	7.28×10^{-8}	8.61×10^{-8}

$$\begin{aligned}
&\sum_{r=1}^{M} d_{s,r,1}\, nu_{rn}\, h_r\, h_{s,1} - \sum_{s=2}^{M} d_{r,s,2}\, v_{ms}\, h_r\, h_s - \kappa\, nu_{rs}\, h_r\, h_s\\
&\quad + \kappa \sum_{\bar{n}=0}^{M}\sum_{\bar{s}=0}^{M}\sum_{n=0}^{M}\sum_{s=0}^{M} G_{r,\bar{s},s}\, G_{r,\bar{n},n}\, v_{\bar{s}\bar{n}}\, v_{rs} h_r\, h_s = 0, \quad 0 \le r \le M-1, 0 \le s \le M-1,
\end{aligned} \tag{74}$$

$$\sum_{n=0}^{M} v_{0n}\, h_0\, J_n^{(\alpha)}(0) = \int_0^1 \eta(x) J_0^{(\alpha)}(x) w_1(x)\, dx, \tag{75}$$

$$\sum_{s=0}^{M} v_{mr}\, h_r J_s^{(\alpha)}(0) = \int_0^1 \xi_0(t) J_r^{(\alpha)}(t) w_1(t)\, dt, \quad 0 \le r \le M-1, \tag{76}$$

$$\sum_{s=0}^{M} v_{mr} h_r J_s^{(\alpha)}(1) = \int_0^1 \xi_1(t) J_r^{(\alpha)}(t) w_1(t)\, dt, \quad 0 \le r \le M-1, \tag{77}$$

where $J_i^{(\alpha)}(0) = ((-1)^i\,(i+\alpha+1))/(\alpha+1)$ and $J_i^{(\alpha)}(1) = 1$.

The proposed tau approach produces the nonlinear system of equations (74)-(77) with the unknowns $\{v_{rs}\}$ of

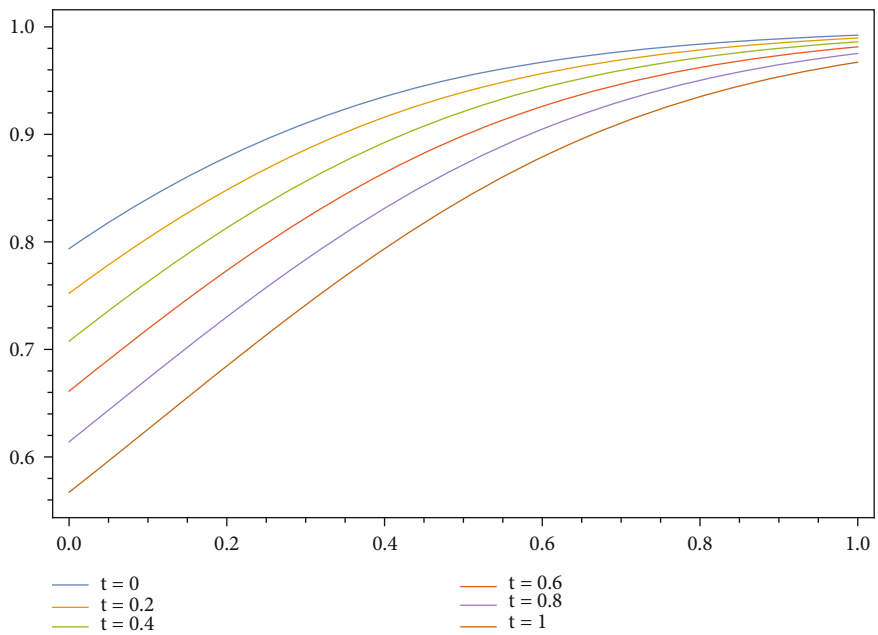

Figure 7: Solution of Example 3 at different values of t.

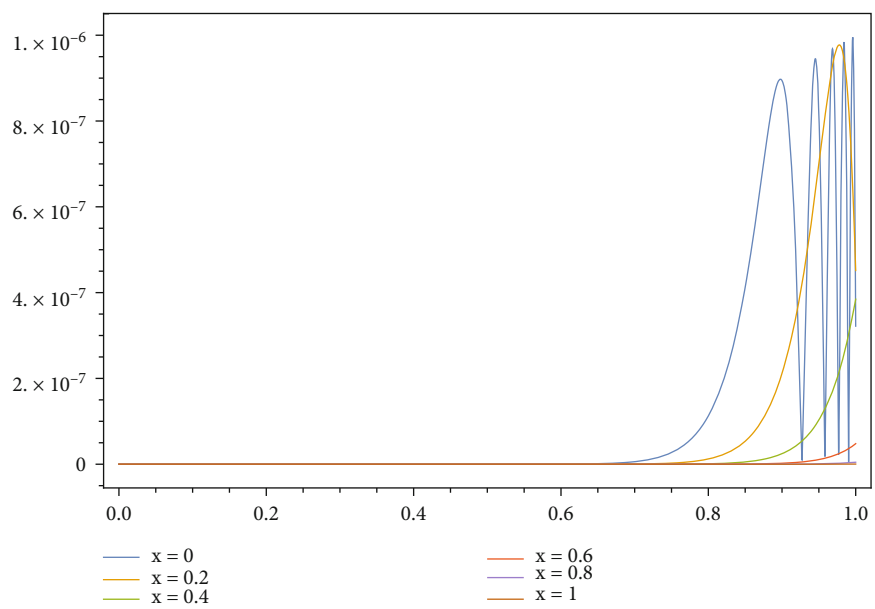

Figure 8: Absolute error of Example 3 at different values of x.

dimension M^2. It is necessary to solve this nonlinear system to obtain the desired approximate solution. This can be accomplished by using a suitable numerical method, such as Newton's iterative technique.

Remark 15. It is very imperative to communique here that if the term $\kappa\mathscr{V}(1-\mathscr{V})$ is replaced by $\kappa\mathscr{V}(1-\mathscr{V}^m)$, where m is any positive integer, then the repeated use of linearization formula (59) will generate a system that is similar to ((73))-((76)). This means our algorithm can be extended to solve this generalized Fisher problem. The details are omitted.

Remark 16. To summarize our proposed numerical algorithm, in Algorithm 1, we list in order the steps required to obtain the desired numerical solution.

6. Numerical Experiments and Comparisons

Example 1. Consider the following nonlinear Fisher equation [32]:

$$\frac{\partial\mathscr{V}}{\partial t} = \frac{\partial^2\mathscr{V}}{\partial x^2} + 6\mathscr{V}(1-\mathscr{V}), \quad (x,t)\in\Omega=(0,1)\times(0,1), \tag{78}$$

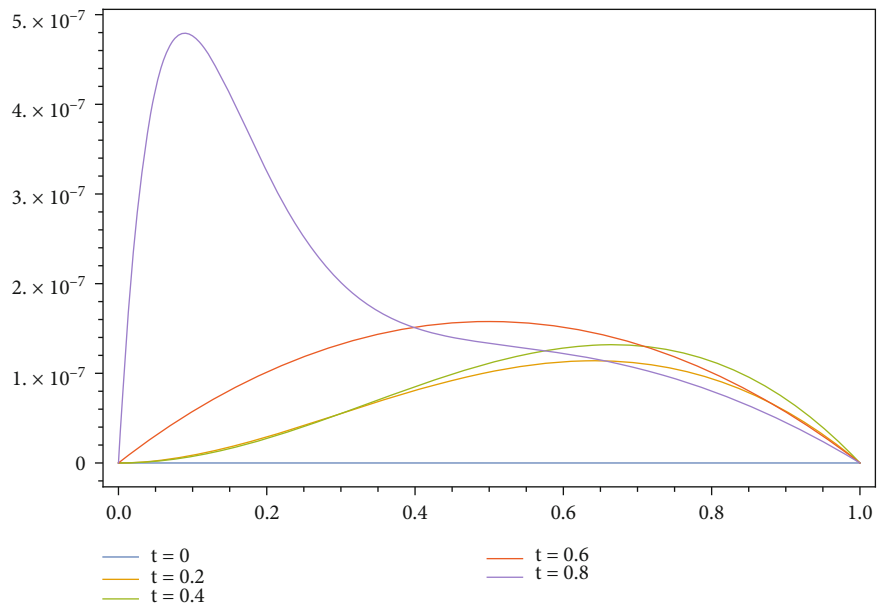

Figure 9: Absolute error of Example 3 at different values of t.

Table 3: MAE for Example 3.

M	$\alpha = 0$	$\alpha = 1/2$	$\alpha = 1$
4	5.27×10^{-3}	2.48×10^{-3}	6.87×10^{-3}
6	3.41×10^{-5}	4.29×10^{-5}	8.63×10^{-5}
8	4.73×10^{-8}	5.27×10^{-7}	9.37×10^{-7}

along with

$$\mathscr{V}(x,0) = (1+e^{x})^{-2}, \quad x \in (0,1), \tag{79}$$

and the boundary conditions:

$$\begin{aligned} \mathscr{V}(0,t) &= \left(1+e^{-5t}\right)^{-2}, \\ \mathscr{V}(1,t) &= \left(1+e^{1-5t}\right)^{-2}, \quad t \in (0,1), \end{aligned} \tag{80}$$

with the exact solution

$$\mathscr{V}(x,t) = \left(1+e^{x-5t}\right)^{-2}. \tag{81}$$

We apply the NJTM for the case corresponding to $\alpha = 0$, $M = 8$. In Figure 1, we depict the approximate solution of Example 1 at different values of x. In Figure 2, we depict the absolute error of Example 1 at different values of x. In Figure 3, we depict the absolute error of Example 1 at different values of t. In Table 1, we report the maximum absolute error (MAE) for different values of M and α.

Example 2. Consider the following nonlinear Fisher equation [32]:

$$\frac{\partial \mathscr{V}}{\partial t} = \frac{\partial^2 \mathscr{V}}{\partial x^2} + \mathscr{V}(1-\mathscr{V}), (x,t) \in \Omega = (0,1) \times (0,1), \tag{82}$$

along with

$$\mathscr{V}(x,0) = \frac{1}{\left(e^{x/\sqrt{6}}+1\right)^2}, \tag{83}$$

and the boundary conditions:

$$\mathscr{V}(0,t) = \frac{1}{\left(e^{-5t/6}+1\right)^2}, \mathscr{V}(1,t) = \frac{1}{\left(e^{(1/\sqrt{6})-(5t/6)}+1\right)^2}, \quad t \in (0,1), \tag{84}$$

with the exact solution

$$\mathscr{V}(x,t) = \frac{1}{\left(e^{(x/\sqrt{6})-(5t/6)}+1\right)^2}. \tag{85}$$

We apply NJTM for the case corresponding to $\alpha = 1/2$, $M = 7$. Figure 4 displays the approximate solutions of Example 2 at different values of t. Additionally, Figure 5 displays the absolute error of Example 2 at different values of x. Figure 6 displays the absolute error of Example 2 at different values of t. Finally, Table 2 reports the MAE for different values of M and α.

Example 3. Consider the following nonlinear Fisher equation ([32, 43]):

$$\frac{\partial \mathscr{V}}{\partial t} = \frac{\partial^2 \mathscr{V}}{\partial x^2} + \mathscr{V}\left(1 - \mathscr{V}^6\right), (x, t) \in \Omega = (0, 1) \times (0, 1), \quad (86)$$

along with

$$\mathscr{V}(x, 0) = \sqrt[3]{\frac{1}{2} - \frac{1}{2}\tanh\left(\frac{3x}{4}\right)}, \quad x \in (0, 1), \quad (87)$$

and the boundary conditions:

$$\begin{aligned}\mathscr{V}(0, t) &= \sqrt[3]{\frac{1}{2}\tanh\left(\frac{15t}{8}\right) + \frac{1}{2}}, \mathscr{V}(1, t) \\ &= \sqrt[3]{\frac{1}{2} - \frac{1}{2}\tanh\left(\frac{3}{4}\left(1 - \frac{5t}{2}\right)\right)}, \quad t \in (0, 1),\end{aligned} \quad (88)$$

with the exact solution

$$\mathscr{V}(x, t) = \sqrt[3]{\frac{1}{2} - \frac{1}{2}\tanh\left(\frac{3}{4}\left(x - \frac{5t}{2}\right)\right)}. \quad (89)$$

We apply NJTM for the case corresponding to $\alpha = 1$, $M = 8$. In Figure 7, we depict the solution of Example 3 at different values of t. Figure 8 shows the absolute error of Example 3 at different values of x, while Figure 9 shows the absolute error of Example 3 at different values of t. The MAE for different values of M and α is reported in Table 3.

7. Concluding Remarks

In this article, a novel linearization formula of a class of Jacobi polynomials that generalizes the third-kind Chebyshev polynomials was established. The establishment of this linearization formula depends on using a new moment formula of these polynomials together with the employment of suitable symbolic computation. The linearization formula and the high-order derivative formula of a certain class of Jacobi polynomials are utilized along with the spectral tau method to develop a new numerical algorithm for treating the nonlinear Fisher equation. We do believe that our theoretical results and the proposed numerical results are new. Furthermore, other types of nonlinear differential equations may be treated using similar techniques. Some illustrative examples were presented accompanied by some comparisons to validate the accuracy and efficiency and the proposed tau algorithm.

Data Availability

No data is associated with this research.

Conflicts of Interest

The authors declare that they have no conflicts of interest.

References

[1] Y. Yang, J. Wang, S. Zhang, and E. Tohidi, "Convergence analysis of space-time Jacobi spectral collocation method for solving time-fractional Schrodinger equations," *Applied Mathematics and Computation*, vol. 387, article 124489, 2020.

[2] G. Deng, Y. Yang, and E. Tohidi, "High accurate pseudo-spectral Galerkin scheme for pantograph type Volterra integro-differential equations with singular kernels," *Applied Mathematics and Computation*, vol. 396, article 125866, 2021.

[3] Y. Yang, G. Rzadkowski, A. Pasban, E. Tohidi, and S. Shateyi, "A high accurate scheme for numerical simulation of two-dimensional mass transfer processes in food engineering," *Alexandria Engineering Journal*, vol. 60, no. 2, pp. 2629–2639, 2021.

[4] B. Zogheib, E. Tohidi, H. M. Baskonus, and C. Cattani, "Method of lines for multi-dimensional coupled viscous Burgers' equations via nodal Jacobi spectral collocation method," *Physica Scripta*, vol. 96, no. 12, article 124011, 2021.

[5] T. J. Rivlin, *Chebyshev Polynomials*, Courier Dover Publications, 2020.

[6] J. C. Mason and D. C. Handscomb, *Chebyshev Polynomials*, Chapman and Hall, New York, NY, CRC, Boca Raton, 2002.

[7] S. D. Oloniiju, S. P. Goqo, and P. Sibanda, "A Chebyshev pseudo-spectral method for the multi-dimensional fractional Rayleigh problem for a generalized Maxwell fluid with Robin boundary conditions," *Applied Numerical Mathematics*, vol. 152, pp. 253–266, 2020.

[8] E. H. Doha, W. M. Abd-Elhameed, and M. A. Bassuony, "On the coefficients of differentiated expansions and derivatives of Chebyshev polynomials of the third and fourth kinds," *Acta Mathematica Scientia*, vol. 35, no. 2, pp. 326–338, 2015.

[9] W. M. Abd-Elhameed and Y. H. Youssri, "New formulas of the high-order derivatives of fifth-kind Chebyshev polynomials: spectral solution of the convection–diffusion equation," *Numerical Methods for Partial Differential Equations*, 2021.

[10] M. Rahman, "A non-negative representation of the linearization coefficients of the product of Jacobi polynomials," *Canadian Journal of Mathematics*, vol. 33, no. 4, pp. 915–928, 1981.

[11] H. Chaggara and W. Koepf, "On linearization coefficients of Jacobi polynomials," *Applied Mathematics Letters*, vol. 23, no. 5, pp. 609–614, 2010.

[12] W. M. Abd-Elhameed, "New formulae between Jacobi polynomials and some fractional Jacobi functions generalizing some connection formulae," *Analysis and Mathematical Physics*, vol. 9, no. 1, pp. 73–98, 2019.

[13] C. Canuto, M. Y. Hussaini, A. Quarteroni, and T. A. Zang, *Spectral Methods in Fluid Dynamics*, Springer-Verlag, 1988.

[14] B. Shizgal, *Spectral Methods in Chemistry and Physics*, Springer, 2015.

[15] J. Hesthaven, S. Gottlieb, and D. Gottlieb, *Spectral Methods for Time-Dependent Problems, volume 21*, Cambridge University Press, 2007.

[16] S. Sabermahani and Y. Ordokhani, "Fibonacci wavelets and Galerkin method to investigate fractional optimal control problems with bibliometric analysis," *Journal of Vibration and Control*, vol. 27, no. 15-16, pp. 1778–1792, 2021.

[17] K. Sadri and H. Aminikhah, "Chebyshev polynomials of sixth kind for solving nonlinear fractional PDEs with proportional delay and its convergence analysis," *Journal of Function Spaces*, vol. 2022, Article ID 9512048, 20 pages, 2022.

[18] M. A. Ramadan, T. Radwan, M. A. Nassar, and M. A. Abd El Salam, "A comparison study of numerical techniques for solving ordinary differential equations defined on a semi-infinite domain using rational Chebyshev functions," *Journal of Function Spaces*, vol. 2021, Article ID 1111417, 12 pages, 2021.

[19] Y. Yang, E. Tohidi, X. Ma, and S. Kang, "Rigorous convergence analysis of Jacobi spectral Galerkin methods for Volterra integral equations with noncompact kernels," *Journal of Computational and Applied Mathematics*, vol. 366, article 112403, 2020.

[20] Y. Yang, G. Deng, and E. Tohidi, "High accurate convergent spectral Galerkin methods for nonlinear weakly singular Volterra integro-differential equations," *Computational and Applied Mathematics*, vol. 40, no. 4, pp. 1–32, 2021.

[21] A. Faghih and P. Mokhtary, "An efficient formulation of Chebyshev tau method for constant coefficients systems of multi-order FDEs," *Journal of Scientific Computing*, vol. 82, no. 1, pp. 1–25, 2020.

[22] F. Mohammadi and C. Cattani, "A generalized fractional-order Legendre wavelet tau method for solving fractional differential equations," *Journal of Computational and Applied Mathematics*, vol. 339, pp. 306–316, 2018.

[23] W. M. Abd-Elhameed and Y. H. Youssri, "Spectral tau algorithm for certain coupled system of fractional differential equations via generalized Fibonacci polynomial sequence," *Iranian Journal of Science and Technology, Transactions A: Science*, vol. 43, no. 2, pp. 543–554, 2019.

[24] A. G. Atta, G. M. Moatimid, and Y. H. Youssri, "Generalized Fibonacci operational tau algorithm for fractional Bagley-Torvik equation," *Progress in Fractional Differentiation and Applications*, vol. 6, no. 3, pp. 215–224, 2020.

[25] F. Costabile and A. Napoli, "Collocation for high order differential equations with two-points Hermite boundary conditions," *Applied Numerical Mathematics*, vol. 87, pp. 157–167, 2015.

[26] F. Costabile and A. Napoli, "A method for high-order multipoint boundary value problems with Birkhoff-type conditions," *International Journal of Computer Mathematics*, vol. 92, no. 1, pp. 192–200, 2015.

[27] V. Saw and S. Kumar, "The Chebyshev collocation method for a class of time fractional convection- diffusion equation with variable coefficients," *Mathematicsl Methods in the Applied Sciences*, vol. 44, no. 8, pp. 6666–6678, 2021.

[28] J. A. Sherratt, "On the transition from initial data to travelling waves in the Fisher-KPP equation," *Dynamics and Stability of Systems*, vol. 13, no. 2, pp. 167–174, 1998.

[29] J. Canosa, "On a nonlinear diffusion equation describing population growth," *IBM Journal of Research and Development*, vol. 17, no. 4, pp. 307–313, 1973.

[30] A. M. Wazwaz and A. Gorguis, "An analytic study of Fisher's equation by using Adomian decomposition method," *Applied Mathematics and Computation*, vol. 154, no. 3, pp. 609–620, 2004.

[31] V. Chandraker, A. Awasthi, and S. Jayaraj, "Implicit numerical techniques for Fisher equation," *Journal of Information and Optimization Sciences*, vol. 39, no. 1, pp. 1–13, 2018.

[32] G. Hariharan, K. Kannan, and K. R. Sharma, "Haar wavelet method for solving Fisher's equation," *Applied Mathematics and Computation*, vol. 211, no. 2, pp. 284–292, 2009.

[33] K. Al-Khaled, "Numerical study of Fisher's reaction-diffusion equation by the Sinc collocation method," *Journal of Computational and Applied Mathematics*, vol. 137, no. 2, pp. 245–255, 2001.

[34] M. M. Khader and M. Adel, "Numerical and theoretical treatment based on the compact finite difference and spectral collocation algorithms of the space fractional-order Fisher's equation," *International Journal of Modern Physics C*, vol. 31, no. 9, article 2050122, 2020.

[35] M. Bastani and D. K. Salkuyeh, "A highly accurate method to solve Fisher's equation," *Pramana*, vol. 78, no. 3, pp. 335–346, 2012.

[36] D. Olmos and B. D. Shizgal, "A pseudospectral method of solution of Fisher's equation," *Journal of Computational and Applied Mathematics*, vol. 193, no. 1, pp. 219–242, 2006.

[37] W. M. Abd-Elhameed and A. M. Alkenedri, "Spectral solutions of linear and nonlinear BVPs using certain Jacobi polynomials generalizing third- and fourth-kinds of Chebyshev polynomials," *Computer Modeling in Engineering & Sciences*, vol. 126, no. 3, pp. 955–989, 2021.

[38] G. E. Andrews, R. Askey, and R. Roy, *Special Functions*, Cambridge University Press, Cambridge, 2013.

[39] W. Koepf, *Hypergeometric Summation*, Springer Universitext Series, 2nd edition, 2014, http://www.hypergeometric-summation.org.

[40] E. H. Doha, W. M. Abd-Elhameed, and M. A. Bassuony, "New algorithms for solving high even-order differential equations using third and fourth Chebyshev-Galerkin methods," *Journal of Computational Physics*, vol. 236, pp. 563–579, 2013.

[41] E. H. Doha and W. M. Abd-Elhameed, "New linearization formulae for the products of Chebyshev polynomials of third and fourth kinds," *The Rocky Mountain Journal of Mathematics*, vol. 46, no. 2, pp. 443–460, 2016.

[42] W. M. Abd-Elhameed, "New product and linearization formulae of Jacobi polynomials of certain parameters," *Integral Transforms and Special Functions*, vol. 26, no. 8, pp. 586–599, 2015.

[43] H. B. Jebreen, "On the numerical solution of Fisher's equation by an efficient algorithm based on multiwavelets," *AIMS Mathematics*, vol. 6, no. 3, pp. 2369–2384, 2020.

Hindawi
Journal of Function Spaces
Volume 2022, Article ID 1541486, 15 pages
https://doi.org/10.1155/2022/1541486

Research Article

A Modified Algorithm Based on Haar Wavelets for the Numerical Simulation of Interface Models

Gule Rana,[1] Muhammad Asif,[2] Nadeem Haider,[2] Rubi Bilal,[1] Muhammad Ahsan,[3] Qasem Al-Mdallal,[4] and Fahd Jarad[5,6]

[1]*Department of Mathematics, Shaheed Benazir Bhutto Women University, Peshawar, Pakistan*
[2]*Department of Mathematics, University of Peshawar, Peshawar, Khyber Pakhtunkhwa, Pakistan*
[3]*Department of Mathematics, University of Swabi, Swabi, Khyber Pakhtunkhwa, Pakistan*
[4]*Department of Mathematical Sciences, UAE University, P.O. Box, 15551 Al Ain, UAE*
[5]*Department of Mathematics, Çankaya University, Ankara 06790, Turkey*
[6]*Department of Medical Research, China Medical University, Taichung 40402, Taiwan*

Correspondence should be addressed to Fahd Jarad; fahd@cankaya.edu.tr

Received 15 September 2021; Revised 20 May 2022; Accepted 13 July 2022; Published 9 August 2022

Academic Editor: Anna Napoli

In this paper, a new numerical technique is proposed for the simulations of advection-diffusion-reaction type elliptic and parabolic interface models. The proposed technique comprises of the Haar wavelet collocation method and the finite difference method. In this technique, the spatial derivative is approximated by truncated Haar wavelet series, while for temporal derivative, the finite difference formula is used. The diffusion coefficients, advection coefficients, and reaction coefficients are considered discontinuously across the fixed interface. The newly established numerical technique is applied to both linear and nonlinear benchmark interface models. In the case of linear interface models, Gauss elimination method is used, whereas for nonlinear interface models, the nonlinearity is removed by using the quasi-Newton linearization technique. The L_∞ errors are calculated for different number of collocation points. The obtained numerical results are compared with the immersed interface method. The stability and convergence of the method are also discussed. On the whole, the numerical results show more efficiency, better accuracy, and simpler applicability of the newly developed numerical technique compared to the existing methods in literature.

1. Introduction

Interface models play an important role in many disciplines including electromagnetic wave propagation, material science, fluid dynamics, and biological systems. The shared boundary between the two intervals in case of one-dimensional domains or between two regions in case of higher-dimensional domains is known as an interface. These domains (intervals or regions) are kept together with the help of suitable jump constraints. These phenomena can be modeled by using partial differential equations (PDEs) or ordinary differential equations (ODEs), where the parameters in these differential equations across the interface separating the two materials or states are discontinuous. Interface model is a mathematical model which considers two identical or different materials at different states having a shared boundary. The example of interface models with same materials in different states is water and ice, while water and oil is an example of interface models with different materials [1, 2]. These models frequently arise in heat conduction, Navier-Stokes flows, crystal growth, wave propagation through nonhomogeneous media, and models of solidification. Most of the interface model equations consist of highly varying coefficients [1, 3, 4]. The approximations of various physical and biomedical models often consist of highly varying coefficients or heterogeneous ODE or PDE models [5].

The solution of these models is a challenge for many standard numerical methods such as finite element method,

finite volume method, and finite difference method. These methods have either poor performance or unable to catch the discontinuity in the solution. Due to the numerous applications of such type of models, several numerical methods have been introduced for the solution of these models with regular and irregular geometries in literature. Some of the numerical methods are immersed boundary method (IBM) [6, 7], immersed interface method (IIM) [1, 8], ghost fluid method (GFM) [9], matched interface and boundary method (MIBM) [10–12], the method based on the integral equations approach [13], and finite element methods [14–17].

Recently, wavelet analysis has got much popularity in the approximation theory. Different wavelets and approximating functions are introduced for approximation purpose. Wavelets have simple and fast algorithms, which result better approximation. Among all these wavelets, Haar wavelet has got great importance due to their simplicity and applications. Haar wavelet contains piecewise constant box functions. The Haar wavelet collocation method (HWCM) got attention of many authors due their simple nature, properties of orthogonality, and compact support. The Haar wavelet contains piecewise constant functions; therefore, complicated models can be approximated very easily using these wavelets. Besides, several types of boundary conditions including local and nonlocal conditions can be utilized. Various applications of HWCM in the approximation theory can be seen in [18–27]. Some of the recent work using Haar wavelets is given in [28–36].

In this article, a new approach based on Haar wavelet and finite difference method is developed for the numerical solution of advection-diffusion-reaction type elliptic and parabolic interface models.

The article is organized as follow. In Section 3, definition of the Haar wavelet and their integrals are presented. In Section 4, construction of the newly proposed numerical method based on Haar wavelet and FDM is given. The convergence and stability analysis of the proposed numerical method are discussed in Sections 5 and 6. In Section 7, numerical validation of the method is given. In the last section, conclusion is presented.

2. Governing Models

2.1. Elliptic Interface Model. Consider the following forms of linear and nonlinear elliptic interface models:

$$\alpha(\eta)v_\eta(\eta) - \left(\beta(\eta)v_\eta(\eta)\right)_\eta + \sigma(\eta)v(\eta) = f(\eta), a < \eta < b, \quad (1)$$

$$\psi\left(v_{\eta\eta}(\eta), v_\eta(\eta), v(\eta), \alpha(\eta), \beta(\eta), \sigma(\eta), \eta\right) = f(\eta), a < \eta < b. \quad (2)$$

At the interface point $\eta = \zeta$, the interval $I = [a, b]$ is divided into two subintervals $I_1 = [a, \zeta]$ and $I_2 = [\zeta, b]$. The functions involved in Equations (1) and (2) are of the form

$$(\alpha(\eta), \beta(\eta), v(\eta), \sigma(\eta), f(\eta)) = \begin{cases} (\alpha_1(\eta), \beta_1(\eta), v_1(\eta), \sigma_1(\eta), f_1(\eta)), & \text{for } \eta \in I_1, \\ (\alpha_2(\eta), \beta_2(\eta), v_2(\eta), \sigma_2(\eta), f_2(\eta)), & \text{for } \eta \in I_2. \end{cases} \quad (3)$$

The Dirichlet boundary conditions at boundary points $\eta = a$ and $\eta = b$ are given by

$$\begin{aligned} v(a) &= \gamma_1, \\ v(b) &= \gamma_2. \end{aligned} \quad (4)$$

The following interface conditions are considered at the interface point $\eta = \zeta$:

$$[v]_\zeta = v_2(\zeta) - v_1(\zeta) = \mu_1, \quad (5)$$

$$\left[\alpha - \beta v_\eta\right]_\zeta = \left(\alpha_2 - \beta_2(\zeta)v_{2\eta}(\zeta)\right) - \left(\alpha_1 - \beta_1(\zeta)v_{1\eta}(\zeta)\right) = \mu_2, \quad (6)$$

where $f_1(\eta)$, $\alpha_1(\eta) > 0$, $\beta_1(\eta) > 0$, and $\sigma_1(\eta) \geq 0$ and $f_2(\eta)$, $\alpha_2(\eta) > 0$, $\beta_2(\eta) > 0$, and $\sigma_2(\eta) \geq 0$ are known functions defined on I_1 and I_2, respectively.

2.2. Parabolic Interface Model. The following forms of linear and nonlinear parabolic interface models are considered:

$$v_t(\eta, t) + \alpha(\eta, t)v_\eta(\eta, t) = \left(\beta(\eta, t)v_\eta(\eta, t)\right)_\eta - \sigma(\eta, t)v(\eta, t) + f(\eta, t), a < \eta < b, 0 \leq t \leq 1, \quad (7)$$

$$\psi\left(v_t(\eta, t), v_{\eta\eta}(\eta, t), v_\eta(\eta, t), v(\eta, t), \alpha(\eta, t), \beta(\eta, t), \sigma(\eta, t), \eta, t\right) = f(\eta, t), a < \eta < b, 0 \leq t \leq 1. \quad (8)$$

The interface point $\eta = \zeta$ divides the interval I into two subintervals I_1 and I_2, where I, I_1, and I_2 are the same as given in the above elliptic problem. The functions involved in Equations (7) and (8) are of the following form:

$$(\alpha(\eta, t), \beta(\eta, t), v(\eta, t), \sigma(\eta, t), f(\eta, t)) = \begin{cases} (\alpha_1(\eta, t), \beta_1(\eta, t), v_1(\eta, t), \sigma_1(\eta, t), f_1(\eta, t)), & \text{for } \eta \in I_1, \\ (\alpha_2(\eta, t), \beta_2(\eta, t), v_2(\eta, t), \sigma_2(\eta, t), f_2(\eta, t)), & \text{for } \eta \in I_2. \end{cases} \quad (9)$$

Subject to the following initial and Dirichlet boundary conditions points $\eta = a$ and $\eta = b$,

$$\begin{aligned} v(\eta, 0) &= v_0(\eta), \text{on } I, \\ v(a, t) &= \gamma_1(t), \\ v(b, t) &= \gamma_2(t). \end{aligned} \quad (10)$$

The following interface conditions are considered at the interface point $\eta = \zeta$:

$$[v]_\zeta = v_2(\zeta, t) - v_1(\zeta, t) = \mu_1(t), \tag{11}$$

$$\begin{aligned}[\alpha - \beta v_\eta]_\zeta &= \left(\alpha_2(\zeta, t) - \beta_2(\zeta, t) v_{2\eta}(\zeta, t)\right) - \left(\alpha_1(\zeta, t) - \beta_1(\zeta, t) v_{1\eta}(\zeta, t)\right) \\ &= \mu_2(t).\end{aligned} \tag{12}$$

The functions $f_1(\eta)$, $\alpha_1(\eta) > 0$, $\beta_1(\eta) > 0$, and $\sigma_1(\eta) \geq 0$ and $f_2(\eta)$, $\alpha_2(\eta) > 0$, $\beta_2(\eta) > 0$, and $\sigma_2(\eta) \geq 0$ are smooth functions defined on I_1 and I_2, respectively.

3. Haar Wavelets

The ith wavelet of the Haar family over $[0, 1)$ is defined as [37]

$$h_i(\eta) = \begin{cases} 1 & \text{for } \eta \in [\delta_1, \delta_2), \\ -1 & \text{for } \eta \in [\delta_2, \delta_3), i = 2, 3, \cdots, \\ 0 & \text{elsewhere}, \end{cases} \tag{13}$$

where

$$\begin{aligned} \delta_1 &= \frac{k}{m}, \\ \delta_2 &= \frac{k + 0.5}{m}, \\ \delta_3 &= \frac{k + 1}{m}. \end{aligned} \tag{14}$$

In the above equations, m and k are integers such that $m = 2^j, j = 0, 1, \cdots$, and $k = 0, 1, \cdots, m - 1$. The level of the resolution of the Haar wavelet and the translation parameter are represented by the integers j and k, respectively. For approximation purposes, we consider a maximal value J of the integer j. The integer J is then called maximal level of resolution. We also define $\mathscr{M} = 2^J$. The equation $i = m + k + 1$ shows the relation among i, m, and k. The minimal and maximal values of i can be obtained from the equation $i = m + k + 1$. If $m = 1$, $k = 0$, then minimal value is $i = 2$ and the maximal value is $i = 2\mathscr{M} = 2^{J+1}$. For $i = 1$, we get $h_1(\eta)$, which is known as scaling function for Haar wavelet family and is defined as

$$h_i(\eta) = \begin{cases} 1 & \text{for } \eta \in [0, 1), \\ 0 & \text{elsewhere}. \end{cases} \tag{15}$$

Any square integrable function $f(\eta)$ over the interval $(0, 1)$ can be expressed as infinite sum of functions of the Haar wavelet family as

$$f(\eta) = \sum_{i=1}^{\infty} a_i h_i(\eta). \tag{16}$$

For approximation purpose, the above series is truncated to a finite sum in the following manner:

$$f(\eta) = \sum_{i=1}^{2\mathscr{M}} a_i h_i(\eta), \tag{17}$$

where $\mathscr{M}$ is the maximal resolution defined above. All other members of the Haar family can be obtained from Equation (13) by the process of dilation and translation. The following notations are introduced for Haar integrals:

$$\begin{aligned} P_{i,1}(\eta) &= \int_0^\eta h_i(z) dz, \\ P_{i,\nu+1}(\eta) &= \int_0^\eta p_{i,\nu}(z) dz, \nu = 1, 2, \cdots. \end{aligned} \tag{18}$$

These integrals can be calculated utilizing Equation (13) and are given below.

$$P_{i,n}(\eta) \begin{cases} 0 & \text{for } \eta \in [0, \delta_1), \\ \frac{1}{n!}(\eta - \delta_1)^n & \text{for } \eta \in [\delta_1, \delta_2), \\ \frac{1}{n!}\left[(\eta - \delta_1)^n - 2(\eta - \delta_2)^n\right] & \text{for } \eta \in [\delta_2, \delta_3), \\ \frac{1}{n!}\left[(\eta - \delta_1)^n - 2(\eta - \delta_2)^n + (\eta - \delta_3)^n\right] & \text{for } \eta \in [\delta_3, 1), \\ n = 1, 2, \cdots \end{cases} \tag{19}$$

where $i = 2, 3, \cdots$. For $i = 1$, we have

$$P_{1,n}(\eta) = \frac{\eta^n}{n!}, n = 1, 2, 3, \cdots. \tag{20}$$

4. Numerical Procedure

In this section, formulation of numerical technique both for elliptic and parabolic advection-diffusion-reaction type interface models is discussed. The interval of study is considered to be $[a, b] = [0, 1]$.

4.1. HWCM for Elliptic Model with Single Interface. In this technique, the higher-order spatial derivative is approximated by truncated Haar series; the approximate expressions for the lower order derivatives and for the unknown function are calculated by integration process. The details of the procedure are given below:

$$v_{1\eta\eta}(\eta) = \sum_{i=1}^{2\mathscr{M}} a_i h_i(\eta), \eta \in I_1. \tag{21}$$

Integrating Equation (21), from η to ζ, we get

$$v_{1\eta} = v_{1\eta}(\zeta) + \sum_{i=1}^{2\mathscr{M}} a_i \left(p_{i,1}(\eta) - p_{i,1}(\zeta)\right), \eta \in I_1. \tag{22}$$

Again integrating from 0 to η, we have

$$v_1(\eta) = \gamma_1 + \eta v_{1\eta}(\zeta) + \sum_{i=1}^{2\mathscr{M}} a_i\left(p_{i,2}(\eta) - \eta p_{i,1}(\zeta)\right), \eta \in I_1. \quad (23)$$

Similarly, we can approximate the second function $v_2(\eta)$ over the second subinterval $I_2 = [\zeta, 1]$ as follows:

$$v_{2\eta\eta}(\eta) = \sum_{i=1}^{2\mathscr{M}} b_i h_i(\eta), \eta \in I_2. \quad (24)$$

Integrating Equation (24), we get the expressions $v_2(\eta)$ and $v_{2\eta}(\eta)$ as follows:

$$v_{2\eta}(\eta) = v_{2\eta}(\zeta) + \sum_{i=1}^{2\mathscr{M}} b_i p_{i,1}(\eta), \eta \in I_2, \quad (25)$$

$$v_2(\eta) = \gamma_2 - (1-\eta) v_{2\eta}(\zeta) + \sum_{i=1}^{2\mathscr{M}} b_i\left(p_{i,2}(\eta) - p_{i,2}(1)\right), \eta \in I_2. \quad (26)$$

After substituting the Haar expression, Equations (5) and (6) become

$$\left(\gamma_2 - (1-\zeta) v_{2\eta}(\zeta) + \sum_{i=1}^{2\mathscr{M}} b_i\left(p_{i,2}(\zeta) - p_{i,2}(1)\right)\right) - \left(\gamma_1 + \zeta v_{1\eta}(\zeta) + \sum_{i=1}^{2\mathscr{M}} a_i\left(p_{i,2}(\zeta) - \zeta p_{i,1}(\zeta)\right)\right) = \mu_1, \quad (27)$$

$$\left(\alpha_2(\zeta) - \beta_2(\zeta)\left(v_{2\eta}(\zeta) + \sum_{i=1}^{2\mathscr{M}} b_i p_{i,1}(\zeta)\right)\right) - \left(\alpha_1(\zeta) - \beta_1(\zeta)\left(v_{1\eta}(\zeta) + \sum_{i=1}^{2\mathscr{M}} a_i\left(p_{i,1}(\zeta) - p_{i,1}(\zeta)\right)\right)\right) = \mu_2. \quad (28)$$

The remaining procedure will be explained separately for both linear and nonlinear cases.

4.1.1. Linear Case. Substituting the values of $v_1(\eta)$, $v_{1\eta}(\eta)$, and $v_{1\eta\eta}(\eta)$ in Equation (1) and simplifying, we have

$$\left(\alpha_1(\eta) - \beta_{1\eta}(\eta)\right)\left(v_{1\eta}(\zeta) + \sum_{i=1}^{2\mathscr{M}} a_i\left(p_{i,1}(\eta) - p_{i,1}(\zeta)\right)\right) - \beta_1(\eta)\sum_{i=1}^{2\mathscr{M}} a_i h_i(\eta) + \sigma_1(\eta)\left(\gamma_1 + \eta v_{1\eta}(\zeta) + \sum_{i=1}^{2\mathscr{M}} a_i\left(p_{i,2}(\eta) - \eta p_{i,1}(\zeta)\right)\right) = f_1(\eta), \eta \in I_1. \quad (29)$$

Similarly, substituting the values of $v_2(\eta)$, $v_{2\eta}(\eta)$, and $v_{2\eta\eta}(\eta)$ in Equation (1), we get

$$\left(\alpha_2(\eta) - \beta_{2\eta}(\eta)\right)\left(v_{2\eta}(\zeta) + \sum_{i=1}^{2\mathscr{M}} b_i p_{i,1}(\eta)\right) - \beta_2(\eta)\sum_{i=1}^{2\mathscr{M}} b_i h_i(\eta) + \sigma_2(\eta) \cdot \left(\gamma_2 - (1-\eta) v_{2\eta}(\zeta) + \sum_{i=1}^{2\mathscr{M}} b_i\left(p_{i,2}(\eta) - p_{i,2}(1)\right)\right) = f_2(\eta), \eta \in I_2. \quad (30)$$

The following discrete points are used for single interface problem:

$$\eta_{c'} = \begin{cases} \dfrac{\zeta\left(c' - 0.5\right)}{2\mathscr{M}}, & \text{for } c' = 1, 2, \cdots, 2\mathscr{M}, \\ \dfrac{\zeta + (1-\zeta)\left(c' - 2\mathscr{M} - 0.5\right)}{2\mathscr{M}}, & \text{for } c' = 2\mathscr{M}+1, 2\mathscr{M}+2, \cdots, 4\mathscr{M}. \end{cases} \quad (31)$$

After discretization, we get the subsequent forms of Equations (29) and (30):

$$\sum_{i=1}^{2\mathscr{M}} a_i\Big(\left(\alpha_1\left(\eta_j\right) - \beta_{1\eta}\left(\eta_j\right)\right)\left(p_{i,1}\left(\eta_j\right) - p_{i,1}(\zeta)\right) - \beta_1\left(\eta_j\right) h_i\left(\eta_j\right) + \sigma_1\left(\eta_j\right)\left(p_{i,2}\left(\eta_j\right) - \eta_j p_{i,1}(\zeta)\right)\Big) + \left(\left(\alpha_1\left(\eta_j\right) - \beta_{1\eta}\left(\eta_j\right)\right) + \sigma_1\left(\eta_j\right)\eta_j\right) u_{1\eta}(\zeta) = f_1\left(\eta_j\right) - \gamma_1 \sigma_1\left(\eta_j\right), j = 1, 2, \cdots, 2\mathscr{M}, \quad (32)$$

$$\sum_{i=1}^{2\mathscr{M}} b_i\Big(\left(\alpha_2\left(\eta_j\right) - \beta_{2\eta}\left(\eta_j\right)\right) p_{i,1}\left(\eta_j\right) - \beta_2\left(\eta_j\right) h_i\left(\eta_j\right) + \sigma_2\left(\eta_j\right)\left(p_{i,2}\left(\eta_j\right) - p_{i,2}(1)\right)\Big) + \left(\left(\alpha_2\left(\eta_j\right) - \beta_{2\eta}\left(\eta_j\right)\right) - \sigma_2\left(\eta_j\right)\left(1 - \eta_j\right)\right) u_{2\eta}(\zeta) = f_2\left(\eta_j\right) - \gamma_2 \sigma_2\left(\eta_j\right), j = 2\mathscr{M}+1, 2\mathscr{M}+2, \cdots, 4\mathscr{M}. \quad (33)$$

Equations (32) and (33) combined with Equations (27) and (28) give a linear system of $4\mathscr{M} + 2$ equations with $4\mathscr{M} + 2$ unknowns $a_i, i = 1, 2, \cdots, 2\mathscr{M}$, $b_i, i = 1, 2, \cdots, 2\mathscr{M}$, $v_{1\eta}(\zeta)$, and $v_{2\eta}(\zeta)$. We can write the above system in matrix form as follows:

$$\mathbf{SX} = \mathbf{Q}, \quad (34)$$

where

$$\mathbf{S}=\begin{bmatrix} s_{11} & \cdots & s_{1,2\mathscr{M}} & 0 & \cdots & 0 & s_{1,4\mathscr{M}+1} & 0 \\ \vdots & \vdots & \vdots & \vdots & \vdots & \vdots & \vdots & \vdots \\ s_{2\mathscr{M},1} & \cdots & s_{2\mathscr{M},2\mathscr{M}} & 0 & \cdots & 0 & s_{2\mathscr{M},4\mathscr{M}+1} & 0 \\ 0 & \cdots & 0 & s_{2\mathscr{M}+1,2\mathscr{M}+1} & \cdots & s_{2\mathscr{M}+1,4\mathscr{M}} & 0 & s_{2\mathscr{M}+1,4\mathscr{M}+2} \\ \vdots & \vdots & \vdots & \vdots & \vdots & \vdots & \vdots & \vdots \\ 0 & \cdots & 0 & s_{4\mathscr{M},2\mathscr{M}+1} & \cdots & s_{4\mathscr{M},4\mathscr{M}} & 0 & s_{4\mathscr{M},4\mathscr{M}+2} \\ s_{4\mathscr{M}+1,1} & \cdots & s_{4\mathscr{M}+1,2\mathscr{M}} & s_{4\mathscr{M}+1,2\mathscr{M}+1} & \cdots & s_{4\mathscr{M}+1,4\mathscr{M}} & s_{4\mathscr{M}+1,4\mathscr{M}+1} & s_{4\mathscr{M}+1,4\mathscr{M}+2} \\ s_{4\mathscr{M}+2,1} & \cdots & s_{4\mathscr{M}+2,2\mathscr{M}} & s_{4\mathscr{M}+2,2\mathscr{M}+1} & \cdots & s_{4\mathscr{M}+2,4\mathscr{M}} & s_{4\mathscr{M}+2,4\mathscr{M}+1} & s_{4\mathscr{M}+2,4\mathscr{M}+2} \end{bmatrix}, \tag{35}$$

$$\mathbf{X}=\left[a_1, a_2,\cdots,a_{2\mathscr{M}}, b_1, b_2,\cdots,b_{2\mathscr{M}}, v_{1\eta}(\zeta), v_{2\eta}(\zeta)\right]^T, \tag{36}$$

$$\mathbf{Q}=\left[q_1, q_2,\cdots q_{4\mathscr{M}+2}.\right]^T. \tag{37}$$

The entries of the matrix $\mathbf{S}$ are given by

$$\begin{aligned} s_{j,i} &= \left(\alpha_1\left(\eta_j\right)-\beta_{1\eta}\left(\eta_j\right)\right)\left(p_{i,1}\left(\eta_j\right)-p_{i,1}(\zeta)\right)-\beta_1\left(\eta_j\right)h_i\left(\eta_j\right) \\ &\quad +\sigma_1\left(\eta_j\right)\left(p_{i,2}\left(\eta_j\right)-\eta_j p_{i,1}(\zeta)\right)\Big) 1\le i,j\le 2\mathscr{M}, \\ s_{j,i} &= \left(\alpha_2\left(\eta_j\right)-\beta_{2\eta}\left(\eta_j\right)\right)p_{i,1}\left(\eta_j\right)-\beta_2\left(\eta_j\right)h_i\left(\eta_j\right) \\ &\quad +\sigma_2\left(\eta_j\right)\left(p_{i,2}\left(\eta_j\right)-p_{i,2}(1)\right)\Big) 2\mathscr{M}+1\le i,j\le 4\mathscr{M}, \\ s_{j,4\mathscr{M}+1} &= \alpha_1\left(\eta_j\right)-\beta_{1\eta}\left(\eta_j\right)+\sigma_1\left(\eta_j\right)\eta_j, 1\le j\le 2\mathscr{M}, \\ s_{j,4\mathscr{M}+2} &= \alpha_2\left(\eta_j\right)-\beta_{2\eta}\left(\eta_j\right)-\sigma_2\left(\eta_j\right)\left(1-\eta_j\right), 2\mathscr{M}+1\le j\le 4\mathscr{M}, \end{aligned}$$

$$s_{4\mathscr{M}+1,i}=\begin{cases} -\left(p_{i,2}(\zeta)-\zeta p_{i,1}(\zeta)\right), & \text{for } i=1,2,\cdots,2\mathscr{M}, \\ \left(p_{i-2\mathscr{M},2}(\zeta)-p_{i-2\mathscr{M},2}(1)\right), & \text{for } i=2\mathscr{M}+1,2\mathscr{M}+2,\cdots,4\mathscr{M}, \\ -\zeta, & \text{for } i=4\mathscr{M}+1, \\ -(1-\zeta), & \text{for } i=4\mathscr{M}+2, \end{cases}$$

$$s_{4\mathscr{M}+2,i}=\begin{cases} \beta_1(\zeta)\left(p_{i,1}(\zeta)-p_{i,1}(\zeta)\right), & \text{for } i=1,2,\cdots,2\mathscr{M}, \\ -\beta_2(\zeta)p_{i-2\mathscr{M},1}(\zeta), & \text{for } i=2\mathscr{M}+1,2\mathscr{M}+2,\cdots,4\mathscr{M}, \\ \beta_1(\zeta), & \text{for } i=4\mathscr{M}+1, \\ -\beta_2(\zeta), & \text{for } i=4\mathscr{M}+2. \end{cases} \tag{38}$$

Finally, we obtained the following entries of the matrix $\mathbf{Q}$:

$$q_j=\begin{cases} f_1\left(\eta_j\right)-\sigma_1\left(\eta_j\right)\gamma_1, & \text{for } j=1,2,\cdots,2\mathscr{M}, \\ f_2\left(\eta_j\right)-\sigma_2\left(\eta_j\right)\gamma_2, & \text{for } j=2\mathscr{M}+1,2\mathscr{M}+2,\cdots,4\mathscr{M}, \\ \mu_1+\gamma_1-\gamma_2, & \text{for } j=4\mathscr{M}+1, \\ \mu_2+\alpha_1(\zeta)-\alpha_2(\zeta), & \text{for } j=4\mathscr{M}+2. \end{cases} \tag{39}$$

Equation (34) can be solved by any linear solver in order to get the unknown Haar coefficients. Now utilizing these unknown Haar coefficients in Equations (23) and (26), we can easily obtain the approximate solution of the problem.

4.1.2. Nonlinear Case. In nonlinear case, first we linearize Equation (2) by using the following quasi-Newton linearization technique [38]:

$$\left(v\frac{dv}{d\eta}\right)^{n+1}=v^n\left(\frac{dv}{d\eta}\right)^{n+1}+v^{n+1}\left(\frac{dv}{d\eta}\right)^{n}-v^n\left(\frac{dv}{d\eta}\right)^{n}. \tag{40}$$

After linearizing Equation (2), substituting the Haar approximations for v and its derivatives and then discretizing, we get

$$\begin{aligned} &\psi\Bigg(\sum_{i=1}^{2\mathscr{M}}a_ih_i\left(\eta_j\right), v_{1\eta}(\zeta)+\sum_{i=1}^{2\mathscr{M}}a_i\left(p_{i,1}\left(\eta_j\right)-p_{i,1}(\zeta)\right), \gamma_1 \\ &\quad +\eta_j v_{1\eta}(\zeta)+\sum_{i=1}^{2\mathscr{M}}a_i\Big(p_{i,2}\left(\eta_j\right) \\ &\quad -\eta_j p_{i,1}(\zeta)\Big), \alpha_1\left(\eta_j\right), \beta_1\left(\eta_j\right), \sigma_1\left(\eta_j\right), \eta_j\Bigg) \\ &= f_1\left(\eta_j\right), j=1,2,\cdots,2\mathscr{M}, \end{aligned} \tag{41}$$

$$\begin{aligned} &\psi\Bigg(\sum_{i=1}^{2\mathscr{M}}b_ih_i\left(\eta_j\right), v_{2\eta}(\zeta)+\sum_{i=1}^{2\mathscr{M}}b_ip_{i,1}\left(\eta_j\right), \gamma_2-\left(1-\eta_j\right)v_{2\eta}(\zeta) \\ &\quad +\sum_{i=1}^{2\mathscr{M}}b_i\left(p_{i,2}\left(\eta_j\right)-p_{i,2}(1)\right), \alpha_2\left(\eta_j\right), \beta_2\left(\eta_j\right), \sigma_2\left(\eta_j\right), \eta_j\Bigg) \\ &= f_2\left(\eta_j\right), j=2\mathscr{M}+1,2\mathscr{M}+2,\cdots,4\mathscr{M}. \end{aligned} \tag{42}$$

Equations (41) and (42) along with Equations (27) and (28) give a linear system of size $(4\mathscr{M}+2)\times(4\mathscr{M}+2)$ with the unknown Haar coefficients a_i, $i=1,2,3,\cdots,2\mathscr{M}$, b_i, $i=1,2,3,\cdots,2\mathscr{M}$ and the values $v_{1\eta}(\zeta)$ and $v_{2\eta}(\zeta)$. The above linear system can be solved by using any linear solver.

4.2. HWCM for Parabolic Model with Single Interface. This is a parabolic interface model. The time derivative is approximated by using the following forward difference formula:

$$v_t(\eta,t)=\frac{v\left(\eta,t^{n+1}\right)-v\left(\eta,t^n\right)}{\Delta t}+\mathscr{O}(\Delta t). \tag{43}$$

Now approximating the highest order spatial derivative $v_{1\eta\eta}(\eta,t)$ over the first subinterval $I_1=[0,\zeta]$ by truncated Haar series,

$$v_{1\eta\eta}(\eta,t)=\sum_{i=1}^{2\mathscr{M}}a_ih_i(\eta), \eta\in I_1. \tag{44}$$

Integrating Equation (44), we get the approximate

expressions for $v_{1\eta}(\eta, t)$ and $v_1(\eta, t)$ as follows:

$$v_{1\eta}(\eta, t) = v_{1\eta}(\zeta, t) + \sum_{i=1}^{2\mathscr{M}} a_i\left(p_{i,1}(\eta) - p_{i,1}(\zeta)\right), \eta \in I_1, \quad (45)$$

$$v_1(\eta, t) = \gamma_1(t) + \eta v_{1\eta}(\zeta, t) + \sum_{i=1}^{2\mathscr{M}} a_i\left(p_{i,2}(\eta) - \eta p_{i,1}(\zeta)\right), \eta \in I_1. \quad (46)$$

Similarly, approximating $v_{2\eta\eta}(\eta, t)$ over the second subinterval $I_2 = [\zeta, 1]$ as follows,

$$v_{2\eta\eta}(\eta, t) = \sum_{i=1}^{2\mathscr{M}} b_i h_i(\eta), \eta \in I_2. \quad (47)$$

Integrating Equation (47), we obtain the approximate expressions for $v_{2\eta}(\eta, t)$ and $v_2(\eta, t)$ as follows:

$$v_{2\eta}(\eta, t) = v_{2\eta}(\zeta, t) + \sum_{i=1}^{2\mathscr{M}} b_i p_{i,1}(\eta), \eta \in I_2, \quad (48)$$

$$v_2(\eta, t) = \gamma_2(t) - (1-\eta) v_{2\eta}(\zeta, t) + \sum_{i=1}^{2\mathscr{M}} b_i\left(p_{i,2}(\eta) - p_{i,2}(1)\right), \eta \in I_2. \quad (49)$$

Substituting the values of $v_1(\zeta, t)$, $v_2(\zeta, t)$, $\alpha_1(\zeta, t)$, $\alpha_2(\zeta, t)$, $\beta_1(\zeta, t)$, and $\beta_2(\zeta, t)$ in Equations (11) and (12), the interface conditions imply that

$$\left(\gamma_2(t) - (1-\zeta) v_{2\eta}(\zeta, t) + \sum_{i=1}^{2M} b_i\left(p_{i,2}(\zeta) - p_{i,2}(1)\right)\right) - \left(\gamma_1(t) + \zeta v_{1\eta}(\zeta, t) + \sum_{i=1}^{2\mathscr{M}} a_i\left(p_{i,2}(\zeta) - \zeta p_{i,1}(\zeta)\right)\right) = \mu_1(t), \quad (50)$$

$$\left(\alpha_2(\zeta, t) - \beta_2(\zeta, t)\left(v_{2\eta}(\zeta, t) + \sum_{i=1}^{2\mathscr{M}} b_i p_{i,1}(\zeta)\right)\right) - \left(\alpha_1(\zeta, t) - \beta_1(\zeta, t)\left(v_{1\eta}(\zeta, t) + \sum_{i=1}^{2\mathscr{M}} a_i\left(p_{i,1}(\zeta) - p_{i,1}(\zeta)\right)\right)\right) = \mu_2(t). \quad (51)$$

The remaining procedure is explained for linear and nonlinear cases separately in the upcoming section.

4.2.1. Linear Case. Substituting Equations (43) and (46) in Equation (7) and simplifying, we have

$$\begin{aligned}&(1 + \Delta t \sigma_1(\eta, t))\left(\gamma_1(t) + \eta v_{1\eta}(\zeta, t) + \sum_{i=1}^{2\mathscr{M}} a_i\left(p_{i,2}(\eta) - \eta p_{i,1}(\zeta)\right)\right)\\ &+ \Delta t\left(\alpha_1(\eta, t) - \beta_{1\eta}(\eta, t)\right)\left(v_{1\eta}(\zeta, t) + \sum_{i=1}^{2\mathscr{M}} a_i\left(p_{i,1}(\eta) - p_{i,1}(\zeta)\right)\right)\\ &- \Delta t \beta_1(\eta, t) \sum_{i=1}^{2\mathscr{M}} a_i h_i(\eta) = \Delta t f_1(\eta, t) + v_{1_0}(\eta), \eta \in I_1.\end{aligned} \quad (52)$$

Similarly by using Equation (43) and Equations (47)–(49) in Equation (7) and simplifying, we have

$$\begin{aligned}&(1 + \Delta t \sigma_2(\eta, t))\left(\gamma_2(t) - (1-\eta) v_{2\eta}(\zeta, t) + \sum_{i=1}^{2\mathscr{M}} b_i\left(p_{i,2}(\eta) - p_{i,2}(1)\right)\right)\\ &+ \Delta t\left(\alpha_2(\eta, t) - \beta_{2\eta}(\eta, t)\right)\left(v_{2\eta}(\zeta, t) + \sum_{i=1}^{2\mathscr{M}} b_i p_{i,1}(\eta)\right)\\ &- \Delta t \beta_2(\eta, t) \sum_{i=1}^{2\mathscr{M}} b_i h_i(\eta) = \Delta t f_2(\eta, t) + v_{2_0}(\eta), \eta \in I_2.\end{aligned} \quad (53)$$

The following nodes are defined for interface conditions at $\eta = \zeta$:

$$\eta_{c'} = \begin{cases} \dfrac{\zeta\left(c' - 0.5\right)}{2\mathscr{M}}, & \text{for } c' = 1, 2, \cdots, 2\mathscr{M}; \\ \dfrac{\zeta + (1-\zeta)\left(c' - 2\mathscr{M} - 0.5\right)}{2\mathscr{M}}, & \text{for } c' = 2\mathscr{M}+1, 2\mathscr{M}+2, \cdots, 4\mathscr{M}. \end{cases} \quad (54)$$

Discretizing, we get the following systems of linear equations:

$$\begin{aligned}&\sum_{i=1}^{2\mathscr{M}} a_i\Big(\left(1 + \Delta t \sigma_1\left(\eta_j, t\right)\right)\left(p_{i,2}\left(\eta_j\right) - \eta_j p_{i,1}(\zeta)\right)\\ &+ \Delta t\left(\alpha_1\left(\eta_j, t\right) - \beta_{1\eta}\left(\eta_j, t\right)\right)\left(p_{i,1}\left(\eta_j\right) - p_{i,1}(\zeta)\right)\\ &- \Delta t \beta_1\left(\eta_j, t\right) h_i\left(\eta_j\right)\Big) + \Big(\left(1 + \Delta t \sigma_1\left(\eta_j, t\right)\right)\eta_j + \Delta t\Big(\alpha_1\left(\eta_j, t\right)\\ &- \beta_{1\eta}\left(\eta_j, t\right)\Big)\Big) v_{1\eta}(\zeta, t) = \Delta t f_1\left(\eta_j, t\right) + v_{1_0}(t)\\ &- \left(1 + \Delta t \sigma_1\left(\eta_j, t\right)\right)\gamma_1(t), j = 1, 2, \cdots, 2\mathscr{M},\end{aligned} \quad (55)$$

$$\begin{aligned}&\sum_{i=1}^{2\mathscr{M}} b_i\Big(\left(1 + \Delta t \sigma_2\left(\eta_j, t\right)\right)\left(p_{i,2}\left(\eta_j\right) - p_{i,2}(1)\right) + \Delta t\left(\alpha_2\left(\eta_j, t\right) - \beta_{2\eta}\left(\eta_j, t\right)\right) p_{i,1}\left(\eta_j\right)\\ &- \Delta t \beta_2\left(\eta_j, t\right) h_i\left(\eta_j\right)\Big) + \Big(\Big(-\left(1 + \Delta t \sigma_2\left(\eta_j, t\right)\right)\left(1 - \eta_j\right)\\ &+ \left(\Delta t\left(\alpha_2\left(\eta_j, t\right) - \beta_{2\eta}\left(\eta_j, t\right)\right)\right) v_{2\eta}(\zeta, t)\\ &= \Delta t f_2\left(\eta_j, t\right) + v_{2_0}(\eta) - \gamma_2(t)\left(1 + \Delta t \sigma_2\left(\eta_j, t\right)\right), j = 2\mathscr{M}+1, 2\mathscr{M}+2, \cdots, 4\mathscr{M}.\end{aligned} \quad (56)$$

Equations (55) and (56) combined with Equations (50)

and (51) give a linear system of size $(4\mathscr{M}+2)\times(4\mathscr{M}+2)$ with $4\mathscr{M}+2$ unknown coefficients $a_i, i=1,2,\cdots,2\mathscr{M}$, $b_i, i=1,2,\cdots,2\mathscr{M}$, $v_{1\eta}(\zeta,t)$, and $v_{2\eta}(\zeta,t)$. In matrix form, the above system can be written as

$$\mathbf{SX}=\mathbf{Q}, \tag{57}$$

where $\mathbf{S}$ and $\mathbf{Q}$ are given in Equations (35) and (37), respectively, and

$$\mathbf{X}=\left[a_1(t),a_2(t),\cdots,a_{2\mathscr{M}}(t),b_1(t),b_2(t),\cdots,b_{2\mathscr{M}}(t),v_{1\eta}(\zeta,t),v_{2\eta}(\zeta,t)\right]^T. \tag{58}$$

The entries of the matrix $\mathbf{S}$ are given by

$$\begin{aligned}
s_{j,i}&=\left(1+\Delta t\sigma_1\left(\eta_j,t\right)\left(p_{i,2}\left(\eta_j\right)-\eta_j p_{i,1}(\zeta)\right)\right.\\
&\quad+\Delta t\left(\alpha_1\left(\eta_j,t\right)-\beta_{1\eta}\left(\eta_j,t\right)\right)\left(p_{i,1}\left(\eta_j\right)-p_{i,1}(\zeta)\right)\\
&\quad-\Delta t\beta_1\left(\eta_j,t\right)h_i\left(\eta_j\right),1\le i,j\le 2\mathscr{M},\\
s_{j,i}&=\left(1+\Delta t\sigma_2\left(\eta_j,t\right)\right)\left(p_{i,2}\left(\eta_j\right)-p_{i,2}(1)\right)+\Delta t\left(\alpha_2\left(\eta_j,t\right)\right.\\
&\quad\left.-\beta_{2\eta}\left(\eta_j,t\right)\right)p_{i,1}\left(\eta_j\right)-\Delta t\beta_2\left(\eta_j,t\right)h_i\left(\eta_j\right),2\mathscr{M}+1\le i,j\le 4\mathscr{M},\\
s_{j,4\mathscr{M}+1}&=\left(1+\Delta t\sigma_1\left(\eta_j,t\right)\right)\eta_j+\Delta t\left(\alpha_1\left(\eta_j,t\right)-\beta_{1\eta}\left(\eta_j,t\right)\right),1\le j\le 2\mathscr{M},\\
s_{j,4\mathscr{M}+2}&=-\left(1+\Delta t\sigma_2\left(\eta_j,t\right)\right)\left(1-\eta_j\right)+\Delta t\left(\alpha_2\left(\eta_j,t\right)\right.\\
&\quad\left.-\beta_{2\eta}\left(\eta_j,t\right)\right),2\mathscr{M}+1\le j\le 4\mathscr{M},\\
s_{4\mathscr{M}+1,i}&=\begin{cases}-\left(p_{i,2}(\zeta)-\zeta p_{i,1}(\zeta)\right), & \text{for } i=1,2,\cdots,2\mathscr{M},\\ \left(p_{i-2M,2}(\zeta)-p_{i-2M,2}(1)\right), & \text{for } i=2\mathscr{M}+1,2\mathscr{M}+2,\cdots,4\mathscr{M},\\ -\zeta, & \text{for } i=4\mathscr{M}+1,\\ -(1-\zeta), & \text{for } i=4\mathscr{M}+2,\end{cases}\\
s_{4\mathscr{M}+2,i}&=\begin{cases}\beta_1(\zeta,t)\left(p_{i,1}(\zeta)-p_{i,1}(\zeta)\right), & \text{for } i=1,2,\cdots,2\mathscr{M},\\ -\beta_2(\zeta,t)p_{i-2\mathscr{M},1}(\zeta), & \text{for } i=2\mathscr{M}+1,2\mathscr{M}+2,\cdots,4\mathscr{M},\\ \beta_1(\zeta,t), & \text{for } i=4\mathscr{M}+1,\\ -\beta_2(\zeta,t), & \text{for } i=4\mathscr{M}+2.\end{cases}
\end{aligned} \tag{59}$$

Finally, we can write the elements of the matrix $\mathbf{Q}$ as follows:

$$q_j=\begin{cases}\Delta t f_1\left(\eta_j,t\right)+v_{1_0}(\eta)-\left(1+\Delta t\sigma_1\left(\eta_j,t\right)\right)\gamma_1(t), & \text{for } j=1,2,\cdots,2\mathscr{M},\\ \Delta t f_2\left(\eta_j,t\right)+v_{2_0}(\eta)-\left(1+\Delta t\sigma_2\left(\eta_j,t\right)\gamma_2(t)\right), & \text{for } j=2\mathscr{M}+1,2\mathscr{M}+2,\cdots,4\mathscr{M},\\ \mu_1(\zeta,t)+\gamma_1(t)-\gamma_2(t), & \text{for } j=4\mathscr{M}+1,\\ \mu_2(\zeta,t)+\alpha_1(\zeta,t)-\alpha_2(\zeta,t), & \text{for } j=4\mathscr{M}+2.\end{cases} \tag{60}$$

From Equation (57), we get

$$X=S^{-1}Q. \tag{61}$$

Solving system (61) by any linear solver, we obtained the values of the unknown Haar coefficients $a_i, i=1,2,\cdots,2\mathscr{M}$, $b_i, i=1,2,\cdots,2\mathscr{M}$, $v_{1\eta}(\zeta,t)$, and $v_{2\eta}(\zeta,t)$. By utilizing these unknown Haar coefficients in Equations (46) and (49), we can easily obtain the approximate solution of the problem.

4.2.2. Nonlinear Case. In nonlinear interface models first, we linearize problem (8) by using the following quasi-Newton Linearization technique [38]:

$$\left(v\frac{\partial v}{\partial\eta}\right)^{n+1}=v^n\left(\frac{\partial v}{\partial\eta}\right)^{n+1}+v^{n+1}\left(\frac{\partial v}{\partial\eta}\right)^{n}-v^n\left(\frac{\partial v}{\partial\eta}\right)^{n}. \tag{62}$$

Now substituting the approximate expressions for higher-order derivatives, unknown function v, and temporal derivative in the linearized equation and discretizing, we obtain the following systems of equations.

$$\begin{aligned}
&\psi\left(v_{1t}(\zeta,t),\sum_{i=1}^{2\mathscr{M}}a_ih_i\left(\eta_j\right),v_{1\eta}(\zeta,t)+\sum_{i=1}^{2\mathscr{M}}a_i\left(p_{i,1}\left(\eta_j\right)-p_{i,1}(\zeta)\right),\gamma_1(t)+\eta_jv_{1\eta}(\zeta,t)\right.\\
&\quad\left.+\sum_{i=1}^{2\mathscr{M}}a_i\left(p_{i,2}\left(\eta_j\right)-\eta_jp_{i,1}(\zeta)\right),\alpha_1\left(\eta_j,t\right),\beta_1\left(\eta_j,t\right),\sigma_1\left(\eta_j,t\right),\eta_j,t\right)\\
&=f_1\left(\eta_j,t\right),j=1,2,\cdots,2\mathscr{M},
\end{aligned} \tag{63}$$

$$\begin{aligned}
&\psi\left(v_{2t}(\zeta,t),\sum_{i=1}^{2\mathscr{M}}b_ih_i\left(\eta_j\right),v_{2\eta}(\zeta,t)+\sum_{i=1}^{2\mathscr{M}}b_ip_{i,1}\left(\eta_j\right),\gamma_2(t)\right.\\
&\quad-\left(1-\eta_j\right)v_{2\eta}(\zeta,t)+\sum_{i=1}^{2\mathscr{M}}b_i\left(p_{i,2}\left(\eta_j\right)\right.\\
&\quad\left.\left.-p_{i,2}(1)\right),\alpha_2\left(\eta_j,t\right),\beta_2\left(\eta_j,t\right),\sigma_2\left(\eta_j,t\right),\eta_j,t\right)\\
&=f_2\left(\eta_j,t\right),j=2\mathscr{M}+1,2\mathscr{M}+2,\cdots,4\mathscr{M}.
\end{aligned} \tag{64}$$

Equations (63) and (64) together with Equations (50) and (51) give a linear system of size $(4\mathscr{M}+2)\times(4\mathscr{M}+2)$. Solving the system by any linear solver, we can get the unknown Haar coefficients. Using these unknown Haar coefficients, we can easily obtain the approximate solution.

5. Convergence

Lemma 1 [39]. *Assume that $v\in C^2(-\infty,\infty)$ with $|v'|\le K,\forall\eta\in(a,b)$, $K>0$, and $v=\sum_{i=0}^{\infty}\lambda_ih_i(x)$, and then, $|\lambda_i|\le K\,2^{-(3j-2)/2}$.*

Lemma 2 [39]. *Let $v\in C^2(-\infty,\infty)$ be continuous on (a,b). Then, the error norm at J^{th} level satisfies*

$$\left\|E_J\right\|^2\le\frac{K^2}{12}2^{-2J}, \tag{65}$$

where $|v'|\le K,\forall\eta\in(a,b)$ and $K>0$, and $\mathscr{M}$ is a positive real number related to the Jth level resolution of the wavelet given by $\mathscr{M}=2^J$.

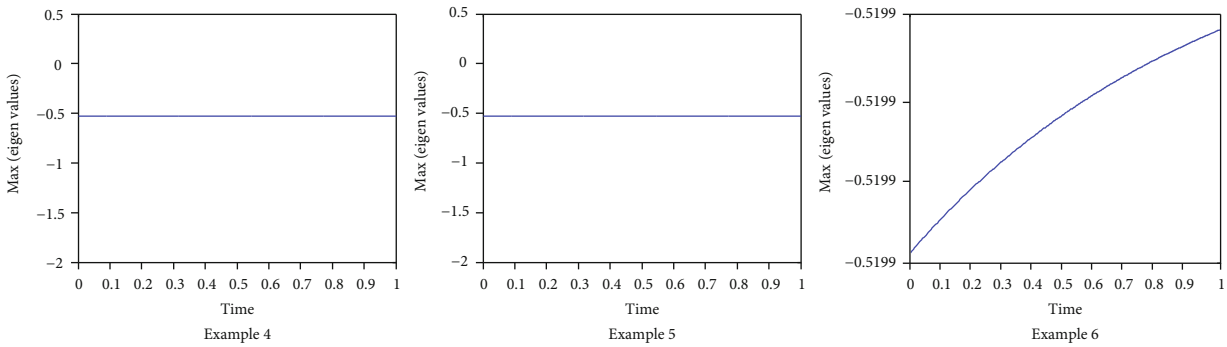

Figure 1: The stability analysis of the proposed method for different examples at $N = 64$, $\Delta t = 0.01/32$, $t = 1$, $a = 0$, and $b = 1$.

Theorem 3. *If $v(\eta)$ is the exact solution and $v^{2.\mathscr{M}}(\eta)$ is the approximate solution of Equation (1), the error norm at J^{th} level resolution is given by*

$$\left\|E_J\right\|_\eta = \left\|v - v^{2.\mathscr{M}}\right\| = \mathcal{O}\left(2^{-3\left(2^J\right)}\right). \tag{66}$$

Proof. The error estimate of the proposed method at J^{th} level resolution is given as

$$\left\|E_J\right\|_\eta = \left\|v - v^{2.\mathscr{M}}\right\| = \left|\sum_{i=2.\mathscr{M}+1}^{\infty} a_i\left(p_{i,2}(\eta) - \eta p_{i,1}(\zeta)\right)\right|, \tag{67}$$

which implies that

$$\begin{aligned}\left\|E_J\right\|_\eta^2 &= \left|\int_{-\infty}^{\infty}\left\langle \sum_{i=2.\mathscr{M}+1}^{\infty} a_i\left(p_{i,2}(\eta) - \eta p_{i,1}(\zeta)\right), \sum_{l=2.\mathscr{M}+1}^{\infty} a_l\left(p_{l,2}(\eta) - \eta p_{l,1}(\zeta)\right)\right\rangle \mathrm{d}\eta\right| \\ &= \left|\sum_{i=2.\mathscr{M}+1}^{\infty}\sum_{l=2.\mathscr{M}+1}^{\infty}\int_a^b a_i a_l\left(p_{i,2}(\eta) - \eta p_{i,1}(\zeta)\right)\left(p_{l,2}(\eta) - \eta p_{l,1}(\zeta)\right)\mathrm{d}\eta\right| \\ &\le \left|\sum_{i=2.\mathscr{M}+1}^{\infty}\sum_{l=2.\mathscr{M}+1}^{\infty} a_i a_l K_{i,l}\right|,\end{aligned} \tag{68}$$

where $K_{i,l} = \mathrm{Sup}_{i,l}\int_a^b\left(p_{i,2}(\eta) - \eta p_{i,1}(\zeta)\right)\left(p_{l,2}(\eta) - \eta p_{l,1}(\zeta)\right)\mathrm{d}\eta$. Now, Equation (68) can be written as

$$\begin{aligned}\left\|E_J\right\|_\eta^2 &\le \sum_{i=2.\mathscr{M}+1}^{\infty}\left|a_i\left(a_{2.\mathscr{M}+1}K_{i,2.\mathscr{M}+1} + a_{2.\mathscr{M}+2}K_{i,2.\mathscr{M}+2} + \cdots\right)\right| \\ &\le \sum_{i=2.\mathscr{M}+1}^{\infty}\left|a_i K_i\left(a_{2.\mathscr{M}+1} + a_{2.\mathscr{M}+2} + \cdots\right)\right|, \text{where } K_i \\ &= \mathrm{Sup}_l K_{i,l} \le \sum_{i=2.\mathscr{M}+1}^{\infty}\left(\left|a_i K_i a_{2.\mathscr{M}+1}\right| + \left|a_i K_i a_{2.\mathscr{M}+2}\right| + \cdots\right) \\ &\le \sum_{i=2.\mathscr{M}+1}^{\infty}\left(\left|a_i K_i a_{2.\mathscr{M}+1}\right| + \left|a_i K_i a_{2.\mathscr{M}+2}\right| + \cdots\right).\end{aligned} \tag{69}$$

Now, using Lemmas 1 and 2, inequality (69) can be written as

$$\left\|E_J\right\|_\eta^2 \le K\frac{2^{-\left(3.2^J+1\right)}}{1 - 2^{-3/2}}\sum_{i=2.\mathscr{M}+1}^{\infty}\left|a_i K_i\right| \le K_1 K\frac{2^{-\left(3.2^J+1\right)}}{1 - 2^{-3/2}} \text{ where } K_1 = \mathrm{Sup}K_i, \tag{70}$$

in which on further simplification and taking squire root, we get

$$\left\|E_J\right\|_\eta \le \sqrt{K_1 K}\frac{2^{-\left(3.2^J+1\right)}}{1 - 2^{-3/2}} \le \mathcal{O}\left(2^{-3\left(2^J\right)}\right). \tag{71}$$

□

It is concluded that error norm is inversely proportional to level of the Haar wavelet resolution J. Hence, the error of the HWCM decreases as J increases, i.e.,

$$\left\|E_J\right\|_\eta \longrightarrow 0 \text{as} J \longrightarrow \infty, \Rightarrow \left\|E_J\right\|_\eta \longrightarrow 0 \text{ as } \mathscr{M} \longrightarrow \infty. \tag{72}$$

Theorem 4. *If $v(\eta, t_p)$ is the exact solution and $v^{2.\mathscr{M}}(\eta, t_p)$ is the approximate solution of Equation (7) and if $p = 0, 1, 2 \cdots P$, where P is a positive integer, then the error norm at J-th level resolution is given by*

$$Error = \left\|E_J\right\|_\eta + \left\|E_J\right\|_{t_p} = \mathcal{O}\left(2^{-3\left(2^J\right)}\right) + \mathcal{O}(\Delta t). \tag{73}$$

Proof. For $p = 0, 1, 2 \cdots P$,

$$\left\|E_J\right\|_\eta = \mathcal{O}\left(2^{-3\left(2^J\right)}\right), \tag{74}$$

see Theorem 3.

For time derivatives, we have used first-order finite difference approximation in Equation (43), so

$$\left\|E_J\right\|_{t_p} = \mathcal{O}(\Delta t). \tag{75}$$

Hence,

$$\text{Error} = \left\|E_J\right\|_\eta + \left\|E_J\right\|_{t_p} = \mathcal{O}\left(2^{-3\left(2^J\right)}\right) + \mathcal{O}(\Delta t). \tag{76}$$

□

Table 1: Analysis of errors for Example 1.

J	N	$\mathbf{E}_c(N)$ proposed technique	CPU time in sec	Eigenvalues	N	IIM	$R_c(N)$
2	16	2.7551×10^{-4}	0.454092	-1.7826	20	6.1×10^{-3}	1.8275
3	32	7.3171×10^{-5}	0.492690	-2.1337	40	1.4×10^{-3}	1.9128
4	64	1.8859×10^{-5}	0.582250	-2.4974	80	3.2779×10^{-4}	1.9560
5	128	4.7873×10^{-6}	1.096531	-2.8811	160	7.9702×10^{-5}	1.9780
6	256	1.2060×10^{-6}	2.806679	-3.2862	320	1.9644×10^{-5}	1.9890

Table 2: Analysis of errors for Example 2.

J	N	$\mathbf{E}_c(N)$ proposed technique	CUP time in sec	Eigenvalues	No. of iterations	$R_c(N)$
1	8	7.1012×10^{-4}	0.009185	-3.2264	4	
2	16	1.9064×10^{-4}	0.031301	-3.2264	4	1.8972
3	32	4.9514×10^{-5}	0.097082	-3.3663	4	1.9449
4	64	1.2626×10^{-5}	0.392260	-3.2264	4	1.9714
5	128	3.1885×10^{-6}	1.514269	-3.3663	4	1.9854
6	256	8.0118×10^{-7}	6.019626	-3.3577	4	1.9927
7	512	2.0081×10^{-7}	23.903250	-3.2264	4	1.9962

6. Stability

In this section, we study the computational stability of the proposed technique. For this purpose, we have observed the maximum eigenvalues of matrix $\mathbf{S}$ at every time step, which represent the corresponding Haar weights. All the maximum eigenvalues of matrix $\mathbf{S}$ stay away from zero (see Figure 1), and this leads to a sufficient condition for the proposed technique to be stable. We can write Equations (1) and (2) in the form

$$v_t = \mathscr{L} v(\eta, t) + f(\eta, t), \tag{77}$$

where $\mathscr{L}$ is the operator.

$$\mathscr{L} v_t = \left[\frac{\partial}{\partial \eta}\left(B(\eta, t)\frac{\partial}{\partial \eta}\right) - \alpha(\eta, t) - \delta(\eta, t)\right] v(\eta, t) + f(\eta, t), \tag{78}$$

$$\{I - \delta t \mathscr{L}\} v(\eta, t) = v(\eta, t_0) + \delta t f(\eta, t), \tag{79}$$

$$v(\eta, t) = \{I - \delta t \mathscr{L}\}^{-1} v(\eta, t_0) + \delta t \{I - \delta t \mathscr{L}\}^{-1} f(\eta, t). \tag{80}$$

Here, t is the next time level and t_0 is the previous time level. After introducing the Haar wavelet, Equation (80) can be written as

$$v(\eta, t) = \{I - \delta t \mathscr{H}\}^{-1} v(\eta, t_0) + \delta t \{I - \delta t \mathscr{H}\}^{-1} f(\eta, t), \tag{81}$$

where $\mathscr{H}$ is the weight Haar matrix for operator $\mathscr{L}$ and I is the identity matrix. If the maximum eigenvalue of $\mathscr{H}$ is λ, then from Equation (81), the stability condition will be [23, 24]

$$\frac{1}{1 - \delta t \lambda} \leq 1. \tag{82}$$

Here, δt is the time step which is always positive, i.e., $\delta t > 0$. We have discussed the following three different cases related to Equation (82).

Case 1. If $\lambda = 0$, then Equation (82) gives

$$\frac{1}{1 - \delta t \lambda} = \frac{1}{1} = 1, \tag{83}$$

which is identically satisfied.

Case 2. If $\lambda < 0$, i.e., $\lambda = -\xi^2$, where $\xi \in \mathbb{R}$, then Equation (82) gives

$$\frac{1}{1 - \delta t \lambda} = \frac{1}{1 + \delta t \xi^2} < 1. \tag{84}$$

The inequality holds because the denominator is greater than the numerator.

Case 3. If $\lambda > 0$, i.e., $\lambda = \xi^2$, then Equation (82) gives

$$\frac{1}{1 - \delta t \lambda} = \frac{1}{1 - \delta t \xi^2} > 1, \tag{85}$$

which is does not holds as the denominator is smaller than the numerator.

Thus, Equation (82) is valid for Cases 1 and 2, which are verified computationally in Figure 1.

Furthermore, examples (1) and (2) are linear and nonlinear steady problems. Therefore, we have found their eigenvalues and listed them in Tables 1 and 2. From the tables, we can observe that all the eigenvalues lie on the left half of the complex plane. Therefore, systems (34) and (42) are stable, because we have a result that state that "A system $AX = B$ will be stable if and only if the real part of all eigenvalues of the matrix A lie on the left half of the complex plane" [40].

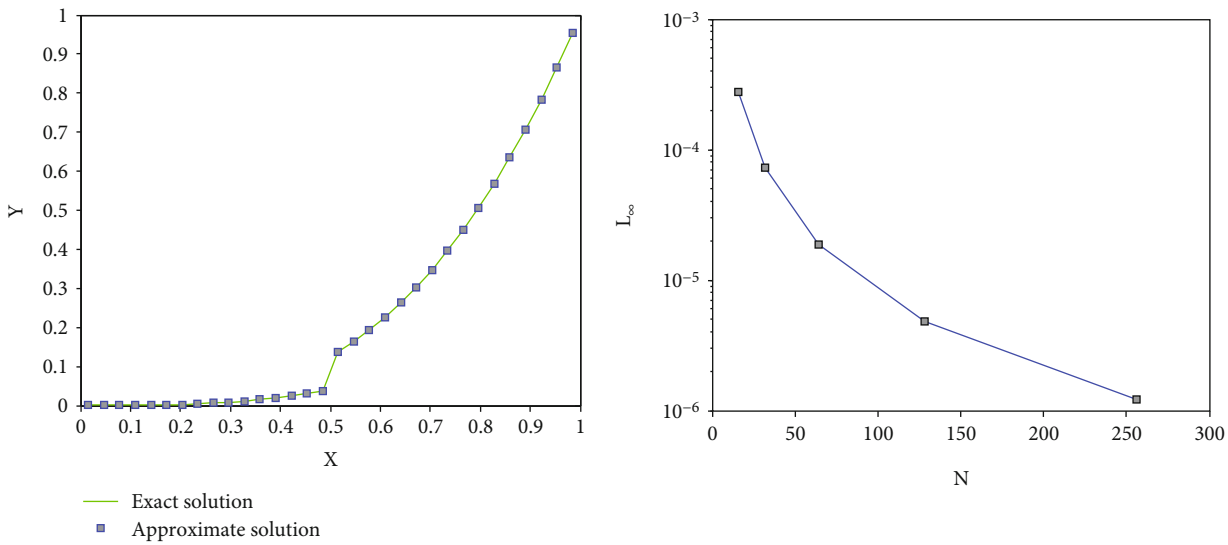

(a) (b)

Figure 2: Comparability of exact and estimated solution for $N = 32$ (a) and plot of $\mathbf{E}_c(\mathcal{T})$ (b) for Example 1.

7. Examples and Discussion

This section is devoted to apply HWCM on some benchmark test models. These problems include parabolic and elliptic advection-diffusion-reaction type linear and nonlinear models with single interface conditions. In nonlinear test models, the quasi-Newton linearization technique given in [41] is utilized. The initial guess for nonlinear elliptic problem is taken 0.1 and stopped the iterations when the criterion of convergence 10^{-5} is satisfied. For calculating experimental convergence rates, we have used the following formula:

$$\mathbf{R}_c(\mathcal{T}) = \frac{\mathrm{Log}[\mathbf{E}_c(\mathcal{T}/2)/\mathbf{E}_c(\mathcal{T})]}{\mathrm{Log}(2)}, \tag{86}$$

where $\mathbf{E}_c(\mathcal{T})$ is the maximum absolute error at $\mathcal{T}$ collocation points.

Example 1. Consider the following initial-boundary value linear elliptic interface model equation [41]:

$$\begin{aligned} v_{1_\eta}(\eta) - \left(\frac{\eta}{3} v_{1_\eta}(\eta)\right)_\eta + v_1(\eta) &= \frac{\eta^3}{3}, \eta \in [0,0.5], \\ \frac{1}{3} v_{2_\eta}(\eta) - \left(\eta v_{2_\eta}(\eta)\right)_\eta + 2v_2(\eta) &= -8\eta^2 + 2\eta^3, \eta \in (0.5,1], \end{aligned} \tag{87}$$

with boundary conditions:

$$\begin{aligned} v_1(0) &= 0, \\ v_2(1) &= 1. \end{aligned} \tag{88}$$

Table 3: Analysis of errors for Example 3.

J	N	Δt	$\mathbf{E}_c(N)$ proposed technique	CPU time in sec	N	IIM
1	8	1/8	1.8394×10^{-3}	0.279452	8	3.7×10^{-2}
2	16	1/16	7.7251×10^{-4}	0.345287	16	7.1×10^{-3}
3	32	1/32	3.5115×10^{-4}	0.612788	32	1.5×10^{-3}
4	64	1/64	1.6775×10^{-4}	2.966826	64	3.0×10^{-4}
5	128	1/128	8.1976×10^{-5}	20.057056	128	1.0×10^{-4}

Table 4: Analysis of errors for Example 4.

J	N	Δt	$\mathbf{E}_c(N)$ proposed technique	CPU time in sec	N	IIM
1	8	0.1/8	1.5×10^{-3}	0.395921	8	1.02×10^{-2}
2	16	0.1/16	7.5054×10^{-4}	0.748104	16	2.4×10^{-3}
3	32	0.1/32	3.7709×10^{-4}	3.148897	32	6.0×10^{-4}
4	64	0.1/64	1.8867×10^{-4}	25.324517	64	1.0×10^{-4}
5	128	0.1/128	9.4324×10^{-5}	194.237104	128	1.0×10^{-4}

and interface conditions:

$$\begin{aligned} [v] &= \frac{1}{3}, \\ [\alpha - \beta v_\eta] &= -1. \end{aligned} \tag{89}$$

The exact solution of the test problem is given by

$$\begin{aligned} v_1(\eta) &= \frac{\eta}{3}, \eta \in [0,0.5], \\ v_2(\eta) &= \eta, \eta \in (0.5,1]. \end{aligned} \tag{90}$$

Table 5: Analysis of errors for Example 5.

J	N	Δt	$\mathbf{E}_c(N)$ proposed technique	CPU time in sec	N	IIM
2	16	0.001/16	3.6548×10^{-6}	34.662755	20	2.9061×10^{-5}
3	32	0.001/32	1.8282×10^{-6}	272.116930	40	6.6497×10^{-6}
4	64	0.001/64	9.1465×10^{-7}	2460.769702	80	1.6343×10^{-6}
5	128	0.001/128	4.5753×10^{-7}	35500.767379	160	4.0802×10^{-7}

Table 6: Analysis of errors Example 6.

J	N	Δt	$\mathbf{E}_c(N)$ proposed technique	CPU time in sec
1	8	0.1/8	6.0232×10^{-4}	0.157302
2	16	0.1/16	1.4666×10^{-4}	1.147091
3	32	0.1/32	3.3345×10^{-5}	11.147277
4	64	0.1/64	6.8252×10^{-6}	81.104287
5	128	0.1/128	1.3904×10^{-6}	588.111313

Example 2. Consider the following initial-boundary value nonlinear elliptic interface problem:

$$\begin{aligned} &v_{1_\eta}(\eta) - \left(\frac{\eta}{v_{1_\eta}}(\eta)\right)_\eta + 2v_1^2(\eta) = 2\eta^2, \eta \in [0,0.5], \\ &\frac{1}{3}v_{2_\eta}(\eta) - \left(2\eta v_{2_\eta}(\eta)\right)_\eta + 2v_2^2(\eta) = e^{-\eta^2}\left(\frac{22}{3}\eta - 8\eta^3 + 2e^{-\eta^2}\right), \eta \in (0.5,1], \end{aligned} \tag{91}$$

with boundary conditions:

$$\begin{aligned} v_1(0) &= 0, \\ v_2(1) &= e^{-1}. \end{aligned} \tag{92}$$

and interface conditions:

$$\begin{aligned} [v] &= e^{-0.25} - \frac{1}{2}, \\ [\alpha - \beta v_\eta] &= e^{-0.25} - \frac{1}{6}. \end{aligned} \tag{93}$$

The exact solution of the test problem is given by

$$\begin{aligned} v_1(\eta) &= \eta, \eta \in [0,0.5], \\ v_2(\eta) &= e^{-\eta^2}, \eta \in (0.5,1]. \end{aligned} \tag{94}$$

Example 3. Suppose the following initial-boundary value linear parabolic problem with single interface conditions [41]:

$$\begin{aligned} &v_{1_t}(\eta,t) + v_{1_\eta}(\eta,t) - \left(\frac{\eta}{3}v_{1_\eta}(\eta,t)\right)_\eta + v_1(\eta,t) = \frac{-\eta^3}{3}\sin(t) + \frac{\eta^3}{3}\cos(t), \eta \in [0,0.5], \\ &v_{2_t}(\eta,t) - \left(\eta v_{2_\eta}(\eta,t)\right)_\eta = -\eta^3 \sin(t) + \left(-9\eta^2\right)\cos(t), \eta \in (0.5,1], \end{aligned} \tag{95}$$

subject to the following initial and boundary conditions:

$$\begin{aligned} v_1(\eta,0) &= \frac{\eta^3}{3} \\ v_1(0,t) &= 0, \\ v_2(1,t) &= \cos(t), \end{aligned} \tag{96}$$

and interface conditions:

$$\begin{aligned} [v] &= (2/3)(0.5)^3 \cos(t), \\ [\alpha - \beta v_\eta] &= (-8/3)(0.5)^3 \cos(t) - 1. \end{aligned} \tag{97}$$

The exact solution of the test problem is given by

$$\begin{aligned} v_1(\eta,t) &= \frac{\eta^3}{3}\cos(t), \eta \in [0,0.5], \\ v_2(\eta,t) &= \eta^3 \cos(t), \eta \in (0.5,1]. \end{aligned} \tag{98}$$

Example 4. Consider another initial-boundary value linear parabolic interface problem [41]:

$$\begin{aligned} &v_{1_t}(\eta,t) + v_{1_\eta}(\eta,t) - \left(\frac{\eta}{3}v_{1_\eta}(\eta,t)\right)_\eta + v_1(\eta,t) \\ &\quad = -(\eta+1)\sin(t) + \left(\frac{5}{3} + \eta\right)\cos(t), \eta \in [0,0.5], \\ &v_{2_t}(\eta,t) - \left(\eta v_{2_\eta}(\eta,t)\right)_\eta = -\eta \sin(t) - \cos(t), \eta \in (0.5,1], \end{aligned} \tag{99}$$

with the following initial and boundary conditions:

$$\begin{aligned} v_1(\eta,0) &= \eta + 1 \\ v_1(0,t) &= \cos(t), \\ v_2(1,t) &= \cos(t), \end{aligned} \tag{100}$$

and interface conditions:

$$\begin{aligned} [v] &= -\cos(t), \\ [\alpha - \beta v_\eta] &= -\frac{1}{3}\cos(t) - 1. \end{aligned} \tag{101}$$

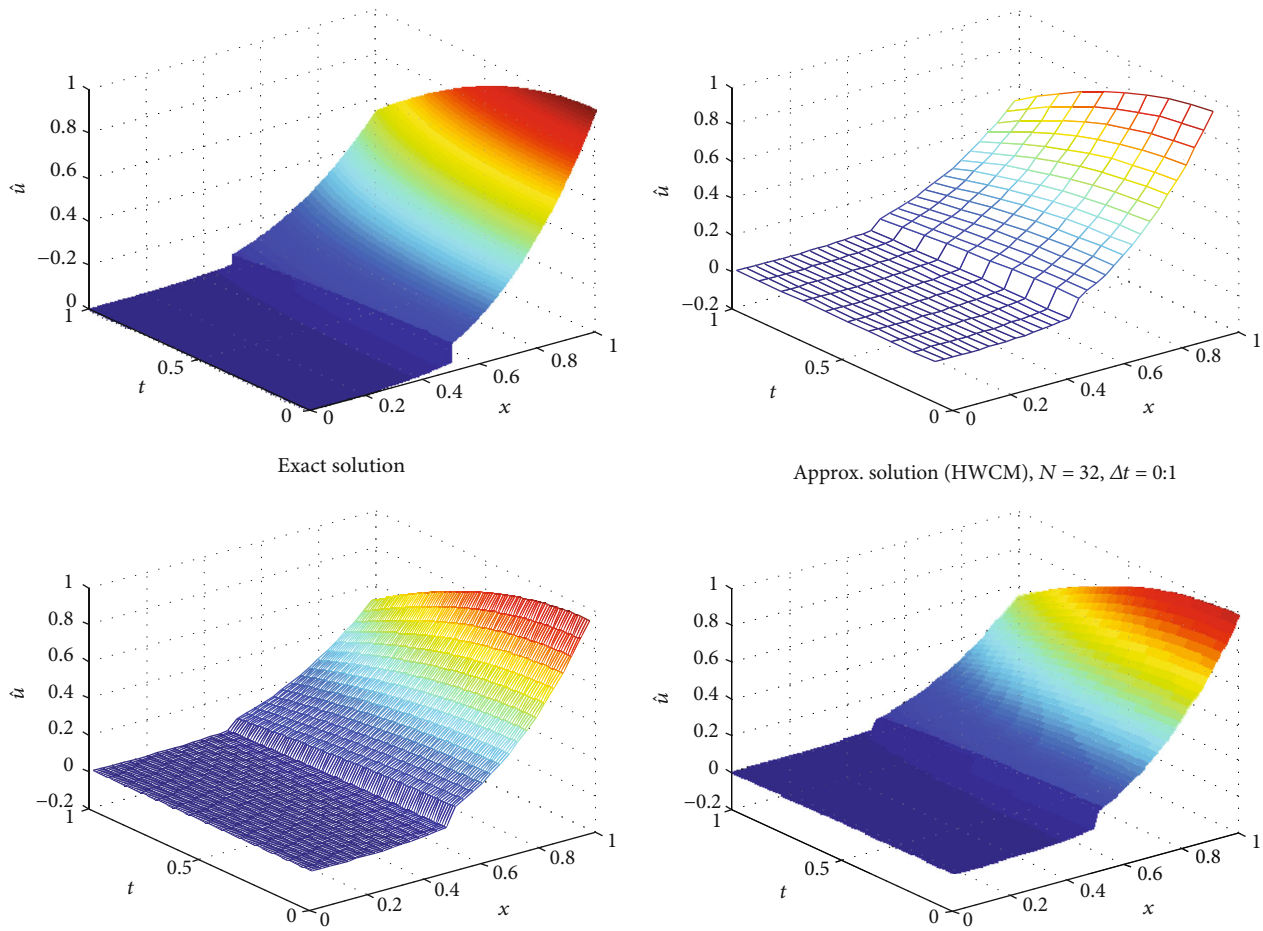

Figure 3: Comparability of exact and estimated results for Example 3.

The exact solution of the test problem is given by

$$v_1(\eta, t) = (\eta + 1)\cos(t), \eta \in [0,0.5],$$
$$v_2(\eta, t) = \eta\cos(t), \eta \in (0.5,1]. \tag{102}$$

Example 5. Consider another linear parabolic interface model:

$$v_{1_t}(\eta, t) + v_{1_\eta}(\eta, t) - \left(\frac{\eta}{3} v_{1_\eta}(\eta, t)\right)_\eta = \frac{2}{3}\cos(t) - \eta\sin(t), \eta \in [0,0.5],$$
$$v_{2_t}(\eta, t) + v_{1_\eta}(\eta, t) - \left(\eta v_{2_\eta}(\eta, t)\right)_\eta = -\left(\eta + \frac{1}{2}\right)\sin(t), \eta \in (0.5,1], \tag{103}$$

with the subsequent initial conditions and boundary conditions:

$$v_1(\eta, 0) = \eta,$$
$$v_1(0, t) = 0,$$
$$v_2(1, t) = \frac{3}{2}\cos(t), \tag{104}$$

and interface conditions:

$$[v] = \frac{1}{2}\cos(t),$$
$$[\alpha - \beta v_\eta] = -\frac{1}{3}\cos(t). \tag{105}$$

The exact solution of the test problem is given by

$$v_1(\eta, t) = \eta\cos(t), \eta \in [0,0.5],$$
$$v_2(\eta, t) = \left(\eta + \frac{1}{2}\right)\cos(t), \eta \in (0.5,1]. \tag{106}$$

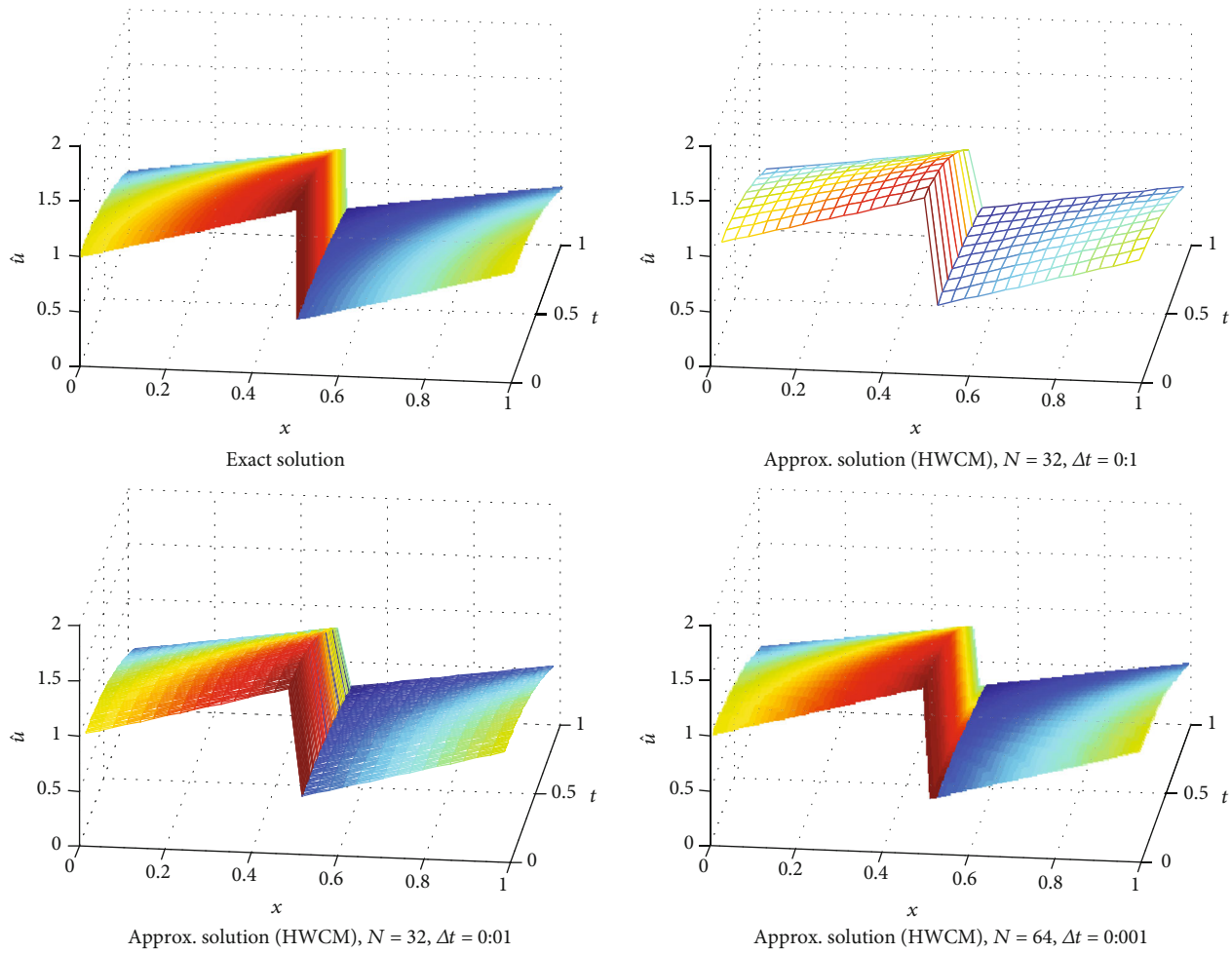

Figure 4: Comparability of exact and estimated results for Example 4.

Example 6. Consider the following nonlinear parabolic interface model:

$$\begin{aligned} &v_{1_t}(\eta,t)+v_{1_\eta}(\eta,t)-\left(\frac{\eta}{3}v_{1_\eta}(\eta,t)\right)_\eta+v_1^2(\eta,t)\\ &\quad=-\eta^4e^{-t}-\frac{4}{3}\eta^3e^{-t}+\eta^8e^{-2t},\eta\in[0,0.5],\\ &v_{2_t}(\eta,t)-\left(\eta v_{2_\eta}(\eta,t)\right)_\eta+v_2^2(\eta,t)\\ &\quad=-\frac{1}{2}\left(\eta^4+\frac{1}{16}\right)e^{-t}-8\eta^3e^{-t}+\frac{1}{4}\left(\eta^8+\frac{\eta^4}{8}+\frac{1}{256}\right)e^{-2t},\eta\in(0.5,1], \end{aligned} \tag{107}$$

subject to the following initial and boundary conditions:

$$\begin{aligned} v_1(\eta,0)&=\eta^4,\\ v_1(0,t)&=0,\\ v_2(1,t)&=\frac{17}{32}e^{-t}, \end{aligned} \tag{108}$$

and interface conditions:

$$\begin{aligned} [v]&=0,\\ [\alpha-\beta v_\eta]&=-\frac{e^{-t}}{24}-1. \end{aligned} \tag{109}$$

The exact solution of the test problem is given by

$$\begin{aligned} v_1(\eta,t)&=\eta^4e^{-t},\eta\in[0,0.5],\\ v_2(\eta,t)&=\frac{1}{2}\left(\eta^4+\frac{1}{16}\right)e^{-t},\eta\in(0.5,1]. \end{aligned} \tag{110}$$

In this section, some numerical experiments comprising linear and nonlinear elliptic and parabolic advection-diffusion-reaction type interface models have been carried out, in order to check the efficiency and better accuracy of the newly proposed numerical technique for these types of models. First, we have discussed elliptic interface models and then parabolic interface models.

In the first two linear and nonlinear elliptic interface models, the errors are decreased to 10^{-6} and 10^{-7} even for small number of grid points. It is worth mentioning that

more accurate numerical results can be obtained if we increase the number grid points. In Table 1, the absolute errors for distinct collocation points are listed. The graph given in Figure 2 also demonstrates that the proposed technique captures the discontinuity very well, where the other methods failed to do so. The computational rate of convergence of the proposed method is approaching to 2, which is theoretically confirmed by Majak et al. [42, 43]. The obtained results are compared with the immersed interface method from literature. The comparability shows that the newly proposed technique is efficient and more accurate for elliptic type interface models than the existing methods. The newly proposed numerical technique is also tested on advection-diffusion-reaction type parabolic interface models, comprising of three linear and one nonlinear models. The obtained point wise absolute errors are mentioned in Tables 3–6. The numerical results are also demonstrated through 3D visualization of the graphs listed in Figures 3 and 4. From the aforementioned figures, it is clear that the newly proposed technique handled the jump discontinuity at 0.5 and 0.7 very well. The approximate results are compared with the immersed interface method from the existing literature. The comparability shows that the proposed technique has better accuracy with simple implementation.

8. Conclusion

In this article, Haar wavelet collocation technique is utilized to solve interface models comprising advection-diffusion-reaction type elliptic and parabolic models with discontinuous coefficients. The newly proposed numerical technique is applicable to both linear and nonlinear interface models. The errors are decreased up to $10^{-}6$ and 10^{-7} for small number of collocation points, which is supposed to be better accuracy for practical problems. The 3D graphs of the estimated and exact solutions also demonstrate that the newly proposed technique handle the jump discontinuity very well, while the other existing techniques failed to capture it. The stability and convergence of the said numerical technique are also proved in the convergence and stability sections, which made the method more powerful. The obtained results are compared with the immersed interface method. The comparability shows that the newly proposed technique is efficient and has better accuracy than immersed interface method.

Data Availability

No data were used to support this study.

Conflicts of Interest

The authors declare that there is no conflict of interests regarding the publication of this paper.

References

[1] Z. Li and K. Ito, "The immersed interface method: numerical solutions of PDEs involving interfaces and irregular domains," *Society for Industrial and Applied Mathematics, (SIAM)*, vol. 33, pp. 3665–3673, 2006.

[2] Z. Li and K. Ito, "Maximum principle preserving schemes for interface problems with discontinuous coefficients," *SIAM Journal of Scientific Computing*, vol. 23, pp. 1225–1242, 2001.

[3] Z. Li and B. Soni, "Fast and accurate numerical approaches for Stefan problems and crystal growth," *Numerical Heat Transfer, Part B: Fundamentals*, vol. 35, pp. 461–484, 1999.

[4] J. B. Bell, P. Colella, and H. M. Glaz, "A second-order projection method for the incompressible Navier-Stokes equations," *Journal of Computational Physics*, vol. 85, no. 2, pp. 257–283, 1989.

[5] X. D. Liu and T. Sideris, "Convergence of the ghost fluid method for elliptic equations with interfaces," *Mathematics of Computation*, vol. 72, no. 244, pp. 1731–1747, 2003.

[6] C. S. Peskin, "Numerical analysis of blood flow in the heart," *Journal of Computational Physics*, vol. 3, no. 25, pp. 220–252, 1977.

[7] C. S. Peskin, *The Immersed Boundary Method. Acta Numerica*, vol. 11, Cambridge University Press, 2002.

[8] J. R. Leveque and Z. Li, "The immersed interface method for elliptic equations with discontinuous coefficients and singular sources," *SIAM Journal on Numerical Analysis*, vol. 31, no. 4, pp. 1019–1044, 1994.

[9] R. P. Fedkiw, T. Aslam, B. Merriman, and S. Osher, "A non-oscillatory Eulerian approach to interfaces in multimaterial flows (the ghost fluid method)," *Journal of Computational Physics*, vol. 152, no. 2, pp. 457–492, 1999.

[10] S. Yu, Y. Zhou, and G. W. Wei, "Matched interface and boundary (MIB) method for elliptic problems with sharp- edged interfaces," *Journal of Computational Physics*, vol. 224, no. 2, pp. 729–756, 2007.

[11] Y. C. Zhou, J. Liu, and D. L. Harry, "A matched interface and boundary method for solving multi-flow Navier-Stokes equations with applications to geodynamics," *Journal of Computational Physics*, vol. 231, no. 1, pp. 223–242, 2012.

[12] Y. Zhou, S. Zhao, M. Feig, and G. W. Wei, "High order matched interface and boundary method for elliptic equations with discontinuous coefficients and singular sources," *Journal of Computational Physics*, vol. 1, no. 213, pp. 1–30, 2006.

[13] A. Mayo, "The fast solution of Poisson's and the biharmonic equations on irregular regions," *SIAM Journal on Numerical Analysis*, vol. 21, no. 2, pp. 285–299, 1984.

[14] W. Feng, X. He, Y. Lin, and X. Zhang, "Immersed finite element method for interface problems with algebraic multigrid solver," *Communications in Computational Physics*, vol. 15, no. 4, pp. 1045–1067, 2014.

[15] Y. Gong, B. Li, and Z. Li, "Immersed-interface finite-element methods for elliptic interface problems with nonhomogeneous jump conditions," *SIAM Journal on Numerical Analysis*, vol. 46, no. 1, pp. 472–495, 2008.

[16] Q. Yang and X. Zhang, "Discontinuous Galerkin immersed finite element methods for parabolic interface problems," *Journal of Computational and Applied Mathematics*, vol. 299, pp. 127–139, 2016.

[17] C. Lehrenfeld and A. Reusken, "Analysis of a high-order unfitted finite element method for elliptic interface problems," *IMA Journal of Numerical Analysis*, vol. 38, pp. 1351–1387, 2017.

[18] C. H. Hsiao and W. J. Wang, "Haar wavelet approach to nonlinear stiff systems," *Mathematics and Computers in Simulation*, vol. 57, no. 6, pp. 347–353, 2001.

[19] C. H. Hsiao, "Haar wavelet approach to linear stiff systems," *Mathematics and Computers in Simulation*, vol. 64, no. 5, pp. 561–567, 2004.

[20] U. Lepik, "Numerical solution of differential equations using Haar wavelets," *Mathematics and Computers in Simulation*, vol. 68, no. 2, pp. 127–143, 2005.

[21] U. Lepik, "Numerical solution of evolution equations by the Haar wavelet method," *Applied Mathematics and Computation*, vol. 185, pp. 695–704, 2007.

[22] M. Ahsan, S. Islam, and I. Hussain, "Haar wavelets multi-resolution collocation analysis of unsteady inverse heat problems," *Inverse Problems in Science and Engineering*, vol. 27, no. 11, pp. 1498–1520, 2019.

[23] S. Islam, M. Ahsan, and I. Hussain, "A multi-resolution collocation procedure for time-dependent inverse heat problems," *International Journal of Thermal Sciiences*, vol. 128, pp. 160–174, 2018.

[24] M. Ahsan, I. Ahmad, M. Ahmad, and I. Hussian, "A numerical Haar wavelet-finite difference hybrid method for linear and non-linear Schrödinger equation," *Mathematics and Computer in Simulation*, vol. 165, pp. 13–25, 2019.

[25] R. Amin, K. Shah, M. Asif, I. Khan, and F. Ullah, "An efficient algorithm for numerical solution of fractional integro-differential equations via Haar wavelet," *Journal of Computational and Applied Mathematics*, vol. 73, article 113028, pp. 1–17, 2020.

[26] I. Aziz, S. Islam, and M. Asif, "Haar wavelet collocation method for three-dimensional elliptic partial differential equations," *Computers and Mathematics with Applications*, vol. 73, no. 9, pp. 2023–2034, 2017.

[27] J. Majak, K. Karjust, M. Eermea, J. Kurnitskia, and B. S. Shvartsman, "New higher order Haar wavelet method: application to FGM structures," *Composite Structures*, vol. 201, pp. 72–78, 2018.

[28] S. Zhi, X. Yan-Hua, and Z. Jun-Ping, "Haar wavelets method for solving Poisson equations with jump conditions in irregular domain," *Advances in Computational Mathematics*, vol. 42, no. 4, pp. 995–1012, 2016.

[29] O. Oruc, "An efficient meshfree method based on Pascal polynomials and multiple-scale approach for numerical solution of 2-D and 3-D second order elliptic interface problems," *Journal of Computational Physics*, vol. 428, article 110070, 2021.

[30] F. Bulut, O. Oruc, and A. Esen, "Higher order Haar wavelet method integrated with strang splitting for solving regularized long wave equation," *Mathematics and Computers in Simulation*, vol. 197, pp. 277–290, 2022.

[31] O. Oruc, A. Esen, and F. Bulut, "Numerical investigation of dynamic Euler-Bernoulli equation via 3-scale Haar wavelet collocation method," *Hacettepe Journal of Mathematics and Statistics*, vol. 50, pp. 159–179, 2021.

[32] O. Oruc, F. Bulut, and A. Esen, "Numerical solution of the KdV equation by Haar wavelet method," *Pranama Journal of Physics*, vol. 87, no. 6, 2016.

[33] O. Oruc, "A non-uniform Haar wavelet method for numerically solving two-dimensional convection-dominated equations and two-dimensional near singular elliptic equations," *Computers and Mathematics with Applications*, vol. 7, no. 77, pp. 1799–1820, 2019.

[34] M. Ratas, J. Majak, and A. Salupere, "Solving nonlinear boundary value problems using the higher order Haar wavelet method," *Mathematics*, vol. 9, no. 21, p. 2809, 2021.

[35] M. Mehrparvar, J. Majak, K. Karjust, and M. Arda, "Free vibration analysis of tapered Timoshenko beam with higher order Haar wavelet method," *Proceedings of the Estonian Academy of Sciences*, vol. 1, no. 71, pp. 77–83, 2022.

[36] M. Ratas, A. Salupere, and J. Majak, "Solving nonlinear PDEs using the higher order Haar wavelet method on nonuniform and adaptive grids," *Mathematical Modelling and Analysis*, vol. 1, no. 26, pp. 147–169, 2021.

[37] M. Asif, N. Haider, Q. A. Mdallal, and I. Khan, "A Haar wavelet collocation approach for solving one and two-dimensional second-order linear and nonlinear hyperbolic telegraph equations," *Numerical Methods for Partial Differential Equations*, vol. 36, no. 6, pp. 1962–1981, 2020.

[38] R. E. Bellman and R. E. Kalaba, *Quasilinearization and Nonlinear Boundary Value Problems*, American, Elsevier, New York, 1965.

[39] M. Kumar and S. Pandit, "A composite numerical scheme for the numerical simulation of coupled Burgers equation," *Computer Physics Communications*, vol. 185, no. 3, pp. 809–817, 2014.

[40] A. Zada, *Asymptotic Behavior of Solutions for a Class of Semi-Linear Differential Systems in Finite Dimensional Spaces*, Abdus Salam School of Mathematical Sciences GC University Lahore, Pakistan, 2010.

[41] N. Aljahdaly, "The immersed interface method for elliptic and parabolic problems with discontinuous coefficients," *American Journal of Numerical Analysis*, vol. 2, pp. 152–166, 2014.

[42] J. Majak, B. Shvartsman, M. Kirs, M. Pohlak, and H. Herranan, "Convergence theorem for the Haar wavelet based discretization method," *Composite Structures*, vol. 126, pp. 227–232, 2015.

[43] J. Majak, B. Shvartsman, K. Karjust, M. Mikola, A. Haavajoe, and M. Pohlak, "On the accuracy of the Haar wavelet discretization method," *Composits B*, vol. 80, pp. 321–327, 2015.

Hindawi
Journal of Function Spaces
Volume 2022, Article ID 8063888, 15 pages
https://doi.org/10.1155/2022/8063888

Review Article

Pell Collocation Method for Solving the Nonlinear Time–Fractional Partial Integro–Differential Equation with a Weakly Singular Kernel

M. Taghipour [1] **and H. Aminikhah** [1,2]

[1] *Department of Applied Mathematics and Computer Science, Faculty of Mathematical Sciences, University of Guilan, P.O. Box 1914, Rasht 41938, Iran*
[2] *Center of Excellence for Mathematical Modelling, Optimization and Combinational Computing (MMOCC), University of Guilan, P.O. Box 1914, Rasht 41938, Iran*

Correspondence should be addressed to H. Aminikhah; aminikhah@guilan.ac.ir

Received 31 December 2021; Accepted 21 April 2022; Published 23 May 2022

Academic Editor: Youssri Hassan Youssri

This article focuses on finding the numerical solution of the nonlinear time–fractional partial integro–differential equation. For this purpose, we use the operational matrices based on Pell polynomials to approximate fractional Caputo derivative, nonlinear, and integro–differential terms; and by collocation points, we transform the problem to a system of nonlinear equations. This nonlinear system can be solved by the fsolve command in Matlab. The method's stability and convergence have been studied. Also included are five numerical examples to demonstrate the veracity of the suggested strategy.

1. Introduction

Nowadays, fractional partial differential equations (FPDEs) have emerged as one of the most crucial issues due to their vast applications in various branches of science, such as medicine [1, 2], control theory [3–5], engineering [6, 7], viscoelasticity [8], mathematical physics [9], geo–hydrology [10], signals [11], stochastic models [12], electrical engineering, [13], and financial economics [14]. Due to the fact that analytical solutions of FPDEs are rarely available, the use of numerical methods is inevitable. Hitherto, a number of numerical methods for FPDEs have been suggested, such as finite difference [15, 16], spectral methods [17–21], homotopy methods [22, 23], and finite element [24, 25]. The nonlinear FPDEs have been extensively analyzed using numerical methods. Dehghan et al. used the homotopy analysis method to construct a scheme for solving the fractional KdV equation [26]. Nikan et al. proposed a meshless technique in order to solve the nonlinear fractional fourth–order diffusion equation [27]. Safari and Azarsa introduced a meshless method based on Muntz polynomials to solve nonlinear and linear space fractional partial differential equations [28]. Yaslan applied the Legender collocation method for solving nonlinear fractional partial differential equations [29].

When it comes to solving differential equations, spectral approaches are extremely effective. The solution to the differential equation is sought as a series of basis polynomials using this method. The Galerkin, Tao, and collocation approximations are the most common spectral methods [30, 31]. For example, Samiee et al. [20] designed a Petrov–Galerkin spectral method for distributed–order PDEs. Agarwal et al. [32] suggested a spectral collocation approach for variable–order fractional integro–differential equations. In [33], the authors used the polynomial–sinc collocation method for solving distributed order fractional differential equations. Abbaszadeh et al. proposed a Crank–Nicolson

Galerkin spectral method for distributed order weakly singular integro–partial differential equations [34].

In the present paper, we offer a numerical technique for solving the nonlinear time–fractional partial integro–differential equation (TFPIDEs) with a weakly singular kernel

$$\begin{aligned}&{}_0^{\mathrm{C}}\mathscr{D}_\eta^\alpha \mathscr{V}(\xi,\eta)+\mathscr{V}(\xi,\eta)\mathscr{V}_\xi(\xi,\eta)\\&\quad=\int_0^\eta(\eta-\mathrm{s})^{\beta-1}\mathscr{V}_{\xi\xi}(\xi,\mathrm{s})\mathrm{ds}+\mathscr{G}(\xi,\eta),\xi\in[0,\mathrm{L}],\eta\in[0,\mathrm{T}],\end{aligned}\tag{1}$$

with initial and boundary conditions

$$\mathscr{V}(0,\eta)=\Phi_1(\eta),\mathscr{V}(L,\eta)=\Phi_2(\eta),0<\eta\le T,\tag{2}$$

$$\mathscr{V}(\xi,0)=\Psi(\xi),0<\xi\le L,\tag{3}$$

where $0<\alpha,\beta<1$, $\mathrm{g}(\xi,\eta)\in\mathrm{C}([0,\mathrm{L}]\times[0,\mathrm{T}])$, and ${}_0^{\mathrm{C}}\mathscr{D}_\eta^\alpha$ signify the fractional operator. This problem appears in the modeling of heat transfer materials with memory, population dynamics [35], and nuclear reaction theory [36].

To the best of the author's knowledge, little work has been done on problem (1). For example, Guo et al. [37] proposed a numerical technique for solving (1)–(3). In the case of $\alpha=1$, Zheng et al. [35] described three semi–implicit compact finite difference schemes for problem (1)–(3). This encourages us to suggest a numerical scheme for the problem (1)–(3). The finite difference schemes are the easiest methods for solving these equations. It is, however, difficult to apply the mathematical study of finite difference methods to nonlinear TFPIDEs. Polynomial spectral techniques are effective tools for solving PDEs. To build spectral methods, many polynomials have been developed (see [38–41]). The coefficients of Pell polynomials are integers, and the number of terms increases slowly. This leads to less CPU time and fewer computational errors. Because of this, the Pell polynomials with both of these two characteristics will be employed.

In this paper, we will focus on the spectral collocation method based on two–variable Pell polynomials. We use them as the basis polynomials to solve the main problem numerically. With the use of operational matrices, the problem is turned into a system of nonlinear equations in the approach based on these polynomials. The error analysis is presented. Several test problems are provided to illustrate the method's efficacy.

The following is the body of the article: Section 2 introduces a number of key themes. To remedy the main problem, we suggest a polynomial spectral technique in Section 3. The error analysis is investigated in Section 4. Section 5 contains the experiments. The conclusion is addressed in Section 6.

2. Definitions

Definition 1 (see [15]). The Riemann–Liouville integral of a function $\mathfrak{z}(\xi,\eta)$ on $(0,L)\times(0,T)$ is defined as follows

$${}_0^{\mathrm{RL}}\mathscr{I}_\eta^\alpha\mathfrak{z}(\xi,\eta)=\frac{1}{\Gamma(\alpha)}\int_0^\eta(\eta-\tau)^{\alpha-1}\mathfrak{z}(\xi,\tau)d\tau,0<\alpha<1.\tag{4}$$

Definition 2 (see [15]). The Riemann–Liouville derivative of a function $\mathfrak{z}(\xi,\eta)$ on $(0,L)\times(0,T)$ is defined as follows

$${}_0^{\mathrm{RL}}\mathscr{D}_\eta^\alpha\mathfrak{z}(\xi,\eta)=\frac{1}{\Gamma(1-\alpha)}\frac{d}{d\eta}\int_0^\eta(\eta-\tau)^{-\alpha}\mathfrak{z}(\xi,\tau)d\tau,0<\alpha<1.\tag{5}$$

Definition 3 (see [15]). The Caputo derivative of a function $\mathfrak{z}(\xi,\eta)$ on $(0,L)\times(0,T)$ is defined as follows

$${}_0^{C}\mathscr{D}_\eta^\alpha\mathfrak{z}(\xi,\eta)=\frac{1}{\Gamma(1-\alpha)}\int_0^\eta(\eta-\tau)^{-\alpha}\mathfrak{z}'(\xi,\tau)d\tau,0<\alpha<1.\tag{6}$$

With respect to these definitions, we have the following properties

$${}_0^{\mathrm{RL}}\mathscr{I}_\eta^\alpha{}_0^{\mathrm{C}}\mathscr{D}_\eta^\alpha\mathfrak{z}(\xi,\eta)=\mathfrak{z}(\xi,\eta)-\mathfrak{z}(\xi,0),0<\alpha<1,0.4\mathrm{cm},\tag{7}$$

$${}_0^{C}\mathscr{D}_\eta^\alpha c=0,\quad c=\text{constant},\tag{8}$$

$${}_0^{C}\mathscr{D}_\eta^\alpha\eta^m=\begin{cases}0,\quad m=0,\\ \dfrac{\Gamma(m+1)}{\Gamma(m+1-\alpha)}\eta^{m-\alpha},m=1,2,\cdots.\end{cases}\tag{9}$$

The following relation can be used to construct Pell polynomials: [42]:

$$\mathscr{P}_{l+2}(\xi)=2\xi\mathscr{P}_{l+1}(\xi)+\mathscr{P}_l(\xi),\mathscr{P}_0(\xi)=0,\mathscr{P}_1(\xi)=1.\tag{10}$$

According to [42], $\mathscr{P}_{\mathrm{n}}(\xi)$ has the following form

$$\mathscr{P}_l(\xi)=\sum_{k=0}^{\lfloor l-1/2\rfloor}\binom{l-k-1}{k}(2\xi)^{l-2k-1}.\tag{11}$$

We can represent a continuous function $\mathscr{V}(\xi)$ via the Pell polynomials as follows:

$$\mathscr{V}(\xi)\approx\mathscr{V}_K(\xi)=\sum_{i=0}^{K}\bar{v}_{i+1}\mathscr{P}_{i+1}(\xi)=\mathscr{V}^T\mathscr{P}_K(\xi),\tag{12}$$

where

$$\mathscr{V}=[\bar{v}_1,\bar{v}_2,\cdots,\bar{v}_{K+1}]^T,\mathscr{P}_K(\xi)=[\mathscr{P}_1(\xi),\mathscr{P}_2(\xi),\cdots,\mathscr{P}_{K+1}(\xi)]^T.\tag{13}$$

Analogously, a function $\mathscr{V}(\xi,\eta)$ defined on $[0,\mathrm{L}]\times[0,\mathrm{T}]$ may be described as follows:

$$\begin{aligned}\mathscr{V}(\xi,\eta)\approx\mathscr{V}_{KJ}(\xi)&=\sum_{i=0}^{K}\sum_{j=0}^{J}\bar{v}_{i+1,j+1}\mathscr{P}_{i+1}(\xi)\mathscr{P}_{j+1}(\eta)\\&=\mathscr{P}_K(\xi)^T\mathscr{W}\mathscr{P}_J(\eta)=\mathscr{V}^T\mathscr{P}_{KJ}(\xi,\eta),\end{aligned}\tag{14}$$

and $\mathscr{W}$ denotes a matrix of suitable dimensions, as well as $\mathscr{V}$ and $\mathscr{P}_{KJ}(\xi,\eta)$ are the following:

$$\mathscr{V} = \left[\bar{v}_{11}, \bar{v}_{12}, \cdots, \bar{v}_{1J+1}, \bar{v}_{21}, \cdots, \bar{u}_{2J+1}, \cdots, \bar{v}_{K1}, \cdots, \bar{v}_{K+1J+1}\right]^T, \tag{15}$$

$$\mathscr{P}_{KJ}(\xi,\eta) = \left[\mathscr{P}_{11}(\xi,\eta), \cdots, \mathscr{P}_{1J+1}(\xi,\eta), \mathscr{P}_{21}(\xi,\eta), \cdots, \mathscr{P}_{2J+1} \cdot (\xi,\eta), \cdots, \mathscr{P}_{K+11}(\xi,\eta), \cdots, \mathscr{P}_{K+1J+1}(\xi,\eta)\right]^T. \tag{16}$$

We may also rephrase $\mathscr{P}_K(\xi), \mathscr{P}_J(\eta)$ in the following way:

$$\mathscr{P}_K(\xi) = \mathscr{Q}_\xi \mathscr{T}(\xi), \tag{17}$$

$$\mathscr{P}_J(\eta) = \mathscr{Q}_\eta \mathscr{T}(\eta), \tag{18}$$

$$\mathscr{T}(\xi) = \left[1, \xi, \cdots, \xi^K\right]^T, \mathscr{T}(\eta) = \left[1, \eta, \cdots, \eta^J\right]^T, \tag{19}$$

where

$$\mathscr{Q}_\xi = \begin{pmatrix} a_{0,0} & 0 & 0 & 0 & \cdots & 0 \\ 0 & a_{1,1} & 0 & 0 & \cdots & 0 \\ a_{2,0} & 0 & a_{2,2} & 0 & \cdots & 0 \\ \vdots & \vdots & \vdots & \vdots & \vdots & \vdots \\ a_{K,1} & 0 & a_{K,3} & \cdots & 0 & a_{K,K} \end{pmatrix},$$

$$\mathscr{Q}_\eta = \begin{pmatrix} a_{0,0} & 0 & 0 & 0 & \cdots & 0 \\ 0 & a_{1,1} & 0 & 0 & \cdots & 0 \\ a_{2,0} & 0 & a_{2,2} & 0 & \cdots & 0 \\ \vdots & \vdots & \vdots & \vdots & \vdots & \vdots \\ a_{J,1} & 0 & a_{J,3} & \cdots & 0 & a_{J,J} \end{pmatrix}, \tag{20}$$

with

$$\left(a_{i,j}\right) = \begin{cases} \begin{pmatrix} i - \left\lfloor \dfrac{i-j}{2} \right\rfloor \\ \left\lfloor \dfrac{i-j}{2} \right\rfloor \end{pmatrix} 2^{i-2\left\lfloor \frac{i-j}{2} \right\rfloor}, & \text{if } i \geq j, i, j = odd \text{ or } i, j = even \\ 0, & otherwise. \end{cases} \tag{21}$$

3. Analysis of the Numerical Method

Here, we find several operational matrices with the help of Pell polynomials, which are useful in developing the suggested technique.

To begin, we estimate the fractional operator as follows:

$$\begin{aligned} {}_0^C\mathscr{D}_\eta^\alpha \mathscr{V}(\xi,\eta) &\approx {}_0^C\mathscr{D}_\eta^\alpha \mathscr{V}_{KJ}(\xi,\eta) \\ &= {}_0^C\mathscr{D}_\eta^\alpha \mathscr{P}_K(\xi)^T \mathscr{W} \mathscr{P}_J(\eta) = \mathscr{P}_K(\xi)^T \mathscr{W}\left({}_0^C\mathscr{D}_\eta^\alpha \mathscr{P}_J(\eta)\right) \\ &= \mathscr{P}_K(\xi)^T \mathscr{W}\left({}_0^C\mathscr{D}_\eta^\alpha \mathscr{Q}_\eta \mathscr{T}(\eta)\right), \end{aligned} \tag{22}$$

$$= \mathscr{P}_K(\xi)^T \mathscr{W} \mathscr{Q}_\eta \left({}_0^C\mathscr{D}_\eta^\alpha T(\eta)\right). \tag{23}$$

Thanks to using relation (9), we obtain

$${}_0^C\mathscr{D}_\eta^\alpha \mathscr{V}_{KJ}(\xi,\eta) = \mathscr{P}_K(\xi)^T \mathscr{W} \mathscr{Q}_\eta \left[0, \frac{\Gamma(2)}{\Gamma(2-\alpha)}\eta^{1-\alpha}, \frac{\Gamma(3)}{\Gamma(3-\alpha)}\eta^{2-\alpha}, \cdots, \frac{\Gamma(J+1)}{\Gamma(J+1-\alpha)}\eta^{J-\alpha}\right]^T, \tag{24}$$

$$= \mathscr{P}_K(\xi)^T \mathscr{W} \mathscr{Q}_\eta \begin{pmatrix} 0 & 0 & 0 & \cdots & 0 \\ 0 & \dfrac{\Gamma(2)}{\Gamma(2-\alpha)}\eta^{-\alpha} & 0 & \cdots & 0 \\ 0 & 0 & \dfrac{\Gamma(3)}{\Gamma(3-\alpha)}\eta^{-\alpha} & \cdots & 0 \\ \vdots & \vdots & \vdots & \vdots & \vdots \\ 0 & 0 & 0 & \cdots & \dfrac{\Gamma(J+1)}{\Gamma(J+1-\alpha)}\eta^{-\alpha} \end{pmatrix} \begin{pmatrix} 1 \\ \eta \\ \eta^2 \\ \vdots \\ \eta^J \end{pmatrix}, \tag{25}$$

$$= \mathscr{P}_K(\xi)^T \mathscr{W} \mathscr{Q}_\eta \mathscr{M}_\alpha \mathscr{Q}_\eta^{-1} \mathscr{P}_J(\eta), \tag{26}$$

where

$$\mathscr{M}_\alpha = \operatorname{diag}\left(0, \frac{\Gamma(2)}{\Gamma(2-\alpha)}\eta^{-\alpha}, \frac{\Gamma(3)}{\Gamma(3-\alpha)}\eta^{-\alpha}, \cdots, \frac{\Gamma(J+1)}{\Gamma(J+1-\alpha)}\eta^{-\alpha}\right). \tag{27}$$

$$ {}_0^C\mathscr{D}_\eta^\alpha \mathscr{V}(\xi,\eta) \approx \mathscr{P}_K(\xi)^T \mathscr{W} \mathscr{Q}_\eta \mathscr{M}_\alpha \mathscr{Q}_\eta^{-1} \mathscr{P}_J(\eta). \tag{28}$$

Next, we approximate the nonlinear and integro–differential terms in equation (1). First, we compute $\mathscr{P}_K{}'(\xi)$ and $\mathscr{P}_K{}''(\xi)$.

$$\begin{aligned}\mathscr{P}_K'(\xi) = \mathscr{Q}_\xi \mathscr{T}'(\xi) &= \mathscr{Q}_\xi \begin{pmatrix} 0 \\ 1 \\ 2\xi \\ \vdots \\ K\xi^{K-1} \end{pmatrix} \\ &= \mathscr{Q}_\xi \begin{pmatrix} 0 & 0 & 0 & 0 & \cdots & 0 & 0 & 0 \\ 1 & 0 & 0 & 0 & \cdots & 0 & 0 & 0 \\ 0 & 2 & 0 & 0 & \cdots & 0 & 0 & 0 \\ 0 & 0 & 3 & 0 & \cdots & 0 & 0 & 0 \\ \vdots & \vdots & \vdots & \vdots & \vdots & \vdots & \vdots & \vdots \\ 0 & 0 & 0 & 0 & \cdots & 0 & N & 0 \end{pmatrix} \begin{pmatrix} 1 \\ \xi \\ \xi^2 \\ \vdots \\ \xi^K \end{pmatrix},\end{aligned} \tag{29}$$

$$= \mathscr{Q}_\xi \mathscr{D}' \mathscr{T}(\xi) = \mathscr{Q}_\xi \mathscr{D}' \mathscr{Q}_\xi^{-1} \mathscr{P}_K(\xi), \tag{30}$$

where

$$\mathscr{D}' = \begin{pmatrix} 0 & 0 & 0 & 0 & \cdots & 0 & 0 & 0 \\ 1 & 0 & 0 & 0 & \cdots & 0 & 0 & 0 \\ 0 & 2 & 0 & 0 & \cdots & 0 & 0 & 0 \\ 0 & 0 & 3 & 0 & \cdots & 0 & 0 & 0 \\ \vdots & \vdots & \vdots & \vdots & \vdots & \vdots & \vdots & \vdots \\ 0 & 0 & 0 & 0 & \cdots & 0 & N & 0 \end{pmatrix}. \tag{31}$$

Similarly, we obtain

$$\mathscr{P}_K'{}'(\xi) = \mathscr{Q}_\xi \mathscr{T}''(\xi) = \mathscr{Q}_\xi \mathscr{D}'' \mathscr{Q}_\xi^{-1} \mathscr{P}_K(\xi), \tag{32}$$

where $\mathscr{D}'' = (d_{i,j})_{1\le i,j\le K+1}$.

$$(d_{i,j}) = \begin{cases} (i-1)(i-2), i \ge 3 & , j = i-2, \\ 0, & \text{otherwise.} \end{cases} \tag{33}$$

If we use (30), we get

$$\begin{aligned}\mathscr{V}(\xi,\eta)\mathscr{V}_\xi(\xi,\eta) &\approx \mathscr{V}_{KJ}(\xi,\eta)\mathscr{V}_{KJx}(\xi,\eta) \\ &= \mathscr{P}_K(\xi)^T \mathscr{W} \mathscr{P}_J(\eta) \mathscr{P}_K(\xi)^T \mathscr{Q}_\xi^{-T} \mathscr{D}'^T \mathscr{Q}_\xi^T \mathscr{W} \mathscr{P}_J(\eta).\end{aligned} \tag{34}$$

For integro–differential term, using (32), we have

$$\begin{aligned}\int_0^\eta (\eta-s)^{\beta-1} \mathscr{V}_{\xi\xi}(\xi,s)\mathrm{d}s &\approx \int_0^\eta (\eta-s)^{\beta-1} \mathscr{P}_K'{}'(\xi)^T \mathscr{W} \mathscr{P}_J(s)\mathrm{d}s \\ &= \int_0^\eta (\eta-s)^{\beta-1} \left(\mathscr{Q}_\xi \mathscr{D}'' \mathscr{Q}_\xi^{-1} \mathscr{P}_K(\xi)\right)^T \mathscr{W} \mathscr{P}_J(s)\mathrm{d}s,\end{aligned} \tag{35}$$

$$= \mathscr{P}_K(\xi)^T \mathscr{Q}_\xi^{-T} \mathscr{D}''^T \mathscr{Q}_\xi^T \mathscr{W} \int_0^\eta (\eta-s)^{\beta-1} \mathscr{Q}_\eta \mathscr{T}(s)\mathrm{d}s, \tag{36}$$

$$= \mathscr{P}_K(\xi)^T \mathscr{Q}_\xi^{-T} \mathscr{D}''^T \mathscr{Q}_\xi^T \mathscr{W} \mathscr{Q}_\eta \int_0^\eta \frac{\left[1, s, \cdots, s^J\right]^T}{(\eta-s)^{1-\beta}}\mathrm{d}s. \tag{37}$$

On the other hand, the following relationship is valid:

$$\int_0^\eta \frac{\xi^k}{(\eta-\xi)^{1-\beta}} d\xi = \frac{\Gamma(k+1)\Gamma(\beta)}{\Gamma(k+\beta+1)}\eta^{k+\beta}, 0 < \beta < 1, k = 0, 1, 2, \cdots. \tag{38}$$

So, by substituting (38) into (37), we have

$$\int_0^\eta (\eta-s)^{\beta-1} \mathscr{V}_{\xi\xi}(\xi,\eta)\mathrm{d}s \approx \mathscr{P}_K(\xi)^T \mathscr{Q}_\xi^{-T} \mathscr{D}''^T \mathscr{Q}_\xi^T \mathscr{W} \mathscr{Q}_\eta \left[\frac{\Gamma(\beta)}{\Gamma(\beta+1)}\eta^\beta, \frac{\Gamma(2)\Gamma(\beta)}{\Gamma(\beta+2)}\eta^{\beta+1}, \cdots, \frac{\Gamma(J+1)\Gamma(\beta)}{\Gamma(\beta+J+1)}\eta^{\beta+J}\right]^T, \tag{39}$$

$$= \mathscr{P}_K(\xi)^T \mathscr{Q}_\xi^{-T} \mathscr{D}''^T \mathscr{Q}_\xi^T \mathscr{W} \mathscr{Q}_\eta \begin{pmatrix} \frac{\Gamma(\beta)}{\Gamma(\beta+1)} & 0 & 0 & \cdots & 0 \\ 0 & \frac{\Gamma(2)\Gamma(\beta)}{\Gamma(\beta+2)} & 0 & \cdots & 0 \\ 0 & 0 & \frac{\Gamma(3)\Gamma(\beta)}{\Gamma(\beta+3)} & \cdots & 0 \\ \vdots & \vdots & \vdots & \vdots & \vdots \\ 0 & 0 & 0 & \cdots & \frac{\Gamma(J+1)\Gamma(\beta)}{\Gamma(\beta+J+1)} \end{pmatrix} \begin{pmatrix} \eta^\beta \\ \eta^{\beta+1} \\ \eta^{\beta+2} \\ \vdots \\ \eta^{\beta+J} \end{pmatrix}, \tag{40}$$

$$= \mathscr{P}_K(\xi)^T \mathscr{Q}_\xi^{-T} \mathscr{D}''^T \mathscr{Q}_\xi^T \mathscr{W} Q_\eta \mathscr{S}\mathscr{T}^\beta(\eta), \tag{41}$$

where

$$\mathcal{S} = \operatorname{diag}\left(\frac{\Gamma(\beta)}{\Gamma(\beta+1)}, \frac{\Gamma(2)\Gamma(\beta)}{\Gamma(\beta+2)}, \cdots, \frac{\Gamma(J+1)\Gamma(1-\beta)}{\Gamma(\beta+J+1)}\right), \tag{42}$$

$$\mathcal{T}^{\beta}(\eta) = \left[\eta^{\beta}, \eta^{\beta+1}, \cdots, \eta^{\beta+J}\right]. \tag{43}$$

Hence, using relations (28), (34), and (41), as a result, we get

$$\begin{cases} \mathcal{R}_1(\xi,\eta) = \mathcal{P}_K(\xi)^T \mathcal{W} \mathcal{Q}_\eta \mathcal{M}_\alpha \mathcal{Q}_\eta^{-1} \mathcal{P}_J(\eta) + \mathcal{P}_K(\xi)^T \mathcal{W} \mathcal{P}_J(\eta) \mathcal{P}_K(\xi)^T \mathcal{Q}_\xi^{-T} \mathcal{D}' T \mathcal{Q}_\xi^T \mathcal{W} \mathcal{P}_J(\eta) - \\ \mathcal{P}_K(\xi)^T \mathcal{Q}_\xi^{-T} \mathcal{D}'^T \mathcal{Q}_\xi^T \mathcal{W} \mathcal{Q}_\eta \mathcal{S} \mathcal{T}^{\beta}(\eta) - \mathcal{G}(\xi,\eta) \approx 0, \\ \mathcal{R}_2(\xi) = \mathcal{P}_K(\xi)^T \mathcal{W} \mathcal{P}_J(0) - \Psi(\xi) \approx 0, \\ \mathcal{R}_3(\eta) = \mathcal{P}_K(0)^T \mathcal{W} \mathcal{P}_J(\eta) - \Phi_1(\eta) \approx 0, \\ \mathcal{R}_4(\eta) = \mathcal{P}_K(L)^T \mathcal{W} \mathcal{P}_J(\eta) - \Phi_2(\eta) \approx 0. \end{cases} \tag{44}$$

Now, from relation (44), we create the nonlinear system below.

$$\begin{cases} \mathcal{R}_1\left(\xi_i, \eta_j\right) \approx 0 & 0 \le i \le K-2, 0 \le j \le J-1, \\ \mathcal{R}_2(\xi_i) \approx 0 & i = 0, 1, \cdots, K, \mathcal{R}_4\left(\eta_j\right) \approx 0 \\ \mathcal{R}_3\left(\eta_j\right) \approx 0 & j = 0, 1, \cdots, J-1, j = 0, 1, \cdots, J-1, \end{cases} \tag{45}$$

where $\xi_i = (2i+1)/2K+2$ and $\eta_j = (2j+1)/2J+2$.

By solving this system, the unknown matrix $\mathcal{W}$ can be determined. It is worth noting that we have used the fsolve command in Matlab.

4. Convergence

Here, we prove that the numerical scheme for solving (1)–(3) is convergent, and we follow references [43, 44]. We assume that

$$G = \operatorname{span}\{\mathcal{P}_1(\xi), \mathcal{P}_2(\xi), \cdots, \mathcal{P}_{K+1}(\xi)\}, \tag{46}$$

$$Q = \operatorname{span}\left\{\mathcal{P}_1(\eta), \mathcal{P}_2(\eta), \cdots, \mathcal{P}_{J+1}(\eta)\right\}, \tag{47}$$

$$G_x = \operatorname{span}\left\{\mathcal{P}_1'(\xi), \mathcal{P}_2'(\xi), \cdots, \mathcal{P}_{K+1}'(\xi)\right\}, \tag{48}$$

$$G_{xx} = \operatorname{span}\left\{\mathcal{P}_1''(\xi), \mathcal{P}_2''(\xi), \cdots, \mathcal{P}_{K+1}''(\xi)\right\}. \tag{49}$$

$$\left\|\mathcal{V}(\xi,\eta) - \mathcal{V}_{KJ}(\xi,\eta)\right\|_2 \le \frac{H_1 LT(L+T)^{K+J+1}}{(K+J+1)!}, \tag{50}$$

$$\left\|\mathcal{V}_\xi(\xi,\eta) - \mathcal{V}_{KJ\xi}(\xi,\eta)\right\|_2 \le \frac{H_2 LT(L+T)^{K+J+1}}{(K+J+1)!}, \tag{51}$$

$$\left\|\mathcal{V}_{\xi\xi}(\xi,\eta) - \mathcal{V}_{KJ\xi\xi}(\xi,\eta)\right\|_2 \le \frac{H_3 LT(L+T)^{K+J+1}}{(K+J+1)!}, \tag{52}$$

Theorem 4. *Let $\mathcal{V}(\xi,\eta) \in C^{K+J+3}([0,L]\times[0,T])$ and $\mathcal{V}_{KJ}(\xi,\eta)$, $\mathcal{V}_{KJ\xi}(\xi,\eta)$, and $\mathcal{V}_{KJ\xi\xi}(\xi,\eta)$ be the best approximations of $\mathcal{V}(\xi,\eta)$, $\mathcal{V}_\xi(\xi,\eta)$, and $\mathcal{V}_{\xi\xi}(\xi,\eta)$ in the spaces $G\times Q$, $G_\xi \times Q$, and $G_{\xi\xi}\times Q$, respectively. The following inequalities are true.*

where $H_i = \max_{k=0,\cdots,J+K+i}|\mathcal{V}^k(\xi,\eta)|$.

$$\begin{aligned} \mathcal{V}(\xi,\eta) &= \mathcal{V}(0,0) + \mathcal{V}_\xi(0,0)\xi + \mathcal{V}_\eta(0,0)\eta + \frac{1}{2!} \\ &\quad \cdot \left(\mathcal{V}_{\xi\xi}(0,0)\xi^2 + 2\mathcal{V}_{\xi\eta}(0,0)\xi\eta + \mathcal{V}_{\eta\eta}(0,0)\eta^2\right) + \cdots, \end{aligned} \tag{53}$$

$$\begin{aligned} &+ \frac{1}{n!}\sum_{i+j=J+K}\binom{n}{j}\mathcal{V}_{\xi^i\eta^j}(0,0)\xi^i\eta^j + R_{J+K,(0,0)}(\xi,\eta) \\ &= P_{J+K,(0,0)}(\xi,\eta) + R_{J+K,(0,0)}(\xi,\eta), \end{aligned} \tag{54}$$

where

$$\begin{aligned} R_{J+K,(0,0)}(\xi,\eta) &= \frac{1}{(J+K)!}\sum_{i+j=J+K+1}\binom{J+K+1}{j}\xi^i\eta^j \\ &\quad \cdot \int_0^1 \mathcal{V}_{\xi^i\eta^j}(m\xi, m\eta)(1-m)^{J+K}dm. \end{aligned} \tag{55}$$

Proof. Using Taylor expansion, we have [45]. □

According to the best approximation theorem

$$\left\|\mathscr{V}(\xi,\eta)-\mathscr{V}_{JK}(\xi,\eta)\right\|_2 \le \left\|\mathscr{V}(\xi,\eta)-P_{J+K,(0,0)}(\xi,\eta)\right\|_2, \tag{56}$$

$$= \left\|\frac{1}{(J+K)!}\sum_{i+j=J+K+1}\binom{J+K+1}{j}\xi^i\eta^j\int_0^1\mathscr{V}_{\xi^i\eta^j}(m\xi,m\eta)(1-m)^{K+K}dm\right\|_2, \tag{57}$$

$$\begin{aligned}
&= \left(\int_0^T\int_0^L\left(\frac{1}{(J+K)!}\sum_{i+j=J+K+1}\binom{J+K+1}{j}\xi^i\eta^j\right.\right.\\
&\quad\left.\left.\cdot\int_0^1\mathscr{V}_{\xi^i\eta^j}(m\xi,m\eta)(1-m)^{J+K}dm\right)^2 d\xi d\eta\right)^{1/2}\\
&\le \left(\int_0^T\int_0^L\left(\frac{H_1}{(J+K+1)!}\sum_{i+j=J+K+1}\binom{J+K+1}{j}\xi^i\eta^j\right)^2 d\xi d\eta\right)^{1/2}\\
&= \frac{H_1}{(J+K+1)!}\left(\int_0^T\int_0^L(\xi+\eta)^{2K+2J+2}d\xi d\eta\right)^{1/2}\\
&\le \frac{H_1LT(L+T)^{J+K+1}}{(J+K+1)!}.
\end{aligned} \tag{58}$$

Similarly, other inequalities can also be proved.

Theorem 5. *Let $\mathscr{V}_{KJ}(\xi,\eta)$ is the exact solution and $\tilde{\mathscr{V}}_{KJ}(\xi,\eta)=\tilde{\mathscr{V}}^T P_{KJ}(\xi,\eta)$ is the approximation solution of equations (45). Then, one has*

$$\left\|\mathscr{V}_{NM}(\xi,\eta)-\tilde{\mathscr{V}}_{NM}(\xi,\eta)\right\|_2 \le \left\|\mathscr{V}-\tilde{\mathscr{V}}\right\|_2 \cdot\sqrt{LT\sum_{r=0}^{K}\sum_{s=0}^{J}\left(\sum_{k=0}^{\lfloor\frac{r}{2}\rfloor}\binom{r-k}{k}(2L)^{r-2k}\right)^2\left(\sum_{k=0}^{\lfloor\frac{s}{2}\rfloor}\binom{s-k}{k}(2T)^{s-2k}\right)^2}. \tag{59}$$

Proof. We have

$$\begin{aligned}
&\left\|\mathscr{V}_{KJ}(\xi,\eta)-\tilde{\mathscr{V}}_{KJ}(\xi,\eta)\right\|_2^2\\
&= \int_0^T\int_0^L\left|\mathscr{V}_{KJ}(\xi,\eta)-\tilde{\mathscr{V}}_{KJ}(\xi,\eta)\right|^2 d\xi d\eta = \int_0^T\int_0^L\\
&= \left|\sum_{r=0}^{K}\sum_{s=0}^{J}\left(\bar{v}_{r+1,s+1}-\tilde{\bar{v}}_{r+1,s+1}\right)\mathscr{P}_{r+1}(\xi)\mathscr{P}_{s+1}(\eta)\right|^2 d\xi d\eta,
\end{aligned} \tag{60}$$

$$\begin{aligned}
&\le \int_0^T\int_0^L\left(\sum_{r=0}^{K}\sum_{s=0}^{J}\left|\bar{v}_{r+1,s+1}-\tilde{\bar{v}}_{r+1,s+1}\right|^2\right)\\
&\quad\cdot\left(\sum_{r=0}^{K}\sum_{s=0}^{J}\left|\mathscr{P}_{r+1}(\xi)\mathscr{P}_{s+1}(\eta)\right|^2\right)d\xi d\eta,
\end{aligned} \tag{61}$$

$$\begin{aligned}
&= \sum_{r=0}^{K}\sum_{s=0}^{J}\left|\bar{v}_{r+1,s+1}-\tilde{\bar{v}}_{r+1,s+1}\right|^2\sum_{r=0}^{K}\sum_{s=0}^{J}\int_0^T\int_0^L\\
&\quad\cdot\left|\mathscr{P}_{r+1}(\xi)\mathscr{P}_{s+1}(\eta)\right|^2 d\xi d\eta,
\end{aligned} \tag{62}$$

$$\begin{aligned}
&= \left\|\mathscr{V}-\tilde{\mathscr{V}}\right\|_2^2\sum_{r=0}^{K}\sum_{s=0}^{J}\int_0^T\int_0^L\left|\sum_{k=0}^{\lfloor\frac{r}{2}\rfloor}\binom{r-k}{k}2^{r-2k}\xi^{r-2k}\right|^2\\
&\quad\cdot\left|\sum_{k=0}^{\lfloor\frac{s}{2}\rfloor}\binom{s-k}{k}2^{s-2k}\eta^{s-2k}\right|^2 d\xi d\eta\\
&\le \left\|\mathscr{V}-\tilde{\mathscr{V}}\right\|_2^2\sum_{r=0}^{K}\sum_{s=0}^{J}\int_0^T\int_0^L\left|\sum_{k=0}^{\lfloor\frac{r}{2}\rfloor}\binom{r-k}{k}2^{r-2k}L^{r-2k}\right|^2\\
&\quad\cdot\left|\sum_{k=0}^{\lfloor\frac{s}{2}\rfloor}\binom{s-k}{k}2^{d-2k}T^{s-2k}\right|^2 d\xi d\eta\\
&= \left\|\mathscr{V}-\tilde{\mathscr{V}}\right\|_2^2 LT\sum_{r=0}^{K}\sum_{s=0}^{J}\left|\sum_{k=0}^{\lfloor\frac{r}{2}\rfloor}\binom{r-k}{k}2^{r-2k}L^{r-2k}\right|^2\\
&\quad\cdot\left|\sum_{k=0}^{\lfloor\frac{s}{2}\rfloor}\binom{s-k}{k}2^{s-2k}T^{s-2k}\right|^2.
\end{aligned} \tag{63}$$

So that

$$\left\|\mathscr{V}_{KJ}(\xi,\eta)-\tilde{\mathscr{V}}_{KJ}(\xi,\eta)\right\|_2 \le \left\|\mathscr{V}-\tilde{\mathscr{V}}\right\|_2 \cdot\sqrt{LT\sum_{r=0}^{K}\sum_{s=0}^{J}\left(\sum_{k=0}^{\lfloor\frac{r}{2}\rfloor}\binom{r-k}{k}(2L)^{r-2k}\right)^2\left(\sum_{k=0}^{\lfloor\frac{s}{2}\rfloor}\binom{s-k}{k}(2T)^{s-2k}\right)^2}. \tag{64}$$

Now, we prove that the presented numerical method is convergent. □

Theorem 6. *Let $S_{KJ}(\xi,\eta)$ be the perturbation term and $\mathscr{V}_{KJ}(\xi,\eta)$ be the approximate solution to the main problem derived using the proposed approach. Then, the perturbation term tends to zero as $K, J \longrightarrow \infty$.*

Proof. Thanks to (9), we deduce that

$$\begin{aligned}
\mathscr{V}(\xi,\eta) &= \Psi(\xi)\,{}_0^{RL}\mathscr{I}_\eta^\alpha\mathscr{V}(\xi,\eta)\mathscr{V}_\xi(\xi,\eta)\\
&\quad+{}_0^{RL}\mathscr{I}_\eta^\alpha\int_0^\eta(\eta-s)^{\beta-1}\mathscr{V}_{\xi\xi}(\xi,s)ds+{}_0^{RL}\mathscr{I}_\eta^\alpha\mathscr{G}(\xi,\eta).
\end{aligned} \tag{65}$$

□

Assume that $\mathscr{V}_{NM}(\xi,\eta)$ is an approximate solution of the above equation. It means that

Table 1: Numerical reports in Example 1.

(ξ_i, η_i)	$\alpha = 0.5$, K = 11	$\alpha = 0.5$, $K = 11$	$\alpha = 0.5$, $K = 9$	$\alpha = 0.5$, $K = 9$
	$\beta = 0.1$, $J = 4$	$\beta = 0.3$, $J = 4$	$\beta = 0.7$, $J = 4$	$\beta = 0.9$, $J = 4$
(0.1,0.1)	$5.2665e-11$	$7.5026e-11$	$9.4157e-10$	$1.5935e-09$
(0.2,0.2)	$8.8713e-10$	$7.0142e-10$	$1.7084e-09$	$4.5505e-09$
(0.3,0.3)	$4.6062e-09$	$3.6713e-09$	$5.8173e-08$	$1.3764e-09$
(0.4,0.4)	$1.4766e-08$	$1.2353e-08$	$3.6620e-07$	$1.2902e-07$
(0.5,0.5)	$3.6426e-08$	$3.1853e-08$	$1.2736e-06$	$6.7104e-07$
(0.6,0.6)	$7.6243e-08$	$6.9345e-08$	$3.4065e-06$	$2.2596e-06$
(0.7,0.7)	$1.4258e-07$	$1.3432e-07$	$7.7630e-06$	$6.0393e-06$
(0.8,0.8)	$2.4555e-07$	$2.3833e-07$	$1.5689e-05$	$1.3673e-05$
(0.9,0.9)	$3.8165e-07$	$3.7801e-07$	$2.5814e-05$	$2.4145e-05$
(1, 1)	$7.3344e-15$	$1.1944e-16$	$1.6793e-15$	$2.1690e-14$

$$\begin{aligned}\mathscr{V}_{KJ}(\xi,\eta) = \Psi(\xi) &- {}_0^{RL}\mathscr{I}_\eta^\alpha \mathscr{V}_{KJ}(\xi,\eta)\mathscr{V}_{KJ\xi}(\xi,\eta)\\ &+ {}_0^{RL}\mathscr{I}_\eta^\alpha \int_0^\eta (\eta-s)^{\beta-1}\mathscr{V}_{KJ\xi\xi}(\xi,s)ds\\ &+ {}_0^{RL}\mathscr{I}_\eta^\alpha \mathscr{G}(\xi,\eta) + S_{KJ}(\xi,\eta),\end{aligned} \tag{66}$$

where S_{KJ} is the perturbation term. From equations (65) and (66), we have

$$\begin{aligned}\mathscr{E}_{KJ}(\xi,\eta) &= -{}_0^{RL}\mathscr{I}_\eta^\alpha\left(\mathscr{V}(\xi,\eta)\mathscr{V}_x(\xi,\eta) - \mathscr{V}_{KJ}(\xi,\eta)\mathscr{V}_{KJ\xi}(\xi,\eta)\right) + {}_0^{RL}\mathscr{I}_\eta^\alpha\int_0^\eta(\eta-s)^{\beta-1}\left(\mathscr{V}_{\xi\xi}(\xi,\eta) - \mathscr{V}_{KJ\xi\xi}(\xi,s)\right)ds - S_{KJ}(\xi,\eta)\\ &= -{}_0^{RL}\mathscr{I}_\eta^\alpha\left(\mathscr{V}_{KJ}(\xi,\eta)\left(\mathscr{V}_\xi(\xi,\eta) - \mathscr{V}_{KJ\xi}(\xi,\eta)\right) + \mathscr{V}_\xi(\xi,\eta)\left(\mathscr{V}(\xi,\eta) - \mathscr{V}_{KJ}(\xi,\eta)\right)\right) + {}_0^{RL}\mathscr{I}_\eta^\alpha\int_0^\eta(\eta-s)^{\beta-1}\left(\mathscr{V}_{\xi\xi}(\xi,\eta) - \mathscr{V}_{KJ\xi\xi}(\xi,s)\right)ds - S_{KJ}(\xi,\eta)\\ &= -{}_0^{RL}\mathscr{I}_\eta^\alpha\left(\mathscr{V}_{KJ}(\xi,\eta)\mathscr{E}_{KJ\xi}(\xi,\eta) + \mathscr{V}_\xi(\xi,\eta)\mathscr{E}_{KJ}(\xi,\eta)\right) + {}_0^{RL}\mathscr{I}_\eta^\alpha\int_0^\eta(\eta-s)^{\beta-1}\mathscr{E}_{KJ\xi\xi}(\xi,\eta)ds - S_{KJ}(\xi,\eta)\\ &= -{}_0^{RL}\mathscr{I}_\eta^\alpha\left(\mathscr{V}_{KJ}(\xi,\eta)\mathscr{E}_{KJ\xi}(\xi,\eta) + \left(\mathscr{V}_\xi(\xi,\eta) - \mathscr{V}_{KJ\xi}(\xi,\eta) + \mathscr{V}_{KJ\xi}(\eta,\eta)\right)\mathscr{E}_{KJ}(\xi,\eta)\right) + {}_0^{RL}\mathscr{I}_\eta^\alpha\int_0^\eta(\eta-s)^{\beta-1}\mathscr{E}_{KJ\xi\xi}(\xi,\eta)ds - S_{KJ}(\xi,\eta)\\ &= -{}_0^{RL}\mathscr{I}_\eta^\alpha\left(\mathscr{V}_{KJ}(\xi,\eta)\mathscr{E}_{KJ\xi}(\xi,\eta) + \mathscr{V}_{KJ\xi}(\xi,\eta)\mathscr{E}_{KJ}(\xi,\eta) + \mathscr{E}_{KJ\xi}(\xi,\eta)\mathscr{E}_{KJ}(\xi,\eta)\right) + {}_0^{RL}\mathscr{I}_\eta^\alpha\int_0^\eta(\eta-s)^{\beta-1}\mathscr{E}_{KJ\xi\xi}(\xi,\eta)ds - S_{KJ}(\xi,\eta),\end{aligned} \tag{67}$$

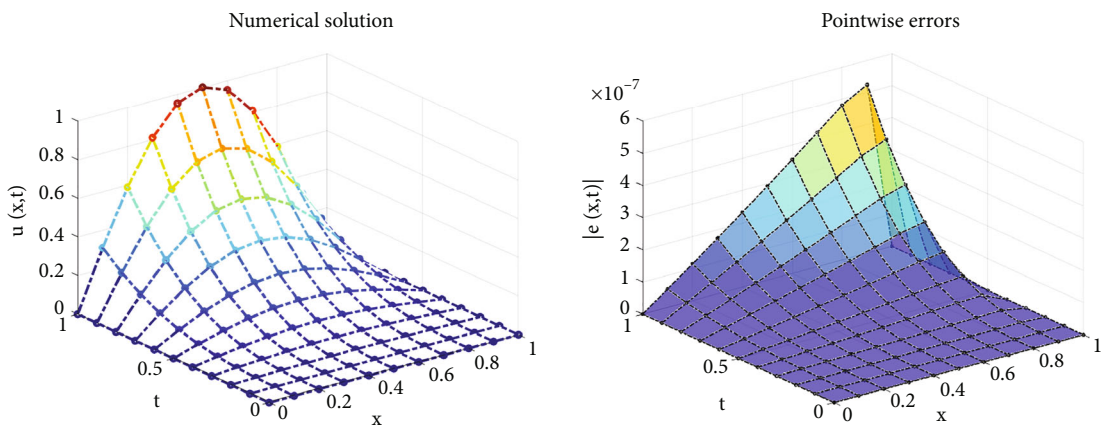

Figure 1: Pictorial results in Example 1 with $\alpha = 0.5$, $\beta = 0.1$, and $N = 11$, $M = 4$.

Table 2: Norm of errors for $\alpha = \beta = 0.5$ and CPU time in Example 1.

	$J = 4, K = 6$	$J = 4, K = 7$	$J = 4, K = 8$	$J = 4, K = 9$	$J = 4, K = 10$
	$\|e\|_\infty$	$\|e\|_\infty$	$\|e\|_\infty$	$\|e\|_\infty$	$\|e\|_\infty$
	$1.7427e-03$	$1.7093e-03$	$3.7497e-05$	$3.7046e-05$	$5.5452e-07$
CPU	0.7787s	1.3037s	1.4066s	1.5607s	1.9541s

Table 3: Numerical results in Example 2.

(ξ_i, η_i)	$\alpha = 0.5$	$\alpha = 0.7$	$\alpha = 0.9$	$\alpha = 1$
	$\beta = 0.5$	$\beta = 0.5$	$\beta = 0.5$	$\beta = 0.5$
(0, 0)	$1.3878e-17$	$1.3878e-17$	$1.3878e-17$	$6.9389e-17$
(0.1,0.1)	$2.9677e-15$	$2.4715e-15$	$2.1732e-15$	$2.4820e-15$
(0.2,0.2)	$1.3601e-14$	$1.0819e-14$	$8.4386e-15$	$8.1749e-15$
(0.3,0.3)	$4.2369e-14$	$3.3196e-14$	$2.4869e-14$	$2.1178e-14$
(0.4,0.4)	$1.0748e-13$	$8.5140e-14$	$6.4282e-14$	$5.2874e-14$
(0.5,0.5)	$2.2699e-13$	$1.8235e-13$	$1.4061e-13$	$1.1730e-13$
(0.6,0.6)	$4.0491e-13$	$3.2892e-13$	$2.5840e-13$	$2.2102e-13$
(0.7,0.7)	$6.1083e-13$	$5.0086e-13$	$3.9917e-13$	$3.4946e-13$
(0.8,0.8)	$7.5499e-13$	$6.2282e-13$	$5.0181e-13$	$4.4802e-13$
(0.9,0.9)	$6.5503e-13$	$5.4298e-13$	$4.4097e-13$	$4.0014e-13$
(1, 1)	$7.5493e-16$	$3.3867e-16$	$1.0991e-15$	$1.0437e-15$

Table 4: Norm of errors for $\alpha = \beta = 0.5$ and CPU time in Example 2.

	$J = 3, K = 3$	$J = 3, K = 4$	$J = 3, K = 5$	$J = 3, K = 6$	$J = 3, K = 7$
	$\|e\|_\infty$	$\|e\|_\infty$	$\|e\|_\infty$	$\|e\|_\infty$	$\|e\|_\infty$
	$1.9604e-12$	$4.9638e-12$	$8.0466e-11$	$1.3686e-13$	$1.4568e-12$
CPU	0.7492s	0.9354s	1.1262s	1.2330s	1.2589s

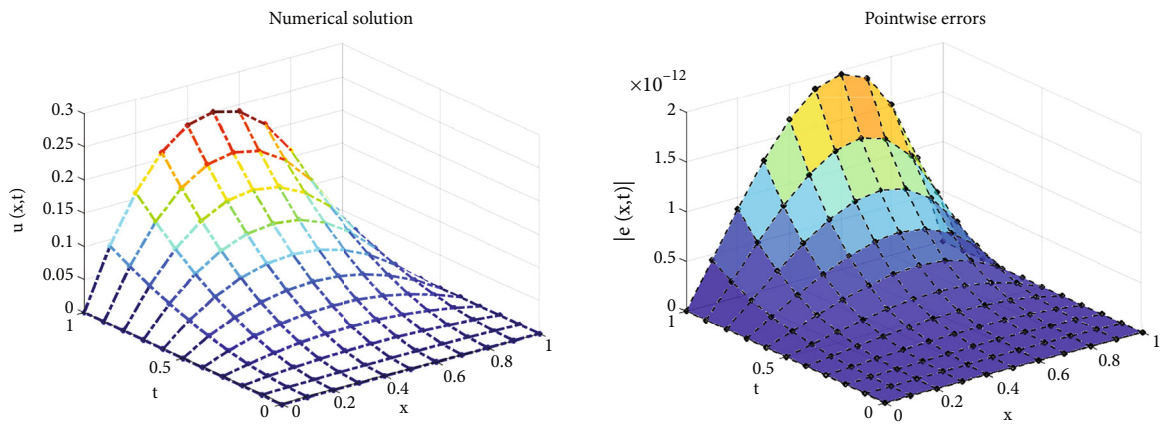

FIGURE 2: Pictorial results in Example 2 for $\alpha = 0.5$, $\beta = 0.5$ and $N = M = 3$.

where $\mathscr{E}_{KJ}(\xi,\eta) = \mathscr{V}(\xi,\eta) - \mathscr{V}_{KJ}(\xi,\eta)$. So that

$$\begin{aligned}\|S_{KJ}(\xi,\eta)\|_2 &\le \left\| {}_{0}^{RL}\mathscr{I}_{\eta}^{\alpha}\mathscr{V}_{KJ}(\xi,\eta)\mathscr{E}_{KJ\xi}(\xi,\eta) + \mathscr{V}_{KJ\xi}(\xi,\eta)\mathscr{E}_{NM}(\xi,\eta) \right.\\ &\quad \left. + \mathscr{E}_{KJ\xi}(\xi,\eta)\mathscr{E}_{NM}(\xi,\eta)\right\|_2 + \|\mathscr{E}_{KJ}(\xi,\eta)\|_2\\ &\quad + \left\| {}_{0}^{RL}\mathscr{I}_{\eta}^{\alpha}\int_0^{\eta}(\eta-s)^{\beta-1}\mathscr{E}_{NM\xi\xi}(\xi,\eta)ds\right\|_2\\ &= \|I_1\|_2 + \|\mathscr{E}_{NM}(\xi,\eta)\|_2 + \|I_2\|.\end{aligned} \tag{68}$$

Now, we compute $\|I_1\|_2$ and $\|I_2\|_2$.

$$\begin{aligned}\|I_2\|_2^2 &= \frac{1}{\Gamma(\alpha)^2}\int_0^T\int_0^L\left|\int_0^{\eta}\int_0^{\tau}(\eta-\tau)^{\alpha-1}(\tau-s)^{\beta-1}\mathscr{E}_{KJ\xi\xi}(\xi,s)dsd\tau\right|^2 d\xi d\eta\\ &\le \frac{1}{\Gamma(\alpha)^2}\int_0^T\int_0^L\left(\int_0^{\eta}\int_0^{\tau}(\eta-\tau)^{\alpha-1}(\tau-s)^{\beta-1}\left|e_{KJ\xi\xi}(\xi,s)\right|dsd\tau\right)^2 d\xi d\eta\\ &\le \frac{1}{\Gamma(\alpha)^2}\int_0^T\int_0^L\left(\int_0^{\eta}\int_0^{\tau}(\eta-\tau)^{2\alpha-2}(\tau-s)^{2\beta-2}dsd\tau\right)\\ &\quad\cdot\left(\int_0^{\eta}\int_0^{\tau}\left|\mathscr{E}_{KJ\xi\xi}(\xi,s)\right|^2dsd\tau\right)d\xi d\eta \le \frac{T}{\Gamma(\alpha)^2}\int_0^T\int_0^L\\ &\quad\cdot\left(\int_0^{\eta}\int_0^{\tau}(\eta-\tau)^{2\alpha-2}(\tau-s)^{2\beta-2}dsd\tau\right)\int_0^T\left|\mathscr{E}_{KJ}(\xi,\eta)\right|^2dsd\xi d\eta\\ &\le \frac{T}{\Gamma(\alpha)^2}\int_0^T\int_0^L\left(T^{2\beta-1}\times t^{2\alpha-1}\right)\int_0^T\left|\mathscr{E}_{KJ}(\xi,\eta)\right|^2dsd\xi d\eta\\ &= \frac{T^{2\beta}}{\Gamma(\alpha)^2}\left(\int_0^T\eta^{2\alpha-1}d\eta\right)\left(\int_0^T\int_0^L\left|\mathscr{E}_{KJ\xi\xi}(\xi,s)\right|^2d\xi ds\right)\\ &= \frac{T^{2\beta+2\alpha}}{\Gamma(\alpha)^2(2\alpha)}\left\|\mathscr{E}_{KJ\xi\xi}(\xi,\eta)\right\|_2^2.\end{aligned} \tag{69}$$

Similarly

$$\|I_1\|_2^2 \le \frac{T^{2\alpha}}{\Gamma(\alpha)^2(2\alpha)}\left\|\mathscr{V}_{KJ}(\xi,\eta)\mathscr{E}_{KJ\xi}(\xi,\eta) + \mathscr{V}_{KJ\xi}(\xi,\eta)\mathscr{E}_{KJ}(\xi,\eta) + \mathscr{E}_{KJ\xi}(\eta,\eta)\mathscr{E}_{KJ}(\xi,\eta)\right\|_2^2. \tag{70}$$

Therefore, we conclude

$$\begin{aligned}\|S_{KJ}(\xi,\eta)\|_2 &\le \sqrt{\frac{T^{2\alpha}}{\Gamma(\alpha)^2(2\alpha)}}\|\mathscr{V}_{KJ}(\xi,\eta)\mathscr{E}_{KJ\xi}(\xi,\eta)\\ &\quad + \mathscr{V}_{KJ\xi}(\xi,\eta)\mathscr{E}_{KJ}(\xi,\eta) + \mathscr{E}_{KJ\xi}(\xi,\eta)\mathscr{E}_{KJ}(\xi,\eta)\|_2\\ &\quad + \|\mathscr{E}_{KJ}(\xi,\eta)\|_2 + \sqrt{\frac{T^{2\beta+2\alpha}}{\Gamma(\alpha)^2(2\alpha)}}\|\mathscr{E}_{KJ\xi\xi}(\xi,\eta)\|_2\\ &\le C_1\|\mathscr{V}_{KJ}(\xi,\eta)\|_2\|\mathscr{E}_{KJ\xi}(\xi,\eta)\|_2\\ &\quad + C_1\|\mathscr{V}_{KJ\xi}(\xi,\eta)\|_2\|\mathscr{E}_{KJ}(\xi,\eta)\|_2\\ &\quad + C_1\|\mathscr{E}_{KJ\xi}(\xi,\eta)\|_2\|\mathscr{E}_{KJ}(\xi,\eta)\|_2 + \|\mathscr{E}_{KJ}(\xi,\eta)\|_2\\ &\quad + C_2\|\mathscr{E}_{KJ\xi\xi}(\xi,\eta)\|_2 \le \frac{C_1H_2LT(L+T)^{n+1}}{(n+1)!}\|\mathscr{V}_{KJ}(\xi,\eta)\|_2\\ &\quad + \frac{C_1H_1LT(L+T)^{n+1}}{(n+1)!}\|\mathscr{V}_{KJx}(\xi,\eta)\|_2\\ &\quad + \frac{C_1H_1H_2L^2T^2(L+T)^{2n+2}}{(n+1)^2} + \frac{H_1LT(L+T)^{n+1}}{(n+1)}\\ &\quad + \frac{C_2H_3LT(L+T)^{n+1}}{(n+1)},\end{aligned} \tag{71}$$

where $n = K + J$. Now $S_{KJ}(\xi,\eta) \longrightarrow 0$ as $K, J \longrightarrow \infty$.

Finally, we provide a theorem about the convergence of the series of Pell polynomials. We follow Atta et al. [38, 40], Abd-Elhameed and Youssri [43, 44], and Youssri [46]. According to [47, 48], a square-integrable function $\mathscr{V}(\xi)$ on $[0, 1]$ has the following Pell expansion

$$\mathscr{V}(\xi) = \sum_{m=0}^{\infty}\bar{v}_{m+1}\mathscr{P}_{m+1}(\xi), \tag{72}$$

where

$$\bar{v}_m = m\sum_{s=0}^{\infty}\frac{(-1)^s b_{2s+m-1}}{2^{2s+m-1}(s+m)}\binom{2s+m-1}{s}, b_s = \frac{\mathscr{V}^s(0)}{s!}. \tag{73}$$

Lemma 7 (see [46]). *Let $I_u(z)$ denote the modified Bessel function of order u of the first kind. The following identity*

Table 5: Numerical results in Example 3.

(ξ_i, η_i)	$\alpha = 0.1$	$\alpha = 0.4$	$\alpha = 0.6$	$\alpha = 0.8$
	$\beta = 0.1$	$\beta = 0.4$	$\beta = 0.6$	$\beta = 0.8$
(0, 0)	$4.7184e-14$	$3.4972e-15$	$5.5511e-15$	$3.9191e-14$
(0.1,0.1)	$3.0197e-14$	$1.8513e-17$	$9.9751e-13$	$5.3904e-14$
(0.2,0.2)	$9.1656e-14$	$1.8249e-15$	$3.8079e-12$	$1.1759e-12$
(0.3,0.3)	$1.9482e-13$	$2.8203e-15$	$8.9047e-12$	$3.4628e-12$
(0.4,0.4)	$4.2674e-13$	$7.0777e-15$	$1.8213e-11$	$6.6157e-12$
(0.5,0.5)	$9.4080e-13$	$1.0436e-14$	$3.9364e-11$	$1.0878e-11$
(0.6,0.6)	$1.9982e-12$	$3.2196e-14$	$8.7362e-11$	$1.6063e-11$
(0.7,0.7)	$3.9228e-12$	$4.3965e-14$	$1.7459e-10$	$1.9690e-11$
(0.8,0.8)	$6.4684e-12$	$8.2379e-14$	$2.8359e-10$	$1.6850e-10$
(0.9,0.9)	$7.9272e-12$	$6.1506e-14$	$3.2058e-10$	$5.0651e-12$
(1, 1)	$5.7618e-12$	$8.9421e-14$	$5.1744e-11$	$3.9714e-12$

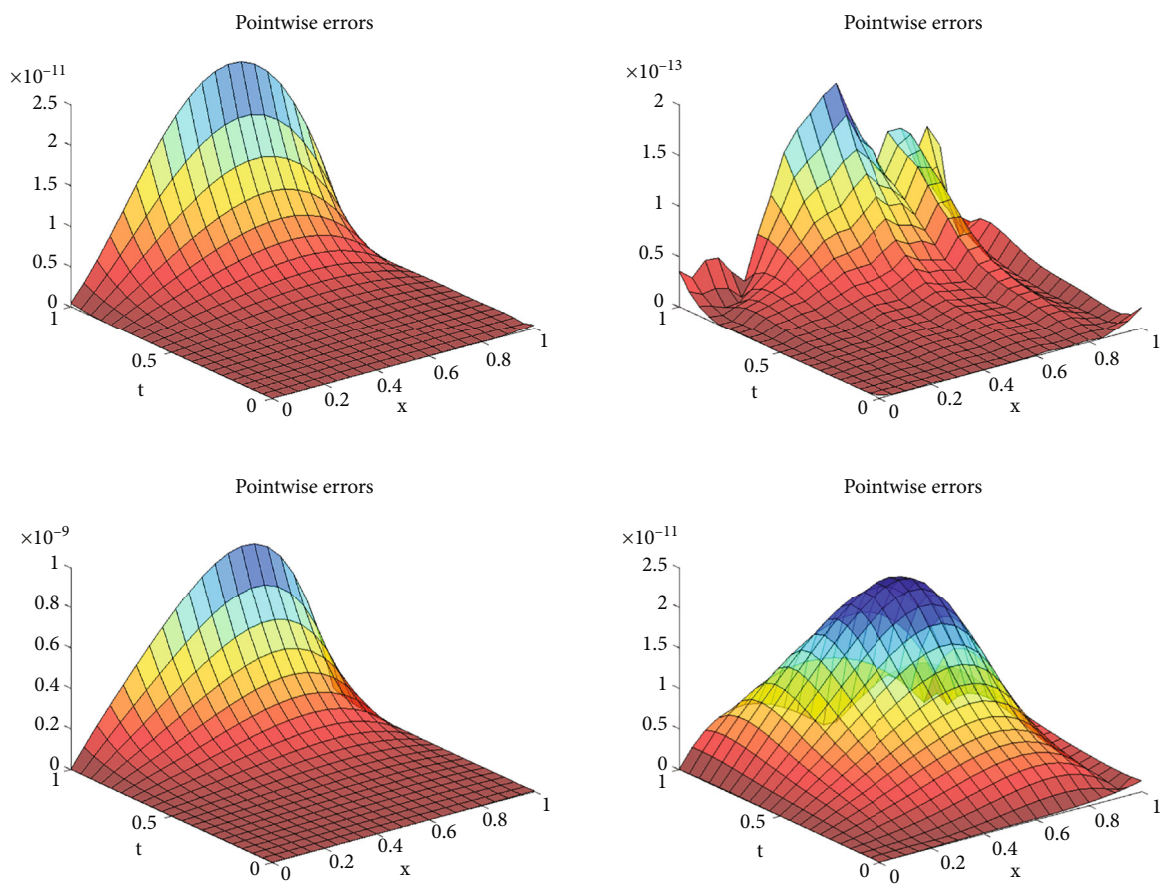

Figure 3: Pictorial results in Example 3 for $J = 4, K = 5$: (a) $(\alpha = 0.1, \beta = 0.1)$, (b) $(\alpha = 0.4, \beta = 0.4)$, (c) $(\alpha = 0.6, \beta = 0.6)$, and (d) $(\alpha = 0.8, \beta = 0.8)$.

holds:

$$\sum_{s=0}^{\infty} \frac{z^s}{s!(s+m+1)!} = t^{-m+1/2} I_{m+1}\left(2\sqrt{z}\right). \tag{74}$$

Lemma 8 (see [46]). *The modified Bessel function of the first kind $I_u z$ satisfies the following inequality:*

$$|I_u(z)| \leq \frac{z^u \cos h(z)}{2^u \Gamma(u+1)}. \tag{75}$$

Table 6: Norm of errors for $\alpha = \beta = 0.5$ and CPU time in Example 3.

	$J = 5, K = 4$	$J = 5, K = 5$	$J = 5, K = 6$	$J = 5, K = 7$	$J = 5, K = 8$
	$\|e\|_\infty$	$\|e\|_\infty$	$\|e\|_\infty$	$\|e\|_\infty$	$\|e\|_\infty$
	$1.7474e-13$	$4.6830e-10$	$5.1812e-10$	$2.2715e-09$	$3.7225e-08$
CPU	0.6941s	1.4075s	1.4990s	1.7516s	2.1537s

Table 7: Numerical reports in Example 4.

(ξ_i, η_i)	$J = 4$	$J = 4$	$J = 4$	$J = 4$
	$K = 6$	$K = 7$	$K = 8$	$K = 9$
$(0, 0)$	$3.9549e-20$	$1.9230e-22$	$6.7320e-20$	$1.1194e-18$
(0.1,0.1)	$1.0519e-10$	$5.3038e-12$	$4.6608e-13$	$2.8112e-12$
(0.2,0.2)	$2.7128e-09$	$1.4373e-10$	$7.5190e-12$	$8.1029e-12$
(0.3,0.3)	$2.6072e-08$	$1.4112e-09$	$6.8470e-11$	$1.6060e-11$
(0.4,0.4)	$1.0383e-07$	$5.6159e-09$	$2.7027e-10$	$3.5035e-11$
(0.5,0.5)	$2.8045e-07$	$1.5208e-08$	$7.3186e-10$	$8.5052e-11$
(0.6,0.6)	$6.1575e-07$	$3.3347e-08$	$1.6119e-09$	$1.9935e-10$
(0.7,0.7)	$1.2047e-06$	$6.5140e-08$	$3.1553e-09$	$4.1556e-10$
(0.8,0.8)	$2.1149e-06$	$1.1777e-07$	$5.7928e-09$	$7.3660e-10$
(0.9,0.9)	$2.8168e-06$	$1.7066e-07$	$8.9641e-09$	$9.7501e-10$
$(1, 1)$	$1.3234e-14$	$2.6645e-15$	$1.0658e-14$	$3.5527e-15$

Table 8: Norm of errors for $\alpha = \beta = 0.5$ and CPU time in Example 4.

	$J = 4, K = 5$	$J = 4, K = 6$	$J = 4, K = 7$	$J = 4, K = 8$	$J = 4, K = 9$
	$\|e\|_\infty$	$\|e\|_\infty$	$\|e\|_\infty$	$\|e\|_\infty$	$\|e\|_\infty$
	$5.4599e-05$	$3.6853e-06$	$2.2397e-07$	$1.1841e-08$	$1.2327e-09$
CPU	0.6648s	1.3185s	1.2689s	1.3789s	1.5100s

Table 9: Norm of errors for $\alpha = 0.5, \beta = 0.5$ in Example 4.

J	K	$\|e\|_2$
4	5	$3.0728e-05$
4	6	$2.0621e-06$
4	7	$1.1742e-07$
4	8	$6.0069e-09$
4	9	$7.7425e-10$

Theorem 9. *Suppose $\mathscr{V}(x) \in L^2[0, 1]$, $\mathscr{V}^{(i)}(0) \le L^i, i \ge 0$, where L is a positive constant and $\mathscr{V}(x) = \sum_{m=0}^{\infty} \bar{v}_{m+1} \mathscr{P}_{m+1}(x)$. Then*

$$|\bar{v}_{m+1}| \le \frac{L^m \cos hL}{2^m m!}, \tag{76}$$

and the approximate solution series converges absolutely. Also, if $E_K(\xi) = \sum_{m=K+1}^{\infty} \bar{v}_{m+1} \mathscr{P}_{m+1}(\xi)$, the following error estimation is satisfied

$$|E_K(\xi)| \le \frac{\cos h(L) e^{L/2} \left(\frac{L}{2}\right)^{K+1}}{(K+1)!}. \tag{77}$$

Proof. From (73), Lemma (7), and Lemma (8), we have

$$\begin{aligned}
|\bar{v}_{m+1}| &= (m+1) \left| \sum_{s=0}^{\infty} \frac{(-1)^s \mathscr{V}^{(2s+m)}(0)}{2^{2s+m}(s+m+1)(2s+m)} \binom{2s+m}{s} \right| \\
&= (m+1) \left| \sum_{s=0}^{\infty} \frac{(-1)^s \mathscr{V}^{(2s+m)}(0)}{2^{2s+m}(s+m+1)s(s+m)} \right| = (m+1) \left| \sum_{s=0}^{\infty} \frac{(-1)^s \mathscr{V}^{(2s+m)}(0)}{2^{2s+m} s(s+m+1)} \right| \\
&\le (m+1) \sum_{s=0}^{\infty} \frac{L^{2s+m}}{2^{2s+m} s(s+m+1)} = (s+1) \times \left(\frac{L}{2}\right)^m \sum_{s=0}^{\infty} \frac{\left(L^2/2^2\right)^s}{s(s+m+1)} \\
&\le (m+1) \times \left(\frac{L}{2}\right)^m \times \left(\frac{L^2}{2^2}\right)^{-m+1/2} \times I_{m+1}\left(\frac{2L}{2}\right) = \frac{2(m+1)}{L} I_{m+1}(L) \\
&\le \frac{2(m+1)}{L} \times \frac{L^{m+1} \cos hL}{2^{m+1} \Gamma(m+2)} = \frac{L^k \cos hL}{2^m m}.
\end{aligned} \tag{78}$$

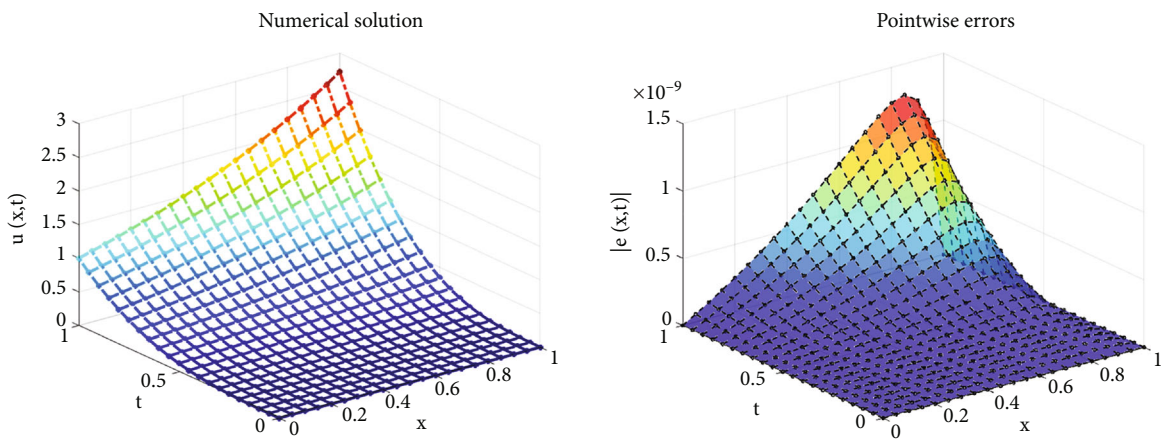

Figure 4: Pictorial results in Example 4 for $\alpha = 0.5$, $\beta = 0.5$ and $K = 9$, $J = 4$.

Table 10: Norm of errors for $\alpha = 0.5$, $\beta = 0.5$ in Example 5.

		$\alpha = \beta = 0.3$	$\alpha = \beta = 0.5$	$\alpha = \beta = 0.7$	$\alpha = \beta = 0.9$
J	K	$\lVert e \rVert_2$	$\lVert e \rVert_2$	$\lVert e \rVert_2$	$\lVert e \rVert_2$
3	5	$7.2576e-05$	$7.1011e-05$	$7.1448e-05$	$6.0514e-05$
3	6	$1.5363e-05$	$1.5000e-05$	$1.4978e-05$	$1.3806e-05$
3	7	$3.8656e-07$	$3.7824e-07$	$3.7609e-07$	$3.4637e-07$
3	8	$5.1965e-08$	$5.0757e-08$	$5.0432e-08$	$3.9225e-08$
3	9	$1.1091e-09$	$2.4799e-09$	$1.6532e-08$	$6.7070e-08$

As a result, the first portion of the theorem is established. □

We now go on to the second section.

$$|\bar{v}_{m+1}\mathscr{P}_{m+1}(\xi)| \le \frac{L^m \cos hL}{2^m m}\mathscr{P}_{m+1}(1), \tag{79}$$

additionally

$$\begin{aligned}\sum_{m=0}^{\infty}\frac{L^m}{2^m m}\mathscr{P}_{m+1}(1) &= \sum_{m=0}^{\infty}\frac{L^m}{2^m m}\times\frac{\left(1+\sqrt{2}\right)^{m+1}-\left(1-\sqrt{2}\right)^{m+1}}{2\sqrt{2}}\\ &= \sum_{m=0}^{\infty}\frac{\left(1+\sqrt{2}\right)}{2\sqrt{2}}\frac{\left(L\left(1+\sqrt{2}\right)/2\right)^m}{m}\\ &\quad-\sum_{m=0}^{\infty}\frac{\left(1-\sqrt{2}\right)}{2\sqrt{2}}\frac{\left(L\left(1-\sqrt{2}\right)/2\right)^m}{m!}\\ &= \frac{\left(1+\sqrt{2}\right)}{2\sqrt{2}}e^{L(1+\sqrt{2})/2}-\frac{\left(1-\sqrt{2}\right)}{2\sqrt{2}}e^{L(1-\sqrt{2})/2}.\end{aligned} \tag{80}$$

As a result, we can conclude that the series is absolutely convergent using the comparison test.

For the third part, we have

$$\begin{aligned}|E_K(\xi)| &\le \cos h(L)\sum_{m=K+1}^{\infty}\frac{L^m}{2^m m} = \cos h(L)\sum_{m=K+1}^{\infty}\frac{(L/2)^m}{m}\\ &= \cos h(L)\frac{\gamma(K+1,(L/2))}{\Gamma(K+1)}e^{L/2},\end{aligned} \tag{81}$$

where $\gamma(K+1, L/2)$ is the lower incomplete gamma function [49], then

$$|E_K(\xi)| \le \cos h(L)\frac{e^{L/2}}{\Gamma(K+1)}\int_0^{L/2}\eta^K e^{-\eta}d\eta \le \frac{\cos h(L)e^{L/2}\left(\frac{L}{2}\right)^{k+1}}{\Gamma(K+1)}. \tag{82}$$

5. Numerical Experiments

Five test problems are offered in this part to demonstrate the correctness and validity of the presented method. On a Windows 10 (64 bit) Intel(R) Core(TM) i7-7500U CPU operating at 2.70 GHz with 8.0 GB of RAM, all computations are done with Matlab R2020b software. In all examples, we use the L_∞ error norm and L_2 error norm

$$\lVert e\rVert_\infty = \max_{\substack{0\le r\le K\\ 0\le s\le J}}\left|\mathscr{V}(\xi_r,\eta_s)-\mathscr{V}_{KJ}(\xi_r,\eta_s)\right|, \lVert e\rVert_2 = \left(h\sum_{s=0}^{n}(e_s^m)^2\right)^{1/2}, \tag{83}$$

Example 1. Consider the following nonlinear time–fractional partial integro–differential equation on $[0, 1] \times [0, 1]$ with the exact solution $\mathscr{V}(\xi, \eta) = \eta^3 \sin(\pi\xi)$

$${}_0^C\mathscr{D}_\eta^\alpha\mathscr{V}(\xi,\eta)+\mathscr{V}(\xi,\eta)\mathscr{V}_\xi(\xi,\eta) = \int_0^\eta(\eta-s)^{\beta-1}\mathscr{V}_{\xi\xi}(\xi,s)ds+\mathscr{G}(\xi,\eta), \tag{84}$$

Table 11: Norm of errors for $\alpha = \beta = 0.5$ and CPU time in Example 5.

	$J = 3, K = 5$	$J = 3, K = 6$	$J = 3, K = 7$	$J = 3, K = 8$	$J = 3, K = 9$
	$\|e\|_\infty$	$\|e\|_\infty$	$\|e\|_\infty$	$\|e\|_\infty$	$\|\|e\|_\infty$
	$1.1228e-04$	$2.3945e-05$	$6.0186e-07$	$8.0155e-08$	$4.0315e-09$
CPU	0.5944s	1.0808s	1.1061s	1.1594s	1.2277s

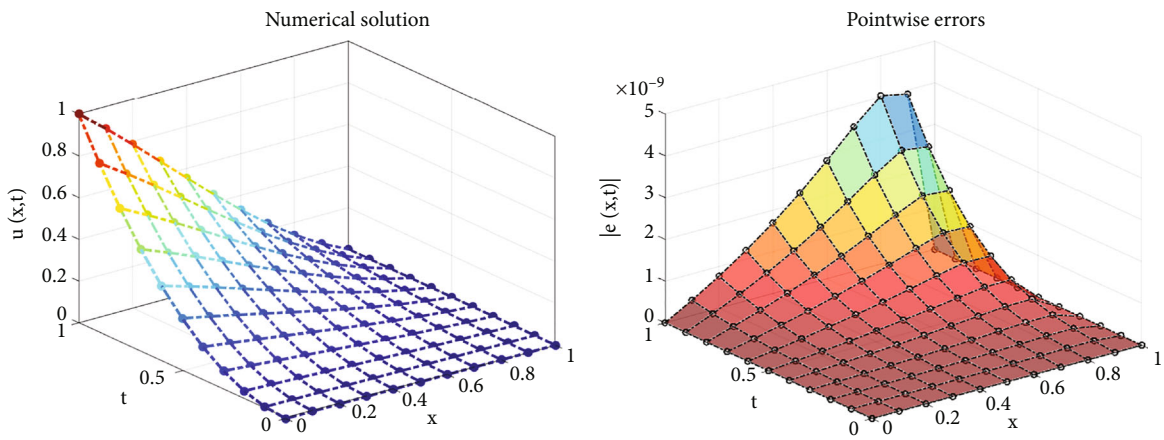

Figure 5: Pictorial results in Example 5 for $\alpha = 0.5$, $\beta = 0.5$ and $K = 9$, $J = 3$.

with conditions (2), (3), and

$$\mathcal{G}(\xi,\eta) = \left(\frac{6\eta^{3-\alpha}}{\Gamma(4-\alpha)} + \frac{6\pi^2\Gamma(\beta)\eta^{3+\beta}}{\Gamma(4+\beta)}\pi\eta^6\cos(\pi\xi)\right)\sin(\pi\xi). \tag{85}$$

We solved this problem numerically using the polynomial spectral scheme provided in this paper. We employed fsolve in Matlab to solve a nonlinear system of equations (45). Table 1 shows the absolute errors for $\alpha = 0.5$ and various β values. We can observe from this table that the recommended strategy is effective. Also, we portrayed the numerical solution and absolute error surfaces in Figure 1. Furthermore, the norm of errors and CPU times is reported in Table 2. Table 1, Table 2, and Figure 1 show that the numerical method provides acceptable results.

Example 2. Consider the following equation

$${}_0^C\mathcal{D}_\eta^\alpha \mathcal{V}(\xi,\eta) + \mathcal{V}(\xi,\eta)\mathcal{V}_\xi(\xi,\eta) = \int_0^\eta (\eta-s)^{\beta-1}\mathcal{V}_{\xi\xi}(\xi,s)ds + \mathcal{G}(\xi,\eta), \tag{86}$$

with conditions (2) and (3). The source term is taken as

$$\mathcal{G}(\xi,\eta) = \frac{2\xi(1-\xi)\eta^{2-\alpha}}{\Gamma(3-\alpha)} + \xi(1-2\xi)(1-\xi)\eta^4 + \frac{4\eta^{\beta+2}}{\beta^3+3\beta^2+2\beta}, \tag{87}$$

and $\mathcal{V}(\xi,\eta) = \eta^2\xi(1-\xi)$.

The absolute errors for equal values of α, β, and $K = J = 3$ are illustrated in Table 3. This table shows quite revealingly that the expressed method has good precision. In addition, we can observe from the table that only a small number of basis functions have produced the necessary outcomes. The CPU times and the norm of errors are provided in Table 4. Figure 2 shows a visualization of the approximate solution as well as absolute errors.

Example 3. Consider the following equation on $[0,1]\times[0,1]$:

$${}_0^C\mathcal{D}_\eta^\alpha \mathcal{V}(\xi,\eta) + \mathcal{V}(\xi,\eta)\mathcal{V}_\xi(\xi,\eta) = \int_0^\eta (\eta-s)^{\beta-1}\mathcal{V}_{\xi\xi}(\xi,s)ds + \mathcal{G}(\xi,\eta), \tag{88}$$

with conditions (2) and (3). The source term is taken as

$$\begin{aligned}\mathcal{G}(\xi,\eta) = {} & \frac{600\xi^3(1-\xi)\eta^{3-\alpha}}{\Gamma(4-\alpha)} - \frac{24\eta^{4-\alpha}}{\Gamma(5-\alpha)} \\ & + 10000\eta^6(1-\eta)^2(3-4\xi)\xi^2\left(\xi^3-\xi^4\right) \\ & - 600\xi(1-2\xi)\left(\frac{6\Gamma(\beta)\eta^{\beta+3}}{\Gamma(4+\beta)} - \frac{24\Gamma(\beta)\eta^{\beta+4}}{\Gamma(5+\beta)}\right).\end{aligned} \tag{89}$$

The exact solution is $\mathcal{V}(\xi,\eta) = 100\xi^3\eta^3(1-\xi)(1-\eta)$.

The numerical results are reported in Table 5. We have chosen $K = 4$, $J = 5$, and for equal α and β, the obtained results are fruitful. This table confirms that the presented method has high performance and produces accurate results. For $\alpha = \beta = 0.5$ and different J and K, the norm of errors and the CPU times are provided in Table 3. The absolute error functions for equal α and β are sketched in Figure 3. These

figures show that the numerical and exact solutions are almost identical (Table 6).

Example 4. Consider the following equation:

$$ {}_0^C\mathcal{D}_\eta^\alpha \mathcal{V}(\xi,\eta) + \mathcal{V}(\xi,\eta)\mathcal{V}_\xi(\xi,\eta) = \int_0^\eta (\eta - s)^{\beta-1}\mathcal{V}_{\xi\xi}(\xi,s)ds + \mathcal{G}(\xi,\eta), \tag{90} $$

with conditions (2), (3), and

$$ \mathcal{G}(\xi,\eta) = \frac{6e^\xi \eta^{3-\alpha}}{\Gamma(4-\alpha)} + \eta^6 e^{2\xi} - \frac{6e^\xi \Gamma(\beta)\eta^{\beta+3}}{\Gamma(4+\beta)}. \tag{91} $$

The exact solution is $\mathcal{V}(\xi,\eta) = \eta^3 e^\xi$.

The absolute errors for $\alpha = \beta = 0.5$ are presented in Table 7. Table 8 illustrates the norm of errors and CPU times for $\alpha = \beta = 0.5$ with various J and K values. Table 9 also contains data on L_2 errors. Numerical solutions and pointwise error graphs are demonstrated in Figure 4. This figure shows the behavior of the numerical solution and the error function. Numerical results are in good settlement with theoretical results.

Example 5. Finally, we investigate the following equation on $[0,1] \times [0,1]$

$$ {}_0^C\mathcal{D}_\eta^\alpha \mathcal{V}(\xi,\eta) + \mathcal{V}(\xi,\eta)\mathcal{V}_\xi(\xi,\eta) = \int_0^\eta (\eta - s)^{\beta-1}\mathcal{V}_{\xi\xi}(\xi,s)ds + \mathcal{G}(\xi,\eta), \tag{92} $$

with conditions (2) and (3). The source term is taken as

$$ \begin{aligned} \mathcal{G}(\xi,\eta) = {} & \frac{2(1-\xi)cos\xi\eta^{2-\alpha}}{\Gamma(3-\alpha)} + \eta^4(1-\xi)\cos\xi(-\sin\xi - \cos\xi + \xi\sin\xi) \\ & - (2\sin\xi + (\xi-1)\cos\xi)\frac{2\Gamma(\beta)\eta^{\beta+2}}{\Gamma(3+\beta)}, \end{aligned} \tag{93} $$

and $\mathcal{V}(\xi,\eta) = \eta^2(1-\xi)\cos\xi$.

In Table 10, the L_2 error is computed for $\alpha = \beta = 0.5$ and different N and M. Table 11 also shows the norm of errors and CPU times. Figure 5 shows the numerical solution and absolute error plots. This figure shows that for $K = 9$ and $J = 4$, the numerical solution is close to the exact solution. Table 10, Table 11, and Figure 5 affirm the validity and efficacy of the presented method.

6. Conclusions

The purpose of this study was to suggest a collocation approach for solving a nonlinear TFPIDE based on Pell polynomials. In the Caputo sense, the fractional derivative is considered. The equation's solution was expressed as a series of Pell polynomials with two variables. An algebraic system of nonlinear equations is obtained using the numerical technique. We proved that the method is convergent. Five test problems are provided to show that the method is efficacious. In numerical results, a small number of basis Pell polynomials is used to obtain good accuracy. In all examples, the CPU time was about one second. All of the tables and graphs demonstrated that the strategy is effective.

Data Availability

All results have been obtained by conducting the numerical procedure and the ideas can be shared for the researchers.

Conflicts of Interest

The authors declare that they have no conflicts of interest.

References

[1] H. Dutta, A. Akdemir, and A. Atangana, *Fractional Order Analysis: Theory, Methods and Applications*, John Wiley and Sons Ltd, 2020.

[2] D. Kumar and J. Singh, *Fractional Calculus in Medical and Health Science*, Taylor & Francis Group, LLC, 2020.

[3] G. A. Anastassiou, *Generalized Fractional Calculus: New Advancements and Applications*, Springer, 2020.

[4] J. C. Trigeassou and N. Maamri, *Analysis, Modeling and Stability of Fractional Order Differential Systems 2*, John Wiley & Sons, 2019.

[5] R. Caponetto, G. Dongola, I. Fortuna, and I. Petras, *Fractional Order Systems: Modeling and Control Applications*, World Scientific, 2010.

[6] A. E. Matouk, "Advanced applications of fractional differential operators to science and technology," *IGI Global*, 2020.

[7] D. Baleanu and A. M. Lopes, *Handbook of Fractional Calculus with Applications, Volume 7 Applications in Engineering*, Life and Social Sciences, Part A, de Gruyter, 2019.

[8] X. J. Yang, F. Gao, and Y. Ju, *General Fractional Derivatives with Applications in Viscoelasticity*, Academic Press, 2020.

[9] E. Shishkina and S. Sitnik, *Transmutations, Singular and Fractional Differential Equations with Applications to Mathematical Physics*, Academic Press, 2020.

[10] A. Atangana, *Fractional Operators with Constant and Variable Order with Application to Geo-Hydrology*, Academic Press, 2017.

[11] D. Valerio and M. D. Ortigueira, *Fractional Signals and Systems*, de Gruyter, 2020.

[12] M. M. Meerschaert and A. Sikorskii, *Stochastic Models for Fractional Calculus*, de Gruyter, 2019.

[13] P. Ostalczyk, D. Sankowski, and J. Nowakowski, *On-Integer Order Calculus and Its Applications*, Springer, 2019.

[14] H. Fallahgoul, S. Focardi, and F. Fabozzi, *Fractional Calculus and Fractional Processes with Applications to Financial Economics: Theory and Application*, Academic Press, 2017.

[15] Z. Z. Sun and G. Gao, *Fractional Differential Equations: Finite Difference Methods*, Walter de Gruyter GmbH & Co KG, 2020.

[16] C. Li and F. Zeng, *Numerical Methods for Fractional Calculus*, Chapman and Hall/CRC, 2019.

[17] W. M. Abd-Elhameed and Y. H. Youssri, "Sixth-kind Chebyshev spectral approach for solving fractional differential equations," *Int. J. Nonlin. Sci. Num.*, vol. 20, no. 2, pp. 191–203, 2019.

[18] W. M. Abd-Elhameed, "Novel expressions for the derivatives of sixth kind Chebyshev polynomials: spectral solution of the non-linear one-dimensional Burgers' equation," *Fractal and Fractional*, vol. 5, no. 2, p. 53, 2021.

[19] W. M. Abd-Elhameed and Y. H. Youssri, "New formulas of the high-order derivatives of fifth-kind Chebyshev polynomials: spectral solution of the convectionâ€'diffusion equation," *Numerical Methods for Partial Differential Equations*, pp. 1–17, 2021.

[20] M. Samiee, E. Kharazmi, M. M. Meerschaert, and M. Zayernouri, "A unified Petrov–Galerkin spectral method and fast solver for distributed-order partial differential equations," *Communications on Applied Mathematics and Computation*, vol. 3, no. 1, pp. 61–90, 2021.

[21] M. Jani, E. Babolian, and D. Bhatta, "A Petrov–Galerkin spectral method for the numerical simulation and analysis of fractional anomalous diffusion," *Mathematical Methods in the Applied Sciences*, vol. 44, no. 2, pp. 2021–2032, 2021.

[22] B. Guo, X. Pu, and F. Huang, *Fractional Partial Differential Equations and Their Numerical Solutions*, World Scientific, 2015.

[23] S. S. Ray, *Nonlinear Differential Equations in Physics: Novel Methods for Finding Solutions*, Springer, 2020.

[24] H. Wang, D. Xu, J. Zhou, and J. Guo, "Weak Galerkin finite element method for a class of time fractional generalized Burgers' equation," *Numerical Methods for Partial Differential Equations*, vol. 37, no. 1, pp. 732–749, 2021.

[25] Y. Zheng and Z. Zhao, "The time discontinuous space-time finite element method for fractional diffusion-wave equation," *Applied Numerical Mathematics*, vol. 150, pp. 105–116, 2020.

[26] M. Dehghan, J. Manafian, and A. Saadatmandi, "Solving nonlinear fractional partial differential equations using the homotopy analysis method," *International Journal*, vol. 26, no. 2, pp. 448–479, 2010.

[27] O. Nikan, Z. Avazzadeh, and J. A. T. Machado, "An efficient local meshless approach for solving nonlinear time-fractional fourth-order diffusion model," *Journal of King Saud University-Science*, vol. 33, no. 1, article 101243, 2021.

[28] F. Safari and P. Azarsa, "Backward substitution method based on Müntz polynomials for solving the nonlinear space fractional partial differential equations," *Mathematical Methods in the Applied Sciences*, vol. 43, no. 2, pp. 847–864, 2020.

[29] H. C. Yaslan, "Legendre collocation method for the nonlinear space–time fractional partial differential equations," *Iranian Journal of Science and Technology, Transactions A: Science*, vol. 44, no. 1, pp. 239–249, 2020.

[30] J. Shen, T. Tang, and L. L. Wang, *Spectral Methods: Algorithms, Analysis and Applications*, Springer Science & Business Media, 2011.

[31] C. Canuto, M. Y. Hussaini, A. Quarteroni, and T. A. Zang, *Spectral Methods in Fluid Dynamics*, Springer Science & Business Media, 2012.

[32] P. Agarwal, A. A. El-Sayed, and J. Tariboon, "Vieta-Fibonacci operational matrices for spectral solutions of variable-order fractional integro-differential equations," *Journal of Computational and Applied Mathematics*, vol. 382, article 113063, 2021.

[33] N. Moshtaghi and A. Saadatmandi, "Polynomial-Sinc collocation method combined with the Legendre-Gauss quadrature rule for numerical solution of distributed order fractional differential equations," *Revista de la Real Academia de Ciencias Exactas, FÃ-sicas y Naturales. Serie A. MatemÃ¡ticas*, vol. 115, no. 2, pp. 1–23, 2021.

[34] M. Abbaszadeh, M. Dehghan, and Y. Zhou, "Crank-Nicolson/Galerkin spectral method for solving two-dimensional time-space distributed-order weakly singular integro-partial differential equation," *Journal of Computational and Applied Mathematics*, vol. 374, article 112739, 2020.

[35] X. Zheng, W. Qiu, and H. Chen, "Three semi-implicit compact finite difference schemes for the nonlinear partial integro-differential equation arising from viscoelasticity," *International Journal of Modelli ng and Simulation*, vol. 41, no. 3, pp. 234–242, 2021.

[36] J. M. Sanz-Serna, "A numerical method for a partial integro-differential equation," *SIAM Journal on Numerical Analysis*, vol. 25, no. 2, pp. 319–327, 1988.

[37] J. Guo, D. Xu, and W. Qiu, "A finite difference scheme for the nonlinear time–fractional partial integro–differential equation," *The European Physical Journal Plus*, vol. 136, no. 1, pp. 1–30, 2021.

[38] A. G. Atta, G. M. Moatimid, and Y. H. Youssri, "Generalized Fibonacci operational collocation approach for fractional initial value problems," *International Journal of Applied and Computational Mathematics*, vol. 5, no. 1, pp. 1–11, 2019.

[39] A. G. Atta, W. M. Abd-Elhameed, G. M. Moatimid, and Y. H. Youssri, "Shifted fifth-kind Chebyshev Galerkin treatment for linear hyperbolic first- order partial differential equations," *Applied Numerical Mathematics*, vol. 167, pp. 237–256, 2021.

[40] A. G. Atta, G. M. Moatimid, and Y. H. Youssri, "Generalized Fibonacci operational tau algorithm for fractional Bagley-Torvik equation," *Prog. Fract. Differ. Appl*, vol. 6, no. 3, pp. 215–224, 2020.

[41] M. Taghipour and H. Aminikhah, "Application of Pell collocation method for solving the general form of time-fractional burgers equations," *Mathematical Sciences*, vol. 1-19, 2022.

[42] A. F. Horadam and J. M. Mahon, "Pell and Pell-Lucas polynomials," *The Fibonacci Quarterly*, vol. 23, no. 1, pp. 7–20, 1985.

[43] W. M. Abd-Elhameed and Y. H. Youssri, "Spectral tau algorithm for certain coupled system of fractional differential equations via generalized Fibonacci polynomial sequence," *Iranian Journal of Science and Technology, Transactions A: Science*, vol. 43, no. 2, pp. 543–554, 2019.

[44] W. M. Abd-Elhameed and Y. H. Youssri, "Generalized Lucas polynomial sequence approach for fractional differential equations," *Nonlinear Dynamics*, vol. 89, no. 2, pp. 1341–1355, 2017.

[45] J. J. Callahan, *Advanced Calculus: A Geometric View*, Springer Science & Business Media, 2010.

[46] Y. H. Youssri, "A new operational matrix of Caputo fractional derivatives of Fermat polynomials: an application for solving the Bagley-Torvik equation," *Adv. Difference Equ.*, vol. 2017, no. 1, pp. 1–17, 2017.

[47] P. F. Byrd, "Expansion of analytic functions in polynomials associated with Fibonacci numbers," *Fibonacci Q.*, vol. 1, article n16, 1963.

[48] M. Taghipour and H. Aminikhah, "A fast collocation method for solving the weakly singular fractional integro-differential equation," *Computational and Applied Mathematics*, vol. 41, no. 4, p. 142, 2022.

[49] G. J. O. Jameson, "The incomplete gamma functions," *The Mathematical Gazette*, vol. 100, no. 548, pp. 298–306, 2016.

Hindawi
Journal of Function Spaces
Volume 2022, Article ID 9734604, 9 pages
https://doi.org/10.1155/2022/9734604

Research Article

Pell Collocation Pseudo Spectral Scheme for One-Dimensional Time-Fractional Convection Equation with Error Analysis

A. S. Mohamed

Department of Mathematics, Faculty of Science, Helwan University, Cairo 11795, Egypt

Correspondence should be addressed to A. S. Mohamed; amany.saad78@yahoo.com

Received 16 October 2021; Revised 1 December 2021; Accepted 2 December 2021; Published 18 May 2022

Academic Editor: Youssri Hassan Youssri

In the current manuscript, we implement the collocation method to obtain an approximate solution of one-dimensional time-fractional convection equation. The operational matrices of Pell polynomials are applied to solve the fractional partial differential equations. In the Caputo sense, we describe the time-fractional derivatives. So, this algorithm allows us to transform the fractional differential equation with initial (boundary) conditions into a system of algebraic equations in a good form. The convergence and error analysis of Pell polynomials are carefully investigated, and some examples are explored to show the comparison and efficiency of our method with others.

1. Introduction

The investigation of differential and integral equations of fractional order is a very important subject. These kinds of equations describe many phenomena in different fields such as mathematics, mechanics, engineering, physics, biology, fluid, and chemistry. It is difficult to evaluate the exact solution of these equations. It had to evaluate the approximate solution instead. For example, the variational iteration method is used to solve fractional wave and Burgers equations, time-fractional partial differential equations, and fractional Klein-Gordon and Black Scholes equations (see [1–3]). The linear space-time-fractional convection-diffusion equations with fractional derivatives for both space and time, the fractional kinetic equations of diffusion or dispersion with time, and space-fractional differential equations with variable diffusivity coefficient are studied by the finite difference method (see [4–6]). The finite element is another method for solving time-fractional partial differential equations, space-fractional partial advection-diffusion equation with non-homogeneous initial-boundary conditions, and linear Riesz space-fractional partial differential equations with a second-order time derivative (see [7–9]).

Various types of ordinary and partial fractional differential (integral) equations can be solved by the well-known methods which are called spectral methods. These methods decrease the number of unknowns and supply small errors. The way of solution in these methods is expressed as expansion of polynomials. One of the spectral methods is shifted Jacobi polynomials which are used to approximate the solution of Volterra-Fredholm integral equation, the space-fractional advection-dispersion equation, and linear multi-term fractional differential equations (see [10–12]). Another spectral method is shifted Chebyshev which is used for solving one-dimensional linear hyperbolic first-order partial differential equations (see [13]). Solving multi-term fractional differential equations and a system of high-order linear differential equations with variable coefficients are using Lucas method (see [14, 15]). Evaluating the solution of Volterra-Fredholm integral equation, multi-term fractional differential equations, multi-term initial value problems, and fractional pantograph differential equations are studied using generalized Lucas polynomials (see [16–19]). Another way of solving such problems is connecting between generalized Lucas polynomials together with third and fourth kinds of Chebyshev polynomials (see [20]). The coupled systems of a fractional differential equation is solved by generalized Fibonacci method (see [21]). However, for multidimensional Burgers-type equations, one- and two-dimensional nonlinear heat-type equations, two-dimensional linear and

nonlinear Sobolev equations, and nonlinear reactionâ€"diffusion Brusselator system with applications in chemical processes, all of them are using mixed Lucas and Fibonacci polynomials (see [22–25]). Also, Fermat polynomials make use for solving the Bagly-Torvik equation (see [26]). In our paper, we shall use Pell collocation (PLC) method to solve partial fractional differential equations and to the best of our knowledge this is the first to be done, also compare our results with the non-uniform L1-discontinuous Galerkin (DG) method (see [27]), and show that our method is more accurate although it takes a longer time.

We considered the fractional derivative in the Caputo sense because it is mathematically rigorous than other derivatives and this was discussed in details (see [17]).

Now our aim is to solve the one-dimensional time-fractional convection equation using Pell polynomials (see [27])

$$\begin{cases} {}_cD_{0,t}^{\lambda} v(y,t) + \beta v_y(y,t) = h(y,t) & (y,t) \in \Lambda \times (0,\tau] \\ v(y,0) = v_0(y), & y \in \Lambda \\ v(d,t) = 0, & t \in (0,\tau] \end{cases}, \tag{1}$$

where $v(y,t)$ is an unknown function, $\Lambda = (d,a)$ is a bounded interval, and β is a non zero given const. $h(y,t) \in L^{\infty}(0,\tau; L^2(\Lambda))$ and $v_0(y) \in L^2(\Lambda)$ are known functions. ${}_cD_{0,t}^{\lambda}$ is the λ-th fractional order Caputo derivative which is given by

$${}_cD_{0,t}^{\lambda} v(y,t) = \frac{1}{\Gamma(1-\lambda)} \int_0^t (t-r)^{-\lambda} \frac{\partial v}{\partial r} dr, 0 < \lambda < 1, \tag{2}$$

We organize this paper as follows: In Section 2, we demonstrate the basic properties and preliminaries of Pell polynomials which will be frequent. Section 3 displays the derivatives of integer and fractional orders for these polynomials. The spectral collocation algorithm for solving one-dimensional time-fractional convection equation is analyzed and described in Section 4. The basic results which show the investigation of convergence, error analysis, and the evaluation of the global error for Pell expansion are included in Section 5. Two numerical examples are demonstrated and we compare the results with another method which will be in Section 6. The last section deals with the conclusions.

2. Preliminaries and Properties of Pell Polynomials

It is known that Pell polynomials are special cases of Fibonacci polynomials and the recurrence form of Pell polynomials is

$$(pL)_{j+1}(y) = 2y(pL)_{j+1}(y) + (pL)_j(y). \tag{3}$$

Another form of this relation is

$$(W)_{j+1}(y) = \rho(y)(W)_{j+1}(y) + \theta(y)(W)_j(y), j \geq 0, \tag{4}$$

with initial conditions

$$(W)_0(y) = 0, (W)_1(y) = 1. \tag{5}$$

The Binet formula of Pell polynomials is

$$(W)_j(y) = \frac{\gamma^j(y) - \eta^j(y)}{\gamma(y) - \eta(y)}, \tag{6}$$

where

$$\gamma(y) = \frac{\rho(y) + \sqrt{\rho^2(y) + 4\theta(y)}}{2}, \eta(y) = \frac{\rho(y) - \sqrt{\rho^2(y) + 4\theta(y)}}{2}. \tag{7}$$

We propose to choose $\rho(y) = 2y$ and $\theta(y) = 1$. Then, Pell polynomials will take the form

$$(pL)_j(y) = \frac{\left(y + \sqrt{y^2+1}\right)^j - \left(y - \sqrt{y^2+1}\right)^j}{2^j\sqrt{y^2+1}}, j \geq 0. \tag{8}$$

The analytical form of these polynomials can be deduced from equation (3) [21], $(pL)_{j+1}(y), j \geq 0$

$$(pL)_{j+1}(y) = \sum_{r=0}^{\lfloor \frac{j}{2} \rfloor} 2^{j-2r} \binom{j-r}{r} y^{j-2r}, \tag{9}$$

where $\lfloor j \rfloor$ is the largest integer less than or equal j From Theorem (4) [21], we have

$$y^j = \frac{1}{2^j} \sum_{r=0}^{\lfloor \frac{j}{2} \rfloor} \frac{(-1)^r \binom{j}{r} (j-2r+1)}{j-r+1} (pL)_{j-2r+1}(y), j \geq 0. \tag{10}$$

3. Integer and Fractional Derivatives of Pell Polynomials

In this section, we get the integer and fractional derivatives of Pell polynomials. This section will be divided into two subsections; the first explores the integer derivatives of Pell polynomials and the second concerns the fractional derivatives of these polynomials.

Let $v(y)$ be expressed in terms of Pell polynomials

$$v(y) = \sum_{j=1}^{\infty} c_j (pL)_j(y). \tag{11}$$

The approximate solution of this function is

$$v(y) \approx v_M(y) = \sum_{j=1}^{M+1} c_j (pL)_j(y) = C^T(PL)(y), \tag{12}$$

where

$$C^T = [c_1, c_2, \cdots, c_{M+1}],$$
$$(PL)(y) = \left[(pL)_1(y), (pL)_2(y), \cdots, (pL)_{M+1}(y)\right]^T. \tag{13}$$

3.1. The Integer Derivatives of Pell Polynomial. The first derivative of $(PL)(y)$ can be written as (see [21])

$$\frac{d(PL)(y)}{dy} = F^{(1)}(PL)(y), \tag{14}$$

where $F^{(1)} = (f_{nm}^{(1)})$ is the $(M+1)\times(M+1)$ matrix of derivatives.

$$f_{nm}^{(1)} = \begin{cases} 2(-1)^{(n-m-1)/2}(m+1), n > m, (n+m)\text{odd} \\ 0 \text{ otherwise} \end{cases}. \tag{15}$$

If $M = 5$, then $F^{(1)}$ has the form

$$F^{(1)} = \begin{bmatrix} 0 & 0 & 0 & 0 & 0 & 0 \\ 2 & 0 & 0 & 0 & 0 & 0 \\ 0 & 4 & 0 & 0 & 0 & 0 \\ -2 & 0 & 6 & 0 & 0 & 0 \\ 0 & -4 & 0 & 8 & 0 & 0 \\ 2 & 0 & -6 & 0 & 10 & 0 \end{bmatrix}. \tag{16}$$

Also, the integer derivatives of $(PL)(y)$ can be easily written in the form (see [21])

$$\frac{d^t(PL)(y)}{dy^t} = F^{(t)}(PL)(y) = \left(F^{(1)}\right)^t(PL)(y). \tag{17}$$

3.2. The Fractional Derivatives of Pell Polynomial. If λ is not an integer, then the fractional derivative of $(PL)(y)$ takes the form (see [21])

$$D^\lambda(PL)(y) = y^{-\lambda}F^{(\lambda)}(PL)(y), \tag{18}$$

where $F^{(\lambda)} = (f_{nm}^{\lambda})$ is the $(M+1)\times(M+1)$ Pell operational matrix of fractional derivatives of order λ, which has the form

$$F^{(\lambda)} = \begin{bmatrix} 0 & 0 & 0 & \cdots & 0 \\ \vdots & \vdots & \vdots & & \vdots \\ \zeta_\lambda(\lceil\lambda\rceil, 1) & \zeta_\lambda(\lceil\lambda\rceil, 2) & 0 & \cdots & 0 \\ \vdots & \vdots & \vdots & & \vdots \\ \zeta_\lambda(i, 1) & \cdots & \zeta_\lambda(i, i) & \cdots & 0 \\ \vdots & \vdots & \vdots & & \vdots \\ \zeta_\lambda(M+1, 1) & \zeta_\lambda(M+1, 2) & \zeta_\lambda(M+1, 3) & \cdots & \zeta_\lambda(M+1, M+1) \end{bmatrix}. \tag{19}$$

f_{nm}^{λ} can be written in the form

$$f_{nm}^{\lambda} = \begin{cases} \zeta_\lambda(n, m), & n \geq \lceil\lambda\rceil, n \geq m \\ 0 & otherwise \end{cases}, \tag{20}$$

where

$$\zeta_\lambda(n, m) = m\xi_m \sum_{l=\lceil\lambda\rceil}^{n} \frac{(-1)^{(1+l-m)/2} l!((n+l-1)/2)!}{((n-l-1)/2)!((1+l-m)/2)!((1+m+l)/2)!\Gamma(1+l-\lambda)},$$
$$\xi_k = \begin{cases} \frac{1}{2}, k = 0, \\ 1, \text{otherwise} \end{cases}. \tag{21}$$

Since $(a)_b = \Gamma(a+b)/\Gamma(a)$,

$$\frac{((n+l-1)/2)!}{((n-l-1)/2)!} = \left(\frac{n-l+1}{2}\right)_l. \tag{22}$$

Clearly, $\zeta_\lambda(n, m)$ can be rewritten in the form

$$\zeta_\lambda(n, m) = m \sum_{l=\lceil\lambda\rceil}^{n} \frac{(-1)^{(1+l-m)/2}\begin{pmatrix} l \\ (1+l-m)/2 \end{pmatrix}((n-l+1)/2)_l}{((1+m+l)/2)\Gamma(1+l-\lambda)}. \tag{23}$$

So the fractional derivative has the relation

$$D^\lambda(pL)_n(y) = y^{-\lambda}\sum_{m=1}^{n}\zeta_\lambda(n, m)(pL)_m(y). \tag{24}$$

4. The Algorithm of the Method

In this section, we study the method for solving one-dimensional time-fractional convection equation with initial (boundary) conditions by using Pell polynomials.

The function $v(y, t)$ of two variables can be expanded in terms of double Pell polynomials

$$v(y, t) = \sum_{k=1}^{\infty}\sum_{\ell=1}^{\infty} c_{k\ell}(pL)_k(y)(pL)_\ell(t), \tag{25}$$

and the approximate solution of this function is

$$v(y, t) \approx \sum_{k=1}^{M+1}\sum_{\ell=1}^{M+1} c_{k\ell}(pL)_k(y)(pL)_\ell(t) = C^T\Psi(y, t), \tag{26}$$

where $c_{k\ell}$, $K, \ell = 1, 2, \cdots, M+1$ are the unknown coefficients

$$C^T = (c_{k\ell})^T = \begin{bmatrix} c_{11} & c_{12} & c_{13} & \cdots & c_{1(M+1)} \\ c_{21} & c_{22} & c_{23} & \cdots & c_{2(M+1)} \\ \vdots & \vdots & \vdots & \cdots & \vdots \\ c_{M1} & c_{M2} & c_{M3} & \cdots & c_{(M+1)(M+1)} \end{bmatrix}, \tag{27}$$

where M is any arbitary positive integer. $(pL)_k(y)$ and $(pL)_\ell(t)$ are Pell polynomials defined in equation (9). Also, $\Psi(y,t)$ is an $(M+1)\times(M+1)$ matrix introduced by

$$\begin{aligned}\Psi(y,t) = [&\psi_{11}(y,t), \psi_{21}(y,t), \cdots, \psi_{M+1}(y,t)\,; \psi_{12}(y,t), \psi_{22} \\ &\cdot (y,t), \cdots, \psi_{(M+1)2}(y,t)\,; \psi_{1(M+1)}(y,t), \psi_{2(M+1)} \\ &\cdot (y,t), \cdots, \psi_{(M+1)(M+1)}(y,t)],\end{aligned} \tag{28}$$

where

$$\psi_{k\ell}(y,t) = (pL)_k(y)(pL)_\ell(t). \tag{29}$$

Substitute equation (26) into equation (1), we obtain

$$\begin{aligned}&{}_cD_{0,t}^{\lambda} \sum_{k=1}^{M+1}\sum_{\ell=1}^{M+1} c_{k\ell}(pL)_k(y)(pL)_\ell(t) \\ &+ \beta\frac{\partial}{\partial y}\sum_{k=1}^{M+1}\sum_{\ell=1}^{M+1} c_{k\ell}(pL)_k(y)(pL)_\ell(t) = h(y,t).\end{aligned} \tag{30}$$

Let

$$\phi_{k\ell}(y,t) = (pL)_k(y)\,{}_cD_{0,t}^{\lambda}(pL)'_\ell(t) + \beta(pL)_\ell(t)\frac{\partial}{\partial y}(pL)'_k(y). \tag{31}$$

Consequently, equation (30) can be rewritten as

$$\sum_{k=1}^{M+1}\sum_{\ell=1}^{M+1} c_{k\ell}\phi_{k\ell}(y,t) = h(y,t). \tag{32}$$

Collocating this equation at $(M+1)\times(M+1)$ roots of Pell polynomials, we have a system of equations

$$\sum_{k=1}^{M+1}\sum_{\ell=1}^{M+1} c_{k\ell}\phi_{k\ell}(y_i,t_j) = h(y_i,t_j),\ i,j = 1,2,\cdots,M+1. \tag{33}$$

The matrix form of this equation is

$$\Phi^T C = H, \tag{34}$$

where $\Phi = (\phi_{k\ell ij}) = \phi_{k\ell}(y_i,t_j)$,$k, \ell, i, j = 1, 2, \cdots, M+1$, and

$$\begin{aligned}H = [&h(y_1,t_1), h(y_2,t_1), \cdots, h(y_{M+1},t_1)\,; h(y_1,t_2), h \\ &\cdot (y_2,t_2), \cdots, h(y_{M+1},t_2)\,; h(y_1,t_{M+1}), h \\ &\cdot (y_2,t_{M+1}), \cdots, h(y_{M+1},t_{M+1})]^T.\end{aligned} \tag{35}$$

Finally, we can determine the constants by

$$C = \left(\Phi^T\right)^{-1} H, \tag{36}$$

with initial (boundary) conditions in the forms

$$\begin{aligned}&C^T(PL)(y)(PL)(0) = v_0(y),\ y \in \Lambda, \\ &C^T(PL)(d)(PL)(t) = 0,\ t \in (0,\tau].\end{aligned} \tag{37}$$

Now we summarize the steps of our scheme in Algorithm 1 below.

5. The Convergence and Error Analysis

In this section, we explore our main results concerning the convergence and error analysis of Pell polynomials for fractional differential equations. Let us start with the following three Lemmas.

Lemma 1. *If $v(y)$ is an infinitely differential function, then it can be expressed in the form of the Pell polynomials.*

$$v(y) = \sum_{k=1}^{\infty}\sum_{\rho=0}^{\infty} \frac{(-1)^\rho k\,(2\rho+k-1)!u_{2\rho+k-1}}{2^{2\rho+k-1}\rho!(\rho+k)!}(pL)_k(y), \tag{38}$$

where $u_j = v^{(j)}(0)/j!$.

Proof. From equation (43) (see [21]).

$$v(y) = \sum_{k=1}^{\infty} c_k G_k^{a,b}(y), \tag{39}$$

where $G_k^{a,b}(y)$ are the generalized Fibonacci polynomials. Taking $a = 2$, $b = 1$, and equations (4.3,5.3) (see [28]), the result holds. □

Lemma 2. *The modified Bessel function satisfies the following inequality.*

$$|I_k(y)| \le \frac{y^k \cosh y}{2^k\Gamma(k+1)}. \tag{40}$$

Proof. See [29]. □

Lemma 3. *The following relations are satisfied.*

$$(pL)_k(y) \le (pL)_k,\ y \in \Lambda, \tag{41}$$

Input $\beta \in R \setminus \{0\}$; the functions $v(y,t)$ and $h(y,t)$.
Step 1. Define Pell polynomials by (9).
Step 2. Compute the basis function of Pell polynomials by (29).
Step 3. Define the basis function vector $\Psi(y,t)$ by (28).
Step 4. Substituting Eqs. (2) and (26) into Eq. (1).
Step 5. Collocating Eq. (32) in $(M+1)\times(M+1)$ roots of the polynomial $(pL)_k(y)(pL)_\ell(t)$.
Step 6. Compute the matrix H using (35).
Step 7. Define the $(M+1)\times(M+1)$ unknown vectors C^T.
Step 8. Use *NSolve* command to solve the system $\Phi^T C = H$.
Output The approximate solution: $v(y,t) = C^T\Psi(y,t)$.

Algorithm 1: Coding algorithm for the proposed scheme.

where

$$\begin{aligned}(pL)_k &= (pL)_k(1) \le 3^k,\\ (pL)_k &= (pL)_k(1) \le 3^{k+1}.\end{aligned} \tag{42}$$

Proof. By simplifying the relation in equation (8) and $y=1$, we obtain the required inequalities. □

The following results are important in itself and will be helpful in discussing the examples given in the coming sections.

Theorem 4. *If $v(y,t) = \sum_{k=1}^{\infty}\sum_{\ell=1}^{\infty} c_{k\ell}(pL)_k(y)(pL)_\ell(t)$ and the exact solution of equation (1) is defined on $\Lambda\times(0,\tau]$, then the following hold:*

$$(1)\quad |c_{k\ell}| \le \frac{\mu^{k+\ell-2}}{2^{k+\ell-2}(k-1)!(\ell-1)!}\cosh^2\mu, \tag{43}$$

where $|v^{(j)}(0,0)| \le \mu^j, j \ge 0$ where μ is a positive constant.

(2) The series converges absolutely

Proof. From Lemma 1.

$$|c_{kl}| \le \sum_{i=0}^{\infty}\sum_{j=0}^{\infty}\frac{k(2i+k-1)!\mathrm{u}_{2i+k-1}}{2^{2i+k-1}i!(i+k)!}\frac{\ell(2j+\ell-1)!\mathrm{u}_{2j+\ell-1}}{2^{2j+\ell-1}j!(j+\ell)!}. \tag{44}$$

Using the given assumptions, we have

$$|c_{kl}| \le k\ell\sum_{i=0}^{\infty}\sum_{j=0}^{\infty}\frac{\mu^{2i+2j+k+\ell-2}}{2^{2i+2j+k+\ell-2}i!j!(i+k)!(j+\ell)!} = \frac{4k\ell}{\mu^2}I_k(\mu)I_\ell(\mu). \tag{45}$$

By applying Lemma 2, we obtain the desired results of the first part. For the second part, from Lemma 3, we obtain

$$\left|c_{k\ell}(pL)_k(y)(pL)_\ell(t)\right| \le \frac{\mu^{k+\ell-2}3^{k+\ell}}{2^{k+\ell-2}(k-1)!(\ell-1)!}\cosh^2\mu. \tag{46}$$

So

$$\begin{aligned}&\sum_{k=1}^{\infty}\sum_{\ell=1}^{\infty}\left|c_{k\ell}(pL)_k(y)(pL)_\ell(t)\right|\\ &\quad\le \left(\cosh^2\mu\right)\sum_{k=1}^{\infty}\sum_{\ell=1}^{\infty}\frac{\mu^{k+\ell-2}3^{k+\ell}}{2^{k+\ell-2}(k-1)!(\ell-1)!} = 9e^{3\mu}\cosh^2\mu.\end{aligned} \tag{47}$$

Thus, the proof completes. □

Theorem 5. *If Theorem 4 is satisfied and the truncation error is $\varepsilon_M(y,t) = v(y,t) - v_{M+1}(y,t)$, where $v_{M+1}(y,t) = \sum_{k=1}^{M+1}\sum_{\ell=1}^{M+1} c_{k\ell}(pL)_k(y)(pL)_\ell(t)$ is the approximate solution of equation (1), then the following estimation is true:*

$$|\varepsilon_M(y,t)| < \frac{18e^{3\mu}}{(M+1)!}\left(\frac{3\mu}{2}\right)^{M+1}\cosh^2\mu. \tag{48}$$

Proof. From the definition of $\varepsilon_M(y,t)$, we have

$$\begin{aligned}\varepsilon_M(y,t) &= \sum_{k=1}^{\infty}\sum_{\ell=1}^{\infty}c_{k\ell}(pL)_k(y)(pL)_\ell(t)\\ &\quad - \sum_{k=1}^{M+1}\sum_{\ell=1}^{M+1}c_{k\ell}(pL)_k(y)(pL)_\ell(t)\\ &= \sum_{k=1}^{M+1}\sum_{\ell=M+2}^{\infty}c_{k\ell}(pL)_k(y)(pL)_\ell(t)\\ &\quad + \sum_{k=M+2}^{\infty}\sum_{\ell=1}^{\infty}c_{k\ell}(pL)_k(y)(pL)_\ell(t).\end{aligned} \tag{49}$$

Using Theorem 4 and Lemma 3 and collecting the summation, we get

$$|\varepsilon_M(y,t)| \le 9e^{3\mu}\left(1 - \frac{(\Gamma(M+1,(3\mu/2)))^2}{(\Gamma(M+1))^2}\right)\cosh^2\mu, \tag{50}$$

where $\Gamma(.)$ and $\Gamma(.,.)$ are gamma and incomplete gamma functions, respectively. So

$$\Gamma(M+1)-\Gamma\left(M+1,\frac{3\mu}{2}\right)<\int_0^{3\mu/2}y^M dy=\frac{(3\mu/2)^{M+1}}{M+1}. \tag{51}$$

Then, the right hand side of the above inequality can be simplified as

$$\begin{aligned}|\varepsilon_M(y,t)|&<\frac{9e^{3\mu}}{(M+1)!}\left(\frac{3\mu}{2}\right)^{M+1}\left(2-\frac{(3\mu/2)^{M+1}}{(M+1)!}\right)\cosh^2\mu,\\&<\frac{18e^{3\mu}}{(M+1)!}\left(\frac{3\mu}{2}\right)^{M+1}\cosh^2\mu.\end{aligned} \tag{52}$$

Thus, the inequality holds. □

Theorem 6. *If $v(y,t)$ satisfies the hypotheses of Theorem 5, and by assuming*

$$\begin{aligned}R_{M+1}(y,t)&=\left|{}_cD_{0,t}^{\lambda}v_{M+1}(y,t)+\beta\left(v_y\right)_{M+1}(y,t)-h(y,t)\right|,\\\mathfrak{R}_{M+1}&=\max_{\substack{y\in\Lambda,\\t\in(0,\tau]}}R_{M+1}(y,t),\end{aligned} \tag{53}$$

and $1+|\beta|\le\sigma$ (a positive constant), then we have the following global error estimation:

$$|\mathfrak{R}_{M+1}|\le\frac{54\sigma e^{3\mu}}{(M+1)!}\left(\frac{3\mu}{2}\right)^{M+1}\cosh^2\mu. \tag{54}$$

Proof. From equation (1), we have

$$h(y,t)={}_cD_{0,t}^{\lambda}v(y,t)+\beta v_y(y,t). \tag{55}$$

So, we obtain

$$R_{M+1}(y,t)\le\left|{}_cD_{0,t}^{\lambda}(v_{M+1}(y,t)-v(y,t))\right|+|\beta||(v_{M+1}(y,t)-v(y,t))|. \tag{56}$$

Using Theorem (2) and Lemma (3), this estimation is transformed to

$$\begin{aligned}R_{M+1}(y,t)\le(1+|\beta|)\left(\cosh^2\mu\right)&\left(\sum_{k=1}^{M+1}\sum_{\ell=M+2}^{\infty}+\sum_{k=M+2}^{\infty}\sum_{\ell=1}^{\infty}\right)\\&\cdot\left(\frac{\mu^{k+\ell-2}3^{k+\ell+1}}{2^{k+\ell-2}(k-1)!(\ell-1)!}\right).\end{aligned} \tag{57}$$

Table 1: Maximum absolute error E with PLC method.

(a)

λ	M	E	M	E	M	E
0.4		0		1.1×10^{-14}		1.2×10^{-13}
0.6	2	0	3	1.8×10^{-15}	4	6.2×10^{-14}
0.8		0		1.6×10^{-15}		8.9×10^{-15}

(b) L^2 errors with L1/DG method

M	$\lambda=0.4$	$\lambda=0.6$	$\lambda=0.8$
64	7.3×10^{-4}	1×10^{-3}	2.1×10^{-3}
128	2.7×10^{-4}	4.2×10^{-4}	9.3×10^{-4}
256	9.5×10^{-5}	1.7×10^{-4}	4.1×10^{-4}
512	3.3×10^{-5}	6.4×10^{-5}	1.8×10^{-4}
1024	1.1×10^{-5}	2.5×10^{-5}	7.9×10^{-5}

(c)

CPU time	C_N
98.436	1.6×10^{-15}
696.998	7.3×10^{-15}
2333.64	9.2×10^{-15}

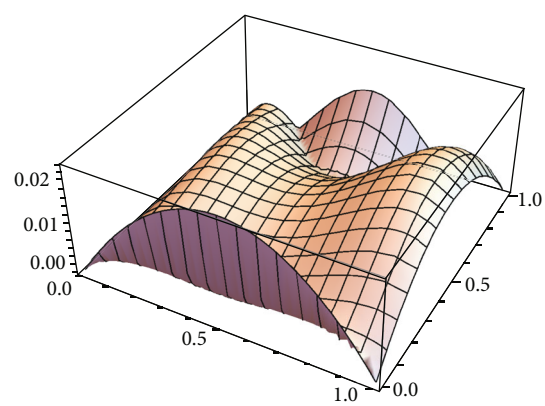

Figure 1: Graph of the numerical solutions at $\lambda=0.4$.

By evaluating the summation, we obtain

$$|\mathfrak{R}_{M+1}|\le27\sigma e^{3\mu}\left(1-\frac{(\Gamma(M+1,(3\mu/2)))^2}{(\Gamma(M+1))^2}\right)\cosh^2\mu. \tag{58}$$

The proof of the required result is similar to the proof in the given last theorem. □

6. Numerical Examples

In this section, we demonstrate two examples using Pell polynomials for solving equation (1). Then, the comparison

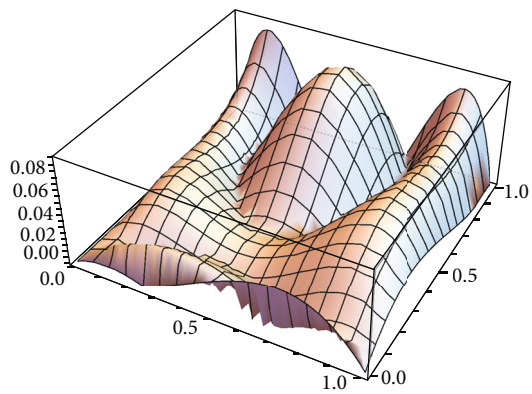

Figure 2: Graph of the numerical solutions at $\lambda = 0.6$.

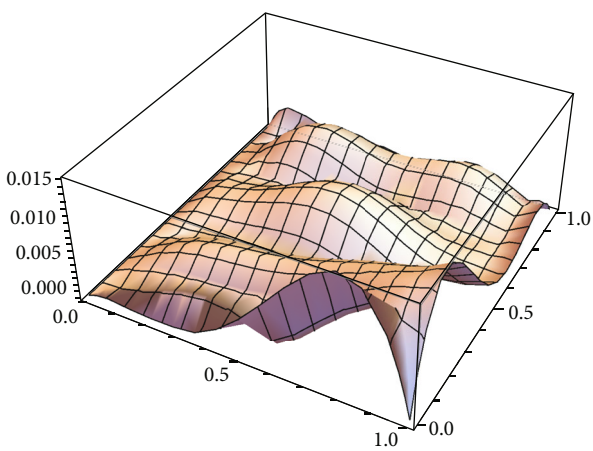

Figure 3: Graph of the numerical solutions at $\lambda = 0.8$.

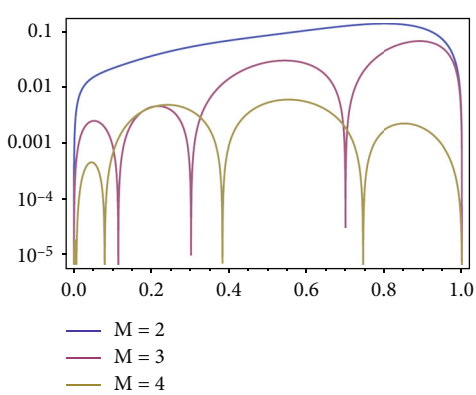

Figure 4: Graph of the absolute errors at M =2, 3, 4.

of the used method and the method in [27] shows the efficiency of our method.

Example 1. Consider the one-dimensional time-fractional convection equation (1) with conditions

$$\begin{aligned} v(y,0) &= 0, y \in (0,1), \\ v(0,t) &= 0, t \in (0,1]. \end{aligned} \tag{59}$$

Table 2: Maximum absolute error E with PLC method

(a)

λ	M	E
0.4		0
0.6	2	2.6×10^{-13}
0.8		5.7×10^{-14}

(b) L^2 errors with L1/DG methods

M	$\lambda = 0.4$	$\lambda = 0.6$	$\lambda = 0.8$
4	2.8×10^{-3}	2.7×10^{-3}	2.7×10^{-3}
8	3.5×10^{-4}	3.5×10^{-4}	3.5×10^{-4}
16	4.4×10^{-5}	4.4×10^{-5}	4.2×10^{-5}
32	5.4×10^{-6}	5.1×10^{-6}	5.2×10^{-6}

(c)

CPU time	C_N
374.563	2.6×10^{-13}
405.828	2.03×10^{-13}
350.329	9.2×10^{-13}

where

$$\begin{aligned} h(y,t) = &\left(\Gamma(\lambda+1) + \frac{2t^{2-\lambda}}{\Gamma(3-\lambda)}\right) \sin(\pi y) \\ &+ \pi\left(t^2 + t^\lambda\right) \cos(\pi y). \end{aligned} \tag{60}$$

The exact solution of this equation is $v(y,t) = (t^2 + t^\lambda) \sin(\pi y)$.

In Table 1, we observe that the absolute errors obtained by Pell collocation (PLC) method at M=2, 3, and 4 are better than obtained by the L1-discontinuous Galerkin (L1/DG) method [27]. Figures 1–3 display the numerical solutions at λ =0.4, 0.6, and 0.8. The absolute errors at the same values are plotted in Figure 4. It is clear that the last figure of the absolute errors decreases drastically with decreasing the number of steps.

Example 2. Consider the one-dimensional time-fractional convection equation (1) with conditions

$$\begin{aligned} v(y,0) &= \begin{cases} y^2(1-y)^2, y \in \left(0, \frac{1}{2}\right) \\ -y^2(1-y)^2, y \in \left(\frac{1}{2}, 1\right) \end{cases}, \\ v(0,t) &= 0, t \in (0,1]. \end{aligned} \tag{61}$$

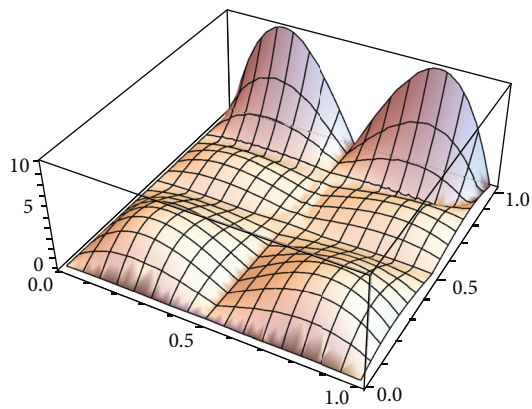

Figure 5: Graph of the numerical solutions at $\lambda = 0.4$.

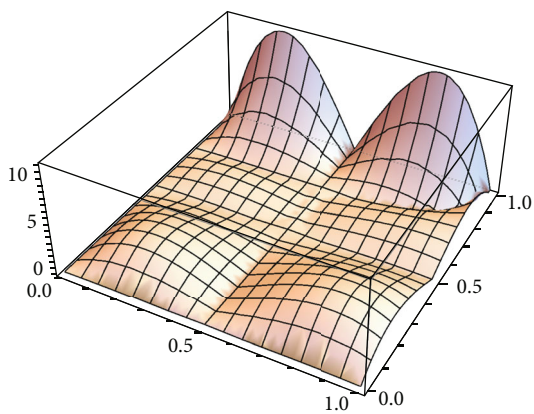

Figure 6: Graph of the numerical solutions at $\lambda = 0.6$.

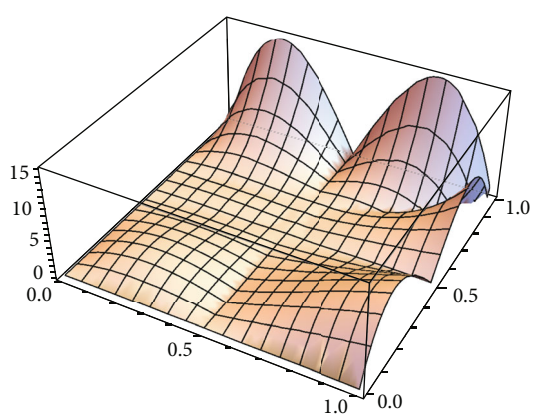

Figure 7: Graph of the numerical solutions at $\lambda = 0.8$.

where

$$h(y,t) = \begin{cases} \left(\Gamma(\lambda+1) + \dfrac{2t^{2-\lambda}}{\Gamma(3-\lambda)}\right) y^2(1-y)^2 + \left(t^2 + t^\lambda + 1\right) 2y(1-y)(1-2y), y \in \left(0, \dfrac{1}{2}\right) \\ -\left(\Gamma(\lambda+1) + \dfrac{2t^{2-\lambda}}{\Gamma(3-\lambda)}\right) y^2(1-y)^2 - \left(t^2 + t^\lambda + 1\right) 2y(1-y)(1-2y), y \in \dfrac{1}{2}, 1\Big) \end{cases}. \tag{62}$$

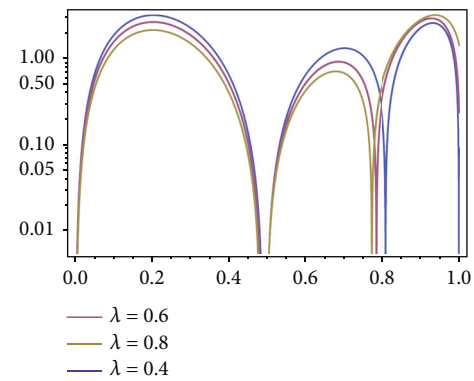

Figure 8: Graph of the absolute errors at $M = 2$ and different values of λ.

The exact solution of this equation is $v(y,t) = \begin{cases} (t^2 + t^\lambda + 1) y^2 (1-y)^2, y \in (0, 1/2) \\ -(t^2 + t^\lambda + 1) y^2 (1-y)^2, y \in 1/2, 1) \end{cases}$.

Table 2 lists the numerical solutions of our method at $M = 2$ and different values of λ. These solutions and the absolute errors are plotted in Figures 5–8. From Figure 8, we observe that the convergence is exponential, and the errors are better with decreasing the number of steps. We notice that the obtained errors are the best and the least.

7. Conclusion

Due to this method, we demonstrate two examples which show the high accuracy of our suggested method and also it is easy to apply. The Mathematica software was agreeable surprised with the results of this method. We also show that any system of linear equations can borrow the given method. The comparison of the method and the non-uniform L1-discontinuous Galerkin (DG) method shows that the spectral solution in ours is more efficient. The truncation and global errors are discussed. Finally, we conclude that the proposed method can solve different kinds of fractional differential equations and integral equations. Finally, Pell polynomial is not the best choice to approximate the solutions of differential equations. I think—as far as I know—the orthogonal Chebyshev polynomials are better.

Data Availability

No data is associated with this research.

Conflicts of Interest

The author declares that she has no competing interest.

Authors' Contributions

The author confirms that this is her own work.

Acknowledgments

The author is very grateful to the anonymous referees for careful reviewing and crucial comments, which enabled me to improve the manuscript.

References

[1] Z. Odibat and S. Momani, "The variational iteration method: an efficient scheme for handling fractional partial differential equations in fluid mechanics," *Computers & Mathematics with Application*, vol. 58, no. 11-12, pp. 2199–2208, 2009.

[2] B. K. Singh and P. Kumar, "Fractional variational iteration method for solving fractional partial differential equations with proportional delay," *International Journal of Differential Equations*, vol. 2017, Article ID 5206380, 11 pages, 2017.

[3] A. A. Elbeleze, A. Kilicman, and M. T. Bachok, "Fractional variational iteration method and its Application to fractional partial differential equation," *Mathematical Problems in Engineering*, vol. 2013, Article ID 543848, 10 pages, 2013.

[4] Y. Zhang, "A finite difference method for fractional partial differential equation," *Applied Mathematics and Computation*, vol. 215, no. 2, pp. 524–529, 2009.

[5] F. Zeng, "Finite difference method for fractional differential equations," *International Journal of Bifurcation and Chaos*, vol. 22, no. 4, article 1230014, p. 28, 2012.

[6] K. A. Mustapha, K. M. Furati, O. M. Knio, and O. P. Le Maitre, "A finite difference method for space fractional differential equations with variable diffusivity coefficient," *Communications on Applied Mathematics and Computation*, vol. 2, no. 4, pp. 671–688, 2020.

[7] Y. Jiang and J. Ma, "High-order finite element methods for time-fractional partial differential equations," *Journal of Computational and Applied Mathematics*, vol. 235, no. 11, pp. 3285–3290, 2011.

[8] Y. Zheng, C. Li, and Z. Zhao, "A note on the finite element method for the space-fractional advection diffusion equation," *Computers & Mathematics with Application*, vol. 59, no. 5, pp. 1718–1726, 2010.

[9] J. Lai, F. Liu, V. V. Anh, and Q. Liu, "A space-time finite element method for solving linear Riesz space fractional partial differential equations," *Numerical Algorithms*, vol. 88, no. 1, pp. 499–520, 2021.

[10] A. S. Mohamed, "Shifted Jacobi collocation method for Volterra-Fredholm integral equation," *Computational Methods for Differential Equations*, vol. 10, no. 2, pp. 408–418, 2021.

[11] A. S. Mohamed and M. M. Mokhtar, "Spectral tau-Jacobi algorithm for space fractional advection-dispersion problem," *Applications ana Applied Mathematics: An International Journal*, vol. 14, no. 1, pp. 548–561, 2019.

[12] E. H. Doha, A. H. Bahraws, and S. S. Ezz-Eldien, "A new Jacobi operational matrix: an application for solving fractional differential equations," *Applied Mathematical Modelling*, vol. 36, no. 10, pp. 4931–4943, 2012.

[13] A. G. Atta, W. M. Abd-Elhameed, G. M. Moatimid, and Y. H. Youssri, "Shifted fifth-kind Chebyshev Galerkin treatment for linear hyperbolic first- order partial differential equations," *Applied Numerical Mathematics*, vol. 167, no. 2021, pp. 237–256, 2021.

[14] W. M. Abd-Elhameed and Y. H. Youssri, "Spectral solutions for fractional differential equations via a novel Lucas operational matrix of fractional derivatives," *Romanian Journal of Physics*, vol. 61, no. 5-6, pp. 795–813, 2016.

[15] C. Muhammed, S. Mehmed, and G. Coskun, "Lucas polynomial approach for system of high-order linear differential equations and residual error estimation," *Mathematical Problems in Engineering*, vol. 2015, Article ID 625984, 14 pages, 2015.

[16] A. S. Mohamed, "Spectral solutions with error analysis of Volterra-Fredholm integral equation via generalized Lucas collocation mathod," *International Journal of Applied and Computational Mathematics*, vol. 7, no. 5, 2021.

[17] W. M. Abd-Elhameed and Y. H. Youssri, "Generalized Lucas polynomial sequence approach for fractional differential equations," *Nonlinear Dynamics*, vol. 89, no. 2, pp. 1341–1355, 2017.

[18] M. M. Mokhtar and A. S. Mohamed, "Lucas polynomials semi-analytic solution for fractional multi-term initial value problems," *Advances in Difference Equations*, vol. 2019, no. 1, 13 pages, 2019.

[19] Y. H. Youssri, W. M. Abd-Elhameed, A. S. Mohamed, and S. M. Sayed, "Generalized Lucas polynomial sequence treatment of fractional pantograph differential equation," *International Journal of Apllied Computational Mathematics*, vol. 7, no. 2, pp. 1–16, 2021.

[20] W. M. Abd-Elhameed and Y. H. Youssri, "Connection formulae between generalized Lucas polynomials and some Jacobi polynomials: application to certain types of fourth-order BVPs," *Applied and Computational Mathematics*, vol. 6, no. 2, pp. 1–19, 2020.

[21] W. M. Abd-Elhameed and Y. H. Youssri, "Spectral tau algorithm for certain coupled system of fractional differential equations via generalized Fibonacci polynomial sequence," *Iranian Journal of Science and Technology, Transactions A: Science*, vol. 43, no. 2, pp. 543–554, 2019.

[22] I. Ali, S. Haq, K. N. Sooppy, and D. Baleanu, "An efficient numerical scheme based on Lucas polynomials for the study of multidimensional Burgers-type equations," *Advances in Difference Equations*, vol. 2021, no. 1, 24 pages, 2021.

[23] I. Ali and S. Haq, "Lucas and Fibonacci polynomials based approach for the study of one- and two-dimensional Burger and heat-type equations," *Arabian Journal of Mathematics*, 2020.

[24] S. Haq and I. Ali, "Approximate solution of two-dimensional Sobolev equation using a mixed Lucas and Fibonacci polynomials," *Engineering with Computers*, pp. 1–11, 2021.

[25] I. Ali, S. Haq, and K. N. Sooppy, "A computational study of two-dimensional reaction-diffusion Brusselator system with applications in chemical processes," *Alexandria Engineering Journal*, vol. 60, no. 5, pp. 4381–4392, 2021.

[26] Y. H. Youssri, "A new operational matrix of Caputo fractional derivatives of Fermat polynomials: an application for solving the Bagley-Torvik equation," *Advances in Difference Equations*, vol. 2017, no. 1, 17 pages, 2017.

[27] Z. Wang, "Non-uniform L1/DG method for one-dimensional time-fractional convection equation," *Computational Methods for Differential Equations*, vol. 9, no. 4, pp. 1069–1082, 2021.

[28] P. F. Byrd, "Expansion of analytic functions in polynomials associated with Fibonacci numbers," *Fibonacci Q*, vol. 1, no. 1, pp. 16–27, 1963.

[29] Y. L. Luke, "Inequalities for generalized hypergeometric functions," *Journal of Approximation Theory*, vol. 5, no. 1, pp. 41–65, 1972.

Hindawi
Journal of Function Spaces
Volume 2022, Article ID 3553021, 26 pages
https://doi.org/10.1155/2022/3553021

Research Article

A Mathematical Analysis on the New Fractal-Fractional Model of Second-Hand Smokers via the Power Law Type Kernel: Numerical Solutions, Equilibrium Points, and Sensitivity Analysis

S. Rezapour,[1,2] **S. Etemad**,[1] **M. Sinan**,[3] **J. Alzabut**,[4,5] **and A. Vinodkumar**[6]

[1]*Department of Mathematics, Azarbaijan Shahid Madani University, Tabriz, Iran*
[2]*Department of Medical Research, China Medical University Hospital, China Medical University, Taichung, Taiwan*
[3]*School of Mathematical Sciences, University of Electronic Science and Technology of China, Chengdu 611731, China*
[4]*Department of Mathematics and Sciences, Prince Sultan University, Riyadh 11586, Saudi Arabia*
[5]*Department of Industrial Engineering, OSTİM Technical University, 06374 Ankara, Turkey*
[6]*Department of Mathematics, Amrita School of Engineering, Amrita Vishwa Vidyapeetham, Coimbatore 641112, India*

Correspondence should be addressed to S. Etemad; sina.etemad@azaruniv.ac.ir

Received 10 December 2021; Accepted 25 March 2022; Published 10 May 2022

Academic Editor: Youssri Hassan Youssri

The second-hand smoke is a phenomenon that needs to be investigated, and its effects on the health of the people are to be examined. To analyze such an issue, the mathematical models are the best tools that help us to study the dynamical behaviors of this phenomenon. For this purpose, in the present paper, we consider a three-compartmental fractal-fractional mathematical model of a specific population of smokers or people that are exposed to second-hand smoke. By assuming some conditions on ϕ-ψ-contractions and compact operators, we prove some theorems in relation to the existence of solutions. The Banach principle for the usual contractions is used for proving the uniqueness of solutions. Next, by some notions of functional analysis, two types of Ulam-Hyers stability for the fractal-fractional second-hand smoker model are established. Moreover, we have a steady-state analysis and obtain equilibrium points and basic reproduction number R_0. Then, we investigate the sensitivity of the fractal-fractional system with respect to each parameter. For numerical simulation, the Adams-Bashforth (AB) method is used to derive numerical schemes for plotting and simulating the approximate solutions. Finally, the obtained solutions are tested with real data and different values of fractal dimensions and fractional orders.

1. Introduction

The notion of the second-hand smoke is considered as the combination of smoke caused by the burning end of a cigarette, the smoke that is exhaled by a smoker, or smoke caused due to other tobacco products [1]. Therefore, being in the exposure of second-hand smoke, it involves an unintentional inhalation of smoke that happens near the people smoking or inhalation in an indoor environment where tobacco has been recently used. The people may be exposed to the second-hand smoke in different places that includes public places, home, private or public transport, workplace, home of relatives, and buses [2, 3]. Nowadays, the exposure to second-hand smoke is considered one of the main risk factor for a class of diseases and harmful health-related results at a vast scale and is evaluated to cause more than 600,000 deaths in each year.

There exists an apparent relation between the factor of the second-hand smoke and an increased danger of stroke. Being in exposure to the second-hand smoke regularly in some public environment increases the chance of stroke by fifty percent [4]. At the same time, the second-hand smoke is as damaging to a fetus as if the mothers were inhaling the smoke directly from a cigarette [5]. Only 30 minutes of exposure to second-hand smoke can result in heart diseases similar to that of habitual smokers [6]. In view of these

items, being in exposure to second-hand smoke is regarded a subject of great concern for all of the people due to its familiar harmful effects on the human health.

Some of researchers have discussed about the adverse effects of second-hand smoke on the health problem as well. In 2011, Lubick et al. [7] conducted a research on the global health burden of the second-hand smoke, and in the same year, Burton [8] focused on an alarming consequence of smoking in indoor places. All the aforementioned studies indicate that the second-hand smoke is a significant problem worldwide.

The importance of this issue led to a number of researches being done in precise mathematical formats, because we have to model these phenomena to study their exact behaviors. Even during the recent years, researchers have modeled many phenomena and diseases by applying new mathematical operators and analyzed such systems numerically and analytically. Their findings help us to take steps about that specific disease and to control the speed of its spread. Instances of such a modeling can be found in [9, 10] by studying electrical circuits and some processes in engineering, in [11–14] for analyzing COVID-19, in [15, 16] for cancer treatment, in [17–19] for investigating different diseases, in [20–22] for controlling some viruses, in [23, 24] for studying some social problems, in [25, 26] for investigating some phenomena in relation to animals and agriculture, etc. More specifically, the operators with Mittag-Leffler-type kernels play an important role in recent mathematical modelings. To see these important phenomena, we can even enumerate some new works in this regard. Khan et al. [27] studied a fractional COVID-19 epidemic model with a convex incidence rate with the help of the Atangana-Baleanu operators in the Caputo sense and analyzed the optimal control on the amount of the infection. In [28], Akgul solved an Atangana-Baleanu fractional differential equation with the reproducing kernel Hilbert space method.

In this direction, the second-hand smoke is also a phenomenon which is important to investigate its effects based on mathematical models. To know some previous works about smoking models, Alkhudhari et al. [29] conducted a research on the global dynamics in relation to smoking on temporary quitters in 2014. One year later, Verma et al. [30] investigated a new model for the smoking cessation and the effects of media campaigns on this issue. Recently in 2019, Adhana et al. [31] studied a model of smoking tobacco in the form of a case study in Ethiopia and analyzed the smoking generation number (SGN) in relation to the given mathematical system. Pulecio-Montoya et al. [32] designed a model of the growth of tobacco consumers and simulated it by the fourth-order Runge-Kutta techniques.

In last decades, Atangana [33] introduced a new advanced kind of derivatives entitled fractal-fractional derivative that connects the two topics of fractional calculus and fractal calculus. Further, he extended the relevant fractal-fractional integral. The construction of such operators is in the form of the convolution of the power-law, exponential-law, and generalized Mittag-Leffler-law type kernels with fractal derivatives. Fractal-fractional operators have two components: one is the fractional order and the second is the fractal dimension (order). Actually, differential equations furnished with the fractal-fractional derivative transfer the order and dimension of the supposed system into a rational order system.

According to this property, we can extend the usual differential equations to generalized systems with arbitrary order of derivatives and dimensions. In other words, the basic aim for defining these derivatives is to study nonlocal BVPs/IVPs in nature that contain fractal behaviors. In this direction, some mathematicians established several results and designed some fractal-fractional models that show better simulations for describing mathematical structures. For instance, Gomez-Aguilar et al. [34] analyzed the transmission of malaria with the help of these fractal-fractional operators. The situation and spread of coronavirus in Pakistan were studied in the form of a fractal-fractional model by Shah et al. in 2020 [35]. Also, one year later, Ali et al. developed another fractal-fractional model of COVID-19 based on the data extracted from Wuhan [36]. In [37], Farman et al. analyzed the solutions of a fractal fractional Atangana-Baleanu model of COVID-19 via the Atangana-Toufik scheme. In other paper, published by Amin et al. [38], the authors used the same fractal-fractional operators for investigating the effect of vaccination to control COVID-19. More recently, Alqhtani and Saad [39] used three types of fractal-fractional operators via the power-law, exponential decay, and Mittag-Leffler kernels for modeling Michaelis-Menten Enzymatic Reaction and compared their numerical results with the classical results. Also, Saad et al. [40] used the Caputo-Fabrizio fractal-fractional derivatives to model the hepatitis C virus infection and analyzed numerical solutions and their chaos with respect to different values of parameters.

In the present study, we will consider a three-compartmental mathematical model of a specific population of smokers or people that are exposured to second-hand smoke, and we will analyze and interpret our findings and model graphically, numerically, and analytically. Also, note that due to the importance of fixed point theory in proving the existence results, most of researchers use the main theorems of this field for confirming the existence of solutions for vide range of mathematical models. For instance, there are different theorems such as the Leray-Schauder fixed point theorem, Krasnoselskii's fixed point theorem [41], some fixed point theorems in partial metric spaces [42], or some special contractions such as F-contractions [43] and ϕ-ψ-contractions [44]. Here, we will use these new contractions for proving the existence of solutions.

We emphasize that the basic contribution and also the novelty of this work is that we compute and obtain our results based on a new model of second-hand smokers designed by the fractal-fractional derivatives for the first time. In the mentioned structure, we use power-law type kernel for this fractal-fractional derivative. Also, for the first time, to prove the existence of solutions, ϕ-admissible maps and ϕ-ψ-contractions play an important role in this study. Moreover, we try to investigate different stability results for the given model and at the end of the paper, we see that

our simulative graphs show the accuracy and applicability of the fractal-fractional operators in comparison to other usual fractional operators. Also, we again emphasize that this is the first work on the application of the fractal-fractional derivatives for modeling dynamics of second-hand smokers. The numerical and graphical results obtained in this work show that we can analyze different qualitative behaviors of mathematical models under the effect of the fractal dimension and fractional order of these new operators and obtain better and more accurate results with the help of real data. This confirms the considerable advantages of the fractal-fractional operators.

This model will be studied from several aspects. In the first place, after describing the suggested fractal-fractional model, we investigate existence theory based on two criteria in relation to ϕ-ψ-contractions and compact operators. The Banach principle for usual contractions is utilized for proving the uniqueness result. Next, by notions of functional analysis, two types of Ulam-Hyers stability of the fractal-fractional system are established. In the sequel, we have a steady-state analysis and obtain equillibria and reproduction number R_0, and then we investigate the sensitivity of the fractal-fractional system with respect to each parameter. For numerical simulation, a fractional type of two-step Lagrange polynomial known as the fractional Adams-Bashforth (AB) method is utilized to derive numerical schemes for plotting and simulating the results. Finally, the obtained solutions are tested with real data and different values of fractal and fractional orders.

2. Preliminaries

In this section, we recall some definitions and properties on the fractal-fractional operators and some self-maps including ϕ-ψ-contractions.

We consider the family Ψ of all increasing functions $\psi : [0,\infty) \longrightarrow [0,\infty)$ such that

$$\sum_{j=1}^{\infty} \psi^j(\mathfrak{t}) < \infty, \psi(\mathfrak{t}) < t, \forall t > 0. \tag{1}$$

Definition 1 (see [44]). Let $\mathcal{F} : \mathbb{X} \longrightarrow \mathbb{X}$ and $\phi : \mathbb{X}^2 \longrightarrow \mathbb{R}_{\geq 0}$, where $\mathbb{X}$ is a normed space. Then,

(1) For $\varkappa_1, \varkappa_2 \in \mathbb{X}$, $\mathcal{F}$ is ϕ-ψ-contraction if

$$\phi(\varkappa_1, \varkappa_2)\mathrm{d}(\mathcal{F}\varkappa_1, \mathcal{F}\varkappa_2) \leq \psi(d(\varkappa_1, \varkappa_2)). \tag{2}$$

(2) $\mathcal{F}$ is ϕ-admissible if

$$\phi(\varkappa_1, \varkappa_2) \geq 1 \Longrightarrow \phi(\mathcal{F}\varkappa_1, \mathcal{F}\varkappa_2) \geq 1. \tag{3}$$

Definition 2 (see [33]). Let a continuous function $\mathcal{F} : (a, b) \longrightarrow [0,\infty)$ be fractal differentiable of fractal order ν. Then, the fractal-fractional derivative of $\mathcal{F}$ equipped with the power-law-type kernel of order ω in the sense of Riemann-Liouville is defined by

$${}^{\mathrm{FFP}}\mathfrak{D}_{a,\mathfrak{t}}^{\omega,\nu}\mathcal{F}(\mathfrak{t}) = \frac{1}{\Gamma(n-\omega)}\frac{\mathrm{d}}{\mathrm{d}\mathfrak{t}^{\nu}}\int_a^{\mathfrak{t}} (\mathfrak{t}-\mathfrak{w})^{n-\omega-1}\mathcal{F}(\mathfrak{w})\mathrm{d}\mathfrak{w}, \tag{4}$$

where $\mathrm{d}\mathcal{F}(\mathfrak{w})/\mathrm{d}\mathfrak{w}^{\nu} = \lim_{\mathfrak{t}\longrightarrow\mathfrak{w}}((F(t)-F(w))/(t^{\nu}-w^{\nu}))$ is the fractal derivative and $n-1 < \omega, \nu \leq n \in \mathbb{N}$.

One can simply observed that by letting $\nu = 1$, the fractal-fractional derivative ${}^{\mathrm{FFP}}\mathfrak{D}_{a,\mathfrak{t}}^{\omega,\nu}$ is the same standard Riemann-Liouville derivative ${}^{\mathrm{RL}}\mathfrak{D}_{a,\mathfrak{t}}^{\omega}$ of order ω.

Definition 3 (see [33]). A continuous function $\mathcal{F}$ defined on (a, b) is fractal-fractional integrable of the fractional and fractal orders ω and ν, respectively, via the power-law-type kernel if the integral

$${}^{FFP}\mathfrak{I}_{a,\mathfrak{t}}^{\omega,\nu}\mathcal{F}(\mathfrak{t}) = \frac{\nu}{\Gamma(\omega)}\int_a^{\mathfrak{t}} \mathfrak{w}^{\nu-1}(\mathfrak{t}-\mathfrak{w})^{\omega-1}\mathcal{F}(\mathfrak{w})\mathrm{d}\mathfrak{w} \tag{5}$$

exists, where $\nu, \omega > 0$.

3. Description of the Model for Second-Hand Smokers

This model of second-hand smoker tobacco involves a system of three differential equations [45]. The compartments are $\mathcal{P}(\mathfrak{t})$, $\mathcal{S}(\mathfrak{t})$, and $\mathcal{Q}(\mathfrak{t})$. It is notable that $\mathcal{P}(\mathfrak{t})$ represents the second-hand smokers or those (at risk of) exposure to others smoking, $\mathcal{Q}(\mathfrak{t})$ denotes a group of persons who have cessated smoking but are at risk because of their previous smoking habit, and $\mathcal{S}(\mathfrak{t})$ is a group of persons who are addicted to tobacco and smoke it yet. The variable as well as parameters used in the model is all nonnegative. Meaning of variables and parameters is given in the sequel. With the above assumptions, and based on [45], the second-hand smoker (SHS) model is provided by a system of ODEs in the form:

$$\begin{cases} \mathcal{P}'(\mathfrak{t}) = \theta - (s + q_1 + r)\mathcal{P}(\mathfrak{t}) - b\mathcal{S}(\mathfrak{t})\mathcal{P}(\mathfrak{t}), \\ \mathcal{S}'(\mathfrak{t}) = b\mathcal{P}(\mathfrak{t})\mathcal{S}(\mathfrak{t}) + r_1\mathcal{Q}(\mathfrak{t})\mathcal{S}(\mathfrak{t}) - (q_1 + q_2 + r_2)\mathcal{S}(\mathfrak{t}), \\ \mathcal{Q}'(\mathfrak{t}) = r_2\mathcal{S}(\mathfrak{t}) - r_1\mathcal{S}(\mathfrak{t})\mathcal{Q}(\mathfrak{t}) - (q_3 + q_1 + \gamma)\mathcal{Q}(\mathfrak{t}), \end{cases} \tag{6}$$

where θ is the number of healthful individuals who are also at risk of smoker people, q_1 stands for the natural mortality rate per total population, s is the death rate of second-hand smoker persons because of exposure to second-hand smoke, q_2 is the death rate of individuals by smoking tobacco, q_3 is the death rate of quit because of smoking habit before transferring to the phase $\mathcal{Q}$, r is the exit rate of second-hand smoker to the healthful individuals, γ is the exit rate of persons who have cessation smoking to the healthful people, b is the infection rate from $\mathcal{P}$ to $\mathcal{S}$, r_2 is the exit rate from $\mathcal{S}$ to $\mathcal{Q}$, and r_1 is the infection rate from $\mathcal{Q}$ to $\mathcal{S}$. The limitations

for these parameters are $\theta > 0$, $0 < s \leq 1$, $0 < q_1 < 1$, and $0 \leq r, b, r_1, q_2, r_2, q_3, \gamma \leq 1$. The initial conditions are $\mathscr{P}(0) = \mathscr{P}_0 \geq 0$, $\mathscr{S}(0) = \mathscr{S}_0 \geq 0$, and $\mathscr{Q}(0) = \mathscr{Q}_0 \geq 0$.

Motivated by the above standard model, we here consider the fractal-fractional model of the second-hand smoker in the following structure:

$$\begin{cases} {}^{FFP}\mathfrak{D}_{0,\mathfrak{t}}^{\omega,\nu}\mathscr{P}(\mathfrak{t}) = \theta - (s + q_1 + r)\mathscr{P}(\mathfrak{t}) - \mathrm{b}\mathscr{S}(t)\mathscr{P}(\mathfrak{t}), \\ {}^{FFP}\mathfrak{D}_{0,\mathfrak{t}}^{\omega,\nu}\mathscr{S}(\mathfrak{t}) = b\mathscr{P}(t)\mathscr{S}(t) + r_1\mathscr{Q}(\mathfrak{t})\mathscr{S}(t) - (q_1 + q_2 + r_2)\mathscr{S}(t), \\ {}^{FFP}\mathfrak{D}_{0,\mathfrak{t}}^{\omega,\nu}\mathscr{Q}(\mathfrak{t}) = \mathrm{r}_2\mathscr{S}(t) - r_1 S(\mathfrak{t})\mathscr{Q}(t) - (q_3 + q_1 + \gamma)\mathscr{Q}(t), \end{cases} \tag{7}$$

subject to

$$\mathscr{P}(0) = \mathscr{P}_0 \geq 0, \mathscr{S}(0) = \mathscr{S}_0 \geq 0, \mathscr{Q}(0) = \mathscr{Q}_0 \geq 0, \tag{8}$$

where ${}^{\mathrm{FFP}}\mathfrak{D}_{0,\mathfrak{t}}^{\omega,\nu}$ is the fractal-fractional derivative with the fractional order $\omega \in (0, 1]$ and the fractal order $\nu \in (0, 1]$ via the power-law-type kernel. We impose several required assumptions on the model: the parameters of (7) are nonnegative and

$$\mathscr{N}(\mathfrak{t}) = \mathscr{P}(\mathfrak{t}) + \mathscr{S}(\mathfrak{t}) + \mathscr{Q}(\mathfrak{t}), \tag{9}$$

where $\mathscr{N}(\mathfrak{t})$ stands for the total population at the time $\mathfrak{t} \in \mathbb{I} := [0, T]$, $(T > 0)$.

4. Existence of Solutions

In this section, the existence criterion is ensured by fixed point theory. Here, for the qualitative analysis, we define the Banach space $\mathbb{X} = \mathbb{M}^3$, where $\mathbb{M} = C(\mathbb{I}, \mathbb{R})$ under the norm

$$\|\mathbb{A}\|_{\mathbb{X}} = \|(\mathscr{P}, \mathscr{S}, \mathscr{Q})\|_{\mathbb{X}} = \max\{|\mathscr{K}(\mathfrak{t})|: \mathfrak{t} \in \mathbb{I}\}, \tag{10}$$

for which $|\mathscr{K}| := |\mathscr{P}| + |\mathscr{S}| + |\mathscr{Q}|$. We rewrite the right-hand side of the fractal-fractional SHS-model (7) as

$$\begin{cases} \mathbb{W}_1(\mathfrak{t}, \mathscr{P}(\mathfrak{t}), \mathscr{S}(\mathfrak{t}), \mathscr{Q}(\mathfrak{t})) = \theta - (s + q_1 + r)\mathscr{P}(\mathfrak{t}) - b\mathscr{S}(\mathfrak{t})\mathscr{P}(\mathfrak{t}), \\ \mathbb{W}_2(\mathfrak{t}, \mathscr{P}(\mathfrak{t}), \mathscr{S}(\mathfrak{t}), \mathscr{Q}(\mathfrak{t})) = b\mathscr{P}(\mathfrak{t})\mathscr{S}(\mathfrak{t}) + r_1\mathscr{Q}(\mathfrak{t})\mathscr{S}(\mathfrak{t}) - (q_1 + q_2 + r_2)\mathscr{S}(\mathfrak{t}), \\ \mathbb{W}_3(\mathfrak{t}, \mathscr{P}(\mathfrak{t}), \mathscr{S}(\mathfrak{t}), \mathscr{Q}(\mathfrak{t})) = r_2\mathscr{S}(\mathfrak{t}) - r_1\mathscr{S}(\mathfrak{t})\mathscr{Q}(\mathfrak{t}) - (q_3 + q_1 + \gamma)\mathscr{Q}(\mathfrak{t}). \end{cases} \tag{11}$$

Since, the integral is differentiable, we write the fractal-fractional SHS-model (7) in the following form:

$$\begin{cases} {}^{RL}\mathfrak{D}_{0,\mathfrak{t}}^{\omega,\nu}\mathscr{P}(\mathfrak{t}) = \nu t^{\nu-1}\mathbb{W}_1(\mathfrak{t}, \mathscr{P}(\mathfrak{t}), \mathscr{S}(\mathfrak{t}), \mathscr{Q}(\mathfrak{t})), \\ {}^{RL}\mathfrak{D}_{0,\mathfrak{t}}^{\omega,\nu}\mathscr{S}(\mathfrak{t}) = \nu t^{\nu-1}\mathbb{W}_2(\mathfrak{t}, \mathscr{P}(\mathfrak{t}), \mathscr{S}(\mathfrak{t}), \mathscr{Q}(\mathfrak{t})), \\ {}^{RL}\mathfrak{D}_{0,\mathfrak{t}}^{\omega,\nu}\mathscr{Q}(\mathfrak{t}) = \nu t^{\nu-1}\mathbb{W}_3(\mathfrak{t}, \mathscr{P}(\mathfrak{t}), \mathscr{S}(\mathfrak{t}), \mathscr{Q}(\mathfrak{t})). \end{cases} \tag{12}$$

By (12), the developed system is illustrated by the following IVP

$${}^{RL}D_{0,t}^{\omega,\nu}A(t) = \nu t^{\nu-1}W(t, A(t)), \omega, \nu \in (0, 1], \tag{13}$$

where

$$\begin{aligned} &\mathbb{A}(\mathfrak{t}) = (\mathscr{P}(\mathfrak{t}), \mathscr{S}(\mathfrak{t}), \mathscr{Q}(\mathfrak{t}))^T, \mathbb{A}_0 = (\mathscr{P}_0, \mathscr{S}_0, \mathscr{Q}_0)^T, \\ &\mathbb{W}(\mathfrak{t}, \mathbb{A}(\mathfrak{t})) = \begin{cases} \mathbb{W}_1(\mathfrak{t}, \mathscr{P}(\mathfrak{t}), \mathscr{S}(\mathfrak{t}), \mathscr{Q}(\mathfrak{t})), \\ \mathbb{W}_2(\mathfrak{t}, \mathscr{P}(\mathfrak{t}), \mathscr{S}(\mathfrak{t}), \mathscr{Q}(\mathfrak{t})), \\ \mathbb{W}_3(\mathfrak{t}, \mathscr{P}(\mathfrak{t}), \mathscr{S}(\mathfrak{t}), \mathscr{Q}(\mathfrak{t})), \mathfrak{t} \in \mathbb{I}. \end{cases} \end{aligned} \tag{14}$$

Now, we operate on both sides of the Equation (13) by the fractal-fractional integral which is given by Definition 3, and we get

$$\mathbb{A}(\mathfrak{t}) = \mathbb{A}(0) + \frac{\nu}{\Gamma(\omega)}\int_0^{\mathfrak{t}} \mathfrak{w}^{\nu-1}(\mathfrak{t} - \mathfrak{w})^{\omega-1}\mathbb{W}(\mathfrak{w}, \mathbb{A}(\mathfrak{w}))\mathrm{d}\mathfrak{w}. \tag{15}$$

In other words, the extended form of the above fractal-fractional integral is represented as

$$\begin{cases} \mathscr{P}(\mathfrak{t}) = \mathscr{P}_0 + \dfrac{\nu}{\Gamma(\omega)}\displaystyle\int_0^{\mathfrak{t}} \mathfrak{w}^{\nu-1}(\mathfrak{t} - \mathfrak{w})^{\omega-1}\mathbb{W}_1(\mathfrak{w}, \mathscr{P}(\mathfrak{w}), \mathscr{S}(\mathfrak{w}), \mathscr{Q}(\mathfrak{w}))\mathrm{d}\mathfrak{w}, \\ \mathscr{S}(\mathfrak{t}) = \mathscr{S}_0 + \dfrac{\nu}{\Gamma(\omega)}\displaystyle\int_0^{\mathfrak{t}} \mathfrak{w}^{\nu-1}(\mathfrak{t} - \mathfrak{w})^{\omega-1}\mathbb{W}_2(\mathfrak{w}, \mathscr{P}(\mathfrak{w}), \mathscr{S}(\mathfrak{w}), \mathscr{Q}(\mathfrak{w}))\mathrm{d}\mathfrak{w}, \\ \mathscr{Q}(\mathfrak{t}) = \mathscr{Q}_0 + \dfrac{\nu}{\Gamma(\omega)}\displaystyle\int_0^{\mathfrak{t}} \mathfrak{w}^{\nu-1}(\mathfrak{t} - \mathfrak{w})^{\omega-1}\mathbb{W}_3(\mathfrak{w}, \mathscr{P}(\mathfrak{w}), \mathscr{S}(\mathfrak{w}), \mathscr{Q}(\mathfrak{w}))\mathrm{d}\mathfrak{w}. \end{cases} \tag{16}$$

To transform into a fixed point problem, we define $G : \mathbb{X} \longrightarrow \mathbb{X}$ by

$$G(\mathbb{A}(\mathfrak{t})) = \mathbb{A}(0) + \frac{\nu}{\Gamma(\omega)}\int_0^{\mathfrak{t}} \mathfrak{w}^{\nu-1}(\mathfrak{t} - \mathfrak{w})^{\omega-1}\mathbb{W}(\mathfrak{w}, \mathbb{A}(\mathfrak{w}))\mathrm{d}\mathfrak{w}. \tag{17}$$

In the preceding, we recall the required fixed point theorem in connection with our aim for proving the existence results.

Theorem 4 (see [44]). *Assume that $(\mathbb{X}, d)$ is a complete metric space, $\phi : \mathbb{X} \times \mathbb{X} \longrightarrow \mathbb{R}$, $\psi \in \Psi$, and $\mathbb{W} : \mathbb{X} \longrightarrow \mathbb{X}$ are an ϕ - ψ -contractive map such that*

(1) $\mathbb{W}$ is ϕ-admissible self map on $\mathbb{X}$

(2) For some $u_0 \in \mathbb{X}$, $\phi(u_0, \mathbb{W}u_0) \geq 1$

(3) For any sequence $\{u_n\}$ in $\mathbb{X}$ with $u_n \longrightarrow u$ and $\phi(u_n, u_{n+1}) \geq 1$ for all $n \geq 1$, we have $\phi(u_n, u) \geq 1$ for all $n \geq 1$

Then, there is a fixed point for $\mathbb{W}$.

Now, the first existence result is proved here under some special operators.

Theorem 5. *Suppose that there are a map $\hbar : \mathbb{R} \times \mathbb{R} \longrightarrow \mathbb{R}$, a continuous function $\mathbb{W} : \mathbb{I} \times \mathbb{X} \longrightarrow \mathbb{X}$, and a nondecreasing function $\psi \in \Psi$. Assume that*

$(\wp_1)$ For any $\mathbb{A}_1, \mathbb{A}_2 \in \mathbb{X}$ and $\mathfrak{t} \in \mathbb{I}$,

$$|\mathbb{W}(\mathfrak{t}, \mathbb{A}_1(\mathfrak{t})) - \mathbb{W}(\mathfrak{t}, \mathbb{A}_2(\mathfrak{t}))| \leq \tilde{\ell}\, \psi(|\mathbb{A}_1(\mathfrak{t}) - \mathbb{A}_2(\mathfrak{t}|), \quad (18)$$

with $\hbar(\mathbb{A}_1(\mathfrak{t}), \mathbb{A}_2(\mathfrak{t})) \geq 0$, where $\tilde{\ell} = \Gamma(\nu + \omega)/\nu T^{\nu+\omega-1}\Gamma(\nu)$.

$(\wp_2)$ There is some $\mathbb{A}_0 \in \mathbb{X}$ such that for each $\mathfrak{t} \in \mathbb{I}$,

$$\hbar(\mathbb{A}_0(\mathfrak{t}), G(\mathbb{A}_0(\mathfrak{t}))) \geq 0, \quad (19)$$

and also the inequality

$$\hbar(\mathbb{A}_1(\mathfrak{t}), \mathbb{A}_2(\mathfrak{t})) \geq 0 \quad (20)$$

gives

$$\hbar(G(\mathbb{A}_1(\mathfrak{t})), G(\mathbb{A}_2(\mathfrak{t}))) \geq 0, \quad (21)$$

for each $\mathbb{A}_1, \mathbb{A}_2 \in \mathbb{X}$ and $\mathfrak{t} \in \mathbb{I}$.

$(\wp_3)$ For each convergent sequence $\{\mathbb{A}_n\}_{n\geq 1}$ that belongs to $\mathbb{X}$ with $\mathbb{A}_n \longrightarrow \mathbb{A}$ and

$$\hbar(\mathbb{A}_n(\mathfrak{t}), \mathbb{A}_{n+1}(\mathfrak{t})) \geq 0, \quad (22)$$

for each n and $\mathfrak{t} \in \mathbb{I}$, we get

$$\hbar(\mathbb{A}_n(\mathfrak{t}), \mathbb{A}(\mathfrak{t})) \geq 0. \quad (23)$$

Then, there is a solution for the fractal-fractional IVP (13), and so there is a solution to the given fractal-fractional SHS-model (7).

Proof. Let $\mathbb{A}_1$ and $\mathbb{A}_2$ be two members belonging to $\mathbb{X}$ with

$$\hbar(\mathbb{A}_1(\mathfrak{t}), \mathbb{A}_2(\mathfrak{t})) \geq 0, \quad (24)$$

for each $\mathfrak{t} \in \mathbb{I}$. Then, by definition of the Beta function, we may write

$$\begin{aligned} |G(\mathbb{A}_1(\mathfrak{t})) - G(\mathbb{A}_2(\mathfrak{t}))| &\leq \frac{\nu}{\Gamma(\omega)} \int_0^{\mathfrak{t}} \mathfrak{w}^{\nu-1}(\mathfrak{t} - \mathfrak{w})^{\omega-1} |\mathbb{W}(\mathfrak{w}, \mathbb{A}_1(\mathfrak{w})) \\ &\quad - \mathbb{W}(\mathfrak{w}, \mathbb{A}_2(\mathfrak{w}))| d\mathfrak{w} \\ &\leq \frac{\nu}{\Gamma(\omega)} \int_0^{t} \mathfrak{w}^{\nu-1}(\mathfrak{t} - \mathfrak{w})^{\omega-1} \tilde{\ell}\psi|(\mathbb{A}_1(\mathfrak{w}) \\ &\quad - \mathbb{A}_2(\mathfrak{w}))| d\mathfrak{w} \\ &\leq \frac{\nu \tilde{\ell} T^{\nu+\omega-1} \mathbb{B}(\nu, \omega)}{\Gamma(\omega)} \psi(\|\mathbb{A}_1 - \mathbb{A}_2\|_{\mathbb{X}}) \\ &= \frac{\nu T^{\nu+\omega-1}\Gamma(\nu)}{\Gamma(\nu + \omega)} \tilde{\ell}\psi(\|\mathbb{A}_1 - \mathbb{A}_2\|_{\mathbb{X}}). \end{aligned} \quad (25)$$

Consequently, we have

$$\begin{aligned} \|G(\mathbb{A}_1) - G(\mathbb{A}_2)\|_{\mathbb{X}} &\leq \frac{\nu T^{\nu+\omega-1}\Gamma(\nu)}{\Gamma(\nu + \omega)} \tilde{\ell}\psi(\|\mathbb{A}_1 - \mathbb{A}_2\|_{\mathbb{X}}) \\ &= \psi(\|\mathbb{A}_1 - \mathbb{A}_2\|_{\mathbb{X}}). \end{aligned} \quad (26)$$

Now, a function $\phi : \mathbb{X} \times \mathbb{X} \longrightarrow [0,\infty)$ is introduced by the rule

$$\phi(\mathbb{A}_1, \mathbb{A}_2) = \begin{cases} 1 & \text{if } \hbar(\mathbb{A}_1(\mathfrak{t}), \mathbb{A}_2(\mathfrak{t})) \geq 0, \\ 0 & \text{otherwise,} \end{cases} \quad (27)$$

for each $\mathbb{A}_1, \mathbb{A}_2 \in \mathbb{X}$. Then, for every $\mathbb{A}_1, \mathbb{A}_2 \in \mathbb{X}$, we will get

$$\phi(\mathbb{A}_1, \mathbb{A}_2)\mathrm{d}(G(\mathbb{A}_1), G(\mathbb{A}_2)) \leq \psi(\mathrm{d}(\mathbb{A}_1, \mathbb{A}_2)). \quad (28)$$

Thus, G is found as an ϕ-ψ-contraction. To verify that G is ϕ-admissible, let $\mathbb{A}_1, \mathbb{A}_2 \in \mathbb{X}$ be arbitrary and $\phi(\mathbb{A}_1, \mathbb{A}_2) \geq 1$. By definition of ϕ, we have

$$\hbar(\mathbb{A}_1(\mathfrak{t}), \mathbb{A}_2(\mathfrak{t})) \geq 0. \quad (29)$$

Then, by $(\mathfrak{P}_2)$, $\hbar(G(\mathbb{A}_1(\mathfrak{t})), G(\mathbb{A}_2(\mathfrak{t}))) \geq 0$ is satisfied. Again, the definition of ϕ gives $\phi(G(\mathbb{A}_1), G(\mathbb{A}_2)) \geq 1$. Thus, G is ϕ-admissible.

On the other hand, the condition $(\mathfrak{P}_2)$ guarantees the existence of $\mathbb{A}_0 \in \mathbb{X}$. In this case, for each $\mathfrak{t} \in \mathbb{I}$, $\hbar(\mathbb{A}_0(\mathfrak{t}), G(\mathbb{A}_0(\mathfrak{t}))) \geq 0$ holds. Clearly, we get $\phi(\mathbb{A}_0, G(\mathbb{A}_0)) \geq 1$. These show that the conditions (1) and (2) of Theorem 4 are fulfilled.

Now, we assume that $\{\mathbb{A}_n\}_{n\geq 1} \subseteq \mathbb{X}$ such that $\mathbb{A}_n \longrightarrow \mathbb{A}$ and for all n, $\phi(\mathbb{A}_n, \mathbb{A}_{n+1}) \geq 1$. By virtue of the definition of the nonnegative function ϕ,

$$\hbar(\mathbb{A}_n(\mathfrak{t}), \mathbb{A}_{n+1}(\mathfrak{t})) \geq 0. \quad (30)$$

Therefore, in the light of hypothesis $(\mathfrak{P}_3)$, we obtain

$$\hbar(\mathbb{A}_n(\mathfrak{t}), \mathbb{A}(\mathfrak{t})) \geq 0. \quad (31)$$

This indicates that $\phi(\mathbb{A}_n, \mathbb{A}) \geq 1$ for every n. This guarantees the condition (3) of Theorem 4. Ultimately, by using Theorem 4, we conclude that there is a fixed point for G like $\mathbb{A}^* \in \mathbb{X}$. This implies that$\mathbb{A}^* = (\mathscr{P}^*, \mathscr{S}^*, \mathscr{Q}^*)^T$ is interpreted as a solution of the fractal-fractional model of second-hand smoker (7), and the proof is completed. □

In the sequel, we use the Leray-Schauder fixed point theorem to prove the existence result.

Theorem 6 (see [41]). *Let $\mathbb{X}$ be a Banach space, $\mathbb{E}$ a bounded convex closed set in $\mathbb{X}$, and $\mathbb{O} \subset \mathbb{E}$ an open set with $0 \in \mathbb{O}$. Then, for the continuous and compact mapping $G : \bar{\mathbb{O}} \longrightarrow \mathbb{E}$, either*

(P1) There is $u \in \bar{\mathbb{O}}$ such that $u = G(u)$ or

(P2) There is $u \in \partial\mathbb{O}$ and $0 < \mu < 1$ such that $u = \mu G(u)$.

Theorem 7. *Suppose that* $\mathbb{W} \in C(\mathbb{I} \times \mathbb{X}, \mathbb{X})$ *and*

(C1) There are $\varphi \in L^1(\mathbb{I}, \mathbb{R}^+)$ *and increasing function* $A \in C([0,\infty), (0,\infty))$ *such that for each* $\mathfrak{t} \in \mathbb{I}$ *and* $\mathbb{A} \in \mathbb{X}$,

$$|\mathbb{W}(\mathfrak{t}, \mathbb{A}(\mathfrak{t}))| \leq \varphi(\mathfrak{t}) A(|\mathbb{A}(\mathfrak{t})|). \tag{32}$$

(C2) There is $\alpha > 0$ *such that*

$$\frac{\alpha}{\mathbb{A}_0 + \left(\nu T^{\nu+\omega-1}\Gamma(\nu)/\Gamma(\nu+\omega)\right)\varphi_0^* A(\alpha)} > 1, \tag{33}$$

where $\varphi_0^* = \sup_{\mathfrak{t}\in\mathbb{I}}|\varphi(\mathfrak{t})|$.

Then, there is a solution for the fractal-fractional problem (13), and so there is a solution for the given fractal-fractional model of second-hand smokers (7) on $\mathbb{I}$.

Proof. To begin the proof, consider $G : \mathbb{X} \longrightarrow \mathbb{X}$ formulated by (17) and the ball

$$N_\varepsilon = \left\{\mathbb{A} \in \mathbb{X} : \|\mathbb{A}\|_{\mathbb{X}} \leq \varepsilon\right\}, \tag{34}$$

for some $\varepsilon > 0$. In the first place, the continuity of $\mathbb{W}$ yields that of the operator G. Now, by (C1), we have

$$\begin{aligned}
|G(\mathbb{A}(\mathfrak{t}))| &\leq |\mathbb{A}(0)| + \frac{\nu}{\Gamma(\omega)}\int_0^{\mathfrak{t}} \mathfrak{w}^{\nu-1}(\mathfrak{t}-\mathfrak{w})^{\omega-1}|\mathbb{W}(\mathfrak{w}, \mathbb{A}(\mathfrak{w}))|d\mathfrak{w} \\
&\leq \mathbb{A}_0 + \frac{\nu}{\Gamma(\omega)}\int_0^{\mathfrak{t}} \mathfrak{w}^{\nu-1}(\mathfrak{t}-\mathfrak{w})^{\omega-1}\varphi(\mathfrak{w})A(|\mathbb{A}(\mathfrak{w})|)d\mathfrak{w} \\
&\leq \mathbb{A}_0 + \frac{\nu T^{\nu+\omega-1}\mathbb{B}(\nu,\omega)}{\Gamma(\omega)}\varphi_0^* A(\|\mathbb{A}\|_{\mathbb{X}}) \\
&\leq \mathbb{A}_0 + \frac{\nu T^{\nu+\omega-1}\Gamma(\nu)}{\Gamma(\nu+\omega)}\varphi_0^* A(\varepsilon),
\end{aligned} \tag{35}$$

for each $\mathbb{A} \in N_\varepsilon$. In consequence, we obtain

$$\|G\mathbb{A}\|_{\mathbb{X}} \leq \mathbb{A}_0 + \frac{\nu T^{\nu+\omega-1}\Gamma(\nu)}{\Gamma(\nu+\omega)}\varphi_0^* A(\varepsilon) < \infty. \tag{36}$$

Hence, G is uniformly bounded on $\mathbb{X}$. In the sequel, the equicontinuity of G is investigated. To prove such a claim, for every $\mathfrak{t}, \mathfrak{t}_* \in [0, T]$ such that $\mathfrak{t} < \mathfrak{t}_*$ and for each $\mathbb{A} \in N_\varepsilon$, by letting

$$\sup_{(\mathfrak{t},\mathbb{A})\in\mathbb{I}\times N_\varepsilon} |\mathbb{W}(\mathfrak{t}, \mathbb{A}(\mathfrak{t}))| = \mathbb{W}^* < \infty, \tag{37}$$

we have

$$\begin{aligned}
&|G(\mathbb{A}(\mathfrak{t}_*)) - G(\mathbb{A}(\mathfrak{t}))| \\
&\leq \left|\frac{\nu}{\Gamma(\omega)}\int_0^{\mathfrak{t}_*} \mathfrak{w}^{\nu-1}(\mathfrak{t}_*-\mathfrak{w})^{\omega-1}\mathbb{W}(\mathfrak{w}, \mathbb{A}(\mathfrak{w}))d\mathfrak{w}\right. \\
&\quad \left. - \frac{\nu}{\Gamma(\omega)}\int_0^{\mathfrak{t}} \mathfrak{w}^{\nu-1}(\mathfrak{t}-\mathfrak{w})^{\omega-1}\mathbb{W}(\mathfrak{w}, \mathbb{A}(\mathfrak{w}))d\mathfrak{w}\right| \\
&\leq \frac{\nu\mathbb{W}^*}{\Gamma(\omega)}\left|\int_0^{\mathfrak{t}_*} \mathfrak{w}^{\nu-1}(\mathfrak{t}_*-\mathfrak{w})^{\omega-1d\mathfrak{w}} - \int_0^{\mathfrak{t}} \mathfrak{w}^{\nu-1}(\mathfrak{t}-\mathfrak{w})^{\omega-1}d\mathfrak{w}\right| \\
&\leq \frac{\nu\mathbb{W}^*\mathbb{B}(\nu,\omega)}{\Gamma(\omega)}\left[\mathfrak{t}_*^{\nu+\omega-1} - \mathfrak{t}^{\nu+\omega-1}\right] \\
&= \frac{\nu\mathbb{W}^*\Gamma(\nu)}{\Gamma(\nu+\omega)}\left[\mathfrak{t}_*^{\nu+\omega-1} - \mathfrak{t}^{\nu+\omega-1}\right],
\end{aligned} \tag{38}$$

which is independent of $\mathbb{A}$, and the right-hand side of (38) converges to 0 as $\mathfrak{t}_* \longrightarrow \mathfrak{t}$. Therefore, this implies that

$$\|G(\mathbb{A}(\mathfrak{t}_*)) - G(\mathbb{A}(\mathfrak{t}))\|_{\mathbb{X}} \longrightarrow 0, \tag{39}$$

as $\mathfrak{t}_* \longrightarrow \mathfrak{t}$. Thus, G is equicontinuous and is compact on N_ε by referring to the Arzelá–Ascoli thoerem. We found that the conditions of Theorem 6 are valid on G. So, one of (P1) or (P2) will be fulfilled. By (C2), set

$$\mathbb{O} := \left\{\mathbb{A} \in \mathbb{X} : \|\mathbb{A}\|_{\mathbb{X}} < \alpha\right\}, \tag{40}$$

for some $\alpha > 0$ via $\mathbb{A}_0 + (\nu T^{\nu+\omega-1}\Gamma(\nu)/\Gamma(\nu+\omega))\varphi_0^* A(\alpha) < \alpha$. With the help of (C1) and by (36), we write

$$\|G\mathbb{A}\|_{\mathbb{X}} \leq \mathbb{A}_0 + \frac{\nu T^{\nu+\omega-1}\Gamma(\nu)}{\Gamma(\nu+\omega)}\varphi_0^* A(\mathbb{A}). \tag{41}$$

Now, we assume the existence of $\mathbb{A} \in \partial\mathbb{O}$ and $0 < \mu < 1$ with $\mathbb{A} = \mu G(\mathbb{A})$. For these selections of $\mathbb{A}$ and μ, and by (41), one may write

$$\begin{aligned}
\alpha = \|\mathbb{A}\|_{\mathbb{X}} = \mu\|G\mathbb{A}\|_{\mathbb{X}} &< \mathbb{A}_0 + \frac{\nu T^{\nu+\omega-1}\Gamma(\nu)}{\Gamma(\nu+\omega)}\varphi_0^* A(\|\mathbb{A}\|_{\mathbb{X}}) \\
&< \mathbb{A}_0 + \frac{\nu T^{\nu+\omega-1}\Gamma(\nu)}{\Gamma(\nu+\omega)}\varphi_0^* A(\alpha) < \alpha,
\end{aligned} \tag{42}$$

and this cannot occur. Therefore, the case (P2) does not hold and G has a fixed–point in $\bar{\mathbb{O}}$ by Theorem 6 which is interpreted as a solution of the fractal-fractional model of second-hand smoker (SHS) (7), and the proof is completed. □

5. Uniqueness result

To prove the uniqueness of solution of the given fractal-fractional model of second-hand smoker (7), we use the Lipschitz property of functions $\mathbb{W}_i$, $(i = 1, 2, 3)$ given by (11).

Lemma 8. *Consider the functions* $\mathscr{P}, \mathscr{S}, \mathscr{Q}, \mathscr{P}^*, \mathscr{S}^*, \mathscr{Q}^* \in \mathbb{M} := C(\mathbb{I}, \mathbb{R})$. *Let*

(H1) $\|\mathscr{P}\| \le \lambda_1$, $\|\mathscr{S}\| \le \lambda_2$, *and* $\|\mathscr{Q}\| \le \lambda_3$ *for some constants* $\lambda_1, \lambda_2, \lambda_3 > 0$.

Then, the functions $\mathbb{W}_1, \mathbb{W}_2, \mathbb{W}_3$ *introduced by (11) are satisfied the Lipschitz property with respect to the corresponding components if* $w_1, w_2, w_3 > 0$, *where*

$$\begin{aligned} w_1 &= s + q_1 + r + b\lambda_2, w_2 \\ &= b\lambda_1 + r_1\lambda_3 + q_1 + q_2 + r_2, w_3 \\ &= r_1\lambda_2 + q_3 + q_1 + \gamma. \end{aligned} \tag{43}$$

Proof. We begin with the function $\mathbb{W}_1$. For each $\mathscr{P}, \mathscr{P}^* \in \mathbb{M} := C(\mathbb{I}, \mathbb{R})$, we have

$$\begin{aligned} &\|\mathbb{W}_1(\mathfrak{t}, \mathscr{P}(\mathfrak{t}), \mathscr{S}(\mathfrak{t}), \mathscr{Q}(\mathfrak{t})) - \mathbb{W}_1(\mathfrak{t}, \mathscr{P}^*(\mathfrak{t}), \mathscr{S}(\mathfrak{t}), \mathscr{Q}(\mathfrak{t}))\| \\ &\quad = \|(\theta - (s + q_1 + r)\mathscr{P}(\mathfrak{t}) - b\mathscr{S}(\mathfrak{t})\mathscr{P}(\mathfrak{t})) \\ &\qquad - (\theta - (s + q_1 + r)\mathscr{P}^*(\mathfrak{t}) - b\mathscr{S}(\mathfrak{t})\mathscr{P}^*(\mathfrak{t}))\| \\ &\quad \le [(q_1 + s + r) + b\|\mathscr{S}(\mathfrak{t})\|]\|\mathscr{P}(\mathfrak{t}) - \mathscr{P}^*(\mathfrak{t})\| \\ &\quad \le [(q_1 + s + r) + b\lambda_2]\|\mathscr{P}(\mathfrak{t}) - \mathscr{P}^*(\mathfrak{t})\| \\ &\quad = w_1\|\mathscr{P}(\mathfrak{t}) - \mathscr{P}^*(\mathfrak{t})\|. \end{aligned} \tag{44}$$

This shows that $\mathbb{W}_1$ is Lipschitz with respect to $\mathscr{P}$ with the Lipschitz constant $w_1 > 0$. For the function $\mathbb{W}_2$, for each $\mathscr{S}, \mathscr{S}^* \in \mathbb{M} := C(\mathbb{I}, \mathbb{R})$, we have

$$\begin{aligned} &\|\mathbb{W}_2(\mathfrak{t}, \mathscr{P}(\mathfrak{t}), \mathscr{S}(\mathfrak{t}), \mathscr{Q}(\mathfrak{t})) - \mathbb{W}_2(\mathfrak{t}, \mathscr{P}(\mathfrak{t}), \mathscr{S}^*(\mathfrak{t}), \mathscr{Q}(\mathfrak{t}))\| \\ &\quad = \|(b\mathscr{P}(\mathfrak{t})\mathscr{S}(\mathfrak{t}) + r_1\mathscr{Q}(\mathfrak{t})\mathscr{S}(\mathfrak{t}) - (q_1 + r_2 + q_2)\mathscr{S}(\mathfrak{t})) \\ &\qquad - (b\mathscr{P}(\mathfrak{t})\mathscr{S}^*(\mathfrak{t}) + r_1\mathscr{Q}(\mathfrak{t})\mathscr{S}^*(\mathfrak{t}) - (q_1 + r_2 + q_2)\mathscr{S}^*(\mathfrak{t}))\| \\ &\quad \le [b\|\mathscr{P}(\mathfrak{t})\| + r_1\|\mathscr{Q}(\mathfrak{t})\| + (q_1 + r_2 + q_2)]\|\mathscr{S}(\mathfrak{t}) - \mathscr{S}^*(\mathfrak{t})\| \\ &\quad \le [b\lambda_1 + r_1\lambda_3 + q_1 + r_2 + q_2]\|\mathscr{S}(\mathfrak{t}) - \mathscr{S}^*(\mathfrak{t})\| \\ &\quad = w_2\|\mathscr{S}(\mathfrak{t}) - \mathscr{S}^*(\mathfrak{t})\|. \end{aligned} \tag{45}$$

This shows that $\mathbb{W}_2$ is Lipschitz with respect to $\mathscr{S}$ with the Lipschitz constant $w_2 > 0$. Now, for each $\mathscr{Q}, \mathscr{Q}^* \in \mathbb{M} := C(\mathbb{I}, \mathbb{R})$, we have

$$\begin{aligned} &\|\mathbb{W}_3(\mathfrak{t}, \mathscr{P}(\mathfrak{t}), \mathscr{S}(\mathfrak{t}), \mathscr{Q}(\mathfrak{t})) - \mathbb{W}_3(\mathfrak{t}, \mathscr{P}(\mathfrak{t}), \mathscr{S}(\mathfrak{t}), \mathscr{Q}^*(\mathfrak{t}))\| \\ &\quad = \|(r_2\mathscr{S}(\mathfrak{t}) - r_1\mathscr{S}(\mathfrak{t})\mathscr{Q}(\mathfrak{t}) - (q_3 + q_1 + \gamma)\mathscr{Q}(\mathfrak{t})) \\ &\qquad - (r_2\mathscr{S}(\mathfrak{t}) - r_1\mathscr{S}(\mathfrak{t})\mathscr{Q}^*(\mathfrak{t}) - (q_3 + q_1 + \gamma)\mathscr{Q}^*(\mathfrak{t}))\| \\ &\quad \le [r_1\|\mathscr{S}(\mathfrak{t})\| + q_3 + q_1 + \gamma]\|\mathscr{Q}(\mathfrak{t}) - \mathscr{Q}^*(\mathfrak{t})\| \\ &\quad \le [r_1\lambda_2 + q_3 + q_1 + \gamma]\|\mathscr{Q}(\mathfrak{t}) - \mathscr{Q}^*(\mathfrak{t})\| \\ &\quad = w_3\|\mathscr{Q}(\mathfrak{t}) - \mathscr{Q}^*(\mathfrak{t})\|. \end{aligned} \tag{46}$$

Accordingly, this shows that $\mathbb{W}_3$ is Lipschitz with respect to $\mathscr{Q}$ with the Lipschitz constant $w_3 > 0$. Above results show that three functions $\mathbb{W}_1, \mathbb{W}_2, \mathbb{W}_3$ are Lipschitzian with respect to the corresponding component with the Lipschitz constants $w_1, w_2, w_3 > 0$, respectively. □

According to the obtained results in Lemma 8, we investigate the uniqueness property for solution to the supposed fractal-fractional system (7).

Theorem 9. *Let (H1) holds. Then, the given fractal-fractional model of second-hand smoker (7) has a unique solution if*

$$\frac{\nu T^{\nu+\omega-1}\Gamma(\nu)}{\Gamma(\nu+\omega)} w_i < 1, i \in \{1, 2, 3\}. \tag{47}$$

Proof. We assume that the conclusion of theorem is not valid. In other words, there is another solution for the given fractal-fractional model of second-hand smoker (7). Assume that $(\mathscr{P}^*(\mathfrak{t}), \mathscr{S}^*(\mathfrak{t}), \mathscr{Q}^*(\mathfrak{t}))$ is another solution with initial conditions $(\mathscr{P}_0, \mathscr{S}_0, \mathscr{Q}_0)$ such that by (16), we have

$$\begin{aligned} \mathscr{P}^*(\mathfrak{t}) &= \mathscr{P}_0 + \frac{\nu}{\Gamma(\omega)}\int_0^{\mathfrak{t}} \mathfrak{w}^{\nu-1}(\mathfrak{t} - \mathfrak{w})^{\omega-1}\mathbb{W}_1(\mathfrak{w}, \mathscr{P}^*(\mathfrak{w}), \mathscr{S}^*(\mathfrak{w}), \mathscr{Q}^*(\mathfrak{w}))\mathrm{d}\mathfrak{w}, \\ \mathscr{S}^*(\mathfrak{t}) &= \mathscr{S}_0 + \frac{\nu}{\Gamma(\omega)}\int_0^{\mathfrak{t}} \mathfrak{w}^{\nu-1}(\mathfrak{t} - \mathfrak{w})^{\omega-1}\mathbb{W}_2(\mathfrak{w}, \mathscr{P}^*(\mathfrak{w}), \mathscr{S}^*(\mathfrak{w}), \mathscr{Q}^*(\mathfrak{w}))\mathrm{d}\mathfrak{w}, \\ \mathscr{Q}^*(\mathfrak{t}) &= \mathscr{Q}_0 + \frac{\nu}{\Gamma(\omega)}\int_0^{\mathfrak{t}} \mathfrak{w}^{\nu-1}(\mathfrak{t} - \mathfrak{w})^{\omega-1}\mathbb{W}_3(\mathfrak{w}, \mathscr{P}^*(\mathfrak{w}), \mathscr{S}^*(\mathfrak{w}), \mathscr{Q}^*(\mathfrak{w}))\mathrm{d}\mathfrak{w}. \end{aligned} \tag{48}$$

Now, we can estimate

$$\begin{aligned} |\mathscr{P}(\mathfrak{t}) - \mathscr{P}^*(\mathfrak{t})| &\le \frac{\nu}{\Gamma(\omega)}\int_0^{\mathfrak{t}} \mathfrak{w}^{\nu-1}(\mathfrak{t} - \mathfrak{w})^{\omega-1} \\ &\qquad \times |\mathbb{W}_1(\mathfrak{w}, \mathscr{P}(\mathfrak{w}), \mathscr{S}(\mathfrak{w}), \mathscr{Q}(\mathfrak{w})) \\ &\qquad - \mathbb{W}_1(\mathfrak{w}, \mathscr{P}^*(\mathfrak{w}), \mathscr{S}^*(\mathfrak{w}), \mathscr{Q}^*(\mathfrak{w}))|\mathrm{d}\mathfrak{w} \\ &\le \frac{\nu}{\Gamma(\omega)}\int_0^{\mathfrak{t}} \mathfrak{w}^{\nu-1}(\mathfrak{t} - \mathfrak{w})^{\omega-1} w_1\|\mathscr{P} - \mathscr{P}^*\|\mathrm{d}\mathfrak{w} \\ &\le \frac{\nu T^{\nu+\omega-1}\Gamma(\nu)}{\Gamma(\nu+\omega)} w_1\|\mathscr{P} - \mathscr{P}^*\|, \end{aligned} \tag{49}$$

and so

$$\left[1 - \frac{\nu T^{\nu+\omega-1}\Gamma(\nu)}{\Gamma(\nu+\omega)} w_1\right]\|\mathscr{P} - \mathscr{P}^*\| \le 0. \tag{50}$$

The latter inequality is true if $\|\mathscr{P} - \mathscr{P}^*\| = 0$, and accordingly, $\mathscr{P} = \mathscr{P}^*$. Similarly, from

$$\|\mathscr{S} - \mathscr{S}^*\| \le \frac{\nu T^{\nu+\omega-1}\Gamma(\nu)}{\Gamma(\nu+\omega)} w_2\|\mathscr{S} - \mathscr{S}^*\|, \tag{51}$$

we get

$$\left[1 - \frac{\nu T^{\nu+\omega-1}\Gamma(\nu)}{\Gamma(\nu+\omega)} w_2\right]\|\mathscr{S} - \mathscr{S}^*\| \le 0. \tag{52}$$

This implies that $\|\mathcal{S}-\mathcal{S}^*\|=0$ and so $\mathcal{S}=\mathcal{S}^*$. Also,

$$\|\mathcal{Q}-\mathcal{Q}^*\| \leq \frac{\nu T^{\nu+\omega-1}\Gamma(\nu)}{\Gamma(\nu+\omega)} w_3 \|\mathcal{Q}-\mathcal{Q}^*\|. \tag{53}$$

This gives

$$\left[1-\frac{\nu T^{\nu+\omega-1}\Gamma(\nu)}{\Gamma(\nu+\omega)} w_3\right] \|\mathcal{Q}-\mathcal{Q}^*\| \leq 0. \tag{54}$$

Hence, $\mathcal{Q}=\mathcal{Q}^*$. Consequently, we get

$$(\mathcal{P}(\mathfrak{t}), \mathcal{S}(\mathfrak{t}), \mathcal{Q}(\mathfrak{t})) = (\mathcal{P}^*(\mathfrak{t}), \mathcal{S}^*(\mathfrak{t}), \mathcal{Q}^*(\mathfrak{t})). \tag{55}$$

This shows that the fractal-fractional model of second-hand smoker (7) has a unique solution, and this completes our proof. □

6. Stability

Here, the stability notion in the sense of the Ulam–Hyers, Ulam–Hyers–Rassias, and their generalized versions is established for the system of fractal-fractional SHS-model (7). For more details on the stability analysis, we refer to [46, 47].

Definition 10. The fractal-fractional model of SHS (7) is Ulam–Hyers stable if there are $0<\mathrm{M}_{\mathbb{W}_i}\in\mathbb{R}$, $(\mathrm{i}\in\{1,2,3\})$ such that for each $\varepsilon_{\mathrm{i}}>0$, and for each $(\mathcal{P}^*, \mathcal{S}^*, \mathcal{Q}^*)\in\mathbb{X}$ satisfying

$$\begin{cases} \left|{}^{\mathrm{FFP}}\mathfrak{D}_{0,\mathfrak{t}}^{\omega,\nu}\mathcal{P}^*(\mathfrak{t}) - \mathbb{W}_1(\mathfrak{t}, \mathcal{P}^*(\mathfrak{t}), \mathcal{S}^*(\mathfrak{t}), \mathcal{Q}^*(\mathfrak{t}))\right| < \varepsilon_1, \\ \left|{}^{FFP}\mathfrak{D}_{0,\mathfrak{t}}^{\omega,\nu}\mathcal{S}^*(\mathfrak{t}) - \mathbb{W}_2(\mathfrak{t}, \mathcal{P}^*(\mathfrak{t}), \mathcal{S}^*(\mathfrak{t}), \mathcal{Q}^*(\mathfrak{t}))\right| < \varepsilon_2, \\ \left|{}^{FFP}\mathfrak{D}_{0,\mathfrak{t}}^{\omega,\nu}\mathcal{Q}^*(\mathfrak{t}) - \mathbb{W}_1(\mathfrak{t}, \mathcal{Q}^*(\mathfrak{t}), \mathcal{S}^*(\mathfrak{t}), \mathcal{Q}^*(\mathfrak{t}))\right| < \varepsilon_3, \end{cases} \tag{56}$$

there is $(\mathcal{P}, \mathcal{S}, \mathcal{Q})\in\mathbb{X}$ satisfying the given fractal-fractional model (7) such that

$$\begin{cases} |\mathcal{P}^*(\mathfrak{t}) - \mathcal{P}(\mathfrak{t})| \leq M_{\mathbb{W}_1}\varepsilon_1, \\ |\mathcal{S}^*(\mathfrak{t}) - \mathcal{S}(\mathfrak{t})| \leq M_{\mathbb{W}_2}\varepsilon_2, \\ |\mathcal{Q}^*(\mathfrak{t}) - \mathcal{Q}(\mathfrak{t})| \leq M_{\mathbb{W}_3}\varepsilon_3. \end{cases} \tag{57}$$

Definition 11. The given fractal-fractional model of second-hand smoker (7) is generalized Ulam–Hyers stable if there are $\mathrm{M}_{\mathbb{W}_{\mathrm{i}}}\in\mathrm{C}(\mathbb{R}^+,\mathbb{R}^+)$, $(\mathrm{i}\in\{1,2,3\})$ with $\mathrm{M}_{\mathbb{W}_{\mathrm{i}}}(0)=0$ such that for each $\varepsilon_{\mathrm{i}}>0$ and for each $(\mathcal{P}^*, \mathcal{S}^*, \mathcal{Q}^*)\in\mathbb{X}$ satisfying the inequalities (56), there is $(\mathcal{P}, \mathcal{S}, \mathcal{Q})\in\mathbb{X}$ as a solution of the given fractal-fractional model of second-hand smoker (7) such that

$$\begin{cases} |\mathcal{P}^*(\mathfrak{t}) - \mathcal{P}(\mathfrak{t})| \leq M_{\mathbb{W}_1}(\varepsilon_1), \\ |\mathcal{S}^*(\mathfrak{t}) - \mathcal{S}(\mathfrak{t})| \leq M_{\mathbb{W}_2}(\varepsilon_2), \\ |\mathcal{Q}^*(\mathfrak{t}) - \mathcal{Q}(\mathfrak{t})| \leq M_{\mathbb{W}_3}(\varepsilon_3). \end{cases} \tag{58}$$

Note that Definition 11 is derived from Definition 10.

Remark 12. Notice that $(\mathcal{P}^*, \mathcal{S}^*, \mathcal{Q}^*)\in\mathbb{X}$ is a solution for (56) if and only if there are $\hbar_1, \hbar_2, \hbar_3\in\mathrm{C}([0,\mathrm{T}],\mathbb{R})$ (depending on $\mathcal{P}^*, \mathcal{S}^*, \mathcal{Q}^*$, respectively) such that for each $\mathfrak{t}\in\mathbb{I}$,

$$|\hbar_i(\mathfrak{t})| < \varepsilon_i. \tag{59}$$

(1) We have

$$\begin{cases} {}^{FFP}\mathfrak{D}_{0,\mathfrak{t}}^{\omega,\nu}\mathcal{P}^*(\mathfrak{t}) - \mathbb{W}_1(\mathfrak{t}, \mathcal{P}^*(\mathfrak{t}), \mathcal{S}^*(\mathfrak{t}), \mathcal{Q}^*(\mathfrak{t})) + \hbar_1(\mathfrak{t}), \\ {}^{FFP}\mathfrak{D}_{0,\mathfrak{t}}^{\omega,\nu}\mathcal{S}^*(\mathfrak{t}) - \mathbb{W}_2(\mathfrak{t}, \mathcal{P}^*(\mathfrak{t}), \mathcal{S}^*(\mathfrak{t}), \mathcal{Q}^*(\mathfrak{t})) + \hbar_2(\mathfrak{t}), \\ {}^{FFP}\mathfrak{D}_{0,\mathfrak{t}}^{\omega,\nu}\mathcal{Q}^*(\mathfrak{t}) - \mathbb{W}_3(\mathfrak{t}, \mathcal{P}^*(\mathfrak{t}), \mathcal{S}^*(\mathfrak{t}), \mathcal{Q}^*(\mathfrak{t})) + \hbar_3(\mathfrak{t}), \end{cases} \tag{60}$$

Definition 13. The given fractal-fractional model of second-hand smoker (7) is Ulam–Hyers–Rassias stable with respect to functions Φ_{i}, $(\mathrm{i}\in\{1,2,3\})$ if there are $0<\mathrm{M}_{(\mathbb{W}_{\mathrm{i}},\Phi_{\mathrm{i}})}\in\mathbb{R}$ such that for each $\varepsilon_{\mathrm{i}}>0$ and for each $(\mathcal{P}^*, \mathcal{S}^*, \mathcal{Q}^*)\in\mathbb{X}$ satisfying

$$\begin{cases} \left|{}^{FFP}\mathfrak{D}_{0,\mathfrak{t}}^{\omega,\nu}\mathcal{P}^*(\mathfrak{t}) - \mathbb{W}_1(\mathfrak{t}, \mathcal{P}^*(\mathfrak{t}), \mathcal{S}^*(\mathfrak{t}), \mathcal{Q}^*(\mathfrak{t}))\right| < \varepsilon_1\Phi_1(\mathfrak{t}), \\ \left|{}^{FFP}\mathfrak{D}_{0,\mathfrak{t}}^{\omega,\nu}\mathcal{S}^*(\mathfrak{t}) - \mathbb{W}_2(\mathfrak{t}, \mathcal{P}^*(\mathfrak{t}), \mathcal{S}^*(\mathfrak{t}), \mathcal{Q}^*(\mathfrak{t}))\right| < \varepsilon_2\Phi_2(\mathfrak{t}), \\ \left|{}^{FFP}\mathfrak{D}_{0,\mathfrak{t}}^{\omega,\nu}\mathcal{Q}^*(\mathfrak{t}) - \mathbb{W}_3(\mathfrak{t}, \mathcal{P}^*(\mathfrak{t}), \mathcal{S}^*(\mathfrak{t}), \mathcal{Q}^*(\mathfrak{t}))\right| < \varepsilon_3\Phi_3(\mathfrak{t}), \end{cases} \tag{61}$$

there is $(\mathcal{P}, \mathcal{S}, \mathcal{Q})\in\mathbb{X}$ as a solution of the given fractal-fractional model of second-hand smoker (7) such that

$$\begin{cases} |\mathcal{P}^*(\mathfrak{t}) - \mathcal{P}(\mathfrak{t})| \leq \varepsilon_1 M_{(\mathbb{W}_1,\Phi_1)}\Phi_1(\mathfrak{t}), \forall\mathfrak{t}\in\mathbb{I}, \\ |\mathcal{S}^*(\mathfrak{t}) - \mathcal{S}(\mathfrak{t})| \leq \varepsilon_2 M_{(\mathbb{W}_2,\Phi_2)}\Phi_2(\mathfrak{t}), \forall\mathfrak{t}\in\mathbb{I}, \\ |\mathcal{Q}^*(\mathfrak{t}) - \mathcal{Q}(\mathfrak{t})| \leq \varepsilon_3 M_{(\mathbb{W}_3,\Phi_3)}\Phi_3(\mathfrak{t}), \forall\mathfrak{t}\in\mathbb{I}. \end{cases} \tag{62}$$

Definition 14. The given fractal-fractional model of second-hand smoker (7) is generalized Ulam–Hyers–Rassias stable with respect to functions Φ_{i} if there are $0<\mathrm{M}_{(\mathbb{W}_{\mathrm{i}},\Phi_{\mathrm{i}})}\in\mathbb{R}$ such that for each $(\mathcal{P}^*, \mathcal{S}^*, \mathcal{Q}^*)\in\mathbb{X}$ satisfying

$$\begin{cases} \left|{}^{FFP}\mathfrak{D}_{0,\mathfrak{t}}^{\omega,\nu}\mathscr{P}^*(\mathfrak{t}) - \mathbb{W}_1(\mathfrak{t},\mathscr{P}^*(\mathfrak{t}),\mathscr{S}^*(\mathfrak{t}),\mathscr{Q}^*(\mathfrak{t}))\right| < \Phi_1(\mathfrak{t}), \\ \left|{}^{FFP}\mathfrak{D}_{0,\mathfrak{t}}^{\omega,\nu}\mathscr{S}^*(\mathfrak{t}) - \mathbb{W}_2(\mathfrak{t},\mathscr{P}^*(\mathfrak{t}),\mathscr{S}^*(\mathfrak{t}),\mathscr{Q}^*(\mathfrak{t}))\right| < \Phi_2(\mathfrak{t}), \\ \left|{}^{FFP}\mathfrak{D}_{0,\mathfrak{t}}^{\omega,\nu}\mathscr{Q}^*(\mathfrak{t}) - \mathbb{W}_3(\mathfrak{t},\mathscr{P}^*(\mathfrak{t}),\mathscr{S}^*(\mathfrak{t}),\mathscr{Q}^*(\mathfrak{t}))\right| < \Phi_3(\mathfrak{t}), \end{cases} \tag{63}$$

there is $(\mathscr{P},\mathscr{S},\mathscr{Q}) \in \mathbb{X}$ as a solution of the given fractal-fractional model of second-hand smoker (7) such that

$$\begin{cases} |\mathscr{P}^*(\mathfrak{t}) - \mathscr{P}(\mathfrak{t})| \le M_{(\mathbb{W}_1,\Phi_1)}\Phi_1(\mathfrak{t}), \\ |\mathscr{S}^*(\mathfrak{t}) - \mathscr{S}(\mathfrak{t})| \le M_{(\mathbb{W}_2,\Phi_2)}\Phi_2(\mathfrak{t}), \\ |\mathscr{Q}^*(\mathfrak{t}) - \mathscr{Q}(\mathfrak{t})| \le M_{(\mathbb{W}_3,\Phi_3)}\Phi_3(\mathfrak{t}). \end{cases} \tag{64}$$

Note that Definition 14 is derived from Definition 13. Also, if we take $\Phi_i(\mathfrak{t}) = 1$, then Definition 13 gives the Ulam-Hyers property for the stability of solutions.

Remark 16. Notice that $(\mathscr{P}^*,\mathscr{S}^*,\mathscr{Q}^*) \in \mathbb{X}$ is a solution for (61) if and only if there are $\hbar_1,\hbar_2,\hbar_3 \in C([0,T],\mathbb{R})$ (depending on $\mathscr{P}^*,\mathscr{S}^*,\mathscr{Q}^*$, respectively) such that $\forall \mathfrak{t} \in \mathbb{I}$,

$$|\hbar_i(\mathfrak{t})| < \varepsilon_i\Phi_i(\mathfrak{T}). \tag{65}$$

(i) We have

$$\begin{cases} {}^{FFP}\mathfrak{D}_{0,\mathfrak{t}}^{\omega,\nu}\mathscr{P}^*(\mathfrak{t}) = \mathbb{W}_1(\mathfrak{t},\mathscr{P}^*(\mathfrak{t}),\mathscr{S}^*(\mathfrak{t}),\mathscr{Q}^*(\mathfrak{t})) + \hbar_1(\mathfrak{t}), \\ {}^{FFP}\mathfrak{D}_{0,\mathfrak{t}}^{\omega,\nu}\mathscr{S}^*(\mathfrak{t}) = \mathbb{W}_2(\mathfrak{t},\mathscr{P}^*(\mathfrak{t}),\mathscr{S}^*(\mathfrak{t}),\mathscr{Q}^*(\mathfrak{t})) + \hbar_2(\mathfrak{t}), \\ {}^{FFP}\mathfrak{D}_{0,\mathfrak{t}}^{\omega,\nu}\mathscr{Q}^*(\mathfrak{t}) = \mathbb{W}_3(\mathfrak{t},\mathscr{P}^*(\mathfrak{t}),\mathscr{S}^*(\mathfrak{t}),\mathscr{Q}^*(\mathfrak{t})) + \hbar_3(\mathfrak{t}). \end{cases} \tag{66}$$

The Ulam–Hyers stability is discussed here to the given fractal-fractional model of second-hand smoker (7).

Theorem 17. *If the assumption (H1) is fulfilled, then the given fractal-fractional model of second-hand smoker (7) is Ulam–Hyers stable on $\mathbb{I} := [0,T]$ and also is generalized Ulam–Hyers stable such that*

$$\frac{\nu T^{\nu+\omega-1}\Gamma(\nu)}{\Gamma(\nu+\omega)}w_i < 1, i \in \{1,2,3\}, \tag{67}$$

where w_i is given by (43).

Proof. Let $\varepsilon_1 > 0$ and $\mathscr{P}^* \in \mathbb{M}$ be arbitrary such that

$$\left|{}^{FFP}\mathfrak{D}_{0,\mathfrak{t}}^{\omega,\nu}\mathscr{P}^*(\mathfrak{t}) - \mathbb{W}_1(\mathfrak{t},\mathscr{P}^*(\mathfrak{t}),\mathscr{S}^*(\mathfrak{t}),\mathscr{Q}^*(\mathfrak{t}))\right| < \varepsilon_1. \tag{68}$$

Then, from Remark 1, we can find a function $\hbar_1(\mathfrak{t})$ satisfying

$${}^{FFP}\mathfrak{D}_{0,\mathfrak{t}}^{\omega,\nu}\mathscr{P}^*(\mathfrak{t}) = \mathbb{W}_1(\mathfrak{t},\mathscr{P}^*(\mathfrak{t}),\mathscr{S}^*(\mathfrak{t}),\mathscr{Q}^*(\mathfrak{t})) + \hbar_1(\mathfrak{t}), \tag{69}$$

with $|\hbar_1(\mathfrak{t})| \le \varepsilon_1$. It follows that

$$\begin{aligned} \mathscr{P}^*(\mathfrak{t}) = \mathscr{P}_0 &+ \frac{\nu}{\Gamma(\omega)}\int_0^{\mathfrak{t}}\mathfrak{w}^{\nu-1}(\mathfrak{t}-\mathfrak{w})^{\omega-1}\mathbb{W}_1(\mathfrak{w},\mathscr{P}^*(\mathfrak{w}),\mathscr{S}^*(\mathfrak{w}),\mathscr{Q}^*(\mathfrak{w}))d\mathfrak{w} \\ &+ \frac{\nu}{\Gamma(\omega)}\int_0^{\mathfrak{t}}\mathfrak{w}^{\nu-1}(\mathfrak{t}-\mathfrak{w})^{\omega-1}\hbar_1(\mathfrak{w})d\mathfrak{w}. \end{aligned} \tag{70}$$

By Theorem 9, let $\mathscr{P} \in \mathbb{M}$ be the unique solution of the given fractal-fractional model of second-hand smoker (7). Then, $\mathscr{P}(\mathfrak{t})$ is defined as

$$\mathscr{P}(\mathfrak{t}) = \mathscr{P}_0 + \frac{\nu}{\Gamma(\omega)}\int_0^{\mathfrak{t}}\mathfrak{w}^{\nu-1}(\mathfrak{t}-\mathfrak{w})^{\omega-1}\mathbb{W}_1(\mathfrak{w},\mathscr{P}(\mathfrak{w}),\mathscr{S}(\mathfrak{w}),\mathscr{Q}(\mathfrak{w}))d\mathfrak{w}. \tag{71}$$

Therefore,

$$\begin{aligned} |\mathscr{P}^*(\mathfrak{t}) - \mathscr{P}(\mathfrak{t})| &\le \frac{\nu}{\Gamma(\omega)}\int_0^{\mathfrak{t}}\mathfrak{w}^{\nu-1}(\mathfrak{t}-\mathfrak{w})^{\omega-1}|\hbar_1(\mathfrak{w})|d\mathfrak{w} \\ &\quad + \frac{\nu}{\Gamma(\omega)}\int_0^{\mathfrak{t}}\mathfrak{w}^{\nu-1}(\mathfrak{t}-\mathfrak{w})^{\omega-1} \\ &\quad \times |\mathbb{W}_1(\mathfrak{w},\mathscr{P}^*(\mathfrak{w}),\mathscr{S}^*(\mathfrak{w}),\mathscr{Q}^*(\mathfrak{w})) \\ &\quad - \mathbb{W}_1(\mathfrak{w},\mathscr{P}(\mathfrak{w}),\mathscr{S}(\mathfrak{w}),\mathscr{Q}(\mathfrak{w}))|d\mathfrak{w} \\ &\le \frac{\nu T^{\nu+\omega-1}\Gamma(\nu)}{\Gamma(\nu+\omega)}\varepsilon_1 + \frac{\nu T^{\nu+\omega-1}\Gamma(\nu)}{\Gamma(\nu+\omega)}w_1\|\mathscr{P}^* - \mathscr{P}\|. \end{aligned} \tag{72}$$

Hence, we get

$$\|\mathscr{P}^* - \mathscr{P}\| \le \frac{\left(\nu T^{\nu+\omega-1}\Gamma(\nu)/\Gamma(\nu+\omega)\right)\varepsilon_1}{1-\left(\nu T^{\nu+\omega-1}\Gamma(\nu)/\Gamma(\nu+\omega)\right)w_1}. \tag{73}$$

If we let $M_{\mathbb{W}_1} = (\nu T^{\nu+\omega-1}\Gamma(\nu))/(\Gamma(\nu+\omega))/(1-(\nu T^{\nu+\omega-1}\Gamma(\nu))/(\Gamma(\nu+\omega))w_1)$, then $\|\mathscr{P}^* - \mathscr{P}\| \le M_{\mathbb{W}_1}\varepsilon_1$. Similarly, we have

$$\|\mathscr{S}^* - \mathscr{S}\| \le M_{\mathbb{W}_2}\varepsilon_2, \|\mathscr{Q}^* - \mathscr{Q}\| \le M_{\mathbb{W}_3}\varepsilon_3, \tag{74}$$

where

$$M_{\mathbb{W}_i} = \frac{\nu T^{\nu+\omega-1}\Gamma(\nu)/\Gamma(\nu+\omega)}{1-\left(\nu T^{\nu+\omega-1}\Gamma(\nu)/\Gamma(\nu+\omega)\right)w_i}, (i \in \{2,3\}). \tag{75}$$

Hence, the Ulam–Hyers stability of the given SHS-model (7) is fulfilled. Next, by assuming

$$M_{\mathbb{W}_i}(\varepsilon_i) = \frac{\left(\nu T^{\nu+\omega-1}\Gamma(\nu)/\Gamma(\nu+\omega)\right)\varepsilon_i}{1-\left(\nu T^{\nu+\omega-1}\Gamma(\nu)/\Gamma(\nu+\omega)\right)w_i}, (i \in \{2,3\}), \tag{76}$$

with $M_{\mathbb{W}_i}(0) = 0$, clearly, the generalized Ulam–Hyers stability is proved. □

Theorem 18. *The condition (H1) is assumed to be held, and*

(H') There are increasing functions $\Phi_i \in C([0,T],\mathbb{R}^+)$, $(i \in \{1,2,3\})$, and $\Lambda_{\Phi_i} > 0$ such that

$$^{FFP}\mathfrak{D}_{0,\mathfrak{t}}^{\omega,\nu}\Phi_i(\mathfrak{t}) < \Lambda_{\Phi_i}\Phi_i(\mathfrak{t}), (i \in \{1,2,3\}), \forall \mathfrak{t} \in \mathbb{I}. \tag{77}$$

Then, the given fractal-fractional model of second-hand smoker (7) is the Ulam–Hyers–Rassias and generalized Ulam–Hyers–Rassias stable.

Proof. For each $\varepsilon_1 > 0$ and for each $\mathscr{P}^* \in \mathbb{M}$ satisfying

$$\left|^{FFP}\mathfrak{D}_{0,\mathfrak{t}}^{\omega,\nu}\mathscr{P}^*(\mathfrak{t}) - \mathbb{W}_1(\mathfrak{t},\mathscr{P}^*(\mathfrak{t}),\mathscr{S}^*(\mathfrak{t}),\mathscr{Q}^*(\mathfrak{t}))\right| < \varepsilon_1\Phi_1(\mathfrak{t}), \tag{78}$$

we can find a function $\hbar_1(\mathfrak{t})$ satisfying

$$^{FFP}\mathfrak{D}_{0,\mathfrak{t}}^{\omega,\nu}\mathscr{P}^*(\mathfrak{t}) = \mathbb{W}_1(\mathfrak{t},\mathscr{P}^*(\mathfrak{t}),\mathscr{S}^*(\mathfrak{t}),\mathscr{Q}^*(\mathfrak{t})) + \hbar_1(\mathfrak{t}), \tag{79}$$

with $|\hbar_1(\mathfrak{t})| \le \varepsilon_1\Phi_1(\mathfrak{t})$. It gives

$$\begin{aligned}\mathscr{P}^*(\mathfrak{t}) = \mathscr{P}_0 &+ \frac{\nu}{\Gamma(\omega)}\int_0^t \mathfrak{w}^{\nu-1}(\mathfrak{t}-\mathfrak{w})^{\omega-1}\mathbb{W}_1(\mathfrak{w},\mathscr{P}^*(\mathfrak{w}),\mathscr{S}^*(\mathfrak{w}),\mathscr{Q}^*(\mathfrak{w}))d\mathfrak{w}\\ &+ \frac{\nu}{\Gamma(\omega)}\int_0^t \mathfrak{w}^{\nu-1}(\mathfrak{t}-\mathfrak{w})^{\omega-1}\hbar_1(\mathfrak{w})d\mathfrak{w}.\end{aligned} \tag{80}$$

By Theorem 9, let $\mathscr{P} \in \mathbb{M}$ be the unique solution of the given fractal-fractional model of second-hand smoker (7). Then, $\mathscr{P}(\mathfrak{t})$ is given by

$$\mathscr{P}(\mathfrak{t}) = \mathscr{P}_0 + \frac{\nu}{\Gamma(\omega)}\int_0^t \mathfrak{w}^{\nu-1}(\mathfrak{t}-\mathfrak{w})^{\omega-1}\mathbb{W}_1(\mathfrak{w},\mathscr{P}(\mathfrak{w}),\mathscr{S}(\mathfrak{w}),\mathscr{Q}(\mathfrak{w}))d\mathfrak{w}. \tag{81}$$

Then, by (77),

$$\begin{aligned}|\mathscr{P}^*(\mathfrak{t}) - \mathscr{P}(\mathfrak{t})| &\le \frac{\nu}{\Gamma(\omega)}\int_0^t \mathfrak{w}^{\nu-1}(\mathfrak{t}-\mathfrak{w})^{\omega-1}|\hbar_1(\mathfrak{w})|d\mathfrak{w}\\ &\quad + \frac{\nu}{\Gamma(\omega)}\int_0^t \mathfrak{w}^{\nu-1}(\mathfrak{t}-\mathfrak{w})^{\omega-1}\\ &\quad \times |\mathbb{W}_1(\mathfrak{w},\mathscr{P}^*(\mathfrak{w}),\mathscr{S}^*(\mathfrak{w}),\mathscr{Q}^*(\mathfrak{w}))\\ &\quad - \mathbb{W}_1(\mathfrak{w},\mathscr{P}(\mathfrak{w}),\mathscr{S}(\mathfrak{w}),\mathscr{Q}(\mathfrak{w}))|d\mathfrak{w}\\ &\le \frac{\varepsilon_1\nu}{\Gamma(\omega)}\int_0^t \mathfrak{w}^{\nu-1}(\mathfrak{t}-\mathfrak{w})^{\omega-1}\Phi_1(\mathfrak{w})d\mathfrak{w}\\ &\quad + \frac{\nu T^{\nu+\omega-1}\Gamma(\nu)}{\Gamma(\nu+\omega)}w_1\|\mathscr{P}^*-\mathscr{P}\|\\ &\le \varepsilon_1\Lambda_{\Phi_1}\Phi_1(\mathfrak{t}) + \frac{\nu T^{\nu+\omega-1}\Gamma(\nu)}{\Gamma(\nu+\omega)}w_1\|\mathscr{P}^*-\mathscr{P}\|.\end{aligned} \tag{82}$$

Accordingly, it gives

$$\|\mathscr{P}^*-\mathscr{P}\| \le \frac{\varepsilon_1\Lambda_{\Phi_1}\Phi_1(\mathfrak{t})}{1-\left(\nu T^{\nu+\omega-1}\Gamma(\nu)/\Gamma(\nu+\omega)\right)w_1}. \tag{83}$$

If we let

$$M_{(\mathbb{W}_1,\Phi_1)} = \frac{\Lambda_{\Phi_1}}{1-\left(\nu T^{\nu+\omega-1}\Gamma(\nu)/\Gamma(\nu+\omega)\right)w_1}, \tag{84}$$

then $\|\mathscr{P}^*-\mathscr{P}\| \le \varepsilon_1 M_{(\mathbb{W}_1,\Phi_1)}\Phi_1(\mathfrak{t})$. Similarly, we have

$$\|\mathscr{S}^*-\mathscr{S}\| \le \varepsilon_2 M_{(\mathbb{W}_2,\Phi_2)}\Phi_2(\mathfrak{t}), \|\mathscr{Q}^*-\mathscr{Q}\| \le \varepsilon_3 M_{(\mathbb{W}_3,\Phi_3)}\Phi_3(\mathfrak{t}), \tag{85}$$

where

$$M_{(\mathbb{W}_i,\Phi_i)} = \frac{\Lambda_{\Phi_i}}{1-\left(\nu T^{\nu+\omega-1}\Gamma(\nu)/\Gamma(\nu+\omega)\right)w_i}, (i \in \{2,3\}). \tag{86}$$

Hence, the given fractal-fractional model of second-hand smoker (7) is stable in the sense of Ulam–Hyers–Rassias. Along with this, by setting $\varepsilon_i = 1, (i \in \{1,2,3\})$, the mentioned fractal-fractional model of second-hand smoker (7) is generalized Ulam–Hyers–Rassias stable. □

7. Steady-State Analysis and Local Stability

Here, we follow our investigation for obtaining equilibrium points of the supposed fractal-fractional system (7).

7.1. Disease-free equilibrium point. Define the following homogeneous system of equations:

$$^{FFP}\mathfrak{D}_{0,\mathfrak{t}}^{\omega,\nu}\mathscr{P}(\mathfrak{t}) = {}^{FFP}\mathfrak{D}_{0,\mathfrak{t}}^{\omega,\nu}\mathscr{S}(\mathfrak{t}) = {}^{FFP}\mathfrak{D}_{0,\mathfrak{t}}^{\omega,\nu}\mathscr{Q}(\mathfrak{t}) = 0, \tag{87}$$

or equivalently

$$\begin{cases} \theta - (s+q_1+r)\mathscr{P}(\mathfrak{t}) - b\mathscr{S}(\mathfrak{t})\mathscr{P}(\mathfrak{t}) = 0, \\ b\mathscr{P}(\mathfrak{t})\mathscr{S}(\mathfrak{t}) + r_1\mathscr{Q}(\mathfrak{t})\mathscr{S}(\mathfrak{t}) - (q_1+q_2+r_2)\mathscr{S}(\mathfrak{t}) = 0, \\ r_2\mathscr{S}(\mathfrak{t}) - r_1\mathscr{S}(\mathfrak{t})\mathscr{Q}(\mathfrak{t}) - (q_3+q_1+\gamma)\mathscr{Q}(\mathfrak{t}) = 0. \end{cases} \tag{88}$$

In this case, the (disease) smoke-free equilibrium point E^0 of the model of second-hand smoker (7) under no infection when $\mathscr{S}^0 = 0$ and $\mathscr{Q}^0 = 0$ is presented by

$$E^0 = \left(\frac{\theta}{s+q_1+r}, 0, 0\right). \tag{89}$$

7.2. Basic Reproduction Number. Here, we calculate the basic reproduction number with the help of the next generation matrix approach [48]. As we know, this quantity denoted by R_0 is considered as the expected value of the rate of infection in each time unit. The infection happens in the susceptible individuals due to the infected individuals, and also, the existence of the endemic equilibrium point to the fractal-fractional second-hand smoker model (7) depends on the value of R_0. To do this, we consider the infected compartments $\mathscr{S}(t)$ and $\mathscr{Q}(t)$. By assuming $\mathscr{Y} = (\mathscr{S}, \mathscr{Q})^T$ and from the infected compartments, we have two vectors say f and v in which we have nonlinear terms in f and the negative of linear terms in v, satisfying

$$\left.\frac{\mathrm{d}\mathscr{Y}}{\mathrm{d}\mathfrak{t}}\right|_{E^0} = f - v, \tag{90}$$

where

$$f = \begin{bmatrix} b\mathscr{S}\mathscr{P} \\ 0 \\ 0 \end{bmatrix}, v = \begin{bmatrix} (q_1+q_2+r_2)\mathscr{S} \\ -\theta + (s+q_1+r)\mathscr{P} + b\mathscr{S}\mathscr{P} \\ -r_2\mathscr{S} + r_1\mathscr{S}\mathscr{Q} + (q_3+q_1+\gamma)\mathscr{Q} \end{bmatrix}. \tag{91}$$

The Jacobian matrices of both matrices f and v are given by

$$\begin{aligned} \mathbb{J}[f] &= \begin{bmatrix} b\mathscr{S} & b\mathscr{P} & 0 \\ 0 & 0 & 0 \\ 0 & 0 & 0 \end{bmatrix}, \mathbb{J}[v] \\ &= \begin{bmatrix} 0 & (q_1+q_2+r_2) & 0 \\ (s+q_1+r)\mathscr{P} + b\mathscr{S} & b\mathscr{P} & 0 \\ 0 & -r_2 + r_1\mathscr{Q} & r_1\mathscr{S} + (q_3+q_1+\gamma) \end{bmatrix}. \end{aligned} \tag{92}$$

Therefore, the Jacobian matrices of both matrices f and v at disease-free equilibrium point E^0 obtained as (89) are given by

$$\begin{aligned} \mathbb{J}[f]\Big|_{E^0} &= \begin{bmatrix} 0 & \dfrac{b\theta}{s+q_1+r} & 0 \\ 0 & 0 & 0 \\ 0 & 0 & 0 \end{bmatrix}, \mathbb{J}[v]\Big|_{E^0} \\ &= \begin{bmatrix} 0 & (q_1+q_2+r_2) & 0 \\ \theta & \dfrac{b\theta}{s+q_1+r} & 0 \\ 0 & -r_2 & (q_3+q_1+\gamma) \end{bmatrix}. \end{aligned} \tag{93}$$

On the other side,

$$\mathbb{J}^{-1}[v]\big|_{E^0} = \begin{bmatrix} -\dfrac{b}{(s+q_1+r)(q_1+q_2+r_2)} & \dfrac{1}{\theta} & 0 \\ \dfrac{1}{q_1+q_2+r_2} & 0 & 0 \\ \dfrac{r_2}{(q_1+q_2+r_2)(q_3+q_1+\gamma)} & 0 & \dfrac{-1}{q_3+q_1+\gamma} \end{bmatrix}. \tag{94}$$

By some simple calculations, we get

$$\mathbb{J}[f]\big|_{E^0} \cdot \mathbb{J}^{-1}[v]\big|_{E^0} = \begin{bmatrix} \dfrac{b\theta}{(s+q_1+r)(q_1+q_2+r_2)} & 0 & 0 \\ 0 & 0 & 0 \\ 0 & 0 & 0 \end{bmatrix}. \tag{95}$$

In the final step, the spectral radius of the next generation matrix $(\mathbb{J}[f]|_{E^0} \cdot \mathbb{J}^{-1}[v]|_{E^0})$ is the basic reproduction number R_0 which is given by

$$R_0 = \rho\left(\mathbb{J}[f]\big|_{E^0} \cdot \mathbb{J}^{-1}[v]\big|_{E^0}\right) = \frac{b\theta}{(s+q_1+r)(q_1+q_2+r_2)}. \tag{96}$$

In Figures 1–4, we plot the dynamics of R_0 by 3D plots and the contours of the basic production number versus different parameters.

7.3. Endemic Equilibrium Point. As we know, the quantity R_0 is a criterion to measure the transmission potential of a infectious disease during a specific time. Whenever $R_0 > 1$, then the fractal-fractional second-hand smoker model (7) involves an endemic equilibrium point $E^* = (\mathscr{P}^*, \mathscr{S}^*, \mathscr{Q}^*)$. To find this point, we must solve the homogeneous system of equation (88) by considering this claim that all state

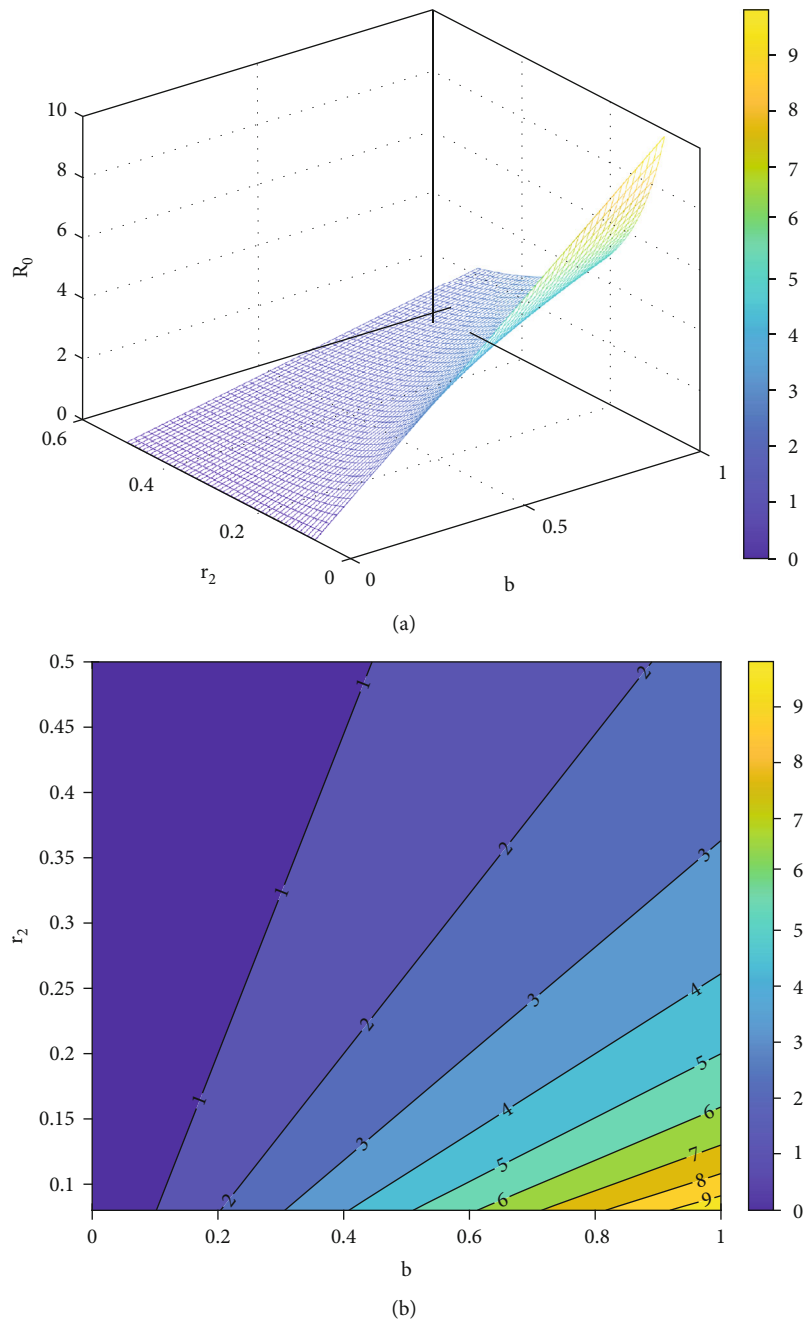

Figure 1: The dynamics of R_0 by 3D plot and the contour of R_0 vs. b and r_2, respectively.

functions $\mathscr{P}(\mathbf{t}), \mathscr{S}(\mathbf{t}), \mathscr{Q}(\mathbf{t})$ are nonzero. Therefore, from the second equation of (88) and by assuming $\mathscr{S}(\mathbf{t}) \neq 0$, we get

$$b\mathscr{P} + r_1\mathscr{Q} = q_1 + q_2 + r_2. \tag{97}$$

Now, we rewrite the first and third equations of (88) as

$$\begin{cases} \theta - [(s + q_1 + r) + b\mathscr{S}]\mathscr{P} = 0, \\ r_2\mathscr{S} - [r_1\mathscr{S} + (q_3 + q_1 + \gamma)]\mathscr{Q} = 0, \end{cases} \tag{98}$$

and we derive the following relations

$$\mathscr{P} = \frac{\theta}{(s + q_1 + r) + b\mathscr{S}}, \mathscr{Q} = \frac{r_2\mathscr{S}}{r_1\mathscr{S} + (q_3 + q_1 + \gamma)}. \tag{99}$$

We substitute above relations into (97) and by assuming the constants $K_1 = s + q_1 + r > 0$, $K_2 = q_1 + q_2 + r_2 > 0$ and $K_3 = q_3 + q_1 + \gamma > 0$, we obtain

$$\frac{b\theta}{K_1 + b\mathscr{S}} + \frac{r_1 r_2 \mathscr{S}}{r_1\mathscr{S} + K_3} - K_2 = 0. \tag{100}$$

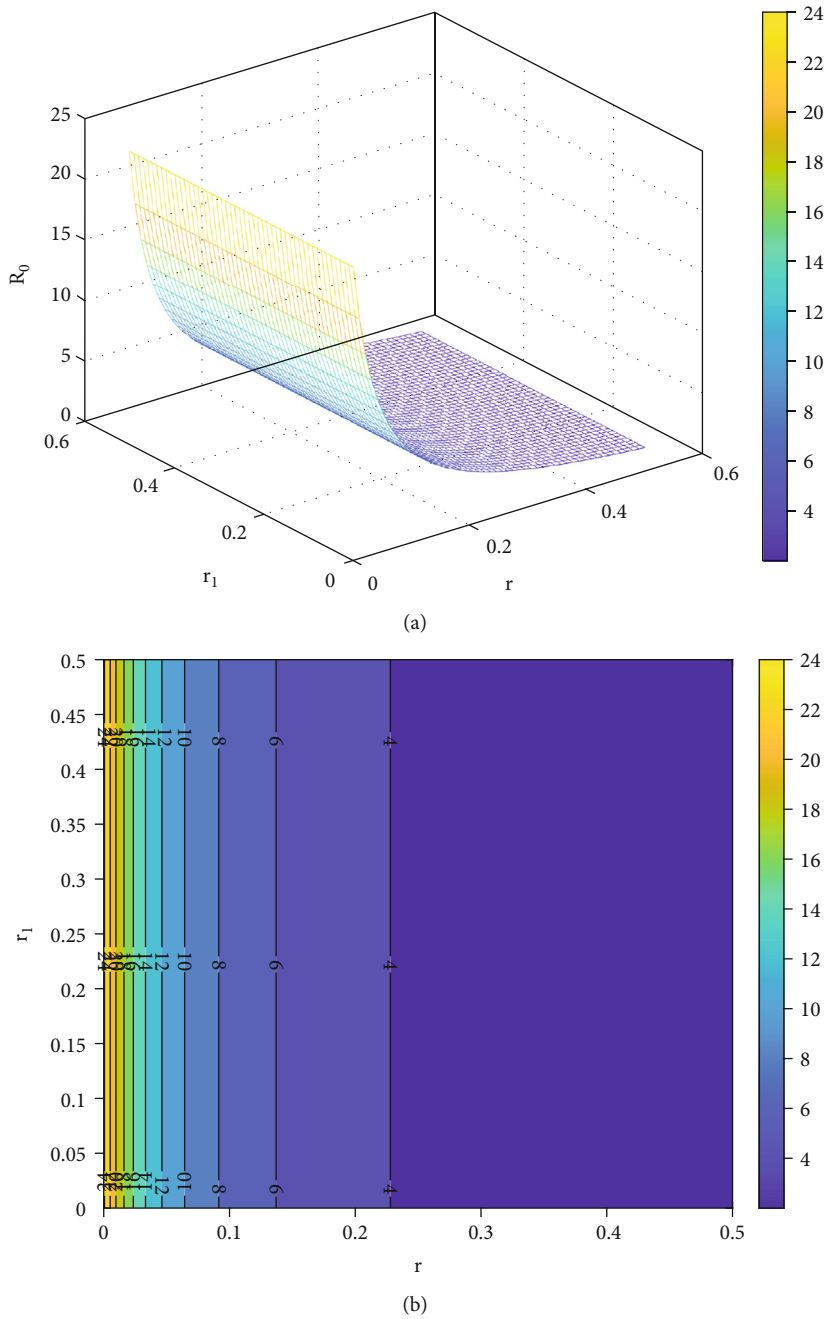

Figure 2: The dynamics of R_0 by 3D plot and the contour of R_0 vs. r and r_1, respectively.

We have

$$\frac{b\theta(r_1\mathcal{S}+K_3)+r_1r_2\mathcal{S}(K_1+b\mathcal{S})-K_2(K_1+b\mathcal{S})(r_1\mathcal{S}+K_3)}{(K_1+b\mathcal{S})(r_1\mathcal{S}+K_3)}=0. \tag{101}$$

Since the denominator of the above equation is nonzero, hence

$$b\theta(r_1\mathcal{S}+K_3)+r_1r_2\mathcal{S}(K_1+b\mathcal{S})-K_2(K_1+b\mathcal{S})(r_1\mathcal{S}+K_3)=0. \tag{102}$$

On the other hand, by the new notation, we know that $R_0=b\theta/K_1K_2$ and so $K_1K_2R_0=b\theta$. Thus, from (102) and by some simple calculations, we derive a quadratic equation with respect to $\mathcal{S}$ as

$$(r_1r_2b-r_1bK_2)\mathcal{S}^2+(r_1r_2K_1-bK_2K_3+r_1K_1K_2(R_0-1))\mathcal{S}+K_1K_2K_3(R_0-1)=0. \tag{103}$$

Set $Y_1=r_1br_2-r_1bK_2$, and

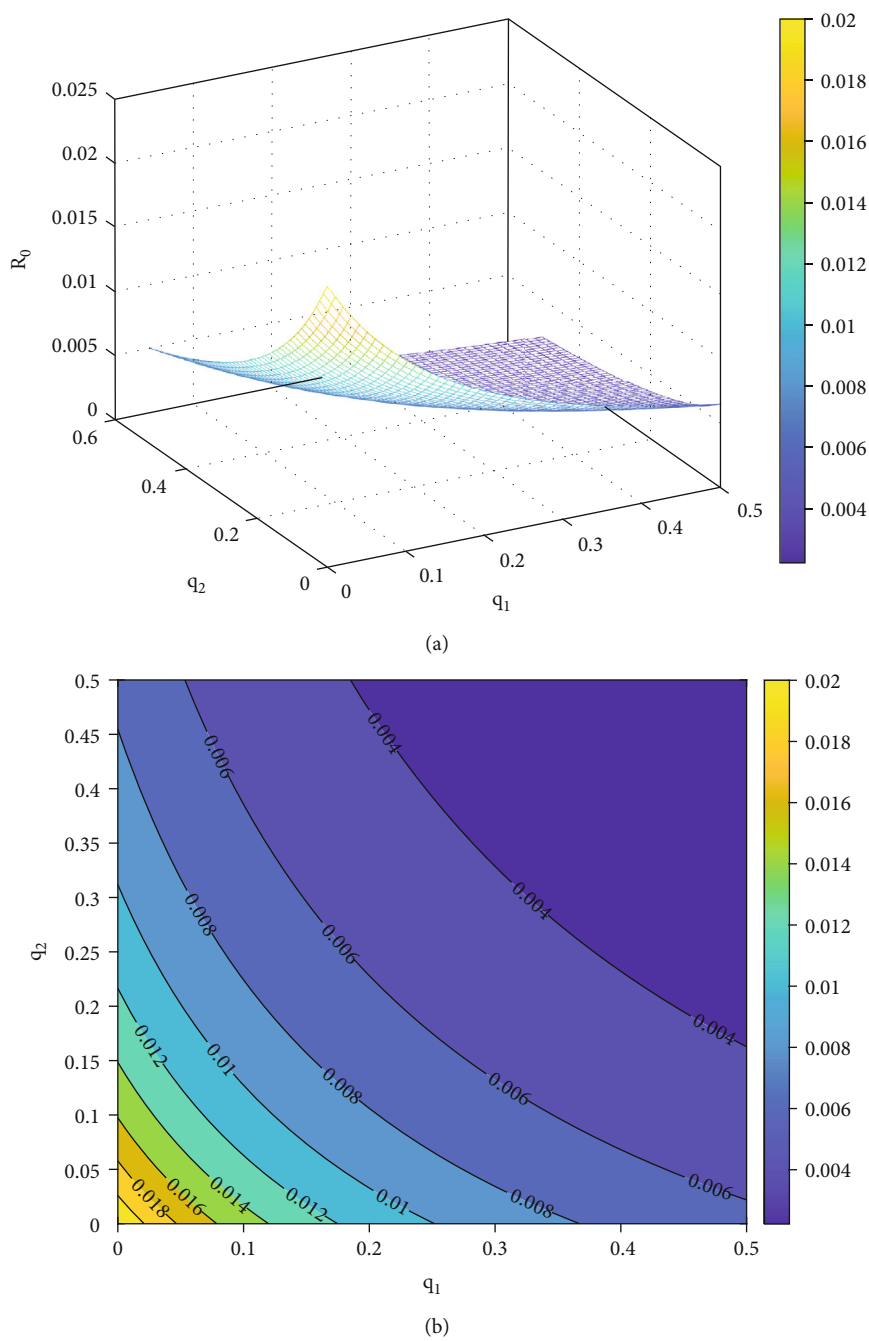

Figure 3: The dynamics of R_0 by 3D plot and the contour of R_0 vs. q_1 and q_2, respectively.

$$Y_2 = r_1 r_2 K_1 - bK_2K_3 + r_1K_1K_2(R_0 - 1), \tag{104}$$

and $Y_3 = K_1K_2K_3(R_0 - 1)$. Consequently, we get

$$\mathcal{S} = \frac{-Y_2 \pm \sqrt{Y_2^2 - 4Y_1Y_3}}{2Y_1}. \tag{105}$$

Since $r_1br_2 < r_1bK_2$, thus $Y_1 < 0$ and if $R_0 > 1$, then

$$\mathcal{S}^* = \frac{-Y_2 - \sqrt{Y_2^2 - 4Y_1Y_3}}{2Y_1}. \tag{106}$$

Simply, $\mathcal{P}^*$ and $\mathcal{Q}^*$ can be obtained by inserting the equation (106) into equation (99), and therefore,

$$\mathcal{P}^* = \frac{\theta}{(s + q_1 + r) + b\left(-Y_2 - \sqrt{Y_2^2 - 4Y_1Y_3}/2Y_1\right)}, \tag{107}$$

$$\mathcal{Q}^* = \frac{r_2\left(-Y_2 - \sqrt{Y_2^2 - 4Y_1Y_3}/2Y_1\right)}{r_1\left(-Y_2 - \sqrt{Y_2^2 - 4Y_1Y_3}/2Y_1\right) + (q_3 + q_1 + \gamma)}. \tag{108}$$

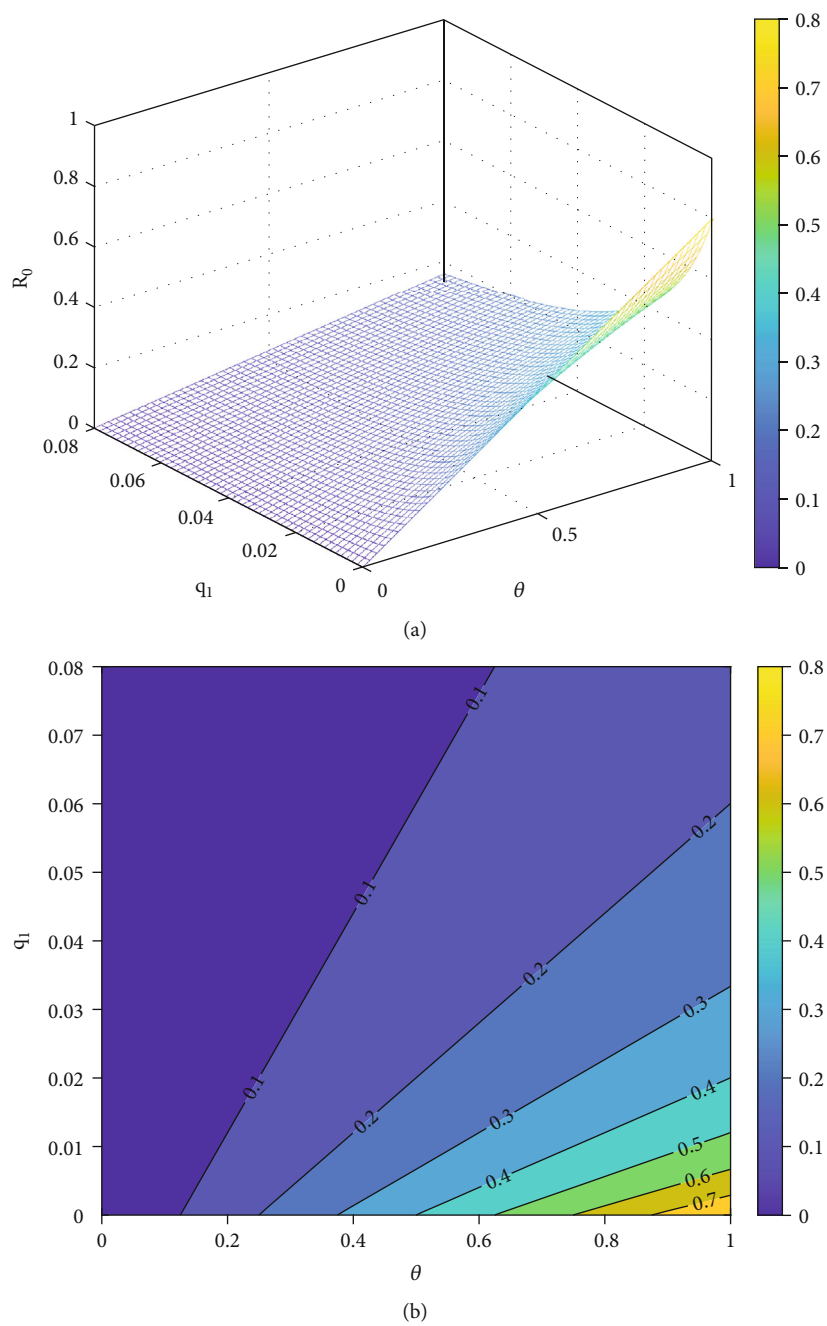

Figure 4: The dynamics of R_0 by 3D plot and the contour of R_0 vs. θ and q_1, respectively.

Theorem 19. *If $R_0 > 1$ or $R_0 = 1$ and $r_1 r_2 K_1 > bK_2K_3$, then there exists $E^* = (\mathscr{P}^*, \mathscr{S}^*, \mathscr{Q}^*)$ as the endemic equilibrium point, where $\mathscr{P}^*$, $\mathscr{S}^*$, and $\mathscr{Q}^*$ are as (106)–(108). Also, If $R_0 < 1$, then this point does not exist.*

Proof. If $R_0 > 1$, then by the above discussions, $E^* = (\mathscr{P}^*, \mathscr{S}^*, \mathscr{Q}^*)$ exists. If $R_0 = 1$, then $Y_2 = r_1 r_2 K_1 - bK_2K_3$ and $Y_3 = 0$. In this case, we have

$$\mathscr{S} = \frac{-Y_2 - |Y_2|}{2Y_1}. \tag{109}$$

On the other side, we know that $Y_1 \neq 0$. Hence, if $Y_2 \leq 0$, then $\mathscr{S} = 0$ and if $Y_2 > 0$, then $\mathscr{S} < 0$. These show the existence of the endemic equilibrium point E^*.

On the other side, $R_0 < 1$ gives $-Y_2 > 0$ and $Y_3 < 0$. Thus, either $\mathscr{S}$ is a complex number or a negative real number, and E^* does not exist. □

In Figures 5 and 6, we show the stability curves of $\mathscr{P}$, $\mathscr{S}$, and $\mathscr{Q}$ at endemic equilibrium point E^* for some values of the fractal and fractional orders.

7.4. Local Asymptotic Stability Analysis. In this place, we aim to investigate the local asymptotic stability of the smoke-free

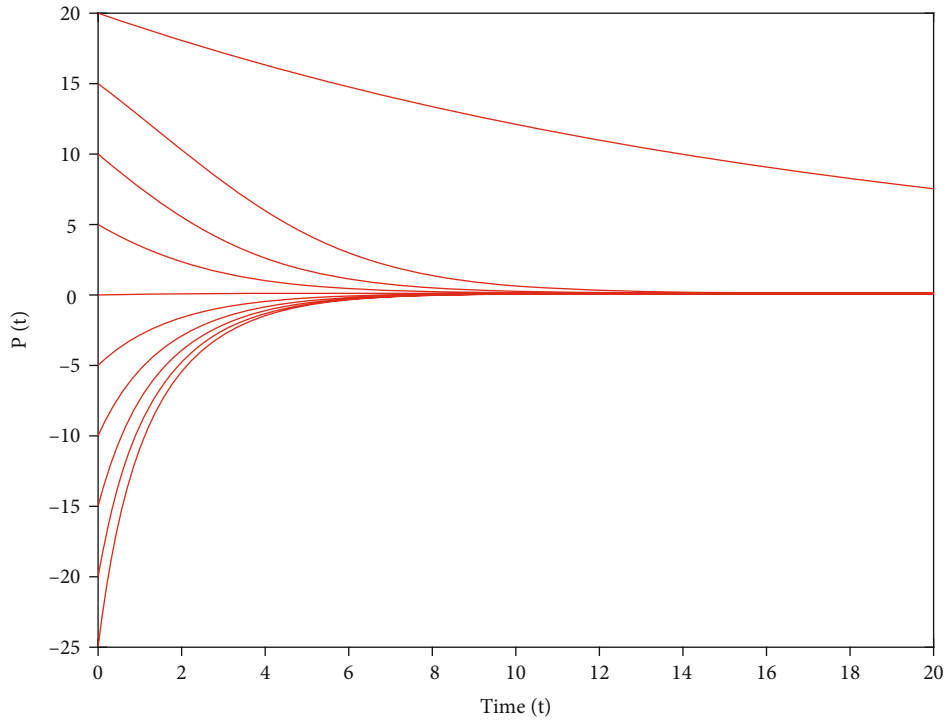

(a)

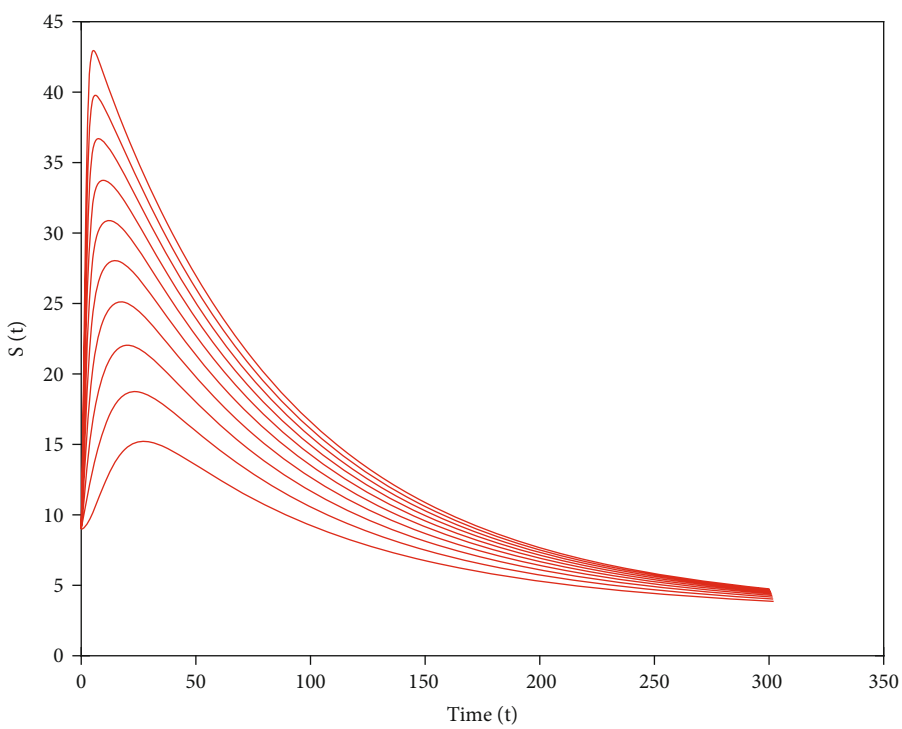

(b)

Figure 5: The stability curves of $\mathscr{P}(\mathbf{t})$ and $\mathscr{S}(\mathbf{t})$ at E^* for $\omega = 0.97$ and $\nu = 0.5$.

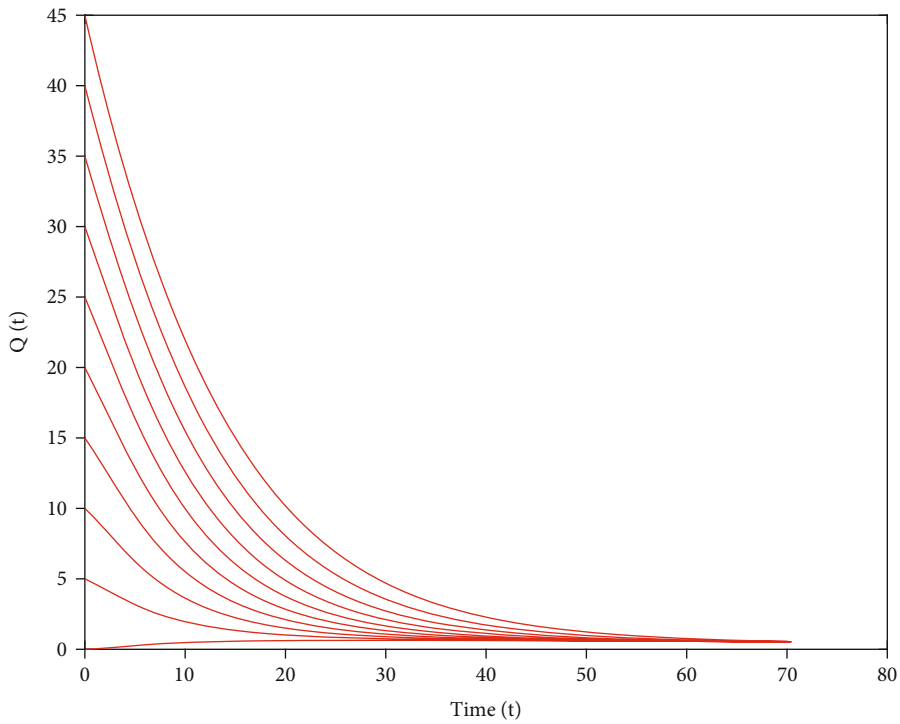

Figure 6: The stability curves of $\mathcal{Q}(t)$ at E^* for $\omega = 0.97$ and $\nu = 0.5$.

point E^0 found in (89) in relation to the fractal-fractional model (7) of second-hand smokers. First, we obtain the Jacobian matrix of the fractal-fractional system (7) as

$$\mathbb{J} = \begin{bmatrix} -(s+q_1+r) - b\mathcal{S} & -b\mathcal{P} & 0 \\ b\mathcal{S} & b\mathcal{P} + r_1\mathcal{Q} - (q_1+q_2+r_2) & r_1\mathcal{S} \\ 0 & r_2 - r_1\mathcal{Q} & -r_1\mathcal{S} - (q_3+q_1+\gamma) \end{bmatrix}. \tag{110}$$

Theorem 20. *The fractal-fractional model (7) of second-hand smokers is locally asymptotically stable at smoke-free equilibrium point E^0 if all roots of the characteristic polynomial* det $(\mathbb{J}(E^0) - \lambda I) = 0$ *are negative or $R_0 < 1$; otherwise, it is unstable.*

Proof. In view of (110), the Jacobian matrix $\mathbb{J}(E^0)$ of the model (7) at smoke-free equilibrium point E^0 is given as

$$\mathbb{J}(E^0) = \begin{bmatrix} -(s+q_1+r) & \dfrac{-b\theta}{s+q_1+r} & 0 \\ 0 & \dfrac{b\theta}{s+q_1+r} - (q_1+q_2+r_2) & 0 \\ 0 & r_2 & -(q_3+q_1+\gamma) \end{bmatrix}. \tag{111}$$

By considering the Jacobian matrix (111) and by det $(\mathbb{J}(E^0) - \lambda I) = 0$, the characteristic polynomial becomes

$$(\lambda + s + q_1 + r)(\lambda + q_3 + q_1 + \gamma)\left(\lambda - \left(\frac{b\theta}{s+q_1+r} - (q_1+q_2+r_2)\right)\right) = 0. \tag{112}$$

The roots of the above polynomial are

$$\lambda_1 = -(s+q_1+r), \lambda_2 = -(q_3+q_1+\gamma), \lambda_3 = \frac{b\theta}{s+q_1+r} - (q_1+q_2+r_2). \tag{113}$$

Since all parameters are assumed to be positive, we clearly have $\lambda_1 < 0$ and $\lambda_2 < 0$. On the other hand, if $R_0 < 1$, then $R_0 - 1 < 0$. So, we can write

$$\frac{b\theta}{(s+q_1+r)(q_1+q_2+r_2)} < 1. \tag{114}$$

Hence,

$$\frac{b\theta}{(s+q_1+r)} < (q_1+q_2+r_2). \tag{115}$$

Consequently, $\lambda_3 = b\theta/(s+q_1+r) - (q_1+q_2+r_2) < 0$. Thus, all of roots are negative, and so the fractal-fractional second-hand smoker model (7) is locally asymptotically stable around the smoke-free equilibrium point E^0. This completes the proof. □

7.5. Sensitivity Analysis. To find out how sensitive the parameters in each model are to the transmission of infections or diseases, the authors use a criterion introduced by Chitnis et al. [49]. Here, to obtain the sensitivity of R_0 in terms of each of its parameters, we compute the partial derivative with respect to every parameter in the reproduction number. In other words, if p is an arbitrary parameter, then the sensitivity index of R_0 versus p is calculated by

$$\mathbb{S}_p^{\mathcal{R}_0} = \frac{p}{\mathcal{R}_0}\left[\frac{\partial \mathcal{R}_0}{\partial p}\right]. \tag{116}$$

Now, according to the above relation, we have

$$\mathbb{S}_b^{\mathcal{R}_0} = \frac{b}{\mathcal{R}_0}\left[\frac{\theta}{(q_1+r_2+q_2)(q_1+r+s)}\right] > 0, \tag{117}$$

$$\mathbb{S}_\theta^{\mathcal{R}_0} = \frac{\theta}{\mathcal{R}_0}\left[\frac{b}{(q_1+r_2+q_2)(q_1+r+s)}\right] > 0, \tag{118}$$

$$\mathbb{S}_s^{\mathcal{R}_0} = \frac{s}{\mathcal{R}_0}\left[-\frac{b\theta}{(q_1+r_2+q_2)(q_1+r+s)^2}\right] < 0, \tag{119}$$

$$\mathbb{S}_{q_1}^{\mathcal{R}_0} = \frac{q_1}{\mathcal{R}_0}\left[-\frac{b\theta}{(q_1+q_2+r_2)(q_1+r+s)^2} - \frac{b\theta}{(q_1+r_2+q_2)^2(q_1+r+s)}\right] < 0, \tag{120}$$

$$\mathbb{S}_r^{\mathcal{R}_0} = \frac{r}{\mathcal{R}_0}\left[-\frac{b\theta}{(q_1+r_2+q_2)(q_1+r+s)^2}\right] < 0, \tag{121}$$

$$\mathbb{S}_{q_2}^{\mathcal{R}_0} = \frac{q_2}{\mathcal{R}_0}\left[-\frac{b\theta}{(q_1+r_2+q_2)^2(q_1+r+s)}\right] < 0, \tag{122}$$

$$\mathbb{S}_{r_2}^{\mathcal{R}_0} = \frac{r_2}{\mathcal{R}_0}\left[-\frac{b\theta}{(q_1+r_2+q_2)^2(q_1+r+s)}\right] < 0. \tag{123}$$

The numeric values for sensitivity indices (120) are given in Table 1.

In Figure 7, when the sign of sensitivity index is positive, then each increase (decrease) in the value of parameters (assuming the remaining parameters to be constant) increases (decreases) the value of R_0. The negative sign in this index gives the inverse result for R_0. In the sensitivity analysis of our second-hand smoker model (7), it is observed that R_0 increases by increasing the values of b, θ and decreases by increasing the values of s, q_1, r, q_2, r_2. For example, $\mathbb{S}_{q_1}^{\mathcal{R}_0} = -0.0061$ means that an increase in q_1 by 10% decreases R_0 by 0.061%. Therefore, to reduce the spread of infections, those parameters having negative sensitivity indices must be minimized in the environment.

Table 1: Sensitivity of the R_0 versus proposed parameters.

Parameter	$\mathbb{S}$	Value	Parameter	$\mathbb{S}$	Value
b	$\mathbb{S}_b^{\mathcal{R}_0}$	+1.0000	θ	$\mathbb{S}_\theta^{\mathcal{R}_0}$	+1.0000
s	$\mathbb{S}_s^{\mathcal{R}_0}$	-9.1621e-05	q_1	$\mathbb{S}_{q_1}^{\mathcal{R}_0}$	-0.0061
r	$\mathbb{S}_r^{\mathcal{R}_0}$	-0.0366	q_2	$\mathbb{S}_{q_2}^{\mathcal{R}_0}$	-0.0018
r_2	$\mathbb{S}_{r_2}^{\mathcal{R}_0}$	-4.0813e-04			

8. Numerical scheme

In this section, we describe the numerical scheme in relation to the fractal-fractional model of second-hand smoker (7). For this, we have taken help from the technique regarding two-step Lagrange polynomials known as the fractional Adams-Bashforth (AB) method [50]. To begin this process, we present the numerical method of fractal-fractional integral equation (16) using a new approach at $\mathfrak{t}_{n+1}$. In other words, we discretize the mentioned equation (16) for $\mathfrak{t} = \mathfrak{t}_{n+1}$, and we have

$$\begin{cases} \mathcal{P}(\mathfrak{t}_{n+1}) = \mathcal{P}_0 + \dfrac{\nu}{\Gamma(\omega)}\displaystyle\int_0^{\mathfrak{t}_{n+1}} (\mathfrak{t}_{n+1}-\mathfrak{w})^{\omega-1}\mathcal{H}_1(\mathfrak{w})\,d\mathfrak{w}, \\ \mathcal{S}(\mathfrak{t}_{n+1}) = \mathcal{S}_0 + \dfrac{\nu}{\Gamma(\omega)}\displaystyle\int_0^{\mathfrak{t}_{n+1}} (\mathfrak{t}_{n+1}-\mathfrak{w})^{\omega-1}\mathcal{H}_2(\mathfrak{w})\,d\mathfrak{w}, \\ \mathcal{Q}(\mathfrak{t}_{n+1}) = \mathcal{Q}_0 + \dfrac{\nu}{\Gamma(\omega)}\displaystyle\int_0^{\mathfrak{t}_{n+1}} (\mathfrak{t}_{n+1}-\mathfrak{w})^{\omega-1}\mathcal{H}_3(\mathfrak{w})\,d\mathfrak{w}, \end{cases} \tag{124}$$

where

$$\begin{cases} \mathcal{H}_1(\mathfrak{w}) = \mathfrak{w}^{\nu-1}\mathbb{W}_1(\mathfrak{w}, \mathcal{P}(\mathfrak{w}), \mathcal{S}(\mathfrak{w}), \mathcal{Q}(\mathfrak{w})), \\ \mathcal{H}_2(\mathfrak{w}) = \mathfrak{w}^{\nu-1}\mathbb{W}_2(\mathfrak{w}, \mathcal{P}(\mathfrak{w}), \mathcal{S}(\mathfrak{w}), \mathcal{Q}(\mathfrak{w})), \\ \mathcal{H}_3(\mathfrak{w}) = \mathfrak{w}^{\nu-1}\mathbb{W}_3(\mathfrak{w}, \mathcal{P}(\mathfrak{w}), \mathcal{S}(\mathfrak{w}), \mathcal{Q}(\mathfrak{w})). \end{cases} \tag{125}$$

By approximating above integrals, we get

$$\begin{cases} \mathcal{P}(\mathfrak{t}_{n+1}) = \mathcal{P}_0 + \dfrac{\nu}{\Gamma(\omega)}\displaystyle\sum_{l=0}^{n}\int_{\mathfrak{t}_l}^{\mathfrak{t}_{l+1}} (\mathfrak{t}_{n+1}-\mathfrak{w})^{\omega-1}\mathcal{H}_1(\mathfrak{w})\,d\mathfrak{w}, \\ \mathcal{S}(\mathfrak{t}_{n+1}) = \mathcal{S}_0 + \dfrac{\nu}{\Gamma(\omega)}\displaystyle\sum_{l=0}^{n}\int_{\mathfrak{t}_l}^{\mathfrak{t}_{l+1}} (\mathfrak{t}_{n+1}-\mathfrak{w})^{\omega-1}\mathcal{H}_2(\mathfrak{w})\,d\mathfrak{w}, \\ \mathcal{Q}(\mathfrak{t}_{n+1}) = \mathcal{Q}_0 + \dfrac{\nu}{\Gamma(\omega)}\displaystyle\sum_{l=0}^{n}\int_{\mathfrak{t}_l}^{\mathfrak{t}_{l+1}} (\mathfrak{t}_{n+1}-\mathfrak{w})^{\omega-1}\mathcal{H}_3(\mathfrak{w})\,d\mathfrak{w}. \end{cases} \tag{126}$$

In the sequel, we approximate the functions $\mathcal{H}_1(\mathfrak{w}), \mathcal{H}_2(\mathfrak{w}), \mathcal{H}_3(\mathfrak{w})$ introduced by (125), on the interval $[\mathfrak{t}_l, \mathfrak{t}_{l+1}]$ via

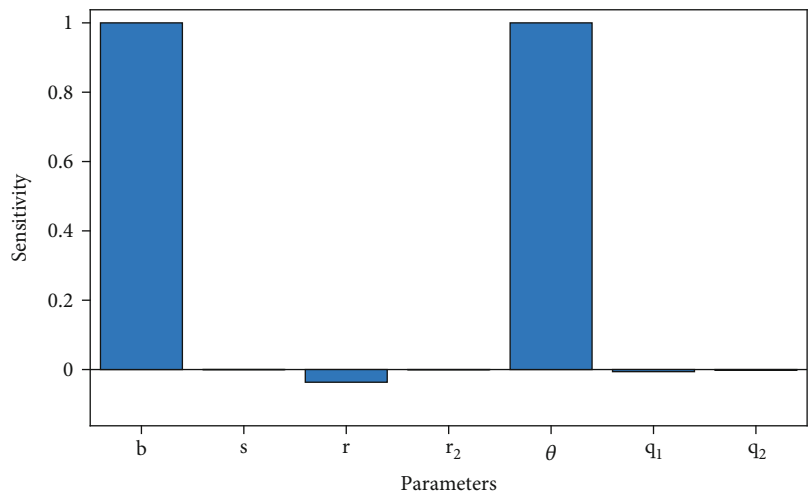

Figure 7: Global sensitivity analysis of model (7) based on R_0 (96) and sensitivity analysis (120).

two-step Lagrange interpolation polynomials with the step size $\mathrm{h} = \mathfrak{t}_l - \mathfrak{t}_{l-1}$ as

$$\begin{aligned}
\mathscr{H}^*_{1,l}(\mathfrak{w}) &\simeq \frac{\mathfrak{w}-\mathfrak{t}_{l-1}}{\mathrm{h}}\mathfrak{t}_l^{\nu-1}\mathbb{W}_1(\mathfrak{w}_l,\mathscr{P}_l,\mathcal{S}_l,\mathcal{Q}_l) - \frac{\mathfrak{w}-\mathfrak{t}_l}{\mathrm{h}}\mathfrak{t}_{l-1}^{\nu-1}\mathbb{W}_1(\mathfrak{w}_{l-1},\mathscr{P}_{l-1},\mathcal{S}_{l-1},\mathcal{Q}_{l-1}),\\
\mathscr{H}^*_{2,l}(\mathfrak{w}) &\simeq \frac{\mathfrak{w}-\mathfrak{t}_{l-1}}{\mathrm{h}}\mathfrak{t}_l^{\nu-1}\mathbb{W}_2(\mathfrak{w}_l,\mathscr{P}_l,\mathcal{S}_l,\mathcal{Q}_l) - \frac{\mathfrak{w}-\mathfrak{t}_l}{\mathrm{h}}\mathfrak{t}_{l-1}^{\nu-1}\mathbb{W}_2(\mathfrak{w}_{l-1},\mathscr{P}_{l-1},\mathcal{S}_{l-1},\mathcal{Q}_{l-1}),\\
\mathscr{H}^*_{3,l}(\mathfrak{w}) &\simeq \frac{\mathfrak{w}-\mathfrak{t}_{l-1}}{\mathrm{h}}\mathfrak{t}_l^{\nu-1}\mathbb{W}_3(\mathfrak{w}_l,\mathscr{P}_l,\mathcal{S}_l,\mathcal{Q}_l) - \frac{\mathfrak{w}-\mathfrak{t}_l}{\mathrm{h}}\mathfrak{t}_{l-1}^{\nu-1}\mathbb{W}_3(\mathfrak{w}_{l-1},\mathscr{P}_{l-1},\mathcal{S}_{l-1},\mathcal{Q}_{l-1}).
\end{aligned} \tag{127}$$

Then, we have

$$\begin{cases}
\mathscr{P}(\mathfrak{t}_{n+1}) = \mathscr{P}_0 + \dfrac{\nu}{\Gamma(\omega)}\displaystyle\sum_{l=0}^{n}\int_{\mathfrak{t}_l}^{\mathfrak{t}_{l+1}}(\mathfrak{t}_{n+1}-\mathfrak{w})^{\omega-1}\mathscr{H}^*_{1,l}(\mathfrak{w})\,\mathrm{d}\mathfrak{w},\\
\mathcal{S}(\mathfrak{t}_{n+1}) = \mathcal{S}_0 + \dfrac{\nu}{\Gamma(\omega)}\displaystyle\sum_{l=0}^{n}\int_{\mathfrak{t}_l}^{\mathfrak{t}_{l+1}}(\mathfrak{t}_{n+1}-\mathfrak{w})^{\omega-1}\mathscr{H}^*_{2,l}(\mathfrak{w})\,\mathrm{d}\mathfrak{w},\\
\mathcal{Q}(\mathfrak{t}_{n+1}) = \mathcal{Q}_0 + \dfrac{\nu}{\Gamma(\omega)}\displaystyle\sum_{l=0}^{n}\int_{\mathfrak{t}_l}^{\mathfrak{t}_{l+1}}(\mathfrak{t}_{n+1}-\mathfrak{w})^{\omega-1}\mathscr{H}^*_{3,l}(\mathfrak{w})\,\mathrm{d}\mathfrak{w}.
\end{cases} \tag{128}$$

By evaluating above integrals directly, the numerical solutions of the given fractal-fractional model of second-hand smoker (7) are given by

$$\begin{aligned}
\mathscr{P}_{n+1} &= \mathscr{P}_0 + \frac{\nu\mathrm{h}^{\omega}}{\Gamma(\omega+2)}\sum_{l=0}^{n}\left[\mathfrak{t}_l^{\nu-1}\mathbb{W}_1(\mathfrak{t}_l,\mathscr{P}_l,\mathcal{S}_l,\mathcal{Q}_l)Y_{(n,l)} - \mathfrak{t}_{l-1}^{\nu-1}\mathbb{W}_1(\mathfrak{t}_{l-1},\mathscr{P}_{l-1},\mathcal{S}_{l-1},\mathcal{Q}_{l-1})\widehat{Y}_{(n,l)}\right],\\
\mathcal{S}_{n+1} &= \mathcal{S}_0 + \frac{\nu\mathrm{h}^{\omega}}{\Gamma(\omega+2)}\sum_{l=0}^{n}\left[\mathfrak{t}_l^{\nu-1}\mathbb{W}_2(\mathfrak{t}_l,\mathscr{P}_l,\mathcal{S}_l,\mathcal{Q}_l)Y_{(n,l)} - \mathfrak{t}_{l-1}^{\nu-1}\mathbb{W}_2(\mathfrak{t}_{l-1},\mathscr{P}_{l-1},\mathcal{S}_{l-1},\mathcal{Q}_{l-1})\widehat{Y}_{(n,l)}\right],\\
\mathcal{Q}_{n+1} &= \mathcal{Q}_0 + \frac{\nu\mathrm{h}^{\omega}}{\Gamma(\omega+2)}\sum_{l=0}^{n}\left[\mathfrak{t}_l^{\nu-1}\mathbb{W}_3(\mathfrak{t}_l,\mathscr{P}_l,\mathcal{S}_l,\mathcal{Q}_l)Y_{(n,l)} - \mathfrak{t}_{l-1}^{\nu-1}\mathbb{W}_3(\mathfrak{t}_{l-1},\mathscr{P}_{l-1},\mathcal{S}_{l-1},\mathcal{Q}_{l-1})\widehat{Y}_{(n,l)}\right],
\end{aligned} \tag{129}$$

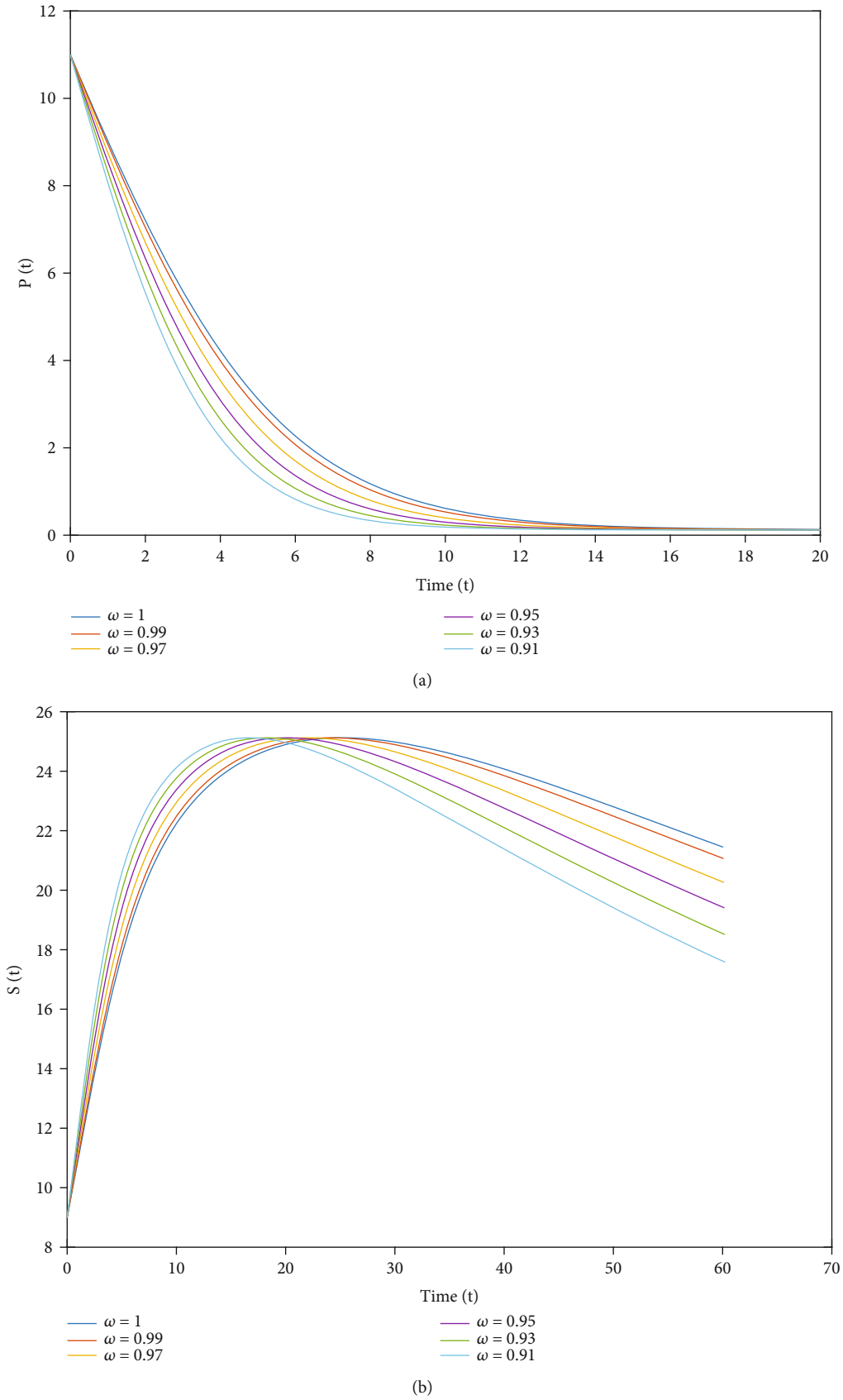

FIGURE 8: The simulation of the functions $\mathscr{P}(\mathbf{t})$ and $\mathscr{S}(\mathbf{t})$ during the time $\mathbf{t}$ for different fractional orders $\omega = 1, 0.99, 0.97, 0.95, 0.93, 0.91$ and fractal dimension $\nu = 0.99$.

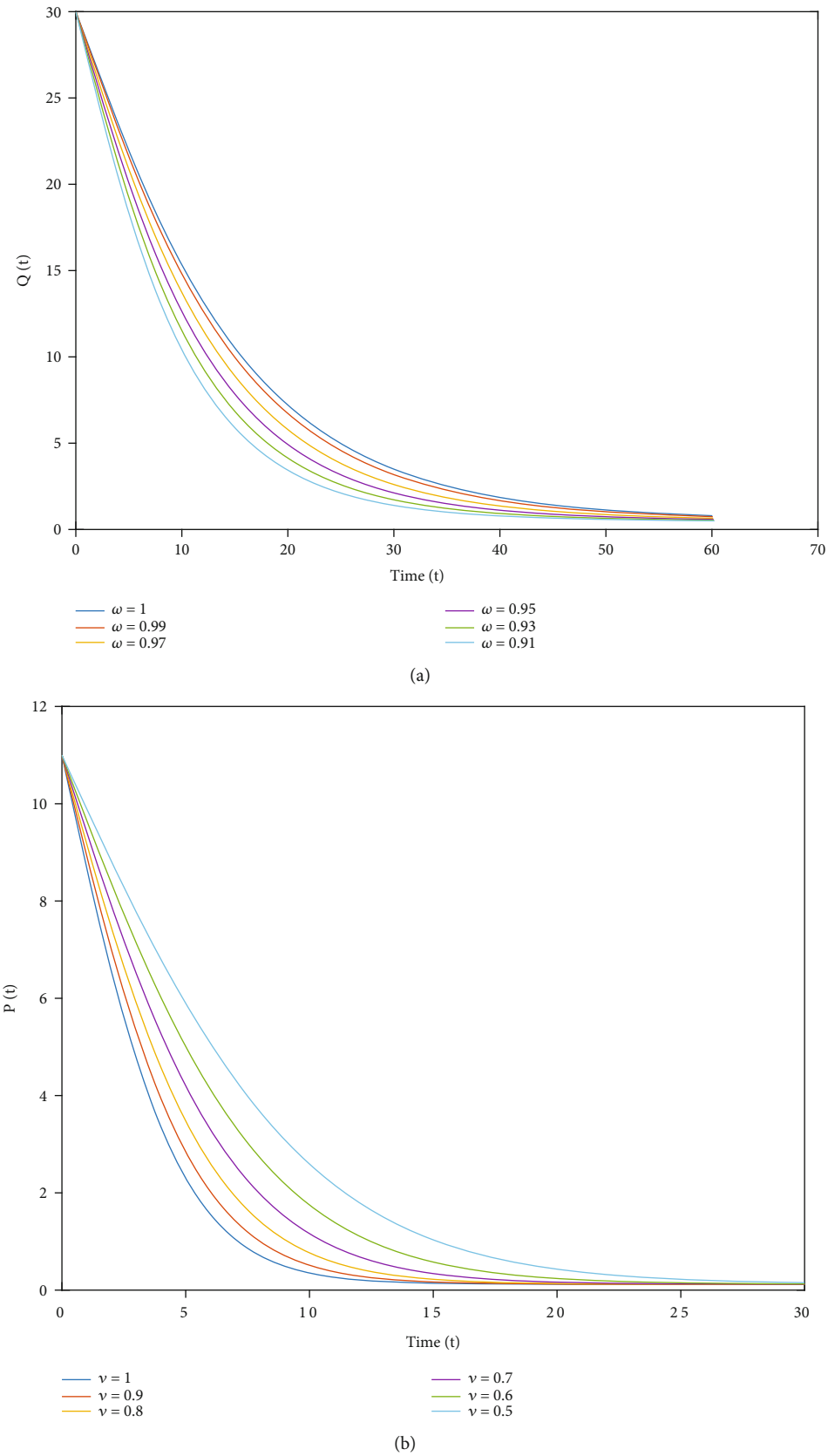

Figure 9: (a) The simulation of the function $\mathcal{Q}(t)$ during the time t for different fractional orders $\omega = 1, 0.99, 0.97, 0.95, 0.93, 0.91$ and fractal dimension $\nu = 0.99$. (b) The simulation of the function $\mathcal{P}(t)$ during the time t for different fractal dimensions $\nu = 1, 0.9, 0.8, 0.7, 0.6, 0.5$ and fractional order $\omega = 0.97$.

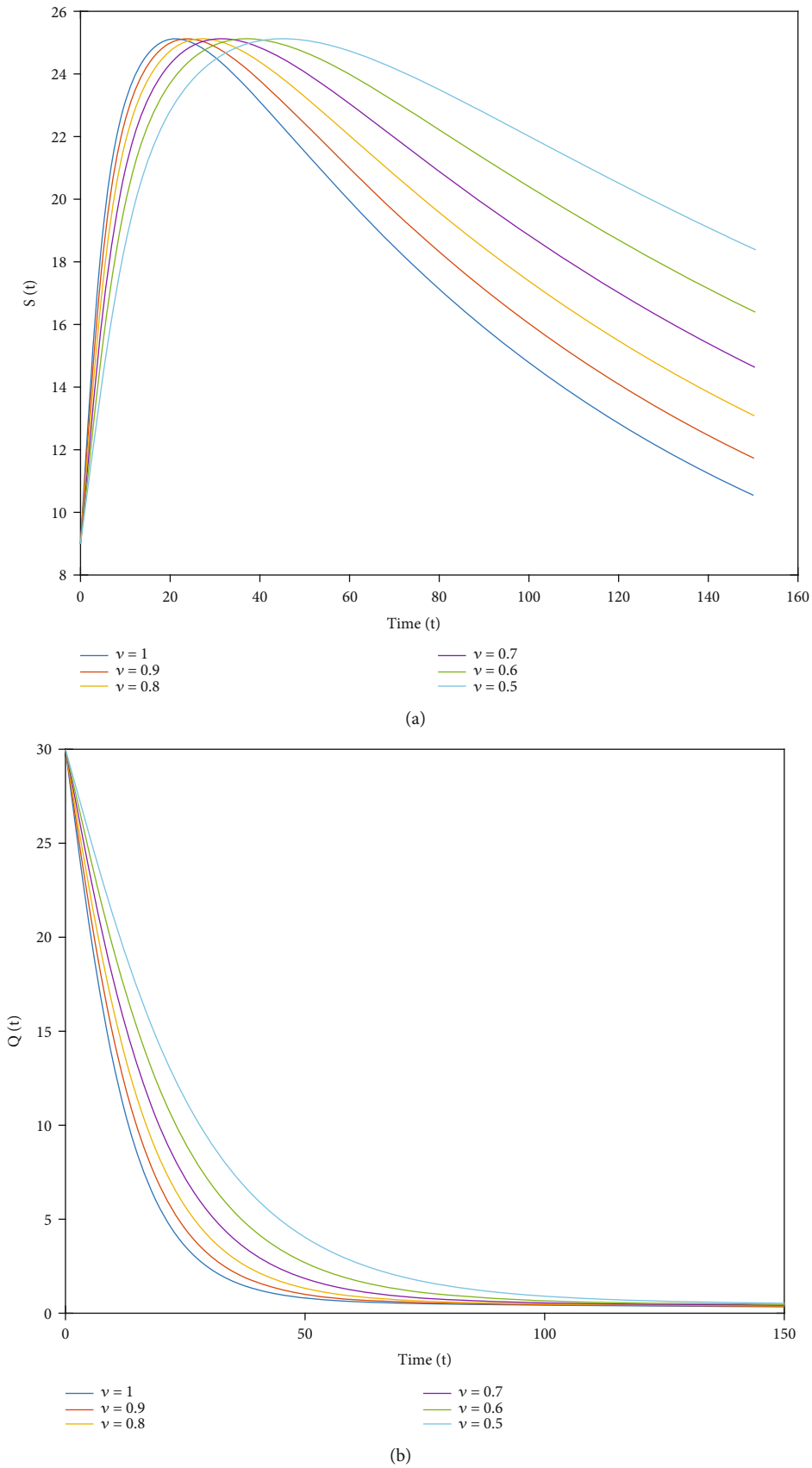

Figure 10: The simulation of the functions $\mathcal{S}(\mathbf{t})$ and $\mathcal{Q}(\mathbf{t})$ during the time $\mathbf{t}$ for different fractal dimensions $\nu = 1, 0.9, 0.8, 0.7, 0.6, 0.5$ and fractional order $\omega = 0.97$.

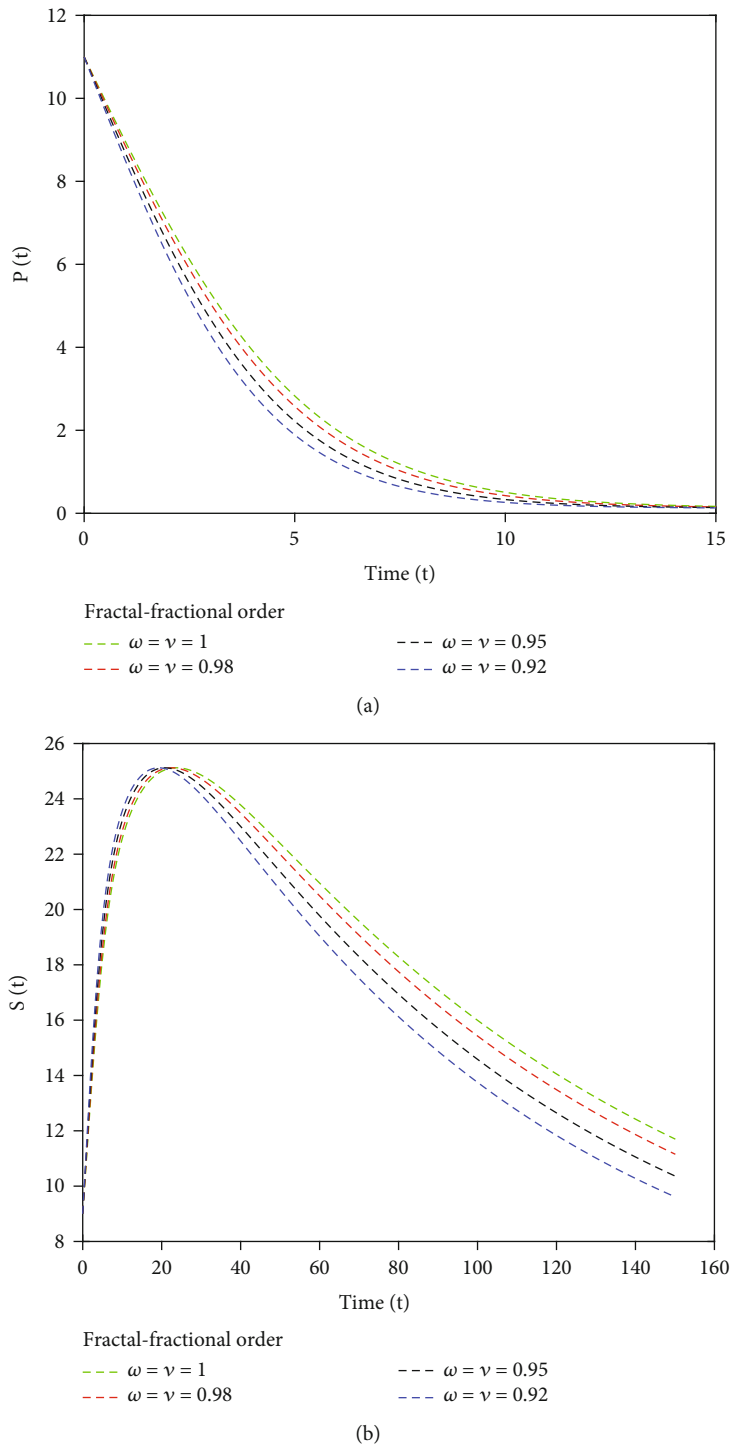

Figure 11: The simulation of the functions $\mathscr{P}(\mathbf{t})$ and $\mathscr{S}(\mathbf{t})$ during the time $\mathbf{t}$ for fractal dimensions and fractional orders $\omega = \nu =$ 1,0.98,0.95,0.92.

where

$$Y_{(n,l)} = (n+1-l)^{\omega}(n-l+2+\omega) - (n-l)^{\omega}(n-l+2+2\omega),$$
$$\widehat{Y}_{(n,l)} = (n+1-l)^{\omega+1} - (n-l)^{\omega}(n-l+1+\omega), \tag{130}$$

where ω is the fractional order of the given fractal-fractional system (7).

9. Simulations

In this section, we simulate and discuss the behavior of the model based on some parameters provided by [45].

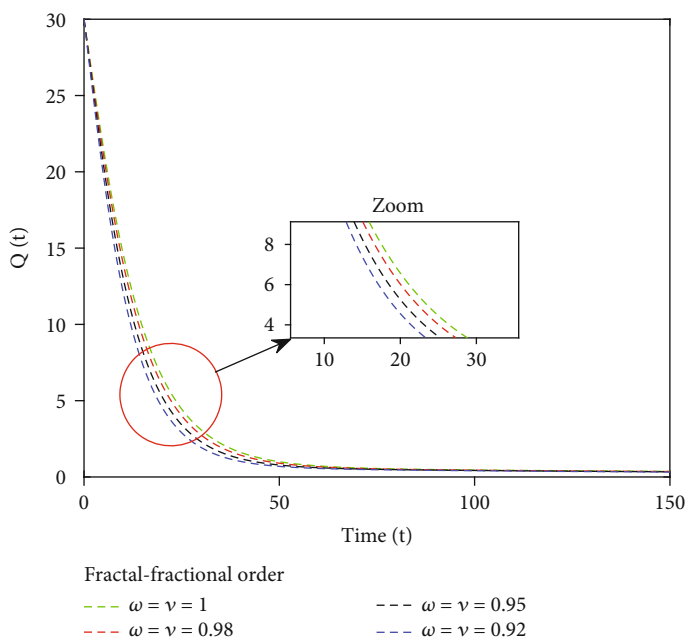

Figure 12: The simulation of the function $\mathcal{Q}(\mathbf{t})$ during the time $\mathbf{t}$ for fractal dimensions and fractional orders $\omega = \nu = 1,0.98,0.95,0.92$.

According to this source, we take $\theta = 0.3$, $s = 0.01$, $q_1 = 0.035$, $r = 0.2$, $b = 0.9001$, $r_1 = 0.009$, $q_2 = 0.01$, $r_2 = 0.01$, $q_3 = 0.1$, and $\gamma = 0.1$. Finally, the initial values for state functions are assumed as $\mathcal{P}(0) = 11$, $\mathcal{S}(0) = 9$, $\mathcal{Q}(0) = 30$. In different figures, we will show the behaviors of three state functions $\mathcal{P}, \mathcal{S}, \mathcal{Q}$ by assuming different values for the fractal order $\nu = 1, 0.9, 0.8, 0.7, 0.6, 0.5$ and fractional orders $\omega = 1.00, 0.99, 0.97, 0.95, 0.93, 0.91$.

More precisely, in Figure 8(a), we see the simulation for different fractional orders $\omega = 1.00,0.99,0.97,0.95,0.93,0.91$ and fractal order $\nu = 0.99$ of the function $\mathcal{P}(\mathbf{t})$ in which the rate of population who addicts to tobacco increases with time $\mathbf{t}$, while in Figure 8(b), the simulation of the function $\mathcal{S}(\mathbf{t})$ for the same values of fractal dimension $\nu = 0.99$ and fractional orders $\omega = 1.00,0.99,0.97,0.95,0.93,0.91$ shows an increase of addiction to tobacco in the population $\mathcal{S}(\mathbf{t})$ by increasing the time $\mathbf{t}$.

In Figure 9(a), we see the simulation for fractional orders $\omega = 1.00,0.99,0.97,0.95,0.93,0.91$ and fractal order $\nu = 0.99$ of the function $\mathcal{Q}(\mathbf{t})$ in which the rate of population who quitting tobacco decreases, while in Figure 9(b), the simulation of the function $\mathcal{P}(t)$ for different fractal orders $\nu = 1,0.9,0.8,0.7,0.6,0.5$ and fractional order $\omega = 0.97$ shows an increase in addiction to tobacco in the population at risk.

In Figure 10, we see the simulation for different fractal orders $\nu = 1,0.9,0.8,0.7,0.6,0.5$ of the functions $\mathcal{S}(\mathbf{t})$ and $\mathcal{Q}(\mathbf{t})$ for fractional order $\omega = 0.97$ in which the addiction to tobacco increases but the population quitting tobacco decreases.

On the other hand, to see the effect of fractional order and fractal dimension simultaneously, we choose different values for these two parameters as $\omega = \nu = 1,0.98,0.95,0.92$. In Figure 11(a), the simulation of the function $\mathcal{P}(\mathbf{t})$ and (Figure 11(b)) the simulation of the function $\mathcal{S}(\mathbf{t})$ during the time $\mathbf{t}$ are plotted. We see that the change in the behavior of curves when the fractal dimension ν and fractional order ω decreases, then the slope of curves increases and finally, the curves reach to a stable status. We see similar behavior for the function $\mathcal{P}(\mathbf{t})$ in Figure 12.

10. Conclusions

Due to the destructive effects of smoking and its resulting smoke on the health of the people in the community, in the present manuscript, we designed a mathematical model of secondhand smokers (SHS) based on three different compartments of the smoker and nonsmoker population and analyzed it numerically and analytically. To model this system, we applied new derivatives entitled the fractal-fractional derivatives with power-law-type kernel. The existence section was proved by ϕ-ψ-contractions and compact operators, and the Banach principle for usual contractions was used for proving the uniqueness result. The stability notion was investigated for solutions of the fractal-fractional SHS-model (7). The steady-state analysis including calculation of equilibrium points and basic reproduction number R_0 was done, and then we compared the sensitivity of the fractal-fractional SHS-system with each parameter. For numerical simulation, the Adams-Bashforth (AB) method was used and simulated the graphs with the help of real data. The effects of each parameter on the overall result of the calculations showed the increase or decrease in the harmful effect of cigarette smoke on people's health. Along with these results, we see accurate and better simulations via the fractal-fractional operators. Our graphs and data showed that our analysis on real data for different fractal dimensions and fractional orders yield similar results in comparison to classical operators. In the next works, we

can conduct comparative research on different fractal-fractional with exponential decay and power-law type kernels.

Data Availability

Data sharing is not applicable to this article as no datasets were generated or analyzed during the current study.

Conflicts of Interest

The authors declare that they have no competing interests.

Authors' Contributions

The authors declare that the study was realized in collaboration with equal responsibility. All authors read and approved the final manuscript.

Acknowledgments

The first and second authors would like to thank Azarbaijan Shahid Madani University. Also, J. Alzabut expresses his sincere thanks to Prince Sultan University and OSTİM Technical University for their endless support.

References

[1] World Health Organization, *Protection from exposure to secondhand tobacco smoke, policy recommendations*, World Health Organization, Geneva, 2007.

[2] J. M. B. Myers, G. K. K. Hershey, R. Deka et al., "Asking the right questions to ascertain early childhood secondhand smoke exposures," *The Journal of Pediatrics*, vol. 160, no. 6, pp. 1050-1051, 2012.

[3] J. Kusel, B. Timm, and I. Lockhart, "The impact of smoking in the home on the health outcomes of non-smoker occupants in the UK," *Tobacco Induced Diseases*, vol. 11, no. 1, pp. 3–10, 2013.

[4] X. Zhang, S. Xo, G. Yang et al., "Association of passive smoking by husbands with prevalence of stroke among Chinese women nonsmokers," *American Journal of Epidemiology*, vol. 161, no. 3, pp. 213–218, 2005.

[5] S. G. Grant, "Qualitatively and quantitatively similar effects of active and passive maternal tobacco smoke exposure on *in utero* mutagenesis at the *HPRT* locus," *BMC Pediatrics*, vol. 5, no. 1, p. 20, 2005.

[6] R. Otsuka, H. Watanabe, K. Hirata et al., "Acute effects of passive smoking on the coronary circulation in healthy young adults," *The Journal of the American Medical Association*, vol. 286, no. 4, pp. 436–441, 2001.

[7] N. Lubick, "Smoking and secondhand smoke: global estimate of SHS burden," *Environmental Health Perspectives*, vol. 119, no. 2, pp. A66–A67, 2011.

[8] A. Burton, "Does the smoke ever really clear? Thirdhand smoke exposure raises new concerns," *Environmental Health Perspectives*, vol. 119, no. 2, pp. A70–A74, 2011.

[9] S. Rezapour, C. T. Deressa, and S. Etemad, "On a memristor-based hyperchaotic circuit in the context of nonlocal and nonsingular kernel fractional operator," *Journal of Mathematics*, vol. 2021, Article ID 6027246, 21 pages, 2021.

[10] N. Sarwar, M. I. Asjad, T. Sitthiwirattham, N. Patanarapeelert, and T. Muhammad, "A Prabhakar fractional approach for the convection flow of casson fluid across an oscillating surface based on the generalized Fourier law," *Symmetry*, vol. 13, no. 11, p. 2039, 2021.

[11] S. Ahmad, A. Ullah, Q. M. Al-Mdallal, H. Khan, K. Shah, and A. Khan, "Fractional order mathematical modeling of COVID-19 transmission," *Solitons & Fractals*, vol. 139, article 110256, 2020.

[12] P. Kumar, V. S. Erturk, and M. Murillo-Arcila, "A new fractional mathematical modelling of COVID-19 with the availability of vaccine," *Results in Physics*, vol. 24, article 104213, 2021.

[13] Z. Zhang, A. Zeb, O. F. Egbelowo, and V. S. Erturk, "Dynamics of a fractional order mathematical model for COVID-19 epidemic," *Advances in Difference Equations*, vol. 2020, no. 1, 2020.

[14] A. Khan, R. Ikram, A. Din, U. W. Humphries, and A. Akgul, "Stochastic COVID-19 SEIQ epidemic model with time-delay," *Results in Physics*, vol. 30, p. 104775, 2021.

[15] M. A. Dokuyucu, E. Celik, H. Bulut, and H. M. Baskonus, "Cancer treatment model with the Caputo-Fabrizio fractional derivative," *The European Physical Journal Plus*, vol. 133, no. 3, p. 92, 2018.

[16] M. El Younoussi, Z. Hajhouji, K. Hattaf, and N. Yousfi, "A new fractional model for cancer therapy with M1 oncolytic virus," *Complexity*, vol. 2021, Article ID 9934070, 12 pages, 2021.

[17] M. Z. Ullah, A. K. Alzahrani, and D. Baleanu, "An efficient numerical technique for a new fractional tuberculosis model with nonsingular derivative operator," *Journal of Taibah University for Science*, vol. 13, no. 1, pp. 1147–1157, 2019.

[18] K. Shah, M. A. Alqudah, F. Jarad, and T. Abdeljawad, "Semi-analytical study of Pine Wilt disease model with convex rate under Caputo-Febrizio fractional order derivative," *Solitons & Fractals*, vol. 135, article 109754, 2020.

[19] D. Baleanu, S. M. Aydogan, H. Mohammadi, and S. Rezapour, "On modelling of epidemic childhood diseases with the Caputo-Fabrizio derivative by using the Laplace Adomian decomposition method," *Alexandria Engineering Journal*, vol. 59, no. 5, pp. 3029–3039, 2020.

[20] H. Khan, J. F. Gomez-Aguilar, A. Alkhazzan, and A. Khan, "A fractional order HIV-TB coinfection model with nonsingular Mittag-Leffler law," *Mathematical Methods in the Applied Sciences*, vol. 43, no. 6, pp. 3786–3806, 2020.

[21] H. Mohammadi, S. Kumar, S. Rezapour, and S. Etemad, "A theoretical study of the Caputo-Fabrizio fractional modeling for hearing loss due to Mumps virus with optimal control," *Solitons & Fractals*, vol. 144, article 110668, 2021.

[22] M. Jleli and B. Samet, "On the well-posedness of a fractional model of HIV infection," *Journal of Function Spaces*, vol. 2020, Article ID 6617245, 9 pages, 2020.

[23] S. A. Khan, K. Shah, G. Zaman, and F. Jarad, "Existence theory and numerical solutions to smoking model under Caputo-Fabrizio fractional derivative," *Chaos*, vol. 29, no. 1, article 013128, 2019.

[24] Z. U. A. Zafar, H. Rezazadeh, M. Inc, K. S. Nisar, T. A. Sulaiman, and A. Yusuf, "Fractional order heroin epidemic dynamics," *Alexandria Engineering Journal*, vol. 60, no. 6, pp. 5157–5165, 2021.

[25] S. Rezapour, S. Etemad, and H. Mohammadi, "A mathematical analysis of a system of Caputo-Fabrizio fractional differential

equations for the anthrax disease model in animals," *Advances in Difference Equations*, vol. 2020, no. 1, 2020.

[26] J. Singh, D. Kumar, and D. Baleanu, "A new analysis of fractional fish farm model associated with Mittag-Leffler type kernel," *International Journal of Biomathematics*, vol. 13, no. 2, article 2050010, 2020.

[27] A. Khan, R. Zarin, U. W. Humphries, A. Akgul, A. Saeed, and T. Gul, "Fractional optimal control of COVID-19 pandemic model with generalized Mittag-Leffler function," *Advances in difference equations*, vol. 2021, no. 1, 2021.

[28] A. Akgul, "A novel method for a fractional derivative with non-local and non-singular kernel," *Solitons Fractals*, vol. 114, pp. 478–482, 2018.

[29] Z. Alkhudhari, S. Al-Sheikh, and S. Al-Tuwairqi, "Global dynamics of a mathematical model on smoking," *International Scholarly Research Notices*, vol. 2014, Article ID 847075, 7 pages, 2014.

[30] V. Verma and M. Agarwal, "Global dynamics of a mathematical model on smoking with media campaigns," *Research Desk*, vol. 4, pp. 500–512, 2015.

[31] M. A. Adhana and T. T. Mekonnen, "A mathematical model analysis of smoking tobacco in the case of Haremaya town; Ethiopia," *International Journal of Research Studies in Science, Engineering and Technology*, vol. 6, no. 2, pp. 14–24, 2019.

[32] A. M. Pulecio-Montoya, L. E. Lopez-Montenegro, and L. M. Benavides, "Analysis of a mathematical model of smoking," *Contemporary Engineering Sciences*, vol. 12, no. 3, pp. 117–129, 2019.

[33] A. Atangana, "Fractal-fractional differentiation and integration: connecting fractal calculus and fractional calculus to predict complex system," *Solitons & Fractals*, vol. 102, pp. 396–406, 2017.

[34] J. F. Gomez-Aguilar, T. Cordova-Fraga, T. Abdeljawad, A. Khan, and H. Khan, "Analysis of fractal-fractional malaria transmission model," *Fractals*, vol. 28, no. 8, article 2040041, 2020.

[35] K. Shah, M. Arfan, I. Mahariq, A. Ahmadian, S. Salahshour, and M. Ferrara, "Fractal-fractional mathematical model addressing the situation of Corona virus in Pakistan," *Results in Physics*, vol. 19, article 103560, 2020.

[36] Z. Ali, F. Rabiei, K. Shah, and T. Khodadadi, "Qualitative analysis of fractal-fractional order COVID-19 mathematical model with case study of Wuhan," *Alexandria Engineering Journal*, vol. 60, no. 1, pp. 477–489, 2021.

[37] M. Farman, A. Akgul, K. S. Nisar et al., "Epidemiological analysis of fractional order COVID-19 model with Mittag-Leffler kernel," *AIMS Mathematics*, vol. 7, no. 1, pp. 756–783, 2021.

[38] M. Amin, M. Farman, A. Akgul, and R. T. Alqahtani, "Effect of vaccination to control COVID-19 with fractal fractional operator," *Alexandria Engineering Journal*, vol. 61, no. 5, pp. 3551–3557, 2022.

[39] M. Alqhtani and K. M. Saad, "Fractal-fractional Michaelis-Menten enzymatic reaction model via different kernels," *Fractal and Fractional*, vol. 6, no. 1, p. 13, 2022.

[40] K. M. Saad, M. Alqhtani, and J. F. Gomez-Aguilar, "Fractal-fractional study of the hepatitis C virus infection model," *Results in Physics*, vol. 19, article 103555, 2020.

[41] A. Granas and J. Dugundji, *Fixed Point Theory*, Springer-Verlag, New York, 2003.

[42] D. Gopal and S. Jain, *Metric Structures and Fixed Point Theory: Fixed Point Theory in Partial Metric Spaces*, Chapman and Hall/CRC, 1st Edition edition, 2021.

[43] V. Joshi and S. Jain, *Metric Structures and Fixed Point Theory: G-Metric Spaces: From the Perspective of F-Contractions and Best Proximity Points*, Chapman and Hall/CRC, 1st Edition edition, 2021.

[44] B. Samet, C. Vetro, and P. Vetro, "Fixed point theorems for α-ψ-contractive type mappings," *Nonlinear Analysis*, vol. 75, no. 4, pp. 2154–2165, 2012.

[45] B. Fekede and B. Mebrate, "Sensitivity and mathematical model analysis on secondhand smoking tobacco," *Journal of the Egyptian Mathematical Society*, vol. 28, no. 1, p. 50, 2020.

[46] S. M. Ulam, *Problems in Modern Mathematics*, Wiley, New York, NY, USA, 1940.

[47] D. Hyers, "On the stability of the linear functional equation," *Proceedings of the National Academy of Sciences of the United States of America*, vol. 27, no. 4, pp. 222–224, 1941.

[48] P. V. D. Driessche and J. Watmough, "Reproduction numbers and sub-threshold endemic equilibria for compartmental models of disease transmission," *Mathematical Biosciences, 2002*, vol. 180, no. 1-2, pp. 29–48, 2002.

[49] N. Chitnis, J. M. Hyman, and J. M. Cushing, "Determining important parameters in the spread of malaria through the sensitivity analysis of a mathematical model," *Bulletin of Mathematical Biology*, vol. 70, no. 5, pp. 1272–1296, 2008.

[50] M. Toufik and A. Atangana, "New numerical approximation of fractional derivative with non-local and non-singular kernel: application to chaotic models," *The European Physical Journal Plus*, vol. 132, no. 10, p. 444, 2017.

Hindawi
Journal of Function Spaces
Volume 2022, Article ID 5431057, 15 pages
https://doi.org/10.1155/2022/5431057

Research Article

Collocation Approach Based on an Extended Cubic *B*-Spline for a Second-Order Volterra Partial Integrodifferential Equation

Reny George,[1] **Muhammad Yaseen**,[2] **and Sana Khan**[2]

[1]*Department of Mathematics, College of Science and Humanities in Al-Kharj, Prince Sattam Bin Abdulaziz University, Al-Kharj 11942, Saudi Arabia*
[2]*Department of Mathematics, University of Sargodha, Sargodha, Pakistan*

Correspondence should be addressed to Reny George; renygeorge02@yahoo.com

Received 4 January 2022; Revised 14 March 2022; Accepted 23 March 2022; Published 30 April 2022

Academic Editor: Youssri Hassan Youssri

This paper focuses on an efficient spline-based numerical technique for numerically addressing a second-order Volterra partial integrodifferential equation. The time derivative is discretized using a finite difference scheme, while the space derivative is approximated using the extended cubic *B*-spline basis. The scheme is also tested for stability study to ensure that the errors do not accumulate. The convergence of the proposed scheme is also investigated. The scheme's key benefit is that the approximate solution is produced as a smooth piecewise continuous function allowing us to approximate the solution at any location in the domain. Numerical study is performed, and the comparison of results is made to previously reported results in the literature to show the efficiency of the suggested scheme.

1. Introduction

Integro-Differential Equations (IDEs) are equations that involve both integrals and derivatives of an unknown function. These equations appear very commonly as mathematical models in various fields. Abel, Lotka, Fredholm, Malthus, Verhulst, and Volterra utilized the integral equations and IDEs [1] to study the problems of physics, economics, and mathematical biology. A vast number of research papers and books are devoted to the ongoing phase of the initiative and growth of IDEs over the last few decades. Special implementation of IDEs to deal with statistical models of spatial-temporal development of epidemics was discussed in [2].

Many methods have been used to approximate IDEs previously. The Jacobi-spectral method was used by Ali [3] to approximate the integrodelay differential equations with a weakly singular kernel. Ogunlaran and Oke [4] presented the numerical solution of first order IDEs. Chrysafinos [5] used the method of wavelet-Galerkin to solve IDEs numerically. Abbas et al. [6] approximated IDEs using the direct method of multiwavelet. The first order linear Fredholm IDEs has recently been solved using the rationalized form of Haar functions by Bhrawy et al. [7]. For the numerical solution of Fredholm IDEs, Behiry and Hashish [8] utilized the wavelet technique. The finite element method was used by Chen et al. [9] to approximate the parabolic IDEs. The parabolic Volterra IDEs were approximated by Fakhar and Dehghan [10] using the spectral technique.

In several problems of applied sciences, partial integro-differential equations (PIDEs) are used to represent the complex systems in physical, chemical, and biological sciences and population dynamics [11–19]. Such systems have been solved analytically as well as numerically. Several researchers have contributed to present the numerical solutions of PIDEs using different numerical schemes such as finite differences, Sinc-collocation method, finite element method, spectral collocation method, Legendre method, Galerkin method, and quasiwavelet-based method. Tang [20] approximated PIDEs by using a finite difference scheme. Dehghan [21] gave an approximate solution to a PIDE arising in viscoelasticity. Zarebnia [22] approximated PIDEs by using Sinc-collocation method. Quasiwavelet methods were used by Long et al. [23] to solve PIDEs numerically. Yang et al. [24] used the Crank-Nicolson/quasiwavelet-based numerical

method to approximate a class of PIDEs. Izadi and Dehghan [10] developed spectral methods for parabolic Volterra IDEs. Legendre multiwavelet collocation method was proposed for the numerical solution of PIDEs by Aziz and Khan [25]. Numerical solution of Volterra partial integrodifferential equations based on Sinc-collocation method was presented by Fahim et al. [26]. Izadi and Dehghan [27] developed an effective pseudospectral Legendre-Galerkin technique to solve a nonlinear PIDE emerging in population dynamics. A piecewise polynomial function of degree $n-1$ is a spline function of order n. B-spline-based numerical methods for curves and surfaces were first proposed in the 1940s but were strengthened in the 1970s by various experts. B-splines come in a variety of shapes and sizes, including uniform, nonuniform, rational, and nonrational. Cubic B-spline is a fourth-order B-spline of degree three. The extended cubic B-spline also has a free parameter that allows for local control of this form of B-spline. Collocation techniques based on B-splines proven to be quite effective at approximating the IDEs. Amir and Shakibi [28] used B-spline interpolation to numerically solve IDEs. Exponential splines were used to find the numerical solutions of linear Fredholm IDEs by Tahernezhad and Jalilian [29]. For approximating linear stochastic IDE of fractional order, Mirzaee and Alipour [30] used a cubic B-spline-based collocation method. For a class of hyperbolic PIDE, Fairweather [31] utilized spline-based collocation technique. Gholamian and Saberi-Nadjafi [32] proposed a cubic B-spline collocation technique for a class of PIDEs. Ali et al. [33] developed a quartic B-spline collocation approach for solving PIDEs with a weakly singular kernel. Trigonometric cubic B-spline-based collocation method was used to solve PIDEs by Ali et al. [34].

In this paper, we consider the following second order Volterra PIDE:

$$\frac{\partial v(x,t)}{\partial t} = \int_0^t (t-z)^{-\gamma} \frac{\partial^2 v(x,z)}{\partial x^2} dz + g(x,t), a \le x \le b, t \ge 0, 0 < \gamma < 1, \tag{1}$$

subjected to initial condition,

$$v(x,0) = \varphi(x), \tag{2}$$

and the boundary conditions,

$$\begin{cases} v(a,t) = 0, \\ v(b,t) = 0, \end{cases} t \ge 0, \tag{3}$$

where $a, b, \varphi(x)$, are given and $0 < \gamma < 1$. Motivated by the popularity of the spline approach, we have utilized the extended cubic B-spline to numerically study the above second order Volterra PIDE.

The rest of the paper is organized as follows. In Section 2, extended cubic B-spline-based collocation method is derived in detail. In Sections 3 and 4, the stability and convergence of the proposed scheme are discussed, respectively. Section 4 compares numerical results with some other numerical techniques available in literature. Section 5 summarizes the conclusions of this study.

2. Derivation of the Scheme

Let $\Delta t = t/Q$ denotes the time, and $h = b - a/N$ denotes the space step sizes, with Q and N being positive integers. Set the partitions, $t^q = q\Delta t (0 \le q \le Q)$ and $x_n = nh (0 \le n \le N)$ of both the temporal and spatial domain. The knots x_j evenly discretize the spatial domain $a \le x \le b$, and the interval $[a, b]$ is divided into N subintervals, $[x_j, x_{j+1}]$ of equal length h, $j = 0, 1, 2, \cdots, N-1$, where $a = x_0 < x_1 < \cdots < x_{n-1} < x_N = b$. The numerical solution $V(x,t)$ to the exact solution $v(x,t)$ of (1) is acquired by

$$V(x,t) = \sum_{j=-1}^{N+1} C_j(t) B_j^4(x,\eta). \tag{4}$$

Here, $C_j(t), j = -1, \cdots N+1$ is time-dependent unknowns that must be evaluated and $B_j^4(x,\eta)$ are extended cubic B-spline (ECuBS) basis functions provided by [35].

$$B_j^4(x,\eta) = \frac{1}{24h^4} \begin{cases} 4h(1-\eta)(x-x_j)^3 + 3\eta(x-x_j)^4, & x \in [x_j, x_{j+1}], \\ (4-\eta)h^4 + 12h^3(x-x_{j+1}) + 6h^2(2+\eta)(x-x_{j+1})^2 & \\ -12h(x-x_{j+1})^3 - 3\eta(x-x_{j+1})^4, & x \in [x_{j+1}, x_{j+2}], \\ (4-\eta)h^4 + 12h^3(x_{j+3}-x) + 6h^2(2+\eta)(x_{j+3}-x)^2 & \\ -12h(x_{j+3}-x)^3 - 3\eta(x_{j+1}-x)^4, & x \in [x_{j+2}, x_{j+3}], \\ 4h(1-\eta)(x_{j+4}-x)^3 + 3\eta(x_{j+4}-x)^4, & x \in [x_{j+3}, x_{j+4}], \\ 0, & \text{otherwise}, \end{cases} \tag{5}$$

where $\eta \in [-8, 1]$. Because of the local support characteristic of ECuBS, only $B_{j-1}^4(x,\eta), B_j^4(x,\eta)$ and $B_{j+1}^4(x,\eta)$ are preserved at the grid point x_j. Consequently, the approximation V^q of $v(s,t)$ at q^{th} time level is given as

$$V(x,t^q) = V^q = \sum_{j=-1}^{N+1} C_j^q(t) B_j^4(x,\eta). \tag{6}$$

The unknowns, $C_j^q(t), j = -1, \cdots, N+1$, are found by using collocation conditions on $B_j^4(x,\eta)$ and the given initial and boundary conditions. As a consequence, the approximations V^q and its essential derivatives are obtained as

$$\begin{cases} V^q = \alpha_1 C_{j-1}^q + \alpha_2 C_j^q + \alpha_1 C_{j+1}^q, \\ (V_x)^q = -\beta_1 C_{j-1}^q + \beta_2 C_j^q + \beta_1 C_{j+1}^q, \\ (V_{xx})^q = \lambda_1 C_{j-1}^q + \lambda_2 C_j^q + \lambda_1 C_{j+1}^q, \end{cases} \tag{7}$$

where $\alpha_1 = 4 - \eta/24, \alpha_2 = 8 + \eta/12, \beta_1 = 1/2h, \beta_2 = 0$, $\lambda_1 = 2 + \eta/2h^2$, and $\lambda_2 = -2 + \eta/h^2$.

Table 1: Error comparison for Example 5 when $\Delta t = 10^{-5}$,and $N = 10$.

Q	ECuBS		TCuBS [34]		CuBS [32]	QBCM [33]	QWM [23]
	L_2	L_∞	L_2	L_∞	L_∞	L_∞	L_∞
50	8.40×10^{-8}	1.13×10^{-7}	5.96×10^{-6}	8.93×10^{-6}	1.24×10^{-6}	1.18×10^{-4}	1.58×10^{-3}
150	1.48×10^{-7}	2.00×10^{-7}	3.09×10^{-5}	4.42×10^{-5}	6.34×10^{-6}	6.75×10^{-4}	7.89×10^{-3}
250	1.90×10^{-7}	2.57×10^{-7}	6.65×10^{-5}	9.45×10^{-5}	1.36×10^{-5}	1.40×10^{-3}	1.61×10^{-2}
350	2.18×10^{-7}	2.98×10^{-7}	1.10×10^{-4}	1.56×10^{-4}	2.25×10^{-5}	2.51×10^{-3}	2.53×10^{-2}
450	2.38×10^{-7}	3.26×10^{-7}	1.60×10^{-4}	2.28×10^{-4}	3.28×10^{-5}	3.70×10^{-3}	3.46×10^{-2}

Discretizing the time derivative in (1) by using forward difference scheme, we obtain

$$\frac{\partial v(x,t)}{\partial t} \approx \frac{V^{q+1}(x) - V^q(x)}{\Delta t}. \tag{8}$$

The term on the RHS of (1) can be written as

$$\int_0^t (t-z)^{-\gamma} v_{xx}(x,z)dz + g(x,t) = \int_0^{t_{q+1}} (t_{q+1}-z)^{-\gamma} v_{xx}(x,z)dz + g(x,t_{q+1}). \tag{9}$$

The first expression on the RHS of (9) is time discretized as

$$\begin{aligned}\int_0^{t_{q+1}} (t_{q+1}-z)^{-\gamma} v_{xx}(x,z)dz &= \int_0^{t_{q+1}} (z)^{-\gamma} v_{xx}(z, t_{q+1}-z)dz,\\ &= \sum_{r=0}^{q} \int_{t_r}^{t_{r+1}} (z)^{-\gamma} v_{xx}(x, t_{q+1}-z)dz,\\ &= \sum_{r=0}^{q} v_{xx}(z, t_{q-r+1}) \int_{t_r}^{t_{r+1}} (z)^{-\gamma} dz,\\ &= \frac{\Delta t^{1-\gamma}}{1-\gamma} \sum_{r=0}^{q} v_{xx}(x, t_{q-r+1}) \left[(r+1)^{1-\gamma} - (r)^{1-\gamma}\right],\\ &= \frac{\Delta t^{1-\gamma}}{1-\gamma} \sum_{r=0}^{q} l_r v_{xx}(x, t_{q-r+1}),\end{aligned} \tag{10}$$

where $l_r = (r+1)^{1-\gamma} - (r)^{1-\gamma}$. Equation (1) becomes

$$\frac{v^{q+1}(x) - v^q(x)}{\Delta t} = \frac{\Delta t^{1-\gamma}}{1-\gamma} \sum_{r=0}^{q} l_r v_{xx}^{q-r+1}(x) + g(x, t_{q+1}). \tag{11}$$

Let $W = \Delta t^{2-\gamma}/1-\gamma$, so that the last equation becomes

$$v^{q+1}(x) - W l_0 v_{xx}^{q+1}(x) = v^q(x) + W \sum_{r=1}^{q} l_r v_{xx}^{q-r+1}(x) + \Delta t g(x, t_{q+1}). \tag{12}$$

The discretization of the space derivative is performed by (8) so that (12) reduces to

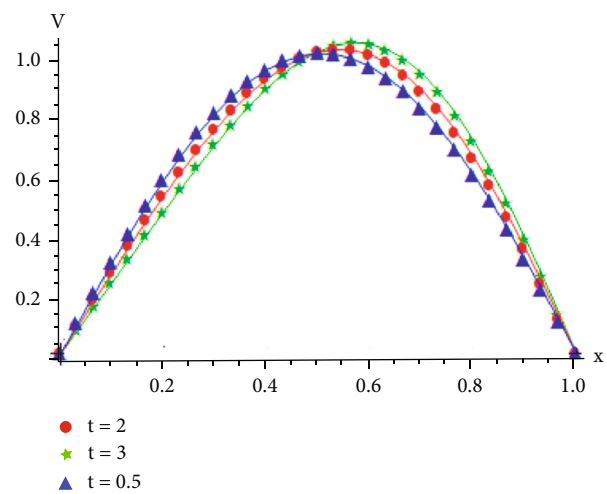

Figure 1: The exact and approximate (triangles, starts, circles) solutions for Example 5 at various times when $h = 0.01$.

$$V^{q+1}(x,\eta) - W V_{xx}^{q+1}(x,\eta) = V^q(x,\eta) + W \sum_{r=1}^{q} l_r V_{xx}^{q-r+1}(x,\eta) + \Delta t g^{q+1}(x). \tag{13}$$

For $x = x_j$, where $j = 0, 1, 2, \cdots, N$, we have

$$V^{q+1}(x_j,\eta) - W V_{xx}^{q+1}(x_j,\eta) = V^q(x_j,\eta) + W \sum_{r=1}^{q} l_r V_{xx}^{q-r+1}(x_j,\eta) + \Delta t g^{q+1}(x_j). \tag{14}$$

Setting

$$G_j = V^q(x_j,\eta) + W \sum_{r=1}^{q} l_r V_{xx}^{q-r+1}(x_j,\eta) + \Delta t g^{q+1}(x_j), \tag{15}$$

we can write, for $j = 0, 1, \cdots, N$,

$$V^{q+1}(x_j,\eta) - W l_0 V_{xx}^{q+1}(x_j,\eta) = G_j \tag{16}$$

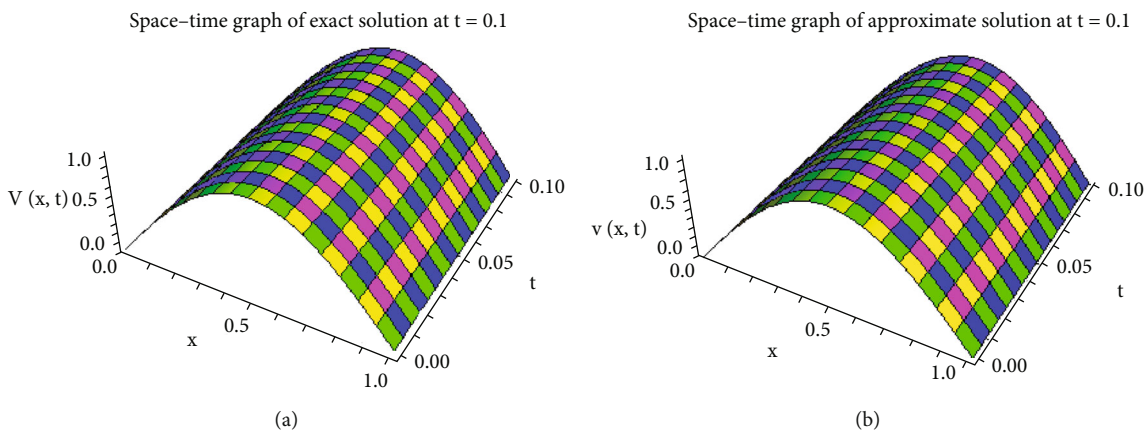

Figure 2: The approximate and exact solutions for Example 5 when $h = 1/60$, $t = 0.1$, $\Delta t = 0.01$.

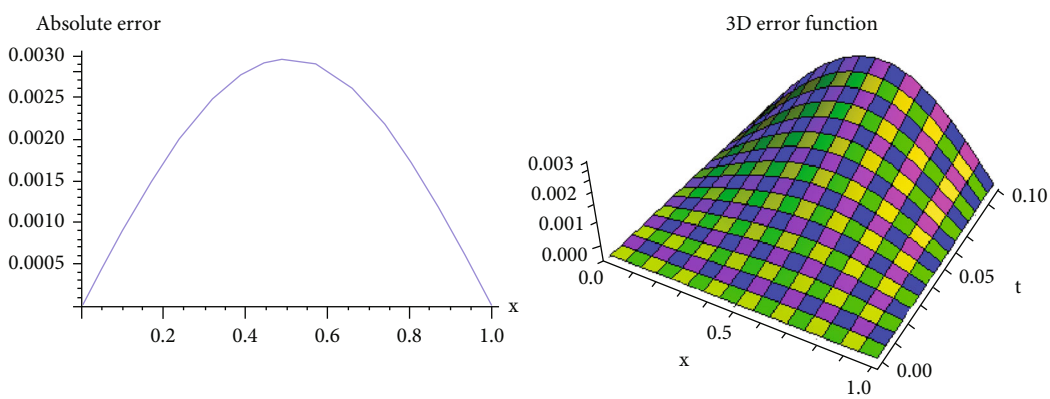

Figure 3: 2D and 3D error profiles for Example 5 when $h = 1/60$, $t = 0.1$, $\Delta t = 0.01$.

This implies that

$$\sum_{j=-1}^{N+1} C_j^{q+1}(t) B_j^4(x_j,\eta) - W \sum_{j=-1}^{N+1} C_j^{q+1}(t) \left(B_j^4\right)''(x_j,\eta) = G_p, \Rightarrow \sum_{j=-1}^{N+1} \left[B_j^4(x_j,\eta) - W\left(B_j^4\right)''(x_j,\eta)\right] C_j^{q+1}(t) = G_j. \tag{17}$$

Equation (17) forms a matrix system of order $(N+1) \times (N+3)$. Approximating the boundary conditions (3) using (7), we obtain two equations from where we remove the unknowns, C_{-1} and C_{N+1}. Consequently, a matrix system of order $(N+1) \times (N+1)$ is generated to acquire the unique solution for this system. The matrix equation for this system is given by

$$SC = G, \tag{18}$$

where the matrices S, C, and G are

$$S = \begin{bmatrix} \omega & 0 & 0 & 0 & \cdots & 0 \\ \rho_1 & \rho_2 & \rho_1 & 0 & \cdots & 0 \\ 0 & \rho_1 & \rho_2 & \rho_1 & \ddots & \vdots \\ \vdots & \ddots & \ddots & \ddots & \ddots & 0 \\ 0 & \cdots & 0 & \rho_1 & \rho_2 & \rho_1 \\ 0 & \cdots & 0 & 0 & 0 & \omega \end{bmatrix}, \tag{19}$$

$$C = \begin{bmatrix} C_0^{q+1} & C_0^{q+1} & \cdots & C_N^{q+1} & C_N^{q+1} \end{bmatrix}^T, \tag{20}$$

$$G = \begin{bmatrix} \vartheta_1(t) & G_0 & G_1 & \cdots & G_N & G_{N+1} & \vartheta_2(t) \end{bmatrix}^T, \tag{21}$$

where $\rho_1 = \alpha_1 - W\lambda_1$ and $\rho_2 = \alpha_2 - W\lambda_2$, $\omega = W\lambda_1/\alpha_1$.

Table 2: Error comparison for Example 6 when $N = 100$,and $\Delta t = 10^{-5}$.

Q	ECuBS		TCuBS [34]		CuBS [32]	
	L_2	L_∞	L_2	L_∞	L_2	L_∞
50	8.37×10^{-10}	1.18×10^{-9}	3.97×10^{-9}	5.61×10^{-9}	6.11×10^{-9}	8.64×10^{-9}
100	5.28×10^{-9}	7.47×10^{-9}	1.41×10^{-8}	1.99×10^{-8}	2.01×10^{-8}	2.84×10^{-8}
150	1.20×10^{-8}	1.71×10^{-8}	2.82×10^{-8}	3.99×10^{-8}	3.93×10^{-8}	5.56×10^{-8}
200	2.08×10^{-8}	2.95×10^{-8}	4.56×10^{-8}	6.45×10^{-8}	6.26×10^{-8}	8.86×10^{-8}
250	3.12×10^{-8}	4.42×10^{-8}	6.59×10^{-8}	9.31×10^{-8}	8.97×10^{-8}	1.27×10^{-8}
300	4.31×10^{-8}	6.10×10^{-8}	8.86×10^{-8}	1.25×10^{-7}	1.20×10^{-7}	1.70×10^{-7}

Initial vector is as follows: the initial condition,

$$v(x_p, 0) = \varphi(x_p), p = 0, 1, 2, 3, \cdots, N \tag{22}$$

can be used to find the initial vector,

$$C^0 = \begin{bmatrix} C_0^0 & C_1^0 & \cdots & C_{N-1}^0 & C_N^0 \end{bmatrix}^T. \tag{23}$$

Equation (22) produces a matrix system of $(N+1) \times (N+1)$ order given as

$$AC^0 = B, \tag{24}$$

where

$$A = \begin{bmatrix} \alpha_1 & \alpha_2 & \alpha_1 & 0 & \cdots & 0 \\ 0 & \alpha_1 & \alpha_2 & \alpha_1 & \cdots & 0 \\ 0 & \ddots & \alpha_1 & \alpha_2 & \alpha_1 & \vdots \\ \vdots & \ddots & \ddots & \ddots & \ddots & \vdots \\ 0 & \cdots & \alpha_1 & \alpha_2 & \alpha_1 & 0 \\ 0 & \cdots & 0 & \alpha_1 & \alpha_2 & \alpha_1 \end{bmatrix},$$
$$C^0 = \begin{bmatrix} c_{-1}^0 & c_0^0 & \cdots & c_N^0 & c_{N+1}^0 \end{bmatrix}^T, \tag{25}$$
$$B = \begin{bmatrix} \varphi(x_0) & \varphi(x_1) & \cdots & \varphi(x_{N-1}) & \varphi(x_N) \end{bmatrix}^T.$$

Once the initial vector C^0 is obtained, the recurrence relation (17) gives the time evolution of vectors C^q, and thus the approximate solution can be calculated.

3. Stability Analysis

In this section, the stability of the proposed method is presented. The proposed scheme is proved stable by using the Von-Neumann stability method. For this purpose, put $g^{q+1}(x) = 0$ in (13) so that

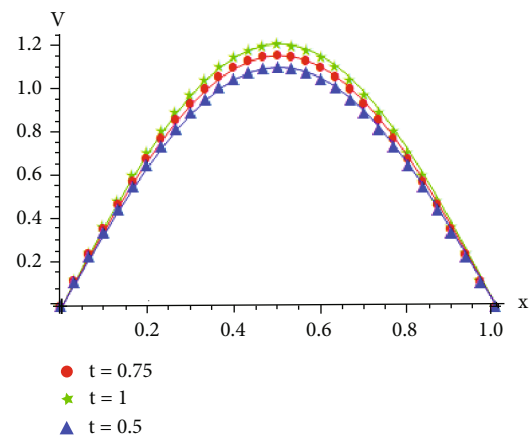

Figure 4: The exact and approximate (triangles, starts, circles) solutions for Example 6 at various times when $h = 0.01$.

$$V^{q+1}(x, \eta) - WV_{xx}^{q+1}(x, \eta) = V^q(x, \eta) + W\sum_{r=1}^{q} l_r V_{xx}^{q-r+1}(x, \eta). \tag{26}$$

Using (8) in (26), we obtain

$$\rho_1 C_{j-1}^{q+1} + \rho_2 C_j^{q+1} + \rho_1 C_{j+1}^{q+1} = \left[\alpha_1 C_{j-1}^q + \alpha_2 C_j^q + \alpha_1 C_{j+1}^q\right] + W\sum_{r=1}^{q} l_r \left[\lambda_1 C_{j-1}^{q-r+1} + \lambda_2 C_j^{q-r+1} + \lambda_1 C_{j+1}^{q-r+1}\right]. \tag{27}$$

Substituting the Fourier mode, $C_j^q = \xi^q e^{\iota j\phi h}$ in (17), where ϕ is the mode number, h is the step size, ξ is the growth factor, $\iota = \sqrt{-1}$, and we obtain

$$K\xi^{q+1} e^{\iota j\phi h} = L\xi^q e^{\iota j\phi h} + \frac{W}{h^2}\sum_{r=1}^{q} M\xi^{q-r+1} e^{\iota j\phi h}, \tag{28}$$

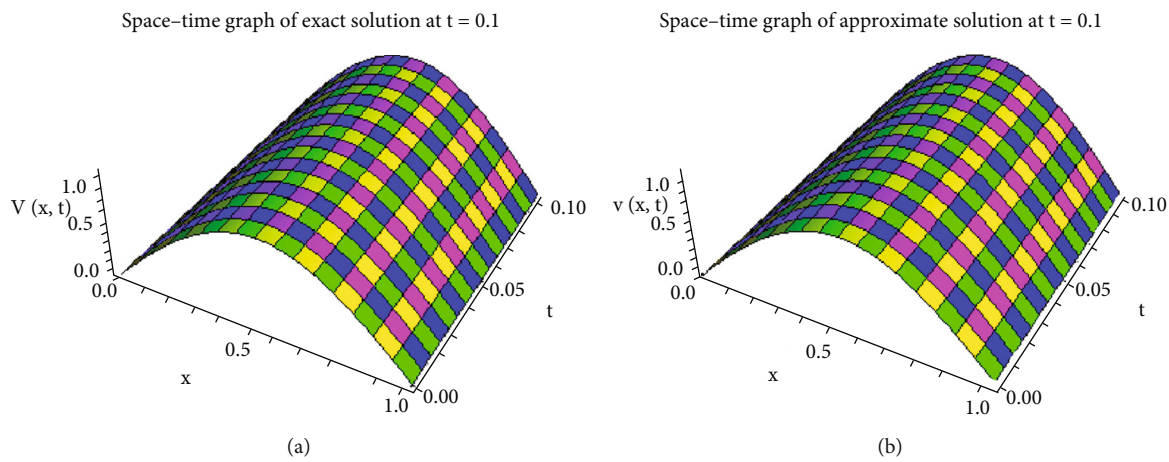

Figure 5: The approximate and exact solutions for Example 6 when $h = 1/60$, $t = 0.1$, $\Delta t = 0.01$.

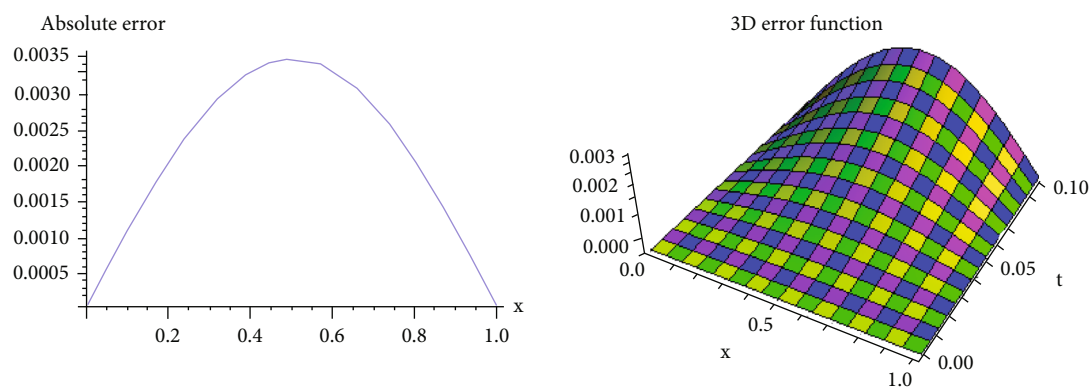

Figure 6: 2D and 3D error profiles for Example 6 when $h = 1/60$, $t = 0.1$, $\Delta t = 0.01$.

where

$$\begin{cases} K = \rho_1\left(e^{-\iota\phi h} + e^{\iota\phi h}\right) + \rho_2, \\ L = \alpha_1\left(e^{-\iota\phi h} + e^{\iota\phi h}\right) + \alpha_2, \\ M = \delta_1\left(e^{-\iota\phi h} + e^{\iota\phi h}\right) + \delta_2, \end{cases} \tag{29}$$

and $\delta_1 = h^2\lambda_1$, $\delta_2 = h^2\lambda_2$. Now, substituting the values of ρ_1, ρ_2, α_1, α_2, δ_1, and δ_2 in (29), we get

$$\begin{cases} K = \left(\frac{4-\eta}{24} - W\left(\frac{2+\eta}{2h^2}\right)\right)(2\cos\phi h) + \left(\frac{8+\eta}{12} - W\left(\frac{2+\eta}{h^2}\right)\right), \\ L = \left(\frac{4-\eta}{24}\right)(2\cos\phi h) + \left(\frac{8+\eta}{12}\right), \\ M = \left(\frac{2+\eta}{2}\right)(2\cos\phi h) - (2+\eta). \end{cases} \tag{30}$$

Rearranging the terms of (28) to obtain

$$\xi^q - \left(\frac{L}{K} + \frac{WM}{Kh^2}\right)\xi^{q-1} - \frac{WM}{Kh^2}\sum_{r=2}^{q} l_r\xi^{q-r} = 0. \tag{31}$$

Letting $b_1 = -L/K - WM/Kh^2$ and $b_r = -(WM/Kh^2)l_r$, and $r = 2, \cdots, q$ in (31) to obtain

$$\xi^q + b_1\xi^{q-1} + b_2\xi^{q-2} + \cdots + b_{q-1}\xi + b_q = 0. \tag{32}$$

It is quite clear from (30) that K and L are positive and $M \le 0$. Thus, the coefficients, $b_1, b_2, \cdots b_q$ are positive. Here, it is necessary to mention the following theorem for further procedure.

Theorem 1 (see [36]). *For all roots ξ_j of an arbitrary polynomial $p(\xi) = a_0\xi^n + \cdots + a_n$ with $a_0 \neq 0$, we have $|\xi_j| \le \max\{1, \sum_{j=1}^{n}|a_j/a_0|\}$.*

It is necessary to prove that all the roots, ξ_j, of (32) satisfy $|\xi_j| \le 1$ for stability. Since from Theorem 1, $a_0 = 1$

Table 3: Error comparison for Example 7 when $N = 50$, and $\Delta t = 10^{-4}$.

Q	ECuBS		TCuBS [34]		CuBS [32]	
	L_2	L_∞	L_2	L_∞	L_2	L_∞
50	1.13×10^{-7}	1.73×10^{-7}	2.73×10^{-7}	4.19×10^{-7}	3.48×10^{-7}	5.34×10^{-7}
100	3.49×10^{-7}	5.21×10^{-7}	8.48×10^{-7}	1.26×10^{-6}	1.08×10^{-6}	1.61×10^{-6}
150	6.75×10^{-7}	9.95×10^{-7}	1.64×10^{-6}	2.42×10^{-6}	2.09×10^{-6}	3.08×10^{-6}
200	1.07×10^{-6}	1.57×10^{-6}	2.61×10^{-6}	3.82×10^{-6}	3.33×10^{-6}	4.87×10^{-6}
250	1.54×10^{-6}	2.27×10^{-6}	3.73×10^{-6}	5.51×10^{-6}	4.76×10^{-6}	7.02×10^{-6}
300	2.05×10^{-6}	3.02×10^{-6}	4.99×10^{-6}	7.33×10^{-6}	6.36×10^{-6}	9.35×10^{-6}

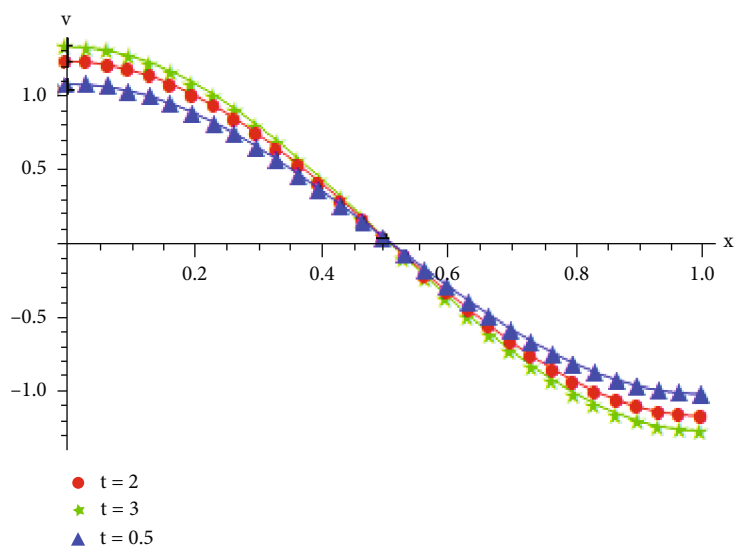

Figure 7: The exact and approximate (triangles, starts, circles) solutions for Example 7 at various times when $h = 0.01$.

and $a_j > 0$, $j = 1, \cdots, q$, we have

$$\sum_{j=1}^{q} \left| \frac{a_j}{a_0} \right| = \left| \frac{-\left(L + \left(WM/h^2\right) \sum_{r=1}^{q} l_r\right)}{K} \right|, \tag{33}$$

where

$\sum_{r=1}^{q} l_r = \sum_{r=1}^{q} [(r+1)^{1-\gamma} - (r)^{1-\gamma}] = (q+1)^{1-\gamma} - 1.()$

Let us assume that $D_\gamma = (q+1)^{1-\gamma} - 1$, then (33) becomes

$$\sum_{j=1}^{q} a_j = \left| -\frac{L + \left(WMD_\gamma/h^2\right)}{K} \right|. \tag{34}$$

From the definition of M in (29), if we let $M = 0$, then $h = 0$. Consequently, (31) becomes

$$\xi^q - \frac{L}{K} \xi^{q-1} = 0 \Rightarrow \xi = 0 \text{ or } \xi = 1. \tag{35}$$

Thus, the required condition for stability is fulfilled that is $|\xi_j| \leq 1$. Next, if $\neq 0 (M < 0)$, then from (34), we have

$$-L - \frac{\mathrm{WMD}_\gamma}{h^2} < K, \tag{36}$$

so that the stability condition, i.e., $(|\xi_j| \leq 1)$ is satisfied. Now, using the values of K, L, and M in above inequality,

$$-(4-\eta) \cos \eta h - (8+\eta) + \frac{6(2+\eta)}{h^2} W\left(D_\gamma - 1\right)(1 - \cos \eta h) < ,0.$$

$$\cos \eta h > \frac{-(8+\eta/6) + \left((2+\eta) W\left(D_\gamma - 1\right)/h^2\right)}{(4-\eta/6) + \left((2+\eta) W\left(D_\gamma - 1\right)/h^2\right)}. \tag{37}$$

This inequality implies the unconditional stability of introduced scheme.

4. Convergence Analysis

The suggested scheme's convergence analysis for spatial and temporal directions is provided separately in this section.

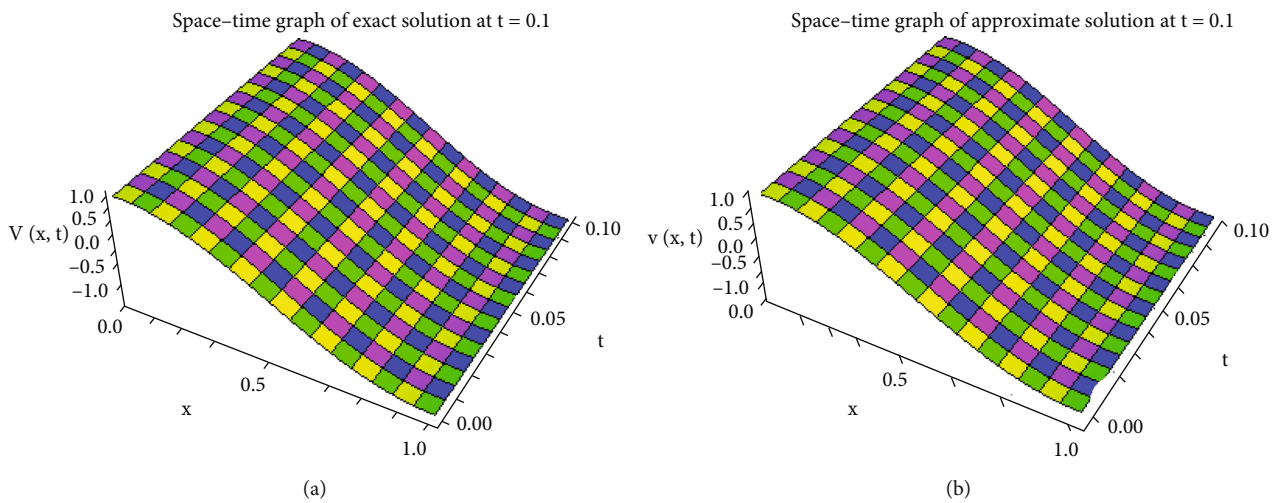

Figure 8: The approximate and exact solutions for Example 7 when $h = 1/60$, $t = 0.1$, $\Delta t = 0.01$.

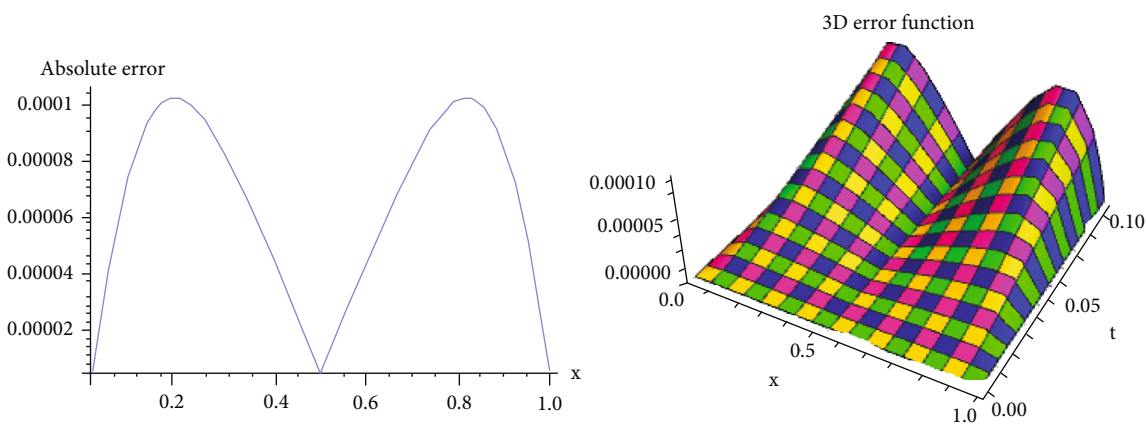

Figure 9: 2D and 3D error profiles for Example 7 when $h = 1/60$, $t = 0.1$, $\Delta t = 0.01$.

The convergence is evaluated independently for spatial and temporal directions for this purpose. The following theorem must be proven for spatial convergence.

Theorem 2. *If $\hat{v}(x)$ is the exact solution of equations (1)–(3) and $\hat{b}(x)$ is the B-spline collocation approximation to $\hat{v}(x)$, the technique is then second order convergent, and*

$$\|\hat{v}(x) - \hat{b}(x)\|_\infty \le \sigma h^2, \tag{38}$$

where $\sigma = \kappa_0 Łh^2 + R$ is a finite constant.

Proof. Assume that $\hat{v}(x)$ is the exact solution of equations (1)–(3), then the approximation, $\hat{b}(x)$ to $\hat{v}(x)$, is given by

$$\hat{b}(x) = \sum_{j=-1}^{N+1} \hat{C}_j(t) B_j^4(x, \eta), \tag{39}$$

where $\hat{C} = (\hat{C}\_1, \hat{C}_0, \cdots, \hat{C}_{N+1})$. Further, suppose that $\tilde{b}(x)$ is the evaluated extended cubic B-spline collocation approximation to $\hat{b}(x)$, namely,

$$\tilde{b}(x) = \sum_{j=-1}^{N+1} \tilde{C}_j(t) B_j^4(x, \eta), \tag{40}$$

where $\tilde{C} = (\tilde{C}_{-1}, \tilde{C}_0, \cdots, \tilde{C}_{N+1})$. To approximate the error, $\|\hat{v}(x) - \hat{b}(x)\|_\infty$, we have to determine the errors, $\|\hat{v}(x) - \tilde{b}(x)\|_\infty$ and $\|\tilde{b}(x) - \hat{b}(x)\|_\infty$ separately. To compute $\tilde{b}(x)$ and $\hat{b}(x)$, the values of vectors $\hat{C}$ and $\tilde{C}$ must be computed from two linear equations,

$$S\hat{C} = \hat{G}, \tag{41}$$

$$S\tilde{C} = \tilde{G}. \tag{42}$$

Table 4: Error comparison for Example 8 when $\gamma = 1/4$, $N = 50$, and $\Delta t = 10^{-4}$.

Q	ECuBS		TCuBS [24]		CuBS [22]	
	L_2	L_∞	L_2	L_∞	L_2	L_∞
50	1.48×10^{-6}	2.88×10^{-6}	2.29×10^{-6}	4.26×10^{-6}	2.46×10^{-6}	4.53×10^{-6}
100	5.15×10^{-6}	8.37×10^{-6}	7.89×10^{-6}	1.24×10^{-5}	8.44×10^{-6}	1.32×10^{-5}
150	1.06×10^{-5}	1.69×10^{-5}	1.61×10^{-5}	2.50×10^{-5}	1.72×10^{-5}	2.67×10^{-5}
200	1.75×10^{-5}	2.66×10^{-5}	2.66×10^{-5}	3.94×10^{-5}	2.84×10^{-5}	4.19×10^{-5}
250	2.58×10^{-5}	3.89×10^{-5}	3.90×10^{-5}	5.74×10^{-5}	4.17×10^{-5}	6.12×10^{-5}
300	3.53×10^{-5}	5.19×10^{-5}	5.33×10^{-5}	7.76×10^{-5}	5.69×10^{-5}	8.29×10^{-5}

Now, by subtracting (42) from (41), we obtain

$$S\left(\tilde{C} - \hat{C}\right) = \tilde{G} - \hat{G}. \tag{43}$$

The specification of matrix S in equation (19) makes S strictly diagonally dominant making it nonsingular. Thus,

$$\left(\tilde{C} - \hat{C}\right) = S^{-1}\left(\tilde{G} - \hat{G}\right). \tag{44}$$

Taking infinity norm of above equation, we obtain

$$\left\|\left(\tilde{C} - \hat{C}\right)\right\|_\infty \le \|S^{-1}\|_\infty \left\|\left(\tilde{G} - \hat{G}\right)\right\|_\infty. \tag{45}$$

Let the sum of ith row of matrix $S = [x_{ij}]_{(N+1)\times(N+1)}$ be $\tau_i (0 \le i \le N)$. Then, we have

$$\begin{aligned} \tau_0 &= \sum_{j=0}^{N} a_{0j} = \omega, \\ \tau_i &= \sum_{j=0}^{N} a_{ij} = \rho_2 + 2\rho_1 \; i = 1, \cdots, N-1, \\ \tau_N &= \sum_{j=0}^{N} a_{Nj} = \omega. \end{aligned} \tag{46}$$

It is well known in the theory of matrices that

$$\sum_{j=0}^{N} x_{ij}^{-1} \tau_j = 1, i = 0, 1, \cdots, N. \tag{47}$$

Here, x_{ij}^{-1} represents the entries of S^{-1}. Then,

$$\|S^{-1}\|_\infty = \sum_{j=0}^{N} \left|x_{ij}^{-1}\right| \le \frac{1}{\tau}, \tag{48}$$

where $\tau = \min_{0\le i\le N} \tau_i = \min(\omega, \rho_2 + 2\rho_1) = \min(W(2 + \eta/2 h^2)(24/4 - \eta), 1)$. Using (48) in (45) to acquire

$$\left\|\left(\tilde{C} - \hat{C}\right)\right\|_\infty \le \frac{1}{\tau} \left\|\left(\tilde{G} - \hat{G}\right)\right\|_\infty. \tag{49}$$

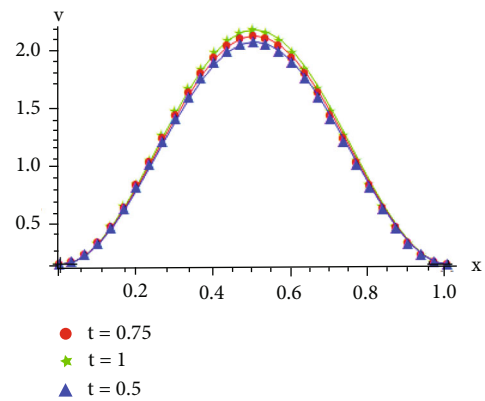

Figure 10: The exact and approximate (triangles, starts, circles) solutions for Example 8 at various times when $h = 0.01$.

Using (15), the upper bound of $\|(\tilde{G} - \hat{G})\|_\infty$ is computed as

$$\begin{aligned} \left|\tilde{G}_i - \hat{G}_i\right| &\le \left|\tilde{v}_i - \hat{v}_i\right| + \Delta t \left|\tilde{g}_i^{q+1} - \hat{g}_i^{q+1}\right| + \frac{W}{h^2} \sum_{r=1}^{q} |l_r| \\ &\left(\delta_1 \left|\tilde{C}_{j-1}^{q-r+1} - \hat{C}_{j-1}^{q-r+1}\right| + \delta_2 \left|\tilde{C}_j^{q-r+1} - \hat{C}_j^{q-r+1}\right| + \delta_1 \left|\tilde{C}_{j+1}^{q-r+1} - \hat{C}_{j+1}^{q-r+1}\right|\right). \end{aligned} \tag{50}$$

To simplify the RHS of (50), we present the following theorem. □

Theorem 3 (see [37, 38]). *If $P(x) \in c^4[a, b]$, $|P^4(x)| \le Ł$, $\forall s \in [a, b]$, the interval $[a, b]$ is partitioned by $\Delta = \{a = x_0 < x_1 < \cdots < x_N = b\}$ into subintervals of length h. If $b(x)$ is the unique spline function interpolates $P(x)$ at knots $x_0, x_1, \cdots, x_N$, then there exists a constant κ_j such that,*

$$\|P^{(l)} - b^{(l)}\| \le \kappa_l Ł h^{4-l} l = 0, 1, 2, 3. \tag{51}$$

Using the aforementioned theorem,

$$\left|\tilde{v}_i - \hat{v}_i\right| = \left|\tilde{b}_i(x) - \hat{b}_i(x)\right| \le \kappa_0 Ł h^4. \tag{52}$$

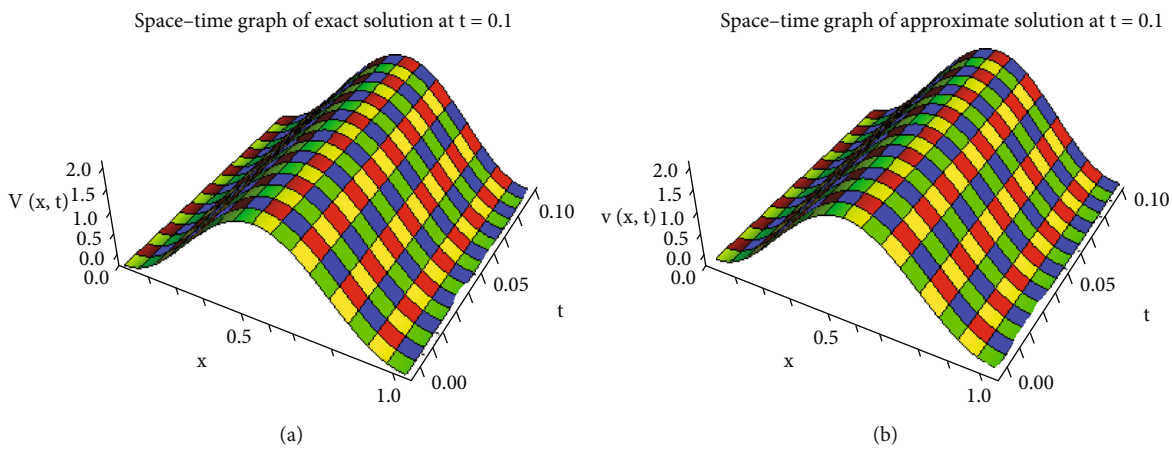

Figure 11: The approximate and exact solutions for Example 8 when $h = 1/60$, $t = 0.1$, $\Delta t = 0.01$.

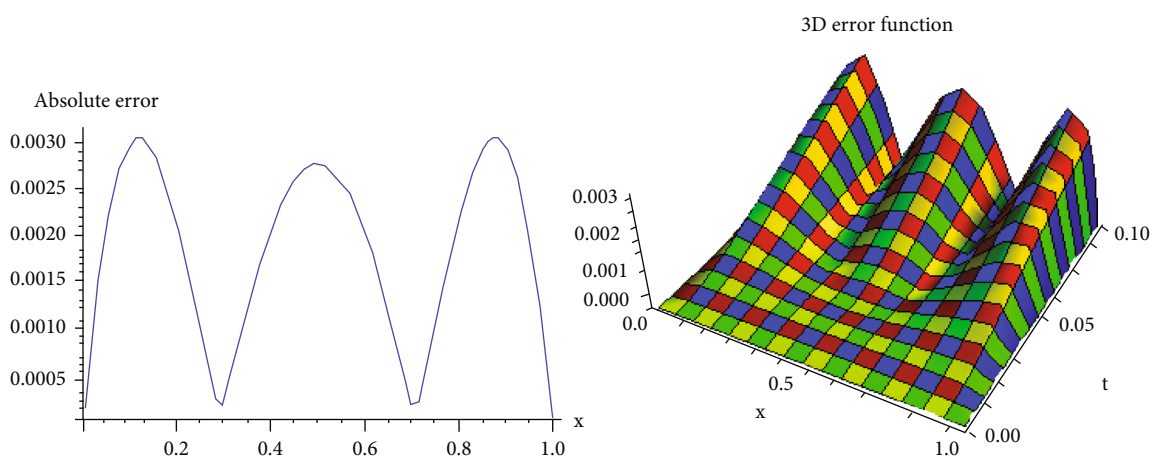

Figure 12: 2D and 3D error profiles for Example 8 when $h = 1/60$, $t = 0.1$, $\Delta t = 0.01$.

Furthermore, $\{l_r\}_{r=1}^{q}$ is a decreasing sequence of positive terms and $l_r \le 1$ for $1 \le r \le n$. Using (52) and letting $\tilde{g}_i^{q+1} = \hat{g}_i^{q+1}$, we can thus write (50) as

$$\left|\tilde{G}_i - \hat{G}_i\right| \le \kappa_0 Łh^4 + \frac{W}{h^2}\sum_{r=1}^{q} d_r. \tag{53}$$

where

$$\left(\delta_1\left|\tilde{C}_{i-1}^{q-r+1} - \hat{C}_{i-1}^{q-r+1}\right| + \delta_2\left|\tilde{C}_i^{q-r+1} - \hat{C}_i^{q-r+1}\right| + \delta_1\left|\tilde{C}_{i+1}^{q-r+1} - \hat{C}_{i+1}^{q-r+1}\right|\right) = d_r. \tag{54}$$

Let $\sum_{r=1}^{q} d_r = D_q$ and $\kappa_0 Łh^4 + (W/h^2)D_q = R_q$, then, (53) becomes

$$\left|\tilde{G}_i - \hat{G}_i\right| \le R_q. \tag{55}$$

Using (55) in (49) to get

$$\left\|\left(\tilde{C} - \hat{C}\right)\right\|_\infty \le \frac{1}{\tau} R_q = Rh^2, \tag{56}$$

where $Rh^2 = (1/\tau)R_q = \max\left((1/W)(2h^2/2 + \eta)(4 - \eta/24), 1\right)$.

To proceed further, we have to follow the next theorem.

Theorem 4 (see [39]). *The B-splines $\{B_{-1}, B_0, B_1, \cdots, B_{N-1}, B_N, B_{N+1}\}$ satisfy the following inequality*

$$\left|\sum_{i=-1}^{N+1} B_i(x)\right| \le 1, 0 \le s \le 1. \tag{57}$$

Now, by subtracting (40) from (39), we have

$$\tilde{b}(x) - \hat{b}(x) = \sum_{j=-1}^{N+1}\left(\tilde{C}_j - \hat{C}_j\right)B_j^4(x). \tag{58}$$

Taking the infinity norm on both sides, we obtain

$$\begin{aligned}\|\tilde{b}(x)-\hat{b}(x)\|_\infty &= \|\sum_{j=-1}^{N+1}\left(\tilde{C}_j-\hat{C}_j\right)B_j^4(x)\|_\infty,\\ &\le \left|\sum_{j=-1}^{N+1}B_j^4(x)\right|\|\left(\tilde{C}_j-\hat{C}_j\right)B_j^4(x)\|_\infty, \le Rh^2,\end{aligned} \tag{59}$$

that is,

$$\|\tilde{b}(x)-\hat{b}(x)\|_\infty \le Rh^2. \tag{60}$$

From Theorem (3) and equation (52), we have

$$\|\hat{v}(x)-\tilde{b}(x)\|_\infty \le \kappa_0 Łh^4. \tag{61}$$

Thus, from (60) and (61), we have

$$\|\hat{v}(x)-\hat{b}(x)\|_\infty \le \|\hat{v}(x)-\tilde{b}(x)\|_\infty + \|\tilde{b}(x)-\hat{b}(x)\|_\infty, \le \kappa_0 Łh^4 + Rh^2 = \sigma h^2, \tag{62}$$

where $\sigma = \kappa_0 Łh^2 + R$.

Now, for temporal convergence, applying Taylor expansion on (16), we have

$$\begin{aligned}&\left(v^q(x)+\Delta t v_t^q(x)+\frac{\Delta t^2}{2}v_{tt}^q(x)+\cdots\right)-T\left(v_{xx}^q(x)+\Delta t v_{xxt}^q(x)+\Delta t v_{xxt}^q(x)+\frac{\Delta t^2}{2!}v_{xxtt}^q(x)+\cdots\right)\\ &\quad = v^q(x)+W\sum_{r=1}^{q}l_r v_{xx}^{q-r+1}(x)+\Delta\left(g^q(x)+\Delta g_t^q(x)\right).\end{aligned} \tag{63}$$

Rearranging terms in above equation, we obtain

$$\begin{aligned}&\Delta t\left(v_t^q-g^q\right)-W\left(l_0 v_{xx}^q+\sum_{r=1}^{q}l_r v_{xx}^{q-r+1}\right)+\Delta v_{xxt}^q\\ &\quad+\frac{\Delta t^2}{2!}v_{xxtt}^q+\frac{\Delta t^2}{2!}\left(v_{xx}^q+g_t^q\right)=O(\Delta t).\end{aligned} \tag{64}$$

Assuming $v(x,t)$ to be the exact and $v^q(x,t)$ the approximate solutions of the equations (1)-(3), we have from (62) and (64) that

$$\|v(x,t)-v^q(x,t)\| \le \rho\left(k+h^2\right), \tag{65}$$

where ρ is a finite constant.

5. Numerical Results

The efficiency and the validity of the suggested methodology are confirmed in this part using various test problems by utilizing the L_2 and L_∞ error norms defined as

$$\begin{aligned}L_2 &= \|V-V_q\|_2 = h\sum_{j=0}^{N}\left|\left(V\left(x_j,t_q\right)-V_j^q\right)^2\right|,\\ L_\infty &= \|V-V_q\|_\infty = \max_j\left|V\left(x_j,t_q\right)-V_j^q\right|.\end{aligned} \tag{66}$$

All numerical calculations have been performed using Mathematica 12.

Example 5 (see [23]). Consider equation (1) with

$$g(x,t)=\frac{2t^{1/2}}{\sqrt{\pi}}\left(\pi^{\frac{5}{2}}\sin(\pi x)-\frac{4t^{3/2}}{\sqrt{\pi}}\sin(2\pi x)\right)-2\pi^{\frac{5}{2}}t^2\sin(2\pi x), \tag{67}$$

subject to the BCs,

$$v(0,t)=v(1,t)=0, 0\le t<1, \tag{68}$$

and the IC,

$$v(x,0)=\sin(\pi x), x\in[0,1]. \tag{69}$$

The analytical solution for this problem is $v(x,t) = \sin(\pi x) - (4t^{5/2}/\sqrt{\pi})\sin(2\pi x)$ with $\gamma = 1/2$. The suggested approach is implemented on the aforementioned problem to get numerical results. The estimated errors are compared to those provided in [23, 32–34] at various time stages in Table 1. Figure 1 presents an efficient comparison of approximate and exact solutions at various time levels. 3D comparison between approximate and exact solution is depicted in Figure 2. Figure 3 exhibits the 2D and 3D error profiles. The comparison reveals that the proposed algorithm has far better accuracy. The numerical solution when $h = 0.05$, $t = 1$, and $\Delta t = 0.01$ is given as

$$V(x,1)=\begin{cases} 1.43183\times 10^{-18}-1.53174x+2.05977\times 10^{-14}x^2+ \\ 25.8542x^3-6.29505x^4, & x\in\left[0,\frac{1}{20}\right), \\ -0.0000243493-1.52879x-0.118318x^2+27.831x^3- \\ 18.1748x^4, & x\in\left[\frac{1}{20},\frac{1}{10}\right), \\ -0.000218991-1.51313x-0.471333x^2+30.9718x^3- \\ 27.9956x^4, & x\in\left[\frac{1}{10},\frac{3}{20}\right), \\ \vdots \\ \vdots \\ 2.92425-32.3551x+104.229x^2-115.32x^3+40.5233x^4, & x\in\left[\frac{17}{20},\frac{9}{10}\right), \\ -6.19315+8.75716x+34.725x^2-63.1058^3+25.817x^4, & x\in\left[\frac{9}{10},\frac{19}{20}\right), \\ -19.686+65.9016x-56.0282x^2+0.949023x^3+8.86352x^4, & x\in\left[\frac{19}{20},1\right). \end{cases} \tag{70}$$

Example 6 (see [32]). Consider the equation (1) with $v(x,t)=(t+1)^2\sin\pi s$ subject to initial and boundary conditions $v(s,0)=\sin\pi s$, $v(0,t)=v(1,t)=0$, respectively. $g(x,t)$ is to be chosen with $\gamma=0.5$.

The suggested technique is applied on the above problem to acquire approximate solutions and absolute errors. Table 2 reports the contrast between the computed errors of present scheme and those of [32, 34] for different time levels. For various time stages, a sharp contrast between exact and approximate solutions is presented in Figure 4. Figure 5 depicts a 3D comparison between exact and approximate solutions. 2D and 3D absolute errors are plotted in Figure 6. The numerical solution when $h=0.05$, $t=1$, and $\Delta t=0.01$ is given as

$$V(x,1)=\begin{cases} 7.69735\times 10^{-18}+12.4842x+3.76073\times 10^{-13}x^2-20.4956x^3+ \\ 0.0307403x^4, & x\in\left[0,\frac{1}{20}\right), \\ -0.0000611671+12.4879x-0.0729451x^2-20.0154x^3+ \\ 0.091464x^4, & x\in\left[\frac{1}{20},\frac{1}{10}\right), \\ -0.00102794+12.5168x-0.361224x^2-19.0661x^3+ \\ 0.149936x^4, & x\in\left[\frac{1}{10},\frac{3}{20}\right), \\ \vdots \\ \vdots \\ -6.76161+44.8042x-56.66x^2+18.4664x^3+0.149936x^4, & x\in\left[\frac{17}{20},\frac{9}{10}\right), \\ -7.50901+47.3382x-59.5702x^2+19.6495x^3+0.091464x^4, & x\in\left[\frac{9}{10},\frac{19}{20}\right), \\ -7.98062+48.8796x-61.3023x^2+20.3726x^3+0.0307403x^4, & x\in\left[\frac{19}{20},1\right). \end{cases} \tag{71}$$

Example 7 (see [32]). Consider an analytic solution of (1)

$$v(x,t) = (t+1)\cos \pi x x \in [0,1]. \tag{72}$$

The initial and boundary conditions are to be evaluated from (72). The function $g(x,t)$ is to be chosen accordingly.

The proposed methodology is utilized to acquire the numerical results for this problem. Table 3 shows the efficiency of the presented scheme by comparing the errors with those presented in [32, 34]. Figures 7 and 8 illustrate the 2D and 3D comparison of the exact to approximate solutions. The graphs are in excellent affirmation. The 2D and 3D error functions for this example are shown in Figure 9. The numerical solution when $h = 0.05$, $t = 1$, and $\Delta t = 0.01$ is given as

$$V(x,1) = \begin{cases} 2 - 0.0163534x - 9.84508x^2 + 0.613676x^3 + 1.95785x^4, & x \in \left[0, \frac{1}{20}\right), \\ 1.99985 - 0.00725949x - 10.0272x^2 + 1.83263x^3 + 1.9096x^4, & x \in \left[\frac{1}{20}, \frac{1}{10}\right), \\ 1.99867 + 0.0280521x - 10.3822x^2 + 3.03508x^3 + 1.81434x^4, & x \in \left[\frac{1}{10}, \frac{3}{20}\right), \\ \vdots \\ \vdots \\ 3.50607 - 4.37378x - 9.60907x^2 + 10.2924x^3 - 1.81434x^4, & x \in \left[\frac{17}{20}, \frac{9}{10}\right), \\ 4.29238 - 6.92536x - 6.92831x^2 + 9.47104x^3 - 1.9096x^4, & x \in \left[\frac{9}{10}, \frac{19}{20}\right), \\ 5.2899 - 10.0341x - 3.74307x^2 + 8.44509x^3 - 1.95785x^4, & x \in \left[\frac{19}{20}, 1\right). \end{cases} \tag{73}$$

Example 8 (see [22]). Consider the equation (1) with IC

$$v(x,0) = 2\sin^2 \pi x, \tag{74}$$

and the BCs,

$$v(0,t) = 0, v(1,t) = 0. \tag{75}$$

The exact solution of this problems is

$$v(x,t) = 2\left(t^2 + t + 1\right)\sin^2 \pi x. \tag{76}$$

$g(x,t)$ is to be chosen accordingly. The introduced algorithm is employed to the aforementioned problem to obtain the numerical results. A comparison of computed errors with those of [22, 24] is discussed in Table 4. In Figure 10, a closed contrast between exact and approximate solution is exhibited. 3D profiles of both exact and approximate solutions are compared in Figure 11. Figure 12 displays the 2D and 3D error portrayals between the approximate and exact solutions. The numerical solution when $h = 0.05$, $t = 1$, and $\Delta t = 0.01$ is given as

$$V(x,1) = \begin{cases} -0.0162085x + 58.9241x^2 - 18.0337x^3 - 11.5028x^4, & x \in \left[0, \frac{1}{20}\right), \\ 0.0043058 - 0.274697x + 64.0995x^2 - 52.6488x^3 - 10.3781x^4, & x \in \left[\frac{1}{20}, \frac{1}{10}\right), \\ 0.0337757 - 1.16093x + 73.0047x^2 - 82.7609x^3 - 8.23736x^4, & x \in \left[\frac{1}{10}, \frac{3}{20}\right), \\ \vdots \\ \vdots \\ -19.1207 + 136.384x - 224.702x^2 + 115.71x^3 - 8.23736x^4, & x \in \left[\frac{17}{20}, \frac{9}{10}\right), \\ 0.802238 + 71.5344x - 156.115x^2 + 94.1611x^3 - 10.3781x^4, & x \in \left[\frac{9}{10}, \frac{19}{20}\right), \\ 29.3714 - 17.7196x - 64.194x^2 + 64.045x^3 - 11.5028x^4, & x \in \left[\frac{19}{20}, 1\right). \end{cases} \tag{77}$$

6. Conclusion

In this study, a numerical technique based on the extended cubic B-spline collocation method for the numerical solution of a second order PIDE is presented. The standard finite difference approach is used to discretize the temporal derivatives, while extended cubic B-splines are used to approximate the spatial derivatives. The stability and convergence of the proposed technique are established to ensure that errors do not magnify. Moreover, experimental outcomes substantiate the validity of the proposed scheme. The scheme's accuracy is confirmed by comparing the numerical results with those computed by some available numerical schemes.

Data Availability

No data were used to support this study.

Conflicts of Interest

The authors declare that they have no conflicts of interest.

Acknowledgments

The authors extend their appreciation to the Deputyship for Research & Innovation, Ministry of Education in Saudi Arabia, for funding this research work through the project number IF-PSAU-2021/01/18696.

References

[1] V. Lakshmikantham and M. Rama, *Theory of Integro-Differential Equations*, vol. 1, CRC Press, 1995.

[2] H. R. Thiem, "A model for the spatial spread of an epidemic," *Journal of Mathematical Biology*, vol. 4, no. 4, pp. 337–351, 1977.

[3] I. Ali, "Jacobi-spectral method for integro-delay differential equations with weakly singular kernels," *Turkish Journal of Mathematics*, vol. 39, pp. 810–819, 2015.

[4] O. M. Ogunlaran and M. O. Oke, "A numerical approach for solving 1st order integro-differential equations," *American Journal of Computational and Applied Mathematics*, vol. 3, no. 4, pp. 214–219, 2013.

[5] K. Chrysafinos, "Approximations of parabolic integro-differential equations using wavelet-Galerkin compression techniques," *BIT Numerical Mathematics*, vol. 47, no. 3, pp. 487–505, 2007.

[6] Z. Abbas, S. Vahdati, K. A. Atan, and L. Nik, "Legendre multi-wavelets direct method for linear integro-differential equations," *Applied Mathematical Sciences*, vol. 3, no. 14, pp. 693–700, 2009.

[7] A. H. Bhrawy, E. Tohidi, and F. Soleymani, "A new Bernoulli matrix method for solving high-order linear and nonlinear Fredholm integro-differential equations with piecewise intervals," *Applied Mathematics and Computation*, vol. 219, no. 2, pp. 482–497, 2012.

[8] S. H. Behiry and H. Hashish, "Wavelet methods for the numerical solution of Fredholm integro-diferential equations," *International Journal of Applied Mathematics*, vol. 11, no. 1, pp. 27–36, 2003.

[9] C. Chen, V. Thome, and L. Wahlbin, "Finite element approximation of a parabolic integro-differential equation with a weakly singular kernel," *Mathematics of Computation*, vol. 58, no. 198, pp. 587–602, 1992.

[10] F. Fakhar-Izadi and M. Dehghan, "The spectral methods for parabolic Volterra integro-differential equations," *Journal of Computational and Applied Mathematics*, vol. 235, no. 14, pp. 4032–4046, 2011.

[11] I. Sloan and V. Thome, "Time discretization of an Integro-differential equation of parabolic type," *SIAM Journal on Numerical Analysis*, vol. 23, no. 5, pp. 1052–1061, 1986.

[12] C. Lubich, "Discretized fractional calculus," *SIAM Journal on Mathematical Analysis*, vol. 17, no. 3, pp. 704–719, 1986.

[13] Z. Sun and X. Wu, "A fully discrete difference scheme for a diffusion-wave system," *Applied Numerical Mathematics*, vol. 56, no. 2, pp. 193–209, 2006.

[14] Y. Lin and C. Xu, "Finite difference/spectral approximations for the time-fractional diffusion equation," *Journal of Computational Physics*, vol. 225, no. 2, pp. 1533–1552, 2007.

[15] S. Larsson, V. Thome, and L. Wahlbin, "Numerical solution of parabolic integro-differential equations by the discontinuous Galerkin method," *Mathematics of Computation*, vol. 67, no. 221, pp. 45–71, 1998.

[16] W. McLean and V. Thome, "Numerical solution of an evolution equation with a positive-type memory term," *The Journal of the Australian Mathematical Society. Series B. Applied Mathematics*, vol. 35, no. 1, pp. 23–70, 1993.

[17] M. A. Ramadan, E. F. Lashien, and W. K. Zahra, "Quintic non-polynomial spline solutions for fourth order two-point boundary value problem," *Communications in Nonlinear Science and Numerical Simulation*, vol. 14, no. 4, pp. 1105–1114, 2009.

[18] M. A. Ramadan, S. F. Talat, and W. K. Zahra, "The use of adomian decomposition method for solving the regularized long-wave equation," *Chaos, Solitons & Fractals*, vol. 26, no. 3, pp. 747–757, 2005.

[19] M. A. Ramadan, E. F. Lashien, and W. K. Zahra, "A class of methods based on a septic non-polynomial spline function for the solution of sixth-order two-point boundary value problems," *International Journal of Computer Mathematics*, vol. 85, no. 5, pp. 759–770, 2008.

[20] T. Tang, "A finite difference scheme for partial integro-differential equations with a weakly singular kernel," *Applied Numerical Mathematics*, vol. 11, no. 4, pp. 309–319, 1993.

[21] M. Dehghan, "Solution of a partial integro-differential equation arising from visco-elasticity," *International Journal of Computer Mathematics*, vol. 83, no. 1, pp. 123–129, 2006.

[22] M. Zarebnia, "Sinc numerical solution for the Volterra integro-differential equation," *Communications in Nonlinear Science and Numerical Simulation*, vol. 15, no. 3, pp. 700–706, 2010.

[23] W. T. Long, D. Xu, and X. Y. Zeng, "Quasi wavelet based numerical method for a class of partial integro- differential equation," *Applied Mathematics and Computation*, vol. 218, no. 24, pp. 11842–11850, 2012.

[24] X. Yang, D. Xu, and H. Zhang, "Crank-Nicolson/quasi-wavelets method for solving fourth order partial integro- differential equation with a weakly singular kernel," *Journal of Computational Physics*, vol. 234, pp. 317–329, 2013.

[25] I. Aziz and I. Khan, "Numerical solution of partial Integro-differential equations of diffusion type," *Mathematical Problems in Engineering*, vol. 2017, 11 pages, 2017.

[26] A. Fahim, M. Araghi, J. Rashidinia, and M. Jalalvand, "Numerical solution of Volterra partial integro-differential equations based on sinc-collocation method," *Advances in Difference Equations*, vol. 2017, no. 1, Article ID 362, 2017.

[27] F. Fakhar-Izadi and M. Dehghan, "An efficient pseudo-spectral Legendre-Galerkin method for solving a nonlinear partial integro-differential equation arising in population dynamics," *Mathematicsl Methods in the Applied Sciences*, vol. 36, no. 12, pp. 1485–1511, 2013.

[28] F. M. Amir and K. Shakibi, "Solving integro-differential equation by using b-spline interpolation," *International Journal of Mathematical Modelling & Computations*, vol. 3, no. 3, pp. 237–244, 2013.

[29] F. Mirzaee and S. Alipour, "Cubic B-spline approximation for linear stochastic integro-differential equation of fractional order," *Journal of Computational and Applied Mathematics*, vol. 366, no. 3, article 112440, 2020.

[30] T. Tahernezhad and R. Jalilian, "Exponential spline for the numerical solutions of Linear Fredholm integro-differential equations," *Advances in Difference Equations*, vol. 2020, no. 1, Article ID 141, 2020.

[31] G. Fairweather, "Spline collocation methods for a class of hyperbolic partial integro-differential equations," *SIAM Journal on Numerical Analysis*, vol. 31, no. 2, pp. 444–460, 1994.

[32] M. Gholamian and J. Saberi-Nadjafi, "Cubic B-splines collocation method for a class of partial integro-differential equation," *Alexandria Engineering Journal*, vol. 57, no. 3, pp. 2157–2165, 2018.

[33] A. Ali, S. Ahmad, S. I. Shah, and F. Haq, "A quartic B-spline collocation technique for the solution of partial integro-differential equations equations with a weakly kernel," *Science International*, vol. 27, no. 4, pp. 2953–2958, 2015.

[34] A. Ali, K. Khan, F. Haq, and S. I. Shah, "A computational modeling based on trigonometric cubic B-spline functions for the approximate solution of a second order partial integro-differential equation," in *Advances in Intelligent Systems and Computing*, Á. Rocha, H. Adeli, L. Reis, and S. Costanzo, Eds., vol. 930 of New Knowledge in Information Systems and Technologies. WorldCIST'19 2019, , pp. 844–854, Springer, 2019.

[35] T. Akram, M. Abbas, A. I. Ismail, N. H. M. Ali, and D. Baleanu, "Extended cubic B-splines in the numerical solution of tme fractional telegraph equation," *Advances in Difference Equations*, vol. 2019, no. 1, 2019.

[36] J. Stoer and R. Bulirsch, *Introduction to Numerical Analysis*, Springer-Verlag, New York, 2nd edition, 1991.

[37] C. de Boor, "On the convergence of odd-degree spline interpolation," *Journal of Approximation Theory*, vol. 1, no. 4, pp. 452–463, 1968.

[38] C. A. Hall, "On error bounds for spline interpolation," *Journal of Approximation Theory*, vol. 1, no. 2, pp. 209–218, 1968.

[39] P. M. Prenter, *Spline and Variational Methods*, Wiley, New-York, 1975.

Hindawi
Journal of Function Spaces
Volume 2022, Article ID 3128586, 13 pages
https://doi.org/10.1155/2022/3128586

Research Article

Generalized Lucas Tau Method for the Numerical Treatment of the One and Two-Dimensional Partial Differential Heat Equation

Y. H. Youssri,[1] **W. M. Abd-Elhameed**,[1] **and S. M. Sayed**[2]

[1]*Department of Mathematics, Faculty of Science, Cairo University, Giza 12613, Egypt*
[2]*Department of Mathematics, Faculty of Science, Helwan University, Cairo 11795, Egypt*

Correspondence should be addressed to Y. H. Youssri; youssri@aucegypt.edu

Received 20 January 2022; Revised 27 March 2022; Accepted 30 March 2022; Published 25 April 2022

Academic Editor: Baowei Feng

This paper is dedicated to proposing two numerical algorithms for solving the one- and two-dimensional heat partial differential equations (PDEs). In these algorithms, generalized Lucas polynomials (GLPs) involving two parameters are utilized as basis functions. The two proposed numerical schemes in one and two- dimensions are based on solving the corresponding integral equation to the heat equation, and after that employing, respectively, the tau and collocation methods to convert the heat equations subject to their underlying conditions into systems of linear algebraic equations that can be treated efficiently via suitable numerical procedures. In this article, the convergence analysis is examined for the proposed generalized Lucas expansion. Five illustrative problems are numerically solved via the two proposed numerical schemes to show the applicability and accuracy of the presented algorithms. Our obtained results compare favourably with the exact solutions.

1. Introduction

Many mathematical models of real-world problems give rise to partial differential equations (*PDEs*) of initial and boundary conditions. *PDEs* are frequently represented as mathematical equations that connect various amounts and their derivatives, e.g., heat transition, a particle's movement in a straight line, the movement of a rocket, a molecule's vibration, and a change in a substance's molecular composition, etc. Every one of these issues is represented by hyperbolic, elliptic, or parabolic partial differential equation (*PPDE*) and might be homogeneous, in one, two, or three dimensions, with non-local boundary conditions in addition to the initial conditions found in the prose. A parabolic *PDE* is used to solve a variety of scientific problems, including ocean acoustic propagation as well as heat diffusion. The hyperbolic *PDE* indicates the wave transformation and sound waves of an elastic string, whereas the elliptic *PDE* describes the Laplace equation.

Fibonacci and Lucas polynomial sequences are crucial and they play vital roles in various disciplines. These sequences are employed to find approximate solutions of different types of DEs. For instance, Fibonacci polynomials were used to treat multi-term fractional DEs in [1]. In [2], Lucas polynomials are employed for the numerical treatment of sinh-Gordon equation. The authors in [3] developed a matrix method using Fibonacci polynomials for the treatment of the generalized pantograph equations with functional arguments. Another approach based on mixed Fibonacci and Lucas polynomials is followed in [4] to obtain numerical solutions of Sobolev equation in two dimensions. Lucas polynomials are employed in [5] to obtain numerical solutions of multidimensional Burgers-type equations. Lucas polynomials were also employed in [6] to solve the fractional-order electro-hydrodynamics flow model.

The Fibonacci and Lucas sequences can be generalized. For example, the authors in [7, 8] introduced two generalized families of Fibonacci and Lucas polynomials. In addition, they employed such generalized sequences to treat some fractional differential equations.

It is well-known that the heat equation is a parabolic *PDE* that describes the distribution of heat. There are two types of heat equations: non-homogeneous and homogeneous. Non-homogeneous heat equations have source terms

in the partial differential equations, whereas homogeneous heat equations do not have source terms. Many authors have researched theoretically and numerically the heat equations. For example, the authors in [9] obtained a numerical solution of the one-dimensional heat equation by using the Chebyshev wavelets method. In [10], the authors treated the same equation using a high-order compact boundary value method. The authors in [11] treated the heat equation using radial basis functions. In [12] a modified Crank-Nicolson scheme Richardson extrapolation is followed to treat the one-dimensional heat equation. Recently, the Chebyshev collocation algorithm is followed in [13] to treat the same equation.

A *PDE* governs the temperature of a rod that is frequently defined as [14]:

$$u_t(\xi, t) = K\, u_{\xi\xi}(\xi, t),\ 0 \le \xi \le L,\ t \ge 0, \tag{1}$$

where $u(\xi, t)$ is the temperature of a rod at position ξ at time t and K is the thermal conductivity of the material, which measures the rod's ability to conduct heat.

The solution's domain is a semi-infinite wire of length L that extends endlessly in time. In practice, the result is found only for a limited time. The solution with equation (1) necessitates the requirements of an initial condition at $t = 0$ as well as boundary conditions at $\xi = 0$, and $\xi = L$.

Initial condition:

$$u(\xi, 0) = g(\xi), \quad 0 \le \xi \le L. \tag{2}$$

Boundary conditions:

$$u(0, t) = S_1(t), \quad t \ge 0, \tag{3}$$

$$u(L, t) = S_2(t), \quad t \ge 0. \tag{4}$$

It is essential to refer here that (1) is called the homogeneous heat equation, whereas the non-homogeneous heat equation is given as:

$$u_t(\xi, t) = K\, u_{\xi\xi}(\xi, t) + g(\xi, t), \quad 0 \le \xi \le L, \quad t \ge 0, \tag{5}$$

where $g(\xi, t)$ is referred to as the heat source.

It is worth mentioning that the heat equation (1) governed by (2)-(4) can be extended to higher-dimensional heat equations. These types of equations were treated analytically and numerically by many authors. For example, the Adomian decomposition method was utilized for handling the two-dimensional heat equation in [14]. In addition, the collocation method together with the finite differences was employed to solve the same type of equations in [15]. Some analytical and numerical studies of a two-dimensional nonlinear heat equation with a source term were presented in [16]. Some other forms of the heat equations were handled in other contributions. For example, the authors in [17] applied the finite difference method of lines to treat the heat equation in three space variables. An Adomian decomposition method is applied to the treatment of a non-linear heat equation in [18]. For some other contributions relating to the heat equation, on can be referred to [19–23].

There are numerous methods that have a significant impact on numerical analysis in general, see for example [24–26]. Among these methods are the spectral methods, which play important roles in dealing with *PDEs* [27, 28], ordinary differential equations (*ODEs*) [29, 30], and fractional differential equations (*FDEs*) [31–34]. The basic idea behind spectral methods is that the proposed approximate solution is written as linear combinations of many basic functions, which may be orthogonal or otherwise. The popular spectral approaches are Galerkin, collocation, and tau. In the context of numerical *DEs*, each version has its own significance. Several authors have made extensive use of the latter methods. The Galerkin approach was followed to treat some types of differential equations. For example, the authors in [35] applied the Galerkin method to obtain spectral solutions of BVPs of even-orders, where the authors in [36] obtained approximate solutions of the fractional telegraph equation via implementing a spectral Legendre-Galerkin algorithm. Regarding the collocation method, it is an advantageous method from its capability for treating any type of differential equations governed by any underlying conditions. For example, it is followed in [37] to treat the initial value problems of any order with the aid of the operational matrices of some orthogonal polynomials. The tau method is different from the tau method in that no restrictions on choosing the basis functions. This of course makes its application to different types of *DEs* is easier than the application of the Galerkin method. So, as a result, it is used for solving several types of differential equations.

The structure of this paper is as follows: Section 2 presents an overview of generalized Lucas polynomials and some of their fundamental properties. In Section 3, a numerical method based on the spectral tau method is applied to solve the one-dimensional partial differential heat equation. An extension to solve the two-dimensional heat equation is proposed in Section 4 based on the application of the collocation method. Section 5 examines the convergence and error analysis of the proposed *GLPs* expansion. Numerical outcomes and comparisons are presented in Section 6 to demonstrate the validity of our proposed methods. Section 7 is made up of a brief outline paper.

2. An Overview on Generalized Lucas Polynomials

The purpose of this section is to give an overview of the (*GLPs*). Furthermore, some of the basic formulas of these polynomials are presented.

The *GLPs* may be constructed with the aid of the following recursive formula:

$$\phi_j^{a,b}(\varepsilon) = a\,\varepsilon\,\phi_{j-1}^{a,b}(\varepsilon) + b\,\phi_{j-2}^{a,b}(\varepsilon), \quad \phi_0^{a,b}(\varepsilon) = 2, \quad \phi_1^{a,b}(\varepsilon) = a\,\varepsilon, \quad j \ge 2, \tag{6}$$

They also may be generated by the following Binet's formula:

$$\phi_j^{a,b}(\varepsilon) = \frac{\left(a\,\varepsilon - \sqrt{a^2\,\varepsilon^2 + 4\,b}\right)^j + \left(a\,\varepsilon + \sqrt{a^2\,\varepsilon^2 + 4\,b}\right)^j}{2^j}, \quad j \geq 0. \tag{7}$$

The first few ones of the $\phi_j^{a,b}(\varepsilon)$ are given as follows:

$$\begin{aligned} &\phi_0^{a,b}(\varepsilon) = 2, \phi_1^{a,b}(\varepsilon) = a\,\varepsilon, \\ &\phi_2^{a,b}(\varepsilon) = a^2\,\varepsilon^2 + 2\,b, \phi_3^{a,b}(\varepsilon) = a^3\,\varepsilon^3 + 3\,a\,b\,\varepsilon. \end{aligned} \tag{8}$$

It is important to point out that this kind of polynomials was employed in [8] to deal with some types of fractional *DEs*.

Some celebrated polynomials can be obtained as special cases of the *GLPs* as a result of the existence of two parameters. In fact, the Lucas polynomials $L_i(\varepsilon)$, Fermat-Lucas polynomials $\mathscr{F}_i(\varepsilon)$, Pell-Lucas polynomials $Q_i(\varepsilon)$, Chebyshev polynomials of the first kind $T_i(\varepsilon)$, and Dickson polynomials of the first kind $D_i^{\alpha}(\varepsilon)$ are special ones of the *GLPs* . Explicitly, we have

$$\begin{aligned} &L_i(\varepsilon) = \phi_i^{1,1}(\varepsilon), \quad \mathscr{F}_i(\varepsilon) = \phi_i^{3,-2}(\varepsilon), \\ &Q_i(\varepsilon) = \phi_i^{2,1}(\varepsilon), \\ &D_i^{\alpha}(\varepsilon) = \phi_i^{1,-\alpha}(\varepsilon). \end{aligned} \tag{9}$$

The *GLPs* have the following analytic formula ([8]):

$$\phi_j^{a,b}(\varepsilon) = j \sum_{r=0}^{\left[\frac{j}{2}\right]} \frac{\binom{j-r}{r} b^r}{j-r} (a\,\varepsilon)^{j-2r}, \quad j \geq 1, \tag{10}$$

where [z] denotes the well-known floor function, which can also be written as:

$$\phi_j^{a,b}(\varepsilon) = j \sum_{k=0}^{j} \frac{2\,\delta_{j+k} \binom{j+k/2}{j-k/2} b^{j-k/2}}{j+k} (a\,\varepsilon)^k, \tag{11}$$

where

$$\delta_n = \begin{cases} 0, & \text{if } n\ odd, \\ 1, & \text{if } n\ even. \end{cases} \tag{12}$$

3. Numerical Treatment of the One-Dimensional Heat Equation

This section focuses on treating the one-dimensional partial differential heat equation We will analyze a numerical solution of the following one-dimensional linear non-homogeneous heat equation ([14]):

$$u_t(\xi, t) = K\,u_{\xi\xi}(\xi, t) + g(\xi, t), \quad 0 \leq \xi \leq L, \quad t \geq 0, \tag{13}$$

governed by the non-homogeneous boundary conditions:

$$u(0, t) = S_1(t), \quad u(L, t) = S_2(t), \quad t \geq 0, \tag{14}$$

and the initial conditions:

$$u(\xi, 0) = f_1(\xi), \quad 0 \leq \xi \leq L. \tag{15}$$

3.1. Integral Equation Corresponding to (13)-(15). Our strategy to solve the one-dimensional heat equation (13) governed by the conditions (14) and (15) is to treat with its corresponding integral equation.

Now, integrating Eq. (13) with respect to the variable t taking into the consideration the initial condition in (15), we get

$$u(\xi, t) = K \int_0^t u_{\xi\xi}(\xi, \varepsilon)\,d\varepsilon + \int_0^t g(\xi, \varepsilon)\,d\varepsilon + f_1(\xi), \tag{16}$$

governed by the non-homogeneous boundary conditions:

$$u(0, t) = S_1(t), \quad u(L, t) = S_2(t), \quad t \geq 0. \tag{17}$$

3.2. Spectral Tau Treatment for the Heat Equation. The objective of the current section is to propose a spectral tau algorithm for numerically solving the corresponding integral form to the linear one-dimensional heat type equation. First, we consider the two families of basis functions $\{\phi_j^{a,b}(\xi)\}_{j\geq 0}$ and $\{\phi_i^{a,b}(t)\}_{i\geq 0}$. Consider the next two spaces:

$$\begin{aligned} &P = \left\{\varepsilon \in \theta^2(\Omega)\colon \varepsilon(0, t) = \varepsilon(L, t) = 0\,; 0 < t \leq \tau\right\}, \\ &P_M = \operatorname{span}\left\{\phi_j^{a,b}(\xi)\,\phi_i^{a,b}(t)\colon j, i = 0, 1, \cdots, M\right\}, \end{aligned} \tag{18}$$

where $\theta^2(\Omega)$; $\Omega = (0, L) \times (0, \tau]$ is the Sobolev space [38].

Now, the following approximation can be assumed for $u(\xi, t)$:

$$u_M(\xi, t) = \sum_{j=0}^{M} \sum_{i=0}^{M} c_{ji}\,\phi_j^{a,b}(\xi)\,\phi_i^{a,b}(t). \tag{19}$$

To use the spectral tau approach to Eq. (16) implies that we first compute the residual of Eq. (13). It is given by

$$\begin{aligned} \mathbf{R}(\xi, t) = &\sum_{j=0}^{M} \sum_{i=0}^{M} c_{ji}\,\phi_j^{a,b}(\xi)\,\phi_i^{a,b}(t) \\ &- \sum_{j=0}^{M} \sum_{i=0}^{M} c_{ji}\partial_{\xi\xi}\,\phi_j^{a,b}(\xi) \int_0^t \phi_i^{a,b}(\varepsilon)\,d\varepsilon - g_2(\xi, t). \end{aligned} \tag{20}$$

The analytic form of $\phi_j^{a,b}(\xi)$ in (11) allows us to express explicitly $D^2\phi_j^{a,b}(\xi)$ and $\int_0^t \phi_i^{a,b}(\varepsilon)\, d\varepsilon$ in the following forms:

$$D^2\phi_j^{a,b}(\xi) = \begin{cases} 0, & \text{if } j = 0, \\ \displaystyle\sum_{k=0}^{j} \frac{2\, j\, k\, (k-1)\, a^k\, b^{j-k/2}\, \delta_{j+k} \begin{pmatrix} j+k/2 \\ j-k/2 \end{pmatrix}}{(j+k)}\, \xi^{k-2}, & \text{if } j \geq 1, \end{cases} \tag{21}$$

$$\begin{aligned} D_t^{-1}\, \phi_i^{(a,b)}(t) &= \int_0^t \phi_i^{a,b}(\varepsilon) d\varepsilon \\ &= \begin{cases} 2t, & \text{if } i = 0, \\ \displaystyle\sum_{k=0}^{i} \frac{2\, i\, a^k\, b^{i-k/2}\, \delta_{i+k} \begin{pmatrix} i+k/2 \\ i-k/2 \end{pmatrix}}{(i+k)\,(k+1)}\, t^{k+1}, & \text{if } i \geq 1. \end{cases} \end{aligned} \tag{22}$$

Based on the two Formulas (21) and (22), the residual in (20) can be rewritten as

$$\begin{aligned} \mathrm{R}(\xi, t) = &\sum_{j=0}^{M} \sum_{i=0}^{M} 4\, j\, i\, c_{ji} \sum_{k=0}^{j} \sum_{k=0}^{i} \\ &\cdot \frac{a^{2k}\, b^{j+i/2-k}\, \delta_{j+k}\, \delta_{i+k} \begin{pmatrix} j+k/2 \\ j-k/2 \end{pmatrix} \begin{pmatrix} i+k/2 \\ i-k/2 \end{pmatrix}}{(j+k)\,(i+k)} \\ &\cdot \left((\xi\, t)^k - \frac{k\,(k-1)\, \xi^{k-2}\, t^{k+1}}{k+1} \right) - g_2(\xi, t), \end{aligned} \tag{23}$$

and therefore, the following system of equations can be acquired after the spectral tau technique is applied (see, [7]).

$$\int_0^\tau \int_0^L \mathrm{R}(\xi, t) \phi_j^{a,b}(\xi) \phi_i^{a,b}(t)\, d\xi\, dt = 0, \quad 0 \leq j, i \leq M-1. \tag{24}$$

In addition, the boundary conditions (14) give:

$$\begin{aligned} &\sum_{j=0}^{M} \sum_{i=0}^{M} c_{ji}\, \phi_j^{a,b}(0)\, \phi_i^{a,b}\left(\frac{k+1}{M+2}\tau\right) \\ &\quad = S_1\left(\frac{k+1}{M+2}\tau\right), \quad 0 \leq k \leq M-1, \end{aligned} \tag{25}$$

$$\begin{aligned} &\sum_{j=0}^{M} \sum_{i=0}^{M} c_{ji}\, \phi_j^{a,b}(L)\, \phi_i^{a,b}\left(\frac{k+1}{M+2}\tau\right) \\ &\quad = S_2\left(\frac{k+1}{M+2}\tau\right), \quad 0 \leq k \leq M. \end{aligned} \tag{26}$$

Eqs. (24), (25), and (26) create a system of linear equations in the dimension $(M+1)^2$ with unknown expansion coefficients c_{ji}. The solution of this system can be found via the Gaussian elimination method.

4. Treatment of the Two-Dimensional Heat Equation

The distribution of heat flow in a two-dimensional space is governed by the following initial boundary value problem (see, [39, 40])

$$u_t(\xi, \eta, t) = \bar{K}\left(u_{\xi\xi}(\xi, \eta, t) + u_{\eta\eta}(\xi, \eta, t)\right); \qquad (\xi, \eta, t) \in \vartheta, \tag{27}$$

subject to the boundary conditions (BCs):

$$\begin{aligned} u(0, \eta, t) &= u(L_1, \eta, t) = 0, \\ u(\xi, 0, t) &= u(\xi, L_2, t) = 0, \end{aligned} \tag{28}$$

and the initial condition (IC):

$$u(\xi, \eta, 0) = g(\xi, \eta), \tag{29}$$

where $u \equiv u(\xi, \eta, t)$ is the temperature of any point located at the position (ξ, η) of a rectangular plate at any time t, $\bar{K}$ is the thermal diffusivity, and $\vartheta = (0, L_1) \times (0, L_2) \times (0, T)$.

We suggest the following approximate spectral solution

$$u_M(\xi, \eta, t) = \sum_{n=0}^{M} \sum_{m=0}^{M} \sum_{\ell=0}^{M} c_{\ell,m,n}\, \phi_\ell^{(a,b)}(\xi)\, \phi_m^{(a,b)}(\eta)\, \phi_n^{(a,b)}(t). \tag{30}$$

By integrating (27) with respect to the variable t and making use of the IC (29), we get

$$u(\xi, \eta, t) = \bar{K} \int_0^t \left(u_{\xi\xi}(\xi, \eta, t) + u_{\eta\eta}(\xi, \eta, t)\right) d\tau + g(\xi, \eta). \tag{31}$$

Now, making use of (21) and (22), we can approximate $\int_0^t (u_{\xi\xi}(\xi, \eta, t) + u_{\eta\eta}(\xi, \eta, t)) d\tau$ in the form:

$$\begin{aligned} &\int_0^t \left(u_{\xi\xi}(\xi, \eta, t) u_{\eta\eta}(\xi, \eta, t)\right) d\tau \\ &\quad \approx \sum_{n=0}^{M} \sum_{m=0}^{M} \sum_{\ell=0}^{M} c_{\ell,m,n}\, D_\xi^2\, \phi_\ell^{(a,b)}(\xi)\, D_\eta^2\, \phi_m^{(a,b)}(\eta)\, D_t^{-1}\, \phi_n^{(a,b)}(t), \end{aligned} \tag{32}$$

where $D_\xi^2\, \phi_\ell^{(a,b)}(\xi)$, $D_\eta^2\, \phi_m^{(a,b)}(\eta)$ can be expressed by (21), and $D_t^{-1}\, \phi_n^{(a,b)}(t)$ can be expressed by (22).

Our strategy to solve numerically (27)-(29) is to utilize the spectral collocation method. For the residual of (31) is given by

$$\begin{aligned} R(\xi,\eta,t) = &\sum_{n=0}^{M}\sum_{m=0}^{M}\sum_{\ell=0}^{M} c_{\ell,m,n}\phi_{\ell}^{(a,b)}(\xi)\phi_{m}^{(a,b)}(\eta)\,\phi_{n}^{(a,b)}(t) \\ &-\bar{K}\sum_{n=0}^{M}\sum_{m=0}^{M}\sum_{\ell=0}^{M} c_{\ell,m,n}D_{\xi}^{2}\phi_{\ell}^{(a,b)}(\xi)D_{\eta}^{2}\phi_{m}^{(a,b)} \\ &\cdot(\eta)D_{t}^{-1}\phi_{n}^{(a,b)}(t) - g(\xi,\eta) \end{aligned} \tag{33}$$

We choose the following Riemann nodes $P_{ijk} = (\xi_i, \eta_j, t_k)$, with

$$\begin{aligned} \xi_i &= \frac{i+1}{M+2}L_1, \\ \eta_j &= \frac{j+1}{M+2}L_2, \\ t_k &= \frac{k+1}{M+2}T \end{aligned} \tag{34}$$

Hence, the application of the spectral collocation method implies that ([41]),

$$R\left(P_{ijk}\right) = 0\,; \quad 0 \le i, j \le M, \quad 0 \le k \le M-4, \tag{35}$$

and the use of the BCs leads to the following constraints:

$$\begin{aligned} u\left(0,\eta_j,t_k\right) &= 0, \quad 0 \le j,k \le M, \\ u\left(L_1,\eta_j,t_k\right) &= 0, \quad 0 \le j,k \le M, \\ u(\xi_i,0,t_k) &= 0, \quad 0 \le i,k \le M, \\ u(\xi_i,L_2,t_k) &= 0, \quad 0 \le i,k \le M. \end{aligned} \tag{36}$$

Now, the above-mentioned equations build a system of algebraic equations of dimension d, where $d = (M+1)^2 (M-3) + 4(M+1)^2 = (M+1)^3$.

Thanks to the Gaussian elimination technique, we get the proposed approximate solution $u_M(\xi,\eta,t)$.

5. Error Analysis and Convergence of the Proposed GLPs Expansion

The goal of this section is to investigate the error analysis and convergence of the GLPs expansion that is used to solve the one-dimensional heat equation (13) governed by the underlying conditions (14) and (15). In the sequel, the next two lemmas are useful.

Lemma 1. *Let $L > 0$ and $\xi \in [0, L]$. For the GLPs, the following inequity is valid:*

$$\left|\phi_j^{a,b}(\xi)\right| \le 2\left(a^3 + 3\,b\,L\right)^{j-1}, \quad j \ge 1. \tag{37}$$

where a and b are positive values.

Proof. We prove by mathematical induction. The inequality is satisfied for $j = 1$, since

$$\left|\phi_1^{a,b}(\xi)\right| = |a\,\xi| \le 2. \tag{38}$$

We now assume that (37) is satisfied for $j = k$

$$\left|\phi_k^{a,b}(\xi)\right| \le 2\left(a^3 + 3\,b\,L\right)^{k-1}. \tag{39}$$

Finally, we demonstrate that validity of (37) for $j = k+1$. Now, we have

$$\begin{aligned} \left|\phi_{k+1}^{a,b}(\xi)\right| &= \left|a\,\xi\,\phi_k^{a,b}(\xi) + b\,\phi_{k-1}^{a,b}(\xi)\right| \\ &\le 2\left|\phi_k^{a,b}(\xi)\right| + |b|\left|\phi_{k-1}^{a,b}(\xi)\right| \\ &= 2\left(a^3 + 3\,b\,L\right)^{k-1} + 2\,|b|\left(a^3 + 3\,b\,L\right)^{k-2} \\ &= 2\left(a^3 + 3\,b\,L\right)^{k}\left[\left(a^3 + 3\,b\,L\right)^{-1} + |b|\left(a^3 + 3\,b\,L\right)^{-2}\right] \\ &\le 2\left(a^3 + 3\,b\,L\right)^{k}. \end{aligned} \tag{40}$$

This ends the proof of Lemma 1. □

Lemma 2. *For all $L > 0$, for every positive integer ν, and $\xi \in [0, L]$, the following inequity is valid for the GLPs:*

$$\left|D^{\nu}\phi_j^{a,b}(\xi)\right| \le \frac{13}{4}\,a^2\left(a^3 + 3\,b\,L\right)^{(j-1)\,\nu}, \tag{41}$$

Proof. By induction on j, we will get started. Assume that the inequality (41) holds for $(j-1)$ and $(j-2)$, and we have to prove that (41) itself holds. Now, our assumption implies that we have the following two inequalities:

$$\left|D^{\nu}\phi_{j-1}^{a,b}(\xi)\right| \le \frac{13}{4}\,a^2\left(a^3 + 3\,b\,L\right)^{(j-2)\,\nu}, \tag{42}$$

$$\left|D^{\nu}\phi_{j-2}^{a,b}(\xi)\right| \le \frac{13}{4}\,a^2\left(a^3 + 3\,b\,L\right)^{(j-3)\,\nu}. \tag{43}$$

In virtue of the recurrence relation (6) and the Inequalities (42) and (43), we get

$$\begin{aligned}\left|D^{\nu}\phi_j^{a,b}(\xi)\right| &= \left|\frac{a\,\xi^{1-\nu}}{\Gamma(2-\nu)}\,\phi_{j-1}^{a,b}(\xi) + a\,\xi\,D^{\nu}\phi_{j-1}^{a,b}(\xi) + b\,D^{\nu}\phi_{j-2}^{a,b}(\xi)\right| \\ &\le \frac{2\,L^{-\nu}}{\Gamma(2-\nu)}\,2\left(a^3+3\,b\,L\right)^{(j-2)} \\ &\quad + 2\left(\frac{13}{4}\,a^2\left(a^3+3\,b\,L\right)^{(j-2)\,\nu}\right) \\ &\quad + |b|\left(\frac{13}{4}\,a^2\left(a^3+3\,b\,L\right)^{(j-3)\,\nu}\right) \\ &= \frac{13\,a^2}{4}\left(a^3+3\,b\,L\right)^{(j-1)\,\nu} \\ &\quad \cdot\left[\frac{16\,L^{-\nu}}{13\,a^2\,\Gamma(2-\nu)}\left(a^3+3\,b\,L\right)^{(j-2-j\,\nu+\nu)}\right. \\ &\quad \left. + 2\left(a^3+3\,b\,L\right)^{-\nu} + |b|\left(a^3+3\,b\,L\right)^{-2\,\nu}\right] \\ &= \frac{13\,a^2}{4}\left(a^3+3\,b\,L\right)^{(j-1)\nu} \\ &\quad \cdot\left[\frac{16}{13\,a^2\,L^{\nu}\,\Gamma(2-\nu)\left(a^3+3\,b\,L\right)^{j\,\nu-\nu-j+2}}\right. \\ &\quad \left. + \frac{2}{\left(a^3+3\,b\,L\right)^{\nu}} + \frac{|b|}{\left(a^3+3\,b\,L\right)^{2\,\nu}}\right] \\ &\le \frac{13\,a^2}{4}\left(a^3+3\,b\,L\right)^{(j-1)\nu}.\end{aligned} \tag{44}$$

Lemma 2 is now proved. □

Theorem 3. *let $\phi_j^{a,b}(\xi)$ and $\phi_i^{a,b}(t)$ belong to the space P, and let $|(\phi_s^{a,b})^{(k)}(0)| \le \ell_s^k$, $k \ge 0$, $s = i, j$. Let $u(\xi, t)$ be expanded as*

$$u(\xi,t) = \sum_{j=0}^{\infty}\sum_{i=0}^{\infty} c_{ji}\,\phi_j^{a,b}(\xi)\phi_i^{a,b}(t). \tag{45}$$

We have the following:

(1) $|c_{ji}| \le |a|^{-j-ji}\ell_j^j\ell_i^i \cosh\left(2|a|^{-1}|b|^{1/2}\ell_j\right)\cosh\left(2|a|^{-1}|b|^{1/2}\ell_i\right)/j!i!$, which ℓ_j, ℓ_i are positive constants.

(2) The Series Comes to a Point of Absolute Convergence.

Proof. The first part of Theorem 3 can be demonstrated by following the same steps that were used in [8]). Now, we prove the remaining part of the theorem. Based on the first part, we have

$$\begin{aligned}|u(\xi,t)| &= \sum_{i=0}^{\infty}\sum_{j=0}^{\infty}\left|c_{ij}\phi_j^{a,b}(\xi)\phi_j^{a,b}(t)\right| \\ &\le \sum_{i=0}^{\infty}\sum_{j=0}^{\infty}\left|\frac{|a|^{-j-i}\ell_j^j\ell_i^i\cosh\left(2|a|^{-1}|b|^{1/2}\ell_j\right)\cosh\left(2|a|^{-1}|b|^{1/2}\ell_j\right)}{j!i!}\phi_j^{a,b}(\xi)\phi_j^{a,b}(t)\right|\end{aligned} \tag{46}$$

In virtue of Lemma 1, we get

$$\begin{aligned}&|u(\xi,t)| \\ &\le \sum_{i=0}^{\infty}\sum_{j=0}^{\infty}\left|\frac{|a|^{-j-i}\,\ell_j^j\,\ell_i^i\,\cosh\left(2\,|a|^{-1}\,|b|^{1/2}\,\ell_j\right)\,\cosh\left(2\,|a|^{-1}\,|b|^{1/2}\,\ell_i\right)}{j!i!}\right. \\ &\quad \left.\cdot\left(4\left(a^3+3\,b\,L\right)^{j+i-2}\right)\right| \\ &\le 4\,e^{\left|a^{-1}\,\ell_j\left(a^3+3\,b\,L\right)\right|+\left|a^{-1}\,\ell_i\left(a^3+3\,b\,L\right)\right|},\end{aligned} \tag{47}$$

then the series comes to a point of absolute convergence. □

Theorem 4. *Let $u(\xi, t)$ that belongs to the space P satisfy the presumptions of Theorem 3, one obtains*

$$|e_M| \le \frac{4\,A\,e^{\zeta}\,e^{\beta}\left[\zeta^{M+1}+\beta^{M+1}\right]}{(M+1)!}, \tag{48}$$

where the constants ζ and β are given as:

$$\begin{aligned}&\zeta = |a|^{-1}\,\ell_j\left(a^3+3\,b\,L\right),\ \beta = |a|^{-1}\,\ell_i\left(a^3+3\,b\,L\right), \text{and} \\ &A = \left(2\,|a|^{-1}\,|b|^{\frac{1}{2}}\,\ell_j\right)^3\left(2\,|a|^{-1}\,|b|^{\frac{1}{2}}\,\ell_i\right)^2.\end{aligned} \tag{49}$$

Proof. If we consider

$$|e_M(\xi,t)| = |u(\xi,t) - u_M(\xi,t)|, \tag{50}$$

then, we have

$$\begin{aligned}|e_M(\xi,t)| &= \left|\sum_{j=0}^{\infty}\sum_{i=0}^{\infty} c_{ji}\,\phi_j^{a,b}(\xi)\,\phi_i^{a,b}(t) - \sum_{j=0}^{M}\sum_{i=0}^{M} c_{ji}\,\phi_j^{a,b}(\xi)\,\phi_i^{a,b}(t)\right| \\ &\le \left|\sum_{j=0}^{M}\sum_{i=M+1}^{\infty} c_{ji}\,\phi_j^{a,b}(\xi)\,\phi_i^{a,b}(t)\right| \\ &\quad + \left|\sum_{j=M+1}^{\infty}\sum_{i=0}^{\infty} c_{ji}\,\phi_j^{a,b}(\xi)\,\phi_i^{a,b}(t)\right| \\ &\le \sum_{j=0}^{M}\sum_{i=M+1}^{\infty}\left|c_{ji}\right|\left|\phi_j^{a,b}(\xi)\right|\left|\phi_i^{a,b}(t)\right| \\ &\quad + \sum_{j=M+1}^{\infty}\sum_{i=0}^{\infty}\left|c_{ji}\right|\left|\phi_j^{a,b}(\xi)\right|\left|\phi_i^{a,b}(t)\right|.\end{aligned} \tag{51}$$

From Theorem 3, we get

$$\begin{aligned}
|e_M(\xi,t)| \le & \sum_{j=0}^{M}\sum_{i=M+1}^{\infty} \\
& \cdot \frac{|a|^{-j-i}\,\ell_j^j\,\ell_i^i\,\cosh\left(2\,|a|^{-1}\,|b|^{1/2}\,\ell_j\right)\,\cosh\left(2\,|a|^{-1}\,|b|^{1/2}\,\ell_i\right)}{j!i!} \\
& \cdot \left|\phi_j^{a,b}(\xi)\right|\left|\phi_i^{a,b}(t)\right| + \sum_{j=M+1}^{\infty}\sum_{i=0}^{\infty} \\
& \cdot \frac{|a|^{-j-i}\,\ell_j^j\,\ell_i^i\,\cosh\left(2\,|a|^{-1}\,|b|^{1/2}\,\ell_j\right)\,\cosh\left(2\,|a|^{-1}\,|b|^{1/2}\,\ell_i\right)}{j!i!} \\
& \cdot \left|\phi_j^{a,b}(\xi)\right|\left|\phi_i^{a,b}(t)\right| \\
\le & A\sum_{j=0}^{M}\sum_{i=M+1}^{\infty}\frac{|a|^{-j-i}\,\ell_j^j\,\ell_i^i}{j!i!}\left|\phi_j^{a,b}(\xi)\right|\left|\phi_i^{a,b}(t)\right| \\
& + A\sum_{j=M+1}^{\infty}\sum_{i=0}^{\infty}\frac{|a|^{-j-i}\,\ell_j^j\,\ell_i^i}{j!i!}\left|\phi_j^{a,b}(\xi)\right|\left|\phi_i^{a,b}(t)\right|.
\end{aligned} \tag{52}$$

Based on Lemma 1, we can write

$$\begin{aligned}
|e_M| \le & A\sum_{j=0}^{M}\sum_{i=M+1}^{\infty}\frac{4\,|a|^{-j-i}\,\ell_j^j\,\ell_i^i}{j!i!}\left(a^3+3\,b\,L\right)^{j+i-2} \\
& + A\sum_{j=M+1}^{\infty}\sum_{i=0}^{\infty}\frac{4\,|a|^{-j-i}\,\ell_j^j\,\ell_i^i}{j!i!}\left(a^3+3bL\right)^{j+i-2} \\
\le & A\sum_{j=0}^{M}\frac{2\,|a|^{-j}\,\ell_j^j}{j!}\left(a^3+3bL\right)^{j}\sum_{i=M+1}^{\infty}\frac{2\,|a|^{-i}\,\ell_i^i}{i!}\left(a^3+3bL\right)^{i} \\
& + A\sum_{j=M+1}^{\infty}\frac{2\,|a|^{-j}\,\ell_j^j}{j!}\left(a^3+3bL\right)^{j} \\
& \cdot \sum_{i=0}^{\infty}\frac{2\,|a|^{-i}\,\ell_i^i}{i!}\left(a^3+3\,b\,L\right)^{i} \\
\le & 4\,A\sum_{j=0}^{M}\frac{\left(|a|^{-1}\,\ell_j\left(a^3+3\,b\,L\right)\right)^{j}}{j!} \\
& \cdot \sum_{i=M+1}^{\infty}\frac{\left(|a|^{-1}\,\ell_i\left(a^3+3\,b\,L\right)\right)^{i}}{i!} \\
& + 4A\sum_{j=M+1}^{\infty}\frac{\left(|a|^{-1}\,\ell_j\left(a^3+3\,b\,L\right)\right)^{j}}{j!} \\
& \cdot \sum_{i=0}^{\infty}\frac{\left(|a|^{-1}\,\ell_i\left(a^3+3\,b\,L\right)\right)^{i}}{i!} \\
\le & 4A\sum_{j=0}^{M}\frac{(\zeta)^j}{j!}\sum_{i=M+1}^{\infty}\frac{(\beta)^i}{i!} + 4A\sum_{j=M+1}^{\infty}\frac{(\zeta)^j}{j!}\sum_{i=0}^{\infty}\frac{(\beta)^i}{i!} \\
\le & 4Ae^{\zeta}e^{\beta}\left[\frac{\Gamma(M+1,\zeta)}{\Gamma(M+1)}\,\frac{\gamma(M+1,\beta)}{\Gamma(M+1)} + \frac{\gamma(M+1,\zeta)}{\Gamma(M+1)}\right] \\
\le & 4\,Ae^{\zeta}e^{\beta}\left[\frac{\gamma(M+1,\zeta)}{\Gamma(M+1)} + \frac{\gamma(M+1,\beta)}{\Gamma(M+1)}\right] \\
\le & \frac{4\,A\,e^{\zeta}\,e^{\beta}}{\Gamma(M+1)}\left[\int_0^{\zeta}x^M\,e^{-x}\,dx + \int_0^{\beta}x^M\,e^{-x}\,dx\right],
\end{aligned} \tag{53}$$

and consequently, this leads to

$$|e_M| \le \frac{4\,A\,e^{\zeta}\,e^{\beta}\left[\zeta^{M+1}+\beta^{M+1}\right]}{(M+1)!}, \tag{54}$$

Because of simple inequity: $e^{-x} \le 1$; $x \ge 0$.

Note: $\gamma(.,.)$, $\Gamma(.,.)$, and $\Gamma(.)$ denote, respectively, lower incomplete gamma, upper incomplete gamma, and gamma functions (see, [42]). □

Table 1: The *MAEs* for Example 5 using the *GLTM*.

t	$M=2$	$M=6$
0.1	$3.54\ \times 10^{-16}$	$9.22\ 10^{-12}$
0.3	$3.33\ \times 10^{-16}$	$1.57\ \times 10^{-11}$
0.5	$3.89\ \times 10^{-16}$	$2.23\ \times 10^{-11}$
0.7	$5.00\ \times 10^{-16}$	$3.17\ \times 10^{-11}$
0.9	0	$4.40\ \times 10^{-11}$
1	0	$5.05\ \times 10^{-11}$

6. Numerical Outcomes and Comparisons

This section presents some examples to demonstrate the accuracy and performance of the following two proposed methods:

(i) The generalized Lucas tau method (*GLTM*) that employed for treating the one-dimensional heat equation.

(ii) The generalized Lucas collocation method (*GLCM*) that employed for treating the two-dimensional heat equation.

The error is represented by E in the maximum norm, that is, in one dimension E is computed by the formula:

$$E = \max\,|u_M(\xi,t) - u(\xi,t)|, 0 \le \xi \le L, t \ge 0, \tag{55}$$

We refer here that Mathematica software was used to perform all of the numerical data.

Example 5 (see [9, 12]). *Consider the following heat equation:*

$$u_t(\xi,t) = u_{\xi\xi}(\xi,t), \quad 0<\xi<1, \quad 0<t<1, \tag{56}$$

with the following initial boundary conditions:

$$u(0,t)=0,\ u(1,t)=e^{-t}\ \sin(1),\ u(\xi,0)=\sin\xi. \tag{57}$$

The exact solution for Eq. (56) is: $u(\xi,t)=e^{-t}\ \sin\xi$. In Table 1, the maximum absolute errors (*MAEs*) obtained

Table 2: Comparison of the *MAEs* of Example 5.

t	$M=4$ *GLTM*	Method in [9]	Method in [12]
0.1	4.71×10^{-13}	1.07×10^{-5}	2.4079×10^{-7}
0.3	4.55×10^{-13}	3.45×10^{-6}	3.0662×10^{-7}
0.5	4.45×10^{-13}	5.13×10^{-6}	2.6652×10^{-7}
0.7	4.33×10^{-13}	7.45×10^{-6}	2.2036×10^{-7}
0.9	4.16×10^{-13}	9.47×10^{-6}	1.8072×10^{-7}
1	4.08×10^{-13}	1.02×10^{-5}	1.6355×10^{-7}

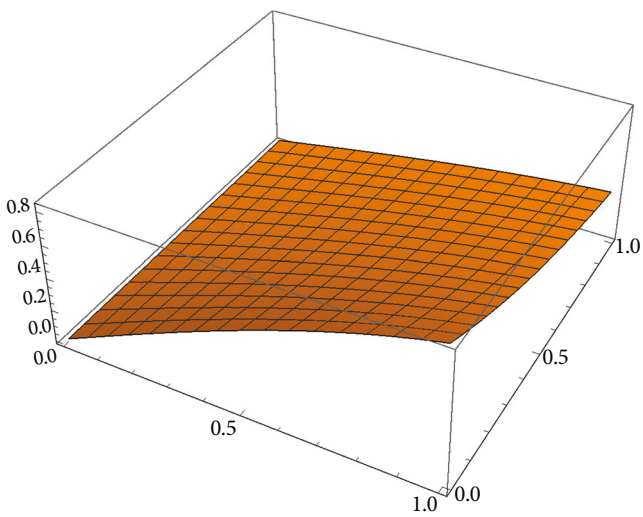

Figure 1: Exact solution for Example 5.

from the application of the *GLTM* are listed for $M=2$ and $M=6$, while in Table 2, we compare the errors resulted from the application of the *GLTM* for the case corresponding to $M=4$ and $a=b=1$ with the best errors resulted from the application of the methods developed in [9, 12]. It is noticed from the obtained results in Table 2 that *GLTM* is more accurate than the two methods that developed in [9, 12]. Figure 1 displays the exact solution. Figure 2 shows the approximate solution for the case corresponding to a = b = 1, whereas Figure 3 shows the resulting *AEs* if the *GLTM* is applied.

Example 6 (see [9]). *Consider the heat equation:*

$$u_t(\xi, t) = u_{\xi\xi}(\xi, t) + \left(2t + t^2\right) \sin \xi, \quad 0 < \xi < 1, \quad 0 < t < 1, \tag{58}$$

governed by the following conditions:

$$u(0, t) = 0, u(1, t) = t^2 \sin(1), u(\xi, 0) = 0. \tag{59}$$

The exact solution of Eq. (58) is: $u(\xi, t) = t^2 \sin \xi$. A comparison of the *MAEs* of Example (55) resulting from the *GLTM* for the choices: $M=4$, $(a=1/2, b=1)$, and (a = b = 1) and the method applied in [9] is shown in

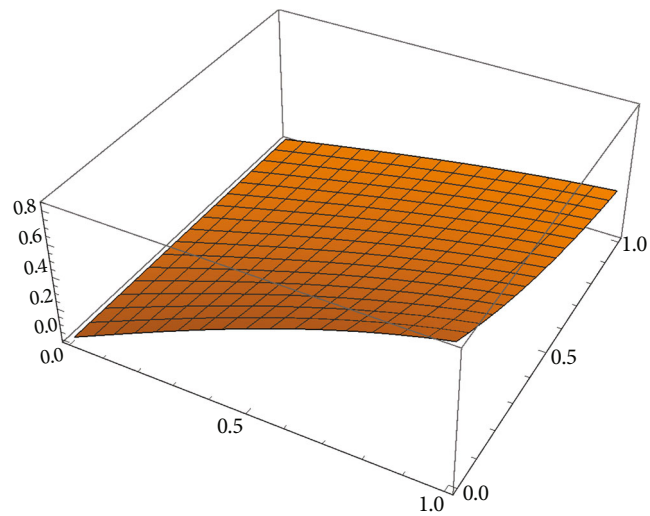

Figure 2: Approximate solution for Example 5.

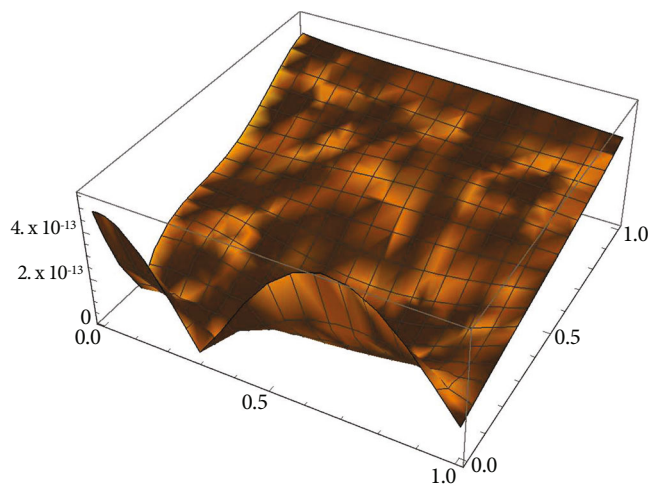

Figure 3: Absolute error for Example 5.

Table 3: Comparison of the *MAEs* of Example 6 for $M=4$.

t	*GLTM* Error $(a=1/2, b=1)$	Error $(a=b=1)$	Method in [9] Error
0.1	1.34×10^{-10}	1.19×10^{-12}	1.40×10^{-3}
0.3	1.55×10^{-10}	1.24×10^{-12}	5.78×10^{-3}
0.5	1.79×10^{-10}	1.25×10^{-12}	5.67×10^{-3}
0.7	1.04×10^{-10}	1.21×10^{-12}	1.10×10^{-3}
0.9	2.40×10^{-10}	1.12×10^{-12}	1.63×10^{-3}
1	2.60×10^{-10}	1.05×10^{-12}	2.27×10^{-3}

Table 3. From the results in Table 3, it is evident that the *GLTM* is more accurate than the method developed in [9]. Furthermore, the exact solution, approximate solution (for the case corresponding to $M=4, a=b=1$), and

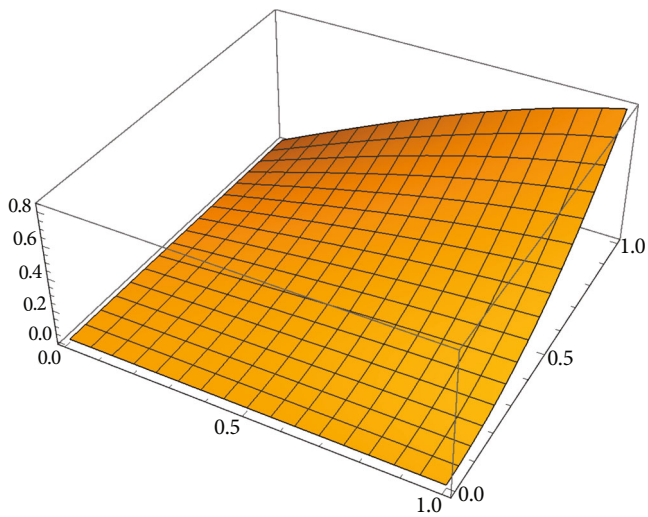

Figure 4: Exact solution for Example 6.

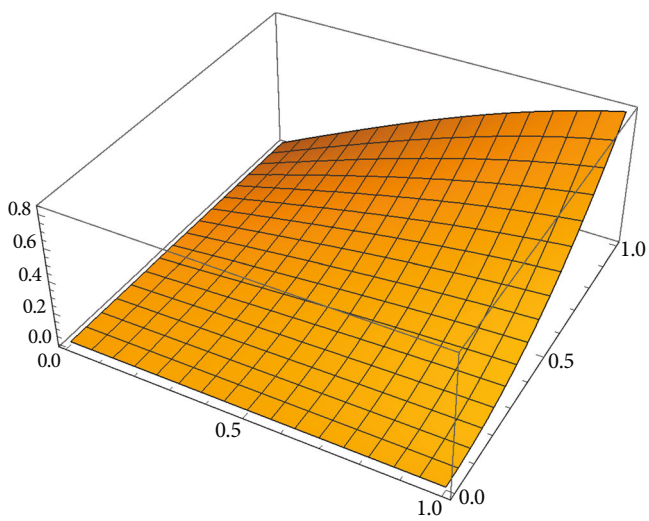

Figure 5: Approximate solution for Example 6.

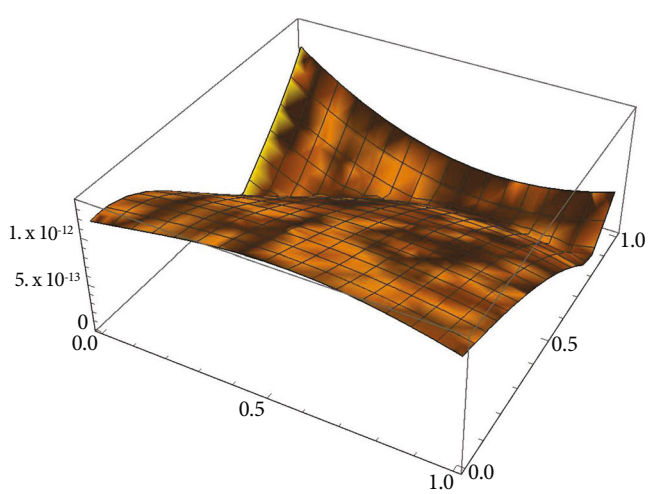

Figure 6: Absolute error for Example 6.

Table 4: Comparison of the *MAEs* of Example 7 for $M = 4$.

t	*GLTM* $(a = 1/2, b = 1)$	*GLTM* $(a = b = 1)$	*GLTM* $(a = 3, b = 1)$	Method in [9]
0.1	5.06×10^{-5}	4.29×10^{-8}	3.87×10^{-10}	6.79×10^{-3}
0.3	5.43×10^{-5}	4.47×10^{-8}	3.86×10^{-10}	3.76×10^{-4}
0.5	5.87×10^{-5}	4.37×10^{-8}	5.76×10^{-10}	2.44×10^{-4}
0.7	6.39×10^{-5}	4.21×10^{-8}	6.53×10^{-10}	3.17×10^{-4}
0.9	6.97×10^{-5}	3.70×10^{-8}	7.69×10^{-10}	3.14×10^{-3}
1	7.29×10^{-5}	3.36×10^{-8}	8.52×10^{-10}	3.32×10^{-3}

Table 5: Comparison of *MAEs* of Example 7.

M	*GLTM*	CN [10]	CBVM [10]
5	4.0×10^{-8}	1.1×10^{-1}	2.8×10^{-2}
10	1.5×10^{-4}	3.0×10^{-2}	3.8×10^{-3}

Table 6: The *MAEs* of Example 7 for $M = 2$.

t	0.1	0.3	0.5	0.7	0.9	1
	9.49×10^{-14}	0	0	0	5.68×10^{-14}	8.53×10^{-14}

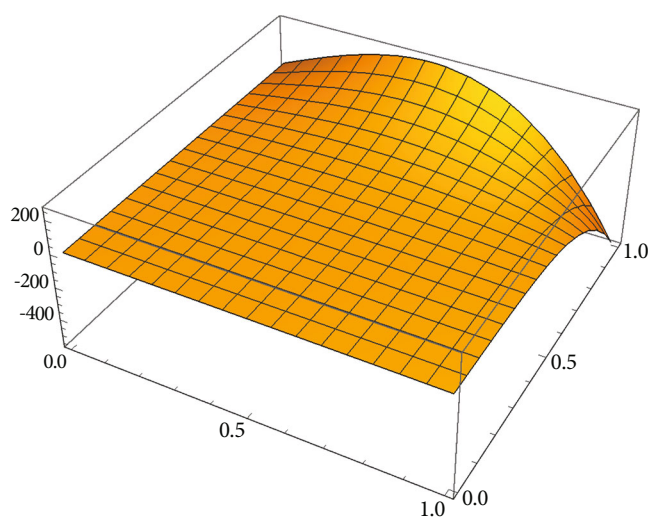

Figure 7: Exact solution for Example 7.

absolute errors of the *GLTM* are displayed, respectively, in Figures 4–6.

Example 7 (see [9, 10]. *The following homogeneous heat equation:*

$$u_t(\xi, t) = u_{\xi\xi}(\xi, t), \quad 0 < \xi < 1, \quad 0 < t < 1, \tag{60}$$

governed by the following conditions:

$$u(0, t) = u(1, t) = 0, u(\xi, 0) = \sin(\pi\xi). \tag{61}$$

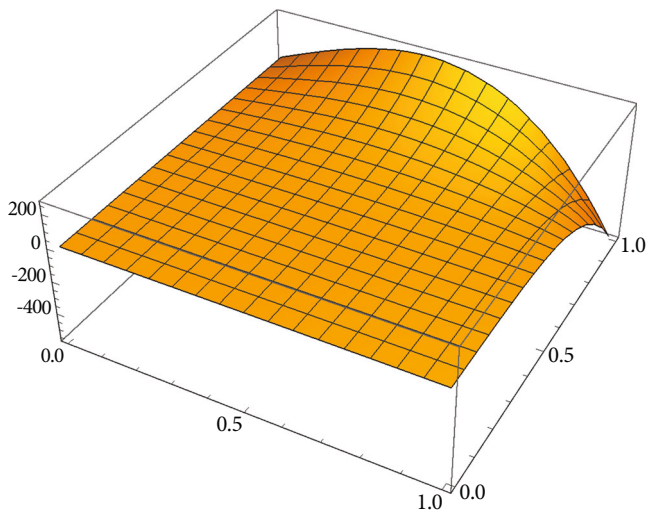

Figure 8: Approximate solution for Example 7.

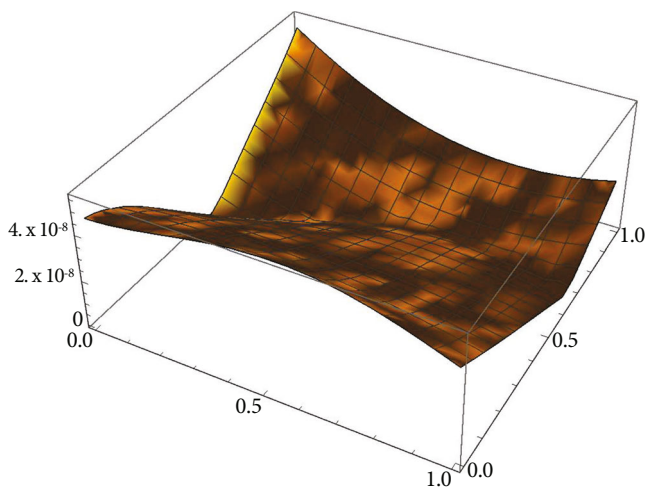

Figure 9: Absolute error for Example 7.

Table 7: Comparison of the *MAEs* of Example 8 for $M = 4$.

t	*GLTM* $(a = 1/2, b = 1)$	*GLTM* $(a = b = 1)$	*GLTM* $(a = 3, b = 1)$	Method in [9]
0.1	1.96×10^{-13}	1.73×10^{-13}	2.89×10^{-14}	8.44×10^{-3}
0.3	1.94×10^{-13}	1.73×10^{-13}	9.24×10^{-15}	8.10×10^{-3}
0.5	1.98×10^{-13}	1.74×10^{-13}	4.07×10^{-14}	7.43×10^{-3}
0.7	2.00×10^{-13}	1.74×10^{-13}	4.51×10^{-14}	9.81×10^{-3}
0.9	1.87×10^{-13}	1.74×10^{-13}	1.94×10^{-14}	1.07×10^{-3}
1	1.89×10^{-13}	1.74×10^{-13}	0	1.15×10^{-3}

The exact solution of (60) is: $u(\xi, t) = e^{-\pi^2 t} \sin(\pi \xi)$. For $M = 4$, and the three choices: $(a = 1/2, b = 1)$, (a = b = 1), and (a = 3, b = 1), we compare the solutions behavior for GLTM and method in [9] as shown in Table 4. In Table 5, the *MAE* for various values of M and a = b = 1 is listed, which illustrates that the *GLTM* is more accurate than the method

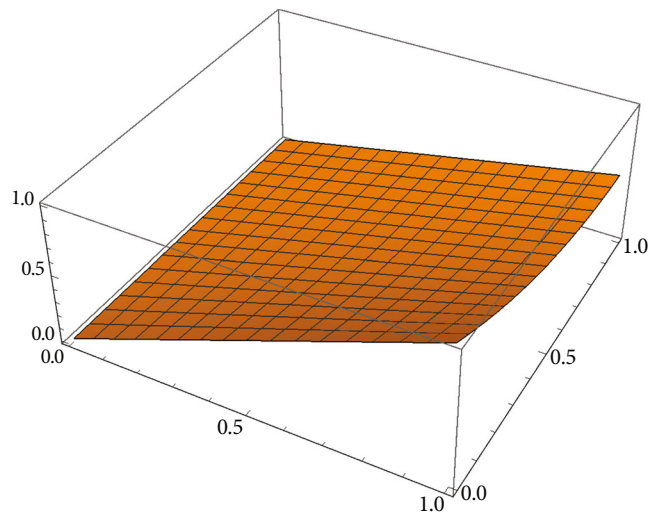

Figure 10: Exact solution for Example 8.

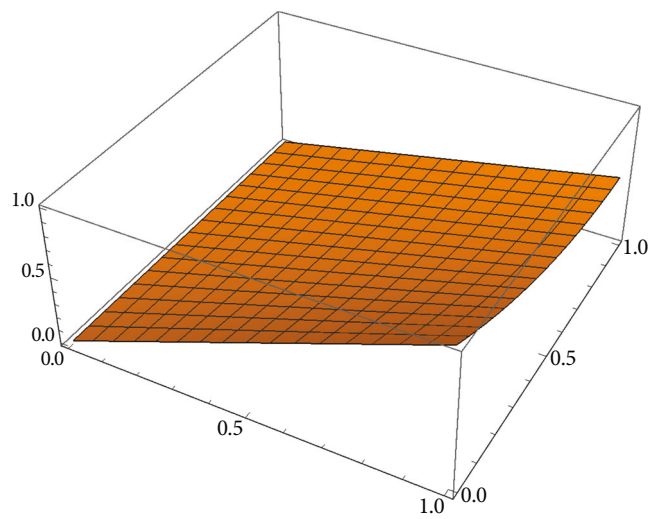

Figure 11: Approximate solution for Example 8.

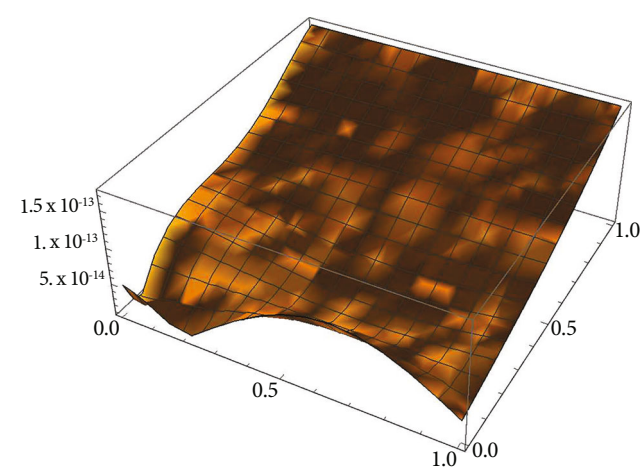

Figure 12: Absolute error for Example 8.

Table 8: The maximum pointwise error at different times of Example 9.

$\xi = \eta$	$t = 1$	$t = 2$	$t = 3$	$t = 4$
$\pi/4$	6.94097×10^{-6}	1.88675×10^{-5}	2.63317×10^{-5}	3.11073×10^{-5}
$\pi/2$	1.22752×10^{-3}	3.33673×10^{-3}	4.65679×10^{-3}	5.50135×10^{-3}
$3\pi/4$	1.49306×10^{-2}	4.05855×10^{-2}	5.66416×10^{-2}	6.69141×10^{-2}

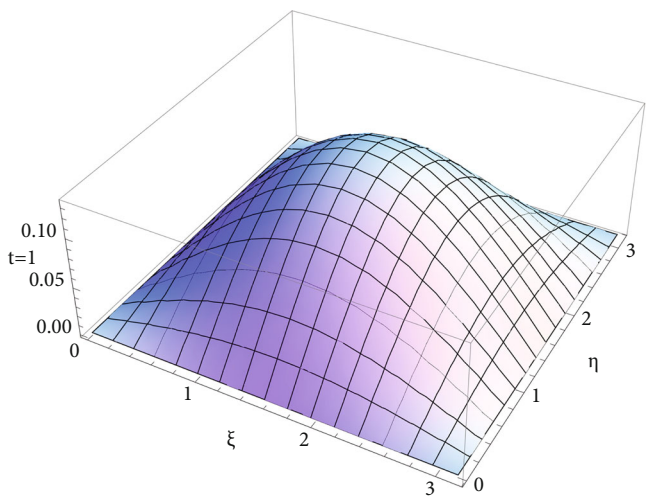

Figure 13: Approximate solution for Example 9 at t = 1.

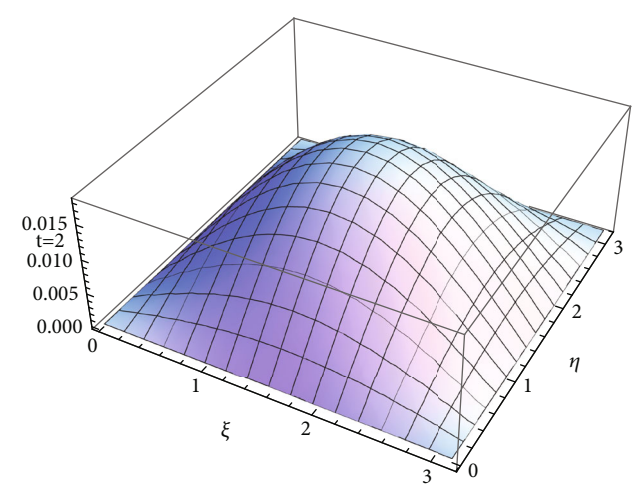

Figure 14: Approximate solution for Example 9 at t = 2.

developed in [9]. Moreover, the approximate solution closes to the exact solution for $M = 2$ and a = b = 1 as shown in Table 6. For the three cases correspond to a = b = 1, Figures 7 and 8 show the difference between the exact and the approximate solutions. Finally, Figure 9 plotted the absolute error when $M = 4$.

Example 8 (see [9]). *Consider the following homogeneous heat equation:*

$$u_t(\xi, t) = u_{\xi\xi}(\xi, t), \quad 0 < \xi < 1, \quad 0 < t < 1, \tag{62}$$

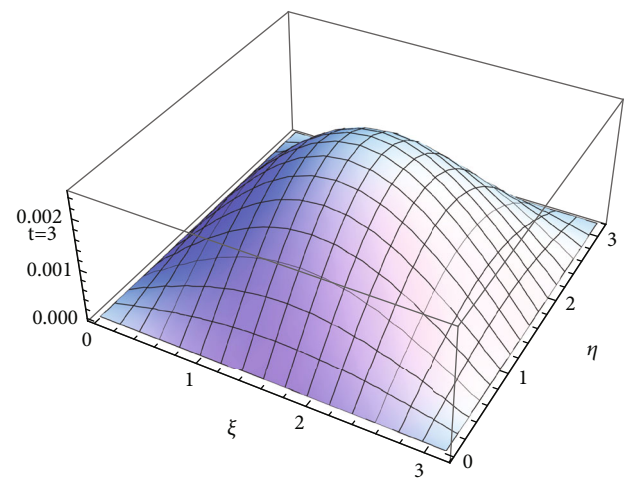

Figure 15: Approximate error for Example 9 at t = 3.

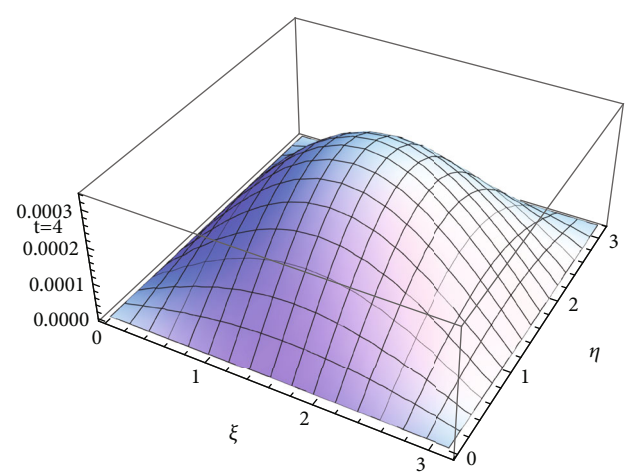

Figure 16: Approximate error for Example 9 at t = 4.

governed by the following conditions:

$$u(0, t) = 0, u(1, t) = \sinh(1)\, e^{-t}, u(\xi, 0) = \sinh \xi. \tag{63}$$

The exact solution of Eq. (62) is given by: $u(\xi, t) = e^{-t} \sinh(\xi)$. We present in Table 7 a comparison between the resulting error from the application of the *GLTM* for the case corresponding to $M = 4$, and for the three choices: $(a = 1/2, b = 1)$, (a = b = 1), and $(a = 3, b = 1)$ with those obtained by the application of the method presented in [9]. In Figures 10–12, the exact solution, approximate solution,

and absolute errors for the case corresponding to $a = b = 1$, resulted from the *GLTM* are, respectively, displayed.

Example 9 (see [39, 40]). *Consider the following two-dimensional heat equation:*

$$u_t(\xi, \eta, t) = u_{\xi\xi}(\xi, \eta, t) + u_{\eta\eta}(\xi, \eta, t), \quad 0 < \xi, \eta < \pi, \quad 0 < t < T, \tag{64}$$

with the boundary conditions:

$$u(0, \eta, t) = u(\pi, \eta, t) = 0, u(\xi, 0, t) = u(\xi, \pi, t) = 0, \tag{65}$$

and the initial condition:

$$u(\xi, \eta, 0) = \sin(\xi) \sin(\eta). \tag{66}$$

The exact solution of Eq. (64) is $u(\xi, \eta, t) = e^{-2t} \sin(\xi) \sin(\eta)$. For different times (t = 1, t = 2, t = 3, and t = 4), we show the maximum pointwise error in Table 8 and the approximate solution in Figures 13, 14, 15, and 16, respectively.

7. Conclusions

In this paper, the generalized Lucas polynomials were utilized along with certain suitable spectral methods for obtaining numerical solutions of one- and two-dimensional heat equations. Two numerical approaches are followed for solving such equations. We showed that the proposed methods are superior if compared to some other methods. We have obtained more precise errors if the retained modes of the approximate expansions are small. Some estimations concerned with the generalized Lucas polynomials were proved and they served to investigate the convergence analysis of the suggested approximate expansion in one dimension. As future work, we plan to use the generalized Lucas polynomials to solve some other types of differential equations. In addition, we plan to use the generalized Lucas polynomials to solve some other types of heat equations.

Data Availability

No data is associated with this research.

Conflicts of Interest

The authors declare that they have no conflicts of interest.

Funding

No funding for this research.

References

[1] W. M. Abd-Elhameed and Y. H. Youssri, "A novel operational matrix of Caputo fractional derivatives of Fibonacci polynomials: Spectral solutions of fractional differential equations," *Entropy*, vol. 18, no. 10, p. 345, 2016.

[2] O. Oruç, "A new numerical treatment based on Lucas polynomials for 1D and 2D sinh-Gordon equation," *Communications in Nonlinear Science and Numerical Simulation*, vol. 57, pp. 14–25, 2018.

[3] A. B. Koç, M. Çakmak, and A. Kurnaz, "A matrix method based on the Fibonacci polynomials to the generalized pantograph equations with functional arguments," *Advances in Mathematical Physics*, vol. 2014, Article ID 694580, 5 pages, 2014.

[4] S. Haq and I. Ali, "Approximate solution of two-dimensional Sobolev equation using a mixed Lucas and Fibonacci polynomials," *Engineering with Computers*, 2021.

[5] I. Ali, S. Haq, K. S. Nisar, and D. Baleanu, "An efficient numerical scheme based on Lucas polynomials for the study of multidimensional Burgers-type equations," *Advances in Difference Equations*, vol. 2021, no. 1, 2021.

[6] M. N. Sahlan and H. Afshari, "Lucas polynomials based spectral methods for solving the fractional order electrohydrodynamics flow model," *Communications in Nonlinear Science and Numerical Simulation*, vol. 107, article 106108, 2022.

[7] W. M. Abd-Elhameed and Y. H. Youssri, "Spectral tau algorithm for certain coupled system of fractional differential equations via generalized Fibonacci polynomial sequence," *Iranian Journal of Science and Technology, Transactions A: Science*, vol. 43, no. 2, pp. 543–554, 2019.

[8] W. M. Abd-Elhameed and Y. H. Youssri, "Generalized Lucas polynomial sequence approach for fractional differential equations," *Nonlinear Dynamics*, vol. 89, no. 2, pp. 1341–1355, 2017.

[9] M. R. Hooshmandasl, M. H. Heydari, and F. M. M. Ghaini, "Numerical solution of the one dimensional heat equation by using Chebyshev wavelets method," *Applied and Computational Mathematics*, vol. 1, no. 6, pp. 1–7, 2012.

[10] H. Sun and J. Zhang, "A high-order compact boundary value method for solving one-dimensional heat equations," *Numerical Methods for Partial Differential Equations*, vol. 19, no. 6, pp. 846–857, 2003.

[11] M. Tatari and M. Dehghan, "A method for solving partial differential equations via radial basis functions: application to the heat equation," *Engineering Analysis with Boundary Elements*, vol. 34, no. 3, pp. 206–212, 2010.

[12] F. E. Merga and H. M. Chemeda, "Modified Crank–Nicolson scheme with Richardson extrapolation for one-dimensional heat equation," *Iranian Journal of Science and Technology, Transactions A: Science*, vol. 45, no. 5, pp. 1725–1734, 2021.

[13] S. H. Lui and S. Nataj, "Chebyshev spectral collocation in space and time for the heat equation," *Electronic Transactions on Numerical Analysis*, vol. 52, pp. 295–319, 2020.

[14] A. M. Wazwaz, "Solitary waves theory," in *Partial Differential Equations and Solitary Waves Theory*, pp. 479–502, Springer, 2009.

[15] J. Kouatchou, "Finite differences and collocation methods for the solution of the two-dimensional heat equation," *Numerical Methods for Partial Differential Equations*, vol. 17, no. 1, pp. 54–63, 2001.

[16] A. Kazakov, L. Spevak, O. Nefedova, and A. Lempert, "On the analytical and numerical study of a two-dimensional nonlinear heat equation with a source term," *Symmetry*, vol. 12, no. 6, p. 921, 2020.

[17] S. Kazem and M. Dehghan, "Application of finite difference method of lines on the heat equation," *Numerical Methods*

for Partial Differential Equations, vol. 34, no. 2, pp. 626–660, 2018.

[18] A. H. Bokhari, G. Mohammad, M. T. Mustafa, and F. D. Zaman, "Adomian decomposition method for a nonlinear heat equation with temperature dependent thermal properties," *Mathematical Problems in Engineering*, vol. 2009, Article ID 926086, 12 pages, 2009.

[19] S. C. Buranay, N. Arshad, and A. H. Matan, "Hexagonal grid computation of the derivatives of the solution to the heat equation by using fourth-order accurate two-stage implicit methods," *Fractal and Fractional*, vol. 5, no. 4, p. 203, 2021.

[20] M. Hajipour, A. Jajarmi, A. Malek, and D. Baleanu, "Positivity-preserving sixth-order implicit finite difference weighted essentially non-oscillatory scheme for the nonlinear heat equation," *Applied Mathematics and Computation*, vol. 325, pp. 146–158, 2018.

[21] A. Hussain, M. Uddin, S. Haq, and H. U. Jan, "Numerical solution of heat equation in polar cylindrical coordinates by the meshless method of lines," *Journal of Mathematics*, vol. 2021, Article ID 8862139, 11 pages, 2021.

[22] W. Zhang, "The extended tanh method and the exp-function method to solve a kind of nonlinear heat equation," *Mathematical Problems in Engineering*, vol. 2010, 12 pages, 2010.

[23] F. Dou, "Wavelet-Galerkin method for identifying an unknown source term in a heat equation," *Mathematical Problems in Engineering*, vol. 2012, Article ID 904183, 22 pages, 2012.

[24] M. Uddin and H. Ali, "The space–time kernel-based numerical method for Burgers' equations," *Mathematics*, vol. 6, no. 10, p. 212, 2018.

[25] M. Uddin, K. Kamran, M. Usman, and A. Ali, "On the Laplace-transformed-based local meshless method for fractional-order diffusion equation," *International Journal for Computational Methods in Engineering Science and Mechanics*, vol. 19, no. 3, pp. 221–225, 2018.

[26] M. Uddin and M. Taufiq, "Approximation of time fractional black-Scholes equation via radial kernels and transformations," *Fractional Differential Calculus*, vol. 9, no. 1, pp. 75–90, 2011.

[27] M. A. Zaky and A. S. Hendy, "An efficient dissipation-preserving Legendre-Galerkin spectral method for the Higgs boson equation in the de Sitter spacetime universe," *Applied Numerical Mathematics*, vol. 160, pp. 281–295, 2021.

[28] D. Fortunato and A. Townsend, "Fast Poisson solvers for spectral methods," *IMA Journal of Numerical Analysis*, vol. 40, no. 3, pp. 1994–2018, 2020.

[29] J. C. Butcher, *Numerical Methods for Ordinary Differential Equations*, John Wiley & Sons, 2016.

[30] J. Zhou, Z. Jiang, H. Xie, and H. Niu, "The error estimates of spectral methods for 1-dimension singularly perturbed problem," *Applied Mathematics Letters*, vol. 100, p. 106001, 2020.

[31] A. Faghih and P. Mokhtary, "An efficient formulation of Chebyshev tau method for constant coefficients systems of multi-order FDEs," *Journal of Scientific Computing*, vol. 82, no. 1, pp. 1–25, 2020.

[32] T. Tang, L.-L. Wang, H. Yuan, and T. Zhou, "Rational spectral methods for PDEs involving fractional Laplacian in unbounded domains," *SIAM Journal on Scientific Computing*, vol. 42, no. 2, pp. A585–A611, 2020.

[33] M. Fei and C. Huang, "Galerkin–Legendre spectral method for the distributed-order time fractional fourth-order partial differential equation," *International Journal of Computer Mathematics*, vol. 97, no. 6, pp. 1183–1196, 2020.

[34] C. Yang and J. Hou, "Jacobi spectral approximation for boundary value problems of nonlinear fractional pantograph differential equations," *Numerical Algorithms*, vol. 86, no. 3, pp. 1089–1108, 2021.

[35] E. H. Doha, W. M. Abd-Elhameed, and A. H. Bhrawy, "New spectral-Galerkin algorithms for direct solution of high even-order differential equations using symmetric generalized Jacobi polynomials," *Collectanea Mathematica*, vol. 64, no. 3, pp. 373–394, 2013.

[36] Y. H. Youssri and W. M. Abd-Elhameed, "Numerical spectral Legendre-Galerkin algorithm for solving time fractional telegraph equation," *Romanian Journal of Physics*, vol. 63, no. 107, 2018.

[37] A. Napoli and W. M. Abd-Elhameed, "An innovative harmonic numbers operational matrix method for solving initial value problems," *Calcolo*, vol. 54, no. 1, pp. 57–76, 2017.

[38] V. Mazya, *Sobolev Spaces*, Springer, 2013.

[39] P. W. Berg and J. L. McGregor, *Elementary Partial Differential Equations*, Holden-Day, 1966.

[40] S. J. Farlow, *Partial Differential Equations for Scientists and Engineers*, Courier Corporation, 1993.

[41] H. Ashry, W. M. Abd-Elhameed, G. M. Moatimid, and Y. H. Youssri, "Spectral treatment of one and two dimensional second-order BVPs via certain modified shifted Chebyshev polynomials," *International Journal of Applied and Computational Mathematics*, vol. 7, no. 6, pp. 1–21, 2021.

[42] E. D. Rainville, *Special Functions*, The Macmillan Company, New York, NY, USA, 1960.

Hindawi
Journal of Function Spaces
Volume 2022, Article ID 3966135, 13 pages
https://doi.org/10.1155/2022/3966135

Research Article

New Fractional Derivative Expression of the Shifted Third-Kind Chebyshev Polynomials: Application to a Type of Nonlinear Fractional Pantograph Differential Equations

Y. H. Youssri,[1] **W. M. Abd-Elhameed**,[1] **and H. M. Ahmed**[2]

[1]*Department of Mathematics, Faculty of Science, Cairo University, Giza 12613, Egypt*
[2]*Department of Mathematics, Faculty of Technology and Education, Helwan University, Helwan, Egypt*

Correspondence should be addressed to Y. H. Youssri; youssri@aucegypt.edu

Received 30 October 2021; Accepted 18 March 2022; Published 11 April 2022

Academic Editor: Salah Mahmoud Boulaaras

The main goal of this paper is to develop a new formula of the fractional derivatives of the shifted Chebyshev polynomials of the third kind. This new formula expresses approximately the fractional derivatives of these polynomials in the Caputo sense in terms of their original ones. The linking coefficients are given in terms of a certain ${}_4F_3(1)$ terminating hypergeometric function. The integer derivatives of the shifted third-kind Chebyshev polynomials can be calculated using this formula after performing some reductions. To solve a nonlinear fractional pantograph differential equation with quadratic nonlinearity, the fractional derivative formula is used in conjunction with the tau technique. The role of the tau method is to convert the pantograph differential equation with its governing initial/boundary conditions into a nonlinear system of algebraic equations that can be treated with the aid of Newton's iterative scheme. To test the method's convergence, certain estimations are included. The proposed numerical method is demonstrated by numerical results to ensure its applicability and efficiency.

1. Introduction

In the last three decades, many searches highlighted descriptions of a variety of phenomena by using fractional differential equations (FDEs) (see, for example, [1–3]). Accordingly, a lot of research was directed to solving these equations. Unfortunately, the exact solutions of many models of FDEs are not always available. So, finding numerical solutions to these equations was the only way to obtain results that are enabling us to study these phenomena in a practical way. In this regard, several numerical approaches for dealing with FDEs have been presented. Among these methods, but not limited to, we find wavelets methods [4, 5], operational matrix methods [6–8], Adomian's decomposition method [9], tau method [10–12], pseudospectral method [13], finite difference method [14], and other methods [15–18].

Throughout the history of numerical analysis research, it has been clarified that orthogonal polynomials are credited with developing these numerical methods. One of the most important orthogonal polynomials that contributed to developing these methods is the Jacobi polynomial. The most famous special cases of Jacobi polynomials are Chebyshev polynomials of first, second, third, and fourth kinds.

Due to the importance of all kinds of Chebyshev polynomials in different branches of mathematics, a great number of authors investigated them from both theoretical and practical points of view. From a theoretical point of view, and for example, regarding the Chebyshev functional, it has an old history in the study (see, for example, [19]) and an extensive repertoire of applications in many fields (see [20]). Furthermore, in the sequence of papers [21–23], the authors have developed some type inequalities related to the Chebyshev functional. From a numerical point of view, the authors in [24] presented a Galerkin operational matrix method for the numerical treatment of linear and nonlinear hyperbolic telegraph type equations based on utilizing certain combinations of Chebyshev polynomials of the first kind. In [25], the fractional derivative formula of the first kind of Chebyshev polynomials was established. In addition, a type of fractional delay differential equations was treated using the spectral tau

method. Chebyshev polynomials of the second kind were used in [26] to find spectral solutions for the fractional Riccati differential equations. Regrading the third- and fourth-kinds of Chebyshev polynomials, they were utilized in many applications. The authors in [27] introduced the operational matrices of derivatives of third- and fourth-kinds Chebyshev polynomials and employed them to numerically solve the Lane-Emden type equations. The authors in [28, 29] have employed such polynomials to treat other types of differential and integral equations. Recently, other two types of Chebyshev polynomials, namely, Chebyshev polynomials of the fifth- and sixth-kinds, were employed in a variety of applications. The author in [12] has established explicit formulas for the derivatives of the sixth-kind Chebyshev polynomials and utilized them to find spectral solution of the nonlinear one-dimensional Burgers' equation.

Spectral methods are among the most widely used numerical techniques that have been developed and adapted to solve various forms of DEs. The use of many properties of orthogonal polynomials has contributed to developing these methods, which enabled researchers to obtain explicit expressions for a general-order derivative of an infinitely differentiable function in terms of those of the function. These expressions enabled them to develop many algorithms to solve these equations (see, for example, [24]). Also, the orthogonality property and the properties of the roots of these polynomials had a clear effect in obtaining high-precision numerical solutions using the different versions of these methods, like the tau method [30, 31], collocation method [32, 33], and Galerkin method [24]. The tau approach offers the benefit of avoiding some problems that the Galerkin method faces. This is because of the freedom with which basis functions can be chosen and the underlying conditions are set as constraints (see [25]).

Delay differential equations (DDEs) and fractional delay differential equations (FDDEs) have vital roles as they arise in several disciplines such as biology, economic, and automatic control (see, [34]). The pantograph differential equations and the fractional pantograph differential equations are important types of DDEs and many authors have interests in them. For example, Sedaghat et al. [35] suggested an approximation to a pantograph equation with the aid of Chebyshev polynomials. The authors in [36] have applied a Taylor method for obtaining an approximate solution of the generalized pantograph equations. The direct operational tau method was employed to solve the pantograph-type equation in [37]. Fractional pantograph differential equations were handled using the generalized fractional-order Bernoulli wavelets in [38]. A wavelet matrix approach was followed in [39] based on using Müntz-Legendre polynomials to treat the fractional pantograph differential equations. For some other contributions regarding the different types of pantograph equations, on can be referred to [40–44].

In this study, an explicit expression for the fractional derivatives of the third-kind Chebyshev polynomials is established. As far as we know, this expression is new, and it generalizes the formula of the integer derivatives of Chebyshev polynomials of the third kind that is previously established. We demonstrate that this formula involves a certain ${}_4F_3(1)$ terminating hypergeometric term. Using the new formula, the tau method is applied to solve the fractional pantograph differential equations.

The following is a breakdown of the current paper's structure. Section 2 is devoted to displaying some definitions of the fractional calculus theory. Moreover, in this section, we present some useful formulas concerned with the third-kind Chebyshev polynomials and their shifted ones. The definitions of the generalized hypergeometric functions and the regularized hypergeometric functions are also presented in this section. Section 3 is interested in deriving in detail a new formula that expresses approximately the fractional derivatives of the shifted third-kind Chebyshev polynomials. Also, in this section, the well-known integer derivative formula of the shifted third-kind Chebyshev polynomials is a specific result of the fractional ones. In Section 4, we describe the proposed numerical algorithm for solving a type of fractional pantograph differential equation with quadratic nonlinearity using the spectral tau method. Some error estimates are given in Section 5 to examine the proposed polynomial series expansion's convergence and error analysis. Some numerical simulations are presented in Section 6 to validate the theoretical results. Finally, Section 7 summarises the findings.

2. Some Essentials and Useful formulas

Some definitions of the fractional calculus theory are presented in this section. In addition, various properties and important formulas for third-kind Chebyshev polynomials and their shifted counterparts are presented. Also, the definitions of the generalized hypergeometric functions and some their basic properties are given.

2.1. Some Definitions of the Fractional Operators

Definition 1. Let I^{μ}denote the Riemann-Liouville fractional integral operator of order μ on the usual Lebesgue space L_1 $[0, 1]$. Then, I^{μ} is defined as

$$I^{\mu} g(t) = \begin{cases} \dfrac{1}{\Gamma(\mu)} \displaystyle\int_0^t (t-\tau)^{\mu-1} g(\tau)\, d\tau, & \mu > 0, \\ g(t), & \mu = 0. \end{cases} \tag{1}$$

The properties below are valid.

(i) $I^{\mu} I^{\beta} = I^{\mu+\beta}$

(ii) $I^{\mu} I^{\beta} = I^{\beta} I^{\mu}$

(iii) $I^{\mu} t^{\gamma} = (\Gamma(\gamma+1)/\Gamma(\gamma+\mu+1)) t^{\gamma+\mu}$

where $\mu, \beta \geq 0$, and $\gamma > -1$.

Definition 2. The Caputo fractional-order derivatives of a function u defined on the interval $I = [0, 1]$ are defined as:

$$\left({}_0^C D_x^\gamma u\right)(x) = \frac{1}{\Gamma(\ell-\gamma)}\int_0^x (x-\tau)^{\ell-\gamma-1} u^{(\ell)}(\tau)d\tau, \gamma > 0, t > 0, \tag{2}$$

where $\ell - 1 \le \gamma < \ell, \ell \in \mathbb{N}$.

The following property is useful

$${}_0^C D_x^\alpha t^\beta = \begin{cases} 0, & \text{for } \beta \in \mathbb{N}_0 \text{ and } \beta < \lceil \alpha \rceil, \\ \dfrac{\Gamma(\beta+1)}{\Gamma(\beta+1-\alpha)} t^{\beta-\alpha}, & \text{for } \beta \in \mathbb{N}_0 \text{ and } \beta \ge \lceil \alpha \rceil, \end{cases} \tag{3}$$

where $\lceil \alpha \rceil$ denotes the lowest integer more than or equal to α and $\mathbb{N}_0 = \{0, 1, 2, \cdots\}$.

2.2. An Account on Third-Kind Chebyshev Polynomials and Their Shifted Ones. The Chebyshev polynomials of the third-kind $V_n(x)$ are polynomials in x that have the following trigonometric definition (see [45])

$$V_n(x) = \frac{\cos(n+1/2)\theta}{\cos(\theta/2)}, \tag{4}$$

with $x = \cos\theta$.

The polynomials $V_n(x)$ are special ones of the Jacobi polynomials. More definitely, we have

$$V_n(x) = \frac{2^{2n}}{\binom{2n}{n}} P_n^{(-1/2,1/2)}(x). \tag{5}$$

With respect to the weight function $w(x) = \sqrt{(1+x)/(1-x)}$, these polynomials are orthogonal on $(-1, 1)$, in the sense that

$$\int_{-1}^1 \sqrt{\frac{1+x}{1-x}} V_m(x) V_n(x) dx = \begin{cases} 0, & m \ne n, \\ \pi, & m = n, \end{cases} \tag{6}$$

and they may be constructed by means of the following recursive formula:

$$V_n(x) = 2x\, V_{n-1}(x) - V_{n-2}(x), V_0(x) = 1, V_1(x) = 2x - 1, n = 2, 3, \cdots. \tag{7}$$

The shifted Chebyshev polynomials of the third kind on $[0, 1]$ are defined as

$$V_n^*(x) = V_n(2x-1). \tag{8}$$

All properties of third-kind Chebyshev polynomials may be readily converted to yield the properties of the analog of their shifted polynomials.

The orthogonality relation of $V_k^*(x)$ on $[0, 1]$ with respect to the weight function $\sqrt{x/(1-x)}$ is given by

$$\int_0^1 \sqrt{\frac{x}{1-x}} V_k^*(x) V_j^*(x) dx = \begin{cases} \dfrac{\pi}{2}, & k = j, \\ 0, & k \ne j. \end{cases} \tag{9}$$

The power form representation of the third-kind Chebyshev polynomials and its inversion formula can be represented respectively as (see [46])

$$V_k^*(x) = \sum_{i=0}^k \frac{2^{2i}(-1)^{k+i}(k+i)!}{(2i+1)!(k-i)!} x^i, \tag{10}$$

and

$$x^r = \frac{(2r+1)!}{2^{2r}} \sum_{\ell=0}^r \frac{1}{(r-\ell)!(\ell+r+1)!} V_\ell^*(x). \tag{11}$$

2.3. An Account on Generalized Hypergeometric Function. We display in this section the definition of the generalized hypergeometric functions and the regularized hypergeometric function which will be essential in the upcoming section.

We recall here the definition of the generalized hypergeometric function given by (see, for example, [46])

$${}_pF_q\left(\begin{matrix} A_1, A_2, \cdots, A_p \\ B_1, B_2, \cdots, B_q \end{matrix} \mid x\right) = \sum_{k=0}^\infty \frac{(A_1)_k (A_2)_k \cdots (A_p)_k}{(B_1)_k (B_2)_k \cdots (B_q)_k} \frac{x^k}{k!}, \tag{12}$$

and the regularized hypergeometric function are defined as

$${}_p\tilde{F}_q\left(\begin{matrix} A_1, A_2, \cdots, A_p \\ B_1, B_2, \cdots, B_q \end{matrix} \mid x\right) = \sum_{k=0}^\infty \frac{(A_1)_k (A_2)_k \cdots (A_p)_k}{\Gamma(B_1+k)\Gamma(B_2+k)\cdots\Gamma(B_q+k)} \frac{x^k}{k!}, \tag{13}$$

where p and q are nonnegative integers. In addition, the constants B_j, $1 \le j \le q$ are all neither zeros nor negative integers.

Note 1. In (12), if one of A_i is a negative integer $(-n)$, the generalized hypergeometric function reduces to a polynomial of degree n.

3. Derivation of the Fractional Derivatives of Chebyshev Polynomials of Third-Kind

This section is confined to deriving in detail the formula that expresses the fractional derivatives of the third-kind Chebyshev polynomials. In addition, the well-known integer derivative formula will be deduced as a special case. For our derivation, the following two lemmas are needed.

Lemma 3. *For every nonnegative integers k, ℓ, r, the following reduction formula is valid*

$$
{}_3F_2\left(\begin{matrix}-\ell, 2k-\ell+1, k-\ell-r+\frac{3}{2}\\ k-\ell+\frac{3}{2}, 2k-2\ell-2r+2\end{matrix}\,\middle|\,1\right) = \frac{2}{\sqrt{\pi}\,(2k+1)} \times \begin{cases} \dfrac{\Gamma((\ell+1)/2)(r)_{\ell/2}}{(k-\ell+3/2)_{\ell/2-1}(k-\ell-r+1)_{\ell/2}}, & \ell \text{ even},\\[2ex] \dfrac{-\Gamma(\ell/2+1)(r)_{(\ell+1)/2}}{(k-\ell+3/2)_{(\ell-1)/2}(k-\ell-r+1)_{(\ell+1)/2}}, & \ell \text{ odd}.\end{cases} \tag{14}
$$

Proof. First, set

$$
Y_{\ell,k,r} = {}_3F_2\left(\begin{matrix}-\ell, 2k-\ell+1, k-\ell-r+\frac{3}{2}\\ k-\ell+\frac{3}{2}, 2k-2\ell-2r+2\end{matrix}\,\middle|\,1\right). \tag{15}
$$

The following recurrence relation of order two can be generated using Zeilberger's approach (see [47]).

$$
\begin{aligned}
&(\ell+1)(2k-\ell)(\ell+2r)(-k+\ell+r+1)(-2k+\ell+2r-1)Y_{\ell,k,r}\\
&\quad -2(2k-2\ell+1)(k-\ell-r)\left(2k(\ell+r+1)-2\ell r-\ell(\ell+1)-2r^2\right)Y_{\ell+1,k,r}\\
&\quad -4(2k-2\ell-1)(2k-2\ell+1)(k-\ell-r-1)(k-\ell-r)^2Y_{\ell+2,k,r}=0,
\end{aligned} \tag{16}
$$

with the initial values

$$
Y_{0,k,r}=1, \quad Y_{1,k,r}=\frac{-r}{(2k+1)(k-r)}. \tag{17}
$$

The recurrence relation (16) can be exactly solved to give

$$
Y_{\ell,k,r} = \frac{2}{\sqrt{\pi}(2k+1)} \begin{cases} \dfrac{\Gamma((\ell+1)/2)(r)_{\ell/2}}{(k-\ell+3/2)_{\ell/2-1}(k-\ell-r+1)_{\ell/2}}, & \ell \text{ even},\\[2ex] \dfrac{-\Gamma(\ell/2+1)(r)_{(\ell+1)/2}}{(k-\ell+3/2)_{(\ell-1)/2}(k-\ell-r+1)_{(\ell+1)/2}}, & \ell \text{ odd}.\end{cases} \tag{18}
$$

This completes the proof of Lemma 3. □

Lemma 4. *Let k, r be any two nonnegative integers with $k \geq r$. The following transformation formula is valid:*

$$
{}_4\tilde{F}_3\left(\begin{matrix}-(k-r), 1, k+r+1, \frac{3}{2}\\ r+\frac{3}{2}, 1-p, p+2\end{matrix}\,\middle|\,1\right) = \frac{(3/2)_p(r-k)_p(k+r+1)_p}{(2p+1)!\Gamma(p+r+3/2)} \times {}_3F_2\left(\begin{matrix}-(k-p-r), p+\frac{3}{2}, k+p+r+1\\ 2p+2, p+r+\frac{3}{2}\end{matrix}\,\middle|\,1\right). \tag{19}
$$

Proof. In the left-hand side of (19), the terminating hypergeometric series can be expressed as

$$
{}_4\tilde{F}_3\left(\begin{matrix}r-k, 1, k+r+1, \frac{3}{2}\\ r+\frac{3}{2}, 1-p, p+2\end{matrix}\,\middle|\,1\right) = \sum_{s=p}^{k-r} \frac{(3/2)_s(r-k)_s(k+r+1)_s}{(s-p)!(s+p+1)!\Gamma(s+r+3/2)}, \tag{20}
$$

which can also be written as

$$
{}_4\tilde{F}_3\left(\begin{matrix}r-k, 1, k+r+1, \frac{3}{2}\\ r+\frac{3}{2}, 1-p, p+2\end{matrix}\,\middle|\,1\right) = \sum_{\ell=0}^{k-p-r} \frac{(3/2)_{p+\ell}(r-k)_{p+\ell}(k+r+1)_{p+\ell}}{\ell!(2p+\ell+1)!\Gamma(p+r+\ell+3/2)}. \tag{21}
$$

In virtue of the identity:

$$
(A)_{p+\ell} = (A)_p(A+p)_\ell, \tag{22}
$$

relation (21) can be written alternatively as

$$
\begin{aligned}
&{}_4\tilde{F}_3\left(\begin{matrix}r-k, 1, k+r+1, \frac{3}{2}\\ r+\frac{3}{2}, 1-p, p+2\end{matrix}\,\middle|\,1\right)\\
&\quad = \frac{(3/2)_p(r-k)_p(k+r+1)_p}{(2p+1)!\Gamma(p+r+3/2)} \sum_{\ell=0}^{k-p-r} \frac{(p+3/2)_\ell(-k+p+r)_\ell(k+p+r+1)_\ell}{(2p+2)_\ell(p+r+3/2)_\ell\,\ell!},
\end{aligned} \tag{23}
$$

which implies the validity of transformation (19).

The key theorem in this section is now stated and proved. □

Theorem 5. *The following formula can be used to approximate the fractional derivatives of the polynomials $V_k^*(x)$ as:*

$$D^{\gamma}V_k^*(x) \simeq \frac{(-1)^{k+n}(2k+1)(k+n)!\Gamma(n-\gamma+3/2)}{\Gamma(n+3/2)(k-n)!} \times \sum_{p=0}^{N} \frac{1}{\Gamma(n-p-\gamma+1)\Gamma(n+p-\gamma+2)} \times {}_4F_3\left(\begin{matrix} 1, n-k, k+n+1, n-\gamma+\frac{3}{2} \\ n+\frac{3}{2}, n-\gamma-p+1, n-\gamma+p+2 \end{matrix} \middle| 1\right) V_p^*(x), \tag{24}$$

where $n = \lceil \gamma \rceil$ is the well-known ceiling notation and N is a sufficiently large positive integer.

Proof. The power form representation of $V_k^*(x)$ in (10), along with relation (2.1) yields

$$D^{\gamma}V_k^*(x) = \sqrt{\pi}\left(k+\frac{1}{2}\right)\sum_{s=n}^{k}\frac{(-1)^{k+s}(k+s)!}{\Gamma(s+3/2)(k-s)!\Gamma(s-\gamma+1)}x^{s-\gamma}. \tag{25}$$

The inversion formula of $V_p^*(x)$ in (11) can be used to approximate $D^{\gamma}V_k^*(x)$ as

$$x^{s-\gamma} \simeq \frac{\Gamma(2s-2\gamma+2)}{2^{2s-2\gamma}}\sum_{\ell=0}^{N}\frac{1}{\Gamma(s-\gamma-\ell+1)\Gamma(s-\gamma+\ell+2)}V_{\ell}^*(x), \tag{26}$$

where N is a sufficiently large positive integer.

The following approximation for $D^{\gamma}V_k^*(x)$ is obtained by inserting (26) into (25)

$$D^{\gamma}V_k^*(x) \simeq (2k+1)\sum_{s=n}^{k}\frac{(-1)^{k+s}(k+s)!\Gamma(s-\gamma+3/2)}{\Gamma(s+3/2)(k-s)!} \times \sum_{\ell=0}^{N}\frac{1}{\Gamma(s-\gamma-\ell+1)\Gamma(s-\gamma+\ell+2)}V_{\ell}^*(x). \tag{27}$$

If the right-hand side of relation (27) is expanded and rearranged, then we get

$$D^{\gamma}V_k^*(x) \simeq (2k+1)\sum_{p=0}^{N}\sum_{\ell=0}^{k-n}\frac{(-1)^{k+n+\ell}(k+n+\ell)!}{\Gamma(\ell+n+3/2)(k-n-\ell)!} \times \frac{\Gamma(\ell+n-\gamma+3/2)}{\Gamma(\ell+n-p-\gamma+1)\Gamma(\ell+n+p-\gamma+2)}V_p^*(x). \tag{28}$$

In hypergeometric form, the last relation can be written as follows:

$$D^{\gamma}V_k^*(x) \simeq \frac{(-1)^{k+n}(2k+1)(k+n)!\Gamma(n-\gamma+3/2)}{\Gamma(n+3/2)(k-n)!} \times \sum_{p=0}^{N}\frac{1}{\Gamma(n-p-\gamma+1)\Gamma(n+p-\gamma+2)} \times {}_4F_3\left(\begin{matrix} 1, n-k, k+n+1, n-\gamma+\frac{3}{2} \\ n+\frac{3}{2}, n-\gamma-p+1, n-\gamma+p+2 \end{matrix} \middle| 1\right) V_p^*(x). \tag{29}$$

This ends the proof of Theorem 5. □

Remark 6. The integer derivatives formula of the polynomials $V_k^*(x)$ may be extracted from Theorem 5 as a special case. The following corollary exhibits this formula.

Corollary 7. *Let r be a positive integer. Then, for all $k \geq r$, one has:*

$$D^{r}V_k^*(x) = \frac{2^{2r}}{(r-1)!}\sum_{\ell=0}^{\lfloor (k-r)/2 \rfloor}\frac{(k-\ell)!(\ell+r-1)!}{\ell!(k-\ell-r)!}V_{k-2\ell-r}^*(x) + \frac{2^{2r}}{(r-1)!}\sum_{\ell=0}^{\lfloor (k-r-1)/2 \rfloor}\frac{(k-\ell-1)!(\ell+r)!}{\ell!(k-\ell-r)!}V_{k-2\ell-r-1}^*(x). \tag{30}$$

Proof. Setting $\gamma = r$, r is a positive integer. In this case $\gamma = n = r$, and therefore, formula (24) can be converted into

$$D^{r}V_k^*(x) = \frac{(-1)^{k+r}\sqrt{\pi}(k+1/2)(k+r)!}{(k-r)!} \times \sum_{p=0}^{k-r} {}_4\tilde{F}_3\left(\begin{matrix} r-k, 1, k+r+1, \frac{3}{2} \\ r+\frac{3}{2}, 1-p, p+2 \end{matrix} \middle| 1\right) V_p^*(x). \tag{31}$$

With the aid of Lemma 4, the last formula reduces to the following one:

$$D^{r}V_k^*(x) = \frac{(-1)^{k+r}\sqrt{\pi}(k+1/2)(k+r)!}{(k-r)!} \times \sum_{p=0}^{k-r}\frac{(3/2)_p(r-k)_p(k+r+1)_p}{(2p+1)!\Gamma(p+r+3/2)} {}_3F_2 \cdot \left(\begin{matrix} -(k-p-r), p+\frac{3}{2}, k+p+r+1 \\ 2p+2, p+r+\frac{3}{2} \end{matrix} \middle| 1\right) V_p^*(x). \tag{32}$$

It is clear that the last relation can be written in the following alternative relation:

$$D^r V_k^*(x) = \frac{(-1)^{k+r}\sqrt{\pi}\,(k+1/2)\,(k+r)!}{(k-r)!} \cdot \sum_{\ell=0}^{k-r} \frac{(3/2)_{k-\ell-r}\,(r-k)_{k-\ell-r}\,(k+r+1)_{k-\ell-r}}{\Gamma(k-\ell+3/2)\,(2k-2\ell-2r+1)!} \times {}_3F_2\left(\begin{matrix}-\ell, 2k-\ell+1, k-\ell-r+\frac{3}{2}\\ k-\ell+\frac{3}{2}, 2k-2\ell-2r+2\end{matrix}\Big|1\right) V_{k-r-\ell}^*(x). \tag{33}$$

In virtue of Lemma 3, the ${}_3F_2(1)$ that appears in (32) can be summed in a closed form, and then, after performing some manipulation, the following formula can be obtained

$$D^r V_k^*(x) = \frac{2^{2r}}{(r-1)!} \sum_{\ell=0}^{\lfloor (k-r)/2 \rfloor} \frac{(k-\ell)!(\ell+r-1)!}{\ell!(k-\ell-r)!} V_{k-2\ell-r}^*(x) + \frac{2^{2r}}{(r-1)!} \sum_{\ell=0}^{\lfloor (k-r-1)/2 \rfloor} \frac{(k-\ell-1)!(\ell+r)!}{\ell!(k-\ell-r)!} V_{k-2\ell-r-1}^*(x). \tag{34}$$

This proves formula (30). □

Remark 8. The result in (30) matches that obtained in [28].

4. Tau Stratagem for Handling a Type of Pantograph Differential Equations with Quadratic Nonlinearity

In this section, we are interested in employing a new expression of the fractional derivatives of the third-kind Chebyshev polynomials along with the application of the spectral tau method to treat the following fractional pantograph differential equation with quadratic nonlinearity ([38, 45, 48]).

$$D^\gamma v(t) + \xi_1 v'(t) + \xi_2 v(t) + \xi_3 v\left(\frac{t}{\tau}\right) + \xi_4 v^2(t) = g(t), t \in (0,1), \tag{35}$$

governed by the boundary conditions:

$$v(0) = \varrho_0, v(1) = \varrho_1, \tag{36}$$

or the initial conditions

$$v(0) = \tilde{\varrho}_0, v'(0) = \tilde{\varrho}_1, \tag{37}$$

where $1 < \gamma \le 2, \tau > 1, \xi_1, \xi_2, \xi_3, \xi_4, \varrho_0, \varrho_1, \tilde{\varrho}_0$, and $\tilde{\varrho}_1$ are real constants, and $g(t)$ is a known continuous source function.

Before moving further with the implementation of our proposed method, the following two lemmas are needed. The first lemma presents the duplication formula of the shifted Chebyshev polynomials of the third kind, whereas the second lemma exhibits the linearization formula of the shifted third-kind Chebyshev polynomials.

Lemma 9. *Let i be any positive integer, and A is a nonzero real number. We have the following formula:*

$$V_i^*(Ax) = A^i(2i+1)! \sum_{p=0}^{i} \frac{1}{p!(2i-p+1)!}\, {}_2F_1 \cdot \left(\begin{matrix}-p, -2i+p-1\\ -2i\end{matrix}\Big|\frac{1}{A}\right) V_{i-p}^*(x). \tag{38}$$

Proof. Formula (37) can be easily obtained by making use of (10) along with (11). □

Lemma 10. *For all nonnegative integers i and j, the following linearization formula is valid ([49])*

$$V_i^*(x)\, V_j^*(x) = \sum_{p=0}^{2\min(i,j)} (-1)^p V_{i+j-p}^*(x). \tag{39}$$

The key idea behind solving (35)–(36) is to use the spectral tau approach. We represent the inner product in $L^2(0,1)$, namely, $(\cdot, \cdot)$

$$(\phi(t), \psi(t))_w = \int_0^1 w(t)\,\phi(t)\,\psi(t)\,dt. \tag{40}$$

If we suppose that the right-hand side of (35) may be written as

$$g(t) = \sum_{i=0}^{\infty} g_i V_i^*(t), \tag{41}$$

the following approximation of $g(t)$ can therefore be considered:

$$g(t) = \sum_{i=0}^{N} g_i V_i^*(t)\,;\, g_i = \frac{2}{\pi}(g, V_i^*(t))_w. \tag{42}$$

We also take into account the approximate solution of (35) as:

$$v(t) \approx v_n(t) = \sum_{i=0}^{n} u_i V_i^*(t) = U.\Phi, \tag{43}$$

where

$$U = (u_0, u_1, \cdots, u_n), \Phi = \begin{pmatrix} V_0^*(t)\\ V_1^*(t)\\ \cdot\\ \cdot\\ \cdot\\ V_n^*(t)\end{pmatrix}. \tag{44}$$

Now, we are going to employ the tau method for solving (35). First, the residual of (35) is given by

$$R_n(t) = D^{\gamma} v_n(t) + \xi_1 D v_n(t) + \xi_2 v_n(t) + \xi_3 v_n\left(\frac{t}{\tau}\right) + \xi_4 v_n^2(t) - g(t). \tag{45}$$

We approximate each term on the right-hand side of (45) in terms of the shifted third-kind Chebyshev polynomials. First, to approximate the term $D^{\gamma} V_i^*(t)$, we make use of Theorem 5, to get

$$D^{\gamma} V_i^*(t) \approx \sum_{p=0}^{N} d_{p,i,\gamma} V_p^*(t), \tag{46}$$

with

$$d_{p,i,\gamma} = \frac{(2i+1)\Gamma(-\gamma+\lceil\gamma\rceil+3/2)(-1)^{\lceil\gamma\rceil+i}(\lceil\gamma\rceil+i)!}{\Gamma(\lceil\gamma\rceil+3/2)(i-\lceil\gamma\rceil)!\Gamma(-p-\gamma+\lceil\gamma\rceil+1)\Gamma(p-\gamma+\lceil\gamma\rceil+2)} \times {}_4F_3\left(\begin{matrix} 1, \lceil\gamma\rceil - i, \lceil\gamma\rceil + i + 1, -\gamma + \lceil\gamma\rceil + \frac{3}{2} \\ \lceil\gamma\rceil + \frac{3}{2}, -\gamma + \lceil\gamma\rceil - p + 1, -\gamma + \lceil\gamma\rceil + p + 2 \end{matrix} \middle| 1\right), \tag{47}$$

and accordingly, we have

$$D^{\gamma} v_n(t) = \sum_{i=0}^{n}\sum_{p=0}^{N} u_i d_{p,i,\gamma} V_p^*(t). \tag{48}$$

Also, Lemma 9 enables one to approximate $V_i^*(t/\tau)$ for any positive integer $\tau > 1$ as

$$V_i^*\left(\frac{t}{\tau}\right) = \sum_{p=0}^{i} \Delta_{i,p} V_{i-p}^*, \tag{49}$$

with

$$\Delta_{i,p} = \frac{(2i+1)!}{\tau^i p!(2i-p+1)!} {}_2F_1\left(\begin{matrix} -p, -2i+p-1 \\ -2i \end{matrix} \middle| \tau\right). \tag{50}$$

In addition, the linearization formula of the third-kind Chebyshev polynomials leads to the following expression for $v_n^2(t)$:

$$v_n^2(t) = \sum_{i=0}^{n}\sum_{j=0}^{n}\sum_{p=0}^{2\min(i,j)} (-1)^p u_i u_j V_{i+j-p}^*(t). \tag{51}$$

Now, in virtue of the three formulas (48), (49), and (51), the residual of (35) can be discretized as

$$\begin{aligned} R_n(t) = {} & \sum_{i=0}^{n}\sum_{p=0}^{N} u_i d_{p,i,\gamma} V_p^*(t) + \xi_1 \sum_{i=0}^{n}\sum_{p=0}^{i-1} u_i d_{p,i,1} V_p^*(t) \\ & + \xi_2 \sum_{i=0}^{n} u_i \phi_i + \xi_3 \sum_{i=0}^{n}\sum_{p=0}^{i} u_i \Delta_{i,p}, V_{i-p}^*(t) \\ & + \xi_4 \sum_{i=0}^{n}\sum_{j=0}^{n}\sum_{p=0}^{2\min(i,j)} (-1)^p u_i u_j V_{i+j-p}^*(t) - \sum_{i=0}^{n} g_i V_i^*(t). \end{aligned} \tag{52}$$

The standard tau technique ([26]) is used in this case to yield

$$\left(R_n(t), V_j^*(t)\right)_w = 0\,; 0 \le j \le n-2, \tag{53}$$

which consequently out-turn

$$\begin{aligned} & \sum_{i=0}^{n}\sum_{p=0}^{N} u_i d_{p,i,\gamma} \left(V_p^*, V_j^*\right)_w + \xi_1 \sum_{i=0}^{n}\sum_{p=0}^{i-1} u_i d_{p,i,1} \left(V_p^*, V_j^*\right)_w \\ & + \xi_2 \sum_{i=0}^{n} u_i \left(V_i^*, V_j^*\right)_w + \xi_3 \sum_{i=0}^{n}\sum_{p=0}^{i} u_i \Delta_{i,p} \left(V_{i-p}^*, V_j^*\right)_w \\ & + \xi_4 \sum_{i=0}^{n}\sum_{j=0}^{n}\sum_{p=0}^{2\min(i,j)} (-1)^p u_i u_j \left(V_{i+j-p}^*, V_j^*\right)_w - \sum_{i=0}^{n} g_i \left(V_i^*, V_j^*\right)_w = 0. \end{aligned} \tag{54}$$

The benefit of the orthogonality relation leads to the following equations

$$\begin{aligned} & \sum_{i=0}^{n}\sum_{p=0}^{N} u_i d_{p,i,\gamma} \delta_{p,j} + \xi_1 \sum_{i=0}^{n}\sum_{p=0}^{i-1} u_i d_{p,i,1} \delta_{p,j} + \xi_2 \sum_{i=0}^{n} u_i \delta_{i,j} + \xi_3 \sum_{i=0}^{n}\sum_{p=0}^{i} u_i \Delta_{i,p} \delta_{i-p,j} \\ & + \xi_4 \sum_{i=0}^{n}\sum_{k=0}^{n}\sum_{p=0}^{2\min(i,k)} (-1)^p u_i u_k \delta_{i+k-p,j} - \sum_{i=0}^{n} g_i \delta_{i,j} = 0, \end{aligned} \tag{55}$$

or equivalently

$$\begin{aligned} & \sum_{i=0}^{n}\sum_{p=0}^{N} u_i d_{p,i,\gamma} \delta_{p,j} + \xi_1 \sum_{i=0}^{n}\sum_{p=0}^{i-1} u_i d_{p,i,1} \delta_{p,j} + \xi_2 u_j + \xi_3 \sum_{i=0}^{n}\sum_{p=0}^{i} u_i \Delta_{i,p} \delta_{i-p,j} \\ & + \xi_4 \sum_{i=0}^{n}\sum_{k=0}^{n}\sum_{p=0}^{2\min(i,k)} (-1)^p u_i u_k \delta_{i+k-p,j} - g_j \\ & = 0\,; j \in \{0, 1, \cdots, n-2\}. \end{aligned} \tag{56}$$

The boundary conditions return

$$\sum_{i=0}^{n} (-1)^i (2i+1) u_i = \varrho_0, \sum_{i=0}^{n} u_i = \varrho_1, \tag{57}$$

while the initial conditions return

$$\sum_{i=0}^{n}(-1)^{i}(2i+1)u_i=\tilde{\mathfrak{Q}}_0,\ \sum_{i=1}^{N}(-1)^{i-1}2(-1)^{i-1}(i)_2(2i+1)\,u_i=3\,\tilde{\mathfrak{Q}}_1. \tag{58}$$

Equations (56)–(57) or (56)–(58) generate a set of algebraic equations with dimension $(n+1)$ in the unknown expansion coefficients u_j that may be solved via Newton's iterative scheme.

5. Error Estimate

This section examines the proposed polynomial series expansion's convergence and error analysis in depth. As a result, several necessary lemmas are employed in this research. Three theorems will also be stated and proved.

In what follows, by writing $A_n \preccurlyeq B_n$, this implies the existence of a generic constant C, such that $A_n \le C\,B_n$.

Lemma 11. *Lat $\gamma \in [1,2)$. One has:*

$$|d_{i,p,\gamma}| \preccurlyeq 4^{6(1+\gamma-i)}\,i^{4(1+\gamma)}. \tag{59}$$

Proof. In virtue of: $\Gamma(r+\beta)\approx r!r^{\beta-1}$ (see, [50]), and after some algebraic computations, we get the result. □

Lemma 12. *We have:*

$$|\Delta_{i,p}| \preccurlyeq \frac{(2i+1)!}{\tau^{i}\,(2i+1-p)!p!}. \tag{60}$$

Proof. Similar to the proof of Lemma 11. □

Lemma 13. *For all $i>0$, we have:*

$$|V_i^*(t)| \le 2i+1. \tag{61}$$

Theorem 14. *For $k>3$, assume that $v(t)$ is C^k-function, and let $v(t)$ can be approximated as:*

$$v(t)\approx v_n(t)=\sum_{i=0}^{n}u_i\,V_i^*(t), \tag{62}$$

then, the following estimate can be obtained

$$|u_i| \preccurlyeq i^{-k}. \tag{63}$$

Proof. We can get the required result by employing steps similar to those used in [25].

If $v(t)$ obeys the assumptions of Theorem 14, we have the following two theorems. □

Theorem 15. *The following truncation error estimate is valid*

$$|v-v_n| \preccurlyeq n^{2-k}. \tag{64}$$

Proof. By the result of Theorem 14and the help of Lemma 13, we get the result. □

Theorem 16. *If we define*

$$\mathscr{E}_n=\left|D^{\gamma}v_n(t)+\xi_1\,v'_n(t)+\xi_2\,v_n(t)+\xi_3\,v_n\left(\frac{t}{\tau}\right)+\xi_4\,v_n^2(t)-g(t)\right|, \tag{65}$$

then, for $1<\tau<4$, we have the following global error estimate:

$$|\mathscr{E}_n| \preccurlyeq \max\left\{n^{3-k},\ \frac{m^2\,n^{4+4\gamma-k}}{2^{12n}},\ \frac{n^{1/2-k}\,\tau^n}{4^n}\right\}. \tag{66}$$

Proof. We have

$$\begin{aligned} &D^{\gamma}v_n(t)+\xi_1\,v'_n(t)+\xi_2\,v_n(t)+\xi_3\,v_n\left(\frac{t}{\tau}\right)+\xi_4\,v_n^2(t)\approx g_n(t),\\ &D^{\gamma}v(t)+\xi_1\,v'(t)+\xi_2\,v(t)+\xi_3\,v\left(\frac{t}{\tau}\right)+\xi_4\,v^2(t)=g(t). \end{aligned} \tag{67}$$

Substitution by (24) into (23), we get

$$\begin{aligned} |\mathscr{E}_n| \le{}& |D^{\gamma}(v-v_n)|+\left|\xi_1\,(v-v_n)'\right|+|\xi_2\,(v-v_n)|\\ &+\left|\xi_3\,(v-v_n)\left(\frac{t}{\tau}\right)\right|+\left|\xi_4\,\left(v^2-v_n^2\right)\right|. \end{aligned} \tag{68}$$

By the boundedness of v and with the help of Theorem 15, we have

$$|\mathscr{E}_n| \preccurlyeq |D^{\gamma}(v-v_n)|+\left|\xi_1\,(v-v_n)'\right|+\left|\xi_3\,(v-v_n)\left(\frac{t}{\tau}\right)\right|+n^{2-k}. \tag{69}$$

Now, we have:

$$\begin{aligned} D(v-v_n)&=\sum_{i=n+1}^{\infty}u_i\,DV_i^*,\\ D^{\gamma}(v-v_n)&=\sum_{i=n+1}^{\infty}\sum_{p=0}^{N}u_i\,d_{p,i,\gamma}\,V_p^*,\\ (v-v_n)\left(\frac{t}{\tau}\right)&=\sum_{i=n+1}^{\infty}\sum_{p=0}^{i}u_i\,\Delta_{i,p}\,V_{i-p}^*. \end{aligned} \tag{70}$$

By the application of Theorem 14, Lemmas 11, 12, and 13, respectively, and after some algebraic manipulation, we get

$$\begin{aligned} (v-v_n)' &\preccurlyeq n^{3-k},\\ D^{\gamma}(v-v_n) &\preccurlyeq \frac{m^2\,n^{4+4\gamma-k}}{2^{12n}},\\ (v-v_n)\left(\frac{t}{\tau}\right) &\preccurlyeq \frac{n^{1/2-k}\,\tau^n}{4^n}, \end{aligned} \tag{71}$$

which ends the proof of the theorem. □

6. Numerical Simulations

This section is confined to presenting four test problems to clarify the accuracy and applicability of the Chebyshev third-kind tau method (C3TM) that derived in Section 4.

Problem 1. Consider the linear fractional pantograph differential equation ([38]):

$$D^{\gamma} v(t) - \frac{3}{4} v(t) - v\left(\frac{1}{2} t\right) = 2 - t^2, t \in (0,1); 1 < \gamma \leq 2,$$
$$v(0) = v'(0) = 0. \tag{72}$$

In case $\gamma = 2$, the exact solution is: $v(t) = t^2$.

First, we discuss the case corresponding to $\gamma = 2$. In this case, after applying our algorithm, with $n = 2$, the following system of equations can be obtained:

$$\begin{aligned} 256\, u_2 + 12\, u_1 - 14\, u_0 &= 11, \\ 5\, u_2 - 3\, u_1 + u_0 &= 0, \\ 5\, u_2 - u_1 &= 0, \end{aligned} \tag{73}$$

which yields

$$u_0 = \frac{5}{8}, u_1 = \frac{5}{16}, u_2 = \frac{1}{16}, \tag{74}$$

and consequently,

$$v(t) = \frac{5}{8}(1) + \frac{5}{16}(-3 + 4t) + \frac{1}{16}\left(5 - 20t + 16t^2\right) = t^2, \tag{75}$$

which is the exact solution.

Second, when $1 < \gamma < 2$. Since the exact solution is not available, we define the following error norm

$$\mathscr{E}_n = \max_{0 \leq t \leq 1} \left| D^{\gamma} v_n(t) - \frac{3}{4} v_n(t) - v_n\left(\frac{1}{2} t\right) - 2 + t^2 \right|. \tag{76}$$

We apply our algorithm with $n = 2, N = 3$. The values of $\mathscr{E}$, for various values of γ, are listed in Table 1.

Note 2. We would like to report here that the authors in [38] obtained an error of order 10^{-17}, when $\gamma = 2$, while, we obtained the exact solution.

Problem 2. Consider the following fractional pantograph differential equation: ([38]):

$$D^{\gamma} v(t) + \frac{5}{6} v(t) - 4\, v\left(\frac{1}{2} t\right) - 9\, v\left(\frac{1}{3} t\right) = t^2 - 1, t \in (0,1); 0 < \gamma \leq 1,$$
$$v(0) = 1. \tag{77}$$

In case $\gamma = 1$, the exact solution is: $v(t) = 12157/1296\, t^3 + 1675/72\, t^2 + 67/6\, t + 1$.

First, we discuss the case corresponding to $\gamma = 1$. In this case, after applying our algorithm, with $n = 3$, we get the following system of equations:

$$\begin{aligned} -292\, u_0 + 672\, u_1 - 144\, u_2 - 4\, u_3 + 9 &= 0, \\ -200\, u_1 + 1104\, u_2 - 648\, u_3 - 15 &= 0, \\ -56\, u_2 + 968\, u_3 - 3 &= 0, \\ u_0 - 3\, u_1 + 5\, u_2 - 7\, u_3 &= 1, \end{aligned} \tag{78}$$

which yields

$$u_0 = \frac{2409095}{82944}, u_1 = \frac{363283}{27648}, u_2 = \frac{205699}{82944}, u_3 = \frac{12157}{82944}, \tag{79}$$

and consequently

$$\begin{aligned} v_3(t) = {} & \frac{2409095}{82944} + \frac{363283}{27648}(4t - 3) + \frac{205699}{82944}\left(16t^2 - 20t + 5\right) \\ & + \frac{12157}{82944}\left(64t^3 - 112t^2 + 56t - 7\right), \end{aligned} \tag{80}$$

and therefore, we get

$$v_3(t) = \frac{12157t^3}{1296} + \frac{1675t^2}{72} + \frac{67t}{6} + 1, \tag{81}$$

which is the exact solution.

Second, when $0 < \gamma < 1$. Since, the exact solution is not available, we define the following error norm

$$\mathscr{E}_n = \max_{0 \leq t \leq 1} \left| D^{\gamma} v_n(t) + \frac{5}{6} v_n(t) - 4\, v_n\left(\frac{1}{2} t\right) - 9\, v_n\left(\frac{1}{3} t\right) - t^2 + 1 \right|. \tag{82}$$

We apply our algorithm with $n = 3, N = 4$. The values of $\mathscr{E}$, for various values of γ are listed in Table 2.

Problem 3. Consider the fractional-delay BVP [25]:

$$v^{(\gamma)}(t) + v'(t) + v\left(\frac{t}{\tau}\right) + v(t) = r(t); t \in (0,1), \tag{83}$$

governed by

$$v(0) = 1, v(1) = \frac{1}{e}, \tag{84}$$

Table 1: Residual error of example 1.

γ	3/2	1.6	1.7	1.8	1.9
$\mathscr{E}$	2.22×10^{-16}	2.22×10^{-16}	2.22×10^{-16}	2.22×10^{-17}	2.22×10^{-18}

Table 2: Residual error of example 2.

γ	0.5	0.6	0.7	0.8	0.9
$\mathscr{E}$	3.56×10^{-13}	4.24×10^{-14}	3.58×10^{-15}	3.94×10^{-15}	2.22×10^{-16}

Table 3: Maximum point-wise error of example 3.

γ	τ	N	4	6	8	10	12	14
	4/3		3.42×10^{-5}	4.76×10^{-7}	5.38×10^{-9}	2.27×10^{-11}	4.68×10^{-14}	2.22×10^{-16}
5/4	2	E	4.51×10^{-5}	5.27×10^{-7}	6.39×10^{-9}	7.95×10^{-11}	6.23×10^{-14}	2.22×10^{-16}
	4		5.37×10^{-5}	8.26×10^{-7}	2.39×10^{-9}	5.95×10^{-11}	7.21×10^{-14}	2.22×10^{-16}
	4/3		$3/27 \times 10^{-5}$	2.25×10^{-7}	5.92×10^{-9}	5.61×10^{-11}	6.34×10^{-14}	2.22×10^{-16}
3/2	2	E	5.13×10^{-5}	7.25×10^{-7}	6.38×10^{-9}	9.34×10^{-11}	2.15×10^{-14}	2.22×10^{-16}
	4		2.87×10^{-5}	2.68×10^{-7}	2.36×10^{-9}	5.27×10^{-11}	2.27×10^{-14}	2.22×10^{-16}
	4/3		4.37×10^{-5}	7.85×10^{-7}	2.96×10^{-9}	3.65×10^{-11}	2.65×10^{-14}	2.22×10^{-16}
7/4	2	E	2.33×10^{-5}	6.64×10^{-7}	2.37×10^{-9}	5.92×10^{-11}	2.84×10^{-14}	2.22×10^{-16}
	4		2.68×10^{-5}	5.61×10^{-7}	3.98×10^{-9}	9.34×10^{-11}	2.38×10^{-14}	2.22×10^{-16}

and $r(t)$ is selected so that $v(t) = \exp(-t)$ is the exact solution. The $C3TM$ is applied for various choices of τ and n. Table 3 lists the maximum point-wise error E that is computed by the following formula:

$$E = \max_{t \in [0,1]} |\text{Exact}(t) - \text{Approximate}(t)|, \tag{85}$$

for $\gamma = 5/4, 3/2, 7/4$ and $\tau = 4/3, 2, 4$. In Figure 1, the log errors are presented in case of $\tau = 2$.

Problem 4. Consider the fractional-delay initial value problem [48]:

$$v^{(\gamma)}(t) + \eta v(t) + \mu v\left(\frac{t}{\tau}\right) = (\eta - 1) \sin t + \mu \sin\left(\frac{t}{\tau}\right); t \in [0, 1], 1 < \gamma \leq 2, \tag{86}$$

governed by the initial conditions:

$$v(0) = v'(0) - 1 = 0, \tag{87}$$

and the exact solution is: $v(t) = \sin t$ for $\gamma = 2$, and η and μ are any real constants. Table 4 presents the errors if $C3TM$ is applied for $n = 15$. We list the maximum absolute residual error defined by:

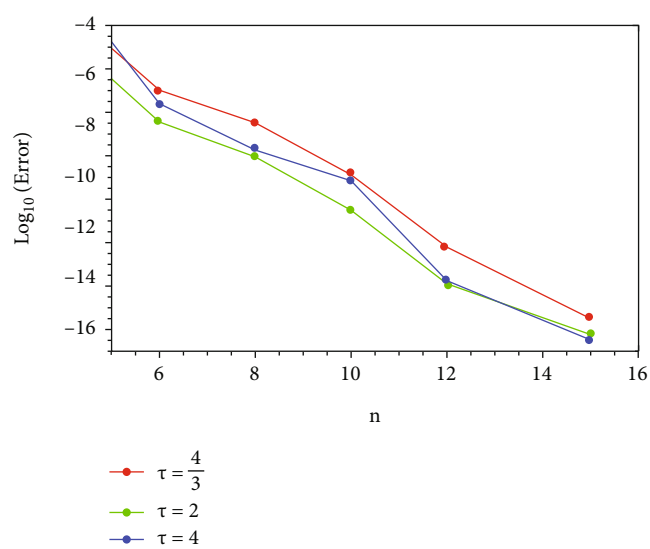

Figure 1: Log errors of example 3.

$$\mathscr{E}_n = \max_{0 \leq t \leq 1} \left| v_n^{(\gamma)}(t) + \eta v_n(t) + \mu v_n\left(\frac{t}{\tau}\right) - (\eta - 1) \sin t - \mu \sin\left(\frac{t}{\tau}\right) \right|, \tag{88}$$

for the case that corresponds to $\eta = 1, \mu = 1/2, \gamma = 2, 7/4, 3/2, 5/4$, and $\tau = 2$, and $\tau = 4$. Figure 2 illustrates the absolute errors for the case $\gamma = 2, n = 15$.

Table 4: The maximum absolute residual error $\mathscr{E}_n$ for various values of γ, for example 4.

n	$\gamma = 2$		$\gamma = 7/4$		$\gamma = 3/2$		$\gamma = 5/4$	
	$\tau = 2$	$\tau = 4$	$\tau = 2$	$\tau = 4$	$\tau = 2$	$\tau = 4$	$\tau = 2$	$\tau = 4$
4	2.2×10^{-3}	4.5×10^{-3}	5.2×10^{-2}	9.8×10^{-3}	7.3×10^{-2}	3.7×10^{-2}	4.4×10^{-2}	2.8×10^{-2}
8	4.6×10^{-7}	5.7×10^{-7}	2.4×10^{-4}	2.9×10^{-4}	3.3×10^{-4}	6.8×10^{-4}	4.2×10^{-4}	1.4×10^{-4}
12	2.8×10^{-10}	4.0×10^{-10}	3.7×10^{-8}	6.2×10^{-8}	5.9×10^{-8}	8.2×10^{-8}	9.2×10^{-8}	6.4×10^{-8}
16	4.4×10^{-16}	4.4×10^{-16}	5.4×10^{-12}	2.4×10^{-12}	5.4×10^{-12}	3.7×10^{-12}	7.5×10^{-12}	8.7×10^{-12}

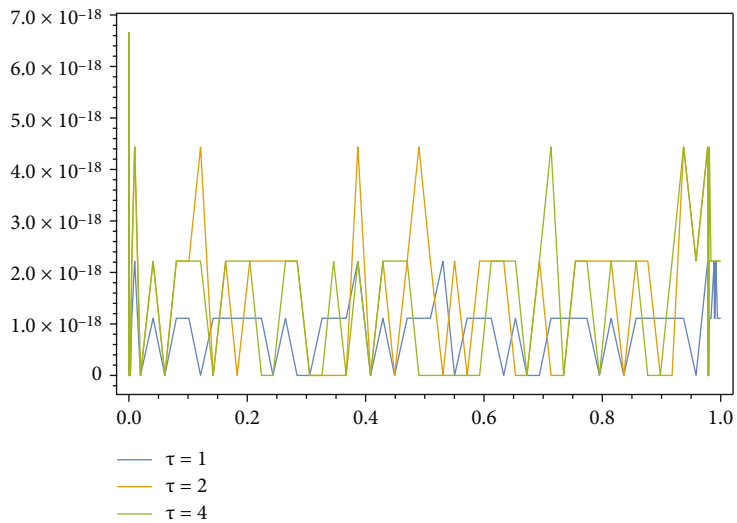

Figure 2: Absolute errors of example 4—$\gamma = 2$, $N = 16$.

7. Conclusion

Herein, we have established a new formula that gives an approximation of the fractional derivatives of the nonsymmetric polynomials, namely, shifted third-kind Chebyshev polynomials in the Caputo sense. We demonstrated that this formula contains a terminating hypergeometric function of type ${}_4F_3(1)$, which can be simplified in the integer case to match the well-known derivative formula of the Chebyshev polynomials of the third kind. A certain nonlinear fractional pantograph differential equation was treated via the application of the spectral tau method depending on the developed fractional derivatives formula. The convergence analysis of the method was investigated. The algorithm was tested through four examples that show the high accuracy and the efficiency of the presented algorithm. We believe that the theoretical results in this paper can be utilized to treat other types of fractional differential equations.

Data Availability

No data is associated with this research.

Conflicts of Interest

The authors declare that they have no conflicts of interest.

References

[1] O. Nikan, A. Golbabai, J. A. T. Machado, and T. Nikazad, "Numerical solution of the fractional Rayleigh–Stokes model arising in a heated generalized second-grade fluid," *Engineering with Computers*, vol. 37, no. 3, pp. 1751–1764, 2021.

[2] D. C. Labora, A. M. Lopes, and J. A. T. Machado, "Time-fractional dependence of the shear force in some beam type problems with negative young modulus," *Applied Mathematical Modelling*, vol. 80, pp. 668–682, 2020.

[3] J. A. T. Machado and A. M. Lopes, "On the mathematical modeling of soccer dynamics," *Communications in Nonlinear Science and Numerical Simulation*, vol. 53, pp. 142–153, 2017.

[4] W. M. Abd-Elhameed and Y. H. Youssri, "New spectral solutions of multi-term fractional order initial value problems with error analysis," *Computer Modeling in Engineering & Sciences*, vol. 105, no. 5, pp. 375–398, 2015.

[5] M. u. Rehman and R. A. Khan, "The Legendre wavelet method for solving fractional differential equations," *Communications in Nonlinear Science and Numerical Simulation*, vol. 16, no. 11, pp. 4163–4173, 2011.

[6] W. M. Abd-Elhameed and Y. H. Youssri, "Spectral solutions for fractional differential equations via a novel Lucas operational matrix of fractional derivatives," *Romanian Journal of Physics*, vol. 61, no. 5-6, pp. 795–813, 2016.

[7] W. M. Abd-Elhameed and Y. H. Youssri, "A novel operational matrix of caputo fractional derivatives of Fibonacci

polynomials: spectral solutions of fractional differential equations," *Entropy*, vol. 18, no. 10, p. 345, 2016.

[8] Y. H. Youssri, "Orthonormal ultraspherical operational matrix algorithm for fractal–fractional Riccati equation with generalized Caputo derivative," *Fractal and Fractional*, vol. 5, no. 3, p. 100, 2021.

[9] D. G. Varsha and H. Jafari, "Solving a multi-order fractional differential equation using Adomian decomposition," *Applied Mathematics and Computation*, vol. 189, no. 1, pp. 541–548, 2007.

[10] M. A. Zaky and J. T. Machado, "Multi-dimensional spectral tau methods for distributed-order fractional diffusion equations," *Computers & Mathematics with Applications*, vol. 79, no. 2, pp. 476–488, 2020.

[11] W. M. Abd-Elhameed and Y. H. Youssri, "Generalized Lucas polynomial sequence approach for fractional differential equations," *Nonlinear Dynamics*, vol. 89, no. 2, pp. 1341–1355, 2017.

[12] W. M. Abd-Elhameed, "Novel expressions for the derivatives of sixth kind Chebyshev polynomials: spectral solution of the non-linear one-dimensional Burgers' equation," *Fractal and Fractional*, vol. 5, no. 2, p. 53, 2021.

[13] M. M. Khader and A. S. Hendy, "The approximate and exact solutions of the fractional-order delay differential equations using Legendre pseudospectral method," *International Journal of Pure and Applied Mathematics*, vol. 74, no. 3, pp. 287–297, 2012.

[14] M. M. Khader, "Fractional Chebyshev finite difference method for solving the fractional-order delay BVPs," *International Journal of Computational Methods*, vol. 12, no. 6, article 1550033, 2015.

[15] M. Cinar, A. Secer, and M. Bayram, "An application of Genocchi wavelets for solving the fractional Rosenau-Hyman equation," *Alexandria Engineering Journal*, vol. 60, no. 6, pp. 5331–5340, 2021.

[16] T. Akram, M. Abbas, M. B. Riaz, A. I. Ismail, and N. M. Ali, "An efficient numerical technique for solving time fractional Burgers equation," *Alexandria Engineering Journal*, vol. 59, no. 4, pp. 2201–2220, 2020.

[17] B. P. Moghaddam, A. Dabiri, A. M. Lopes, and J. A. T. Machado, "Numerical solution of mixed-type fractional functional differential equations using modified Lucas polynomials," *Computational and Applied Mathematics*, vol. 38, no. 2, pp. 1–12, 2019.

[18] A. Jannelli, "Numerical solutions of fractional differential equations arising in engineering sciences," *Mathematics*, vol. 8, no. 2, p. 215, 2020.

[19] P. I. Chebyshev, "Sur les expressions approximatives des integrales definies par les autres prises entre les mêmes limites," *In Proceedings of the Kharkov Mathematical Society*, vol. 2, pp. 93–98, 1882.

[20] P. Cerone, *On Chebyshev Functional Bounds*, In Proc. Hindawi Publ. Corp, New York, 2006.

[21] M. E. Özdemir, E. Set, A. O. Akdemir, and M. Z. Sarkaya, "Some new Chebyshev type inequalities for functions whose derivatives belongs to L_p spaces," *Afrika Matematika*, vol. 26, no. 7, pp. 1609–1619, 2015.

[22] A. O. Akdemir, S. I. Butt, M. Nadeem, and M. A. Ragusa, "New general variants of Chebyshev type inequalities via generalized fractional integral operators," *Mathematics*, vol. 9, no. 2, p. 122, 2021.

[23] S. I. Butt, M. Nadeem, and G. Farid, "On Caputo fractional derivatives via exponential s-convex functions," *Turkish Journal of Science*, vol. 5, no. 2, pp. 140–146, 2020.

[24] W. M. Abd-Elhameed, E. H. Doha, Y. H. Youssri, and M. A. Bassuony, "New Tchebyshev-Galerkin operational matrix method for solving linear and nonlinear hyperbolic telegraph type equations," *Numerical Methods for Partial Differential Equations*, vol. 32, no. 6, pp. 1553–1571, 2016.

[25] W. M. Abd-Elhameed, J. A. T. Machado, and Y. H. Youssri, "Hypergeometric fractional derivatives formula of shifted Chebyshev polynomials: tau algorithm for a type of fractional delay differential equations," *International Journal of Nonlinear Sciences and Numerical Simulation*, 2021.

[26] W. M. Abd-Elhameed and Y. H. Youssri, "Explicit shifted second-kind Chebyshev spectral treatment for fractional Riccati differential equation," *Computer Modeling in Engineering & Sciences*, vol. 121, no. 3, pp. 1029–1049, 2019.

[27] E. H. Doha, W. M. Abd-Elhameed, and M. A. Bassuony, "On using third and fourth kinds Chebyshev operational matrices for solving Lane-Emden type equations," *Romanian Journal of Physics*, vol. 60, no. 3-4, pp. 281–292, 2015.

[28] E. H. Doha, W. M. Abd-Elhameed, and M. A. Bassuony, "On the coefficients of differentiated expansions and derivatives of Chebyshev polynomials of the third and fourth kinds," *Acta Mathematica Scientia*, vol. 35, no. 2, pp. 326–338, 2015.

[29] M. R. A. Sakran, "Numerical solutions of integral and integro-differential equations using Chebyshev polynomials of the third kind," *Applied Mathematics and Computation*, vol. 351, pp. 66–82, 2019.

[30] E. H. Doha and W. M. Abd-Elhameed, "Accurate spectral solutions for the parabolic and elliptic partial differential equations by the ultraspherical tau method," *Journal of Computational and Applied Mathematics*, vol. 181, no. 1, pp. 24–45, 2005.

[31] F. Mohammadi and C. Cattani, "A generalized fractional-order Legendre wavelet tau method for solving fractional differential equations," *Journal of Computational and Applied Mathematics*, vol. 339, pp. 306–316, 2018.

[32] A. Napoli and W. M. Abd-Elhameed, "An innovative harmonic numbers operational matrix method for solving initial value problems," *Calcolo*, vol. 54, no. 1, pp. 57–76, 2017.

[33] Y. H. Youssri, "Two Fibonacci operational matrix pseudo-spectral schemes for nonlinear fractional Klein–Gordon equation," *International Journal of Modern Physics C*, no. article 2250049, 2022.

[34] R. L. Magin, "Fractional calculus models of complex dynamics in biological tissues," *Computers & Mathematics with Applications*, vol. 59, no. 5, pp. 1586–1593, 2010.

[35] S. Sedaghat, Y. Ordokhani, and M. Dehghan, "Numerical solution of the delay differential equations of pantograph type via Chebyshev polynomials," *Communications in Nonlinear Science and Numerical Simulation*, vol. 17, no. 12, pp. 4815–4830, 2012.

[36] M. Sezer and A. Akyüz-Dascoglu, "A Taylor method for numerical solution of generalized pantograph equations with linear functional argument," *Journal of Computational and Applied Mathematics*, vol. 200, no. 1, pp. 217–225, 2007.

[37] D. Trif, "Direct operational tau method for pantograph-type equations," *Applied Mathematics and Computation*, vol. 219, no. 4, pp. 2194–2203, 2012.

[38] P. Rahimkhani, Y. Ordokhani, and E. Babolian, "Numerical solution of fractional pantograph differential equations by using generalized fractional-order Bernoulli wavelet," *Journal of Computational and Applied Mathematics*, vol. 309, pp. 493–510, 2017.

[39] P. Rahimkhani, Y. Ordokhani, and E. Babolian, "Müntz-Legendre wavelet operational matrix of fractional-order integration and its applications for solving the fractional pantograph differential equations," *Numerical Algorithms*, vol. 77, no. 4, pp. 1283–1305, 2018.

[40] H. Alrabaiah, I. Ahmad, R. Amin, and K. Shah, "A numerical method for fractional variable order pantograph differential equations based on Haar wavelet," *Engineering with Computers*, 2021.

[41] H. Jafari, M. Mahmoudi, and M. H. Noori Skandari, "A new numerical method to solve pantograph delay differential equations with convergence analysis," *Advances in Difference Equations*, vol. 2021, 12 pages, 2021.

[42] C. Yang and J. Hou, "Jacobi spectral approximation for boundary value problems of nonlinear fractional pantograph differential equations," *Numerical Algorithms*, vol. 86, no. 3, pp. 1089–1108, 2021.

[43] Y. H. Youssri, W. M. Abd-Elhameed, A. S. Mohamed, and S. M. Sayed, "Generalized Lucas polynomial sequence treatment of fractional pantograph differential equation," *International Journal of Applied and Computational Mathematics*, vol. 7, no. 2, pp. 1–16, 2021.

[44] C. C. Hou, T. E. Simos, and I. T. Famelis, "Neural network solution of pantograph type differential equations," *Mathematical Methods in the Applied Sciences*, vol. 43, no. 6, pp. 3369–3374, 2020.

[45] J. C. Mason and D. C. Handscomb, *Chebyshev Polynomials*, CRC Press, 2002.

[46] G. E. Andrews, R. Askey, and R. Roy, *Special Functions*, Cambridge University Press, Cambridge, 1999.

[47] W. Koepf, *Hypergeometric Summation: An Algorithmic Approach to Summation and Special Function Identities*, Vieweg, Braunschweig, Germany, 1998.

[48] H. Brunner, Q. Huang, and H. Xie, "Discontinuous Galerkin methods for delay differential equations of pantograph type," *SIAM Journal on Numerical Analysis*, vol. 48, no. 5, pp. 1944–1967, 2010.

[49] E. H. Doha and W. M. Abd-Elhameed, "New linearization formulae for the products of Chebyshev polynomials of third and fourth kinds," *Rocky Mountain Journal of Mathematics*, vol. 46, no. 2, pp. 443–460, 2016.

[50] N. Batir, "Inequalities for the gamma function," *Archiv der Mathematik*, vol. 91, no. 6, pp. 554–563, 2008.

Hindawi
Journal of Function Spaces
Volume 2022, Article ID 7667370, 9 pages
https://doi.org/10.1155/2022/7667370

Research Article

Existence and Uniqueness of the Solution for an Inverse Problem of a Fractional Diffusion Equation with Integral Condition

Taki-Eddine Oussaeif,[1] **Benaoua Antara**,[1] **Adel Ouannas**,[1] **Iqbal M. Batiha**,[2,3] **Khaled M. Saad**,[4] **Hadi Jahanshahi**,[5] **Awad M. Aljuaid**,[6] **and Ayman A. Aly**[7]

[1]*Department of Mathematics and Computer Science, University of Larbi Ben M'hidi, Oum El Bouaghi, Algeria*
[2]*Department of Mathematics, Faculty of Science and Technology, Irbid National University, 2600 Irbid, Jordan*
[3]*Nonlinear Dynamics Research Center (NDRC), Ajman University, Ajman, UAE*
[4]*Department of Mathematics, Faculty of Applied Science, Taiz University, Taiz, Yemen*
[5]*Department of Mechanical Engineering, University of Manitoba, Winnipeg, Canada R3T 5V6*
[6]*Department of Industrial Engineering, College of Engineering, Taif University, P.O. Box 11099, Taif 21944, Saudi Arabia*
[7]*Department of Mechanical Engineering, College of Engineering, Taif University, P.O. Box 11099Taif 21944, Saudi Arabia*

Correspondence should be addressed to Khaled M. Saad; khaledma_sd@hotmail.com

Received 14 September 2021; Revised 27 December 2021; Accepted 21 February 2022; Published 6 April 2022

Academic Editor: Youssri Hassan Youssri

The solvability of the fractional partial differential equation with integral overdetermination condition for an inverse problem is investigated in this paper. We analyze the direct problem solution by using the "energy inequality" method. Using the fixed point technique, the existence and uniqueness of the solution of the inverse problem on the data are established.

1. Introduction

This work devoted to study the solvability of a pair of functions $\{u, f\}$ satisfying the following fractional parabolic problem:

$$ {}^{C}D_t^{\alpha} u - \Delta u + \beta u = f(t) g(x, t)\,;\, x \in \Omega, t \in [0, T], \tag{1} $$

with the initial condition

$$ u(x, 0) = \varphi(x), x \in \Omega, \tag{2} $$

the boundary condition

$$ u(x, t) = 0, (x, t) \in \partial\Omega \times [0, T], \tag{3} $$

and the nonlocal condition

$$ \int_{\Omega} v(x) u(x, t) dx = \theta(t), t \in [0, T]. \tag{4} $$

Here, Ω is a bounded domain in $\mathbb{R}^n$ with smooth boundary $\partial\Omega$.. The functions g, φ, and θ are known functions, and β is a positive constant. And $\boldsymbol{\Gamma}(\cdot)$ denotes the gamma function. For any positive integer $0 < \alpha < 1$, the left Caputo derivative is defined as

$$ {}^{C}D_t^{\alpha} u(x, t) := \frac{1}{\Gamma(1-\alpha)} \int_0^t \frac{\partial u(x, \tau)}{\partial \tau} \frac{1}{(t-\tau)^{\alpha}} d\tau. \tag{5} $$

Inverse parabolic equation problems occur naturally in many fields, and there is extensive literature on inverse heat equation problems (see [1–4], and references therein). The form (4) is an additional information of problem.

In engineering and physics, the parameter recognition in a partial differential equation from the data of the integral overdetermination condition plays an important role [5–10]. From a physical point of view, these conditions can be interpreted by a system averaging the domain of spatial variables as measurements of the temperature $u(x,t)$.

Note that nonlocal problems related with integral overdetermination [11, 12]. Studies have shown that when we deal with these kinds of nonclassical problems, classical approaches sometimes do not work [13, 14]. To date, different methods for addressing problems resulting from nonlocal problem have been suggested. The choice of approach depends on the form of nonlocal boundary value that are involved.

We note that several authors have studied the inverse parabolic problem with condition of type (4) and its special solubility (see, for example, [3, 4, 15–20]). There are also several articles dedicated to the study of the existence and uniqueness of inverse problem solutions for different parabolic equations with unknown source functions. Inverse problems related by determining unknown function in source term of a parabolic equation with overdetermination condition [21, 22].

In recent years, fractional differential equations have created growing interest from engineers and scientists and have great importance in modeling complex phenomena. Because FDEs have memory, nonlocal space, and time relationships, using these equations, complex phenomena can be modelled [23–28].

Namely, in the present paper, a new research on the inverse problem of a fractional parabolic equation is discussed, for which the solvability of the problem (1)–(4) is reduced to the concept of a fixed point technique. This work is divided into four sections; we start with an introduction then we give some definitions of function space and important lemmas. The third section is devoted to studying the solvability of the direct fractional parabolic problem. Finally, in the last section, we prove the existence and uniqueness of the solution to the main problem.

2. Functional Space

Definition 1. Let us introduce certain notations used below, we set

$$g^*(t) = \int_\Omega v(x) g(x,t)\,dx,\ Q_T = \Omega \times [0,T]. \tag{6}$$

We denote by $C((0,T), L_2(\Omega))$ the space is composed of all continuous functions on $(0,T)$ with values in $L_2(\Omega)$. For any $0<\alpha<1$, the Caputo and Riemann-Liouville derivatives are defined, respectively, as follows:

(i) The left Caputo derivatives:

$$^{C}D_t^\alpha u(x,t) := \frac{1}{\Gamma(1-\alpha)} \int_0^t \frac{\partial u(x,\tau)}{\partial \tau} \frac{1}{(t-\tau)^\alpha}\,d\tau. \tag{7}$$

(ii) The left Riemann-Liouville derivatives:

$$^{R}D_t^\alpha u(x,t) := \frac{1}{\Gamma(1-\alpha)} \frac{\partial}{\partial t} \int_0^t \frac{u(x,\tau)}{(t-\tau)^\alpha}\,d\tau. \tag{8}$$

(iii) The right Riemann-Liouville derivatives:

$$^{R}_{t}D^\alpha u(x,t) := \frac{1}{\Gamma(1-\alpha)} \frac{\partial}{\partial t} \int_t^T \frac{u(x,\tau)}{(\tau-t)^\alpha}\,d\tau. \tag{9}$$

Many authors believe that the Caputo version is more natural because it makes it easier to manage inhomogeneous initial conditions. Then, the following relationship is related to the two concepts (7) and (8), which can be checked by a direct calculation:

$$^{R}D_t^\alpha u(x,t) = {}^{C}D_t^\alpha u(x,t) + \frac{u(x,0)}{\Gamma(1-\alpha)t^\alpha}. \tag{10}$$

Definition 2 (see [29]). For any real $\sigma>0$, we define the space $^{l}H_0^\sigma(I)$ as the closure of $C_0^\infty(I)$ with respect to the following norm $\|\cdot\|_{^{l}H_0^\sigma(I)}$:

$$\|u\|_{^{l}H^\sigma(I)} := \left(\|u\|^2_{L_2(I)} + |u|^2_{lH_0^\sigma(I)}\right)^{1/2}, \tag{11}$$

where

$$|u|^2_{^{l}H^\sigma(I)} := \left\|{}^{R}_{0}D_t^\sigma u\right\|^2_{L_2(I)}. \tag{12}$$

Definition 3. For any real $\sigma>0$, we define the space $^{r}H_0^\sigma(I)$ as the closure of $C_0^\infty(I)$ with respect to the following norm $\|\cdot\|_{^{r}H_0^\sigma(I)}$:

$$\|u\|_{^{r}H_0^\sigma(I)} := \left(\|u\|^2_{L_2(I)} + |u|^2_{rH_0^\sigma(I)}\right)^{1/2}, \tag{13}$$

where

$$|u|^2_{^{r}H_0^\sigma(I)} := \left\|{}^{R}_{t}\partial_T^\sigma u\right\|^2_{L_2(I)}. \tag{14}$$

Lemma 4 (see [29, 30]). *For any real $\sigma \in \mathbb{R}_+$, if $u \in {}^{l}H^\alpha(I)$ and $v \in C_0^\infty(I)$, then*

$$\left({}^{R}D_t^\sigma u(t), v(t)\right)_{L^2(I)} = \left(u(t), {}^{R}_{t}D^\sigma v(t)\right)_{L^2(I)}. \tag{15}$$

Lemma 5 (see [29, 30]). *For $0<\sigma<2$, $\sigma \neq 1$, $u \in H_0^{\sigma/2}(I)$, on a*

$$^{R}D_t^\sigma u(t) = {}^{R}D_t^{\sigma/2}\,{}^{R}D_t^{\sigma/2} u(t). \tag{16}$$

Lemma 6 (see [29, 30]). *For $\sigma \in \mathbb{R}_+, \sigma \neq n + (1/2)$, the seminorms $|.|_{l_{H^\sigma(I)}}, |.|_{r_{H^\sigma(I)}}$ and $|.|_{c_{H^\sigma(I)}}$ are equivalent. Then, we pose*

$$|\cdot|_{l_{H^\sigma(I)}} = \tilde{}|\cdot|_{r_{H^\sigma(I)}} = \tilde{}|\cdot|_{c_{H^\sigma(I)}}. \tag{17}$$

Lemma 7 (see [29]). *For any real $\sigma > 0$, the space ${}^lH_0^\sigma(I)$ with respect to the norm (11) is complete.*

Definition 8. We denote by $L_2(0, T, L_2(0, d)) := L_2(Q)$ the space of square functions, integrated with the scalar product in the Bochner sense,

$$(u, w)_{L_2(0,T,L_2(0,d))} = \int_0^T ((u, \cdot), (w, \cdot))_{L_2(0,d)} dt. \tag{18}$$

Since the space $L_2(0, d)$ is a Hilbert space, it can be shown that $L_2(0, T, L_2(0, d))$ is a Hilbert space as well. Let $C^\infty(0, T)$ denote the space of infinitely differentiable functions on $(0, T)$ and $C_0^\infty(0, T)$ denote the space of infinitely differentiable functions with compact support in $(0, T)$.

3. Solvability of the Direct Fractional Parabolic Problem

3.1. Position of Problem. In the rectangular domain $Q = (0, d) \times (0, T) = \Omega \times I$, with $d, T < \infty$ and $0 < \alpha < 1$, we shall study the existence and uniqueness of solutions $u = u(x, t)$ to the following fractional parabolic problem:

$$\begin{cases} {}^CD_t^\alpha u(x,t) - \left(\dfrac{\partial^2 u(x,t)}{\partial x^2}\right) + bu(x,t) = \tilde{f}(x,t) & \text{in } Q, \\ u(x,0) = \varphi(x) & \forall x \in (0,d), \\ u(0,t) = u(d,t) = 0 & \forall t \in (0,T). \end{cases} \tag{19}$$

We consider the following fractional parabolic equation of the type

$$\mathscr{L}u = {}^CD_t^\alpha u - \frac{\partial^2 u}{\partial x^2} + bu = \tilde{f}, \tag{20}$$

with the initial condition

$$\ell u = u(x, 0) = \varphi(x), \forall x \in (0, d), \tag{21}$$

and Dirichlet condition

$$u(0, t) = u(d, t) = 0, \forall t \in (0, T), \tag{22}$$

where $b \in \mathbb{R}_*^+$; $\tilde{f}$ and φ are known functions.

We shall assume that the function φ satisfies a compatibility conditions, i.e.,

$$\varphi(0) = \varphi(d) = 0. \tag{23}$$

Now, introducing a new function

$$v(x, t) = u(x, t) - U(x) \Rightarrow u(x, t) = v(x, t) + U(x), \tag{24}$$

where

$$\varphi(x) = U(x). \tag{25}$$

So, we get

$$\begin{cases} {}^CD_t^\alpha v(x,t) - \left(\dfrac{\partial^2 v(x,t)}{\partial x^2}\right) + bv(x,t) = \tilde{f}(x,t) - \mathscr{L}\varphi(x) = f(x,t) & \text{in } Q, \\ v(x,0) = 0 & \forall x \in (0,d), \\ v(0,t) = v(d,t) = 0 & \forall t \in (0,T). \end{cases} \tag{26}$$

Such that

$${}^CD_t^\alpha v(x, t) - \frac{\partial^2 v(x, t)}{\partial x^2} + bv(x, t) = f(x, t), \tag{27}$$

with the initial condition

$$\ell v = v(x, 0) = 0, \quad \forall \mathrm{x} \in (0, \mathrm{d}), \tag{28}$$

the boundary condition of Dirichlet type

$$v(0, t) = v(d, t) = 0, \quad \forall t \in (0, T), \tag{29}$$

where

$$f(x, t) = \tilde{f}(x, t) + \frac{\partial^2 \varphi(x)}{\partial x^2} - b\varphi(x). \tag{30}$$

3.2. A Priori Estimate. In this section, we illustrate the existence and uniqueness of the problem's solution (27)–(29) as a solution of the operator equation

$$Lv = \mathscr{F}, \tag{31}$$

where $L = (\mathscr{L}, \ell)$, with domain of definition B consisting of functions $v \in L^2(Q)$, such that v, ${}^C D_t^\alpha v, (\partial v/\partial x) \in L^2(Q)$, and v verify (29).

The operator L is considered from B to F, where B is the Banach space consisting of all functions $v(x,t)$ having a finite norm

$$\|v\|_B^2 = \left\| {}^C D_t^{\alpha/2} v \right\|_{L^2(Q)}^2 + \|v\|_{L^2(Q)}^2 + \left\| \frac{\partial v}{\partial x} \right\|_{L^2(Q)}^2, \tag{32}$$

and F is the Hilbert space consisting of all elements Fourier $= (f, 0)$ for which the norm $L^2(Q)$ is finite.

Theorem 9. *For any function $u \in B$, we have the inequality*

$$\|v\|_B \le k \|Lv\|_{L^2(Q)}, \tag{33}$$

where k is a positive constant independent of v.

Proof. Multiplying equation (27) by the following function:

$$Mv = v(x,t), \tag{34}$$

and integrating over $Q = (0,d) \times (0,T)$, we get

$$\begin{aligned} &\int_Q \mathscr{L} v \cdot M v dxdt \\ &= \int_Q {}^C D_t^\alpha v(x,t) \cdot v(x,t) dxdt - \int_Q \frac{\partial^2 v(x,t)}{\partial x^2} v(x,t) dxdt \\ &\quad + \int_Q b \cdot v^2(x,t) dxdt = \int_Q f(x,t) \cdot v(x,t) dxdt. \end{aligned} \tag{35}$$

As $v(x,0) = 0$, so by applying Lemmas 4, 5, and 6 becomes

$$\begin{aligned} &\int_Q {}^C D_t^\alpha v(x,t).v(x,t) dxdt \\ &= \left({}^C D_t^\alpha v(x,t), v(x,t) \right)_{L^2(Q)} \\ &= \left({}^R D_t^{(\alpha/2)} {}^R D_t^{\alpha/2} v(x,t), \quad v(x,t) \right)_{L^2(Q)} \\ &\cdot \left({}^R D_t^{\alpha/2} v(x,t), \quad {}^R_t D^{\alpha/2} v(x,t) \right)_{L^2(Q)} \\ &= |u|^2_{{}^c H^\alpha(Q)} 2 \cong |u|^2_{{}^l H^\alpha(Q)} \\ &\qquad \text{(According to Lemma 2)} \\ &= \left\| {}^C D_t^{\alpha/2} v \right\|_{L^2(Q)}^2, \quad \text{(According to Lemma 1)} \\ &\qquad \text{(According to Lemma 3)} \end{aligned} \tag{36}$$

and by integration by parts over $(0,d)$, we get

$$-\int_Q \frac{\partial^2 v(x,t)}{\partial x^2} v(x,t) dxdt = \int_Q \left(\frac{\partial v(x,t)}{\partial x} \right)^2 dxdt. \tag{37}$$

So, we obtain

$$\begin{aligned} &\int_Q \left({}^R D_t^\alpha v(x,t) - \frac{\partial^2 v(x,t)}{\partial x^2} + b v(x,t) \right) \cdot M v dxdt \\ &\cong \left\| R D_t^{\alpha/2} v \right\|_{L^2(Q)}^2 + \int_Q \left(\frac{\partial v(x,t)}{\partial x} \right)^2 dxdt + \int_Q b v^2(x,t) dxdt \\ &\le \frac{1}{2\varepsilon} \int_Q |f(x,t)|^2 dxdt + \frac{\varepsilon}{2} \int_Q |v(x,t)|^2 dxdt. \end{aligned} \tag{38}$$

So, we get

$$\begin{aligned} &\left\| {}^C D_t^{\alpha/2} v \right\|_{L^2(Q)}^2 + \int_Q \left(\frac{\partial v(x,t)}{\partial x} \right)^2 dxdt + \int_Q \left(b - \frac{\varepsilon}{2} \right) v^2(x,t) dxdt \\ &\le \frac{1}{2\varepsilon} \int_Q |f(x,t)|^2 dxdt, \end{aligned} \tag{39}$$

which give

$$\begin{aligned} &\left\| {}^C D_t^{\alpha/2} v \right\|_{L^2(Q)}^2 + \int_Q \left(\frac{\partial v(x,t)}{\partial x} \right)^2 dxdt + \int_Q \left(b - \frac{\varepsilon}{2} \right) v^2(x,t) dxdt \\ &\le \frac{1}{2\varepsilon} \int_Q |f(x,t)|^2 dxdt. \end{aligned} \tag{40}$$

So, we have

$$\left\| {}^C D_t^{\alpha/2} v \right\|_{L^2(Q)}^2 \le \frac{1}{2\varepsilon} \|f\|_{L^2(Q)}^2. \tag{41}$$

On the other hand, we have

$$\left\| \frac{\partial v}{\partial x} \right\|_{L^2(Q)}^2 \le \frac{1}{2\varepsilon} \|f\|_{L^2(Q)}^2. \tag{42}$$

Also, we have

$$\|v\|_{L^2(Q)}^2 \le \frac{1}{2\varepsilon(b - (\varepsilon/2))} \|f\|_{L^2(Q)}^2. \tag{43}$$

By combining (41), (42), and (43), for $\varepsilon < b/2$, we get

$$\begin{aligned} &\left\| {}^C D_t^{\alpha/2} v \right\|_{L^2(Q)}^2 + \left\| \frac{\partial v}{\partial x} \right\|_{L^2(Q)}^2 + \|v\|_{L^2(Q)}^2 \\ &\le \frac{1}{2\varepsilon} \left(1 + \frac{1}{(b - (\varepsilon/2))} \right) \|f\|_{L^2(Q)}^2. \end{aligned} \tag{44}$$

Finally, it follows that

$$\left\|{}^{C}D_t^{\alpha/2}v\right\|_{L^2(Q)}^2 + \left\|\frac{\partial v}{\partial x}\right\|_{L^2(Q)}^2 + \|v\|_{L^2(Q)}^2 \leq C\|f\|_{L^2(Q)}^2, \quad (45)$$

with

$$C = \frac{1}{2\varepsilon}\left(1 + \frac{1}{(b-(\varepsilon/2))}\right). \quad (46)$$

Therefore, we obtain that

$$\|v\|_B \leq k\|Lv\|_F, \text{ where } k = \sqrt{C}. \quad (47)$$

Hence, the uniqueness of the solution. □

Remark 10. This inequality $\|v\|_B \leq k\|Lv\|_F$ gives the uniqueness of the solution, indeed:

Let v_1 and v_2 two solutions, so

$$\begin{cases} Lv_1 = \mathscr{F} \\ Lv_2 = \mathscr{F} \end{cases} \Rightarrow L(v_1 - v_2) = 0, \quad (48)$$

then

$$\|v_1 - v_2\|_B \leq k\|0\|_F \Rightarrow \|v_1 - v_2\|_B \leq 0 \Rightarrow v_1 - v_2 = 0, \quad (49)$$

which gives the uniqueness of the solution.

Proposition 11. *The operator L from B to F admits a closure.*

Proof. Let $(v_n)_{n\in\mathbb{N}} \subset D(L)$ be a sequence such that:

$$\begin{aligned} v_n &\longrightarrow 0 \text{ in } B, \\ Lv_n &\longrightarrow \mathscr{F} \text{ in } F, \end{aligned} \quad (50)$$

it must be shown that

$$f \equiv 0. \quad (51)$$

The convergence of v_n toward 0 in B entails that

$$v_n \longrightarrow 0 \text{ in} (C_0^\infty(Q_T))'. \quad (52)$$

As the continuity of the fractional derivation(2) and the derivation of the first order (as a particular case of the fractional derivative) of $(C_0^\infty(Q_T))'$ in $(C_0^\infty(Q_T))'$, then (52) implies

$$\mathscr{L}u_n \longrightarrow 0 \text{ in} (C_0^\infty(Q_T))'. \quad (53)$$

On the other hand, the convergence of $\mathscr{L}v_n$ to f in $F = L^2(Q_T)$ implies that

$$\mathscr{L}u_n \longrightarrow f \text{ in} (C_0^\infty(Q_T))'. \quad (54)$$

By virtue of the uniqueness of the limit in $(C_0^\infty(Q_T))'$, we conclude between (53) and (54) that

$$f \equiv 0. \quad (55)$$

Hence, the operator L is closable. □

Definition 12. Let $\bar{L}$ the closure of L and $D(\bar{L})$ the definition domain of $\bar{L}$. The solution of the equation

$$\bar{L}v = \mathscr{F}, \quad (56)$$

is called generalized strong solution of the problem (27)–(29).

Theorem 9 is valid for a generalized strong solution, i.e., we have the following inequality:

$$\|v\|_B \leq k\left\|\bar{L}v\right\|_F, \forall v \in D(\bar{L}). \quad (57)$$

Consequently, this last inequality entails the following corollaries:

Corollary 13. *The strong solution of the problem (27)–(29) is unique and depends continuously on $f \in F$.*

Corollary 14. *The range $R(\bar{L})$ of the operator $\bar{L}$ is equal to the closure $\overline{R(L)}$ of $R(L)$.*

Proof. Let $z \in \overline{R(L)}$, then there exists a Cauchy sequence $(z_n)_n$ in F consists of the elements of the set $R(L)$ such that

$$\lim_{n\longrightarrow+\infty} z_n = z. \quad (58)$$

So there is a corresponding sequence $(v_n)_n \subset D(L)$ such that

$$Lv_n = z_n. \quad (59)$$

From the estimate (41), we obtain

$$\left\|v_p - v_q\right\|_B \leq k\left\|Lv_p - Lv_q\right\|_F \longrightarrow 0, \text{ when } p, q \longrightarrow +\infty. \quad (60)$$

We can deduce that $(v_n)_n$ is a Cauchy sequence in B, so there is $v \in B$

$$\lim_{n\longrightarrow+\infty} v_n = v \text{ in } B. \quad (61)$$

By virtue of the definition of $\bar{L}$ ($\lim_{n\longrightarrow+\infty} v_n = v$ in B; if $\lim_{n\longrightarrow+\infty} Lv_n = \lim_{n\longrightarrow+\infty} z_n = z$, so $\lim_{n\longrightarrow+\infty} \bar{L}v_n = z$ and as $\bar{L}$ is closed so $\bar{L}v = z$), the function v verifies that

$$v \in D(\bar{L}), \quad \bar{L}v = z. \quad (62)$$

Thus, $z \in R(\bar{L})$, then

$$\overline{R(L)} \subset R(\bar{L}). \tag{63}$$

So we conclude here that $R(\bar{L})$ is closed because it is complete (any complete subspace of a metric space (not necessarily complete) is closed).

It remains to show the opposite inclusion.

Let $z \in R(\bar{L})$, then there is a sequence of $(z_n)_n$ in F consists of the elements of the set $R(\bar{L})$ such that

$$\lim_{n \longrightarrow +\infty} z_n = z, \tag{64}$$

where $z \in R(\bar{L})$, because $R(\bar{L})$ is closed subset of a complete space F; then, $R(\bar{L})$ is complete.

So there is a corresponding sequence $(v_n)_n \subset D(\bar{L})$ such that

$$\bar{L}v_n = z_n. \tag{65}$$

From the estimate (57), we obtain

$$\|v_p - v_q\|_B \leq k\|\bar{L}v_p - \bar{L}v_q\|_F \longrightarrow 0, \text{if } p, q \longrightarrow +\infty. \tag{66}$$

We can deduce that $(v_n)_n$ is a Cauchy sequence in B, so there is $v \in B$

$$\lim_{n \longrightarrow +\infty} v_n = v \text{in} B. \tag{67}$$

Once more, there is a corresponding sequence $(L(v_n))_n \in R(L)$ such that

$$Lv_n = \bar{L}v_n \text{ over } R(L), \forall n. \tag{68}$$

Then

$$\lim_{n \longrightarrow +\infty} Lv_n = z. \tag{69}$$

Consequently, $z \in \overline{R(L)}$, and then, we conclude that

$$R(\bar{L}) \subset \overline{R(L)}. \tag{70}$$

□

3.3. Existence of Solution. To show the existence of solutions, we prove that $R(L)$ is dense in F for all $u \in B$ and for arbitrary $\mathscr{F} = (f, 0) \in F$.

Theorem 15. *The problem (27)–(29) admits a solution.*

Proof. The scalar product of F is defined by

$$(Lv, W)_F = \int_{Q_T} \mathscr{L}v \cdot w dxdt, \quad \text{where} \quad W = (w, 0) \in D(L). \tag{71}$$

If we put $w \in R(L)^{\perp}$, we have

$$\int_{Q_T} \left({}^C D_t^{\alpha} v(x,t) - \frac{\partial^2 v(x,t)}{\partial x^2} + bv(x,t) \right) \cdot w(x,t) dxdt = 0, \tag{72}$$

where ${}^C D_t^{\alpha} v$, $\partial v / \partial x$, $v \in L^2(Q_T)$, with v satisfies the boundary conditions of (27)–(29). From (72), we get the equality

$$\int_{Q_T} {}^C D_t^{\alpha} v(x,t) \cdot w(x,t) dxdt - \int_{Q_T} \frac{\partial^2 v(x,t)}{\partial x^2} \cdot w(x,t) dxdt + b \int_{Q_T} v(x,t) \cdot w(x,t) dxdt = 0. \tag{73}$$

And from the equality (73), we give the function w in terms of v as follows:

$$w = v, \tag{74}$$

then $w \in L^2(Q_T)$.

Replacing w in (73) by its representation (74) and integrating by parts each term of (73) and by taking the condition of v, we obtain

$$\int_{Q_T} \left(CD_t^{\alpha/2} v(x,t) \right)^2 dxdt + \int_{Q_T} bv^2(x,t) dxdt \leq -\int_{Q_T} \left(\frac{\partial v(x,t)}{\partial x} \right)^2 dxdt \leq 0, \tag{75}$$

then

$$\left\| {}^C D_t^{\alpha/2} v \right\|^2_{L^2(Q_T)} + b\|v\|^2_{L^2(Q_T)} \leq 0. \tag{76}$$

Hence

$$\|v\|_{L^2(Q_T)} = 0. \tag{77}$$

And thus, $v = 0$ in Q_T which gives $w = 0$ in Q_T. This proves Theorem 15. So $\overline{R(L)} = F$. □

4. Existence and Uniqueness of the Solution of Main Problem

We are finding a solution in the form of the original inverse problem. $\{u, f\} = \{z, f\} + \{y, 0\}$ where y is the solution of the direct problem

$${}^C D_t^{\alpha} y - \Delta y + \beta y = 0. \quad (x,t) \in Q_T, \tag{78}$$

$$y(x,0) = \varphi(x), \quad x \in \Omega, \tag{79}$$

$$y(x,t) = 0, \quad (x,t) \in \partial\Omega \times [0,T], \tag{80}$$

while the pair $\{z, f\}$ is the solution of the inverse problem

$$^{C}D_t^{\alpha} z - \Delta z + \beta z = f(t) g(x, t). \quad (x, t) \in Q, \tag{81}$$

$$z(x, 0) = 0, \quad x \in \Omega, \tag{82}$$

$$z(x, t) = 0, \quad (x, t) \in \partial\Omega \times [0, T], \tag{83}$$

$$\int_{\Omega} v(x) z(x, t) dx = E(t), t \in [0, T], \tag{84}$$

where

$$E(t) = \theta(t) - \int_{\Omega} v(x) y(x, t) dx. \tag{85}$$

We will assume that the functions that appear in the problem data are measurable and fulfill the following conditions:

$$\begin{cases} g \in C((0, T), L_2(\Omega)), v \in W_2^1(\Omega), E \in W_2^2(0, T), \\ \|g(x, t)\| \leqslant m; |g^*(\mathrm{t})| \geqslant p > 0, \quad \text{for} \quad p \in \mathbb{R}, (\mathrm{x}, \mathrm{t}) \in \mathrm{Q_T}, \\ \varphi(x) \in W_2^1(\Omega) \quad \text{where} \quad g^* \quad \text{is} \quad \text{defind} \quad \text{in} \quad (5). \end{cases} \tag{86}$$

The correspondence between f and z can be seen as one way of defining the linear operator.

$$A : L_2(0, T) \longrightarrow L_2(0, T), \tag{87}$$

with the values

$$(Af)(t) = \frac{1}{g^*} \left\{ \int_{\Omega} \nabla z \nabla v dx \right\}. \tag{88}$$

In this view, the linear equation of the second form for the function is rational to refer to f over the space $L_2(0, T)$:

$$f = Af + W, \tag{89}$$

where

$$W = \frac{CD_t^{\alpha} E + \beta E}{g^*}. \tag{90}$$

Remark 16. As $\{u, f\} = \{z, f\} + \{y, 0\}$ where y is the solution of the direct problem (78)–(80). Obviously, the previous section implies that y exists and is unique, but instead of demonstrating the solvability of the initial problem (1)–(4), we demonstrate the existence and uniqueness of the inverse problem (81)–(84) solution.

Theorem 17. *Suppose the input of the inverse problem data (81)–(84) satisfies (H). Then, the following assertions are valid: (i) if the inverse problem (81)–(84) is solvable, then so is equation (89). And (ii) if equation (89) has a solution and the condition of compatibility has*

$$E(0) = 0, \tag{91}$$

holds, then a solution to the inverse problem exists.

Proof.

(i) Suppose that the inverse problem (81)–(84) is solvable. We denote its solution by $\{z, f\}$. Multiplying the function v scalarly in $L_2(\Omega)$ both sides of (81), we get

$$^{C}D_t^{\alpha} \int_{\Omega} zv dx + \int_{\Omega} \nabla z \nabla v dx + \beta \int_{\Omega} zv dx = \int_{\Omega} f(t) g^*(x, t). \tag{92}$$

With (84) and (88), from (92), it follows that $f = Af + ((CD_t^{\alpha} E + \beta E)/g^*)$. This gives that f solves equation (89).

(ii) Equation (89) has a solution in space, according to the assumption, $L_2(0, T)$, say f. The resulting relationship (81)–(83) can be viewed as a direct problem with a unique solution $z \in W_2^1(Q_T)$ when inserting this function in (81). Let us show that the z function also satisfies the condition of integral overdetermination (84). By equation (92), the function z is subject to the following relation

$$^{C}D_t^{\alpha} E + \beta E + \int_{\Omega} \nabla z \nabla v dx = f(t) g^*(t). \tag{93}$$

Subtracting equation (92) from equation (93), we get

$$^{C}D_t^{\alpha} \int_{\Omega} zv dx + \beta \int_{\Omega} zv dx = {}^{C}D_t^{\alpha} E + \beta E. \tag{94}$$

Integrating the preceding differential equation and taking into account the compatibility condition (89), we find that the overdetermination condition (84) is satisfied by z and the function pair $\{z, f\}$ is a solution to the inverse problem (81)–(84).

This completes the theorem's proof. □

Now, we are touching on some properties of operator A.

Lemma 18. *Let the condition (H) hold. Then, there exists a positive ε for which A is a contracting operator in $L_2(0, T)$.*

Proof. Obviously, (88) yields the estimate

$$\|Af\|_{L_2(0,T)} \leq \frac{k}{p} \left(\int_0^T \|\nabla z(.,\tau)\|_{L_2(\Omega)}^2 d\tau \right)^{1/2}, \tag{95}$$

where

$$k = \|\nabla v\|_{L_2(\Omega)}. \tag{96}$$

Multiplying both sides of (81) by z scalarly in $L_2(Q_T)$ and integrating the resulting by parts with use of (82), we get

$$\begin{aligned}&\left\|{}^C D_t^{\alpha/2} z\right\|^2_{L_2(Q_T)} + \|\nabla z\|^2_{L_2(Q_T)} + \beta\|z\|^2_{L_2(Q_T)}\\ &\quad = \int_0^T \left(f(t)\int_\Omega g(x,t) z dx\right) dt.\end{aligned} \tag{97}$$

Thus, by using the Cauchy's ε-inequality, we obtain

$$\begin{aligned}&\left\|{}^C D_t^{\alpha/2} z\right\|^2_{L_2(Q_T)} + \|\nabla z\|^2_{L_2(Q_T)} + \beta\|z\|^2_{L_2(Q_T)}\\ &\quad \le \frac{m|\Omega|}{2\varepsilon}\int_0^T |f(t)|^2 dt + \frac{\varepsilon}{2}\|z\|^2_{L_2(Q_T)}.\end{aligned} \tag{98}$$

Choosing $0 < \varepsilon < 2\beta$, we get

$$\begin{aligned}&\left\|{}^C D_t^{\alpha/2} z\right\|^2_{L_2(Q_T)} + \|\nabla z\|^2_{L_2(Q_T)} + \left(\beta - \frac{\varepsilon}{2}\right)\|z\|^2_{L_2(Q_T)}\\ &\quad \le \frac{m|\Omega|}{2\varepsilon}\int_0^T |f(\tau)|^2 dt.\end{aligned} \tag{99}$$

Omitting some terms on the left-hand side (99) leads to

$$\|\nabla z\|^2_{L_2(Q_T)} = \int_0^T \|\nabla z(.,\tau)\|^2_{L_2(\Omega)} d\tau \le \frac{m|\Omega|}{2\varepsilon}\int_0^T |f(\tau)|^2 dt. \tag{100}$$

According to (95) and (100), we can obtain the following estimate:

$$\|Af\|_{L_2(0,T)} \le \delta\int_0^T |f(\tau)|^2 dt, \quad 0 \leqslant t \leqslant T, \tag{101}$$

where

$$\delta = \frac{k\sqrt{m}|\Omega|}{p\sqrt{2\varepsilon}}. \tag{102}$$

So, we obtain

$$\|Af\|_{L_2(0,T)} \le \delta\|f\|_{L_2(0,T)}. \tag{103}$$

It is obvious from the above that there is positive ε such that

$$\delta < 1. \tag{104}$$

Inequality (103) shows that the operator A is a contracting mapping on $L_2(0, T)$. □

The following result may be useful with respect to the particular solvability of the inverse problem concerned.

Theorem 19. *Let the compatibility condition (91) and the condition (H) hold. Then, the inverse problem (81)–(84) has a unique solution $\{z, f\}$.*

Proof. This means that the equation (89) has a unique solution f in $L_2(0, T)$.

The existence of a solution to the inverse problem (81)–(84) is verified, according to Lemma 6.

The uniqueness of this solution has yet to be proven.

Suppose the contrary that there are two distinct solutions $\{z_1, f_1\}$ and $\{z_2, f_2\}$ of the under consideration inverse problem.

Also, the linear operator A is contracting on $L_2(0, T)$ from Lemma 18, which gives that $f_1 = f_2$; then, by the theorem of the uniqueness of the solution of main direct problem (78)–(80), we will just have $z_1 = z_2$. □

Corollary 20. *The solution f to equation (91) depends continuously, under the conditions of Theorem 19, on the data W.*

Proof. Let V_1 and V_2 twosets of data that satisfy Theorem 19's assumptions.

Let f and g be solutions of the equation (89) corresponding to the data V_1 and V_2, respectively. According to (103), we have

$$\begin{aligned}f &= Af + V_1,\\ g &= Ag + V_2.\end{aligned} \tag{105}$$

Let us estimate the difference first, $f - g$. It is easy to see with the use of (103) that

$$\begin{aligned}\|f - g\|_{L_2(0,T)} &= \|(Af + V_1) - (Ag + V_2)\|_{L_2(0,T)}\\ &= \|A(f - g) + (V_1 - V_2)\|_{L_2(0,T)}\\ &\leqslant \delta\|f - g\|_{L_2(0,T)} + \|(V_1 - V_2)\|_{L_2(0,T)},\end{aligned} \tag{106}$$

so, we get

$$\|f - g\|_{L_2(0,T)} \leqslant \frac{1}{(1-\delta)}\|(V_1 - V_2)\|_{L_2(0,T)}. \tag{107}$$

□

5. Conclusion and Perspectives

This work contains a new inverse problem by investigating the fractional derivatives where we develop the method of fixed point and energy inequality method for proving the solvability of an inverse fractional problem. We note that our work extends to the existence of open problems as a study of the nonlinear case of this problem and the numerical part.

Data Availability

No data were used to support this study.

Disclosure

An earlier version of this manuscript has been presented as online conference in Modern Fractional Calculus and Its Applications (OCMFCA-2020) Biruni University Istanbul Turkey.

Conflicts of Interest

The authors declare no conflict of interest.

Acknowledgments

The research was supported by the Taif University Researchers Supporting Project number (TURSP-2020/77), Taif University, Taif, Saudi Arabia.

References

[1] M. I. Ivanchov, *Inverse Problems for Equations of Parabolic Type*, VNTL, Lviv, 2003.

[2] A. G. Ramm, *Inverse Problems*, Springer, New York, 2005.

[3] T.-E. Oussaeif and A. Bouziani, "Inverse problem of a hyperbolic equation with an integral overdetermination condition," *Electronic Journal of Differential Equations*, vol. 138, pp. 1–7, 2016.

[4] T.-E. Oussaeif and A. Bouziani, "An inverse coefficient problem for a parabolic equation under nonlocal boundary and integral overdetermination conditions," *International Journal of Partial Differential Equations and Applications*, vol. 2, no. 3, pp. 38–43, 2014.

[5] J. Cannon, Y. Lin, and S. Wang, "Determination of a control parameter in a parabolic partial differential equation," *The ANZIAM Journal*, vol. 33, pp. 149–163, 1991.

[6] J. Cannon, Y. Lin, and S. Wang, "Determination of source parameter in parabolic equations," *Meccanica*, vol. 27, no. 2, pp. 85–94, 1992.

[7] A. Fatullayev, N. Gasilov, and I. Yusubov, "Simultaneous determination of unknown coefficients in a parabolic equation," *Applicable Analysis*, vol. 87, no. 10-11, pp. 1167–1177, 2008.

[8] M. Ivanchov and N. Pabyrivska, "Simultaneous determination of two coefficients of a parabolic equation in the case of nonlocal and integral conditions," *Ukrainian Mathematical Journal*, vol. 53, no. 5, pp. 674–684, 2001.

[9] M. Ismailov and F. Kanca, "An inverse coefficient problem for a parabolic equation in the case of nonlocal boundary and overdetermination conditions," *Mathematicsl Methods in the Applied Sciences*, vol. 34, no. 6, pp. 692–702, 2011.

[10] F. Kanca and M. Ismailov, "The inverse problem of finding the time-dependent diffusion coefficient of the heat equation from integral overdetermination data," *Inverse Problems in Science and Engineering*, vol. 20, no. 4, pp. 463–476, 2012.

[11] V. L. Kamynin, "Unique solvability of the inverse problem of determination of the leading coefficient in a parabolic equation," *Differential Equations*, vol. 47, no. 1, pp. 91–101, 2011.

[12] J. R. Cannon and Y. Lin, "An inverse problem of finding a parameter in a semi-linear heat equation," *Journal of Mathematical Analysis and Applications*, vol. 145, no. 2, pp. 470–484, 1990.

[13] A. Bouziani, "Solution forte d'un problem mixte avec condition non locales pour une classe d'equations hyperboliques," *Bulletin de la Classe des sciences (Académie royale de Belgique)*, vol. 8, pp. 53–70, 1997.

[14] N. I. Ionkin, "Solution of one boundary value problem of heat conduction theory with a nonclassical boundary condition," *Differentsial'nye Uravneniya*, vol. 13, no. 2, pp. 294–304, 1977.

[15] A. I. Prilepko and D. G. Orlovski, "Determination of the parameter of an evolution equation and inverse problems of mathematical physics. II," *Differential Equations (journal)*, vol. 21, pp. 694–700, 1985.

[16] J. R. Cannon and Y. Lin, "/Determination of a parameter $p(t)$ in some quasilinear parabolic differential equations," *Inverse Problems*, vol. 4, no. 1, pp. 35–45, 1988.

[17] A. B. Kostin, "Inverse Problem for the Heat Equation with Integral Overdetermination," in *Inverse Problems for Mathematical Modelling of Physical Processes. Collection of Scientific Reports*, pp. 45–49, Moscow Institute of Engineering Physics, Moscow, 1991.

[18] V. L. Kamynin, ""On convergence of the solutions of inverse problems for parabolic equations with weakly converging coefficients", elliptic and parabolic problems (Pont- a-Mousson, 1994)," *Pitman Research Notes in Mathematics Series*, vol. 325, pp. 130–151, 1995.

[19] T.-E. Oussaeif and A. Bouziani, "Existence and uniqueness of solutions to parabolic fractional differential equations with integral conditions," *Electronic Journal of Differential Equations*, vol. 179, pp. 1–10, 2014.

[20] A. Lopushanskyi, H. Lopushanska, and V. Rapita, "Inverse problem in the space of generalized functions," *Ukrainian Mathematical Journal*, vol. 68, article 269282, 2016.

[21] A. I. Prilepko, D. G. Orlovsky, and I. A. Vasin, *Methods for Solving Inverse Problems in Mathematical Physics*, Marcel Dekker Inc, 1999.

[22] V. L. Kamynin and I. A. Vasin, "Asymptotic behaviour of the solutions of inverse problems for parabolic equations with irregular coefficients," *Sbornik: Mathematics*, vol. 188, no. 3, pp. 371–387, 1997.

[23] K. B. Oldham and J. Spanier, *The Fractional Calculus*, Academic Press, New York, 1974.

[24] A. A. Kilbas, H. M. Srivastava, and J. J. Trujillo, *Theory and Applications of Fractional Differential Equations*, Elsevier, Amsterdam, 2006.

[25] J. H. He, "Nonlinear Oscillation with Fractional Derivative and Its Applications," in *International Conference on Vibrating Engineering'98*, pp. 288–291, Dalian, China, 1998.

[26] J. H. He, "Some applications of nonlinear fractional differential equations and their approximations," *Bulletin of Science and Technology*, vol. 15, pp. 86–90, 1999.

[27] J. H. He, "Approximate analytical solution for seepage flow with fractional derivatives in porous media," *Computer Methods in Applied Mechanics and Engineering*, vol. 167, no. 1-2, pp. 57–68, 1998.

[28] R. Metzler and J. Klafter, "The random walk's guide to anomalous diffusion: a fractional dynamics approach," *Physics Reports*, vol. 339, no. 1, pp. 1–77, 2000.

[29] X. J. Li and C. J. Xu, "A space-time spectral method for the time fractional diffusion equation," *SIAM Journal on Numerical Analysis*, vol. 47, no. 3, pp. 2108–2131, 2009.

[30] X. J. Li and C. J. Xu, "Existence and uniqueness of the weak solution of the space-time fractional diffusion equation and a spectral method approximation," *Communications in Computational Physics*, vol. 8, no. 5, pp. 1016–1051, 2010.

Hindawi
Journal of Function Spaces
Volume 2022, Article ID 1079214, 11 pages
https://doi.org/10.1155/2022/1079214

Research Article

Theory of Fractional Hybrid Problems in the Frame of ψ-Hilfer Fractional Operators

Saeed M. Ali,[1] **Wedad Albalawi**,[2] **Mohammed S. Abdo**,[3] **Heba Y. Zahran**,[4,5,6] **and Abdel-Haleem Abdel-Aty**[7,8]

[1]*Department of Basic Engineering Sciences, College of Engineering, Imam Abdulrahman Bin Faisal University, P.O. Box 1982, Dammam 34151, Saudi Arabia*
[2]*Department of Mathematical Sciences, College of Science, Princess Nourah bint Abdulrahman University, P.O. Box 84428, Riyadh 11671, Saudi Arabia*
[3]*Department of Mathematics, Hodeidah University, P.O. Box 3114, Al-Hudaydah, Yemen*
[4]*Laboratory of Nano-Smart Materials for Science and Technology (LNSMST), Department of Physics, Faculty of Science, King Khalid University, P.O. Box 9004, Abha 61413, Saudi Arabia*
[5]*Research Center for Advanced Materials Science (RCAMS), King Khalid University, P.O. Box 9004, Abha 61413, Saudi Arabia*
[6]*Nanoscience Laboratory for Environmental and Biomedical Applications (NLEBA), Metallurgical Lab. 1, Department of Physics, Faculty of Education, Ain Shams University, Roxy, Cairo 11757, Egypt*
[7]*Department of Physics, College of Sciences, University of Bisha, P.O. Box 344, Bisha 61922, Saudi Arabia*
[8]*Physics Department, Faculty of Science, Al-Azhar University, Assiut 71524, Egypt*

Correspondence should be addressed to Mohammed S. Abdo; msabdo@hoduniv.net.ye

Received 16 December 2021; Revised 15 February 2022; Accepted 17 February 2022; Published 20 March 2022

Academic Editor: Youssri Hassan Youssri

In the present manuscript, we develop and extend a qualitative analysis for two classes of boundary value problems for nonlinear hybrid fractional differential equations with hybrid boundary conditions involving a ψ-Hilfer fractional order derivative introduced by Sousa and de Oliveira (2018). First, we derive the equivalent fractional integral equations to the proposed problems from some properties of the ψ-fractional calculus. Next, we establish the existence theorems in the weighted spaces via equivalent fractional integral equations with the help of Dhage's fixed-point theorem (2004). Besides, for an adequate choice of the kernel ψ, we recover most of all the preceding results on fractional hybrid equations. Finally, two examples are constructed to make our main findings effective.

1. Introduction

Recently, a lot of keen interest in the topic of fractional calculus (FC) has been shown by many researchers and investigators in view of its theoretical development and extensive applications in the applied and natural sciences. Different types of differential and integral operators of arbitrary orders have been introduced by Kilbas et al. [1]. In the same regard, Atangana and Baleanu [2] proposed a new fractional derivative (FD) based on a nonsingular and nonlocal kernel. On the advanced improvement of the FC without a singular kernel of the sinc function, the Yang-Gao-Machado-Baleanu FD was introduced in [3]. Some properties of the FD without a singular kernel were introduced by Lozada and Nieto [4].

Hilfer in [5] proposed a generalization of the Riemann-Liouville fractional derivative (RLFD) and Caputo fractional derivative (CFD) when the author deliberated fractional time evolution in physical phenomena. The author named it a generalized FD, whereas more recently, it was named the Hilfer fractional derivative (HFD). This operator carries two parameters (α, β) that may be decreased to the RLFD and CFD definitions if $\beta = 0$ and $\beta = 1$, respectively. So, such

a derivative incorporates between the RLFD and CFD. Some important laws and applications of this operator are obtained in [6, 7] and the references therein.

Initial value problems (IVPs) involving the HFD were investigated by many authors, like Furati et al. [8], Gu and Trujillo [9], and Wang and Zhang [10]. Some existence and uniqueness results of IVPs for ψ-Hilfer-type coupled hybrid equations were obtained in [11]. Boundary value problems (BVPs) with the nonlocal conditions and the HFD were studied in [12]. The authors in [13] investigated the existence and stability of the solution of BVPs for ψ-Hilfer-type fractional integrodifferential equations with boundary conditions (BCs).

ψ-Fractional derivatives (ψ-FDs) have been considered in [1] to be a generalization of RLFD. Some properties of these operators have been given by Agrawal in [14]. These operators are different from the other classical operators because the kernel is shown to be linked to another function ψ. For instance, Almeida [15] gave a new generalization of CFD with some interesting properties. In addition, the authors in [16] introduced a generalized type of the Laplace transform of generalized fractional operators in the frame of both RLFD and CFD.

The new version of the HFD with respect to another function ψ has been introduced by Sousa and de Oliveira [17]. Recently, the investigation of diverse qualitative properties of solutions to several fractional differential equations (FDEs) involving generalized FDs has become the key theme of applied mathematics research. Many interesting results concerning the existence and stability of solutions by using various kinds of fixed-point techniques were formulated; e.g., Abdo et al. [18, 19] investigated various types of the Ulam-Hyers stability for ψ-Hilfer fractional problems with infinite delay and without infinite delay, respectively. The Ulam-Hyers-Rassias stability for FDEs using the ψ-Hilfer operator was discussed by Sousa and de Oliveira [20].

On the other hand, hybrid-type FDEs have attained a considerable saucepan of interest and investigations of several researchers. This category of hybrid FDEs comprises the perturbations of primitive differential equations in various manners. For instance, Dhage and Lakshmikantham [21] considered the following IVPs for hybrid DEs:

$$\begin{cases} \dfrac{d}{d\vartheta}\left(\dfrac{\varkappa(\vartheta)}{\mathbf{q}(\vartheta,\varkappa(\vartheta))}\right) = \mathbf{p}(\vartheta,\varkappa(\vartheta)), \text{a.e.}\vartheta \in \mho := [0,b], \\ \varkappa(\vartheta)|_{\vartheta=\vartheta_0} = \varkappa_0 \in \mathbb{R}, \end{cases} \tag{1}$$

where $\mathbf{p} \in C(\mho\times\mathbb{R},\mathbb{R})$ and $\mathbf{q} \in C(\mho\times\mathbb{R},\mathbb{R}\setminus\{0\})$. Zhao et al. [22] studied the following hybrid FDEs with RLFD:

$$\begin{cases} {}^{RL}\mathfrak{D}_{0^+}^{\theta_1}\left(\dfrac{\varkappa(\vartheta)}{\mathbf{q}(\vartheta,\varkappa(\vartheta))}\right) = \mathbf{p}(\vartheta,\varkappa(\vartheta)), \text{a.e.}\vartheta \in \mho, \\ \varkappa(\vartheta)|_{\vartheta=\vartheta_0} = \varkappa_0 \in \mathbb{R}, \end{cases} \tag{2}$$

where $\mathbf{p} \in C(\mho\times\mathbb{R},\mathbb{R})$ and $\mathbf{q} \in C(\mho\times\mathbb{R},\mathbb{R}\setminus\{0\})$.

On the other hand, Benchohra et al. [23] considered the following BVP for the Caputo-type FDE:

$$\begin{cases} {}^{C}\mathfrak{D}_{0^+}^{\theta_1}\varkappa(\vartheta) = \mathbf{p}(\vartheta,\varkappa(\vartheta)), \vartheta \in \mho, \\ c_1\varkappa(\vartheta)|_{\vartheta=0} + c_2\varkappa(\vartheta)|_{\vartheta=b} = d, \end{cases} \tag{3}$$

where $0 < \theta_1 < 1, c_1, c_2, d \in \mathbb{R}$ with $c_1 + c_2 \neq 0$, and $\mathbf{p} \in C(\mho\times\mathbb{R},\mathbb{R})$.

Hilal and Kajouni [24] considered the BVP for Caputo-type hybrid FDEs with BC:

$$\begin{cases} {}^{C}\mathfrak{D}_{0^+}^{\theta_1}\left(\dfrac{\varkappa(\vartheta)}{\mathbf{q}(\vartheta,\varkappa(\vartheta))}\right) = \mathbf{p}(\vartheta,\varkappa(\vartheta)), \vartheta \in \mho, \\ c_1\left.\dfrac{\varkappa(\vartheta)}{\mathbf{q}(\vartheta,\varkappa(\vartheta))}\right|_{\vartheta=0} + c_2\left.\dfrac{\varkappa(\vartheta)}{\mathbf{q}(\vartheta,\varkappa(\vartheta))}\right|_{\vartheta=b} = d, \end{cases} \tag{4}$$

where $0 < \theta_1 < 1, c_1, c_2, d \in \mathbb{R}$ with $c_1 + c_2 \neq 0$, $\mathbf{p} \in C(\mho\times\mathbb{R},\mathbb{R})$, and $\mathbf{q} \in C(\mho\times\mathbb{R},\mathbb{R}\setminus\{0\})$.

However, as far as we could possibly know, no one considered the existence of solution for the hybrid-type BVPs involving HFD with respect to ψ. Here, we discuss the existence theorems of BVPs for Hilfer-type FDE with respect to ψ and BCs:

$$\begin{cases} \mathfrak{D}_{a^+}^{\theta_1,\theta_2;\psi}\varkappa(\vartheta) = \mathbf{p}(\vartheta,\varkappa(\vartheta)), \vartheta \in (a,b], \\ c_1\mathfrak{I}_{a^+}^{1-\theta;\psi}\varkappa(\vartheta)|_{\vartheta=a} + c_2\varkappa(\vartheta)|_{\vartheta=b} = d. \end{cases} \tag{5}$$

Also, we consider the Hilfer-type hybrid FDE with respect to ψ and hybrid BCs:

$$\begin{cases} \mathfrak{D}_{a^+}^{\theta_1,\theta_2;\psi}\left(\dfrac{\varkappa(\vartheta)-\mathbb{z}(\vartheta,\varkappa(\vartheta))}{\mathbf{q}(\vartheta,\varkappa(\vartheta))}\right) = \mathbf{p}(\vartheta,\varkappa(\vartheta)), \vartheta \in (a,b], \\ c_1\mathfrak{I}_{a^+}^{1-\theta;\psi}\left.\left(\dfrac{\varkappa(\vartheta)-\mathbb{z}(\vartheta,\varkappa(\vartheta))}{\mathbf{q}(\vartheta,\varkappa(\vartheta))}\right)\right|_{\vartheta=a} + c_2\left.\left(\dfrac{\varkappa(\vartheta)-\mathbb{z}(\vartheta,\varkappa(\vartheta))}{\mathbf{q}(\vartheta,\varkappa(\vartheta))}\right)\right|_{\vartheta=b} = d, \end{cases} \tag{6}$$

where $0 < \theta_1 < 1$ and $0 \le \theta_2 \le 1$, $\theta = \theta_1 + \theta_2(1-\theta_1), c_1, c_2, d \in \mathbb{R}$, $\mathfrak{D}_{a^+}^{\theta_1,\theta_2;\psi}$, and $\mathfrak{I}_{a^+}^{1-\theta;\psi}$ are the HFD and RLFD with respect to ψ, respectively, $\mathbf{p}, \mathbb{z} \in C(I\times\mathbb{R},\mathbb{R})$, $\mathbf{q} \in C(I\times\mathbb{R},\mathbb{R}\setminus\{0\})$, and $I = [a,b]$.

Observe that the considered problems (5) and (6) are the first investigations of hybrid FDEs with hybrid BCs involving ψ-HFD. Moreover, we have chosen this operator, besides the fact that it is a global operator and it generalizes more than twenty the freedom of choice of the ordinary differential operator; some of its advantages have been explained in Remark 3. So, we are sure that the obtained results will be a beneficial contribution and an extension of the current results in the literature. We will also refer here to some recent results related to the subject of our study (see [25–31]).

The rest of the work is displayed as follows. In Section 2, we give some advantageous preliminaries related to our work. In Section 3, we derive the equivalent solutions to linear problems corresponding to the proposed problems. Then, we prove the existence of solutions to given problems

via Dhage's fixed-point theorem. Finally, two examples to justify reported results are offered in Section 4.

2. Preliminaries

Let us initially present some imperative definitions and primer ideas related to our work.

Let $\theta = \theta_1 + \theta_2(1-\theta_1)$ where, $0 < \theta_1 < 1$ and $0 \le \theta_2 \le 1$, and let $I = [a, b], I' = (a, b]$. Consider the functional spaces $C(I, \mathbb{R})$ and $C^{\psi}_{1-\theta}(I, \mathbb{R})$ as follows:

$$C(I, \mathbb{R}) = \{\varphi : I \longrightarrow \mathbb{R} : \varphi \text{ is continuous}\},$$
$$C^{\psi}_{1-\theta}(I, \mathbb{R}) = \left\{\varphi : I' \longrightarrow \mathbb{R} : (\psi(\vartheta) - \psi(a))^{1-\theta}\varphi(\vartheta) \in C(I, \mathbb{R})\right\}, \tag{7}$$

equipped with the norms

$$\|\varphi\|_C := \max\{|\varphi(\vartheta)| : \vartheta \in I\},$$
$$\|\varphi\|_{C^{\psi}_{1-\theta}} = \left\|(\psi(\vartheta) - \psi(a))^{1-\theta}\varphi(\vartheta)\right\|_C. \tag{8}$$

Obviously, $(C^{\psi}_{1-\theta}(I, \mathbb{R}), \|\cdot\|_{C^{\psi}_{1-\theta}})$ is the Banach space.

In the next expressions, we will consider ψ to be an increasing function such that $\psi'(\vartheta) \neq 0$ for all $\vartheta \in I$.

Definition 1 (see [1]). Let $\theta_1 > 0\ (\theta_1 \in \mathbb{R}), \varphi \in L^1(I, \mathbb{R})$, and $\psi \in C^1(I, \mathbb{R})$. Then, ψ-RL fractional integral of φ is defined by

$$\mathfrak{I}^{\theta_1;\psi}_{a^+}\varphi(\vartheta) = \frac{1}{\Gamma(\theta_1)}\int_a^{\vartheta}\psi'(s)(\psi(\vartheta) - \psi(s))^{\theta_1 - 1}\varphi(s)ds. \tag{9}$$

Definition 2 (see [17]). Let $n - 1 < \theta_1 < n \in \mathbb{N}$, $0 \le \theta_2 \le 1$, and $\psi, \varphi \in C^n(I, \mathbb{R})$. Then, the ψ-HFD of φ is defined by

$$\mathfrak{D}^{\theta_1,\theta_2;\psi}_{a^+}\varphi(\vartheta) = \mathfrak{I}^{\theta_2(n-\theta_1);\psi}_{a^+}\left(\frac{1}{\psi'(\vartheta)}\frac{d}{d\vartheta}\right)^n \mathfrak{I}^{(1-\theta_2)(n-\theta_1);\psi}_{a^+}\varphi(\vartheta). \tag{10}$$

Specifically, if $0 < \theta_1 < 1$, we have

$$\mathfrak{D}^{\theta_1,\theta_2;\psi}_{a^+}\varphi(\vartheta) = \mathfrak{I}^{\theta_2(1-\theta_1);\psi}_{a^+}\left(\frac{1}{\psi'(\vartheta)}\frac{d}{d\vartheta}\right)\mathfrak{I}^{(1-\theta_2)(1-\theta_1);\psi}_{a^+}\varphi(\vartheta). \tag{11}$$

Remark 3. The operator $\mathfrak{D}^{\theta_1,\theta_2;\psi}_{a^+}$ is an interpolator of the following FDs:

(i) Classical HFD (for $\psi(\vartheta) \longrightarrow \vartheta$, see [5]), Hilfer-Hadamard FD (for $\psi(\vartheta) \longrightarrow \log\vartheta$, see [32]), and Hilfer-Katugampola FD (for $\psi(\vartheta) \longrightarrow \vartheta^{\rho}, \rho > 0$, see [33])

(ii) Standard RLFD (for $\psi(\vartheta) \longrightarrow \vartheta, \theta_2 \longrightarrow 0$, see [1]) and standard CFD (for $\psi(\vartheta) \longrightarrow \vartheta, \theta_2 \longrightarrow 1$, see [1])

(iii) Generalized RLFD (for $\theta_2 \longrightarrow 0$, see [1]) and generalized CFD (for $\theta_2 \longrightarrow 1$, see [15])

(iv) Generalized Liouville (for $\theta_2 \longrightarrow 0, a = 0$, see [1]) and generalized Weyl (for $\theta_2 \longrightarrow 0, a = -\infty$, see [34])

Lemma 4 (see [1, 17]). *Let $\theta_1, \theta_2 > 0, \eta > 0$, and $\mathscr{K}_{\psi}(\vartheta, a) := [\psi(\vartheta) - \psi(a)]$. Then,*

$$\mathfrak{I}^{\theta_1;\psi}_{a^+}\left[\mathscr{K}^{\eta-1}_{\psi}(\vartheta, a)\right] = \frac{\Gamma(\eta)}{\Gamma(\eta + \theta_1)}\left[\mathscr{K}^{\theta_1+\eta-1}_{\psi}(\vartheta, a)\right],$$
$$\mathfrak{D}^{\theta_1,\theta_2;\psi}_{a^+}\left[\mathscr{K}^{\theta-1}_{\psi}(\vartheta, a)\right] = 0, \tag{12}$$

$$\mathfrak{I}^{\theta_1;\psi}_{a^+}\mathfrak{I}^{\theta_2;\psi}_{a^+}\varphi(\vartheta) = \mathfrak{I}^{\theta_1+\theta_2;\psi}_{a^+}\varphi(\vartheta), \textit{for } \varphi \in C(I, \mathbb{R}).$$

Lemma 5 (see [17]). *Let $0 < \theta_1 < 1$ and $0 \le \theta_2 \le 1$, where $\theta = \theta_1 + \theta_2(1 - \theta_1)$. If $\mathfrak{I}^{1-\theta;\psi}_{a^+}\varphi(\vartheta) \in C(I, \mathbb{R})$, then*

$$\mathfrak{I}^{\theta_1;\psi}_{a^+}\mathfrak{D}^{\theta_1,\theta_2;\psi}_{a^+}\varphi(\vartheta) = \varphi(\vartheta) - \frac{\mathfrak{I}^{1-\theta;\psi}_{a^+}\varphi(a)}{\Gamma(\theta)}(\psi(\vartheta) - \psi(a))^{\theta-1},$$
$$\mathfrak{D}^{\theta_1,\theta_2;\psi}_{a^+}\mathfrak{I}^{\theta_1;\psi}_{a^+}\varphi(\vartheta) = \varphi(\vartheta). \tag{13}$$

Lemma 6 (see [17]). *Let $n - 1 \le \theta < n$ and $\varphi \in C_{\theta}(I, \mathbb{R})$. Then, $\mathfrak{I}^{\theta_1;\psi}_{a^+}$ is bounded in $C_{\theta}(I, \mathbb{R})$. Moreover, we have*

$$\mathfrak{I}^{\theta_1;\psi}_{a^+}\varphi(a) = \lim_{\vartheta \longrightarrow a^+}\mathfrak{I}^{\theta_1;\psi}_{a^+}\varphi(\vartheta) = 0, n - 1 \le \theta < \theta_1. \tag{14}$$

Theorem 7 [35]. *Let K be a nonempty, convex, closed subset of the Banach algebra $\mathscr{L}$. Let the operators $B_1, B_2 : \mathscr{L} \longrightarrow \mathscr{L}$, and $B_3 : K \longrightarrow \mathscr{L}$ such that (i) B_1 and B_2 are Lipschitzian, with Lipschitz constants κ_1 and κ_2, respectively; (ii) B_3 is continuous and compact; (iii) $\omega = B_1\varpi_1 B_3\varpi_2 + B_2\varpi_2 \in K \Rightarrow \varpi_2 \in K$ for each $\varpi_1 \in K$; and (iv) $\kappa_1 M + \kappa_2 < 1$, where $M = \|B_3(K)\|$. Then, there exists $w \in K$ such that $B_1 w B_3 w + B_2 w = w$.*

3. Main Results

In this section, we pay attention to deriving equivalent solutions to linear problems associated with problems (5) and (6); then, we prove the existence of solution to problems (5) and (6) using Dhage's fixed-point technique.

3.1. Fractional Integral Equations (FIEs). The forthcoming results give the equivalent of solution formulas for the proposed problems. For brevity, we set the following symbols:

$$\mathscr{K}^{\theta-1}_{\psi}(\vartheta, a) = (\psi(\vartheta) - \psi(a))^{\theta-1}, F^{\theta}_{\psi}(\vartheta, s) = \psi'(s)(\psi(\vartheta) - \psi(s))^{\theta-1}, \tag{15}$$

$$\frac{1}{\Gamma(\theta_1)}\int_a^{\vartheta} F_{\psi}^{\theta_1}(\vartheta,s)ds = \frac{1}{\Gamma(\theta_1)}\int_a^{\vartheta}\psi'(s)(\psi(\vartheta)-\psi(s))^{\theta_1-1}ds = \frac{(\psi(\vartheta)-\psi(a))^{\theta_1}}{\Gamma(\theta_1+1)} = \frac{\mathscr{K}_{\psi}^{\theta_1}(\vartheta,a)}{\Gamma(\theta_1+1)}, \tag{16}$$

$$\begin{aligned}\frac{1}{\Gamma(\theta_1)}&\int_a^{\vartheta} F_{\psi}^{\theta_1}(\vartheta,s)\mathscr{K}_{\psi}^{\theta-1}(s,a)ds \\ &= \frac{1}{\Gamma(\theta_1)}\int_a^{\vartheta}\psi'(s)(\psi(\vartheta)-\psi(s))^{\theta_1-1}(\psi(s)-\psi(a))^{\theta-1}ds \\ &= \mathfrak{I}_{a^+}^{\theta_1;\psi}[\psi(\vartheta)-\psi(a)]^{\theta-1} = \frac{\Gamma(\theta)}{\Gamma(\theta+\theta_1)}[\psi(\vartheta)-\psi(a)]^{\theta_1+\theta-1} \\ &= \frac{\Gamma(\theta)}{\Gamma(\theta+\theta_1)}\mathscr{K}_{\psi}^{\theta_1+\theta-1}(\vartheta,a).\end{aligned} \tag{17}$$

Lemma 8. *Let $0<\theta_1<1, 0\le\theta_2\le 1$, where $\theta=\theta_1+\theta_2-\theta_1\theta_2$, and $H: I' \longrightarrow \mathbb{R}$ is continuous. Then, the function $\varkappa \in C_{1-\theta,\psi}(I,\mathbb{R})$ is a solution of the linear fractional BVP:*

$$\begin{cases}\mathfrak{D}_{a^+}^{\theta_1,\theta_2;\psi}\varkappa(\vartheta) = H(\vartheta), \vartheta\in I', \\ c_1\mathfrak{I}_{a^+}^{1-\theta;\psi}\varkappa(\vartheta)|_{\vartheta=a} + c_2\varkappa(\vartheta)|_{\vartheta=b} = d,\end{cases} \tag{18}$$

if and only if $\varkappa$ satisfies the FIE:

$$\begin{aligned}\varkappa(\vartheta) = &\frac{\mathscr{K}_{\psi}^{\theta-1}(\vartheta,a)}{\Pi_b}\left[d - c_2\left(\mathfrak{I}_{a^+}^{\theta_1;\psi}H(s)\right)(b)\right] \\ &+ \left(\mathfrak{I}_{a^+}^{\theta_1;\psi}H(s)\right)(\vartheta), \vartheta\in I',\end{aligned} \tag{19}$$

where $\Pi_b := c_1\Gamma(\theta) + c_2\mathscr{K}_{\psi}^{\theta-1}(b,a) \neq 0$.

Proof. Let $\varkappa\in C_{1-\theta,\psi}(I,\mathbb{R})$ be a solution of (18). We need to prove that $\varkappa$ is also a solution of (19). By the definition of $C_{1-\theta,\psi}(I,\mathbb{R})$ and Lemma 6, we have $\mathfrak{I}_{a^+}^{1-\theta;\psi}\varkappa(\vartheta)\in C(I,\mathbb{R})$.

Now, by applying $\mathfrak{I}_{a^+}^{\theta_1;\psi}$ to the first equation in (18) and using Lemma 5, we can write

$$\varkappa(\vartheta) = \frac{\mathfrak{I}_{a^+}^{1-\theta;\psi}\varkappa(a^+)}{\Gamma(\theta)}(\psi(\vartheta)-\psi(a))^{\theta-1} + \left(\mathfrak{I}_{a^+}^{\theta_1;\psi}H(s)\right)(\vartheta). \tag{20}$$

Set $Y_0 := \mathfrak{I}_{a^+}^{1-\theta;\psi}\varkappa(a^+)$. Then,

$$\varkappa(\vartheta) = \frac{Y_0}{\Gamma(\theta)}(\psi(\vartheta)-\psi(a))^{\theta-1} + \left(\mathfrak{I}_{a^+}^{\theta_1;\psi}H(s)\right)(\vartheta). \tag{21}$$

Taking the limit $\vartheta\longrightarrow b$, we get

$$\varkappa(b) = \frac{Y_0}{\Gamma(\theta)}(\psi(b)-\psi(a))^{\theta-1} + \left(\mathfrak{I}_{a^+}^{\theta_1;\psi}H(s)\right)(b). \tag{22}$$

From the mixed boundary conditions $c_1Y_0 + c_2\varkappa(b) = d$, we get

$$Y_0 = \frac{d}{c_1} - \frac{c_2}{c_1}\left[\frac{Y_0}{\Gamma(\theta)}(\psi(b)-\psi(a))^{\theta-1} + \left(\mathfrak{I}_{a^+}^{\theta_1;\psi}H(s)\right)(b)\right], \tag{23}$$

which implies

$$Y_0 = \frac{\Gamma(\theta)}{c_1\Gamma(\theta) + c_2\mathscr{K}_{\psi}^{\theta-1}(b,a)}\left[d - c_2\left(\mathfrak{I}_{a^+}^{\theta_1;\psi}H(s)\right)(b)\right]. \tag{24}$$

Then, (21) becomes

$$\varkappa(\vartheta) = \frac{\mathscr{K}_{\psi}^{\theta-1}(\vartheta,a)}{\Pi_b}\left[d - c_2\left(\mathfrak{I}_{a^+}^{\theta_1;\psi}H(s)\right)(b)\right] + \left(\mathfrak{I}_{a^+}^{\theta_1;\psi}H(s)\right)(\vartheta), \tag{25}$$

which shows that formula (19) is satisfied, where

$$\left(\mathfrak{I}_{a^+}^{\theta_1;\psi}H(s)\right)(r) = \frac{1}{\Gamma(\theta_1)}\int_a^r\psi'(s)(\psi(r)-\psi(s))^{\theta_1-1}H(s)ds. \tag{26}$$

Conversely, let $\varkappa\in C_{1-\theta,\psi}(I,\mathbb{R})$ satisfy (19) which can be written as (25). In (19), taking the limit as $\vartheta\longrightarrow a$ and $\vartheta\longrightarrow b$ and then using Lemma 6, we get

$$\begin{aligned}c_1\mathfrak{I}_{a^+}^{1-\theta;\psi}\varkappa(\vartheta)|_{\vartheta=a} + c_2\varkappa(\vartheta)|_{\vartheta=b} &= \frac{c_1\Gamma(\theta)}{\Pi_b}\left[d - c_2\left(\mathfrak{I}_{a^+}^{\theta_1;\psi}H(s)\right)(b)\right] \\ &+ \frac{c_2\mathscr{K}_{\psi}^{\theta-1}(b,a)}{\Pi_b}\left[d - c_2\left(\mathfrak{I}_{a^+}^{\theta_1;\psi}H(s)\right)(b)\right] \\ &+ c_2\left(\mathfrak{I}_{a^+}^{\theta_1;\psi}H(s)\right)(b) = \left(\frac{c_1\Gamma(\theta)}{\Pi_b} + \frac{c_2\mathscr{K}_{\psi}^{\theta-1}(b,a)}{\Pi_b}\right)d \\ &- \frac{c_1c_2\Gamma(\theta)}{c_1\Gamma(\theta)+c_2\mathscr{K}_{\psi}^{\theta-1}(b,a)}\left(\mathfrak{I}_{a^+}^{\theta_1;\psi}H(s)\right)(b) \\ &+ \left(c_2 - \frac{c_2c_2\mathscr{K}_{\psi}^{\theta-1}(b,a)}{\Pi_b}\right)\left(\mathfrak{I}_{a^+}^{\theta_1;\psi}H(s)\right)(b) = d.\end{aligned} \tag{27}$$

In another direction, by applying $\mathfrak{D}_{a^+}^{\theta_1,\theta_2;\psi}$ on (19) and using Lemmas 4 and 5, we obtain

$$\begin{aligned}\mathfrak{D}_{a^+}^{\theta_1,\theta_2;\psi}\varkappa(\vartheta) &= \frac{\mathfrak{D}_{a^+}^{\theta_1,\theta_2;\psi}\mathscr{K}_{\psi}^{\theta-1}(\vartheta,a)}{\Pi_b}\left[d - c_2\left(\mathfrak{I}_{a^+}^{\theta_1;\psi}H(s)\right)(b)\right] \\ &+ \mathfrak{D}_{a^+}^{\theta_1,\theta_2;\psi}\left(\mathfrak{I}_{a^+}^{\theta_1;\psi}H(s)\right)(\vartheta) \\ &= \left(\mathfrak{D}_{a^+}^{\theta_1,\theta_2;\psi}\mathfrak{I}_{a^+}^{\theta_1;\psi}H(s)\right)(\vartheta) = H(\vartheta).\end{aligned} \tag{28}$$

This finishes the proof. □

Lemma 9. *Let $0 < \theta_1 < 1, 0 \le \theta_2 \le 1$, where $\theta = \theta_1 + \theta_2 - \theta_1\theta_2$, and let $H, Z \in C(I', \mathbb{R})$ and $W \in C(I', \mathbb{R} \setminus \{0\})$. Then, the function $\varkappa \in C_{1-\theta,\psi}(I, \mathbb{R})$ is a solution of the following linear fractional hybird BVP:*

$$\begin{cases} \mathfrak{D}_{a^+}^{\theta_1,\theta_2;\psi}\left(\dfrac{\varkappa(\vartheta) - Z(\vartheta)}{W(\vartheta)}\right) = H(\vartheta), \vartheta \in I', \\ c_1 \mathfrak{I}_{a^+}^{1-\theta;\psi}\left(\dfrac{\varkappa(\vartheta) - Z(\vartheta)}{W(\vartheta)}\right)\Bigg|_{\vartheta=a} + c_2\left(\dfrac{\varkappa(\vartheta) - Z(\vartheta)}{W(\vartheta)}\right)\Bigg|_{\vartheta=b} = d, \end{cases} \tag{29}$$

if and only if $\varkappa$ satisfies the FIE:

$$\varkappa(\vartheta) = W(\vartheta)\left(\frac{\mathscr{K}_\psi^{\theta-1}(\vartheta, a)}{\Pi_b}\left[d - c_2\left(\mathfrak{I}_{a^+}^{\theta_1;\psi}H(s)\right)(b)\right] + \left(\mathfrak{I}_{a^+}^{\theta_1;\psi}H(s)\right)(\vartheta)\right) + Z(\vartheta), \tag{30}$$

where Π_b is defined as in Lemma 8.

Proof. Let $\varkappa \in C_{1-\theta,\psi}(I, \mathbb{R})$ be a solution of (29). We need to prove that $\varkappa$ is also a solution of (30). By the definition of $C_{1-\theta,\psi}(I, \mathbb{R})$ and Lemma 6, we have $\mathfrak{I}_{a^+}^{1-\theta;\psi}\varkappa(\vartheta) \in C(I, \mathbb{R})$.

Now, by applying $\mathfrak{I}_{a^+}^{\theta_1;\psi}$ on the first equation of (29) and using Lemma 5, we can write

$$\frac{\varkappa(\vartheta) - Z(\vartheta)}{W(\vartheta)} = \frac{(\psi(\vartheta) - \psi(a))^{\theta-1}}{\Gamma(\theta)}\mathfrak{I}_{a^+}^{1-\theta;\psi}\left(\frac{\varkappa(a) - Z(a)}{W(a)}\right) + \left(\mathfrak{I}_{a^+}^{\theta_1;\psi}H(s)\right)(\vartheta). \tag{31}$$

Set $Y_1 = \mathfrak{I}_{a^+}^{1-\theta;\psi}((\varkappa(a) - Z(a))/W(a))$; it follows that

$$\varkappa(\vartheta) = W(\vartheta)\left(\frac{Y_1}{\Gamma(\theta)}(\psi(\vartheta) - \psi(a))^{\theta-1} + \left(\mathfrak{I}_{a^+}^{\theta_1;\psi}H(s)\right)(\vartheta)\right) + Z(\vartheta). \tag{32}$$

Taking the limit $\vartheta \longrightarrow b$, we get

$$\varkappa(b) = W(b)\left(\frac{Y_1}{\Gamma(\theta)}(\psi(b) - \psi(a))^{\theta-1} + \left(\mathfrak{I}_{a^+}^{\theta_1;\psi}H(s)\right)(b)\right) + Z(b), \tag{33}$$

which implies

$$\frac{\varkappa(b) - Z(b)}{W(b)} = \frac{Y_1}{\Gamma(\theta)}(\psi(b) - \psi(a))^{\theta-1} + \left(\mathfrak{I}_{a^+}^{\theta_1;\psi}H(s)\right)(b). \tag{34}$$

To determine the constant Y_1, we use the BC of (29). It was followed by

$$Y_1 = \frac{d}{c_1} - \frac{c_2}{c_1}\left[\frac{Y_1}{\Gamma(\theta)}(\psi(b) - \psi(a))^{\theta-1} + \left(\mathfrak{I}_{a^+}^{\theta_1;\psi}H(s)\right)(b)\right], \tag{35}$$

which implies

$$Y_1 = \frac{\Gamma(\theta)}{c_1\Gamma(\theta) + c_2\mathscr{K}_\psi^{\theta-1}(b, a)}\left[d - c_2\left(\mathfrak{I}_{a^+}^{\theta_1;\psi}H(s)\right)(b)\right]. \tag{36}$$

Then, (32) becomes

$$\varkappa(\vartheta) = W(\vartheta)\left(\frac{\mathscr{K}_\psi^{\theta-1}(\vartheta, a)}{\Pi_b}\left[d - c_2\left(\mathfrak{I}_{a^+}^{\theta_1;\psi}H(s)\right)(b)\right] + \left(\mathfrak{I}_{a^+}^{\theta_1;\psi}H(s)\right)(\vartheta)\right) + Z(\vartheta), \tag{37}$$

which shows that formula (30) is satisfied.

Conversely, let $\varkappa \in C_{1-\theta,\psi}(I, \mathbb{R})$ satisfy (29) which can be written as (37). In (30), taking the limit as $\vartheta \longrightarrow a$ and $\vartheta \longrightarrow b$ and then using Lemma 6, we get

$$c_1 \mathfrak{I}_{a^+}^{1-\theta;\psi}\left(\frac{\varkappa(\vartheta) - Z(\vartheta)}{W(\vartheta)}\right)\Bigg|_{\vartheta=a} + c_2\left(\frac{\varkappa(\vartheta) - Z(\vartheta)}{W(\vartheta)}\right)\Bigg|_{\vartheta=b} = d. \tag{38}$$

In the same context, we have from (30) that

$$\frac{\varkappa(\vartheta) - Z(\vartheta)}{W(\vartheta)} = \frac{\mathscr{K}_\psi^{\theta-1}(\vartheta, a)}{\Pi_b}\left[d - c_2\left(\mathfrak{I}_{a^+}^{\theta_1;\psi}H(s)\right)(b)\right] + \left(\mathfrak{I}_{a^+}^{\theta_1;\psi}H(s)\right)(\vartheta). \tag{39}$$

Operate $\mathfrak{D}_{a^+}^{\theta_1,\theta_2;\psi}$ on both sides of (39); then, use Lemmas 4 and 5 to get

$$\begin{aligned} &\mathfrak{D}_{a^+}^{\theta_1,\theta_2;\psi}\left(\frac{\varkappa(\vartheta) - Z(\vartheta)}{W(\vartheta)}\right) \\ &= \frac{\left(\mathfrak{D}_{a^+}^{\theta_1,\theta_2;\psi}\mathscr{K}_\psi^{\theta-1}(s, a)\right)(\vartheta)}{\Pi_b}\left[d - c_2\left(\mathfrak{I}_{a^+}^{\theta_1;\psi}H(s)\right)(b)\right] \\ &\quad + \left(\mathfrak{D}_{a^+}^{\theta_1,\theta_2;\psi}\mathfrak{I}_{a^+}^{\theta_1;\psi}H(s)\right)(\vartheta) = \left(\mathfrak{D}_{a^+}^{\theta_1,\theta_2;\psi}\mathfrak{I}_{a^+}^{\theta_1;\psi}H(s)\right)(\vartheta) \\ &= H(\vartheta). \end{aligned} \tag{40}$$

This finishes the proof. □

3.2. Existence Theorems. In this portion, we prove the existence theorems to problems (5) and (6) in the weighted space by means of Dhage's fixed-point technique.

By a solution of (6), we mean a function $\varkappa \in C_{1-\theta,\psi}(I, \mathbb{R})$ such that

(1) the function $(\varkappa(\vartheta)-\mathbb{z}(\vartheta,\varkappa(\vartheta)))/\mathbf{q}(\vartheta,\varkappa(\vartheta)) \in C_{1-\theta,\psi}(I,\mathbb{R})$ if $[\psi(\vartheta)-\psi(a)]^{1-\theta}((\varkappa(\vartheta)-\mathbb{z}(\vartheta,\varkappa(\vartheta)))/\mathbf{q}(\vartheta,\varkappa(\vartheta))) \in C(I,\mathbb{R})$

(2) $\varkappa$ satisfies the equations in (6)

Before pursuing the main findings, we state the following assumptions:

(A_1) Let $\mathbf{q}: I' \times \mathbb{R} \longrightarrow \mathbb{R}\setminus\{0\}, \mathbb{z}: I' \times \mathbb{R} \longrightarrow \mathbb{R}$, and $\mathbf{p}: I' \times \mathbb{R} \longrightarrow \mathbb{R}$ be continuous functions such that $\mathbf{q}(\cdot,\varkappa(\cdot))$, $\mathbb{z}(\cdot,\varkappa(\cdot)), \mathbf{p}(\cdot,\varkappa(\cdot)) \in C^{\psi}_{1-\theta}(I,\mathbb{R})$, for each $\varkappa \in C^{\psi}_{1-\theta}(I,\mathbb{R})$.

(A_2) There exist two positive functions $\mu_{\mathbf{q}}, \mu_{\mathbb{z}} \in C(I,\mathbb{R})$ such that

$$\begin{aligned}|\mathbf{q}(\vartheta,\varkappa)-\mathbf{q}(\vartheta,\bar{\varkappa})| &\le \mu_{\mathbf{q}}|\varkappa-\bar{\varkappa}|,\\ |\mathbb{z}(\vartheta,\varkappa)-\mathbb{z}(\vartheta,\bar{\varkappa})| &\le \mu_{\mathbb{z}}|\varkappa-\bar{\varkappa}|,\end{aligned} \tag{41}$$

for each $\vartheta \in I'$ and $\varkappa, \bar{\varkappa} \in \mathbb{R}$.

(A_3) There exist $\rho, \sigma \in C(I,\mathbb{R})$ such that

$$|\mathbf{p}(\vartheta,\varkappa)| \le \rho(\vartheta)+\sigma(\vartheta)\|\varkappa\|_{C^{\psi}_{1-\theta}}, \text{ for each } (\vartheta,\varkappa) \in I' \times \mathbb{R}. \tag{42}$$

(A_4) There exists a constant $\mu > 0$ such that

$$\mu \ge \frac{\mathbf{q}_0 R+\mathbb{z}_0}{1-\left(\left\|\mu_{\mathbf{q}}\right\|_C R+\|\mu_{\mathbb{z}}\|_C\right)}, \left\|\mu_{\mathbf{q}}\right\|_C R+\|\mu_{\mathbb{z}}\|_C < 1, \tag{43}$$

$$R := \left(\frac{\mathscr{K}^{\theta-1}_{\psi}(b,a)}{\Pi_b}d+\left(\frac{\mathscr{K}^{\theta-1}_{\psi}(b,a)|c_2|}{\Pi_b}+1\right)\frac{\mathscr{K}^{\theta_1}_{\psi}(b,a)}{\Gamma(\theta_1+1)}\left(\|\rho\|_C+\|\sigma\|_C\mu\right)\right), \tag{44}$$

where $\mathbf{q}_0 := \max_{\vartheta\in I}|(\psi(\vartheta)-\psi(a))^{1-\theta}\mathbf{q}(\vartheta,0)|$ and $\mathbb{z}_0 := \max_{\vartheta\in I}|(\psi(\vartheta)-\psi(a))^{1-\theta}\mathbb{z}(\vartheta,0)|$.

As a result of Lemma 8, we present the next lemma.

Lemma 10. *Let $0<\theta_1<1, 0\le\theta_2\le 1$, where $\theta=\theta_1+\theta_2-\theta_1\theta_2$ and $p: I' \times \mathbb{R} \longrightarrow \mathbb{R}$ are continuous. Then, the nonlinear fractional BVP*

$$\begin{cases}\mathfrak{D}^{\theta_1,\theta_2;\psi}_{a^+}\varkappa(\vartheta)=\mathbf{p}(\vartheta,\varkappa(\vartheta)), \vartheta\in I',\\ c_1\mathfrak{J}^{1-\theta;\psi}_{a^+}\varkappa(\vartheta)|_{\vartheta=a}+c_2\varkappa(\vartheta)|_{\vartheta=b}=d\end{cases} \tag{45}$$

is equivalent to

$$\begin{aligned}\varkappa(\vartheta)=&\frac{\mathscr{K}^{\theta-1}_{\psi}(\vartheta,a)}{\Pi_b}\left(d-\frac{c_2}{\Gamma(\theta_1)}\int_a^b F^{\theta_1}_{\psi}(b,s)\mathbf{p}(s,\varkappa(s))ds\right)\\ &+\frac{1}{\Gamma(\theta_1)}\int_a^{\vartheta}F^{\theta_1}_{\psi}(\vartheta,s)\mathbf{p}(s,\varkappa(s))ds, \vartheta\in I'.\end{aligned} \tag{46}$$

As a result of Lemma 9, we present the next lemma.

Lemma 11. *Let $0<\theta_1<1$, $0\le\theta_2\le 1$, where $\theta=\theta_1+\theta_2-\theta_1\theta_2$ and $p: I' \times \mathbb{R} \longrightarrow \mathbb{R}$ are continuous. Then, the nonlinear fractional hybrid BVP*

$$\begin{cases}\mathfrak{D}^{\theta_1,\theta_2;\psi}_{a^+}\left(\dfrac{\varkappa(\vartheta)-\mathbb{z}(\vartheta,\varkappa(\vartheta))}{\mathbf{q}(\vartheta,\varkappa(\vartheta))}\right)=\mathbf{p}(\vartheta,\varkappa(\vartheta)), \vartheta\in I',\\ c_1\mathfrak{J}^{1-\theta;\psi}_{a^+}\left(\dfrac{\varkappa(\vartheta)-\mathbb{z}(\vartheta,\varkappa(\vartheta))}{\mathbf{q}(\vartheta,\varkappa(\vartheta))}\right)\Bigg|_{\vartheta=a}+c_2\left(\dfrac{\varkappa(\vartheta)-\mathbb{z}(\vartheta,\varkappa(\vartheta))}{\mathbf{q}(\vartheta,\varkappa(\vartheta))}\right)\Bigg|_{\vartheta=b}=d\end{cases} \tag{47}$$

is equivalent to

$$\begin{aligned}\varkappa(\vartheta)=&\,\mathbb{z}(\vartheta,\varkappa(\vartheta))+\mathbf{q}(\vartheta,\varkappa(\vartheta))\\ &\cdot\left[\frac{\mathscr{K}^{\theta-1}_{\psi}(\vartheta,a)}{\Pi_b}\left(d-\frac{c_2}{\Gamma(\theta_1)}\int_a^b F^{\theta_1}_{\psi}(b,s)\mathbf{p}(s,\varkappa(s))ds\right)\right.\\ &\left.+\frac{1}{\Gamma(\theta_1)}\int_a^{\vartheta}F^{\theta_1}_{\psi}(\vartheta,s)\mathbf{p}(s,\varkappa(s))ds\right].\end{aligned} \tag{48}$$

Theorem 12. *Suppose that (A_1)–(A_4) hold. Then, problem (6) has at least one solution in $C^{\psi}_{1-\theta}(I,\mathbb{R})$.*

Proof. Set

$$B_{\mu}=\left\{\varkappa\in C^{\psi}_{1-\theta}(I,\mathbb{R}): \|\varkappa\|_{C^{\psi}_{1-\theta}}\le\mu\right\}. \tag{49}$$

Obviously, B_{μ} is a convex, closed, bounded subset of $C_{1-\theta,\psi}(I,\mathbb{R})$. By Lemma 11, problem (6) is equivalent to

$$\begin{aligned}\varkappa(\vartheta)=&\,\mathbb{z}(\vartheta,\varkappa(\vartheta))+\mathbf{q}(\vartheta,\varkappa(\vartheta))\\ &\cdot\left[\frac{\mathscr{K}^{\theta-1}_{\psi}(\vartheta,a)}{\Pi_b}\left(d-\frac{c_2}{\Gamma(\theta_1)}\int_a^b F^{\theta_1}_{\psi}(b,s)\mathbf{p}(s,\varkappa(s))ds\right)\right.\\ &\left.+\frac{1}{\Gamma(\theta_1)}\int_a^{\vartheta}F^{\theta_1}_{\psi}(\vartheta,s)\mathbf{p}(s,\varkappa(s))ds\right], \vartheta\in I'.\end{aligned} \tag{50}$$

Define the operators $A, B: C^{\psi}_{1-\theta}(I,\mathbb{R}) \longrightarrow C^{\psi}_{1-\theta}(I,\mathbb{R})$ and $C: B_{\mu} \longrightarrow C^{\psi}_{1-\theta}(I,\mathbb{R})$ by

$$\begin{aligned}A\varkappa(\vartheta)&=\mathbf{q}(\vartheta,\varkappa(\vartheta)), \vartheta\in I',\\ B\varkappa(\vartheta)&=\mathbb{z}(\vartheta,\varkappa(\vartheta)), \vartheta\in I',\\ C\varkappa(\vartheta)&=\frac{\mathscr{K}^{\theta-1}_{\psi}(\vartheta,a)}{\Pi_b}\left(d-\frac{c_2}{\Gamma(\theta_1)}\int_a^b F^{\theta_1}_{\psi}(b,s)\mathbf{p}(s,\varkappa(s))ds\right)\\ &\quad+\frac{1}{\Gamma(\theta_1)}\int_a^{\vartheta}F^{\theta_1}_{\psi}(\vartheta,s)\mathbf{p}(s,\varkappa(s))ds, \vartheta\in I'.\end{aligned} \tag{51}$$

Then, we can express equation (50) as follows:

$$\varkappa(\vartheta)=B\varkappa(\vartheta)+C\varkappa(\vartheta)\cdot A\varkappa(\vartheta), \vartheta\in I'. \tag{52}$$

Now, we will show that A, B, and C meet all the requirements for Theorem 7. This will be accomplished in a series of next steps.

Step 1. $A, B : C^{\psi}_{1-\theta}(I,\mathbb{R}) \longrightarrow C^{\psi}_{1-\theta}(I,\mathbb{R})$ are Lipschitzian on $C^{\psi}_{1-\theta}(I,\mathbb{R})$.

Let $\varkappa, \omega \in C^{\psi}_{1-\theta}(I,\mathbb{R})$ and $\vartheta \in I'$. Then, by (A_2), we have

$$\begin{aligned}\|A\varkappa - A\omega\|_{C^{\psi}_{1-\theta}} &= \max_{\vartheta\in I}\left|[\psi(\vartheta)-\psi(a)]^{1-\theta}(A\varkappa(\vartheta)-A\omega(\vartheta))\right| \\ &= \max_{\vartheta\in I}[\psi(\vartheta)-\psi(a)]^{1-\theta}|\mathbf{q}(\vartheta,\varkappa(\vartheta))-\mathbf{q}(\vartheta,\omega(\vartheta))| \\ &\le \max_{\vartheta\in I}[\psi(\vartheta)-\psi(a)]^{1-\theta}\mu_{\mathbf{q}}(\vartheta)|\varkappa(\vartheta)-\omega(\vartheta)| \\ &\le \left\|\mu_{\mathbf{q}}\right\|_C\|\varkappa-\omega\|_{C^{\psi}_{1-\theta}}.\end{aligned} \tag{53}$$

Therefore, A is Lipschitzian on $C^{\psi}_{1-\theta}(I,\mathbb{R})$ with the Lipschitz constant $\|\mu_{\mathbf{q}}\|_C$.

Similarly, we conclude that B is Lipschitzian on $C^{\psi}_{1-\theta}(I,\mathbb{R})$ with the Lipschitz constant $\|\mu_{\mathbb{z}}\|_C$, i.e.,

$$\|B\varkappa - B\omega\|_{C^{\psi}_{1-\theta}} \le \|\mu_{\mathbb{z}}\|_C\|\varkappa-\omega\|_{C^{\psi}_{1-\theta}}. \tag{54}$$

Step 2. $C : B_{\mu} \longrightarrow C^{\psi}_{1-\theta}(I,\mathbb{R})$ is completely continuous.

First, we show that $C : B_{\mu} \longrightarrow C^{\psi}_{1-\theta}(I,\mathbb{R})$ is continuous. Let $\{\varkappa_n\}$ be a sequence such that $\varkappa_n \longrightarrow \varkappa$ in B_{μ}. Then,

$$\begin{aligned}&\lim_{n\longrightarrow\infty}\left|[\psi(\vartheta)-\psi(a)]^{1-\theta}(C\varkappa_n(\vartheta)-C\varkappa(\vartheta))\right| \\ &\le \frac{1}{\Pi_b}\frac{c_2}{\Gamma(\theta_1)}\int_a^b F_{\psi}^{\theta_1}(b,s)\lim_{n\longrightarrow\infty}|\mathbf{p}(s,\varkappa_n(s))-\mathbf{p}(s,\varkappa(s))|ds \\ &\quad+\frac{\mathcal{K}_{\psi}^{1-\theta}(\vartheta,a)}{\Gamma(\theta_1)}\int_a^{\vartheta}F_{\psi}^{\theta_1}(\vartheta,s)\lim_{n\longrightarrow\infty}|\mathbf{p}(s,\varkappa_n(s))-\mathbf{p}(s,\varkappa(s))|ds \\ &= \frac{1}{\Pi_b}\frac{c_2}{\Gamma(\theta_1)}\int_a^b F_{\psi}^{\theta_1}(b,s)\mathcal{K}_{\psi}^{\theta-1}(s,a) \\ &\quad\times\lim_{n\longrightarrow\infty}\mathcal{K}_{\psi}^{1-\theta}(s,a)|\mathbf{p}(s,\varkappa_n(s))-\mathbf{p}(s,\varkappa(s))|ds \\ &\quad+\frac{\mathcal{K}_{\psi}^{1-\theta}(\vartheta,a)}{\Gamma(\theta_1)}\int_a^{\vartheta}F_{\psi}^{\theta_1}(\vartheta,s)\mathcal{K}_{\psi}^{\theta-1}(s,a) \\ &\quad\times\lim_{n\longrightarrow\infty}\mathcal{K}_{\psi}^{1-\theta}(s,a)|\mathbf{p}(s,\varkappa_n(s))-\mathbf{p}(s,\varkappa(s))|ds.\end{aligned} \tag{55}$$

Since $\mathbf{p}(\cdot,\varkappa(\cdot))$ is a continuous function with $\mathbf{p}(\cdot,\varkappa(\cdot)) \in C^{\psi}_{1-\theta}(I,\mathbb{R})$, we have

$$\begin{aligned}&\lim_{n\longrightarrow\infty}\left|[\psi(\vartheta)-\psi(a)]^{1-\theta}(C\varkappa_n(\vartheta)-C\varkappa(\vartheta))\right| \\ &\le \frac{1}{\Pi_b}\frac{c_2}{\Gamma(\theta_1)}\int_a^b F_{\psi}^{\theta_1}(b,s)\mathcal{K}_{\psi}^{\theta-1}(s,a)\lim_{n\longrightarrow\infty}\|\mathbf{p}(\cdot,\varkappa_n(\cdot))-\mathbf{p}(\cdot,\varkappa(\cdot))\|_{C^{\psi}_{1-\theta}}ds \\ &\quad+\frac{\mathcal{K}_{\psi}^{1-\theta}(\vartheta,a)}{\Gamma(\theta_1)}\int_a^{\vartheta}F_{\psi}^{\theta_1}(\vartheta,s)\mathcal{K}_{\psi}^{\theta-1}(s,a)\lim_{n\longrightarrow\infty}\|\mathbf{p}(\cdot,\varkappa_n(\cdot))-\mathbf{p}(\cdot,\varkappa(\cdot))\|_{C^{\psi}_{1-\theta}}ds.\end{aligned} \tag{56}$$

Since ψ is increasing and using (17), we obtain

$$\begin{aligned}&\lim_{n\longrightarrow\infty}\left|[\psi(\vartheta)-\psi(a)]^{1-\theta}(C\varkappa_n(\vartheta)-C\varkappa(\vartheta))\right| \\ &\le\left(\frac{c_2}{\Pi_b}+\mathcal{K}_{\psi}^{1-\theta}(b,a)\right)\frac{\Gamma(\theta)}{\Gamma(\theta+\theta_1)}\mathcal{K}_{\psi}^{\theta_1+\theta-1}(b,a) \\ &\quad\times\lim_{n\longrightarrow\infty}\|\mathbf{p}(\cdot,\varkappa_n(\cdot))-\mathbf{p}(\cdot,\varkappa(\cdot))\|_{C^{\psi}_{1-\theta}}\longrightarrow 0 \text{ as } n\longrightarrow\infty.\end{aligned} \tag{57}$$

This shows that $C : B_{\mu} \longrightarrow C^{\psi}_{1-\theta}(I,\mathbb{R})$ is continuous on B_{μ}.

Next, we show that $C(B_{\mu})$ is uniformly bounded in B_{μ}. Indeed, for any $\varkappa \in B_{\mu}$, we have

$$\begin{aligned}\|C\varkappa\|_{C^{\psi}_{1-\theta}} &= \max_{\vartheta\in I}\left|[\psi(\vartheta)-\psi(a)]^{1-\theta}C\varkappa(\vartheta)\right| \le \frac{d}{\Pi_b} \\ &\quad+\left|\frac{c_2}{\Pi_b}\right|\frac{1}{\Gamma(\theta_1)}\int_a^b F_{\psi}^{\theta_1}(b,s)\max_{\vartheta\in I}|\mathbf{p}(s,\varkappa(s))|ds \\ &\quad\cdot+\frac{\mathcal{K}_{\psi}^{1-\theta}(\vartheta,a)}{\Gamma(\theta_1)}\int_a^{\vartheta}F_{\psi}^{\theta_1}(\vartheta,s)\max_{\vartheta\in I}|\mathbf{p}(s,\varkappa(s))|ds \\ &\le \frac{d}{\Pi_b}+\left|\frac{c_2}{\Pi_b}\right|\frac{1}{\Gamma(\theta_1)}\int_a^b F_{\psi}^{\theta_1}(b,s)\max_{\vartheta\in I}\left(\rho(s)+\sigma(s)\|\varkappa\|_{C^{\psi}_{1-\theta}}\right)ds \\ &\quad+\frac{\mathcal{K}_{\psi}^{1-\theta}(\vartheta,a)}{\Gamma(\theta_1)}\int_a^{\vartheta}F_{\psi}^{\theta_1}(\vartheta,s)\max_{\vartheta\in I}\left(\rho(s)+\sigma(s)\|\varkappa\|_{C^{\psi}_{1-\theta}}\right)ds \\ &\le \frac{d}{\Pi_b}+\left|\frac{c_2}{\Pi_b}\right|\frac{\mathcal{K}_{\psi}^{\theta}(b,a)}{\Gamma(\theta_1+1)}\left(\|\rho\|_C+\|\sigma\|_C\|\varkappa\|_{C^{\psi}_{1-\theta}}\right) \\ &\quad+\frac{\mathcal{K}_{\psi}^{1}(b,a)}{\Gamma(\theta_1+1)}\left(\|\rho\|_C+\|\sigma\|_C\|\varkappa\|_{C^{\psi}_{1-\theta}}\right)\le\frac{d}{\Pi_b} \\ &\quad+\left[\left|\frac{c_2}{\Pi_b}\right|\mathcal{K}_{\psi}^{\theta_1}(b,a)+\mathcal{K}_{\psi}^{1}(b,a)\right]\frac{\left(\|\rho\|_C+\|\sigma\|_C\mu\right)}{\Gamma(\theta_1+1)}.\end{aligned} \tag{58}$$

By (44), then $\|C\varkappa\|_{C^{\psi}_{1-\theta}} \le R$ for each $\varkappa \in B_{\mu}$.

Now, we prove that $C(B_{\mu})$ is an equicontinuous set in $C^{\psi}_{1-\theta}(I,\mathbb{R})$.

Let $\varkappa \in B_{\mu}$ and $\vartheta_1, \vartheta_2 \in I'$ with $\vartheta_1 < \vartheta_2$. Then,

$$\begin{aligned}&\left|[\psi(\vartheta_2)-\psi(a)]^{1-\theta}C\varkappa(\vartheta_2)-[\psi(\vartheta_1)-\psi(a)]^{1-\theta}C\varkappa(\vartheta_1)\right| \\ &=\left|\frac{\mathcal{K}_{\psi}^{1-\theta}(\vartheta_2,a)}{\Gamma(\theta_1)}\int_a^{\vartheta_2}F_{\psi}^{\theta_1}(\vartheta_2,s)\mathbf{p}(s,\varkappa(s))ds\right. \\ &\quad\left.-\frac{\mathcal{K}_{\psi}^{1-\theta}(\vartheta_1,a)}{\Gamma(\theta_1)}\int_a^{\vartheta_1}F_{\psi}^{\theta_1}(\vartheta_1,s)\mathbf{p}(s,\varkappa(s))ds\right| \\ &=\left|\frac{\mathcal{K}_{\psi}^{1-\theta}(\vartheta_2,a)}{\Gamma(\theta_1)}\int_a^{\vartheta_2}F_{\psi}^{\theta_1}(\vartheta_2,s)\mathcal{K}_{\psi}^{\theta-1}(s,a)\left|[\psi(s)-\psi(a)]^{1-\theta}\mathbf{p}(s,\varkappa(s))\right|ds\right. \\ &\quad\left.-\frac{\mathcal{K}_{\psi}^{1-\theta}(\vartheta_1,a)}{\Gamma(\theta_1)}\int_a^{\vartheta_1}F_{\psi}^{\theta_1}(\vartheta_1,s)\mathcal{K}_{\psi}^{\theta-1}(s,a)\left|[\psi(s)-\psi(a)]^{1-\theta}\mathbf{p}(s,\varkappa(s))\right|ds\right|.\end{aligned} \tag{59}$$

Since $\mathbf{p}(\cdot,\varkappa(\cdot)) \in C^{\psi}_{1-\theta}(I,\mathbb{R})$ for any $\varkappa \in C^{\psi}_{1-\theta}(I,\mathbb{R})$ and

$[\psi(\cdot)-\psi(a)]^{1-\theta}\mathbf{p}(\cdot,\varkappa(\cdot))\in C(I,\mathbb{R})$, there exist $\xi\in\mathbb{R}$ such that

$$\left|[\psi(s)-\psi(a)]^{1-\theta}\mathbf{p}(s,\varkappa(s))\right|\le\xi \text{ for all } \vartheta\in I'. \tag{60}$$

Hence,

$$\begin{aligned}
&\left|[\psi(\vartheta_2)-\psi(a)]^{1-\theta}C\varkappa(\vartheta_2)-[\psi(\vartheta_1)-\psi(a)]^{1-\theta}C\varkappa(\vartheta_1)\right|\\
&\quad\le\left|\frac{\mathscr{K}_\psi^{1-\theta}(\vartheta_2,a)}{\Gamma(\theta_1)}\xi\int_a^{\vartheta_2}F_\psi^{\theta_1}(\vartheta_2,s)\mathscr{K}_\psi^{\theta-1}(s,a)ds\right.\\
&\qquad\left.-\frac{\mathscr{K}_\psi^{1-\theta}(\vartheta_1,a)}{\Gamma(\theta_1)}\xi\int_a^{\vartheta_1}F_\psi^{\theta_1}(\vartheta_1,s)\mathscr{K}_\psi^{\theta-1}(s,a)ds\right|\\
&\quad=\left|\mathscr{K}_\psi^{1-\theta}(\vartheta_2,a)\frac{\xi\Gamma(\theta)}{\Gamma(\theta+\theta_1)}[\psi(\vartheta_2)-\psi(a)]^{\theta_1+\theta-1}\right.\\
&\qquad\left.-\mathscr{K}_\psi^{1-\theta}(\vartheta_1,a)\frac{\xi\Gamma(\theta)}{\Gamma(\theta+\theta_1)}[\psi(\vartheta_1)-\psi(a)]^{\theta_1+\theta-1}\right|\\
&\quad=\left|\frac{\xi\Gamma(\theta)}{\Gamma(\theta+\theta_1)}\left([\psi(\vartheta_2)-\psi(a)]^{\theta_1}-[\psi(\vartheta_1)-\psi(a)]^{\theta_1}\right)\right|.
\end{aligned} \tag{61}$$

The continuity of ψ shows that $|[\psi(\vartheta_2)-\psi(a)]^{1-\theta}C\varkappa(\vartheta_2)-[\psi(\vartheta_1)-\psi(a)]^{1-\theta}C\varkappa(\vartheta_1)|\longrightarrow 0$ as $|\vartheta_2-\vartheta_1|\longrightarrow 0$.

This confirms that $C(B_\mu)$ is an equicontinuous set in $C_{1-\theta}^{\psi}(I,\mathbb{R})$. As a result of the Arzelà-Ascoli theorem, C is completely continuous.

Step 3. $A\varkappa C\omega+B\varkappa\in B_\mu$ for $\varkappa\in C_{1-\theta}^{\psi}(I,\mathbb{R})$ and $\omega\in B_\mu$.

Let $\varkappa\in C_{1-\theta}^{\psi}(I,\mathbb{R})$, and $\omega\in B_\mu$ such that $\varkappa=A\varkappa C\omega+B\varkappa$. Then,

$$\begin{aligned}
|\varkappa(\vartheta)|&\le|A\varkappa(\vartheta)||C\omega(\vartheta)|+|B\varkappa(\vartheta)|\le(|\mathbf{q}(\vartheta,\varkappa(\vartheta))-\mathbf{q}(\vartheta,0)|+|\mathbf{q}(\vartheta,0)|)\\
&\quad\times\left(\frac{\mathscr{K}_\psi^{\theta-1}(\vartheta,a)}{\Pi_b}d+\frac{\mathscr{K}_\psi^{\theta-1}(\vartheta,a)}{\Pi_b}\frac{|c_2|}{\Gamma(\theta_1)}\int_a^b F_\psi^{\theta_1}(b,s)|\mathbf{p}(s,\omega(s))|ds\right.\\
&\quad\left.+\frac{1}{\Gamma(\theta_1)}\int_a^{\vartheta}F_\psi^{\theta_1}(\vartheta,s)|\mathbf{p}(s,\omega(s))|d\varkappa\right)+|\mathbb{z}(\vartheta,\varkappa(\vartheta))-\mathbb{z}(\vartheta,0)|\\
&\quad+|\mathbb{z}(\vartheta,0)|\le\left(\mu_{\mathbf{q}}(\vartheta)|\varkappa(\vartheta)|+|\mathbf{q}(\vartheta,0)|\right)\\
&\quad\times\left(\frac{\mathscr{K}_\psi^{\theta-1}(\vartheta,a)}{\Pi_b}d+\frac{\mathscr{K}_\psi^{\theta-1}(\vartheta,a)}{\Pi_b}|c_2|\left(\mathfrak{I}_{a^+}^{\theta_1;\psi}\left(\rho(s)+\sigma(s)\|\omega\|_{C_{1-\theta}^{\psi}}\right)\right)(b)\right.\\
&\quad\left.+\left(\mathfrak{I}_{a^+}^{\theta_1;\psi}\left(\rho(s)+\sigma(s)\|\omega\|_{C_{1-\theta}^{\psi}}\right)\right)(\vartheta)\right)+\mu_{\mathbb{z}}(\vartheta)|\varkappa(\vartheta)|+|\mathbb{z}(\vartheta,0)|\\
&\le\mathscr{K}_\psi^{\theta-1}(\vartheta,a)\left(\left\|\mu_{\mathbf{q}}\right\|_C\|\varkappa\|_{C_{1-\theta}^{\psi}}+\mathbf{q}_0\right)\\
&\quad\times\left(\frac{\mathscr{K}_\psi^{\theta-1}(\vartheta,a)}{\Pi_b}d+\frac{\mathscr{K}_\psi^{\theta-1}(\vartheta,a)}{\Pi_b}\frac{|c_2|\mathscr{K}_\psi^{\theta_1}(b,a)}{\Gamma(\theta_1+1)}\left(\|\rho\|_C+\|\sigma\|_C\|\omega\|_{C_{1-\theta}^{\psi}}\right)\right.\\
&\quad\left.+\left(\|\rho\|_C+\|\sigma\|_C\|\omega\|_{C_{1-\theta}^{\psi}}\right)\frac{\mathscr{K}_\psi^{\theta_1}(\vartheta,a)}{\Gamma(\theta_1+1)}\right)\\
&\quad+\mathscr{K}_\psi^{\theta-1}(\vartheta,a)\left(\|\mu_{\mathbb{z}}\|_C\|\varkappa\|_{C_{1-\theta}^{\psi}}+\mathbb{z}_0\right).
\end{aligned} \tag{62}$$

Therefore,

$$\|\varkappa\|_{C_{1-\theta}^{\psi}}\le\left(\left\|\mu_{\mathbf{q}}\right\|_C\|\varkappa\|_{C_{1-\theta}^{\psi}}+\mathbf{q}_0\right)R+\|\mu_{\mathbb{z}}\|_C\|\varkappa\|_{C_{1-\theta}^{\psi}}+\mathbb{z}_0, \tag{63}$$

which implies

$$\|\varkappa\|_{C_{1-\theta}^{\psi}}\le\frac{\mathbf{q}_0R+\mathbb{z}_0}{1-\left(\left\|\mu_{\mathbf{q}}\right\|_C R+\|\mu_{\mathbb{z}}\|_C\right)}\le\mu. \tag{64}$$

Step 4. Condition (iv) in Theorem 7 holds. That is, $\kappa_1 M+\kappa_2<1$.

From Step 2 and (44), we have

$$\begin{aligned}
M&=\|C(B_\mu)\|=\sup_{\varkappa\in B_\mu}\left\{\sup_{\vartheta\in I}|C\varkappa(\vartheta)|\right\}\\
&\le\left(\frac{\mathscr{K}_\psi^{\theta-1}(b,a)}{\Pi_b}d+\left(\frac{\mathscr{K}_\psi^{\theta-1}(b,a)|c_2|}{\Pi_b}+1\right)\frac{\mathscr{K}_\psi^{\theta_1}(b,a)}{\Gamma(\theta_1+1)}\left(\|\rho\|_C+\|\sigma\|_C\mu\right)\right)\\
&=R.
\end{aligned} \tag{65}$$

Hence,

$$\left\|\mu_{\mathbf{q}}\right\|_C M+\|\mu_{\mathbb{z}}\|_C\le\left\|\mu_{\mathbf{q}}\right\|_C R+\|\mu_{\mathbb{z}}\|_C<1, \tag{66}$$

where $\kappa_1=\|\mu_{\mathbf{q}}\|_C$ and $\kappa_2=\|\mu_{\mathbb{z}}\|_C$. Thus, all the assumptions of Theorem 7 are fulfilled, so the equation $\varkappa=A\varkappa C\varkappa+B\varkappa$ has a solution in B_μ. As a result, problem (6) has a solution on I. □

Theorem 13. *Suppose that (A_1)–(A_4) hold. Then, the ψ-Hilfer problem (5) has at least one solution on I.*

Proof. The proof of this theorem is quite similar to that of Theorem 12 with consideration that $\mathbb{z}(\vartheta,\varkappa(\vartheta))\equiv 0$ and $\mathbf{q}(\vartheta,\varkappa(\vartheta))\equiv 1$ in problem (6). Thus, we omit the details. □

Remark 14.

(1) The conditions (A_2) and (A_3) are also correct if we replace the functions $\rho,\sigma,\mu_{\mathbf{q}},\mu_{\mathbb{z}}\in C(I,\mathbb{R})$ with constants

(2) Problem (6) reduces to problem (5) when $\mathbb{z}(\vartheta,\varkappa(\vartheta))\equiv 0$ and $\mathbf{q}(\vartheta,\varkappa(\vartheta))\equiv 1$. Consequently, Theorem 12 is applied to problem (5)

(3) Problem (5) reduces to problem (3) when $\psi(\vartheta)=\vartheta$, $a=0$, and $\theta_2=1$ (see [23])

(4) Problem (6) reduces to problem (4) when $\psi(\vartheta)=\vartheta$, $a=0$, $\theta_2=1$, and $\mathbb{z}(\vartheta,\varkappa(\vartheta))\equiv 0$ (see [24])

(5) In particular, if $\psi(\vartheta)=\vartheta$, then the obtained results correspond to Caputo-type FDE and RL-type FDE, for $\theta_2=1$ and $\theta_2=0$, respectively

(6) The corresponding fractional problems involving the Hilfer-Katugampola type and Hilfer-Hadamard type appear as a special case of our proposed problems for $\psi(\vartheta) = \vartheta^{\rho}$, $\rho > 0$, and $\psi(\vartheta) = \log \vartheta$, respectively

4. Examples

In this part, we construct two examples to explain the main results.

Example 15. Consider the ψ-Hilfer hybrid FDE with hybrid BC:

$$\begin{cases} \mathfrak{D}_{a^+}^{\theta_1,\theta_2;\psi}\left(\dfrac{\varkappa(\vartheta) - \mathbb{z}(\vartheta,\varkappa(\vartheta))}{\mathbf{q}(\vartheta,\varkappa(\vartheta))}\right) = \mathbf{p}(\vartheta,\varkappa(\vartheta)), \vartheta \in (0,1], \\ c_1 \mathfrak{I}_{a^+}^{1-\theta;\psi}\left(\dfrac{\varkappa(\vartheta) - \mathbb{z}(\vartheta,\varkappa(\vartheta))}{\mathbf{q}(\vartheta,\varkappa(\vartheta))}\right)\Bigg|_{\vartheta=a} + c_2\left(\dfrac{\varkappa(\vartheta) - \mathbb{z}(\vartheta,\varkappa(\vartheta))}{\mathbf{q}(\vartheta,\varkappa(\vartheta))}\right)\Bigg|_{\vartheta=b} = d. \end{cases} \tag{67}$$

Define $\mathbb{z} : (0,1] \times \mathbb{R} \longrightarrow \mathbb{R}$, $\mathbf{q} : (0,1] \times \mathbb{R} \longrightarrow \mathbb{R} \setminus \{0\}$, and $\mathbf{p} : (0,1] \times \mathbb{R} \longrightarrow \mathbb{R}$ by

$$\begin{aligned} \mathbb{z}(\vartheta,\varkappa(\vartheta)) &= \frac{1}{2}\cos\left(\frac{\vartheta}{3}\right)\left(\frac{\varkappa(\vartheta)}{1+\varkappa(\vartheta)} + e^{-\vartheta}\right), \\ \mathbf{q}(\vartheta,\varkappa(\vartheta)) &= \left(1 + \frac{\sin\vartheta}{12}\varkappa(\vartheta)\right), \\ \mathbf{p}(\vartheta,\varkappa(\vartheta)) &= \frac{\psi(\vartheta)-\psi(0)}{100}\left(\frac{\varkappa(\vartheta)}{1+\varkappa(\vartheta)} + 2\right). \end{aligned} \tag{68}$$

It is easy to show that for any $\varkappa, \omega \in \mathbb{R}$, we have

$$\begin{aligned} |\mathbb{z}(\vartheta,\varkappa(\vartheta)) - \mathbb{z}(\vartheta,\omega(\vartheta))| &\le \frac{1}{2}\cos\left(\frac{\vartheta}{3}\right)|\varkappa(\vartheta) - \omega(\vartheta)|, \\ |\mathbf{q}(\vartheta,\varkappa(\vartheta)) - \mathbf{q}(\vartheta,\omega(\vartheta))| &\le \frac{\sin\vartheta}{12}|\varkappa(\vartheta) - \omega(\vartheta)|, \end{aligned} \tag{69}$$

and for each $\varkappa \in C_{1-\theta}^{\psi}([0,1],\mathbb{R})$, we have

$$\begin{aligned} |\mathbf{p}(\vartheta,\varkappa(\vartheta))| &\le \frac{\psi(\vartheta)-\psi(0)}{100}|\varkappa(\vartheta)| + \frac{\psi(\vartheta)-\psi(0)}{50} \\ &\le \frac{[\psi(\vartheta)-\psi(0)]^{\theta}}{100}\|\varkappa\|_{1-\theta;\psi} + \frac{\psi(\vartheta)-\psi(0)}{50}. \end{aligned} \tag{70}$$

Hence, the hypotheses (A_1)–(A_3) hold with $\mu_{\mathbf{q}}(\vartheta) = \sin\vartheta/12$, $\mu_{\mathbb{z}}(\vartheta) = (1/2)\cos(\vartheta/3)$, $\rho(\vartheta) = [\psi(\vartheta)-\psi(0)]^{\theta}/100$, and $\sigma(\vartheta) = (\psi(\vartheta)-\psi(0))/50$. Then, $\|\mu_{\mathbf{q}}\|_C = 1/12$, $\|\mu_{\mathbb{z}}\|_C = 1/2$, $\mathbf{q}_0 = \max_{\vartheta\in 0,1]}|(\psi(\vartheta)-\psi(0))^{1-\theta}|$, and $\mathbb{z}_0 = \max_{\vartheta\in 0,1]}|(\psi(\vartheta)-\psi(0))^{1-\theta}\cos(\vartheta/3)e^{-\vartheta}|$. Taking $\theta_1 = 1/2$, $\theta_2 = 0$, $\theta = 1/2$, $c_1 = 1/3$, $c_2 = 1/3$, $d = 1$, and $\psi(\vartheta) = \vartheta$, we get $\|\rho\|_C = 1/100$, $\|\sigma\|_C = 1/50$, $\mathbf{q}_0 = 1$, and $\mathbb{z}_0 = (1/e)\cos(1/3)$. From the condition (A_4), $\|\mu_{\mathbf{q}}\|_C R + \|\mu_{\mathbb{z}}\|_C < 1$ when $R < 6$, and $\mu \ge 1/(1-((1/12)R + (1/2)))(R + (1/e)\cos(1/3))$. Also, $\Pi_b \ne 0$; it follows from (44) that $R = (3/(1+\sqrt{\pi})) + ((1/(1+\sqrt{\pi})) + 1)((1/50\sqrt{\pi}) + (1/25\sqrt{\pi})\mu) < 6$. Hence, $\mu < (2 - 149\sqrt{\pi} - 300\pi)/(-4 - 2\sqrt{\pi})$. Using the MATLAB program, μ satisfies the inequality $64.17 < \mu < 159.65$. Hence, all assumptions of Theorem 12 are satisfied, so problem (67) has at least one solution on $(0,1]$.

Example 16. As a special case when $\mathbb{z}(\vartheta,\varkappa(\vartheta)) = 0$ and $q(\vartheta,\varkappa(\vartheta)) = 1$, we consider the ψ-Hilfer FDE with BC:

$$\begin{cases} \mathfrak{D}_{0^+}^{1/2,\vartheta}\varkappa(\vartheta) = \dfrac{\varkappa(\vartheta)}{1+\varkappa(\vartheta)} + \dfrac{1}{100}, \vartheta \in (0,1], \\ 100\left[\mathfrak{I}_{a^+}^{1-\theta;\psi}\varkappa(\vartheta)|_{\vartheta=0} + \varkappa(\vartheta)|_{\vartheta=1}\right] = 1. \end{cases} \tag{71}$$

Comparing problem (71) with problem (5), we obtain

$$\begin{aligned} \theta_1 &= \frac{1}{2}, \\ \theta_2 &= 1, \\ c_1 = c_2 &= 100, \\ d &= 1, \\ \psi(\vartheta) &= \vartheta, \\ \mathbf{p}(\vartheta,\varkappa(\vartheta)) &= \frac{\varkappa(\vartheta)}{1+\varkappa(\vartheta)} + \frac{1}{100}. \end{aligned} \tag{72}$$

It is obvious that $\theta = 1$, and in this case, the space $C_{1-\theta}^{\psi}([0,1],\mathbb{R})$ is reduced to the space of continuous functions $C([0,1],\mathbb{R})$. Hence, (A_1) holds. It is easy to show that for each $\varkappa \in \mathbb{R}$, we have

$$|\mathbf{p}(\vartheta,\varkappa(\vartheta))| \le |\varkappa(\vartheta)| + \frac{1}{100} \le \|\varkappa\|_C + \frac{1}{100}. \tag{73}$$

Thus, the hypothesis (A_3) holds with $\rho(\vartheta) = 1/100$, and $\sigma(\vartheta) = 1$. Then, $\|\mu_{\mathbf{q}}\|_C = 1$, $\|\mu_{\mathbb{z}}\|_C = 0$, $\mathbf{q}_0 = 1$, and $\mathbb{z}_0 = 0$. So, we get $\|\rho\|_C = 1/100$, $\|\sigma\|_C = 1$. From the condition (A_4), we have $\mu \ge R/(1-R)$. Finally, we need to show that $R < 1$. Indeed, from (44), we have $R = (1/200) + (3/100\sqrt{\pi}) + (3/\sqrt{\pi})\mu$. It follows that there exists $\mu > 0$ with $\mu < 1/600(199\sqrt{\pi} - 6)$ such that $R < 1$. Therefore, problem (71) can be applied to Theorem 12.

5. Concluding Remarks

We have acquired further existence results for the solution of BVPs for the ψ-Hilfer problem (6), and the ψ-Hilfer hybrid problem (5) relies on the reduction of proposed problems to FIEs. Dhage's hybrid fixed-point theorem in the Banach algebra has been applied. The reported results in the current paper are also valid for the hybrid FDEs involving RLFD and CFD, and they are also true for special cases of the function ψ. We confirm that the obtained results of this work are recent and generalize some of the previous results in the literature. More precisely, when taking different values of

function ψ and parameter θ_2, the studied problems cover several problems involving classical fractional operators such as RLFD, CFD, HFD, Hilfer-Katugampola FD, and Hilfer-Hadamard FD, as mentioned in Remark 14, which have been incorporated into the operators used in our investigation. Using these investigations, other qualitative analyses of the solution such as stability and continuous dependence results can be discussed, and this is what we desire to think about in a future paper.

Data Availability

Data are available upon request.

Conflicts of Interest

The authors declare that they have no conflict regarding the publication of this paper.

Acknowledgments

The authors thank the Research Center for Advanced Materials Science (RCAMS)" at King Khalid University, Saudi Arabia, for funding this work under the grant number KKU/RCAMS/G013-21. The authors extend their appreciation to the Deputyship for Research & Innovation, Ministry of Education, in Saudi Arabia, for funding this research work through the project number IFP-KKU-2020/9. This work was funded under the Princess Nourah bint Abdulrahman University Researchers Supporting Project number PNURSP2022R157, Princess Nourah bint Abdulrahman University, Riyadh, Saudi Arabia.

References

[1] A. A. Kilbas, H. M. Srivastava, and J. J. Trujillo, *Theory and Applications of Fractional Differential Equations*, Elsevier B.V, Amsterdam, 2006.

[2] A. Atangana and D. Baleanu, "New fractional derivative with non-local and non-singular kernel," *Thermal Science*, vol. 20, no. 2, pp. 757–763, 2016.

[3] X. J. Yang, F. Gao, J. T. Machado, and D. Baleanu, "A new fractional derivative involving the normalized sinc function without singular kernel," *The European Physical Journal Special Topics*, vol. 226, no. 16-18, pp. 3567–3575, 2017.

[4] J. Lozada and J. J. Nieto, "Properties of a new fractional derivative without singular kernel," *Progress in Fractional Differentiation and Applications*, vol. 1, no. 1, pp. 87–92, 2015.

[5] R. Hilfer, *Applications of Fractional Calculus in Physics*, World Scientific Publishing Co. Inc, River Edge, NJ, Singapore, 2000.

[6] R. Hilfer, "Fractional time evolution," in *Applications of Fractional Calculus in Physics*, vol. 87, World Sci. Publ, River Edge, NJ, 2000.

[7] R. Hilfer, "Mathematical and physical interpretations of fractional derivatives and integrals," *Handbook of Fractional Calculus with Applications*, vol. 1, pp. 47–85, 2019.

[8] K. M. Furati, M. D. Kassim, and N. Tatar, "Existence and uniqueness for a problem involving Hilfer fractional derivative," *Computers & Mathematcs with Applications*, vol. 64, no. 6, pp. 1616–1626, 2012.

[9] H. Gu and J. J. Trujillo, "Existence of mild solution for evolution equation with Hilfer fractional derivative," *Applied Mathematics and Computation*, vol. 257, pp. 344–354, 2015.

[10] J. Wang and Y. Zhang, "Nonlocal initial value problems for differential equations with Hilfer fractional derivative," *Applied Mathematics and Computation*, vol. 266, pp. 850–859, 2015.

[11] A. D. Mali, K. D. Kucche, and J. V. da Costa Sousa, "On coupled system of nonlinear ψ-Hilfer hybrid fractional differential equations," in *International Journal of Nonlinear Sciences and Numerical Simulation*, Walter de Gruyter GmbH, Berlin/Boston, 2021.

[12] S. Asawasamrit, A. Kijjathanakorn, S. K. Ntouyas, and J. Tariboon, "Nonlocal boundary value problems for Hilfer fractional differential equations," *Bulletin of the Korean Mathematical Society*, vol. 55, no. 6, pp. 1639–1657, 2018.

[13] S. T. M. Thabet, M. S. Abdo, and B. Ahmad, "The existence and Ulamâ Hyers stability results for ψ-Hilfer fractional integrodifferential equations," *Journal of Pseudo-Differential Operators and Applications*, vol. 11, no. 4, pp. 1757–1780, 2020.

[14] O. P. Agrawal, "Some generalized fractional calculus operators and their applications in integral equations," *Fractional Calculus and Applied Analysis*, vol. 15, no. 4, pp. 700–711, 2012.

[15] R. Almeida, "A Caputo fractional derivative of a function with respect to another function," *Communications in Nonlinear Science and Numerical Simulation*, vol. 44, pp. 460–481, 2017.

[16] F. Jarad and T. Abdeljawad, "Generalized fractional derivatives and Laplace transforms," *Discrete and Continuous Dynamical Systems: Series S*, vol. 13, no. 3, pp. 709–722, 2020.

[17] J. V. C. Sousa and E. C. de Oliveira, "On the ψ-Hilfer fractional derivative," *Communications in Nonlinear Science and Numerical Simulation*, vol. 60, pp. 72–91, 2018.

[18] M. S. Abdo, H. A. Wahash, and S. K. Panchal, "Ulam-Hyers-Mittag-Leffler stability for a ψ-Hilfer problem with fractional order and infinite delay," *Results in Applied Mathematics*, vol. 7, article 100115, 2020.

[19] H. A. Wahash, M. S. Abdo, and S. K. Panchal, "Fractional integrodifferential equations with nonlocal conditions and generalized Hilfer fractional derivative," *Ufa Mathematical Journal*, vol. 11, no. 1, pp. 3–21, 2019.

[20] J. V. C. Sousa and E. C. de Oliveira, "On the Ulam–Hyers–Rassias stability for nonlinear fractional differential equations using the ψ-Hilfer operator," *Journal of Fixed Point Theory and Applications*, vol. 20, p. 96, 2018.

[21] B. C. Dhage and V. Lakshmikantham, "Basic results on hybrid differential equations," *Nonlinear Analysis: Real World Applications*, vol. 4, pp. 414–424, 2010.

[22] Y. Zhao, S. Sun, Z. Han, and Q. Li, "Theory of fractional hybrid differential equations," *Computers & Mathematcs with Applications*, vol. 62, no. 3, pp. 1312–1324, 2011.

[23] M. Benchohra, S. Hamani, and S. K. Ntouyas, "Boundary value problems for differential equations with fractional order," *Surveys in Mathematics and its Applications*, vol. 3, pp. 1–12, 2008.

[24] K. Hilal and A. Kajouni, "Boundary value problem for hybrid differential equations with fractional order," *Advances in Difference Equations*, vol. 183, 19 pages, 2015.

[25] M. Abdelhakem, D. Abdelhamied, M. G. Alshehri, and M. El-Kady, "Shifted Legendre fractional pseudospectral differentiation matrices for solving fractional differential problems," *Fractals*, vol. 2021, article 2240038, 2021.

[26] M. Abdelhakem, D. Mahmoud, D. Baleanu, and M. El-kady, "Shifted ultraspherical pseudo-Galerkin method for approximating the solutions of some types of ordinary fractional problems," *Advances in Difference Equations*, vol. 2021, 18 pages, 2021.

[27] M. Abdelhakem, H. Moussa, D. Baleanu, and M. El-Kady, "Shifted Chebyshev schemes for solving fractional optimal control problems," *Journal of Vibration and Control*, vol. 25, pp. 2143–2150, 2019.

[28] B. P. Moghaddam, A. Dabiri, and J. A. T. Machado, "Application of variable-order fractional calculus in solid mechanics," *Applications in Engineering, Life and Social Sciences, Part A*, vol. 7, pp. 207–224, 2019.

[29] B. P. Moghaddam and J. A. Tenreiro Machado, "Time analysis of forced variable-order fractional Van der Pol oscillator," *The European Physical Journal Special Topics*, vol. 226, no. 16, pp. 3803–3810, 2017.

[30] S. Etemad, M. Matar, M. A. Ragusa, and S. Rezapour, "Ripled fixed points and existence study to a tripled impulsive fractional differential system via measures of noncompactness," *Mathematics*, vol. 10, no. 1, p. 25, 2022.

[31] M. Matar, M. Ahmad, A. Zada, S. Etemad, and S. Rezapour, "On the existence and stability of two positive solutions of a hybrid differential system of arbitrary fractional order via Avery–Anderson–Henderson criterion on cones," *Advances in Difference Equations*, vol. 2021, 23 pages, 2021.

[32] M. D. Kassim and N. E. Tatar, "Well-posedness and stability for a differential problem with Hilfer-Hadamard fractional derivative," *Abstract and Applied Analysis*, vol. 2013, Article ID 605029, 12 pages, 2013.

[33] D. S. Oliveira and E. C. de Oliveira, "Hilfer-Katugampola fractional derivative," *Computational and Applied Mathematics*, vol. 37, no. 3, pp. 3672–3690, 2018.

[34] R. Hilfer, "Threefold introduction to fractional derivatives, anomalous transport," in *Foundations and Applications*, pp. 1–17, Wiley-VCH, Weinheim, Germany, 2008.

[35] B. C. Dhage, "A fixed point theorem in Banach algebras with applications to functional integral equations," *Kyungpook National University*, vol. 44, pp. 145–155, 2004.

Hindawi
Journal of Function Spaces
Volume 2022, Article ID 5128343, 18 pages
https://doi.org/10.1155/2022/5128343

Research Article

Structure Preserving Numerical Analysis of Reaction-Diffusion Models

Nauman Ahmed,[1,2] **Muhammad Aziz-ur Rehman**,[2] **Waleed Adel**,[3,4] **Fahd Jarad**,[5,6] **Mubasher Ali**,[7] **Muhammad Rafiq**,[8] **and Ali Akgül**[9]

[1]*Department of Mathematics and Statistics, The University of Lahore, Lahore, Pakistan*
[2]*Department of Mathematics, University of Management and Technology, Lahore, Pakistan*
[3]*Department of Mathematics and Engineering Physics, Faculty of Engineering, Mansoura University, Mansoura, Egypt*
[4]*Université Française d'Egypte, Ismailia Desert Road, El Shorouk, Cairo, Egypt*
[5]*Department of Mathematics, Çankaya University, 06790 Etimesgut, Ankara, Turkey*
[6]*Department of Medical Research, China Medical University, Taichung 40402, Taiwan*
[7]*School of Engineering and Digital Arts, University of Kent, Canterbury Kent, UK*
[8]*Department of Mathematics, Faculty of Sciences, University of Central Punjab, Lahore, Pakistan*
[9]*Siirt University, Art and Science Faculty, Department of Mathematics, TR-56100, Siirt, Turkey*

Correspondence should be addressed to Fahd Jarad; fahd@cankaya.edu.tr

Received 30 October 2021; Accepted 28 January 2022; Published 20 March 2022

Academic Editor: Youssri Hassan Youssri

In this paper, we examine two structure preserving numerical finite difference methods for solving the various reaction-diffusion models in one dimension, appearing in chemistry and biology. These are the finite difference methods in splitting environment, namely, operator splitting nonstandard finite difference (OS-NSFD) methods that effectively deal with nonlinearity in the models and computationally efficient. Positivity of both the proposed splitting methods is proved mathematically and verified with the simulations. A comparison is made between proposed OS-NSFD methods and well-known classical operator splitting finite difference (OS-FD) methods, which demonstrates the advantages of proposed methods. Furthermore, we applied proposed NSFD splitting methods on several numerical examples to validate all the attributes of the proposed numerical designs.

1. Introduction

A system of differential equations represents the dynamics of real-life phenomenon. These systems can be applied in the field of physics, chemistry, fluid dynamics, engineering, economics, biological sciences etc. Initially, only temporal systems were used to observe the dynamics of different situations. But, for studying the most general behaviors of such systems, we can include the additional quantities such as advection and diffusion in the systems of differential equations. These systems depict the generic situations of the temporal and spatial models [1–3]. Reaction-diffusion equations are considered as one of the most important equations that are used in the modeling of chemical and biological systems. Certain phenomena such as population densities, concentration of chemical substance, and pressure of fluid are described by the state variables of such systems. Therefore, the positivity of state variables is an important requirement for the discrete scheme and should not produce nonphysical oscillations and negative solutions. There is not much work in the literature for positivity preserving and chaos-free numerical methods for chemical reaction models. In this study, we have designed two operator splitting positivity preserving and chaos-free numerical schemes for various reaction diffusion models arising in chemistry and biology.

In this paper, three different models of reaction diffusion equations in one-space dimension are considered for the

study. The main aim of this work is to find the numerical solutions of these models with reliable numerical techniques. These proposed techniques preserve the structure of continuous systems in one dimension.

First of all, among these important models, we consider the Brusselator system that is used in describing the simulations of nonlinear oscillations in chemical reaction-diffusion processes [4–7]. The importance of oscillation in a biochemical system is very significant and was first introduced by Turning et al. [8]. They showed that when some phenomena are considered with diffusion term, a stable spatial pattern is obtained. Also, this system appears in a wide variety of models, such as ozone formation during oxygen atoms collision and enzymatic reactions. The reaction diffusion Brusselator system contains a couple of variables which intervene with reactions, and this process produces chemicals whose concentrations are then controlled. This model has been revealed as the trimolecular model.

Due to the importance of such models, many powerful and efficient techniques have been proposed for solving this system. Such models with nonlinear evolution terms are very hard to solve with the aid of analytical methods. Therefore, numerical methods are needed while dealing with such models. For example, Mittal et al. [9–11] investigated the solution of the one-dimensional Brusselator system using the differential quadrature technique. The behaviour of one-dimensional version of the Brusselator system is studied in [12] with the aid of collocation method based on the radial bases functions. A B-spline approach with a modification was introduced by Jiwari and Yuan in [13] for the Brusselator system with one and two dimensions. Also, a three dimensional form of this system was first solved in [14] using the modified B-spline differential quadrature method. Lin et al. [15] studied the inhomogeneous Brusselator model with cross diffusion process by using a finite volume element approximation and performed the stability analysis for the method and addressed the formation of turning patterns. A new exact solution for this system was driven using the exp-function method in [16]. For more details about the methods for solving the Brusselator model, see [17–20] and references therein.

The Brusselator reaction-diffusion model in one dimension is given as follows:

$$\frac{\partial \psi_1}{\partial t} = \varepsilon_{\psi_1} \frac{\partial^2 \psi_1}{\partial x^2} + \vartheta_2 - (\vartheta_1 + 1)\psi_1 + (\psi_1)^2 \psi_2, \tag{1}$$

$$\frac{\partial \psi_2}{\partial t} = \varepsilon_{\psi_2} \frac{\partial^2 \psi_2}{\partial x^2} + \vartheta_1 \psi_1 - (\psi_1)^2 \psi_2, \tag{2}$$

with initial conditions

$$\psi_1(x,0) = \alpha(x), \quad 0 \le x \le L, \tag{3}$$

$$\psi_2(x,0) = \beta(x), \quad 0 \le x \le L, \tag{4}$$

and homogeneous Neumann boundary conditions

$$\frac{\partial \psi_1(0,t)}{\partial x} = \frac{\partial \psi_1(L,t)}{\partial x} = 0, \quad t > 0, \tag{5}$$

$$\frac{\partial \psi_2(0,t)}{\partial x} = \frac{\partial \psi_2(L,t)}{\partial x} = 0, \quad t > 0. \tag{6}$$

As discussed earlier that $\psi_1(x,t)$ and $\psi_2(x,t)$ are the concentrations of the chemical substances or species, ϑ_1 and ϑ_2 represent the concentrations' constants that appear in the reaction process, and ε_{ψ_1} and ε_{ψ_2} are the diffusion constants. The equilibrium point of systems (1) and (2) is $(\psi_1^*, \psi_2^*) = (\vartheta_2, \vartheta_1/\vartheta_2)$. The point (ψ_1^*, ψ_2^*) is stable if $1 - \vartheta_1 + \vartheta_2^2 \ge 0$ and unstable if $1 - \vartheta_1 + \vartheta_2^2 < 0$. The solution to the system represented by equations (1) and (2) describes the positivity criteria as ψ_1 and ψ_2 are the concentrations of the two species [21]. Therefore, negative values of the solution of this model are meaningless. The numerical technique applied to find the solution of system by the coupled equation in (1) and (2) must preserve the positivity.

The finite-difference technique is an important tool to solve the nonlinear model involving differential equations. Because finding the analytical solution of such models is not an easy task. Therefore, various authors used finite-difference numerical schemes to solve several mathematical models involving ordinary differential equations or partial differential equations [22–28].

The nonstandard finite difference method (NSFD) is a powerful technique for solving different type of nonlinear continuous models which was first presented by Mickens back in 1993 [29]. Over the years, this method proved that it can treat continuous dynamical models that should preserve positivity property. For example, Ahmed et al. [30] adapt the NSFD scheme for solving different types of such models including the SEIR reaction diffusion model. Detailed discussion regarding NSFD and positivity preserving techniques can be found in [31–37].

The paper is organized as follows: in Section 2, four numerical techniques are presented for solving the Brusselator model. In Section 3, the stability and accuracy of the presented methods are introduced. Section 4 is devoted for illustrating the positivity of the purposed schemes. The applications of various reaction-diffusion systems along with the comparison of the four presented methods are presented in Section 5. Lastly, Section 6 provides conclusion for the study.

2. Numerical Techniques

In this section, we will introduce four techniques for solving systems (1)and(2) subjected to condition (3) and homogeneous Neumann boundary conditions. These numerical methods can be divided into two classical methods named as forward and backward operator splitting methods and two nonclassical methods named as explicit and implicit OS-NSFD methods. Each of these method has its own pros and cons. These methods are explained as follows.

2.1. Forward Euler Operator Splitting Method. In the current section, the first method is introduced which is a splitting method based on a finite difference scheme. The splitting

techniques are computationally efficient and handle the complexity and nonlinearity of the differential equations. The main idea of these methods is to split the main equation into two-equation system. The nonlinear reaction steps are described as

$$\begin{aligned}\frac{1}{2}\frac{\partial\psi_1}{\partial t} &= \vartheta_2 - (\vartheta_1 + 1)\psi_1 + (\psi_1)^2\psi_2,\\ \frac{1}{2}\frac{\partial\psi_2}{\partial t} &= \vartheta_1\psi_1 - (\psi_1)^2\psi_2.\end{aligned} \tag{7}$$

Here, ϑ_1 and ϑ_2 represent the concentrations's constants that appears in the reaction process. These last mentioned equations are then utilized for the solution of the linear part of the diffusion equation at the first half step for time as

$$\begin{aligned}\frac{1}{2}\frac{\partial\psi_1}{\partial t} &= \varepsilon_{\psi_1}\frac{\partial^2\psi_1}{\partial x^2},\\ \frac{1}{2}\frac{\partial\psi_2}{\partial t} &= \varepsilon_{\psi_2}\frac{\partial^2\psi_2}{\partial x^2},\end{aligned} \tag{8}$$

that are used for the second equal time step.

For the finite difference approximations, divide $[0, L] \times [0, T]$ into $M \times N$ with $\omega = L/M$ and $\kappa = T/N$.

Grid points are $x_i = i\omega, i = 0, 1, 2, \ldots, M$, $t_n = n\kappa, n = 0, 1, 2, \ldots, N$, and $\psi_{1_i}^n$ and $\psi_{2_i}^n$ describe the difference approximations of $\psi_1(i\omega, n\kappa)$ and $\psi_2(i\omega, n\kappa)$, respectively. Then, the proposed scheme is used to solve these equations in the form:

$$\begin{aligned}\overline{\psi_{1i}}^{n+(1/2)} &= \psi_{1_i}^n + \kappa\vartheta_2 - \kappa(\vartheta_1 + 1)\psi_{1_i}^n + \kappa\left(\psi_{1_i}^n\right)^2 u_{2_i}^n,\\ \overline{\psi_{2i}}^{n+(1/2)} &= \psi_{2_i}^n + \kappa\vartheta_1\psi_{1_i}^n - \kappa\left(\psi_{1_i}^n\right)^2\psi_{2_i}^n,\end{aligned} \tag{9}$$

where $\overline{\psi}_{1_i}^{n+(1/2)}$ and $\overline{\psi}_{2_i}^{n+(1/2)}$ demonstrate the concentrations at the first equal step of time and $\psi_1(t_{n+(1/2)}) = \psi_1(t_n + (1/2)\omega)$ and $\psi_2(t_{n+(1/2)}) = \psi_2(t_n + (1/2)\omega)$. At the next step of time, the form is

$$\psi_{1_i}^{n+1} = \overline{\psi}_{1_i}^{n+(1/2)} + \lambda_1\left(\overline{\psi}_{1_{i-1}}^{n+(1/2)} - 2\overline{\psi}_{1_i}^{n+(1/2)} + \overline{\psi}_{1_{i+1}}^{n+(1/2)}\right), \tag{10}$$

$$\psi_{2_i}^{n+1} = \overline{\psi}_{2_i}^{n+(1/2)} + \lambda_2\left(\overline{\psi}_{2_{i-1}}^{n+(1/2)} - 2\overline{\psi}_{2_i}^{n+(1/2)} + \overline{\psi}_{2_{i+1}}^{n+(1/2)}\right). \tag{11}$$

The boundary condition (5) is incorporated in (10) and (11) by using central difference approximation as

$$\begin{aligned}&\frac{\psi_{1_{i+1}}^n - \psi_{1_{i-1}}^n}{2\omega} = 0, \quad \text{which implies that}\\ &\psi_{1_1}^n = \psi_{1_{-1}}^n,\\ &\psi_{1_{M+1}}^n = \psi_{1_{M-1}}^n,\end{aligned} \tag{12}$$

with initial conditions as

$$\begin{aligned}\psi_{1_i}^0 &= \alpha(x_i),\\ \psi_{2_i}^0 &= \beta(x_i).\end{aligned} \tag{13}$$

2.2. Backward Euler Operator Splitting Method. Now, in this section, we will implement the backward Euler OS-FD technique to solve the Brusselator system. The procedure for the first half step of time is given as

$$\overline{\psi_{1i}}^{n+(1/2)} = \psi_{1_i}^n + \kappa\vartheta_2 - \kappa(\vartheta_1 + 1)\psi_{1_i}^n + \kappa\left(\psi_{1_i}^n\right)^2\psi_{2_i}^n, \tag{14}$$

$$\overline{\psi_{2i}}^{n+(1/2)} = \psi_{2_i}^n + \kappa\vartheta_1\psi_{1_i}^n - \kappa\left(\psi_{1_i}^n\right)^2\psi_{2_i}^n, \tag{15}$$

which is identical to the last scheme. At the next equal step of time, the final form for the above mentioned scheme is

$$-\lambda_1\psi_{1_{i-1}}^{n+1} + (1 + 2\lambda_1)\psi_{1_i}^{n+1} - \lambda_1\psi_{1_{i-1}}^{n+1} = \overline{\psi}_{1_i}^{n+(1/2)}, \tag{16}$$

$$-\lambda_2\psi_{2_{i-1}}^{n+1} + (1 + 2\lambda_2)\psi_{2_i}^{n+1} - \lambda_2\psi_{2_{i-1}}^{n+1} = \overline{\psi}_{2_i}^{n+(1/2)}. \tag{17}$$

The boundary condition (5) is incorporated in (16) and (17) by using central difference approximation as

$$\begin{aligned}&\frac{\psi_{1_{i+1}}^n - \psi_{1_{i-1}}^n}{2\omega} = 0, \quad \text{which implies that}\\ &\psi_{1_1}^n = \psi_{1_{-1}}^n,\\ &\psi_{1_{M+1}}^n = \psi_{1_{M-1}}^n,\end{aligned} \tag{18}$$

with initial conditions as,

$$\begin{aligned}\psi_{1_i}^0 &= \alpha(x_i),\\ \psi_{2_i}^0 &= \beta(x_i).\end{aligned} \tag{19}$$

2.3. Operator Splitting Nonstandard Explicit Finite Difference Method. Here, we turn our attention to construct a novel method based on a nonstandard finite difference and an operator splitting method named as (OS-NSFD) explicit scheme. For this, we apply the rules defined by Mickens [29] and the designed OS-NSFD technique at the first half time step is described as

$$\overline{\psi}_{1_i}^{n+(1/2)} = \frac{\psi_{1_i}^n + \kappa\vartheta_2 + \kappa\left(\psi_{1_i}^n\right)^2\psi_{2_i}^n}{1 + \kappa(\vartheta_1 + 1)}, \tag{20}$$

$$\overline{\psi}_{2_i}^{n+(1/2)} = \frac{\psi_{2_i}^n + \kappa\vartheta_1\psi_{1_i}^n}{1 + \kappa\left(\psi_{1_i}^n\right)^2}. \tag{21}$$

For the second equal time step, the strategy for aforementioned technique is

$$\psi_{1_i}^{n+1} = (1 - 2\lambda_1)\overline{\psi}_{1_i}^{n+(1/2)} + \lambda_1\left(\overline{\psi}_{1_{i-1}}^{n+(1/2)} + \overline{\psi}_{1_{i+1}}^{n+(1/2)}\right), \tag{22}$$

$$\psi_{2_i}^{n+1} = (1 - 2\lambda_2)\overline{\psi}_{2_i}^{n+(1/2)} + \lambda_2\left(\overline{\psi}_{2_{i-1}}^{n+(1/2)} + \overline{\psi}_{2_{i+1}}^{n+(1/2)}\right). \tag{23}$$

The boundary condition (5) is incorporated in (22) and (23) by using central difference approximation as

$$\frac{\psi^n_{1_{i+1}} - \psi^n_{1_{i-1}}}{2\omega} = 0, \quad \text{which implies that}$$
$$\psi^n_{1_1} = \psi^n_{1_{-1}}, \tag{24}$$
$$\psi^n_{1_{M+1}} = \psi^n_{1_{M-1}},$$

with initial conditions as

$$\psi^0_{1_i} = \alpha(x_i),$$
$$\psi^0_{2_i} = \beta(x_i). \tag{25}$$

2.4. Operator Splitting Nonstandard Implicit Finite Difference Method. This section is devoted for the second proposed novel scheme named as OS-NSFD implicit scheme. The designed OS-NSFD implicit technique at the first half step of time is

$$\overline{\psi}^{n+(1/2)}_{1_i} = \frac{\psi^n_{1_i} + \kappa\vartheta_2 + \kappa\left(\psi^n_{1_i}\right)^2\psi^n_{2_i}}{1 + \kappa\left(\vartheta_1 + 1\right)}, \tag{26}$$

$$\overline{\psi}^{n+(1/2)}_{2_i} = \frac{\psi^n_{2_i} + \kappa\vartheta_1\psi^n_{1_i}}{1 + \kappa\left(\psi^n_{1_i}\right)^2}. \tag{27}$$

For the next step, the final form of current technique is

$$-\lambda_1\psi^{n+1}_{1_{i-1}} + \left(1 + 2\lambda_1\right)\psi^{n+1}_{1_i} - \lambda_1\psi^{n+1}_{1_{i-1}} = \overline{\psi}^{n+(1/2)}_{1_i}, \tag{28}$$

$$-\lambda_2\psi^{n+1}_{2_{i-1}} + \left(1 + 2\lambda_2\right)\psi^{n+1}_{2_i} - \lambda_2\psi^{n+1}_{2_{i-1}} = \overline{\psi}^{n+(1/2)}_{2_i}. \tag{29}$$

The boundary condition (5) is incorporated in (28) and (29) by using central difference approximation as

$$\frac{\psi^n_{1_{i+1}} - \psi^n_{1_{i-1}}}{2\omega} = 0, \quad \text{which implies that}$$
$$\psi^n_{1_1} = \psi^n_{1_{-1}}, \tag{30}$$
$$\psi^n_{1_{M+1}} = \psi^n_{1_{M-1}},$$

with initial conditions as

$$\psi^0_{1_i} = \alpha(x_i),$$
$$\psi^0_{2_i} = \beta(x_i). \tag{31}$$

In all above numerical schemes, the value of $\lambda_1 = \varepsilon_{\psi_1}(\kappa/\omega^2)$ and $\lambda_2 = \varepsilon_{\psi_2}(\kappa/\omega^2)$.

3. Stability and Consistency of Underlying Techniques

In this section, the stability along with the consistency of the solution for all the above operator splitting methods is investigated. In all of these methods, the time derivative has an accuracy of $O(\kappa)$ when solved exactly for the reaction step. The diffusion step, in the same way, has an $O(\omega^2)$ accuracy, and the accumulative accuracy for all the techniques is first order and second order in time and space, respectively. The reaction steps are proven to be unconditionally stable for all the methods illustrated above when solving in an exact way [38,39]. In forward Euler OS-FD and explicit NSFD techniques represented in equations (22) and (23), the stability region is

$$\lambda_i \le \frac{1}{2}, \quad (i = 1, 2, 3). \tag{32}$$

In addition, for the Euler OS-FD and implicit NSFD methods, the stability for the diffusion process is found to be stable without any conditions.

Next, we will study the positivity of the solution by considering all of the above schemes.

4. Positivity of the Proposed Schemes

This section is concerned with the validation of positivity of the designed NSFD explicit and implicit techniques. The following theorem verifies that the proposed explicit technique retains the positivity of the solution.

Theorem 1. *The solution of the proposed explicit techniques in the given formulas (20), (21), (26), and (27) at the reaction step with the assumptions of nonnegative initial conditions, i.e.,*

$$\psi^n_{1i,} \ge 0, \psi^n_{2i} \ge 0 \Rightarrow \psi^{n+(1/2)}_{1i} \ge 0, \psi^{n+(1/2)}_{2i} \ge 0. \tag{33}$$

Theorem 1 verifies that the property of positivity of the solution is preserved by the proposed OS-NSFD schemes at the reaction step.

Remark 1. A positive solution is achieved by using the explicit NSFD method represented in equations (22) and (23) if

$$1 - 2\lambda_i \ge 0, \quad i = 1, 2. \tag{34}$$

From the above expression, it is clear that

$$\lambda_i \le \frac{1}{2}, \quad (i = 1, 2), \tag{35}$$

which is the same stability condition as (32) of the OS-NSFD explicit method. This proves that the OS-NSFD explicit method can preserve positivity within its stability region.

We, then utilize the M-matrix theory [40] which helps in proving the positivity property for the proposed OS-NSFD implicit method (28)-(29).

Theorem 2. *For any $\omega > 0$ and $\kappa > 0$, systems (28) and (29) are positive, i.e., $\psi^n_1 > 0$ and $\psi^n_2 > 0$ for all $n = 0, 1, 2 \ldots$.*

Proof. Systems (28) and (29) can be written as

$$\Theta\psi_1^{n+1} = \psi_1^n, \tag{36}$$

$$\Phi\psi_2^{n+1} = \psi_2^n. \tag{37}$$

In the above equations, Θ and Φ are the square matrices as follows:

$$\Theta = \begin{pmatrix} \Theta_3 & \Theta_1 & 0 & \cdots & \cdots & \cdots & \cdots & 0 \\ \Theta_2 & \Theta_3 & \Theta_2 & \ddots & & & & \vdots \\ 0 & \Theta_2 & \Theta_3 & \Theta_2 & \ddots & & & \vdots \\ \vdots & \ddots & \ddots & \ddots & \ddots & \ddots & & \vdots \\ \vdots & & \ddots & \ddots & \ddots & \ddots & \ddots & \vdots \\ \vdots & & & \ddots & \Theta_2 & \Theta_3 & \Theta_2 & 0 \\ \vdots & & & & \ddots & \Theta_2 & \Theta_3 & \Theta_2 \\ 0 & \cdots & \cdots & \cdots & \cdots & 0 & \Theta_1 & \Theta_3 \end{pmatrix}, \tag{38}$$

$$\Phi = \begin{pmatrix} \Phi_3 & \Phi_1 & 0 & \cdots & \cdots & \cdots & \cdots & 0 \\ \Phi_2 & \Phi_3 & \Phi_2 & \ddots & & & & \vdots \\ 0 & \Phi_2 & \Phi_3 & \Phi_2 & \ddots & & & \vdots \\ \vdots & \ddots & \ddots & \ddots & \ddots & \ddots & & \vdots \\ \vdots & & \ddots & \ddots & \ddots & \ddots & \ddots & \vdots \\ \vdots & & & \ddots & \Phi_2 & \Phi_3 & \Phi_2 & 0 \\ \vdots & & & & \ddots & \Phi_2 & \Phi_3 & \Phi_2 \\ 0 & \cdots & \cdots & \cdots & \cdots & 0 & \Phi_1 & \Phi_3 \end{pmatrix}. \tag{39}$$

The off-diagonal entries of Θ are $\Theta_1 = -2\lambda_1$ and $\Theta_2 = -\lambda_1$, and diagonal entries are $\Theta_3 = 1 + 2\lambda_1$. The off-diagonal entries of Φ are $\Phi_1 = -2\lambda_1$ and $\Phi_2 = -\lambda_1$, and diagonal entries are $\Phi_3 = 1 + 2\lambda_2$. Thus, Θ, and Φ are M-matrices. Therefore, expressions (36) and (37) can be written as

$$\psi_1^{n+1} = \Theta^{-1}\psi_1^n, \tag{40}$$

$$\psi_2^{n+1} = \Phi^{-1}\psi_2^n. \tag{41}$$

If we consider that $\psi_1^n > 0$ and $\psi_2^n > 0$, then we get that $\psi_1^{n+1} > 0$ and $\psi_2^{n+1} > 0$, with the aid of the property of M-matrix and Theorem 1. So, the result is then proved by induction. From this theorem, we conclude that the implicit OS-NSFD preserves the property of positivity unconditionally. □ □

5. Application

To support our claims regarding the proposed OS-NSFD techniques, we will implement these schemes to several reaction diffusion models along with the famous Brusselator model.

5.1. Brusselator Model. For the application of the proposed and classical methods under study, we chose the following numerical test. The graphical behaviour of the solution for each of the proposed four methods are demonstrated through the following figures for solving systems (1) and (2). As discussed above, systems (1) and (2) have a positive solution and converge toward the equilibrium point if the condition $1 - \vartheta_1 + \vartheta_2^2 \geq 0$ is satisfied and unstable if $1 - \vartheta_1 + \vartheta_2^2 < 0$.

First, Figures 1 and 2 demonstrates the simulated results for the first method which is the forward Euler OS-FD technique at various step sizes. It can be noticed from these figures that this method gives nonconsistent data with systems (1) and (2). This proves that this method gives negative values of the concentrations which is meaningless. Also, the solution diverge from the equilibrium point which contradict with the physical behavior of the solution.

The second method is tested on the same example which is the backward Euler OS-FD method with the same value of parameters as in the first method for the sake of comparison. The behavior of the solution is illustrated in Figures 3 and 4. These figures show that this method, like the first method, fails to preserve the positivity of the solution and also gives divergence.

The graphical behaviour of the state variables show that the forward Euler and backward Euler OS-FD method are not the reliable techniques to solve the nonlinear autocatalytic chemical reaction model. As they provide us with the negative solutions for the small step sizes.

Due to the failure of the two abovementioned methods, the NSFD methods are presented to overcome this issue. Figures 5 and 6 show the graphs of the solution using the explicit OS-NSFD method. For the sake of comparison with the other methods, we use the same values of the parameters which are used in the previous two methods and took the value of ϑ_1 and ϑ_2 such that $1 - \vartheta_1 + \vartheta_2^2 \geq 0$. From these figures, unlike the other methods, we observe that this method preserves the positivity and all the important properties of the glycolysis continuous model and converges toward the equilibrium point.

The graphs in Figures 7 and 8 demonstrate the concentrations by using the implicit OS-NSFD method. This behavior is also shown to be consistent with the explicit OS-NSFD method. This method like the previous method also preserves positivity and chaos-free properties and converges towards the equilibrium point which is stable under the condition $1 - \vartheta_1 + \vartheta_2^2 \geq 0 > 0$.

Now, the simulations by using both designed OS-NSFD techniques are given by considering the values of parameters ϑ_1 and ϑ_2 so that $1 - \vartheta_1 + \vartheta_2^2 > 0$.

As mentioned before, the stability of the Brusselator system is preserved with the condition $1 - \vartheta_1 + \vartheta_2^2 > 0$. Figures 9 and 10 prove this fact that the two new presented OS-NSFD methods are consistent with the continuous model when the stability condition holds and are inconsistent when $1 - \vartheta_1 + \vartheta_2^2 < 0$. Figures 9 and 10 reflect the inconsistent behavior when the stability criterion does not hold, while the other while the other parameters and step sizes and kept fixed. This fact has been proven that stability criteria is very important in the stability analysis.

Now, we consider $T = 1$ and $M = 100$. Figure 11 depicts log-log graphs of the error versus the computational time. We presented the four schemes, and the graphs correspond

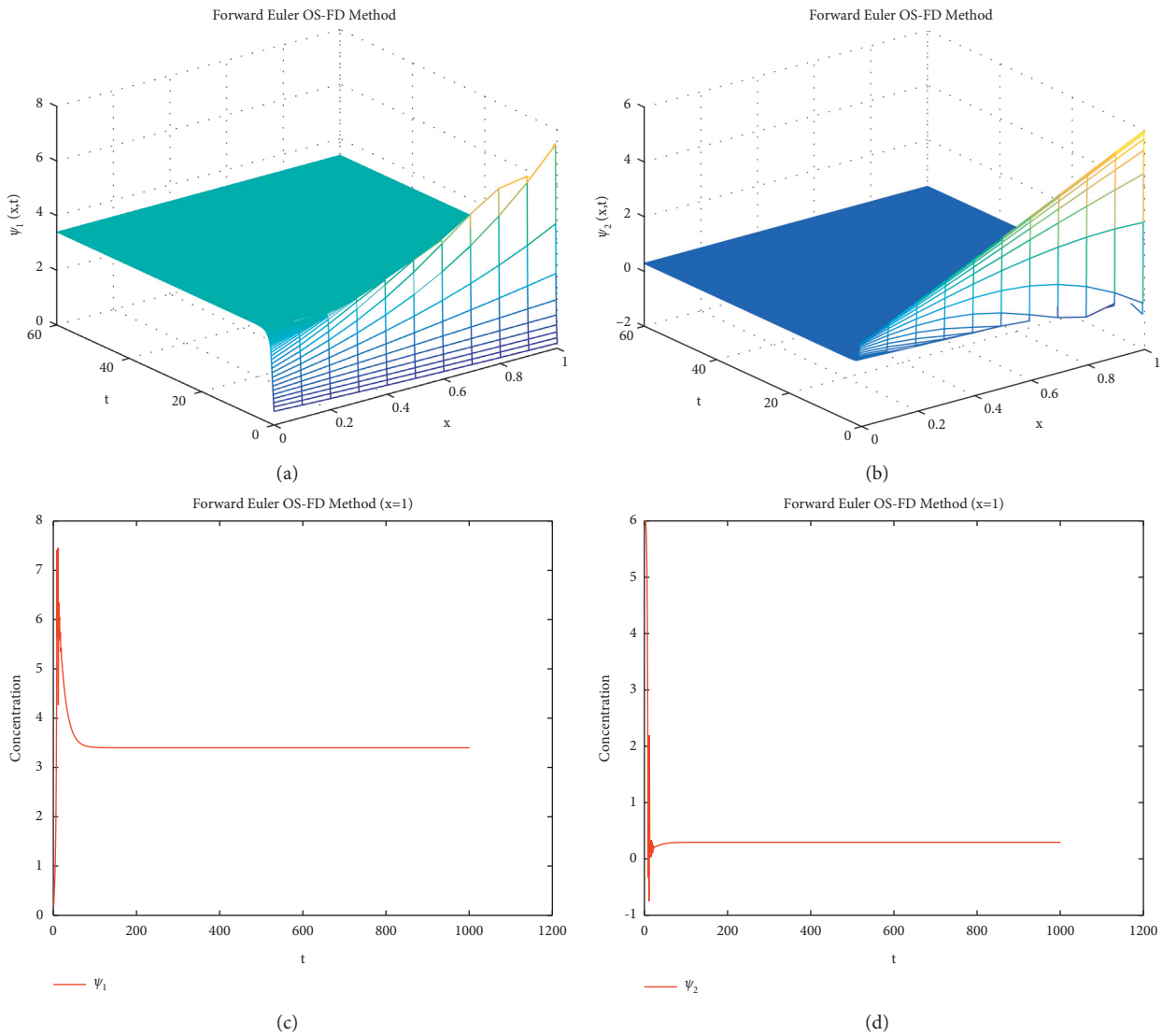

Figure 1: Mesh graphs and plot graphs of ψ_1 and ψ_2 (concentration profile) using forward Euler OS-FD method at $\kappa = 0.1, \vartheta_1 = 1, \vartheta_2 = 3.4, \lambda_1 = \lambda_2 = 0.0006$, and $\varepsilon_{\psi_1} = \varepsilon_{\psi_1} = 10^{-4}$. (a) Solution graph of ψ_1. (b) Solution graph of ψ_2. (c) Plot graph of ψ_1. (d) Plot graph of ψ_2.

to the solutions when we estimate the concentration profiles ψ_1 and ψ_2 of the Brusselator system. The result demonstrates that the OS-NSFD explicit and implicit schemes are approximately as efficient as forward Euler OS-FD and backward Euler OS-FD schemes. Obviously, the former technique stands out in terms of its capability to preserve the structure of the relevant solutions of the Brusselator model under investigation. It is worth pointing out that the approximation to the exact solution was obtained using $N = 20000$.

Finally, four numerical methods are used to solve the underlying model, namely, the forward Euler operator splitting method, backward Euler operator splitting method, nonstandard finite difference explicit operator splitting method, and nonstandard finite difference implicit operator splitting method. The extensively used numerical Euler methods (backward and forward) are used to solve the underlying models. The obtained solutions are analyzed and compared with the newly developed methods. The failure of the classical methods motivated us to develop new numerical methods. The new techniques are structure-preserving and reliable numerical methods that give positive and bounded solutions. The computed solutions converge towards the exact steady-state. So, the numerical analysis demonstrates that the NSFD methods are the reliable tool to solve the nonlinear models.

5.2. Susceptible-Infected-Recovered Epidemic Model. For the second application, we consider nonlinear reaction-diffusion system of infectious disease dynamics. The system is known as susceptible-infected-recovered (SIR) epidemic [41],

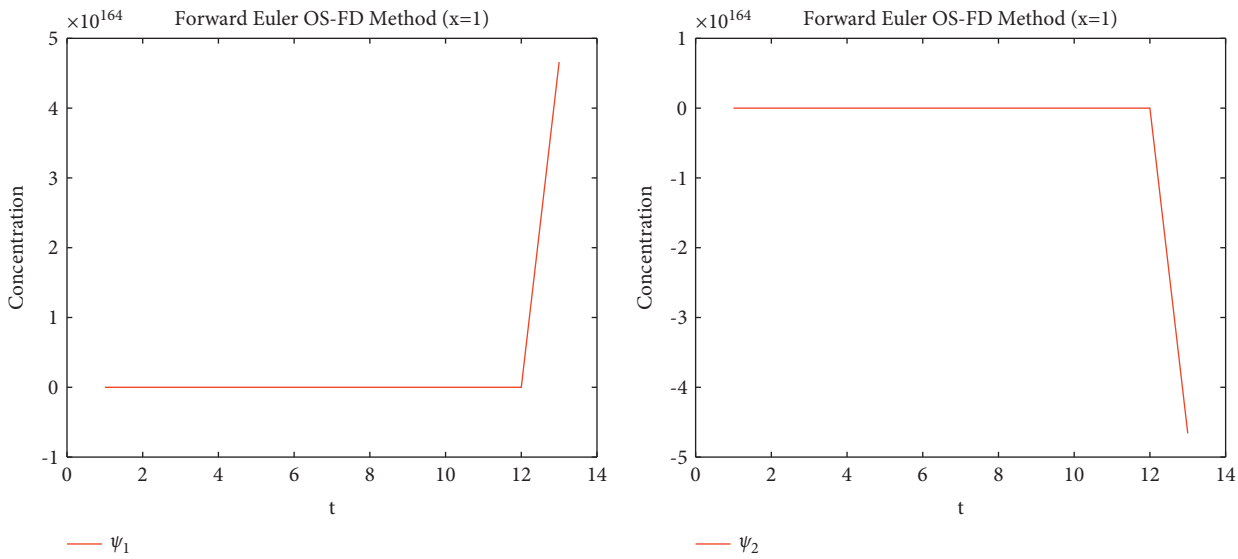

(a) (b)

Figure 2: Plot graphs of ψ_1 and ψ_2 implementing the forward Euler OS-FD technique at $\kappa = 0.1, \vartheta_1 = 1, \vartheta_2 = 3.4, \lambda_1 = \lambda_2 = 0.001$, and $\varepsilon_{\psi_1} = \varepsilon_{\psi_1} = 10^{-4}$. (a) Plot graph of ψ_1. (b) Plot graph of ψ_2.

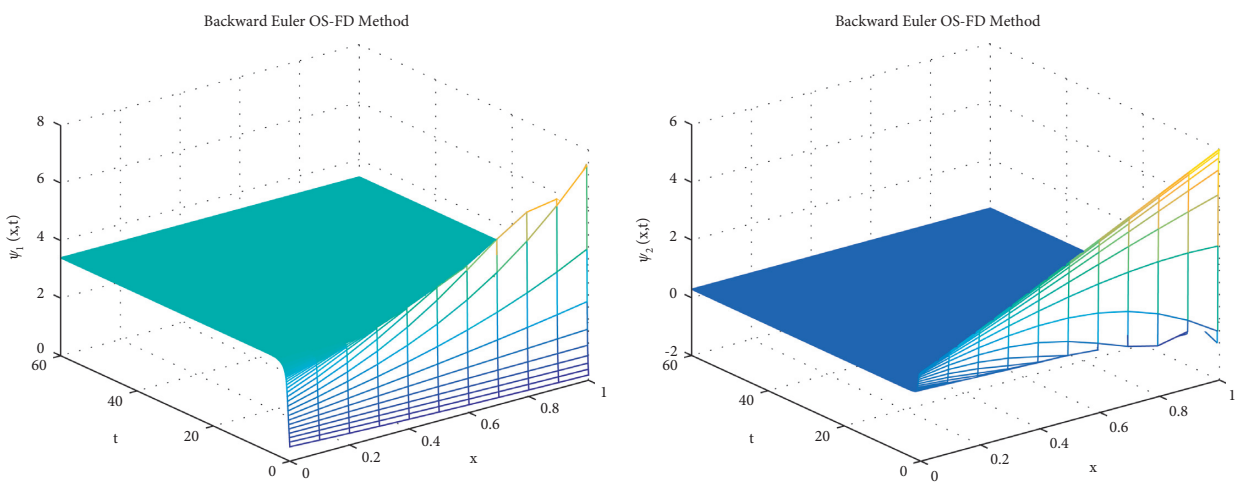

(a) (b)

Figure 3: Continued.

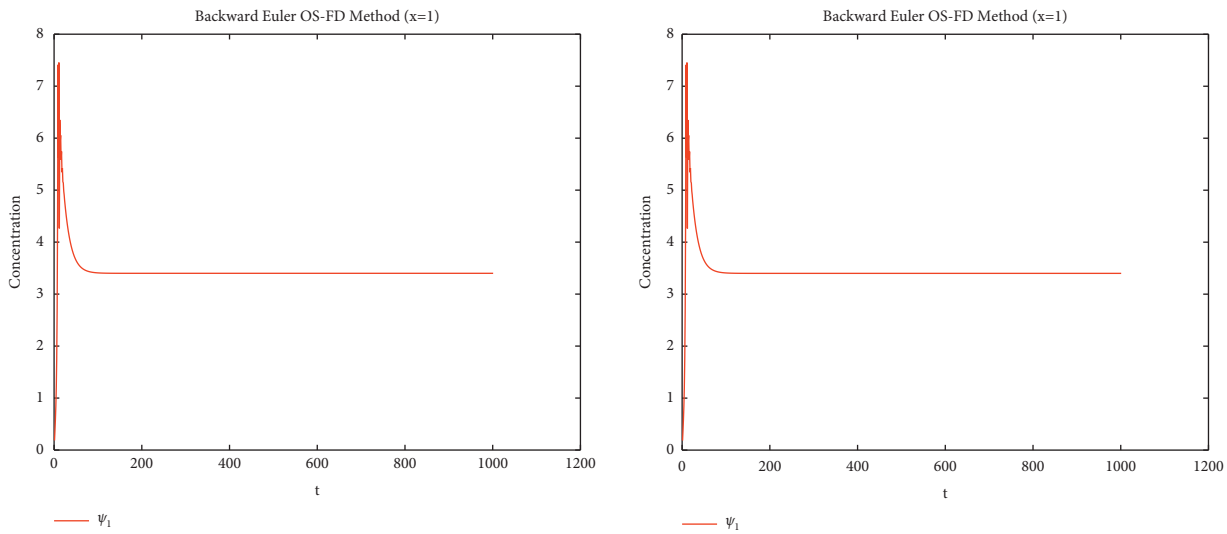

(c) (d)

Figure 3: Solution graphs and plot graphs of ψ_1 and ψ_2 implementing backward Euler OS-FD technique at $\kappa = 0.1, \vartheta_1 = 1, \vartheta_2 = 3.4, \lambda_1 = \lambda_2 = 0.0006$, and $\varepsilon_{\psi_1} = \varepsilon_{\psi_1} = 10^{-4}$. (a) Solution graph of ψ_1. (b) Solution graph of ψ_2. (c) Plot graph of ψ_1. (d) Plot graph of ψ_2.

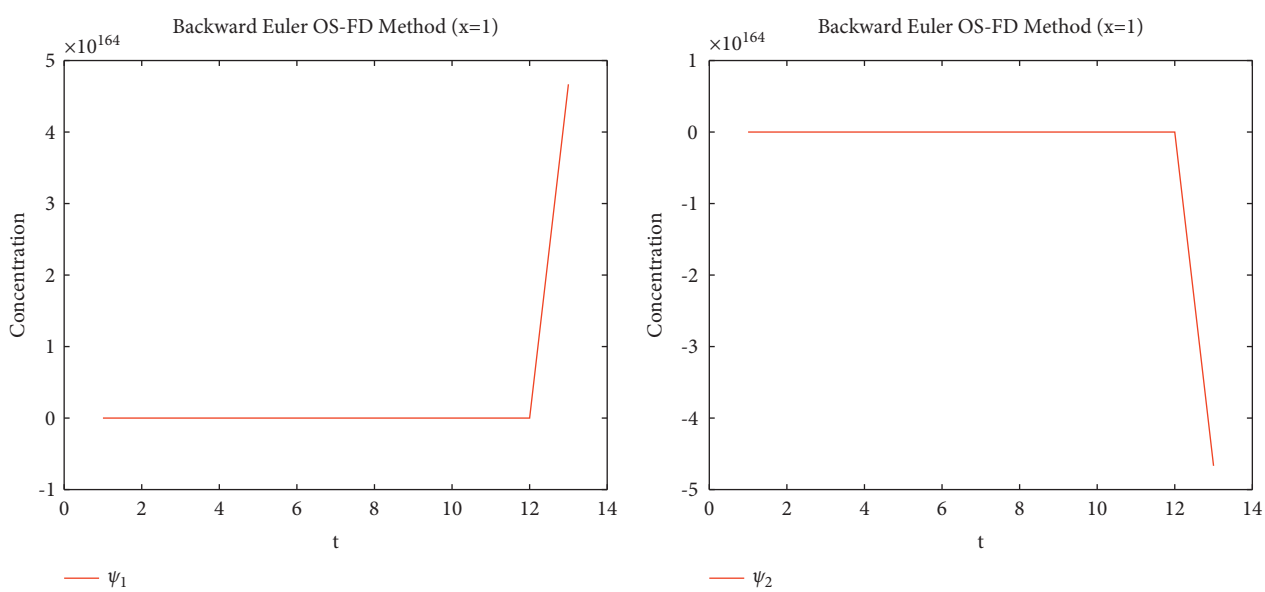

(a) (b)

Figure 4: Plot graphs of ψ_1 and ψ_2 implementing the backward Euler OS-FD method at $\kappa = 0.01, \vartheta_1 = 1, \vartheta_2 = 3.4, \lambda_1 = \lambda_2 = 0.001$, and $\varepsilon_{\psi_1} = \varepsilon_{\psi_1} = 10^{-4}$. (a) Plot graph of ψ_1. (b) Plot graph of ψ_2.

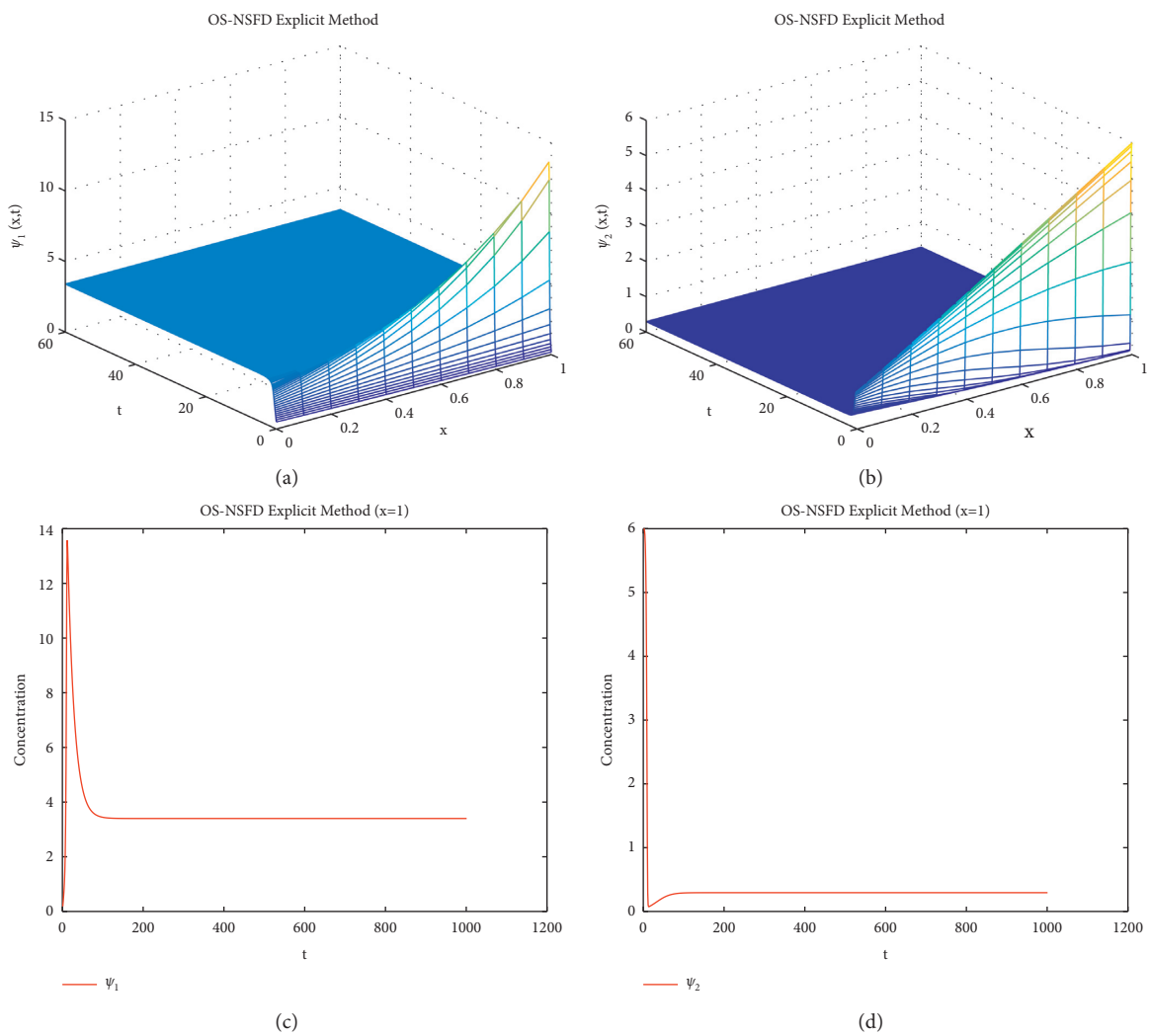

FIGURE 5: Mesh graphs and plot graphs of ψ_1 and ψ_2 implementing NSFD explicit splitting method at $\kappa = 0.1, \vartheta_1 = 1, \vartheta_2 = 3.4, \lambda_1 = \lambda_2 = 0.0006$, and $\varepsilon_{\psi_1} = \varepsilon_{\psi_1} = 10^{-4}$. (a) Mesh graph of ψ_1. (b) Mesh graph of ψ_2. (c) Plot graph of ψ_1. (d) Plot graph of ψ_2.

$$\frac{\partial \psi_1}{\partial t} = \varepsilon_{\psi_1} \frac{\partial^2 \psi_1}{\partial x^2} + \vartheta_1 N - \vartheta_1 \psi_1 - \vartheta_3 \psi_1 \psi_2, \tag{42}$$

$$\frac{\partial \psi_2}{\partial t} = \varepsilon_{\psi_2} \frac{\partial^2 \psi_2}{\partial x^2} - (\vartheta_1 + \vartheta_2)\psi_2 + \vartheta_3 \psi_1 \psi_2, \tag{43}$$

with initial conditions

$$\begin{aligned} \psi_1(x,0) &= \begin{cases} 325000x, & 0 \le x \le \frac{1}{2}, \\ 325000(1-x), & \frac{1}{2} \le x \le 1, \end{cases} \\ \psi_2(x,0) &= \begin{cases} 7500x, & 0 \le x \le \frac{1}{2}, \\ 7500(1-x), & \frac{1}{2} \le x \le 1, \end{cases} \end{aligned} \tag{44}$$

and homogeneous Neumann boundary conditions. In systems (42) and (43), $\psi_1 = \psi_1(x,t)$ and $\psi_2 = \psi_2(x,t)$ are susceptible and infected population densities. ϑ_1 is the parameter which represents natural birth and death rate. ϑ_2 indicates the rate of recovery from infected to recovered class. The transmission coefficient from susceptibility to disease is denoted by ϑ_3.

The epidemic systems (42) and (43) have two stable fixed points, disease-free point (DFP) and endemic point (EP). DFP is the point when disease eradicates from the population. The DFP of systems (42)and(43) $\epsilon_0 = (N, 0)$. The EP is the point when disease persists in the population. The EP of systems (42)and(43) is $\epsilon_* = (\psi_{1*}, \psi_{2*})$, where $\psi_{1*} = (\vartheta_1 + \vartheta_2)/\vartheta_3$ and $\vartheta_{2*} = (\vartheta_1 N/(\vartheta_1 + \vartheta_2)) - (\vartheta_1/\vartheta_3)$.

The basic reproductive number of the epidemic system (42)and(43) is $\mathscr{B}_0 = N\vartheta_3/\vartheta_1 + \vartheta_2$ when $d_{\psi_i} = 0, i = 1, 2$. $\mathscr{B}_0$ is very important quantity which decides whether disease is eradicated or persisted. If $\mathscr{B}_0 < 1$, then disease will wipe out, and the disease is present if $\mathscr{B}_0 > 1$.

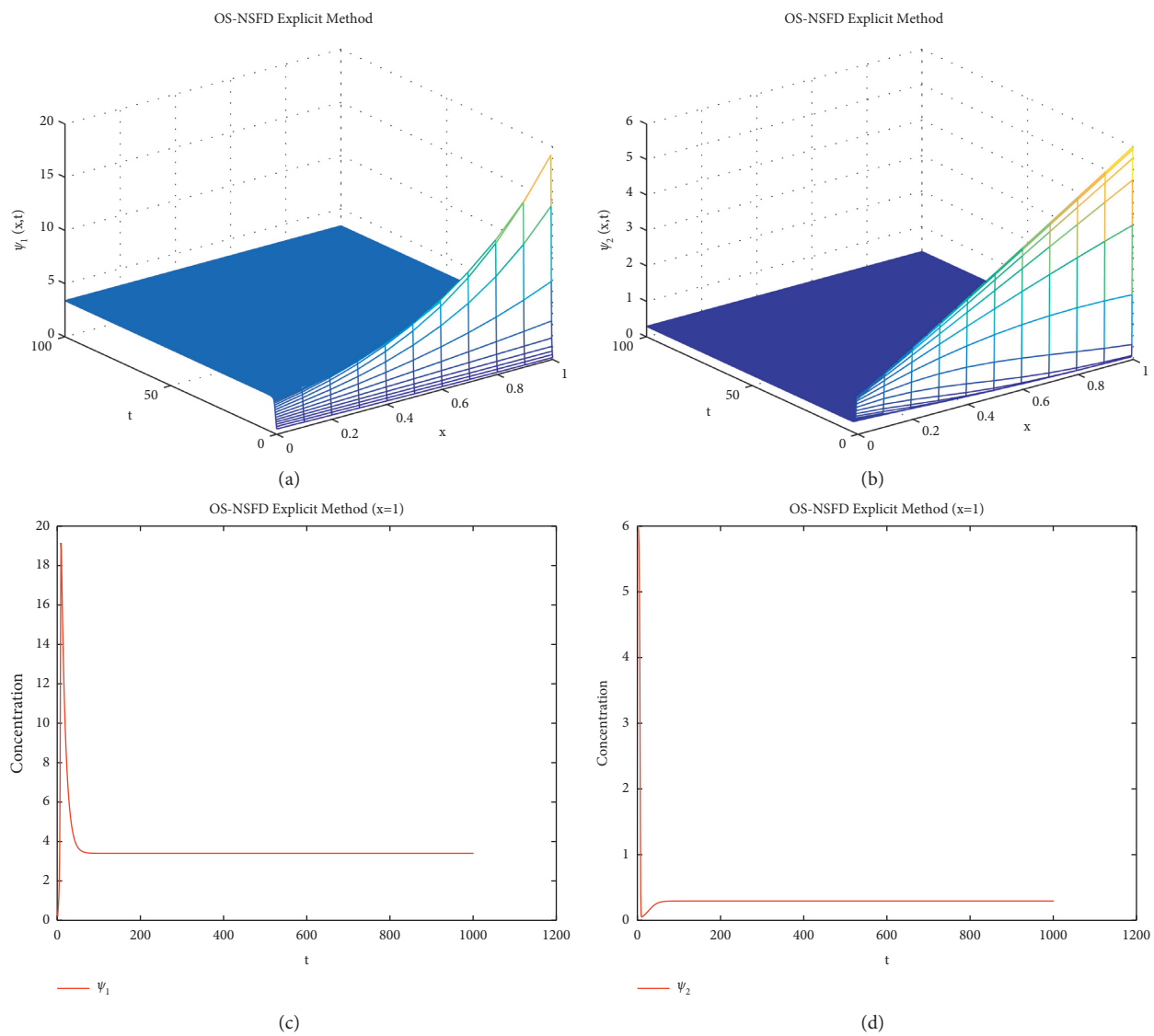

Figure 6: Mesh and plot graphs of ψ_1 and ψ_2 implementing NSFD explicit splitting technique at $\kappa = 0.1, \vartheta_1 = 1, \vartheta_2 = 3.4, \lambda_1 = \lambda_2 = 0.001$, and $\varepsilon_{\psi_1} = \varepsilon_{\psi_1} = 10^{-4}$. (a) Mesh graph of ψ_1. (b) Mesh graph of ψ_2. (c) Plot graph of ψ_1. (d) Plot graph of ψ_2.

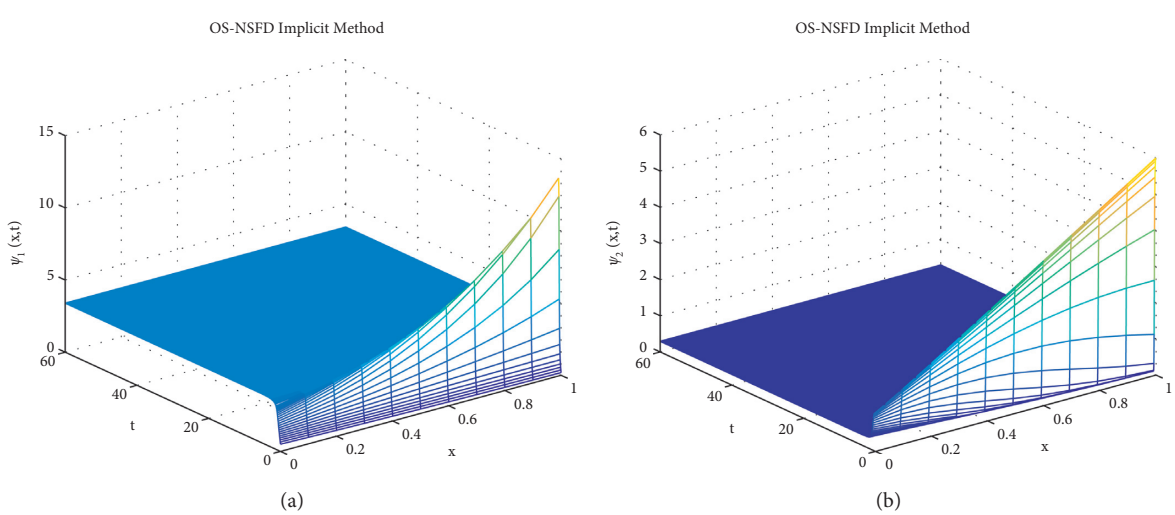

Figure 7: Continued.

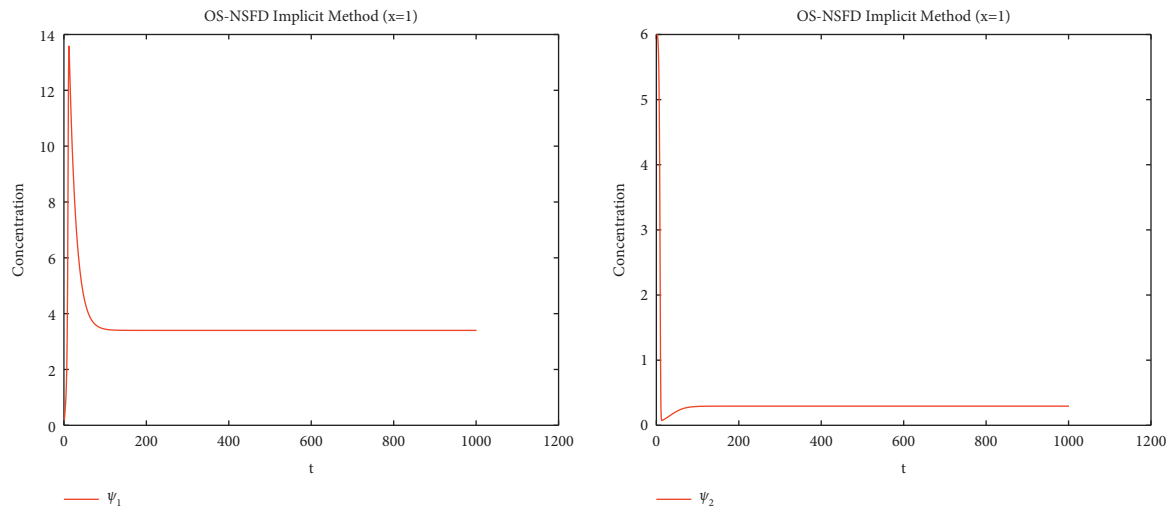

(c) (d)

Figure 7: Mesh graphs and plot graphs of ψ_1 and ψ_2 implementing NSFD implicit splitting technique at $\kappa = 0.1, \vartheta_1 = 1, \vartheta_2 = 3.4, \lambda_1 = \lambda_2 = 0.0006$, and $\varepsilon_{\psi_1} = \varepsilon_{\psi_1} = 10^{-4}$. (a) Mesh graph of ψ_1. (b) Mesh graph of ψ_2. (c) Plot graph of ψ_1. (d) Plot graph of ψ_2.

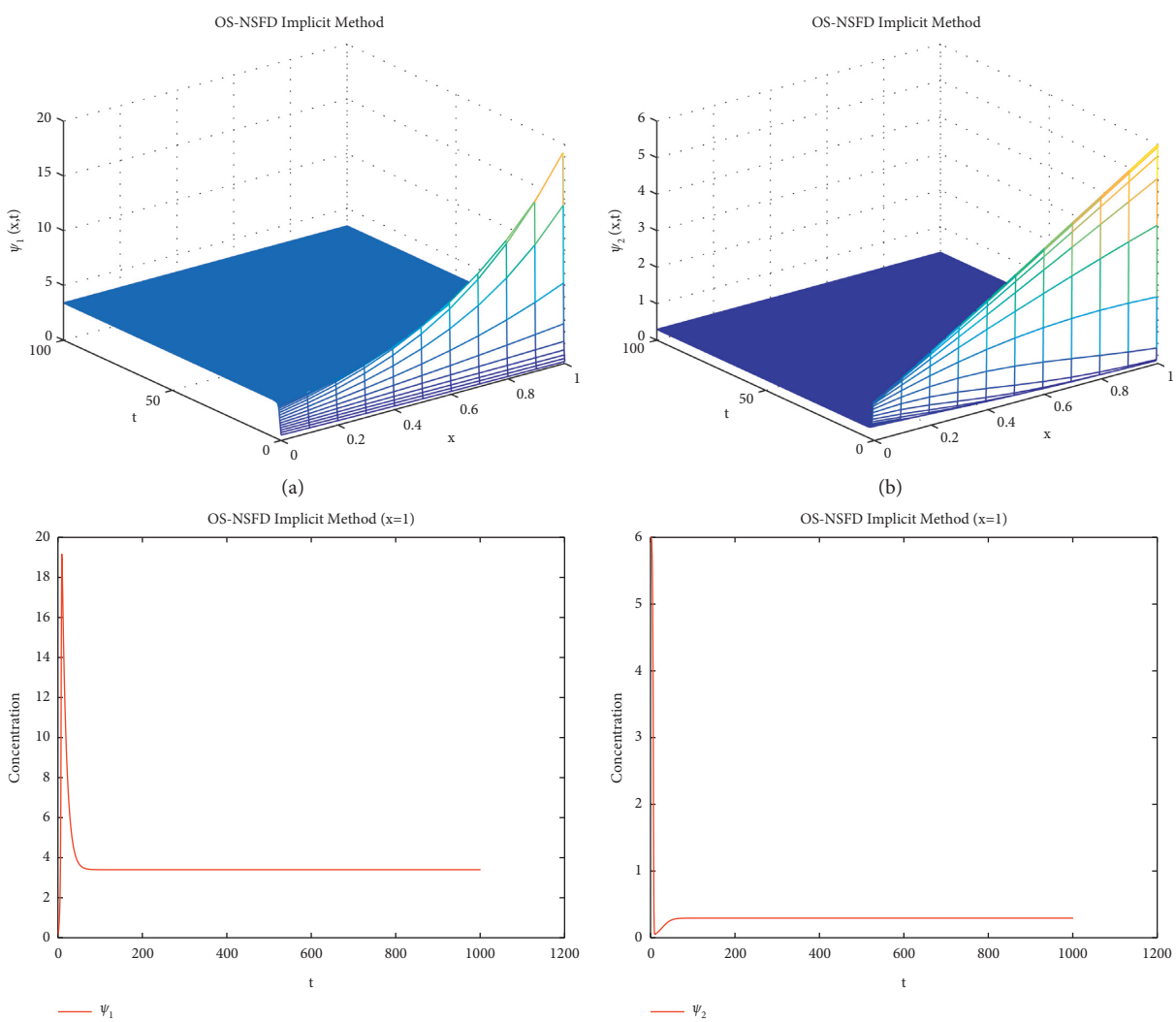

(a) (b)

(c) (d)

Figure 8: Mesh and plot graphs of ψ_1 and ψ_2 implementing NSFD implicit splitting method at $\kappa = 0.1, \vartheta_1 = 1, \vartheta_2 = 3.4, \lambda_1 = \lambda_2 = 0.001$, and $\varepsilon_{\psi_1} = \varepsilon_{\psi_1} = 10^{-4}$. (a) Solution graph of ψ_1. (b) Solution graph of ψ_2. (c) Plot graph of ψ_1. (d) Plot graph of ψ_2.

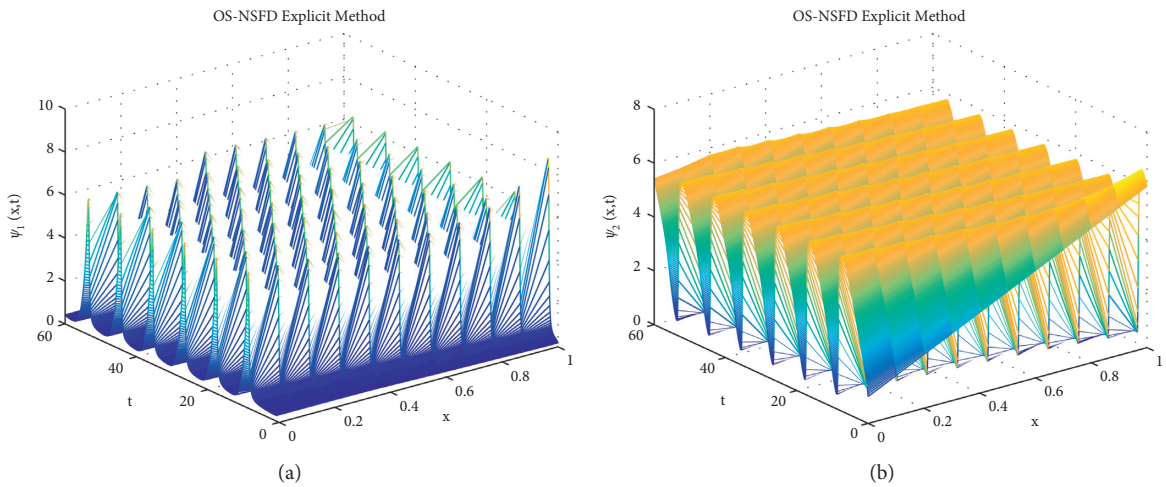

Figure 9: Solution graphs of ψ_1 and ψ_2 implementing NSFD explicit splitting technique at $\kappa = 0.1, \vartheta_1 = 3.4, \vartheta_2 = 1, \lambda_1 = \lambda_2 = 0.0006$, and $\varepsilon_{\psi_1} = \varepsilon_{\psi_1} = 10^{-4}$. (a) Solution graph of ψ_1. (b) Solution graph of ψ_2.

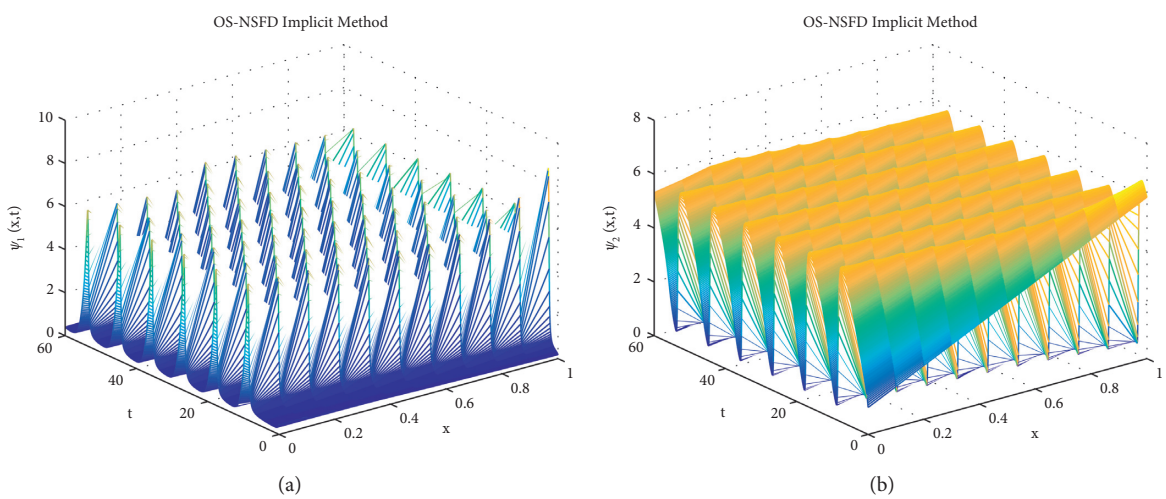

Figure 10: Solution graphs of ψ_1 and ψ_2 implementing NSFD implicit splitting method at $\kappa = 0.1, \vartheta_1 = 1, \vartheta_2 = 3.4, \lambda_1 = \lambda_2 = 0.0006$, and $\varepsilon_{\psi_1} = \varepsilon_{\psi_1} = 10^{-4}$. (a) Solution graph of ψ_1. (b) Solution graph of ψ_2.

In the above experiment, we use the following numerical values of parameters involved in the above system. $N = 3 \times 10^{-05}$, $\vartheta_1 = 0.04$, $\vartheta_2 = 24$, and $\varepsilon_{\psi_1} = \varepsilon_{\psi_2} = 0.01$. First, we depict the simulations of OS-NSFD explicit and implicit schemes at DFP. For the DFP, we take the value $\vartheta_3 = 9.2 \times 10^{-07}$ so that $\mathscr{B}_0 < 1$.

The simulations in the Figures 12 and 13 describe that the proposed splitting methods show positive solution as well as preserves the stability of fixed point DFP $\epsilon_0 = (N, 0) = (3 \times 10^{-05})$ under the condition $\mathscr{B}_0 < 1$. This shows that the designed NSFD splitting techniques do not show the contrived chaos.

Also, the graphs for susceptible and infected individuals reflect the positive and bounded solutions. It is notable that those graphs converge towards the exact fixed points for the step sizes, and other parameter values are mentioned above.

Next, we present the simulations of OS-NSFD explicit and implicit schemes at EP. For the EP, we use the value $\vartheta_3 = 1.4 \times 10^{-03}$ so that $\mathscr{B}_0 > 1$.

As we have taken the values of parameters so that $\mathscr{B}_0 > 1$. This implicates that SIR epidemic model converges toward EP $\epsilon_* = (\psi_{1*}, \psi_{2*})$. The simulation executed in Figures 14 and 15 illustrate the positive behavior and convergence to the EP $\epsilon_* = (\psi_{1*}, \psi_{2*})$ of NSFD explicit and implicit splitting schemes. In the light of the above discussion, it can be concluded that OS-NSFD explicit and implicit methods are reliable numerical methods for the solution of reaction diffusion models. Because these methods confine all the

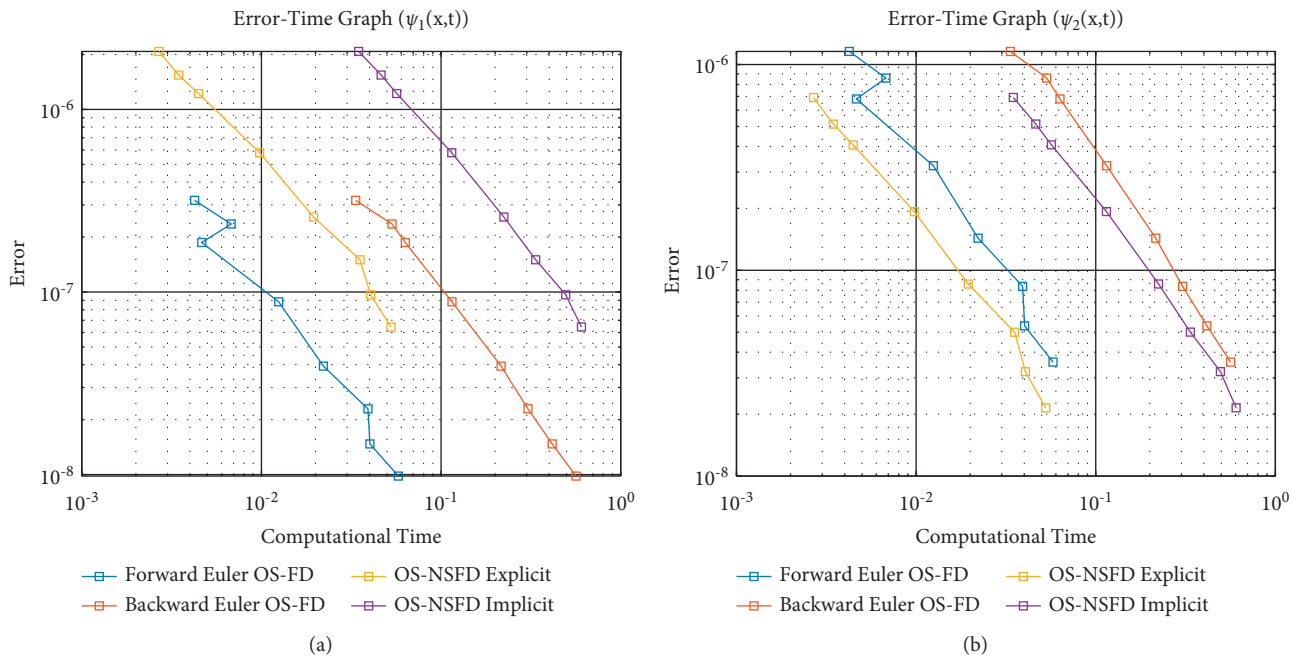

Figure 11: Log-log graphs. The error versus the computational time when solving the system subjected to the initial data. Three schemes are employed: forward Euler OS-FD technique, backward Euler OS-FD technique, OS-NSFD explicit technique, and OS-NSFD implicit technique. The graphs correspond to the solutions when the functions ψ_1 and ψ_2 of the Brusselator model are estimated. The parameters employed are $L = 1, T = 1, \vartheta_1 = 0.05, \vartheta_2 = 0.02, M = 100$, and $\varepsilon_{\psi_1} = \varepsilon_{\psi_1} = 10^{-4}$. The exact solution was approximated using $N = 20000$. (a) Error time graph for ψ_1. (b) Error time graph for ψ_2.

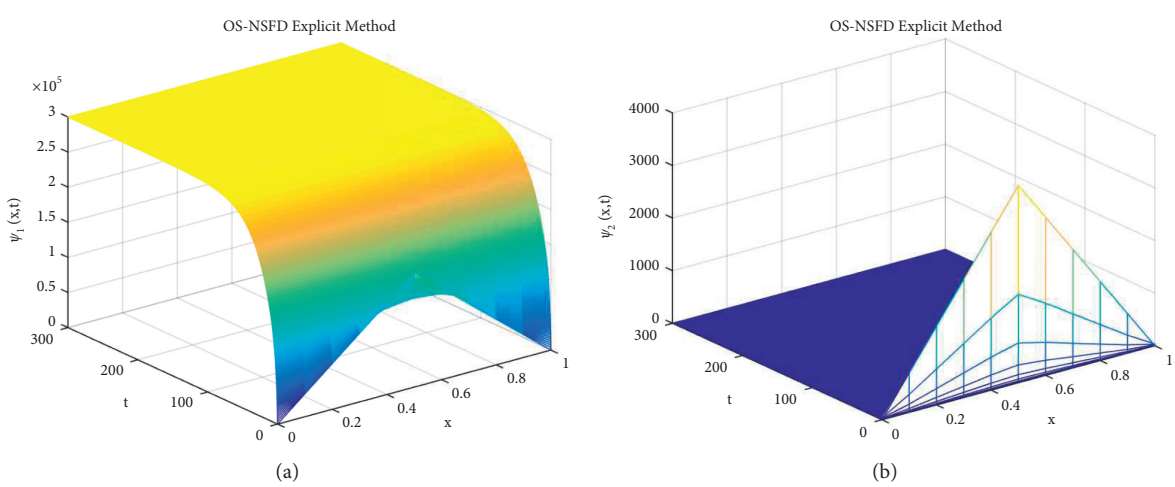

Figure 12: Solution graphs of ψ_1 and ψ_2 (susceptible and infected population densities) using the NSFD explicit splitting method at $\kappa = 0.1, \lambda_1 = \lambda_2 = 0.05$. (a) Solution graph of ψ_1. (b) Solution graph of ψ_2.

important features of reaction diffusion systems like as positivity, boundedness, and stability at equilibrium points.

6. Schnakenberg Model

Schnakenberg model is autocatalytic in nature given in 1979 [42]. The Schnakenberg model is a coupled reaction diffusion system [43] given as

$$\frac{\partial \psi_1}{\partial t} = \frac{\partial^2 \psi_1}{\partial x^2} + \vartheta_3\left(\vartheta_1 - \psi_1 + (\psi_1)^2 \psi_2\right), \tag{45}$$

$$\frac{\partial \psi_2}{\partial t} = \varepsilon_{\psi_2} \frac{\partial^2 \psi_2}{\partial x^2} + \vartheta_3\left(\vartheta_2 - (\psi_1)^2 \psi_2\right), \tag{46}$$

with initial conditions

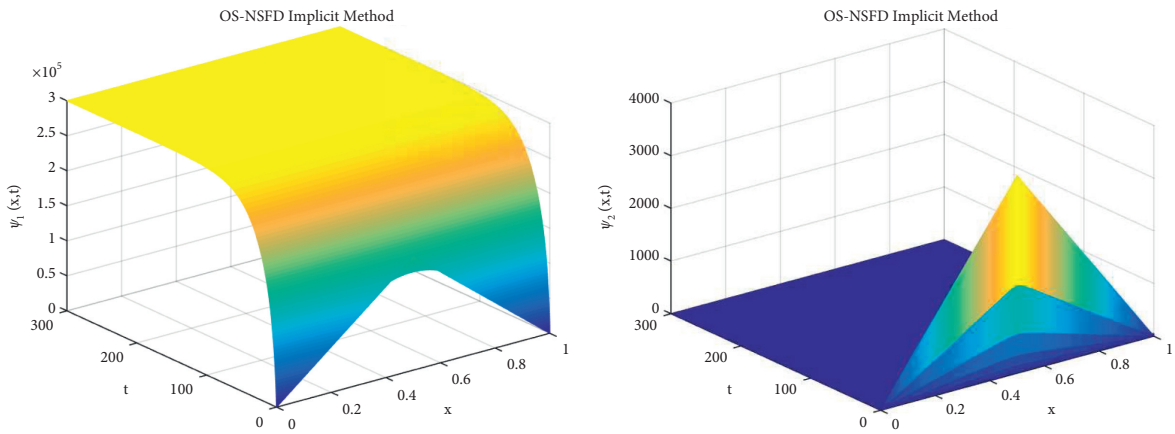

(a) (b)

Figure 13: Solution graphs of ψ_1 and ψ_2 (susceptible and infected population densities) using NSFD implicit splitting method at $\kappa = 0.002, \lambda_1 = \lambda_2 = 125$. (a) Solution graph of ψ_1. (b) Solution graph of ψ_2.

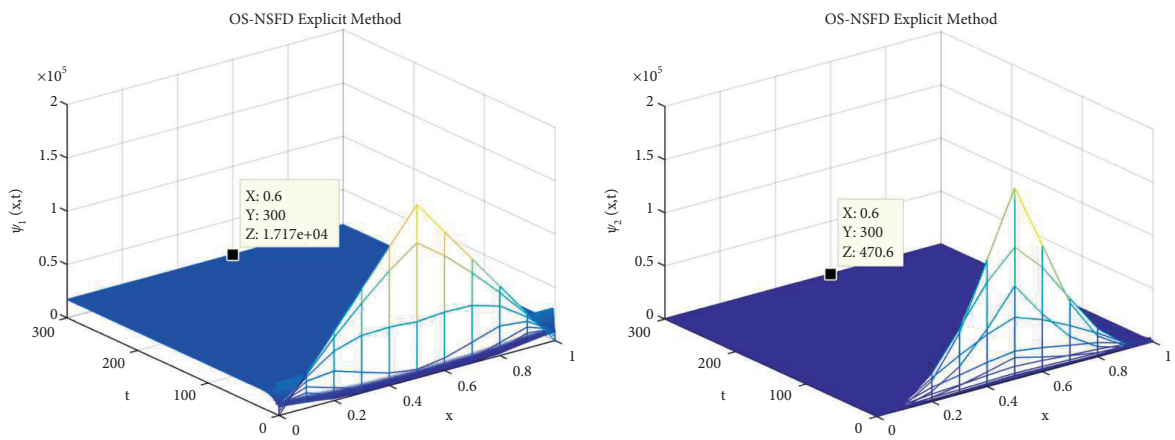

(a) (b)

Figure 14: Solution graphs of ψ_1 and ψ_2 (susceptible and infected population densities) using the NSFD explicit splitting method at $\kappa = 0.1, \lambda_1 = \lambda_2 = 0.05$. (a) Solution graph of ψ_1. (b) Solution graph of ψ_2.

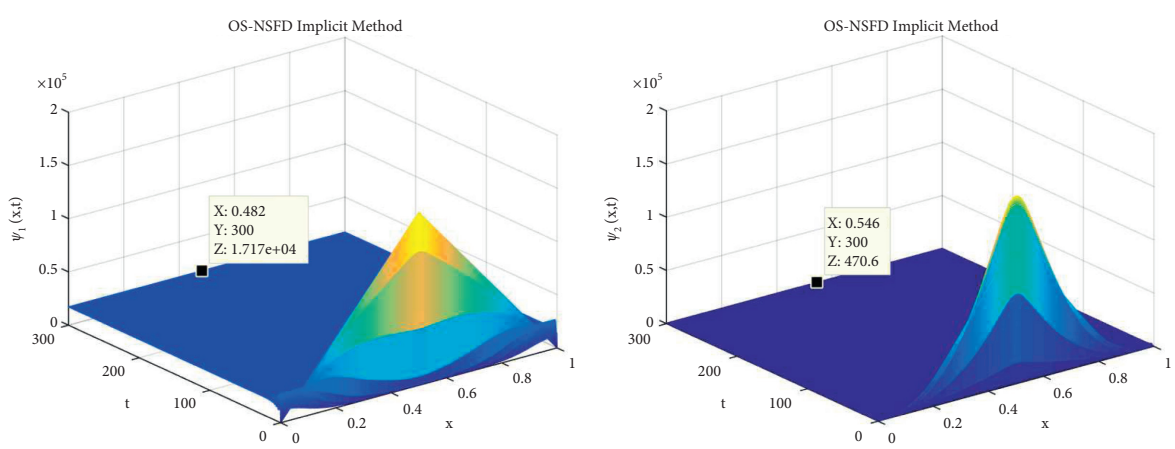

(a) (b)

Figure 15: Solution graphs of ψ_1 and ψ_2 (susceptible and infected population densities) using the NSFD implicit splitting method at $\kappa = 0.002, \lambda_1 = \lambda_2 = 125$. (a) Solution graph of ψ_1. (b) Solution graph of ψ_2.

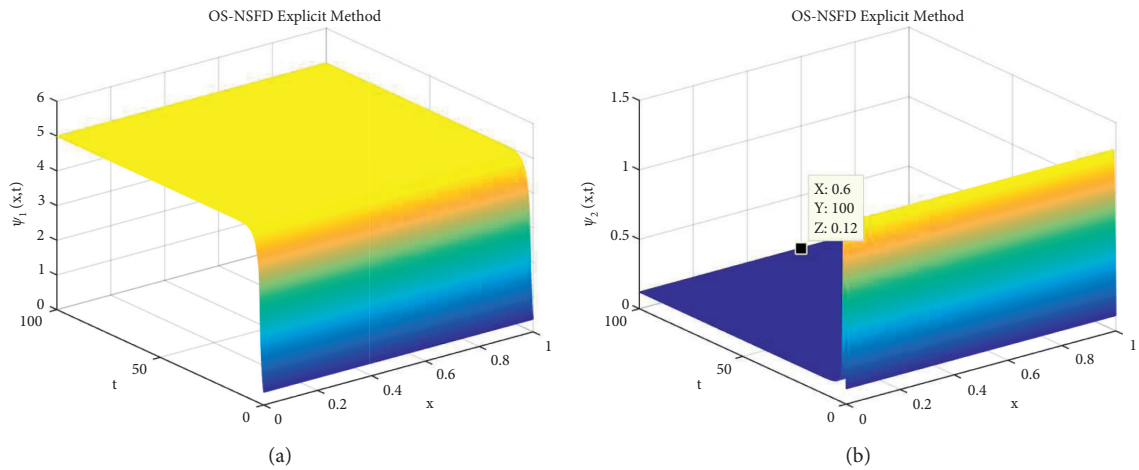

Figure 16: Mesh graphs of ψ_1 and ψ_2 (chemical concentration) using NSFD explicit splitting method at $\kappa = 0.1, \lambda_1 = 0.1, \lambda_2 = 0.00001$. (a) Mesh graph of ψ_1. (b) Mesh graph of ψ_2.

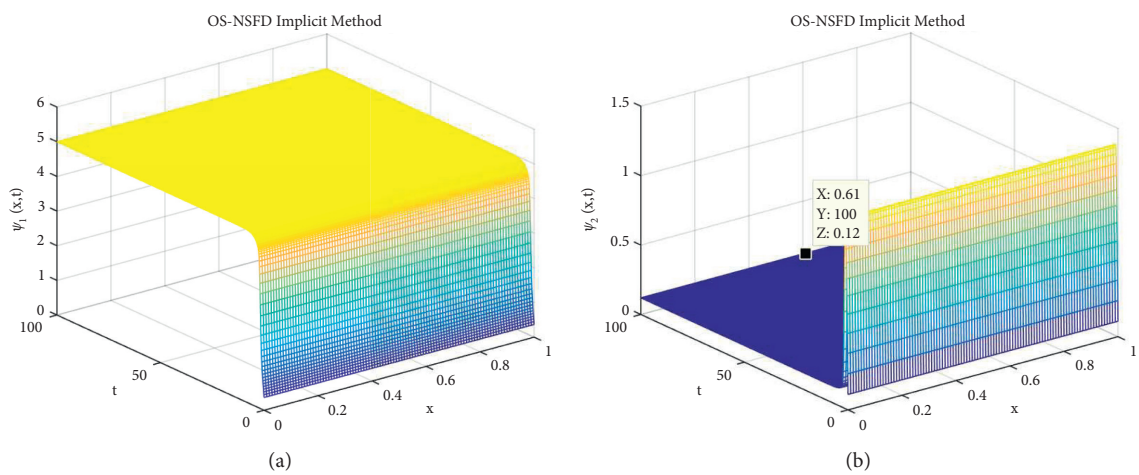

Figure 17: Mesh graphs of ψ_1 and ψ_2 (chemical concentration) using NSFD implicit splitting method at $\kappa = 0.01, \lambda_1 = 1000, \lambda_2 = 0.1$. (a) Mesh graph of ψ_1. (b) Mesh graph of ψ_2.

$$\psi_1(x,0) = e^{-(1+0.001x)}, \tag{47}$$

$$\psi_2(x,0) = \frac{1}{9}, \tag{48}$$

and no flux boundary conditions.

Here, ψ_1 and ψ_2 demonstrate the chemical concentrations of the two species. ϑ_1 and ϑ_2 are chemical kinetic positive constants, and ϑ_3 is the positive constant for the model which is dimensionless. The equilibrium point of systems (45)and(46) is (ψ_1^*, ψ_2^*), where $\psi_1^* = (\vartheta_1 + \vartheta_2)$ and $\psi_2^* = \vartheta_2/(\vartheta_1 + \vartheta_2)$. The equilibrium point is stable under the condition $\vartheta_2 - \vartheta_1 < (\vartheta_1 + \vartheta_2)^3$ [43]. If this condition violates, then the point (ψ_1^*, ψ_2^*) is unstable.

Now, we present the simulations of the above experiment. First, we take the values of parameters $\vartheta_1 = 2$, $\vartheta_2 = 3$, $\vartheta_3 = 0.5$, and $\varepsilon_{\psi_2} = 10^{-04}$ such that the condition $\vartheta_2 - \vartheta_1 < (\vartheta_1 + \vartheta_2)^3$ satisfies. For these numerical values, the equilibrium point is $(\psi_1^*, \psi_2^*) = (5, 0.12)$.

The graphs in Figures 16 and 17 show the consistent behavior of both OS-NSFD explicit and implicit schemes. Both schemes show that the graphs converge towards the point $(\psi_1^*, \psi_2^*) = (5, 0.12)$. We are not presenting the graphical solution with forward Euler and backward Euler splitting schemes, but it is confirmed that the schemes will present the inconsistent behavior for different values of parameters as shown earlier for the Brusselator model.

Now, we choose the values of parameters $\vartheta_1 = 0.1$, $\vartheta_2 = 0.4$, $\vartheta_3 = 0.5$, and $\varepsilon_{\psi_2} = 10^{-04}$ such that the condition $\vartheta_2 - \vartheta_1 < (\vartheta_1 + \vartheta_2)^3$ violates.

As we discussed earlier that systems (45) and (46) show the unstable behavior if the condition $\vartheta_2 - \vartheta_1 < (\vartheta_1 + \vartheta_2)^3$ does not satisfy. The graphs in Figures 18 and 19 clarify that OS-NSFD explicit and implicit schemes also reveal the unstable behavior which is possessed by the continuous system.

It is important to note that all the parameters and step sizes are kept same during the simulations. It is the stability

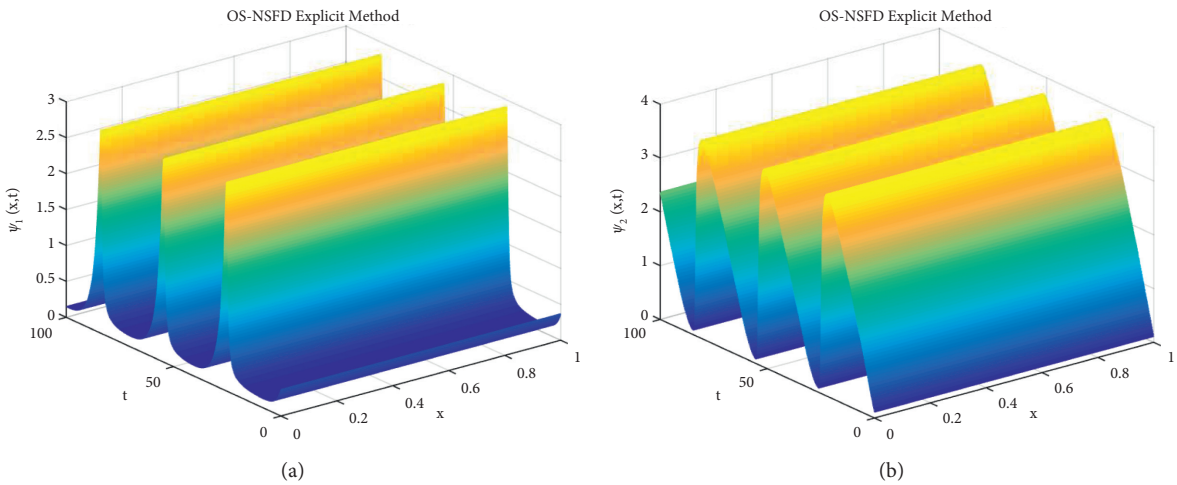

Figure 18: Mesh graphs of ψ_1 and ψ_2 (chemical concentration) using the NSFD explicit splitting method at $\kappa = 0.1, \lambda_1 = 0.1, \lambda_2 = 0.00001$. (a) Mesh graph of ψ_1. (b) Mesh graph of ψ_2.

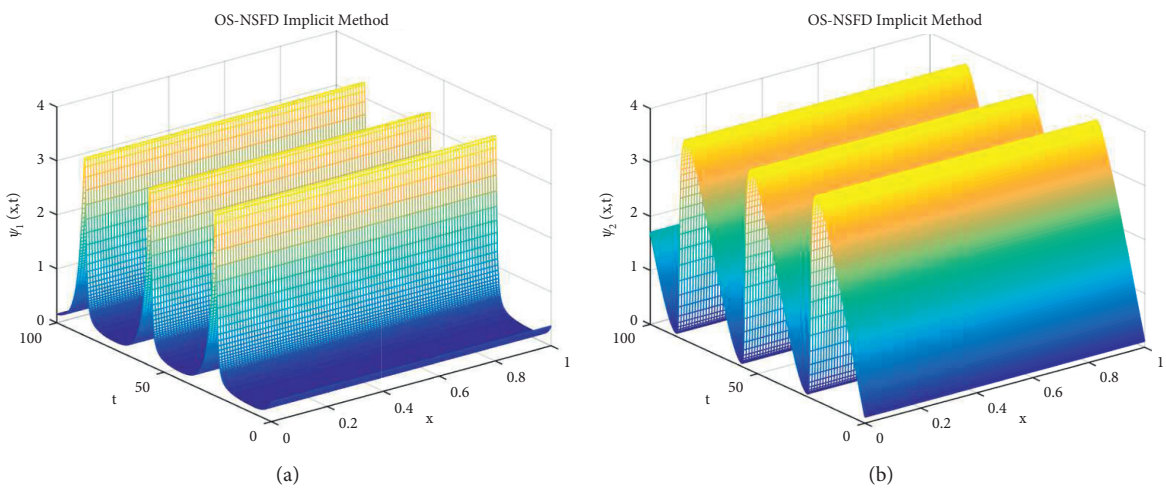

Figure 19: Mesh graphs of ψ_1 and ψ_2 (chemical concentration) using the NSFD implicit splitting method at $\kappa = 0.01, \lambda_1 = 1000, \lambda_2 = 0.1$. (a) Mesh graph of ψ_1. (b) Mesh graph of ψ_2.

condition that also plays an important role in describing the stability of the system.

7. Conclusion

In this article, four numerical schemes based on finite difference approximation are presented for solving different reaction-diffusion models in one-space dimension. It has been observed that two classical methods fail to provide accurate solution. Also, these schemes do not hold the positivity condition of the unknown variables in the continuous system. To overcome this issue, two new positivity preserving techniques have been proposed, based on OS-NSFD schemes. Our proposed methods not only provide the positive solution but also retain the essential physical attributes of the state variables. The designed schemes are applied on the Brusselator model, Schnakenberg model, and SIR epidemic model. The simulations are carried out to obtain the graphical solutions. The numerical results ascertained that the newly designed NSFD splitting schemes have some prominent features of the solution such as positivity of the solutions and stability at equilibrium points of the continuous system. One of the main significance is that the designed schemes do not generate the contrived chaos.

The OS-NSFD methods grant the positive solution irrespective of the step sizes. So, these schemes are unconditionally positivity preserving. Also, these schemes are time efficient and consistent.

The successful implementation of NSFD splitting schemes on three different problems show that our proposed schemes are futuristic and these techniques can be applied on various physical reaction diffusion problem in the fields of physical science, engineering, fluid mechanics, economics, and many more.

Data Availability

No data were used to support this work.

Conflicts of Interest

The authors declare no conflicts of interest.

References

[1] Z. Korpinar, M. Inc, M. S. Alshomrani, and D. Baleanu, "The deterministic and stochastic solutions of the Schrodinger equation with time conformable derivative in birefrigent fibers," *AIMS Mathematics*, vol. 5, no. 3, pp. 2326–2345, 2020.

[2] M. Partohaghighi, M. Inc, M. Bayram, and D. Baleanu, "On numerical solution of the time fractional advection-diffusion equation involving atangana-baleanu-caputo derivative," *Open Physics*, vol. 17, no. 1, pp. 816–822, 2019.

[3] M. M. A. Khater, D.-C. Lu, R. A. M. Attia, and M. Inç, "Analytical and approximate solutions for complex nonlinear schrödinger equation via generalized auxiliary equation and numerical schemes," *Communications in Theoretical Physics*, vol. 71, no. 11, p. 1267, 2019.

[4] R. Lefever and G. Nicolis, "Chemical instabilities and sustained oscillations," *Journal of Theoretical Biology*, vol. 30, no. 2, pp. 267–284, 1971.

[5] I. Prigogine and G. Nicolis, "Self-organisation in nonequilibrium systems: towards a dynamics of complexity," *Bifurcation Analysis*, Springer, Netherlands, pp. 3–12, 1985.

[6] I. Prigogine and R. Lefever, "Symmetry breaking instabilities in dissipative systems. II," *The Journal of Chemical Physics*, vol. 48, no. 4, pp. 1695–1700, 1968.

[7] J. J. Tyson, "Some further studies of nonlinear oscillations in chemical systems," *The Journal of Chemical Physics*, AIP Publishing), vol. 58, no. 9, pp. 3919–3930, 1973.

[8] A. Turing, "The chemical basis of morphogenesis," *Bulletin of Mathematical Biology*, vol. 52, no. 1-2, pp. 153–197, 1990.

[9] S. Kumar, R. Jiwari, and R. C. Mittal, "Numerical simulation for computational modelling of reaction diffusion Brusselator model arising in chemical processes," *Journal of Mathematical Chemistry*, Springer Science and Business Media, vol. 57, , pp. 149–179, 2019.

[10] R. C. Mittal and R. Rohila, "A study of one dimensional nonlinear diffusion equations by Bernstein polynomial based differential quadrature method," *Journal of Mathematical Chemistry*, vol. 55, no. 2, pp. 673–695, 2016.

[11] R. C. Mittal and R. Rohila, "Numerical simulation of reaction-diffusion systems by modified cubic B-spline differential quadrature method," *Chaos, Solitons & Fractals*, vol. 92, pp. 9–19, 2016.

[12] S. Siraj-ul-Islam, A. Ali, and S. Haq, "A computational modeling of the behavior of the two-dimensional reaction-diffusion Brusselator system," *Applied Mathematical Modelling*, vol. 34, no. 12, pp. 3896–3909, 2010.

[13] R. Jiwari and J. Yuan, "A computational modeling of two dimensional reaction-diffusion Brusselator system arising in chemical processes," *Journal of Mathematical Chemistry*, Springer Science and Business Media, vol. 52, no. 6, pp. 1535–1551, 2014.

[14] S. Dahiya and R. C. Mittal, "A modified cubic B-spline differential quadrature method for three-dimensional non-linear diffusion equations," *Open Physics*, vol. 15, no. 1, pp. 453–463, 2017.

[15] Z. Lin, R. Ruiz-Baier, and C. Tian, "Finite volume element approximation of an inhomogeneous Brusselator model with cross-diffusion," *Journal of Computational Physics*, vol. 256, pp. 806–823, 2014.

[16] F. Khani, F. Samadi, and S. Hamedi-Nezhad, "New exact solutions of the brusselator reaction diffusion model using the exp-function method," *Mathematical Problems in Engineering*, vol. 2009, pp. 1–9, 2009.

[17] R. C. Mittal and R. Jiwari, "Numerical solution of two-dimensional reaction-diffusion Brusselator system," *Applied Mathematics and Computation*, vol. 217, no. 12, pp. 5404–5415, 2011.

[18] H. y. Alfifi, "Semi-analytical solutions for the brusselator reaction-diffusion model," *ANZIAM Journal*, vol. 59, no. 2, pp. 167–182, 2017.

[19] S. Alkhalaf, "Third-order approximate solution of chemical reaction-diffusion brusselator system using optimal homotopy asymptotic method," *Advances in Mathematical Physics*, vol. 2017, pp. 1–8, 2017.

[20] M. Ghergu and V. Rădulescu, "Turing patterns in general reaction-diffusion systems of brusselator type," *Communications in Contemporary Mathematics*, vol. 12, no. 4, pp. 661–679, 2010.

[21] Z. U. A. Zafar, K. Rehan, M. Mushtaq, and M. Rafiq, "Numerical treatment for nonlinear Brusselator chemical model," *Journal of Difference Equations and Applications*, vol. 23, no. 3, pp. 521–538, 2016.

[22] M. A. Zaky and A. S. Hendy, "An efficient dissipation-preserving Legendre-Galerkin spectral method for the Higgs boson equation in the de Sitter spacetime universe," *Applied Numerical Mathematics*, vol. 160, pp. 281–295, 2021.

[23] M. Abbaszadeh, M. Dehghan, M. A. Zaky, and A. S. Hendy, "Interpolating stabilized element free galerkin method for neutral delay fractional damped diffusion-wave equation," *Journal of Function Spaces*, vol. 2021, Article ID 6665420, 11 pages, 2021.

[24] A. K. Omran, M. A. Zaky, A. S. Hendy, and V. G. Pimenov, "An efficient hybrid numerical scheme for nonlinear multi-term caputo time and riesz space fractional-order diffusion equations with delay," *Journal of Function Spaces*, vol. 2021, Article ID 5922853, , 2021.

[25] A. S. Hendy, M. A. Zaky, and M. Abbaszadeh, "Long time behavior of Robin boundary sub-diffusion equation with fractional partial derivatives of Caputo type in differential and difference settings," *Mathematics and Computers in Simulation*, vol. 190, pp. 1370–1378, 2021.

[26] S. Nandal, M. A. Zaky, and R. H. De Staeien, "Numerical simulation for a multidimensional fourth-order nonlinear fractional subdiffusion model with time delay," *Mathematics*, vol. 9, no. 23, p. 3050, 2021.

[27] A. S. Hendy, M. A. Zaky, R. M. Hafeez, and R. H. De Staeien, "The impact of memory effect on space fractional strong quantum couplers with tunable decay behavior and its numerical simulation," *Scientific Reports*, vol. 11, no. 1, pp. 1–15, 2021.

[28] H. Selvitopi, M. A. Zaky, and A. S. Hendy, "Crank-Nicolson/finite element approximation for the Schrödinger equation in the de Sitter spacetime," *Physica Scripta*, vol. 96, no. 12, Article ID 124010, 2021.

[29] R. E. Mickens, *Nonstandard Finite Difference Models of Differential Equations*, World Scientific, Singapore, 1993.

[30] N. Ahmed, T. S.S., M. Rafiq, M. A. Rehman, M. Ali, and M. O. Ahmad, "Positivity preserving operator splitting nonstandard finite difference methods for SEIR reaction

diffusion model," *Open Mathematics*, vol. 17, no. 1, pp. 313–330, 2019.

[31] M. Zhang and Q. Zhang, "A positivity preserving numerical method for stochastic R&D model," *Applied Mathematics and Computation*, vol. 351, pp. 193–203, 2019.

[32] N. Ahmed, M. Rafiq, M. A. Rehman, M. S. Iqbal, and M. Ali, "Numerical modeling of three dimensional Brusselator reaction diffusion system," *AIP Advances*, vol. 9, no. 1, Article ID 015205, 2019.

[33] J. Tan, H. Yang, W. Men, and Y. Guo, "Construction of positivity preserving numerical method for jump-diffusion option pricing models," *Journal of Computational and Applied Mathematics*, vol. 320, pp. 96–100, 2017.

[34] N. Ahmed, Z. Wei, D. Baleanu, M. Rafiq, and M. A. Rehman, "Spatio-temporal numerical modeling of reaction-diffusion measles epidemic system," *Chaos: An Interdisciplinary Journal of Nonlinear Science*, vol. 29, no. 10, Article ID 103101, 2019.

[35] N. Ahmed, M. Jawaz, M. Rafiq, M. A. Rehman, M. Ali, and M. O. Ahmad, "Numerical treatment of an epidemic model with spatial diffusion," *Journal of Applied Environmental and Biological Sciences*, vol. 8, no. 6, pp. 17–29, 2018.

[36] N. Ahmed, M. Rafiq, M. A. Rehman, M. Ali, and M. O. Ahmad, "Numerical modeling of SEIR measles dynamics with diffusion," *Communications in Mathematics and Applications*, vol. 9, pp. 315–326, 2018.

[37] N. Ahmed, N. Shahid, Z. Iqbal et al., "Numerical modeling of SEIQV epidemic model with saturated incidence rate," *Journal of Applied Environmental and Biological Sciences*, vol. 8, 2018.

[38] R. C. Harwood, *Operator Splitting Method and Applications for Semilinear Parabolic Partial Differential Equations*, George Fox University, USA, 2011.

[39] R. C. Harwood, V. S. Manoranjan, and D. B. Edwards, "Lead-acid battery model under discharge with a fast splitting method," *IEEE Transactions on Energy Conversion*, vol. 26, no. 4, pp. 1109–1117, 2011.

[40] T. Fujimoto and R. Ranade, "Two characterizations of inverse-positive matrices: the Hawkins-Simon condition and the Le Chatelier-Braun principle," *The Electronic Journal of Linear Algebra*, vol. 11, no. 1, 2004.

[41] S. Chinviriyasit and W. Chinviriyasit, "Numerical modelling of an SIR epidemic model with diffusion," *Applied Mathematics and Computation*, vol. 216, no. 2, pp. 395–409, 2010.

[42] J. Schnakenberg, "Simple chemical reaction systems with limit cycle behaviour," *Journal of Theoretical Biology*, vol. 81, pp. 389–400, 1979.

[43] Z. Hammouch, T. Mekkaoui, and F. B. M. Belgacem, "Numerical simulations for a variable order fractional Schnakenberg model," *AIP Conference Proceedings*, vol. 1637, 2014.

Hindawi
Journal of Function Spaces
Volume 2022, Article ID 8316404, 17 pages
https://doi.org/10.1155/2022/8316404

Research Article

Extended Split-Step Fourier Transform Approach for Accurate Characterization of Soliton Propagation in a Lossy Optical Fiber

Neveen G. A. Farag,[1] **Ahmed H. Eltanboly**,[1] **M. S. El-Azab**,[1] **and S. S. A. Obayya**[2,3]

[1]*Mathematics and Engineering Physics Department, Faculty of Engineering, Mansoura University, Mansoura 35516, Egypt*
[2]*Centre for Photonics and Smart Materials, Zewail City of Science and Technology, October Gardens, 6th of October City, Giza 12578, Egypt*
[3]*Electronics and Communications Engineering Department, Faculty of Engineering, Mansoura University, Mansoura 35516, Egypt*

Correspondence should be addressed to Neveen G. A. Farag; eng_neveen@hotmail.com

Received 1 December 2021; Revised 31 January 2022; Accepted 17 February 2022; Published 8 March 2022

Academic Editor: Youssri Hassan Youssri

In this paper, we present a novel extension of the well-known split-step Fourier transform (SSFT) approach for solving the one-dimensional nonlinear Schrödinger equation (NLSE), which incorporates the fiber loss term. While this essential equation governs the pulse propagation in a lossy optical fiber, it is not supported by an exact analytical solution. In this regard, extended versions of the Fourier pseudospectral method (FPSM) and Hopscotch method (HSM) are effectively established as well to cope with the fiber losses effects associated with the pulses' propagation through the fiber optics, and thus, numerous comparisons are exhaustively conducted among these three compelling numerical approaches to validate their reliability, stability, and accuracy. Based on this, the MATLAB numerical findings bolster that the extended version of the SSFT approach demonstrates superior performance over the other suggested schemes in simulating the solitons propagation in a lossy optical fiber.

1. Introduction

A soliton, or what is also known as a solitary wave, is a self-reinforcing wave packet that sustains both its form and velocity while propagation, regardless of the travelling distance or presence of obstacles. This shape conservation property makes it potentially compatible with the long-distance expansive data transmission [1]. Moreover, a cancellation of nonlinear and dispersive effects in the propagation medium, which is a basic feature that invariably occurs in the optical fibers, causes solitons. In other words, the term soliton refers to any optical pulse that resists changing when it is transferred from the source to the destination due to a sensitive balance between the nonlinear and linear effects in the medium [2]. Therefore, the solitons are utterly beneficial in transporting information through optical fibers in a variety of modern communication systems because they demonstrate a robust grasp in achieving high bit rate transmission while minimizing error possibilities. This occurs due to their propagation without any distortion or shape changing while moving through a lossless medium, which guarantees retaining the information stored in them until they reach the desired location [3]. This means that solitons pulses have incredibly stable characteristics in propagation through the transmission path due to its powerful resistance to the distortion effects, which resulted from the nonlinearity and dispersion and inherited in the optical fibers. However, the only serious damage that may change their shapes while propagation is the attenuation caused by the fiber losses. Thus, numerous researchers have suggested to compensate these fiber losses by the aid of the amplification in order to mitigate the functionality of the all-optical transmission system [4].

The optical fiber, where the solitons always propagate, is an extremely fine and thin pure glass that is usually made of pure silica. This fascinating fiber simulates the function of a waveguide in transmitting light pulses through the fiber ends because it comprises a transparent core surrounded by a lower refraction index transparent cladding material; this unique structure, presented in Figure 1 [5], confines the light

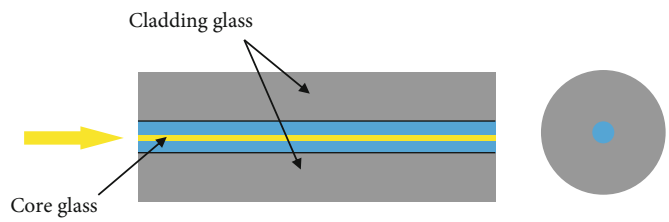

Figure 1: A schematic diagram of a single-mode fiber optics.

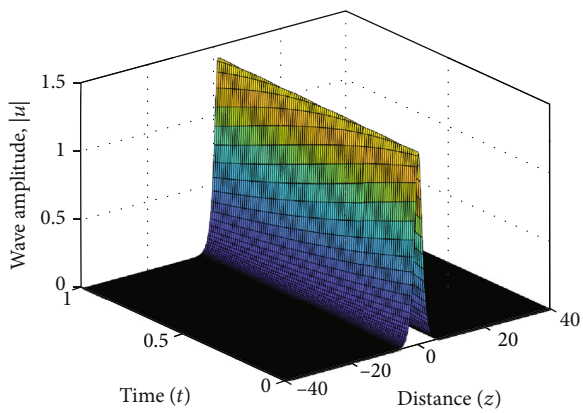

Figure 2: A 3D plot of the 1D CNLSE exact solution.

wave in the core region in accordance with the total internal reflection phenomenon. Hence, optical fibers are eminently used in the communications field, especially for long distance and higher band width transmission. In contrast, transmission through the metal wires experiences higher losses and encounters electromagnetic interference, which negatively impacts the quality of the transmitted data [6].

The propagation of the optical pulses through the optical fiber, which is a nonlinear medium, is modeled by the 1D nonlinear Schrödinger equation (NLSE). Thus, this crucial second-order partial differential equation is highly compatible with depicting the unidirectional propagation of the light waves in single-mode fiber optics [7]. More importantly, although it is remarkably noticed that the NLSE can be solved using both exact and numerical solutions, its analytical solution is extremely tough and tedious to be found, abreast of being provided for a limited set of initial conditions [8]. As a result of this, the numerical solutions of the NLSE frequently demonstrate a significant role in solving and approximating the equation and, likewise, understanding the equation's physical behavior [9].

Moreover, the exact analytical solutions of NLSE can only be obtained in the case of the soliton solutions, if and only if the attenuation term is neglected, whereas, for the other solutions, which are not solitons, or in the presence of fiber losses that must occur in any realistic optical fiber, the exact solutions are not easily to be reached. In other words, the exact analytical solution can only be found for some specific input pulses, most commonly, the hyperbolic secant and tangent functions. Therefore, the numerical solutions are widely used to unravel this equation. More specifically, the split-step Fourier transform is suggested for its high processing speed, stability, and accuracy, along with other techniques such as the Fourier pseudospectral method and the Hopscotch approach, as employed elsewhere for solving other equations [10–16], which will be comprehensively explained within this framework. Besides, other numerical approaches have recently been developed to report the 1D NLSE by several authors, for more details, see [17–26]. Additionally, analytical approximations to solve the NLSE might exist by implementing plenty of linearization techniques. For instance, perturbation methods tailored for modulation instability, small-signal analysis, variational method, and an approach based on Volterra series, all these methods can provide accurate approximations for any arbitrary modulated input signal [17, 18].

On the other hand, opting for a numerical approach to solve this equation should be classified under two main categories, which are either the finite difference methods (FDMs) or the function approximation methods (FAMs), which are divided into both the spectral and pseudospectral methods. In the FDMs, the unknown function is approximated at discrete points in the space-time plane, while replacing the partial derivatives with difference relations employed by Taylor series. Whereas in the FAMs, the basic goal is to approximate the exact solution using an appropriate chosen basis function, a trigonometric function is usually selected. This notable strategy eventually constitutes the finite element method that is categorized as a spectral method [27]. Furthermore, the main distinguished difference between the pseudospectral and spectral methods is that the pseudospectral methods are computed in a discrete space, which resembles the behavior of the FDMs [28, 29].

In this paper, the aim is to seek feasible solutions for the NLSE, incorporating the fiber loss term. More specifically, due to the harmful impact of the fiber losses on changing the authentic form of the transmitted pulse that can obviously be noticed as an attenuation in both the pulse's amplitude and power, an urgent need has emerged to include the fiber losses in our consideration. Furthermore, this attenuation should efficiently be measured and hence compensated using amplifiers in order not to hinder the accurate reception of the pulses at the destination. In other words, including the loss term to our attention in the simulation of the soliton propagation is extremely vital, as recently followed elsewhere [30]. Otherwise, numerical errors may arise, which shall likely lead to biased results that do not genuinely represent the physical phenomenon. For example, failing to correctly model the degradation of the pulse's amplitude and power due to the attenuation was caused by the loss effects. Despite the losses problem in

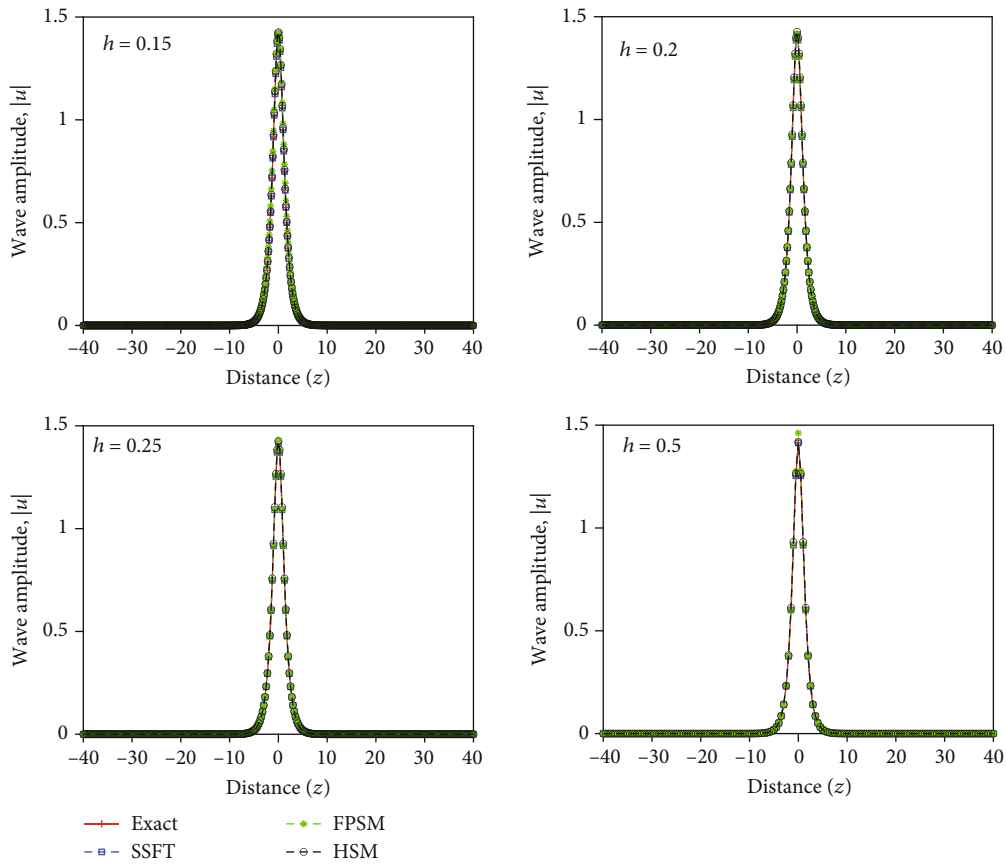

Figure 3: A comparison of the split-step Fourier transform (SSFT), the Fourier pseudospectral method (FPSM), the Hopscotch method (HSM), and the exact solution at $\tau = 0.001$ and $t = 20$ over a space domain z from -40 to 40, whereas using different values of h.

optical fibers has previously attracted a great deal of interest, we exhibit in the present work, for the first time, a method that renders the least sum of square errors along with the fastest computational speed based on an extended version of a well-known split-step strategy. Therefore, our primary target was the meticulous inclusion of the loss term in our suggested numerical methods named split-step Fourier transform (SSFT), Fourier pseudospectral method (FPSM), and Hopscotch method (HSM); the first two methods are pseudospectral methods, while the last one is an explicit finite difference method. Based on this, an extension for each of the three proposed approaches was developed so that their approximate solutions agree with the effects generated by the fiber losses, thereby broadening the validity range of the suggested schemes. Furthermore, in an attempt to substantiate the performance of the extended approaches, plenty of numerical assessments were conducted to track the behavior of both the pulse's shape and power. In this regard, we fundamentally focus on the bright and dark one soliton propagation in fiber optics abreast of demonstrating and testing each of the suggested methods of solutions.

This paper is organized as follows. Following this introduction, which is illustrated in Section 1, the mathematical preliminaries are explained in detail in Section 2. Section 3 is devoted to annotating the modified numerical approaches, while Section 4 elaborates on the error and convergence discussion. In Section 5, the numerical results that were achieved are exhibited, rigorously highlighting the attenuation effect caused by the presence of the fiber losses through the drawing of copious graphs and illustrative comparisons. Eventually, Section 6 culminates with the overall conclusion that summarizes the research work presented in this paper.

2. Mathematical Preliminaries

2.1. The NLSE for Lossy Optical Fiber. The 1D NLSE, which governs the pulse propagation in the z direction through a lossy optical fiber, comprises four rudimentary terms, the first-order spatial partial derivative term, the second-order temporal partial derivative term, the nonlinear term, and the unknown function term. Moreover, this outstanding equation mainly relies on some crucial parameters such as the Kerr nonlinear coefficient, the power attenuation constant, and the group velocity dispersion parameter, as illustrated by either Equation (1) or (2):

$$\frac{\partial u(z,t)}{\partial z} = -i\frac{\beta_2}{2}\frac{\partial^2 u(z,t)}{\partial t^2} + i\gamma|u(z,t)|^2 u(z,t) - \frac{\alpha}{2}u(z,t), \tag{1}$$

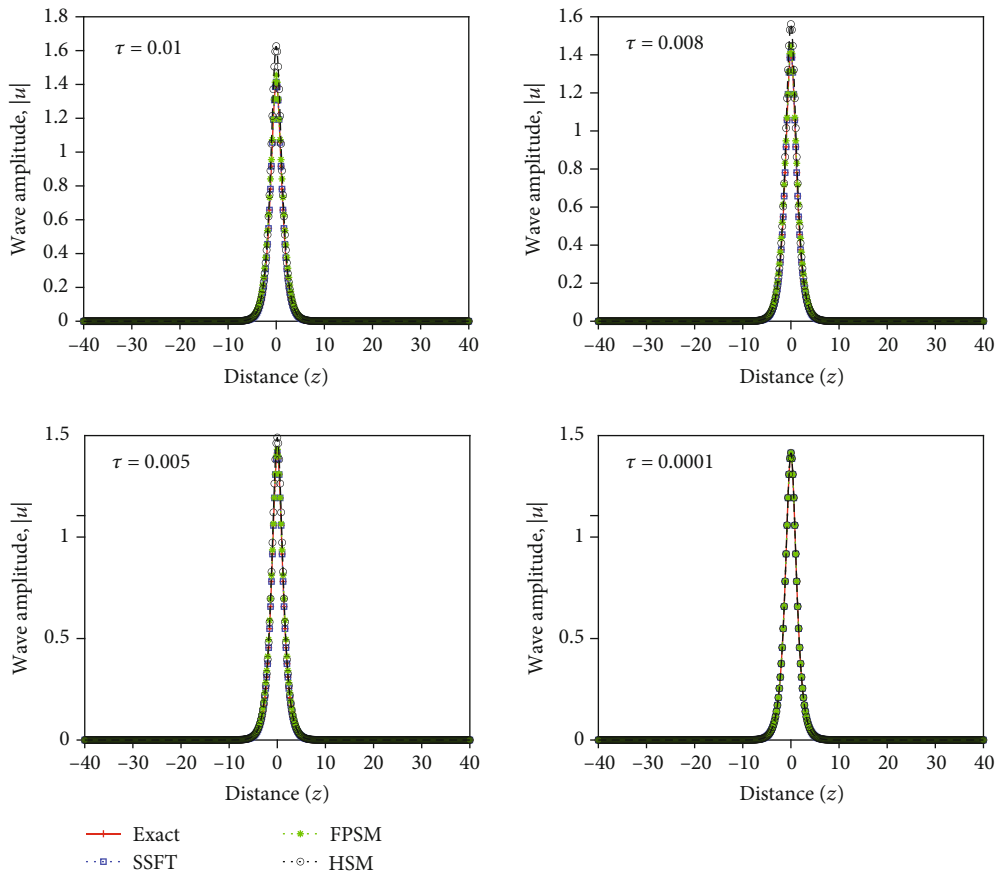

Figure 4: A comparison of the split-step Fourier transform (SSFT) and the Fourier pseudospectral method (FPSM), the Hopscotch method (HSM), and the exact solution at $h = 0.2$ and $t = 20$ over a space domain z from -40 to 40, whereas using different values τ.

Table 1: A comparison among the sum of squares error (SSE) of the split-step Fourier transform (SSFT), the Fourier pseudospectral method (FPSM), and the Hopscotch scheme (HSM), computed for different time values t from 35 to 105.When $h = 0.2$ and $\tau = 0.001$.

Time, t	SSE-SSFT	CPU time (s)	SSE-FPSM	CPU time (s)	SSE-HSM	CPU time (s)
35	$1.6336e-21$	2.7994	$2.7847e-03$	2.8612	$6.5206e-03$	3.7639
45	$2.6725e-21$	3.2639	$4.6158e-03$	3.6818	$1.1120e-02$	4.8691
55	$3.914e-21$	3.9879	$6.9139e-03$	4.3797	$1.7156e-02$	5.9605
65	$5.439e-21$	4.8138	$9.6827e-03$	5.2361	$2.4774e-02$	6.9654
75	$7.2441e-21$	5.4023	$1.2926e-02$	5.884	$3.4139e-02$	8.0312
85	$9.2143e-21$	6.1936	$1.6647e-02$	6.6282	$4.5442e-02$	9.2682
95	$1.141e-20$	6.9974	$2.0851e-02$	7.4995	$5.8899e-02$	10.181
105	$1.3794e-20$	7.8761	$2.5540e-02$	8.5734	$7.4759e-02$	11.307

Table 2: A comparison among the sum of squares error (SSE) of the split-step Fourier transform (SSFT), the Fourier pseudospectral method (FPSM), and the Hopscotch scheme (HSM), computed for different time values t from 35 to 105. When $h = 0.2$ and $\tau = 0.0001$.

Time, t	SSE–SSFT	CPU time (s)	SSE-FPSM	CPU time (s)	SSE-HSM	CPU time (s)
35	$1.4036e-19$	24.941	$2.7610e-05$	27.572	$5.9491e-05$	36.65
45	$2.3119e-19$	32.435	$4.5653e-05$	36.867	$9.8615e-05$	46.599

Table 3: A comparison among the sum of squares error (SSE) of the split-step Fourier transform (SSFT), the Fourier pseudospectral method (FPSM), and the Hopscotch scheme (HSM), computed for different time values t from 35 to 105. When $h = 0.2$ and $\tau = 0.008$.

Time, t	SSE-SSFT	CPU time (s)	SSE-FPSM	CPU time (s)	SSE-HSM	CPU time (s)
35	$1.9435e-23$	0.35126	$1.9046e-01$	0.43022	$1.5158e+00$	0.63134
45	$3.1307e-23$	0.44921	$3.2239e-01$	0.51259	$1.0684e+01$	0.70445

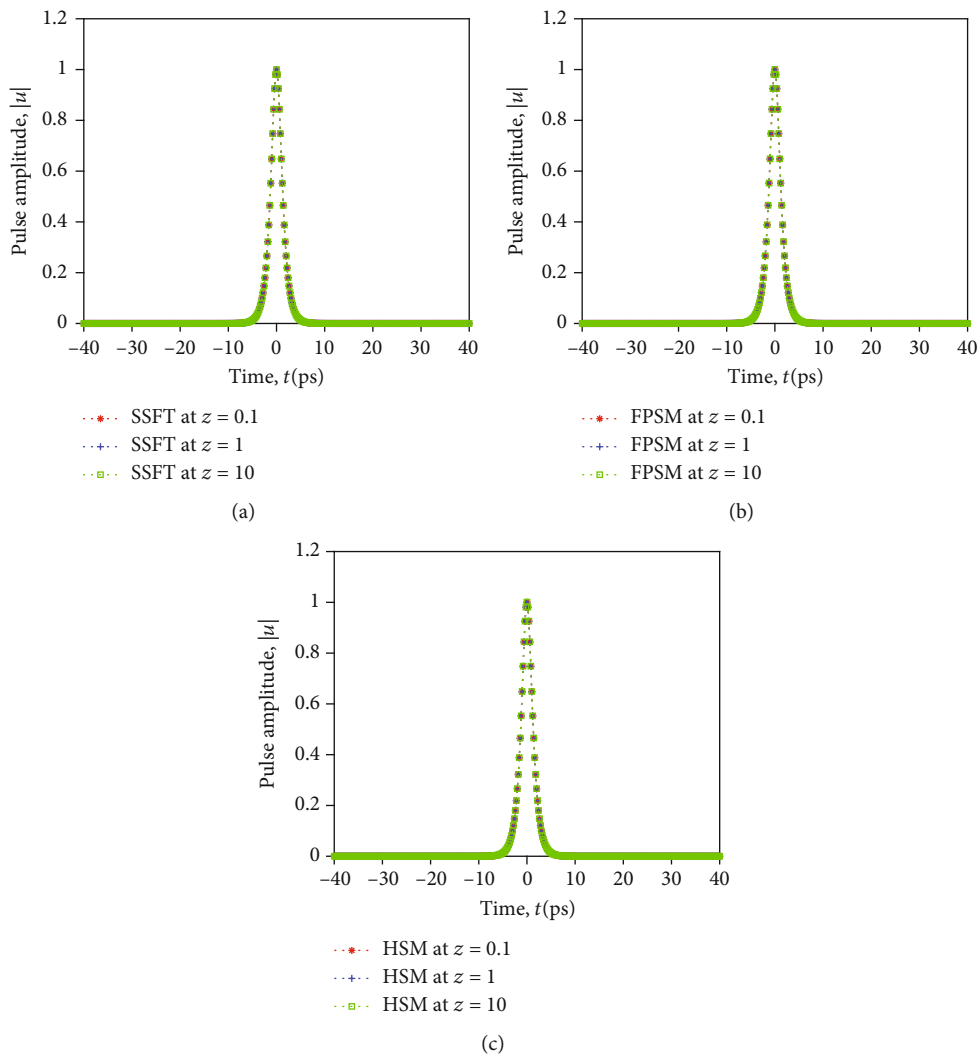

Figure 5: A comparison of the split-step Fourier transform (SSFT) (a), the Fourier pseudospectral method (FPSM) (b), and the Hopscotch method (HSM) (c) approximate solutions at for a lossless optical fiber when the input pulse is a bright soliton at distances $z = 0.1, 1, 10$ km, respectively.

$$i\frac{\partial u(z,t)}{\partial z} = \frac{\beta_2}{2}\frac{\partial^2 u(z,t)}{\partial t^2} - \gamma|u(z,t)|^2 u(z,t) - i\frac{\alpha}{2}u(z,t), \tag{2}$$

where $u(z,t)$ is the spatial-temporal varying amplitude of the optical pulse, z is the longitudinal coordinate of the fiber, and t is the normalized time with respect to a reference frame that moves with the pulse at a speed equal to the group velocity $v_g = 1/\beta_1$. This frame is also called the retarded frame, such that $t = \zeta - (z/v_g)$, where ζ is the present or physical time; both z and t are dimensionless in distance and time, respectively, α is the power attenuation constant, γ is the Kerr nonlinear coefficient, and β_2 is the first-order group velocity dispersion (GVD) parameter or the second-order dispersion coefficient [19, 20], which can be computed using the following formula:

$$\beta_2 = \frac{-\lambda^2 D}{2\pi c}. \tag{3}$$

It is significant to highlight that λ represents the reference wavelength, c is the speed of light, and D is the fiber dispersion parameter at a given wavelength. In addition to

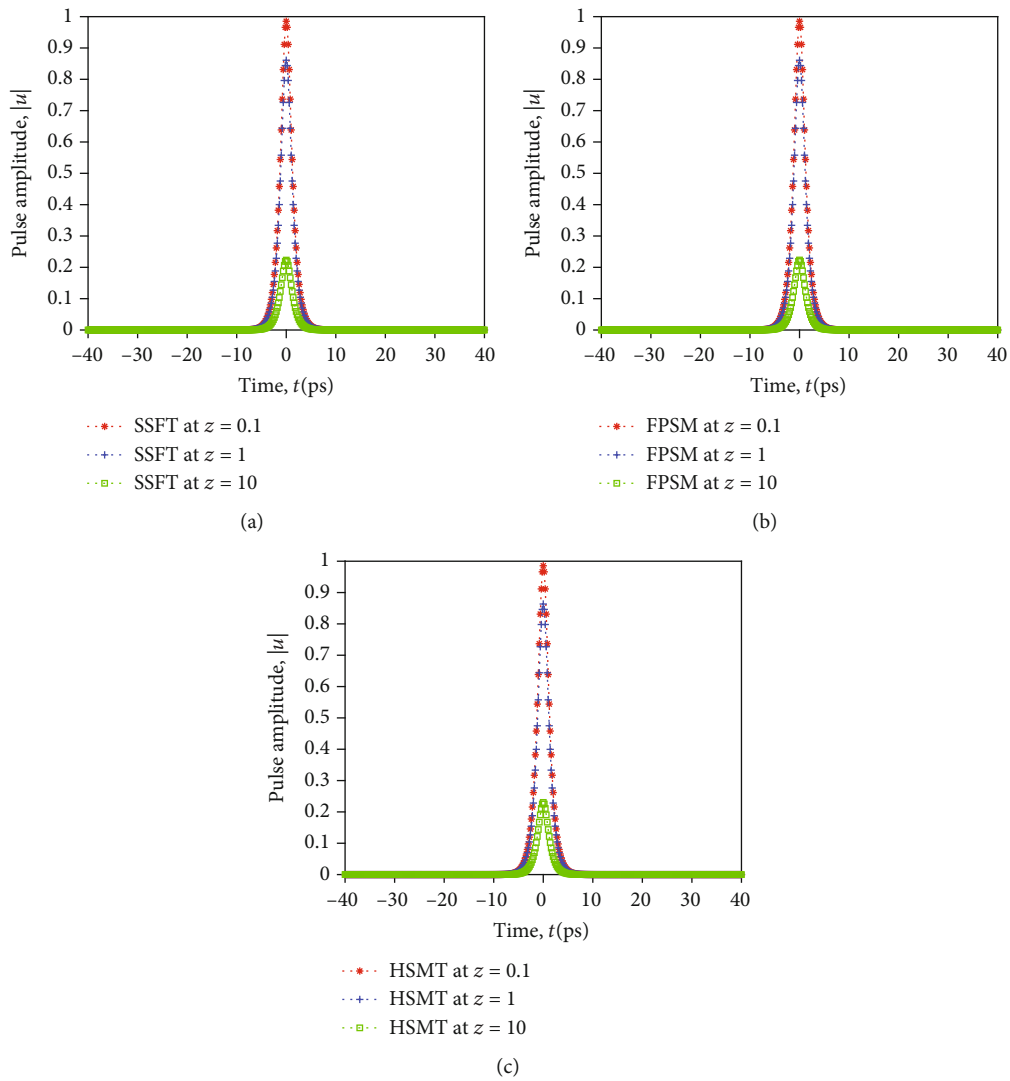

Figure 6: A comparison of the split-step Fourier transform (SSFT) (a), the Fourier pseudospectral method (FPSM) (b), and the Hopscotch method (HSM) (c) approximate solutions at for a lossy optical fiber $\alpha = 0.3$ dB/km when the input pulse is a bright soliton at distances $z = 0.1, 1, 10$ km, respectively.

this, the sign of the GVD determines three different regimes as mentioned below:

(i) When $\beta_2 = 0$, the GV is an extremum. Such points are called the zero-dispersion wavelength (ZDW)

(ii) When $\beta_2 < 0$, the GV increases with the frequency, and it is called anomalous dispersion. This regime supports bright solitons

(iii) When $\beta_2 > 0$, the GV decreases with the frequency, and it is called normal dispersion. This regime supports dark solitons

It is obviously noted that the reason of having different velocities for the spectral components of a pulse is the physical behavior of the group velocity (GV), which depends on the frequency. This change in the velocities frequently produces a pulse temporal distortion [31]. Moreover, elaborating the concept of GVD in nonlinear optical fiber is ubiquitously important because of its inevitable effect in shaping the pulse propagation through fiber. When the dispersion is constant, the shape of a well-prepared pulse remains the same, while its propagation through the nonlinear fiber, creating a soliton; the accurate compensation between the nonlinear effects and the linear dispersion in the fiber is the cause of this fixed dispersion.

Likewise, illustrating the fiber loss term is amazingly beneficial as a measure of the power loss during the transmission process inside the fiber. Assuming that the length of the fiber is L, the input power is P_o, and the transmitted power is P_t; α is the attenuation real positive constant. Then, the fiber losses can be calculated using the following formula [6]:

$$\alpha_{dB} = -\frac{10}{L}\log\left(\frac{P_t}{P_o}\right) = -\frac{10}{L}\log\left(\exp\left(-\alpha L\right)\right) = 4{,}343\alpha. \quad (4)$$

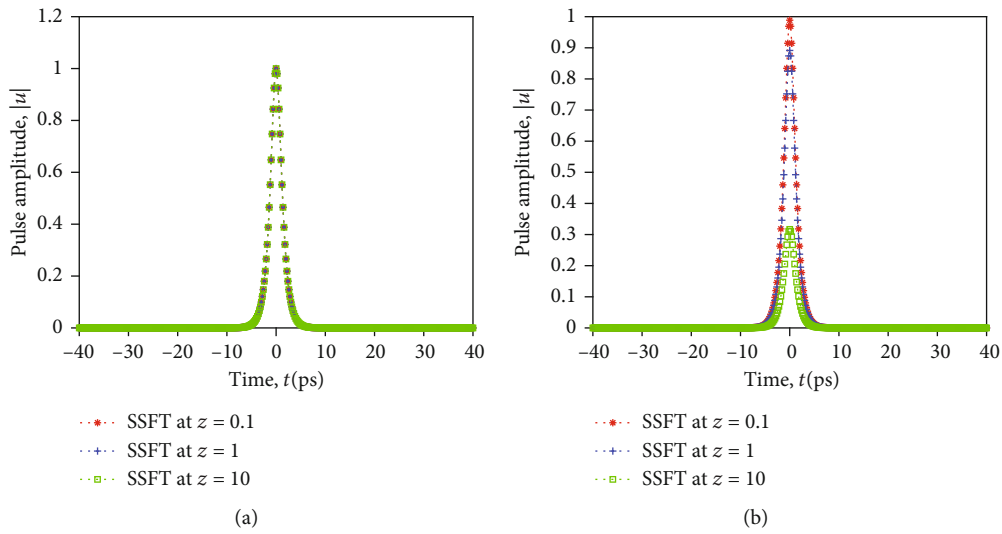

Figure 7: A comparison of the split-step Fourier transform (SSFT) approximate solutions at a higher value of GVD of $\beta_2 = -20\,\text{ps}^2/\text{km}$ for a lossless (a) and lossy optical fiber (b) when the input pulse is a bright soliton at distances $z = 0.1, 1, 10$ km, respectively.

Obtaining a more realistic model to simulate and govern the actual wave propagation through the optical fiber requires a generalization of Equation (1). This generalization must include other terms and parameters to demonstrate additional effects. Additionally, the perturbed or generalized nonlinear Schrödinger equation (PNLSE) models this realistic pulses' propagation. If the perturbation does not exist, the PNLSE will be reduced to the canonical nonlinear Schrödinger equation (CNLSE), presented in Equation (8), which has an exact analytical solution that can be obtained using different regimes. On the contrary, when the perturbations take place, its governed equation cannot analytically be solved. It is essential to address different types of optical fiber perturbations, for instance, higher-order and nonlinear dispersion, shock effect, stimulated Raman scattering, self-steepening effects, dissipation, amplification, along with others [32].

The dominance of either the dispersion or the nonlinearity effects might depend on the values of the initial pulse's half-width at half amplitude T_0 and the initial peak power P_o of the incident pulse. Thus, introducing two length scales, which are the dispersion length L_D and the nonlinear length L_{NL} is crucially advantageous because the relative magnitude of these two lengths, along with the fiber length L, can control the pulses' evolution to some extent. In this regard, we apply a special normalization scale to the time, space, and pulse amplitude as shown below:

$$T = \frac{t}{T_0}, \quad Z = \frac{z}{L}, \quad U(Z,T) = \frac{u(Z,T)}{\sqrt{P_o}\exp\left(-(\alpha Z/2)\right)}. \tag{5}$$

These transformations yield

$$i\frac{\partial U(Z,T)}{\partial Z} = \frac{L}{L_D}\frac{\operatorname{sgn}(\beta_2)}{2}\frac{\partial^2 U(Z,T)}{\partial T^2} - \exp(-\alpha L Z)\frac{L}{L_{NL}}|U(Z,T)|^2 U(Z,T), \tag{6}$$

where $\operatorname{sgn}(\beta_2)$ is the sign of the β_2 coefficient, $L_D = {T_0}^2/|\beta_2|$, and $L_{NL} = 1/\gamma P_o$, where L_D is called the dispersion length that quantifies the pulse broadening per unit length, whereas L_{NL} is defined as the nonlinear length that quantifies the nonlinear phase shift per unit length.

Equation (6) is another formula to represent the NLSE, which might mostly be used in the fabrication process of the fiber optics because this special formalism comprises the fiber real parameters, such as the fiber length, the initial pulse power, and the initial half-width of the input pulse. Nevertheless, this equation may not commonly be employed in the simulations [17, 31].

Moreover, it is fundamental to define the soliton order parameter η by the following relation [25]:

$$\eta^2 = \frac{L_D}{L_{NL}} = \frac{\gamma P_o {T_0}^2}{|\beta_2|}, \tag{7}$$

when η has an integer value; it indicates a soliton pulse solution, either bright or dark, depending on the group velocity dispersion parameter's sign β_2. This integer value manifests that the dispersion and the nonlinear effects compensate each other, achieving a balance that results in an unchanged and undistorted wave during propagation, which is called a soliton.

2.2. Exact Analytical Solution for Solving the CNLSE. To confidently navigate the validation of the proposed numerical

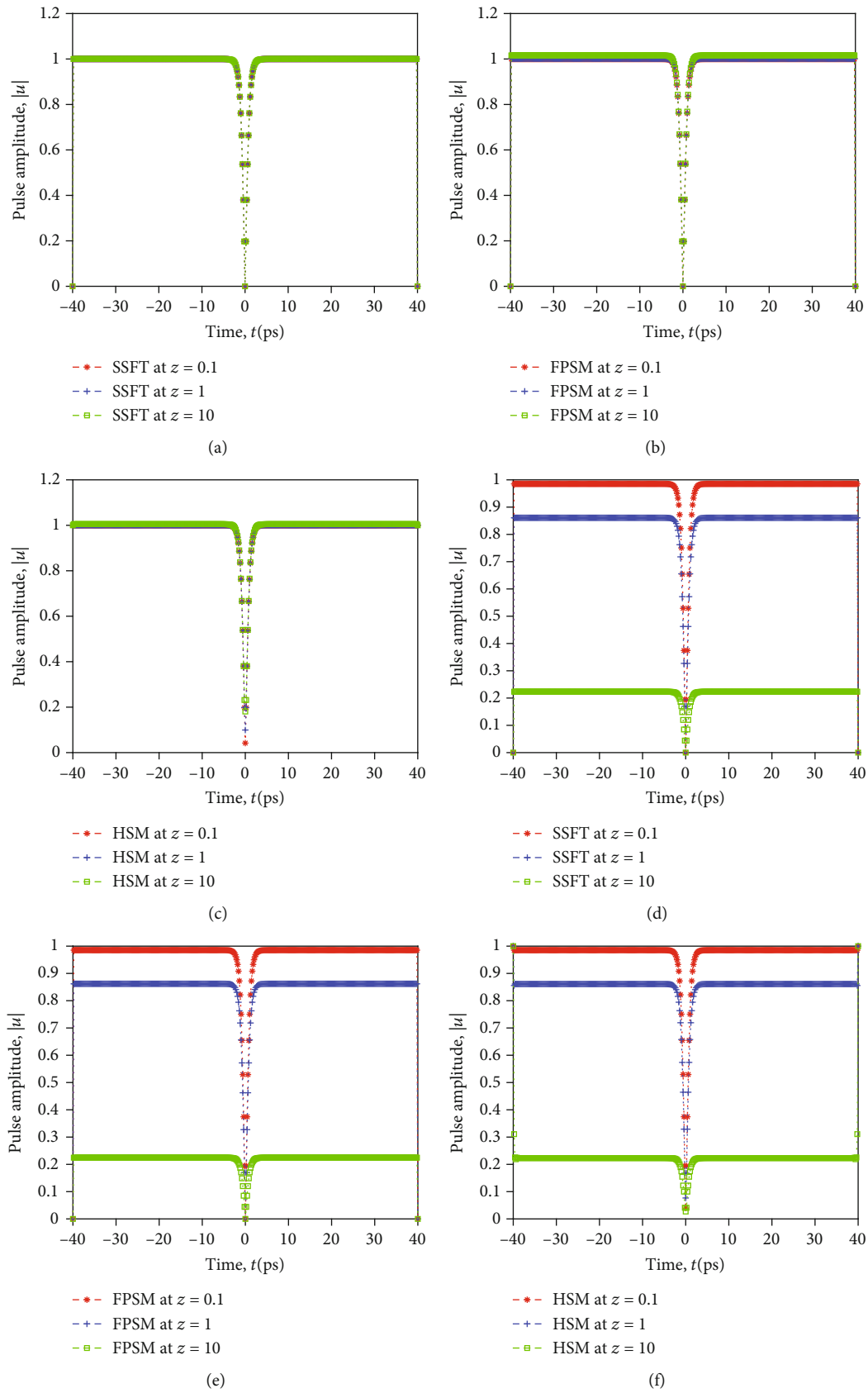

Figure 8: A comparison of the split-step Fourier transform (SSFT), the Fourier pseudospectral method (FPSM), and the Hopscotch method (HSM) approximate solution for a lossless (a, b, c) and lossy (d, e, f) optical fiber when the input pulse is a dark soliton at distances $z = 0.1, 1, 10$ km, respectively.

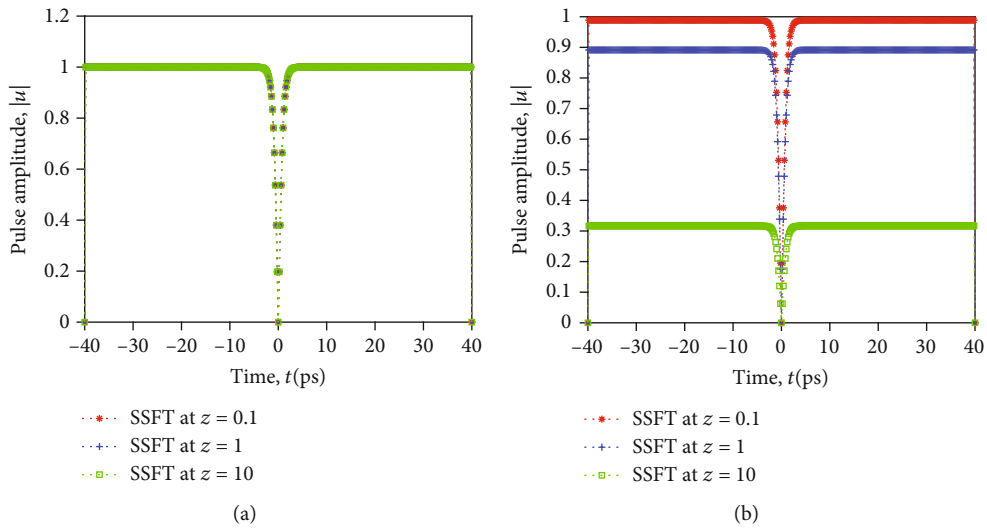

Figure 9: The split-step Fourier transform (SSFT) approximate solution for a lossless (a) and lossy (b) optical fiber at a higher value of GVD of $\beta_2 = +20\,\mathrm{ps}^2/\mathrm{km}$ when the input pulse is a dark soliton at distances $z = 0.1, 1, 10$ km, respectively.

schemes, a fundamental initiative is to evoke the genuine NLSE along with its exact soliton solution for the comparison purpose. This equation resembles the NLSE under study in this research paper.

However, an interchange between the spatial and temporal variables occurs in each of the first- and second-order derivatives. Beside this, the attenuation term is neglected. Furthermore, it is a nonlinear second-order partial differential equation that is widely used in numerous applications abreast of the optical fiber field. The original NLSE is represented as shown below [33]:

$$i\frac{\partial u(z,t)}{\partial t} + \frac{\partial^2 u(z,t)}{\partial z^2} + \gamma|u(z,t)|^2 u(z,t) = 0. \tag{8}$$

Similar to Equation (2), the unknown function $u(z,t)$ represents a wave. The second-order derivative $\partial^2 u(z,t)/\partial z^2$ represents the dispersion, while the nonlinear term $\gamma|u(z,t)|^2 u(z,t)$ represents the nonlinearity of the problem.

In this work, we shall consider and select the single bright soliton solution, shown in Equation (9), also named the envelope solution, among all the other approved exact analytical solutions because of its popularity, along with its simplicity, as it has comprehensively been derived and utilized in a plenty of previously published research articles [14, 26, 33, 34]:

$$u(z,t) = (2\lambda)^{0.5} e^{i\left(0.5cz + \left(\lambda - 0.25c^2\right)t + \Phi o\right)} \operatorname{sech}\left((\lambda)^{0.5}(z - ct - zo)\right), \tag{9}$$

where $zo, \Phi o, c$, and λ are the initial position, initial phase, propagation speed, and soliton amplitude, respectively.

2.3. Numerical Approaches for Solving the CNLSE. In this section, three powerful numerical techniques are presented to report the CNLSE, represented in Equation (8). The three methods are the SSFT, FPSM, and HSM [12, 16, 27, 35–40].

2.3.1. The Split-Step Fourier Transform. This method is a straightforward and fast numerical technique that belongs to the pseudospectral family. Moreover, it is unconditionally stable, standing on the split of the NLSE into two subsequent linear and nonlinear partial equations. Moreover, this easy implemented scheme has a unique significance because it represents the effects of the dispersion and nonlinearity separately in this problem.

Rearranging the terms of Equation (8), on the form of $\partial_t u(z,t) = (\mathrm{L} + \mathrm{N})u(z,t)$, to isolate the linear and nonlinear terms yields

$$\begin{aligned} i\partial_t u(z,t) &= -\partial_{zz}^2 u(z,t) - \gamma|u(z,t)|^2 u(z,t), \\ u(z,0) &= u_0(z). \end{aligned} \tag{10}$$

Assuming that the linear operator is $L = i\partial_{zz}^2$ and the nonlinear operator is $N = \gamma i|u(z,t)|^2$. Then, we split it into two parts to solve the problem as follows.

Part one, the nonlinear step is introduced as: $\partial_t u(z,t) = Nu(z,t)$, where $N = \gamma i|u(z,t+\tau)|^2 \approx \gamma i|u(z,t)|^2$. Hence, the analytical solution will be given as shown below:

$$u(z,t+\tau) = \exp\,(i\tau N)u(z,t) = \exp\,\left(i\tau\gamma|u(z,t)|^2\right)u(z,t). \tag{11}$$

Part two, the linear step is introduced as $i\partial_t u(z,t) = \mathrm{L}u(z,t)$. We apply Fourier transform, to both sides to convert the PDE into an ODE in the frequency domain to facilitate its solution, as follows:

$$\partial_t \hat{u} = -ik^2 \hat{u}. \tag{12}$$

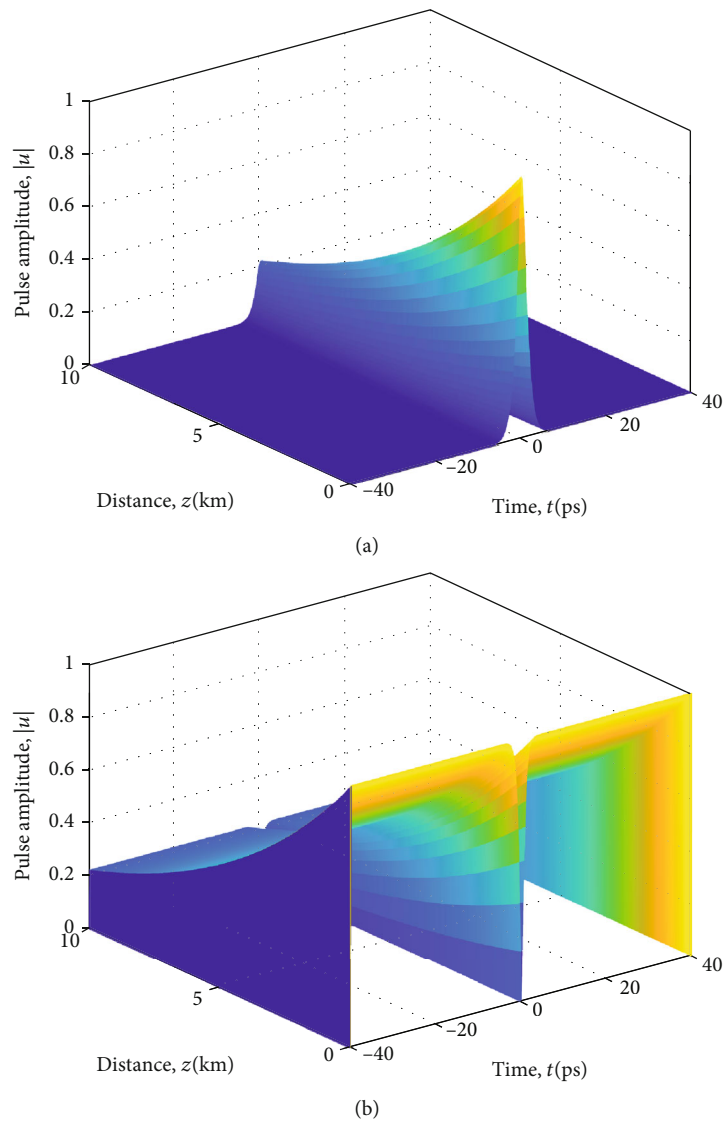

Figure 10: Three-dimension graphs of the split-step Fourier transform (SSFT) approximate solution for a lossy optical fiber $\alpha = 0.3$ dB/km when the input pulse is a bright soliton (a) and a black dark soliton (b), respectively, at a distance $z = 10$ km.

Equation (14) demonstrates the analytical solution of the previous equation but computed in the frequency domain:

$$\hat{u}(z, t+\tau) = \exp\left(-ik^2\tau\right).\hat{u}(z, t). \tag{13}$$

Eventually, we apply the inverse Fourier transform to both sides to obtain the final equation represented below:

$$u(z, t+\tau) = F^{-1}\left(\exp\left(-ik^2\tau\right).F\left(\exp\left(i\tau\gamma|u(z,t)|^2\right)u(z,t)\right)\right). \tag{14}$$

2.3.2. The Fourier Pseudospectral Method. This approach is deemed to be a member of the pseudospectral family as well, and it can only be applied to the periodic functions over the interval $x \in [-P, P]$. Its key pillar stands on implementing Fourier transform for the space second-order derivative, while discretizing the first-order time derivative using an appropriate finite difference relation.

In the first stage, we replace the temporal first derivative by the following difference relation:

$$\frac{\partial u}{\partial t} = \frac{u(z, t+\tau) - u(z, t)}{\tau}. \tag{15}$$

In the second stage, we substitute the above relation into Equation (8) to get the following equation:

$$i\frac{u(z, t+\tau) - u(z, t)}{\tau} = -F^{-1}\left(i^2k^2\frac{\pi^2}{P^2}F(u)\right) - \gamma|u(z,t)|^2u(z,t), \tag{16}$$

Table 4: A comparison of the pulse powers using the split-step Fourier transform (SSFT), the Fourier pseudospectral method (FPSM), and the Hopscotch scheme (HSM), at a distance $z = 20$ km, computed at different attenuation constants values α from 0.1 to 0.45 dB/km.

α (dB/km)	Power (w)-SSFT	CPU time (s)	Power (w)-FPSM	CPU time (s)	Power (w)-HSM	CPU time (s)
0.1	$1.3534e-01$	1.1251	$1.3579e-01$	1.2936	$1.4115e-01$	2.9371
0.15	$4.9787e-02$	1.1236	$5.0051e-02$	1.2766	$5.3130e-02$	2.9356
0.2	$1.8316e-02$	1.1046	$1.8436e-02$	1.296	$2.0022e-02$	2.85
0.25	$6.7379e-03$	1.1287	$6.7884e-03$	1.3048	$7.5516e-03$	2.9818
0.3	$2.4788e-03$	1.108	$2.4988e-03$	1.3188	$2.8516e-03$	2.9684
0.35	$9.1188e-04$	1.1347	$9.1961e-04$	1.2802	$1.0824e-03$	3.0699
0.4	$3.3546e-04$	1.1467	$3.3838e-04$	1.2865	$4.1209e-04$	3.1696
0.45	$1.2341e-04$	1.1515	$1.2450e-04$	1.2792	$1.5625e-04$	3.0975

Table 5: A comparison of the pulse powers using the split-step Fourier transform (SSFT), the Fourier pseudospectral method (FPSM), and the Hopscotch method (HSM), at an attenuation constant $\alpha = 0.2$ dB/km, computed at different distances z from 1 to 60 km.

z (km)	Power (w)-SSFT	CPU time (s)	Power (w)-FPSM	CPU time (s)	Power (w)-HSM	CPU time (s)
1	$8.1873e-01$	0.066308	$8.1890e-01$	0.07973	$8.2207e-01$	0.20215
5	$3.6788e-01$	0.31196	$3.6802e-01$	0.35977	$3.7538e-01$	0.82056
10	$1.3534e-01$	0.55666	$1.3557e-01$	0.65937	$1.4107e-01$	1.5985
20	$1.8316e-02$	1.1563	$1.8436e-02$	1.2707	$2.0021e-02$	3.0384
30	$2.4788e-03$	1.6731	$2.5091e-03$	2.0559	$2.8636e-03$	4.5262
40	$3.3546e-04$	2.2148	$3.4151e-04$	2.5027	$4.1551e-04$	5.8678
50	$4.5400e-05$	2.7437	$4.6481e-05$	3.1548	$6.3139e-05$	7.2459
60	$6.1442e-06$	3.3364	$6.3267e-06$	3.7705	$1.3284e-05$	9.1225

$$u(z,t+\tau) - u(z,t) = \tau i F^{-1}\left(i^2 k^2 \frac{\pi^2}{P^2} F(u)\right) + i\tau\gamma |u(z,t)|^2 u(z,t), \tag{17}$$

$$u(z,t+\tau) = u(z,t) - \tau i F^{-1}\left(k^2 \frac{\pi^2}{P^2} F(u)\right) + i\tau\gamma |u(z,t)|^2 u(z,t). \tag{18}$$

The solution exhibited in Equation (18) is only stable for values of $\tau/(h)^2 < 1/\pi^2$.

Despite this, applying the Fornberg and Whitham principles yields an unconditionally stable solution, as follows:

$$\begin{aligned} u(z,t+\tau) = u(z,t) - \mathrm{iF}^{-1}\left(\sin\left(k^2 \frac{\pi^2}{P^2}\tau\right) F(u(z,t))\right) \\ + i\tau\gamma |u(z,t)|^2 u(z,t). \end{aligned} \tag{19}$$

2.3.3. The Hopscotch Method. This scheme is a fast explicit finite difference method, which operates on replacing the nonlinear term by an average formula computed at the row j, as shown in Equation (20). Besides, it is also an unconditionally stable approach with a truncation error of $O(h^2) + O(\tau^2)$ [27]; thus, the order of convergence is 2 in both time and distance.

$$(u)_{ij} = \left(\frac{\left|u_{i-1,j}\right|^2 * u_{i-1,j} + \left|u_{i+1,j}\right|^2 u_{i+1,j}}{2}\right). \tag{20}$$

We substitute the previous equation and the other appropriate difference relations in Equation (8), subject to the boundary and initial conditions, which yields

$$\begin{aligned} i\frac{u_{i,j+1} - u_{i,j}}{\tau} + \frac{u_{i+1,j} + u_{i-1,j} - 2u_{i,j}}{h^2} \\ + \gamma \frac{\left|u_{i-1,j}\right|^2 * u_{i-1,j} + \left|u_{i+1,j}\right|^2 u_{i+1,j}}{2} = 0, \end{aligned}$$

$$\begin{aligned} u_{i,j+1} = u_{i,j} + i\tau \frac{u_{i+1,j} + u_{i-1,j} - 2u_{i,j}}{h^2} \\ + i\gamma \frac{\tau}{2}\left(\left|u_{i-1,j}\right|^2 * u_{i-1,j} + \left|u_{i+1,j}\right|^2 u_{i+1,j}\right). \end{aligned} \tag{21}$$

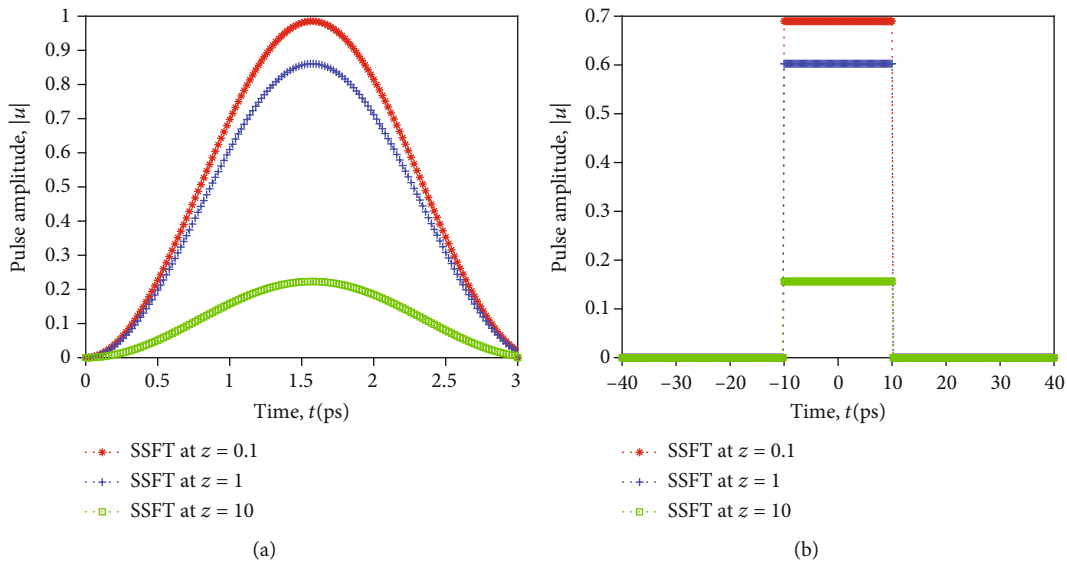

Figure 11: The split-step Fourier transform (SSFT) approximate solution for a lossy optical fiber $\alpha = 0.3$ dB/km when the input pulse is a sine squared function (a) and a rectangular pulse (b) at distances $z = 0.1, 1, 10$ km, respectively.

Therefore, the final explicit formula is given by Equation (22), where $\lambda = \tau/h^2$,

$$u_{i,j+1} = (1 - 2i\lambda)u_{i,j} + i\lambda\left(u_{i+1,j} + u_{i-1,j}\right) + i\gamma\frac{\tau}{2}\left(\left|u_{i-1,j}\right|^2 * u_{i-1,j} + \left|u_{i+1,j}\right|^2 u_{i+1,j}\right). \tag{22}$$

3. Modified Numerical Approaches for Solving the Lossy Fiber Optics

In this section, two main actions were implemented to obtain the modified versions. First, we have successfully incorporated the loss term in the three suggested numerical schemes, which are the SSFT, FSSM, and HSM. This unique insertion is utterly essential in the simulation process because it guarantees preserving a high accuracy level for the obtained approximate solutions that should effectively be employed to model the propagation of the solitons. Second, an interchange has taken place between the temporal and spatial variables to cope with the requirements of the problem, under study in this article. As a result, extended versions of each of the three proposed numerical techniques are derived to solve the 1D NLSE, comprising the attenuation term, presented in Equation (1) or (2). Thereafter, comparing their resulted approximate solutions to corroborate their reliability and creditability, here, the exact analytical solution is an inadequate trend because the exact solution cannot smoothly be obtained for this kind of equation, especially after inserting the term that is responsible for the fiber losses. Roughly speaking, these modifications seek an insightful approximation of the attenuation amount to eradicate its undesired effects by using compensating amplifiers, which guarantees the healthy delivery of the transmitted signals.

3.1. The Extended Split-Step Fourier Transform. Starting with the NLSE presented in Equation (1) and rewriting it as shown below:

$$\partial_z u(z,t) = (\mathrm{L} + \mathrm{N})u(z,t). \tag{23}$$

While applying the initial condition $u(0,\mathrm{t}) = u_0(t)$. Then, define the time independent linear operator as $L = -i(\beta_2/2)\partial_{tt}^2 - (\alpha/2)$, and the nonlinear operator as $N = i\gamma|u(z,t)|^2$.

First, the analytical solution of the nonlinear part will be given by the following equation:

$$u(z+h,t) = \exp\left(ih\gamma|u(z,t)|^2\right)u(z,t). \tag{24}$$

Second, the analytical solution of the linear part can be computed in the frequency domain, using the following relation:

$$\hat{u}(z+h,t) = \exp\left(i\frac{\beta_2}{2}k^2h\right).\exp\left(-\frac{\alpha}{2}h\right).\hat{u}(z,t). \tag{25}$$

Then, plugging Equation (24) into the previous equation:

$$\hat{u}(\mathrm{z}+h,t) = \exp\left(i\frac{\beta_2}{2}k^2h\right).\exp\left(-\frac{\alpha}{2}h\right).F \cdot \left(\exp\left(ih\gamma|u(z,t)|^2\right)u(z,t)\right). \tag{26}$$

Hence, the final equation can be written as

$$u(z+h,t) = F^{-1}\left(\exp\left(i\frac{\beta_2}{2}k^2h\right).\exp\left(-\frac{\alpha}{2}h\right).F \cdot \left(\exp\left(ih\gamma|u(z,t)|^2\right)u(z,t)\right)\right). \tag{27}$$

3.2. The Extended Fourier Pseudospectral Method. Commencing with the NLSE over the interval $t \in [-P, P]$. First, replacing the spatial first-order derivative by the following difference relation:

$$\frac{\partial u}{\partial z} = \frac{u(z+h,t) - u(z,t)}{h}. \tag{28}$$

Second, substituting the above relation into Equation (1) to get the following equation:

$$\begin{aligned}\frac{u(z+h,t) - u(z,t)}{h} &= -i\frac{\beta_2}{2}F^{-1}\left(i^2k^2\frac{\pi^2}{P^2}F(u)\right)\\ &\quad + i\gamma|u(z,t)|^2u(z,t) - \frac{\alpha}{2}u(z,t),\end{aligned}$$

$$\begin{aligned}u(z+h,t) - u(z,t) &= -i\frac{\beta_2}{2}hF^{-1}\left(i^2k^2\frac{\pi^2}{P^2}F(u)\right)\\ &\quad + i\gamma h|u(z,t)|^2u(z,t) - \frac{\alpha}{2}hu(z,t).\end{aligned} \tag{29}$$

Then, substituting the difference relation in Equation (28), the initial condition $u(0,\mathrm{t}) = u_0(t)$, and the Fourier transform of the second derivative term into Equation (1) to obtain the following equation:

$$\begin{aligned}u(z+h,t) &= u(z,t) + h\frac{\beta_2}{2}\mathrm{iF}^{-1}\left(k^2\frac{\pi^2}{P^2}F(u)\right)\\ &\quad + i\gamma h\left|u(z,t)^2\right|u(z,t) - \frac{\alpha}{2}hu(z,t).\end{aligned} \tag{30}$$

Equation (30) is only stable for values of $h/\tau^2 < 1/\pi^2$.

Despite this, making a modification in the previous equation by using the Fornberg and Whitham principles [27] yields an unconditionally stable solution, presented

$$\begin{aligned}u(z+h,t) &= u(z,t) + \frac{\beta_2}{2}\mathrm{iF}^{-1}\left(\sin\left(k^2\frac{\pi^2}{P^2}h\right)F(u(z,t))\right)\\ &\quad + i\gamma h\left|u(z,t)^2\right|u(z,t) - \frac{\alpha}{2}hu(z,t).\end{aligned} \tag{31}$$

3.3. The Extended Hopscotch Method. To kick off, we replace the nonlinear term by an average formula computed at the column i as illustrated below:

$$(u)_{ij} = \left(\frac{\left|u_{i,j-1}\right|^2 * u_{i,j-1} + \left|u_{i,j+1}\right|^2 u_{i,j+1}}{2}\right). \tag{32}$$

Substituting the appropriate FDM average and difference relations in Equation (1), subject to the initial and boundary conditions, to obtain

$$\begin{aligned}&\frac{u_{i+1,j} - u_{i,j}}{h} + \frac{u_{i,j+1} + u_{i,j-1} - 2u_{i,j}}{\tau^2}\\ &\quad + i\gamma\frac{\left|u_{i,j-1}\right|^2 * u_{i,j-1} + \left|u_{i,j+1}\right|^2 u_{i,j+1}}{2}\\ &\quad - \frac{\alpha}{2}h\left(\frac{u_{i,j-1} + u_{i,j+1}}{2}\right) = 0,\end{aligned}$$

$$\begin{aligned}u_{i+1,j} &= u_{i,j} - i\frac{\beta_2}{2}h\left(\frac{u_{i,j+1} + u_{i,j-1} - 2u_{i,j}}{\tau^2}\right)\\ &\quad + i\gamma\frac{h}{2}\left(\left|u_{i,j-1}\right|^2 * u_{i,j-1} + \left|u_{i,j+1}\right|^2 u_{i,j+1}\right).\end{aligned} \tag{33}$$

The final explicit formula for this unconditionally stable approach is given by

$$\begin{aligned}u_{i+1,j} &= (1 + i\beta_2\lambda)u_{i,j} - i\frac{\beta_2}{2}\lambda\left(u_{i,j+1} + u_{i,j-1}\right)\\ &\quad + i\gamma\frac{h}{2}\left(\left|u_{i,j-1}\right|^2 * u_{i,j-1} + \left|u_{i,j+1}\right|^2 u_{i,j+1}\right)\\ &\quad - \frac{\alpha}{4}h\left(u_{i,j-1} + u_{i,j+1}\right),\end{aligned} \tag{34}$$

where $\lambda = h/\tau^2$.

4. The Error and Convergence Discussion

The convergent statement states that the numerical solutions collapse onto the exact analytical solution, when the limit $\tau \longrightarrow 0$; hence, the error reaches zero accordingly at all time indices. In other words, if we shrink the temporal step towards zero smaller and smaller, the absolute error, which is the difference between the exact and approximate solution, will go smaller and smaller as well. The convergence of the three numerical schemes is verified numerically in the fifth section under systematic temporal mesh refinement [41].

5. Numerical Results

Here, our strategy is to first investigate the behavior of our original proposed numerical approaches against the exact analytical solution for the CNLSE, which models the pulse propagation in a lossless optical fiber. Then, the extended versions of these numerical techniques are intensively employed to solve the PNLSE, associated with the fiber loss term.

5.1. Numerical Tests for the CNLSE. In this section, plenty of designated numerical examples are conducted, as recently followed elsewhere [42–47], to examine how efficient, fast, and accurate the proposed numerical techniques are, especially when compared with the exact analytical solution. Particularly, MATLAB software was used to run these tests, which were performed to measure the accuracy among

various numerical approaches, estimate the error, and decide on the most reliable and fastest approach for solving the 1D NLSE. In all the proposed methods, the NLSE is discretely solved at different values of time and space [28]. For the numerical experiment, we discretize the space domain x from -40 to 40, setting the parameters, in Equation (9), γ nad λ, to one unit and c, xo, and Φo to zero, respectively. This leads to the hyperbolic secant initial condition [37]:

$$u(z,0) = (2)^{0.5} e^{i(0.5z)} \operatorname{sech}(z). \tag{35}$$

Associated with the zero boundary conditions is shown below:

$$\begin{aligned} u(L,t) &= 0, \\ u(-L,t) &= 0, \end{aligned} \tag{36}$$

occurring at $z = -L, L$, and for $t \geq 0$.

Our simulation strategy stands on employing various spatial steps h when the other parameters are fixed, and subsequently, adapting various temporal steps τ while not changing the rest of the parameters. These steps sizes are dimensionless, and their values determine the accuracy of the experiment. In particular, the smaller their values, the more precise the approximate numerical solution becomes. Figure 2 demonstrates the graph of the exact bright one soliton solution in three dimensions to provide a rigorous focus during the comparison process on the actual shape of this pulse.

First, by using numerous space steps at a time step $\tau = 0.001$ computed at time $t = 20$, we have compared the exact solution, previously presented in Equation (9), and the three suggested methods, which are the split-step Fourier method, Fourier pseudospectral method, and Hopscotch method, in the graphs presented in Figure 3. Second, although the same process has been repeated, the values of the used time step have been changed instead of the space step, which sustained a constant value of 0.2, computed at the same time $t = 20$. The graphs are presented in Figure 4.

Eventually, drawing a comparison to estimate the sum of squares error (SSE) [48] of all the mentioned numerical techniques and their exact solution, shown in Table 1, at the selected spatial step $h = 0.2$, temporal step $\tau = 0.001$, and space domain x from -40 to 40, while selecting a domain of time values from 35 to 105. In specific, the SSE is computed by $\sum_{i=1}^{n} (u_i - u_{ex})^2$, where u_i is the discrete numerical approximate solution over the predefined domain x and u_{ex} is the discrete exact analytical solution over the same predefined spatial domain at a specific time value. As endorsed by Figures 3 and 4, the three proposed approaches are accuracy adjustable. The smaller the temporal and spatial steps sizes, the more efficacy they achieve. Besides, as advocated by Table 1, the SSFT approach exhibits the smallest sum of squares error over the other demonstrated schemes. Precisely, the errors are approximately in terms of 10e-21 when the time step is 10e-3, which substantiate that this method almost renders the exact solution itself. However, we can achieve less computational time by adjusting a higher value of temporal step size, in a trade off with the accuracy of the scheme that will be decreased accordingly, as demonstrated in Tables 2 and 3. Additionally, it is obviously noticed from Tables 1–3, using a fixed space step size while employing different values of time steps $\tau = 0.008$, $\tau = 0.001$, and $\tau = 0.0001$, that the obtained error diminishes when the temporal step size value decreases in an attempt to approach zero, which advocates the convergence behavior of our three proposed schemes [41].

5.2. Numerical Tests for the PNLSE. Here, we shall divert our attention to the PNLSE presented in Equation (1), in which the fiber loss term deliberately appears so that we intensively investigate this perturbation effect on the shape of the transmitted pulse.

In order to examine such an effect, our numerical experiments have been performed on both types of solitons solutions, single bright and dark solitons.

To perform these tests, we shall use an initial bright pulse soliton of [25]:

$$u(0,t) = \sqrt{P_o} \operatorname{sech}\left(\frac{t}{T_0}\right). \tag{37}$$

On the other hand, using an initial dark pulse soliton of

$$u(0,t) = \sqrt{P_o}\left(\frac{1}{B^2} - \operatorname{sech}^2\left(\mathrm{B}\frac{t}{T_0}\right)\right)^{0.5}. \tag{38}$$

Setting P_o and T_o to one unit for both initial conditions. In Equation (38), B is called the darkness coefficient. In general, the value of this coefficient varies between zero and one $0 < B \leq 1$.

Opting for $B = 1$, this soliton is called a "black soliton." In contrast, a grey soliton is produced, for any other value of B [4]. Since the exact solution cannot be obtained for these kinds of equations, the three proposed approaches were examined for a lossy optical fiber. Generally, the simulation process is divided into three fundamental consecutive stages.

In the first stage, our simulation is focused on the anomalous dispersion, generating bright solitons for an optical fiber of length $L = 10$ km. Moreover, this assessment was performed, adhering to the following parameters $\beta_2 = -1$ ps^2/km, $\gamma = 1\,\mathrm{W}^{-1}\cdot\mathrm{km}^{-1}$, when $\alpha = 0$ dB/km followed by $\alpha = 0.3$ dB/km. The graphs, representing the pulse at different distances $z = 0.1, 1, 10$ km, are shown in Figures 5 and 6, respectively. Likewise, repeating the previous experiment for the same fiber but with different parameters' values and higher GVD such that $\beta_2 = -20$ ps^2/km, $\gamma = 2.5\,\mathrm{W}^{-1}\,\mathrm{km}^{-1}$, and $\alpha = 0$ dB/km. Since the split-step Fourier transform scheme is the only method that has endured under this assessment, the graph of its approximate solution is shown in Figure 7(a). Subsequently, the experiment was conducted for a lossy optical fiber at the same length and parameters, when $\alpha = 0.23$ dB/km. Figure 7(b) exhibits the pulses' shapes at different distances using the split-step Fourier transform as well.

In the second stage of this simulation, our goal is to test the normal dispersion, introducing dark solitons pulses. For this purpose, the approach was examined on the same length of optical fiber, when $\beta_2 = +1\,\mathrm{ps}^2/\mathrm{km}$, and $\gamma = 1\,\mathrm{W}^{-1}\,\mathrm{km}^{-1}$, and for both values of attenuation constant $\alpha = 0$ and 0.3 dB/km. The three numerical schemes were tested, and their results are illustrated in Figure 8. Similarly, we have repeated the previous experiment but with other parameters' values such that $\beta_2 = +20\,\mathrm{ps}^2/\mathrm{km}$, $\gamma = 2.5\,\mathrm{W}^{-1}\mathrm{km}^{-1}$, and for both $\alpha = 0$ and 0.23 dB/km. The results, by using the split-step Fourier transform, are presented in Figure 9. In Figures 10(a) and 10(b), we have plotted the split-step Fourier transform numerical solution in 3D for a lossy optical fiber $\alpha = 0.3$ dB/km when the input pulse is a single bright and dark soliton, respectively, at a distance $z = 10$ km.

For a single bright soliton, a comparison is conducted in Table 4, using the three proposed numerical schemes, to present the variation of the pulse power values at a distance $z = 20$ km, computed for different attenuation constants, while Table 5 demonstrates the attenuation effect on the transmitted pulse power, using the same numerical approaches, when the attenuation constant is $\alpha = 0.2$ dB/km but over different distances z from 1 to 60 km. The final stage is dedicated to applying the same test but for various initial conditions, associated with different input pulses, which cannot be supported with the exact solution that is only valid for some special initial pulses. This means other signals rather than the bright and dark solitons, such as the sine squared function, which is a periodic travelling wave, and the rectangular pulse in the presence of attenuation. Figure 11 presents the outcome of this experiment, by using the split-step Fourier transform to approximate the solution.

As evident by all the obtained numerical results, our suggested approach, which is the extended split-step Fourier transform, has a leading behavior in modeling the soliton propagation through a lossy optical fiber, especially when compared to the other proposed numerical approaches. Based on the previously obtained findings, Figures 5 and 8(a)–8(c) reinforced that the input signal has retained its shape and amplitude while propagation, in the absence of the losses, creating a soliton. On the contrary, when the fiber losses existed, the transmitted pulse has suffered from attenuation, which can be noticed as a decrease in the amplitude and power of the pulse [49], as supported by Figures 6 and 8(d)–8(f), whereas Figure 10 bolstered that this amplitude degradation gradually occurs in an exponential form over the propagation distance. Hence, amplifiers are widely used to overcome such a perturbed effect. Moreover, when the GVD parameter maintained a value less than 4, the three proposed schemes have provided a reliable solution for this problem, as referred in Figures 5, 6, and 8. Nevertheless, when this parameter was assigned a value greater than or equal to five, the extended split-step Fourier transform was the only approach that has provided reasonable behavior under this experiment and achieved the best accuracy among the other proposed techniques, as explained in Figures 7 and 9. Eventually, Table 4 endorsed that increasing the fiber losses has inversely decreased the transmitted pulse power. Meanwhile, transmitting the pulse through longer propagation distance in a lossy optical fiber has conversely attenuated the power of the initial pulse, as illustrated by Table 5.

Despite the three extended numerical approaches have achieved slightly close results, as clearly shown in Tables 4 and 5, our superior approach, the extended SSFT, has corroborated the fastest performance, through achieving the least elapsed time among the other extended versions of the other demonstrated techniques.

6. Conclusion

To recapitulate, although the pulse propagation through a lossy optical fiber is modeled by the well-known 1D NLSE, the exact solution of this equation cannot invariably be reached, especially after comprising the attenuation term. Thus, an extended version of the SSFT approach was successfully developed in this paper by including the fiber loss effects to accurately obtain an approximate numerical solution that simulates this notable phenomenon. This precise inclusion is extremely crucial because these losses, associated with any realistic optical fiber, cannot be ignored due to their inevitable repercussions in decreasing the amplitude and power of the soliton during propagation over the transmission path. Additionally, to advocate the efficacy and accuracy of our proposed approach, two other extensions of numerical schemes were introduced, named the FPSM and HSM, and assessed by drawing a plethora of graphs and tables for the comparison purpose. Eventually, the performed experiments findings have corroborated that our remarkable approach, the extended SSFT, has provided prominence performance when compared to its suggested counterparts, in the presence and absence of fiber losses. In specific, when the losses were utterly neglected, our approach has achieved the least sum of squares error, whereas when the losses were considered, this superb approach has demonstrated compatible results with the other proposed approaches, along with rendering the least processing time, which places it in the first rank as the fastest scheme. Moreover, it was the only technique to survive when handling higher values of the GVD parameter. Therefore, the extended SSFT is deemed to be an accurate, straightforward, and fast approach for manipulating this significant problem.

Data Availability

The data used to support the findings of this study are available upon request from the corresponding author.

Disclosure

This research was accomplished as a part of the authors' employment at their respected institutions.

Conflicts of Interest

The authors declare that they have no potential conflict of interest.

References

[1] L. F. Mollenauer and J. P. Gordon, *Solitons in Optical Fibers: Fundamentals and Applications*, Elsevier, 2006.

[2] C. Mahnke, A. Hause, and F. Mitschke, "On the creation of solitons in amplifying optical fibers," *International Journal of Optics*, vol. 2018, Article ID 9452540, 11 pages, 2018.

[3] S. Y. Al-Dabagh and M. S. Abdalla, "Numerical solutions aspect of nonlinear Schrödinger equation in monomode optical fiber," in *2006 2nd International Conference on Information & Communication Technologies*, vol. 2, pp. 2099–2103, Damascus, Syria, April 2006.

[4] H. Apithy, Y. Bouslimani, and H. Hamam, "Split-step algorithm-based propagation modelling of dark soliton-like pulses," *International Journal of Modelling and Simulation*, vol. 27, no. 1, pp. 68–73, 2007.

[5] P. Chou, "Fiber optics part 2: single-mode fiber vs. multimode-fiber, Cisco blogs," 2018, https://blogs.cisco.com/sp/fiberopticspt2singlemultifiber.

[6] D. Felice, "A study of a nonlinear Schrödinger equation for optical fibers," 2016, https://arxiv.org/abs/1612.00358.

[7] F. Copie, S. Randoux, and P. Suret, "The physics of the one-dimensional nonlinear Schrodinger equation in fiber optics: rogue waves, modulation instability and self-focusing phenomena," *Reviews in Physics*, vol. 5, article 100037, 2020.

[8] Y. Y. Choy, W. N. Tan, K. G. Tay, and C. T. Ong, "Crank-Nicolson implicit method for the nonlinear Schrödinger equation with variable coefficient," *AIP Conference Proceedings*, vol. 1605, no. 1, pp. 76–82, 2014.

[9] E. Kersale, "Analytic solutions of partial differential equations-MATH3414," School of Mathematics, University of Leeds, 2003.

[10] G. M. Muslu and H. A. Erbay, "A split-step Fourier method for the complex modified Korteweg-de Vries equation," *Computers & Mathematics with Applications*, vol. 45, no. 1-3, pp. 503–514, 2003.

[11] D. O. Liceaga, *Pseudospectral solutions of reaction-diffusion equations that model excitable media: convergence of solutions and applications*, Doctoral dissertation, University of British Columbia, 2007.

[12] C. Harley, "Hopscotch method: The numerical solution of the Frank-Kamenetskii partial differential equation," *Applied Mathematics and Computation*, vol. 217, no. 8, pp. 4065–4075, 2010.

[13] H. N. Hassan and H. K. Saleh, "Fourier spectral methods for solving some nonlinear partial differential equations," *International Journal of Open Problems in Computer Science and Mathematics*, vol. 6, no. 2, pp. 144–179, 2013.

[14] X. Kang, K. Cheng, and C. Guo, "A second-order Fourier pseudospectral method for the generalized regularized long wave equation," *Advances in Difference Equations*, vol. 2015, no. 1, Article ID 339, 2015.

[15] M. Saleh and E. Kovács, "New explicit asymmetric hopscotch methods for the heat conduction equation," *Proceedings of the 1st Online Conference on Algorithms*, MDPI, Basel, Switzerland, 2021.

[16] N. G. Farag, A. H. Eltanboly, M. S. El-Azab, and S. Obayya, "Pseudo-spectral approach for extracting optical solitons of the complex Ginzburg Landau equation with six nonlinearity forms," *Optik*, vol. 254, p. 168662, 2022.

[17] M. Aleshams, A. Zarifkar, and M. H. Sheikhi, "Split-step Fourier transform method in modeling of pulse propagation in dispersive nonlinear optical fibers," in *Proceedings of CAOL 2005. Second International Conference on Advanced Optoelectronics and Lasers, 2005*, vol. 2, pp. 124–126, Yalta, Ukraine, September 2005.

[18] E. Forestieri and M. Secondini, "Solving the nonlinear Schrödinger equation," in *Optical Communication Theory and Techniques*, pp. 3–11, Springer, Boston, MA, 2005.

[19] A. V. Ramprasad and M. Meenakshi, "A study on the propagation characteristics of pulses in optical fiber communication systems," in *2006 IFIP International Conference on Wireless and Optical Communications Networks*, p. 5, Bangalore, India, April 2006.

[20] S. V. Siddamal, R. M. Banakar, and B. C. Jinaga, "Split step method in the analysis and modeling of optical fiber communication system," in *International Conference on Advances in Computing, Communication and Control*, pp. 254–261, Springer, Berlin, Heidelberg, 2011.

[21] R. Deiterding, R. Glowinski, H. Oliver, and S. Poole, "A reliable split-step Fourier method for the propagation equation of ultra-fast pulses in single-mode optical fibers," *Journal of Lightwave Technology*, vol. 31, no. 12, pp. 2008–2017, 2013.

[22] J. Shao, X. Liang, and S. Kumar, "Comparison of split-step Fourier schemes for simulating fiber optic communication systems," *IEEE Photonics Journal*, vol. 6, no. 4, pp. 1–15, 2014.

[23] R. Deiterding and S. W. Poole, "Robust split-step Fourier methods for simulating the propagation of ultra-short pulses in single-and two-mode optical communication fibers," in *Splitting Methods in Communication, Imaging, Science, and Engineering*, pp. 603–625, Springer, Cham, 2016.

[24] L. Ladányi, Ľ. Scholtz, and J. Müllerová, "Numerical simulations of dispersion effects in chirped Gaussian and soliton pulses," *Optical and Quantum Electronics*, vol. 49, no. 3, p. 105, 2017.

[25] H. E. Ibarra-Villalon, O. Pottiez, A. Gomez-Vieyra, J. P. Lauterio-Cruz, and Y. E. Bracamontes-Rodriguez, "Numerical approaches for solving the nonlinear Schrödinger equation in the nonlinear fiber optics formalism," *Journal of Optics*, vol. 22, no. 4, article 043501, 2020.

[26] A. Semenova, S. A. Dyachenko, A. O. Korotkevich, and P. M. Lushnikov, "Comparison of split-step and Hamiltonian integration methods for simulation of the nonlinear Schrodinger type equations," *Journal of Computational Physics*, vol. 427, article 110061, 2021.

[27] T. R. Taha and M. I. Ablowitz, "Analytical and numerical aspects of certain nonlinear evolution equations. II. Numerical, nonlinear Schrodinger equation," *Journal of Computational Physics*, vol. 55, no. 2, pp. 203–230, 1984.

[28] J. Ohlsson, P. Schlatter, C. Mavriplis, and D. S. Henningson, "The spectral-element and pseudo-spectral methods: a comparative study," in *Spectral and High Order Methods for Partial Differential Equations*, pp. 459–467, Springer, Berlin, Heidelberg, 2011.

[29] L. N. Trefethen, "Spectral methods in MATLAB," in *Society for industrial and applied mathematics*, Philadelphia, Pa.: Society for Industrial and Applied Mathematics (SIAM, 3600 Market Street, Floor 6, Philadelphia, PA 19104), 2000.

[30] C. Dall'Agnol, P. L. Natti, E. R. Cirilo, N. M. L. Romeiro, and É. R. T. Natti, "Soliton propagation in lossy optical fibers," 2021, https://arxiv.org/abs/2110.10069.

[31] C. Mas Arabi, "Nonlinear propagation in optical fibers: from soliton radiations to multimode instabilities," Doctoral dissertation, Lille 1, 2018.

[32] M. Eguchi, K. Hayata, and M. Koshiba, "Analysis of soliton pulse propagation in an optical fiber using the finite- element method," *Electronics and Communications in Japan (Part II: Electronics)*, vol. 73, no. 3, pp. 81–91, 1990.

[33] V. E. Zakharov and S. V. Manakov, "On the complete integrability of a nonlinear Schrödinger equation," *Theoretical and Mathematical Physics*, vol. 19, no. 3, pp. 551–559, 1974.

[34] J. R. Buchanan and Z. Shao, *A First Course in Partial Differential Equations*, World Scientific Publishing Company, 2017.

[35] J. C. Washburne, *A distributed surface temperature and energy balance model of a semi-arid watershed*, Doctoral dissertation, The University of Arizona, 1994.

[36] S. C. Tsang and K. W. Chow, "The evolution of periodic waves of the coupled nonlinear Schrodinger equations," *Mathematics and Computers in Simulation*, vol. 66, no. 6, pp. 551–564, 2004.

[37] A. I. Mahdy, "Fourier pseudospectral solution for a 2D nonlinear paraxial envelope equation of laser interactions in plasmas," *Journal of Applied Mathematics and Physics*, vol. 4, no. 12, pp. 2186–2202, 2016.

[38] J. M. Carcione, "A generalization of the Fourier pseudospectral method," *Geophysics*, vol. 75, no. 6, pp. A53–A56, 2010.

[39] P. Suarez, *An Introduction to the Split Step Fourier Method Using MATLAB*, 2016.

[40] N. G. Farag, A. H. Eltanboly, M. S. EL-Azab, and S. S. A. Obayya, "On the analytical and numerical solutions of the one-dimensional nonlinear Schrodinger equation," *Mathematical Problems in Engineering*, vol. 2021, Article ID 3094011, 15 pages, 2021.

[41] E. Love and W. J. Rider, "On the convergence of finite difference methods for PDE under temporal refinement," *Computers & Mathematics with Applications*, vol. 66, no. 1, pp. 33–40, 2013.

[42] J. A. Machado, A. Babaei, and B. P. Moghaddam, "Highly accurate scheme for the Cauchy problem of the generalized Burgers-Huxley equation," *Acta Polytechnica Hungarica*, vol. 13, no. 6, 2016.

[43] M. Abdelhakem and Y. H. Youssri, "Two spectral Legendre's derivative algorithms for Lane-Emden, Bratu equations, and singular perturbed problems," *Applied Numerical Mathematics*, vol. 169, pp. 243–255, 2021.

[44] B. P. Moghaddam and Z. S. Mostaghim, "A novel matrix approach to fractional finite difference for solving models based on nonlinear fractional delay differential equations," *Ain Shams Engineering Journal*, vol. 5, no. 2, pp. 585–594, 2014.

[45] E. M. Abo-Eldahab, R. Adel, H. M. Mobarak, and M. Abdelhakem, "The effects of magnetic field on boundary layer nano-fluid flow over stretching sheet," *Applied Mathematics & Information Sciences*, vol. 15, no. 6, pp. 731–741, 2021.

[46] M. Abdelhakem, T. Alaa-Eldeen, D. Baleanu, M. G. Alshehri, and M. El-Kady, "Approximating real-life BVPs via Chebyshev polynomials' first derivative pseudo-Galerkin method," *Fractal and Fractional*, vol. 5, no. 4, p. 165, 2021.

[47] M. Abdelhakem, M. Biomy, S. A. Kandil, and D. Baleanu, "A numerical method based on Legendre differentiation matrices for higher order ODEs," *Information Sciences Letters*, vol. 9, no. 3, p. 3, 2020.

[48] D. Steinley, "Validating clusters with the lower bound for sum-of-squares error," *Psychometrika*, vol. 72, no. 1, pp. 93–106, 2007.

[49] C. F. de Oliveira, P. L. Natti, E. R. Cirilo, N. M. L. Romeiro, and É. R. T. Natti, "Numerical stability of solitons waves through splices in quadratic optical media," *Acta Scientiarum Technology*, vol. 42, no. 1, article e46881, 2020.

Hindawi
Journal of Function Spaces
Volume 2022, Article ID 1581362, 11 pages
https://doi.org/10.1155/2022/1581362

Research Article

A β-Convolution Theorem Associated with the General Quantum Difference Operator

Enas M. Shehata [1] **and Rasha M. El Zafarani** [2]

[1]*Department of Mathematics and Computer Science, Faculty of Science, Menoufia University, Shibin El-Kom 32511, Egypt*
[2]*Department of Mathematics, Faculty of Science, Ain Shams University, Cairo, Egypt*

Correspondence should be addressed to Enas M. Shehata; enas.soliman@science.menofia.edu.eg

Received 26 October 2021; Accepted 9 December 2021; Published 24 February 2022

Academic Editor: Youssri Hassan Youssri

In this paper, we prove some properties of the β-partial derivative. We define the β-convolution of two functions associated with the general quantum difference operator, $D_\beta f(t) = (f(\beta(t)) - f(t))/(\beta(t) - t)$; β is a strictly increasing continuous function. Moreover, we study the shift, the associative law, and the β-differentiability of the β-convolution. Furthermore, we prove the β-convolution theorem and give some applications.

1. Introduction and Preliminaries

The classical convolution of two real functions u and v is defined by

$$(u * v)(t) = \int_0^t u(t-s)v(s)ds, \tag{1}$$

where $u(t-s) = f(t,s)$ is the usual shift of the function u defined on $\mathbb{R}$ which is considered as the unique solution of the first-order partial differential equation

$$\frac{\partial}{\partial t} f(t,s) = -\frac{\partial}{\partial s} f(t,s), t, s \in \mathbb{R}, f(t,0) = u(t), t \in \mathbb{R}. \tag{2}$$

The convolution theorem highly extends the potential of Laplace transform in solving ordinary differential equations. Furthermore, the operation of the convolution is needed in understanding many topics such as partial differential equations, Green's functions, and forming the general solution of some kinds of boundary value problems. See [1–4] for some applications of the convolution in electrical engineering, physics, and theory of distribution. The classical convolution theorem says that the Laplace transform of the convolution $u * v$ of the two functions u and v is equal to the Laplace transform of u multiplied by the Laplace transform of v. Recently, there are many versions of the convolution theorem such as h-convolution theorem, q-convolution theorem, convolution theorem on time scale, and (q,h)-convolution theorem on discrete time scale, see, e.g., [5–8]. Bohner and Guseinov [9] studied the convolution theorem on a time scale $\mathbb{T}$, where the convolution of two functions $u, v : \mathbb{T} \longrightarrow \mathbb{R}$ is defined by

$$(u * v)(t) = \int_{t_0}^t \hat{u}(t, \sigma(s))v(s)\Delta s, \ t, t_0 \in \mathbb{T}. \tag{3}$$

Here, $\hat{u}(t,s)$ is the shift of the given function u defined on $\mathbb{T}$ which is considered as the unique solution of the shifting problem

$$u\wedge^{\Delta_t}(t, \sigma(s)) = -u\wedge^{\Delta_s}(t,s), t, s \in \mathbb{T}, \hat{u}(t, t_0) = u(t), t, t_0 \in \mathbb{T}, \tag{4}$$

where Δ is the delta differentiation and σ is the forward jump operator in $\mathbb{T}$. In [7], the convolution theorem of two

positive real functions $u_1(t)$ and $u_2(t)$ is defined by

$$\mathscr{L}_q\{u_1(t) * u_2(t)\} = \mathscr{L}_q\{u_1(t)\}\mathscr{L}_q\{u_2(t)\}, \tag{5}$$

where $\mathscr{L}_q\{u(t)\} = \int_0^\infty e_q^{-st} u(t)dt$, $s \in \mathbb{C}$, $R(s) > 0$, and

$$u_1(t) * u_2(t) = \int_0^t u_1(\tau)u_2(t-\tau)d\tau. \tag{6}$$

It should be noted that, here in [7], the Laplace transform denoted by $\mathscr{L}_q$ and the related convolution are defined by the usual integral; however, the q-exponential e_q^{-st} is used in the form $[1+(q-1)st]^{-1/(q-1)}$, $t \geq 0$, $q > 1$. In [10], the q-convolution is defined by

$$u_1(t) * u_2(t) = \int_0^t u_1(\tau)u_2(t-\tau)d_q\tau. \tag{7}$$

Hamza et al. [11] defined the general quantum β-difference operator D_β by:

$$D_\beta f(t) = \begin{cases} \dfrac{f(\beta(t)) - f(t)}{\beta(t) - t}, & t \neq s_0, \\ f'(s_0), & t = s_0, \end{cases} \tag{8}$$

where the function β is a strictly increasing and continuous defined on an interval $I \subseteq \mathbb{R}$, β has only one fixed point $s_0 \in I$, and the inequality $(t - s_0)(\beta(t) - t) \leq 0$ holds for all $t \in I$, accordingly $s_0 = \lim_{k\longrightarrow\infty}\beta^k(t)$, $\beta^k(t) = \beta \circ \beta \circ \cdots \circ \beta(t)$ (k-times). A function f is said to be β-differentiable on I, if the ordinary derivative $f'(s_0)$ exists. The β-difference operator D_β produces the Jackson q-difference operator, the Hahn difference operator, and the power quantum difference operator when $\beta(t) = qt$, $\beta(t) = qt + \omega$, and $\beta(t) = qt^n$, respectively; $t \in I$, $q \in (0,1)$, $\omega > 0$, and n is odd number, see [12–14]. Quantum difference operators consider a good tool in dealing with sets of nondifferentiable functions in the usual concept; furthermore, it has an interesting role due to their applications in several sciences, see, e.g., [15–18]. Recent quantum calculus applications can be found in [19–21].

The β-integral of $f : I \longrightarrow \mathbb{R}$ is defined in [11] by

$$\int_a^c f(t)d_\beta t = \int_{s_0}^c f(t)d_\beta t - \int_{s_0}^a f(t)d_\beta t, a, c \in I, \tag{9}$$

where

$$F(x) = \int_{s_0}^x f(t)d_\beta t = \sum_{k=0}^\infty \left(\beta^k(x) - \beta^{k+1}(x)\right) f\left(\beta^k(x)\right), x \in I, \tag{10}$$

provided that the series in the right hand side converges. Furthermore, if f is continuous at s_0, then F exists and is continuous at s_0, and $D_\beta F(x)$ exists for all $x \in I$, $D_\beta F(x) = f(x)$. The β-exponential functions are defined, in [22], by

$$\begin{aligned} e_{\lambda,\beta}(t) &= \frac{1}{\prod_{k=0}^\infty \left[1 - \lambda\left(\beta^k(t)\right)\left(\beta^k(t) - \beta^{k+1}(t)\right)\right]}, \\ E_{\lambda,\beta}(t) &= \prod_{k=0}^\infty \left[1 + \lambda\left(\beta^k(t)\right)\left(\beta^k(t) - \beta^{k+1}(t)\right)\right]. \end{aligned} \tag{11}$$

If the function $f : I \longrightarrow \mathbb{R}$ is β-differentiable and $D_\beta f(t) = 0$ for all $t \in I$, then f is constant function and

$$f(t) = f(s_0), \text{for all } t \in I, \tag{12}$$

see [11]. In [23] (p. 126), the β-partial derivative of $f(t, y)$ with respect to t is defined by

$$\frac{\partial_\beta}{\partial_\beta t} f(t, y) = \frac{f(\beta(t), y) - f(t, y)}{\beta(t) - t}, t \neq s_0. \tag{13}$$

Also, if $F(t) := \int_{s_0}^b f(t, y)d_\beta y$, $b, t \in I$. Then, $D_\beta F(t)$ at $t \neq s_0$ exists and is given by

$$D_\beta F(t) = \int_{s_0}^b \frac{\partial_\beta}{\partial_\beta t} f(t, y)d_\beta y. \tag{14}$$

Moreover, the Leibniz's rule is proved in [23] such that if $F(t) := \int_{s_0}^t f(t, y)d_\beta y$, then $D_\beta F(t)$ at $t \neq s_0$ exists and is given by

$$D_\beta F(t) = f(\beta(t), t) + \int_{s_0}^t \frac{\partial_\beta}{\partial_\beta t} f(t, y)d_\beta y. \tag{15}$$

The general quantum Laplace transform $\mathscr{L}_\beta$ and its inverse $\mathscr{L}_\beta^{-1}$ and some of their properties were deduced in [24]. The β-Laplace transform $\mathscr{L}_\beta$ is defined by:

$$\mathscr{L}_\beta\{f(t)\} := \int_{s_0}^\infty f(t)e_{\ominus_\beta z,\beta}(\beta(t))d_\beta t, \tag{16}$$

such that the improper β-integral, see [24] (Definition 3.5), in (16) exists, where $s_0 \in I$, $f \in V([s_0,\infty), \mathbb{C})$, which is the set of β-integrable functions over each compact subinterval of $[s_0, \infty)$, and z satisfies $1 + z(\beta(t) - t) \neq 0$. The function f is said to be of exponential order $\lambda > 0$, if there exist a constant $M > 0$ such that $|f(t)| \leq Me_{\lambda,\beta}(t)$ for all $t \in [s_0,\infty)$. Let $p, q : I \longrightarrow \mathbb{C}$ be continuous functions at s_0 and satisfy the condition $1 + (\beta(t) - t)p(t) \neq 0$ for all $t \in I$, then the following properties hold [24]:

(i_1) $e_{\ominus_\beta p,\beta}(t) = 1/e_{p,\beta}(t)$

(i_2) $e_{\ominus_\beta p,\beta}(\beta(t)) = e_{\ominus_\beta p,\beta}(t)/(1 + (\beta(t) - t)p(t)) = -((\ominus_\beta p)(t)/p(t))e_{\ominus_\beta p,\beta}(t)$

(i_3) $D_\beta(e_{\ominus_\beta p,\beta}(t)) = (\ominus_\beta p)(t)e_{\ominus_\beta p,\beta}(t)$

where $(\ominus_\beta p)(t) = -p(t)/(1 + (\beta(t) - t)p(t))$.

Recently, Cardoso [25] investigated the β-Lagrange's identity for the β-Sturm-Liouville eigenvalue problem and proved that it is self-adjoint in $L^2_\beta([a,b])$. For more results in β-calculus, we refer the readers to see [26–29].

The current paper is organized as follows. In Section 2, we introduce some properties of the β-partial derivative. In Section 3, we define the β-convolution of two functions and study their shift, associativity, and the β-differentiability. Moreover, we prove the β-convolution theorem and give some applications.

2. β-Partial Derivative

In this section, we introduce some properties of the β-partial derivative.

Theorem 1. *Let $f, g : I \times I \longrightarrow \mathbb{R}$. Assume that the β-partial derivatives of $f(t,\tau)$, $g(t,\tau)$, $t,\tau \in I$ with respect to t at $t \neq s_0$ exist. Then:*

(i) The β-partial derivative of the product $(fg)(t,\tau)$ with respect to t at $t \neq s_0$ is given by

$$\begin{aligned}\frac{\partial_\beta}{\partial_\beta t}(fg)(t,\tau) &= \left[\frac{\partial_\beta}{\partial_\beta t}f(t,\tau)\right]g(\beta(t),\tau) + f(t,\tau)\left[\frac{\partial_\beta}{\partial_\beta t}g(t,\tau)\right]\\ &= \left[\frac{\partial_\beta}{\partial_\beta t}f(t,\tau)\right]g(t,\tau) + f(\beta(t),\tau)\left[\frac{\partial_\beta}{\partial_\beta t}g(t,\tau)\right],\end{aligned} \tag{17}$$

where $(fg)(t,\tau) = f(t,\tau)g(t,\tau)$.

(ii) The β-partial derivative of $(f/g)(t,\tau)$ with respect to t at $t \neq s_0$ is given by

$$\frac{\partial_\beta}{\partial_\beta t}\left(\frac{f}{g}\right)(t,\tau) = \frac{\left[(\partial_\beta/\partial_\beta t)f(t,\tau)\right]g(t,\tau) - f(t,\tau)\left[(\partial_\beta/\partial_\beta t)g(t,\tau)\right]}{g(t,\tau)g(\beta(t),\tau)}, \tag{18}$$

provided that $g(t,\tau)g(\beta(t),\tau) \neq 0$.

Proof. (i).

$$\begin{aligned}\frac{\partial_\beta}{\partial_\beta t}(fg)(t,\tau) &= \frac{(fg)(\beta(t),\tau) - (fg)(t,\tau)}{\beta(t) - t}\\ &= \frac{f(\beta(t),\tau) - f(t,\tau)}{\beta(t) - t}g(\beta(t),\tau) + f(t,\tau)\\ &\quad \cdot \frac{g(\beta(t),\tau) - g(t,\tau)}{\beta(t) - t}\\ &= \left[\frac{\partial_\beta}{\partial_\beta t}f(t,\tau)\right]g(\beta(t),\tau) + f(t,\tau)\left[\frac{\partial_\beta}{\partial_\beta t}g(t,\tau)\right].\end{aligned} \tag{19}$$

Similarly, we can prove that

$$\frac{\partial_\beta}{\partial_\beta t}(fg)(t,\tau) = \left[\frac{\partial_\beta}{\partial_\beta t}f(t,\tau)\right]g(t,\tau) + f(\beta(t),\tau)\left[\frac{\partial_\beta}{\partial_\beta t}g(t,\tau)\right]. \tag{20}$$

In the same way, we can prove (ii). □

Lemma 2. *Let $f : I \times I \longrightarrow \mathbb{R}$ and assume that the β-partial derivative of $f(t,\tau)$, $t,\tau \in I$ with respect to τ exists and is continuous at (t,s_0). Then*

$$\int_\tau^{\beta(\tau)} f(t,y)d_\beta y = (\beta(\tau) - \tau)f(t,\tau). \tag{21}$$

Proof. Let $F(t,\tau) = \int_{s_0}^{\tau} f(t,y)d_\beta y$. Since $F(t,\tau)$ is continuous at (t,s_0) and $(\partial_\beta/\partial_\beta\tau)F(t,\tau) = f(t,\tau)$, then

$$\begin{aligned}\int_\tau^{\beta(\tau)} f(t,y)d_\beta y &= \int_{s_0}^{\beta(\tau)} f(t,y)d_\beta y - \int_{s_0}^{\tau} f(t,y)d_\beta y\\ &= F(t,\beta(\tau)) - F(t,\tau).\end{aligned} \tag{22}$$

Since $F(t,\beta(\tau)) - F(t,\tau) = (\beta(\tau) - \tau)(\partial_\beta/\partial_\beta\tau)F(t,\tau)$, then

$$\int_\tau^{\beta(\tau)} f(t,y)d_\beta y = (\beta(\tau) - \tau)f(t,\tau). \tag{23}$$

□

Lemma 3. *Let $f : I \times I \longrightarrow \mathbb{R}$. If the β-partial derivative of $f(t,\tau)$, $t,\tau \in I$ with respect to t exists and is continuous at (s_0,τ), then*

$$\int_a^b \frac{\partial_\beta}{\partial_\beta t}f(t,\tau)d_\beta t = f(b,\tau) - f(a,\tau) \text{ for all } a,b \in I. \tag{24}$$

Proof. We have

$$\begin{aligned}\int_{s_0}^b \frac{\partial_\beta}{\partial_\beta t}f(t,\tau)d_\beta t &= \sum_{k=0}^{\infty}\left(\beta^k(b) - \beta^{k+1}(b)\right)\frac{\partial_\beta}{\partial_\beta t}f\left(\beta^k(b),\tau\right)\\ &= \sum_{k=0}^{\infty}\left[f\left(\beta^k(b),\tau\right) - f\left(\beta^{k+1}(b),\tau\right)\right]\\ &= \lim_{n\longrightarrow\infty}\sum_{k=0}^{n}\left[f\left(\beta^k(b),\tau\right) - f\left(\beta^{k+1}(b),\tau\right)\right]\\ &= f(b,\tau) - f(s_0,\tau).\end{aligned} \tag{25}$$

Similarly,

$$\int_{s_0}^a \frac{\partial_\beta}{\partial_\beta t}f(t,\tau)d_\beta t = f(a,\tau) - f(s_0,\tau). \tag{26}$$

Hence,

$$\int_a^b \frac{\partial_\beta}{\partial_\beta t} f(t,\tau) d_\beta t = f(b,\tau) - f(a,\tau). \tag{27}$$

□

Lemma 4 (integration by parts). *Let $f, g : I \times I \longrightarrow \mathbb{R}$. Assume that the β-partial derivatives of $f(t,\tau), g(t,\tau)$, $t, \tau \in I$ with respect to t exist and are both continuous at (s_0, τ). Then*

$$\int_a^b f(t,\tau)\left[\frac{\partial_\beta}{\partial_\beta t} g(t,\tau)\right] d_\beta t = f(b,\tau)g(b,\tau) - f(a,\tau)g(a,\tau) - \int_a^b \left[\frac{\partial_\beta}{\partial_\beta t} f(t,\tau)\right] g(\beta(t),\tau) d_\beta t, a, b \in I. \tag{28}$$

Proof. Since

$$\frac{\partial_\beta}{\partial_\beta t}(fg)(t,\tau) = f(t,\tau)\left[\frac{\partial_\beta}{\partial_\beta t} g(t,\tau)\right] + g(\beta(t),\tau)\left[\frac{\partial_\beta}{\partial_\beta t} f(t,\tau)\right]. \tag{29}$$

Then

$$\int_a^b f(t,\tau)\frac{\partial_\beta}{\partial_\beta t} g(t,\tau) d_\beta t = \int_a^b \frac{\partial_\beta}{\partial_\beta t}(fg)(t,\tau) d_\beta t - \int_a^b \left[\frac{\partial_\beta}{\partial_\beta t} f(t,\tau)\right] g(\beta(t),\tau) d_\beta t, a, b \in I. \tag{30}$$

By Lemma 3, we get

$$\int_a^b \frac{\partial_\beta}{\partial_\beta t}(fg)(t,\tau) d_\beta t = f(b,\tau)g(b,\tau) - f(a,\tau)g(a,\tau). \tag{31}$$

Therefore,

$$\int_a^b f(t,\tau)\left[\frac{\partial_\beta}{\partial_\beta t} g(t,\tau)\right] d_\beta t = f(b,\tau)g(b,\tau) - f(a,\tau)g(a,\tau) - \int_a^b \left[\frac{\partial_\beta}{\partial_\beta t} f(t,\tau)\right] g(\beta(t),\tau) d_\beta t, a, b \in I. \tag{32}$$

□

3. The β-Convolution Theorem

In the following, we define the β-convolution of two functions and prove some of its properties. Furthermore, we prove the β-convolution theorem and give some applications.

Definition 5. Consider the β-shifting problem

$$\frac{\partial_\beta}{\partial_\beta t} z(t,\beta(\tau)) = -\frac{\partial_\beta}{\partial_\beta \tau} z(t,\tau), t, \tau \in I, t \geq \tau \geq s_0, \tag{33}$$

$$z(t, s_0) = f(t), t \in I, t \geq s_0. \tag{34}$$

We denote the shift of a function $f \in V([s_0,\infty), \mathbb{C})$ by $\widehat{f}(t,\tau)$, $t, \tau \in I$ which is the solution of (33).

We will assume in this paper that the problem (33) has a unique solution $z = \widehat{f}$.

Definition 6 (β-convolution). The β-convolution $f * g$ of two functions $f, g \in V([s_0,\infty), \mathbb{C})$ is defined by

$$(f * g)(t) = \int_{s_0}^t \widehat{f}(t,\beta(\tau)) g(\tau) d_\beta \tau, t \in I, \tag{35}$$

where $\widehat{f}$ is the shift of f given in Definition 5.

Note that in the case of $\beta(t) = qt$, $s_0 = 0$, we get the q-shifting problem

$$\frac{\partial_q}{\partial_q t} z(t, q\tau) = -\frac{\partial_q}{\partial_q \tau} z(t,\tau), z(t,0) = f(t), \tag{36}$$

and the q-convolution

$$(f * g)(t) = \int_0^t \widehat{f}(t, q\tau) g(\tau) d_q \tau, \tag{37}$$

we refer the reader to see [6]. Furthermore, in the case of $\beta(t) = t$, we get the usual shifting problem

$$\frac{\partial}{\partial t} z(t,\tau) = -\frac{\partial}{\partial \tau} z(t,\tau), z(t, s_0) = f(t), \tag{38}$$

with the unique solution $z(t,\tau) = f(t-\tau) = \widehat{f}(t,\tau)$ which is the usual shift, and we get the classical convolution

$$(f * g)(t) = \int_0^t f(t-\tau) g(\tau) d\tau. \tag{39}$$

Lemma 7. *Let $\widehat{f}$ be the shift of f. Then, $\widehat{f}(t,t) = f(s_0)$ for all $t \in I$.*

Proof. Let $\widehat{f}$ be the shift of f. Set $\widehat{f}(t,t) = F(t)$. From the β-shifting problem (33), we have

$$0 = \frac{\partial_\beta}{\partial_\beta t}\widehat{f}(t,\beta(\tau)) + \frac{\partial_\beta}{\partial_\beta \tau}\widehat{f}(t,\tau) = \frac{\widehat{f}(\beta(t),\beta(\tau)) - \widehat{f}(t,\beta(\tau))}{\beta(t) - t} + \frac{\widehat{f}(t,\beta(\tau)) - \widehat{f}(t,\tau)}{\beta(\tau) - \tau}. \tag{40}$$

Take $t=\tau$, consequently

$$0=\frac{\widehat{f}(\beta(t),\beta(t))-\widehat{f}(t,\beta(t))}{\beta(t)-t}+\frac{\widehat{f}(t,\beta(t))-\widehat{f}(t,t)}{\beta(t)-t}$$
$$=\frac{\widehat{f}(\beta(t),\beta(t))-\widehat{f}(t,t)}{\beta(t)-t}=\frac{F(\beta(t))-F(t)}{\beta(t)-t}=D_\beta F(t),\ t\neq s_0. \tag{41}$$

By equation (12), $\widehat{f}(t,t)=F(t)=F(s_0)$, for all $t\in I$. Moreover, from the initial condition (33), $F(s_0)=f(s_0)$. Then, $\widehat{f}(t,t)=f(s_0)$ for all $t\in I$. □

Lemma 8. *Define the function F by*

$$F(t,\tau):=\int_\tau^t \widehat{f}(t,\beta(y))\widehat{g}(y,\tau)d_\beta y. \tag{42}$$

Then, $(\partial_\beta/\partial_\beta t)F(t,\tau)$ and $(\partial_\beta/\partial_\beta \tau)F(t,\tau)$ exist and are given by:

$$\frac{\partial_\beta}{\partial_\beta t}F(t,\tau)=\widehat{f}(\beta(t),\beta(t))\widehat{g}(t,\tau)+\int_\tau^t\left[\frac{\partial_\beta}{\partial_\beta t}\widehat{f}(t,\beta(y))\right]\widehat{g}(y,\tau)d_\beta y,$$
$$\frac{\partial_\beta}{\partial_\beta \tau}F(t,\tau)=\int_\tau^t \widehat{f}(t,\beta(y))\left[\frac{\partial_\beta}{\partial_\beta \tau}\widehat{g}(y,\tau)\right]d_\beta y-\widehat{f}(t,\beta(\tau))\widehat{g}(\tau,\beta(\tau)). \tag{43}$$

Proof. We have

$$F(t,\tau)=\int_{s_0}^t \widehat{f}(t,\beta(y))\widehat{g}(y,\tau)d_\beta y-\int_{s_0}^\tau \widehat{f}(t,\beta(y))\widehat{g}(y,\tau)d_\beta y. \tag{44}$$

Then,

$$\frac{\partial_\beta}{\partial_\beta t}F(t,\tau)=\frac{\partial_\beta}{\partial_\beta t}\left[\int_{s_0}^t \widehat{f}(t,\beta(y))\widehat{g}(y,\tau)d_\beta y\right]-\frac{\partial_\beta}{\partial_\beta t}\left[\int_{s_0}^\tau \widehat{f}(t,\beta(y))\widehat{g}(y,\tau)d_\beta y\right],$$

$$\frac{\partial_\beta}{\partial_\beta \tau}F(t,\tau)=\frac{\partial_\beta}{\partial_\beta \tau}\left[\int_{s_0}^t \widehat{f}(t,\beta(y))\widehat{g}(y,\tau)d_\beta y\right]-\frac{\partial_\beta}{\partial_\beta \tau}\left[\int_{s_0}^\tau \widehat{f}(t,\beta(y))\widehat{g}(y,\tau)d_\beta y\right]. \tag{45}$$

Now,

$$\begin{aligned}
&\frac{\partial_\beta}{\partial_\beta t}\left[\int_{s_0}^t \widehat{f}(t,\beta(y))\widehat{g}(y,\tau)d_\beta y\right]\\
&=\frac{1}{\beta(t)-t}\left\{\sum_{k=0}^\infty\left(\beta^{k+1}(t)-\beta^{k+2}(t)\right)\widehat{f}\left(\beta(t),\beta^{k+2}(t)\right)\right.\\
&\quad\cdot\widehat{g}\left(\beta^{k+1}(t),\tau\right)-\sum_{k=0}^\infty\left(\beta^{k}(t)-\beta^{k+1}(t)\right)\widehat{f}\left(t,\beta^{k+1}(t)\right)\\
&\quad\left.\cdot\widehat{g}\left(\beta^{k}(t),\tau\right)\right\}=\frac{1}{\beta(t)-t}\left\{\sum_{k=1}^\infty\left(\beta^{k}(t)-\beta^{k+1}(t)\right)\right.\\
&\quad\cdot\left[\widehat{f}\left(\beta(t),\beta^{k+1}(t)\right)\widehat{g}\left(\beta^{k}(t),\tau\right)-\widehat{f}\left(t,\beta^{k+1}(t)\right)\right.\\
&\quad\left.\left.\cdot\widehat{g}\left(\beta^{k}(t),\tau\right)\right]\right\}-\frac{(t-\beta(t))\widehat{f}(t,\beta(t))\widehat{g}(t,\tau)}{\beta(t)-t}\\
&=\frac{1}{\beta(t)-t}\left\{\sum_{k=0}^\infty\left(\beta^{k}(t)-\beta^{k+1}(t)\right)\left[\widehat{f}\left(\beta(t),\beta^{k+1}(t)\right)\right.\right.\\
&\quad\left.\left.\cdot\widehat{g}\left(\beta^{k}(t),\tau\right)-\widehat{f}\left(t,\beta^{k+1}(t)\right)\widehat{g}\left(\beta^{k}(t),\tau\right)\right]\right\}\\
&\quad-\frac{t-\beta(t)}{\beta(t)-t}\left[\widehat{f}(\beta(t),\beta(t))\widehat{g}(t,\tau)-\widehat{f}(t,\beta(t))\widehat{g}(t,\tau)\right]\\
&\quad+\widehat{f}(t,\beta(t))\widehat{g}(t,\tau)=\widehat{f}(\beta(t),\beta(t))\widehat{g}(t,\tau)\\
&\quad+\int_{s_0}^t\left[\frac{\partial_\beta}{\partial_\beta t}\widehat{f}(t,\beta(y))\right]\widehat{g}(y,\tau)d_\beta y.
\end{aligned} \tag{46}$$

Similarly,

$$\frac{\partial_\beta}{\partial_\beta t}\left[\int_{s_0}^\tau \widehat{f}(t,\beta(y))\widehat{g}(y,\tau)d_\beta y\right]=\int_{s_0}^\tau\left[\frac{\partial_\beta}{\partial_\beta t}\widehat{f}(t,\beta(y))\right]\widehat{g}(y,\tau)d_\beta y. \tag{47}$$

Therefore,

$$\begin{aligned}
\frac{\partial_\beta}{\partial_\beta t}F(t,\tau)&=\widehat{f}(\beta(t),\beta(t))\widehat{g}(t,\tau)+\int_{s_0}^t\left[\frac{\partial_\beta}{\partial_\beta t}\widehat{f}(t,\beta(y))\right]\\
&\quad\cdot\widehat{g}(y,\tau)d_\beta y-\int_{s_0}^\tau\left[\frac{\partial_\beta}{\partial_\beta t}\widehat{f}(t,\beta(y))\right]\widehat{g}(y,\tau)d_\beta y\\
&=\widehat{f}(\beta(t),\beta(t))\widehat{g}(t,\tau)+\int_\tau^t\left[\frac{\partial_\beta}{\partial_\beta t}\widehat{f}(t,\beta(y))\right]\\
&\quad\cdot\widehat{g}(y,\tau)d_\beta y.
\end{aligned} \tag{48}$$

Using the same technique, we obtain

$$\begin{aligned}\frac{\partial_\beta}{\partial_\beta \tau}F(t,\tau) &= \int_{s_0}^{\tau}\widehat{f}(t,\beta(y))\left[\frac{\partial_\beta}{\partial_\beta \tau}\widehat{g}(y,\tau)\right]d_\beta y - \widehat{f}(t,\beta(\tau))\widehat{g}(\tau,\beta(\tau)) \\ &\quad - \int_{s_0}^{t}\widehat{f}(t,\beta(y))\left[\frac{\partial_\beta}{\partial_\beta \tau}\widehat{g}(y,\tau)\right]d_\beta y \\ &= \int_{\tau}^{t}\widehat{f}(t,\beta(y))\left[\frac{\partial_\beta}{\partial_\beta \tau}\widehat{g}(y,\tau)\right]d_\beta y - \widehat{f}(t,\beta(\tau))\widehat{g}(\tau,\beta(\tau)).\end{aligned} \tag{49}$$

□

Theorem 9. *The shift of the β-convolution of two functions f, g is given by*

$$(\widehat{f * g})(t,\tau) = \int_{\tau}^{t}\widehat{f}(t,\beta(y))\widehat{g}(y,\tau)d_\beta y. \tag{50}$$

Proof. We aim to prove that the integral in equation (50) is a solution of the β-shifting problem (33). Set

$$F(t,\tau) = \int_{\tau}^{t}\widehat{f}(t,\beta(y))\widehat{g}(y,\tau)d_\beta y. \tag{51}$$

Take $\tau = s_0$, then

$$F(t,s_0) = \int_{s_0}^{t}\widehat{f}(t,\beta(y))\widehat{g}(y,s_0)d_\beta y. \tag{52}$$

From the initial condition of the shift problem (33), we get $\widehat{g}(y,s_0) = g(y)$. Consequently,

$$F(t,s_0) = \int_{s_0}^{t}\widehat{f}(t,\beta(y))g(y)d_\beta y = (f * g)(t). \tag{53}$$

Using Lemmas 7 and 8, we get

$$\begin{aligned}&\frac{\partial_\beta}{\partial_\beta t}F(t,\beta(\tau)) + \frac{\partial_\beta}{\partial_\beta \tau}F(t,\tau) \\ &\quad = -\int_{\beta(\tau)}^{t}\left[\frac{\partial_\beta}{\partial_\beta y}\widehat{f}(t,y)\right]\widehat{g}(y,\beta(\tau))d_\beta y + f(s_0)\widehat{g}(t,\beta(\tau)) \\ &\qquad + \int_{\tau}^{t}\widehat{f}(t,\beta(y))\left[\frac{\partial_\beta}{\partial_\beta \tau}\widehat{g}(y,\tau)\right]d_\beta y - \widehat{f}(t,\beta(\tau))\widehat{g}(\tau,\beta(\tau)).\end{aligned} \tag{54}$$

We have, using the integration by parts,

$$\begin{aligned}&\int_{\beta(\tau)}^{t}\left[\frac{\partial_\beta}{\partial_\beta y}\widehat{f}(t,y)\right]\widehat{g}(y,\beta(\tau))d_\beta y \\ &\quad = \widehat{f}(t,t)\widehat{g}(t,\beta(\tau)) - \widehat{f}(t,\beta(\tau))\widehat{g}(\beta(\tau),\beta(\tau)) \\ &\qquad - \int_{\beta(\tau)}^{t}\widehat{f}(t,\beta(y))\left[\frac{\partial_\beta}{\partial_\beta y}\widehat{g}(y,\beta(\tau))\right]d_\beta y \\ &\quad = f(s_0)\widehat{g}(t,\beta(\tau)) - \widehat{f}(t,\beta(\tau))g(s_0) \\ &\qquad + \int_{\beta(\tau)}^{t}\widehat{f}(t,\beta(y))\left[\frac{\partial_\beta}{\partial_\beta \tau}\widehat{g}(y,\tau)\right]d_\beta y.\end{aligned} \tag{55}$$

Consequently,

$$\begin{aligned}&\frac{\partial_\beta}{\partial_\beta t}F(t,\beta(\tau)) + \frac{\partial_\beta}{\partial_\beta \tau}F(t,\tau) \\ &\quad = -f(s_0)\widehat{g}(t,\beta(\tau)) + \widehat{f}(t,\beta(\tau))g(s_0) - \int_{\beta(\tau)}^{t}\widehat{f}(t,\beta(y)) \\ &\qquad \cdot \left[\frac{\partial_\beta}{\partial_\beta \tau}\widehat{g}(y,\tau)\right]d_\beta y + f(s_0)\widehat{g}(t,\beta(\tau)) - \widehat{f}(t,\beta(\tau))\widehat{g}(\tau,\beta(\tau)) \\ &\qquad + \int_{\tau}^{t}\widehat{f}(t,\beta(y))\left[\frac{\partial_\beta}{\partial_\beta \tau}\widehat{g}(y,\tau)\right]d_\beta y = \widehat{f}(t,\beta(\tau))g(s_0) \\ &\qquad + \int_{\tau}^{\beta(\tau)}\widehat{f}(t,\beta(y))\left[\frac{\partial_\beta}{\partial_\beta \tau}\widehat{g}(y,\tau)\right]d_\beta y - \widehat{f}(t,\beta(\tau))\widehat{g}(\tau,\beta(\tau)).\end{aligned} \tag{56}$$

By using Lemma 2, we get

$$\begin{aligned}&\frac{\partial_\beta}{\partial_\beta t}F(t,\beta(\tau)) + \frac{\partial_\beta}{\partial_\beta \tau}F(t,\tau) = \widehat{f}(t,\beta(\tau))g(s_0) + (\beta(\tau) - \tau) \\ &\qquad \cdot \widehat{f}(t,\beta(\tau))\left[\frac{\partial_\beta}{\partial_\beta \tau}\widehat{g}(\tau,\tau)\right] - \widehat{f}(t,\beta(\tau))\widehat{g}(\tau,\beta(\tau)) \\ &\quad = \widehat{f}(t,\beta(\tau))g(s_0) + \widehat{f}(t,\beta(\tau))[\widehat{g}(\tau,\beta(\tau)) - \widehat{g}(\tau,\tau)] \\ &\qquad - \widehat{f}(t,\beta(\tau))\widehat{g}(\tau,\beta(\tau)) = 0.\end{aligned} \tag{57}$$

Therefore,

$$\frac{\partial_\beta}{\partial_\beta t}F(t,\beta(\tau)) = -\frac{\partial_\beta}{\partial_\beta \tau}F(t,\tau). \tag{58}$$

Hence, $F(t,\tau) = (\widehat{f * g})(t,\tau)$ is the solution of equation (58). □

The proof of the following Lemma 10 will be omitted since it is a direct consequence of Definitions 5 and 6 and the linearity of the β-integral.

Lemma 10. *The β-convolution $f * g$ defined in (35) satisfies the following properties:*

(i) $c(f * g) = cf * g = f * cg,\ c \in \mathbb{R}$

(ii) $f * (g + h) = f * g + f * h$

(iii) $f * (ag + bh) = a(f * g) + b(f * h),\ a, b \in \mathbb{R}$

Lemma 11. *Let $w : J \times J \longrightarrow \mathbb{R}$ be continuous function at (s_0, s_0), $s_0 \in J$, and J is a compact subinterval of I, where $w(y, \tau) = \widehat{f}(t, \beta(y))\widehat{g}(y, \beta(\tau))h(\tau)$. Then,*

$$\int_{s_0}^{t}\int_{\beta(\tau)}^{t} \widehat{f}(t, \beta(y))\widehat{g}(y, \beta(\tau))h(\tau)d_\beta y d_\beta \tau = \int_{s_0}^{t}\int_{s_0}^{y} \widehat{f}(t, \beta(y))\widehat{g}(y, \beta(\tau))h(\tau)d_\beta \tau d_\beta y. \tag{59}$$

Proof. First, we refer the reader to see Fubini's Theorem in [23] (p. 132). Now, let

$$W(t, \tau) = \int_{\beta(\tau)}^{t} w(y, \tau)d_\beta y,\ \phi_1(t) = \int_{s_0}^{t} W(t, \tau)d_\beta \tau,$$
$$G(y) = \int_{s_0}^{y} w(y, \tau)d_\beta \tau,\ \phi_2(t) = \int_{s_0}^{t} G(y)d_\beta y. \tag{60}$$

Then,

$$D_\beta \phi_1(t) = \int_{s_0}^{t} \frac{\partial_\beta}{\partial_\beta t} W(t, \tau)d_\beta \tau,$$

$$\frac{\partial_\beta}{\partial_\beta t} W(t, \tau) = \frac{1}{\beta(t) - t}\left\{\sum_{k=0}^{\infty}\left(\beta^{k+1}(t) - \beta^{k+2}(t)\right)w\left(\beta^{k+1}(t), \tau\right) - \sum_{k=0}^{\infty}\left(\beta^{k}(t) - \beta^{k+1}(t)\right)w\left(\beta^{k}(t), \tau\right)\right\} = w(t, \tau). \tag{61}$$

Therefore, $D_\beta \phi_1(t) = \int_{s_0}^{t} w(t, \tau)d_\beta \tau$. Also,

$$D_\beta \phi_2(t) = D_\beta\left[\int_{s_0}^{t} G(y)d_\beta y\right] = G(t) = \int_{s_0}^{t} w(t, \tau)d_\beta \tau = D_\beta \phi_1(t). \tag{62}$$

Hence, $\phi_1(t) = \phi_2(t),\ t \in I$. □

Theorem 12 (Associativity of the β-convolution). *The β-convolution is associative, that is,*

$$(f * g) * h = f * (g * h). \tag{63}$$

Proof. Using Theorem 9 and Lemma 11, we have

$$\begin{aligned}((f * g) * h)(t) &= \int_{s_0}^{t} (\widehat{f * g})(t, \beta(\tau))h(\tau)d_\beta \tau \\ &= \int_{s_0}^{t}\int_{\beta(\tau)}^{t} \widehat{f}(t, \beta(y))\widehat{g}(y, \beta(\tau))h(\tau)d_\beta y d_\beta \tau \\ &= \int_{s_0}^{t}\int_{s_0}^{y} \widehat{f}(t, \beta(y))\widehat{g}(y, \beta(\tau))h(\tau)d_\beta \tau d_\beta y \\ &= \int_{s_0}^{t} \widehat{f}(t, \beta(y))(g * h)(y)d_\beta y = (f * (g * h))(t).\end{aligned} \tag{64}$$

□

Theorem 13. *Let f and g be β-differentiable functions, then we have*

$$D_\beta(f * g)(t) = f(t)g(s_0) + \left(f * D_\beta g\right)(t). \tag{65}$$

Proof. We have

$$(f * g)(t) = \int_{s_0}^{t} \widehat{f}(t, \beta(\tau))g(\tau)d_\beta \tau, \quad t \in I. \tag{66}$$

Using Lemma 8, then,

$$D_\beta(f * g)(t) = \int_{s_0}^{t}\left[\frac{\partial_\beta}{\partial_\beta t}\widehat{f}(t, \beta(\tau))\right]g(\tau)d_\beta \tau + \widehat{f}(\beta(t), \beta(t))g(t). \tag{67}$$

By Definition 5 and Lemma 7

$$\frac{\partial_\beta}{\partial_\beta t}\widehat{f}(t, \beta(\tau)) = -\frac{\partial_\beta}{\partial_\beta \tau}\widehat{f}(t, \tau),$$
$$\widehat{f}(\beta(t), \beta(t)) = f(s_0), \tag{68}$$

therefore,

$$D_\beta(f * g)(t) = -\int_{s_0}^{t}\left[\frac{\partial_\beta}{\partial_\beta \tau}\widehat{f}(t, \tau)\right]g(\tau)d_\beta \tau + f(s_0)g(t). \tag{69}$$

We get, by the integration by parts,

$$\begin{aligned}D_\beta(f * g)(t) &= -\widehat{f}(t, t)g(t) + \widehat{f}(t, s_0)g(s_0) + \int_{s_0}^{t} \widehat{f}(t, \beta(\tau))\left[\frac{\partial_\beta}{\partial_\beta \tau}g(\tau)\right] \\ &\quad \cdot d_\beta \tau + f(s_0)g(t) = -f(s_0)g(t) + f(t)g(s_0) \\ &\quad + \int_{s_0}^{t} \widehat{f}(t, \beta(\tau))\left[\frac{\partial_\beta}{\partial_\beta \tau}g(\tau)\right]d_\beta \tau + f(s_0)g(t) \\ &= f(t)g(s_0) + \int_{s_0}^{t} \widehat{f}(t, \beta(\tau))\left[\frac{\partial_\beta}{\partial_\beta \tau}g(\tau)\right]d_\beta \tau.\end{aligned} \tag{70}$$

Since $(\partial_\beta/\partial_\beta\tau)g(\tau) = D_\beta g(\tau)$, then,

$$\begin{aligned} D_\beta(f*g)(t) &= f(t)g(s_0) + \int_{s_0}^{t} \widehat{f}(t,\beta(\tau))\left(D_\beta g(\tau)\right)d_\beta\tau \\ &= f(t)g(s_0) + \left(f * D_\beta g\right)(t). \end{aligned} \tag{71}$$

This completes the proof of equation of (65). □

Corollary 14. *For all $k \in \mathbb{N}_0$, we have*

$$D_\beta^k(f*g) = f*\left(D_\beta^k g\right) + \sum_{r=0}^{k-1}\left(D_\beta^r f\right)\left(D_\beta^{k-1-r} g\right)(s_0). \tag{72}$$

Proof. Using the induction, for $k=1$ equation (72) is equation (65). Suppose that for $k = m \in \mathbb{N}_0$ equation (72) is true, i.e.

$$D_\beta^m(f*g)(t) = \left(f*D_\beta^m g\right)(t) + \sum_{r=0}^{m-1}\left(D_\beta^r f\right)(t)\left(D_\beta^{m-1-r} g\right)(s_0). \tag{73}$$

Then, by using equation (65) and from the linearity of D_β, we get

$$\begin{aligned} D_\beta^{m+1}(f*g)(t) &= D_\beta\left[\left(f*D_\beta^m g\right)(t) + \sum_{r=0}^{m-1}\left(D_\beta^r f\right)(t)\left(D_\beta^{m-1-r} g\right)(s_0)\right] \\ &= f(t)\left(D_\beta^m g\right)(s_0) + \left(f*D_\beta^{m+1} g\right)(t) + \sum_{r=0}^{m-1}\left(D_\beta^{r+1} f\right) \\ &\quad \cdot (t)\left(D_\beta^{m-1-r} g\right)(s_0) = \left(f*D_\beta^{m+1} g\right)(t) \\ &\quad + \sum_{r=0}^{m}\left(D_\beta^r f\right)(t)\left(D_\beta^{m-r} g\right)(s_0). \end{aligned} \tag{74}$$

Therefore, equation (72) is true for $k = m+1$, and thus, it holds for any $k \in \mathbb{N}$. □

Lemma 15. *Let Ψ be a function defined by*

$$\Psi(\tau) = \int_\tau^\infty \frac{\widehat{f}(t,\tau)}{e_{z,\beta}(\beta(t),\tau)} d_\beta t. \tag{75}$$

Then, Ψ is constant, where $e_{z,\beta}(\beta(t),\tau) = e_{z,\beta}(\beta(t))/e_{z,\beta}(\tau)$.

Proof. We will show that $D_\beta\Psi(\tau) \equiv 0$ for all τ, then Ψ is constant.

By using Theorem 1 and Lemma 8, we find

$$\begin{aligned} D_\beta\Psi(\tau) &= \int_\tau^\infty \frac{\left[(\partial_\beta/\partial_\beta\tau)\widehat{f}(t,\tau)\right]e_{z,\beta}(\beta(t),\tau) - (\ominus_\beta z)(\tau)e_{z,\beta}(\beta(t),\tau)\widehat{f}(t,\tau)}{e_{z,\beta}(\beta(t),\tau)e_{z,\beta}(\beta(t),\beta(\tau))} \\ &\quad \cdot d_\beta t - \frac{\widehat{f}(\tau,\beta(\tau))}{e_{z,\beta}(\beta(\tau),\beta(\tau))}. \end{aligned} \tag{76}$$

Since $(\partial_\beta/\partial_\beta\tau)\widehat{f}(t,\tau) = -(\partial_\beta/\partial_\beta t)\widehat{f}(t,\beta(\tau))$, $e_{z,\beta}(\beta(\tau),\beta(\tau)) = 1$, we get

$$\begin{aligned} D_\beta\Psi(\tau) &= \int_\tau^\infty \left[\frac{-(\partial_\beta/\partial_\beta t)\widehat{f}(t,\beta(\tau))}{e_{z,\beta}(\beta(t),\beta(\tau))} + \frac{[z/(1+z(\beta(\tau)-\tau))]\widehat{f}(t,\tau)}{e_{z,\beta}(\beta(t),\beta(\tau))}\right] \\ &\quad \cdot d_\beta t - \widehat{f}(\tau,\beta(\tau)) = -\int_\tau^\infty \frac{(\partial_\beta/\partial_\beta t)\widehat{f}(t,\beta(\tau))}{e_{z,\beta}(\beta(t),\beta(\tau))} d_\beta t \\ &\quad + z\left[\int_\tau^\infty \frac{\widehat{f}(t,\tau)}{e_{z,\beta}(\beta(t),\tau)} d_\beta t\right] - \widehat{f}(\tau,\beta(\tau)) = z\Psi(\tau) \\ &\quad - \int_\tau^\infty \frac{(\partial_\beta/\partial_\beta t)\widehat{f}(t,\beta(\tau))}{e_{z,\beta}(\beta(t),\beta(\tau))} d_\beta t - \widehat{f}(\tau,\beta(\tau)) = z\Psi(\tau) \\ &\quad - \int_\tau^{\beta(\tau)} \frac{(\partial_\beta/\partial_\beta t)\widehat{f}(t,\beta(\tau))}{e_{z,\beta}(\beta(t),\beta(\tau))} d_\beta t - \int_{\beta(\tau)}^\infty \frac{(\partial_\beta/\partial_\beta t)\widehat{f}(t,\beta(\tau))}{e_{z,\beta}(\beta(t),\beta(\tau))} \\ &\quad \cdot d_\beta t - \widehat{f}(\tau,\beta(\tau)). \end{aligned} \tag{77}$$

Also, since $\widehat{f}(\beta(\tau),\beta(\tau)) = f(s_0)$ and

$$\begin{aligned} &\left[\frac{\partial_\beta}{\partial_\beta t}\widehat{f}(t,\beta(\tau))\right]e_{\ominus_\beta z,\beta}(\beta(t),\beta(\tau)) \\ &\quad = \frac{\partial_\beta}{\partial_\beta t}\left[\widehat{f}(t,\beta(\tau))e_{\ominus_\beta z,\beta}(t,\beta(\tau))\right] \\ &\qquad - (\ominus_\beta z)(t)e_{\ominus_\beta z,\beta}(t,\beta(\tau))\widehat{f}(t,\beta(\tau)). \end{aligned} \tag{78}$$

Hence, by Lemma 3, we get

$$\int_\tau^{\beta(\tau)} \frac{(\partial_\beta/\partial_\beta t)\widehat{f}(t,\beta(\tau))}{e_{z,\beta}(\beta(t),\beta(\tau))} d_\beta t - \widehat{f}(\tau,\beta(\tau)) = f(s_0),$$

$$\begin{aligned} &\int_{\beta(\tau)}^\infty \left[\frac{\partial_\beta}{\partial_\beta t}\widehat{f}(t,\beta(\tau))\right]e_{\ominus_\beta z,\beta}(\beta(t),\beta(\tau))d_\beta t \\ &\quad = \int_{\beta(\tau)}^\infty \frac{\partial_\beta}{\partial_\beta t}\left[\widehat{f}(t,\beta(\tau))e_{\ominus_\beta z,\beta}(t,\beta(\tau))\right]d_\beta t \\ &\qquad - \int_{\beta(\tau)}^\infty (\ominus_\beta z)(t)e_{\ominus_\beta z,\beta}(t,\beta(\tau))\widehat{f}(t,\beta(\tau))d_\beta t \\ &\quad = -f(s_0) + z\int_{\beta(\tau)}^\infty \widehat{f}(t,\beta(\tau))e_{\ominus_\beta z,\beta}(\beta(t),\beta(\tau))d_\beta t \\ &\quad = -f(s_0) + z\Psi(\beta(\tau)). \end{aligned} \tag{79}$$

Therefore,

$$\begin{aligned} D_\beta \Psi(\tau) &= z\Psi(\tau) - f(s_0) + f(s_0) - z\Psi(\beta(\tau)) \\ &= -z[\Psi(\beta(\tau)) - \Psi(\tau)] = -z(\beta(\tau) - \tau) D_\beta \Psi(\tau), \end{aligned} \tag{80}$$

and then $[1 + (\beta(\tau) - \tau)z] D_\beta \Psi(\tau) = 0$, i.e., $D_\beta \Psi(\tau) = 0$. □

Now, we prove the β-convolution theorem.

Theorem 16 (β-Convolution theorem). *Let $f, g \in V([s_0, \infty), \mathbb{C})$ be two functions of exponential order and their β-convolution $f * g$ is defined by (35). Then,*

$$\mathscr{L}_\beta\{f * g\} = \mathscr{L}_\beta\{f\} \cdot \mathscr{L}_\beta\{g\}. \tag{81}$$

Proof. We have

$$\begin{aligned} \mathscr{L}_\beta\{f * g\} &= \int_{s_0}^{\infty} \frac{(f * g)(t)}{e_{z,\beta}(\beta(t))} d_\beta t = \int_{s_0}^{\infty} \frac{1}{e_{z,\beta}(\beta(t))} \\ &\quad \cdot \int_{s_0}^{t} \widehat{f}(t, \beta(\tau)) g(\tau) d_\beta \tau d_\beta t. \end{aligned} \tag{82}$$

Then,

$$\begin{aligned} \mathscr{L}_\beta\{f * g\} &= \int_{s_0}^{\infty} \frac{g(\tau)}{e_{z,\beta}(\beta(\tau))} \left[\int_{\beta(\tau)}^{\infty} \frac{\widehat{f}(t, \beta(\tau)) e_{z,\beta}(\beta(\tau))}{e_{z,\beta}(\beta(t))} d_\beta t \right] d_\beta \tau \\ &= \int_{s_0}^{\infty} \frac{g(\tau)}{e_{z,\beta}(\beta(\tau))} \Psi(\beta(\tau)) d_\beta \tau \\ &= \int_{s_0}^{\infty} g(\tau) e_{\ominus_\beta z,\beta}(\beta(\tau)) \Psi(\beta(\tau)) d_\beta \tau. \end{aligned} \tag{83}$$

Using Lemma 15, equation (12), we get $\Psi(\tau) = \Psi(\beta(\tau)) = \Psi(s_0)$. Moreover,

$$\begin{aligned} \Psi(s_0) &= \int_{s_0}^{\infty} \frac{\widehat{f}(t, s_0) e_{z,\beta}(s_0)}{e_{z,\beta}(\beta(t))} d_\beta t \\ &= \int_{s_0}^{\infty} f(t) e_{\ominus_\beta z,\beta}(\beta(t)) d_\beta t = \mathscr{L}_\beta\{f\}. \end{aligned} \tag{84}$$

Hence, $\mathscr{L}_\beta\{f * g\} = \mathscr{L}_\beta\{f\} \cdot \mathscr{L}_\beta\{g\}$. □

Corollary 17. *Let $\widehat{f}$ be the shift of f, $\tau \in I$ with $\tau \geq s_0$. Define the function χ_τ by*

$$\chi_\tau(t) = \begin{cases} 0, & t < \tau, \\ 1, & t \geq \tau. \end{cases} \tag{85}$$

Then

$$\mathscr{L}_\beta\left\{\chi_\tau \widehat{f}(\cdot, \tau)\right\} = e_{\ominus_\beta z,\beta}(\tau) \mathscr{L}_\beta\{f\}. \tag{86}$$

Proof.

$$\begin{aligned} \mathscr{L}_\beta\left\{\chi_\tau \widehat{f}(\cdot, \tau)\right\} &= \int_{s_0}^{\infty} \chi_\tau(t) \widehat{f}(t, \tau) e_{\ominus_\beta z,\beta}(\beta(t)) d_\beta t \\ &= \int_{\tau}^{\infty} \widehat{f}(t, \tau) e_{\ominus_\beta z,\beta}(\beta(t)) d_\beta t \\ &= e_{\ominus_\beta z,\beta}(\tau) \int_{\tau}^{\infty} \widehat{f}(t, \tau) e_{\ominus_\beta z,\beta}(\beta(t), \tau) d_\beta t \\ &= e_{\ominus_\beta z,\beta}(\tau) \Psi(\tau), \end{aligned} \tag{87}$$

where Ψ is defined in equation (75). Then, by Lemma 15, $\Psi(\tau) \equiv \Psi(s_0) = \mathscr{L}_\beta\{f\}$. □

3.1. Applications on the β-Convolution Theorem. Here, we apply the β-convolution theorem to find the following:

(1) $e_{\lambda,\beta}(t) * e_{\mu,\beta}(t)$,

(2) $t * e_{\lambda,\beta}(t)$,

(3) $\sin_{\lambda,\beta}(t) * \sin_{\lambda,\beta}(t)$.

(1) We have by the β-convolution Theorem 16 and [24] (Theorem 3.10) that

$$\begin{aligned} \mathscr{L}_\beta\{e_{\lambda,\beta}(t) * e_{\mu,\beta}(t)\} &= \frac{1}{(z-\lambda)(z-\mu)} = \frac{1}{(\lambda-\mu)(z-\lambda)} \\ &\quad - \frac{1}{(\lambda-\mu)(z-\mu)}. \end{aligned} \tag{88}$$

Then, by [24] (Corollary 3.22), we get

$$\begin{aligned} e_{\lambda,\beta}(t) * e_{\mu,\beta}(t) &= \frac{1}{(\lambda-\mu)} \mathscr{L}_\beta^{-1}\left\{\frac{1}{(z-\lambda)}\right\} - \frac{1}{(\lambda-\mu)} \\ &\quad \cdot \mathscr{L}_\beta^{-1}\left\{\frac{1}{(z-\mu)}\right\} = \frac{1}{(\lambda-\mu)} \left[e_{\lambda,\beta}(t) - e_{\mu,\beta}(t)\right]. \end{aligned} \tag{89}$$

(2) We have $\mathscr{L}_\beta\{t\} = 1/z^2$ by [24] (Example 3.23), then

$$\mathscr{L}_\beta\{t * e_{\lambda,\beta}(t)\} = \mathscr{L}_\beta\{t\} \cdot \mathscr{L}_\beta\{e_{\lambda,\beta}(t)\} = \frac{1}{z^2(z-\lambda)}. \tag{90}$$

Therefore,

$$t * e_{\lambda,\beta}(t) = \mathscr{L}_\beta^{-1}\left\{\frac{1}{z^2(z-\lambda)}\right\} = -\frac{1}{\lambda^2}\mathscr{L}_\beta^{-1}\left\{\frac{1}{z}\right\} - \frac{1}{\lambda}\mathscr{L}_\beta^{-1}\left\{\frac{1}{z^2}\right\} + \frac{1}{\lambda^2}\mathscr{L}_\beta^{-1}\left\{\frac{1}{z-\lambda}\right\} = -\frac{1}{\lambda^2} - \frac{1}{\lambda}t + \frac{1}{\lambda^2}e_{\lambda,\beta}(t). \tag{91}$$

(3) Since

$$\mathscr{L}_\beta\left\{\sin_{\lambda,\beta}(t) * \sin_{\lambda,\beta}(t)\right\} = \mathscr{L}_\beta\left\{\sin_{\lambda,\beta}(t)\right\} \cdot \mathscr{L}_\beta\left\{\sin_{\lambda,\beta}(t)\right\}. \tag{92}$$

From [24] (Example 3.13), we have

$$\mathscr{L}_\beta\left\{\sin_{\lambda,\beta}(t) * \sin_{\lambda,\beta}(t)\right\} = \frac{\lambda^2}{\left(z^2+\lambda^2\right)^2}. \tag{93}$$

By [24] (Theorem 3.21),

$$\mathscr{L}_\beta^{-1}\left\{\frac{1}{\left(z^2+\lambda^2\right)^2}\right\} = \frac{\sin_{\lambda,\beta}(t)}{2\lambda^3} - \frac{\cos_{\lambda,\beta}(t)}{2\lambda^2}\int_{s_0}^{t}\frac{1}{1+\lambda^2(\beta(\tau)-\tau)^2} \cdot d_\beta\tau - \frac{\sin_{\lambda,\beta}(t)}{2\lambda}\int_{s_0}^{t}\frac{(\beta(\tau)-\tau)}{1+\lambda^2(\beta(\tau)-\tau)^2}d_\beta\tau. \tag{94}$$

Hence,

$$\sin_{\lambda,\beta}(t) * \sin_{\lambda,\beta}(t) = \mathscr{L}_\beta^{-1}\left\{\frac{\lambda^2}{\left(z^2+\lambda^2\right)^2}\right\} = \lambda^2\mathscr{L}_\beta^{-1}\left\{\frac{1}{\left(z^2+\lambda^2\right)^2}\right\} = \frac{\sin_{\lambda,\beta}(t)}{2\lambda} - \frac{\cos_{\lambda,\beta}(t)}{2}\int_{s_0}^{t}\frac{1}{1+\lambda^2(\beta(\tau)-\tau)^2}d_\beta\tau - \frac{\lambda\sin_{\lambda,\beta}(t)}{2}\int_{s_0}^{t}\frac{(\beta(\tau)-\tau)}{1+\lambda^2(\beta(\tau)-\tau)^2}d_\beta\tau. \tag{95}$$

4. Conclusion

In this paper, some properties of the β-partial derivative corresponding to $D_\beta f(t) = (f(\beta(t)) - f(t))/(\beta(t) - t)$, $\beta(t) \neq t$, were introduced. The associated β-convolution of two functions was presented, and also the shift, associativity, and β-differentiability of the β-convolution were studied. Moreover, the β-convolution theorem and some applications were introduced.

Data Availability

All the data are included in the article.

Conflicts of Interest

The authors declare that they have no competing interests.

Authors' Contributions

All authors contributed equally and significantly in writing this article. All authors read and approved the final manuscript.

References

[1] P. Blanchard and E. Brüning, *Mathematical Methods in Physics: Distributions, Hilbert Space Operators, Variational Methods, and Applications in Quantum Physics*, vol. 69, Birkhäuser, 2015.

[2] V. K. Khanna, *Digital Signal Processing*, S. Chand Publishing, 2009.

[3] T. Sundius, "Computer fitting of Voigt profiles to Raman lines," *Journal of Raman Spectroscopy*, vol. 1, no. 5, pp. 471–488, 1973.

[4] L. Wang, S. L. Jacques, and L. Zheng, "Conv–convolution for responses to a finite diameter photon beam incident on multi-layered tissues," *Computer Methods and Programs in Biomedicine*, vol. 54, no. 3, pp. 141–150, 1997.

[5] M. Bohner and A. Peterson, *Dynamic Equations on Time Scales, an Introduction with Applications*, Springer Science +Business Media, Lic, 2001.

[6] M. Bohner and G. S. Guseinov, "The h-Laplace and q-Laplace transforms," *Journal of Mathematical Analysis and Applications*, vol. 365, no. 1, pp. 75–92, 2010.

[7] S. R. Naik and H. J. Haubold, "On the q-Laplace transform and related special functions," *Axioms*, vol. 5, no. 3, p. 24, 2016.

[8] M. R. S. Rahmat, "The (q, h)-Laplace transform on discrete time scales," *Computers and Mathematics with Applications*, vol. 62, no. 1, pp. 272–281, 2011.

[9] M. Bohner and G. S. Guseinov, "The convolution on time scales," in *Abstract and Applied Analysis (Vol. 2007)*, Hindawi, 2007.

[10] S. K. Al-Omari, "The q-Sumudu transform and its certain properties in a generalized q-calculus theory," *Advances in Difference Equations*, vol. 2021, no. 1, p. 14, 2021.

[11] A. E. Hamza, A. M. Sarhan, E. M. Shehata, and K. A. Aldowah, "A general quantum difference calculus," *Advances in Difference Equations*, vol. 2015, 2015.

[12] M. H. Annaby, A. E. Hamza, and K. A. Aldowah, "Hahn difference operator and associated Jackson-Nörlund integerals," *Journal of Optimization Theory and Applications*, vol. 154, pp. 133–153, 2012.

[13] V. Kac and P. Cheung, *Quantum Calculus*, Springer, New York, 2002.

[14] K. A. Aldwoah, A. B. Malinowska, and D. F. M. Torres, "The power quantum calculus and variational problems," *Dynamics of Continuous, Discrete and Impulsive Systems*, vol. 19, pp. 93–116, 2012.

[15] F. Ben Adda and J. Cresson, "Quantum derivatives and the Schrodinger equation," *Chaos, Solitons & Fractals*, vol. 19, no. 5, pp. 1323–1334, 2004.

[16] R. Almeida and D. F. Torres, "Nondifferentiable variational principles in terms of a quantum operator," *Mathematical*

Methods in the Applied Sciences, vol. 34, no. 18, pp. 2231–2241, 2011.

[17] R. Almeida and D. F. Torres, "Fractional variational calculus for nondifferentiable functions," *Computers & Mathematics with Applications*, vol. 61, no. 10, pp. 3097–3104, 2011.

[18] R. Askey and J. Wilson, "Some basic hypergeometric orthogonal polynomials that generalize the Jacobi polynomials," *Memoirs of the American Mathematical Society*, vol. 54, pp. 1–55, 1985.

[19] A. M. Alanazi, A. Ebaid, W. M. Alhawiti, and G. Muhiuddin, "The falling body problem in quantum calculus," *Frontiers in Physics*, vol. 8, p. 43, 2020.

[20] M. Arif, O. Barkub, H. M. Srivastava, S. Abdullah, and S. A. Khan, "Some Janowski type harmonic q-starlike functions associated with symmetrical points," *Mathematics*, vol. 8, no. 4, p. 629, 2020.

[21] H. M. Srivastava, M. Arif, and M. Raza, "Convolution properties of meromorphically harmonic functions defined by a generalized convolution q-derivative operator," *AIMS Mathematics*, vol. 6, no. 6, pp. 5869–5885, 2021.

[22] A. E. Hamza, A. M. Sarhan, and E. M. Shehata, "Exponential, trigonometric and hyperbolic functions associated with a general quantum difference operator," *Advances in Dynamical Systems and Applications*, vol. 12, no. 1, pp. 25–38, 2017.

[23] A. E. Hamza, E. M. Shehata, and P. Agarwal, "Leibniz's Rule and Fubini's Theorem Associated with a General Quantum Difference Operator," in *Computational Mathematics and Variational Analysis*, pp. 121–134, Springer, Cham, 2020.

[24] E. M. Shehata, N. Faried, and R. M. El Zafarani, "A general quantum Laplace transform," *Advances in Difference Equations*, vol. 2020, 2020.

[25] J. L. Cardoso, "A β-Sturm–Liouville problem associated with the general quantum operator," *Journal of Difference Equations and Applications*, vol. 27, no. 4, pp. 579–595, 2021.

[26] J. L. Cardoso, "Variations around a general quantum operator," *The Ramanujan Journal*, vol. 54, no. 3, pp. 555–569, 2021.

[27] A. M. C. B. d. Cruz and N. Martins, "General quantum variational calculus," *Statistics, Optimization & Information Computing*, vol. 6, no. 1, pp. 22–41, 2018.

[28] N. Faried, E. M. Shehata, and R. M. El Zafarani, "On homogenous second order linear general quantum difference equations," *Journal of Inequalities and Applications*, vol. 2017, 2017.

[29] N. Faried, E. M. Shehata, and R. M. El Zafarani, "Theory of nth-order linear general quantum difference equations," *Advances in Difference Equations*, vol. 2018, no. 1, 2018.

Hindawi
Journal of Function Spaces
Volume 2022, Article ID 8522231, 15 pages
https://doi.org/10.1155/2022/8522231

Research Article

Discrete Maximum Principle and Energy Stability of the Compact Difference Scheme for Two-Dimensional Allen-Cahn Equation

Yu Bo,[1] Dan Tian,[2] Xiao Liu,[1] and Yuanfeng Jin[1]

[1]*College of Science, Yanbian University, Yanji 133002, China*
[2]*Public Course Department, Xi'an Traffic Engineering Institute, Xi'an 710000, China*

Correspondence should be addressed to Yuanfeng Jin; yfkim@ybu.edu.cn

Received 5 November 2021; Accepted 13 December 2021; Published 10 February 2022

Academic Editor: Youssri Hassan Youssri

The Allen-Cahn model is discussed mainly in the phase field simulation. The compact difference method will be used to numerically approximate the two-dimensional nonlinear Allen-Cahn equation with initial and boundary value conditions, and then, a fully discrete compact difference scheme with second-order accuracy in time and fourth-order in space is established. And its numerical solution satisfies the discrete maximum principle under the constraints of reasonable space and time steps. On this basis, the energy stability of the scheme is investigated. Finally, numerical examples are given to illustrate the theoretical results.

1. Introduction

The phase field problem is a mathematical model described by partial differential equations. The numerical simulation of the phase field has always been an important field of research at home and abroad because of its important theoretical and practical significance. In 1979, the Allen-Cahn equation is considered to describe the antiphase boundary of the crystal movement by Allen and Cahn, which describes fluid dynamics problems and reaction diffusion problems in materials science, and the same model on the study of many diffusion phenomena is proposed such as the competition and repulsion of biological populations and the migration process of river beds. For describing the motion of the antiphase boundary in the crystal, since this type of phase field model does not have an accurate solution, different numerical methods are used to simulate. At present, numerical approximation methods about these phase field models include the finite difference method [1–5], finite element method [6–8], and spectral method [9, 10], etc.

In the paper, the compact difference method is applied to approximate the two-dimensional nonlinear Allen-Cahn equations with initial boundary conditions numerically.

$$\begin{cases} \dfrac{\partial u}{\partial t} = \varepsilon^2 \Delta u - f(u), & (x, y) \in \Omega, t \in [0, T], \\ u(x, y, 0) = u_0(x, y), & (x, y) \in \bar{\Omega}, \\ u|_{\partial\Omega} = 0, & t \in [0, T], \end{cases} \tag{1}$$

where u represents the concentration of a metal component in a binary alloy, the positive parameter ε is the interface width, and the nonlinear term $f(u) = u^3 - u$.

The energy function on the L^2 space is defined as

$$E(u) = \oint_{\Omega} \left(F(u) - \frac{1}{2}\varepsilon^2 u \Delta u \right) dx. \tag{2}$$

Here, $F(u) = (1/4)(u^2 - 1)^2$. One of the intrinsic properties of the Allen-Cahn equation is the energy function that decreases with time:

$$\frac{d}{dt}E(u) \le 0, \quad \forall t > 0. \tag{3}$$

In 2016, Zhang and Hou [3] considered three discrete schemes of the Allen-Cahn equation that included the stable first-order linear explicit-implicit scheme, stable second-order nonlinear Crank-Nicolson scheme, and stable second-order linear Leap-Frog scheme and proved the discrete maximum principle and energy stability under the condition of these three schemes; a compact difference scheme with second-order accuracy in time and fourth-order accuracy in space for one-dimensional Allen-Cahn equation was established by Tian et al. [2] in 2018, and the energy stability of the scheme was investigated; Wu et al. [11] proposed two ADI schemes for the two-dimensional Allen-Cahn equation: the second-order ADI scheme and fourth-order compact ADI scheme, and the analysis of stability and maximum principle were given, respectively, in 2019; then, Deng et al. [12] adopted the finite difference method in time and barycentric interpolation collocation method in space for the two-dimensional Allen-Cahn equation in 2020, obtained the spatial high precision error, and verified the law of energy decline; the Crank-Nicolson difference scheme with second-order accuracy in time and space for the two-dimensional Allen-Cahn equation was established by Zhang et al. [1] in 2021, which proved the existence and convergence of the solution, and finally verified the discrete maximum principle with a numerical example. Based on the existing finite difference methods and inspired by reference [2], a compact difference scheme with second-order accuracy in time and fourth-order accuracy in space is established for the two-dimensional Allen-Cahn equation. Then, the discrete maximum principle and discrete energy stability are mainly investigated. Compared with the previous work about two-dimensional Allen-Cahn equations, this paper obtains higher accuracy in space than before, and the compact difference method is applied and realized in two-dimensional equations for the first time, which will add an effective and feasible method to this kind of research.

2. Establishment of a Compact Difference Scheme for the Two-Dimensional Allen-Chan Equation

Firstly, several commonly used numerical differential formulas are given:

Let $h > 0$ and c be two constants.

Lemma 1 (see [2]). *If $g(x) \in C^2[c-h, c+h]$, then*

$$g(c) = \frac{1}{2}[g(c-h) + g(c+h)] - \frac{h^2}{2}g''(\xi_1), \quad c-h < \xi_1 < c+h. \tag{4}$$

Lemma 2 (see [2]). *If $g(x) \in C^3[c-h, c+h]$, then*

$$g'(c) = \frac{1}{2h}[g(c+h) - g(c-h)] - \frac{h^2}{6}g''(\xi_2), \quad c-h < \xi_2 < c+h. \tag{5}$$

Lemma 3 (see [2]). *If $g(x) \in C^6[c-h, c+h]$, then*

$$\begin{aligned}\frac{1}{12}\left[g''(c-h) + 10g''(c) + g''(c+h)\right] &= \frac{1}{h^2}[g(c+h) - 2g(c) + g(c-h)] + \frac{h^4}{240}g^{(6)}(\xi_3), \\ &\qquad c-h < \xi_3 < c+h.\end{aligned} \tag{6}$$

In this section, a compact difference scheme will be establish for the following two-dimensional Allen-Cahn equation as

$$\begin{cases} \dfrac{\partial u}{\partial t} = \varepsilon^2\left(\dfrac{\partial^2 u}{\partial x^2} + \dfrac{\partial^2 u}{\partial y^2}\right) - f(u), & (x, y) \in \Omega, t \in [0, T], \\ u(x, y, 0) = u_0(x, y), & (x, y) \in \bar{\Omega}, \\ u|_{\partial\Omega} = 0, & t \in [0, T], \end{cases} \tag{7}$$

where $\Omega = [0, 1] \times [0, 1]$.

Let us divide the interval $[0, 1]$ into M equal parts and $[0, T]$ into N equal parts, the space step is $h = 1/M$, and time step is $\tau = T/N$, where $x_i = ih$, $0 \le i \le M$, $y_j = jh$, $0 \le j \le M$, and $t_n = n\tau$, $0 \le n \le N$. $\Omega_h = \{(x_i, y_j) | 0 \le i, j \le M\}$ and $\Omega_\tau = \{t_n | 0 \le n \le N\}$. Let $f_{ij}^{n+1/2} = f(u(x_i, y_j, t_{n+1/2}))$ and $(x_i, y_j, t_{n+1/2})$ be called the node.

Suppose $u = \{u_{ij}^n | 0 \le i, j \le M, 0 \le n \le N\}$ is a grid function on $\Omega_h \times \Omega_\tau$, let

$$\begin{aligned} t_{n+1/2} &= \frac{1}{2}(t_n + t_{n+1}), \\ \delta_t u_{ij}^{n+1/2} &= \frac{1}{\tau}\left(u_{ij}^{n+1} -_{ij}^{n}\right), \\ \delta_x^2 u_{ij}^n &= \frac{1}{h^2}\left(u_{i+1,j}^n - 2u_{ij}^n + u_{i-1,j}^n\right), \\ \delta_y^2 u_{ij}^n &= \frac{1}{h^2}\left(u_{i,j+1}^n - 2u_{ij}^n + u_{i,j-1}^n\right), \\ u_{ij}^{n+1/2} &= \frac{1}{2}\left(u_{ij}^n + u_{ij}^{n+1}\right), \\ \left(u_{ij}^{n+1/2}\right)^3 &= \frac{1}{2}\left[\left(u_{ij}^n\right)^3 + \left(u_i^{n+1}\right)^3\right]. \end{aligned} \tag{8}$$

Suppose $u = \{u_{ij} | 0 \le i, j \le M\}$ is a grid function on Ω_h, the operator is defined by

$$(\mathscr{A}u)_{ij} = \begin{cases} \frac{1}{12}\left(u_{i-1,j} + 10u_{ij} + u_{i+1,j}\right), \\ 1 \le i \le M-1, \quad 0 \le j \le M, \\ u_{ij}, \quad i = 0, M, \quad 0 \le j \le M, \end{cases} \tag{9}$$

$$(\mathscr{B}u)_{ij} = \begin{cases} \frac{1}{12}\left(u_{i,j-1} + 10u_{ij} + u_{i,j+1}\right), \\ 1 \le j \le M-1, \quad 0 \le i \le M, \\ u_{ij}, \quad j = 0, M, \quad 0 \le i \le M, \end{cases} \tag{10}$$

$$v = \frac{\partial^2 u}{\partial x^2}, \tag{11}$$

$$w = \frac{\partial^2 u}{\partial y^2}. \tag{12}$$

Then, we get the following equation:

$$\frac{\partial u}{\partial t} = \varepsilon^2 v + \varepsilon^2 w - f(u). \tag{13}$$

Define the grid functions as

$$\begin{aligned} U_{i,j}^n &= u\left(x_i, y_j, t_n\right), \quad 0 \le i, j \le M, \quad 0 \le n \le N, \\ V_{i,j}^n &= v\left(x_i, y_j, t_n\right), \quad 0 \le i, j \le M, \quad 0 \le n \le N, \\ W_{i,j}^n &= w\left(x_i, y_j, t_n\right), \quad 0 \le i, j \le M, \quad 0 \le n \le N. \end{aligned} \tag{14}$$

Considering differential Equation (13) at the point $(x_i, y_j, t_{n+1/2})$,

$$\begin{aligned} \frac{\partial u}{\partial t}\left(x_i, y_j, t_{n+1/2}\right) &= \varepsilon^2 v\left(x_i, y_j, t_{n+1/2}\right) + \varepsilon^2 w\left(x_i, y_j, t_{n+1/2}\right) \\ &\quad - f\left(u\left(x_i, y_j, t_{n+1/2}\right)\right), 0 \le i, j \le M, \quad 0 \le n \le N-1. \end{aligned} \tag{15}$$

Using Taylor expansion,

$$\begin{aligned} \frac{\partial u}{\partial t}\left(x_i, y_j, t_{n+1/2}\right) &= \frac{1}{\tau}\left[u\left(x_i, y_j, t_{n+1}\right) - u\left(x_i, y_j, t_n\right)\right] \\ &\quad - \frac{\tau^2}{24} \cdot \frac{\partial^3 u}{\partial t^3}\left(x_i, y_j, t_{n+1/2}\right) + O\left(\tau^4\right) \\ &= \delta_t U_{i,j}^{n+1/2} - \frac{\tau^2}{24} \cdot \frac{\partial^3 u}{\partial t^3}\left(x_i, y_j, t_{n+1/2}\right) + O\left(\tau^4\right), \end{aligned}$$

$$v\left(x_i, y_j, t_{n+1/2}\right) = V_{i,j}^{n+1/2} - \frac{\tau^2}{8} \cdot \frac{\partial^2 v}{\partial t^2}\left(x_i, y_j, t_{n+1/2}\right) + O\left(\tau^4\right),$$

$$w\left(x_i, y_j, t_{n+1/2}\right) = W_{i,j}^{n+1/2} - \frac{\tau^2}{8} \cdot \frac{\partial^2 w}{\partial t^2}\left(x_i, y_j, t_{n+1/2}\right) + O\left(\tau^4\right). \tag{16}$$

Substituting the above three equations into (15),

$$\begin{aligned} \delta_t U_{i,j}^{n+1/2} &= \varepsilon^2 V_{i,j}^{n+1/2} + \varepsilon^2 W_{i,j}^{n+1/2} - f_{i,j}^{n+1/2} \\ &\quad + \frac{\tau^2}{24} \cdot \frac{\partial^3 u}{\partial t^3}\left(x_i, y_j, t_{n+1/2}\right) \\ &\quad - \frac{\varepsilon^2 \tau^2}{8}\left[\frac{\partial^2 v}{\partial t^2}\left(x_i, y_j, t_{n+1/2}\right) + \frac{\partial^2 w}{\partial t^2}\left(x_i, y_j, t_{n+1/2}\right)\right] \\ &\quad + O\left(\tau^4\right). \end{aligned} \tag{17}$$

Denoted by

$$g(x, y, t) = \frac{1}{24} \cdot \frac{\partial^3 u}{\partial t^3}(x, y, t) - \frac{\varepsilon^2}{8}\left[\frac{\partial^2 v}{\partial t^2}(x, y, t) + \frac{\partial^2 w}{\partial t^2}(x, y, t)\right]. \tag{18}$$

Then,

$$\delta_t U_{i,j}^{n+1/2} = \varepsilon^2 V_{i,j}^{n+1/2} + \varepsilon^2 W_{i,j}^{n+1/2} - f_{i,j}^{n+1/2} + \tau^2 g_{i,j}^{n+1/2} + O\left(\tau^4\right). \tag{19}$$

Acting the operator $\mathscr{A}\mathscr{B}$ on both sides of the equation

above,

$$\mathscr{A}\mathscr{B}\delta_t U_{i,j}^{n+1/2} = \varepsilon^2 \mathscr{A}\mathscr{B} V_{i,j}^{n+1/2} + \varepsilon^2 \mathscr{A}\mathscr{B} W_{i,j}^{n+1/2} - \mathscr{A}\mathscr{B} f_{i,j}^{n+1/2} + \tau^2 \mathscr{A}\mathscr{B} g_{i,j}^{n+1/2} + O(\tau^4), \quad 1 \le i, j \le M-1, 0 \le n \le N-1. \tag{20}$$

Considering differential Equation (11) at the point (x_i, y_j, t_n),

$$v\left(x_i, y_j, t_n\right) = \frac{\partial^2 u}{\partial x^2}\left(x_i, y_j, t_n\right), \quad 0 \le i, j \le M, 0 \le n \le N. \tag{21}$$

Based on Lemma 3,

$$\mathscr{A} V_{i,j}^n = \delta_x^2 U_{i,j}^n + \frac{h^4}{240}\frac{\partial^6 u}{\partial x^6}\left(x_i, y_j, t_n\right) + O\left(h^6\right), \quad 1 \le i \le M-1, 0 \le j \le M, 0 \le n \le N. \tag{22}$$

Acting the two equations superscripted as n and $n+1$ and dividing by 2,

$$\begin{aligned}\mathscr{A} V_{i,j}^{n+1/2} &= \frac{1}{2}\left(\mathscr{A} V_{i,j}^n + \mathscr{A} V_{i,j}^{n+1}\right) = \frac{1}{2}\left(\delta_x^2 U_{i,j}^n + \delta_x^2 U_{i,j}^{n+1}\right) \\ &+ \frac{h^4}{240}\cdot\frac{1}{2}\left[\frac{\partial^6 u}{\partial x^6}\left(x_i, y_j, t_n\right) + \frac{\partial^6 u}{\partial x^6}\left(x_i, y_j, t_{n+1}\right)\right] \\ &+ O\left(h^6\right) = \delta_x^2 U_{i,j}^{n+1/2} + \frac{h^4}{240}\frac{\partial^6 u}{\partial x^6}\left(x_i, y_j, t_{n+1/2}\right) \\ &+ O\left(\tau^2 + \tau^2 h^4 + h^6\right), \quad 1 \le i \le M-1, 0 \le j \le M, 0 \le n \le N-1.\end{aligned} \tag{23}$$

Acting the operator $\mathscr{B}$ on both sides of the equation above,

$$\begin{aligned}\mathscr{A}\mathscr{B} V_{i,j}^{n+1/2} &= \mathscr{B}\delta_x^2 U_{i,j}^{n+1/2} + \frac{h^4}{240}\mathscr{B}\frac{\partial^6 u}{\partial x^6}\left(x_i, y_j, t_{n+1/2}\right) \\ &+ O\left(\tau^2 + \tau^2 h^4 + h^6\right), \quad 1 \le i, j \le M-1, 0 \le n \le N-1.\end{aligned} \tag{24}$$

Similarly, considering differential Equation (12) at the point (x_i, y_j, t_n), then

$$\begin{aligned}\mathscr{A}\mathscr{B} W_{i,j}^{n+1/2} &= \mathscr{A}\delta_y^2 U_{i,j}^{n+1/2} + \frac{h^4}{240}\mathscr{A}\frac{\partial^6 u}{\partial y^6}\left(x_i, y_j, t_{n+1/2}\right) \\ &+ O\left(\tau^2 + \tau^2 h^4 + h^6\right), \quad 1 \le i, j \le M-1, 0 \le n \le N-1.\end{aligned} \tag{25}$$

Substituting (24) and (25) into (20),

$$\begin{aligned}\mathscr{A}\mathscr{B}\delta_t U_{i,j}^{n+1/2} &= \varepsilon^2\left(\mathscr{B}\delta_x^2 U_{i,j}^{n+1/2} + \mathscr{A}\delta_y^2 U_{i,j}^{n+1/2}\right) - \mathscr{A}\mathscr{B} f_{i,j}^{n+1/2} \\ &+ \varepsilon^2\frac{h^4}{240}\left[\mathscr{B}\frac{\partial^6 u}{\partial x^6}\left(x_i, y_j, t_{n+1/2}\right) + \mathscr{A}\frac{\partial^6 u}{\partial y^6}\left(x_i, y_j, t_{n+1/2}\right)\right] \\ &+ \tau^2\mathscr{A}\mathscr{B} g_{i,j}^{n+1/2} + O\left(\tau^4 + \tau^2 h^4 + h^6\right), \quad 1 \le i, j \le M-1, 0 \le n \le N-1.\end{aligned} \tag{26}$$

Here,

$$\begin{aligned}R_{i,j}^{n+1/2} &= \varepsilon^2\frac{h^4}{240}\left[\mathscr{B}\frac{\partial^6 u}{\partial x^6}\left(x_i, y_j, t_{n+1/2}\right) + \mathscr{A}\frac{\partial^6 u}{\partial y^6}\left(x_i, y_j, t_{n+1/2}\right)\right] \\ &+ \tau^2\mathscr{A}\mathscr{B} g_{i,j}^{n+1/2} + O\left(\tau^4 + \tau^2 h^4 + h^6\right).\end{aligned} \tag{27}$$

Then,

$$\mathscr{A}\mathscr{B}\delta_t U_{i,j}^{n+1/2} = \varepsilon^2\left(\mathscr{B}\delta_x^2 U_{i,j}^{n+1/2} + \mathscr{A}\delta_y^2 U_{i,j}^{n+1/2}\right) - \mathscr{A}\mathscr{B} f_{i,j}^{n+1/2} + R_{i,j}^{n+1/2}, \quad 1 \le i, j \le M-1, 0 \le n \le N-1. \tag{28}$$

Omitting the small term $R_{i,j}^{n+1/2}$ and substituting the following equation into (28),

$$\begin{aligned}f\left(u\left(x_i, y_j, t_{n+1/2}\right)\right) &= \left(u_{i,j}^{n+1/2}\right)^3 - u_{i,j}^{n+1/2} \\ &= \frac{\left(u_{ij}^{n+1}\right)^3 + \left(u_{ij}^n\right)^3}{2} - \frac{u_{ij}^{n+1} + u_{ij}^n}{2}.\end{aligned} \tag{29}$$

Then, the two-dimensional Allen-Cahn Equation (7)

corresponding compact difference scheme is obtained.

$$\begin{aligned}&\mathscr{A}\mathscr{B}\frac{u_{ij}^{n+1}-u_{ij}^{n}}{\tau}+\mathscr{A}\mathscr{B}\left[\frac{\left(u_{ij}^{n+1}\right)^{3}+\left(u_{ij}^{n}\right)^{3}}{2}-\frac{u_{ij}^{n+1}+u_{ij}^{n}}{2}\right]\\&=\frac{\varepsilon^{2}}{2}\left(\mathscr{B}\delta_{x}^{2}u_{ij}^{n+1}+\mathscr{B}\delta_{x}^{2}u_{ij}^{n}+\mathscr{A}\delta_{y}^{2}u_{ij}^{n+1}+\mathscr{A}\delta_{y}^{2}u_{ij}^{n}\right),\quad 1\le i,j\\&\le M-1,0\le n\le N-1.\end{aligned}\tag{30}$$

Finally, the spatial derivative is discretized by the central finite difference scheme for the two-dimensional Allen-Cahn equation, the D_2 is expressed as the corresponding discrete matrix, and

$$D_2=BD_1+D_1A.\tag{31}$$

Here,

$$D_1=\frac{1}{h^2}\begin{pmatrix}-2&1&0&\cdots&0\\1&-2&1&\cdots&0\\0&1&-2&\cdots&0\\\vdots&\vdots&\vdots&&\vdots\\0&0&0&\cdots&-2\end{pmatrix}_{(M-1)\times(M-1)}.\tag{32}$$

Meanwhile, let $M-1$ be the number of nodes inside the interval after spatial dispersion and h be the space step.

$$B=A=\begin{pmatrix}\frac{10}{12}&\frac{1}{12}&0&\cdots&0\\\frac{1}{12}&\frac{10}{12}&\frac{1}{12}&\cdots&0\\0&\frac{1}{12}&\frac{10}{12}&\cdots&0\\\vdots&\vdots&\vdots&&\vdots\\0&0&0&\cdots&\frac{10}{12}\end{pmatrix}_{(M-1)\times(M-1)}.\tag{33}$$

Then, the discrete matrix D_2 satisfies the following properties:

(a) D_2 is symmetric.

(b) D_2 is semi-negative definite, such as

$$U^{T}D_{2}U\le 0.\tag{34}$$

(c) The elements in D_2 satisfy

$$d_{ii}<0,\quad -d_{ii}\ge\max_{1\le i\le M-1}\sum_{j=1,j\ne i}^{M-1}\left|d_{ij}\right|.\tag{35}$$

Let

$$C=AB.\tag{36}$$

Matrix C satisfies the following properties:

(a) C is symmetric.

(b) C is positive definite, such as

$$U^{T}CU>0.\tag{37}$$

(c) The elements in C satisfy

$$c_{ij}>0,\quad c_{ii}\ge\max_{1\le i\le M-1}\sum_{j=1,j\ne i}^{M-1}\left|c_{ij}\right|.\tag{38}$$

Substituting the matrix D_2 and C into (30), we get the compact difference scheme:

$$\begin{aligned}&C\frac{U^{n+1}-U^{n}}{\tau}+C\left[\frac{\left(U^{n+1}\right)^{3}-U^{n+1}}{2}+\frac{\left(U^{n}\right)^{3}-U^{n}}{2}\right]\\&=\frac{\varepsilon^{2}\left(D_{2}U^{n+1}+D_{2}U^{n}\right)}{2}.\end{aligned}\tag{39}$$

Here,

$$\begin{aligned}U^{n}&:=\left\{u_{ij}^{n}\middle|1\le i,j\le M-1\right\},\\\left(U^{n}\right)^{3}&:=\left\{\left(u_{ij}^{n}\right)^{3}\middle|1\le i,j\le M-1\right\}.\end{aligned}\tag{40}$$

Multiplying C^{-1} to both sides of the above equation,

$$\begin{aligned}&\frac{U^{n+1}-U^{n}}{\tau}+\left[\frac{\left(U^{n+1}\right)^{3}-U^{n+1}}{2}+\frac{\left(U^{n}\right)^{3}-U^{n}}{2}\right]\\&=\frac{\varepsilon^{2}}{2}C^{-1}D_{2}\left(U^{n+1}+U^{n}\right),\quad 0\le n\le N-1.\end{aligned}\tag{41}$$

Matrix $C^{-1}D_2$ satisfies the following properties:

(a) $C^{-1}D_2$ is symmetric.

(b) $C^{-1}D_2$ is negative definite, such as

$$U^T C^{-1} D_2 U \le 0. \tag{42}$$

3. Discrete Maximum Principle of Compact Difference Scheme for Two-Dimensional Allen-Cahn Equation

Theorem 4. *Assuming that the initial value of the Allen-Cahn problem satisfies* $\max_{(x,y)\epsilon\bar{\Omega}} |u_0(x,y)| \le 1$, *when the step ratio satisfies* $5/24 < \lambda < 5/12$ *and the time step satisfies* $0 < \tau \le \min\{(4/5)\lambda - 1/6, 1 - (12/5)\lambda\}$, *we have* $\|U^n\|_\infty \le 1$, *for* $\forall n \ge 1$.

Proof. Obviously, $\|U^0\|_\infty \le \|u_0\| \le 1$. Assuming that $\|U^n\|_\infty \le 1$, then $\|U^{n+1}\|_\infty \le 1$ needs to be proved. Expanding the established compact difference scheme,

$$\begin{aligned}
&\frac{1}{\tau}\Bigg[\Bigg(\frac{1}{144}u_{i-1,j-1}^{n+1} + \frac{10}{144}u_{i,j-1}^{n+1} + \frac{1}{144}u_{i+1,j-1}^{n+1} + \frac{10}{144}u_{i-1,j}^{n+1} \\
&\quad + \frac{100}{144}u_{i,j}^{n+1} + \frac{10}{144}u_{i+1,j}^{n+1} + \frac{1}{144}u_{i-1,j+1}^{n+1} + \frac{10}{144}u_{i,j+1}^{n+1} + \frac{1}{144}u_{i+1,j+1}^{n+1}\Bigg) \\
&\quad - \Bigg(\frac{1}{144}u_{i-1,j-1}^{n} + \frac{10}{144}u_{i,j-1}^{n} + \frac{1}{144}u_{i+1,j-1}^{n} + \frac{10}{144}u_{i-1,j}^{n} + \frac{100}{144}u_{i,j}^{n} \\
&\quad + \frac{10}{144}u_{i+1,j}^{n} + \frac{1}{144}u_{i-1,j+1}^{n} + \frac{10}{144}u_{i,j+1}^{n} + \frac{1}{144}u_{i+1,j+1}^{n}\Bigg)\Bigg] \\
&\quad + \frac{1}{2}\Bigg[\Bigg(\frac{1}{144}\left(u_{i-1,j-1}^{n+1}\right)^3 + \frac{10}{144}\left(u_{i,j-1}^{n+1}\right)^3 + \frac{1}{144}\left(u_{i+1,j-1}^{n+1}\right)^3 \\
&\quad + \frac{10}{144}\left(u_{i-1,j}^{n+1}\right)^3 + \frac{100}{144}\left(u_{i,j}^{n+1}\right)^3 + \frac{10}{144}\left(u_{i+1,j}^{n+1}\right)^3 + \frac{1}{144}\left(u_{i-1,j+1}^{n+1}\right)^3 \\
&\quad + \frac{10}{144}\left(u_{i,j+1}^{n+1}\right)^3 + \frac{1}{144}\left(u_{i+1,j+1}^{n+1}\right)^3\Bigg) + \Bigg(\frac{1}{144}\left(u_{i-1,j-1}^{n}\right)^3 \\
&\quad + \frac{10}{144}\left(u_{i,j-1}^{n}\right)^3 + \frac{1}{144}\left(u_{i+1,j-1}^{n}\right)^3 + \frac{10}{144}\left(u_{i-1,j}^{n}\right)^3 + \frac{100}{144}\left(u_{i,j}^{n}\right)^3 \\
&\quad + \frac{10}{144}\left(u_{i+1,j}^{n}\right)^3 + \frac{1}{144}\left(u_{i-1,j+1}^{n}\right)^3 + \frac{10}{144}\left(u_{i,j+1}^{n}\right)^3 \\
&\quad + \frac{1}{144}\left(u_{i+1,j+1}^{n}\right)^3\Bigg)\Bigg] - \frac{1}{2}\Bigg[\Bigg(\frac{1}{144}u_{i-1,j-1}^{n+1} + \frac{10}{144}u_{i,j-1}^{n+1} + \frac{1}{144}u_{i+1,j-1}^{n+1} \\
&\quad + \frac{10}{144}u_{i-1,j}^{n+1} + \frac{100}{144}u_{i,j}^{n+1} + \frac{10}{144}u_{i+1,j}^{n+1} + \frac{1}{144}u_{i-1,j+1}^{n+1} + \frac{10}{144}u_{i,j+1}^{n+1} \\
&\quad + \frac{1}{144}u_{i+1,j+1}^{n+1}\Bigg) + \Bigg(\frac{1}{144}u_{i-1,j-1}^{n} + \frac{10}{144}u_{i,j-1}^{n} + \frac{1}{144}u_{i+1,j-1}^{n} \\
&\quad + \frac{10}{144}u_{i-1,j}^{n} + \frac{100}{144}u_{i,j}^{n} + \frac{10}{144}u_{i+1,j}^{n} + \frac{1}{144}u_{i-1,j+1}^{n} + \frac{10}{144}u_{i,j+1}^{n} \\
&\quad + \frac{1}{144}u_{i+1,j+1}^{n}\Bigg)\Bigg] = \frac{\varepsilon^2}{2}\frac{1}{h^2}\Bigg[\Bigg(\frac{2}{12}u_{i-1,j-1}^{n+1} + \frac{8}{12}u_{i,j-1}^{n+1} + \frac{2}{12}u_{i+1,j-1}^{n+1} \\
&\quad + \frac{8}{12}u_{i-1,j}^{n+1} - \frac{40}{12}u_{i,j}^{n+1} + \frac{8}{12}u_{i+1,j}^{n+1} + \frac{2}{12}u_{i-1,j+1}^{n+1} + \frac{8}{12}u_{i,j+1}^{n+1} + \frac{2}{12}u_{i+1,j+1}^{n+1}\Bigg) \\
&\quad + \Bigg(\frac{2}{12}u_{i-1,j-1}^{n} + \frac{8}{12}u_{i,j-1}^{n} + \frac{2}{12}u_{i+1,j-1}^{n} + \frac{8}{12}u_{i-1,j}^{n} - \frac{40}{12}u_{i,j}^{n} + \frac{8}{12}u_{i+1,j}^{n} \\
&\quad + \frac{2}{12}u_{i-1,j+1}^{n} + \frac{8}{12}u_{i,j+1}^{n} + \frac{2}{12}u_{i+1,j+1}^{n}\Bigg)\Bigg].
\end{aligned} \tag{43}$$

Multiplying τ to both sides of the above equation and letting $\lambda = \varepsilon^2(\tau/h^2)$,

$$\begin{aligned}
&\left[\frac{100}{144}\left(1 - \frac{\tau}{2}\right) + \frac{5}{3}\lambda\right]u_{i,j}^{n+1} + \frac{100}{144}\frac{\tau}{2}\left(u_{i,j}^{n+1}\right)^3 \\
&\quad + \left[\frac{10}{144}\left(1 - \frac{\tau}{2}\right) - \frac{1}{3}\lambda\right]u_{i-1,j}^{n+1} + \frac{10}{144}\frac{\tau}{2}\left(u_{i-1,j}^{n+1}\right)^3 \\
&\quad + \left[\frac{10}{144}\left(1 - \frac{\tau}{2}\right) - \frac{1}{3}\lambda\right]u_{i+1,j}^{n+1} + \frac{10}{144}\frac{\tau}{2}\left(u_{i+1,j}^{n+1}\right)^3 \\
&\quad + \left[\frac{10}{144}\left(1 - \frac{\tau}{2}\right) - \frac{1}{3}\lambda\right]u_{i,j-1}^{n+1} + \frac{10}{144}\frac{\tau}{2}\left(u_{i,j-1}^{n+1}\right)^3 \\
&\quad + \left[\frac{10}{144}\left(1 - \frac{\tau}{2}\right) - \frac{1}{3}\lambda\right]u_{i,j+1}^{n+1} + \frac{10}{144}\frac{\tau}{2}\left(u_{i,j+1}^{n+1}\right)^3 \\
&\quad + \left[\frac{1}{144}\left(1 - \frac{\tau}{2}\right) - \frac{1}{12}\lambda\right]u_{i-1,j-1}^{n+1} + \frac{1}{144}\frac{\tau}{2}\left(u_{i-1,j-1}^{n+1}\right)^3 \\
&\quad + \left[\frac{1}{144}\left(1 - \frac{\tau}{2}\right) - \frac{1}{12}\lambda\right]u_{i+1,j-1}^{n+1} + \frac{1}{144}\frac{\tau}{2}\left(u_{i+1,j-1}^{n+1}\right)^3 \\
&\quad + \left[\frac{1}{144}\left(1 - \frac{\tau}{2}\right) - \frac{1}{12}\lambda\right]u_{i-1,j+1}^{n+1} + \frac{1}{144}\frac{\tau}{2}\left(u_{i-1,j+1}^{n+1}\right)^3 \\
&\quad + \left[\frac{1}{144}\left(1 - \frac{\tau}{2}\right) - \frac{1}{12}\lambda\right]u_{i+1,j+1}^{n+1} + \frac{1}{144}\frac{\tau}{2}\left(u_{i+1,j+1}^{n+1}\right)^3 \\
&\quad = \left[\frac{100}{144}\left(1 + \frac{\tau}{2}\right) - \frac{5}{3}\lambda\right]u_{i,j}^{n} - \frac{100}{144}\frac{\tau}{2}\left(u_{i,j}^{n}\right)^3 \\
&\quad + \left[\frac{10}{144}\left(1 + \frac{\tau}{2}\right) + \frac{1}{3}\lambda\right]u_{i-1,j}^{n} - \frac{10}{144}\frac{\tau}{2}\left(u_{i-1,j}^{n}\right)^3 \\
&\quad + \left[\frac{10}{144}\left(1 + \frac{\tau}{2}\right) + \frac{1}{3}\lambda\right]u_{i+1,j}^{n} - \frac{10}{144}\frac{\tau}{2}\left(u_{i+1,j}^{n}\right)^3 \\
&\quad + \left[\frac{10}{144}\left(1 + \frac{\tau}{2}\right) + \frac{1}{3}\lambda\right]u_{i,j-1}^{n} - \frac{10}{144}\frac{\tau}{2}\left(u_{i,j-1}^{n}\right)^3 \\
&\quad + \left[\frac{10}{144}\left(1 + \frac{\tau}{2}\right) + \frac{1}{3}\lambda\right]u_{i,j+1}^{n} - \frac{10}{144}\frac{\tau}{2}\left(u_{i,j+1}^{n}\right)^3 \\
&\quad + \left[\frac{1}{144}\left(1 + \frac{\tau}{2}\right) + \frac{1}{12}\lambda\right]u_{i-1,j-1}^{n} - \frac{1}{144}\frac{\tau}{2}\left(u_{i-1,j-1}^{n}\right)^3 \\
&\quad + \left[\frac{1}{144}\left(1 + \frac{\tau}{2}\right) + \frac{1}{12}\lambda\right]u_{i+1,j-1}^{n} - \frac{1}{144}\frac{\tau}{2}\left(u_{i+1,j-1}^{n}\right)^3 \\
&\quad + \left[\frac{1}{144}\left(1 + \frac{\tau}{2}\right) + \frac{1}{12}\lambda\right]u_{i-1,j+1}^{n} - \frac{1}{144}\frac{\tau}{2}\left(u_{i-1,j+1}^{n}\right)^3 \\
&\quad + \left[\frac{1}{144}\left(1 + \frac{\tau}{2}\right) + \frac{1}{12}\lambda\right]u_{i+1,j+1}^{n} - \frac{1}{144}\frac{\tau}{2}\left(u_{i+1,j+1}^{n}\right)^3.
\end{aligned} \tag{44}$$

Shifting terms on both sides of the equation,

$$\begin{aligned}
&\left[\frac{100}{144}\left(1-\frac{\tau}{2}\right)+\frac{5}{3}\lambda\right]u_{i,j}^{n+1}+\frac{100}{144}\frac{\tau}{2}\left(u_{i,j}^{n+1}\right)^3\\
&=\left[\frac{1}{3}\lambda-\frac{10}{144}\left(1-\frac{\tau}{2}\right)\right]u_{i-1,j}^{n+1}-\frac{10}{144}\frac{\tau}{2}\left(u_{i-1,j}^{n+1}\right)^3\\
&\quad+\left[\frac{1}{3}\lambda-\frac{10}{144}\left(1-\frac{\tau}{2}\right)\right]u_{i+1,j}^{n+1}-\frac{10}{144}\frac{\tau}{2}\left(u_{i+1,j}^{n+1}\right)^3\\
&\quad+\left[\frac{1}{3}\lambda-\frac{10}{144}\left(1-\frac{\tau}{2}\right)\right]u_{i,j-1}^{n+1}-\frac{10}{144}\frac{\tau}{2}\left(u_{i,j-1}^{n+1}\right)^3\\
&\quad+\left[\frac{1}{3}\lambda-\frac{10}{144}\left(1-\frac{\tau}{2}\right)\right]u_{i,j+1}^{n+1}-\frac{10}{144}\frac{\tau}{2}\left(u_{i,j+1}^{n+1}\right)^3\\
&\quad+\left[\frac{1}{12}\lambda-\frac{1}{144}\left(1-\frac{\tau}{2}\right)\right]u_{i-1,j-1}^{n+1}-\frac{1}{144}\frac{\tau}{2}\left(u_{i-1,j-1}^{n+1}\right)^3\\
&\quad+\left[\frac{1}{12}\lambda-\frac{1}{144}\left(1-\frac{\tau}{2}\right)\right]u_{i+1,j-1}^{n+1}-\frac{1}{144}\frac{\tau}{2}\left(u_{i+1,j-1}^{n+1}\right)^3\\
&\quad+\left[\frac{1}{12}\lambda-\frac{1}{144}\left(1-\frac{\tau}{2}\right)\right]u_{i-1,j+1}^{n+1}-\frac{1}{144}\frac{\tau}{2}\left(u_{i-1,j+1}^{n+1}\right)^3\\
&\quad+\left[\frac{1}{12}\lambda-\frac{1}{144}\left(1-\frac{\tau}{2}\right)\right]u_{i+1,j+1}^{n+1}-\frac{1}{144}\frac{\tau}{2}\left(u_{i+1,j+1}^{n+1}\right)^3\\
&\quad+\left[\frac{100}{144}\left(1+\frac{\tau}{2}\right)-\frac{5}{3}\lambda\right]u_{i,j}^{n}-\frac{100}{144}\frac{\tau}{2}\left(u_{i,j}^{n}\right)^3\\
&\quad+\left[\frac{10}{144}\left(1+\frac{\tau}{2}\right)+\frac{1}{3}\lambda\right]u_{i-1,j}^{n}-\frac{10}{144}\frac{\tau}{2}\left(u_{i-1,j}^{n}\right)^3\\
&\quad+\left[\frac{10}{144}\left(1+\frac{\tau}{2}\right)+\frac{1}{3}\lambda\right]u_{i+1,j}^{n}-\frac{10}{144}\frac{\tau}{2}\left(u_{i+1,j}^{n}\right)^3\\
&\quad+\left[\frac{10}{144}\left(1+\frac{\tau}{2}\right)+\frac{1}{3}\lambda\right]u_{i,j-1}^{n}-\frac{10}{144}\frac{\tau}{2}\left(u_{i,j-1}^{n}\right)^3\\
&\quad+\left[\frac{10}{144}\left(1+\frac{\tau}{2}\right)+\frac{1}{3}\lambda\right]u_{i,j+1}^{n}-\frac{10}{144}\frac{\tau}{2}\left(u_{i,j+1}^{n}\right)^3\\
&\quad+\left[\frac{1}{144}\left(1+\frac{\tau}{2}\right)+\frac{1}{12}\lambda\right]u_{i-1,j-1}^{n}-\frac{1}{144}\frac{\tau}{2}\left(u_{i-1,j-1}^{n}\right)^3\\
&\quad+\left[\frac{1}{144}\left(1+\frac{\tau}{2}\right)+\frac{1}{12}\lambda\right]u_{i+1,j-1}^{n}-\frac{1}{144}\frac{\tau}{2}\left(u_{i+1,j-1}^{n}\right)^3\\
&\quad+\left[\frac{1}{144}\left(1+\frac{\tau}{2}\right)+\frac{1}{12}\lambda\right]u_{i-1,j+1}^{n}-\frac{1}{144}\frac{\tau}{2}\left(u_{i-1,j+1}^{n}\right)^3\\
&\quad+\left[\frac{1}{144}\left(1+\frac{\tau}{2}\right)+\frac{1}{12}\lambda\right]u_{i+1,j+1}^{n}-\frac{1}{144}\frac{\tau}{2}\left(u_{i+1,j+1}^{n}\right)^3.
\end{aligned}\tag{45}$$

For the right side of Equation (45), the n-layer terms are processed firstly.

Then, the sum of the n-layer terms is L. Let $\|U^n\|_\infty \le 1$.

$$f(x)=\left[\frac{100}{144}\left(1+\frac{\tau}{2}\right)-\frac{5}{3}\lambda\right]x-\frac{100}{144}\frac{\tau}{2}x^3,\quad x\in[0,1].\tag{46}$$

Thus,

$$f(0)=0,\quad f(1)=\frac{25}{36}-\frac{5}{3}\lambda=\frac{5}{3}\left(\frac{5}{12}-\lambda\right).\tag{47}$$

Since

$$\begin{aligned}
f'(x)&=\frac{25}{36}\left(1+\frac{\tau}{2}\right)-\frac{5}{3}\lambda-\frac{25\tau}{24}x^2,\\
f''(x)&=-\frac{25\tau}{12}x\le 0.
\end{aligned}\tag{48}$$

$f'(x)$ is monotonicity decreasing,

$$\begin{aligned}
f'(0)&=\frac{25}{36}\left(1+\frac{\tau}{2}\right)-\frac{5}{3}\lambda,\\
f'(1)&=\frac{25}{36}\left(1+\frac{\tau}{2}\right)-\frac{5}{3}\lambda-\frac{25\tau}{24}.
\end{aligned}\tag{49}$$

When $\tau\le 1-(12/5)\lambda$, $f'(1)\ge 0$, therefore, $f'(x)\ge 0$.

Thus, $f(x)$ is monotonicity increasing. $\forall x\in[0,1]$, $f(0)\le f(x)\le f(1)$, namely,

$$f(x)\le\frac{25}{36}-\frac{5}{3}\lambda,\quad \lambda\le\frac{5}{12}.\tag{50}$$

Let

$$g(x)=\left[\frac{10}{144}\left(1+\frac{\tau}{2}\right)+\frac{1}{3}\lambda\right]x-\frac{10}{144}\frac{\tau}{2}x^3,\quad x\in[0,1].\tag{51}$$

Then,

$$g(0)=0,\quad g(1)=\frac{5}{72}+\frac{1}{3}\lambda.\tag{52}$$

Since

$$\begin{aligned}
g'(x)&=\frac{5}{72}\left(1+\frac{\tau}{2}\right)+\frac{1}{3}\lambda-\frac{5\tau}{48}x^2,\\
g''(x)&=-\frac{5\tau}{24}x\le 0.
\end{aligned}\tag{53}$$

$g'(x)$ is monotonicity decreasing,

$$\begin{aligned}
g'(0)&=\frac{5}{72}\left(1+\frac{\tau}{2}\right)+\frac{1}{3}\lambda,\\
g'(1)&=\frac{5}{72}\left(1+\frac{\tau}{2}\right)+\frac{1}{3}\lambda-\frac{5\tau}{48}.
\end{aligned}\tag{54}$$

When $\tau\le 1+(24/5)\lambda$, $g'(1)\ge 0$, we have $g'(x)\ge 0$.

Thus, $g(x)$ is monotonicity increasing. $\forall x\in[0,1]$, then $g(0)\le g(x)\le g(1)$, namely,

$$g(x)\le\frac{5}{72}+\frac{1}{3}\lambda.\tag{55}$$

Let

$$h(x)=\left[\frac{1}{144}\left(1+\frac{\tau}{2}\right)+\frac{1}{12}\lambda\right]x-\frac{1}{144}\frac{\tau}{2}x^3,\quad x\in[0,1]. \tag{56}$$

Then,

$$h(0)=0,\quad h(1)=\frac{1}{144}+\frac{1}{12}\lambda. \tag{57}$$

Since

$$\begin{aligned}h'(x)&=\frac{1}{144}\left(1+\frac{\tau}{2}\right)+\frac{1}{12}\lambda-\frac{\tau}{96}x^2,\\ h''(x)&=-\frac{\tau}{48}x\le 0.\end{aligned} \tag{58}$$

$h'(x)$ is monotonicity decreasing,

$$\begin{aligned}h'(0)&=\frac{1}{144}\left(1+\frac{\tau}{2}\right)+\frac{1}{12}\lambda,\\ h'(1)&=\frac{1}{144}\left(1+\frac{\tau}{2}\right)+\frac{1}{12}\lambda-\frac{\tau}{96}.\end{aligned} \tag{59}$$

When $\tau\le 1+12\lambda$, $h'(1)\ge 0$, we have $h'(x)\ge 0$.

Thus, $h(x)$ is monotonicity increasing. $\forall x\in[0,1]$, $h(0)\le h(x)\le h(1)$, that is,

$$h(x)\le\frac{1}{144}+\frac{1}{12}\lambda. \tag{60}$$

According to (50), (55), and (60), when $\tau\le 1-(12/5)\lambda$,

$$\begin{aligned}f(x)&\le\frac{25}{36}-\frac{5}{3}\lambda,\quad \lambda\le\frac{5}{12},\\ g(x)&\le\frac{5}{72}+\frac{1}{3}\lambda,\\ h(x)&\le\frac{1}{144}+\frac{1}{12}\lambda.\end{aligned} \tag{61}$$

Then,

$$L\le f(1)+4g(1)+4h(1)=1. \tag{62}$$

Next, the eight items in the $n+1$ layer on the right side of equation (45) are dealt.

Let

$$p(y)=\left[\frac{\lambda}{3}-\frac{10}{144}\left(1-\frac{\tau}{2}\right)\right]y-\frac{10}{144}\frac{\tau}{2}y^3. \tag{63}$$

Then,

$$p'(y)=\frac{\lambda}{3}-\frac{10}{144}\left(1-\frac{\tau}{2}\right)-\frac{5\tau}{48}y^2. \tag{64}$$

When $p'(y)=0$, the maximum point is obtained,

$$y_1=\sqrt{\frac{48}{5\tau}}\cdot\sqrt{\frac{1}{3}\left(\lambda-\frac{5}{24}\right)+\frac{5\tau}{144}},\quad \lambda\ge\frac{5}{24}. \tag{65}$$

Since $p(y)$ is an odd function and monotonicity increasing in the interval of $(-y_1,y_1)$, then $|p(y)|\le|p(y_1)|$.

Let

$$q(y)=\left[\frac{\lambda}{12}-\frac{1}{144}\left(1-\frac{\tau}{2}\right)\right]y-\frac{1}{144}\frac{\tau}{2}y^3. \tag{66}$$

Then,

$$q'(y)=\frac{\lambda}{12}-\frac{1}{144}\left(1-\frac{\tau}{2}\right)-\frac{\tau}{96}y^2. \tag{67}$$

When $q'(y)=0$, the maximum point is obtained,

$$y_2=\sqrt{\frac{96}{\tau}}\cdot\sqrt{\frac{1}{12}\left(\lambda-\frac{1}{12}\right)+\frac{\tau}{288}},\quad \lambda\ge\frac{1}{12}. \tag{68}$$

Since $q(y)$ is an odd function and monotonicity increasing in the interval of $(-y_2,y_2)$, then $|q(y)|\le|q(y_2)|$.

Substituting (62), (63), and (66) into (45), then

$$\begin{aligned}&\left[\frac{100}{144}\left(1-\frac{\tau}{2}\right)+\frac{5}{3}\lambda\right]u_{ij}^{n+1}+\frac{100}{144}\frac{\tau}{2}\left(u_{ij}^{n+1}\right)^3\\ &\quad\le p\left(u_{i-1,j}^{n+1}\right)+p\left(u_{i+1,j}^{n+1}\right)+p\left(u_{i,j-1}^{n+1}\right)+p\left(u_{i,j+1}^{n+1}\right)\\ &\qquad+q\left(u_{i-1,j-1}^{n+1}\right)+q\left(u_{i+1,j-1}^{n+1}\right)+q\left(u_{i-1,j+1}^{n+1}\right)\\ &\qquad+q\left(u_{i+1,j+1}^{n+1}\right)+1,\quad 1\le i,j\le N-1.\end{aligned} \tag{69}$$

Suppose $\|U^{n+1}\|_\infty=|U_{i_0,j_0}^{n+1}|=m$.

On the one hand, for the right eight terms of Equation (69), taking the absolute value of both sides of the equation by definition (63), according to the triangle inequality,

$$\begin{aligned}\left|p\left(u_{i-1,j}^{n+1}\right)\right|&=\left|\left[\frac{\lambda}{3}-\frac{10}{144}\left(1-\frac{\tau}{2}\right)\right]u_{i-1,j}^{n+1}-\frac{5\tau}{144}\left(u_{i-1,j}^{n+1}\right)^3\right|\\ &\le\left[\frac{\lambda}{3}-\frac{5}{72}\left(1-\frac{\tau}{2}\right)\right]\left|u_{i-1,j}^{n+1}\right|+\frac{5\tau}{144}\left|u_{i-1,j}^{n+1}\right|^3\\ &\le\left[\frac{\lambda}{3}-\frac{5}{72}\left(1-\frac{\tau}{2}\right)\right]m+\frac{5\tau}{144}m^3.\end{aligned} \tag{70}$$

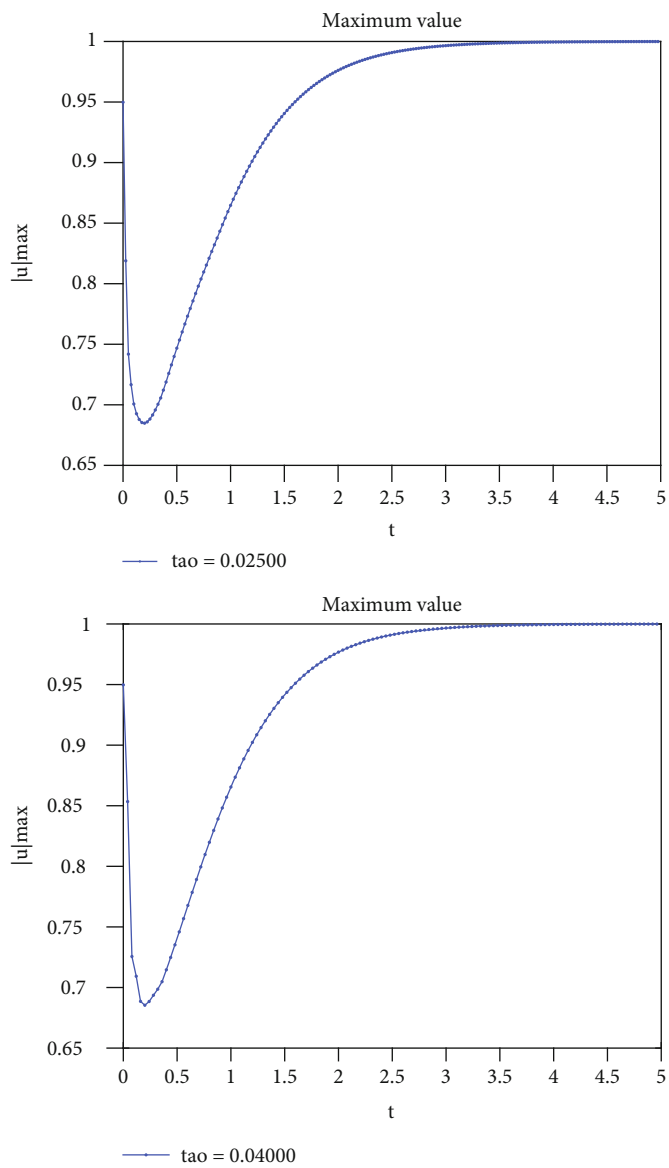

FIGURE 1: When $\tau = 0.025, 0.04$, the maximum of the scheme is (30).

Similarly,

$$\begin{aligned}
\left|p\left(u_{i+1,j}^{n+1}\right)\right| &\le \left[\frac{\lambda}{3} - \frac{5}{72}\left(1-\frac{\tau}{2}\right)\right]m + \frac{5\tau}{144}m^3,\\
\left|p\left(u_{i,j-1}^{n+1}\right)\right| &\le \left[\frac{\lambda}{3} - \frac{5}{72}\left(1-\frac{\tau}{2}\right)\right]m + \frac{5\tau}{144}m^3,\\
\left|p\left(u_{i,j+1}^{n+1}\right)\right| &\le \left[\frac{\lambda}{3} - \frac{5}{72}\left(1-\frac{\tau}{2}\right)\right]m + \frac{5\tau}{144}m^3.
\end{aligned} \tag{71}$$

Taking the absolute value of both sides of the equation by definition (66), according to the triangle inequality,

$$\begin{aligned}
\left|q\left(u_{i-1,j-1}^{n+1}\right)\right| &= \left|\left[\frac{\lambda}{12} - \frac{1}{144}\left(1-\frac{\tau}{2}\right)\right]u_{i-1,j-1}^{n+1} - \frac{\tau}{288}\left(u_{i-1,j-1}^{n+1}\right)^3\right|\\
&\le \left[\frac{\lambda}{12} - \frac{1}{144}\left(1-\frac{\tau}{2}\right)\right]\left|u_{i-1,j-1}^{n+1}\right| + \frac{\tau}{288}\left|u_{i-1,j-1}^{n+1}\right|^3\\
&\le \left[\frac{\lambda}{12} - \frac{1}{144}\left(1-\frac{\tau}{2}\right)\right]m + \frac{\tau}{288}m^3.
\end{aligned} \tag{72}$$

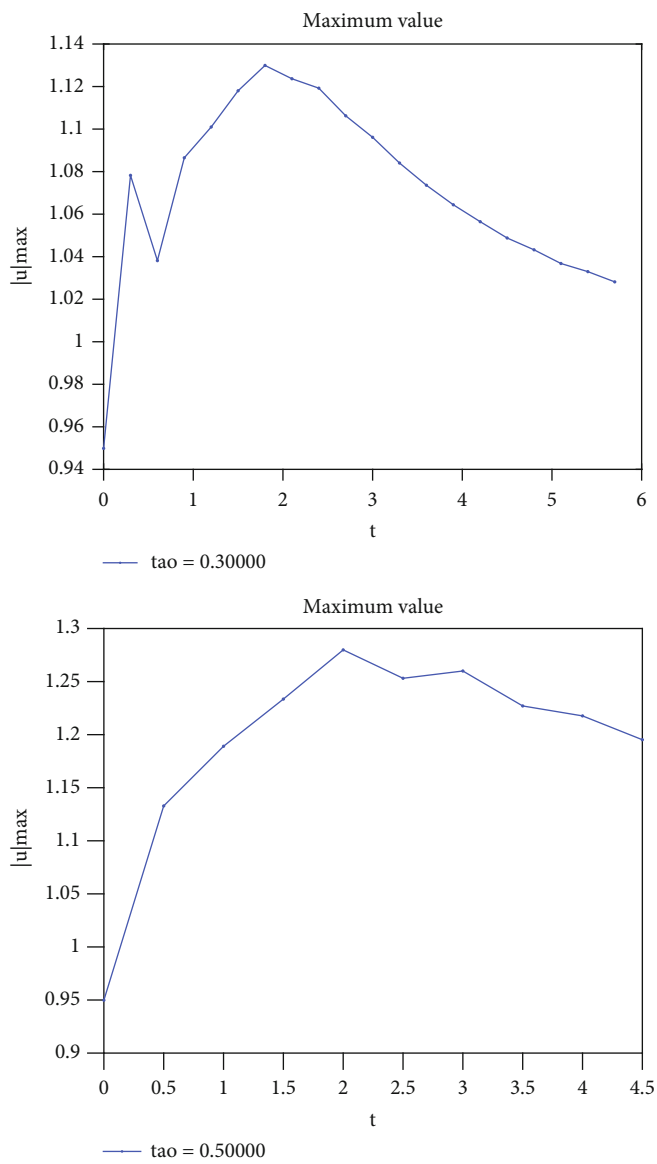

FIGURE 2: When $\tau = 0.3, 0.5$, the maximum of the scheme is (30).

Similarly,

$$\begin{aligned}
\left|q\left(u_{i+1,j-1}^{n+1}\right)\right| &\le \left[\frac{\lambda}{12} - \frac{1}{144}\left(1-\frac{\tau}{2}\right)\right]m + \frac{\tau}{288}m^3,\\
\left|q\left(u_{i-1,j+1}^{n+1}\right)\right| &\le \left[\frac{\lambda}{12} - \frac{1}{144}\left(1-\frac{\tau}{2}\right)\right]m + \frac{\tau}{288}m^3,\\
\left|q\left(u_{i+1,j+1}^{n+1}\right)\right| &\le \left[\frac{\lambda}{12} - \frac{1}{144}\left(1-\frac{\tau}{2}\right)\right]m + \frac{\tau}{288}m^3.
\end{aligned} \tag{73}$$

Taking $i = i_0, j = j_0$ for the left side of (69), substituting (70) and (72) into the right side of (69),

$$\begin{aligned}
&\left[\frac{100}{144}\left(1-\frac{\tau}{2}\right) + \frac{5}{3}\lambda\right]m + \frac{100}{144}\frac{\tau}{2}m^3\\
&\quad \le 4\left\{\left[\frac{\lambda}{3} - \frac{5}{72}\left(1-\frac{\tau}{2}\right)\right]m + \frac{5\tau}{144}m^3\right\}\\
&\qquad + 4\left\{\left[\frac{\lambda}{12} - \frac{1}{144}\left(1-\frac{\tau}{2}\right)\right]m + \frac{\tau}{288}m^3\right\} + 1,
\end{aligned} \tag{74}$$

namely,

$$\left(1-\frac{\tau}{2}\right)m + \frac{7\tau}{36}m^3 \le 1. \tag{75}$$

When $\tau \le 1$, then $M \le 1/(1-\tau/2) \le 2$, $|u_{i_0,j_0}^{n+1}| \in (0,2)$.

Let $y_0 = (-y_1, y_1) \cap (-y_2, y_2)$, suppose $y_0 = 2$, then $p(y)$ and $q(y)$ are monotonicity increasing in the interval of $(-2,2)$. For

$$p'(y) = \frac{\lambda}{3} - \frac{10}{144}\left(1-\frac{\tau}{2}\right) - \frac{5\tau}{48}y^2 \ge 0, \tag{76}$$

then

$$\frac{5\tau}{48}y^2 \le \frac{\lambda}{3} - \frac{10}{144}\left(1-\frac{\tau}{2}\right) = \frac{1}{3}\left(\lambda - \frac{5}{24}\right) + \frac{5\tau}{144}. \tag{77}$$

Since $y \in (-2,2)$, then

$$\frac{5\tau}{12} \le \frac{1}{3}\left(\lambda - \frac{5}{24}\right). \tag{78}$$

So,

$$\tau \le \frac{4}{5}\lambda - \frac{1}{6}. \tag{79}$$

Similarly, for

$$q'(y) = \frac{\lambda}{12} - \frac{1}{144}\left(1-\frac{\tau}{2}\right) - \frac{\tau}{96}y^2 \ge 0, \tag{80}$$

then

$$\frac{\tau}{96}y^2 \le \frac{\lambda}{12} - \frac{1}{144}\left(1-\frac{\tau}{2}\right) = \frac{1}{12}\left(\lambda - \frac{1}{12}\right) + \frac{\tau}{288}. \tag{81}$$

Since $y \in (-2,2)$, then

$$\frac{\tau}{24} \le \frac{1}{12}\left(\lambda - \frac{1}{12}\right). \tag{82}$$

That means that

$$\tau \le 2\lambda - \frac{1}{6}. \tag{83}$$

In conclusion, according to (65), (68), (79), and (83), we obtain $\tau \le (4/5)\lambda - 1/6$ $(\lambda \ge 5/24)$.

On the other hand, taking $i = i_0, j = j_0$ in (69), thus

$$\begin{aligned}&\left[\frac{100}{144}\left(1-\frac{\tau}{2}\right) + \frac{5}{3}\lambda\right]\left|u_{i_0,j_0}^{n+1}\right| + \frac{50\tau}{144}\left(\left|u_{i_0,j_0}^{n+1}\right|\right)^3,\\ &\le 4p\left(\left|u_{i_0,j_0}^{n+1}\right|\right) + 4q\left(\left|u_{i_0,j_0}^{n+1}\right|\right) + 1.\end{aligned} \tag{84}$$

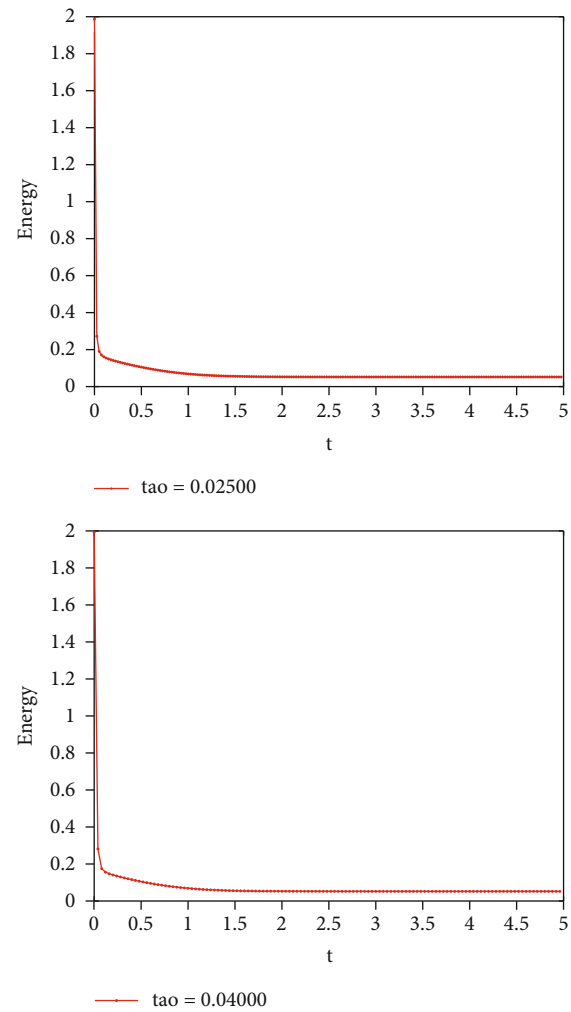

Figure 3: When $\tau = 0.025, 0.04$, the energy of the scheme is (30).

According to (63) and (66),

$$\begin{aligned}&\left[\frac{25}{36}\left(1-\frac{\tau}{2}\right) + \frac{5}{3}\lambda\right]m + \frac{25\tau}{72}m^3,\\ &\le \left[\frac{5}{3}\lambda - \frac{11}{36}\left(1-\frac{\tau}{2}\right)\right]m - \frac{11\tau}{72}m^3 + 1,\end{aligned} \tag{85}$$

namely,

$$\left(1-\frac{\tau}{2}\right)m + \frac{\tau}{2}m^3 \le 1. \tag{86}$$

$m \le 1$ is obtained.

Consequently, when $0 < \tau \le \min\{(4/5)\lambda - 1/6, 1 - (12/5)\lambda\}$, $5/24 < \lambda < 5/12$, then $\|U^{n+1}\|_\infty \le 1$.□ □

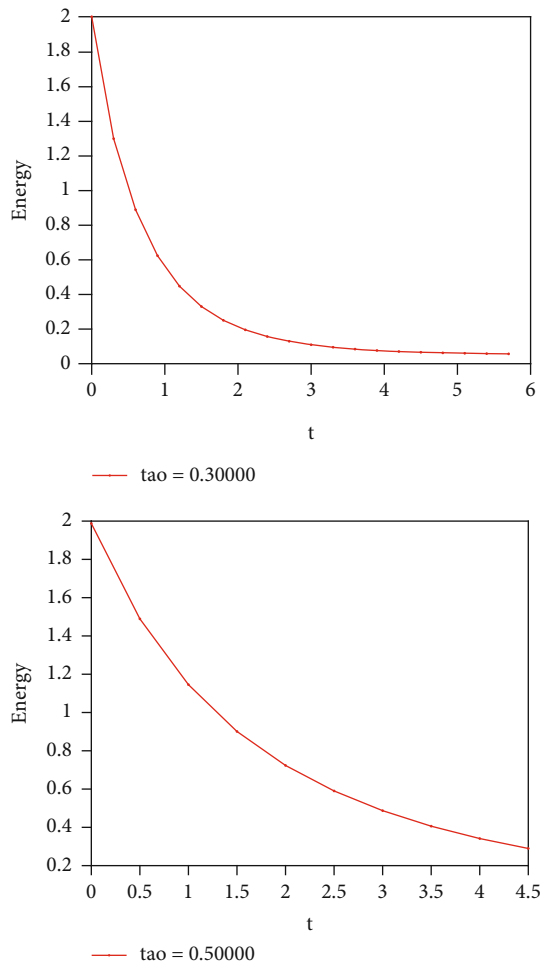

FIGURE 4: When $\tau = 0.3, 0.5$, the energy of the scheme is (30).

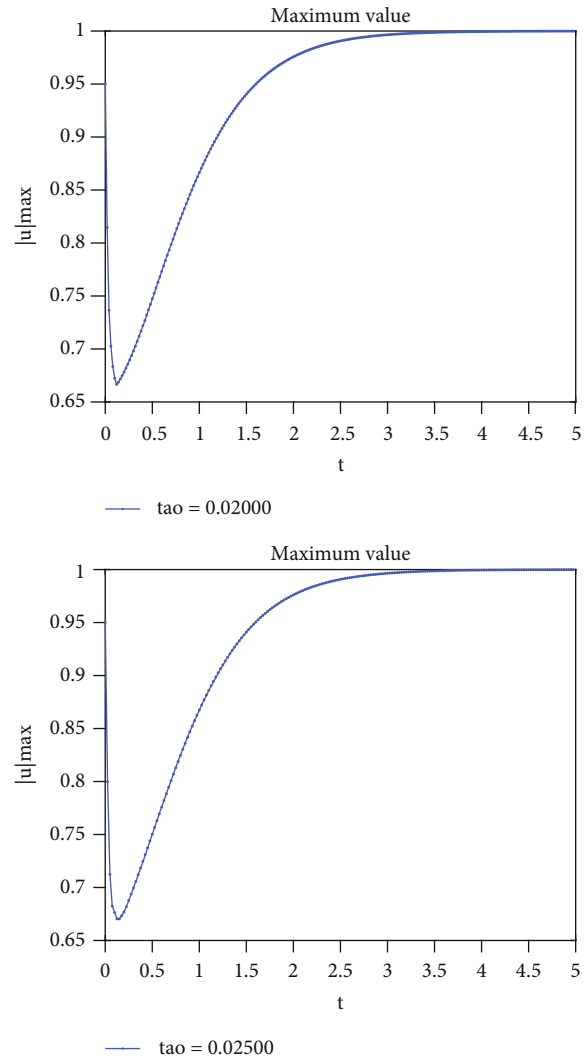

FIGURE 5: When $\tau = 0.02, 0.025$, the maximum of the scheme is (30).

4. Two-Dimensional Discrete Energy Stability

Lemma 5 (see [2]). $\forall a, b \in [-1, 1]$,

$$\begin{aligned}(a^3 - a)(a - b) + (a - b)^2 &\geq \frac{1}{4}\left[(a^2 - 1)^2 - (b^2 - 1)^2\right],\\ (a^3 - b)(a - b) + (a - b)^2 &\geq \frac{1}{4}\left[(a^2 - 1)^2 - (b^2 - 1)^2\right].\end{aligned} \tag{87}$$

According to the energy function that is defined by (2), discrete energy function of compact difference scheme (41) is defined by

$$E(u) = \frac{1}{4} \cdot h^2 \cdot \sum_{i=1}^{M-1}\sum_{j=1}^{M-1}\left(u_{ij}^2 - 1\right)^2 - \frac{\varepsilon^2}{2} \cdot h^2 \cdot u^T C^{-1} D_2 u. \tag{88}$$

Theorem 6. *Assuming that the initial value of the Allen-Cahn problem satisfies* $\max_{(x,y)\epsilon\bar{\Omega}} |u_0(x, y)| \leq 1$, *then the numerical solution obtained by scheme (41) satisfies discrete energy decaying under the condition of 4:*

$$E\left(U^{n+1}\right) \leq E\left(U^n\right). \tag{89}$$

Proof.

$$\begin{aligned}\frac{E\left(U^{n+1}\right) - E\left(U^n\right)}{h^2} = \frac{1}{4}\sum_{i=1}^{M-1}\sum_{j=1}^{M-1}&\left[\left(\left(U_{ij}^{n+1}\right)^2 - 1\right)^2 - \left(\left(U_{ij}^{n}\right)^2 - 1\right)^2\right]\\ &- \frac{\varepsilon^2}{2}\left(\left(U^{n+1}\right)^T C^{-1} D_2 U^{n+1} - \left(U^n\right)^T C^{-1} D_2 U^n\right).\end{aligned} \tag{90}$$

In view of Theorem 4, $\|U^n\|_\infty \leq 1$ and $\|U^{n+1}\|_\infty \leq 1$.

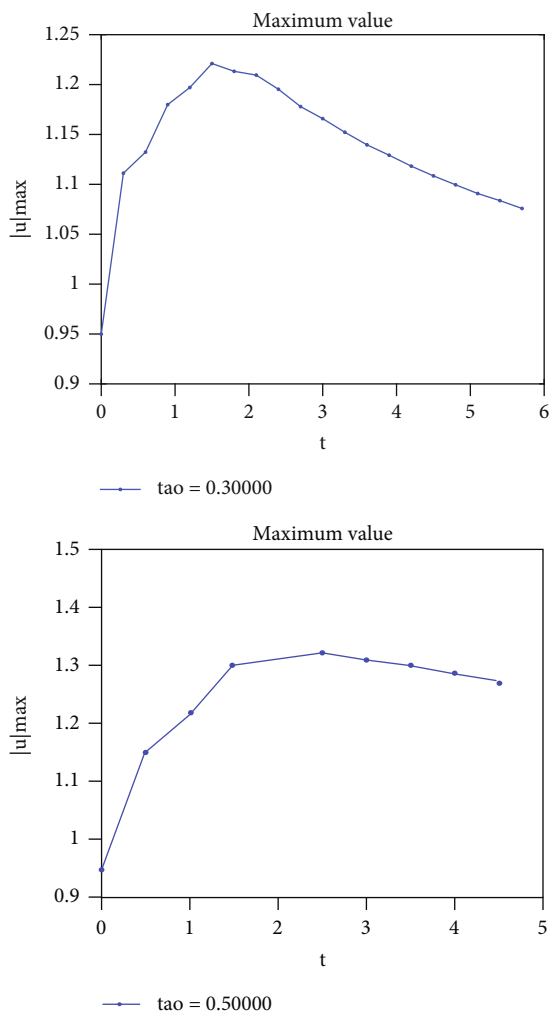

FIGURE 6: When $\tau = 0.3, 0.5$, the maximum of the scheme is (30).

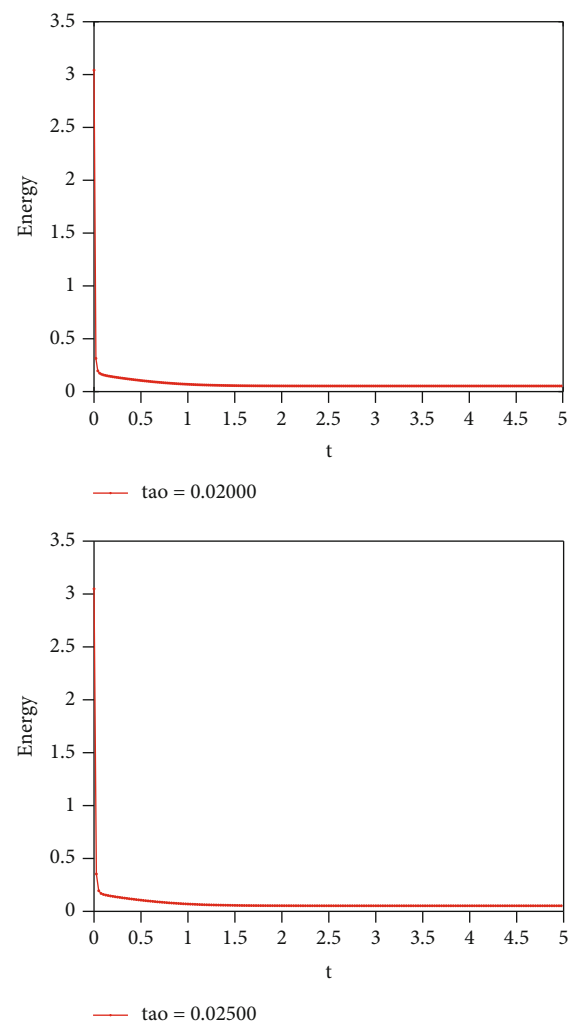

FIGURE 7: When $\tau = 0.02, 0.025$, the energy of the scheme is (30).

Therefore, using Lemma 5,

$$\begin{aligned}
&\frac{1}{4}\sum_{i=1}^{M-1}\sum_{j=1}^{M-1}\left[\left(\left(U_{ij}^{n+1}\right)^2-1\right)^2-\left(\left(U_{ij}^{n}\right)^2-1\right)^2\right] \\
&\quad\le \sum_{i=1}^{M-1}\sum_{j=1}^{M-1}\left[\frac{1}{2}\left(\left(U_{ij}^{n+1}\right)^3-U_{ij}^{n+1}\right)\left(U_{ij}^{n+1}-U_{ij}^{n}\right)\right. \\
&\qquad\left.+\frac{1}{2}\left(\left(U_{ij}^{n}\right)^3-U_{ij}^{n}\right)\left(U_{ij}^{n+1}-U_{ij}^{n}\right)+\left(U_{ij}^{n+1}-U_{ij}^{n}\right)^2\right].
\end{aligned} \tag{91}$$

Since the matrix $C^{-1}D_2$ is symmetric,

$$\begin{aligned}
&\frac{\varepsilon^2}{2}\left(U^{n+1}-U^{n}\right)^T C^{-1}D_2\left(U^{n+1}+U^{n}\right) \\
&\quad=\frac{\varepsilon^2}{2}\left(\left(U^{n+1}\right)^T C^{-1}D_2U^{n+1}-\left(U^{n}\right)^T C^{-1}D_2U^{n}\right).
\end{aligned} \tag{92}$$

Substituting (91) and (92) into (90),

$$\begin{aligned}
\frac{E\left(U^{n+1}\right)-E\left(U^{n}\right)}{h^2}\le{}& \sum_{i=1}^{M-1}\sum_{j=1}^{M-1}\left[\frac{1}{2}\left(\left(U_{ij}^{n+1}\right)^3-U_{ij}^{n+1}\right)\left(U_{ij}^{n+1}-U_{ij}^{n}\right)\right. \\
&+\frac{1}{2}\left(\left(U_{ij}^{n}\right)^3-U_{ij}^{n}\right)\left(U_{ij}^{n+1}-U_{ij}^{n}\right)+\left(U_{ij}^{n+1}-U_{ij}^{n}\right)^2 \\
&-\frac{\varepsilon^2}{2}\left(U^{n+1}-U^{n}\right)^T C^{-1}D_2\left(U^{n+1}+U^{n}\right).
\end{aligned} \tag{93}$$

Multiplying (41) by $U^{n+1}-U^{n}$, summing up for i from 1 to $M-1$ and same for j,

$$\begin{aligned}
&\sum_{i=1}^{M-1}\sum_{j=1}^{M-1}\left[\frac{1}{2}\left(\left(U_{ij}^{n+1}\right)^3-U_{ij}^{n+1}\right)\left(U_{ij}^{n+1}-U_{ij}^{n}\right)\right. \\
&\quad\left.+\frac{1}{2}\left(\left(U_{ij}^{n}\right)^3-U_{ij}^{n}\right)\left(U_{ij}^{n+1}-U_{ij}^{n}\right)+\frac{1}{\tau}\left(U_{ij}^{n+1}-U_{ij}^{n}\right)^2\right] \\
&\quad=\frac{\varepsilon^2}{2}\left(U^{n+1}-U^{n}\right)^T C^{-1}D_2\left(U^{n+1}+U^{n}\right).
\end{aligned} \tag{94}$$

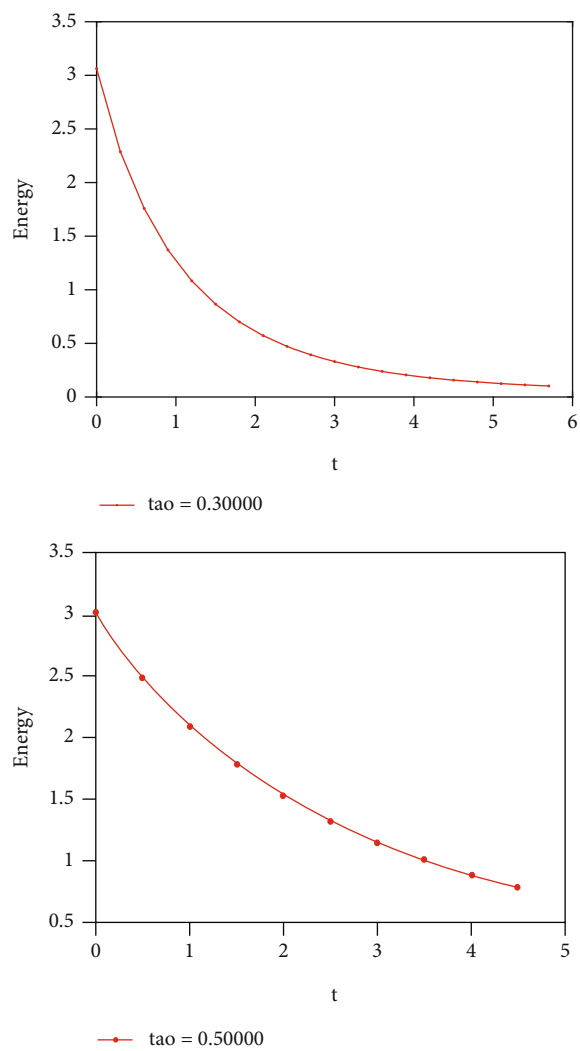

FIGURE 8: When $\tau = 0.3, 0.5$, the energy of the scheme is (30).

Substituting (94) into (93),

$$\begin{aligned}\frac{E(U^{n+1})-E(U^n)}{h^2} \le & \sum_{i=1}^{M-1}\sum_{j=1}^{M-1}\left[\frac{1}{2}\left(\left(U_{ij}^{n+1}\right)^3-U_{ij}^{n+1}\right)\left(U_{ij}^{n+1}-U_{ij}^n\right)\right. \\ & \left.+\frac{1}{2}\left(\left(U_{ij}^n\right)^3-U_{ij}^n\right)\left(U_{ij}^{n+1}-U_{ij}^n\right)+\left(U_{ij}^{n+1}-U_{ij}^n\right)^2\right] \\ & -\sum_{i=1}^{M-1}\sum_{j=1}^{M-1}\left[\frac{1}{2}\left(\left(U_{ij}^{n+1}\right)^3-U_{ij}^{n+1}\right)\right. \\ & \cdot\left(U_{ij}^{n+1}-U_{ij}^n\right)+\frac{1}{2}\left(\left(U_{ij}^n\right)^3-U_{ij}^n\right)\left(U_{ij}^{n+1}-U_{ij}^n\right) \\ & \left.+\frac{1}{\tau}\left(U_{ij}^{n+1}-U_{ij}^n\right)^2\right].\end{aligned} \tag{95}$$

Then,

$$\frac{E(U^{n+1})-E(U^n)}{h^2} \le \left(1-\frac{1}{\tau}\right)\sum_{i=1}^{M-1}\sum_{j=1}^{M-1}\left(U_{ij}^{n+1}-U_{ij}^n\right)^2. \tag{96}$$

Since $0<\tau\le\min\{(4/5)\lambda-1/6, 1-(12/5)\lambda\}$, $5/24<\lambda<5/12$, the right side of inequality is negative.

Then, $E(U^{n+1})\le E(U^n)$ is proved. □

5. Numerical Examples

In this part, some numerical examples are given to verify the theoretical results of the previous sections which are discrete numerical maximum principle and energy stability. Considering a two-dimensional problem with homogeneous Riemann boundary conditions, and selecting the initial condition as

$$u_0(x) = 0.9 * \text{rand}(\cdot) + 0.05, \tag{97}$$

here, rand $(\cdot)$ is a random sequence in the interval of $(0, 1)$.

If given $\epsilon^2 = 0.001, h = 0.01$, by $\lambda = \varepsilon^2(\tau/h^2)$, using the conditions of Theorem 4, $5/24 \le \lambda \le 5/12, 0 < \tau \le \min\{(4/5)\lambda - 1/6, 1-(12/5)\lambda\}$, we can get $1/48 < \tau < 1/24$. Taking different values for time step τ, the results are shown in the following figures.

It can be observed from Figure 1 that the discrete scheme (30) satisfies the maximum principle when the time step τ is 0.025 or 0.04, and from Figure 2, the discrete scheme (30) does not satisfy the maximum principle when the time step τ is 0.3 or 0.5. In addition, it satisfies the stability of discrete energy decaying according to Figures 3 and 4.

Then, if given $\epsilon^2 = 0.001, h = 0.008$; similarly, we can get $1/75 < \tau < 2/75$. The results are shown in the following figures.

It can be observed from Figure 5 that the discrete scheme (30) satisfies the maximum principle when the time step τ is 0.02 or 0.025, and from Figure 6, the discrete scheme (30) does not satisfy the maximum principle when the time step τ is 0.3 or 0.5. In addition, it satisfies the stability of discrete energy decaying according to Figures 7 and 8.

6. Conclusions

In this paper, the two-dimensional nonlinear Allen-Cahn equation is discretized by using the central finite difference method in space and using two operators $\mathscr{A}$ and $\mathscr{B}$ in time, and then, the fully discrete compact difference scheme with second-order accuracy in time and fourth-order in space is established as below:

$$\begin{aligned}\mathscr{A}\mathscr{B}\frac{u_{ij}^{n+1}-u_{ij}^n}{\tau}+\mathscr{A}\mathscr{B}\left[\frac{\left(u_{ij}^{n+1}\right)^3+\left(u_{ij}^n\right)^3}{2}-\frac{u_{ij}^{n+1}+u_{ij}^n}{2}\right] \\ =\frac{\varepsilon^2}{2}\left(\mathscr{B}\delta_x^2u_{ij}^{n+1}+\mathscr{B}\delta_x^2u_{ij}^n+\mathscr{A}\delta_y^2u_{ij}^{n+1}+\mathscr{A}\delta_y^2u_{ij}^n\right),\end{aligned}$$

$$1\le i\le M-1, 0\le n\le N-1. \tag{98}$$

Constructing the discrete matrix,

$$D_2 = BD_1 + D_1A,$$
$$C = AB. \tag{99}$$

Then, using the matrix instead of the operator, the following compact difference equation (39) can be obtained:

$$C\frac{U^{n+1} - U^n}{\tau} + C\left[\frac{\left(U^{n+1}\right)^3 - U^{n+1}}{2} + \frac{\left(U^n\right)^3 - U^n}{2}\right] = \frac{\varepsilon^2\left(D_2U^{n+1} + D_2U^n\right)}{2}. \tag{100}$$

It proved that when $5/24 < \lambda < 5/12$, $0 < \tau \le \min\left\{(4/5)\lambda - 1/6, 1 - (12/5)\lambda\right\}$, the discrete scheme satisfies the maximum principle $\|U^n\|_\infty \le 1$, for $\forall n \ge 1$.

Secondly, the discrete energy function of the compact difference scheme (88) of the two-dimensional Allen-Cahn equation is

$$E(u) = \frac{1}{4}\cdot h^2 \cdot \sum_{i=1}^{M-1}\sum_{j=1}^{M-1}\left(u_{ij}^2 - 1\right)^2 - \frac{\varepsilon^2}{2}\cdot h^2 \cdot u^T C^{-1} D_2 u. \tag{101}$$

The numerical solution obtained by scheme (39) satisfies the stability of discretization energy decaying under the conditions and conclusions of discretization maximization.

$$E\left(U^{n+1}\right) \le E\left(U^n\right). \tag{102}$$

Data Availability

The data used to support the findings of this study are included within the article.

Conflicts of Interest

The authors declare that they have no conflicts of interest.

Acknowledgments

The work is supported by the National Natural Science Foundation of China (11761074), the Natural Science Foundation of Jilin Province (2020122336JC), and the Program for Young and Middle-Aged Leading Talents in Scientific and Technological Innovation of Jilin Province (20200301053RQ).

References

[1] X. Zhang, Y. F. Jin, H. Y. Qiao, and C. H. Li, "Crank-Nicolson difference scheme for two dimensional Allen-Cahn equation," *Acta Mathematicae Applicatae Sinica*, vol. 44, no. 2, pp. 238–250, 2021.

[2] D. Tian, Y. F. Jin, and G. Lv, *Discrete maximum principle and energy stability of compact difference scheme for the Allen-Cahn equation*, Preprints, 2018.

[3] J. Q. Zhang and T. L. Hou, "Discrete maximum principle and energy stability of finite difference methods for one-dimensional Allen-Cahn equations," *Journal of Beihua University*, vol. 17, no. 2, pp. 159–164, 2016.

[4] S. Y. Zhai, X. L. Feng, and Y. N. He, "Numerical simulation of the three dimensional Allen-Cahn equation by the high-order compact ADI method," *Computer Physics Communications*, vol. 185, no. 10, pp. 2449–2455, 2014.

[5] D. Jeong, S. Lee, D. Lee, J. Shin, and J. Kim, "Comparison study of numerical methods for solving the Allen-Cahn equation," *Computational Materials Science*, vol. 111, pp. 131–136, 2016.

[6] F. Wu, *The Direct Discontinuous Galerkin Method for Allen-Cahn Equations*, Xiangtan University, 2019.

[7] R. H. Guo, *Local Discontinuous Galerkin Methods and Fast Solvers for Phase Field Models*, University of Science and Technology of China, 2014.

[8] X. F. Xiao, D. W. Gui, and X. L. Feng, "A highly efficient operator-splitting finite element method for 2D/3D nonlinear Allen-Cahn equation," *International Journal of Numerical Methods for Heat and Fluid Flow*, vol. 27, no. 2, pp. 530–542, 2017.

[9] T. T. Li, *Allen-Cahn and Cahn-Hilliard Equations Using Spectral Methods*, Huazhong University of Science and Technology, 2015.

[10] H. G. Lee and J. Y. Lee, "A semi-analytical Fourier spectral method for the Allen–Cahn equation," *Computers and Mathematics with Applications*, vol. 68, no. 3, pp. 174–184, 2014.

[11] L. Y. Wu, J. Y. Wang, and S. Y. Zhai, "Two ADI schemes for solving two-dimensional Allen-Cahn equations," *Journal of Huaqiao University*, vol. 40, no. 3, pp. 412–420, 2019.

[12] Y. F. Deng, Z. F. Yao, J. Y. Wang, and Z. F. Weng, "Two dimensional Allen-Cahn equations solved by finite difference method/collocation method," *Journal of Huaqiao University*, vol. 41, no. 5, pp. 690–694, 2020.

Hindawi
Journal of Function Spaces
Volume 2022, Article ID 4773005, 16 pages
https://doi.org/10.1155/2022/4773005

Research Article

Study of Nonlocal Boundary Value Problem for the Fredholm–Volterra Integro-Differential Equation

K. R. Raslan,[1] Khalid K. Ali,[1] Reda Gamal Ahmed,[1] Hind K. Al-Jeaid,[2] and Amira Abd-Elall Ibrahim[3]

[1]*Department of Mathematics, Faculty of Science, Al-Azhar University, Nasr-City, Cairo, Egypt*
[2]*Department of Mathematical Sciences, Umm Al-Qura University, Makkah, KSA, Saudi Arabia*
[3]*October High Institute for Engineering and Technology, 6th of October City, Egypt*

Correspondence should be addressed to Khalid K. Ali; khalidkaram2012@yahoo.com

Received 30 October 2021; Revised 22 December 2021; Accepted 31 December 2021; Published 7 February 2022

Academic Editor: Youssri Hassan Youssri

In this paper, the existence and uniqueness of the Fredholm–Volterra integro-differential equation with the nonlocal condition will be studied. Also, we study the continuous dependence of the initial data. The numerical solution of the problem will be studied using the central difference approximations and trapezoidal rule to transform the Volterra–Fredholm integro-differential equation into a system of algebraic equations which can be solved together to get the solution. Finally, we solve some examples numerically to show the accuracy of the proposed method.

1. Introduction

Recently, some researchers were interested in studying the existence and uniqueness of different types of integro-differential equation with the different conditions. El-Sayed et al. studied the existence of solutions to some integro-differential equations with infinite point and integral conditions, and they have also studied some properties of these solutions [1–4]. There are also many authors interested in studying the numerical solution for integral and integro-differential equations. Mirzaee and Piroozfar used modified Simpson's quadrature rule for solving linear Fredholm integral equations of the second kind [5]. Rahman et al. solved the system of linear Volterra Integral equations of the second kind using Simpson's quadrature rule [6]. Garba and Bichi studied the numerical solution for first-order Fredholm integro-differential equation using finite difference-composite Simpson method [7]. Ibrahim et al. studied the existence of a unique solution to nonlinear Fredholm integro-differential equation of the second order, and they introduced the exact solution using the direct computation method, introduced numerical solution using the combination of the finite difference method with the composite Simpson method to transform the Fredholm integro-differential equation into a system of nonlinear algebraic equations, and also computed the error estimation for the scheme to show the accuracy of the presented method [8]. Pandey used the finite difference method and the composite trapezoidal quadrature method to solve the Fredholm integro-differential equation [9]. Saadati et al. solved the linear Volterra and Fredholm integro-differential equation using the combination of the trapezoidal rule and the finite difference method and compared it with the variational iteration method (VIM). The result of comparison shows that VIM is better than the trapezoidal method [10]. Ishak and Norazura Ahmed obtained the numerical solution for the first-order Volterra integro-differential equation using the trapezoidal method and compared the results with the Euler method. The results of comparisons show that the trapezoidal method is better than the Euler method [11]. Raftari used the homotopy perturbation method (HPM) and the finite difference method to solve the Volterra integro-differential equation of the first order. The results of applying these methods demonstrate the validity and applicability of these techniques.

In this paper, we study the nonlocal boundary value problem for the Fredholm–Volterra integro-differential equation:

$$u''(x) = F\left(x, u(x), \int_a^b f(x,t,u'(t))(x,t,u'(t))\mathrm{d}t, \int_a^x g(x,t,u'(t))\mathrm{d}t\right), \quad x \in [a,b], \tag{1}$$

with the nonlocal condition

$$\begin{aligned} \sum_{j=0}^{m} a_j u(\tau_j) &= \mu_0, \\ u'(a) &= \rho_0, \\ a_j &\geq 0, \\ \tau_j &\in [a,b]. \end{aligned} \tag{2}$$

We study the existence of solution $u(x) \in C[a,b]$. We study the continuous dependence of the unique solution on μ_0 and on the nonlocal parameter a_j.

As applications, the nonlocal problem of the Fredholm–Volterra integro-differential equation (1) with the integral condition

$$\int_a^b u(s)\mathrm{d}\phi(s) = \mu_0 \tag{3}$$

will be studied.

This paper is organized as follows. In Section 2, we discuss the integral representation. We discuss the existence of solution and the nonlocal integral condition in Section 3. We discuss the uniqueness of the solution in Section 4. In Section 5, we discuss the continuous dependence on μ_0 and a_j. In Section 6, we present the methodology of numerical technique and numerical examples. Section 7 gives the conclusion.

2. Integral Representation

Consider nonlocal problems (1) and (2) with the following assumptions:

(1) F: $[a,b] \times \mathbb{R}^3 \longrightarrow \mathbb{R}$ satisfies Caratheodory condition, i.e., F is measurable in x for any $\xi, \alpha, \gamma \in \mathbb{R}$ and continuous for almost all $x \in [a,b]$. There exist a function $M_1(x) \in L^1[a,b]$ and a positive constant $C_1 > 0$, such that

$$|F(x,\xi,\alpha,\gamma)| \leq M_1(x) + C_1|\xi| + C_1|\alpha| + C_1|\gamma|. \tag{4}$$

(2) f: $[a,b] \times [a,b] \times \mathbb{R} \longrightarrow \mathbb{R}$ satisfies Caratheodory condition, i.e., f is measurable in x for any $v(t) \in \mathbb{R}$ and continuous for almost all $x \in [a,b]$. There exist a function $M_2(x,t) \in L^1[a,b]$ and a positive constant $C_2 > 0$, such that

$$|f(x,t,v(t))| \leq M_2(x,t) + C_2|v(t)|. \tag{5}$$

(3) g: $[a,b] \times [a,b] \times \mathbb{R} \longrightarrow \mathbb{R}$ satisfies Caratheodory condition. There exist a function $M_3(x,t) \in L^1[a,b]$ and a positive constant $C_3 > 0$, such that

$$|g(x,t,v(t))| \leq M_3(x,t) + C_3|v(t)|. \tag{6}$$

(4)

$$\begin{aligned} \sup_{x\in[a,b]} \int_a^x M_1(\theta)\mathrm{d}\theta &\leq N_1, \\ \sup_{\theta\in[a,b]} \int_a^b M_2(\theta,t)\mathrm{d}t &\leq N_2, \\ \sup_{\theta\in[a,b]} \int_a^\theta M_3(\theta,t)\mathrm{d}t &\leq N_3. \end{aligned} \tag{7}$$

(5) $(2C_1b^2 + C_1C_2b^2 + C_1C_3b^2) < 1$.

Lemma 1. *Let $\beta = \sum_{j=0}^{m} a_j \neq 0$, and we can represent the solution of nonlocal problems (1) and (2), if it exists by the integral equation*

$$u(x) = \beta^{-1}\left[\mu_0 - \sum_{j=0}^{m} a_j \int_a^{\tau_j} v(s)\mathrm{d}s\right] + \int_a^x v(s)\mathrm{d}s, \tag{8}$$

where

$$v(x) = \rho_0 + \int_a^x F\left(\theta, \beta^{-1}\left[\mu_0 - \sum_{j=0}^{m} a_j \int_a^{\tau_j} v(s)\mathrm{d}s\right] + \int_a^\theta v(s)\mathrm{d}s, \int_a^b f(\theta,t,v(t))\mathrm{d}t, \int_a^\theta g(\theta,t,v(t))\mathrm{d}t\right)\mathrm{d}\theta. \tag{9}$$

Proof. Integrating both sides of (1), we get

$$u'(x) = u'(a) + \int_a^x F\left(\theta, u(\theta), \int_a^b f(\theta, t, u'(t))\mathrm{d}t, \int_a^\theta g(\theta, t, u'(t))\mathrm{d}t\right)\mathrm{d}\theta, \quad x \in [a, b]. \tag{10}$$

Let $u'(x) = v(x)$ in (10), and we obtain

$$v(x) = \rho_0 + \int_a^x F\left(\theta, u(\theta), \int_a^b f(\theta, t, v(t))\mathrm{d}t, \int_a^\theta g(\theta, t, v(t))\mathrm{d}t\right)\mathrm{d}\theta, \quad x \in [a, b], \tag{11}$$

where

$$u(x) = u(a) + \int_a^x v(s)\mathrm{d}s, \quad x \in [a, b], \tag{12}$$

and using nonlocal condition (2), we get

$$\sum_{j=0}^m a_j u(\tau_j) = u(a)\sum_{j=0}^m a_j + \sum_{j=0}^m a_j \int_a^{\tau_j} v(s)\mathrm{d}s, \tag{13}$$

and then

$$u(a) = \beta^{-1}\left[\mu_0 - \sum_{j=0}^m a_j \int_a^{\tau_j} v(s)\mathrm{d}s\right]. \tag{14}$$

We obtain (8) and (9) from (11), (12), and (14). This completes the proof. □

3. Existence of Solution

Definition 1. By a solution of Fredholm–Volterra integral equation (9), *we mean a function* $u(x) \in C[a, b]$ *that satisfies* (5).

Theorem 1. *Let the assumptions (1)–(5) hold. Then, Fredholm–Volterra integral equation (9) has at least one solution* $u(x) \in C[a, b]$.

Proof. Define the operator E associated with integral *equation* (9) by

$$Ev(x) = \rho_0 + \int_a^x F\left(\theta, \beta^{-1}\left[\mu_0 - \sum_{j=0}^m a_j \int_a^{\tau_j} v(s)\mathrm{d}s\right] + \int_a^\theta v(s)ds\ , \int_a^b f(\theta, t, v(t))\mathrm{d}t, \int_a^\theta g(\theta, t, v(t))\mathrm{d}t\right)\mathrm{d}\theta. \tag{15}$$

Let $Q_r = \{v(x) \in \mathbb{R}: \|v\|_C \le r\}$, where $r = (|\rho_0| + N_1 + C_1 b\beta^{-1}|\mu_0| + C_1 bN_2 + C_1 bN_3)/(1 - (2C_1 b^2 + C_1 C_2 b^2 + C_1 C_3 b^2))$.

Then, we have that for $v(x) \in Q_r$,

$$\begin{aligned}
\|Ev(x)\|_C &\le |\rho_0| + \int_a^x \left|F\left(\theta, \beta^{-1}\left[\mu_0 - \sum_{j=0}^m a_j \int_a^{\tau_j} v(s)\mathrm{d}s\right] + \int_a^\theta v(s)\mathrm{d}s, \int_a^b f(\theta, t, v(t))\mathrm{d}t, \int_a^\theta g(\theta, t, v(t))\mathrm{d}t\right)\mathrm{d}\theta\right|, \\
&\le |\rho_0| + \int_a^x \left[M_1(\theta) + C_1\beta^{-1}\left|\mu_0 - \sum_{j=0}^m a_j \int_a^{\tau_j} v(s)\mathrm{d}s\right| + C_1\int_a^\theta |v(s)|\mathrm{d}s + C_1\int_a^b f|(\theta, t, v(t))|\mathrm{d}t + C_1\int_a^\theta g|(\theta, t, v(t))|\mathrm{d}t\right]\mathrm{d}\theta \\
&\le |\rho_0| + N_1 + \int_a^x \begin{bmatrix} C_1\beta^{-1}|\mu_0| + C_1\beta^{-1}\sum_{j=0}^m a_j \int_a^{\tau_j} |v(s)|\mathrm{d}s + C_1\int_a^\theta |v(s)|\mathrm{d}s \\ +C_1\int_a^b |M_2(\theta, t)|\mathrm{d}t + C_1C_2\int_a^b |v(t)|\mathrm{d}t + C_1\int_a^\theta |M_3(\theta, t)|\mathrm{d}t + C_1C_3\int_a^\theta |v(t)|\mathrm{d}t \end{bmatrix}\mathrm{d}\theta \\
&\le |\rho_0| + N_1 + \int_a^x \left[C_1\beta^{-1}|\mu_0| + C_1 b\|v\| + C_1 b\|v\| + C_1N_2 + C_1C_2 b\|v\| + C_1N_3 + C_1C_3 b\|v\|\right]\mathrm{d}\theta \\
&\le |\rho_0| + N_1 + C_1 b\beta^{-1}|\mu_0| + 2C_1 b^2 r + C_1 bN_2 + C_1C_2 b^2 r + C_1 bN_3 + C_1C_3 b^2 r = r.
\end{aligned} \tag{16}$$

This proves that $E\colon Q_r \longrightarrow Q_r$ and the class of functions $Ev(x)$ is uniformly bounded in Q_r.

Now, let $x_1, x_2 \in [a,b]$ such that $|x_2 - x_1| < \delta$; then,

$$\begin{aligned}
\left|Ev(x_2) - Ev(x_1)\right| &= \left|\rho_0 + \int_a^{x_2} F\left(\theta, \beta^{-1}\left[\mu_0 - \sum_{j=0}^{m} a_j \int_a^{\tau_j} v(s)\mathrm{d}s\right] + \int_a^{\theta} v(s)\mathrm{d}s, \int_a^b f(\theta,t,v(t))\mathrm{d}t, \int_a^{\theta} g(\theta,t,v(t))\mathrm{d}t\right)\mathrm{d}\theta\right. \\
&\quad \left. -\rho_0 - \int_a^{x_1} F\left(\theta, \beta^{-1}\left[\mu_0 - \sum_{j=0}^{m} a_j \int_a^{\tau_j} v(s)\mathrm{d}s\right] + \int_a^{\theta} v(s)\mathrm{d}s, \int_a^b f(\theta,t,v(t))\mathrm{d}t, \int_a^{\theta} g(\theta,t,v(t))\mathrm{d}t\right)d\theta\right| \\
&= \left|\int_a^{x_1} F\left(\theta, \beta^{-1}\left[\mu_0 - \sum_{j=0}^{m} a_j \int_a^{\tau_j} v(s)\mathrm{d}s\right] + \int_a^{\theta} v(s)\mathrm{d}s, \int_a^b f(\theta,t,v(t))\mathrm{d}t, \int_a^{\theta} g(\theta,t,v(t))\mathrm{d}t\right)\mathrm{d}\theta\right. \\
&\quad + \int_{x_1}^{x_2} F\left(\theta, \beta^{-1}\left[\mu_0 - \sum_{j=0}^{m} a_j \int_a^{\tau_j} v(s)\mathrm{d}s\right] + \int_a^{\theta} v(s)\mathrm{d}s, \int_a^b f(\theta,t,v(t))\mathrm{d}t, \int_a^{\theta} g(\theta,t,v(t))\mathrm{d}t\right)d\theta \\
&\quad \left. - \int_a^{x_1} F\left(\theta, \beta^{-1}\left[\mu_0 - \sum_{j=0}^{m} a_j \int_a^{\tau_j} v(s)\mathrm{d}s\right] + \int_a^{\theta} v(s)\mathrm{d}s, \int_a^b f(\theta,t,v(t))\mathrm{d}t, \int_a^{\theta} g(\theta,t,v(t))\mathrm{d}t\right)d\theta\right| \\
&\le \int_{x_1}^{x_2}\left|F\left(\theta, \beta^{-1}\left[\mu_0 - \sum_{j=0}^{m} a_j \int_a^{\tau_j} v(s)\mathrm{d}s\right] + \int_a^{\theta} v(s)\mathrm{d}s, \int_a^b f(\theta,t,v(t))\mathrm{d}t, \int_a^{\theta} g(\theta,t,v(t))\mathrm{d}t\right)\right|d\theta \\
&\le \int_{x_1}^{x_2} M_1(\theta)\mathrm{d}\theta + \left(C_1\beta^{-1}\mu_0 + 2C_1 br + C_1 N_2 + C_1 C_2 br + C_1 N_3 + C_1 C_3 br\right)\delta.
\end{aligned} \tag{17}$$

This means that the class of functions $Ev(x)$ is equicontinuous in Q_r. □

Let $v_n(x) \in Q_r$, $v_n(x) \longrightarrow v(x)\,(n \longrightarrow \infty)$; then, from the continuity of the three functions F, f, and g, we obtain $F(x,\xi_n,\alpha_n,\gamma_n) \longrightarrow F(x,\xi,\alpha,\gamma)$, $f(x,t,v_n(t)) \longrightarrow f(x,t,v(t))$ and $g(x,t,v_n(t)) \longrightarrow g(x,t,v(t))$ as $n \longrightarrow \infty$. Also,

$$\lim_{n\longrightarrow\infty} Ev_n(x) = \lim_{n\longrightarrow\infty}\left[\rho_0 + \int_a^{x} F\left(\theta, \beta^{-1}\left[\mu_0 - \sum_{j=0}^{m} a_j \int_a^{\tau_j} v_n(s)\mathrm{d}s\right] + \int_a^{\theta} v_n(s)\mathrm{d}s, \int_a^b f(\theta,t,v_n(t))\mathrm{d}t, \int_a^{\theta} g(\theta,t,v_n(t))\mathrm{d}t\right)\mathrm{d}\theta\right]. \tag{18}$$

Using assumptions (1)–(3) and Lebesgue dominated convergence theorem [13], we obtain

$$\lim_{n\longrightarrow\infty} Ev_n(x) = \rho_0 + \int_a^{x} \lim_{n\longrightarrow\infty} F\left(\theta, \beta^{-1}\left[\mu_0 - \sum_{j=0}^{m} a_j \int_a^{\tau_j} v_n(s)\mathrm{d}s\right] + \int_a^{\theta} v_n(s)\mathrm{d}s, \int_a^b f(\theta,t,v_n(t))\mathrm{d}t, \int_a^{\theta} g(\theta,t,v_n(t))\mathrm{d}t\right)\mathrm{d}\theta = Ev(x). \tag{19}$$

Then, $Ev_n(x) \longrightarrow Ev(x)$ as $n \longrightarrow \infty$. This means that the operator E is continuous in Q_r. Then, by Schauder fixed point theorem [14], there exists at least one solution $v(x) \in C[a,b]$ of integral equation (9). Thus, based on Lemma 1, nonlocal problems (1) and (2) possess a solution $u(x) \in C[a,b]$.

3.1. Nonlocal Integral Condition. Let $v(x) \in C[a,b]$ be the solution of integral equation (9). Let $a_j = \phi(x_j) - \phi(x_{j-1})$, ϕ be increasing function, $\tau_j \in (x_{j-1}, x_j)$, and $a = x_0 < x_1 < x_2 < \ldots < x_N = b$; then, as $m \longrightarrow \infty$, nonlocal condition (2) will be

$$\sum_{j=0}^{m}\left(\phi\left(x_j\right)-\phi\left(x_{j-1}\right)\right)u\left(\tau_j\right)=\mu_0, \tag{20}$$

$$\lim_{m\longrightarrow\infty}\sum_{j=0}^{m}\left(\phi\left(x_j\right)-\phi\left(x_{j-1}\right)\right)u\left(\tau_j\right)=\int_a^b u(s)\mathrm{d}(s)=\mu_0. \tag{21}$$

Theorem 2. *Let the assumptions (1)–(5) hold; then, nonlocal problems (1) and (3) have at least one solution given by*

$$u(x)=\frac{1}{\phi(b)-\phi(a)}\left(\mu_0-\int_a^b\int_a^\theta v(s)\mathrm{d}s\mathrm{d}\phi(\theta)\right)+\int_a^x v(s)\mathrm{d}s, \tag{22}$$

where

$$v(x)=\rho_0+\int_a^x F\left(\theta,\frac{1}{\phi(b)-\phi(a)}\left(\mu_0-\int_a^b\int_a^\theta v(s)\mathrm{d}s\mathrm{d}\phi(\theta)\right)+\int_a^\theta v(s)\mathrm{d}s,\int_a^b f(\theta,t,v(t))dt\ ,\int_a^\theta g(\theta,t,v(t))\mathrm{d}t\right)\mathrm{d}\theta\right). \tag{23}$$

Proof. As $m\longrightarrow\infty$, the solution of nonlocal problems (1) and (3) will be

$$\begin{aligned}u(x)&=\lim_{m\longrightarrow\infty}\left[\beta^{-1}\left[\mu_0-\sum_{j=0}^{m}a_j\int_a^{\tau_j}v(s)\mathrm{d}s\right]+\int_a^x v(s)\mathrm{d}s\right]\\&=\frac{1}{\phi(b)-\phi(a)}\left[\mu_0-\lim_{m\longrightarrow\infty}\sum_{j=0}^{m}\int_a^{\tau_j}v(s)\mathrm{d}s\left(\phi\left(x_j\right)-\phi\left(x_{j-1}\right)\right)\right]+\int_a^x v(s)\mathrm{d}s\\&=\frac{1}{\phi(b)-\phi(a)}\left[\mu_0-\int_a^b\int_a^\theta v(s)\mathrm{d}s\mathrm{d}\phi(\theta)\right]+\int_a^x v(s)\mathrm{d}s,\end{aligned} \tag{24}$$

where

$$v(x)=\rho_0+\int_a^x F\left(\theta,\frac{1}{\phi(b)-\phi(a)}\left(\mu_0-\int_a^b\int_a^\theta v(s)\mathrm{d}s\mathrm{d}\phi(\theta)\right)+\int_a^\theta v(s)\mathrm{d}s,\int_a^b f(\theta,t,v(t))\mathrm{d}t,\int_a^\theta g(\theta,t,v(t))\mathrm{d}t\right)\mathrm{d}\theta. \tag{25}$$

□

4. Uniqueness of the Solution

Let F, f, and g satisfy the following assumptions:

(i) F: $[a,b]\times\mathbb{R}^3\longrightarrow\mathbb{R}$ is measurable in x for any $\xi,\alpha,\gamma\in\mathbb{R}$ and satisfies the Lipschitz condition

$$\begin{aligned}&\left|F(x,\xi,\alpha,\gamma)-F(x,\nu,\alpha_1,\gamma_1)\right|\\&\quad\le C_1|\xi-\nu|+C_1\left|\alpha-\alpha_1\right|+C_1\left|\gamma-\gamma_1\right|.\end{aligned} \tag{26}$$

(ii) f: $[a,b]\times[a,b]\times\mathbb{R}\longrightarrow\mathbb{R}$ is measurable in x for any $v(t)\in\mathbb{R}$ and satisfies the Lipschitz condition

$$|f(x,t,v(t))-f(x,t,w(t))|\le C_2|v(t)-w(t)|. \tag{27}$$

(iii) g: $[a,b]\times[a,b]\times\mathbb{R}\longrightarrow\mathbb{R}$ is measurable in x for any $v(t)\in\mathbb{R}$ and satisfies the Lipschitz condition

$$|g(x,t,v(t))-g(x,t,w(t))|\le C_3|v(t)-w(t)|. \tag{28}$$

Theorem 3. *Let the assumptions (i) – (iii) hold; then, the solution of Fredholm–Volterra integral equation (9) is unique.*

Proof. Let $v(x),w(x)$ be two solutions of Fredholm–Volterra integral *equation* (9); then,

$$|v(x)-w(x)|\le\int_a^x|F\left(\theta,\beta^{-1}\left[\mu_0-\sum_{j=0}^{m}a_j\int_a^{\tau_j}v(s)\mathrm{d}s\right]+\int_a^\theta v(s)\mathrm{d}s,\int_a^b f(\theta,t,v(t))\mathrm{d}t,\int_a^\theta f(\theta,t,v(t))\mathrm{d}t\right)\mathrm{d}\theta$$

$$
\begin{aligned}
&- F\left(\theta, \beta^{-1}\left[\mu_0 - \sum_{j=0}^{m} a_j \int_a^{\tau_j} w(s)\mathrm{d}s\right] + \int_a^{\theta} w(s)\mathrm{d}s, \int_a^b f(\theta, t, w(t))\mathrm{d}t, \int_a^{\theta} g(\theta, t, w(t))\mathrm{d}t\right)|d\theta \\
&\leq \int_a^x \left[C_1\left|\beta^{-1}\sum_{j=0}^{m} a_j \int_a^{\tau_j} w(s) - v(s)\mathrm{d}s + \int_a^{\theta} v(s) - w(s)\mathrm{d}s\right|\right. \\
&\quad + C_1\left|\int_a^b (f(\theta, t, v(t)) - f(\theta, t, w(t)))dt\right| + C_1\left|\int_a^{\theta} (g(\theta, t, v(t)) - g(\theta, t, w(t)))\mathrm{d}t\right| \\
&\leq C_1 \int_a^x \left[\beta^{-1}\sum_{j=0}^{m} a_j \int_a^{\tau_j} |w(s) - v(s)|\mathrm{d}s + \int_a^{\theta} |w(s) - v(s)|\mathrm{d}s\right. \\
&\quad \left. + \int_a^b |f(\theta, t, v(t)) - f(\theta, t, w(t))|\mathrm{d}t + \int_a^{\theta}\int_a^b |g(\theta, t, v(t)) - g(\theta, t, w(t))|\mathrm{d}t\right]\mathrm{d}\theta \\
&\leq C_1\|w - v\|b^2 + C_1\|w - v\|b^2 + C_1 \int_a^x \int_a^b C_2|v(t) - w(t)|\mathrm{d}t\mathrm{d}\theta \\
&\quad + C_1 \int_a^x \int_a^{\theta} C_3|v(t) - w(t)|\mathrm{d}t\mathrm{d}\theta \\
&\leq 2C_1\|w - v\|b^2 + C_1C_2b^2\|w - v\| + C_1C_3b^2\|w - v\| \\
&\leq \left(2C_1b^2 + C_1C_2b^2 + C_1C_3b^2\right)\|w - v\|.
\end{aligned} \tag{29}
$$

Hence,

$$
\left[1 - \left(2C_1b^2 + C_1C_2b^2 + C_1C_3b^2\right)\right]\|w - v\| \leq 0. \tag{30}
$$

Since $2C_1b^2 + C_1C_2b^2 + C_1C_3b^2 < 1$, then $w(x) = v(x)$ and the solution of Fredholm–Volterra integral equation (9) is unique. Thus, based on Lemma 1, nonlocal problems (1) and (2) possess a unique solution $u(x) \in C[a, b]$. □

5. Continuous Dependence

5.1. Continuous Dependence on μ_0

Definition 2. The solution $u(x) \in C[a, b]$ *of nonlocal Fredholm–Volterra problems* (1) and (2) *depends continuously on* μ_0, *if*

$$
\forall \varepsilon > 0, \quad \exists \quad \delta(\varepsilon) \quad s.t \quad \left|\mu_0 - \mu_0^*\right| < \delta \Rightarrow \left\|u - u^*\right\| < \varepsilon, \tag{31}
$$

where u^* is the solution of the nonlocal problem

$$
u^{*}\prime\prime(x) = F\left(x, u^*(x), \int_a^b f\left(x, t, u^{*'}(t)\right)\mathrm{d}t, \int_a^x g\left(x, t, u^{*'}(t)\right)\mathrm{d}t\right), \quad x \in [a, b], \tag{32}
$$

with the nonlocal condition

$$
\begin{gathered}
\sum_{j=0}^{m} a_j u^*\left(\tau_j\right) = \mu_0^*, \quad u^{*'}(a) = \rho_0, \\
a_j \geqslant 0, \quad \tau_j \in [a, b].
\end{gathered} \tag{33}
$$

Theorem 4. *Let the assumptions (1)–(5) of Theorem 1hold; then, the solution of nonlocal Fredholm–Volterra problems (1) and (2) depends continuously on* μ_0.

Proof. Let $u(x)$, $u^*(x)$ be two solutions of nonlocal Fredholm–Volterra problems (1) and (2) *and* (23)–(33), respectively. Then,

$$
\begin{aligned}
\left|v(x) - v^*(x)\right| = |\int_a^x &\left[F\left(\theta, \beta^{-1}\left[\mu_0 - \sum_{j=0}^{m} a_j \int_a^{\tau_j} v(s)ds\right] + \int_a^{\theta} v(s)\mathrm{d}s, \int_a^b f(\theta, t, v(t))\mathrm{d}t, \int_a^{\theta} g(\theta, t, v(t))\mathrm{d}t\right)\right. \\
&\left. -F\left(\theta, \beta^{-1}\left[\mu_0^* - \sum_{j=0}^{m} a_j \int_a^{\tau_j} v^*(s)\mathrm{d}s\right] + \int_a^{\theta} v^*(s)ds\ , \int_a^b f\left(\theta, t, v^*(t)\right)\mathrm{d}t, \int_a^{\theta} g\left(\theta, t, v^*(t)\right)\mathrm{d}t\right)\right]\mathrm{d}\theta|
\end{aligned}
$$

$$
\begin{aligned}
&\leq \int_a^x |F\left(\theta, \beta^{-1}\left[\mu_0 - \sum_{j=0}^m a_j \int_a^{\tau_j} v(s)\mathrm{d}s\right] + \int_a^\theta v(s)\mathrm{d}s, \int_a^b f(\theta, t, v(t))\mathrm{d}t, \int_a^\theta g(\theta, t, v(t))\mathrm{d}t\right) \\
&\quad - F\left(\theta, \beta^{-1}\left[\mu_0^* - \sum_{j=0}^m a_j \int_a^{\tau_j} v^*(s)\mathrm{d}s\right] + \int_a^\theta v^*(s)\mathrm{d}s, \int_a^b f(\theta, t, v^*(t))\mathrm{d}t, \int_a^\theta g(\theta, t, v^*(t))\mathrm{d}t\right)|\mathrm{d}\theta \\
&\leq \int_a^x \left[C_1\left|\beta^{-1}(\mu_0 - \mu_0^*) + \beta^{-1}\sum_{j=0}^m a_j \int_a^{\tau_j}(v^*(s) - v(s))\mathrm{d}s + \int_a^\theta v(s) - v^*(s)\mathrm{d}s\right|\right. \\
&\quad \left. + C_1\left|\int_a^b (f(\theta, t, v(t)) - f(\theta, t, v^*(t)))\mathrm{d}t\right| + C_1\left|\int_a^\theta (g(\theta, t, v(t)) - g(\theta, t, v^*(t)))\mathrm{d}t\right|\right]\mathrm{d}\theta \\
&\leq \int_a^x \left[C_1\beta^{-1}|\mu_0 - \mu_0^*| + C_1\beta^{-1}\sum_{j=0}^m a_j \int_a^{\tau_j}|v^*(s) - v(s)|\mathrm{d}s + C_1\int_a^\theta |v(s) - v^*(s)|\mathrm{d}s\right. \\
&\quad \left. + C_1\int_a^b |f(\theta, t, v(t)) - f(\theta, t, v^*(t))|\mathrm{d}t + C_1\int_a^\theta |g(\theta, t, v(t)) - g(\theta, t, v^*(t))|\mathrm{d}t\right]\mathrm{d}\theta \\
&\leq C_1\beta^{-1}|\mu_0 - \mu_0^*|b + C_1\|v - v^*\|b^2 + C_1\|v - v^*\|b^2 \\
&\quad + C_1\int_a^x\int_a^b C_2|v(t) - v^*(t)|\mathrm{d}t + C_1\int_a^x\int_a^\theta C_3|v(t) - v^*(t)|\mathrm{d}t\mathrm{d}\theta \\
&\leq C_1 b\beta^{-1}\delta + 2C_1\|v - v^*\|b^2 + C_1C_2b^2\|v - v^*\| + C_1C_3b^2\|v - v^*\|.
\end{aligned} \tag{34}
$$

Hence,

$$
\|v - v^*\| \leq \frac{C_1 b\beta^{-1}\delta}{1 - \left(2C_1b^2 + C_1C_2b^2 + C_1C_3b^2\right)}. \tag{35}
$$

Since

$$
|u(x) - u^*(x)| = \beta^{-1}\left[\mu_0 - \sum_{j=0}^m a_j \int_a^{\tau_j} v(s)\mathrm{d}s\right] + \int_a^x v(s)\mathrm{d}s - \beta^{-1}\left[\mu_0^* - \sum_{j=0}^m a_j \int_a^{\tau_j} v^*(s)\mathrm{d}s\right] + \int_a^x v^*(s)\mathrm{d}s\beta^{-1}|\mu_0 - \mu_0^*| + 2b\|v - v^*\|, \tag{36}
$$

then

$$
\|u - u^*\| \leq \beta^{-1}\delta + \frac{2C_1b^2\beta^{-1}\delta}{1 - \left(2C_1b^2 + C_1C_2b^2 + C_1C_3b^2\right)} = \varepsilon. \tag{37}
$$

Therefore, the solution of nonlocal Fredholm–Volterra problems (1) and (2) depends continuously on μ_0. □

5.2. Continuous Dependence on a_j

Definition 3. The solution $u(x) \in C[a, b]$ of nonlocal Fredholm–Volterra problems (1) and (2) *depends continuously on a_j, if*

$$
\forall \varepsilon > 0, \quad \exists \quad \delta(\varepsilon) \quad s.t \quad |a_j - a_j^*| < \delta \Rightarrow \|u - u^*\| < \varepsilon, \tag{38}
$$

where $u^*(x)$ is the solution of the nonlocal problem

$$
u^{*\prime\prime}(x) = F\left(x, u^*(x), \int_a^b f\left(x, t, u^{*\prime}(t)\right)\mathrm{d}t, \int_a^x g\left(x, t, u^{*\prime}(t)\right)\mathrm{d}t\right), \quad x \in [a, b], \tag{39}
$$

with the nonlocal condition

$$\sum_{j=0}^{m} a_j^* u^*\left(\tau_j\right) = \mu_0, \quad u^{*'}(a) = \rho_0, \quad a_j \geqslant 0, \quad \tau_j \in [a,b]. \tag{40}$$

Theorem 5. *Let the assumptions (1)–(5) ofTheorem 1hold; then, the solution of nonlocal problems (1) and (2) depends continuously on a_j.*

Proof. Let $\beta^* = \sum_{j=0}^{m} a_j^* \neq 0$ and $v(x), v^*(x)$ be two solutions of nonlocal Fredholm–Volterra problems (1) and (2) *and* (39)–(40), respectively. Then,

$$\begin{aligned}
\left|v(x) - v^*(x)\right| \leq & \int_a^x \Bigg| F\left(\theta, \beta^{-1}\left[\mu_0 - \sum_{j=0}^{m} a_j \int_a^{\tau_j} v(s)\mathrm{d}s\right] + \int_a^\theta v(s)\mathrm{d}s, \int_a^b f(\theta,t,v(t))\mathrm{d}t, \int_a^\theta g(\theta,t,v(t))\mathrm{d}t\right) \\
& - F\left(\theta, \beta^{*-1}\left[\mu_0 - \sum_{j=0}^{m} a_j^* \int_a^{\tau_j} v^*(s)\mathrm{d}s\right] + \int_a^\theta v^*(s)\mathrm{d}s, \int_a^b f(\theta,t,v^*(t))\mathrm{d}t, \int_a^\theta g(\theta,t,v^*(t))\mathrm{d}t\right)\Bigg| \mathrm{d}\theta \\
\leq & \int_a^x \Bigg[C_1 |\beta^{-1}(\mu_0) - \beta^{*-1}(\mu_0) + \beta^{*-1} \sum_{j=0}^{m} a_j^* \int_a^{\tau_j} v^*(s)\mathrm{d}s - \beta^{-1} \sum_{j=0}^{m} a_j \int_a^{\tau_j} v(s)\mathrm{d}s \\
& + \int_a^\theta v(s)\mathrm{d}s - \int_a^\theta v^*(s)\mathrm{d}s| + C_1 \left| \int_a^b \left(f(\theta,t,v(t)) - f(\theta,t,v^*(t))\right)\mathrm{d}t \right| \\
& + C_1 \left| \int_a^\theta \left(g(\theta,t,v(t)) - g(\theta,t,v^*(t))\right)\mathrm{d}t \right| \Bigg] \mathrm{d}\theta \\
\leq & \int_a^x \Bigg[C_1 \left|\beta^{-1}(\mu_0) - \beta^{*^{-1}}(\mu_0)\right| + C_1 \beta^{*^{-1}} \sum_{j=0}^{m} a_j^* \int_a^{\tau_j} \left|v^*(s) - v(s)\right| \mathrm{d}s \\
& + C_1 \beta^{*-1} \left(\sum_{j=0}^{m} \left|a_j^* - a_j\right| \right) \int_a^{\tau_j} |v(s)|\mathrm{d}s + C_1 \beta^{-1} \beta^{*^{-1}} \sum_{j=0}^{m} \left|a_j - a_j^*\right| \sum_{j=0}^{m} a_j \int_a^{\tau_j} |v(s)|\mathrm{d}s \\
& + C_1 \int_a^\theta \left|v(s) - v^*(s)\right| \mathrm{d}s + C_1 \int_a^b \left|f(\theta,t,v(t)) - f(\theta,t,v^*(t))\right| \mathrm{d}t \\
& + C_1 \int_a^\theta \left|g(\theta,t,v(t)) - g(\theta,t,v^*(t))\right| \mathrm{d}t \Bigg] \mathrm{d}\theta \\
\leq & C_1 \beta^{-1} \beta^{*^{-1}} m\delta\mu_0 + C_1 \left\|v - v^*\right\| b^2 + C_1 \beta^{*^{-1}} m\delta \|v\| b^2 + C_1 \beta^{*^{-1}} m\delta \|v\| b^2 \\
& + C_1 \left\|v - v^*\right\| b^2 + C_1 C_2 b^2 \left\|v - v^*\right\| + C_1 C_3 b^2 \left\|v - v^*\right\| \\
\leq & C_1 \beta^{-1} \beta^{*^{-1}} m\delta\mu_0 + 2C_1 \beta^{*^{-1}} m\delta \|v\| b^2 + \left(2C_1 b^2 + C_1 C_2 b^2 + C_1 C_3 b^2\right) \left\|v - v^*\right\|.
\end{aligned} \tag{41}$$

Hence,

$$\left\|v - v^*\right\| \leq \frac{C_1 \beta^{-1} \beta^{*^{-1}} m\delta\mu_0 + 2C_1 \beta^{*^{-1}} m\delta \|v\| b^2}{\left[1 - \left(2C_1 b^2 + C_1 C_2 b^2 + C_1 C_3 b^2\right)\right]}. \tag{42}$$

Since

$$\begin{aligned}
\left|u(x) - u^*(x)\right| = & \Bigg| \frac{1}{\sum_{j=0}^{m} a_j} \left[\mu_0 - \sum_{j=0}^{m} a_j \int_a^{\tau_j} v(s)\mathrm{d}s\right] + \int_a^x v(s)\mathrm{d}s - \frac{1}{\sum_{j=0}^{m} a_j^*} \\
& \left[\mu_0 - \sum_{j=0}^{m} a_j^* \int_a^{\tau_j} v^*(s)\mathrm{d}s\right] + \int_a^x v^*(s)\mathrm{d}s \Bigg| \leq \frac{m\delta\left|\mu_0\right|}{\beta\beta^*} + 2\, m\delta b \beta^{*^{-1}} r + 2b\left\|v - v^*\right\|,
\end{aligned} \tag{43}$$

then

$$\|u-u^*\| \le \frac{m\delta|\mu_0|}{\beta\beta^*} + 2\,m\delta b\beta^{*\,-1}r + 2b \frac{C_1\beta^{-1}\beta^{*\,-1}m\delta\mu_0 + 2C_1\beta^{*\,-1}m\delta\|v\|b^2}{\left[1-\left(2C_1b^2+C_1C_2b^2+C_1C_3b^2\right)\right]} = \epsilon. \tag{44}$$

Thus, the solution of nonlocal Fredholm–Volterra problems (1) and (2) depends continuously on a_j. □

6. Methodology of Numerical Technique

In this section, we wish to determine the numerical solution of equation (1). We divide the domain $[a,x]$ and $[a,b]$ of equation (1) into N finite points as $a = x_0 < x_1 < \ldots < x_{N-1} < x_N = x = b$. We use uniform step length $h = ((b-a)/N) = ((x_i - a)/i)$, $i \ge 1$, as $x_j = a + jh = t_j$, $j = 0, 1, 2, \ldots, N$. Then, we use the trapezoidal rule to approximate the integral parts of (1) as follows [10]:

$$\int_a^b k(x_i,t_j)u'(t_j)\mathrm{d}t \simeq \frac{h}{2}\left[k(x_i,t_0)u'(t_0) + 2\sum_{j=1}^{N-1} k(x_i,t_j)u'(t_j) + k(x_i,t_N)u'(t_N)\right], \tag{45}$$

$$\int_a^{x_i} K(x_i,t_j)u'(t_j)\mathrm{d}t \simeq \frac{h_i}{2}\left[K(x_i,t_0)u'(t_0) + 2\sum_{j=1}^{N-1} K(x_i,t_j)u'(t_j) + K(x_i,t_N)u'(t_N)\right], \tag{46}$$

where $K(x_i,t_j) = 0$ for $t_j \le x_i$, $j \ge 1$.

Then, we use central difference approximations to approximate the derivative parts of (1) as

$$u_i'' \simeq \frac{u_{i+1} - 2u_i + u_{i-1}}{h^2}, \qquad u_i' \simeq \frac{u_{i+1} - u_{i-1}}{2h}, \tag{47}$$

where $u_i'' = u''(x_i)$, $u_i' = u'(x_i)$.

6.1. Numerical Examples. Now, we apply Theorem 1 on some examples of the nonlocal Fredholm–Volterra integro-differential equation and we solve it numerically by using the finite difference-trapezoidal method. The results obtained are tabulated in Tables 1–4, and all results for these examples are obtained by using Wolfram Mathematica.

Example 1. Consider the equation

$$\begin{aligned} u''(x) - \frac{1}{8}u^2(x) &= \frac{1}{240}\left(-2x^5 - 6x^2\sin(2x) + 9x\sin^2(x) + 3\sin^3(x)\cos(x)\right) \\ &- \frac{1}{48}x\left(\frac{3}{2} - e^{-\sin(1)}\right) - \frac{1}{8}\cos^2(x) - \cos(x) + \frac{1}{48}\int_0^1\left(tx + x\cos(t)e^{u'(t)}\right)\mathrm{d}t \\ &+ \frac{1}{40}\int_0^x\left(tx + \sin(x)u'^2(t)\right)\mathrm{d}t, u(0.4) + u(0.6) = 1.746, u'(0) = 0. \end{aligned} \tag{48}$$

The exact solution of this problem is $u(x) = \cos(x)$.

Firstly, we apply the assumptions of Theorem 1 to prove that this example has a continuous solution:

$$\begin{aligned} &F\left(x, u(x), \int_a^b f(x,t,u'(t))\mathrm{d}t, \int_a^x g(x,t,u'(t))\mathrm{d}t\right) \\ &= \frac{1}{240}\left(-2x^5 - 6x^2\sin(2x) + 9x\sin^2(x) + 3\sin^3(x)\cos(x)\right) - \frac{1}{48}x\left(\frac{3}{2} - e^{-\sin(1)}\right) - \frac{1}{8}\cos^2(x) - \cos(x) \\ &+ \frac{1}{8}u^2(x) + \frac{1}{48}\int_0^1\left(tx + x\cos(t)e^{u'(t)}\right)\mathrm{d}t + \frac{1}{40}\int_0^x\left(tx + \sin(x)u'^2(t)\right)\mathrm{d}t. \end{aligned} \tag{49}$$

Table 1: The exact and numerical solutions of example 1.

x_i	Numerical solution	Exact solution	Absolute error
0.0	1.00007	1.00000	7.1195 E-5
0.1	0.99507	0.99500	6.7119 E-5
0.2	0.98012	0.98007	5.5076 E-5
0.3	0.95537	0.95534	3.6189 E-5
0.4	0.92108	0.92106	1.3545 E-5
0.5	0.87758	0.87758	6.6020 E-6
0.6	0.82532	0.82534	1.3545 E-5
0.7	0.76485	0.76484	9.2025 E-6
0.8	0.69679	0.69671	8.5149 E-5
0.9	0.62186	0.62161	2.4584 E-4
1.0	0.54083	0.54030	5.3145 E-4

Table 2: The exact and numerical solutions of example 2.

x_i	Approximate solution	Exact solution	Absolute error
−1.0	−0.845787	−0.841471	4.31629 E-3
−0.8	−0.720890	−0.717356	3.53409 E-3
−0.6	−0.567342	−0.564642	2.69934 E-3
−0.4	−0.391242	−0.389418	1.82331 E-3
−0.2	−0.199588	−0.198669	9.18883 E-4
0.0	0.000000	0.000000	0.00000
0.2	0.199588	0.198669	9.18883 E-4
0.4	0.391242	0.389418	1.82331 E-3
0.6	0.567342	0.564642	2.69934 E-3
0.8	0.720890	0.717356	3.53409 E-3
1.0	0.845787	0.841471	4.31629 E-3

Table 3: The exact and numerical solutions of example 3.

x_i	Approximate solution	Exact solution	Absolute error
0.0	0.99967	1.00000	3.20617 E-4
0.1	1.00468	1.00500	3.24861 E-4
0.2	1.01972	1.02007	3.49559 E-4
0.3	1.04493	1.04534	4.06892 E-4
0.4	1.08056	1.08107	5.09384 E-4
0.5	1.12696	1.12763	6.70039 E-4
0.6	1.18456	1.18547	9.02486 E-4
0.7	1.25395	1.25517	1.22112 E-3
0.8	1.33579	1.33743	1.64126 E-3
0.9	1.43091	1.43309	2.17931 E-3
1.0	1.54023	1.54308	2.85299 E-3

Table 4: The exact and numerical solutions of example 4.

x_i	Approximate solution	Exact solution	Absolute error
0.0	1.00094	1.	9.4143 E-4
0.1	1.10594	1.10517	7.7156 E-4
0.2	1.222	1.2214	5.9439 E-4
0.3	1.35027	1.34986	4.0876 E-4
0.4	1.49204	1.49182	2.1332 E-4
0.5	1.64873	1.64872	6.5459 E-6
0.6	1.82191	1.82212	2.1332 E-4
0.7	2.0133	2.01375	4.4832 E-4
0.8	2.22484	2.22554	7.0085 E-4
0.9	2.45863	2.4596	9.7372 E-4
1.0	2.71701	2.71828	1.2703 E-3

Then,

$$\begin{aligned}
&\left|F\left(x, u(x), \int_a^b f(x,t,u'(t))\mathrm{d}t, \int_a^x g(x,t,u'(t))\mathrm{d}t\right)\right| \leq \\
&\left|\frac{1}{240}\left(-2x^5 - 6x^2\sin(2x) + 9x\sin^2(x) + 3\sin^3(x)\cos(x)\right) - \frac{1}{48}x\left(\frac{3}{2} - e^{-\sin(1)}\right) - \frac{1}{8}\cos^2(x) - \cos(x)\right| \\
&+ \frac{1}{8}\left|u^2(x)\right| + \frac{1}{8}\int_0^1 \frac{1}{6}\left|tx + x\cos(t)e^{u'(t)}\right|\mathrm{d}t + \frac{1}{8}\int_0^x \frac{1}{5}\left|tx + \sin(x)u'^2(t)\right|\mathrm{d}t,
\end{aligned} \tag{50}$$

and also

$$\begin{aligned}
\left|f(x,t,u'(t)\mathrm{d}t)\right| &\leq \frac{1}{6}(xt) + \frac{1}{6}\left|e^{u'(t)}\right|, \\
\left|g(x,t,u'(t)\mathrm{d}t)\right| &\leq \frac{1}{5}(xt) + \frac{1}{5}\left|u'^2(t)\right|,
\end{aligned} \tag{51}$$

where $M_1(x) = (1/240)(-2x^5 - 6x^2\sin(2x) + 9x\sin^2(x) + 3\sin^3(x)\cos(x)) - (1/48)x((3/2) - e^{-\sin(1)}) - (1/8)\cos^2(x) - \cos(x) \in L^1[a,b]$, $M_2(x,t) = (1/6)(xt) \in L^1[a,b]$, $M_3(x,t) = (1/5)(xt) \in L^1[a,b]$, $C_1 = (1/8)$, $C_2 = (1/6)$, $C_3 = (1/5)$, $b = 1$; then, $2C_1b^2 + C_1C_2b^2 + C_1C_3b^2 = (2/8) + (1/48) + (1/40) = (71/240) < 1$. It is clear that the assumptions (1)–(5) of Theorem 1 hold; therefore, the given nonlocal problem has a continuous solution.

Now, we use the finite difference-trapezoidal method with $N = 10$ to find the numerical solution of this problem. Table 1 and Figure 1 give the comparison between the numerical and exact solutions of this problem.

Through our observation of Table 1, the interval $[0, 1]$ was divided into 10 subintervals of equal length. We obtain solutions at the endpoints of subintervals and show that the method used is effective, and this is evident from the absolute error that was calculated for the difference between the numerical and real solutions. Also, by looking at Figure 1, we find that the numerical solution and the real solution are very close, which means that the numerical solutions are good.

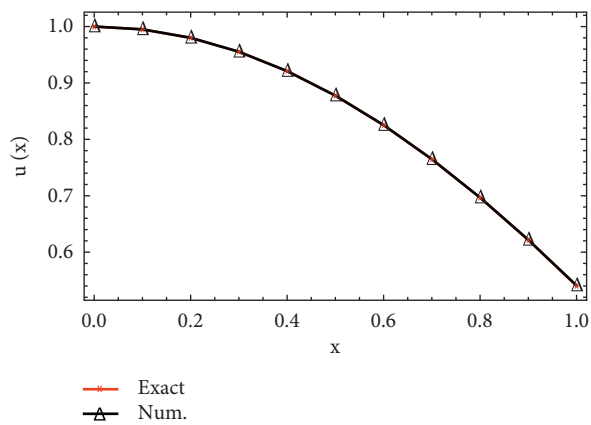

Figure 1: Comparison between the numerical and exact solutions of example 1.

Example 2. Consider the equation

$$\begin{aligned} u''(x) - \frac{1}{7}u(x) = {} & \frac{1}{56}\left(-\frac{1}{2}\left(x^2 + 2\sin(x) - 1\right)\cos(x) - \sin(x)\left(x\sin(x) - \sin(1) - \cos(1)\right)\right) \\ & - \frac{8\sin(x)}{7} + \frac{1}{70}\int_{-1}^{1}\left(tx + \sin(xt)u'(t)\right)\mathrm{d}t \\ & + \frac{1}{56}\int_{-1}^{x}\left(t\cos(x) + t\sin(x)u'(t)\right)\mathrm{d}t, \quad u(-1) + u(1) = 0,\ u'(-1) = \cos(-1). \end{aligned} \tag{52}$$

The exact solution of this problem is $u(x) = \sin(x)$.

Firstly, we apply the assumptions of Theorem 1 to prove that this example has a continuous solution:

$$\begin{aligned} & F\left(x, u(x), \int_a^b f(x,t,u'(t))\mathrm{d}t, \int_a^x g(x,t,u'(t))\mathrm{d}t\right) \\ & = \frac{1}{56}\left(-\frac{1}{2}\left(x^2 + 2\sin(x) - 1\right)\cos(x) - \sin(x)\left(x\sin(x) - \sin(1) - \cos(1)\right)\right) - \frac{8\sin(x)}{7} + \frac{1}{7}u(x) \\ & + \frac{1}{70}\int_{-1}^{1}\left(tx + \sin(xt)u'(t)\right)\mathrm{d}t + \frac{1}{56}\int_{-1}^{x}\left(t\cos(x) + t\sin(x)u'(t)\right)\mathrm{d}t. \end{aligned} \tag{53}$$

Then,

$$\begin{aligned} & \left|F\left(x, u(x), \int_a^b f(x,t,u'(t))\mathrm{d}t, \int_a^x g(x,t,u'(t))\mathrm{d}t\right)\right| \le \\ & \left|\frac{1}{56}\left(-\frac{1}{2}\left(x^2 + 2\sin(x) - 1\right)\cos(x) - \sin(x)\left(x\sin(x) - \sin(1) - \cos(1)\right)\right) - \frac{8\sin(x)}{7}\right| \\ & + \frac{1}{7}|u(x)| + \frac{1}{7}\int_{-1}^{1}\frac{1}{10}\left|tx + \sin(xt)u'(t)\right|\mathrm{d}t + \frac{1}{7}\int_{-1}^{x}\frac{1}{8}\left|t\cos(x) + t\sin(x)u'(t)\right|\mathrm{d}t, \end{aligned} \tag{54}$$

and also

$$\begin{aligned}\left|f\left(x,t,u'(t)\mathrm{d}t\right)\right| &\le \frac{1}{10}|tx| + \frac{1}{10}\left|u'(t)\right|,\\ \left|g\left(x,t,u'(t)\mathrm{d}t\right)\right| &\le \frac{1}{8}|t\ \cos(x)| + \frac{1}{8}\left|u'(t)\right|,\end{aligned} \tag{55}$$

where

$$\begin{aligned}M_1(x) &= \frac{1}{56}\left(-\frac{1}{2}\left(x^2 + 2\ \sin(x) - 1\right)\cos(x) - \sin(x)(x\ \sin(x) - \sin(1) - \cos(1))\right) - \frac{8\ \sin(x)}{7} \in L^1[a,b],\\ M_2(x,t) &= \frac{1}{10}(tx) \in L^1[a,b],\\ M_3(x,t) &= \frac{1}{8}(t\ \cos(x)) \in L^1[a,b],\\ C_1 &= \frac{1}{7},\\ C_2 &= \frac{1}{10},\\ C_3 &= \frac{1}{8},\\ b &= 1.\end{aligned} \tag{56}$$

Then, $2C_1b^2 + C_1C_2b^2 + C_1C_3b^2 = (2/7) + (1/70) + (1/56) = (89/280) < 1$. It is clear that the assumptions (1)–(5) of Theorem 1 hold; therefore, the given nonlocal problem has a continuous solution.

Now, we use the finite difference-trapezoidal method with $N = 10$ to find the numerical solution of this problem. Table 2 and Figure 2 give the comparison between the numerical and exact solutions of this problem.

Through our observation of Table 2, the interval $[-1, 1]$ was divided into 10 subintervals of equal length. We obtain solutions at the endpoints of subintervals and show that the method used is effective, and this is evident from the absolute error that was calculated for the difference between the numerical and real solutions. Also, by looking at Figure 2, we find that the numerical solution and the real solution are very close, which means that the numerical solutions are good.

Example 3. Consider the equation

$$\begin{aligned}u''(x) - \frac{1}{12}u(x) &= \frac{1}{60}\left(-\frac{x^3}{2} - \sinh(x)(x\cosh(x) - \sinh(x)\right) + \frac{11\cosh(x)}{12} + \frac{1}{84}\left(-\frac{\sinh(x)}{2} - \frac{\cosh(x)}{e}\right)\\ &\quad + \frac{1}{84}\int_0^1 (t\sinh(x) + t\cosh(x)u'(t))\mathrm{d}t + \frac{1}{60}\int_0^x (tx + t\sinh(x)u'(t))\mathrm{d}t,\\ \int_0^1 u(x)\mathrm{d}x &= \sinh(1), \quad u'(0) = 0.\end{aligned} \tag{57}$$

The exact solution of this problem is $u(x) = \cosh(x)$.

Firstly, we apply the assumptions of Theorem 1 to prove that this example has a continuous solution:

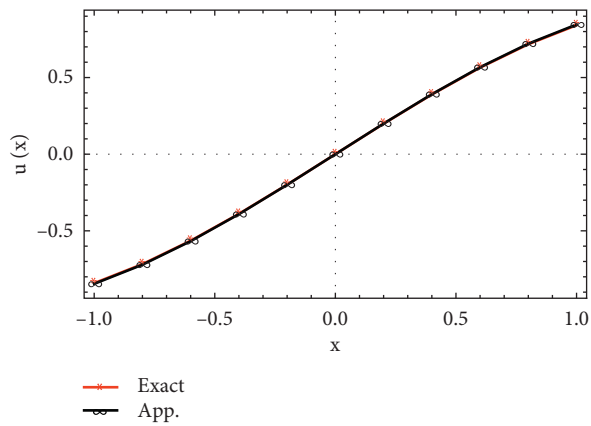

Figure 2: Comparison between the numerical and exact solutions of example 2.

$$F\left(x, u(x), \int_a^b f(x,t,u'(t))\mathrm{d}t, \int_a^x g(x,t,u'(t))\mathrm{d}t\right) = \frac{1}{60}\left(-\frac{x^3}{2} - \sinh(x)(x\cosh(x) - \sinh(x))\right) + \frac{11\cosh(x)}{12} + \frac{1}{84}\left(-\frac{\sinh(x)}{2} - \frac{\cosh(x)}{e}\right) + \frac{1}{12}u(x) + \frac{1}{84}\int_0^1 (t\sinh(x) + t\cosh(x)u'(t))\mathrm{d}t + \frac{1}{60}\int_0^x (tx + t\sinh(x)u'(t))\mathrm{d}t. \tag{58}$$

Then,

$$\left|F\left(x, u(x), \int_a^b f(x,t,u'(t))\mathrm{d}t, \int_a^x g(x,t,u'(t))\mathrm{d}t\right)\right| \leq \left|\frac{1}{60}\left(-\frac{x^3}{2} - \sinh(x)(x\cosh(x) - \sinh(x))\right) + \frac{11\cosh(x)}{12} + \frac{1}{84}\left(-\frac{\sinh(x)}{2} - \frac{\cosh(x)}{e}\right)\right| + \frac{1}{12}|u(x)| + \frac{1}{12}\int_0^1 \frac{1}{7}\left|t\sinh(x) + t\cosh(x)u'(t)\right|\mathrm{d}t + \frac{1}{12}\int_0^x \frac{1}{5}\left|tx + t\sinh(x)u'(t)\right|\mathrm{d}t, \tag{59}$$

and also

$$\left|f(x,t,u'(t)\mathrm{d}t)\right| \leq \frac{1}{7}|t\sinh(x)| + \frac{1}{7}\left|u'(t)\right|, \qquad \left|g(x,t,u'(t)\mathrm{d}t)\right| \leq \frac{1}{5}|tx| + \frac{1}{5}\left|u'(t)\right|, \tag{60}$$

where

$$M_1(x) = \frac{1}{60}\left(-\frac{x^3}{2} - \sinh(x)(x\cosh(x) - \sinh(x))\right) + \frac{11\cosh(x)}{12} + \frac{1}{84}\left(-\frac{\sinh(x)}{2} - \frac{\cosh(x)}{e}\right) \in L^1[a,b],$$

$$M_2(x,t) = \frac{1}{7}(t\sinh(x)) \in L^1[a,b],$$

$$\begin{aligned} M_3(x,t) &= \frac{1}{5}(tx) \in L^1[a,b], \\ C_1 &= \frac{1}{12}, \\ C_2 &= \frac{1}{7}, \\ C_3 &= \frac{1}{5}, \\ b &= 1. \end{aligned} \tag{61}$$

Then, $2C_1b^2 + C_1C_2b^2 + C_1C_3b^2 = (2/12) + (1/84) + (1/60) = (41/210) < 1$. It is clear that the assumptions (1)–(5) of Theorem 1 hold; therefore, the given nonlocal problem has a continuous solution.

Now, we use the finite difference-trapezoidal method with $N = 10$ to find the numerical solution of this problem. Table 3 and Figure 3 give the comparison between the numerical and exact solutions of this problem.

Through our observation of Table 3, the interval $[0,1]$ was divided into 10 subintervals of equal length. We obtain solutions at the endpoints of subintervals and show that the method used is effective, and this is evident from the absolute error that was calculated for the difference between the numerical and real solutions. Also, by looking at Figure 3, we find that the numerical solution and the real solution are very close, which means that the numerical solutions are good.

Example 4. Consider the equation

$$\begin{aligned} u''(x) - \frac{1}{9}u^2(x) &= -\frac{1}{144}(x + 2e^x - 2)x^2 - \frac{1}{324}\left(e^2x + x + 2\right)x + e^x - \frac{e^{2x}}{9} \\ &\quad + \frac{1}{81}\int_0^1\left(xt + x^2tu'^2(t)\right)\mathrm{d}t + \frac{1}{72}\int_0^x\left(tx + x^2u'(t)\right)\mathrm{d}t, \\ u(0.4) + u(0.6) &= 3.31394, \quad u'(0) = 1. \end{aligned} \tag{62}$$

The exact solution of this problem is $u(x) = e^x$.

Firstly, we apply the assumptions of Theorem 1 to prove that this example has a continuous solution:

$$\begin{aligned} &F\left(x, u(x), \int_a^b f(x,t,u'(t))\mathrm{d}t, \int_a^x g(x,t,u'(t))\mathrm{d}t\right) = \\ &\quad -\frac{1}{144}(x + 2e^x - 2)x^2 - \frac{1}{324}\left(e^2x + x + 2\right)x + e^x - \frac{e^{2x}}{9} \\ &\quad + \frac{1}{9}u^2(x) + \frac{1}{81}\int_0^1\left(xt + x^2tu'^2(t)\right)\mathrm{d}t + \frac{1}{72}\int_0^x\left(tx + x^2u'(t)\right)\mathrm{d}t. \end{aligned} \tag{63}$$

Then,

$$\begin{aligned} &\left|F\left(x, u(x), \int_a^b f(x,t,u'(t))\mathrm{d}t, \int_a^x g(x,t,u'(t))\mathrm{d}t\right)\right| \\ &\le \left|-\frac{1}{144}(x + 2e^x - 2)x^2 - \frac{1}{324}\left(e^2x + x + 2\right)x + e^x - \frac{e^{2x}}{9}\right| \\ &\quad + \frac{1}{9}\left|u^2(x)\right| + \frac{1}{9}\int_0^1\frac{1}{9}\left|xt + x^2tu'^2(t)\right|\mathrm{d}t + \frac{1}{9}\int_0^x\frac{1}{8}\left|tx + x^2u'(t)\right|\mathrm{d}t, \end{aligned} \tag{64}$$

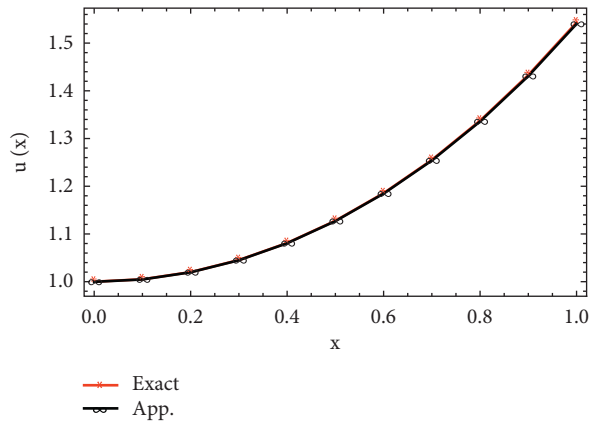

Figure 3: Comparison between the numerical and exact solutions of example 3.

and also

$$\left|f\left(x,t,u'\left(t\right)\mathrm{d}t\right)\right| \leq \frac{1}{9}\left|tx\right| + \frac{1}{9}\left|u'\left(t\right)\right|,$$
$$\left|g\left(x,t,u'\left(t\right)\mathrm{d}t\right)\right| \leq \frac{1}{8}\left|tx\right| + \frac{1}{8}\left|u'\left(t\right)\right|, \tag{65}$$

where

$$M_1\left(x\right) = -\frac{1}{144}\left(x + 2e^x - 2\right)x^2 - \frac{1}{324}\left(e^2x + x + 2\right)x + e^x - \frac{e^{2x}}{9} \in L^1\left[a,b\right],$$
$$M_2\left(x,t\right) = \frac{1}{9}\left(tx\right) \in L^1\left[a,b\right],$$
$$M_3\left(x,t\right) = \frac{1}{8}\left(tx\right) \in L^1\left[a,b\right],$$
$$C_1 = \frac{1}{9},$$
$$C_2 = \frac{1}{9},$$
$$C_3 = \frac{1}{8},$$
$$b = 1. \tag{66}$$

Then, $2C_1b^2 + C_1C_2b^2 + C_1C_3b^2 = (2/9) + (1/81) + (1/72) = (161/684) < 1$. It is clear that the assumptions (1)–(5) of Theorem 1 hold; therefore, the given nonlocal problem has a continuous solution.

Now, we use the finite difference-trapezoidal method with $N = 10$ to find the numerical solution of this problem. Table 4 and Figure 4 give the comparison between the numerical and exact solutions of this problem.

Through our observation of Table 4, the interval $[0,1]$ was divided into 10 subintervals of equal length. We obtain solutions at the endpoints of subintervals and show that the method used is effective, and this is evident from the absolute error that was calculated for the difference between the numerical and real solutions. Also, by looking at Figure 4, we find that the numerical solution and the real solution are very close, which means that the numerical solutions are good.

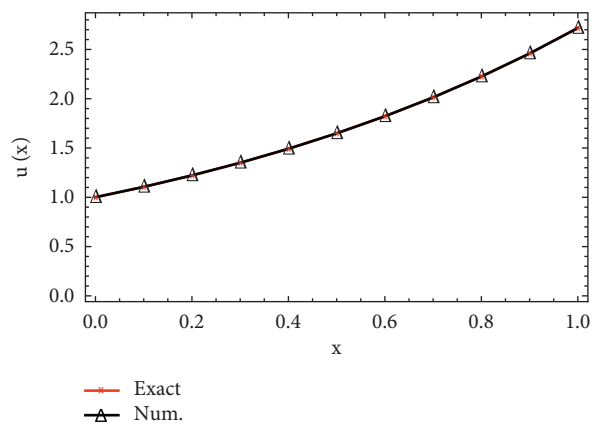

Figure 4: Comparison between the numerical and exact solutions of example 4.

7. Conclusion

The existence and uniqueness of the nonlocal boundary value problem for the Fredholm–Volterra integro-differential equation with the nonlocal condition and the integral condition have been studied. The continuous dependence of the solution on μ_0 and a_j has been introduced. Also, we used the central difference approximations and trapezoidal rule to obtain a numerical solution for problems. The error estimation has been derived in this paper. Finally, we solve some numerical examples to illustrate the accuracy of the proposed method [12].

Data Availability

No data were used to support this study.

Conflicts of Interest

The authors declare that they have no conflicts of interest.

Authors' Contributions

This study was realized in collaboration with equal responsibility. All authors read and approved the final manuscript.

References

[1] A. M. A. El-Sayed and R. G. Ahmed, "Existence of solutions for a functional integro-differential equation with infinite point and integral conditions," *International Journal of Algorithms, Computing and Mathematics*, vol. 5, no. 4, p. 108, 2019.

[2] A. M. A. El-Sayed and R. Gamal, "Infinite point and Riemann-Stieltjes integral conditions for an integro-differential equation," *Nonlinear Analysis Modelling and Control*, vol. 24, pp. 733–754, 2019.

[3] A. M. A. El-sayed, H. El-Owaidy, and R. Gamal Ahmed, "Solvability of a boundary value problem of self-reference functional differential equation with infinite point and integral conditions," *The Journal of Mathematics and Computer Science*, vol. 21, no. 04, pp. 296–308, 2020.

[4] A. M. A. El-Sayed and R. G. Ahmed, "Solvability of a coupled system of functional integro-differential equations with infinite point and Riemann-Stieltjes integral conditions," *Applied Mathematics and Computation*, vol. 370, Article ID 124918, 2020.

[5] F. Mirzaee and S. Piroozfar, "Numerical solution of linear Fredholm integral equations via modified Simpson's quadrature rule," *Journal of King Saud University Science*, vol. 23, no. 1, pp. 7–10, 2011.

[6] I. Rahman, M. M. Parvez, and S. Ghosh, "A new technique for numerical solution of system of Volterra integral equations of the second kind by Simpson's quadrature rule," *Journal of Computer and Mathematical Sciences*, vol. 8, pp. 332–339, 2017.

[7] B. D. Garba and S. L. Bichi, "On solving linear Fredholm integro-differential equations via finite difference-Simpson's approach," *Malaya Journal of Matematik*, vol. 8, no. 2, pp. 469–472, 2020.

[8] A. A. Ibrahim, A. A. S. Zaghrout, K. R. Raslan, and K. K. Ali, "On the analytical and numerical study for nonlinear Fredholm integro-differential equations," *Appl. Math. Inf. Sci*, vol. 14, pp. 921–929, 2020.

[9] P. K. Pandey, "Numerical solution of Linear Fredholm integro-differential equations by non-standard finite difference method," *Applications and Applied Mathematics*, vol. 10, pp. 1019–1026, 2015.

[10] R. Saadati, B. Raftari, H. Adibi, S. M. Vaezpour, and S. Shakeri, "A comparison between the variational iteration method and Trapezoidal rule for solving linear integro-differential equations," *World Applied Sciences Journal*, vol. 4, pp. 321–325, 2008.

[11] F. Ishak and S. Norazura Ahmed, "Developement of extended Trapeziodal method for numerical solution of Volterra integro-differential equations," *International Journal of Mathematics and Computer Science*, vol. 10, pp. 579–582, 2016.

[12] B. Raftari, "Numerical solutions of the linear Volterra integro-differential equations: Homotopy perturbation method and finite difference method," *World Applied Sciences Journal*, vol. 9, pp. 7–12, 2010.

[13] A. N. Kolomogorov and S. V. Fomin, *Inroductory Real Analysis*, Dover Puble. Inc, Downers Grove, IL, USA, 1975.

[14] K. Goeble and W. A. Kirk, *Topics in Metric Fixed Point Theory*, Cambirdge Universty Press, Cambridge, UK, 1990.

Hindawi
Journal of Function Spaces
Volume 2022, Article ID 3438289, 9 pages
https://doi.org/10.1155/2022/3438289

Research Article

A Numerical Method for the Variable-Order Time-Fractional Wave Equations Based on the H2N2 Approximation

Xiao Liu, Yu Bo, and Yuanfeng Jin

College of Science, Yanbian University, Yanji 133002, China

Correspondence should be addressed to Yuanfeng Jin; yfkim@ybu.edu.cn

Received 1 October 2021; Revised 18 November 2021; Accepted 24 November 2021; Published 17 January 2022

Academic Editor: Youssri Hassan Youssri

Aiming at the initial boundary value problem of variable-order time-fractional wave equations in one-dimensional space, a numerical method using second-order central difference in space and H2N2 approximation in time is proposed. A finite difference scheme with second-order accuracy in space and $3-\gamma^*$ order accuracy in time is obtained. The stability and convergence of the scheme are further discussed by using the discrete energy analysis method. A numerical example shows the effectiveness of the results.

1. Introduction

In recent years, due to the non-locality of fractional calculus, more and more problems in physical science, electromagnetism, electrochemistry, diffusion and general transport theory can be described by the fractional calculus approach, among which the Riemann-Liouville fractional derivative and the Caputo fractional derivative are the most widely used [1–4]. At the same time, more and more researchers found that a variety of important dynamical problems exhibit fractional-order behavior that may vary with time, space, or other conditions. This phenomenon indicates that variable-order fractional calculus is a natural choice to provide an effective mathematical framework for the description of complex problems.

In 2020, Shen et al. proposed a new numerical approximation method—the H2N2 approximation [5] for the numerical differential formula of the Caputo fractional derivative of $\gamma \in (1,2)$ and applied it for the constant-order time-fractional wave equations in the following multidimensional space

$$\begin{cases} {}_0^C D_t^{\gamma} u(x,t) = \Delta u + q(x,t),\ x \in \Omega, t \in (0,T], \\ u(x,0) = \varphi(x),\ u_t(x,0) = \psi(x),\ x \in \Omega, \\ u(x,t) = 0, \quad x \in \partial\Omega, t \in [0,T], \end{cases} \tag{1}$$

where $q(x,t), \varphi(x), \psi(x)$ are given sufficiently smooth functions, $\Omega = \prod_{j=1}^{d}(l^{(j)}, r^{(j)}) \subset R^d$, $\partial\Omega$ is the boundary of Ω, $x = (x^{(1)}, x^{(2)}, \cdots, x^{(d)}) \in \Omega$, $\Delta u = \sum_{j=1}^{d} \partial_{x^{(j)}}^2 u$. When $x \in \partial\Omega$, $\varphi(x)$ and $\psi(x)$ satisfy consistency conditions $\varphi(x) = \psi(x) = 0$. It was proved that the proposed scheme has the accuracy of order of $(3-\gamma)$ in time and 2 in space, and it is clear that its theoretical analysis is similar to the L1 method applied in solving the constant-order time-fractional slow diffusion equations.

Motivated by the above literature [6–9], in this work, we consider the numerical solution of the following variable-order time-fractional wave equations in one-dimensional space

$${}_0^C D_t^{\gamma(t)} u(x,t) = u_{xx}(x,t) + f(x,t), x \in (0,L), t \in (0,T]. \tag{2}$$

$$u(x,0) = \varphi(x), u_t(x,0) = \psi(x), x \in (0,L). \tag{3}$$

$$u(0,t) = 0, u(L,t) = 0, t \in [0,T]. \tag{4}$$

where $1 < \gamma(t) < 2, {}_0^C D_t^{\gamma(t)} u(x,t)$ is the variable-order Caputo fractional derivative, $f(x,t), \varphi(x), \psi(x)$ are given sufficiently smooth functions and satisfy $\varphi(0) = \psi(0), \varphi(L) = \psi(L)$. Suppose its solution function $u \in C^{(4,3)}([0,L] \times [0,T])$.

The rest of this paper is organized as follows. In the next section, some necessary notations are introduced. In Section 3, the H2N2-based finite difference scheme for the variable-order time-fractional wave equations is derived. In Section 4, the stability and convergence of the difference scheme are studied. In Section 5, a numerical result is listed to verify the theoretical prediction and the effectiveness of the difference scheme. Finally, a brief conclusion is provided.

2. Preliminary Knowledge and Relevant Lemmas

Definition 1 (see [10]). Suppose the function $f(t)$ is defined on the interval $[0, T], 1 < \gamma(t) < 2$, then the variable-order Caputo fractional derivative is defined as

$$ {}_0^C D_t^{\gamma(t)} f(t) = \frac{1}{\Gamma(2-\gamma(t))} \int_0^t f''(s)(t-s)^{1-\gamma(t)} ds. \tag{5} $$

Next, mesh the solution intervals $[0, L]$ and $[0, T]$, take integers M and N, denote $h = L/M$, $\tau = T/N$, h and τ are called space step and time step, respectively. Denote $x_i = ih (0 \le i \le M)$, $t_k = k\tau (0 \le k \le N)$, $\Omega_h = \{x_i | 0 \le i \le M\}$, $\Omega_\tau = \{t_k | 0 \le k \le N\}$. Define the following grid function spaces

$$ \begin{aligned} U_h &= \{u \mid u = (u_0, u_1, \cdots, u_M)\}, \\ \widehat{U}_h &= \{u | u \in U_h, u_0 = u_M = 0\}. \end{aligned} \tag{6} $$

For grid function $u = \{u_i^k \mid 0 \le i \le M, 0 \le k \le N\}$ defined on $\Omega_h \times \Omega_\tau$, introduce the following notations

$$ \begin{aligned} \delta_x u_{i-1/2}^k &= \frac{1}{h}\left(u_i^k - u_{i-1}^k\right), \\ \delta_x^2 u_i^k &= \frac{1}{h^2}\left(u_{i+1}^k - 2u_i^k + u_{i-1}^k\right), \\ \delta_t u_i^{k+1/2} &= \frac{1}{\tau}\left(u_i^{k+1} - u_i^{k-1}\right), \\ \delta_t^2 u_i^k &= \frac{1}{\tau}\left(\delta_t u_i^{k+1/2} - \delta_t u_i^{k-1/2}\right). \end{aligned} \tag{7} $$

For any grid functions $u, v \in \widehat{U}_h$, denote the following notations

$$ \begin{aligned} (u, v) &= h \sum_{i=1}^{M-1} u_i v_i, \quad \|u\| = \sqrt{(u, u)}, \\ (\delta_x u, \delta_x v) &= h \sum_{i=0}^{M-1} (\delta_x u_{i+1/2})(\delta_x v_{i+1/2}), \\ \|u\|_\infty &= \max_{0 \le i \le M} |u_i|, \quad \|\delta_x u\| = \sqrt{(\delta_x u, \delta_x u)}. \end{aligned} \tag{8} $$

For any function $f(t)$ defined on the interval $[0, t_1]$, using the data $(t_0, f(t_0)), (t_1, f(t_1)), (t_0, f'(t_0))$ to make the quadratic Hermite interpolation polynomial of $f(t)$

$$ H_{2,0}(t) = f(t_0) + f'(t_0)(t - t_0) + \frac{1}{\tau}\left(\delta_t f^{1/2} - f'(t_0)\right)(t - t_0)^2. \tag{9} $$

Taking the twice derivative arrives at

$$ H_{2,0}''(t) = \frac{2}{\tau}\left(\delta_t f^{1/2} - f'(t_0)\right). \tag{10} $$

For any function $f(t)$ defined on the interval $[t_{k-1}, t_{k+1}]$ $(1 \le k \le N-1)$, using three points $(t_{k-1}, f(t_{k-1})), (t_k, f(t_k)), (t_{k+1}, f(t_{k+1}))$ to make the quadratic Newton interpolation polynomial of $f(t)$

$$ \begin{aligned} N_{2,k}(t) = f(t_{k-1}) &+ \left(\delta_t f^{k-1/2}\right)(t - t_{k-1}) \\ &+ \frac{1}{2}\left(\delta_t^2 f^k\right)(t - t_{k-1})(t - t_k). \end{aligned} \tag{11} $$

Taking the second-order derivative yields

$$ N_{2,k}''(t) = \delta_t^2 f^k. \tag{12} $$

On the basis of the above interpolation polynomial, we next discuss the high-precision approximation formula of the variable-order Caputo fractional derivative.

Here, we denote $f^l = f(t_l)$, $\gamma_{n-1/2} = \gamma(t_{n-1/2})$, $t_{n-1/2} = t_n - \tau/2$. Suppose $f(t) \in C^3[t_0, t_n]$ and $1 < \gamma(t) < 2$, then at the half-grid point $t_{n-1/2}$, we have

$$ \begin{aligned} {}_0^C D_t^{\gamma_{n-1/2}} f(t_{n-1/2}) &= \frac{1}{\Gamma(2-\gamma_{n-1/2})} \left[\int_{t_0}^{t_{1/2}} f''(t)(t_{n-1/2} - t)^{1-\gamma_{n-1/2}} dt \right. \\ &\quad \left. + \sum_{k=1}^{n-1} \int_{t_{k-1/2}}^{t_{k+1/2}} f''(t)(t_{n-1/2} - t)^{1-\gamma_{n-1/2}} dt\right] \\ &\approx \frac{1}{\Gamma(2-\gamma_{n-1/2})} \left[\int_{t_0}^{t_{1/2}} H_{2,0}''(t)(t_{n-1/2} - t)^{1-\gamma_{n-1/2}} dt \right. \\ &\quad \left. + \sum_{k=1}^{n-1} \int_{t_{k-1/2}}^{t_{k+1/2}} N_{2,k}''(t)(t_{n-1/2} - t)^{1-\gamma_{n-1/2}} dt\right] = \frac{1}{\Gamma(2-\gamma_{n-1/2})} \\ &\quad \cdot \left[\int_{t_0}^{t_{1/2}} \frac{2}{\tau}\left(\delta_t f^{1/2} - f'(t_0)\right)(t_{n-1/2} - t)^{1-\gamma_{n-1/2}} dt \right. \\ &\quad \left. + \sum_{k=1}^{n-1} \int_{t_{k-1/2}}^{t_{k+1/2}} \left(\delta_t^2 f^k\right)(t_{n-1/2} - t)^{1-\gamma_{n-1/2}} dt\right] = \frac{1}{\Gamma(2-\gamma_{n-1/2})} \\ &\quad \cdot \left[\frac{2}{\tau}\int_{t_0}^{t_{1/2}} (t_{n-1/2} - t)^{1-\gamma_{n-1/2}} dt \cdot \left(\delta_t f^{1/2} - f'(t_0)\right) \right. \\ &\quad \left. + \frac{1}{\tau}\sum_{k=1}^{n-1} \int_{t_{k-1/2}}^{t_{k+1/2}} (t_{n-1/2} - t)^{1-\gamma_{n-1/2}} dt \cdot \left(\delta_t f^{k+1/2} - \delta_t f^{k-1/2}\right)\right] \\ &= \frac{1}{\Gamma(2-\gamma_{n-1/2})} \left[b_{n-1}^{(n,\gamma_{n-1/2})}\left(\delta_t f^{1/2} - f'(t_0)\right) + \sum_{k=1}^{n-1} b_{n-k-1}^{(n,\gamma_{n-1/2})} \right. \\ &\quad \left. \cdot \left(\delta_t f^{k+1/2} - \delta_t f^{k-1/2}\right)\right] = \frac{1}{\Gamma(2-\gamma_{n-1/2})} \\ &\quad \cdot \left[b_0^{(n,\gamma_{n-1/2})} \delta_t f^{n-1/2} - \sum_{k=1}^{n-1}\left(b_{n-k-1}^{(n,\gamma_{n-1/2})} - b_{n-k}^{(n,\gamma_{n-1/2})}\right)\delta_t f^{k-1/2} \right. \\ &\quad \left. - b_{n-1}^{(n,\gamma_{n-1/2})} f'(t_0)\right] \equiv D_t^{\gamma_{n-1/2}} f(t_{n-1/2}). \end{aligned} \tag{13} $$

Here

$$b_{n-1}^{(n,\gamma_{n-1/2})} = \frac{2}{\tau}\int_{t_0}^{t_{1/2}} (t_{n-1/2}-t)^{1-\gamma_{n-1/2}}dt, \tag{14}$$

$$b_{n-k-1}^{(n,\gamma_{n-1/2})} = \frac{1}{\tau}\int_{t_{k-1/2}}^{t_{k+1/2}} (t_{n-1/2}-t)^{1-\gamma_{n-1/2}}dt, \tag{15}$$

where $1 \le k \le n-1$.

Then, it can be calculated that

$$b_k^{(n,\gamma_{n-1/2})} = \begin{cases} \dfrac{\tau^{1-\gamma_{n-1/2}}}{2-\gamma_{n-1/2}}\left[(k+1)^{2-\gamma_{n-1/2}} - k^{2-\gamma_{n-1/2}}\right], & 0 \le k \le n-2, \\ 2\dfrac{\tau^{1-\gamma_{n-1/2}}}{2-\gamma_{n-1/2}}\left[\left(n-\dfrac{1}{2}\right)^{2-\gamma_{n-1/2}} - (n-1)^{2-\gamma_{n-1/2}}\right], & k = n-1. \end{cases} \tag{16}$$

Denote

$$r_n = {}_0^C D_t^{\gamma_{n-1/2}} f(t_{n-1/2}) - D_t^{\gamma_{n-1/2}} f(t_{n-1/2}), \tag{17}$$

we have

$$|r_n| \le C_0 \max_{t_0 \le t \le t_n} \left|f'''(t)\right| \tau^{3-\gamma_{n-1/2}}. \tag{18}$$

Here, $C_0 = 1/8\Gamma(2-\gamma_{n-1/2}) + 1/12\Gamma(3-\gamma_{n-1/2}) + (\gamma_{n-1/2} - 1)/2\Gamma(4-\gamma_{n-1/2})$, the proof process is similar to Theorem 2.1 in Reference [5].

Lemma 2. *For any $n \ge 2$, according to $b_k^{(n,\gamma_{n-1/2})}$ defined by (14)–(15), we have*

$$\frac{\tau^{1-\gamma_{n-1/2}}}{(n-1/2)^{\gamma_{n-1/2}-1}} < b_{n-1}^{(n,\gamma_{n-1/2})} < b_{n-2}^{(n,\gamma_{n-1/2})} < \cdots < b_1^{(n,\gamma_{n-1/2})} < b_0^{(n,\gamma_{n-1/2})} = \frac{\tau^{1-\gamma_{n-1/2}}}{2-\gamma_{n-1/2}}. \tag{19}$$

Proof. According to the formula (14)–(15), we have

$$b_{n-1}^{(n,\gamma_{n-1/2})} = \frac{2\tau^{1-\gamma_{n-1/2}}}{2-\gamma_{n-1/2}}\left[\left(n-\frac{1}{2}\right)^{2-\gamma_{n-1/2}} - (n-1)^{2-\gamma_{n-1/2}}\right], \tag{20}$$

$$b_{n-k-1}^{(n,\gamma_{n-1/2})} = \frac{\tau^{1-\gamma_{n-1/2}}}{2-\gamma_{n-1/2}}\left[(n-k)^{2-\gamma_{n-1/2}} - (n-k-1)^{2-\gamma_{n-1/2}}\right], \quad 1 \le k \le n-1. \tag{21}$$

When $k = n-1$, it can be obtained by calculation

$$b_0^{(n,\gamma_{n-1/2})} = \frac{\tau^{1-\gamma_{n-1/2}}}{2-\gamma_{n-1/2}}. \tag{22}$$

From equations (20) and (21), we have

$$\begin{aligned} b_{n-1}^{(n,\gamma_{n-1/2})} &= 2\tau^{1-\gamma_{n-1/2}}\int_{n-1}^{n-1/2} \xi^{1-\gamma_{n-1/2}}d\xi, \\ b_k^{(n,\gamma_{n-1/2})} &= \tau^{1-\gamma_{n-1/2}}\int_{k}^{k+1} \xi^{1-\gamma_{n-1/2}}d\xi, \\ &0 \le k \le n-2. \end{aligned} \tag{23}$$

Therefore, it can be obtained

$$b_{n-1}^{(n,\gamma_{n-1/2})} < b_{n-2}^{(n,\gamma_{n-1/2})} < \cdots < b_1^{(n,\gamma_{n-1/2})} < b_0^{(n,\gamma_{n-1/2})} = \frac{\tau^{1-\gamma_{n-1/2}}}{2-\gamma_{n-1/2}}. \tag{24}$$

When $n \ge 2$, we have

$$\begin{aligned} \left(1-\frac{1}{2n-1}\right)^{2-\gamma_{n-1/2}} &= 1 - \frac{2-\gamma_{n-1/2}}{2n-1} \\ &+ \frac{(2-\gamma_{n-1/2})(1-\gamma_{n-1/2})}{2!}\left(-\frac{1}{2n-1}\right)^2 \\ &+ \frac{(2-\gamma_{n-1/2})(1-\gamma_{n-1/2})(-\gamma_{n-1/2})}{3!} \\ &\cdot \left(-\frac{1}{2n-1}\right)^3 + \cdots. \end{aligned} \tag{25}$$

From the above formula

$$\begin{aligned} &\left(n-\frac{1}{2}\right)^{2-\gamma_{n-1/2}} - (n-1)^{2-\gamma_{n-1/2}} - \frac{2-\gamma_{n-1/2}}{2(n-1/2)^{\gamma^{n-1/2-1}}} \\ &= \left(n-\frac{1}{2}\right)^{2-\gamma_{n-1/2}}\left[1 - \frac{2-\gamma_{n-1/2}}{2(n-1/2)} - \left(1-\frac{1}{2n-1}\right)^{2-\gamma_{n-1/2}}\right] \\ &= \left(n-\frac{1}{2}\right)^{2-\gamma_{n-1/2}}\left[-\frac{(2-\gamma_{n-1/2})(1-\gamma_{n-1/2})}{2!}\left(-\frac{1}{2n-1}\right)^2\right. \\ &\quad \left. - \frac{(2-\gamma_{n-1/2})(1-\gamma_{n-1/2})(-\gamma_{n-1/2})}{3!}\left(-\frac{1}{2n-1}\right)^3 - \cdots\right] > 0. \end{aligned} \tag{26}$$

And when $n = 1$, we have

$$\left(\frac{1}{2}\right)^{2-\gamma_{n-1/2}} - \frac{2-\gamma_{n-1/2}}{2\cdot(1/2)^{\gamma_{n-1/2}-1}} = \frac{\gamma_{n-1/2}-1}{2^{2-\gamma_{n-1/2}}} > 0. \tag{27}$$

Therefore, it can be seen that

$$b_{n-1}^{(n,\gamma_{n-1/2})} > \frac{2\tau^{1-\gamma_{n-1/2}}}{2-\gamma_{n-1/2}} \cdot \frac{2-\gamma_{n-1/2}}{2(n-1/2)^{\gamma_{n-1/2}-1}} = \frac{\tau^{1-\gamma_{n-1/2}}}{(n-1/2)^{\gamma_{n-1/2}-1}}. \tag{28}$$

To sum up, Lemma 2 is proved. □

Lemma 3 (see [11]). *If the function $f \in C^4[x_{i-1}, x_{i+1}]$, $\lambda \in (x_{i-1}, x_{i+1})$, there is*

$$f''(x_i) = \frac{f(x_{i-1}) - 2f(x_i) + f(x_{i+1})}{h^2} - \frac{h^2}{12} f^{(4)}(\lambda). \tag{29}$$

Lemma 4. *For any positive integer m and any $\psi, V_1, V_2, \cdots, V_N \in \widehat{U}_h$, when*

$$(t_{n+1/2} - t)^{\gamma_{n+1/2}-1} \geq (t_{n-1/2} - t)^{\gamma_{n-1/2}-1}, t \in (0, t_{n-1/2}), t_{n+1/2} \leq T, \tag{30}$$

we have

$$\sum_{n=1}^{m}\left(b_0^{(n,\gamma_{n-1/2})} V^n - \sum_{k=1}^{n-1}\left(b_{n-k-1}^{(n,\gamma_{n-1/2})} - b_{n-k}^{(n,\gamma_{n-1/2})}\right) V^k - b_{n-1}^{(n,\gamma_{n-1/2})}\psi, V^n\right) \geq \frac{1}{2}\left(\sum_{k=1}^{m} b_{m-k}^{(m,\gamma_{m-1/2})}\left\|V^k\right\|^2 - \sum_{n=1}^{m} b_{n-1}^{(n,\gamma_{n-1/2})}\|\psi\|^2\right), \tag{31}$$

where $1 \leq m \leq N$.

Proof. On the basis of [12], it can be seen from the condition

$$\begin{aligned}
&\sum_{n=1}^{m}\left(b_0^{(n,\gamma_{n-1/2})} V^n - \sum_{k=1}^{n-1}\left(b_{n-k-1}^{(n,\gamma_{n-1/2})} - b_{n-k}^{(n,\gamma_{n-1/2})}\right) V^k - b_{n-1}^{(n,\gamma_{n-1/2})}\psi, V^n\right) \\
&= \sum_{n=1}^{m}\left(b_0^{(n,\gamma_{n-1/2})}\|V^n\|^2 - \sum_{k=1}^{n-1}\left(b_{n-k-1}^{(n,\gamma_{n-1/2})} - b_{n-k}^{(n,\gamma_{n-1/2})}\right)\left(V^k, V^n\right)\right. \\
&\quad \left. - b_{n-1}^{(n,\gamma_{n-1/2})}(\psi, V^n)\right) \geq \sum_{n=1}^{m}\left[b_0^{(n,\gamma_{n-1/2})}\|V^n\|^2 - \frac{1}{2}\sum_{k=1}^{n-1}\right. \\
&\quad \left. \cdot\left(b_{n-k-1}^{(n,\gamma_{n-1/2})} - b_{n-k}^{(n,\gamma_{n-1/2})}\right)\left(\left\|V^k\right\|^2 + \|V^n\|^2\right) - \frac{1}{2} b_{n-1}^{(n,\gamma_{n-1/2})}\left(\|\psi\|^2 + \|V^n\|^2\right)\right] \\
&= \frac{1}{2}\sum_{n=1}^{m}\left[\left(2b_0^{(n,\gamma_{n-1/2})} - \sum_{k=1}^{n-1}\left(b_{n-k-1}^{(n,\gamma_{n-1/2})} - b_{n-k}^{(n,\gamma_{n-1/2})}\right) - b_{n-1}^{(n,\gamma_{n-1/2})}\right)\|V^n\|^2\right. \\
&\quad \left. - \sum_{k=1}^{n-1}\left(b_{n-k-1}^{(n,\gamma_{n-1/2})} - b_{n-k}^{(n,\gamma_{n-1/2})}\right)\left\|V^k\right\|^2 - b_{n-1}^{(n,\gamma_{n-1/2})}\|\psi\|^2\right] \\
&= \frac{1}{2}\sum_{n=1}^{m}\left[b_0^{(n,\gamma_{n-1/2})}\|V^n\|^2 - \sum_{k=1}^{n-1} b_{n-k-1}^{(n,\gamma_{n-1/2})}\left\|V^k\right\|^2 + \sum_{k=1}^{n-1} b_{n-k}^{(n,\gamma_{n-1/2})}\left\|V^k\right\|^2\right. \\
&\quad \left. - b_{n-1}^{(n,\gamma_{n-1/2})}\|\psi\|^2\right] = \frac{1}{2}\sum_{n=1}^{m}\left[\sum_{k=1}^{n} b_{n-k}^{(n,\gamma_{n-1/2})}\left\|V^k\right\|^2 - \sum_{k=1}^{n-1} b_{n-k-1}^{(n,\gamma_{n-1/2})}\left\|V^k\right\|^2\right. \\
&\quad \left. - b_{n-1}^{(n,\gamma_{n-1/2})}\|\psi\|^2\right] = \frac{1}{2}\left[\sum_{k=1}^{m}\sum_{n=k}^{m} b_{n-k}^{(n,\gamma_{n-1/2})}\left\|V^k\right\|^2 - \sum_{k=1}^{m-1}\sum_{n=k+1}^{m} b_{n-k-1}^{(n,\gamma_{n-1/2})}\left\|V^k\right\|^2\right. \\
&\quad \left. - \sum_{n=1}^{m} b_{n-1}^{(n,\gamma_{n-1/2})}\|\psi\|^2\right] = \frac{1}{2}\left[b_0^{(m,\gamma_{m-1/2})}\|V^m\|^2\right. \\
&\quad \left. + \sum_{k=1}^{m-1}\left(\sum_{n=k}^{m} b_{n-k}^{(n,\gamma_{n-1/2})} - \sum_{n=k+1}^{m} b_{n-k-1}^{(n,\gamma_{n-1/2})}\right)\left\|V^k\right\|^2 - \sum_{n=1}^{m} b_{n-1}^{(n,\gamma_{n-1/2})}\|\psi\|^2\right] \\
&= \frac{1}{2}\left[b_0^{(m,\gamma_{m-1/2})}\|V^m\|^2 + \sum_{k=1}^{m-1} b_{m-k}^{(m,\gamma_{m-1/2})}\left\|V^k\right\|^2\right. \\
&\quad \left. + \sum_{k=1}^{m-1}\sum_{n=k}^{m-1}\left(b_{n-k}^{(n,\gamma_{n-1/2})} - b_{n-k}^{(n+1,\gamma_{n+1/2})}\right)\left\|V^k\right\|^2 - \sum_{n=1}^{m} b_{n-1}^{(n,\gamma_{n-1/2})}\|\psi\|^2\right].
\end{aligned} \tag{32}$$

When $\gamma(t)$ satisfies the following condition

$$\begin{aligned}
&b_{n-k}^{(n,\gamma_{n-1/2})} - b_{n-k}^{(n+1,\gamma_{n+1/2})} \\
&= \frac{1}{\tau}\int_{t_{k-3/2}}^{t_{k-1/2}}\left[(t_{n-1/2} - t)^{1-\gamma_{n-1/2}} - (t_{n+1/2} - t)^{1-\gamma_{n+1/2}}\right] dt,
\end{aligned} \tag{33}$$

namely

$$(t_{n+1/2} - t)^{\gamma_{n+1/2}-1} \geq (t_{n-1/2} - t)^{\gamma_{n-1/2}-1}. \tag{34}$$

Then, we have

$$\begin{aligned}
&\sum_{n=1}^{m}\left(b_0^{(n,\gamma_{n-1/2})} V^n - \sum_{k=1}^{n-1}\left(b_{n-k-1}^{(n,\gamma_{n-1/2})} - b_{n-k}^{(n,\gamma_{n-1/2})}\right)\cdot V^k - b_{n-1}^{(n,\gamma_{n-1/2})}\psi, V^n\right) \\
&\geq \frac{1}{2}\left(\sum_{k=1}^{m} b_{m-k}^{(m,\gamma_{m-1/2})}\left\|V^k\right\|^2 - \sum_{n=1}^{m} b_{n-1}^{(n,\gamma_{n-1/2})}\|\psi\|^2\right).
\end{aligned} \tag{35}$$

□

Remark 5. Consider the function

$$g(x, y) = x^y, \quad x > 0,\ y > 0. \tag{36}$$

We have

$$\begin{aligned}
\frac{\partial g(x, y)}{\partial x} &= yx^{y-1} > 0, \\
\frac{\partial g(x, y)}{\partial y} &= x^y Inx = \begin{cases} <0, & x \in (0, 1), \\ >0, & x > 1. \end{cases}
\end{aligned} \tag{37}$$

If $T \leq 1$ and $\gamma(t)$ is an non-increasing function on $[0, T]$, then $t_{n+1/2} - t \in (0, 1)$, $t_{n-1/2} - t \in (0, 1)$ and $\gamma_{n+1/2} \leq \gamma_{n-1/2}$, consequently

$$(t_{n+1/2} - t)^{\gamma_{n+1/2}-1} \geq (t_{n-1/2} - t)^{\gamma_{n-1/2}-1}, t \in (0, t_{n-1/2}), t_{n+1/2} \leq T. \tag{38}$$

(30) is valid.

If $T > 1$, $\gamma(t)$ is an non-increasing function on the interval $[0, 1]$ and $\gamma(t)$ is a constant on the interval $[1, T]$, (30) is also valid.

Lemma 6 (see [11]). *For any $\varepsilon > 0, a, b \geq 0$, there is*

$$ab \leq \varepsilon a^2 + \frac{1}{4\varepsilon} b^2. \tag{39}$$

Lemma 7 (see [11]). *For any grid function $u \in \widehat{U}_h$, there is*

$$\|u\|_\infty \leq \frac{\sqrt{L}}{2}\|\delta_x u\|. \tag{40}$$

Lemma 8 (see [13]). *Suppose $\{F^k \mid k \geq 0\}, \{G^k \mid k \geq 1\}$ are two non-negative sequences, $\{G^k\}$ does not decrease with k, if*

$$F^k \leq C\tau \sum_{l=0}^{k} F^l + G^k, \quad k = 1, 2, \cdots, \tag{41}$$

where C is an non-negative constant, when $\tau \leq 2/3C$, then

$$F^k \leq \exp\,(3Ck\tau)\left(C\tau F^0 + 3G^k\right), \quad k = 1, 2, \cdots. \tag{42}$$

3. Establishment of the Difference Scheme

Denote $U_i^n = u(x_i, t_n), 0 \leq i \leq M, 0 \leq n \leq N$; $\varphi_i = \varphi(x_i), \psi_i = \psi(x_i)$, consider (2) at the point $(x_i, t_{n-1/2})$, we have

$$\begin{aligned} {}_0^C D_t^{\gamma_{n-1/2}} u(x_i, t_{n-1/2}) = u_{xx}(x_i, t_{n-1/2}) + f(x_i, t_{n-1/2}), \quad 1 \leq i \\ \leq M-1,\ 1 \leq n \leq N. \end{aligned} \tag{43}$$

Applying (13) to approximate the temporal fractional derivative and central difference quotient (29) to approximate the spatial derivative, we can obtain

$$\begin{aligned} &\frac{1}{\Gamma(2-\gamma_{n-1/2})}\left[b_0^{(n,\gamma_{n-1/2})}\delta_t U_i^{n-1/2} - \sum_{k=1}^{n-1} \cdot\left(b_{n-k-1}^{(n,\gamma_{n-1/2})} - b_{n-k}^{(n,\gamma_{n-1/2})}\right)\delta_t U_i^{k-1/2} - b_{n-1}^{(n,\gamma_{n-1/2})}\psi_i\right] \\ &= \delta_x^2 U_i^{n-1/2} + f_i^{n-1/2} + R_i^{n-1/2}, \quad 1 \leq i \leq M-1,\ 1 \leq n \leq N. \end{aligned} \tag{44}$$

There exists a positive constant C_1 such that

$$\left|R_i^{n-1/2}\right| \leq C_1\left(\tau^{3-\gamma_{n-1/2}} + h^2\right), \quad 1 \leq i \leq M-1,\ 1 \leq n \leq N. \tag{45}$$

Noticing the initial and boundary value conditions (3) and (4), we have

$$\begin{cases} U_i^0 = \varphi_i, \quad 1 \leq i \leq M-1. \\ U_0^n = 0, \quad U_M^n = 0, \quad 0 \leq n \leq N. \end{cases} \tag{46}$$

Omitting the small term $R_i^{n-1/2}$ in the equation and replacing the grid function U_i^n by its numerical approximation u_i^n, we construct the difference scheme for solving the problems (2)–(4) as follows

$$\begin{aligned} &\frac{1}{\Gamma(2-\gamma_{n-1/2})}\left[b_0^{(n,\gamma_{n-1/2})}\delta_t u_i^{n-1/2} - \sum_{k=1}^{n-1} \cdot\left(b_{n-k-1}^{(n,\gamma_{n-1/2})} - b_{n-k}^{(n,\gamma_{n-1/2})}\right)\delta_t u_i^{k-1/2} - b_{n-1}^{(n,\gamma_{n-1/2})}\psi_i\right] \\ &= \delta_x^2 u_i^{n-1/2} + f_i^{n-1/2}, \quad 1 \leq i \leq M-1,\ 1 \leq n \leq N. \end{aligned} \tag{47}$$

$$u_i^0 = \varphi_i, \quad 1 \leq i \leq M-1. \tag{48}$$

$$u_0^n = 0, \quad u_M^n = 0,\ 0 \leq n \leq N. \tag{49}$$

4. Stability and Convergence of the Difference Scheme

Theorem 9. *Suppose $\{u_i^n \mid 0 \leq i \leq M, 0 \leq n \leq N\}$ is the solution of the following difference scheme*

$$\begin{aligned} &\frac{1}{\Gamma(2-\gamma_{n-1/2})}\left[b_0^{(n,\gamma_{n-1/2})}\delta_t u_i^{n-1/2} - \sum_{k=1}^{n-1} \cdot\left(b_{n-k-1}^{(n,\gamma_{n-1/2})} - b_{n-k}^{(n,\gamma_{n-1/2})}\right)\delta_t u_i^{k-1/2} - b_{n-1}^{(n,\gamma_{n-1/2})}\psi_i\right] \\ &= \delta_x^2 u_i^{n-1/2} + p_i^{n-1/2}, \quad 1 \leq i \leq M-1,\ 1 \leq n \leq N, \end{aligned} \tag{50}$$

$$u_i^0 = \varphi_i, \quad 1 \leq i \leq M-1, \tag{51}$$

$$u_0^n = 0, \quad u_M^n = 0,\ 0 \leq n \leq N, \tag{52}$$

where $p_i^{n-1/2}$ is a given perturbation term, when $\tau < 2/3c_0$, it holds that

$$\|\delta_x u^n\|^2 \leq \exp\,(3c_0 T)\left(c_0\tau\left\|\delta_x u^0\right\|^2 + 3Q^n\right), \quad 1 \leq n \leq N. \tag{53}$$

c_0 and Q^n are given in (56) and (64), respectively.

Proof. Taking an inner product (50) with $\Gamma(2-\gamma_{n-1/2})\delta_t u^{n-1/2}$ and summing n from 1 to m, we have

$$\begin{aligned} &\sum_{n=1}^{m}\left[b_0^{(n,\gamma_{n-1/2})}\|\delta_t u^{n-1/2}\|^2 - \sum_{k=1}^{n-1}\left(b_{n-k-1}^{(n,\gamma_{n-1/2})} - b_{n-k}^{(n,\gamma_{n-1/2})}\right)\left(\delta_t u^{k-1/2}, \delta_t u^{n-1/2}\right) - b_{n-1}^{(n,\gamma_{n-1/2})}\left(\psi, \delta_t u^{n-1/2}\right)\right] \\ &= \sum_{n=1}^{m}\Gamma(2-\gamma_{n-1/2})\left(\delta_x^2 u^{n-1/2}, \delta_t u^{n-1/2}\right) + \sum_{n=1}^{m}\Gamma(2-\gamma_{n-1/2})\left(p^{n-1/2}, \delta_t u^{n-1/2}\right), \quad 1 \leq m \leq N. \end{aligned} \tag{54}$$

Noticing that

$$\begin{aligned}
&\sum_{n=1}^{m}\Gamma(2-\gamma_{n-1/2})\left(\delta_x^2u^{n-1/2},\delta_tu^{n-1/2}\right)\\
&\quad=-\frac{1}{2\tau}\sum_{n=1}^{m}\Gamma(2-\gamma_{n-1/2})\left(\|\delta_xu^n\|^2-\|\delta_xu^{n-1}\|^2\right)\\
&\quad=-\frac{1}{2\tau}\sum_{n=1}^{m}\Big\{\Gamma(2-\gamma_n)\|\delta_xu^n\|^2-\Gamma(2-\gamma_{n-1})\|\delta_xu^{n-1}\|^2\\
&\qquad-[\Gamma(2-\gamma_n)-\Gamma(2-\gamma_{n-1/2})]\|\delta_xu^n\|^2-[\Gamma(2-\gamma_{n-1/2})\\
&\qquad-\Gamma(2-\gamma_{n-1})]\|\delta_xu^{n-1}\|^2\Big\}\le-\frac{1}{2\tau}\sum_{n=1}^{m}\\
&\qquad\cdot\left(\Gamma(2-\gamma_n)\|\delta_xu^n\|^2-\Gamma(2-\gamma_{n-1})\|\delta_xu^{n-1}\|^2\right)\\
&\qquad+\frac{1}{2\tau}\sum_{n=1}^{m}[\Gamma(2-\gamma_n)-\Gamma(2-\gamma_{n-1/2})]\|\delta_xu^n\|^2\\
&\qquad+\frac{1}{2\tau}\sum_{n=1}^{m}[\Gamma(2-\gamma_{n-1/2})-\Gamma(2-\gamma_{n-1})]\|\delta_xu^{n-1}\|^2\\
&\quad\le-\frac{1}{2\tau}\sum_{n=1}^{m}\left(\Gamma(2-\gamma_n)\|\delta_xu^n\|^2-\Gamma(2-\gamma_{n-1})\|\delta_xu^{n-1}\|^2\right)\\
&\qquad+\frac{1}{4}c_0\sum_{n=1}^{m}\left(\|\delta_xu^n\|^2+\|\delta_xu^{n-1}\|^2\right),
\end{aligned}\tag{55}$$

where

$$c_0=\max_{0\le t\le T}\left|\frac{d}{dt}\Gamma(2-\gamma(t))\right|.\tag{56}$$

Applying Lemma 4, we have

$$\begin{aligned}
&\frac{1}{2}\left(\sum_{k=1}^{m}b_{m-k}^{(m,\gamma_{m-1/2})}\left\|\delta_tu^{k-1/2}\right\|^2-\sum_{n=1}^{m}b_{n-1}^{(n,\gamma_{n-1/2})}\|\psi\|^2\right)\\
&\quad\le-\frac{1}{2\tau}\sum_{n=1}^{m}\left(\Gamma(2-\gamma_n)\|\delta_xu^n\|^2-\Gamma(2-\gamma_{n-1})\|\delta_xu^{n-1}\|^2\right)\\
&\qquad+\frac{1}{4}c_0\sum_{n=1}^{m}\left(\|\delta_xu^n\|^2+\|\delta_xu^{n-1}\|^2\right)+\sum_{n=1}^{m}\Gamma(2-\gamma_{n-1/2})\\
&\qquad\times\left(p^{n-1/2},\delta_tu^{n-1/2}\right),\quad 1\le m\le N.
\end{aligned}\tag{57}$$

Then, we have

$$\begin{aligned}
&\frac{1}{2}\sum_{k=1}^{m}b_{m-k}^{(m,\gamma_{m-1/2})}\left\|\delta_tu^{k-1/2}\right\|^2+\frac{1}{2\tau}\left(\Gamma(2-\gamma_m)\|\delta_xu^m\|^2-\|\delta_xu^0\|^2\right)\\
&\quad\le\frac{1}{2}\sum_{n=1}^{m}b_{n-1}^{(n,\gamma_{n-1/2})}\|\psi\|^2+\sum_{n=1}^{m}\Gamma(2-\gamma_{n-1/2})\left(p^{n-1/2},\delta_tu^{n-1/2}\right)\\
&\qquad+\frac{1}{2}c_0\sum_{n=0}^{m}\|\delta_xu^n\|^2,\quad 1\le m\le N.
\end{aligned}\tag{58}$$

By Lemma 2, noticing that

$$b_{m-k}^{(m,\gamma_{m-1/2})}>\frac{\tau^{1-\gamma_{m-1/2}}}{(m-1/2)^{\gamma_{m-1/2}-1}}=t_{m-1/2}^{1-\gamma_{m-1/2}},\ b_{n-1}^{(n,\gamma_{n-1/2})}<\frac{\tau^{1-\gamma_{n-1/2}}}{2-\gamma_{n-1/2}}.\tag{59}$$

Then

$$\begin{aligned}
&\frac{1}{2}t_{m-1/2}^{1-\gamma_{m-1/2}}\sum_{k=1}^{m}\left\|\delta_tu^{k-1/2}\right\|^2+\frac{\Gamma(2-\gamma_m)}{2\tau}\|\delta_xu^m\|^2\\
&\quad\le\frac{1}{2\tau}\|\delta_xu^0\|^2+\frac{1}{2}\sum_{n=1}^{m}\frac{\tau^{1-\gamma_{n-1/2}}}{2-\gamma_{n-1/2}}\|\psi\|^2+\sum_{n=1}^{m}\Gamma(2-\gamma_{n-1/2})\\
&\qquad\cdot\left(\frac{t_{m-1/2}^{1-\gamma_{m-1/2}}}{2\Gamma(2-\gamma_{n-1/2})}\|\delta_tu^{n-1/2}\|^2+\frac{\Gamma(2-\gamma_{n-1/2})}{2t_{m-1/2}^{1-\gamma_{m-1/2}}}\|p^{n-1/2}\|^2\right)\\
&\qquad+\frac{1}{2}c_0\sum_{n=0}^{m}\|\delta_xu^n\|^2.
\end{aligned}\tag{60}$$

We use the Cauchy inequality for the inner product $(p^{n-1/2},\delta_tu^{n-1/2})$, the above equation can be simplified

$$\begin{aligned}
\frac{\Gamma(2-\gamma_m)}{2\tau}\|\delta_xu^m\|^2&\le\frac{1}{2\tau}\|\delta_xu^0\|^2+\frac{1}{2}\sum_{n=1}^{m}\frac{\tau^{1-\gamma_{n-1/2}}}{2-\gamma_{n-1/2}}\|\psi\|^2\\
&\quad+\sum_{n=1}^{m}\frac{\Gamma^2(2-\gamma_{n-1/2})}{2t_{m-1/2}^{1-\gamma_{m-1/2}}}\|p^{n-1/2}\|^2\\
&\quad+\frac{1}{2}c_0\sum_{n=0}^{m}\|\delta_xu^n\|^2.
\end{aligned}\tag{61}$$

Multiplying by $2\tau/\Gamma(2-\gamma_m)$, then we have

$$\begin{aligned}
\|\delta_xu^m\|^2\le\frac{1}{\Gamma(2-\gamma_m)}&\Bigg(\|\delta_xu^0\|^2+\tau\sum_{n=1}^{m}\frac{\tau^{1-\gamma_{n-1/2}}}{2-\gamma_{n-1/2}}\|\psi\|^2\\
&+\tau t_{m-1/2}^{\gamma_{m-1/2}-1}\sum_{n=1}^{m}\Gamma^2(2-\gamma_{n-1/2})\|p^{n-1/2}\|^2+\tau c_0\sum_{n=0}^{m}\|\delta_xu^n\|^2\Bigg).
\end{aligned}\tag{62}$$

Note that Γ is decreasing on the interval $(0,1]$. Since $0<2-\gamma(t)\le1$, $\Gamma(2-\gamma(t))^{-1}\le1$. Then

$$\begin{aligned}
\|\delta_xu^m\|^2&\le\|\delta_xu^0\|^2+\tau\sum_{n=1}^{m}\frac{\tau^{1-\gamma_{n-1/2}}}{2-\gamma_{n-1/2}}\|\psi\|^2\\
&\quad+\tau t_{m-1/2}^{\gamma_{m-1/2}-1}\sum_{n=1}^{m}\Gamma^2(2-\gamma_{n-1/2})\|p^{n-1/2}\|^2\\
&\quad+\tau c_0\sum_{n=0}^{m}\|\delta_xu^n\|^2.
\end{aligned}\tag{63}$$

Let

$$Q^m = \left\|\delta_x u^0\right\|^2 + \tau \sum_{n=1}^{m} \frac{\tau^{1-\gamma_{n-1/2}}}{2-\gamma_{n-1/2}} \|\psi\|^2 + \tau t_{m-1/2}^{\gamma_{m-1/2}-1} \sum_{n=1}^{m} \Gamma^2 \cdot (2-\gamma_{n-1/2}) \left\|p^{n-1/2}\right\|^2, \quad 1 \le m \le N. \tag{64}$$

Then

$$\|\delta_x u^m\|^2 \le \tau c_0 \sum_{n=0}^{m} \|\delta_x u^n\|^2 + Q^m. \tag{65}$$

It is easy to know Q^m does not decrease with m. According to Lemma 8, when $\tau < 2/3c_0$, we have

$$\|\delta_x u^m\|^2 \le \exp\left(3c_0 T\right)\left(c_0 \tau \left\|\delta_x u^0\right\|^2 + 3Q^m\right), \quad 1 \le m \le N. \tag{66}$$

Theorem 9 is proved. We can say that the difference scheme is stable. □

Theorem 10. *Assume $\{u(x_i, t_n)\}$ and $\{u_i^n\}$ are solutions of problems (2)–(4) and difference scheme (47)–(49), respectively. Denote*

$$e_i^n = u(x_i, t_n) - u_i^n, \quad 0 \le i \le M, \quad 0 \le n \le N. \tag{67}$$

Then, there exists a positive constant C_2, when $\tau < 2/3c_0$, $n\tau \le T$, such that

$$\|e^n\|_\infty \le \frac{\sqrt{L}}{2} C_2 \left(\tau^{3-\gamma^*} + h^2\right), \quad 0 \le n \le N, \tag{68}$$

where $C_2 = \sqrt{3TL} C_1 \exp\left(3c_0 T/2\right)$ and $\gamma^* = \max_{0 \le t \le T} \gamma(t)$.

Proof. Subtracting (44) and (46) from (47)–(49), we obtain the system of error equations

$$\begin{cases} \dfrac{1}{\Gamma(2-\gamma_{n-1/2})}\left[b_0^{(n,\gamma_{n-1/2})} \delta_t e_i^{n-1/2} - \displaystyle\sum_{k=1}^{n-1}\left(b_{n-k-1}^{(n,\gamma_{n-1/2})} - b_{n-k}^{(n,\gamma_{n-1/2})}\right)\delta_t e_i^{k-1/2}\right] = \delta_x^2 e_i^{n-1/2} + R_i^{n-1/2}, \\ 1 \le i \le M-1, \quad 1 \le n \le N, \\ e_i^0 = 0, \quad 1 \le i \le M-1, \\ e_0^n = 0, \quad e_M^n = 0, \quad 0 \le n \le N. \end{cases} \tag{69}$$

Applying Theorem 9 and (45), it yields

$$\|\delta_x e^n\|^2 \le C_2^2 \left(\tau^{3-\gamma^*} + h^2\right)^2, \tag{70}$$

where $\gamma^* = \max_{0 \le t \le T} \gamma(t)$.

Applying Lemma 7, it yields

$$\|e^n\|_\infty \le \frac{\sqrt{L}}{2} \|\delta_x e^n\| \le \frac{\sqrt{L}}{2} C_2 \left(\tau^{3-\gamma^*} + h^2\right). \tag{71}$$

The proof is ended. □

Table 1: Errors and temporal convergence orders, $M = 1000$.

$\gamma(t)$	τ	$E(h,\tau)$	Order_τ
$2-t^2$	1/512	$8.7295e-4$	0
	1/1024	$4.2265e-4$	1.05
	1/2048	$2.0502e-4$	1.04
	1/4096	$9.9746e-5$	1.04
$1+e^{-t}$	1/512	$4.0772e-4$	0
	1/1024	$1.8602e-4$	1.13
	1/2048	$8.5528e-5$	1.12
	1/4096	$3.9764e-5$	1.10
$\frac{6+\cos t}{4}$	1/512	$3.8173e-4$	0
	1/1024	$1.5945e-4$	1.26
	1/2048	$6.6746e-5$	1.26
	1/4096	$2.8186e-5$	1.24

5. Numerical Example

In order to verify the accuracy of the finite difference scheme, several different types of variable-order index $\gamma(t) \in (1,2)$ are used to solve the variable-order fractional wave equations (2)–(4) in 1D case. The scheme is implemented in MATLAB (R2019a).

Here, we take $L = \pi$, $T = 1$. The source term of equation (2)

$$f(x,t) = \left(\frac{6}{\Gamma(4-\gamma(t))} t^{3-\gamma(t)} + \frac{6}{\Gamma(3-\gamma(t))} t^{2-\gamma(t)} + t^3 + 3t^2 + 1\right) \sin x, \tag{72}$$

Table 2: Errors and spatial convergence orders, $N = 20000$.

$\gamma(t)$	h	$E(h,\tau)$	Order_h
$2-t^2$	$\pi/5$	$3.2641e-2$	0
	$\pi/10$	$8.6512e-3$	1.92
	$\pi/20$	$2.1801e-3$	1.99
	$\pi/40$	$5.5869e-4$	1.96
$1+e^{-t}$	$\pi/5$	$3.1901e-2$	0
	$\pi/10$	$8.4489e-3$	1.92
	$\pi/20$	$2.1209e-3$	1.99
	$\pi/40$	$5.3548e-4$	1.99
$\frac{6+\cos t}{4}$	$\pi/5$	$3.0356e-2$	0
	$\pi/10$	$8.0401e-3$	1.92
	$\pi/20$	$2.0164e-3$	2.00
	$\pi/40$	$5.0707e-4$	1.99

the initial value

$$u(x,0) = \sin x, \quad x \in [0,\pi], \tag{73}$$

the boundary value

$$u(0,t) = u(\pi,t) = 0, \quad t \in [0,1], \tag{74}$$

the exact solution is given by

$$u(x,t) = \left(t^3 + 3t^2 + 1\right) \sin x. \tag{75}$$

Define the error of the numerical solution

$$E(h,\tau) = \max_{0\le k\le N} \left\| U^k - u^k \right\|_\infty, \tag{76}$$

the temporal convergence order

$$\text{Order}_\tau = \log_2\left(\frac{E(h,2\tau)}{E(h,\tau)}\right), \tag{77}$$

the spatial convergence order

$$\text{Order}_h = \log_2\left(\frac{E(2h,\tau)}{E(h,\tau)}\right). \tag{78}$$

Denote $M = 1000$, for different $\gamma(t) = 2 - t^2$, $1 + e^{-t}$, $(6 + \cos t)/4$. The time step τ is varied from 1/512 to 1/4096, where $N = 512$, 1024, 2048, 4096. Table 1 shows the errors and temporal convergence orders of the difference scheme (47)–(49). It can be seen from Table 1 that the difference scheme (47)–(49) has a precision of approximately $3 - \gamma^*$ order in time. The computational results are in good agreement with theoretical results.

Take a fixed and sufficiently small time step $\tau = 1/20000$, for different $\gamma(t) = 2 - t^2$, $1 + e^{-t}$, $(6 + \cos t)/4$, verify space step h from $\pi/5$ to $\pi/40$, where $N = 20000$, $M = 5, 10, 20, 40$. Table 2 shows the errors and spatial convergence orders of the difference scheme (47)–(49). It can be seen from Table 2 that the difference scheme (47)–(49) in the space has an accuracy of approximately 2 order, which is consistent with the theoretical results.

6. Conclusions

In this paper, we consider a numerical approximation method for the variable-order Caputo fractional derivative—H2N2 approximation, and give the corresponding calculation formula. Secondly, we use this formula to solve the one-dimensional variable-order time-fractional wave equations and discuss the stability and convergence of the equations by the discrete energy analysis method. Finally, a numerical example verifies the effectiveness of the scheme.

Data Availability

The data used to support the findings of this study are included within the article.

Conflicts of Interest

The authors declare that they have no conflicts of interest.

Acknowledgments

The work is supported by the National Natural Science Foundation of China (11761074), the Natural Science Foundation of Jilin Province (2020122336JC), and the Program for Young and Middle-aged Leading Talents in Scientific and Technological Innovation of Jilin Province (20200301053RQ).

References

[1] X. Zhao, Z. Z. Sun, and G. E. Karniadakis, "Second-order approximations for variable order fractional derivatives: Algorithms and applications," *Journal of Computational Physics*, vol. 293, pp. 184–200, 2015.

[2] Z. W. Fang, H. W. Sun, and H. Wang, "A fast method for variable-order Caputo fractional derivative with applications to time-fractional diffusion equations," *Computers and Mathematics with Applications*, vol. 80, no. 5, pp. 1443–1458, 2020.

[3] S. Chen, F. Liu, P. Zhuang, and V. Anh, "Finite difference approximations for the fractional Fokker-Planck equation," *Applied Mathematical Modelling*, vol. 33, no. 1, pp. 256–273, 2009.

[4] J. W. Guo, *The Research on the Asymptotic Expansions of Solutions to Two Kinds of Variable-Order Fractional Equations and Related Numerical Algorithms*, Tianjin Normal University, 2020.

[5] J. Y. Shen, C. P. Li, and Z. Z. Sun, "An H2N2 interpolation for Caputo derivative with order in (1, 2) and its application to time-fractional wave equations in more than one space dimension," *Journal of Scientific Computing*, vol. 83, no. 2, pp. 1–29, 2020.

[6] R. L. Du, A. A. Alikhanov, and Z. Z. Sun, "Temporal second order difference schemes for the multi-dimensional variable-order time fractional sub-diffusion equations," *Computers*

Mathematics with Applications, vol. 79, no. 10, pp. 2952–2972, 2020.

[7] H. F. Ding, "The development of higher-order numerical differential formulas of Caputo derivative and their applications (I)," *Computers and Mathematics with Applications*, vol. 84, pp. 203–223, 2021.

[8] Y. F. Liu, *A Compact Finite Difference Scheme for Variable Order Time Diffusion Equation*, Shandong University, 2018.

[9] X. M. Ma, *Finite Difference/Spectral Methods for Variable-Order Fractional Diffusion Equations*, Xiamen University, 2017.

[10] H. G. Sun, W. Chen, H. Wei, and Y. Q. Chen, "A comparative study of constant-order and variable-order fractional models in characterizing memory property of systems," *The European Physical Journal Special Topics*, vol. 193, no. 1, pp. 185–192, 2011.

[11] Z. Z. Sun, *Numerical Methods for Partial Differential Equations*, Science Press, Beijing, 2012.

[12] Z. Z. Sun, C. C. Ji, and R. L. Du, "A new analytical technique of the L-type difference schemes for time fractional mixed subdiffusion and diffusion-wave equations," *Applied Mathematics Letters*, vol. 102, 2020.

[13] R. Liu, *Finite Difference Methods for Solving A Class of Multi-Term Time Fractional Diffusion-Wave Equations with the Spatial Fourth-Order Derivative*, Nanjing University of Posts and Telecommunications, 2018.

Hindawi
Journal of Function Spaces
Volume 2022, Article ID 9512048, 20 pages
https://doi.org/10.1155/2022/9512048

Research Article

Chebyshev Polynomials of Sixth Kind for Solving Nonlinear Fractional PDEs with Proportional Delay and Its Convergence Analysis

Khadijeh Sadri [1,2] **and Hossein Aminikhah** [1,2]

[1] *Department of Applied Mathematics and Computer Science, Faculty of Mathematical Sciences, University of Guilan, P.O. Box 41938-19141, Rasht, Iran*
[2] *Center of Excellence for Mathematical Modelling, Optimization and Combinational Computing (MMOCC), University of Guilan, P.O. Box 41938-19141, Rasht, Iran*

Correspondence should be addressed to Hossein Aminikhah; aminikhah@guilan.ac.ir

Received 27 October 2021; Accepted 6 December 2021; Published 7 January 2022

Academic Editor: Youssri Hassan Youssri

This work devotes to solving a class of delay fractional partial differential equations that arises in physical, biological, medical, and climate models. For this, a numerical scheme is implemented that applies operational matrices to convert the main problem into a system of algebraic equations; then, solving the resultant system leads to an approximate solution. The two-variable Chebyshev polynomials of the sixth kind, as basis functions in the proposed method, are constructed by the one-variable ones, and their operational matrices are derived. Error bounds of approximate solutions and their fractional and classical derivatives are computed. With the aid of these bounds, a bound for the residual function is estimated. Three illustrative examples demonstrate the simplicity and efficiency of the proposed method.

1. Introduction

Mathematical modeling of some physical and biological phenomena leads to delay fractional differential equations (DFDEs) [1–3]. The independent variables t and x represent time and position in space or size of cells, and so on. The solutions can stand for temperature densities of cells, chemicals, etc. Hardly obtaining exact solutions to these equations necessitates mathematicians to construct some vigorous numerical and semianalytical schemes to handle solving these problems. Nevertheless, few methods exist for solving delay partial differential equations. The interest of scientists and mathematicians in DFDEs has resulted in the presentation of efficient schemes to solve this category of equations. For example, Pimenov and Hendy presented a difference scheme for a class of fractional diffusion equations with fixed time delay [4]. A compact difference scheme was constructed in [5] for the numerical solution of one-dimensional fractional parabolic differential equations with delay. Hendy et al. [6] introduced a Crank–Nicolson difference approximation for solving multiterm time-fractional diffusion equations with delay. Nandal and Pandey constructed a linearized compact difference scheme for fourth-order nonlinear fractional subdiffusion with time delay [7].

One of the most popular methods for solving diverse functional equations is the spectral method. The nature of the spectral methods has been joined with the orthogonal polynomials and functions. Orthogonal polynomials are utilized as basis functions in many numerical methods; hence, addressing the properties of orthogonal polynomials is important. For example, some properties of the generalized Gegenbauer polynomials were studied in [8, 9]. Bracciali et al. dealt with a class of Sobolev orthogonal polynomials and Hahn polynomials on the unit circle in [10]. Asymptotic approximations of Jacobi polynomials and their zeros were given in [11]. The shifted Chebyshev polynomials of the third kind were proposed in [12] to solve multiterm variable-order fractional differential equations. The

Chebyshev polynomials of the first kind were used by Vlasic et al. [13] as basis functions to introduce a spline-like parametric model for compressive imaging. Nemati et al. [14] applied the second-kind Chebyshev polynomials for fractional integrodifferential equations with weakly singular kernels. Dahmen and Glorieux applied an extension of the Legendre polynomial method to model coupled Lamb wave parameters for defect detection in anisotropic composite three-layer with Kelvin–Voigt viscoelasticity [15]. A Legendre orthogonal polynomial method was proposed to calculate the reflection and transmission coefficients of plane wave at the liquid interface of a liquid-loaded functionally gradient material plate [16]. Masjed–Jamei [17] presented two new classes of orthogonal polynomials which are called Chebyshev polynomials of fifth and sixth kinds. Abd-Elhameed and Youssri presented a new numerical algorithm based on the sixth-kind Chebyshev polynomials for solving some linear and nonlinear fractional-order differential equations [18]. In [19], a new orthogonal wavelet based on the sixth-kind Chebyshev polynomials was constructed to obtain the solution of fractional optimal control problems. Abd-Elhameed used the sixth-kind Chebyshev polynomials for obtaining a numerical solution of nonlinear one-dimensional Burgers' equations [20]. Atta et al. [21] employed shifted fifth-kind Chebyshev polynomials for the numerical solution of one-dimensional linear hyperbolic partial differential equations. A sixth-kind Chebyshev collocation method was considered in [22] for solving a class of variable-order fractional nonlinear quadratic integrodifferential equations. Bivariate Chebyshev polynomials of the fifth kind were utilized in [23] for variable-order time-fractional partial integrodifferential equations with the weakly singular kernel. Sadri and Aminikhah [24] employed fifth-kind Chebyshev polynomials for solving multiterm variable-order time-fractional diffusion-wave equations.

Recently, spectral methods coupled with operational matrices have attracted the attention of many mathematicians and researchers. The advantage of applying operational matrices is to express the derivatives of the orthogonal polynomials as basis functions in terms of the linear combinations of original polynomials and rewrite these combinations as a sparse matrix form which decreases the computational costs [14, 20, 21, 24, 25]. In the current work, a class of time-fractional partial differential equations with the proportional delay as the following form is considered [26, 27]:

$$ {}_0^C\mathscr{D}_t^\sigma \mathbf{u}(x,t) + \mathscr{L}[\mathbf{u}(x,t)] + \mathscr{N}[\mathbf{u}(q_1x, q_2t)] = \mathbf{Q}(x,t), (x,t) \in \Omega, \tag{1} $$

with the conditions

$$ \begin{aligned} \mathbf{u}(x,0) &= h(x), \\ \mathbf{u}(0,t) &= g_1(t), \\ \mathbf{u}_x(x,t) &= g_2(t), \end{aligned} \tag{2} $$

where ${}_0^CD_t^\sigma$, $0 < \sigma \le 1$ is the Caputo operator, $\Omega = [0,1] \times [0,1]$, $0 < q_i \le 1, i = 1, 2$, and $\mathscr{L}$ and $\mathscr{N}$ are linear and nonlinear differential operators, respectively. In [26, 27], the homotopy perturbation and natural decomposition methods have been applied for solving problems (1) and (2). The two above-mentioned methods provided approximate solutions based on the Taylor expansions of time parts of the solutions which have only good accuracy for the classical case $\sigma = 1$ [26, 27]. The goal of the present paper is to construct a scheme using the sixth-kind Chebyshev polynomials; hence, integral operational matrices of integer and fractional orders are derived. Moreover, an operational matrix is constructed to show the relation between the original basis and its delay form. Then, obtained matrices are utilized to obtain corresponding operational matrices for the two-variable basis. Resultant matrices accompanying the collocation method convert the main problem (1) and (2) into a system of algebraic equations, the solving of which leads to an approximate solution. It is worth noting that the obtained nonlinear algebraic system can be solved using Newton's iteration method.

The rest of the paper is structured as follows: Section 2 recalls some basic definitions of fractional calculus and its properties. The one- and two-variable Chebyshev polynomials of the sixth kind are introduced, and their operational matrices are constructed in Section 3. The idea of the proposed method is described and the error analysis is presented in Section 4. The accuracy and efficiency of the scheme are successfully demonstrated by implementing the algorithm on three examples in Section 5. Finally, a conclusion is given in Section 6.

2. Preliminaries

In this section, some definitions that are useful throughout the paper are presented.

Definition 1. A real function $f(t), t > 0$ belongs to the space $C_q, q \in \mathbb{R}$ if a real number $p > q$ exists such that $f(t) = t^p f_1(t)$ where $f_1(t) \in [0,\infty)$, and it belongs to the space C_q^n, $n \in \mathbb{N}$ if and only if $f^{(n)}(t) \in C_q$ [28].

Definition 2. Suppose that $f(t) \in C_q, t > 0$ and $q > -1$. The Riemann-Liouville fractional integral of the order $\sigma > 0$ is defined as [28]

$$ {}_0^{RL}\mathscr{I}_t^\sigma f(t) = \begin{cases} \dfrac{1}{\Gamma(\sigma)} \displaystyle\int_0^t (t-s)^{\sigma-1} f(s)ds, & \sigma > 0, \\ f(t), & \sigma = 0. \end{cases} \tag{3} $$

Definition 3. The Caputo fractional derivative of the order $\sigma > 0$ of the funcion $f(t) \in C_q, t > 0$ and $q > -1$ is given by the following expression [28]:

$$ {}_0^C\mathscr{D}_t^\sigma f(t) = \begin{cases} \dfrac{1}{\Gamma(m-\sigma)} \displaystyle\int_0^t (t-s)^{m-\sigma-1} \dfrac{d^m f(s)}{ds^m} ds, & m-1 < \sigma \le m, \\ f(t), & \sigma = 0. \end{cases} \tag{4} $$

The following properties of these operators hold:

$$ \begin{gathered} {}_0^C\mathscr{D}_t^\sigma t^m = \begin{cases} \dfrac{\Gamma(m+1)\, t^{m-\sigma}}{\Gamma(m-\sigma+1)}, & m \ge \sigma, \\ 0, & m < \sigma, \end{cases} \\ {}_0^{RL}\mathscr{I}_t^\sigma t^m = \frac{\Gamma(m+1)\, t^{m+\sigma}}{\Gamma(m+\sigma+1)}, \\ {}_0^C\mathscr{D}_t^{\sigma_1}\, {}_0^C\mathscr{D}_t^{\sigma_2} f(t) = {}_0^C\mathscr{D}_t^{\sigma_1+\sigma_2} f(t), \\ {}_0^C\mathscr{D}_t^{\sigma}\, {}_0^{RL}\mathscr{I}_t^{\sigma} f(t) = f(t), \\ {}_0^{RL}\mathscr{I}_t^{\sigma}\, {}_0^C\mathscr{D}_t^{\sigma} \mathrm{f}(t) = \mathrm{f}(t) - \mathrm{f}(0), \quad 0 < \sigma < 1. \end{gathered} \tag{5} $$

3. Sixth-Kind Chebyshev Polynomials and Their Operational Matrices

The family of Chebyshev polynomials has found popularity in different spectral and pseudospectral methods [12–14, 18, 19, 21]. A class of the Chebyshev polynomials, called sixth-kind Chebyshev polynomials, was proposed for the first time in [18] to solve fractional ordinary differential equations. In this section, first, the shifted form of these polynomials is introduced over $[0, 1]$; then, two-variable Chebyshev polynomials of the sixth kind are constructed using them.

3.1. One-Variable Chebyshev Polynomials of the Sixth Kind. The following recurrence relation holds for the sixth-kind Chebyshev polynomials

$$ \begin{gathered} \bar{\mathscr{Y}}_j(z) = z\bar{\mathscr{Y}}_{j-1}(z) - \theta_{j+1}\bar{\mathscr{Y}}_{j-2}(z), \quad j \ge 2, z \in [-1, 1], \\ \bar{\mathscr{Y}}_0(z) = 1, \bar{\mathscr{Y}}_1(z) = z, \end{gathered} \tag{6} $$

where

$$ \theta_j = \frac{j(j+1) + (-1)^j(2j+1) + 1}{4j(j+1)}. \tag{7} $$

These polynomials are orthogonal with respect to the weight function $\bar{w}(z) = z^2\sqrt{1-z^2}$, that is,

$$ \int_{-1}^1 \bar{\mathscr{Y}}_i(z)\bar{\mathscr{Y}}_j(z) z^2 \sqrt{1-z^2} dz = \bar{\hbar}_i \delta_{ij}, \tag{8} $$

where

$$ \bar{\hbar}_i = \begin{cases} \dfrac{\pi}{2^{2i+3}}, & i \text{ even}, \\ \dfrac{\pi(i+3)}{2^{2i+3}(i+1)}, & i \text{ odd}. \end{cases} \tag{9} $$

By the change of variable $z = 2t - 1$, the shifted Chebyshev polynomials $\mathscr{Y}_i(t) = \bar{\mathscr{Y}}_i(2t-1)$ are orthogonal regarding the weight function $w(t) = (2t-1)^2\sqrt{t-t^2}$ on the interval $[0, 1]$,

$$ \int_0^1 \mathscr{Y}_i(t)\mathscr{Y}_j(t)(2t-1)^2\sqrt{t-t^2} dt = \hbar_i \delta_{ij}, \tag{10} $$

and

$$ \bar{\hbar}_i = \begin{cases} \dfrac{\pi}{2^{2i+5}}, & i \text{ even}, \\ \dfrac{\pi(i+3)}{2^{2i+5}(i+1)}, & i \text{ odd}. \end{cases} \tag{11} $$

The series form of the shifted Chebyshev polynomials of the sixth kind is as follows:

$$ \mathscr{Y}_j(t) = \sum_{r=0}^{j} \varsigma_{r,j} t^r, \tag{12} $$

where

$$ \varsigma_{r,j} = \frac{2^{2r-j}}{(2r+1)!} \begin{cases} \displaystyle\sum_{l=\lfloor (r+1)/2 \rfloor}^{j/2} \frac{(-1)^{(j/2)+l+r}(2l+r+1)!}{(2l-r+1)!}, & j \text{ even}, \\ \dfrac{2}{j+1} \displaystyle\sum_{l=\lceil r/2 \rceil}^{(j-1)/2} \frac{(-1)^{((j+1)/2)+l+r}(l+1)(2l+r+2)!}{(2l-r+1)!}, & j \text{ odd}. \end{cases} \tag{13} $$

Every square-integrable function $v(t) \in L_w^2(I)$, $I = [0, 1]$ can be expanded in the shifted sixth-kind Chebyshev polynomials as

$$ v(t) = \sum_{j=0}^{\infty} V_j \mathscr{Y}_j(t), \quad t \in I, \tag{14} $$

where the coefficients V_j are computed as

$$ V_j = \frac{1}{\hbar_j} \int_0^1 v(t)\, \mathscr{Y}_j(t)\, w(t) dt. \tag{15} $$

The first few coefficients in (14) practically keep information of function $v(t)$. In other words, a finite series can present an approximation to $v(t)$ as

$$v(t) \approx v_N(t) = \sum_{j=0}^{N} V_j \mathscr{Y}_j(t) = \mathbf{Y}^T(t)V = V^T\mathbf{Y}(t), \tag{16}$$

where V and $\mathbf{Y}(t)$ are the $(N+1)\times 1$ vectors as follows:

$$\begin{aligned} V &= [V_0 V_1 \cdots V_N]^T, \\ \mathbf{Y}(t) &= [\mathscr{Y}_0(t)\mathscr{Y}_1(t) \cdots \mathscr{Y}_N(t)]^T. \end{aligned} \tag{17}$$

3.2. Operational Matrices of One-Variable Basis. In this subsection, integral operational matrices of integral and fractional orders are obtained for the one-variable basis. Furthermore, the relation between the main basis and its delay form is given as a matrix. For this, some useful lemma and theorems are stated and proved.

Lemma 4. *If $\nu \in \mathbb{R}^+$, then*

$$\begin{aligned} \int_0^1 t^\nu \mathscr{Y}_k(t)w(t)dt = \sum_{m=0}^{k} \varsigma_{m,k}\Gamma\left(\frac{3}{2}\right)\Bigg\{&\frac{4\Gamma(\nu+m+(7/2))}{\Gamma(\nu+m+5)} \\ &- \frac{4\Gamma(\nu+m+(5/2))}{\Gamma(\nu+m+4)} + \frac{\Gamma(\nu+m+(3/2))}{\Gamma(\nu+m+3)}\Bigg\}. \end{aligned} \tag{18}$$

Proof. By the series form of the shifted sixth-kind Chebyshev polynomials in (12) and the weight function $w(t)$, one has

$$\begin{aligned} \int_0^1 t^\nu \mathscr{Y}_k(t)w(t)dt &= \int_0^1 t^\nu \left(\sum_{m=0}^{k} \varsigma_{m,k} t^m\right)(2t-1)^2\sqrt{t-t^2}dt \\ &= \sum_{m=0}^{k} \varsigma_{m,k}\int_0^1 \left(4t^{\nu+m+(5/2)} - 4t^{\nu+m+(3/2)} + x^{\nu+m+(1/2)}\right)(1-t)^{(1/2)}dt \\ &= \sum_{m=0}^{k} \varsigma_{m,k}\Bigg(4B\left(\nu+m+\frac{7}{2},\frac{3}{2}\right) \\ &\quad - 4B\left(\nu+m+\frac{5}{2},\frac{3}{2}\right) + B\left(\nu+m+\frac{3}{2},\frac{3}{2}\right)\Bigg), \end{aligned} \tag{19}$$

where $B(r,s)$ is the well-known beta function, so, the desired result is achieved. □

Theorem 5. *If $\mathbf{Y}(t)$ is the basis vector in (17), the integral of $\mathbf{Y}(t)$ can be computed as*

$$\int_0^t \mathbf{Y}(s)ds \approx \mathbf{P}\mathbf{Y}(t), \quad t \in I, \tag{20}$$

where $\mathbf{P}$ is the $(N+1)\times(N+1)$ integral operational matrix of the integer-order in the following form:

$$\boldsymbol{P} = \begin{bmatrix} \pi(0,0) & \pi(0,1) & \cdots & \pi(0,N) \\ \pi(1,0) & \pi(1,1) & \cdots & \pi(1,N) \\ \vdots & \vdots & \ddots & \vdots \\ \pi(j,0) & \pi(j,1) & \cdots & \pi(j,N) \\ \vdots & \vdots & \ddots & \vdots \\ \pi(N,0) & \pi(N,1) & \cdots & \pi(N,N) \end{bmatrix}, \tag{21}$$

where the entries $\pi(j,k)$ are computed as

$$\begin{aligned} \pi(j,k) = &\sum_{r=0}^{j} \frac{\varsigma_{r,j}\Gamma(3/2)}{(r+1)\hbar_k}\sum_{m=0}^{k}\varsigma_{m,k} \\ &\cdot\left(\frac{4\Gamma(r+m+(9/2))}{\Gamma(r+m+6)} - \frac{4\Gamma(r+m+(7/2))}{\Gamma(r+m+5)} + \frac{\Gamma(r+m+(5/2))}{\Gamma(r+m+4)}\right), \\ &j = 0,1,\cdots,N, k = 0,1,\cdots,N. \end{aligned} \tag{22}$$

Proof. Integrating the elements of the vector $\mathbf{Y}(t)$ yields

$$\int_0^t \mathscr{Y}_j(s)ds = \sum_{r=0}^{j}\varsigma_{r,j}\int_0^t s^r ds = \sum_{r=0}^{j}\varsigma_{r,j}\frac{t^{r+1}}{r+1}, \quad j = 0,1,\cdots,N. \tag{23}$$

Now, t^{r+1} is approximated in terms of the shifted sixth-kind Chebyshev polynomials

$$t^{r+1} \approx \sum_{k=0}^{N}\rho_{k,r+1}\mathscr{Y}_k(t), \tag{24}$$

where

$$\rho_{k,r+1} = \frac{1}{\hbar_k}\int_0^1 t^{r+1}\mathscr{Y}_k(t)w(t)dt. \tag{25}$$

Using Lemma 4, the integral part of (25) is computed as follows:

$$\begin{aligned} \int_0^1 t^{r+1}\mathscr{Y}_k(t)w(t)dt = \sum_{m=0}^{k}\varsigma_{m,k}\Gamma\left(\frac{3}{2}\right)\Bigg(&\frac{4\Gamma(r+m+(9/2))}{\Gamma(r+m+6)} \\ &- \frac{4\Gamma(r+m+(7/2))}{\Gamma(r+m+5)} + \frac{\Gamma(r+m+(5/2))}{\Gamma(r+m+4)}\Bigg). \end{aligned} \tag{26}$$

Therefore, (23) is written as

$$\begin{aligned} \int_0^t \mathscr{Y}_j(s)ds \approx \sum_{k=0}^{N}\Bigg\{\sum_{r=0}^{j}\frac{\varsigma_{r,j}\Gamma(3/2)}{(r+1)\hbar_k}\sum_{m=0}^{k}\varsigma_{m,k}\Bigg(&\frac{4\Gamma(r+m+(9/2))}{\Gamma(r+m+6)} \\ &- \frac{4\Gamma(r+m+(7/2))}{\Gamma(r+m+5)} + \frac{\Gamma(r+m+(5/2))}{\Gamma(r+m+4)}\Bigg)\Bigg\}\mathscr{Y}_k(t). \end{aligned} \tag{27}$$

By rewriting the last series as a matrix form, the desired result is achieved. □

Theorem 6. *Assume that $\mathbf{Y}(t)$ is the basis vector in (17) and ${}_0^{RL}\mathcal{I}_t^{\sigma}$ is the Riemann-Liouville integral operator of the order σ, $0<\sigma<1$. Then, one has*

$$ {}_0^{RL}\mathcal{I}_t^{\sigma}\mathbf{Y}(t) \approx \mathbf{P}^{(\sigma)}\mathbf{Y}(t), \tag{28} $$

where $\mathbf{P}^{(\sigma)}$ is the $(N+1)\times(N+1)$ fractional operational matrix of the order σ as follows:

$$ \boldsymbol{P}^{(\sigma)} = \begin{bmatrix} \pi^{(\sigma)}(0,0) & \pi^{(\sigma)}(0,1) & \cdots & \pi^{(\sigma)}(0,N) \\ \pi^{(\sigma)}(1,0) & \pi^{(\sigma)}(1,1) & \cdots & \pi^{(\sigma)}(1,N) \\ \vdots & \vdots & \ddots & \vdots \\ \pi^{(\sigma)}(i,0) & \pi^{(\sigma)}(i,1) & \cdots & \pi^{(\sigma)}(i,N) \\ \vdots & \vdots & \ddots & \vdots \\ \pi^{(\sigma)}(N,0) & \pi^{(\sigma)}(N,1) & \cdots & \pi^{(\sigma)}(N,N) \end{bmatrix}, \tag{29} $$

where the entries $\pi^{(\sigma)}(i,k)$ are computed as

$$ \begin{aligned} \pi^{(\sigma)}(i,k) = {} & \sum_{r=0}^{i} \frac{\varsigma_{r,i}\Gamma(r+\sigma+1)\Gamma(3/2)}{\Gamma(r+\sigma+2)\hbar_k} \sum_{m=0}^{k} \varsigma_{m,k} \\ & \cdot \left(\frac{4\Gamma(r+m+(7/2))}{\Gamma(r+m+5)} - \frac{4\Gamma(r+m+(5/2))}{\Gamma(r+m+4)} + \frac{\Gamma(r+m+(3/2))}{\Gamma(r+m+3)} \right), \\ & i=0,1,\cdots,N, k=0,1,\cdots,N. \end{aligned} \tag{30} $$

Proof. The proof process is similar to Theorem 5. Noting the definition of ${}_0^{RL}\mathcal{I}_t^{\sigma}$ and its properties in (5), the fractional integral of $\mathcal{Y}_i(t)$ is computed as

$$ {}_0^{RL}\mathcal{I}_t^{\sigma}\mathcal{Y}_i(t) = \sum_{r=0}^{i} \frac{\varsigma_{r,i}\Gamma(r+\sigma+1)t^{r+\sigma}}{\Gamma(r+\sigma+2)}, \quad i=0,1,\cdots,N. \tag{31} $$

Now, $t^{r+\sigma}$ is approximated by the Chebyshev polynomials of the sixth kind as

$$ t^{r+\sigma} \approx \sum_{k=0}^{N} \rho_{k,r}\mathcal{Y}_k(t), \text{s.t.} \rho_{k,r} = \frac{1}{\hbar_k}\int_0^1 t^{r+\sigma}\mathcal{Y}_k(t)w(t)dt. \tag{32} $$

By Lemma 4 and pursuing the proof process in Theorem 5, Equation (31) is written as

$$ \begin{aligned} {}_0^{RL}\mathcal{I}_t^{\sigma}\mathcal{Y}_i(t) \approx {} & \sum_{k=0}^{N} \left\{ \sum_{r=0}^{i} \frac{\varsigma_{r,i}\Gamma(r+\sigma+1)\Gamma(3/2)}{\Gamma(r+\sigma+2)\hbar_k} \times \sum_{m=0}^{k} \varsigma_{m,k} \right. \\ & \cdot \left(\frac{4\Gamma(r+\sigma+m+(7/2))}{\Gamma(r+\sigma+m+5)} - \frac{4\Gamma(r+\sigma+m+(5/2))}{\Gamma(r+\sigma+m+4)} \right. \\ & \left. \left. + \frac{\Gamma(r+\sigma+m+(3/2))}{\Gamma(r+\sigma+m+3)} \right) \right\} \mathcal{Y}_k(t), i=0,1,\cdots,N. \end{aligned} \tag{33} $$

□

Theorem 7. *Assume that $\mathbf{Y}(t)$ is the basis vector and $\mathbf{Y}(qt)$, $0<q<1$ is its delay form. $\mathbf{Y}(qt)$ can be approximated in $\mathbf{Y}(t)$ as*

$$ \mathbf{Y}(qt) \approx \mathbf{L}\mathbf{Y}(t), \tag{34} $$

where $\mathbf{L}$ is a $(N+1)\times(N+1)$ matrix as follows:

$$ \mathbf{L} = \begin{bmatrix} 1 & 0 & 0 & \cdots & 0 \\ l_0^{(1)} & q & 0 & \cdots & 0 \\ l_0^{(2)} & l_1^{(2)} & q & \cdots & 0 \\ \vdots & \vdots & \vdots & \ddots & \vdots \\ l_0^{(N)} & l_1^{(N)} & l_2^{(N)} & \cdots & q^N \end{bmatrix}, \tag{35} $$

and $l_k^{(j)}$ is computed from the following recurrence formulas:

$$ \begin{cases} l_0^{(j+1)} = (q-1)l_0^{(j)} + q\theta_2 l_1^{(j)} - \theta_j l_0^{(j-1)}, & j=1,2,\cdots,N-1, \\ l_k^{(j+1)} = q l_{k-1}^{(j)} + (q-1)l_k^{(j)} + q\theta_{k+1} l_{k+1}^{(j)} - \theta_j l_k^{(j-1)}, & k=1,2,\cdots,j-1, \\ l_j^{(j+1)} = q l_{j-1}^{(j)} + (q-1)q^j, & j=1,2,\cdots,N-1, \end{cases} \tag{36} $$

with the starting values $l_j^{(j)} = q^j, j=0,1,\cdots,N$, and $l_0^{(1)} = q-1$.

Proof. Consider the following recurrence formula obtained from Equation (6)

$$ \mathcal{Y}_{j+1}(qt) = (2qt-1)\mathcal{Y}_j(qt) - \theta_{j+1}\mathcal{Y}_{j-1}(qt), \quad j \geq 1. \tag{37} $$

Also, the following auxiliary relation is obtained from formula (6):

$$ 2t\mathcal{Y}_j(t) = \mathcal{Y}_{j+1}(t) + \mathcal{Y}_j(t) + \theta_{j+1}\mathcal{Y}_{j-1}(t), \quad j \geq 1. \tag{38} $$

Now, $\mathcal{Y}_j(qt)$ can be expanded in terms of the Chebyshev polynomials of the sixth kind as follows:

$$\mathcal{Y}_j(qt) = \sum_{k=0}^{j} l_k^{(j)} \mathcal{Y}_k(t), \quad j = 0, 1, \cdots, N. \tag{39}$$

From the first few polynomials in Equation (39), it is easily obtained $l_0^{(1)} = q - 1$, $l_j^{(j)} = q^j, j = 0, 1, \cdots, N$. Using auxiliary relation (38) and substituting Equation (39) into Equation (37), one gets

$$\begin{aligned}\sum_{k=0}^{j+1} l_k^{(j+1)} \mathcal{Y}_k(t) &= q \sum_{k=0}^{j} l_k^{(j)} (\mathcal{Y}_{k+1}(t) + \mathcal{Y}_k(t) + \theta_{k+1} \mathcal{Y}_{k-1}(t)) \\ &\quad - \theta_{j+1} \sum_{k=0}^{j-1} l_k^{(j-1)} \mathcal{Y}_k(t) - \sum_{k=0}^{j} l_k^{(j)} \mathcal{Y}_k(t) \\ &= \sum_{k=0}^{j} l_k^{(j)} (q\mathcal{Y}_{k+1}(t) + (q-1)\mathcal{Y}_k(t) \\ &\quad + q\theta_{k+1} \mathcal{Y}_{k-1}(t)) - \theta_{j+1} \sum_{k=0}^{j-1} l_k^{(j-1)} \mathcal{Y}_k(t).\end{aligned} \tag{40}$$

Equating coefficients of $\mathcal{Y}_k(t)$ on both sides of the last equality leads to recurrence formula (36). □

3.3. Two-Variable Chebyshev Polynomials of the Sixth Kind. Two-variable Chebyshev polynomials are constructed by one-variable ones on the domain $\Omega = [0, 1] \times [0, 1]$ as

$$\mathcal{W}_{ij}(x, t) = \mathcal{Y}_i(x) \mathcal{Y}_j(t), \quad i, j = 0, 1, \cdots, \quad (x, t) \in \Omega. \tag{41}$$

These polynomials are orthogonal regarding the weight function $\omega(x, t) = w(x)w(t)$ on Ω,

$$\int_0^1 \int_0^1 \mathcal{W}_{ij}(x, t) \mathcal{W}_{kl}(x, t) \omega(x, t)\, dx\, dt = \hbar_i \hbar_j \delta_{ik} \delta_{jl}, \tag{42}$$

where $\hbar_i$ and $\hbar_j$ are calculated by (11). The function $V(x, t) \in L_\omega^2(\Omega)$ is expanded as

$$V(x, t) = \sum_{i=0}^{\infty} \sum_{j=0}^{\infty} V_{ij} \mathcal{W}_{ij}(x, t), \quad (x, t) \in \Omega, \tag{43}$$

and a truncated series of (43) is considered as an approximation to the function $V(x, t)$,

$$\begin{aligned}V(x, t) \approx V_N(x, t) &= \sum_{i=0}^{N} \sum_{j=0}^{N} V_{ij} \mathcal{W}_{ij}(x, t) \\ &= \sum_{i=0}^{(N+1)^2-1} V_i^* \mathcal{W}_i^*(x, t) = \mathbf{V}^T \mathbf{W}(x, t) = \mathbf{W}^T(x, t)\mathbf{V},\end{aligned} \tag{44}$$

where $V_i^* = V_{rs}, \mathcal{W}_i^*(x, t) = \mathcal{W}_{rs}(x, t)$ such that $r = \lfloor i/(N+1) \rfloor, s = i - r(N+1)$, and $\mathbf{V}, \mathbf{W}(x, t)$ are the $(N+1)^2 \times 1$ vectors as

$$\begin{aligned}\mathbf{V} &= [V_{00} V_{01} \cdots V_{0N} V_{10} V_{11} \cdots V_{1N} \cdots V_{N0} V_{N1} \cdots V_{NN}]^T, \\ \mathbf{W}(x, t) &= [\mathcal{W}_{00}(x, t) \mathcal{W}_{01}(x, t) \cdots \mathcal{W}_{0N}(x, t) \mathcal{W}_{10} \mathcal{W}_{11}(x, t) \\ &\quad \cdots \mathcal{W}_{1N}(x, t) \cdots \mathcal{W}_{N0}(x, t) \mathcal{W}_{N1}(x, t) \cdots \mathcal{W}_{NN}(x, t)]^T.\end{aligned} \tag{45}$$

3.4. Operational Matrices of Two-Variable Basis. Consider the two-variable basis $\mathbf{W}(x, t)$ in (45). The integral operational matrices of $\mathbf{W}(x, t)$ with respect to variables x and t are obtained, respectively, as

$$\begin{aligned}\int_0^x \mathbf{W}(s, t) ds &\approx \mathbb{P}_{(x)}^{(1)} \mathbf{W}(x, t) = (\mathbf{P} \otimes \mathbf{I}) \mathbf{W}(x, t), \\ \int_0^t \mathbf{W}(x, \tau) d\tau &\approx \mathbb{P}_{(t)}^{(1)} \mathbf{W}(x, t) = (\mathbf{I} \otimes \mathbf{P}) \mathbf{W}(x, t),\end{aligned} \tag{46}$$

where $\mathbb{P}_{(x)}^{(1)}$ and $\mathbb{P}_{(t)}^{(1)}$ are the $(N+1)^2 \times (N+1)^2$ integral operational matrices related to x and t, respectively, $\mathbf{P}$ is the operational matrix in Theorem 5, and $\mathbf{I}$ is the $(N+1) \times (N+1)$ identity matrix. Similarly, the fractional integral of $\mathbf{W}(x, t)$ of the order σ with respect to t can be computed as

$${}_0^{RL}\mathcal{I}_t^{\sigma} \mathbf{W}(x, t) \approx \mathbb{P}_{(t)}^{(\sigma)} \mathbf{W}(x, t) = \left(\mathbf{I} \otimes \mathbf{P}^{(\sigma)}\right) \mathbf{W}(x, t), \tag{47}$$

where $\mathbb{P}_{(t)}^{(\sigma)}$ is the $(N+1)^2 \times (N+1)^2$ fractional integral operational matrix of the order σ related to t, $\mathbf{P}^{(\sigma)}$ is the operational matrix in Theorem 6, and $\mathbf{I}$ is the $(N+1) \times (N+1)$ identity matrix. Now, the relationship of the vectors $\mathbf{W}(x, qt)$, $\mathbf{W}(qx, t)$, and $\mathbf{W}(qx, qt)$ to the basis vector $\mathbf{W}(x, t)$ is specified.

By setting $t = qt$ in $\mathbf{W}(x, t)$, the vector $\mathbf{W}(x, qt)$ is rewritten as follows:

$$\begin{aligned}\mathbf{W}(x, qt) &= [\mathcal{Y}_0(x)\mathcal{Y}_0(qt), \mathcal{Y}_0(x)\mathcal{Y}_1(qt), \cdots, \mathcal{Y}_0 \\ &\quad \cdot (x)\mathcal{Y}_N(qt), \mathcal{Y}_1(x)\mathcal{Y}_0(qt), \mathcal{Y}_1(x)\mathcal{Y}_1(qt), \cdots, \mathcal{Y}_{1\ T} \\ &\quad \cdot (x)\mathcal{Y}_N(qt), \cdots, \mathcal{Y}_N \\ &\quad \cdot (x)\mathcal{Y}_0(qt), \mathcal{Y}_N(x)\mathcal{Y}_1(qt), \cdots, \mathcal{Y}_N(x)\mathcal{Y}_N(qt)] \\ &= [\mathcal{Y}_0(x)[\mathcal{Y}_0(qt), \mathcal{Y}_1(qt), \cdots, \mathcal{Y}_N(qt)], \mathcal{Y}_1(x) \\ &\quad \cdot[\mathcal{Y}_0(qt), \mathcal{Y}_1(qt), \cdots, \mathcal{Y}_N(qt)], \cdots, \mathcal{Y}_N(x) \\ &\quad \cdot[\mathcal{Y}_0(qt), \mathcal{Y}_1(qt), \cdots, \mathcal{Y}_N(qt)]]^T \\ &= [\mathcal{Y}_0(x)\mathbf{Y}(qt), \mathcal{Y}_1(x)\mathbf{Y}(qt), \cdots, \mathcal{Y}_N(x)\mathbf{Y}(qt)]^T \\ &\approx [\mathcal{Y}_0(x)\mathbf{L}\mathbf{Y}(t), \mathcal{Y}_1(x)\mathbf{L}\mathbf{Y}(t), \cdots, \mathcal{Y}_N(x)\mathbf{L}\mathbf{Y}(t)]^T \\ &= \begin{bmatrix} \mathbf{L} & O_{N+1} & \cdots & O_{N+1} \\ O_{N+1} & \mathbf{L} & \cdots & O_{N+1} \\ \vdots & \vdots & \ddots & \vdots \\ O_{N+1} & O_{N+1} & \cdots & \mathbf{L} \end{bmatrix} \begin{bmatrix} \mathcal{Y}_0(x)\mathcal{Y}_0(t) \\ \vdots \\ \mathcal{Y}_N(x)\mathcal{Y}_0(t) \\ \vdots \\ \mathcal{Y}_N(x)\mathcal{Y}_N(t) \end{bmatrix} \\ &= (\mathbf{I} \otimes \mathbf{L})\mathbf{W}(x, t) = \mathfrak{L}^{**}\mathbf{W}(x, t),\end{aligned} \tag{48}$$

where $\mathbf{L}$ is the matrix in Theorem 7, O_{N+1} is the $(N+1)\times(N+1)$ zero matrix, and $\mathfrak{L}^{**}$ is the $(N+1)^2\times(N+1)^2$ delay matrix. Similarly, it is found that

$$\begin{aligned}\mathbf{W}(qx,t)&\approx(\mathbf{L}\otimes\mathbf{I})\mathbf{W}(x,t)=\mathfrak{L}^{*}\mathbf{W}(x,t),\\ \mathbf{W}(qx,qt)&\approx\mathfrak{L}^{*}\mathfrak{L}^{**}\mathbf{W}(x,t)=\mathfrak{L}\mathbf{W}(x,t),\ \mathfrak{L}=\mathfrak{L}^{*}\mathfrak{L}^{**},\end{aligned}\tag{49}$$

where $\mathfrak{L}^{*}$ and $\mathfrak{L}$ are $(N+1)^2\times(N+1)^2$ matrices.

3.5. Solution Method. To describe the methodology, three forms of Equations (1) and (2) are considered [26, 27]:

Form I:

$$\begin{aligned}&{}_0^C\mathscr{D}_t^{\sigma}\mathbf{u}(x,t)-\frac{\partial^2\mathbf{u}(x,t)}{\partial x^2}-\frac{\partial\mathbf{u}(x,(t/2))}{\partial x}\mathbf{u}\left(\frac{x}{2},\frac{t}{2}\right)-\frac{1}{2}\mathbf{u}(x,t)\\ &=0,\quad 0<\sigma\leqslant 1,\quad (x,t)\in\Omega,\\ &\mathbf{u}(x,0)=x,\quad \mathbf{u}(0,t)=0,\quad \mathbf{u}_x(0,t)=\exp(t).\end{aligned}\tag{50}$$

According to the highest orders of derivatives regarding x and t, the following approximation is considered:

$$\frac{\partial^3\mathbf{u}(x,t)}{\partial x^2\partial t}\approx\mathbf{W}^T(x,t)\mathbf{C}.\tag{51}$$

Integrating (51) concerning t and x, respectively, leads to the following approximations:

$$\frac{\partial^2\mathbf{u}(x,t)}{\partial x^2}\approx\mathbf{W}^T(x,t)\mathbb{P}_{(t)}^{(1)^T}\mathbf{C}+\frac{\partial^2\mathbf{u}(x,0)}{\partial x^2}\approx\mathbf{W}^T(x,t)\mathbb{P}_{(t)}^{(1)^T}\mathbf{C},\tag{52}$$

$$\begin{aligned}\frac{\partial\mathbf{u}(x,t)}{\partial x}&\approx\mathbf{W}^T(x,t)\mathbb{P}_{(x)}^{(1)^T}\mathbb{P}_{(t)}^{(1)^T}\mathbf{C}+\frac{\partial\mathbf{u}(0,t)}{\partial x}\\ &\approx\mathbf{W}^T(x,t)\mathbb{P}_{(x)}^{(1)^T}\mathbb{P}_{(t)}^{(1)^T}\mathbf{C}+\mathbf{W}^T(x,t)F,\end{aligned}\tag{53}$$

$$\begin{aligned}\mathbf{u}(x,t)&\approx\mathbf{W}^T(x,t)\left(\mathbb{P}_{(x)}^{(1)^T}\right)^2\mathbb{P}_{(t)}^{(1)^T}\mathbf{C}+\mathbf{W}^T(x,t)\mathbb{P}_{(x)}^{(1)^T}F+\mathbf{u}(0,t)\\ &\approx\mathbf{W}^T(x,t)\left(\mathbb{P}_{(x)}^{(1)^T}\right)^2\mathbb{P}_{(t)}^{(1)^T}\mathbf{C}+\mathbf{W}^T(x,t)\mathbb{P}_{(x)}^{(1)^T}F.\end{aligned}\tag{54}$$

Now, twice integrating approximation (51) with respect to x leads to an approximation for $(\partial\mathbf{u}(x,t))/\partial t$:

$$\begin{aligned}\frac{\partial^2\mathbf{u}(x,t)}{\partial x\partial t}&\approx\mathbf{W}^T(x,t)\mathbb{P}_{(x)}^{(1)^T}\mathbf{C}+\mathbf{W}^T(x,t)F,\\ \frac{\partial\mathbf{u}(x,t)}{\partial t}&\approx\mathbf{W}^T(x,t)\left(\mathbb{P}_{(x)}^{(1)^T}\right)^2\mathbf{C}+\mathbf{W}^T(x,t)\mathbb{P}_{(x)}^{(1)^T}F.\end{aligned}\tag{55}$$

To obtain an approximation to ${}_0^C\mathscr{D}_t^{\sigma}\mathbf{u}(x,t)$, approximation (55) is rewritten as follows:

$$\begin{aligned}\frac{\partial\mathbf{u}(x,t)}{\partial t}&=\frac{\partial^{1-\sigma}\partial^{\sigma}\mathbf{u}(x,t)}{\partial t^{1-\sigma}\partial t^{\sigma}}\\ &\approx\mathbf{W}^T(x,t)\left(\mathbb{P}_{(x)}^{(1)^T}\right)^2\mathbf{C}+\mathbf{W}^T(x,t)\mathbb{P}_{(x)}^{(1)^T}F.\end{aligned}\tag{56}$$

By applying the Riemann-Liouville operator of the order $1-\sigma$ to both sides of (56), one gets

$$\begin{aligned}{}_0^C\mathscr{D}_t^{\sigma}\mathbf{u}(x,t)&\approx\mathbf{W}^T(x,t)\mathbb{P}_{(t)}^{(1-\sigma)^T}\left(\mathbb{P}_{(x)}^{(1)^T}\right)^2\mathbf{C}\\ &\quad+\mathbf{W}^T(x,t)\mathbb{P}_{(t)}^{(1-\sigma)^T}\mathbb{P}_{(x)}^{(1)^T}F+{}_0^C\mathscr{D}_t^{\sigma}\mathbf{u}(x,0).\end{aligned}\tag{57}$$

Fractionally differentiating approximation (54) and setting $t=0$ lead to

$${}_0^C\mathscr{D}_t^{\sigma}\mathbf{u}(x,0)\approx{}_0^C\mathscr{D}_t^{\sigma}\mathbf{W}^T(x,t)\left(\mathbb{P}_{(x)}^{(1)^T}\right)^2\mathbb{P}_{(t)}^{(1)^T}\mathbf{C}+{}_0^C\mathscr{D}_t^{\sigma}\mathbf{W}^T(x,t)\mathbb{P}_{(x)}^{(1)^T}F|_{t=0}=0.\tag{58}$$

Approximation (58) equals zero because after fractionally differentiating $\mathbf{W}(x,t)$ related to t, all components of the basis vector involve terms as $t^{\mu}, 1-\sigma<\mu<N-\sigma$ or are zero.

The terms with delays can be approximated as

$$\begin{aligned}\frac{\partial\mathbf{u}(x,t/2)}{\partial x}&\approx\mathbf{W}^T\left(x,\frac{t}{2}\right)\mathbb{P}_{(x)}^{(1)^T}\mathbb{P}_{(t)}^{(1)^T}\mathbf{C}+\mathbf{W}^T\left(x,\frac{t}{2}\right)F\\ &\approx\mathbf{W}^T(x,t)\mathfrak{L}^{**T}\mathbb{P}_{(x)}^{(1)^T}\mathbb{P}_{(t)}^{(1)^T}\mathbf{C}+\mathbf{W}^T(x,t)\mathfrak{L}^{**T}F,\end{aligned}\tag{59}$$

$$\begin{aligned}\mathbf{u}\left(\frac{x}{2},\frac{t}{2}\right)&\approx\mathbf{W}^T\left(\frac{x}{2},\frac{t}{2}\right)\left(\mathbb{P}_{(x)}^{(1)^T}\right)^2\mathbb{P}_{(t)}^{(1)^T}\mathbf{C}+\mathbf{W}^T\left(\frac{x}{2},\frac{t}{2}\right)\mathbb{P}_{(x)}^{(1)^T}F\\ &\approx\mathbf{W}^T(x,t)\mathfrak{L}^{T}\left(\mathbb{P}_{(x)}^{(1)^T}\right)^2\mathbb{P}_{(t)}^{(1)^T}\mathbf{C}+\mathbf{W}^T(x,t)\mathfrak{L}^{T}\mathbb{P}_{(x)}^{(1)^T}F.\end{aligned}\tag{60}$$

Substituting approximations (52)–(60) into Equation (50) results in the following residual function:

$$\begin{aligned}\mathscr{R}_N(x,t)&=\mathbf{W}^T(x,t)\mathbb{P}_{(t)}^{(1-\sigma)^T}\left(\mathbb{P}_{(x)}^{(1)^T}\right)^2\mathbf{C}\\ &\quad+\mathbf{W}^T(x,t)\mathbb{P}_{(t)}^{(1-\sigma)^T}\mathbb{P}_{(x)}^{(1)^T}F-\mathbf{W}^T(x,t)\mathbb{P}_{(t)}^{(1)^T}\mathbf{C}\\ &\quad-\left(\mathbf{W}^T(x,t)\mathfrak{L}^{**T}\mathbb{P}_{(x)}^{(1)^T}\mathbb{P}_{(t)}^{(1)^T}\mathbf{C}+\mathbf{W}^T(x,t)\mathfrak{L}^{**T}F\right)\\ &\quad\cdot\left(\mathbf{W}^T(x,t)\mathfrak{L}^{T}\left(\mathbb{P}_{(x)}^{(1)^T}\right)^2\mathbb{P}_{(t)}^{(1)^T}\mathbf{C}+\mathbf{W}^T(x,t)\mathfrak{L}^{T}\mathbb{P}_{(x)}^{(1)^T}F\right)\\ &\quad-\frac{1}{2}\left(\mathbf{W}^T(x,t)\left(\mathbb{P}_{(x)}^{(1)^T}\right)^2\mathbf{C}+\mathbf{W}^T(x,t)\mathbb{P}_{(x)}^{(1)^T}F\right)\approx 0.\end{aligned}\tag{61}$$

Form II:

$$
\begin{gathered}
{}_0^C\mathscr{D}_t^\sigma \mathbf{u}(x,t) - \frac{\partial^2 \mathbf{u}(x,t/2)}{\partial x^2}\mathbf{u}\left(x,\frac{t}{2}\right) + \mathbf{u}(x,t) = 0, \quad 0<\sigma\leqslant 1, \quad (x,t)\in\Omega, \\
\mathbf{u}(x,0) = x^2, \quad \mathbf{u}(0,t)=0, \quad \mathbf{u}_x(0,t)=0.
\end{gathered} \tag{62}
$$

The functions in Equation (62) are approximated based on what was done for Equation (50):

$$
\begin{gathered}
\frac{\partial^3 \mathbf{u}(x,t)}{\partial x^2\,\partial t} \approx \mathbf{W}^T(x,t)\,\mathbf{C}, \\
\frac{\partial^2 \mathbf{u}(x,t)}{\partial x^2} \approx \mathbf{W}^T(x,t)\,\mathbb{P}_{(t)}^{(1)T}\,\mathbf{C} + \frac{\partial^2 \mathbf{u}(x,0)}{\partial x^2} \approx \mathbf{W}^T(x,t)\,\mathbb{P}_{(t)}^{(1)T}\,\mathbf{C} + \mathbf{W}^T(x,t)\,F, \\
\mathbf{u}(x,t) \approx \mathbf{W}^T(x,t)\left(\mathbb{P}_{(x)}^{(1)T}\right)^2\mathbb{P}_{(t)}^{(1)T}\,\mathbf{C} + \mathbf{W}^T(x,t)\left(\mathbb{P}_{(x)}^{(1)T}\right)^2 F, \\
{}_0^C\mathscr{D}_t^\sigma \mathbf{u}(x,t) \approx \mathbf{W}^T(x,t)\,\mathbb{P}_{(t)}^{(1-\sigma)T}\left(\mathbb{P}_{(x)}^{(1)T}\right)^2\mathbf{C}, \\
\frac{\partial^2 \mathbf{u}(x,t/2)}{\partial x^2} \approx \mathbf{W}^T(x,t)\,\mathfrak{L}^{**T}\mathbb{P}_{(t)}^{(1)T}\,\mathbf{C} + \mathbf{W}^T(x,t)\,\mathfrak{L}^{**T}\,F, \\
\mathbf{u}\left(x,\frac{t}{2}\right) \approx \mathbf{W}^T(x,t)\,\mathfrak{L}^{**T}\left(\mathbb{P}_{(x)}^{(1)T}\right)^2\mathbb{P}_{(t)}^{(1)T}\,\mathbf{C} + \mathbf{W}^T(x,t)\,\mathfrak{L}^{**T}\mathbb{P}_{(x)}^{(1)T}\,F.
\end{gathered} \tag{63}
$$

Substituting approximations (63) into Equation (62) leads to the following residual function:

$$
\begin{aligned}
\mathscr{R}_N(x,t) = {} & \mathbf{W}^T(x,t)\mathbb{P}_{(t)}^{(1-\sigma)T}\left(\mathbb{P}_{(x)}^{(1)T}\right)^2\mathbf{C} \\
& - \left(\mathbf{W}^T(x,t)\mathfrak{L}^{**T}\mathbb{P}_{(t)}^{(1)T}\mathbf{C} + \mathbf{W}^T(x,t)\mathfrak{L}^{**T}F\right) \\
& \times \left(\mathbf{W}^T(x,t)\mathfrak{L}^{**T}\left(\mathbb{P}_{(x)}^{(1)T}\right)^2\mathbb{P}_{(t)}^{(1)T}\mathbf{C} + \mathbf{W}^T(x,t)\mathfrak{L}^{**T}\mathbb{P}_{(x)}^{(1)T}F\right) \\
& + \mathbf{W}^T(x,t)\left(\mathbb{P}_{(x)}^{(1)T}\right)^2\mathbb{P}_{(t)}^{(1)T}\mathbf{C} + \mathbf{W}^T(x,t)\left(\mathbb{P}_{(x)}^{(1)T}\right)^2 F \approx 0.
\end{aligned} \tag{64}
$$

Form III:

$$
\begin{gathered}
{}_0^C\mathscr{D}_t^\sigma \mathbf{u}(x,t) - \frac{\partial^2 \mathbf{u}(x/2,t/2)}{\partial x^2}\frac{\partial \mathbf{u}(x/2,t/2)}{\partial x} + \frac{\partial \mathbf{u}(x,t)}{\partial x} + \mathbf{u}(x,t) \\
= 0, \quad 0<\sigma\leqslant 1, \quad (x,t)\in\Omega,
\end{gathered}
$$

$$
\mathbf{u}(x,0) = x^2, \quad \mathbf{u}(0,t)=0, \quad \mathbf{u}_x(0,t)=0. \tag{65}
$$

The following approximations can be obtained for the functions in Equation (65):

$$
\begin{gathered}
\frac{\partial^3 \mathbf{u}(x,t)}{\partial x^2\,\partial t} \approx \mathbf{W}^T(x,t)\,\mathbf{C}, \\
\frac{\partial^2 \mathbf{u}(x,t)}{\partial x^2} \approx \mathbf{W}^T(x,t)\,\mathbb{P}_{(t)}^{(1)T}\,\mathbf{C} + \frac{\partial^2 \mathbf{u}(x,0)}{\partial x^2} \approx \mathbf{W}^T(x,t)\,\mathbb{P}_{(t)}^{(1)T}\,\mathbf{C} + \mathbf{W}^T(x,t)\,F, \\
\frac{\partial \mathbf{u}(x,t)}{\partial x} \approx \mathbf{W}^T(x,t)\mathbb{P}_{(x)}^{(1)T}\mathbb{P}_{(t)}^{(1)T}\,\mathbf{C} + \mathbf{W}^T(x,t)\mathbb{P}_{(x)}^{(1)T}F, \\
\mathbf{u}(x,t) \approx \mathbf{W}^T(x,t)\left(\mathbb{P}_{(x)}^{(1)T}\right)^2\mathbb{P}_{(t)}^{(1)T}\,\mathbf{C} + \mathbf{W}^T(x,t)\left(\mathbb{P}_{(x)}^{(1)T}\right)^2 F, \\
{}_0^C\mathscr{D}_t^\sigma \mathbf{u}(x,t) \approx \mathbf{W}^T(x,t)\mathbb{P}_{(t)}^{(1-\sigma)T}\left(\mathbb{P}_{(x)}^{(1)T}\right)^2\mathbf{C}, \\
\frac{\partial^2 \mathbf{u}(x/2,t/2)}{\partial x^2} \approx \mathbf{W}^T(x,t)\,\mathfrak{L}^T\mathbb{P}_{(t)}^{(1)T}\,\mathbf{C} + \mathbf{W}^T(x,t)\,\mathfrak{L}^T\,F, \\
\frac{\partial \mathbf{u}(x/2,t/2)}{\partial x} \approx \mathbf{W}^T(x,t)\,\mathfrak{L}^T\mathbb{P}_{(x)}^{(1)T}\mathbb{P}_{(t)}^{(1)T}\,\mathbf{C} + \mathbf{W}^T(x,t)\,\mathfrak{L}^T\mathbb{P}_{(x)}^{(1)T}\,F.
\end{gathered} \tag{66}
$$

By substituting approximations (66) into Equation (65), one gets the following residual function:

$$
\begin{aligned}
\mathscr{R}_N(x,t) = {} & \mathbf{W}^T(x,t)\mathbb{P}_{(t)}^{(1-\sigma)T}\left(\mathbb{P}_{(x)}^{(1)T}\right)^2\mathbf{C} \\
& - \left(\mathbf{W}^T(x,t)\mathfrak{L}^T\mathbb{P}_{(t)}^{(1)T}\mathbf{C} + \mathbf{W}^T(x,t)\mathfrak{L}^T F\right) \\
& \times \left(\mathbf{W}^T(x,t)\mathfrak{L}^T\mathbb{P}_{(x)}^{(1)T}\mathbb{P}_{(t)}^{(1)T}\mathbf{C} + \mathbf{W}^T(x,t)\mathfrak{L}^T\mathbb{P}_{(x)}^{(1)T}F\right) \\
& + \mathbf{W}^T(x,t)\mathbb{P}_{(x)}^{(1)T}\mathbb{P}_{(t)}^{(1)T}\mathbf{C} + \mathbf{W}^T(x,t)\mathbb{P}_{(x)}^{(1)T}F \\
& + \mathbf{W}^T(x,t)\left(\mathbb{P}_{(x)}^{(1)T}\right)^2\mathbb{P}_{(t)}^{(1)T}\mathbf{C} + \mathbf{W}^T(x,t)\left(\mathbb{P}_{(x)}^{(1)T}\right)^2 F \approx 0.
\end{aligned} \tag{67}
$$

The residual functions in Equations (61), (64), and (65) are collocated at collocation nodes $\{(x_i,t_j)\}_{i,j=0}^{\infty}$, which x_i and t_j are roots of $\mathscr{Y}_{N+1}(x)$ and $\mathscr{Y}_{N+1}(t)$, respectively. Hence, a nonlinear system involving $(N+1)^2$ algebraic equations is achieved that can be solved by the Newton's iteration method. Therefore, the coefficient vector $\mathbf{C}$ is determined approximately; then, an approximate solution, $\mathbf{u}(x,t)$, is achieved. To better describe the solution method, pursuing Algorithm 1 for Equation (50) is suggested.

4. Error Analysis

It is found that the value of the error function $\mathscr{E}_N(x,t)$ decreases when values of N increase. First, some error bounds are obtained for the unknown function $\mathbf{u}(x,t)$ and its derivatives.

Theorem 8. *Assume that $\partial^{i+j}u(x,t)/\partial x^i\partial t^j \in C(\Omega)$, $i,j=0,1,\cdots,N+1$, $\Theta_N = span\{\mathscr{W}_{ij}(x,t), i,j=0,1,\cdots,N\}$, and $u_N(x,t)$ is the approximate solution obtained from the method belonging to Θ_N, and*

$$
\tau_N = \sup_{(x,t)\in\Omega}\left|\frac{\partial^{2(N+1)}\mathbf{u}(x,t)}{\partial x^{N+1}\partial t^{N+1}}\right|. \tag{68}
$$

Input: σ, N
Step 1. Derive operational matrices P, $P^{(\sigma)}$, and L from (21), (29), and (36).
Step 2. Construct the operational matrices $\mathbb{P}_{(x)}^{(1)}$, $\mathbb{P}_{(t)}^{(1)}$, $\mathbb{P}_{(t)}^{(\sigma)}$, $\mathfrak{L}$, $\mathfrak{L}^*$, $\mathfrak{L}^{**}$ from (46)-(49).
Step 3. Consider the approximation $\partial^3\mathbf{u}(x,t)/\partial x^2\partial t \approx \mathbf{W}^T(x,t)\mathbf{C}$ in (51).
Step 4. Find approximations to $\partial^2\mathbf{u}(x,t)/\partial x^2$, $\partial\mathbf{u}(x,t)/\partial x$, $\mathbf{u}(x,t)$, and $\partial\mathbf{u}(x,t)/\partial t$ from (52)-(55).
Step 5. Find an approximation to ${}_0^C\mathscr{D}_t^\sigma\mathbf{u}(x,t)$ from (57).
Step 6. Determine the residual function from (61).
Step 7. Obtain roots of $\mathscr{Y}_{N+1}(x)$ and $\mathscr{Y}_{N+1}(t)$ $(x_i, t_j, i, j = 0, 1, \cdots, N)$ using fsolve command in Maple.
Step 8. Collocate the residual function at tensor points (x_i, t_j), $i, j = 0, 1, \cdots, N$.
Step 9. Solve the resultant non-linear system in Step 8 by Newton's iteration method and obtain the unknown vector $\mathbf{C}$.
Step 10. Find $\mathbf{u}_N(x,t)$ from (54).
Output: $\mathbf{u}_N(x,t)$

Algorithm 1: Solution method

Then, the error bound of the $\mathbf{u}_N(x,t)$ can be obtained as

$$\|\mathbf{u}(x,t)-\mathbf{u}_N(x,t)\|_{L_\omega^2(\Omega)} \le \frac{\mathscr{A}_0\tau_N\sqrt{\pi}}{2^{5/2}N^{3/2}\Gamma(N+2)^2}. \tag{69}$$

Proof. Define the bivariate Taylor expansion of $\mathbf{u}_N(x,t)$ as

$$\mathscr{T}_N(x,t) = \sum_{i=0}^{N}\sum_{j=0}^{N-i}\left[\frac{\partial^{i+j}\mathbf{u}(x,t)}{\partial x^i\partial t^j}\right]_{(0,0)}\frac{x^it^j}{\Gamma(i+1)\Gamma(j+1)}, \tag{70}$$

and

$$\mathbf{u}(x,t)-\mathscr{T}_N(x,t) = \frac{x^{N+1}t^{N+1}}{\Gamma(N+2)^2}\frac{\partial^{2(N+1)}\mathbf{u}(\xi,\eta)}{\partial x^{N+1}\partial t^{N+1}}, (\xi,\eta)\in\Omega. \tag{71}$$

Since $\mathbf{u}_N(x,t)$ is the best approximate solution of $\mathbf{u}(x,t)$ from Θ_N and according to Equation (71), one gets

$$\begin{aligned}
\|\mathbf{u}(x,t)-\mathbf{u}_N(x,t)\|_{L_\omega^2(\Omega)}^2 &\le \|\mathbf{u}(x,t)-\mathscr{T}_N(x,t)\|_{L_\omega^2(\Omega)}^2\\
&\le \int_0^1\int_0^1 \frac{\tau_N^2x^{2(N+1)}t^{2(N+1)}}{\Gamma(N+2)^4}\omega(x,t)dxdt\\
&= \frac{\tau_N^2}{\Gamma(N+2)^4}\int_0^1\left(4x^{2N+9/2}(1-x)^{1/2}-4x^{2N+7/2}(1-x)^{1/2}+4x^{2N+5/2}(1-x)^{1/2}\right)dx\\
&\quad\times\int_0^1\left(4t^{2N+9/2}(1-t)^{1/2}-4t^{2N+7/2}(1-t)^{1/2}+4t^{2N+5/2}(1-t)^{1/2}\right)dt\\
&= \frac{\tau_N^2\pi}{4\Gamma(N+2)^4}\left(\frac{4\Gamma(2N+(11/2))}{\Gamma(2N+7)}-\frac{4\Gamma(2N+(9/2))}{\Gamma(2N+6)}+\frac{\Gamma(2N+(7/2))}{\Gamma(2N+5)}\right)^2.
\end{aligned} \tag{72}$$

By the Stirling formula [29], some bounds are computed for the last equality:

$$\begin{aligned}
\|\mathbf{u}(x,t)-\mathbf{u}_N(x,t)\|_{L_\omega^2(\Omega)} &\le \frac{\tau_N\sqrt{\pi}}{2\Gamma(N+2)^2}\\
&\quad\cdot\left(4\alpha_1(2N)^{-3/2}-4\alpha_2(2N)^{-3/2}+\alpha_3(2N)^{-3/2}\right)\\
&\le \frac{\mathscr{A}_0\tau_N\sqrt{\pi}}{2^{5/2}N^{3/2}\Gamma(N+2)^2},
\end{aligned} \tag{73}$$

where $\mathscr{A}_0 = 4\alpha_1 - 4\alpha_2 + \alpha_3$. Therefore, the desired result is achieved. □

Theorem 9. *Assume that $u(x,t)$, $u_N(x,t)$, and $\partial^{i+j}u(x,t)/\partial x^i\partial t^j$, $i, j = 0, 1, \cdots, N$ satisfy the condition of Theorem 8, and set*

$$\theta_{N,k} = \sup_{(x,t)\in\Omega}\left|\frac{\partial^{2N-k+2}\mathbf{u}(x,t)}{\partial x^{2N-k+1}\partial t^{N+1}}\right|, \quad k = 1, 2. \tag{74}$$

Then,

$$\left\|\frac{\partial^k\mathbf{u}(x,t)}{\partial x^k}-\frac{\partial^k\mathbf{u}_N(x,t)}{\partial x^k}\right\|_{L_\omega^2(\Omega)} \le \frac{\mathscr{A}_{1,k}\theta_{N,k}\sqrt{\pi}}{2^{5/2}(N(N-k))^{3/4}\Gamma(N-k+2)\Gamma(N+2)}, \quad k = 1, 2. \tag{75}$$

Proof. The bivariate Taylor expansion of $\partial^k\mathbf{u}(x,t)/\partial x^k$ leads to

$$\frac{\partial^k\mathbf{u}(x,t)}{\partial x^k}-\frac{\partial^k\mathbf{u}_N(x,t)}{\partial x^k} = \frac{x^{N-k+1}t^{N+1}}{\Gamma(N-k+2)\Gamma(N+2)}\frac{\partial^{2N-k+2}\mathbf{u}(\xi',\eta')}{\partial x^{N-k+1}\partial t^{N+1}}, \quad (\xi',\eta')\in\Omega, k = 1, 2. \tag{76}$$

Therefore, by taking L^2-norm and using Equation (74) and Stirling formula, one has

$$\begin{aligned}
&\left\|\frac{\partial^k \mathbf{u}(x,t)}{\partial x^k}-\frac{\partial^k \mathbf{u}_N(x,t)}{\partial x^k}\right\|^2_{L^2_\omega(\Omega)}\\
&\quad\le \int_0^1\int_0^1 \frac{\theta_{N,k}^2 x^{2(N-k+1)} t^{2(N+1)}}{\Gamma(N-k+2)^2\Gamma(N+2)^2}\omega(x,t)dxdt\\
&\quad= \frac{\theta_{N,k}^2\pi}{4\Gamma(N-k+2)^2\Gamma(N+2)^2}\\
&\qquad\times\left(\frac{4\Gamma(2(N-k)+(11/2))}{\Gamma(2(N-k)+7)}-\frac{4\Gamma(2(N-k)+(9/2))}{\Gamma(2(N-k)+6)}\right.\\
&\qquad\left.+\frac{\Gamma(2(N-k)+(7/2))}{\Gamma(2(N-k)+5)}\right)\times\left(\frac{4\Gamma(2N+(11/2))}{\Gamma(2N+7)}\right.\\
&\qquad\left.-\frac{4\Gamma(2N+(9/2))}{\Gamma(2N+6)}+\frac{\Gamma(2N+(7/2))}{\Gamma(2N+5)}\right)\\
&\le \frac{\theta_{N,k}^2\pi}{4\Gamma(N-k+2)\Gamma(N+2)}\\
&\quad\cdot\left(4\beta_1(N-k)^{-3/2}-4\beta_2(N-k)^{-3/2}+\beta_3(N-k)^{-3/2}\right)\\
&\quad\times\left(4\gamma_1N^{-3/2}-4\gamma_2N^{-3/2}+\gamma_3N^{-3/2}\right)\\
&\le \frac{\mathscr{A}_{1,k}^2\theta_{N,k}^2\pi}{4\Gamma(N-k+2)^2\Gamma(N+2)^2}(2(N-k))^{-3/2}(2N)^{-3/2},
\end{aligned}\tag{77}$$

where $\mathscr{A}_{1,k}^2=(4\beta_1-4\beta_2+\beta_3)(4\gamma_1-4\gamma_2+\gamma_3)$. □

Theorem 10. *Assume that ${}_0^C\mathscr{D}_t^\sigma u(x,t)\in C(\Omega)$ and the conditions of Theorem 8 hold. Then,*

$$\begin{aligned}
&\left\|{}_0^C\mathscr{D}_t^\sigma \mathbf{u}(x,t)-{}_0^C\mathscr{D}_t^\sigma \mathbf{u}_N(x,t)\right\|_{L^2_\omega(\Omega)}\\
&\quad\le \frac{\mathscr{A}_2\tau_N\sqrt{\pi}}{2^{5/2}\Gamma(N+2)\Gamma(N-\sigma+2)(N(N-\sigma))^{3/4}}.
\end{aligned}\tag{78}$$

Proof. According to Equation (71) and properties of the Caputo operator in (5), one can write

$$\left|{}_0^C\mathscr{D}_t^\sigma \mathbf{u}(x,t)-\mathbf{u}_N(x,t)\right|\le\frac{\tau_N x^{N+1}t^{N-\sigma+1}}{\Gamma(N-\sigma+1)\Gamma(N+2)}.\tag{79}$$

Taking L^2-norm yields

$$\begin{aligned}
&\left\|{}_0^C\mathscr{D}_t^\sigma \mathbf{u}(x,t)-{}_0^C\mathscr{D}_t^\sigma \mathbf{u}_N(x,t)\right\|_{L^2_\omega(\Omega)}\\
&\quad\le\int_0^1\int_0^1\frac{\tau_N^2x^{2(N+1)}t^{2(N-\sigma+1)}}{\Gamma(N-\sigma+2)^2\Gamma(N+2)^2}\omega(x,t)dxdt\\
&\quad=\frac{\tau_N^2\pi}{4\Gamma(N-\sigma+2)^2\Gamma(N+2)^2}\\
&\qquad\times\left(\frac{4\Gamma(2N+(11/2))}{\Gamma(2N+7)}-\frac{4\Gamma(2N+(9/2))}{\Gamma(2N+6)}+\frac{\Gamma(2N+(7/2))}{\Gamma(2N+5)}\right)\\
&\qquad\times\left(\frac{4\Gamma(2(N-\sigma)+(11/2))}{\Gamma(2(N-\sigma)+7)}-\frac{4\Gamma(2(N-\sigma)+(9/2))}{\Gamma(2(N-\sigma)+6)}\right.\\
&\qquad\left.+\frac{\Gamma(2(N-\sigma)+(7/2))}{\Gamma(2(N-\sigma)+5)}\right)\\
&\quad\le\frac{\mathscr{A}_2\tau_N^2\pi}{4\Gamma(N-\sigma+2)^2\Gamma(N+2)^2}(2N)^{-3/2}(2(N-\sigma))^{-3/2}.
\end{aligned}\tag{80}$$

□

Corollary 11. *Some error bounds for functions with proportional delays can be obtained using the resultant bounds in Theorems 8, 9, and 10.*

$$\begin{aligned}
&\left\|\mathbf{u}\left(x,\frac{t}{2}\right)-\mathbf{u}_N\left(x,\frac{t}{2}\right)\right\|_{L^2_\omega(\Omega)}\le\frac{\mathscr{A}_0\tau_N\sqrt{\pi}}{2^{N+(7/2)}N^{3/2}\Gamma(N+2)^2},\\
&\left\|\mathbf{u}\left(\frac{x}{2},\frac{t}{2}\right)-\mathbf{u}_N\left(\frac{x}{2},\frac{t}{2}\right)\right\|_{L^2_\omega(\Omega)}\le\frac{\mathscr{A}_0\tau_N\sqrt{\pi}}{2^{2N+(9/2)}N^{3/2}\Gamma(N+2)^2},\\
&\left\|\frac{\partial\mathbf{u}(x,t/2)}{\partial x}-\frac{\partial\mathbf{u}_N(x,t/2)}{\partial x}\right\|_{L^2_\omega(\Omega)}\le\frac{\mathscr{A}_{1,1}\theta_{N,1}\sqrt{\pi}}{2^{N+(7/2)}(N(N-1))^{3/4}\Gamma(N+1)\Gamma(N+2)},\\
&\left\|\frac{\partial^2\mathbf{u}(x,t/2)}{\partial x^2}-\frac{\partial^2\mathbf{u}_N(x,t/2)}{\partial x^2}\right\|_{L^2_\omega(\Omega)}\le\frac{\mathscr{A}_{1,2}\theta_{N,2}\sqrt{\pi}}{2^{N+(7/2)}(N(N-2))^{3/4}\Gamma(N)\Gamma(N+2)},\\
&\left\|\frac{\partial\mathbf{u}(x/2,t/2)}{\partial x}-\frac{\partial\mathbf{u}_N(x/2,t/2)}{\partial x}\right\|_{L^2_\omega(\Omega)}\le\frac{\mathscr{A}_{1,1}\theta_{N,1}\sqrt{\pi}}{2^{2N+(9/2)}(N(N-1))^{3/4}\Gamma(N+1)\Gamma(N+2)},\\
&\left\|\frac{\partial^2\mathbf{u}(x/2,t/2)}{\partial x^2}-\frac{\partial^2\mathbf{u}_N(x/2,t/2)}{\partial x^2}\right\|_{L^2_\omega(\Omega)}\le\frac{\mathscr{A}_{1,2}\theta_{N,2}\sqrt{\pi}}{2^{2N+(9/2)}(N(N-2))^{3/4}\Gamma(N)\Gamma(N+2)}.
\end{aligned}\tag{81}$$

Now, Theorems 8, 9, and 10 and Corollary 11 are applied to show that the error of the method becomes sufficiently small when N is sufficiently large. For this, three equations (50), (62), and (65) in Section 4 are called again. Moreover, consider the following bounds:

$$\begin{aligned}
&\left\|\mathbf{u}_N\left(\frac{x}{2},\frac{t}{2}\right)\right\|_{L^2_\omega(\Omega)}\le\mathscr{U}_1,\ \left\|\frac{\partial\mathbf{u}_N(x,t/2)}{\partial x}\right\|_{L^2_\omega(\Omega)}\le\mathscr{U}_2,\ \left\|\frac{\partial^2\mathbf{u}_N(x,t/2)}{\partial x^2}\right\|_{L^2_\omega(\Omega)}\le\mathscr{U}_3,\\
&\left\|\mathbf{u}_N\left(x,\frac{t}{2}\right)\right\|_{L^2_\omega(\Omega)}\le\mathscr{U}_4,\ \left\|\frac{\partial\mathbf{u}_N(x/2,t/2)}{\partial x}\right\|_{L^2_\omega(\Omega)}\le\mathscr{U}_5,\ \left\|\frac{\partial^2\mathbf{u}_N(x/2,t/2)}{\partial x^2}\right\|_{L^2_\omega(\Omega)}\le\mathscr{U}_6.
\end{aligned}\tag{82}$$

Form I. Suppose $\mathrm{u}_N(x,t)$ is the best approximate solution from Θ_N which is obtained from the proposed scheme. Therefore, it satisfies the following equation:

$$ {}_0^C\mathcal{D}_t^\sigma \mathbf{u}_N(x,t) - \frac{\partial^2 \mathbf{u}_N(x,t)}{\partial x^2} - \frac{\partial \mathbf{u}_N(x,t/2)}{\partial x}\mathbf{u}_N\left(\frac{x}{2},\frac{t}{2}\right) - \frac{1}{2}\mathbf{u}_N(x,t) = \mathcal{E}_N(x,t), \tag{83} $$

where $\mathcal{E}_N(x,t)$ is the error term. Subtracting Equation (83) from Equation (50) leads to the following equation:

$$ \begin{aligned} \mathcal{E}_N(x,t) &= \left({}_0^C\mathcal{D}_t^\sigma \mathbf{u}(x,t) - {}_0^C\mathcal{D}_t^\sigma \mathbf{u}_N(x,t)\right) \\ &\quad - \left(\frac{\partial^2 \mathbf{u}(x,t)}{\partial x^2} - \frac{\partial^2 \mathbf{u}_N(x,t)}{\partial x^2}\right) \\ &\quad - \left(\frac{\partial \mathbf{u}(x,t/2)}{\partial x}\mathbf{u}\left(\frac{x}{2},\frac{t}{2}\right) - \frac{\partial \mathbf{u}_N(x,t/2)}{\partial x}\mathbf{u}_N\left(\frac{x}{2},\frac{t}{2}\right)\right) \\ &\quad - \frac{1}{2}(\mathbf{u}(x,t) - \mathbf{u}_N(x,t)) \\ &= \left({}_0^C\mathcal{D}_t^\sigma \mathbf{u}(x,t) - {}_0^C\mathcal{D}_t^\sigma \mathbf{u}_N(x,t)\right) \\ &\quad - \left(\frac{\partial^2 \mathbf{u}(x,t)}{\partial x^2} - \frac{\partial^2 \mathbf{u}_N(x,t)}{\partial x^2}\right) \\ &\quad - \left(\frac{\partial \mathbf{u}(x,t/2)}{\partial x} - \frac{\partial \mathbf{u}_N(x,t/2)}{\partial x}\right)\left(\mathbf{u}\left(\frac{x}{2},\frac{t}{2}\right) - \mathbf{u}_N\left(\frac{x}{2},\frac{t}{2}\right) + \mathbf{u}_N\left(\frac{x}{2},\frac{t}{2}\right)\right) - \frac{\partial \mathbf{u}_N(x,t/2)}{\partial x}\left(\mathbf{u}\left(\frac{x}{2},\frac{t}{2}\right) - \mathbf{u}_N\left(\frac{x}{2},\frac{t}{2}\right)\right) \\ &\quad - \frac{1}{2}\left(\mathbf{u}(x,t) - \mathbf{u}_N(x,t)\right). \end{aligned} \tag{84} $$

So, one has

$$ \begin{aligned} \|\mathcal{E}_N(x,t)\|_{L^2_\omega(\Omega)} &\frac{\mathcal{A}_2\tau_N\sqrt{\pi}}{2^{5/2}\Gamma(N+2)\Gamma(N-\sigma+2)(N(N-\sigma))^{3/4}} \\ &+ \frac{\mathcal{A}_{1,2}\theta_{N,2}\sqrt{\pi}}{2^{5/2}\Gamma(N)\Gamma(N+2)(N(N-2))^{3/4}} \\ &+ \frac{\mathcal{A}_{1,1}\theta_{N,1}\sqrt{\pi}}{2^{N+7/2}\Gamma(N+1)\Gamma(N+2)(N(N-1))^{3/4}} \\ &\cdot \left(\frac{\mathcal{A}_0\tau_N\sqrt{\pi}}{2^{2N+9/2}\Gamma(N+1)^2N^{3/2}} + \mathcal{U}_1\right) + \mathcal{U}_2\frac{\mathcal{A}_0\tau_N\sqrt{\pi}}{2^{2N+9/2}\Gamma(N+1)^2N^{3/2}} \\ &+ \frac{1}{2}\frac{\mathcal{A}_0\tau_N\sqrt{\pi}}{2^{5/2}\Gamma(N+1)^2N^{3/2}}. \end{aligned} \tag{85} $$

Form II. If $\mathbf{u}_N(x,t)$ is the solution obtained from the proposed algorithm for Equation (62), then it satisfies the following equation:

$$ \mathcal{E}_N(x,t) = {}_0^C\mathcal{D}_t^\sigma \mathbf{u}_N(x,t) - \frac{\partial^2 \mathbf{u}_N(x,t/2)}{\partial x^2}\mathbf{u}_N\left(x,\frac{t}{2}\right) + \mathbf{u}_N(x,t). \tag{86} $$

Subtracting Equation (86) from Equation (62) leads to

$$ \begin{aligned} \mathcal{E}_N(x,t) &= \left({}_0^C\mathcal{D}_t^\sigma \mathbf{u}(x,t) - {}_0^C\mathcal{D}_t^\sigma \mathbf{u}_N(x,t)\right) \\ &\quad - \left(\frac{\partial^2 \mathbf{u}(x,t/2)}{\partial x^2}\mathbf{u}\left(x,\frac{t}{2}\right) - \frac{\partial^2 \mathbf{u}_N(x,t/2)}{\partial x^2}\mathbf{u}_N\left(x,\frac{t}{2}\right)\right) \\ &\quad + (\mathbf{u}(x,t) - \mathbf{u}_N(x,t)) \\ &= \left({}_0^C\mathcal{D}_t^\sigma \mathbf{u}(x,t) - {}_0^C\mathcal{D}_t^\sigma \mathbf{u}_N(x,t)\right) \\ &\quad - \left(\frac{\partial^2 \mathbf{u}(x,t/2)}{\partial x^2} - \frac{\partial^2 \mathbf{u}_N(x,t/2)}{\partial x^2}\right)\left(\mathbf{u}\left(x,\frac{t}{2}\right) - \mathbf{u}_N\left(x,\frac{t}{2}\right) + \mathbf{u}_N\left(x,\frac{t}{2}\right)\right) - \frac{\partial^2 \mathbf{u}_N(x,t/2)}{\partial x^2}\left(\mathbf{u}\left(x,\frac{t}{2}\right) - \mathbf{u}_N\left(x,\frac{t}{2}\right)\right) \\ &\quad + (\mathbf{u}(x,t) - \mathbf{u}_N(x,t)). \end{aligned} \tag{87} $$

Then, one has

$$ \begin{aligned} \|\mathcal{E}_N(x,t)\|_{L^2_\omega(\Omega)} &\le \frac{\mathcal{A}_2\tau_N\sqrt{\pi}}{2^{5/2}\Gamma(N+2)\Gamma(N-\sigma+2)(N(N-\sigma))^{3/4}} \\ &\quad + \frac{\mathcal{A}_{1,2}\theta_{N,2}\sqrt{\pi}}{2^{N+(7/2)}\Gamma(N)\Gamma(N+2)(N(N-2))^{3/4}} \\ &\quad \cdot \left(\frac{\mathcal{A}_0\tau_N\sqrt{\pi}}{2^{N+(7/2)}\Gamma(N+2)^2N^{3/2}} + \mathcal{U}_4\right) \\ &\quad + \mathcal{U}_3\frac{\mathcal{A}_0\tau_N\sqrt{\pi}}{2^{N+(7/2)}\Gamma(N+2)^2N^{3/2}} \\ &\quad + \frac{\mathcal{A}_0\tau_N\sqrt{\pi}}{2^{5/2}\Gamma(N+2)^2N^{3/2}}. \end{aligned} \tag{88} $$

Form III. If $\mathbf{u}_N(x,t)$ is an approximate solution obtained from the suggested algorithm for Equation (65), then one has

$$ \begin{aligned} \mathcal{E}_N(x,t) &= {}_0^C\mathcal{D}_t^\sigma \mathbf{u}_N(x,t) - \frac{\partial^2 \mathbf{u}_N(x/2,t/2)}{\partial x^2}\frac{\partial \mathbf{u}_N(x/2,t/2)}{\partial x} \\ &\quad + \frac{\partial \mathbf{u}_N(x,t)}{\partial x} + \mathbf{u}_N(x,t). \end{aligned} \tag{89} $$

Subtracting (89) from Equation (65) leads to

$$ \begin{aligned} \mathcal{E}_N(x,t) &= \left({}_0^C\mathcal{D}_t^\sigma \mathbf{u}_N(x,t) - {}_0^C\mathcal{D}_t^\sigma \mathbf{u}_N(x,t)\right) \\ &\quad - \left(\frac{\partial^2 \mathbf{u}(x/2,t/2)}{\partial x^2}\frac{\partial \mathbf{u}(x/2,t/2)}{\partial x} - \frac{\partial^2 \mathbf{u}_N(x/2,t/2)}{\partial x^2}\frac{\partial \mathbf{u}_N(x/2,t/2)}{\partial x}\right) \\ &\quad + \left(\frac{\partial \mathbf{u}(x,t)}{\partial x} - \frac{\partial \mathbf{u}_N(x,t)}{\partial x}\right) + (\mathbf{u}(x,t) - \mathbf{u}_N(x,t)) \\ &= \left({}_0^C\mathcal{D}_t^\sigma \mathbf{u}_N(x,t) - {}_0^C\mathcal{D}_t^\sigma \mathbf{u}_N(x,t)\right) \\ &\quad - \left(\frac{\partial^2 \mathbf{u}(x/2,t/2)}{\partial x^2} - \frac{\partial^2 \mathbf{u}_N(x/2,t/2)}{\partial x^2}\right) \\ &\quad \cdot \left(\frac{\partial \mathbf{u}(x/2,t/2)}{\partial x} - \frac{\partial \mathbf{u}_N(x/2,t/2)}{\partial x} + \frac{\partial \mathbf{u}_N(x/2,t/2)}{\partial x}\right) \end{aligned} $$

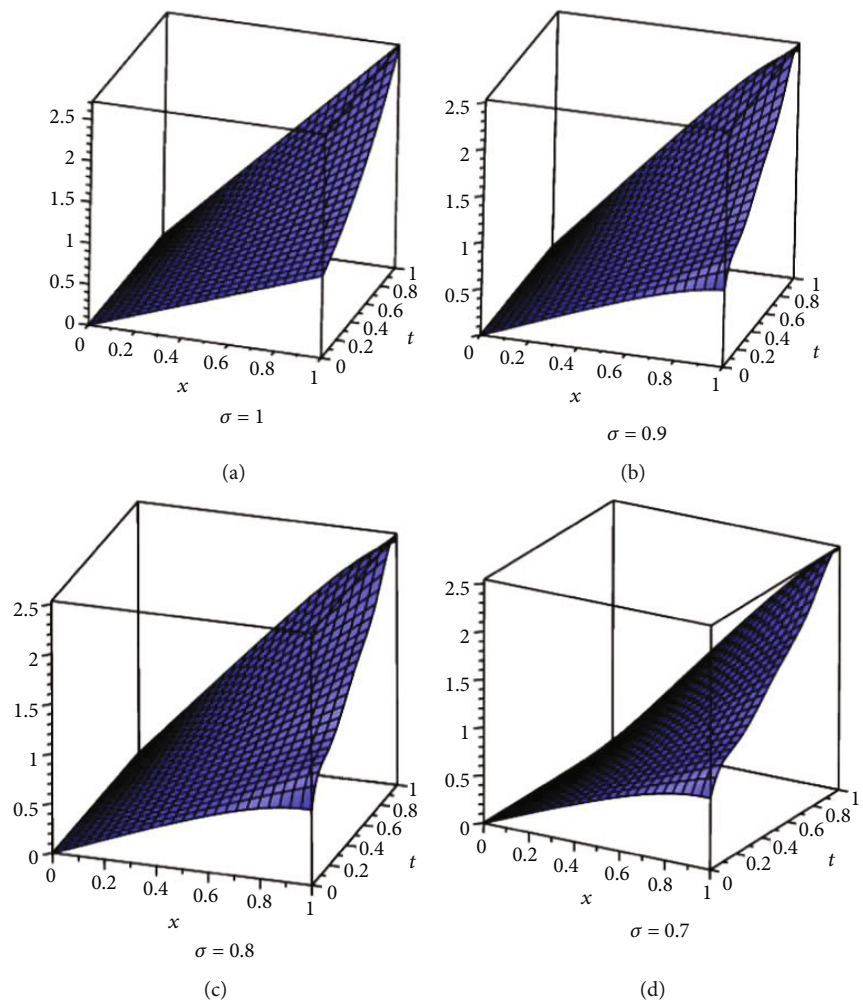

Figure 1: Surface behavior of solutions of Example 1 for $N = 6$ and various values of σ.

$$- \frac{\partial^2 \mathbf{u}_N(x/2, t/2)}{\partial x^2} \left(\frac{\partial \mathbf{u}(x/2, t/2)}{\partial x} - \frac{\partial \mathbf{u}_N(x/2, t/2)}{\partial x} \right) + \left(\frac{\partial \mathbf{u}(x, t)}{\partial x} - \frac{\partial \mathbf{u}_N(x, t)}{\partial x} \right) + (\mathbf{u}(x, t) - \mathbf{u}_N(x, t)). \tag{90}$$

By taking L^2-norm, one gets

$$\begin{aligned} \|\mathscr{E}_N(x, t)\|_{L^2_\omega(\Omega)} & \frac{\mathscr{A}_2 \tau_N \sqrt{\pi}}{2^{5/2} \Gamma(N+2) \Gamma(N-\sigma+2) (N(N-\sigma))^{3/4}} \\ & + \frac{\mathscr{A}_{1,2} \theta_{N,2} \sqrt{\pi}}{2^{2N+(9/2)} \Gamma(N) \Gamma(N+2) (N(N-2))^{3/4}} \\ & \cdot \left(\mathscr{U}_5 + \frac{A_{1,1} \theta_{N,1} \sqrt{\pi}}{2^{2N+(9/2)} \Gamma(N+1) \Gamma(N+2) (N(N-1))^{3/4}} \right) \\ & + \mathscr{U}_6 \frac{A_{1,1} \theta_{N,1} \sqrt{\pi}}{2^{2N+(9/2)} \Gamma(N+1) \Gamma(N+2) (N(N-1))^{3/4}} \\ & + \frac{A_{1,1} \theta_{N,1} \sqrt{\pi}}{2^{5/2} \Gamma(N+1) \Gamma(N+2) (N(N-1))^{3/4}} \\ & + \frac{\mathscr{A}_0 \tau_N \sqrt{\pi}}{2^{5/2} \Gamma(N+2)^2 N^{3/2}}. \end{aligned} \tag{91}$$

As seen from the right-hand sides of inequalities (85), (88), and (91), $\mathscr{E}_N(x, t)$ will decrease by choosing appropriate values of N, i.e., the error bound will be sufficiently small for the sufficiently large values of N.

5. Numerical Examples

To demonstrate the accuracy and validity of the proposed method, three given examples in Refs. [26, 27] are solved in this section. These equations have been solved using the homotopy perturbation and natural transformation decomposition methods in [26, 27], respectively. The approximate solutions are compared to the exact ones and those reported by [26, 27], maximum absolute errors are calculated, and results are reported in tables and figures.

Example 1. Consider Equation (50) with the exact solution $\mathbf{u}(x, t) = x \exp(t)$ for $\sigma = 1$ and its corresponding residual function Equation (61) that is collocated at roots of the

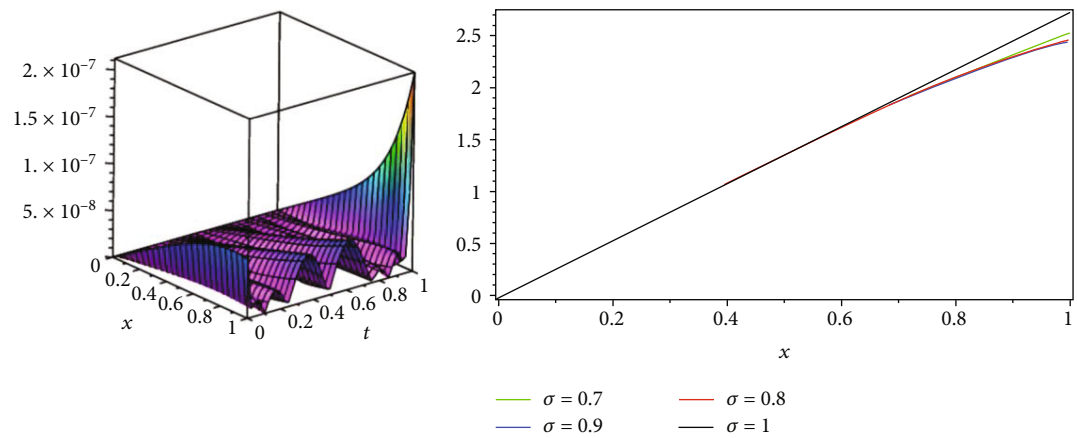

(a) (b)

Figure 2: (a) Absolute error function for Example 1 for $N = 6$, $\sigma = 1$. (b) Plots of solutions for different values of σ, $N = 6, t = 1$.

Table 1: Numerical results of Example 1 for $N = 6$ and various values of σ.

x_i	t_j	$\sigma = 0.7$	$\sigma = 0.8$	$\sigma = 0.9$	$\sigma = 1$	Exact	Error
0.25	0.25	0.3199866	0.3203102	0.3206518	0.3210064	0.3210064	1.3966×10^{-9}
	0.50	0.4114050	0.4116834	0.4119457	0.4121803	0.4121803	8.0055×10^{-10}
	0.75	0.5285656	0.5288107	0.5290395	0.5292500	0.5292500	9.2143×10^{-10}
	1.00	0.6788737	0.6790652	0.6792634	0.6795704	0.6795705	2.5998×10^{-8}
0.50	0.25	0.6337580	0.6362631	0.6389749	0.6420127	0.6420127	2.5203×10^{-9}
	0.50	0.8187531	0.8209753	0.8229275	0.8243606	0.8243606	1.4904×10^{-9}
	0.75	1.0528606	1.0547361	1.0565811	1.0585000	1.0585000	8.8651×10^{-10}
	1.00	1.3512839	1.3521827	1.3540014	1.3591409	1.3591409	5.3534×10^{-8}
0.75	0.25	0.9340411	0.9417454	0.9507790	0.9630191	0.9630191	1.9619×10^{-9}
	0.50	1.2215925	1.2293426	1.2350774	1.2365410	1.2365410	7.2547×10^{-10}
	0.75	1.5672652	1.5729640	1.5793773	1.5877500	1.5877500	5.3519×10^{-10}
	1.00	1.9936484	1.9888627	1.9937973	2.0387113	2.0387114	9.5450×10^{-8}
1.0	0.25	1.2085347	1.2227737	1.2437234	1.2840254	1.2840254	4.6333×10^{-9}
	0.50	1.6298471	1.6506066	1.6612803	1.6487213	1.6487213	6.2784×10^{-9}
	0.75	2.0608936	2.0714857	2.0878337	2.1170000	2.1170000	2.3318×10^{-9}
	1.00	2.5193819	2.4585462	2.4518089	2.7182816	2.7182818	2.1185×10^{-7}

Chebyshev polynomials of the sixth kind. Therefore, an approximate solution is obtained. The surface plots of approximate solutions are depicted in Figure 1, and the absolute error function is seen in Figure 2(a) for $N = 6$ and $\sigma = 0.7, 0.8, 0.9, 1$. Also, the figures of approximate solutions at $t = 1$ are seen in Figure 2(b) for $N = 6$ and $\sigma = 0.7, 0.8, 0.9, 1$. The values of the approximate solution at the selected points are listed in Table 1 which compared to the values of the exact one for $N = 6$ and various values of σ. The results are compared to those reported in [26, 27] in Table 2. As seen, the proposed method presents better accuracy. Besides, the maximum absolute errors of approximate solutions are computed for different values of N and $\sigma = 1$, and results are observed in Table 3. Increasing N leads to the decrease of the values of the errors.

Example 2. Consider the nonlinear fractional partial differential equation with the proportional delay in (62) and its corresponding residual function in Equation (64). The

Table 2: Numerical results of Example 1 for $N = 6$, $\sigma = 1$.

x_i	t_j	Method in [26]	Method in [27]	Chebyshev method	Exact
0.25	0.25	0.3210042	0.3210042	0.3210064	0.3210064
	0.50	0.4121094	0.4121094	0.4121803	0.4121803
	0.75	0.5286865	0.5286865	0.5292500	0.5292500
	1.00	0.6770833	0.6770833	0.6795704	0.6795705
0.50	0.25	0.6420085	0.6420085	0.6420127	0.6420127
	0.50	0.8242188	0.8242187	0.8243606	0.8243606
	0.75	1.0573730	1.0573730	1.0585000	1.0585000
	1.00	1.3541667	1.3541667	1.3591409	1.3591409
0.75	0.25	0.9630127	0.9630127	0.9630191	0.9630191
	0.50	1.236328	1.2363281	1.2365410	1.2365410
	0.75	1.586060	1.5860596	1.5877500	1.5877500
	1.00	2.0312500	2.0312490	2.0387113	2.0387114

Table 3: Maximum absolute errors of Example 1 for $\sigma = 1$ and various values of N.

N	4	5	6	7	8
Error	7.5579×10^{-5}	4.5135×10^{-6}	2.1185×10^{-7}	7.7009×10^{-9}	3.6459×10^{-10}

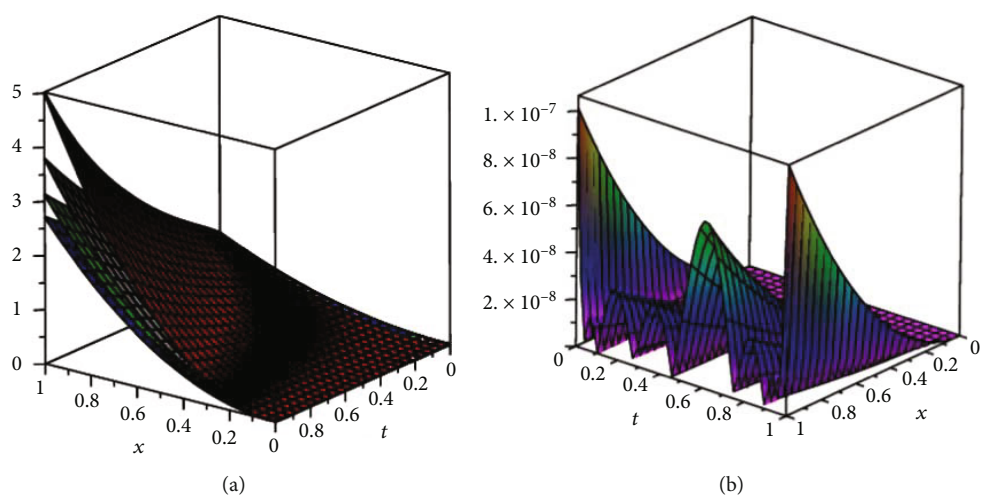

Figure 3: (a) Surface solutions for $N = 6$ and $\sigma = 1$ (blue), $\sigma = 0.9$ (green), $\sigma = 0.8$ (gray), and $\sigma = 0.7$ (red). (b) Absolute error function of Example 2 for $N = 6$, $\sigma = 1$.

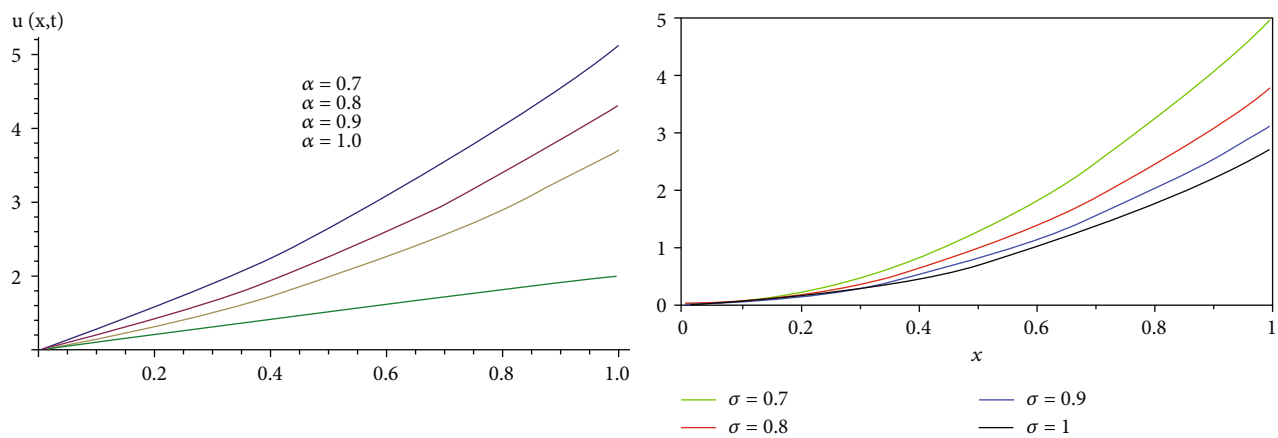

(a) (b)

Figure 4: Left: approximate solutions depicted in [26]. Right: obtained solutions from the proposed method for different values of σ, $N = 6$, $t = 1$ for Example 2.

Table 4: Numerical results of Example 2 for various values of σ, $N = 6$.

x_i	t_j	$\sigma = 0.7$	$\sigma = 0.8$	$\sigma = 0.9$	$\sigma = 1$	Exact	Error
0.25	0.25	0.1013235	0.0914426	0.0849036	0.0802516	0.0802516	8.0280×10^{-10}
	0.50	0.1493151	0.1266051	0.1125784	0.1030451	0.1030451	1.5944×10^{-9}
	0.75	0.2164930	0.1734092	0.1485001	0.1323125	0.1323125	1.9099×10^{-10}
	1.00	0.3137011	0.2372436	0.1956991	0.1698926	0.1698926	6.6257×10^{-9}
0.50	0.25	0.4052941	0.3657705	0.3396142	0.3210064	0.3210064	3.2112×10^{-9}
	0.50	0.5972605	0.5064204	0.4503138	0.4121803	0.4121803	6.3777×10^{-9}
	0.75	0.8659720	0.6936368	0.5940005	0.5292500	0.5292500	7.6358×10^{-10}
	1.00	1.2548043	0.9489743	0.7827965	0.6795704	0.6795705	2.6504×10^{-8}
0.75	0.25	0.9119117	0.8229837	0.7641321	0.7222643	0.7222643	7.2249×10^{-9}
	0.50	1.3438362	1.1394460	1.0132059	0.9274057	0.9274057	1.4348×10^{-8}
	0.75	1.9484370	1.5606829	1.3365010	1.1908125	1.1908125	1.7060×10^{-9}
	1.00	2.8233096	2.1351921	1.7612922	1.5290335	1.5290335	5.9679×10^{-8}
1.0	0.25	0.3371509	1.4630821	1.3584570	1.2840254	1.2840254	1.2842×10^{-8}
	0.50	2.3890421	2.0256818	1.8012550	1.6487214	1.6487213	2.5483×10^{-8}
	0.75	3.4638880	2.7745474	2.3760019	2.1170000	2.117000	2.9197×10^{-9}
	1.00	5.0192169	3.7958971	3.1311862	2.7182817	2.7182818	1.0649×10^{-7}

Table 5: Numerical results of Example 2 for $N = 6$, $\sigma = 1$.

x_i	t_j	Method in [26]	Method in [27]	Chebyshev Method	Exact
0.25	0.25	0.0802511	0.0802516	0.0802516	0.0802516
	0.50	0.1030273	0.1030451	0.1030451	0.1030451
	0.75	0.1321716	0.1323123	0.1323125	0.1323125
	1.00	0.1692708	0.1698909	0.1698926	0.1698926
0.50	0.25	0.3210042	0.3210064	0.3210064	0.3210064
	0.50	0.4121094	0.4121803	0.4121803	0.4121803
	0.75	0.5286865	0.5292493	0.5292500	0.5292500
	1.00	0.6770833	0.6795635	0.6795704	0.6795705
0.75	0.25	0.7222595	–	0.7222643	0.7222643
	0.50	0.9272461	–	0.9274057	0.9274057
	0.75	1.1895447	–	1.1908125	1.1908125
	1.00	1.5234375	–	1.5290335	1.5290335
1.00	0.25	–	1.2840254	1.2840254	1.2840254
	0.50	–	1.6487212	1.6487213	1.6487213
	0.75	–	2.1169973	2.1170000	2.1170000
	1.00	–	2.7182540	2.7182817	2.7182818

Table 6: Maximum absolute errors of Example 2 for $\sigma = 1$ and various values of N.

N	4	5	6	7	8
Error	2.3903×10^{-5}	2.3083×10^{-6}	1.0149×10^{-7}	1.6453×10^{-8}	2.8933×10^{-9}

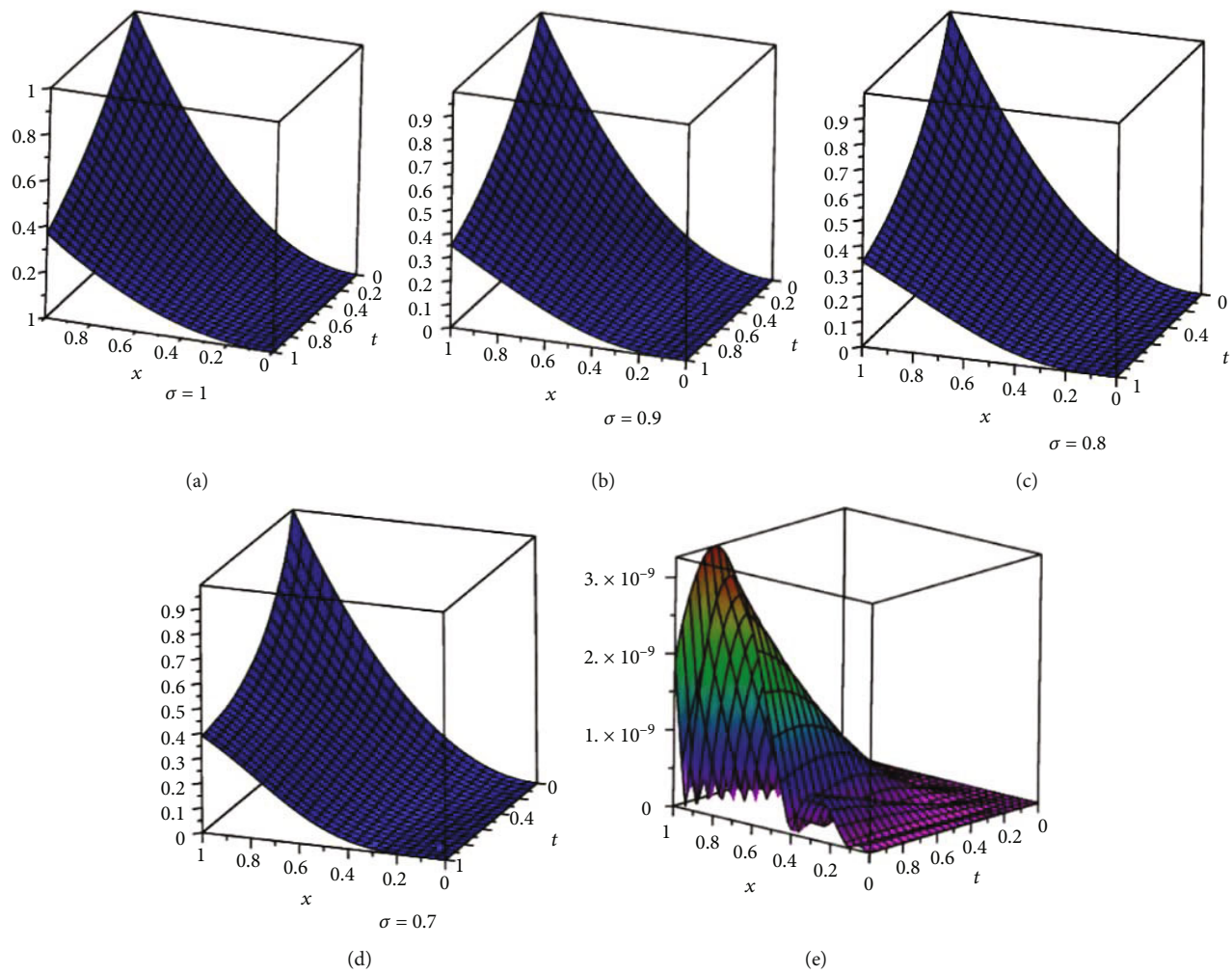

Figure 5: (a)–(d) Surface solutions for $N = 8$ and $\sigma = 1,0.9,0.8,0.7$. (e) Absolute error function of Example 3 for $N = 8$, $\sigma = 1$.

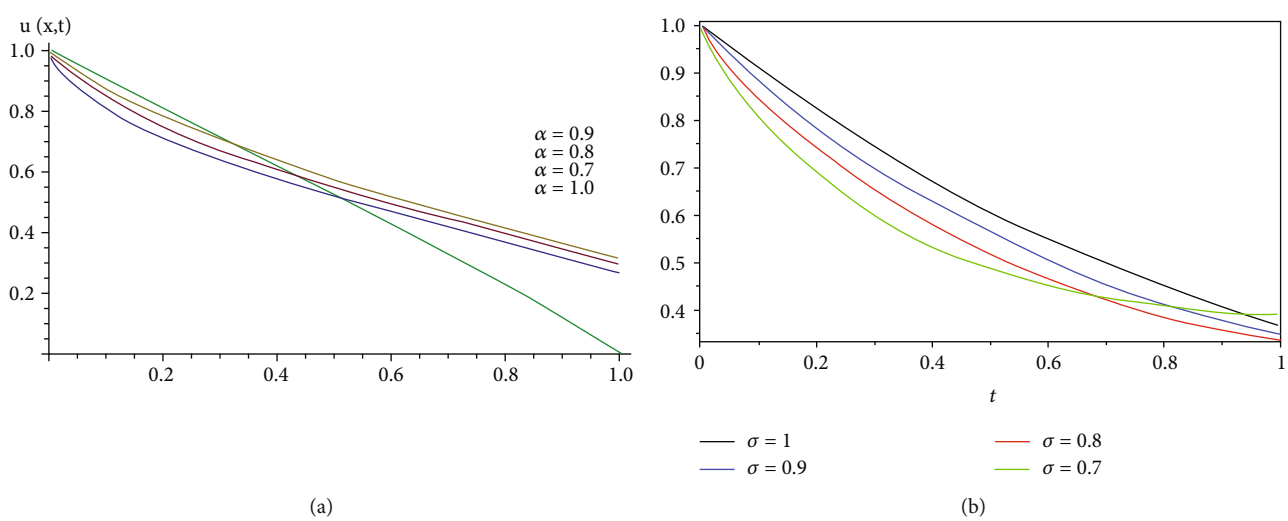

Figure 6: Left: approximate solutions depicted in [26]. Right: obtained solutions from the proposed method for different values of σ, $N = 8$, $x = 1$ for Example 3.

exact solution is $\mathbf{u}(x,t) = x^2 \exp(t)$ if $\sigma = 1$. The 3D figures of the approximate solutions are depicted in Figure 3(a) for $N = 6$ and $\sigma = 0.7,0.8,0.9,1$. The plot of the absolute error function is seen in Figure 3(b). The approximate solutions are plotted at $t = 1$ and compared to those presented by [26] in Figure 4 for $N = 6$ and $\sigma =$

Table 7: Numerical results of Example 3 for various values of σ, $N = 8$.

x_i	t_j	$\sigma = 0.7$	$\sigma = 0.8$	$\sigma = 0.9$	$\sigma = 1$	Exact	Error
0.25	0.25	0.0357780	0.0420024	0.0456542	0.0486750	0.0486750	7.6753×10^{-12}
	0.50	0.0205174	0.0286599	0.0333034	0.0379082	0.0379082	1.6649×10^{-10}
	0.75	0.0112779	0.0189974	0.0238430	0.0295229	0.0295229	3.8695×10^{-10}
	1.00	0.0069793	0.0127259	0.0169906	0.0229925	0.0229925	5.6253×10^{-10}
0.50	0.25	0.1660490	0.1748887	0.1854495	0.1947002	0.1947002	1.1877×10^{-10}
	0.50	0.1279483	0.1353176	0.1441304	0.1516327	0.1516327	7.2917×10^{-10}
	0.75	0.0946332	0.1052157	0.1124282	0.1180916	0.1180916	1.1956×10^{-9}
	1.00	0.0696568	0.0820349	0.0872306	0.0919699	0.0919699	1.2032×10^{-9}
0.75	0.25	0.3660803	0.3889022	0.4149060	0.4380754	0.4380754	2.6901×10^{-10}
	0.50	0.2980705	0.2987502	0.3193789	0.3411735	0.3411735	4.0079×10^{-10}
	0.75	0.2559271	0.2423933	0.2546668	0.2657062	0.2657062	1.0422×10^{-9}
	1.00	0.2239921	0.2048991	0.2081581	0.2069322	0.2069322	3.1164×10^{-9}
1.0	0.25	0.6401432	0.6932895	0.7398243	0.7788008	0.7788008	6.2071×10^{-11}
	0.50	0.4874058	0.5155939	0.5609473	0.6065307	0.6065307	1.5635×10^{-9}
	0.75	0.4145884	0.4015728	0.4331895	0.4723665	0.4723666	3.2396×10^{-9}
	1.00	0.3913723	0.3364194	0.3492084	0.3678794	0.3678794	1.8734×10^{-9}

Table 8: Numerical results of Example 3 for $N = 8$, $\sigma = 1$.

x_i	t_j	Method in [26]	Method in [27]	Chebyshev method	Exact
0.25	0.25	0.0486755	0.0486750	0.0486750	0.0486750
	0.50	0.0379232	0.0379081	0.0379082	0.0379082
	0.75	0.0296326	0.0295228	0.0295229	0.0295229
	1.00	0.0234375	0.0229911	0.0229925	0.0229925
0.50	0.25	0.1947021	0.1947002	0.1947002	0.1947002
	0.50	0.1516927	0.1516326	0.1516327	0.1516327
	0.75	0.1185303	0.1180911	0.1180916	0.1180916
	1.00	0.0937500	0.0919643	0.0919699	0.0919699
0.75	0.25	0.4380798	–	0.4380754	0.4380754
	0.50	0.3413086	–	0.3411735	0.3411735
	0.75	0.2666931	–	0.2657062	0.2657062
	1.00	0.2109375	–	0.2069322	0.2069322
1.00	0.25	–	0.7788008	0.7788008	0.7788008
	0.50	–	0.6065306	0.6065307	0.6065307
	0.75	–	0.4723643	0.4723665	0.4723665
	1.00	–	0.3678571	0.3678794	0.3678794

0.7,0.8,0.9,1. As seen, our obtained solutions converge faster to the exact one. The values of the resultant solution at the selected points are listed in Table 4 which compared to the values of the exact solution for $N = 6$ and various values of σ. The obtained results are compared to those reported in [26, 27] in Table 5. As seen, the proposed method presents better accuracy. The maximum absolute errors are seen in Table 6 for $\sigma = 1$ and $N = 4, 5, 6, 7, 8$.

Example 3. Consider Form III in (65) and residual function (67). The exact solution is $\mathbf{u}(x,t) = x^2 \exp(-t)$ if $\sigma = 1$. The three-dimensional figures of the approximate solutions are depicted in Figures 5(a)–5(d) for $N = 8$ and $\sigma = 0.7, 0.8, 0.9, 1$. The plot of the absolute error function is seen in Figure 5(e) for $N = 8$ and $\sigma = 1$. The obtained solutions are plotted in Figure 6 at $t = 1$ for $N = 8$ and $\sigma = 0.7, 0.8, 0.9, 1$ which are compared to those presented by [27]. The values of the resultant solution at the selected points are listed in Table 7 which are compared to the values of the exact one for $N = 8$ and various values of σ. As $\sigma \longrightarrow 1$, the numerical solutions converge to the exact one. The obtained results are compared to those reported in [26, 27] in Table 8 for $N = 8$ and $\sigma = 1$. As seen, the proposed method presents better accuracy.

6. Conclusion

This paper deals with numerically solving a class of fractional partial differential equations with proportional delays on the domain $\Omega = [0,1] \times [0,1]$. A spectral collocation approach, based on the sixth-kind Chebyshev polynomials as basis functions, has been considered to solve this class of equations. The two-variable Chebyshev polynomials of the sixth kind were introduced, and their integral operational matrices were derived. The relationship between the delay Chebyshev polynomials and the original basis was stated in a matrix form called delay operational matrix. The numerical results were reported in tables and figures and confirmed the accuracy and good agreement of the approximate solutions with exact ones. An error analysis has been presented which showed that the method error becomes small when N is properly selected. The picked examples were also solved by homotopy perturbation and natural decomposition methods in [26, 27], and values of approximate solutions were reported at some selected points. It was clear from Tables 2, 5, and 8; the proposed method is more efficient. Therefore, the sixth-kind Chebyshev polynomials can be used to numerically solve other fractional functional equations.

Data Availability

All results have been obtained by conducting the numerical procedure, and the ideas can be shared for the researchers.

Conflicts of Interest

The authors declare that they have no conflicts of interest.

References

[1] J. Wu, *Theory and Applications of Partial Functional Differential Equations*, Springer-Verlag, New York, NY, USA, 1996.

[2] F. Shakeri and M. Dehghan, "Solution of delay differential equations via a homotopy perturbation method," *Mathematical and Computer Modeling*, vol. 48, no. 3-4, pp. 486–498, 2008.

[3] A. D. Polyanin and A. I. Zhurov, "Functional constraints method for constructing exact solutions to delay reaction-diffusion equations and more complex nonlinear equations," *Communications in Nonlinear Science and Numerical Simulation*, vol. 19, no. 3, pp. 417–430, 2014.

[4] V. G. Pimenov and A. S. Hendy, "A numerical solution for a class of time fractional diffusion equations with delay," *International Journal of Applied Mathematics and Computer Science*, vol. 27, no. 3, pp. 477–488, 2017.

[5] A. S. Hendy, V. G. Pimenov, and J. E. Macias-Diaz, "Convergence and stability estimates in difference setting for time-fractional parabolic equations with functional delay," *Numerical Methods for Partial Differential Equations*, vol. 36, no. 1, pp. 118–132, 2020.

[6] A. S. Hendy, M. A. Zaky, and R. H. De Staelen, "A general framework for the numerical analysis of high-order finite difference solvers for nonlinear multi-term time-space fractional partial differential equations with time delay," *Applied Numerical Mathematics*, vol. 169, pp. 108–121, 2021.

[7] S. Nandal and D. N. Pandey, "Numerical solution of nonlinear fourth order fractional sub-diffusion wave equation with time delay," *Applied Mathematics and Computation*, vol. 369, article 124900, 2020.

[8] Y. Xu, "An integral formula for generalized Gegenbauer polynomials and Jacobi polynomials," *Advances in Applied Mathematics*, vol. 29, no. 2, pp. 328–343, 2002.

[9] A. Draux, M. Sadik, and B. Moalla, "Markov-Bernstein inequalities for generalized Gegenbauer weight," *Applied Numerical Mathematics*, vol. 61, no. 12, pp. 1301–1321, 2011.

[10] C. F. Bracciali, J. V. da Silva, and A. Sri Ranga, "A class of Sobolev orthogonal polynomials on the unit circle and associated continuous dual Hahn polynomials: bounds, asymptotics and zeros," *Journal of Approximation Theory*, vol. 268, article 105604, 2021.

[11] A. Gil, J. Segura, and N. M. Temme, "Asymptotic expansions of Jacobi polynomials and of the nodes and weights of Gauss-Jacobi quadrature for large degree and parameters in terms of elementary functions," *Journal of Mathematical Analysis and Applications*, vol. 494, no. 2, article 124642, 2021.

[12] S. N. Tural-Polat and A. T. Dincel, "Numerical solution method for multi-term variable order fractional differential equations by shifted Chebyshev polynomials of the third kind," *Alexandria Engineering Journal*, 2021.

[13] T. Vlasic, I. Ralasic, A. Tafro, and D. Sersic, "Spline-like Chebyshev polynomial model for compressive imaging," *Journal of Visual Communication and Image Representation*, vol. 61, article 102731, 2019.

[14] S. Nemati, S. Sedaghat, and I. Mohammadi, "A fast numerical algorithm based on the second kind Chebyshev polynomials for fractional integro-differential equations with weakly singular kernels," *Journal of Computational and Applied Mathematics*, vol. 308, pp. 231–242, 2016.

[15] S. Dahmen and C. Glorieux, "Optimization of coupled Lamb wave parameters for defect detection in anisotropic composite three-layer with Kelvin-Voigt viscoelasticity using Legendre polynomial method," *Composite Structures*, vol. 272, article 114158, 2021.

[16] G. Jie, L. Yan, S. Guorong, L. Mingkun, and Z. Mingfang, "Legendre orthogonal polynomial method in calculating reflection and transmission coefficients of fluid-loaded functionally gradient plates," *Wave Motion*, vol. 104, article 102754, 2021.

[17] M. Masjed–Jamei, "Some new classes of orthogonal polynomials and special functions: a symmetric generalization of Sturm–Liouville problems and its consequences," PdD thesis, 2006.

[18] W. M. Abd-Elhameed and Y. H. Youssri, "Sixth-kind Chebyshev spectral approach for solving fractional differential equations," *International Journal of Nonlinear Sciences and Numerical Simulation*, vol. 20, no. 2, pp. 191–203, 2019.

[19] X. Xu, L. Xiong, and F. Zhou, "Solving fractional optimal control problems with inequality constraints by a new kind of Chebyshev wavelets method," *Journal of Computational Science*, vol. 54, article 101412, 2021.

[20] W. M. Abd-Elhameed, "Novel expressions for the derivatives of sixth kind Chebyshev polynomials: spectral solution of the non-linear one-dimensional Burgers' equation," *Fractal and Fractional*, vol. 5, no. 2, p. 53, 2021.

[21] A. G. Atta, W. M. Abd-Elhameed, G. M. Moatimid, and Y. H. Youssri, "Shifted fifth-kind Chebyshev Galerkin treatment for linear hyperbolic first- order partial differential equations," *Applied Numerical Mathematics*, vol. 167, pp. 237–256, 2021.

[22] A. Babaei, H. Jafari, and S. Banihashemi, "Numerical solution of variable order fractional nonlinear quadratic integro- differential equations based on the sixth-kind Chebyshev collocation method," *Journal of Computational and Applied Mathematics*, vol. 377, article 112908, 2020.

[23] K. Sadri, K. Hosseini, D. Baleanu, A. Ahmadian, and S. Salahshour, "Bivariate Chebyshev polynomials of the fifth kind for variable-order time-fractional partial integro-differential equations with weakly singular kernel," *Advances in Difference Equations*, vol. 2021, no. 1, 2021.

[24] K. Sadri and H. Aminikhah, "A new efficient algorithm based on fifth-kind Chebyshev polynomials for solving multi-term variable-order time-fractional diffusion-wave equation," *International Journal of Computer Mathematics*, pp. 1–27, 2021.

[25] W. M. Abd-Elhameed and Y. H. Youssri, "New formulas of the high-order derivatives of fifth-kind Chebyshev polynomials: spectral solution of the convection-diffusion equation," *Numerical Methods for Partial Differential Equations*, pp. 1–17, 2021.

[26] M. G. Sakar, F. Uludag, and F. Erdogan, "Numerical solution of time-fractional nonlinear PDEs with proportional delays by homotopy perturbation method," *Applied Mathematical Modeling*, vol. 40, no. 13-14, pp. 6639–6649, 2016.

[27] R. Shah, H. Khan, P. Kumam, M. Arif, and D. Baleanu, "Natural transform decomposition method for solving fractional-order partial differential equations with proportional delay," *Mathematics*, vol. 7, no. 6, p. 532, 2019.

[28] I. Podlubny, *Fractional Differential Equations: An Introduction to Fractional Derivatives, Fractional Differential Equations, to Methods of Their Solution and Some of Their Applications*, vol. 198, Elsevier, Amsterdam, The Netherlands, 1998.

[29] B. Y. Guo and L. L. Wang, "Jacobi approximations in non-uniformly Jacobi-weighted Sobolev spaces," *Journal of Approximate Theory*, vol. 128, no. 1, pp. 1–41, 2004.

Hindawi
Journal of Function Spaces
Volume 2021, Article ID 9984473, 11 pages
https://doi.org/10.1155/2021/9984473

Research Article

Nonuniform Finite Difference Scheme for the Three-Dimensional Time-Fractional Black–Scholes Equation

Sangkwon Kim,[1] Chaeyoung Lee,[1] Wonjin Lee,[2] Soobin Kwak,[1] Darae Jeong,[3] and Junseok Kim[1]

[1]*Department of Mathematics, Korea University, Seoul 02841, Republic of Korea*
[2]*Department of Financial Engineering, Korea University, Seoul 02841, Republic of Korea*
[3]*Department of Mathematics, Kangwon National University, Gangwon-do 24341, Republic of Korea*

Correspondence should be addressed to Junseok Kim; cfdkim@korea.ac.kr

Received 24 September 2021; Accepted 29 November 2021; Published 24 December 2021

Academic Editor: Youssri Hassan Youssri

In this study, we present an accurate and efficient nonuniform finite difference method for the three-dimensional (3D) time-fractional Black–Scholes (BS) equation. The operator splitting scheme is used to efficiently solve the 3D time-fractional BS equation. We use a nonuniform grid for pricing 3D options. We compute the three-asset cash-or-nothing European call option and investigate the effects of the fractional-order α in the time-fractional BS model. Numerical experiments demonstrate the efficiency and fastness of the proposed scheme.

1. Introduction

We consider the following 3D version of the time-fractional Black–Scholes (BS) model [1]:

$$\begin{aligned}&\frac{\partial^\alpha u}{\partial t^\alpha}(x,y,z,t)+\mathscr{L}_{\mathrm{BS}}u(x,y,z,t)\\&\quad=0\quad\text{for }(x,y,z,t)\in\Omega\times[0,T),\end{aligned}\tag{1}$$

$$u(x,y,z,T)=u_T(x,y,z),\tag{2}$$

where $u(x,y,z,t)$ is the option value at time t and $u_T(x,y,z)$ is the payoff function at time $t=T$,

$$\frac{\partial^\alpha u}{\partial t^\alpha}(x,y,z,t)=\frac{1}{\Gamma(1-\alpha)}\frac{d}{dt}\int_t^T\frac{u(x,y,z,\xi)-u(x,y,z,T)}{(\xi-t)^\alpha}d\xi,\tag{3}$$

where $0<\alpha<1$ and

$$\begin{aligned}\mathscr{L}_{\mathrm{BS}}=&\frac{1}{2}\sigma_x^2x^2\frac{\partial^2u}{\partial x^2}+\frac{1}{2}\sigma_y^2y^2\frac{\partial^2u}{\partial y^2}+\frac{1}{2}\sigma_z^2z^2\frac{\partial^2u}{\partial z^2}\\&+\rho_{xy}\sigma_x\sigma_yxy\frac{\partial^2u}{\partial x\partial y}+\rho_{yz}\sigma_y\sigma_zyz\frac{\partial^2u}{\partial y\partial z}\\&+\rho_{zx}\sigma_z\sigma_xzx\frac{\partial^2u}{\partial z\partial x}+rx\frac{\partial u}{\partial x}+ry\frac{\partial u}{\partial y}+rz\frac{\partial u}{\partial z}-ru.\end{aligned}\tag{4}$$

Here, x, y, and z, and σ_x, σ_y, and σ_z are the prices and volatilities of the underlying assets x, y, and z, respectively. Additionally, ρ_{xy}, ρ_{yz}, and ρ_{zx} are the correlation values between two subscript asset variables, and r is the interest rate. Black and Scholes published in 1973 their paper which described the BS model and option pricing formula [2]. This has become an important fundamental topic for studying financial engineering and financial theory. However, the option pricing formula is based on the assumption that the returns of asset prices follow a Gaussian distribution. This means that the volatility of the underlying asset price is

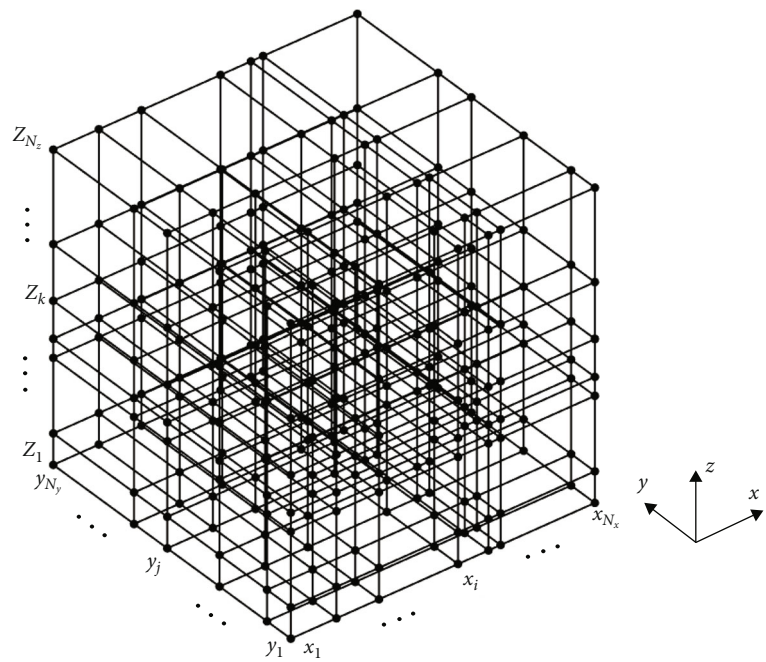

Figure 1: Three-dimensional nonuniform mesh.

constant until the time to maturity of the option contracts. This has become a weakness of this formula. Many researchers and traders have found that rare events such as drastic drops in financial markets are much more frequent than would be anticipated based on Gaussian distributions and that the distribution of the returns of asset prices has a fat tail. Therefore, in real financial markets, many researchers have begun to develop models that more accurately reflect real market. The study of stable distribution has arisen naturally during the study of heavy-tailed distributions and has been applied in finance to develop models of extreme events that occur rarely. Because a stable probability distribution captures unpredictable events well, it is now more suitable for financial markets than the BS model. Time-fractional analysis is closely connected to stable probability distributions [3]. Many researchers in the financial field have attempted to generalize the BS model in the fractional-order based on the fact that fractional derivatives and integrals provide powerful tools for explaining the memory and hereditary traits of different substances. The use of the fractional BS model for the high volatility of the stock market is one such generalization. There are two types of fractional derivatives as space-fractional [4, 5] and time-fractional derivatives [6, 7]. Regarding the time-fractional model, researchers have focused on the analytical [8–10] and numerical [11–13] methods. The finite difference method (FDM) is known as the most famous evaluation tool in quantitative finance and is more stable than Monte Carlo simulation (MCS). FDM has been applied in various studies [14, 15]. One researcher who has solved a two-dimensional time-fractional BS model using an implicit FDM proposed a fast biconjugate gradient stabilized scheme to solve the linear system to speed up computation and save storage space [16]. Option derivatives, European vanilla

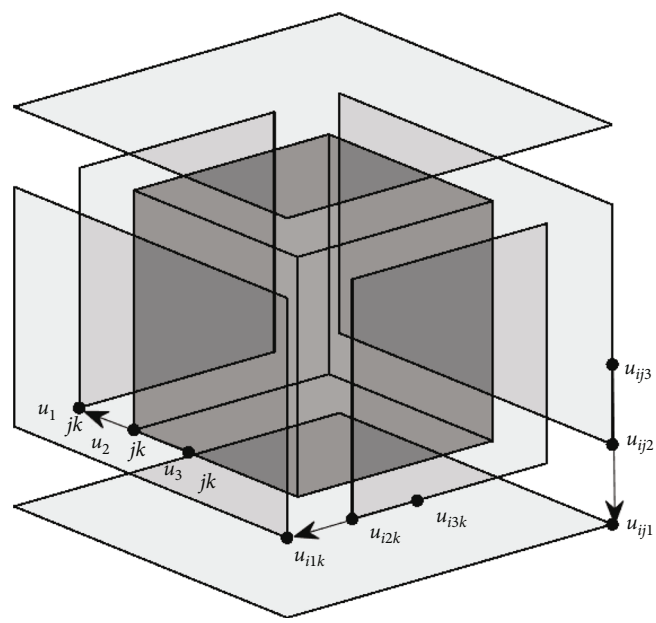

Figure 2: Schematic illustration of the linear boundary condition.

options [17], and double barrier options [18] are analytically priced under the time-fractional BS equation. In [19], the authors developed a homotopy perturbation method to obtain the analytical solutions for the fractional BS equation. Khajehnasiri and Safavi presented the Boubaker operation matrix for the time fractional derivative which approximates the solution of the fractional BS [20]. The authors in [21] proposed a novel operator splitting scheme for pricing American options using the time-fractional BS equation. They provided the effects of the fractional orders and the comparison of fractional equations through the numerical analysis. The paper also used the FDM of the Crank–Nicolson scheme for pricing European

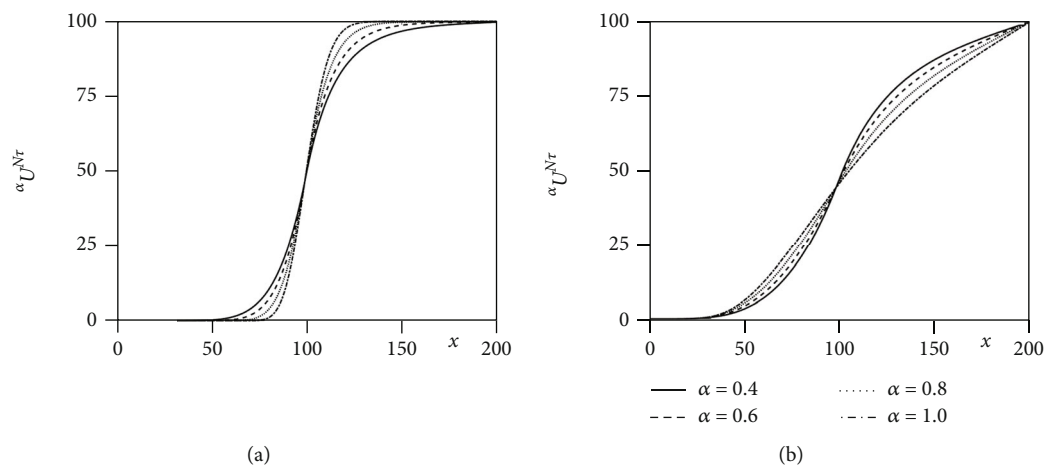

Figure 3: Numerical results for cash-or-nothing option for different fractional-orders $\alpha = 0.4, 0.6, 0.8$, and 1.0 with maturity times (a) $T = 0.1$ and (b) $T = 2.5$.

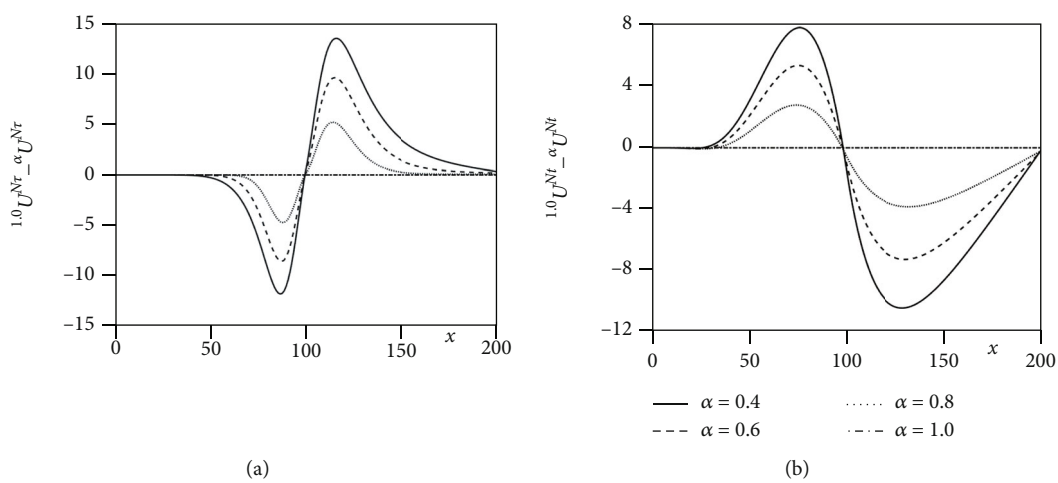

Figure 4: Differences in the numerical solutions between $\alpha = 1.0$ and $\alpha = 0.4, 0.6, 0.8$, and 1.0 for maturity times (a) $T = 0.1$ and (b) $T = 2.5$.

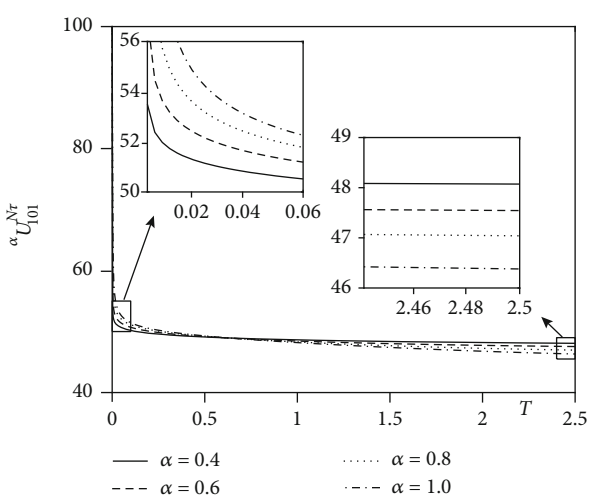

Figure 5: Numerical solution at $x = 100$ for maturity $0 \le T \le 2.5$ with $\alpha = 0.4, 0.6, 0.8$, and 1.0.

options based on the fractional BS equation [22]. They demonstrated that the proposed scheme has unconditional stability and convergent property through the numerical results. In [23], the authors represented that the fractional partial differential equation (PDE) has been successfully applied in option pricing problems and it is more suitable for empirical financial markets. They used a fast preconditioned iterative method for pricing rainbow options based on a two-dimensional fractional PDE. This method demonstrated the accuracy and efficiency of numerical studies. The author in [24] proposed the application of homotopy analysis method (HAM) for pricing European call option based on time-fractional BS equation. He demonstrated the accuracy, effectiveness, and suitability of HAM through comparative tests. The pricing equation based on a space-time fractional PDE is presented in [25]. The author calculated European call and put options based on space-time fractional BS equation using the technique of Adomian decomposition method under the FDM. In [26], option derivatives were numerically priced using the θ-method for the time-fractional BS equation. These schemes are both first-order and second-order accurate in

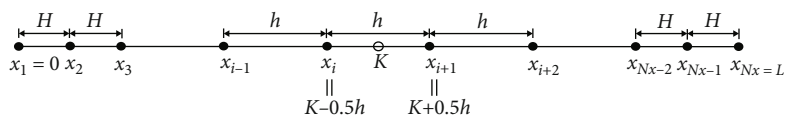

Figure 6: Mesh with a mesh size h for the convergence test.

Table 1: Three-asset cash-or-nothing option prices with varying h and time step $\Delta\tau$.

	$h = 8$	$h = 4$	$h = 2$	$h = 1$
$\Delta\tau = 0.1/10$	21.5301	22.6046	22.9076	22.9860
$\Delta\tau = 0.1/20$	21.4572	22.5433	22.8548	22.9358
$\Delta\tau = 0.1/40$	21.4689	22.5894	22.9176	23.0039
$\Delta\tau = 0.1/80$	21.5070	22.6675	23.0157	23.1082
$\Delta\tau = 0.1/160$	21.5490	22.7479	23.1167	23.2161

time and space, respectively. De Staelen and Hendy [27] improved the spatial fourth-order scheme with a temporal accuracy order of $2-\alpha$ and performed stability and convergence analysis on their proposed scheme. Golbabai and Nikan [28] numerically solved the time-fractional BS equation using the moving least-squares method. The authors in [29] solved the fractional three-dimensional (3D) chaotic process using the Adams–Bashforth–Moulton (ABM) method. They implemented an alternative numerical method based on the ABM method to reduce the computational cost and demonstrated that the proposed method is efficient and effective. She et al. [30] modified an $L1$ scheme to solve the time-fractional BS equation. The modified $L1$ time method is based on a change of variable and then obtains optimal error estimates. In [31], the authors removed the convection term with exponential transformation, transforming the time-fractional BS model into a time-fractional subdiffusion model, and then applied L 1 -2 formula for the Caputo time-fractional derivative. This scheme applied a quadratic B-spline collocation scheme for space. By using the compact quadratic spline collocation (QSC) scheme, this scheme yields $3-\alpha$-order and 4-order convergence in time and space, respectively. The complexity of calculations and CPU time are very important when applying numerical methods to solve high-dimensional problems. Although numerical studies have been conducted on the one-asset [26–28] and two-asset [16, 32] options, there is a lack of research on higher-dimensional numerical methods of more than two assets. Therefore, in this paper, we present the 3D time-fractional BS equation for pricing three-asset cash-or-nothing European call option. Let us consider the following change of the variable $\tau = T - t$; then,

$$\begin{aligned}\frac{\partial^\alpha u}{\partial t^\alpha}(x,y,z,t) &= \frac{1}{\Gamma(1-\alpha)}\frac{d}{dt}\int_t^T \frac{u(x,y,z,\xi)-u(x,y,z,T)}{(\xi-t)^\alpha}d\xi \\ &= \frac{-1}{\Gamma(1-\alpha)}\frac{d}{d\tau}\int_{T-\tau}^T \frac{u(x,y,z,\xi)-u(x,y,z,T)}{(\xi-T+\tau)^\alpha}d\xi \\ &= \frac{-1}{\Gamma(1-\alpha)}\frac{d}{d\tau}\int_0^\tau \frac{u(x,y,z,T-\eta)-u(x,y,z,T)}{(\tau-\eta)^\alpha}d\eta,\end{aligned} \tag{5}$$

where $\eta = T - \xi$ is used. Let $U(x,y,z,\tau) = u(x,y,z,T-\tau)$; then, Equation (5) becomes

$$\begin{aligned}&\frac{-1}{\Gamma(1-\alpha)}\frac{d}{d\tau}\int_0^\tau \frac{U(x,y,z,\eta)-U(x,y,z,0)}{(\tau-\eta)^\alpha}d\eta \\ &= \frac{-1}{\Gamma(1-\alpha)}\left[\frac{d}{d\tau}\int_0^\tau \frac{U(x,y,z,\eta)}{(\tau-\eta)^\alpha}d\eta - \frac{d}{d\tau}\int_0^\tau \frac{U(x,y,z,0)}{(\tau-\eta)^\alpha}d\eta\right] \\ &= \frac{-1}{\Gamma(1-\alpha)}\left[\frac{d}{d\tau}\int_0^\tau \frac{U(x,y,z,\eta)}{(\tau-\eta)^\alpha}d\eta - \frac{U(x,y,z,0)}{\tau^\alpha}\right] \\ &= \frac{-1}{\Gamma(1-\alpha)}\frac{d}{d\tau}\int_0^\tau \frac{\partial U(x,y,z,\eta)}{\partial\eta}\frac{(\tau-\eta)^{1-\alpha}}{1-\alpha}d\eta \\ &= \frac{-1}{\Gamma(1-\alpha)}\int_0^\tau \frac{\partial U(x,y,z,\eta)}{\partial\eta}(\tau-\eta)^{-\alpha}d\eta,\end{aligned} \tag{6}$$

where we have used the integration by parts and the Leibniz integral rule. Therefore, after the change of variables, Equation (1) becomes

$$\frac{1}{\Gamma(1-\alpha)}\int_0^\tau (\tau-\eta)^{-\alpha}\frac{\partial U(x,y,z,\eta)}{\partial\eta}d\eta = \mathscr{L}_{\mathrm{BS}}U(x,y,z,\tau), \tag{7}$$

with the initial condition $U(x,y,z,0) = u_T(x,y,z)$ for $(x,y,z,\tau) \in \Omega \times (0,T]$. When we solve the 3D time-fractional BS equation, there are difficulties in terms of memory shortage and computational cost because of the nonlocal property of the temporal derivative, which is the left hand side term in Equation (7). Therefore, we need efficient numerical schemes for this type of time-fractional PDE. First, the numerical scheme should be stable so that relatively large time steps can be used; otherwise, the computational cost will increase exponentially. Second, at each time step, the numerical solution scheme should be fast. To satisfy these conditions, in this study, we present an accurate and efficient nonuniform finite difference method for the 3D time-fractional BS model.

This paper is organized as follows. In Section 2, the proposed numerical scheme is described. In Section 3, numerical results are presented. In Section 4, conclusions are drawn. In the appendix, we provide the MATLAB code for the numerical implementation for the three-asset cash-or-nothing option.

2. Numerical Solutions

Let $\Omega = (0,L_x)\times(0,L_y)\times(0,L_z)$ be the computational domain discretized in nonuniform intervals $h_i^x = x_{i+1} - x_i$, $h_j^y = y_{j+1} - y_j$, and $h_k^z = z_{k+1} - z_k$ for $i = 1,\cdots,N_x - 1$, $j = 1,$

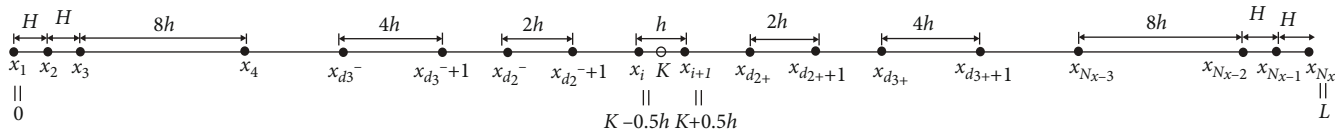

Figure 7: Piecewise-uniform mesh Ω_x.

Table 2: Option prices with respect to α.

α	0.1	0.2	0.3	0.4	0.5
Price	20.6535	21.3818	22.0402	22.6076	23.0786
α	0.6	0.7	0.8	0.9	1.0
Price	23.4597	23.7645	24.0086	24.2053	24.3633

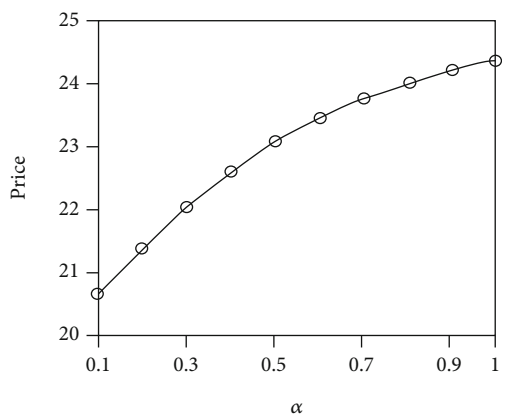

Figure 8: Plot of option prices with respect to α.

$\cdots, N_y - 1$, and $k = 1, \cdots, N_z - 1$. Here, $x_1 = y_1 = z_1 = 0, x_{N_x} = L_x, y_{N_y} = L_y$, and $z_{N_z} = L_z$. $\Delta\tau = T/N_\tau$ is the time step, and N_τ is the number of time steps. Figure 1 illustrates an example of a three-dimensional nonuniform mesh.

Let U_{ijk}^n be the numerical approximation of $U(x_i, y_j, z_k, n\Delta\tau)$ and $\tau_p = p\Delta\tau$. The left hand side term in Equation (7) can be approximated by the following numerical quadrature formula:

$$\begin{aligned}
&\frac{1}{\Gamma(1-\alpha)}\int_0^{\tau_{n+1}} (\tau_{n+1}-\eta)^{-\alpha}\frac{\partial U\left(x_i, y_j, z_k, \eta\right)}{\partial \eta}d\eta \\
&= \frac{1}{\Gamma(1-\alpha)}\sum_{p=1}^{n+1}\int_{\tau_{p-1}}^{\tau_p} (\tau_{n+1}-\eta)^{-\alpha}\frac{\partial U\left(x_i, y_j, z_k, \eta\right)}{\partial \eta}d\eta \\
&\approx \frac{1}{\Gamma(2-\alpha)}\sum_{p=1}^{n+1}\left[\left(\tau_{n+1}-\tau_{p-1}\right)^{1-\alpha} - \left(\tau_{n+1}-\tau_p\right)^{1-\alpha}\right] \\
&\cdot \frac{U_{ijk}^p - U_{ijk}^{p-1}}{\Delta\tau} = \frac{1}{(\Delta\tau)^\alpha\Gamma(2-\alpha)}\sum_{p=1}^{n+1}\left[(n+2-p)^{1-\alpha}\right. \\
&\left. - (n+1-p)^{1-\alpha}\right]\left(U_{ijk}^p - U_{ijk}^{p-1}\right).
\end{aligned} \tag{8}$$

Therefore, we propose the following discretization of Equation (7) using Equation (8).

$$\begin{aligned}
&\frac{1}{(\Delta\tau)^\alpha\Gamma(2-\alpha)}\sum_{p=1}^{n+1}\left[(n+2-p)^{1-\alpha}\right. \\
&\left. - (n+1-p)^{1-\alpha}\right]\left(U_{ijk}^p - U_{ijk}^{p-1}\right) \\
&= \left(\mathscr{L}_{\mathrm{BS}}^x U\right)_{ijk}^{n+(1/3)} + \left(\mathscr{L}_{\mathrm{BS}}^y U\right)_{ijk}^{n+(2/3)} + \left(\mathscr{L}_{\mathrm{BS}}^z U\right)_{ijk}^{n+1},
\end{aligned} \tag{9}$$

where

$$\begin{aligned}
\left(\mathscr{L}_{\mathrm{BS}}^x U\right)_{ijk}^{n+(1/3)} &= \frac{(\sigma_x x_i)^2}{2}D_{xx}U_{ijk}^{n+(1/3)} + rx_iD_xU_{ijk}^{n+(1/3)} \\
&\quad + \sigma_x\sigma_y\rho_{xy}x_iy_jD_{xy}U_{ijk}^n + \sigma_y\sigma_z\rho_{yz}y_jz_kD_{yz}U_{ijk}^n \\
&\quad + \sigma_z\sigma_x\rho_{zx}z_kx_iD_{zx}U_{ijk}^n - \frac{1}{3}rU_{ijk}^{n+(1/3)}, \\
\left(\mathscr{L}_{\mathrm{BS}}^y U\right)_{ijk}^{n+(2/3)} &= \frac{\left(\sigma_y y_j\right)^2}{2}D_{yy}U_{ijk}^{n+(2/3)} + ry_jD_yU_{ijk}^{n+(2/3)} \\
&\quad - \frac{1}{3}rU_{ijk}^{n+(2/3)}, \\
\left(\mathscr{L}_{\mathrm{BS}}^z U\right)_{ijk}^{n+1} &= \frac{(\sigma_z z_k)^2}{2}D_{zz}U_{ijk}^{n+1} + rz_kD_zU_{ijk}^{n+1} - \frac{1}{3}rU_{ijk}^{n+1}.
\end{aligned} \tag{10}$$

The numerical derivatives are defined as

$$\begin{aligned}
D_xU_{ijk} &= -\frac{h_i^xU_{i-1,jk}}{h_{i-1}^x(h_{i-1}^x+h_i^x)} + \frac{(h_i^x - h_{i-1}^x)U_{ijk}}{h_{i-1}^xh_i^x} + \frac{h_{i-1}^xU_{i+1,jk}}{h_i^x(h_{i-1}^x+h_i^x)}, \\
D_{xx}U_{ijk} &= \frac{2U_{i-1,jk}}{h_{i-1}^x(h_{i-1}^x+h_i^x)} - \frac{2U_{ijk}}{h_{i-1}^xh_i^x} + \frac{2U_{i+1,jk}}{h_i^x(h_{i-1}^x+h_i^x)}, \\
D_{xy}U_{ijk} &= \frac{U_{i+1,j+1,k} - U_{i-1,j+1,k} - U_{i+1,j-1,k} + U_{i-1,j-1,k}}{h_i^xh_j^y + h_{i-1}^xh_j^y + h_i^xh_{j-1}^y + h_{i-1}^xh_{j-1}^y},
\end{aligned} \tag{11}$$

and the other terms are similarly defined. Additional details can be found in [33, 34]. We solve the discrete Equation (9) using the operator splitting method. First, let

$$\begin{aligned}
&\frac{1}{(\Delta\tau)^\alpha\Gamma(2-\alpha)}\sum_{p=1}^{n+1}\left[(n+2-p)^{1-\alpha} - (n+1-p)^{1-\alpha}\right] \\
&\cdot \left(U_{ijk}^p - U_{ijk}^{p-1}\right) = F_{ijk}^n + \frac{U_{ijk}^{n+1} - U_{ijk}^n}{(\Delta\tau)^\alpha\Gamma(2-\alpha)},
\end{aligned} \tag{12}$$

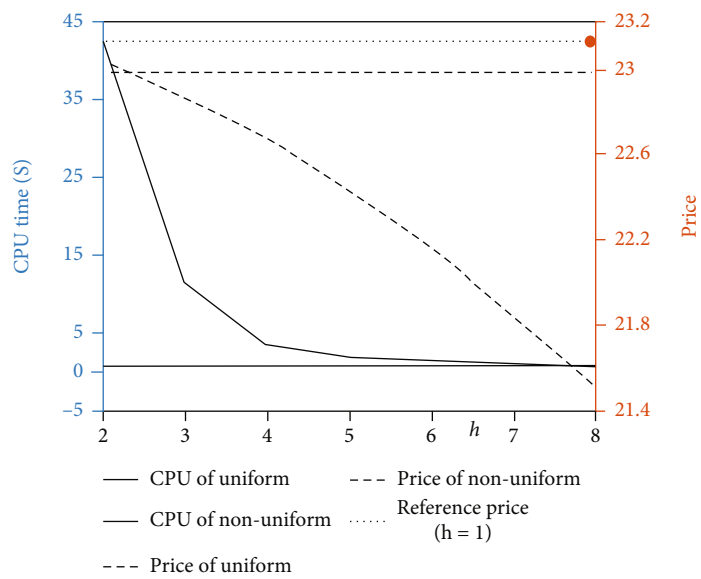

Figure 9: CPU time and price of three-asset cash-or-nothing option for nonuniform mesh with $m_1 = 1, m_2 = 2$, and $m_3 = 3, m_4 = 1$ and uniform mesh with respect to $h = 2, 3, \cdots, 8$.

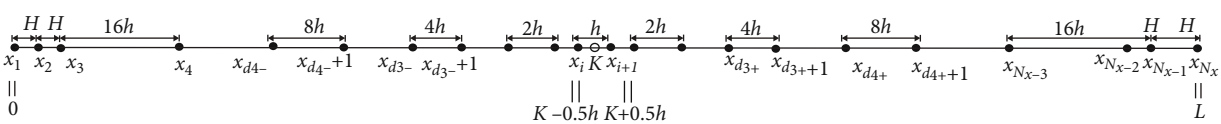

Figure 10: Nonuniform mesh in a comparison test.

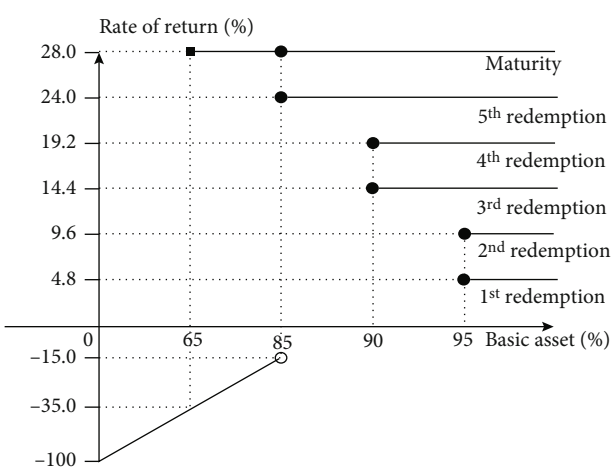

Figure 11: ELS payoff structure.

where

$$F_{ijk}^{n} = \frac{1}{(\Delta\tau)^{\alpha}\Gamma(2-\alpha)} \sum_{p=1}^{n} \left[(n+2-p)^{1-\alpha} - (n+1-p)^{1-\alpha}\right] \left(U_{ijk}^{p} - U_{ijk}^{p-1}\right). \tag{13}$$

Let $\delta\tau = (\Delta\tau)^{\alpha}\Gamma(2-\alpha)$ for simplicity of exposition; then we sequentially solve the following equations [34]:

$$\frac{U_{ijk}^{n+(1/3)} - U_{ijk}^{n}}{\delta\tau} = \left(\mathscr{L}_{\mathrm{BS}}^{x} U\right)_{ijk}^{n+(1/3)} - F_{ijk}^{n}, \tag{14}$$

$$\frac{U_{ijk}^{n+(2/3)} - U_{ijk}^{n+(1/3)}}{\delta\tau} = \left(\mathscr{L}_{\mathrm{BS}}^{y} U\right)_{ijk}^{n+(2/3)}, \tag{15}$$

$$\frac{U_{ijk}^{n+1} - U_{ijk}^{n+(2/3)}}{\delta\tau} = \left(\mathscr{L}_{\mathrm{BS}}^{z} U\right)_{ijk}^{n+1}, \tag{16}$$

for $1 \le i \le N_x$, $1 \le j \le N_y$, and $1 \le k \le N_z$. Note that if we sum up these three equations (14)–(16), then we obtain Equation (9). For the detailed numerical solution, algorithm with source program code of Equations (14)–(16) can be found in [34]. We use the linear boundary condition, specifically, for example, in the case of Equation (14) (see Figure 2):

$$\begin{aligned} U_{1jk}^{n+(1/3)} &= 2U_{2jk}^{n+(1/3)} - U_{3jk}^{n+(1/3)}, \\ U_{N_x jk}^{n+(1/3)} &= 2U_{N_x-1,jk}^{n+(1/3)} - U_{N_x-2,jk}^{n+(1/3)}, \\ &\text{for } j = 2, \cdots, N_y - 1, k = 2, \cdots, N_z - 1, \end{aligned}$$

$$\begin{aligned} U_{i1k}^{n+(1/3)} &= 2U_{i2k}^{n+(1/3)} - U_{i3k}^{n+(1/3)}, \\ U_{iN_y k}^{n+(1/3)} &= 2U_{i,N_y-1,k}^{n+(1/3)} - U_{i,N_y-2,k}^{n+(1/3)}, \\ &\text{for } i = 1, \cdots, N_x, k = 2, \cdots, N_z - 1, \end{aligned}$$

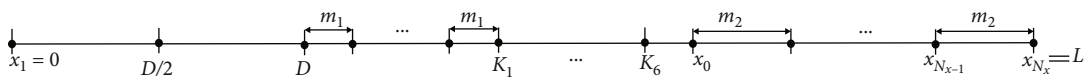

Figure 12: Nonuniform mesh for the three-asset ELS.

$$\begin{aligned} U_{ij1}^{n+(1/3)} &= 2U_{ij2}^{n+(1/3)} - U_{ij3}^{n+(1/3)}, \\ U_{ijN_z}^{n+(1/3)} &= 2U_{ij,N_z-1}^{n+(1/3)} - U_{ij,N_z-2}^{n+(1/3)}, \\ &\text{for } i = 1, \cdots, N_x, j = 1, \cdots, N_y. \end{aligned} \tag{17}$$

3. Numerical Experiments

Numerical experiments were conducted using MATLAB R2020b software on an Intel(R) Core(TM) i7-7700 CPU @3.60 GHz machine with 8 GB of memory.

3.1. Effect of Fractional-Order α. In this subsection, we investigate the effects of the fractional-order α by considering one-asset cash-or-nothing European call option. The payoff function of cash-or-nothing European call option is defined as

$$U^0(x) = \begin{cases} c, & \text{if } C \geq K, \\ 0, & \text{otherwise,} \end{cases} \tag{18}$$

where the strike price is $K = 100$ and the cash is $C = 100$. The parameter values are $r = 0.03$, $\sigma = 0.3$, and $\Delta\tau = 1/365$. We use a uniform mesh $h = 1$ with $L = 200$. Let ${}^{\alpha}U_i^n$ be the numerical approximation of the solution, where $i = 1, \cdots, N_x$, $n = 0, \cdots, N_\tau$, and $0 < \alpha \leq 1$. A linear boundary condition can be applied. Figure 3 illustrates the numerical solutions of cash-or-nothing European call option for different fractional-orders $\alpha = 0.4, 0.6, 0.8$, and 1.0. Figures 3(a) and 3(b) show the numerical results with a relatively short maturity $T = 0.1$ and long maturity $T = 2.5$, respectively. We can observe the different solution profiles according to α.

Figures 4(a) and 4(b) show the differences in the numerical solutions between $\alpha = 1.0$ and $\alpha = 0.4, 0.6, 0.8, 1.0$, i.e., ${}^{1.0}U^{N\tau} - {}^{\alpha}U^{N\tau}$, for $T = 0.1$ and $T = 2.5$, respectively. The lower the α for a short maturity option, the higher the price of the option is in in the money (ITM) and undervalued in out of the money (OTM), see Figure 4(a). However, for long maturity option, the result is contrary to the result of short maturity option (see Figure 4(b)).

Figure 5 shows numerical solutions at $x = 100$ with $\alpha = 0.4, 0.6, 0.8$, and 1.0 as maturity increases, $0 \leq T \leq 2.5$. For short maturity times, the solutions with lower α values diffuse rapidly, but as the maturity time increases, the solutions with lower α values diffuse slowly. The results of the two subaxes in Figure 5 can be interpreted similarly to Figure 4.

3.2. Three-Asset Options with Nonuniform Mesh

3.2.1. Cash-or-Nothing Option. We investigated three-asset cash-or-nothing European call option with the following payoff function:

$$U^0(x, y, z) = \begin{cases} c, & \text{if } x \geq K_1, y \geq K_2, z \geq K_3, \\ 0, & \text{otherwise,} \end{cases} \tag{19}$$

where the strike prices are $K_1 = K_2 = K_3 = 100$ and the cash is $c = 100$. The parameter values are $T = 0.1$, $r = 0.03$, $L = M = N = 200$, $\sigma_x = 0.3$, $\sigma_y = 0.3$, $\sigma_z = 0.3$, and $\rho_{xy} = 0.5$, $\rho_{yz} = 0.5$, and $\rho_{zx} = 0.5$. Figure 6 shows the mesh structure with a mesh size h for the convergence test. Note that we straddle the strike point such that the strike point is in the middle of two neighboring points. If $x_2 < h$, then we reset $x_2 = 0.5x_3$ so that we can apply the linear boundary condition. Similarly, if $x_{N_x} - x_{N_x-1} < h$, then we reset $x_{N_x-1} = 0.5(x_{N_x} + x_{N_x-2})$.

Table 1 presents the three-asset cash-or-nothing European call option prices with various variable h and time step $\Delta\tau$. Here, we use $\alpha = 0.5$. We can confirm that the option prices obtained with each h value converge as the time step $\Delta\tau$ becomes smaller. We adopt the reference solution $U(x_i, y_j, z_k, T)$ which uses $h = 1$ and time step $\Delta\tau = 0.1/80$.

We consider the piecewise-uniform mesh $\Omega_x = \Omega_1 \cup \Omega_2 \cup \Omega_3 \cup \Omega_4 \cup \Omega_5$ with

$$\begin{aligned} \Omega_1 &= \{D_1^-, D_1^- + h, D_1^- + 2h, \cdots, D_1^+\}, \\ \Omega_2 &= \{D_2^-, D_2^- + (2h), \cdots, D_1^-\} \cup \{D_1^+, D_1^+ + (2h), \cdots, D_2^+\}, \\ \Omega_3 &= \{D_3^-, D_3^- + (4h), \cdots, D_2^-\} \cup \{D_2^+, D_2^+ + (4h), \cdots, D_3^+\}, \\ \Omega_4 &= \{D_4^-, D_4^- + (8h), \cdots, D_3^-\} \cup \{D_3^+, D_3^+ + (8h), \cdots, D_4^+\}, \\ \Omega_5 &= \{0, 0.5D_4^-, D_4^-\} \cup \{D_4^+, D_4^+ + 0.5(L - D_4^+), L\}. \end{aligned} \tag{20}$$

Here, $D_i^{\pm}$ are the upper and lower bounds of each uniform mesh and are defined as follows:

$$\begin{aligned} D_1^- &= K_1 - (0.5 + m_1)h, D_1^+ = K_1 + (0.5 + m_1)h, \\ D_2^- &= D_1^- - (2h)m_2, D_2^+ = D_1^+ + (2h)m_2, \\ D_3^- &= D_2^- - (4h)m_3, D_3^+ = D_2^+ + (4h)m_3, \\ D_4^- &= D_3^- - (8h)m_4, D_4^+ = D_3^+ + (8h)m_4, \end{aligned} \tag{21}$$

where $2 \times m_i$ is the number of points in mesh Ω_i for $i = 1, 2, 3, 4$. In particular, $m_4 = \lfloor D_3^-/(8h) \rfloor - 1$ where $\lfloor x \rfloor$ is the maximum integer not greater than x. From now on, we use $m_1 = 5$, $m_2 = 5$, and $m_3 = 4$ in our numerical experiments. Figure 7 shows the piecewise-uniform mesh structure defined as Ω_x for pricing the three-asset cash-or-nothing option considered in this section. $d_i^{\pm}$, which is defined in Figure 7, is an index of the point x with the $D_i^{\pm}$ values defined above.

```
clear;clc;
L=200; xvol=0.3; yvol=0.3; zvol=0.3; r=0.03; rho xy=0.5; rho yz=0.5;
rho zx=0.5;K1=100;K2=100;K3=100;T=0.1; dt=0.1/80;Nt=ceil(T/dt);
h=1;m1=5;m2=5;m3=4; xr=K1+0.5*h:h:K1+0.5*h+m1;
xr=[xr(1:end-1) xr(end):2*h:xr(end)+2*h*m2];
xr=[xr(1:end-1) xr(end):4*h:xr(end)+4*h*m3];
m4=floor((L-xr(end))/8);
xr=[xr(1:end-1) xr(end):8*h:xr(end)+8*h*m4];
if xr(end)<L
xr(end)=(xr(end-1)+L)/2; xr(end+1)=L;
end
x=[flipl r(L-xr) xr]; y=x; z=x;
Nx=length(x);Ny=length(y);Nz=length(z); hx=diff(x); hy=diff(y);
hz=diff(z);
U=zeros(Nx,Ny,Nz,Nt+1);U(x>=K1, y>=K2, z>=K3, 1)=100;V=U;
alp=0.5; s=1.0/(dt^alp*gamma(2-alp));
ax=zeros(1,Nx-2); dx=ax; cx=ax;
for i=2:Nx-1
ax(i-1)=r*x(i)*hx(i)/(hx(i-1)*(hx(i-1)+hx(i))) ...
-(xvol*x(i))^2/(hx(i-1)*(hx(i-1)+hx(i)));
dx(i-1)=s+(xvol*x(i))^2/(hx(i-1)*hx(i)) ...
-r*x(i)*(hx(i)-hx(i-1))/(hx(i-1)*hx(i))+r/3;
cx(i-1)=-r*x(i)*hx(i-1)/(hx(i)*(hx(i-1)+hx(i))) ...
-(xvol*x(i))^2/(hx(i)*(hx(i-1)+hx(i)));
end
dx(1)=dx(1)++2*ax(1); cx(1)=cx(1)-ax(1);
ax(Nx-2)=ax(Nx-2)-cx(Nx-2); dx(Nx-2)=dx(Nx-2)++2*cx(Nx-2);
bx=ax; by=ax; bz=ax;
for n=1:Nt
F=zeros(Nx-2,Ny-2,Nz-2);
if n>1
for j=1:n-1
F=F+((n-j+1)^(1-alp)-(n-j)^(1-alp))*(U(2:Nx-1,2:Ny-1,2:Nz-1,j+1) ...
-U(2:Nx-1,2:Ny-1,2:Nz-1,j));
end
end
V(:,:,:,n)=U(:,:,:,n);
for j=2:Ny-1
for k=2:Nz-1
for i=2:Nx-1
bx(i-1)=s*V(i,j,k,n)-s*F(i-1,j-1,k-1) ...
+(rho xy*xvol*yvol*x(i)*y(j)*(V(i+1,j+1,k,n)+V(i-1,j-1,k,n) ...
-V(i-1,j+1,k,n)-V(i+1,j-1,k,n))/((hx(i)*hy(j))+(hx(i-1)*hy(j)) ...
+(hx(i)*hy(j-1))+(hx(i-1)*hy(j-1))) ...
+rho yz*yvol*zvol*y(j)*z(k)*(V(i,j+1,k+1,n)+V(i,j-1,k-1,n) ...
-V(i,j-1,k+1,n)-V(i,j+1,k-1,n))/((hy(j)*hz(k))+(hy(j-1)*hz(k)) ...
+(hy(j)*hz(k-1))+(hy(j-1)*hz(k-1))) ...
+rho zx*xvol*zvol*x(i)*z(k)*(V(i+1,j,k+1,n)+V(i-1,j,k-1,n) ...
-V(i-1,j,k+1,n)-V(i+1,j,k-1,n))/((hx(i)*hz(k))+(hx(i-1)*hz(k)) ...
+(hx(i)*hz(k-1))+(hx(i-1)*hz(k-1)))));
end
U(2:Nx-1,j,k,n+1)=thomas3(ax,dx,cx,bx);
end
end
U(1,2:Ny-1,2:Nz-1,n+1)=2*U(2,2:Ny-1,2:Nz-1,n+1) ...
-U(3,2:Ny-1,2:Nz-1,n+1);
U(:,1,2:Nz-1,n+1)=2*U(:,2,2:Nz-1,n+1)-U(:,3,2:Nz-1,n+1);
U(:,:,1,n+1)=2*U(:,:,2,n+1)-U(:,:,3,n+1);
U(Nx,2:Ny-1,2:Nz-1,n+1)=2*U(Nx-1,2:Ny-1,2:Nz-1,n+1) ...
-U(Nx-2,2:Ny-1,2:Nz-1,n+1);
```

Listing 1: Continued.

```
U( : ,Ny , 2 :Nz -1 , n+1)=2*U( : ,Ny-1 , 2 :Nz -1 , n+1) -U( : ,Ny-2 , 2 :Nz -1 , n+1) ;
U( : , : ,Nz , n+1)=2*U( : , : ,Nz -1 , n+1) -U( : , : ,Nz -2 , n+1) ;
f o r k=2:Nz -1
f o r i =2:Nx-1
f o r j =2:Ny-1
by ( j -1 )=s *U( i , j , k , n+1) ;
end
V( i , 2 :Ny-1 , k , n+1)=thomas3 ( ax , dx , cx , by ) ;
end
end
V( 1 , 2 :Ny-1 , 2 :Nz -1 , n+1)=2*V( 2 , 2 :Ny-1 , 2 :Nz -1 , n+1) . . .
-V( 3 , 2 :Ny-1 , 2 :Nz -1 , n+1) ;
V( : , 1 , 2 :Nz -1 , n+1)=2*V( : , 2 , 2 :Nz -1 , n+1) -V( : , 3 , 2 :Nz -1 , n+1) ;
V( : , : , 1 , n+1)=2*V( : , : , 2 , n+1) -V( : , : , 3 , n+1) ;
V(Nx , 2 :Ny-1 , 2 :Nz -1 , n+1)=2*V(Nx-1 , 2 :Ny-1 , 2 :Nz -1 , n+1) . . .
-V(Nx-2 , 2 :Ny-1 , 2 :Nz -1 , n+1) ;
V( : ,Ny , 2 :Nz -1 , n+1)=2*V( : ,Ny-1 , 2 :Nz -1 , n+1) -V( : ,Ny-2 , 2 :Nz -1 , n+1) ;
V( : , : ,Nz , n+1)=2*V( : , : ,Nz -1 , n+1) -V( : , : ,Nz -2 , n+1) ;
f o r j =2:Ny-1
f o r i =2:Nx-1
f o r k=2:Nz -1
bz (k -1 )=s *V( i , j , k , n+1) ;
end
U( i , j , 2 :Nz -1 , n+1)=thomas3 ( ax , dx , cx , bz ) ;
end
end
U( 1 , 2 :Ny-1 , 2 :Nz -1 , n+1)=2*U( 2 , 2 :Ny-1 , 2 :Nz -1 , n+1) . . .
-U( 3 , 2 :Ny-1 , 2 :Nz -1 , n+1) ;
U( : , 1 , 2 :Nz -1 , n+1)=2*U( : , 2 , 2 :Nz -1 , n+1) -U( : , 3 , 2 :Nz -1 , n+1) ;
U( : , : , 1 , n+1)=2*U( : , : , 2 , n+1) -U( : , : , 3 , n+1) ;
U(Nx , 2 :Ny-1 , 2 :Nz -1 , n+1)=2*U(Nx-1 , 2 :Ny-1 , 2 :Nz -1 , n+1) . . .
-U(Nx-2 , 2 :Ny-1 , 2 :Nz -1 , n+1) ;
U( : ,Ny , 2 :Nz -1 , n+1)=2*U( : ,Ny-1 , 2 :Nz -1 , n+1) -U( : ,Ny-2 , 2 :Nz -1 , n+1) ;
U( : , : ,Nz , n+1)=2*U( : , : ,Nz -1 , n+1) -U( : , : ,Nz -2 , n+1) ;
end
f i g u r e ( 1 ) ; c l f ; colormap ( [ 0 0 0 ] ) ;
mesh ( x , y ,U( : , : , min ( f i n d ( z>100) )++1,n+1) ) ;
Pr i c e=i n t e rp 3 (y , x , z ,U( : , : , : , Nt+1) ,K1,K2,K3)
f u n c t i on x=thomas3 ( alpha , beta ,gamma, f )
n=length ( f ) ;
f o r i =2:n
mult=alpha ( i ) / be ta ( i -1 ) ;
be ta ( i )=be ta ( i ) -mult*gamma( i -1 ) ;
f ( i )=f ( i ) -mult* f ( i -1 ) ;
end
x (n)=f (n) / be ta (n) ;
f o r i=n -1 : -1 : 1
x ( i )=( f ( i ) -gamma( i ) *x ( i+1) ) / be ta ( i ) ;
end
end
```

Listing 1: MATLAB code for cash-or-nothing.

Given the same option, Table 2 lists the option prices with respect to α. Here, $h = 1$ and $\Delta\tau = 0.1/80$ are taken and the other parameters are the same as in the test above. The code for the numerical implementation for this test is provided in the appendix.

Figure 8 shows the option prices according to the value of α. For $T = 0.1$, the option prices obtained tend to be undervalued as α decreases, as is the case with one underlying asset.

Figure 9 shows the CPU time and prices of three-asset cash-or-nothing option. In Figure 9, the dotted curve is the reference price of using the uniform mesh with mesh size $h = 1$. We use the maturity time $T = 0.1$, and the other parameters are the same as in the tests previously. In Figure 9, the solid and dashed curves are the CPU time and prices, respectively, with respect to uniform mesh with mesh size $h = 2, 3, \cdots, 8$. Here, the uniform mesh is

constructed as shown in Figure 6. Figure 10 was constructed in a similar manner to Figure 7. Here, we add a piecewise-uniform mesh with a step size $16h$. Likewise, we define $D_5^{\pm} = D_4^{\pm} \pm (16h)m_5$, and $m_5 = \lfloor D_4^{-}/(16h) \rfloor - 1$. We compute the CPU time and price of using the nonuniform mesh with $m_1 = 1, m_2 = 2, m_3 = 3$, and $m_4 = 1$, which is constructed in Figure 10. We can confirm that the difference between the reference and numerical solutions obtained with each mesh is greater when using the uniform mesh, despite using the number of same grid points when the uniform mesh size is $h = 8$. Additionally, the elapsed time is similar to using the uniform mesh. In other words, nonuniform meshes are faster and more accurate compared to uniform mesh.

3.2.2. Equity-Linked Security. We consider a three-asset equity-linked security (ELS) option that contains knock-in-barrier (D). The complex profit structure of ELS complicates pricing. To briefly explain return of ELS on one asset, if the underlying asset price is higher than the predetermined exercise prices $(K_1, K_2, \cdots, K_6)$ on the early exercise date before maturity, the contract provides the specific returns $(c_1, c_2, \cdots, c_6)$ and is terminated. Otherwise, the contract will continue on the next early exercise date. If the contract is not terminated by maturity, it depends on whether the underlying asset touched the knock-in-barrier. If the underlying asset did not touch the knock-in-barrier, it provides dummy return (d) and otherwise suffers losses. The payoff structure of ELS is illustrated in Figure 11.

For $\alpha = 0.8$, we performed the comparison test with the uniform mesh under the same conditions considered in Section 3.2 [35] on the nonuniform mesh. For additional information on numerical testing, please refer to the thesis [35]. The nonuniform mesh was constructed using the piecewise-uniform mesh, as shown in Figure 12, with fixed points $(0, D/2, D, K_1, K_2, \cdots, K_6, x0, L)$ and $m_1 = 5, m_2 = 20$, where $x0$ is the current underlying price.

When using a nonuniform grid as shown in Figure 12, the ELS price is 8767 and the elapsed time is 15.3783. When comparing this result to the result obtained using the uniform mesh ($h = 2$), the relative error of the price is 0.0205 and the elapsed time is 470 times shorter.

4. Conclusions

In this study, we presented an efficient and accurate nonuniform FDM for the 3D time-fractional BS equation. In numerical experiments, we investigated the effects of the fractional-order α by considering one-asset cash-or-nothing European call option. The lower the value of α, and the shorter the maturity of the option, and the larger the difference in option prices between the $\alpha = 1.0$ and $\alpha < 1.0$ except for at the money (ATM). Because of the complexity of calculations and CPU time for computation on high-dimensional options takes longer, there is a lack of research on higher-dimensional numerical methods with more than three assets in the time-fractional BS equation. We used the nonuniform implicit FDM with operator splitting scheme for pricing three-asset cash-or-nothing options and ELS. Here, we use the operator splitting method to solve the discrete system of equations and linear boundary conditions efficiently. Based on the use of the nonuniform implicit FDM, the numerical solution computation could be fast, and the numerical scheme could be stable even if relatively large time steps are used. Our results suggest that the proposed method is faster and more accurate than the uniform mesh. We demonstrated the efficiency and fastness of the proposed method through numerical experiments. Although there have been theoretical analyses (stability analysis, truncation error, and convergence analysis) of the one-dimensional time-fractional BS equation [1, 27], there is a lack of research on multidimensional theoretical analysis of the time-fractional BS equation. Therefore, for future work, we will perform the theoretical analysis of the multidimensional time-fractional BS equation and compute various financial assets based on the multidimensional time-fractional BS equation using the proposed method and continue to improve our method.

Appendix

The following Listing 1 is a MATLAB code for pricing the three-asset cash-or-nothing European call option.

Data Availability

No data were used to support this study.

Conflicts of Interest

The authors declare that they have no conflicts of interest.

Acknowledgments

The corresponding author (J.S. Kim) was supported by the Brain Korea 21 FOUR from the Ministry of Education of the Republic of Korea.

References

[1] J. Huang, Z. Cen, and J. Zhao, "An adaptive moving mesh method for a time-fractional Black–Scholes equation," *Advances in Difference Equations*, vol. 2019, no. 1, 14 pages, 2019.

[2] F. Black and M. Scholes, "The pricing of options and corporate liabilities," *Journal of Political Economy*, vol. 81, no. 3, pp. 637–654, 1973.

[3] A. A. Tateishi, H. V. Ribeiro, and E. K. Lenzi, "The role of fractional time-derivative operators on anomalous diffusion," *Frontiers in Physics*, vol. 5, 2017.

[4] Y. Chen, H. Gu, and L. Ma, "Variational method to -Laplacian fractional Dirichlet problem with instantaneous and noninstantaneous impulses," *Journal of Function Spaces*, vol. 2020, Article ID 8598323, 8 pages, 2020.

[5] D. Prathumwan and K. Trachoo, "On the solution of two-dimensional fractional Black–Scholes equation for European put option," *Advances in Difference Equations*, vol. 2020, no. 1, 9 pages, 2020.

[6] Y. Kumar and V. K. Singh, "Computational approach based on wavelets for financial mathematical model governed by distributed order fractional differential equation," *Mathematics and Computers in Simulation*, vol. 190, pp. 531–569, 2021.

[7] M. X. Zhou, A. S. V. Kanth, K. Aruna et al., "Numerical solutions of time fractional Zakharov-Kuznetsov equation via natural transform decomposition method with nonsingular kernel derivatives," *Journal of Function Spaces*, vol. 2021, Article ID 9884027, 17 pages, 2021.

[8] S. Kumar, A. Yildirim, Y. Khan, H. Jafari, K. Sayevand, and L. Wei, "Analytical solution of fractional Black–Scholes European option pricing equation by using Laplace transform," *Journal of Fractional Calculus and Applications*, vol. 2, no. 8, pp. 1–9, 2012.

[9] J. S. Duan, L. Lu, L. Chen, and Y. L. An, "Fractional model and solution for the Black–Scholes equation," *Mathematical Methods in the Applied Sciences*, vol. 41, no. 2, pp. 697–704, 2018.

[10] K. Zhang, "Existence and uniqueness of analytical solution of time-fractional Black–Scholes type equation involving hyper-Bessel operator," *Mathematical Methods in the Applied Sciences*, vol. 44, no. 7, pp. 6164–6177, 2021.

[11] M. M. Khader, "The numerical solution for BVP of the liquid film flow over an unsteady stretching sheet with thermal radiation and magnetic field using the finite element method," *International Journal of Modern Physics C*, vol. 30, no. 11, pp. 1950080–1950088, 2019.

[12] Y. Gu and H. Sun, "A meshless method for solving three-dimensional time fractional diffusion equation with variable-order derivatives," *Applied Mathematical Modelling*, vol. 78, pp. 539–549, 2020.

[13] P. Roul, "A high accuracy numerical method and its convergence for time-fractional Black-Scholes equation governing European options," *Applied Numerical Mathematics*, vol. 151, pp. 472–493, 2020.

[14] M. M. Khader, "Fourth-order predictor-corrector FDM for the effect of viscous dissipation and Joule heating on the Newtonian fluid flow," *Computers & Fluids*, vol. 182, pp. 9–14, 2019.

[15] M. M. Khader and R. P. Sharma, "Evaluating the unsteady MHD micropolar fluid flow past stretching/shirking sheet with heat source and thermal radiation: implementing fourth order predictor-corrector FDM," *Mathematics and Computers in Simulation*, vol. 181, pp. 333–350, 2021.

[16] H. Zhang, F. Liu, S. Chen, and M. Shen, "A fast and high accuracy numerical simulation for a fractional Black–Scholes model on two assets," *Annals of Applied Mathematics*, vol. 36, no. 1, pp. 91–110, 2020.

[17] W. Wyss, "The fractional Black–Scholes equation," *Fractional Calculus and Applied Analysis*, vol. 3, no. 1, pp. 51–61, 2000.

[18] W. Chen, X. Xu, and S. P. Zhu, "Analytically pricing double barrier options based on a time-fractional Black- Scholes equation," *Computers & Mathematics with Applications*, vol. 69, no. 12, pp. 1407–1419, 2015.

[19] A. N. Fall, S. N. Ndiaye, and N. Sene, "Black-Scholes option pricing equations described by the Caputo generalized fractional derivative," *Chaos, Solitons & Fractals*, vol. 125, pp. 108–118, 2019.

[20] A. A. Khajehnasiri and M. Safavi, "Solving fractional Black-Scholes equation by using Boubaker functions," *Mathematical Methods in the Applied Sciences*, vol. 4, no. 11, pp. 8505–8515, 2021.

[21] C. Chen, Z. Wang, and Y. Yang, "A new operator splitting method for American options under fractional Black- Scholes models," *Computers & Mathematics with Applications*, vol. 77, no. 8, pp. 2130–2144, 2019.

[22] G. Krzyżanowski, M. Magdziarz, and Ł. Płociniczak, "A weighted finite difference method for subdiffusive Black-Scholes model," *Computers & Mathematics with Applications*, vol. 80, no. 5, pp. 653–670, 2020.

[23] X. Chen, D. Ding, S. L. Lei, and W. Wang, "A fast preconditioned iterative method for two-dimensional options pricing under fractional differential models," *Computers & Mathematics with Applications*, vol. 79, no. 2, pp. 440–456, 2020.

[24] S. E. Fadugba, "Homotopy analysis method and its applications in the valuation of European call options with time-fractional Black-Scholes equation," *Chaos, Solitons & Fractals*, vol. 141, article 110351, 2020.

[25] L. Song, "A space-time fractional derivative model for European option pricing with transaction costs in fractal market," *Chaos, Solitons & Fractals*, vol. 103, pp. 123–130, 2017.

[26] X. Zhang, S. Shuzhen, W. Lifei, and Y. Xiaozhong, "θ-Difference numerical method for solving time-fractional Black–Scholes equation. Highlights of Science paper online," *China Science and Technology Papers*, vol. 7, no. 13, pp. 1287–1295, 2014.

[27] R. H. De Staelen and A. S. Hendy, "Numerically pricing double barrier options in a time-fractional Black-Scholes model," *Computers & Mathematics with Applications*, vol. 74, no. 6, pp. 1166–1175, 2017.

[28] A. Golbabai and O. Nikan, "A computational method based on the moving least-squares approach for pricing double barrier options in a time-fractional Black-Scholes model," *Computational Economics*, vol. 55, no. 1, pp. 119–141, 2020.

[29] M. S. Hashemi, M. Inc, and A. Yusuf, "On three-dimensional variable order time fractional chaotic system with nonsingular kernel," *Chaos, Solitons & Fractals*, vol. 133, article 109628, 2020.

[30] M. She, L. Li, R. Tang, and D. Li, "A novel numerical scheme for a time fractional Black-Scholes equation," *Journal of Applied Mathematics and Computing*, vol. 66, no. 1-2, pp. 853–870, 2021.

[31] Z. Tian, S. Zhai, H. Ji, and Z. Weng, "A compact quadratic spline collocation method for the time-fractional Black-Scholes model," *Journal of Applied Mathematics and Computing*, vol. 66, no. 1-2, pp. 327–350, 2021.

[32] W. Chen and S. Wang, "A 2nd-order ADI finite difference method for a 2D fractional Black-Scholes equation governing European two asset option pricing," *Mathematics and Computers in Simulation*, vol. 171, pp. 279–293, 2020.

[33] J. Bodeau, G. Riboulet, and T. Roncalli, "Non-uniform grids for PDE in finance," 2000, https://papers.ssrn.com/sol3/papers.cfm?abstract_id=1031941.

[34] S. Kim, D. Jeong, C. Lee, and J. Kim, "Finite difference method for the multi-asset Black–Scholes equations," *Mathematics*, vol. 8, no. 3, p. 391, 2020.

[35] W. Lee, *An efficient finite difference method for the three-dimensional time-fractional Black–Scholes equation*, Graduate School, Korea University, 2021.

Hindawi
Journal of Function Spaces
Volume 2021, Article ID 2444920, 15 pages
https://doi.org/10.1155/2021/2444920

Research Article

Numerical, Approximate Solutions, and Optimal Control on the Deathly Lassa Hemorrhagic Fever Disease in Pregnant Women

M. Higazy,[1,2] A. El-Mesady,[2] A. M. S. Mahdy,[1,3] Sami Ullah,[4,5] and A. Al-Ghamdi[6]

[1]*Department of Mathematics and Statistics, College of Science, Taif University, P.O. Box 11099, Taif 21944, Saudi Arabia*
[2]*Department of Physics and Engineering Mathematics, Faculty of Electronic Engineering, Menoufia University, Menouf 32952, Egypt*
[3]*Department of Mathematics, Faculty of Science, Zagazig University, Zagazig, Egypt*
[4]*Research Center for Advanced Materials Science (RCAMS), King Khalid University, P.O. Box 9004, Abha 61413, Saudi Arabia*
[5]*Department of Chemistry, College of Science, King Khalid University, P.O. Box 9004, Abha 61413, Saudi Arabia*
[6]*Department of Physics, Faculty of Science, King Abdulaziz University, Jeddah 21589, Saudi Arabia*

Correspondence should be addressed to A. El-Mesady; ahmed.ibrahiem81@el-eng.menofia.edu.eg

Received 26 October 2021; Revised 13 November 2021; Accepted 22 November 2021; Published 15 December 2021

Academic Editor: Youssri Hassan Youssri

This paper is devoted to the model of Lassa hemorrhagic fever (LHF) disease in pregnant women. This disease is a biocidal fever and epidemic. LHF disease in pregnant women has negative impacts that were initially appeared in Africa. In the present study, we find an approximate solution to the fractional-order model that describes the fatal LHF disease. Laplace transforms coupled with the Adomian decomposition method (ADM) are applied. In addition, the fractional-order LHF model is numerically simulated in terms of a varied fractional order. Furthermore, a fractional order optimal control for the LHF model is studied.

1. Introduction

Infectious diseases remain a major threat to human health and welfare throughout history. Their spread is affected by several factors such as mode of transmission, infectious agent, infectious periods, incubation period, susceptibility, and resistance [1]. Some devastating infectious diseases like Lassa fever are endemic in many parts of the world and continue to emerge.

Lassa fever, also known as Lassa hemorrhagic fever (LHF), is an animal-borne, or zoonotic, acute viral hemorrhagic illness caused by Lassa virus, a member of the family *Arenaviridae*. The reservoir is the rats *Mastomys natalensis*, *M. erythroleucus*, and *Hylomyscus pamfi*. Food contaminated with rodent urine, saliva, or feces is the main cause of human cases. Human-to-human transmission can occur via exposure to the blood, feces, urine, saliva, or vomitus of infected patients [2, 3]. The incubation period is ca. 2-21 days. LHF is basically endemic in some countries of West Africa, and outbreaks have occurred in Benin, Ghana, Guinea, Liberia, Nigeria, Sierra Leone, and Togo. Cases have been imported to Germany, United Kingdom, United States, and Sweden. This disease with high mortality rates (e.g., 80% among pregnant women) is likely affecting between 100,000 and 300,000 people every year, and it kills around 5,000 people, almost all in West Africa alone [4, 5].

Fractional Calculus (FC) is a fruitful field of mathematical research with numerous applications in engineering [6], nanotechnology [7], optics [8], human diseases [9], and chaos soliton theory [10]. Application of FC is also adopted in biology, heat transfer, system identification, genetic algorithms, traffic systems, telecommunications, physics as well as finance, and economics [11–20].

Herein, we are interested in the paradigm showing the nature of LHF, since it is lethal and transmissible [1, 2, 21, 22]. Using mathematical modeling to probe this fatal illness may provide insight, answers, and guidance useful for controlling its spread, and the originating applications. The given model is studied through Caputo fractional operator. In this model, the Caputo fractional operator is used since

it permits both initial and boundary conditions to involve in modeling problems. The Caputo fractional operator can be applied on sufficiently differentiable functions only. One of the advantages of the fractional derivative of Caputo compared with the fractional derivative 3 of Riemann-Liouville is that the fractional derivative of Caputo for the constant is equal to zero. We develop an approximate solution to the fractional-order model describing the LHF affecting pregnant women using the Laplace transform coupled with the ADM. Numerical simulations are also presented. A fractional optimal control for the SIRD model is ultimately offered. For a good survey on the approximating of the differential equations, see [23–26]. Some recent research fractional optimal controls can be found in [27–29]. Atangana [21] studied the LHF using beta differential operator, where the model was proposed as follows in (1). Table 1 shows the meaning of the parameters in the model (1).

$$\begin{aligned}
{}_0^A D_t^\beta S(t) &= -u_1 S(t)I(t) + (\mu - l)N + \omega R(t) + (u_2 - l)S(t),\\
{}_0^A D_t^\beta I(t) &= u_1 S(t)I(t) - (\omega + u_2)I(t) - u_2 S(t),\\
{}_0^A D_t^\beta R(t) &= u_2 I(t) - \omega R(t),\\
{}_0^A D_t^\beta D(t) &= \omega I(t) + (l - \mu)N + lS(t),
\end{aligned} \tag{1}$$

where ${}_0^A D_t^\beta g(t) = (t + 1/\Gamma(\beta))^{1-\beta} \lim_{h \longrightarrow 0} g(t+h) - g(t)/h$.

Also, the model has been studied by Goyal et al. [22]. The q-homotopy analysis transform method (q-HATM) has been applied for solving the LHF model [30]. The LHF model via Atangana-Baleanu fractional derivative has been studied in [31]. The SIR model has been studied through Caputo-Fabrizio fractional operator in [32].

In this paper, we reconsider the system (1) by the following fractional sense of the system (1)

$$D^{(\alpha_1)}S(t) = -u_1 SI + (\mu - l)N + \omega R + (u_2 - l)S, \tag{2}$$

$$D^{(\alpha_2)}I(t) = u_1 SI - (\omega + u_2)I - u_2 S, \tag{3}$$

$$D^{(\alpha_3)}R(t) = u_2 I - \omega R, \tag{4}$$

$$D^{(\alpha_4)}D(t) = \omega I + (l - \mu)N + lS, \tag{5}$$

where $D^{(r)}$ is the Caputo fractional derivative of order r.

We organize the rest of our paper as follows. In Section 2, we provide some basic mathematical concepts that will be necessary for our work. Also, the description of the proposed model is presented. We then follow by presenting the series solution for the proposed model in Section 3. We provide the approximate solution construction in Section 4. The numerical solution of the proposed model, having arbitrary order, is given in Section 5. The optimal control case is studied in Section 6. In Section 7, a concise conclusion of our paper results is presented.

Table 1: The meaning of the parameters in the model (1).

Parameters	Meaning
$S(t)$	Susceptible pregnant women population
$I(t)$	Infected pregnant women population
$R(t)$	Recovery of pregnant women population
$D(t)$	The population of pregnant women dying in that country
u_1	The rate at which the women are infected
N	The total number of adult women in the given country
μ	The rate at which the women are pregnant
ω	The rate of death of pregnant women with LHF
l	The rate of death of pregnant women with another disease or with natural death
u_2	The rate of recovery of pregnant women from LHF

2. Preliminaries

For studying the proposed model (2), we present in this section the basic definitions concerned with fractional calculus. For a good survey on the basic definitions and several applications on fractional calculus, see [6, 7, 33].

2.1. Some Important Definitions

Definition 1. The Riemann–Liouville integral is represented by

$$I^\alpha z(t) = \frac{1}{\Gamma(\alpha)} \int_0^t (t - x)^{\alpha - 1} z(x)dx, \tag{6}$$

where Γ is the known gamma function and $\alpha \in (0, 1)$ is the order of this fractional integral.

Definition 2. The Caputo-type fractional derivative of order α is defined as

$$D^{(\alpha)}z(t) = \frac{1}{\Gamma(k - \alpha)} \int_0^t (t - x)^{k - \alpha - 1} z^{(k)}(x)dx, \tag{7}$$

Definition 3. The Laplace transform of Caputo fractional derivative of order α [33] is given by

$$\begin{aligned}
\mathscr{L}\left\{D^{(\alpha)}z(t)\right\} = s^\alpha Z(s) - \sum_{i=0}^{m-1} s^{\alpha - i - 1} z^{(i)}(0)\,;\, m - 1 < \alpha\\
< m, m \in N\,;\, Z(s) = \mathscr{L}\{z(t)\}.
\end{aligned} \tag{8}$$

2.2. Mathematical Formulation and Description for the Proposed Model. The meaning of the parameters is shown in Table 1. Now, the description and the mathematical formulation of the model can be shown as follows.

With time t, we can express the rate of change in susceptible population as follows

$$D^{(\alpha_1)}S(t) = -u_1 SI + (\mu - l)N + \omega R + (u_2 - l)S. \tag{9}$$

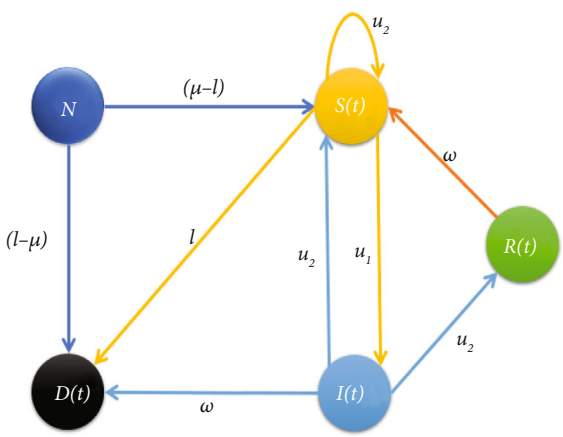

Figure 1: Signal flow graph of the studied LHF model.

With time t, we can express the rate of change in the population of the infected pregnant women as follows

$$D^{(\alpha_2)}I(t) = u_1 SI - (\omega + u_2)I - u_2 S. \tag{10}$$

Here, $u_1 SI$ is the number of pregnant women excluded from the group of susceptible.

With time t, the rate of change in recovery population is written as

$$D^{(\alpha_3)}R(t) = u_2 I - \omega R. \tag{11}$$

Finally, the rate of change of dying population with time t is given as

$$D^{(\alpha_4)}D(t) = \omega I + (l - \mu)N + lS. \tag{12}$$

Hence, the mathematical model for the LHF is given by model (2), with initial conditions

$$S(0) = S_0, I(0) = I_0, R(0) = R_0, D(0) = D_0. \tag{13}$$

Also $0 < \alpha_i < 1, i \in \{1, 2, 3, 4\}$. Here, $S(t)$, $I(t)$, $R(t)$, and $D(t)$ are sufficiently differentiable functions. Model (2) has not yet been studied by using the Laplace transform coupled with the ADM. Also, we introduce numerical simulations and fractional optimal controls for the SIRD model.

The interaction between different compartments of LHF model (2) can be viewed via the following signal flow graph shown in Figure 1.

2.3. Calculating the Basic Reproduction Number R_0. Basic reproduction number R_0 is the expected production of newly infected females, in a totally susceptible women, by meeting a typical infective woman. The local stability and instability of the disease-free equilibrium (DFE) depend on the value of R_0. Also, it defines the local stability threshold for the DFE. Moreover, it is a very important tool for controlling the disease, and it is an essential epidemiological criteria of disease. When $R_0 < 1$, the DFE is locally asymptotically stable; a small number of infections into the population may cause it to evolve into an endemic prevalence. From another point of view, when $R_0 > 1$, the DFE is locally unstable; a sufficiently small number of infected women will produce an outbreak. Here, R_0 is estimated from the paradigm of nonlinear FDE's (2) via the next-generation matrix method [34].

Since the Jacobian matrix is

$$J = \begin{pmatrix} -u_1 I + (u_2 - l) & -u_1 S & \omega & 0 \\ u_1 I - u_2 & u_1 S - \omega - u_2 & 0 & 0 \\ 0 & u_2 & -\omega & 0 \\ l & \omega & 0 & 0 \end{pmatrix}. \tag{14}$$

At the disease-free equilibrium point $(\mu - l/lN, 0, 0, 0)$ and $u_2 = 0$ then by putting the model in the $F - V$ form [34] where

$$F = \begin{pmatrix} \frac{u_1(\mu - l)N}{l} & 0 \\ 0 & 0 \end{pmatrix}, V = \begin{pmatrix} \omega & 0 \\ 0 & \omega \end{pmatrix}, V^{-1} = \begin{pmatrix} \frac{1}{\omega} & 0 \\ 0 & \frac{1}{\omega} \end{pmatrix}, \tag{15}$$

then

$$FV^{-1} = \begin{pmatrix} \frac{u_1(\mu - l)N}{l\omega} & 0 \\ 0 & 0 \end{pmatrix}. \tag{16}$$

Then, the basic reproduction number of the given paradigm is $R_0 = u_1(\mu - l)/\omega lN$. If $R_0 < 1$, then, infection cannot develop because an infected woman infects less than one new woman during their infectious period on average. Conversely, if $R_0 > 1$, the disease can enter the population because on average each infected woman will infect more than one new woman.

3. Series Solution for the Proposed Model

Applying Laplace transformation of (2) gives

$$\begin{cases} \mathscr{L}\left\{D^{(\alpha_1)}S(t)\right\} = \mathscr{L}\{-u_1 SI + (\mu - l)N + \omega R + (u_2 - l)S\}, \\ \mathscr{L}\left\{D^{(\alpha_2)}I(t)\right\} = \mathscr{L}\{u_1 SI - (\omega + u_2)I - u_2 S\}, \\ \mathscr{L}\left\{D^{(\alpha_3)}R(t)\right\} = \mathscr{L}\{u_2 I - \omega R\}, \\ \mathscr{L}\left\{D^{(\alpha_4)}D(t)\right\} = \mathscr{L}\{\omega I + (l - \mu)N + lS\}, \end{cases} \tag{17}$$

which gives

$$\begin{cases} s^{\alpha_1}S^*(s) - s^{\alpha_1-1}S(0) = \mathscr{L}\{-u_1SI + (\mu - l)N + \omega R + (u_2 - l)S\}, \\ s^{\alpha_2}I^*(s) - s^{\alpha_2-1}I(0) = \mathscr{L}\{u_1SI - (\omega + u_2)I - u_2S\}, \\ s^{\alpha_3}R^*(s) - s^{\alpha_3-1}R(0) = \mathscr{L}\{u_2I - \omega R\}, \\ s^{\alpha_4}D^*(s) - s^{\alpha_4-1}D(0) = \mathscr{L}\{\omega I + (l - \mu)N + lS\}, \end{cases} \tag{18}$$

where $S^*(s) = \mathscr{L}\{S(t)\}, I^*(s) = \mathscr{L}\{I(t)\}, R^*(s) = \mathscr{L}\{R(t)\}$, $D^*(s) = \mathscr{L}\{D(t)\}$.

By dividing the ith equation of (18) by s^{α_i}, we get

$$\begin{cases} S^*(s) = \dfrac{1}{s}S(0) + \dfrac{1}{s^{\alpha_1}}\mathscr{L}\{-u_1SI + (\mu - l)N + \omega R + (u_2 - l)S\}, \\ I^*(s) = \dfrac{1}{s}I(0) + \dfrac{1}{s^{\alpha_2}}\mathscr{L}\{u_1SI - (\omega + u_2)I - u_2S\}, \\ R^*(s) = \dfrac{1}{s}R(0) + \dfrac{1}{s^{\alpha_3}}\mathscr{L}\{u_2I - \omega R\}, \\ D^*(s) = \dfrac{1}{s}D(0) + \dfrac{1}{s^{\alpha_4}}\mathscr{L}\{\omega I + (l - \mu)N + lS\}. \end{cases} \tag{19}$$

Taking the inverse of Laplace transformation on (19) gives

$$\begin{cases} S(t) = S(0) + \mathscr{L}^{-1}\left[\dfrac{1}{s^{\alpha_1}}\mathscr{L}\{-u_1SI + (\mu - l)N + \omega R + (u_2 - l)S\}\right], \\ I(t) = I(0) + \mathscr{L}^{-1}\left[\dfrac{1}{s^{\alpha_2}}\mathscr{L}\{u_1SI - (\omega + u_2)I - u_2S\}\right], \\ R(t) = R(0) + \mathscr{L}^{-1}\left[\dfrac{1}{s^{\alpha_3}}\mathscr{L}\{u_2I - \omega R\}\right], \\ D(t) = D(0) + \mathscr{L}^{-1}\left[\dfrac{1}{s^{\alpha_4}}\mathscr{L}\{\omega I + (l - \mu)N + lS\}\right]. \end{cases} \tag{20}$$

Now, we will find the series solution by putting

$$\begin{aligned} S(t) &= \sum_{k=0}^{\infty} S_k(t), I(t) = \sum_{k=0}^{\infty} I_k(t), \\ R(t) &= \sum_{k=0}^{\infty} R_k(t), D(t) = \sum_{k=0}^{\infty} D_k(t). \end{aligned} \tag{21}$$

Decomposing the terms $S(t)I(t)$ gives

$$S(t)I(t) = \sum_{k=0}^{\infty} G_k(t). \tag{22}$$

The polynomial $G_k(t)$ is known as "Adomian polynomial" with the form

$$G_k(t) = \frac{1}{k!}\left[\left(\frac{d}{d\varepsilon}\right)^k\left[\sum_{r=0}^{k}\varepsilon^r S_r(t)\sum_{r=0}^{k}\varepsilon^r I_r(t)\right]\right]_{\varepsilon=0}. \tag{23}$$

By substituting from (21) and (22) into (20), we get

$$\mathscr{L}(S_0) = \frac{S_0}{s}, \mathscr{L}(I_0) = \frac{I_0}{s}, \mathscr{L}(R_0) = \frac{R_0}{s}, \mathscr{L}(D_0) = \frac{D_0}{s}, \tag{24}$$

$$\begin{aligned} \mathscr{L}(S_1) &= \frac{1}{s^{\alpha_1}}\mathscr{L}\{-u_1G_0 + (\mu - l)N + \omega R_0 + (u_2 - l)S_0\}, \\ \mathscr{L}(I_1) &= \frac{1}{s^{\alpha_2}}\mathscr{L}\{u_1G_0 - (\omega + u_2)I_0 - u_2S_0\}, \\ \mathscr{L}(R_1) &= \frac{1}{s^{\alpha_3}}\mathscr{L}\{u_2I_0 - \omega R_0\}, \\ \mathscr{L}(D_1) &= \frac{1}{s^{\alpha_4}}\mathscr{L}\{\omega I_0 + (l - \mu)N + lS_0\}, \end{aligned} \tag{25}$$

$$\begin{aligned} \mathscr{L}(S_2) &= \frac{1}{s^{\alpha_1}}\mathscr{L}\{-u_1G_1 + \omega R_1 + (u_2 - l)S_1\}, \\ \mathscr{L}(I_2) &= \frac{1}{s^{\alpha_2}}\mathscr{L}\{u_1G_1 - (\omega + u_2)I_1 - u_2S_1\}, \\ \mathscr{L}(R_2) &= \frac{1}{s^{\alpha_3}}\mathscr{L}\{u_2I_1 - \omega R_1\}, \mathscr{L}(D_2) = \frac{1}{s^{\alpha_4}}\mathscr{L}\{\omega I_1 + lS_1\}, \end{aligned} \tag{26}$$

$$\begin{aligned} \mathscr{L}(S_3) &= \frac{1}{s^{\alpha_1}}\mathscr{L}\{-u_1G_2 + \omega R_2 + (u_2 - l)S_2\}, \\ \mathscr{L}(I_3) &= \frac{1}{s^{\alpha_2}}\mathscr{L}\{u_1G_2 - (\omega + u_2)I_2 - u_2S_2\}, \\ \mathscr{L}(R_3) &= \frac{1}{s^{\alpha_3}}\mathscr{L}\{u_2I_2 - \omega R_2\}, \mathscr{L}(D_3) = \frac{1}{s^{\alpha_4}}\mathscr{L}\{\omega I_2 + lS_2\}, \end{aligned} \tag{27}$$

$$\begin{aligned} \mathscr{L}(S_4) &= \frac{1}{s^{\alpha_1}}\mathscr{L}\{-u_1G_3 + \omega R_3 + (u_2 - l)S_3\}, \\ \mathscr{L}(I_4) &= \frac{1}{s^{\alpha_2}}\mathscr{L}\{u_1G_3 - (\omega + u_2)I_3 - u_2S_3\}, \\ \mathscr{L}(R_4) &= \frac{1}{s^{\alpha_3}}\mathscr{L}\{u_2I_3 - \omega R_3\}, \mathscr{L}(D_4) = \frac{1}{s^{\alpha_4}}\mathscr{L}\{\omega I_3 + lS_3\}, \\ &\vdots \end{aligned} \tag{28}$$

$$\begin{aligned} \mathscr{L}(S_k) &= \frac{1}{s^{\alpha_1}}\mathscr{L}\{-u_1G_{k-1} + \omega R_{k-1} + (u_2 - l)S_{k-1}\}, \\ \mathscr{L}(I_k) &= \frac{1}{s^{\alpha_2}}\mathscr{L}\{u_1G_{k-1} - (\omega + u_2)I_{k-1} - u_2S_{k-1}\}, \\ \mathscr{L}(R_k) &= \frac{1}{s^{\alpha_3}}\mathscr{L}\{u_2I_{k-1} - \omega R_{k-1}\}, \\ \mathscr{L}(D_k) &= \frac{1}{s^{\alpha_4}}\mathscr{L}\{\omega I_{k-1} + lS_{k-1}\}. \end{aligned} \tag{29}$$

Note that $k \in \{2, 3, 4, .. \cdots\}$ in (29).

4. Approximate Solution

4.1. Construction of the Approximate Solution. Hereafter, we will discuss an approximate solution for the proposed model. Taking the inverse of Laplace transformation for (24), (25), (26), and (27) gives

$$\mathscr{L}^{-1}\left\{\frac{S_0}{s}\right\}=S_0,\ \mathscr{L}^{-1}\left\{\frac{I_0}{s}\right\}=I_0,\quad \mathscr{L}^{-1}\left\{\frac{R_0}{s}\right\}=R_0,\ \mathscr{L}^{-1}\left\{\frac{D_0}{s}\right\}=D_0, \tag{30}$$

$$S_1=at^{\alpha_1},\ a=\frac{-u_1G_0+(\mu-l)N+\omega R_0+(u_2-l)S_0}{\Gamma(\alpha_1+1)}, \tag{31}$$

$$I_1=bt^{\alpha_2},\ b=\frac{u_1G_0-(\omega+u_2)I_0-u_2S_0}{\Gamma(\alpha_2+1)}, \tag{32}$$

$$R_1=ct^{\alpha_3},\ c=\frac{u_2I_0-\omega R_0}{\Gamma(\alpha_3+1)}, \tag{33}$$

$$D_1=d^1t^{\alpha_4},\ d^1=\frac{\omega I_0+(l-\mu)N+lS_0}{\Gamma(\alpha_4+1)}, \tag{34}$$

$$S_2=dt^{2\alpha_1}+et^{\alpha_1+\alpha_2}+\mathrm{f}t^{\alpha_1+\alpha_3}, \tag{35}$$

$$d=a((u_2-l)-u_1I_0)\frac{\Gamma(\alpha_1+1)}{\Gamma(2\alpha_1+1)},\quad e=-u_1S_0b\frac{\Gamma(\alpha_2+1)}{\Gamma(\alpha_1+\alpha_2+1)},\ f=c\omega\frac{\Gamma(\alpha_3+1)}{\Gamma(\alpha_1+\alpha_3+1)}, \tag{36}$$

$$I_2=gt^{\alpha_1+\alpha_2}+ht^{2\alpha_2},\ g=a(u_1I_0-u_2)\frac{\Gamma(\alpha_1+1)}{\Gamma(\alpha_1+\alpha_2+1)},\quad h=b(u_1S_0-(\omega+u_2))\frac{\Gamma(\alpha_2+1)}{\Gamma(2\alpha_2+1)}, \tag{37}$$

$$R_2=it^{\alpha_2+\alpha_3}+jt^{2\alpha_3},\ i=u_2b\frac{\Gamma(\alpha_2+1)}{\Gamma(\alpha_2+\alpha_3+1)},\quad j=-\omega c\frac{\Gamma(\alpha_3+1)}{\Gamma(2\alpha_3+1)}, \tag{38}$$

$$D_2=pt^{\alpha_2+\alpha_4}+qt^{\alpha_1+\alpha_4},\ p=\omega b\frac{\Gamma(\alpha_2+1)}{\Gamma(\alpha_2+\alpha_4+1)},\quad q=la\frac{\Gamma(\alpha_1+1)}{\Gamma(\alpha_1+\alpha_4+1)}, \tag{39}$$

$$S_3=rt^{2\alpha_1+\alpha_2}+st^{3\alpha_1}+r_1t^{\alpha_1+2\alpha_2}+ut^{2\alpha_1+\alpha_3}+vt^{\alpha_1+\alpha_2+\alpha_3}+wt^{\alpha_1+2\alpha_3}, \tag{40}$$

$$\begin{aligned}
&r=(-u_1gS_0-u_1I_0e-u_1ab+e(u_2-l))\frac{\Gamma(\alpha_1+\alpha_2+1)}{\Gamma(2\alpha_1+\alpha_2+1)},\\
&s=((-u_1I_0d)+d(u_2-l))\frac{\Gamma(2\alpha_1+1)}{\Gamma(3\alpha_1+1)},\\
&r_1=-u_1hS_0\frac{\Gamma(2\alpha_2+1)}{\Gamma(\alpha_1+2\alpha_2+1)},\\
&\cdot\ u=(-u_1I_0f+f(u_2-l))\frac{\Gamma(\alpha_1+\alpha_3+1)}{\Gamma(2\alpha_1+\alpha_3+1)},\\
&\cdot\ v=i\omega\frac{\Gamma(\alpha_2+\alpha_3+1)}{\Gamma(\alpha_1+\alpha_2+\alpha_3+1)},\ w=j\omega\frac{\Gamma(2\alpha_3+1)}{\Gamma(\alpha_1+2\alpha_3+1)},
\end{aligned} \tag{41}$$

$$I_3=xt^{\alpha_1+2\alpha_2}+yt^{3\alpha_2}+zt^{2\alpha_1+\alpha_2}+a_1t^{\alpha_1+\alpha_2+\alpha_3}, \tag{42}$$

$$\begin{aligned}
x&=(u_1S_0g+eu_1I_0-g(\omega+u_2)\\
&\quad+u_1ab-u_2e)\frac{\Gamma(\alpha_1+\alpha_2+1)}{\Gamma(\alpha_1+2\alpha_2+1)},\\
y&=(u_1S_0h-h(\omega+u_2))\frac{\Gamma(2\alpha_2+1)}{\Gamma(3\alpha_2+1)},\\
z&=(du_1I_0-u_2d)\frac{\Gamma(2\alpha_1+1)}{\Gamma(2\alpha_1+\alpha_2+1)},\\
a_1&=f(u_1I_0-u_2)\frac{\Gamma(\alpha_1+\alpha_3+1)}{\Gamma(\alpha_1+\alpha_2+\alpha_3+1)},
\end{aligned} \tag{43}$$

$$R_3=b_1t^{\alpha_1+\alpha_2+\alpha_3}+c_1t^{2\alpha_2+\alpha_3}+d_1t^{\alpha_2+2\alpha_3}+e_1t^{3\alpha_3}, \tag{44}$$

$$\begin{aligned}
&b_1=gu_2\frac{\Gamma(\alpha_1+\alpha_2+1)}{\Gamma(\alpha_1+\alpha_2+\alpha_3+1)},\ c_1=hu_2\frac{\Gamma(2\alpha_2+1)}{\Gamma(2\alpha_2+\alpha_3+1)},\\
&d_1=-\omega i\frac{\Gamma(\alpha_2+\alpha_3+1)}{\Gamma(\alpha_2+2\alpha_3+1)},\ e_1=-\omega j\frac{\Gamma(2\alpha_3+1)}{\Gamma(3\alpha_3+1)},
\end{aligned} \tag{45}$$

$$D_3=f_1t^{\alpha_1+\alpha_2+\alpha_4}+g_1t^{2\alpha_2+\alpha_4}+h_1t^{2\alpha_1+\alpha_4}+i_1t^{\alpha_1+\alpha_3+\alpha_4}, \tag{46}$$

$$\begin{aligned}
&f_1=(g\omega+le)\frac{\Gamma(\alpha_1+\alpha_2+1)}{\Gamma(\alpha_1+\alpha_2+\alpha_4+1)},\ g_1=\omega h\frac{\Gamma(2\alpha_2+1)}{\Gamma(2\alpha_2+\alpha_4+1)},\\
&h_1=ld\frac{\Gamma(2\alpha_1+1)}{\Gamma(2\alpha_1+\alpha_4+1)},\ i_1=lf\frac{\Gamma(\alpha_1+\alpha_3+1)}{\Gamma(\alpha_1+\alpha_3+\alpha_4+1)}.
\end{aligned} \tag{47}$$

Since $S(t)=\sum_{k=0}^{\infty}S_k(t)$, $I(t)=\sum_{k=0}^{\infty}I_k(t)$, $R(t)=\sum_{k=0}^{\infty}R_k(t)$, $D(t)=\sum_{k=0}^{\infty}D_k(t)$, then, if we take the first four terms from the above series and take into consideration the equations from (30) to (46), we get

$$\begin{aligned}
S(t)&=S_0+S_1+S_2+S_3=S_0+at^{\alpha_1}+dt^{2\alpha_1}\\
&\quad+et^{\alpha_1+\alpha_2}+\mathrm{f}t^{\alpha_1+\alpha_3}+rt^{2\alpha_1+\alpha_2}+st^{3\alpha_1}\\
&\quad+r_1t^{\alpha_1+2\alpha_2}+ut^{2\alpha_1+\alpha_3}+vt^{\alpha_1+\alpha_2+\alpha_3}+wt^{\alpha_1+2\alpha_3},
\end{aligned} \tag{48}$$

$$\begin{aligned}
I(t)&=I_0+I_1+I_2+I_3=I_0+bt^{\alpha_2}+gt^{\alpha_1+\alpha_2}\\
&\quad+ht^{2\alpha_2}+xt^{\alpha_1+2\alpha_2}+yt^{3\alpha_2}+zt^{2\alpha_1+\alpha_2}+a_1t^{\alpha_1+\alpha_2+\alpha_3},
\end{aligned} \tag{49}$$

$$R(t) = R_0 + R_1 + R_2 + R_3 = R_0 + ct^{\alpha_3} + it^{\alpha_2+\alpha_3} + jt^{2\alpha_3} + b_1 t^{\alpha_1+\alpha_2+\alpha_3} + c_1 t^{2\alpha_2+\alpha_3} + d_1 t^{\alpha_2+2\alpha_3} + e_1 t^{3\alpha_3}, \tag{50}$$

$$D(t) = D_0 + D_1 + D_2 + D_3 = D_0 + d^1 t^{\alpha_4} + pt^{\alpha_2+\alpha_4} + qt^{\alpha_1+\alpha_4} + f_1 t^{\alpha_1+\alpha_2+\alpha_4} + g_1 t^{2\alpha_2+\alpha_4} + h_1 t^{2\alpha_1+\alpha_4} + i_1 t^{\alpha_1+\alpha_3+\alpha_4}. \tag{51}$$

After the compensation by the values of $a, b, c, d^1, d, e, f, g, h, i, j, p, q, r, r_1, s, u, v, w, x, y, z, a_1, b_1, c_1, d_1, e_1, f_1, g_1, h_1, i_1$, we obtain $S(t) = S_0 + S_1 + S_2 + S_3 =$

$$\begin{aligned}
&S_0 + \left(\frac{-u_1G_0 + (\mu - l)N + \omega R_0 + (u_2 - l)S_0}{\Gamma(\alpha_1+1)}\right)t^{\alpha_1} + \left(\left(\frac{-u_1G_0 + (\mu - l)N + \omega R_0 + (u_2 - l)S_0}{\Gamma(\alpha_1+1)}\right)((u_2 - l) - u_1I_0)\frac{\Gamma(\alpha_1+1)}{\Gamma(2\alpha_1+1)}\right)t^{2\alpha_1} \\
&- \left(u_1S_0\left(\frac{u_1G_0 - (\omega + u_2)I_0 - u_2S_0}{\Gamma(\alpha_2+1)}\right)\frac{\Gamma(\alpha_2+1)}{\Gamma(\alpha_1+\alpha_2+1)}\right)t^{\alpha_1+\alpha_2} + \left(\left(\frac{u_2I_0 - \omega R_0}{\Gamma(\alpha_3+1)}\right)\omega\frac{\Gamma(\alpha_3+1)}{\Gamma(\alpha_1+\alpha_3+1)}\right)t^{\alpha_1+\alpha_3} \\
&+ \left(\begin{array}{c}
-u_1\left(\left(\frac{-u_1G_0 + (\mu - l)N + \omega R_0 + (u_2 - l)S_0}{\Gamma(\alpha_1+1)}\right)(u_1I_0 - u_2)\frac{\Gamma(\alpha_1+1)}{\Gamma(\alpha_1+\alpha_2+1)}\right)S_0 \\
-u_1I_0\left(-u_1S_0\left(\frac{u_1G_0 - (\omega + u_2)I_0 - u_2S_0}{\Gamma(\alpha_2+1)}\right)\frac{\Gamma(\alpha_2+1)}{\Gamma(\alpha_1+\alpha_2+1)}\right) \\
-u_1\left(\frac{-u_1G_0 + (\mu - l)N + \omega R_0 + (u_2 - l)S_0}{\Gamma(\alpha_1+1)}\right)\left(\frac{u_1G_0 - (\omega + u_2)I_0 - u_2S_0}{\Gamma(\alpha_2+1)}\right) \\
+\left(-u_1S_0\left(\frac{u_1G_0 - (\omega + u_2)I_0 - u_2S_0}{\Gamma(\alpha_2+1)}\right)\frac{\Gamma(\alpha_2+1)}{\Gamma(\alpha_1+\alpha_2+1)}\right)(u_2 - l)
\end{array}\right)\frac{\Gamma(\alpha_1+\alpha_2+1)}{\Gamma(2\alpha_1+\alpha_2+1)}t^{2\alpha_1+\alpha_2} \\
&+ \left(\begin{array}{c}
\left(-u_1I_0\left(\frac{-u_1G_0 + (\mu - l)N + \omega R_0 + (u_2 - l)S_0}{\Gamma(\alpha_1+1)}\right)((u_2 - l) - u_1I_0)\frac{\Gamma(\alpha_1+1)}{\Gamma(2\alpha_1+1)}\right) \\
+\left(\left(\frac{-u_1G_0 + (\mu - l)N + \omega R_0 + (u_2 - l)S_0}{\Gamma(\alpha_1+1)}\right)((u_2 - l) - u_1I_0)\frac{\Gamma(\alpha_1+1)}{\Gamma(2\alpha_1+1)}\right)(u_2 - l)
\end{array}\right)\frac{\Gamma(2\alpha_1+1)}{\Gamma(3\alpha_1+1)}t^{3\alpha_1} + \left(\begin{array}{c}
-u_1I_0\left(\left(\frac{u_2I_0 - \omega R_0}{\Gamma(\alpha_3+1)}\right)\omega\frac{\Gamma(\alpha_3+1)}{\Gamma(\alpha_1+\alpha_3+1)}\right) \\
+\left(\left(\frac{u_2I_0 - \omega R_0}{\Gamma(\alpha_3+1)}\right)\omega\frac{\Gamma(\alpha_3+1)}{\Gamma(\alpha_1+\alpha_3+1)}\right)(u_2 - l)
\end{array}\right) \\
&\cdot \frac{\Gamma(\alpha_1+\alpha_3+1)}{\Gamma(2\alpha_1+\alpha_3+1)}t^{2\alpha_1+\alpha_3} + \left(u_2\left(\frac{u_1G_0 - (\omega + u_2)I_0 - u_2S_0}{\Gamma(\alpha_2+1)}\right)\frac{\Gamma(\alpha_2+1)}{\Gamma(\alpha_2+\alpha_3+1)}\right)\omega\frac{\Gamma(\alpha_2+\alpha_3+1)}{\Gamma(\alpha_1+\alpha_2+\alpha_3+1)}t^{\alpha_1+\alpha_2+\alpha_3} + \left(-\omega\left(\frac{u_2I_0 - \omega R_0}{\Gamma(\alpha_3+1)}\right)\frac{\Gamma(\alpha_3+1)}{\Gamma(2\alpha_3+1)}\right) \\
&\cdot \omega\frac{\Gamma(2\alpha_3+1)}{\Gamma(\alpha_1+2\alpha_3+1)}t^{\alpha_1+2\alpha_3} - u_1\left(\left(\left(\frac{u_1G_0 - (\omega + u_2)I_0 - u_2S_0}{\Gamma(\alpha_2+1)}\right)(u_1S_0 - (\omega + u_2))\frac{\Gamma(\alpha_2+1)}{\Gamma(2\alpha_2+1)}\right)\right)S_0\frac{\Gamma(2\alpha_2+1)}{\Gamma(\alpha_1+2\alpha_2+1)}t^{\alpha_1+2\alpha_2},
\end{aligned} \tag{52}$$

$$\begin{aligned}
I(t) = I_0 + I_1 + I_2 + I_3 &= I_0 + \left(\frac{u_1G_0 - (\omega + u_2)I_0 - u_2S_0}{\Gamma(\alpha_2+1)}\right)t^{\alpha_2} + \left(\frac{-u_1G_0 + (\mu - l)N + \omega R_0 + (u_2 - l)S_0}{\Gamma(\alpha_1+1)}\right) \\
&\cdot (u_1I_0 - u_2)\frac{\Gamma(\alpha_1+1)}{\Gamma(\alpha_1+\alpha_2+1)}t^{\alpha_1+\alpha_2} + \left(\left(\frac{u_1G_0 - (\omega + u_2)I_0 - u_2S_0}{\Gamma(\alpha_2+1)}\right)(u_1S_0 - (\omega + u_2))\frac{\Gamma(\alpha_2+1)}{\Gamma(2\alpha_2+1)}\right)t^{2\alpha_2} \\
&+ \left(\left(\begin{array}{c}
u_1S_0\left(\left(\frac{-u_1G_0 + (\mu - l)N + \omega R_0 + (u_2 - l)S_0}{\Gamma(\alpha_1+1)}\right)(u_1I_0 - u_2)\frac{\Gamma(\alpha_1+1)}{\Gamma(\alpha_1+\alpha_2+1)}\right) \\
+\left(-u_1S_0\left(\frac{u_1G_0 - (\omega + u_2)I_0 - u_2S_0}{\Gamma(\alpha_2+1)}\right)\frac{\Gamma(\alpha_2+1)}{\Gamma(\alpha_1+\alpha_2+1)}\right)u_1I_0 \\
-\left(\left(\frac{-u_1G_0 + (\mu - l)N + \omega R_0 + (u_2 - l)S_0}{\Gamma(\alpha_1+1)}\right)(u_1I_0 - u_2)\frac{\Gamma(\alpha_1+1)}{\Gamma(\alpha_1+\alpha_2+1)}\right)(\omega + u_2) \\
+u_1\left(\frac{-u_1G_0 + (\mu - l)N + \omega R_0 + (u_2 - l)S_0}{\Gamma(\alpha_1+1)}\right)\left(\frac{u_1G_0 - (\omega + u_2)I_0 - u_2S_0}{\Gamma(\alpha_2+1)}\right) \\
-u_2\left(-u_1S_0\left(\frac{u_1G_0 - (\omega + u_2)I_0 - u_2S_0}{\Gamma(\alpha_2+1)}\right)\frac{\Gamma(\alpha_2+1)}{\Gamma(\alpha_1+\alpha_2+1)}\right)
\end{array}\right)\frac{\Gamma(\alpha_1+\alpha_2+1)}{\Gamma(\alpha_1+2\alpha_2+1)}\right)t^{\alpha_1+2\alpha_2} \\
&+ \left(\left(\begin{array}{c}
u_1S_0\left(\left(\frac{u_1G_0 - (\omega + u_2)I_0 - u_2S_0}{\Gamma(\alpha_2+1)}\right)(u_1S_0 - (\omega + u_2))\frac{\Gamma(\alpha_2+1)}{\Gamma(2\alpha_2+1)}\right) \\
-\left(\left(\frac{u_1G_0 - (\omega + u_2)I_0 - u_2S_0}{\Gamma(\alpha_2+1)}\right)(u_1S_0 - (\omega + u_2))\frac{\Gamma(\alpha_2+1)}{\Gamma(2\alpha_2+1)}\right)(\omega + u_2)
\end{array}\right)\frac{\Gamma(2\alpha_2+1)}{\Gamma(3\alpha_2+1)}\right)t^{3\alpha_2} \\
&+ \left((u_1I_0 - u_2)\left(\left(\frac{-u_1G_0 + (\mu - l)N + \omega R_0 + (u_2 - l)S_0}{\Gamma(\alpha_1+1)}\right)((u_2 - l) - u_1I_0)\frac{\Gamma(\alpha_1+1)}{\Gamma(2\alpha_1+1)}\right)\frac{\Gamma(2\alpha_1+1)}{\Gamma(2\alpha_1+\alpha_2+1)}\right)t^{2\alpha_1+\alpha_2} \\
&+ \left(\left(\left(\frac{u_2I_0 - \omega R_0}{\Gamma(\alpha_3+1)}\right)\omega\frac{\Gamma(\alpha_3+1)}{\Gamma(\alpha_1+\alpha_3+1)}\right)(u_1I_0 - u_2)\frac{\Gamma(\alpha_1+\alpha_3+1)}{\Gamma(\alpha_1+\alpha_2+\alpha_3+1)}\right)t^{\alpha_1+\alpha_2+\alpha_3},
\end{aligned} \tag{53}$$

$$\begin{aligned}
R(t) = R_0 + R_1 + R_2 + R_3 = R_0 &+ \left(\frac{u_2 I_0 - \omega R_0}{\Gamma(\alpha_3+1)}\right) t^{\alpha_3} + \left(u_2\left(\frac{u_1 G_0 - (\omega+u_2) I_0 - u_2 S_0}{\Gamma(\alpha_2+1)}\right)\frac{\Gamma(\alpha_2+1)}{\Gamma(\alpha_2+\alpha_3+1)}\right) t^{\alpha_2+\alpha_3} \\
&- \left(\omega\left(\frac{u_2 I_0 - \omega R_0}{\Gamma(\alpha_3+1)}\right)\frac{\Gamma(\alpha_3+1)}{\Gamma(2\alpha_3+1)}\right) t^{2\alpha_3} + \left(\left(\frac{-u_1 G_0 + (\mu-l)N + \omega R_0 + (u_2-l)S_0}{\Gamma(\alpha_1+1)}\right)(u_1 I_0 - u_2)\frac{\Gamma(\alpha_1+1)}{\Gamma(\alpha_1+\alpha_2+1)}\right) \\
&\cdot u_2 \frac{\Gamma(\alpha_1+\alpha_2+1)}{\Gamma(\alpha_1+\alpha_2+\alpha_3+1)} t^{\alpha_1+\alpha_2+\alpha_3} + \left(\left(\frac{u_1 G_0 - (\omega+u_2) I_0 - u_2 S_0}{\Gamma(\alpha_2+1)}\right)(u_1 S_0 - (\omega+u_2))\frac{\Gamma(\alpha_2+1)}{\Gamma(2\alpha_2+1)}\right) \\
&\cdot u_2 \frac{\Gamma(2\alpha_2+1)}{\Gamma(2\alpha_2+\alpha_3+1)} t^{2\alpha_2+\alpha_3} - \omega\left(u_2\left(\frac{u_1 G_0 - (\omega+u_2) I_0 - u_2 S_0}{\Gamma(\alpha_2+1)}\right)\frac{\Gamma(\alpha_2+1)}{\Gamma(\alpha_2+\alpha_3+1)}\right)\frac{\Gamma(\alpha_2+\alpha_3+1)}{\Gamma(\alpha_2+2\alpha_3+1)} t^{\alpha_2+2\alpha_3} \\
&- \omega\left(-\omega\left(\frac{u_2 I_0 - \omega R_0}{\Gamma(\alpha_3+1)}\right)\frac{\Gamma(\alpha_3+1)}{\Gamma(2\alpha_3+1)}\right)\frac{\Gamma(2\alpha_3+1)}{\Gamma(3\alpha_3+1)} t^{3\alpha_3},
\end{aligned} \tag{54}$$

$$\begin{aligned}
D(t) = D_0 + D_1 + D_2 + D_3 = D_0 &+ \left(\frac{\omega I_0 + (l-\mu)N + l S_0}{\Gamma(\alpha_4+1)}\right) t^{\alpha_4} + \left(\omega\left(\frac{u_1 G_0 - (\omega+u_2) I_0 - u_2 S_0}{\Gamma(\alpha_2+1)}\right)\frac{\Gamma(\alpha_2+1)}{\Gamma(\alpha_2+\alpha_4+1)}\right) t^{\alpha_2+\alpha_4} \\
&+ \left(l\left(\frac{-u_1 G_0 + (\mu-l)N + \omega R_0 + (u_2-l)S_0}{\Gamma(\alpha_1+1)}\right)\frac{\Gamma(\alpha_1+1)}{\Gamma(\alpha_1+\alpha_4+1)}\right) t^{\alpha_1+\alpha_4} \\
&+ \left(\begin{array}{c} \left(\left(\frac{-u_1 G_0 + (\mu-l)N + \omega R_0 + (u_2-l)S_0}{\Gamma(\alpha_1+1)}\right)(u_1 I_0 - u_2)\frac{\Gamma(\alpha_1+1)}{\Gamma(\alpha_1+\alpha_2+1)}\right)\omega \\ + l\left(-u_1 S_0\left(\frac{u_1 G_0 - (\omega+u_2) I_0 - u_2 S_0}{\Gamma(\alpha_2+1)}\right)\frac{\Gamma(\alpha_2+1)}{\Gamma(\alpha_1+\alpha_2+1)}\right) \end{array}\right)\frac{\Gamma(\alpha_1+\alpha_2+1)}{\Gamma(\alpha_1+\alpha_2+\alpha_4+1)} t^{\alpha_1+\alpha_2+\alpha_4} \\
&+ \omega\left(\left(\frac{u_1 G_0 - (\omega+u_2) I_0 - u_2 S_0}{\Gamma(\alpha_2+1)}\right)(u_1 S_0 - (\omega+u_2))\frac{\Gamma(\alpha_2+1)}{\Gamma(2\alpha_2+1)}\right)\frac{\Gamma(2\alpha_2+1)}{\Gamma(2\alpha_2+\alpha_4+1)} t^{2\alpha_2+\alpha_4} \\
&+ l\left(\left(\frac{-u_1 G_0 + (\mu-l)N + \omega R_0 + (u_2-l)S_0}{\Gamma(\alpha_1+1)}\right)((u_2-l) - u_1 I_0)\frac{\Gamma(\alpha_1+1)}{\Gamma(2\alpha_1+1)}\right)\frac{\Gamma(2\alpha_1+1)}{\Gamma(2\alpha_1+\alpha_4+1)} t^{2\alpha_1+\alpha_4} \\
&+ l\left(\left(\frac{u_2 I_0 - \omega R_0}{\Gamma(\alpha_3+1)}\right)\omega\frac{\Gamma(\alpha_3+1)}{\Gamma(\alpha_1+\alpha_3+1)}\right)\frac{\Gamma(\alpha_1+\alpha_3+1)}{\Gamma(\alpha_1+\alpha_3+\alpha_4+1)} t^{\alpha_1+\alpha_3+\alpha_4}.
\end{aligned} \tag{55}$$

Now, by taking the first three terms of $S(t)$, $I(t)$, $R(t)$, and $D(t)$ and putting $\alpha_1 = \alpha_2 = \alpha_3 = \alpha_4 = \alpha, u_1 = 0.4$, $\mu = 0.3$, $N = 1000$, $l = 0.2$, $\omega = 0.8$, $u_2 = 0.2$, $S(0) = 900$, $I(0) = 10$, $R(0) = D(0) = 0$, in the proposed model yield (see [30]).

$$S(t) = S_0 + S_1 + S_2 = 900 - \frac{3500}{\Gamma(\alpha+1)} t^{\alpha} - \frac{1213598.4}{\Gamma(2\alpha+1)} t^{2\alpha}, \tag{56}$$

$$I(t) = I_0 + I_1 + I_2 = 10 + \frac{3410}{\Gamma(\alpha+1)} t^{\alpha} + \frac{1210890}{\Gamma(2\alpha+1)} t^{2\alpha}, \tag{57}$$

$$R(t) = R_0 + R_1 + R_2 = 0 + \frac{2}{\Gamma(\alpha+1)} t^{\alpha} + \frac{680.4}{\Gamma(2\alpha+1)} t^{2\alpha}, \tag{58}$$

$$D(t) = D_0 + D_1 + D_2 = 0 + \frac{88}{\Gamma(\alpha+1)} t^{\alpha} + \frac{2028}{\Gamma(2\alpha+1)} t^{2\alpha}. \tag{59}$$

Figure 2 exhibits the dynamical behavior of $S(t)$, $I(t)$, $R(t)$, and $D(t)$ against various fractional orders ($\alpha = 0,7$; 0.8; 0.9; 1).

4.2. Convergence and Error Analysis. It is clear that the previous solution is a series. This solution converges rapidly and uniformly to the exact solution. We will use classical techniques to prove the convergence of the series (21), and hence, we can get the sufficient conditions for the convergence of the used method.

Theorem 4. *Suppose $\wp$ is the Banach space and $\sigma : \wp \longrightarrow \wp$ is a contractive nonlinear operator with for all $x, x' \in \wp$, $\|\sigma(x) - \sigma(x')\| \le \lambda\|x - x'\|$, $0 < \lambda < 1$. Then, based on Banach contraction principle, there is a unique point x such that $\sigma x = x$, where $x = (s, i, r, d)$. By applying the ADM, the series in (21) can be written as follows:*

$$x_n = \sigma x_{n-1}, x_{n-1} = \sum_{k=1}^{n-1} x_k, n = 1, 2, 3, \cdots, \tag{60}$$

and suppose that $x_0 = x_0 \in A_j(x)$ where $A_j(x) = \{x' \in \wp : \|x - x'\| < j\}$, then, we obtain

$$x_n \in A_j(x); \tag{61}$$

$$\lim_{n \longrightarrow \infty} x_n = x. \tag{62}$$

Proof. For the first part $(a) x_n \in A_j(x)$; by the mathematical induction if $n = 1$, we obtain

$$\|x_0 - x\| = \|\sigma(x_0) - \sigma(x)\| \le \lambda\|x_0 - x\|. \tag{63}$$

Suppose the result is true at $n - 1$, hence,

$$\|x_0 - x\| \le \lambda^{n-1}\|x_0 - x\|. \tag{64}$$

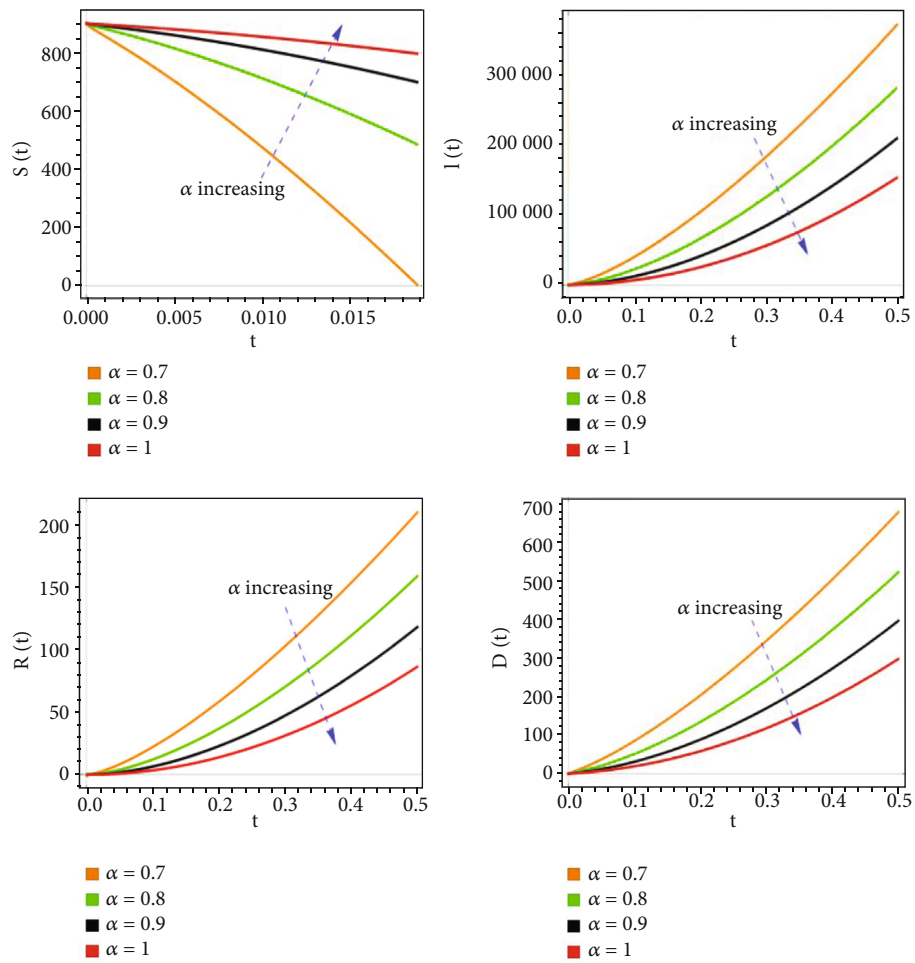

Figure 2: The behavior of $S(t), I(t), R(t)$, and $D(t)$ populations versus time with different fractional derivative orders.

We have

$$\begin{aligned}\|x_n - x\| &= \|\sigma(x_{n-1}) - \sigma(x)\| \le \lambda\|x_{n-1} - x\| \\ &\le \lambda^n\|x_0 - x\|,\end{aligned} \tag{65}$$

$$\|x_n - x\| \le \lambda^n\|x_0 - x\| \le \lambda^n j < j. \tag{66}$$

This shows that $x_n \in A_j(x)$..□ □

For the second part (b) $\lim_{n\longrightarrow\infty} x_n = x$.

Since $\|x_n - x\| \le \lambda^n\|x_0 - x\|$ and $\lim_{n\longrightarrow\infty} \lambda^n = 0$. So, we obtain $\lim_{n\longrightarrow\infty}\|x_n - x\| = 0 \Rightarrow \lim_{n\longrightarrow\infty} x_n = x$.

5. Fractional-Order Numerical Simulations of the SIRD System

First, we recall the basics of the applied numerical technique that have been given for the numerical simulation of fractional IVPs with Caputo derivatives (2). The technique is an extension of the well-known Adams-Bashforth-Moulton (ABM) integrator which is common for the numerical simulation of 1st order differential equations [35]. This technique comes from the idea that the IVP is equal to the equation of Volterra integral. The fractional ABM technique is fully presented by the following formulas (all other states can be found same as S). Assuming that $[0, T]$ is the domain of the solution and $n = 0, 1, 2, \cdots, N$, $h = T/N$, $t_n = nh$:

$$\begin{aligned}S(t_{n+1}) &= \sum_{i=0}^{\lceil\alpha\rceil-1} S_0^{(i)} \frac{t_{n+1}^{\ i+1}}{i!} + \frac{h^\alpha}{\Gamma(\alpha+2)}\psi_1(t_{n+1}, S^p(t_{n+1})) \\ &\quad + \frac{h^\alpha}{\Gamma(\alpha+2)}\sum_{j=0}^{n}\Lambda_{j,n+1}\psi_1(t_j, S(t_j)), S^p(t_{n+1}) \\ &= \sum_{i=0}^{\lceil\alpha\rceil-1} S_0^{(i)} \frac{t_{n+1}^{\ i+1}}{i!} + \frac{1}{\Gamma(\alpha)}\sum_{k=0}^{n}\Xi_{k,n+1}\psi_1(t_k, S(t_k)),\end{aligned} \tag{67}$$

where

$$\Lambda_{j,n+1} = \begin{cases} n^{\alpha+1} - (n-\alpha)(n+1)^\alpha, & \text{if } j = 0, \\ (n-j+2)^{\alpha+1} + (n-j)^{\alpha+1} - 2(n-j+1)^{\alpha+1}, & \text{if } 1 \le j \le n, \\ 1 & \text{if } j = n+1, \end{cases} \tag{68}$$

$$\Xi_{j,n+1} = \frac{h^\alpha}{\alpha}\left((n+1-j)^\alpha - (n-j)^\alpha\right). \tag{69}$$

A complete study of the stability of the method has been produced in [36].

In this part, we have found the numerical simulation of the proposed paradigm via the predictor-corrector PECE method of ABM [35] coded in MATLAB. The behavior of the obtained solution is shown by taking suitable values of the parameters as in [30]: $u_1 = 0.4$, $\mu = 0.3$, $N = 1000$, $l = 0.2$, $\omega = 0.8$, $u_2 = 0.2$, $S(0) = 900$, $I(0) = 10$, $R(0) = D(0) = 0$, and $\alpha_1 = \alpha_2 = \alpha_3 = \alpha_4 = \alpha$. In Figure 3, the behavior of $S(t)$ and $I(t)$ populations versus time with different fractional derivative orders is shown. In Figure 4, the behavior of $R(t)$ and $D(t)$ populations versus time with different fractional derivative orders is shown. In Figure 5, the dynamics of the populations in $I(t), R(t)$ and $D(t)$ 3D space with different fractional derivative orders are shown. In Figure 6, the dynamics of the populations in $S(t), I(t)$ and $D(t)$ 3D-space with different fractional derivative orders are shown. In Figure 7, the dynamics of the populations in $S(t)$,$I(t)$, and $R(t)$ 3D space with different fractional derivative orders are shown. In Figure 8, the dynamics of the populations in $S(t)$,$R(t)$, and $D(t)$ 3D space with different fractional derivative orders are shown. In Figure 9, the Lyapunov exponents concerning the fraction derivative order α are displayed. From Figure 9, we can conclude that the system is unstable in the transient period since LE1 is positive. But as shown LE1 loses its positivity after a short period which indicates that the system settles to its fixed point. In Figure 10, we show the 3D dynamics of the infected population concerning both time and infection rate at fractional derivative order 0.95. In Figure 11, we show the 3D dynamics of the susceptible population concerning both time and infection rate at fractional derivative order 0.95. There is a quick convergence between the obtained and the exact solution. In complex models, it is well known that a small variation in physical behavior stimulates several new results to understand and analyze nature in a systematic manner.

6. Fractional Optimal Control (FOCP) for SIRD Paradigm

In this position, we discuss the optimal control of the fractional-order SIRD paradigm:

$$\begin{aligned} D^\alpha S(t) &= -u_1 SI + (\mu - 1)N + \omega R + (u_2 - l)S, \\ D^\alpha I(t) &= u_1 SI - (\omega + u_2)I - u_2 S, \\ D^\alpha R(t) &= u_2 I - \omega R, \\ D^\alpha D(t) &= \omega I + (l - \mu)N + lS. \end{aligned} \tag{70}$$

According to references [37–40], consider the model (70) inside R^4. The proposed control functions can be formulated as follows:

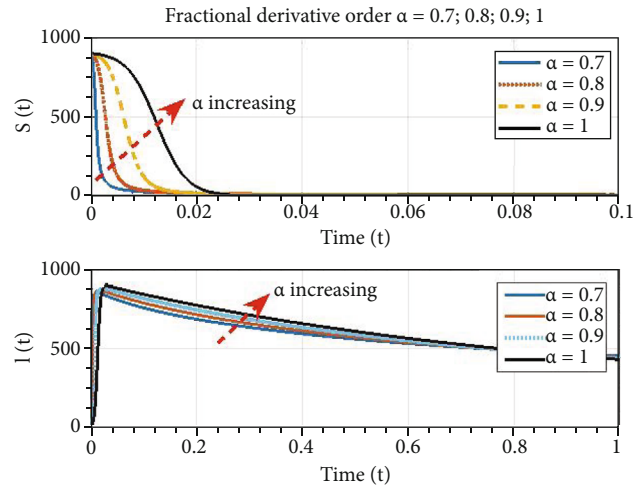

Figure 3: The behavior of $S(t)$ and $I(t)$ populations versus time with different fractional derivative orders.

$$\begin{aligned} \Psi = \{(u_1(.), u_2(.)) \in (L^\infty \times L^\infty) | 0 \le u_1(.), u_2(.) \\ \le 1, \forall t \in [0, T_f] = [0, 1]\}, \end{aligned} \tag{71}$$

and T_f refers to the end of the time period, $u_1(.)$ provides the rate of susceptibility per year, and $u_2(.)$ provides the rate of curing from infection population to recovered population per year. $u_1(.)$ with $u_2(.)$ is the control functions. Here, the function space L^∞ norm is defined as $\|x\|_\infty = \max_i |x_i|$. This concept of the L^∞ norm considered to be equal to taking the limit as $p \longrightarrow \infty$ of the L^p norm.

The following is the definition of the objective function (the control variables are squared)

$$J(u_1, u_2) = \int_0^{T_f} \left[aI(t) + bu_1^2(t) + c\,u_2^2(t)\right] dt. \tag{72}$$

Such that a, b, and c clarify, respectively, the quantity of infectious, a per year rate of susceptible, and a per year rate of progress from infective to recovered.

Finding the optimal controls $u_1(.)$ and $u_2(.)$ is the basic goal in FOCPs, in order to minimize the predefined objective function:

$$J(u_1, u_2) = \int_0^{T_f} \psi[S, I, R, D, u_1, u_2, t] dt, \tag{73}$$

where $\psi[S, I, R, D, u_1, u_2, t] = [a\,I(t) + b\,u_1^2(t) + c\,u_2^2(t)]$, subjected to the constraint

$$D^\alpha S = \eta_1, D^\alpha I = \eta_2, D^\alpha R = \eta_3, D^\alpha D = \eta_4, \tag{74}$$

where $\eta_i = \eta_i(S, I, R, D, u_1, u_2, t)$, $i = 1, 2, 3, 4$.

The initial conditions are as follows:

$$S(0) = S_1, I(0) = I_1, R(0) = R_1, D(0) = D_1. \tag{75}$$

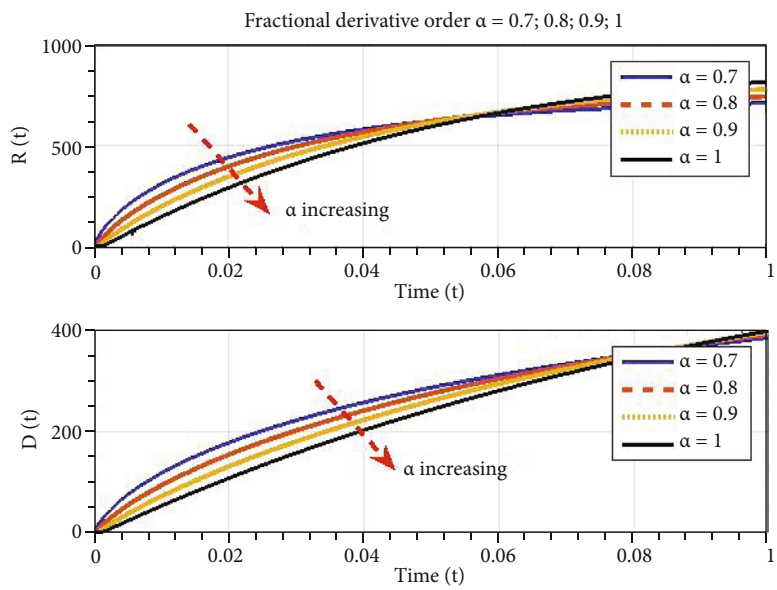

Figure 4: The behavior of $R(t)$ and $D(t)$ populations versus time with different fractional derivative orders.

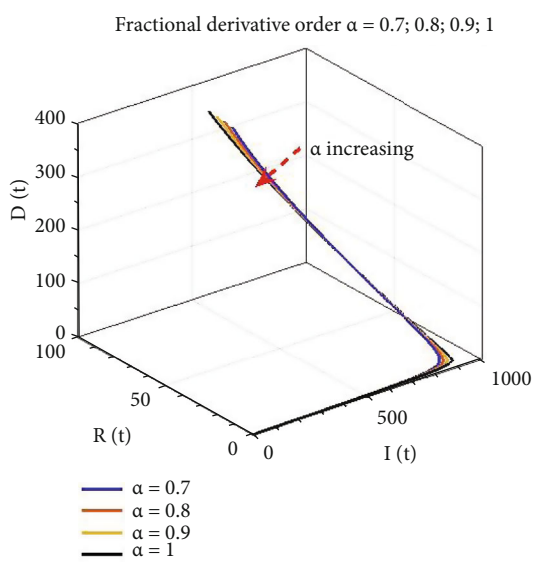

Figure 5: The dynamics of the populations in $I(t)$,$R(t)$, and $D(t)$ 3D space with different fractional derivative orders.

To construct the FOCP, consider the selected objective function defined in [41–44]:

$$\overset{*}{J} = \int_0^{T_f} \left[H(S, I, R, D, u_1, u_2, t) - \sum_{i=1}^{4} \lambda_i \eta_i (S, I, R, D, u_1, u_2, t) \right] dt, \tag{76}$$

Such that $i = 1, 2, 3, 4$.

In equation (77), (78), we write the Hamiltonian of the cost (objective) function (76) and the control of the fractional-order SIRD paradigm (70):

$$H(S, I, R, D, u_1, u_2, t) = \psi(S, I, R, C, u_1, u_2, t) + \sum_{i=1}^{4} \lambda_i \eta_i (S, I, R, D, u_1, u_2, t), \tag{77}$$

then

$$\begin{aligned} H = {} & a\,I + b\,u_1^2 + c\,u_2^2 + \lambda_1[-u_1 SI + (\mu - 1)N \\ & + \omega R + (u_2 - l)S] + \lambda_3[u_2 I - \omega R] \\ & + \lambda_2[u_1 SI - (\omega + u_2)I - u_2 S] \\ & + \lambda_4[\omega I + (l - \mu)N + lS]. \end{aligned} \tag{78}$$

From (76) and (78), following the method in [37, 39, 43–45], the FOPC's necessary and sufficient conditions are formulated as

$$D^\alpha \lambda_1 = \frac{\partial H}{\partial S}, D^\alpha \lambda_2 = \frac{\partial H}{\partial I}, D^\alpha \lambda_3 = \frac{\partial H}{\partial R}, D^\alpha \lambda_4 = \frac{\partial H}{\partial D}, \tag{79}$$

$$\frac{\partial H}{\partial u_k} = 0, k = 1, 2 \Rightarrow \frac{\partial H}{\partial u_1} = 0, \frac{\partial H}{\partial u_2} = 0, \tag{80}$$

$$D^\alpha S = \frac{\partial H}{\partial \lambda_1}, D^\alpha I = \frac{\partial H}{\partial \lambda_2}, D^\alpha R = \frac{\partial H}{\partial \lambda_3}, D^\alpha D = \frac{\partial H}{\partial \lambda_4}, \tag{81}$$

additionally,

$$\lambda_i, (T_f) = 0, \tag{82}$$

where λ_i, $i = 1, 2, 3, 4$ represent the Lagrange multipliers. In equations (79) and (80), the necessary conditions using FOPC Hamiltonian are represented.

The main result is recorded in Theorem 5.

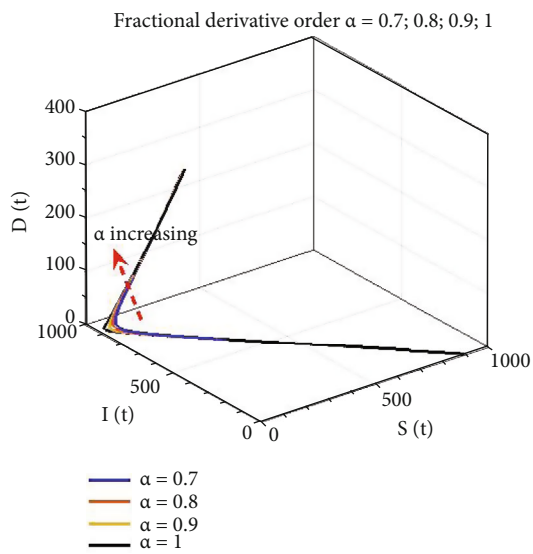

Figure 6: The dynamics of the populations in $S(t)$,$I(t)$, and $D(t)$ 3D space with different fractional derivative orders.

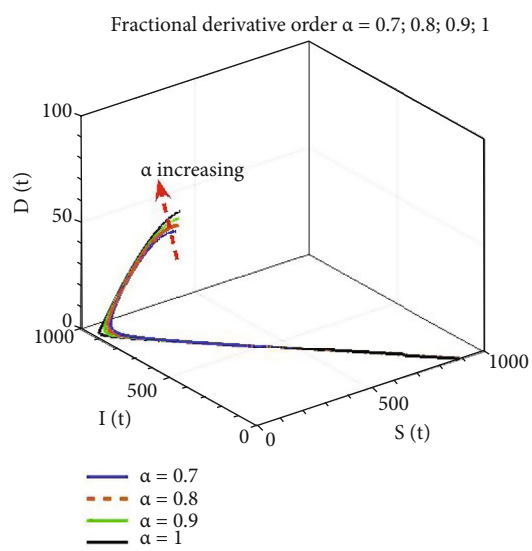

Figure 7: The dynamics of the populations in $S(t)$,$I(t)$, and $R(t)$ 3D space with different fractional derivative orders.

Theorem 5. *If u_1 and u_2 are optimal controls related to the controlled states S^*, I^*, R^* and D^*, then, the adjoint variables $\lambda_i^*, i = 1, 2, 3, 4$ exist that satisfy the following conditions:*

(i) Adjoint conditions (costate conditions)

Considering the related conditions represented in the recorded theorem and using equations (82), see [37, 39, 43, 44], we obtain the following four conditions that can be formulated as

$$D^\alpha \lambda_1^* = \lambda_1^*[-u_1 I^* + (u_2 - l)] + \lambda_2^*[u_1 I^* - u_2] + \lambda_4^*[l], \tag{83}$$

$$\begin{aligned} D^\alpha \lambda_2^* = a + \lambda_1^*[-u_1 S^*] + \lambda_2^*[u_1 S^* - (\omega + u_2)] \\ + \lambda_3^*[u_2] + \lambda_4^*[\omega], \end{aligned} \tag{84}$$

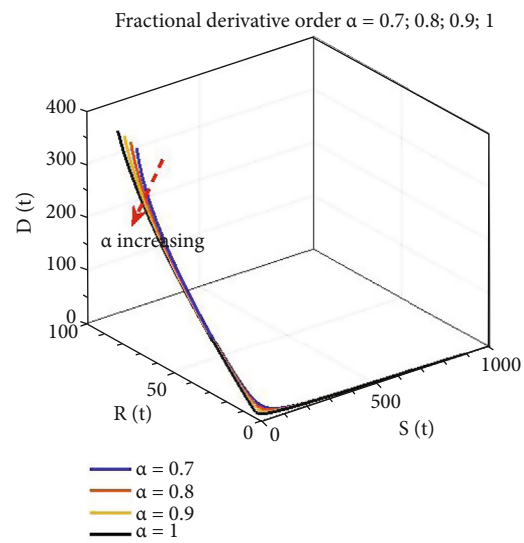

Figure 8: The dynamics of the populations in $S(t)$,$R(t)$, and $D(t)$ 3D space with different fractional derivative orders.

$$D^\alpha \lambda_3^* = \lambda_1^*[\omega] + \lambda_3^*[-\omega], \tag{85}$$

$$D^\alpha \lambda_4^* = 0. \tag{86}$$

(ii) Transversality conditions

$$\lambda_i^*(T_f) = 0, i = 1, 2, 3, 4. \tag{87}$$

(iii) Conditions of optimality

$$\begin{aligned} &H(S^*, I^*, R^*, D^*, u_1^*, u_2^*, \lambda_i) \\ &= \min_{0 \le u_1^*, u_2^* \le 1} H^*(S^*, I^*, R^*, D^*, u_1^*, u_2^*, \lambda_i), \end{aligned} \tag{88}$$

moreover, by applying equations (80), the control functions u_1^*, u_2^* are given as follows:

$$\frac{\partial H}{\partial u_1} = 0 \Rightarrow u_1 = \frac{[\lambda_1^* - \lambda_2^*] S^* I^*}{2b}, \tag{89}$$

$$\frac{\partial H}{\partial u_2} = 0 \Rightarrow u_2 = \frac{[\lambda_2^* - \lambda_3^*] I^* + [\lambda_2^* - \lambda_1^*] S^*}{2c}, \tag{90}$$

$$u_1^* = \min\left\{1, \max\left\{0, \frac{[\lambda_1^* - \lambda_2^*] S^* I^*}{2b}\right\}\right\}, \tag{91}$$

$$v_2^* = \min\left\{1, \max\left\{0, \frac{[\lambda_2^* - \lambda_3^*] I^* + [\lambda_2^* - \lambda_1^*] S^*}{2c}\right\}\right\}. \tag{92}$$

Proof. The system of costate conditions (83)–(86) is produced from equation (81) such that the Hamiltonian H^* is presented as

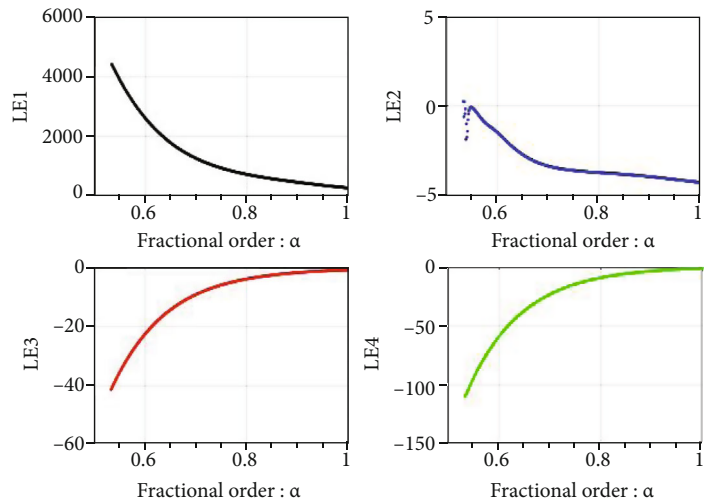

Figure 9: The exponents of Lyapunov as a function of the fractional derivative order α.

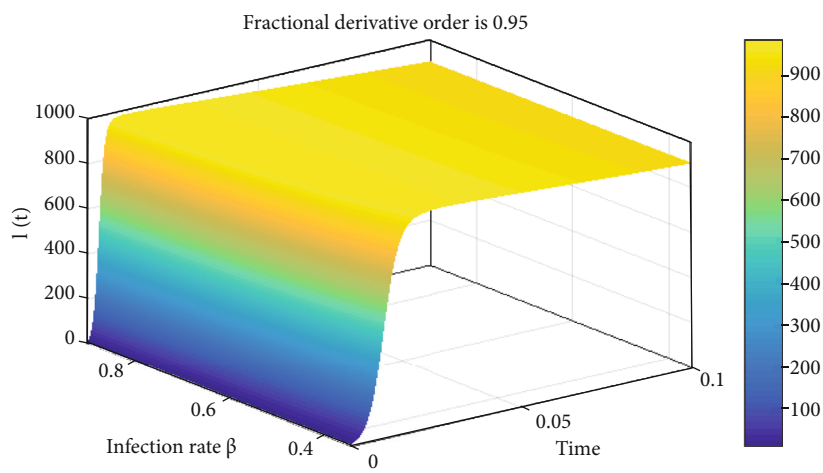

Figure 10: 3D dynamics of the infected population versus both time and infection rate at fractional derivative order 0.95.

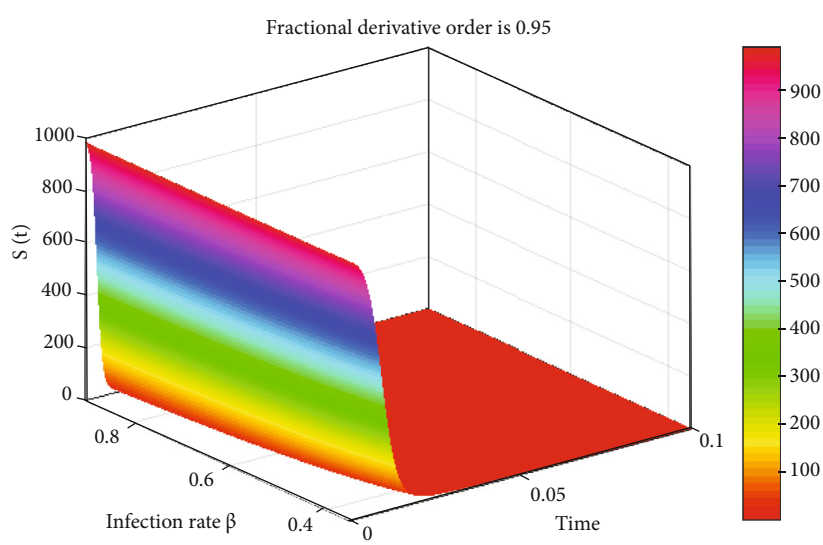

Figure 11: 3D dynamics of the susceptible population versus both time and infection rate at fractional derivative order 0.95.

$$H^* = a I^* + b u_1^{*2} + c u_2^{*2} + \lambda_1^* D^\alpha S^* + \lambda_2^* D^\alpha I^* + \lambda_3^* D^\alpha R^* + \lambda_4^* D^\alpha D^*. \tag{93}$$

Furthermore, the conditions in equation (82) are guaranteed, and the optimal control given by equations (91)–(92) can be produced via equation (80).□ □

Substituting v_i^*, $i = 1, 2$ in (70), the state system is formulated as follows:

$$\begin{aligned} D^\alpha S^*(t) &= -u_1^* S^* I^* + (\mu - 1)N + \omega R^* + (u_2^* - l)S^*, \\ D^\alpha I^*(t) &= u_1^* S^* I^* - (\omega + u_2^*)I^* - u_2^* S^*, \\ D^\alpha R^*(t) &= u_2^* I^* - \omega R^*, \\ D^\alpha D^*(t) &= \omega I^* + (l - \mu)N + l S^*. \end{aligned} \tag{94}$$

For more details about FOC, see [37, 39, 40, 44].

The existence of the control system (83)–(86) is to be proved here, the same can be found in [37–43] as follows:

Let

$$g_1(\lambda_1^*, \lambda_2^*, \lambda_3^*, \lambda_4^*) = \lambda_1^*[-u_1^* I^* + (u_2^* - l)] + \lambda_2^*[u_1^* I^* - u_2^*] + \lambda_4^*[l], \tag{95}$$

$$g_2(\lambda_1^*, \lambda_2^*, \lambda_3^*, \lambda_4^*) = a + \lambda_1^*[-u_1^* S^*] + \lambda_2^*[u_1^* S^* - (\omega + u_2^*)] + \lambda_3^*[u_2^*] + \lambda_4^*[\omega], \tag{96}$$

$$g_3(\lambda_1^*, \lambda_2^*, \lambda_3^*, \lambda_4^*) = \lambda_1^*[\omega] + \lambda_3^*[-\omega], g_4(\lambda_1^*, \lambda_2^*, \lambda_3^*, \lambda_4^*) = 0. \tag{97}$$

Let $\Omega = \{\lambda_r^* \in R : |\lambda_r^*| \le k, r = 1, 2, 3, 4, t \in [0, T]\}$.

We have, at $\Omega : \partial g_1/\partial\lambda_1^* = -u_1^* I^* + (u_2^* - l), \partial g_1/\partial\lambda_2^* = u_1^* I^* - u_2^*, \partial g_1/\partial\lambda_3^* = 0, \partial g_1/\partial\lambda_4^* = l,\ \partial g_2/\partial\lambda_1^* = -u_1^* S^*,\ \partial g_2/\partial\lambda_2^* = u_1^* S^* - (\omega + u_2^*), \partial g_2/\partial\lambda_3^* = u_2^*, \partial g_2/\partial\lambda_4^* = \omega,$

$$\frac{\partial g_3}{\partial\lambda_1^*} = \omega, \frac{\partial g_3}{\partial\lambda_2^*} = 0, \frac{\partial g_3}{\partial\lambda_3^*} = -\omega, \frac{\partial g_3}{\partial\lambda_4^*} = 0, \tag{98}$$

$$\frac{\partial g_4}{\partial\lambda_1^*} = \frac{\partial g_4}{\partial\lambda_2^*} = \frac{\partial g_4}{\partial\lambda_3^*} = \frac{\partial g_4}{\partial\lambda_4^*} = 0, \tag{99}$$

$$\left|\frac{\partial g_1}{\partial\lambda_3^*}\right| \le k_1 \Rightarrow g_1 = g_{13}, \left|\frac{\partial g_1}{\partial\lambda_4^*}\right| \le g_1 \Rightarrow g_1 = k_{13}, \left|\left|\frac{\partial g_1}{\partial\lambda_1^*}\right| \le k_{11}, \frac{\partial g_1}{\partial\lambda_2^*}\right| \le k_{12}, \tag{100}$$

$$\left|\frac{\partial g_2}{\partial\lambda_1^*}\right| \le k_{21}, \cdots \left|\left|\frac{\partial g_2}{\partial\lambda_3^*}\right| \le k_{23}, \left|\frac{\partial g_2}{\partial\lambda_4^*}\right| \le k_{24}, \frac{\partial g_2}{\partial\lambda_2^*}\right| \le k_{22}, \cdots \tag{101}$$

$$\left|\frac{\partial g_3}{\partial\lambda_1^*}\right| \le k_2, \left|\frac{\partial g_3}{\partial\lambda_2^*}\right| \le k_2 \Rightarrow g_3 = k_{31}, \left|\frac{\partial g_3}{\partial\lambda_3^*}\right| \le k_{33}, \left|\frac{\partial g_3}{\partial\lambda_4^*}\right| \le k_{34}, \tag{102}$$

$$\left|\frac{\partial g_4}{\partial\lambda_1^*}\right| \le k_{41}, \left|\left|\frac{\partial g_4}{\partial\lambda_3^*}\right| \le k_{43}, \left|\frac{\partial g_4}{\partial\lambda_4^*}\right| \le k_{44}, \frac{\partial g_4}{\partial\lambda_2^*}\right| \le k_{42}, \tag{103}$$

where $k_1, k_2, k_3, k_4,\ k_5 k_{22}, k_{23}, k_{24}, k_2, k_{31}, k_{33}, k_{34}, k_{41}, k_{42}, k_{43}$, and k_{44} are constants greater than zero. Hence, each of the four functions f_1, f_2, and f_4 agrees with the Lipschitz z conditions. Then, each of the four kernels f_1, f_2 is continuous respecting the four features, then. See for instance [37–43] for more information about the existence and uniqueness.

7. Conclusion

In this work, we have provided the approximate solution constructions for the fractional-order LHF model. In addition, the numerical simulations of the fractional-order LHF model have been experimented with many arbitrary orders. Also, an optimal control case has been investigated. The outcomes acquired by utilizing Laplace transform combined with the ADM are very compatible with results existing in the previous research. Further, the applied method for finding the numerical solution of the proposed model is introduced without considering any perturbation, discretization, or transformations. The current examination enlightens the considered nonlinear manner that rely upon the time history and the time moment by applying the idea of fractional order differentiation. Moreover, the obtained results show that Laplace transform combined with the ADM is amazingly deliberate, more powerful, and exceptionally precise, and which can be applied to break down the different classes of nonlinear marvels that emerge in science and innovation. For future work, we suggest generalizing the studied LHF model to show the effect of the infection from other sources as animals, men, and children.

Data Availability

The data used to support the findings of this study are available from the corresponding author on request.

Conflicts of Interest

The authors declare no conflict of interest.

Authors' Contributions

Conceptualization was done by M.H.; methodology was done by M.H, A.E., and A.M.; software was done by M.H, A.E., and A.M.; validation was done by M.H, A.E., S.U., A.G., and A.M.; formal analysis was done by M.H, A.E., S.U., A.G., and A.M.; investigation was done by M.H, A.E., S.U., A.G., and A.M.; resources was done by M.H, A.E., S.U., A.G., and A.M.; data curation was done by M.H, A.E., S.U., A.G., and A.M.; writing—original draft preparation was done by M.H. and A.E.; writing—review and editing was done by M.H. and A.E.; visualization was done by M.H. and A.E.; supervision was done by M.H.; project administration was done by M.H.; funding acquisition was

done by A.G. and S.U. All authors have read and agreed to the published version of the manuscript.

Acknowledgments

The authors acknowledge the support and funding of Research Center for Advanced Material Science (RCAMS) at King Khalid University through Grant No. RCAMS/KKU/008-21.

References

[1] J. M. van Seventer and N. S. Hochberg, "Principles of infectious diseases: transmission, diagnosis, prevention, and control," *Public Health*, pp. 22–39, 2017.

[2] O. Ogbu, E. Ajuluchukwu, and C. J. Uneke, "Lassa fever in West African sub-region: an overview," *Journal of Vector Borne Diseases*, vol. 44, no. 1, pp. 1–11, 2007.

[3] J. D. Frame, J. M. Baldwin Jr., D. J. Gocke, and J. M. Troup, "Lassa fever, a new virus disease of man from West Africa," *The American Journal of Tropical Medicine and Hygiene*, vol. 19, no. 4, pp. 670–676, 1970.

[4] I. Faith, O. A. A. SM, O. Ifeanyi et al., "An assessment of onset-to-intervention time and outcome of Lassa fever during an outbreak in Edo State, Nigeria," *International Journal of Prevention and Treatment*, vol. 7, no. 1, pp. 1–5, 2018.

[5] H. U. Ekechi, C. Ibeneme, B. Ogunniyi et al., "Factors associated with a confirmed Lassa fever outbreak in Eguare community of Esan West, Edo State, Nigeria: January-March, 2019," *Journal of Interventional Epidemiology and Public Health*, vol. 3, no. 1, 2020.

[6] J. A. Tenreiro Machado, M. F. Silva, R. S. Barbosa et al., "Some applications of fractional calculus in engineering," *Mathematical Problems in Engineering*, vol. 2010, Article ID 639801, 34 pages, 2010.

[7] D. Baleanu, Z. B. Guvenc, and J. A. T. Machado, *New Trends in Nanotechnology and Fractional Calculus Applications*, Springer Dordrecht Heidelberg, London, New York, 2010.

[8] H. Bulut, T. A. Sulaiman, H. M. Baskonus, H. Rezazadeh, M. Eslami, and M. Mirzazadeh, "Optical solitons and other solutions to the conformable space-time fractional Fokas-Lenells equation," *Optik*, vol. 172, pp. 20–27, 2018.

[9] P. Veeresha, D. G. Prakasha, and H. M. Baskonus, "Solving smoking epidemic model of fractional order using a modified homotopy analysis transform method," *The Mathematical Scientist*, vol. 13, no. 2, pp. 115–128, 2019.

[10] D. Baleanu, G. C. Wu, and S. D. Zeng, "Chaos analysis and asymptotic stability of generalized Caputo fractional differential equations," *Chaos, Solitons & Fractals*, vol. 102, pp. 99–105, 2017.

[11] R. S. Barbosa, J. A. T. Machado, and I. M. Ferreira, "PID controller tuning using fractional calculus concepts," *Fractional Calculus & Applied Analysis*, vol. 7, no. 2, pp. 119–134, 2004.

[12] M. F. Silva, J. A. T. Machado, and A. M. Lopes, "Position/force control of a walking robot," *Machine Intelligence and Robot Control*, vol. 5, pp. 33–44, 2003.

[13] M. F. Silva, J. A. T. Machado, and A. M. Lopes, "Comparison of fractional and integer order control of an hexapod robot," in *Proceedings of International Design Engineering Technical Conferences and Computers and Information in Engineering Conference, vol. 5 of 19th Biennial Conference on Mechanical Vibration and Noise*, pp. 667–676, Chicago, Ill, USA, 2003.

[14] R. S. Barbosa, J. A. T. Machado, and I. M. Ferreira, "Tuning of PID controllers based on Bode's ideal transfer function," *Nonlinear Dynamics*, vol. 38, no. 1–4, pp. 305–321, 2004.

[15] F. Duarte and J. A. T. Machado, "Chaotic phenomena and fractional-order dynamics in the trajectory control of redundant manipulators," *Nonlinear Dynamics*, vol. 29, no. 1/4, pp. 315–342, 2002.

[16] M. F. Silva and J. A. T. Machado, "Fractional order PDαjoint control of legged robots," *Journal of Vibration and Control*, vol. 12, no. 12, pp. 1483–1501, 2006.

[17] J. A. T. Machado, I. S. Jesus, J. B. Cunha, and J. K. Tar, "Fractional dynamics and control of distributed parameter systems," *Intelligent Systems at the Service of Mankind*, vol. 2, pp. 295–305, 2006.

[18] J. A. T. Machado, "Discrete-time fractional-order controllers," *Fractional Calculus & Applied Analysis*, vol. 4, no. 1, pp. 47–66, 2001.

[19] A. I. El-Mesady, Y. S. Hamed, and A. M. Alsharif, "Jafari transformation for solving a system of ordinary differential equations with medical application," *Fractal and Fractional*, vol. 5, no. 3, p. 130, 2021.

[20] N. H. Sweilam, S. M. al-Mekhlafi, A. O. Albalawi, and J. A. Tenreiro Machado, "Optimal control of variable-order fractional model for delay cancer treatments," *Applied Mathematical Modelling*, vol. 89, pp. 1557–1574, 2021.

[21] A. Atangana, "A novel model for the Lassa hemorrhagic fever: deathly disease for pregnant women," *Neural Computing and Applications*, vol. 26, no. 8, pp. 1895–1903, 2015.

[22] M. Goyal, H. M. Baskonus, and A. Prakash, "An efficient technique for a time fractional model of Lassa hemorrhagic fever spreading in pregnant women," *The European Physical Journal Plus*, vol. 134, no. 10, pp. 1–10, 2019.

[23] M. Abdelhakem, T. Alaa-Eldeen, D. Baleanu, M. G. Alshehri, and M. El-Kady, "Approximating real-life BVPs via Chebyshev polynomials' first derivative pseudo-Galerkin method," *Fractal and Fractional*, vol. 5, no. 4, p. 165, 2021.

[24] M. Abdelhakem and Y. H. Youssri, "Two spectral Legendre's derivative algorithms for Lane-Emden, Bratu equations, and singular perturbed problems," *Applied Numerical Mathematics*, vol. 169, pp. 243–255, 2021.

[25] Y. H. Youssri, W. M. Abd-Elhameed, and M. Abdelhakem, "A robust spectral treatment of a class of initial value problems using modified Chebyshev polynomials," *Mathematical Methods in the Applied Sciences*, vol. 44, no. 11, pp. 9224–9236, 2021.

[26] M. Abdelhakem, M. Biomy, A. S. Kandil, and D. Baleanu, "A numerical method based on Legendre differentiation matrices for higher order ODEs," *Information Sciences Letters*, vol. 9, no. 3, pp. 175–180, 2020.

[27] M. Abdelhakem, D. Abdelhamied, A. Mg, and E.-K. Ma, "Shifted Legendre fractional pseudospectral differentiation matrices for solving fractional differential problems," *Fractals*, no. article 2240038, 2021.

[28] M. Abdelhakem, D. Mahmoud, D. Baleanu, and M. el-kady, "Shifted ultraspherical pseudo-Galerkin method for approximating the solutions of some types of ordinary fractional problems," *Advances in Difference Equations*, vol. 2021, no. 1, 18 pages, 2021.

[29] M. Abdelhakem, H. Moussa, D. Baleanu, and M. El-Kady, "Shifted Chebyshev schemes for solving fractional optimal control problems," *Journal of Vibration and Control*, vol. 25, no. 15, pp. 2143–2150, 2019.

[30] W. Gao, P. Veeresha, D. G. Prakasha, H. M. Baskonus, and G. Yel, "New approach for the model describing the deathly disease in pregnant women using Mittag-Leffler function," *Chaos, Solitons & Fractals*, vol. 134, article 109696, 2020.

[31] S. Jain and A. Atangana, "Analysis of Lassa hemorrhagic fever model with non-local and non-singular fractional derivatives," *International Journal of Biomathematics*, vol. 11, no. 8, p. 1850100, 2018.

[32] A. Yusuf, T. Sulaiman, and P. Kumar, *A New Study of Lassa Hemorrhagic Fever Model via Caputo-Fabrizio Derivative*, Authorea, 2020.

[33] Y. A. Amer, A. M. S. Mahdy, T. T. Shwayaa, and E. S. M. Youssef, "Laplace transform method for solving nonlinear biochemical reaction model and nonlinear Emden-Fowler system," *Journal of Engineering and Applied Sciences*, vol. 13, no. 17, 2018.

[34] P. van den Driessche and J. Watmough, "Reproduction numbers and sub-threshold endemic equilibria for compartmental models of disease transmission," *Mathematical Biosciences*, vol. 180, no. 1-2, pp. 29–48, 2002.

[35] K. Diethelm and A. D. Freed, "The FracPECE subroutine for the numerical solution of differential equations of fractional order," in *Research and Scientific Computing 1998*, S. Heinzel and T. Plesser, Eds., pp. 57–71, Society for scientific data processing, Göttingen, 1999.

[36] R. Garrappa, "On linear stability of predictor–corrector algorithms for fractional differential equations," *International Journal of Computer Mathematics*, vol. 87, no. 10, pp. 2281–2290, 2010.

[37] A. M. S. Mahdy, K. A. Gepreel, K. Lotfy, and A. A. El-Bary, "A numerical method for solving the Rubella ailment disease model," *International Journal of Modern Physics C*, vol. 32, no. 7, pp. 1–15, 2021.

[38] K. A. Gepreel, M. Higazy, and A. M. S. Mahdy, "Optimal control, signal flow graph, and system electronic circuit realization for nonlinear Anopheles mosquito model," *International Journal of Modern Physics C*, vol. 31, no. 9, pp. 1–18, 2020.

[39] A. M. S. Mahdy, M. S. Mohamed, K. Lotfy, M. Alhazmi, A. A. El-Bary, and M. H. Raddadi, "Numerical solution and dynamical behaviors for solving fractional nonlinear rubella ailment disease model," *Results in Physics*, vol. 39, pp. 1–10, 2018.

[40] N. H. Sweilam, S. M. Al-Mekhlafi, and D. Baleanu, "Optimal control for a fractional tuberculosis infection model including the impact of diabetes and resistant strains," *Journal of Advanced Research*, vol. 24, pp. 125–137, 2019.

[41] A. Jajarmi, B. Ghanbari, and D. Baleanu, "A new and efficient numerical method for the fractional modeling and optimal control of diabetes and tuberculosis co-existence," *Chaos*, vol. 29, no. 9, article 093111, 2019.

[42] M. Higazy, F. M. Allehiany, and E. E. Mahmoud, "Numerical study of fractional order COVID-19 pandemic transmission model in context of ABO blood group," *Results in Physics*, vol. 22, article 103852, 2021.

[43] G. Yel and H. M. Baskonus, "Solitons in conformable time-fractional Wu-Zhang system arising in coastal design," *Pramana*, vol. 93, no. 4, pp. 1–10, 2019.

[44] W. Gao, H. F. Ismael, A. M. Husien, H. Bulut, and H. M. Baskonus, "Optical soliton solutions of the cubic-quartic nonlinear Schrödinger and resonant nonlinear Schrödinger equation with the parabolic law," *Applied Sciences*, vol. 10, no. 1, p. 219, 2020.

[45] A. M. S. Mahdy, M. Higazy, and M. S. Mohamed, "Optimal and memristor-based control of a nonlinear fractional tumor-immune model," *Materials & Continua*, vol. 67, no. 3, pp. 3463–3486, 2021.

Hindawi
Journal of Function Spaces
Volume 2021, Article ID 7767848, 22 pages
https://doi.org/10.1155/2021/7767848

Research Article

On Comparative Analysis for the Black-Scholes Model in the Generalized Fractional Derivatives Sense via Jafari Transform

Saima Rashid,[1] Sobia Sultana,[2] Rehana Ashraf,[3] and Mohammed K. A. Kaabar[4,5]

[1]*Department of Mathematics, Government College University, Faisalabad 38000, Pakistan*
[2]*Department of Mathematics, Imam Mohammad Ibn Saud Islamic University, Riyadh 12211, Saudi Arabia*
[3]*Department of Mathematics, Lahore College Women University, 54000 Lahore, Pakistan*
[4]*Gofa Camp, Near Gofa Industrial College and German Adebabay, Nifas Silk-Lafto, 26649 Addis Ababa, Ethiopia*
[5]*Institute of Mathematical Sciences, Faculty of Science, University of Malaya, Kuala Lumpur 50603, Malaysia*

Correspondence should be addressed to Mohammed K. A. Kaabar; mohammed.kaabar@wsu.edu

Received 3 October 2021; Revised 16 November 2021; Accepted 23 November 2021; Published 8 December 2021

Academic Editor: Youssri Hassan Youssri

The Black-Scholes model is well known for determining the behavior of capital asset pricing models in the finance sector. The present article deals with the Black-Scholes model via the Caputo fractional derivative and Atangana-Baleanu fractional derivative operator in the Caputo sense, respectively. The Jafari transform is merged with the Adomian decomposition method and new iterative transform method. It is worth mentioning that the Jafari transform is the unification of several existing transforms. Besides that, the convergence and uniqueness results are carried out for the aforesaid model. In mathematical terms, the variety of equations and their solutions have been discovered and identified with various novel features of the projected model. To provide additional context for these ideas, numerous sorts of illustrations and tabulations are presented. The precision and efficacy of the proposed technique suggest its applicability for a variety of nonlinear evolutionary problems.

1. Introduction

Recently, the subject of fractional calculus has garnered considerable prominence. Several well-known mathematicians have contributed to this field by proposing numerous fractional operators in various texts. The conclusions of contemporary calculus are often substantially more precise than those of ancient ones. It has presented the dynamic behavior of a variety of real-world situations that take place between two integers. Additionally, fractional operators have more dimensionality than integer differential operators such as Caputo, Liouville, Hadamard, Coimbra, Davison, Riesz, Riemann and Liouville, Weyl, and Jumarie, Caputo and Fabrizio [1], Atangana and Baleanu [2], and Scherer et al. [3] are some well-known fractional derivative formulations, see [4–9]. Furthermore, the Liouville-Caputo and AB operators are considered to be the best fractional filters in this field of research.

Several methods that assess fractional differential equations (FDEs) for their reliability and trustworthiness are actively considered in [10, 11]. Certain popular approximate-analytical approaches including Adomian decomposition method [12], new iterative transform method [13], homotopy perturbation method [14], Haar wavelet method [15], Padé approximation [16], reproducing kernel Hilbert space method [17], new Legendre wavelet decomposition method [18], Bäcklund transformation method [19], and Lie symmetry analysis [20].

Fischer Black and Myron Scholes developed a mathematical model for the capital asset pricing model in 1973. The revolutionary Black–Scholes model (BSM) is the foundation of modern financial theory which is remarkable to discuss contemporary economics without referencing the innovative BSM.

The purpose of this research is to obtain new solutions by employing both decomposition method and Jafari iterative transform method into a BSM. In banking and finance, the fractional formulation of BSM is represented by [16]:

$$\mathbf{D}_{\varsigma}^{\vartheta}\mathcal{U} + \frac{\varpi^2}{2}\mathcal{S}^2\frac{\partial^2\mathcal{U}}{\partial\mathcal{S}^2} + \zeta\mathcal{S}\frac{\partial\mathcal{U}}{\partial\mathcal{S}} - \zeta\mathcal{U} = 0, \tag{1}$$

subject to the playoff mapping

$$\mathcal{U}(\mathcal{S},\mathcal{T}) = \max\,(\mathcal{S} - E, 0), \tag{2}$$

where $\mathcal{U}(\mathcal{S},\varsigma)$ represents the option's value at $\mathcal{S}$ asset values at time ς and $\mathcal{T}$ is the expiry period. The fundamental stock price is indicated by the letter E. The risk-free mortgage to expiry is represented by the variable ζ. The volatility of a financial commodity is represented by the constant ϖ. We also include the necessary hypotheses: a constant risk-free interest rate u, no processing fees, the ability to purchase and sell an unlimited number of stocks, and no prohibitions on speculative trading. Finally, we include European options. Furthermore, it is remarkable that $\mathcal{U}(0,\varsigma) = 0$ and $\mathcal{U}(\mathcal{S},\mathcal{T}) \approx \mathcal{S}$ as $\mathcal{S} \mapsto \infty$. The BSM in (1) can then be represented as a parabolic diffusion equation. Introducing the subsequent transformations

$$\mathcal{S} = E\ \exp\,(\mathbf{w}_1), \varsigma = \mathcal{T} - \frac{2\tau}{\varpi^2}, \mathcal{U} = E\mathcal{Q}(\mathbf{w}_1,\varsigma), \tag{3}$$

then, Equation (1) reduces to

$$\mathbf{D}_{\varsigma}^{\vartheta}\mathcal{Q}(\mathbf{w}_1,\varsigma) = \frac{\partial^2\mathcal{Q}(\mathbf{w}_1,\varsigma)}{\partial\mathbf{w}_1^2} + (\eta - 1)\frac{\partial\mathcal{Q}(\mathbf{w}_1,\varsigma)}{\partial\mathbf{w}_1} - \eta\mathcal{Q}(\mathbf{w}_1,\varsigma), \tag{4}$$

subject to initial conditions

$$\mathcal{Q}(\mathbf{w}_1, 0) = \max\,(\exp\,(\mathbf{w}_1) - 1, 0), \tag{5}$$

where η signifies the equilibrium between the free relationship in inflation and stock volatility. In [20], Cen and Le introduced the generalized fractional BSM. The BSM is described this way:

$$\begin{aligned}\mathbf{D}_{\varsigma}^{\vartheta}\mathcal{Q}(\mathbf{w}_1,\varsigma) = {}& -0.08(2 + \sin\mathbf{w}_1)^2\mathbf{w}_1^2\frac{\partial^2\mathcal{Q}(\mathbf{w}_1,\varsigma)}{\partial\mathbf{w}_1^2} \\ & - 0.06\mathbf{w}_1\frac{\partial\mathcal{Q}(\mathbf{w}_1,\varsigma)}{\partial\mathbf{w}_1} + 0.06\mathcal{Q}(\mathbf{w}_1,\varsigma),\end{aligned} \tag{6}$$

subject to initial conditions

$$\mathcal{Q}(\mathbf{w}_1, 0) = \max\,(\mathbf{w}_1 - 25\exp\,(-0.06), 0). \tag{7}$$

The fractional BSM with one commodity has been explored extensively [21, 22]. The fractional BSM is an extended variant of the classical BSM that extends the model's limitations. Meng and Wang [23] used the BSM to investigate fractional opportunity valuation. The covered call price for bank international trade in China was calculated using the fractional BSM. Their findings suggest that when it comes to evaluating the influence of the pricing system, the fractional BSM outperforms the classical BSM [24]. Fall et al. [14] estimated the Black-Scholes option pricing equations via the homotopy perturbation method. Matadi and Zondi [25] contemplated the invariant solutions of BSM via theOrnstein-Uhlenbeck process. Kumar et al. [26] demonstrated numerical computation of fractional BSM arising in the financial market. Yavuz and Özdemir [27] proposed a diverse approach to the European option pricing model with a new fractional operator.

Amidst Gorge Adomian's massive boost in 1980, the Adomian decomposition method introduced a well-noted terminology. It has been intensively implemented for a diverse set of nonlinear PDEs, for instance, Fisher's model [28] and Zakharov–Kuznetsov equation [29]. The ADM was determined to be significantly related to a variety of integral transforms, including Laplace, Swai, Mohand, Aboodh, and Elzaki. Very recently, Jafari [30] propounded a well-known integral transform which is known as the Jafari transform. The dominant feature of this transformation is that it has the ability to recapture several existing transformations, see Remark 8.

In 2006, Yavuz and Özdemir [27] expounded a new iterative transform method (NITM) that is intensively employed by numerous researchers due to its frequent applicability in fractional ODES and PDEs. The recursive technique tends to the exact solution if it exists via successive approximations. A small proportion of estimates can be employed for analytical reasons with a reasonable level of accuracy for particular problems. The NITM does not need some restricted hypothesis for handling nonlinearity factors. For example, in [28], the authors employed NITM to find the numerical solution of the fifth- and sixth-order nonlinear boundary value problems, Rashid et al. [29] applied NITM to obtain the solution of the fractional Fornberg-Whitham equation, and Jafari [30] constructed the Laplace decomposition algorithm via NITM.

Owing to the aforementioned trend, to obtain the explicit solution of the time-fractional BSM, we employ the Jafari transform decomposition technique (JDM) and Jafari iterative transform method (JITM). The Jafari transform merged the Adomian decomposition method and a new iterative method in an efficient manner to develop novel algorithmic approaches. The Jafari transform is the refinement of several existing transforms, see Remark 8. Both projected schemes yield analytical solutions in a convergent series form. Mathematical characterizations of the BSM are illustrated via the AB fractional derivative operator in the Caputo sense. Simulation and tabulation studies depict a clear picture of the proposed approaches. The analytical solution, especially for fractional PDEs, is a useful mechanism for analyzing the behaviors of solutions that are challenging to numerically solve. The analytical solution can be used to investigate macroeconomic behaviors.

This article's entire content is divided into seven parts, which are described in the following order: Section 2 summarises and presents the core concepts and terminology of the singular power law fractional derivative and nonsingular Atangana-Baleanu fractional derivative in the Caputo sense. In Section 3, two novel algorithms are developed via the new integral transform. In Section 4, convergence and uniqueness analyses are discussed and presented for the proposed model. Section 5 is the main part of the proposed work where we present a debate on the results and their

interpretation. Finally, concluding remarks are presented in Section 7.

2. Preliminaries

In this section, we present some essential concepts, notions, and definitions concerning fractional derivative operators depending on power and Mittag-Leffler as a kernel, along with the detailed consequences of the Jafari transform.

Definition 1 (see [1]). The Caputo fractional derivative (CFD) is described as follows:

$$ {}_0^c\mathbf{D}_\varsigma^\vartheta(\mathcal{Q}(\varsigma)) = \begin{cases} \dfrac{1}{\Gamma(r-\vartheta)}\displaystyle\int_0^\varsigma \dfrac{\mathcal{Q}^{(r)}(\mathbf{w}_1)}{(\varsigma-\mathbf{w}_1)^{\vartheta+1-r}}d\mathbf{w}_1, & r-1<\vartheta<r, \\ \dfrac{d^r}{d\varsigma^r}\mathcal{Q}(\varsigma), & \vartheta = r. \end{cases} \tag{8} $$

Definition 2 (see [2]). The Atangana-Baleanu fractional derivative operator in the Caputo form (ABC) is stated as follows:

$$ {}_{\eta_1}^{ABC}\mathbf{D}_\varsigma^\vartheta(\mathcal{Q}(\varsigma)) = \frac{\mathbb{A}(\vartheta)}{1-\vartheta}\int_{\eta_1}^\varsigma \mathcal{Q}'(\varsigma)E_\vartheta\left[-\frac{\vartheta(\varsigma-\mathbf{w}_1)^\vartheta}{1-\vartheta}\right]d\mathbf{w}_1, \tag{9} $$

where $\mathcal{Q}\in\mathscr{H}^1(a_1,a_2)$(Sobolev space), $a_1<a_2$, $\vartheta\in[0,1]$ and $\mathbb{A}(\vartheta)$ signifies a normalization function as $\mathbb{A}(\vartheta)=\mathbb{A}(0)=\mathbb{A}(1)=1$.

Definition 3 (see [2]). The fractional integral of the ABC operator is described as follows:

$$ {}_{\eta_1}^{\mathrm{ABC}}\mathcal{J}_\varsigma^\vartheta(\mathcal{Q}(\varsigma)) = \frac{1-\vartheta}{\mathbb{A}(\vartheta)}\mathcal{Q}(\varsigma) + \frac{\vartheta}{\Gamma(\vartheta)\mathbb{A}(\vartheta)}\int_{\eta_1}^\varsigma \mathcal{Q}(\mathbf{w}_1)(\varsigma-\mathbf{w}_1)^{\vartheta-1}d\mathbf{w}_1. \tag{10} $$

Definition 4 (see [30]). Consider an integrable mapping $\mathcal{Q}(\varsigma)$ defined on a set $\mathscr{P}$, then

$$ \mathscr{P} = \{\mathcal{Q}(\varsigma)\colon \exists M>0, \kappa>0, |\mathcal{Q}(\varsigma)|<M\exp(\kappa\varsigma), if\, \varsigma\geq 0\}. \tag{11} $$

Definition 5 (see [30]). Suppose the mappings $\phi(\mathfrak{s}), \psi(\mathfrak{s})$: $\mathbb{R}^+\mapsto\mathbb{R}^+$ such that $\psi(\mathfrak{s})\neq 0\forall\mathfrak{s}\in\mathbb{R}^+$. The Jafari transform of the mapping $\mathcal{Q}(\varsigma)$ presented by $\mathbf{Q}(\mathfrak{s})$ is described as

$$ \mathbb{J}\{\mathcal{Q}(\varsigma),\mathfrak{s}\} = \mathbf{Q}(\mathfrak{s}) = \phi(\mathfrak{s})\int_0^\infty \mathcal{Q}(\varsigma)\exp(-\psi(\mathfrak{s})\varsigma)d\varsigma. \tag{12} $$

Theorem 6 (see [30]) (convolution property). *For Jafari transform, the subsequent holds true:*

$$ \mathbb{J}\{\mathcal{Q}_1 * \mathcal{Q}_2\} = \frac{1}{\phi(\mathfrak{s})}\mathbf{Q}_1(\mathfrak{s}) * \mathbf{Q}_2(\mathfrak{s}). \tag{13} $$

Definition 7. The Jafari transform of the CFD operator is stated as follows:

$$ \mathbb{J}\left\{{}_0^c\mathbf{D}_\varsigma^\vartheta(\mathcal{Q}(\varsigma)),\mathfrak{s}\right\} = \psi^\vartheta(\mathfrak{s})\mathbf{Q}(\mathfrak{s}) - \phi(\mathfrak{s})\sum_{\kappa=0}^{\vartheta-1}\psi^{\vartheta-\kappa-1}(\mathfrak{s})\mathcal{Q}^{(\kappa)}(0), \quad r-1<\vartheta<r, \phi, \psi>0. \tag{14} $$

Remark 8. Definition 7 leads to the following conclusions:

(1) Taking $\phi(\mathfrak{s})=1$ and $\psi(\mathfrak{s})=\mathfrak{s}$, then we acquire the Laplace transform [35]

(2) Taking $\phi(\mathfrak{s})1/\mathfrak{s}$ and $\psi(\mathfrak{s})=1/\mathfrak{s}$, then we acquire the α-Laplace transform [36]

(3) Taking $\phi(\mathfrak{s})=1/\mathfrak{s}$ and $\psi(\mathfrak{s})=1/\mathfrak{s}$, then we acquire the Sumudu transform [37]

(4) Taking $\phi(\mathfrak{s})=1/\mathfrak{s}$ and $\psi(\mathfrak{s})=1$, then we acquire the Aboodh transform [38]

(5) Taking $\phi(\mathfrak{s})=\mathfrak{s}$ and $\psi(\mathfrak{s})=\mathfrak{s}^2$, then we acquire the Pourreza transform [39, 40]

(6) Taking $\phi(\mathfrak{s})=\mathfrak{s}$ and $\psi(\mathfrak{s})=1/\mathfrak{s}$, then we acquire the Elzaki transform [41]

(7) Taking $\phi(\mathfrak{s})=\mathbf{w}_2$ and $\psi(\mathfrak{s})=\mathfrak{s}/\mathbf{w}_2$, then we acquire the natural transform [42]

(8) Taking $\phi(\mathfrak{s})=\mathfrak{s}^2$ and $\psi(\mathfrak{s})=\mathfrak{s}$, then we acquire the Mohand transform [43]

(9) Taking $\phi(\mathfrak{s})=1/\mathfrak{s}^2$ and $\psi(\mathfrak{s})=1/\mathfrak{s}$, then we acquire the Sawi transform [44]

(10) Taking $\phi(\mathfrak{s})=1$ and $\psi(\mathfrak{s})=1/\mathfrak{s}$, then we get the Kamal transform [45].

(11) Taking $\phi(\mathfrak{s})=\mathfrak{s}^\alpha$ and $\psi(\mathfrak{s})=1/\mathfrak{s}$, then we acquire the G_transform [46, 47]

Definition 9 (see [48]). The Jafari transform of the ABC fractional derivative operator is described as

$$ \mathbb{J}\left\{{}_0^{\mathrm{ABC}}\mathbf{D}_\varsigma^\vartheta(\mathcal{Q}(\varsigma)),\mathfrak{s}\right\}(\vartheta) = \frac{\mathbb{A}(\vartheta)\psi^\vartheta(\mathfrak{s})}{\vartheta+(1-\vartheta)\psi^\vartheta(\mathfrak{s})}\left(\mathbf{Q}(\mathfrak{s}) - \frac{\phi(\mathfrak{s})}{\psi(\mathfrak{s})}\mathcal{Q}(0)\right). \tag{15} $$

Remark 10. Definition 9 leads to the following conclusions:

(1) Taking $\phi(\mathfrak{s})=1$ and $\psi(\mathfrak{s})=\mathfrak{s}$, then we acquire the Laplace transform of ABC fractional derivative operator [2, 49]

(2) Taking $\phi(\mathfrak{s}) = \mathfrak{s}$ and $\psi(\mathfrak{s}) = 1/\mathfrak{s}$, then we acquire the Elzaki transform of ABC fractional derivative operator [50]

(3) Taking $\phi(\mathfrak{s}) = \psi(\mathfrak{s}) = 1/\mathfrak{s}$, then we get the Sumudu transform of ABC fractional derivative operator [51]

(4) Taking $\phi(\mathfrak{s}) = 1$ and $\psi(\mathfrak{s}) = \mathfrak{s}/\mathbf{w}_2$, then we get the Shehu transform of ABC fractional derivative operator [51]

Definition 11 (see [52]). The Mittag-Leffler function for a single parameter is described as

$$E_\vartheta(z) = \sum_{\kappa=0}^{\infty} \frac{z^\kappa}{\Gamma(\kappa\vartheta + 1)}, \vartheta, z \in \mathbb{C}, \Re(\vartheta) \geq 0. \tag{16}$$

3. New Semianalytical Approach for Nonlinear PDEs

Consider the generic fractional form of PDE:

$$\mathbf{D}_\varsigma^\vartheta \mathcal{Q}(\mathbf{w}_1, \varsigma) + \mathbb{L}\mathcal{Q}(\mathbf{w}_1, \varsigma) + \mathbb{N}\mathcal{Q}(\mathbf{w}_1, \varsigma) = \mathbf{F}(\mathbf{w}_1, \varsigma), \varsigma > 0, 0 < \vartheta \leq 1, \tag{17}$$

with ICs

$$\mathcal{Q}(\mathbf{w}_1, 0) = \mathcal{G}(\mathbf{w}_1), \tag{18}$$

where $\mathbf{D}_\varsigma^\vartheta = \partial^\vartheta \mathcal{Q}(\mathbf{w}_1, \varsigma)/\partial\varsigma^\vartheta$ symbolizes the Caputo and ABC fractional derivative of order $\vartheta \in (0, 1]$ while $\mathbb{L}$ and $\mathbb{N}$ denotes the linear and nonlinear factors, respectively. Also, $\mathbf{F}(\mathbf{w}_1, \varsigma)$ represents the source term.

3.1. Configuration of Jafari Decomposition Method. Taking into account the Jafari transform to (17), we acquire

$$\mathbb{J}\left[\mathbf{D}_\varsigma^\vartheta \mathcal{Q}(\mathbf{w}_1, \varsigma) + \bar{\mathbb{L}}\mathcal{Q}(\mathbf{w}_1, \varsigma) + \overline{\mathbb{N}}\mathcal{Q}(\mathbf{w}_1, \varsigma)\right] = \mathbb{J}[\mathbf{F}(\mathbf{w}_1, \varsigma)]. \tag{19}$$

Firstly, the differentiation rule of Jafari transform with respect to CFD was applied; then, we apply the ABC fractional derivative operator as follows:

$$\begin{aligned}\psi^\vartheta(\varsigma)\mathcal{U}(\mathbf{w}_1, \varsigma) = \phi(\varsigma) &\sum_{q=0}^{n-1} \psi^{\vartheta-1-q}(\varsigma)\mathcal{Q}^{(q)}(0) \\ &+ \mathbb{J}\left[\bar{\mathbb{L}}\mathcal{Q}(\mathbf{w}_1, \varsigma) + \overline{\mathbb{N}}\mathcal{Q}(\mathbf{w}_1, \varsigma)\right] \\ &+ \mathbb{J}[\mathbf{F}(\mathbf{w}_1, \varsigma)],\end{aligned} \tag{20}$$

$$\begin{aligned}&\frac{\psi^\vartheta(\varsigma)\mathbb{A}(\vartheta)}{\vartheta + (1-\vartheta)\psi^\vartheta(\varsigma)}\mathcal{U}(\mathbf{w}_1, \varsigma) \\ &= \frac{\phi(\varsigma)}{\psi(\varsigma)}\frac{\psi^\vartheta(\varsigma)\mathbb{A}(\vartheta)}{\vartheta + (1-\vartheta)\psi^\vartheta(\varsigma)}\mathcal{Q}(0) \\ &\quad + \mathbb{J}\left[\bar{\mathbb{L}}\mathcal{Q}(\mathbf{w}_1, \varsigma) + \overline{\mathbb{N}}\mathcal{Q}(\mathbf{w}_1, \varsigma)\right] + \mathbb{J}[\mathbf{F}(\mathbf{w}_1, \varsigma)].\end{aligned} \tag{21}$$

The inverse Jafari transform of (20) and (21), respectively, yields

$$\begin{aligned}\mathcal{Q}(\mathbf{w}_1, \varsigma) = \mathbb{J}^{-1}&\left[\phi(\varsigma)\sum_{q=0}^{n-1}\psi(\varsigma)^{\vartheta-q-1}\mathcal{Q}^{(q)}(0) + \frac{1}{\psi^\vartheta(\varsigma)}\mathbb{J}[\mathbf{F}(\mathbf{w}_1, \varsigma)]\right] \\ &- \mathbb{J}^{-1}\left[\frac{1}{\psi^\vartheta(\varsigma)}\mathbb{J}\left[\bar{\mathbb{L}}\mathcal{Q}(\mathbf{w}_1, \varsigma) + \overline{\mathbb{N}}\mathcal{Q}(\mathbf{w}_1, \varsigma)\right]\right].\end{aligned}$$

$$\begin{aligned}\mathcal{Q}(\mathbf{w}_1, \varsigma) = \mathbb{J}^{-1}&\left[\frac{\phi(\varsigma)}{\psi(\varsigma)}\mathcal{Q}(0) + \frac{\vartheta + (1-\vartheta)\psi^\vartheta(\varsigma)}{\psi^\vartheta(\varsigma)\mathbb{A}(\vartheta)}\mathbb{J}[\mathbf{F}(\mathbf{w}_1, \varsigma)]\right] \\ &- \mathbb{J}^{-1}\left[\frac{\vartheta + (1-\vartheta)\psi^\vartheta(\varsigma)}{\psi^\vartheta(\varsigma)\mathbb{A}(\vartheta)}\mathbb{J}\left[\bar{\mathbb{L}}\mathcal{Q}(\mathbf{w}_1, \varsigma) + \overline{\mathbb{N}}\mathcal{Q}(\mathbf{w}_1, \varsigma)\right]\right].\end{aligned} \tag{22}$$

Therefore, the Jafari decomposition method was utilized to derive the solution of (17) by satisfying the assumption that $\mathcal{Q}(\mathbf{w}_1, \varsigma)$ has a solution of this equation which can be expressed as

$$\mathcal{Q}(\mathbf{w}_1, \varsigma) = \sum_{q=0}^{\infty} \mathcal{Q}_q(\mathbf{w}_1, \varsigma). \tag{23}$$

Thus, the nonlinear term $\overline{\mathbb{N}}(\mathbf{w}_1, \varsigma)$ can be evaluated by the Adomian decomposition method prescribed as

$$\overline{\mathbb{N}}\mathcal{Q}(\mathbf{w}_1, \varsigma) = \sum_{q=0}^{\infty} \tilde{A}_q(\mathcal{Q}_0, \mathcal{Q}_1, \cdots), q = 0, 1, \cdots, \tag{24}$$

where

$$\tilde{A}_q(\mathcal{Q}_0, \mathcal{Q}_1, \cdots) = \frac{1}{q!}\left[\frac{d^q}{d\vartheta^q}\overline{\mathbb{N}}\left(\sum_{j=0}^{\infty}\vartheta^j\mathcal{Q}_j\right)\right]_{\vartheta=0}, q > 0. \tag{25}$$

Inserting (23) and (24) into (26) and (27), respectively, we have

$$\begin{aligned}\sum_{q=0}^{\infty}\mathcal{Q}_q(\mathbf{w}_1, \varsigma) &= \mathcal{G}(\mathbf{w}_1) + \tilde{\mathcal{G}}(\mathbf{w}_1) \\ &\quad - \mathbb{J}^{-1}\left[\frac{1}{\psi^\vartheta(\varsigma)}\mathbb{J}\left[\bar{\mathbb{L}}\mathcal{Q}(\mathbf{w}_1, \varsigma) + \sum_{q=0}^{\infty}\tilde{A}_q\right]\right],\end{aligned} \tag{26}$$

$$\begin{aligned}\sum_{q=0}^{\infty}\mathcal{Q}_q(\mathbf{w}_1, \varsigma) &= \mathcal{G}(\mathbf{w}_1) + \tilde{\mathcal{G}}(\mathbf{w}_1) \\ &\quad - \mathbb{J}^{-1}\left[\frac{\vartheta + (1-\vartheta)\psi^\vartheta(\varsigma)}{\mathbb{A}(\vartheta)\psi^\vartheta(\varsigma)}\mathbb{J}\left[\bar{\mathbb{L}}\mathcal{Q}(\mathbf{w}_1, \varsigma) + \sum_{q=0}^{\infty}\tilde{A}_q\right]\right].\end{aligned} \tag{27}$$

Consequently, the recursive technique for (26) and (18) are established as

$$\mathcal{Q}_0(\mathbf{w}_1,\varsigma)=\mathcal{G}(\mathbf{w}_1)+\tilde{\mathcal{G}}(\mathbf{w}_1), q=0,$$

$$\mathcal{Q}_{q+1}(\mathbf{w}_1,\varsigma)=-\mathbb{J}^{-1}\left[\frac{1}{\psi^{\vartheta}(\varsigma)}\mathbb{J}\left[\bar{\mathbb{L}}\left(\mathcal{Q}_q(\mathbf{w}_1,\varsigma)\right)+\sum_{q=0}^{\infty}\tilde{A}_q\right]\right], q\geq 1,$$

$$\mathcal{Q}_{q+1}(\mathbf{w}_1,\varsigma)=-\mathbb{J}^{-1}\left[\frac{\vartheta+(1-\vartheta)\psi^{\vartheta}(\varsigma)}{\mathbb{A}(\vartheta)\psi^{\vartheta}(\varsigma)}\mathbb{J}\left[\bar{\mathbb{L}}\left(\mathcal{Q}_q(\mathbf{w}_1,\varsigma)\right)+\sum_{q=0}^{\infty}\tilde{A}_q\right]\right], q\geq 1. \tag{28}$$

3.2. Construction of Jafari Iterative Transform Method. With the aid of Jafari transform to (17) along with the IC (18), we obtain

$$\mathbb{J}\left[\mathbf{D}_{\varsigma}^{\vartheta}\mathcal{Q}(\mathbf{w}_1,\varsigma)+\bar{\mathbb{L}}\mathcal{Q}(\mathbf{w}_1,\varsigma)+\overline{\mathbb{N}}\mathcal{Q}(\mathbf{w}_1,\varsigma)\right]=\mathbb{J}[\mathbf{F}(\mathbf{w}_1,\varsigma)]. \tag{29}$$

First, we apply the differentiation rule of Jafari transform for CFD, and then, we consider for ABC fractional derivative operator, respectively, we get

$$\begin{aligned}\mathbb{J}[\mathcal{Q}(\mathbf{w}_1,\varsigma)]&=\frac{\phi(\varsigma)}{\psi^{\vartheta}(\varsigma)}\sum_{q=0}^{n-1}\psi^{\vartheta-1-q}(\varsigma)\mathcal{Q}^{(q)}(\psi,0)\\&-\frac{1}{\psi^{\vartheta}(\varsigma)}\mathbb{J}\left[\bar{\mathbb{L}}\mathcal{Q}(\mathbf{w}_1,\varsigma)+\overline{\mathbb{N}}\mathcal{Q}(\mathbf{w}_1,\varsigma)\right]\\&+\frac{1}{\psi^{\vartheta}(\varsigma)}\mathbb{J}[\mathbf{F}(\mathbf{w}_1,\varsigma)],\end{aligned} \tag{30}$$

$$\begin{aligned}\mathbb{J}[\mathcal{Q}(\mathbf{w}_1,\varsigma)]&=\frac{\phi(\varsigma)}{\psi^{\vartheta}(\varsigma)}\sum_{q=0}^{n-1}\psi^{\vartheta-1-q}(\varsigma)\mathcal{Q}^{(q)}(\psi,0)\\&-\frac{\psi^{\vartheta}(\varsigma)(1-\vartheta)+\vartheta}{\mathbb{A}(\vartheta)\psi^{\vartheta}(\varsigma)}\mathbb{J}\left[\bar{\mathbb{L}}\mathcal{Q}(\mathbf{w}_1,\varsigma)+\overline{\mathbb{N}}\mathcal{Q}(\mathbf{w}_1,\varsigma)\right]\\&+\frac{\psi^{\vartheta}(\varsigma)(1-\vartheta)+\vartheta}{\mathbb{A}(\vartheta)\psi^{\vartheta}(\varsigma)}\mathbb{J}[\mathbf{F}(\mathbf{w}_1,\varsigma)].\end{aligned} \tag{31}$$

By the virtue of the inverse Jafari transform of (30) and (31), respectively, this yields

$$\begin{aligned}\mathcal{Q}(\mathbf{w}_1,\varsigma)&=\mathcal{G}(\psi)+\mathbb{J}^{-1}\left\{\frac{1}{\psi^{\vartheta}(\varsigma)}\mathbb{J}[\mathbf{F}(\mathbf{w}_1,\varsigma)]\right\}\\&-\mathbb{J}^{-1}\left\{\frac{1}{\psi^{\vartheta}(\varsigma)}\mathbb{J}\left[\bar{\mathbb{L}}\mathcal{Q}(\mathbf{w}_1,\varsigma)+\overline{\mathbb{N}}\mathcal{Q}(\mathbf{w}_1,\varsigma)\right]\right\},\end{aligned} \tag{32}$$

$$\begin{aligned}\mathcal{Q}(\mathbf{w}_1,\varsigma)&=\mathcal{G}(\psi)+\mathbb{J}^{-1}\left\{\frac{\psi^{\vartheta}(\varsigma)(1-\vartheta)+\vartheta}{\mathbb{A}(\vartheta)\psi^{\vartheta}(\varsigma)}\mathbb{J}[\mathbf{F}(\mathbf{w}_1,\varsigma)]\right\}\\&-\mathbb{J}^{-1}\left\{\frac{\psi^{\vartheta}(\varsigma)(1-\vartheta)+\vartheta}{\mathbb{A}(\vartheta)\psi^{\vartheta}(\varsigma)}\mathbb{J}\left[\bar{\mathbb{L}}\mathcal{Q}(\mathbf{w}_1,\varsigma)+\overline{\mathbb{N}}\mathcal{Q}(\mathbf{w}_1,\varsigma)\right]\right\}.\end{aligned} \tag{33}$$

Using the fact of an iterative process, we find

$$\mathcal{Q}(\mathbf{w}_1,\varsigma)=\sum_{q=0}^{\infty}\mathcal{Q}_q(\mathbf{w}_1,\varsigma). \tag{34}$$

Also, the operator $\bar{\mathbb{L}}$ is linear; therefore,

$$\bar{\mathbb{L}}\left(\sum_{q=0}^{\infty}\mathcal{Q}_q(\mathbf{w}_1,\varsigma)\right)=\sum_{q=0}^{\infty}\bar{\mathbb{L}}\left[\mathcal{Q}_q(\mathbf{w}_1,\varsigma)\right], \tag{35}$$

and the nonlinearity $\overline{\mathbb{N}}$ dealt by (see [27])

$$\begin{aligned}\overline{\mathbb{N}}\left(\sum_{q=0}^{\infty}\mathcal{Q}_q(\mathbf{w}_1,\varsigma)\right)&=\overline{\mathbb{N}}(\mathcal{Q}_0(\mathbf{w}_1,\varsigma))+\sum_{q=1}^{\infty}\left[\overline{\mathbb{N}}\left(\sum_{\kappa=0}^{q}\mathcal{Q}_q(\mathbf{w}_1,\varsigma)\right)\right.\\&\left.-\overline{\mathbb{N}}\left(\sum_{\kappa=0}^{q-1}\mathcal{Q}_q(\mathbf{w}_1,\varsigma)\right)\right]\\&=\overline{\mathbb{N}}(\mathcal{Q}_0)+\sum_{q=1}^{\infty}D_q,\end{aligned} \tag{36}$$

where $D_q=\overline{\mathbb{N}}(\sum_{\kappa=0}^{q}\mathcal{Q}_q)-\overline{\mathbb{N}}(\sum_{\kappa=0}^{q-1}\mathcal{Q}_q)$.

Plugging (37), (39), and (36) into (32) and (33), respectively, we attain

$$\begin{aligned}\sum_{q=0}^{\infty}\mathcal{Q}_q(\mathbf{w}_1,\varsigma)&=\mathcal{G}(\psi)+\mathbb{J}^{-1}\left\{\frac{1}{\psi^{\vartheta}(\varsigma)}\mathbb{J}[\mathbf{F}(\mathbf{w}_1,\varsigma)]\right\},\\&-\mathbb{J}^{-1}\left\{\frac{1}{\psi^{\vartheta}(\varsigma)}\mathbb{J}\left[\bar{\mathbb{L}}\left(\sum_{\kappa=0}^{q}\mathcal{Q}_q(\mathbf{w}_1,\varsigma)\right)\right.\right.\\&\left.\left.+\overline{\mathbb{N}}(\mathcal{Q}_0)+\sum_{\kappa=1}^{q}D_q\right]\right\},\end{aligned} \tag{37}$$

$$\begin{aligned}\sum_{q=0}^{\infty}\mathcal{Q}_q(\mathbf{w}_1,\varsigma)&=\mathcal{G}(\psi)+\mathbb{J}^{-1}\left\{\frac{\psi^{\vartheta}(\varsigma)(1-\vartheta)+\vartheta}{\mathbb{A}(\vartheta)\psi^{\vartheta}(\varsigma)}\mathbb{J}[\mathbf{F}(\mathbf{w}_1,\varsigma)]\right\},\\&-\mathbb{J}^{-1}\left\{\frac{\psi^{\vartheta}(\varsigma)(1-\vartheta)+\vartheta}{\mathbb{A}(\vartheta)\psi^{\vartheta}(\varsigma)}\mathbb{J}\left[\bar{\mathbb{L}}\left(\sum_{q=0}^{q}\mathcal{Q}_q(\mathbf{w}_1,\varsigma)\right)\right.\right.\\&\left.\left.+\overline{\mathbb{N}}(\mathcal{Q}_0)+\sum_{q=1}^{q}D_q\right]\right\}.\end{aligned} \tag{38}$$

Finally, we derive the following iterative process for CFD:

$$\mathcal{Q}_0(\boldsymbol{w}_1,\varsigma)=\mathcal{G}(\psi)+\mathbb{J}^{-1}\left\{\frac{1}{\psi^{\vartheta}(\varsigma)}\mathcal{L}[\boldsymbol{F}(\boldsymbol{w}_1,\varsigma)]\right\},$$
$$\mathcal{Q}_1(\boldsymbol{w}_1,\varsigma)=-\mathbb{J}^{-1}\left\{\frac{1}{\psi^{\vartheta}(\varsigma)}\mathbb{J}\left[\bar{\mathbb{L}}(\mathcal{Q}_0(\boldsymbol{w}_1,\varsigma))+\overline{\mathbb{N}}(\mathcal{Q}_0(\boldsymbol{w}_1,\varsigma))\right]\right\},$$
$$\vdots$$
$$\mathcal{Q}_{q+1}(\boldsymbol{w}_1,\varsigma)=-\mathbb{J}^{-1}\left\{\frac{1}{\psi^{\vartheta}(\varsigma)}\mathbb{J}\left[\bar{\mathbb{L}}\left(\mathcal{Q}_q(\boldsymbol{w}_1,\varsigma)\right)+D_q\right]\right\}. \tag{39}$$

Again, the iterative process for ABC fractional derivative operator is presented as follows:

$$\mathcal{Q}_0(\boldsymbol{w}_1,\varsigma)=\mathcal{G}(\psi)+\mathbb{J}^{-1}\left\{\frac{\psi^{\vartheta}(\varsigma)(1-\vartheta)+\vartheta}{\mathbb{A}(\vartheta)\psi^{\vartheta}(\varsigma)}\mathcal{L}[\boldsymbol{F}(\boldsymbol{w}_1,\varsigma)]\right\},$$
$$\mathcal{Q}_1(\boldsymbol{w}_1,\varsigma)=-\mathbb{J}^{-1}\left\{\frac{\psi^{\vartheta}(\varsigma)(1-\vartheta)+\vartheta}{\mathbb{A}(\vartheta)\psi^{\vartheta}(\varsigma)}\mathbb{J}\left[\bar{\mathbb{L}}(\mathcal{Q}_0(\boldsymbol{w}_1,\varsigma))+\overline{\mathbb{N}}(\mathcal{Q}_0(\boldsymbol{w}_1,\varsigma))\right]\right\},$$
$$\vdots$$
$$\mathcal{Q}_{q+1}(\boldsymbol{w}_1,\varsigma)=-\mathbb{J}^{-1}\left\{\frac{\psi^{\vartheta}(\varsigma)(1-\vartheta)+\vartheta}{\mathbb{A}(\vartheta)\psi^{\vartheta}(\varsigma)}\mathbb{J}\left[\bar{\mathbb{L}}\left(\mathcal{Q}_q(\boldsymbol{w}_1,\varsigma)\right)+D_q\right]\right\}. \tag{40}$$

Finally, (37), (39), and (40) produce the q-term solution in series representation, stated as

$$\mathcal{Q}(\mathbf{w}_1,\varsigma)\neg\mathcal{Q}_0(\mathbf{w}_1,\varsigma)+\mathcal{Q}_1(\mathbf{w}_1,\varsigma)+\mathcal{Q}_2(\mathbf{w}_1,\varsigma)+\cdots+\mathcal{Q}_q(\mathbf{w}_1,\varsigma),\ q\in\mathbb{N}. \tag{41}$$

4. Convergence and Uniqueness Analyses of BSM via ABC Fractional Derivative Operator

The subsequent subsections will highlight how sufficient requirements guarantee the emergence of a unique solution. Our anticipated existence of solutions in the case of JDM is followed by [53].

Theorem 12 (uniqueness theorem). *Equation (24) has a unique solution whenever $0<\varepsilon<1$, where $\varepsilon=(\mathcal{K}_1+\mathcal{K}_2+\mathcal{K}_3)/\mathbb{A}(\vartheta)[\vartheta(\varsigma^{(\vartheta)}/\Gamma(\vartheta+1))+(1-\vartheta)]$.*

Proof. Assuming all continuous functions on the Banach space are denoted by $\Omega=(\mathbb{C}[\mathcal{J}],\|\bullet\|)$. Also, suppose that $\mathcal{J}=[0,\mathcal{T}]$ have the norm $\|\bullet\|$. Now, we define a function $\mathcal{V}:\Omega\mapsto\Omega$ such that

$$\mathcal{Q}_{\ell+1}(\mathbf{w}_1,\varsigma)=\mathcal{Q}(\mathbf{w}_1,\varsigma)+\mathbb{J}^{-1}\left[\frac{\psi^{\vartheta}(\varsigma)(1-\vartheta)+\vartheta}{\mathbb{A}(\vartheta)\psi^{\vartheta}(\varsigma)}\mathbb{J}[\mathbb{L}[\mathcal{Q}_{\ell}(\mathbf{w}_1,\varsigma)]+\bar{P}[\mathcal{Q}_{\ell}(\mathbf{w}_1,\varsigma)]+\mathbb{N}[\mathcal{Q}_{\ell}(\mathbf{w}_1,\varsigma)]]\right],\ \ell\geq 0, \tag{42}$$

where $\mathbb{L}[\mathcal{Q}(\mathbf{w}_1,\varsigma)]\equiv\partial^3\mathcal{Q}(\mathbf{w}_1,\varsigma)/\partial\mathbf{w}_1^2$ and $\bar{P}[\mathcal{Q}(\mathbf{w}_1,\varsigma)]\equiv\partial\mathcal{Q}(\mathbf{w}_1,\varsigma)/\partial\mathbf{w}_1$. Here, suppose that $\mathbb{L}[\mathcal{Q}(\mathbf{w}_1,\varsigma)]$ and $\mathbb{N}[\mathcal{Q}(\mathbf{w}_1,\varsigma)]$ are also Lipschitzian with $|\bar{P}\mathcal{Q}-\bar{P}\widehat{\mathcal{Q}}|<\mathcal{K}_1|\mathcal{Q}-\widehat{\mathcal{Q}}|$ and $|\mathbb{L}\mathcal{Q}-\mathbb{L}\widehat{\mathcal{Q}}|<\mathcal{K}_2|\mathcal{Q}-\widehat{\mathcal{Q}}|$, where $\mathcal{K}_1$ and $\mathcal{K}_2$ are Lipschitz constant, respectively, and $\mathcal{Q},\widehat{\mathcal{Q}}$ are distinct functional values.

$$\begin{aligned}
\|\mathcal{V}\mathcal{Q}-\mathcal{V}\widehat{\mathcal{Q}}\| &= \max_{\varsigma\in\mathcal{J}}\left|\begin{array}{l}\mathbb{J}^{-1}\left[\frac{\psi^{\vartheta}(\varsigma)(1-\vartheta)+\vartheta}{\mathbb{A}(\vartheta)\psi^{\vartheta}(\varsigma)}\mathbb{J}\left[\mathbb{L}[\mathcal{Q}(\mathbf{w}_1,\varsigma)]+\bar{P}[\mathcal{Q}(\mathbf{w}_1,\varsigma)]+\mathbb{N}[\mathcal{Q}(\mathbf{w}_1,\varsigma)]\right]\right]\\ -\mathbb{J}^{-1}\left[\frac{\psi^{\vartheta}(\varsigma)(1-\vartheta)+\vartheta}{\mathbb{A}(\vartheta)\psi^{\vartheta}(\varsigma)}\mathbb{J}\left[\mathbb{L}\left[\widehat{\mathcal{Q}}(\mathbf{w}_1,\varsigma)\right]+\bar{P}\left[\widehat{\mathcal{Q}}(\mathbf{w}_1,\varsigma)\right]+\mathbb{N}\left[\widehat{\mathcal{Q}}(\mathbf{w}_1,\varsigma)\right]\right]\right]\end{array}\right| \leq \max_{\varsigma\in\mathcal{J}}\left|\begin{array}{l}\mathbb{J}^{-1}\left[\frac{\psi^{\vartheta}(\varsigma)(1-\vartheta)+\vartheta}{\mathbb{A}(\vartheta)\psi^{\vartheta}(\varsigma)}\mathbb{J}\left[\mathbb{L}[\mathcal{Q}(\mathbf{w}_1,\varsigma)]-\mathbb{L}\left[\widehat{\mathcal{Q}}(\mathbf{w}_1,\varsigma)\right]\right]\right]\\ +\mathbb{J}^{-1}\left[\frac{\psi^{\vartheta}(\varsigma)(1-\vartheta)+\vartheta}{\mathbb{A}(\vartheta)\psi^{\vartheta}(\varsigma)}\mathbb{J}\left[\bar{P}[\mathcal{Q}(\mathbf{w}_1,\varsigma)]-\bar{P}\left[\widehat{\mathcal{Q}}(\mathbf{w}_1,\varsigma)\right]\right]\right]\\ +\mathbb{J}^{-1}\left[\frac{\psi^{\vartheta}(\varsigma)(1-\vartheta)+\vartheta}{\mathbb{A}(\vartheta)\psi^{\vartheta}(\varsigma)}\mathbb{J}\left[\mathbb{N}[\mathcal{Q}(\mathbf{w}_1,\varsigma)]-\mathbb{N}\left[\widehat{\mathcal{Q}}(\mathbf{w}_1,\varsigma)\right]\right]\right]\end{array}\right|\\
&\leq \max_{\varsigma\in\mathcal{J}}\left[\begin{array}{l}\mathcal{K}_1\mathbb{J}^{-1}\left[\frac{\psi^{\vartheta}(\varsigma)(1-\vartheta)+\vartheta}{\mathbb{A}(\vartheta)\psi^{\vartheta}(\varsigma)}\mathbb{J}\,|\,\mathcal{Q}(\mathbf{w}_1,\varsigma)-\widehat{\mathcal{Q}}(\mathbf{w}_1,\varsigma)\,|\right]\\ +\mathcal{K}_2\mathbb{J}^{-1}\left[\frac{\psi^{\vartheta}(\varsigma)(1-\vartheta)+\vartheta}{\mathbb{A}(\vartheta)\psi^{\vartheta}(\varsigma)}\mathbb{J}\,|\,\mathcal{Q}(\mathbf{w}_1,\varsigma)-\widehat{\mathcal{Q}}(\mathbf{w}_1,\varsigma)\,|\right]\\ +\mathcal{K}_3\mathbb{J}^{-1}\left[\frac{\psi^{\vartheta}(\varsigma)(1-\vartheta)+\vartheta}{\mathbb{A}(\vartheta)\psi^{\vartheta}(\varsigma)}\mathbb{J}\,|\,\mathcal{Q}(\mathbf{w}_1,\varsigma)-\widehat{\mathcal{Q}}(\mathbf{w}_1,\varsigma)\,|\right]\end{array}\right] \leq \max_{\varsigma\in\mathcal{J}}(\mathcal{K}_1+\mathcal{K}_2+\mathcal{K}_3)\mathbb{J}^{-1}\left[\frac{\psi^{\vartheta}(\varsigma)(1-\vartheta)+\vartheta}{\mathbb{A}(\vartheta)\psi^{\vartheta}(\varsigma)}\mathbb{J}\,|\,\mathcal{Q}(\mathbf{w}_1,\varsigma)-\widehat{\mathcal{Q}}(\mathbf{w}_1,\varsigma)\,|\right]\\
&\leq (\mathcal{K}_1+\mathcal{K}_2+\mathcal{K}_3)\mathbb{J}^{-1}\left[\frac{\psi^{\vartheta}(\varsigma)(1-\vartheta)+\vartheta}{\mathbb{A}(\vartheta)\psi^{\vartheta}(\varsigma)}\mathbb{J}\|\mathcal{Q}(\mathbf{w}_1,\varsigma)-\widehat{\mathcal{Q}}(\mathbf{w}_1,\varsigma)\|\right]=(\mathcal{K}_1+\mathcal{K}_2+\mathcal{K}_3)\mathbb{J}^{-1}\left[\frac{\psi^{\vartheta}(\varsigma)(1-\vartheta)+\vartheta}{\mathbb{A}(\vartheta)\psi^{\vartheta}(\varsigma)}\frac{\phi(\mathfrak{s})}{\psi(\mathfrak{s})}\|\mathcal{Q}(\mathbf{w}_1,\varsigma)-\widehat{\mathcal{Q}}(\mathbf{w}_1,\varsigma)\|\right]\\
&=\frac{(\mathcal{K}_1+\mathcal{K}_2+\mathcal{K}_3)}{\mathbb{A}(\vartheta)}\left[\vartheta\frac{\varsigma^{(\vartheta)}}{\Gamma(\vartheta+1)}+(1-\vartheta)\right]\|\mathcal{Q}(\mathbf{w}_1,\varsigma)-\widehat{\mathcal{Q}}(\mathbf{w}_1,\varsigma)\|.
\end{aligned} \tag{43}$$

Since $0<\varepsilon<1$, the mapping is contraction. Consequently, by the Banach contraction fixed point theorem, (17) has a unique. This gives the desired result. □

Theorem 13 (convergence analysis). *The general form solution of (17) will be convergent.*

Proof. Assume that $\widehat{W}_\ell$ be the nth partial sum, i.e., $\widehat{W}_\ell = \sum_{m=0}^{\ell} \mathcal{Q}_\ell(\mathbf{w}_1,\varsigma)$. Here, we prove that a Cauchy sequence $\{\widehat{W}_\ell\}$ in Banach space U.

We acquire by considering a new form of Adomian polynomials.

$$\begin{aligned}\bar{R}\left(\widehat{W}_\ell\right) &= \tilde{\mathscr{H}}_\ell + \sum_{p=0}^{\ell-1} \tilde{\mathscr{H}}_p,\\ \mathbb{N}\left(\widehat{W}_\ell\right) &= \tilde{\mathscr{H}}_\ell + \sum_{c=0}^{\ell-1} \tilde{\mathscr{H}}_c.\end{aligned} \tag{44}$$

Now,

$$\begin{aligned}\|\widehat{W}_\ell - \widehat{W}_q\| &= \max_{\varsigma\in\mathscr{J}}|\widehat{W}_\ell - \widehat{W}_q| = \max_{\varsigma\in\mathscr{J}}\Big|\sum_{m=q+1}^{\ell} \widehat{\mathcal{Q}}(\mathbf{w}_1,\varsigma)\Big|, (m=1,2,3,\cdots)\\
&\le \max_{\varsigma\in\mathscr{J}}\Bigg|\mathbb{J}^{-1}\left[\frac{\psi^{\vartheta}(\varsigma)(1-\vartheta)+\vartheta}{\mathbb{A}(\vartheta)\psi^{\vartheta}(\varsigma)}\mathbb{J}\left[\sum_{m=q+1}^{\ell}\mathbb{L}[\mathcal{Q}_{\ell-1}(\mathbf{w}_1,\varsigma)]\right]\right]\\
&\quad+\mathbb{J}^{-1}\left[\frac{\psi^{\vartheta}(\varsigma)(1-\vartheta)+\vartheta}{\mathbb{A}(\vartheta)\psi^{\vartheta}(\varsigma)}\mathbb{J}\left[\sum_{m=q+1}^{\ell}\bar{P}[\mathcal{Q}_{\ell-1}(\mathbf{w}_1,\varsigma)]\right]\right]\\
&\quad+\mathbb{J}^{-1}\left[\frac{\psi^{\vartheta}(\varsigma)(1-\vartheta)+\vartheta}{\mathbb{A}(\vartheta)\psi^{\vartheta}(\varsigma)}\mathbb{J}\left[\sum_{m=q+1}^{\ell}\tilde{\mathscr{H}}_{\ell-1}(\mathbf{w}_1,\varsigma)\right]\right]\Bigg|\\
&= \max_{\varsigma\in\mathscr{J}}\Bigg|\mathbb{J}^{-1}\left[\frac{\psi^{\vartheta}(\varsigma)(1-\vartheta)+\vartheta}{\mathbb{A}(\vartheta)\psi^{\vartheta}(\varsigma)}\mathbb{J}\left[\sum_{m=q}^{\ell-1}\mathbb{L}[\mathcal{Q}_{\ell}(\mathbf{w}_1,\varsigma)]\right]\right]\\
&\quad+\mathbb{J}^{-1}\left[\frac{\psi^{\vartheta}(\varsigma)(1-\vartheta)+\vartheta}{\mathbb{A}(\vartheta)\psi^{\vartheta}(\varsigma)}\mathbb{J}\left[\sum_{m=q}^{\ell-1}\bar{P}[\mathcal{Q}_{\ell}(\mathbf{w}_1,\varsigma)]\right]\right]\\
&\quad+\mathbb{J}^{-1}\left[\frac{\psi^{\vartheta}(\varsigma)(1-\vartheta)+\vartheta}{\mathbb{A}(\vartheta)\psi^{\vartheta}(\varsigma)}\mathbb{J}\left[\sum_{m=q}^{\ell-1}\tilde{\mathscr{H}}_{\ell}(\mathbf{w}_1,\varsigma)\right]\right]\Bigg|\\
&\le \max_{\varsigma\in\mathscr{J}}\Bigg|\mathbb{J}^{-1}\left[\frac{\psi^{\vartheta}(\varsigma)(1-\vartheta)+\vartheta}{\mathbb{A}(\vartheta)\psi^{\vartheta}(\varsigma)}\mathbb{J}\left[\sum_{m=q}^{\ell-1}\mathbb{L}\left(\widehat{W}_{\ell-1}\right)-\mathbb{L}\left(\widehat{W}_{q-1}\right)\right]\right]\\
&\quad+\mathbb{J}^{-1}\left[\frac{\psi^{\vartheta}(\varsigma)(1-\vartheta)+\vartheta}{\mathbb{A}(\vartheta)\psi^{\vartheta}(\varsigma)}\mathbb{J}\left[\sum_{m=q}^{\ell-1}\bar{P}\left(\widehat{W}_{\ell-1}\right)-\bar{P}\left(\widehat{W}_{q-1}\right)\right]\right]\\
&\quad+\mathbb{J}^{-1}\left[\frac{\psi^{\vartheta}(\varsigma)(1-\vartheta)+\vartheta}{\mathbb{A}(\vartheta)\psi^{\vartheta}(\varsigma)}\mathbb{J}\left[\sum_{m=q}^{\ell-1}\mathbb{N}\left(\widehat{W}_{\ell-1}\right)-\mathbb{N}\left(\widehat{W}_{q-1}\right)\right]\right]\Bigg|\\
&\le \max_{\varsigma\in\mathscr{J}}\Bigg|\mathbb{J}^{-1}\left[\frac{\psi^{\vartheta}(\varsigma)(1-\vartheta)+\vartheta}{\mathbb{A}(\vartheta)\psi^{\vartheta}(\varsigma)}\mathbb{J}\left[\mathbb{L}\left(\widehat{W}_{\ell-1}\right)-\mathbb{L}\left(\widehat{W}_{q-1}\right)\right]\right]\\
&\quad+\mathbb{J}^{-1}\left[\frac{\psi^{\vartheta}(\varsigma)(1-\vartheta)+\vartheta}{\mathbb{A}(\vartheta)\psi^{\vartheta}(\varsigma)}\mathbb{J}\left[\bar{P}\left(\widehat{W}_{\ell-1}\right)-\bar{P}\left(\widehat{W}_{q-1}\right)\right]\right]\\
&\quad+\mathbb{J}^{-1}\left[\frac{\psi^{\vartheta}(\varsigma)(1-\vartheta)+\vartheta}{\mathbb{A}(\vartheta)\psi^{\vartheta}(\varsigma)}\mathbb{J}\left[\mathbb{N}\left(\widehat{W}_{\ell-1}\right)-\mathbb{N}\left(\widehat{W}_{q-1}\right)\right]\right]\Bigg|\\
&\le \mathscr{K}_1\max_{\varsigma\in\mathscr{J}}\mathbb{J}^{-1}\left|\left[\frac{\psi^{\vartheta}(\varsigma)(1-\vartheta)+\vartheta}{\mathbb{A}(\vartheta)\psi^{\vartheta}(\varsigma)}\mathbb{J}\left[\left(\widehat{W}_{\ell-1}\right)-\left(\widehat{W}_{q-1}\right)\right]\right]\right|\\
&\quad+\mathscr{K}_2\max_{\varsigma\in\mathscr{J}}\left|\mathbb{J}^{-1}\left[\frac{\psi^{\vartheta}(\varsigma)(1-\vartheta)+\vartheta}{\mathbb{A}(\vartheta)\psi^{\vartheta}(\varsigma)}\mathbb{J}\left[\left(\widehat{W}_{\ell-1}\right)-\left(\widehat{W}_{q-1}\right)\right]\right]\right|\\
&\quad+\mathscr{K}_3\max_{\varsigma\in\mathscr{J}}\left|\mathbb{J}^{-1}\left[\frac{\psi^{\vartheta}(\varsigma)(1-\vartheta)+\vartheta}{\mathbb{A}(\vartheta)\psi^{\vartheta}(\varsigma)}\mathbb{J}\left[\left(\widehat{W}_{\ell-1}\right)-\left(\widehat{W}_{q-1}\right)\right]\right]\right|\\
&= (\mathscr{K}_1+\mathscr{K}_2+\mathscr{K}_3)\mathbb{J}^{-1}\left[\frac{\psi^{\vartheta}(\varsigma)(1-\vartheta)+\vartheta}{\mathbb{A}(\vartheta)\psi^{\vartheta}(\varsigma)}\frac{\phi(\mathfrak{s})}{\psi^{\vartheta}(\mathfrak{s})}\right]\left\|\widehat{W}_{\ell-1}-\widehat{W}_{q-1}\right\|.\\
&= \frac{(\mathscr{K}_1+\mathscr{K}_2+\mathscr{K}_3)}{\mathbb{A}(\vartheta)}\left[\vartheta\frac{\varsigma^{\vartheta}}{\Gamma(\vartheta+1)}+(1-\vartheta)\right]\left\|\widehat{W}_{\ell-1}-\widehat{W}_{q-1}\right\|.\end{aligned} \tag{45}$$

Consider $n=q+1$, then,

$$\begin{aligned}\|\widehat{W}_{q+1}-\widehat{W}_q\| &\le \varepsilon\|\widehat{W}_q-\widehat{W}_{q-1}\| \le \varepsilon^2\|\widehat{W}_{q-1}-\widehat{W}_{q-2}\|\\ &\le\cdots\le\varepsilon^q\|\widehat{W}_1-\widehat{W}_0\|,\end{aligned} \tag{46}$$

where $\varepsilon = (\mathscr{K}_1+\mathscr{K}_2+\mathscr{K}_3)/\mathbb{A}(\vartheta)[\vartheta(\varsigma^{\vartheta}/\Gamma(\vartheta+1))+(1-\vartheta)]$. Now, from triangular inequality we have

$$\begin{aligned}\|\widehat{W}_\ell-\widehat{W}_q\| &\le \|\widehat{W}_{q+1}-\widehat{W}_q\|+\|\widehat{W}_{q+2}-\widehat{W}_{q+1}\|+\cdots+\|\widehat{W}_\ell-\widehat{W}_{\ell-1}\|\\
&\le \left[\varepsilon^q+\varepsilon^{q+1}+\cdots+\varepsilon^{\ell-1}\right]\|\widehat{W}_1-\widehat{W}_0\|\\
&\le \varepsilon^q\left(\frac{1-\varepsilon^{\ell-q}}{\varepsilon}\right)\|\mathcal{Q}_1\|,\end{aligned} \tag{47}$$

since $0<\varepsilon<1$, we have $(1-\varepsilon^{\ell-q})<1$, then,

$$\|\widehat{W}_\ell-\widehat{W}_q\| \le \frac{\varepsilon^q}{1-\varepsilon}\max_{\varsigma\in\mathscr{J}}\|\mathcal{Q}_1\|. \tag{48}$$

Therefore, $|\mathcal{Q}_1|<\infty$ (since $\mathcal{Q}(\mathbf{w}_1,\varsigma)$ is bounded). Furthermore, as $q\mapsto\infty$, then $\|\widehat{W}_\ell-\widehat{W}_q\|\mapsto 0$. Thus, $\{\widehat{W}_1\}$ is a Cauchy sequence in K. Consequently, the series $\sum_{n=0}^{\infty}\mathcal{Q}_\ell$ is convergent and this yields the immediate consequence. □

Theorem 14 (see [53]) (error estimate). *The absolute error of the series solution (17) to (24) is calculated as*

$$\max_{\varsigma\in\mathscr{J}}\Big|\mathcal{Q}(\mathbf{w}_1,\varsigma)-\sum_{\ell=1}^{q}\mathcal{Q}_\ell(\mathbf{w}_1,\varsigma)\Big| \le \frac{\varepsilon^q}{1-\varepsilon}\max_{\varsigma\in\mathscr{J}}\|\mathcal{Q}_1\|. \tag{49}$$

5. Physical Interpretation of Time-Fractional Black-Scholes Models

In this section, we compute the approximate analytical solution of BSM via the CFD and ABC fractional derivative operators by using the Jafari decomposition method.

5.1. Jafari Decomposition Method

Example 1 (see [16]). Assume the time-fractional one-dimensional BSM (4) subject to IC (5).

Case 1. Firstly, we solve the (4) by using Caputo fractional derivative operator incorporating the Jafari decomposition method.

Applying Jafari transform to both sides of (4), we have

$$\mathbb{J}\left[\mathbf{D}_{\varsigma}^{\vartheta}\mathcal{Q}(\mathbf{w}_1,\varsigma)\right] = \mathbb{J}\left[\frac{\partial^2\mathcal{Q}(\mathbf{w}_1,\varsigma)}{\partial\mathbf{w}_1^2} + (\eta-1)\frac{\partial\mathcal{Q}(\mathbf{w}_1,\varsigma)}{\partial\mathbf{w}_1} - \eta\mathcal{Q}(\mathbf{w}_1,\varsigma)\right]. \tag{50}$$

Using the differentiation rule of Jafari transform, we have

$$\begin{aligned}\psi^{\vartheta}(\varsigma)\mathbb{J}[\mathcal{Q}(\mathbf{w}_1,\varsigma)] &= \phi(\varsigma)\sum_{q=0}^{q-1}\psi^{\vartheta-1-q}(\varsigma)\mathcal{Q}^{(q)}(0)\\ &+ \mathbb{J}\left[\frac{\partial^2\mathcal{Q}(\mathbf{w}_1,\varsigma)}{\partial\mathbf{w}_1^2} + (\eta-1)\frac{\partial\mathcal{Q}(\mathbf{w}_1,\varsigma)}{\partial\mathbf{w}_1} - \eta\mathcal{Q}(\mathbf{w}_1,\varsigma)\right].\end{aligned} \tag{51}$$

In view of (5), we get

$$\begin{aligned}\mathbb{J}[\mathcal{Q}(\mathbf{w}_1,\varsigma)] &= \frac{\phi(\varsigma)}{\psi^{\vartheta}(\varsigma)}\max(\exp(\mathbf{w}_1)-1,0)\\ &+ \frac{1}{\psi^{\vartheta}(\varsigma)}\mathbb{J}\left[\frac{\partial^2\mathcal{Q}(\mathbf{w}_1,\varsigma)}{\partial\mathbf{w}_1^2} + (\eta-1)\frac{\partial\mathcal{Q}(\mathbf{w}_1,\varsigma)}{\partial\mathbf{w}_1} - \eta\mathcal{Q}(\mathbf{w}_1,\varsigma)\right].\end{aligned} \tag{52}$$

Employing the inverse Jafari transform on both sides yields

$$\begin{aligned}\mathcal{Q}(\mathbf{w}_1,\varsigma) &= \mathbb{J}^{-1}\left[\frac{\phi(\varsigma)}{\psi^{\vartheta}(\varsigma)}\max(\exp(\mathbf{w}_1)-1,0)\right]\\ &+ \mathbb{J}^{-1}\left[\frac{1}{\psi^{\vartheta}(\varsigma)}\mathbb{J}\left[\frac{\partial^2\mathcal{Q}(\mathbf{w}_1,\varsigma)}{\partial\mathbf{w}_1^2} + (\eta-1)\frac{\partial\mathcal{Q}(\mathbf{w}_1,\varsigma)}{\partial\mathbf{w}_1} - \eta\mathcal{Q}(\mathbf{w}_1,\varsigma)\right]\right].\end{aligned} \tag{53}$$

With the help of Jafari decomposition method, we find

$$\begin{aligned}\mathcal{Q}_0(\mathbf{w}_1,\varsigma) &= \mathbb{J}^{-1}\left[\frac{\phi(\varsigma)}{\psi^{\vartheta}(\varsigma)}\max(\exp(\mathbf{w}_1)-1,0)\right]\\ &= \max(\exp(\mathbf{w}_1)-1,0).\end{aligned} \tag{54}$$

Here, we surmise that the unknown function $\mathcal{Q}(\mathbf{w}_1,\varsigma)$ can be written by an infinite series of the form

$$\mathcal{Q}(\mathbf{w}_1,\varsigma) = \sum_{q=0}^{\infty}\mathcal{Q}_q(\mathbf{w}_1,\varsigma),$$

$$\begin{aligned}\sum_{q=0}^{\infty}\mathcal{Q}_{q+1}(\mathbf{w}_1,\varsigma) &= \mathbb{J}^{-1}\left[\frac{1}{\psi^{\vartheta}(\varsigma)}\mathbb{J}\left[\sum_{q=0}^{\infty}(\mathcal{Q}(\mathbf{w}_1,\varsigma))_{\mathbf{w}_1\mathbf{w}_1}\right.\right.\\ &\left.\left.+(\eta-1)\sum_{q=0}^{\infty}(\mathcal{Q}(\mathbf{w}_1,\varsigma))_{\mathbf{w}_1} - \eta\sum_{q=0}^{\infty}(\mathcal{Q}(\mathbf{w}_1,\varsigma))\right]\right],\\ &q=0,1,2,\cdots,\end{aligned}$$

$$\begin{aligned}\mathcal{Q}_1(\mathbf{w}_1,\varsigma) &= \mathbb{J}^{-1}\left[\frac{1}{\psi^{\vartheta}(\varsigma)}\mathbb{J}\left[(\mathcal{Q}_0(\mathbf{w}_1,\varsigma))_{\mathbf{w}_1\mathbf{w}_1} + (\eta-1)(\mathcal{Q}_0(\mathbf{w}_1,\varsigma))_{\mathbf{w}_1} + \eta\mathcal{Q}_0\right]\right]\\ &= [\eta\max(\exp(\mathbf{w}_1),0) - \eta\max(\exp(\mathbf{w}_1-1),0)]\mathbb{J}^{-1}\left[\frac{\phi(\mathfrak{s})}{\psi^{\vartheta+1}(\mathfrak{s})}\right]\\ &= [\eta\max(\exp(\mathbf{w}_1),0) - \eta\max(\exp(\mathbf{w}_1-1),0)]\frac{\varsigma^{\vartheta}}{\Gamma(\vartheta+1)},\end{aligned}$$

$$\begin{aligned}\mathcal{Q}_2(\mathbf{w}_1,\varsigma) &= \mathbb{J}^{-1}\left[\frac{1}{\psi^{\vartheta}(\varsigma)}\mathbb{J}\left[(\mathcal{Q}_1(\mathbf{w}_1,\varsigma))_{\mathbf{w}_1\mathbf{w}_1} + (\eta-1)(\mathcal{Q}_1(\mathbf{w}_1,\varsigma))_{\mathbf{w}_1} + \eta\mathcal{Q}_1\right]\right]\\ &= \left[-\eta^2\max(\exp(\mathbf{w}_1),0) + \eta^2\max(\exp(\mathbf{w}_1-1),0)\right]\frac{\varsigma^{2\vartheta}}{\Gamma(2\vartheta+1)},\end{aligned}$$

$$\begin{aligned}\mathcal{Q}_3(\mathbf{w}_1,\varsigma) &= \mathbb{J}^{-1}\left[\frac{1}{\psi^{\vartheta}(\varsigma)}\mathbb{J}\left[(\mathcal{Q}_2(\mathbf{w}_1,\varsigma))_{\mathbf{w}_1\mathbf{w}_1} + (\eta-1)(\mathcal{Q}_2(\mathbf{w}_1,\varsigma))_{\mathbf{w}_1} + \eta\mathcal{Q}_2\right]\right]\\ &= \left[-\eta^3\max(\exp(\mathbf{w}_1),0) + \eta^3\max(\exp(\mathbf{w}_1-1),0)\right]\frac{\varsigma^{3\vartheta}}{\Gamma(3\vartheta+1)}.\\ &\vdots.\end{aligned} \tag{55}$$

The approximate solution for Example 1 is expressed as

$$\begin{aligned}\mathcal{Q}(\mathbf{w}_1,\varsigma) &= \mathcal{Q}_0(\mathbf{w}_1,\varsigma) + \mathcal{Q}_1(\mathbf{w}_1,\varsigma) + \mathcal{Q}_2(\mathbf{w}_1,\varsigma) + \mathcal{Q}_3(\mathbf{w}_1,\varsigma) + \cdots,\\ &= \max(\exp(\mathbf{w}_1-1),0)\left[1 - \frac{\eta\varsigma^{\vartheta}}{\Gamma(\vartheta+1)} + \frac{\eta^2\varsigma^{2\vartheta}}{\Gamma(2\vartheta+1)}\right.\\ &\left.- \frac{\eta^3\varsigma^{3\vartheta}}{\Gamma(3\vartheta+1)} + \cdots\right] + \max(\exp(\mathbf{w}_1),0)\\ &\cdot\left[1 - 1 + \frac{\eta\varsigma^{\vartheta}}{\Gamma(\vartheta+1)} - \frac{\eta^2\varsigma^{2\vartheta}}{\Gamma(2\vartheta+1)} + \frac{\eta^3\varsigma^{3\vartheta}}{\Gamma(3\vartheta+1)} + \cdots\right]\\ &= \max(\exp(\mathbf{w}_1-1),0)E_{\vartheta}\left(-\eta(\varsigma)^{\vartheta}\right)\\ &+ \max(\exp(\mathbf{w}_1),0)E_{\vartheta}\left(1-\eta(\varsigma)^{\vartheta}\right).\end{aligned} \tag{56}$$

Case 2. Now, we solve(4) by using the ABC fractional derivative operator incorporating the Jafari decomposition method.

Considering (50) and using the differentiation rule of Jafari transform, we have

$$\begin{aligned}\frac{\psi^{\vartheta}(\varsigma)\mathbb{A}(\vartheta)}{\vartheta+(1-\vartheta)\psi^{\vartheta}(\varsigma)}\mathbb{J}[\mathcal{Q}(\mathbf{w}_1,\varsigma)] &= \phi(\varsigma)\sum_{q=0}^{q-1}\psi^{\vartheta-1-q}(\varsigma)\mathcal{Q}^{(q)}(0)\\ &+ \mathbb{J}\left[\frac{\partial^2\mathcal{Q}(\mathbf{w}_1,\varsigma)}{\partial\mathbf{w}_1^2} + (\eta-1)\frac{\partial\mathcal{Q}(\mathbf{w}_1,\varsigma)}{\partial\mathbf{w}_1} - \eta\mathcal{Q}(\mathbf{w}_1,\varsigma)\right].\end{aligned} \tag{57}$$

In view of (5), we get

$$\mathbb{J}[\mathcal{Q}(\mathbf{w}_1,\varsigma)] = \frac{\phi(\varsigma)}{\psi^{\vartheta}(\varsigma)}\max\left(\exp\left(\mathbf{w}_1\right)-1,0\right)+\frac{\vartheta+(1-\vartheta)\psi^{\vartheta}(\varsigma)}{\psi^{\vartheta}(\varsigma)\mathbb{A}(\vartheta)} \cdot \mathbb{J}\left[\frac{\partial^2\mathcal{Q}(\mathbf{w}_1,\varsigma)}{\partial\mathbf{w}_1^2}+(\eta-1)\frac{\partial\mathcal{Q}(\mathbf{w}_1,\varsigma)}{\partial\mathbf{w}_1}-\eta\mathcal{Q}(\mathbf{w}_1,\varsigma)\right]. \tag{58}$$

Employing the inverse Jafari transform on both sides of the above equation yields

$$\begin{aligned}\mathcal{Q}(\mathbf{w}_1,\varsigma) &= \mathbb{J}^{-1}\left[\frac{\phi(\varsigma)}{\psi^{\vartheta}(\varsigma)}\max\left(\exp\left(\mathbf{w}_1\right)-1,0\right)\right]\\ &+\mathbb{J}^{-1}\left[\frac{\vartheta+(1-\vartheta)\psi^{\vartheta}(\varsigma)}{\psi^{\vartheta}(\varsigma)\mathbb{A}(\vartheta)}\mathbb{J}\left[\frac{\partial^2\mathcal{Q}(\mathbf{w}_1,\varsigma)}{\partial\mathbf{w}_1^2}\right.\right.\\ &\left.\left.+(\eta-1)\frac{\partial\mathcal{Q}(\mathbf{w}_1,\varsigma)}{\partial\mathbf{w}_1}-\eta\mathcal{Q}(\mathbf{w}_1,\varsigma)\right]\right].\end{aligned} \tag{59}$$

By the Jafari decomposition method, we find:

$$\begin{aligned}Q_0(\mathbf{w}_1,\varsigma) &= \mathbb{J}^{-1}\left[\frac{\phi(\varsigma)}{\psi^{\vartheta}(\varsigma)}\max\left(\exp\left(\mathbf{w}_1\right)-1,0\right)\right]\\ &= \max\left(\exp\left(\mathbf{w}_1\right)-1,0\right).\end{aligned} \tag{60}$$

Here, we surmise that the unknown function $\mathcal{Q}(\mathbf{w}_1,\varsigma)$ can be written by an infinite series of the form:

$$\mathcal{Q}(\mathbf{w}_1,\varsigma)=\sum_{q=0}^{\infty}\mathcal{Q}_{\mathrm{q}}(\mathbf{w}_1,\varsigma),$$

$$\begin{aligned}\sum_{q=0}^{\infty}\mathcal{Q}_{q+1}(\mathbf{w}_1,\varsigma) &= \mathbb{J}^{-1}\left[\frac{\vartheta+(1-\vartheta)\psi^{\vartheta}(\varsigma)}{\psi^{\vartheta}(\varsigma)\mathbb{A}(\vartheta)}\mathbb{J}\left[\sum_{q=0}^{\infty}\left(\mathcal{Q}(\mathbf{w}_1,\varsigma)\right)_{\mathbf{w}_1\mathbf{w}_1}\right.\right.\\ &\left.\left.+(\eta-1)\sum_{q=0}^{\infty}\left(\mathcal{Q}(\mathbf{w}_1,\varsigma)\right)_{\mathbf{w}_1}-\eta\sum_{q=0}^{\infty}\left(\mathcal{Q}(\mathbf{w}_1,\varsigma)\right)\right]\right],\\ &q=0,1,2,\cdots,\end{aligned}$$

$$\begin{aligned}\mathcal{Q}_1(\mathbf{w}_1,\varsigma) &= \mathbb{J}^{-1}\left[\frac{\vartheta+(1-\vartheta)\psi^{\vartheta}(\varsigma)}{\psi^{\vartheta}(\varsigma)\mathbb{A}(\vartheta)}\mathbb{J}\left[\left(\mathcal{Q}_0(\mathbf{w}_1,\varsigma)\right)_{\mathbf{w}_1\mathbf{w}_1}+(\eta-1)\left(\mathcal{Q}_0(\mathbf{w}_1,\varsigma)\right)_{\mathbf{w}_1}+\eta\mathcal{Q}_0\right]\right]\\ &= \frac{\left[\eta\max\left(\exp\left(\mathbf{w}_1\right),0\right)-\eta\max\left(\exp\left(\mathbf{w}_1-1\right),0\right)\right]}{\mathbb{A}(\vartheta)}\left[\vartheta\frac{\varsigma^{\vartheta}}{\Gamma(\vartheta+1)}+(1-\vartheta)\right],\end{aligned}$$

$$\begin{aligned}\mathcal{Q}_2(\mathbf{w}_1,\varsigma) &= \mathbb{J}^{-1}\left[\frac{\vartheta+(1-\vartheta)\psi^{\vartheta}(\varsigma)}{\psi^{\vartheta}(\varsigma)\mathbb{A}(\vartheta)}\mathbb{J}\left[\left(\mathcal{Q}_1(\mathbf{w}_1,\varsigma)\right)_{\mathbf{w}_1\mathbf{w}_1}+(\eta-1)\left(\mathcal{Q}_1(\mathbf{w}_1,\varsigma)\right)_{\mathbf{w}_1}+\eta\mathcal{Q}_1\right]\right]\\ &= -\frac{\left[\eta^2\max\left(\exp\left(\mathbf{w}_1\right),0\right)+\eta^2\max\left(\exp\left(\mathbf{w}_1-1\right),0\right)\right]}{\mathbb{A}^2(\vartheta)}\\ &\cdot\left[\vartheta^2\frac{\varsigma^{2\vartheta}}{\Gamma(2\vartheta+1)}+2\vartheta(1-\vartheta)\frac{\varsigma^{\vartheta}}{\Gamma(\vartheta+1)}+(1-\vartheta)^2\right],\end{aligned}$$

$$\begin{aligned}\mathcal{Q}_3(\mathbf{w}_1,\varsigma) &= \mathbb{J}^{-1}\left[\frac{\vartheta+(1-\vartheta)\psi^{\vartheta}(\varsigma)}{\psi^{\vartheta}(\varsigma)\mathbb{A}(\vartheta)}\mathbb{J}\left[\left(\mathcal{Q}_2(\mathbf{w}_1,\varsigma)\right)_{\mathbf{w}_1\mathbf{w}_1}+(\eta-1)\left(\mathcal{Q}_2(\mathbf{w}_1,\varsigma)\right)_{\mathbf{w}_1}+\eta\mathcal{Q}_2\right]\right]\\ &= -\frac{\left[\eta^3\max\left(\exp\left(\mathbf{w}_1\right),0\right)+\eta^3\max\left(\exp\left(\mathbf{w}_1-1\right),0\right)\right]}{\mathbb{A}^3(\vartheta)}\\ &\times\left[\vartheta^3\frac{\varsigma^{3\vartheta}}{\Gamma(3\vartheta+1)}+3\vartheta^2(1-\vartheta)\frac{\varsigma^{2\vartheta}}{\Gamma(2\vartheta+1)}+3\vartheta(1-\vartheta)^2\frac{\varsigma^{\vartheta}}{\Gamma(\vartheta+1)}+(1-\vartheta)^3\right].\\ &\vdots.\end{aligned} \tag{61}$$

The approximate solution for Example 1 is expressed as:

$$\begin{aligned}\mathcal{Q}(\mathbf{w}_1,\varsigma) &= \mathcal{Q}_0(\mathbf{w}_1,\varsigma)+\mathcal{Q}_1(\mathbf{w}_1,\varsigma)+\mathcal{Q}_2(\mathbf{w}_1,\varsigma)+\mathcal{Q}_3(\mathbf{w}_1,\varsigma)+\cdots,\\ &= \max\left(\exp\left(\mathbf{w}_1-1\right),0\right)\left[1-\frac{\eta}{\mathbb{A}(\vartheta)}\left[\vartheta\frac{\varsigma^{\vartheta}}{\Gamma(\vartheta+1)}+\vartheta\right]\right.\\ &\left.-\frac{\eta^2}{\mathbb{A}^2(\vartheta)}\left[\vartheta^2\frac{\varsigma^{2\vartheta}}{\Gamma(2\vartheta+1)}+2\vartheta(1-\vartheta)\frac{\varsigma^{\vartheta}}{\Gamma(\vartheta+1)}+(1-\vartheta)^2\right]-\cdots\right]\\ &+\max\left(\exp\left(\mathbf{w}_1\right),0\right)\left[-\frac{\eta}{\mathbb{A}(\vartheta)}\left[\vartheta\frac{\varsigma^{\vartheta}}{\Gamma(\vartheta+1)}+\vartheta\right]\right.\\ &\left.-\frac{\eta^2}{\mathbb{A}^2(\vartheta)}\left[\vartheta^2\frac{\varsigma^{2\vartheta}}{\Gamma(2\vartheta+1)}+2\vartheta(1-\vartheta)\frac{\varsigma^{\vartheta}}{\Gamma(\vartheta+1)}+(1-\vartheta)^2\right]-\cdots\right].\end{aligned} \tag{62}$$

The integer-order solution of Example 1 can be obtained with the aid of Taylor series expansion and setting $\vartheta=1$ as follows:

$$\begin{aligned}\mathcal{Q}(\mathbf{w}_1,\varsigma) &= \max\left(\exp\left(\mathbf{w}_1-1\right),0\right)\exp\left(-\eta\varsigma\right)\\ &+\max\left(\exp\left(\mathbf{w}_1\right),0\right)\left[1-\exp\left(-\eta\varsigma\right)\right].\end{aligned} \tag{63}$$

Example 2 (see [20]). Assume the time-fractional one-dimensional BSM (6) subject to IC (7).

Case 1. Firstly, we solve the (6) in the sense of Caputo fractional derivative operator incorporating the Jafari decomposition method.

Applying Jafari transform to both sides of (6), we have

$$\begin{aligned}\mathbb{J}\left[\mathbf{D}_{\varsigma}^{\vartheta}\mathcal{Q}(\mathbf{w}_1,\varsigma)\right] &= \mathbb{J}\left[-0.08\left(2+\sin\mathbf{w}_1\right)^2\mathbf{w}_1^2\frac{\partial^2\mathcal{Q}(\mathbf{w}_1,\varsigma)}{\partial\mathbf{w}_1^2}\right.\\ &\left.-0.06\mathbf{w}_1\frac{\partial\mathcal{Q}(\mathbf{w}_1,\varsigma)}{\partial\mathbf{w}_1}+0.06\mathcal{Q}(\mathbf{w}_1,\varsigma)\right].\end{aligned} \tag{64}$$

Using the differentiation rule of Jafari transform, we have

$$\begin{aligned}\psi^{\vartheta}(\varsigma)\mathbb{J}[\mathcal{Q}(\mathbf{w}_1,\varsigma)] &= \phi(\varsigma)\sum_{q=0}^{q-1}\psi^{\vartheta-1-q}(\varsigma)\mathcal{Q}^{(q)}(0)\\ &+\mathbb{J}\left[-0.08\left(2+\sin\mathbf{w}_1\right)^2\mathbf{w}_1^2\frac{\partial^2\mathcal{Q}(\mathbf{w}_1,\varsigma)}{\partial\mathbf{w}_1^2}\right.\\ &\left.-0.06\mathbf{w}_1\frac{\partial\mathcal{Q}(\mathbf{w}_1,\varsigma)}{\partial\mathbf{w}_1}+0.06\mathcal{Q}(\mathbf{w}_1,\varsigma)\right].\end{aligned} \tag{65}$$

In view of (7), we get

$$\begin{aligned}\mathbb{J}[\mathcal{Q}(\mathbf{w}_1,\varsigma)] &= \frac{\phi(\varsigma)}{\psi^{\vartheta}(\varsigma)}\max\left(\mathbf{w}_1-25\exp\left(-0.06\right),0\right)+\frac{1}{\psi^{\vartheta}(\varsigma)}\\ &\cdot\mathbb{J}\left[-0.08\left(2+\sin\mathbf{w}_1\right)^2\mathbf{w}_1^2\frac{\partial^2\mathcal{Q}(\mathbf{w}_1,\varsigma)}{\partial\mathbf{w}_1^2}-0.06\mathbf{w}_1\frac{\partial\mathcal{Q}(\mathbf{w}_1,\varsigma)}{\partial\mathbf{w}_1}+0.06\mathcal{Q}(\mathbf{w}_1,\varsigma)\right].\end{aligned} \tag{66}$$

Employing the inverse Jafari transform on both sides yields

$$\begin{aligned}\mathcal{Q}(\mathbf{w}_1,\varsigma) &= \mathbb{J}^{-1}\left[\frac{\phi(\varsigma)}{\psi^{\vartheta}(\varsigma)}\max\left(\mathbf{w}_1-25\exp\left(-0.06\right),0\right)\right]\\ &+\mathbb{J}^{-1}\left[\frac{1}{\psi^{\vartheta}(\varsigma)}\mathbb{J}\left[-0.08(2+\sin\mathbf{w}_1)^2\mathbf{w}_1^2\frac{\partial^2\mathcal{Q}(\mathbf{w}_1,\varsigma)}{\partial\mathbf{w}_1^2}\right.\right.\\ &\left.\left.-0.06\mathbf{w}_1\frac{\partial\mathcal{Q}(\mathbf{w}_1,\varsigma)}{\partial\mathbf{w}_1}+0.06\mathcal{Q}(\mathbf{w}_1,\varsigma)\right]\right].\end{aligned}\tag{67}$$

By the Jafari decomposition method, we find

$$\begin{aligned}Q_0(\mathbf{w}_1,\varsigma) &= \mathbb{J}^{-1}\left[\frac{\phi(\varsigma)}{\psi^{\vartheta}(\varsigma)}\max\left(\mathbf{w}_1-25\exp\left(-0.06\right),0\right)\right]\\ &=\max\left(\mathbf{w}_1-25\exp\left(-0.06\right),0\right).\end{aligned}\tag{68}$$

Here, we surmise that the unknown function $\mathcal{Q}(\mathbf{w}_1,\varsigma)$ can be written by an infinite series of the form:

$$\mathcal{Q}(\mathbf{w}_1,\varsigma)=\sum_{q=0}^{\infty}\mathcal{Q}_q(\mathbf{w}_1,\varsigma),$$

$$\begin{aligned}\sum_{q=0}^{\infty}\mathcal{Q}_{q+1}(\mathbf{w}_1,\varsigma) &= \mathbb{J}^{-1}\left[\frac{1}{\psi^{\vartheta}(\varsigma)}\mathbb{J}\left[-0.08(2+\sin\mathbf{w}_1)^2\mathbf{w}_1^2\sum_{q=0}^{\infty}\left(\mathcal{Q}(\mathbf{w}_1,\varsigma)\right)_{\mathbf{w}_1\mathbf{w}_1}\right.\right.\\ &\left.\left.-0.06\mathbf{w}_1\sum_{q=0}^{\infty}\left(\mathcal{Q}(\mathbf{w}_1,\varsigma)\right)_{\mathbf{w}_1}+0.06\sum_{q=0}^{\infty}\left(\mathcal{Q}(\mathbf{w}_1,\varsigma)\right)\right]\right],\\ &\forall q=0,1,2,\cdots,\end{aligned}$$

$$\begin{aligned}\mathcal{Q}_1(\mathbf{w}_1,\varsigma) &= \mathbb{J}^{-1}\left[\frac{1}{\psi^{\vartheta}(\varsigma)}\mathbb{J}\left[-0.08(2+\sin\mathbf{w}_1)^2\mathbf{w}_1^2\left(\mathcal{Q}_0(\mathbf{w}_1,\varsigma)\right)_{\mathbf{w}_1\mathbf{w}_1}\right.\right.\\ &\left.\left.-0.06\mathbf{w}_1\left(\mathcal{Q}_0(\mathbf{w}_1,\varsigma)\right)_{\mathbf{w}_1}-0.06\mathcal{Q}_0\right]\right]\\ &=\left[-0.06\mathbf{w}_1+0.06\max\left(\mathbf{w}_1-25\exp\left(-0.06\right),0\right)\right]\mathbb{J}^{-1}\left[\frac{\phi(\mathfrak{z})}{\psi^{\vartheta+1}(\mathfrak{z})}\right]\\ &=\left[-0.06\mathbf{w}_1+0.06\max\left(\mathbf{w}_1-25\exp\left(-0.06\right),0\right)\right]\frac{\varsigma^{\vartheta}}{\Gamma(\vartheta+1)},\end{aligned}$$

$$\begin{aligned}\mathcal{Q}_2(\mathbf{w}_1,\varsigma) &= \mathbb{J}^{-1}\left[\frac{1}{\psi^{\vartheta}(\varsigma)}\mathbb{J}\left[-0.08(2+\sin\mathbf{w}_1)^2\mathbf{w}_1^2\left(\mathcal{Q}_1(\mathbf{w}_1,\varsigma)\right)_{\mathbf{w}_1\mathbf{w}_1}\right.\right.\\ &\left.\left.-0.06\mathbf{w}_1\left(\mathcal{Q}_1(\mathbf{w}_1,\varsigma)\right)_{\mathbf{w}_1}-0.06\mathcal{Q}_1\right]\right]\\ &=\left[-0.0036\mathbf{w}_1+0.0036\max\left(\mathbf{w}_1-25\exp\left(-0.06\right),0\right)\right]\frac{\varsigma^{2\vartheta}}{\Gamma(2\vartheta+1)},\end{aligned}$$

$$\begin{aligned}\mathcal{Q}_3(\mathbf{w}_1,\varsigma) &= \mathbb{J}^{-1}\left[\frac{1}{\psi^{\vartheta}(\varsigma)}\mathbb{J}\left[-0.08(2+\sin\mathbf{w}_1)^2\mathbf{w}_1^2\left(\mathcal{Q}_2(\mathbf{w}_1,\varsigma)\right)_{\mathbf{w}_1\mathbf{w}_1}\right.\right.\\ &\left.\left.-0.06\mathbf{w}_1\left(\mathcal{Q}_2(\mathbf{w}_1,\varsigma)\right)_{\mathbf{w}_1}-0.06\mathcal{Q}_2\right]\right]\\ &=\left[-0.000216\mathbf{w}_1+0.00216\max\left(\mathbf{w}_1-25\exp\left(-0.06\right),0\right)\right]\\ &\cdot\frac{\varsigma^{3\vartheta}}{\Gamma(3\vartheta+1)},\\ &\vdots.\end{aligned}\tag{69}$$

The approximate solution for Example 2 is expressed as

$$\begin{aligned}\mathcal{Q}(\mathbf{w}_1,\varsigma) &= \mathcal{Q}_0(\mathbf{w}_1,\varsigma)+\mathcal{Q}_1(\mathbf{w}_1,\varsigma)+\mathcal{Q}_2(\mathbf{w}_1,\varsigma)+\mathcal{Q}_3(\mathbf{w}_1,\varsigma)\\ &+\cdots,=\max\left(\mathbf{w}_1-25\exp\left(-0.06\right),0\right)\\ &+\left(\mathbf{w}_1-\max\left(\mathbf{w}_1-25\exp\left(-0.06\right)\right)\right)\\ &\times\left[1-1-\frac{0.06\varsigma^{\vartheta}}{\Gamma(\vartheta+1)}-\frac{0.0036\varsigma^{2\vartheta}}{\Gamma(2\vartheta+1)}-\frac{0.000216\varsigma^{3\vartheta}}{\Gamma(3\vartheta+1)}+\cdots\right]\\ &=\max\left(\mathbf{w}_1-25\exp\left(-0.06\right),0\right)\\ &+\left(\mathbf{w}_1-\max\left(\mathbf{w}_1-25\exp\left(-0.06\right),0\right)\right)\left[1-E_{\vartheta}\left(0.06(\varsigma)^{\vartheta}\right)\right].\end{aligned}\tag{70}$$

Case 2. Now, we solve the (6) by using ABC fractional derivative operator incorporating the Jafari decomposition method.

Considering (64) and using the differentian rule of Jafari transform, we have

$$\begin{aligned}\frac{\psi^{\vartheta}(\varsigma)\mathbb{A}(\vartheta)}{\vartheta+(1-\vartheta)\psi^{\vartheta}(\varsigma)}\mathbb{J}[\mathcal{Q}(\mathbf{w}_1,\varsigma)] &= \phi(\varsigma)\sum_{q=0}^{q-1}\psi^{\vartheta-1-q}(\varsigma)\mathcal{Q}^{(q)}(0)\\ &+\mathbb{J}\left[-0.08(2+\sin\mathbf{w}_1)^2\mathbf{w}_1^2\frac{\partial^2\mathcal{Q}(\mathbf{w}_1,\varsigma)}{\partial\mathbf{w}_1^2}\right.\\ &\left.-0.06\mathbf{w}_1\frac{\partial\mathcal{Q}(\mathbf{w}_1,\varsigma)}{\partial\mathbf{w}_1}+0.06\mathcal{Q}(\mathbf{w}_1,\varsigma)\right].\end{aligned}\tag{71}$$

In view of (7), we get

$$\begin{aligned}\mathbb{J}[\mathcal{Q}(\mathbf{w}_1,\varsigma)] &= \frac{\phi(\varsigma)}{\psi^{\vartheta}(\varsigma)}\max\left(\mathbf{w}_1-25\exp\left(-0.06\right),0\right)+\frac{\vartheta+(1-\vartheta)\psi^{\vartheta}(\varsigma)}{\psi^{\vartheta}(\varsigma)\mathbb{A}(\vartheta)}\\ &\cdot\mathbb{J}\left[-0.08(2+\sin\mathbf{w}_1)^2\mathbf{w}_1^2\frac{\partial^2\mathcal{Q}(\mathbf{w}_1,\varsigma)}{\partial\mathbf{w}_1^2}-0.06\mathbf{w}_1\frac{\partial\mathcal{Q}(\mathbf{w}_1,\varsigma)}{\partial\mathbf{w}_1}\right.\\ &\left.+0.06\mathcal{Q}(\mathbf{w}_1,\varsigma)\right].\end{aligned}\tag{72}$$

Employing the inverse Jafari transform on both sides yields:

$$\begin{aligned}\mathcal{Q}(\mathbf{w}_1,\varsigma) &= \mathbb{J}^{-1}\left[\frac{\phi(\varsigma)}{\psi^{\vartheta}(\varsigma)}\max\left(\mathbf{w}_1-25\exp\left(-0.06\right),0\right)\right]\\ &+\mathbb{J}^{-1}\left[\frac{\vartheta+(1-\vartheta)\psi^{\vartheta}(\varsigma)}{\psi^{\vartheta}(\varsigma)\mathbb{A}(\vartheta)}\mathbb{J}\left[-0.08(2+\sin\mathbf{w}_1)^2\mathbf{w}_1^2\right.\right.\\ &\left.\left.\cdot\frac{\partial^2\mathcal{Q}(\mathbf{w}_1,\varsigma)}{\partial\mathbf{w}_1^2}-0.06\mathbf{w}_1\frac{\partial\mathcal{Q}(\mathbf{w}_1,\varsigma)}{\partial\mathbf{w}_1}+0.06\mathcal{Q}(\mathbf{w}_1,\varsigma)\right]\right].\end{aligned}\tag{73}$$

By the Jafari decomposition method, we find:

$$\begin{aligned}Q_0(\mathbf{w}_1,\varsigma) &= \mathbb{J}^{-1}\left[\frac{\phi(\varsigma)}{\psi^{\vartheta}(\varsigma)}\max\left(\mathbf{w}_1-25\exp\left(-0.06\right),0\right)\right]\\ &=\max\left(\mathbf{w}_1-25\exp\left(-0.06\right),0\right).\end{aligned}\tag{74}$$

Table 1: The exact, JDM_{CFD}, and JDM_{ABC} solutions of Example 1 at various fractional orders with varying values of $\mathbf{w}_1$ and ς.

$\mathbf{w}_1$	ς	$\vartheta = 0.7$	$\vartheta = 0.8$	$\vartheta = 0.9$	$\vartheta = 1(JDM_{CFD})$	$\vartheta = 1(JDM_{ABC})$	Exact
	00.1	0.5038479597	0.4840895398	0.4674596860	0.4538001114	0.4538001114	0.4537994222
	00.2	0.6142259772	0.5911676480	0.5697105760	0.5502060671	0.5502060671	0.5501940469
0.2	00.3	0.6585618567	0.6371931313	0.6161005539	0.5956319295	0.5956319295	0.5955719039
	00.4	0.6956692898	0.6956692898	0.6576549272	0.6380690943	0.6380690943	0.6378819374
	00.5	0.7281682904	0.7121411619	0.6954314260	0.6777823827	0.6777823827	0.6773315511
	00.1	0.6801236061	0.6534525291	0.6310045745	0.6125660773	0.6125660773	0.6125651470
	00.2	0.7502173029	0.7220537959	0.6958460689	0.6720232080	0.6720232080	0.6720085265
0.4	00.3	0.8043692685	0.7782694482	0.7525069160	0.7275064817	0.7275064817	0.7274331662
	00.4	0.8496923896	0.8267500270	0.8032615422	0.7793393519	0.7793393519	0.7791107578
	00.5	0.8893867586	0.8698111796	0.8494018620	0.8278452719	0.8278452719	0.8272946248
	00.1	0.8307048482	0.7981287212	0.7707107275	0.7707107275	0.7707107275	0.7481887600
	00.2	0.9163174827	0.8819184976	0.8499083077	0.8208109997	0.8208109997	0.8207930676
0.6	00.3	0.9824588428	0.9505804504	0.9191140225	0.8885784232	0.8885784232	0.8884888755
	00.4	1.037816628	1.009794763	0.9811058630	0.9518872337	0.9518872337	0.9516080283
	00.5	1.086299440	1.062389774	1.037461777	1.011132498	1.011132498	1.010459936
	00.1	1.014625193	0.9748366216	0.9413482084	0.9138412031	0.9138412031	0.9138398152
	00.2	1.119192701	1.077177686	1.038080351	1.002540819	1.002540819	1.002518917
0.8	00.3	1.199977940	1.161041584	1.122608402	1.085312137	1.085312137	1.085202763
	00.4	1.267592092	1.233366109	1.198325407	1.162637693	1.162637693	1.162296670
	00.5	1.326809132	1.297605800	1.267158676	1.235000022	1.235000022	1.234178553
	00.1	1.239266009	1.190668138	1.149765298	1.116168166	1.116168166	1.116166471
	00.2	1.366985052	1.315667796	1.267914204	1.224506122	1.224506122	1.224479370
1.0	00.3	1.465656366	1.418099393	1.371156999	1.325603238	1.325603238	1.325469648
	00.4	1.548240477	1.506436767	1.463637957	1.420048885	1.420048885	1.419632359
	00.5	1.620568333	1.584899303	1.547711101	1.508432433	1.508432433	1.507429089

Here, we surmise that the unknown function $\mathcal{Q}(\mathbf{w}_1, \varsigma)$ can be written by an infinite series of the form:

$$\mathcal{Q}(\mathbf{w}_1, \varsigma) = \sum_{q=0}^{\infty} \mathcal{Q}_q(\mathbf{w}_1, \varsigma),$$

$$\begin{aligned}\sum_{q=0}^{\infty} \mathcal{Q}_{q+1}(\mathbf{w}_1, \varsigma) &= \mathbb{J}^{-1}\left[\frac{\vartheta + (1-\vartheta)\psi^{\vartheta}(\varsigma)}{\psi^{\vartheta}(\varsigma)\mathbb{A}(\vartheta)} \mathbb{J}\left[-0.08(2+\sin \mathbf{w}_1)^2 \mathbf{w}_1^2 \sum_{q=0}^{\infty} \cdot (\mathcal{Q}(\mathbf{w}_1, \varsigma))_{\mathbf{w}_1\mathbf{w}_1} - 0.06\mathbf{w}_1 \sum_{q=0}^{\infty} (\mathcal{Q}(\mathbf{w}_1, \varsigma))_{\mathbf{w}_1} + 0.06 \sum_{q=0}^{\infty} (\mathcal{Q}(\mathbf{w}_1, \varsigma))\right]\right], q = 0, 1, 2, \cdots,\end{aligned}$$

$$\begin{aligned}\mathcal{Q}_1(\mathbf{w}_1, \varsigma) &= \mathbb{J}^{-1}\left[\frac{\vartheta + (1-\vartheta)\psi^{\vartheta}(\varsigma)}{\psi^{\vartheta}(\varsigma)\mathbb{A}(\vartheta)} \mathbb{J}\left[-0.08(2+\sin \mathbf{w}_1)^2 \mathbf{w}_1^2 (\mathcal{Q}_0(\mathbf{w}_1, \varsigma))_{\mathbf{w}_1\mathbf{w}_1} - 0.06\mathbf{w}_1 (\mathcal{Q}_0(\mathbf{w}_1, \varsigma))_{\mathbf{w}_1} - 0.06\mathcal{Q}_0\right]\right] \\ &= \frac{[-0.06\mathbf{w}_1 + 0.06 \max(\mathbf{w}_1 - 25\exp(-0.06), 0)]}{\mathbb{A}(\vartheta)} \cdot \left[\vartheta \frac{\varsigma^{\vartheta}}{\Gamma(\vartheta+1)} + (1-\vartheta)\right],\end{aligned}$$

$$\begin{aligned}\mathcal{Q}_2(\mathbf{w}_1, \varsigma) &= \mathbb{J}^{-1}\left[\frac{\vartheta + (1-\vartheta)\psi^{\vartheta}(\varsigma)}{\psi^{\vartheta}(\varsigma)\mathbb{A}(\vartheta)} \mathbb{J}\left[-0.08(2+\sin \mathbf{w}_1)^2 \mathbf{w}_1^2 (\mathcal{Q}_1(\mathbf{w}_1, \varsigma))_{\mathbf{w}_1\mathbf{w}_1} - 0.06\mathbf{w}_1 (\mathcal{Q}_1(\mathbf{w}_1, \varsigma))_{\mathbf{w}_1} - 0.06\mathcal{Q}_1\right]\right] \\ &= \frac{[-0.0036\mathbf{w}_1 + 0.0036 \max(\mathbf{w}_1 - 25\exp(-0.06), 0)]}{\mathbb{A}^2(\vartheta)} \cdot \left[\vartheta^2 \frac{\varsigma^{2\vartheta}}{\Gamma(2\vartheta+1)} + 2\vartheta(1-\vartheta)\frac{\varsigma^{\vartheta}}{\Gamma(\vartheta+1)} + (1-\vartheta)^2\right],\end{aligned}$$

$$\begin{aligned}\mathcal{Q}_3(\mathbf{w}_1, \varsigma) &= \mathbb{J}^{-1}\left[\frac{\vartheta + (1-\vartheta)\psi^{\vartheta}(\varsigma)}{\psi^{\vartheta}(\varsigma)\mathbb{A}(\vartheta)} \mathbb{J}\left[-0.08(2+\sin \mathbf{w}_1)^2 \mathbf{w}_1^2 (\mathcal{Q}_2(\mathbf{w}_1, \varsigma))_{\mathbf{w}_1\mathbf{w}_1} - 0.06\mathbf{w}_1 (\mathcal{Q}_2(\mathbf{w}_1, \varsigma))_{\mathbf{w}_1} - 0.06\mathcal{Q}_2\right]\right] \\ &= -\frac{[-0.000216\mathbf{w}_1 + 0.00216 \max(\mathbf{w}_1 - 25\exp(-0.06), 0)]}{\mathbb{A}^3(\vartheta)} \times \left[\vartheta^3 \frac{\varsigma^{3\vartheta}}{\Gamma(3\vartheta+1)} + 3\vartheta^2(1-\vartheta)\frac{\varsigma^{2\vartheta}}{\Gamma(2\vartheta+1)} + 3\vartheta(1-\vartheta)^2 \cdot \frac{\varsigma^{\vartheta}}{\Gamma(\vartheta+1)} + (1-\vartheta)^3\right].\end{aligned}$$

$$\vdots \,. \tag{75}$$

Table 2: The exact, $\mathrm{JITM}_{\mathrm{CFD}}$, and $\mathrm{JITM}_{\mathrm{ABC}}$ solutions of Example 3 at various fractional orders with varying $\mathbf{w}_1$ and ς.

$\mathbf{w}_1$	ς	$\vartheta = 0.75$	$\vartheta = 0.85$	$\vartheta = 0.95$	$\vartheta = 1(\mathrm{JITM}_{\mathrm{CFD}})$	$\vartheta = 1(\mathrm{JITM}_{\mathrm{ABC}})$	Exact
	00.6	0.7508677004	0.7372780991	0.7227692296	0.7150366162	0.7150366162	0.7141141271
	00.7	0.7792390784	0.7681866657	0.7564519988	0.7500966158	0.7500966158	0.7484099736
00.2	00.8	0.8059972934	0.7971941227	0.7881505824	0.7832272030	0.7832272030	0.7803872090
	00.9	0.8316666049	0.8247731367	0.8182127671	0.8146931992	0.8146931992	0.8102025856
	11.0	0.8566680138	0.8513290369	0.8469638545	0.8447594256	0.8447594256	0.8380022585
	00.6	0.9171118804	0.9005135041	0.8827923308	0.8733476954	0.8733476954	0.8722209647
	00.7	0.9517647598	0.9382653126	0.9239325579	0.9161700757	0.9161700757	0.9141100062
00.4	00.8	0.9844473175	0.9736951006	0.9626492954	0.9566358662	0.9566358662	0.9531670898
	00.9	1.015799885	1.007380184	0.9993673307	0.9950685208	0.9950685208	0.9895836730
	11.0	1.046336675	1.039815634	1.034483988	1.031791493	1.031791493	1.023538270
	00.6	1.120162980	1.099889677	1.078244987	1.066709284	1.066709284	1.065333092
	00.7	1.162488102	1.145999840	1.128493774	1.119012657	1.119012657	1.116496482
0.6	00.8	1.202406668	1.189273881	1.175782504	1.168437685	1.168437685	1.164200912
	00.9	1.240700781	1.230416935	1.220630014	1.215379436	1.215379436	1.208680227
	11.0	1.277998501	1.270033683	1.263521596	1.260232974	1.260232974	1.250152466
	00.6	1.368170153	1.343408286	1.316971402	1.302881661	1.302881661	1.301200776
	00.7	1.419866175	1.399727366	1.378345408	1.366765146	1.366765146	1.363691883
0.8	00.8	1.468622821	1.452582399	1.436103994	1.427133012	1.427133012	1.421958205
	00.9	1.515395356	1.502834639	1.490880866	1.484467795	1.484467795	1.476285363
	11.0	1.560950894	1.551222644	1.543268762	1.539252031	1.539252031	1.526939670
	00.6	1.671086799	1.640842586	1.608552502	1.591343254	1.591343254	1.589290217
	00.7	1.734228462	1.709630866	1.683514884	1.669370718	1.669370718	1.665617027
1.0	00.8	1.793779965	1.774188148	1.754061379	1.743104197	1.743104197	1.736783674
	00.9	1.850908068	1.835566372	1.820966001	1.813133059	1.813133059	1.803139015
	11.0	1.906549727	1.894667615	1.884952723	1.880046676	1.880046676	1.865008325

The approximate solution for Example 2 is expressed as:

$$\begin{aligned}\mathcal{Q}(\mathbf{w}_1,\varsigma) &= \mathcal{Q}_0(\mathbf{w}_1,\varsigma) + \mathcal{Q}_1(\mathbf{w}_1,\varsigma) + \mathcal{Q}_2(\mathbf{w}_1,\varsigma) + \mathcal{Q}_3(\mathbf{w}_1,\varsigma) + \cdots,\\ &= \max\left(\mathbf{w}_1 - 25\exp(-0.06), 0\right)\\ &\quad - \frac{0.06\mathbf{w}_1 - 0.06\max\left(\mathbf{w}_1 - 25\exp(-0.06), 0\right)}{\mathbb{A}(\vartheta)}\\ &\quad \cdot \left[\vartheta\frac{\varsigma^{\vartheta}}{\Gamma(\vartheta+1)} + \vartheta\right]\\ &\quad - \frac{0.0036\mathbf{w}_1 - 0.0036\max\left(\mathbf{w}_1 - 25\exp(-0.06), 0\right)}{\mathbb{A}^2(\vartheta)}\\ &\quad \cdot \left[\vartheta^2\frac{\varsigma^{2\vartheta}}{\Gamma(2\vartheta+1)} + 2\vartheta(1-\vartheta)\frac{\varsigma^{\vartheta}}{\Gamma(\vartheta+1)} + (1-\vartheta)^2\right] - \cdots.\end{aligned} \tag{76}$$

The integer-order solution of Example 2 can be obtained with the aid of Taylor series expansion and setting $\vartheta = 1$ as follows:

$$\begin{aligned}\mathcal{Q}(\mathbf{w}_1,\varsigma) &= \max\left(\mathbf{w}_1 - 25\exp(-0.06), 0\right)\\ &\quad + \left(\mathbf{w}_1 - \max\left(\mathbf{w}_1 - 25\exp(-0.06), 0\right)\right)\\ &\quad \cdot \left[1 - \exp(-0.06\varsigma)\right].\end{aligned} \tag{77}$$

5.2. Jafari Iterative Transform Method

Example 3 (see[16]). Assume the time-fractional one-dimensional BSM (4) subject to IC (5).

Case 1. First, we surmise the Caputo fractional derivative operator for (4) with the new iterative transform method via the Jafari transform.

Implementing the Jafari transform to (4) with IC (5), we have:

$$\begin{aligned}\psi^{\vartheta}(\varsigma)\mathbb{J}[\mathcal{Q}(\mathbf{w}_1,\varsigma)] &= \phi(\varsigma)\sum_{q=0}^{q-1}\psi^{\vartheta-1-q}(\varsigma)\mathcal{Q}^{(q)}(0)\\ &\quad + \mathbb{J}\left[\frac{\partial^2\mathcal{Q}(\mathbf{w}_1,\varsigma)}{\partial\mathbf{w}_1^2} + (\eta-1)\frac{\partial\mathcal{Q}(\mathbf{w}_1,\varsigma)}{\partial\mathbf{w}_1} - \eta\mathcal{Q}(\mathbf{w}_1,\varsigma)\right].\end{aligned} \tag{78}$$

Correspondingly, we get

$$\begin{aligned}\mathbb{J}[\mathcal{Q}(\mathbf{w}_1,\varsigma)] &= \frac{\phi(\varsigma)}{\psi^{\vartheta}(\varsigma)}\max\left(\exp(\mathbf{w}_1) - 1, 0\right) + \frac{1}{\psi^{\vartheta}(\varsigma)}\\ &\quad \cdot \mathbb{J}\left[\frac{\partial^2\mathcal{Q}(\mathbf{w}_1,\varsigma)}{\partial\mathbf{w}_1^2} + (\eta-1)\frac{\partial\mathcal{Q}(\mathbf{w}_1,\varsigma)}{\partial\mathbf{w}_1} - \eta\mathcal{Q}(\mathbf{w}_1,\varsigma)\right].\end{aligned} \tag{79}$$

Table 3: The comparsion analysis among HPM [14], $\mathrm{JDM}_{\mathrm{CFD}}$, and $\mathrm{JDM}_{\mathrm{ABC}}$ of Example 1 for approximated results of $\mathcal{Q}(\mathbf{w}_1, \varsigma)$ and absolute error $E_{\mathrm{abs}} = \|E^{\mathrm{exact}} - E^{\mathrm{approx}}\|$ at $\vartheta = 1$ with varying values of $\mathbf{w}_1$ and ς.

$\mathbf{w}_1$	ς	$\|\mathrm{Exact} - \mathrm{HPM}\|$	$\|\mathrm{Exact} - \mathrm{JDM}_{\mathrm{CFD}}\|$	$\|\mathrm{Exact} - \mathrm{JDM}_{\mathrm{ABC}}\|$
	0.1	$768.9000000 \times 10^{-7}$	$761.7000000 \times 10^{-9}$	$761.7000000 \times 10^{-9}$
	0.2	13.099020×10^{-5}	$12.0202000 \times 10^{-6}$	$12.0202000 \times 10^{-6}$
0.2	0.3	$64.2248000 \times 10^{-5}$	$60.0256000 \times 10^{-6}$	$60.0256000 \times 10^{-6}$
	0.4	$189.107690 \times 10^{-5}$	$187.1569000 \times 10^{-6}$	$187.1569000 \times 10^{-6}$
	0.5	$455.4455000 \times 10^{-5}$	$450.8316000 \times 10^{-6}$	$450.8316000 \times 10^{-6}$
	0.1	$933.050000 \times 10^{-8}$	$930.3000000 \times 10^{-9}$	$930.3000000 \times 10^{-9}$
	0.2	$15.7634000 \times 10^{-5}$	$14.6815000 \times 10^{-6}$	$14.6815000 \times 10^{-6}$
0.4	0.3	$75.9988000 \times 10^{-5}$	$73.3155000 \times 10^{-6}$	$73.3155000 \times 10^{-6}$
	0.4	$230.5679000 \times 10^{-5}$	$228.5941000 \times 10^{-6}$	$228.5941000 \times 10^{-6}$
	0.5	$554.5621000 \times 10^{-5}$	$550.6471000 \times 10^{-6}$	$550.6471000 \times 10^{-6}$
	0.1	2.0098000×10^{-5}	1.1363000×10^{-6}	1.1363000×10^{-6}
	0.2	$16.4534000 \times 10^{-5}$	$17.9321000 \times 10^{-6}$	$17.9321000 \times 10^{-6}$
0.6	0.3	$90.6658000 \times 10^{-5}$	$89.5477000 \times 10^{-6}$	$89.5477000 \times 10^{-6}$
	0.4	$220.3489000 \times 10^{-5}$	$279.2054000 \times 10^{-6}$	$279.2054000 \times 10^{-6}$
	0.5	$660.9890000 \times 10^{-5}$	$672.5620000 \times 10^{-6}$	$672.5620000 \times 10^{-6}$
	0.1	2.0094000×10^{-5}	1.3879000×10^{-6}	1.3879000×10^{-6}
	0.2	$23.0020000 \times 10^{-5}$	$21.9020000 \times 10^{-6}$	$21.9020000 \times 10^{-6}$
0.8	0.3	$111.5690000 \times 10^{-5}$	$109.3740000 \times 10^{-6}$	$109.3740000 \times 10^{-6}$
	0.8	$345.9980000 \times 10^{-5}$	$341.0230000 \times 10^{-6}$	$341.0230000 \times 10^{-6}$
	0.5	$824.0000000 \times 10^{-5}$	$821.4690000 \times 10^{-6}$	$821.4690000 \times 10^{-6}$
	0.1	$2.346789233 \times 10^{-6}$	$1.695175303 \times 10^{-6}$	$1.695175303 \times 10^{-6}$
	0.2	$3.700000000 \times 10^{-4}$	$2.675000000 \times 10^{-5}$	$2.675000000 \times 10^{-5}$
1.0	0.3	$2.888600000 \times 10^{-3}$	$1.336000000 \times 10^{-4}$	$1.336000000 \times 10^{-4}$
	0.4	$5.120000000 \times 10^{-3}$	$4.165000000 \times 10^{-4}$	$4.165000000 \times 10^{-4}$
	0.5	$2.000000000 \times 10^{-2}$	$1.003000000 \times 10^{-3}$	$1.003000000 \times 10^{-3}$

Employing the suggested analytical method, we obtain

$$\begin{aligned}\mathcal{Q}_0(\mathbf{w}_1, \varsigma) &= \mathbb{J}^{-1}\left[\frac{\phi(\varsigma)}{\psi^{\vartheta}(\varsigma)} \max\left(\exp\left(\mathbf{w}_1\right) - 1, 0\right)\right] \\ &= \max\left(\exp\left(\mathbf{w}_1\right) - 1, 0\right),\end{aligned}$$

$$\begin{aligned}\mathcal{Q}_1(\mathbf{w}_1, \varsigma) &= \mathbb{J}^{-1}\left[\frac{1}{\psi^{\vartheta}(\varsigma)} \mathbb{J}\left[\left(\mathcal{Q}_0(\mathbf{w}_1, \varsigma)\right)_{\mathbf{w}_1\mathbf{w}_1} + (\eta - 1)\left(\mathcal{Q}_0(\mathbf{w}_1, \varsigma)\right)_{\mathbf{w}_1} + \eta \mathcal{Q}_0\right]\right] \\ &= \left[\eta \max\left(\exp\left(\mathbf{w}_1\right), 0\right) - \eta \max\left(\exp\left(\mathbf{w}_1 - 1\right), 0\right)\right] \mathbb{J}^{-1}\left[\frac{\phi(\mathfrak{s})}{\psi^{\vartheta+1}(\mathfrak{s})}\right] \\ &= \left[\eta \max\left(\exp\left(\mathbf{w}_1\right), 0\right) - \eta \max\left(\exp\left(\mathbf{w}_1 - 1\right), 0\right)\right] \frac{\varsigma^{\vartheta}}{\Gamma(\vartheta + 1)},\end{aligned}$$

$$\begin{aligned}\mathcal{Q}_2(\mathbf{w}_1, \varsigma) &= \mathbb{J}^{-1}\left[\frac{1}{\psi^{\vartheta}(\varsigma)} \mathbb{J}\left[\left(\mathcal{Q}_1(\mathbf{w}_1, \varsigma)\right)_{\mathbf{w}_1\mathbf{w}_1} + (\eta - 1)\left(\mathcal{Q}_1(\mathbf{w}_1, \varsigma)\right)_{\mathbf{w}_1} + \eta \mathcal{Q}_1\right]\right] \\ &= \left[-\eta^2 \max\left(\exp\left(\mathbf{w}_1\right), 0\right) + \eta^2 \max\left(\exp\left(\mathbf{w}_1 - 1\right), 0\right)\right] \frac{\varsigma^{2\vartheta}}{\Gamma(2\vartheta + 1)},\end{aligned}$$

$$\begin{aligned}\mathcal{Q}_3(\mathbf{w}_1, \varsigma) &= \mathbb{J}^{-1}\left[\frac{1}{\psi^{\vartheta}(\varsigma)} \mathbb{J}\left[\left(\mathcal{Q}_2(\mathbf{w}_1, \varsigma)\right)_{\mathbf{w}_1\mathbf{w}_1} + (\eta - 1)\left(\mathcal{Q}_2(\mathbf{w}_1, \varsigma)\right)_{\mathbf{w}_1} + \eta \mathcal{Q}_2\right]\right] \\ &= \left[-\eta^3 \max\left(\exp\left(\mathbf{w}_1\right), 0\right) + \eta^3 \max\left(\exp\left(\mathbf{w}_1 - 1\right), 0\right)\right] \frac{\varsigma^{3\vartheta}}{\Gamma(3\vartheta + 1)}.\end{aligned}$$

$$\vdots\,. \tag{80}$$

Table 4: The exact, JDM_{CFD}, and JDM_{ABC} solutions of Example 2 at various fractional-orders with varying $\mathbf{w}_1$ and ς.

$\mathbf{w}_1$	ς	$\vartheta = 0.7$	$\vartheta = 0.8$	$\vartheta = 0.9$	$\vartheta = 1(JDM_{CFD})$	$\vartheta = 1(JDM_{ABC})$	Exact
	0.1	0.0026121375	0.0020293922	0.0015639815	0.0011964072	0.0011964072	0.001196407
	0.2	0.0042204353	0.0035172577	0.0029075880	0.0023856576	0.0023856576	0.0023856574
0.2	0.3	0.0055797208	0.0048449971	0.0041732529	0.0035677944	0.0035677944	0.003567793
	0.4	0.0067961194	0.0060754949	0.0053880675	0.0047428608	0.0047428608	0.0047428580
	0.5	0.0079145429	0.0072365565	0.0065645469	0.0059109000	0.0059109000	0.0059108933
	0.1	0.0052242750	0.0040587845	0.0031279630	0.0023928144	0.0023928144	0.0023928143
	0.2	0.0084408706	0.0070345154	0.0058151760	0.0047713152	0.0047713152	0.0047713148
0.4	0.3	0.011159441	0.0096899942	0.0083465059	0.0071355888	0.0071355888	0.0071355870
	0.4	0.013592238	0.012150989	0.010776135	0.0094857216	0.0094857216	0.0094857160
	0.5	0.015829085	0.014473113	0.013129093	0.011821800	0.011821800	0.0118217866
	0.1	0.0078364125	0.0060881767	0.0046919445	0.0035892216	0.0035892216	0.0035892215
	0.2	0.012661305	0.010551773	0.0087227641	0.0071569728	0.0071569728	0.0071569722
0.6	0.3	0.016739162	0.014534991	0.012519758	0.010703383	0.010703383	0.0107033805
	0.4	0.020388358	0.018226484	0.016164202	0.014228582	0.014228582	0.0142285741
	0.5	0.023743628	0.021709669	0.019693640	0.017732700	0.017732700	0.0177326799
	0.1	0.010448550	0.0081175690	0.0062559261	0.0047856288	0.0047856288	0.0047856287
	0.2	0.016881741	0.014069030	0.011630352	0.0095426304	0.0095426304	0.0095426296
0.8	0.3	0.022318883	0.019379988	0.016693011	0.016693011	0.016693011	0.0142711740
	0.4	0.027184477	0.024301979	0.021552270	0.018971443	0.018971443	0.0189714321
	0.5	0.031658171	0.028946226	0.026258187	0.023643600	0.023643600	0.0236435732
	0.1	0.013060687	0.010146961	0.0078199076	0.0059820360	0.0059820360	0.005982035
	0.2	0.021102176	0.017586288	0.014537940	0.011928288	0.011928288	0.011928287
1.0	0.3	0.027898604	0.024224985	0.020866264	0.017838972	0.017838972	0.017838967
	0.4	0.033980597	0.030377474	0.026940337	0.023714304	0.023714304	0.023714290
	0.5	0.039572714	0.036182782	0.032822734	0.029554500	0.029554500	0.029554466

The series form solution is

$$\mathcal{Q}(\mathbf{w}_1, \varsigma) = \mathcal{Q}_0(\mathbf{w}_1, \varsigma) + \mathcal{Q}_1(\mathbf{w}_1, \varsigma) + \mathcal{Q}_2(\mathbf{w}_1, \varsigma) + \mathcal{Q}_3(\mathbf{w}_1, \varsigma) + \cdots. \tag{81}$$

Consequently, we have

$$\begin{aligned}\mathcal{Q}(\mathbf{w}_1, \varsigma) &= \mathcal{Q}_0(\mathbf{w}_1, \varsigma) + \mathcal{Q}_1(\mathbf{w}_1, \varsigma) + \mathcal{Q}_2(\mathbf{w}_1, \varsigma) + \mathcal{Q}_3(\mathbf{w}_1, \varsigma) + \cdots, \\ &= \max(\exp(\mathbf{w}_1 - 1), 0)\left[1 - \frac{\eta\varsigma^{\vartheta}}{\Gamma(\vartheta+1)} + \frac{\eta^2\varsigma^{2\vartheta}}{\Gamma(2\vartheta+1)} - \frac{\eta^3\varsigma^{3\vartheta}}{\Gamma(3\vartheta+1)} + \cdots\right] \\ &\quad + \max(\exp(\mathbf{w}_1), 0)\left[1 - 1 + \frac{\eta\varsigma^{\vartheta}}{\Gamma(\vartheta+1)} - \frac{\eta^2\varsigma^{2\vartheta}}{\Gamma(2\vartheta+1)} + \frac{\eta^3\varsigma^{3\vartheta}}{\Gamma(3\vartheta+1)} + \cdots\right] \\ &= \max(\exp(\mathbf{w}_1 - 1), 0) E_{\vartheta}\left(-\eta(\varsigma)^{\vartheta}\right) + \max(\exp(\mathbf{w}_1), 0) E_{\vartheta}\left(1 - \eta(\varsigma)^{\vartheta}\right).\end{aligned} \tag{82}$$

Case 2. Now, we consider the ABC fractional derivative operator for (4) with the new iterative transform method via the Jafari transform.

Implementing the Jafari transform to (4) with IC (5), we have

$$\begin{aligned}\frac{\psi^{\vartheta}(\varsigma)\mathbb{A}(\vartheta)}{\vartheta + (1-\vartheta)\psi^{\vartheta}(\varsigma)} \mathbb{J}[\mathcal{Q}(\mathbf{w}_1, \varsigma)] &= \phi(\varsigma) \sum_{q=0}^{q-1} \psi^{\vartheta-1-q}(\varsigma) \mathcal{Q}^{(q)}(0) \\ &\quad + \mathbb{J}\left[\frac{\partial^2 \mathcal{Q}(\mathbf{w}_1, \varsigma)}{\partial \mathbf{w}_1^2} + (\eta - 1)\frac{\partial \mathcal{Q}(\mathbf{w}_1, \varsigma)}{\partial \mathbf{w}_1} - \eta \mathcal{Q}(\mathbf{w}_1, \varsigma)\right].\end{aligned} \tag{83}$$

Correspondingly, we get

$$\begin{aligned}\mathbb{J}[\mathcal{Q}(\mathbf{w}_1, \varsigma)] &= \frac{\phi(\varsigma)}{\psi^{\vartheta}(\varsigma)} \max(\exp(\mathbf{w}_1) - 1, 0) + \frac{\vartheta + (1-\vartheta)\psi^{\vartheta}(\varsigma)}{\psi^{\vartheta}(\varsigma)\mathbb{A}(\vartheta)} \\ &\quad \cdot \mathbb{J}\left[\frac{\partial^2 \mathcal{Q}(\mathbf{w}_1, \varsigma)}{\partial \mathbf{w}_1^2} + (\eta - 1)\frac{\partial \mathcal{Q}(\mathbf{w}_1, \varsigma)}{\partial \mathbf{w}_1} - \eta \mathcal{Q}(\mathbf{w}_1, \varsigma)\right].\end{aligned} \tag{84}$$

Table 5: The exact, $\mathrm{JITM}_{\mathrm{CFD}}$, and $\mathrm{JITM}_{\mathrm{ABC}}$ solutions of Example 4 at various fractional orders with varying $\mathbf{w}_1$ and ς.

$\mathbf{w}_1$	ς	$\vartheta = 0.75$	$\vartheta = 0.85$	$\vartheta = 0.97$	$\vartheta = 1(\mathrm{JITM}_{\mathrm{CFD}})$	$\vartheta = 1(\mathrm{JITM}_{\mathrm{ABC}})$	Exact
	00.6	0.0086548678	0.0080282318	0.0073906661	0.0070719552	0.0070719552	0.0070719413
	00.7	0.0096825555	0.0091221078	0.0085297821	0.0082260696	0.0082260696	0.0082260438
00.2	00.8	0.010667397	0.010185717	0.0096537610	0.0093732864	0.0093732864	0.0093732425
	00.9	0.011615667	0.011222842	0.010763853	0.010513648	0.010513648	0.0105135787
	11.0	0.012532107	0.012236387	0.011861042	0.011647200	0.011647200	0.0116470932
	00.6	0.017309735	0.016056463	0.014781332	0.014143910	0.014143910	0.0141438826
	00.7	0.019365111	0.018244215	0.017059564	0.016452139	0.016452139	0.0164520877
00.4	00.8	0.021334795	0.020371435	0.019307522	0.018746572	0.018746572	0.0187464851
	00.9	0.023231334	0.022445684	0.021527707	0.021027297	0.021027297	0.0210271574
	11.0	0.025064214	0.024472774	0.023722084	0.023294400	0.023294400	0.0232941865
	00.6	0.025964603	0.024084695	0.022171998	0.021215865	0.021215865	0.0212158239
	00.7	0.029047666	0.027366323	0.025589346	0.024678208	0.024678208	0.0246781316
0.6	00.8	0.032002192	0.030557153	0.028961283	0.028119859	0.028119859	0.0281197277
	00.9	0.034847002	0.033668527	0.032291560	0.031540946	0.031540946	0.031540736
	11.0	0.037596321	0.036709162	0.035583126	0.034941600	0.034941600	0.0349412798
	00.6	0.034619471	0.032112927	0.029562664	0.028287820	0.028287820	0.0282877652
	00.7	0.038730222	0.036488431	0.034119128	0.032904278	0.032904278	0.032904175
0.8	00.8	0.042669590	0.040742871	0.038615044	0.037493145	0.037493145	0.0374929703
	00.9	0.046462669	0.044891369	0.043055414	0.042054595	0.042054595	0.042054314
	11.0	0.050128428	0.048945549	0.047444168	0.046588800	0.046588800	0.0465883731
	00.6	0.043274339	0.040141159	0.036953330	0.035359776	0.035359776	0.035359706
	00.7	0.048412777	0.045610539	0.042648910	0.041130348	0.041130348	0.041130219
1.0	00.8	0.053336988	0.050928588	0.048268805	0.046866432	0.046866432	0.046866212
	00.9	0.058078336	0.056114211	0.053819267	0.052568244	0.052568244	0.052567893
	11.0	0.062660535	0.061181937	0.059305210	0.058236000	0.058236000	0.058235466

Employing the suggested analytical method, we obtain

$$\begin{aligned}\mathcal{Q}_0(\mathbf{w}_1,\varsigma) &= \mathbb{J}^{-1}\left[\frac{\phi(\varsigma)}{\psi^{\vartheta}(\varsigma)}\max\left(\exp\left(\mathbf{w}_1\right)-1,0\right)\right]\\ &= \max\left(\exp\left(\mathbf{w}_1\right)-1,0\right),\end{aligned}$$

$$\begin{aligned}\mathcal{Q}_1(\mathbf{w}_1,\varsigma) &= \mathbb{J}^{-1}\left[\frac{\vartheta+(1-\vartheta)\psi^{\vartheta}(\varsigma)}{\psi^{\vartheta}(\varsigma)\mathbb{A}(\vartheta)}\mathbb{J}\left[\left(\mathcal{Q}_0(\mathbf{w}_1,\varsigma)\right)_{\mathbf{w}_1\mathbf{w}_1}+(\eta-1)\left(\mathcal{Q}_0(\mathbf{w}_1,\varsigma)\right)_{\mathbf{w}_1}+\eta\mathcal{Q}_0\right]\right]\\ &= \frac{\left[\eta\max\left(\exp\left(\mathbf{w}_1\right),0\right)-\eta\max\left(\exp\left(\mathbf{w}_1-1\right),0\right)\right]}{\mathbb{A}(\vartheta)}\left[\vartheta\frac{\varsigma^{\vartheta}}{\Gamma(\vartheta+1)}+(1-\vartheta)\right],\end{aligned}$$

$$\begin{aligned}\mathcal{Q}_2(\mathbf{w}_1,\varsigma) &= \mathbb{J}^{-1}\left[\frac{\vartheta+(1-\vartheta)\psi^{\vartheta}(\varsigma)}{\psi^{\vartheta}(\varsigma)\mathbb{A}(\vartheta)}\mathbb{J}\left[\left(\mathcal{Q}_1(\mathbf{w}_1,\varsigma)\right)_{\mathbf{w}_1\mathbf{w}_1}+(\eta-1)\left(\mathcal{Q}_1(\mathbf{w}_1,\varsigma)\right)_{\mathbf{w}_1}+\eta\mathcal{Q}_1\right]\right]\\ &= -\frac{\left[\eta^2\max\left(\exp\left(\mathbf{w}_1\right),0\right)+\eta^2\max\left(\exp\left(\mathbf{w}_1-1\right),0\right)\right]}{\mathbb{A}^2(\vartheta)}\\ &\quad\cdot\left[\vartheta^2\frac{\varsigma^{2\vartheta}}{\Gamma(2\vartheta+1)}+2\vartheta(1-\vartheta)\frac{\varsigma^{\vartheta}}{\Gamma(\vartheta+1)}+(1-\vartheta)^2\right],\end{aligned}$$

$$\begin{aligned}\mathcal{Q}_3(\mathbf{w}_1,\varsigma) &= \mathbb{J}^{-1}\left[\frac{\vartheta+(1-\vartheta)\psi^{\vartheta}(\varsigma)}{\psi^{\vartheta}(\varsigma)\mathbb{A}(\vartheta)}\mathbb{J}\left[\left(\mathcal{Q}_2(\mathbf{w}_1,\varsigma)\right)_{\mathbf{w}_1\mathbf{w}_1}+(\eta-1)\left(\mathcal{Q}_2(\mathbf{w}_1,\varsigma)\right)_{\mathbf{w}_1}+\eta\mathcal{Q}_2\right]\right]\\ &= -\frac{\left[\eta^3\max\left(\exp\left(\mathbf{w}_1\right),0\right)+\eta^3\max\left(\exp\left(\mathbf{w}_1-1\right),0\right)\right]}{\mathbb{A}^3(\vartheta)}\\ &\quad\times\left[\vartheta^3\frac{\varsigma^{3\vartheta}}{\Gamma(3\vartheta+1)}+3\vartheta^2(1-\vartheta)\frac{\varsigma^{2\vartheta}}{\Gamma(2\vartheta+1)}+3\vartheta(1-\vartheta)^2\frac{\varsigma^{\vartheta}}{\Gamma(\vartheta+1)}+(1-\vartheta)^3\right].\end{aligned}$$

$$\vdots\,. \tag{85}$$

The series form solution is

$$\mathcal{Q}(\mathbf{w}_1,\varsigma) = \mathcal{Q}_0(\mathbf{w}_1,\varsigma)+\mathcal{Q}_1(\mathbf{w}_1,\varsigma)+\mathcal{Q}_2(\mathbf{w}_1,\varsigma)+\mathcal{Q}_3(\mathbf{w}_1,\varsigma)+\cdots. \tag{86}$$

Consequently, we have

$$\begin{aligned}\mathcal{Q}(\mathbf{w}_1,\varsigma) &= \mathcal{Q}_0(\mathbf{w}_1,\varsigma)+\mathcal{Q}_1(\mathbf{w}_1,\varsigma)+\mathcal{Q}_2(\mathbf{w}_1,\varsigma)+\mathcal{Q}_3(\mathbf{w}_1,\varsigma)+\cdots,\\ &= \max\left(\exp\left(\mathbf{w}_1-1\right),0\right)\left[1-\frac{\eta}{\mathbb{A}(\vartheta)}\left[\vartheta\frac{\varsigma^{\vartheta}}{\Gamma(\vartheta+1)}+\vartheta\right]\right.\\ &\quad\left.-\frac{\eta^2}{\mathbb{A}^2(\vartheta)}\left[\vartheta^2\frac{\varsigma^{2\vartheta}}{\Gamma(2\vartheta+1)}+2\vartheta(1-\vartheta)\frac{\varsigma^{\vartheta}}{\Gamma(\vartheta+1)}+(1-\vartheta)^2\right]-\cdots\right]\\ &\quad+\max\left(\exp\left(\mathbf{w}_1\right),0\right)\left[-\frac{\eta}{\mathbb{A}(\vartheta)}\left[\vartheta\frac{\varsigma^{\vartheta}}{\Gamma(\vartheta+1)}+\vartheta\right]\right.\\ &\quad\left.-\frac{\eta^2}{\mathbb{A}^2(\vartheta)}\left[\vartheta^2\frac{\varsigma^{2\vartheta}}{\Gamma(2\vartheta+1)}+2\vartheta(1-\vartheta)\frac{\varsigma^{\vartheta}}{\Gamma(\vartheta+1)}+(1-\vartheta)^2\right]-\cdots\right].\end{aligned} \tag{87}$$

Example 4 (see [20]). Assume the time-fractional one-dimensional BSM (6) subject to IC (7).

Table 6: The comparsion analysis among HPM [14], $\mathrm{JDM}_{\mathrm{CFD}}$, and $\mathrm{JDM}_{\mathrm{ABC}}$ of Example 2 for approximated results of $\mathcal{Q}(\mathbf{w}_1, \varsigma)$ and absolute error $E_{\mathrm{abs}} = \|E^{\mathrm{exact}} - E^{\mathrm{approx}}\|$ at $\vartheta = 1$ with varying $\mathbf{w}_1$ and ς.

$\mathbf{w}_1$	ς	$\|\mathrm{Exact} - \mathrm{HPM}\|$	$\|\mathrm{Exact} - \mathrm{JDM}_{\mathrm{CFD}}\|$	$\|\mathrm{Exact} - \mathrm{JDM}_{\mathrm{ABC}}\|$
0.2	0.1	3.00450×10^{-10}	2.00000×10^{-11}	2.00000×10^{-11}
	0.2	2.00000×10^{-9}	1.80000×10^{-10}	1.80000×10^{-10}
	0.3	9.50000×10^{-9}	8.80000×10^{-10}	8.80000×10^{-10}
	0.4	3.89000×10^{-8}	2.76000×10^{-9}	2.76000×10^{-9}
	0.5	7.70000×10^{-8}	6.70000×10^{-9}	6.70000×10^{-9}
0.4	0.1	5.780000×10^{-10}	4.00000×10^{-11}	4.00000×10^{-11}
	0.2	4.80000×10^{-9}	3.60000×10^{-10}	3.60000×10^{-10}
	0.3	2.98000×10^{-8}	1.76000×10^{-9}	1.76000×10^{-9}
	0.4	6.45000×10^{-8}	5.52000×10^{-9}	5.52000×10^{-9}
	0.5	2.47000×10^{-7}	1.34000×10^{-8}	1.34000×10^{-8}
0.6	0.1	7.96600×10^{-10}	6.00000×10^{-11}	6.00000×10^{-11}
	0.2	6.785000×10^{-9}	5.40000×10^{-10}	5.40000×10^{-10}
	0.3	3.98000×10^{-8}	2.64000×10^{-9}	2.64000×10^{-9}
	0.4	9.31000×10^{-8}	8.28000×10^{-9}	8.28000×10^{-9}
	0.5	3.003000×10^{-7}	2.01000×10^{-8}	2.01000×10^{-8}
0.8	0.1	9.890000×10^{-10}	8.00000×10^{-11}	8.00000×10^{-11}
	0.2	9.80000×10^{-9}	7.20000×10^{-10}	7.20000×10^{-10}
	0.3	4.94000×10^{-8}	3.52000×10^{-9}	3.52000×10^{-9}
	0.4	2.89000×10^{-7}	1.10400×10^{-8}	1.10400×10^{-8}
	0.5	3.60089×10^{-7}	2.68000×10^{-8}	2.68000×10^{-8}
1.0	0.1	2.9900×10^{-9}	1.00000×10^{-10}	1.00000×10^{-10}
	0.2	11.00011×10^{-9}	9.00000×10^{-10}	9.00000×10^{-10}
	0.3	6.40000×10^{-8}	4.40000×10^{-9}	4.40000×10^{-9}
	0.4	2.87000×10^{-7}	1.38000×10^{-8}	1.38000×10^{-8}
	0.5	4.89000×10^{-7}	3.35000×10^{-8}	3.35000×10^{-8}

Case 1. First, we surmise the Caputo fractional derivative operator for (6) with the new iterative transform method via the Jafari transform.

Implementing the Jafari transform to (6) with IC (7), we have

$$\begin{aligned}\psi^{\vartheta}(\varsigma)\mathbb{J}[\mathcal{Q}(\mathbf{w}_1,\varsigma)] &= \phi(\varsigma)\sum_{q=0}^{q-1}\psi^{\vartheta-1-q}(\varsigma)\mathcal{Q}^{(q)}(0)\\ &+ \mathbb{J}\left[-0.08(2+\sin\mathbf{w}_1)^2\mathbf{w}_1^2\frac{\partial^2\mathcal{Q}(\mathbf{w}_1,\varsigma)}{\partial\mathbf{w}_1^2}\right.\\ &\left.-0.06\mathbf{w}_1\frac{\partial\mathcal{Q}(\mathbf{w}_1,\varsigma)}{\partial\mathbf{w}_1}+0.06\mathcal{Q}(\mathbf{w}_1,\varsigma)\right].\end{aligned} \tag{88}$$

Correspondingly, we get:

$$\begin{aligned}\mathbb{J}[\mathcal{Q}(\mathbf{w}_1,\varsigma)] &= \frac{\phi(\varsigma)}{\psi^{\vartheta}(\varsigma)}\max\left(\mathbf{w}_1-25\exp\left(-0.06\right),0\right)+\frac{1}{\psi^{\vartheta}(\varsigma)}\\ &\cdot\mathbb{J}\left[-0.08(2+\sin\mathbf{w}_1)^2\mathbf{w}_1^2\frac{\partial^2\mathcal{Q}(\mathbf{w}_1,\varsigma)}{\partial\mathbf{w}_1^2}\right.\\ &\left.-0.06\mathbf{w}_1\frac{\partial\mathcal{Q}(\mathbf{w}_1,\varsigma)}{\partial\mathbf{w}_1}+0.06\mathcal{Q}(\mathbf{w}_1,\varsigma)\right].\end{aligned} \tag{89}$$

Employing the suggested analytical method, we obtain

$$\begin{aligned}\mathcal{Q}_0(\mathbf{w}_1,\varsigma) &= \mathbb{J}^{-1}\left[\frac{\phi(\varsigma)}{\psi^{\vartheta}(\varsigma)}\max\left(\mathbf{w}_1-25\exp\left(-0.06\right),0\right)\right]\\ &= \max\left(\mathbf{w}_1-25\exp\left(-0.06\right),0\right),\end{aligned}$$

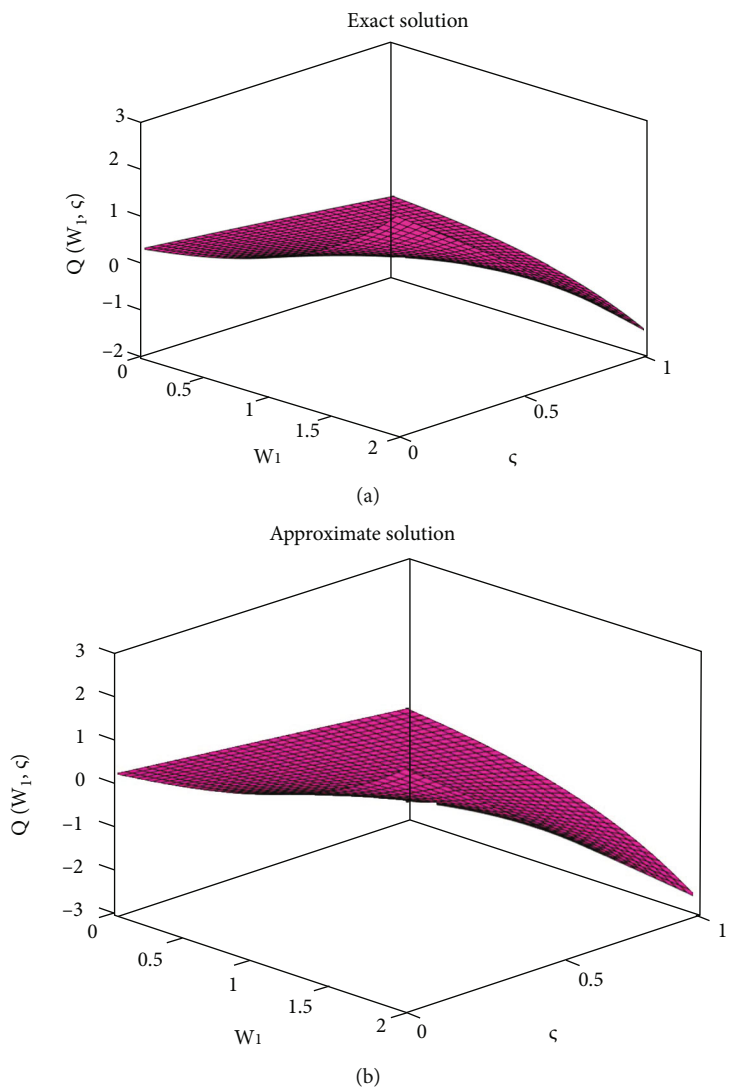

Figure 1: Three-dimensional illustration of the exact and approximate solution via CFD of Example 1 when $\vartheta = 1$.

$$\begin{aligned}\mathcal{Q}_1(\mathbf{w}_1,\varsigma) &= \mathbb{J}^{-1}\left[\frac{1}{\psi^{\vartheta}(\varsigma)}\mathbb{J}\left[-0.08(2+\sin\mathbf{w}_1)^2\mathbf{w}_1^2(\mathcal{Q}_0(\mathbf{w}_1,\varsigma))_{\mathbf{w}_1\mathbf{w}_1}\right.\right.\\ &\quad\left.\left.-0.06\mathbf{w}_1(\mathcal{Q}_0(\mathbf{w}_1,\varsigma))_{\mathbf{w}_1}-0.06\mathcal{Q}_0\right]\right]\\ &= [-0.06\mathbf{w}_1+0.06\max(\mathbf{w}_1-25\exp(-0.06),0)]\,\mathbb{J}^{-1}\left[\frac{\phi(\mathfrak{s})}{\psi^{\vartheta+1}(\mathfrak{s})}\right]\\ &= [-0.06\mathbf{w}_1+0.06\max(\mathbf{w}_1-25\exp(-0.06),0)]\frac{\varsigma^{\vartheta}}{\Gamma(\vartheta+1)},\end{aligned}$$

$$\begin{aligned}\mathcal{Q}_2(\mathbf{w}_1,\varsigma) &= \mathbb{J}^{-1}\left[\frac{1}{\psi^{\vartheta}(\varsigma)}\mathbb{J}\left[-0.08(2+\sin\mathbf{w}_1)^2\mathbf{w}_1^2(\mathcal{Q}_1(\mathbf{w}_1,\varsigma))_{\mathbf{w}_1\mathbf{w}_1}\right.\right.\\ &\quad\left.\left.-0.06\mathbf{w}_1(\mathcal{Q}_1(\mathbf{w}_1,\varsigma))_{\mathbf{w}_1}-0.06\mathcal{Q}_1\right]\right]\\ &= [-0.0036\mathbf{w}_1+0.0036\max(\mathbf{w}_1-25\exp(-0.06),0)]\frac{\varsigma^{2\vartheta}}{\Gamma(2\vartheta+1)},\end{aligned}$$

$$\begin{aligned}\mathcal{Q}_3(\mathbf{w}_1,\varsigma) &= \mathbb{J}^{-1}\left[\frac{1}{\psi^{\vartheta}(\varsigma)}\mathbb{J}\left[-0.08(2+\sin\mathbf{w}_1)^2\mathbf{w}_1^2(\mathcal{Q}_2(\mathbf{w}_1,\varsigma))_{\mathbf{w}_1\mathbf{w}_1}\right.\right.\\ &\quad\left.\left.-0.06\mathbf{w}_1(\mathcal{Q}_2(\mathbf{w}_1,\varsigma))_{\mathbf{w}_1}-0.06\mathcal{Q}_2\right]\right]\\ &= [-0.000216\mathbf{w}_1+0.00216\max(\mathbf{w}_1-25\exp(-0.06),0)]\frac{\varsigma^{3\vartheta}}{\Gamma(3\vartheta+1)}.\\ &\vdots\,.\end{aligned} \tag{90}$$

The series form solution is

$$\mathcal{Q}(\mathbf{w}_1,\varsigma) = \mathcal{Q}_0(\mathbf{w}_1,\varsigma)+\mathcal{Q}_1(\mathbf{w}_1,\varsigma)+\mathcal{Q}_2(\mathbf{w}_1,\varsigma)+\mathcal{Q}_3(\mathbf{w}_1,\varsigma)+\cdots. \tag{91}$$

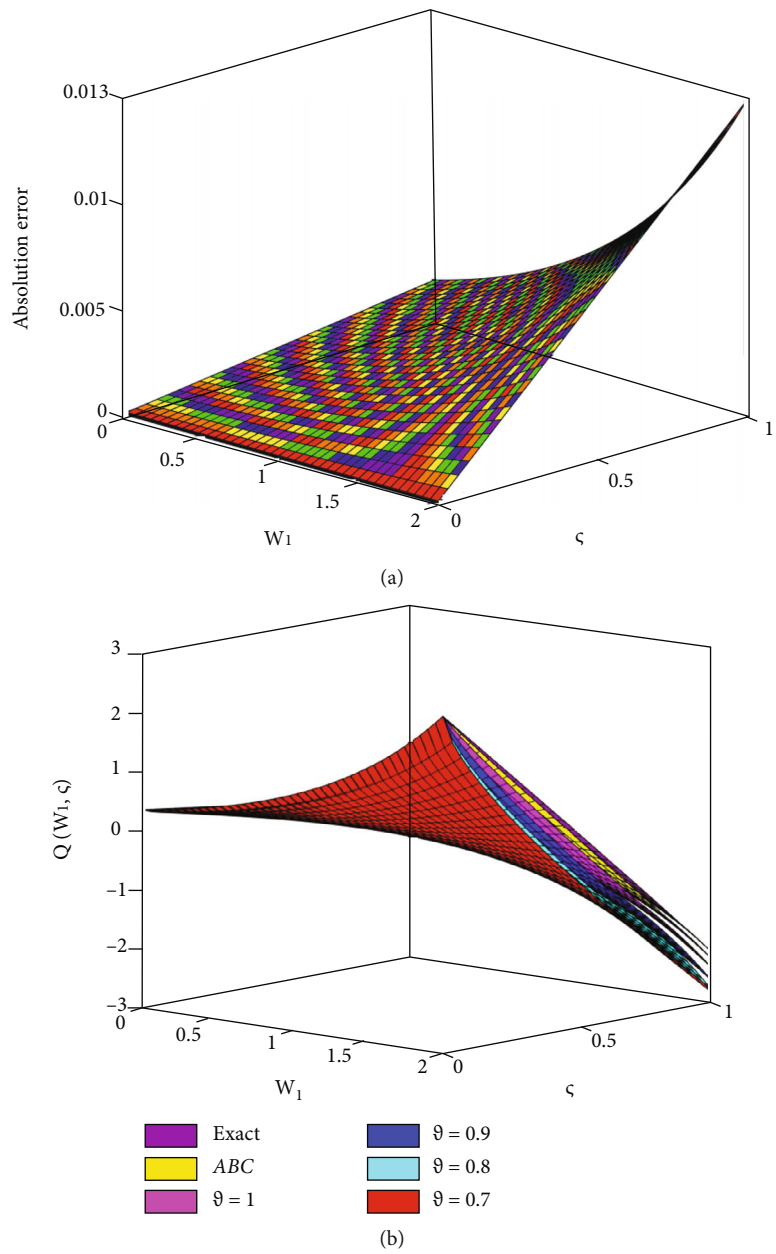

Figure 2: Three-dimensional illustration of the absolute error and multiple surface plots of Example 1 via CFD for varying fractional orders.

Consequently, we have

$$\begin{aligned}\mathcal{Q}(\mathbf{w}_1,\varsigma) &= \mathcal{Q}_0(\mathbf{w}_1,\varsigma) + \mathcal{Q}_1(\mathbf{w}_1,\varsigma) + \mathcal{Q}_2(\mathbf{w}_1,\varsigma) + \mathcal{Q}_3(\mathbf{w}_1,\varsigma)+\cdots,\\ &= \max\left(\mathbf{w}_1 - 25\exp(-0.06), 0\right) + \left(\mathbf{w}_1 - \max\left(\mathbf{w}_1 - 25\exp(-0.06)\right)\right)\\ &\quad\times\left[1 - 1 - \frac{0.06\varsigma^{\vartheta}}{\Gamma(\vartheta+1)} - \frac{0.0036\varsigma^{2\vartheta}}{\Gamma(2\vartheta+1)} - \frac{0.000216\varsigma^{3\vartheta}}{\Gamma(3\vartheta+1)}+\cdots\right]\\ &= \max\left(\mathbf{w}_1 - 25\exp(-0.06), 0\right) + \left(\mathbf{w}_1 - \max\left(\mathbf{w}_1 - 25\exp(-0.06)\right)\right)\\ &\quad\cdot\left[1 - E_{\vartheta}\left(0.06(\varsigma)^{\vartheta}\right)\right].\end{aligned} \tag{92}$$

Case 2. Now, we consider the ABC fractional derivative operator for (6) with the new iterative transform method via the Jafari transform.

Implementing the Jafari transform to (6) with IC (7), we have

$$\begin{aligned}\frac{\psi^{\vartheta}(\varsigma)\mathbb{A}(\vartheta)}{\vartheta + (1-\vartheta)\psi^{\vartheta}(\varsigma)}\mathbb{J}[\mathcal{Q}(\mathbf{w}_1,\varsigma)] &= \phi(\varsigma)\sum_{q=0}^{q-1}\psi^{\vartheta-1-q}(\varsigma)\mathcal{Q}^{(q)}(0)\\ &+ \mathbb{J}\left[-0.08(2+\sin\mathbf{w}_1)^2\mathbf{w}_1^2\frac{\partial^2\mathcal{Q}(\mathbf{w}_1,\varsigma)}{\partial\mathbf{w}_1^2}\right.\\ &\left.- 0.06\mathbf{w}_1\frac{\partial\mathcal{Q}(\mathbf{w}_1,\varsigma)}{\partial\mathbf{w}_1} + 0.06\mathcal{Q}(\mathbf{w}_1,\varsigma)\right].\end{aligned} \tag{93}$$

Correspondingly, we get

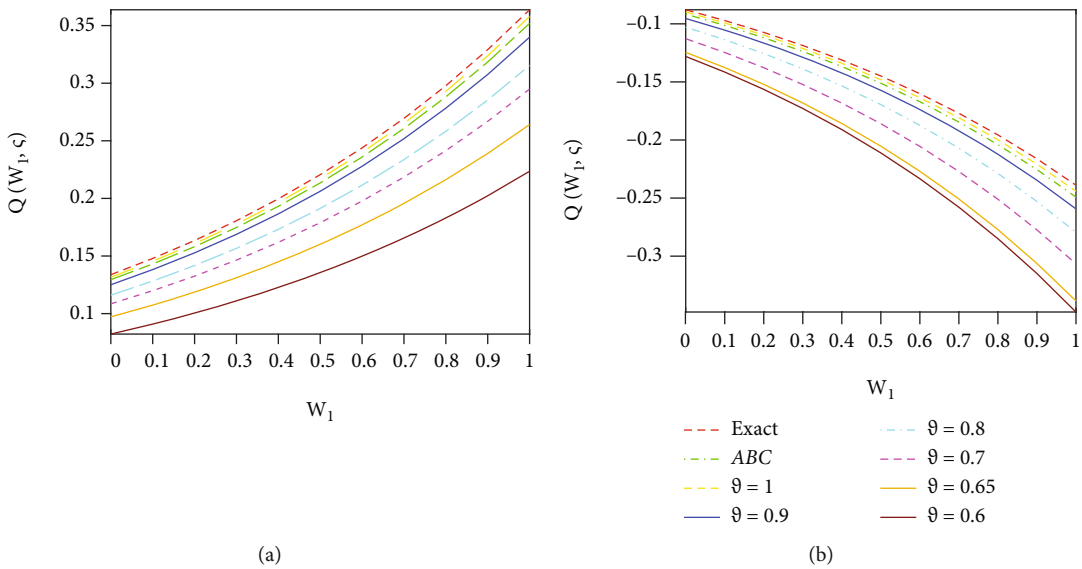

Figure 3: Two-dimensional illustration of the exact, approximate solution via CFD, and ABC fractional derivative operator of Example 1 with varying fractional orders at (a) $\varsigma = 0.7$ and (b) $\varsigma = 0.3$.

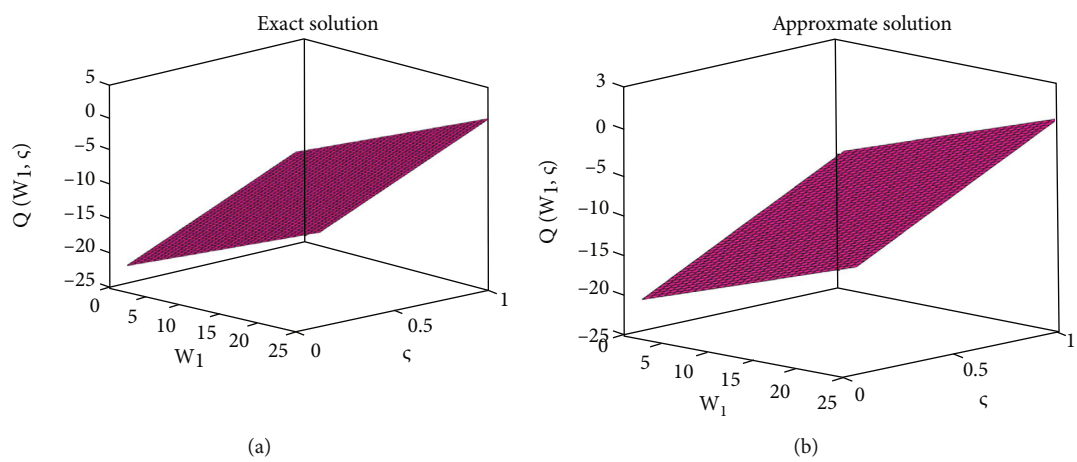

Figure 4: Three-dimensional illustration of the exact and approximate solution via CFD of Example 1 when $\vartheta = 1$.

$$\mathbb{J}[\mathcal{Q}(\mathbf{w}_1,\varsigma)] = \frac{\phi(\varsigma)}{\psi^{\vartheta}(\varsigma)} \max\left(\mathbf{w}_1 - 25\exp(-0.06), 0\right) + \frac{\vartheta + (1-\vartheta)\psi^{\vartheta}(\varsigma)}{\psi^{\vartheta}(\varsigma)\mathbb{A}(\vartheta)} \mathbb{J}\left[-0.08(2+\sin\mathbf{w}_1)^2\mathbf{w}_1^2\frac{\partial^2\mathcal{Q}(\mathbf{w}_1,\varsigma)}{\partial\mathbf{w}_1^2} - 0.06\mathbf{w}_1\frac{\partial\mathcal{Q}(\mathbf{w}_1,\varsigma)}{\partial\mathbf{w}_1} + 0.06\mathcal{Q}(\mathbf{w}_1,\varsigma)\right]. \tag{94}$$

Employing the suggested analytical method, we obtain

$$\mathcal{Q}_0(\mathbf{w}_1,\varsigma) = \mathbb{J}^{-1}\left[\frac{\phi(\varsigma)}{\psi^{\vartheta}(\varsigma)} \max\left(\mathbf{w}_1 - 25\exp(-0.06), 0\right)\right] = \max\left(\mathbf{w}_1 - 25\exp(-0.06), 0\right),$$

$$\begin{aligned}\mathcal{Q}_1(\mathbf{w}_1,\varsigma) &= \mathbb{J}^{-1}\left[\frac{\vartheta + (1-\vartheta)\psi^{\vartheta}(\varsigma)}{\psi^{\vartheta}(\varsigma)\mathbb{A}(\vartheta)} \mathbb{J}\left[-0.08(2+\sin\mathbf{w}_1)^2\mathbf{w}_1^2(\mathcal{Q}_0(\mathbf{w}_1,\varsigma))_{\mathbf{w}_1\mathbf{w}_1} - 0.06\mathbf{w}_1(\mathcal{Q}_0(\mathbf{w}_1,\varsigma))_{\mathbf{w}_1} - 0.06\mathcal{Q}_0\right]\right] \\ &= \frac{\left[-0.06\mathbf{w}_1 + 0.06\max\left(\mathbf{w}_1 - 25\exp(-0.06), 0\right)\right]}{\mathbb{A}(\vartheta)} \cdot \left[\vartheta\frac{\varsigma^{\vartheta}}{\Gamma(\vartheta+1)} + (1-\vartheta)\right],\end{aligned}$$

$$\begin{aligned}\mathcal{Q}_2(\mathbf{w}_1,\varsigma) &= \mathbb{J}^{-1}\left[\frac{\vartheta + (1-\vartheta)\psi^{\vartheta}(\varsigma)}{\psi^{\vartheta}(\varsigma)\mathbb{A}(\vartheta)} \mathbb{J}\left[-0.08(2+\sin\mathbf{w}_1)^2\mathbf{w}_1^2(\mathcal{Q}_1(\mathbf{w}_1,\varsigma))_{\mathbf{w}_1\mathbf{w}_1} - 0.06\mathbf{w}_1(\mathcal{Q}_1(\mathbf{w}_1,\varsigma))_{\mathbf{w}_1} - 0.06\mathcal{Q}_1\right]\right] \\ &= \frac{\left[-0.0036\mathbf{w}_1 + 0.0036\max\left(\mathbf{w}_1 - 25\exp(-0.06), 0\right)\right]}{\mathbb{A}^2(\vartheta)} \cdot \left[\vartheta^2\frac{\varsigma^{2\vartheta}}{\Gamma(2\vartheta+1)} + 2\vartheta(1-\vartheta)\frac{\varsigma^{\vartheta}}{\Gamma(\vartheta+1)} + (1-\vartheta)^2\right],\end{aligned}$$

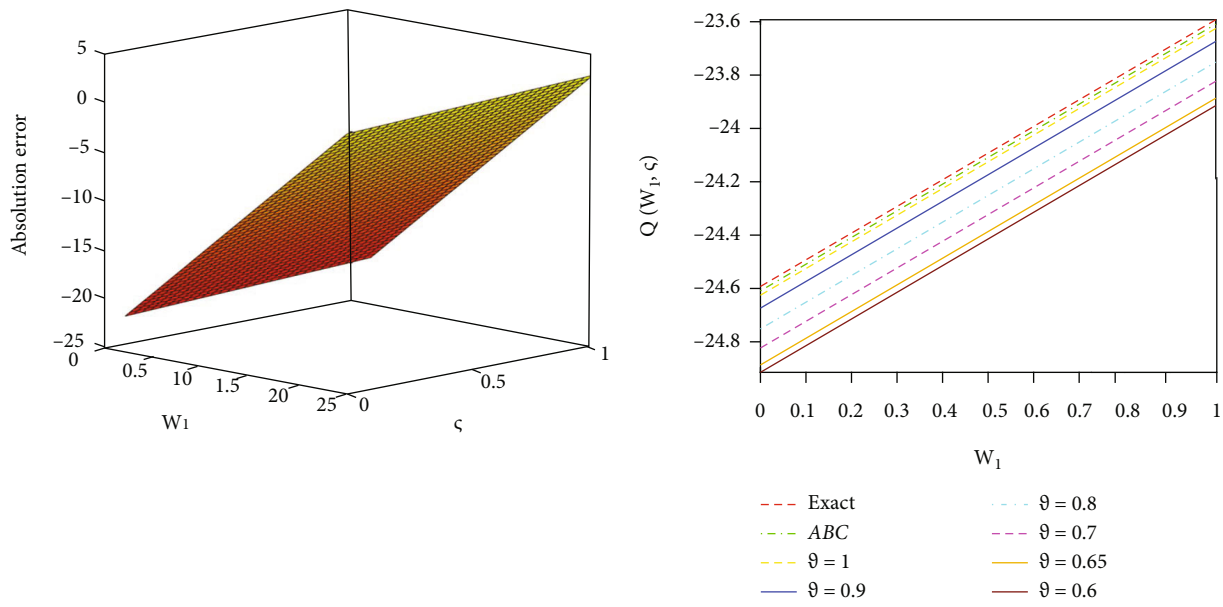

(a) (b)

Figure 5: (a) Three-dimensional illustration of the absolute error plot of Example 1 when $\vartheta = 1$. (b) Two-dimensional illustration of the of Example 1 for varying fractional orders when $\varsigma = 0.7$.

$$\begin{aligned}
\mathcal{Q}_3(\mathbf{w}_1,\varsigma) &= \mathbb{J}^{-1}\left[\frac{\vartheta+(1-\vartheta)\psi^{\vartheta}(\varsigma)}{\psi^{\vartheta}(\varsigma)\mathbb{A}(\vartheta)}\mathbb{J}\left[-0.08(2+\sin\mathbf{w}_1)^2\mathbf{w}_1^2(\mathcal{Q}_2(\mathbf{w}_1,\varsigma))_{\mathbf{w}_1\mathbf{w}_1}\right.\right.\\
&\quad\left.\left.-0.06\mathbf{w}_1(\mathcal{Q}_2(\mathbf{w}_1,\varsigma))_{\mathbf{w}_1}-0.06\mathcal{Q}_2\right]\right]\\
&= -\frac{[-0.000216\mathbf{w}_1+0.00216\max(\mathbf{w}_1-25\exp(-0.06),0)]}{\mathbb{A}^3(\vartheta)}\\
&\quad\times\left[\vartheta^3\frac{\varsigma^{3\vartheta}}{\Gamma(3\vartheta+1)}+3\vartheta^2(1-\vartheta)\frac{\varsigma^{2\vartheta}}{\Gamma(2\vartheta+1)}\right.\\
&\quad\left.+3\vartheta(1-\vartheta)^2\frac{\varsigma^{\vartheta}}{\Gamma(\vartheta+1)}+(1-\vartheta)^3\right].\\
&\quad\vdots\,.
\end{aligned}\tag{95}$$

The series form solution is

$$\mathcal{Q}(\mathbf{w}_1,\varsigma) = \mathcal{Q}_0(\mathbf{w}_1,\varsigma)+\mathcal{Q}_1(\mathbf{w}_1,\varsigma)+\mathcal{Q}_2(\mathbf{w}_1,\varsigma)+\mathcal{Q}_3(\mathbf{w}_1,\varsigma)+\cdots.\tag{96}$$

Consequently, we have

$$\begin{aligned}
\mathcal{Q}(\mathbf{w}_1,\varsigma) &= \mathcal{Q}_0(\mathbf{w}_1,\varsigma)+\mathcal{Q}_1(\mathbf{w}_1,\varsigma)+\mathcal{Q}_2(\mathbf{w}_1,\varsigma)+\mathcal{Q}_3(\mathbf{w}_1,\varsigma)\\
&\quad+\cdots,=\max(\mathbf{w}_1-25\exp(-0.06),0)\\
&\quad-\frac{0.06\mathbf{w}_1-0.06\max(\mathbf{w}_1-25\exp(-0.06),0)}{\mathbb{A}(\vartheta)}\left[\vartheta\frac{\varsigma^{\vartheta}}{\Gamma(\vartheta+1)}+\vartheta\right]\\
&\quad-\frac{0.0036\mathbf{w}_1-0.0036\max(\mathbf{w}_1-25\exp(-0.06),0)}{\mathbb{A}^2(\vartheta)}\\
&\quad\cdot\left[\vartheta^2\frac{\varsigma^{2\vartheta}}{\Gamma(2\vartheta+1)}+2\vartheta(1-\vartheta)\frac{\varsigma^{\vartheta}}{\Gamma(\vartheta+1)}+(1-\vartheta)^2\right]-\cdots.
\end{aligned}\tag{97}$$

6. Results and Discussion

Two distinctive techniques have been used to analyse the exact approximate solution of time-fractional BSM in this investigation. With MATLAB package 21, exact analytical solutions for the Black–Scholes option pricing models are presented via the CFD and ABC fractional derivative operators at any order for varying values of space and time.

For the solution in Examples 1 and 3, we conducted simulation studies for several Brownian movements with varied values of $\mathbf{w}1$ and ς in Tables 1 and 2. Table 3 exibits a numerical comparative analysis of the Homotopy perturbation approach and the Jafari decomposition method in perspective of absolute error for (4) taking into consideration both fractional derivative operators.

The findings of a simulation study for the BSM considered in Examples 2 and 4 are shown in Tables 4 and 5. The comparative analysis of the homotopy perturbation with the projected methods is represented in Table 6. This comparison clearly illustrates that the synthesised trajectories are more powerful and effective than the existing ones.

Figure 1 depicts the behavior of the Jafari decomposition method's outcome from $\mathcal{Q}(\mathbf{w}1,\varsigma)$ for Example 1. Figures 1(a) and 1(b) demonstrates the behavior of exact and approximate solutions of Black-Scholes option pricing models via the CFD operator, whereas Figures 2(a) and 2(b) depicts the absolute errors behavior and fractional-order variation of $\mathcal{Q}(\mathbf{w}_1,\varsigma)$. The different fractional orders at $\vartheta = 0.7, 0.8, 0.9, 1$ behave analogously. In the same way, Figures 3(a) and 3(b) represent the two-dimensional options graphically of the obtained result $\mathcal{Q}(\mathbf{w}_1,\varsigma)$ for (4) at $\varsigma = 0.7$ and $\varsigma = 0.3$.

Continuing in the same manner, Figures 4(a) and 4(b) illustrates the exact -approximate consequences $\mathcal{Q}(\mathbf{w}_1,\varsigma)$

for (1.6) by the use of Jafari decomposition method the values of the options graphically. Figures 5(a) and 5(b) show the absolute error and response of acquired data for (6) with various standard and Brownian motions of 0.6,0.65,0.7,0.8,0.9, and 1, respectively. Thus, we conclude that the order of the profile pictures increases as the value of the time-dependent variable increases. It is worth mentioning that the fractional order has an acceleration effect on the diffusion processes.

7. Conclusions

This article has investigated the more general integral transform with the Adomian decomposition method and new iterative transform method. The Caputo and ABC fractional derivative operators have been implemented to deal with the BSM. Several distinct solutions have been proposed with the assumption of fractional orders. Various representations have been used to understand these solutions, which have clarified the significant properties of the fractional models in consideration. Without any restrictive assumptions, discretization, or linearization, the proposed methodology locates solutions. Elegance and originality have been invoked to describe our trajectory. Contrasting proposed findings to those acquired in earlier scholarly articles demonstrate the specificality of our solutions in the European option pricing model. The strategy's powerful and successful implementation is explored and validated in order to demonstrate its applicability to additional nonlinear evolution equations that arise in banking and finance issues.

Data Availability

No data were used to support this study.

Conflicts of Interest

The authors declare that they have no competing interests.

Authors' Contributions

All authors read and approved the final manuscript.

References

[1] M. Caputo and M. Fabrizio, "A new definition of fractional derivative without singular kernel," *Progress in Fractional Differentiation and Applications*, vol. 73, pp. 1–13, 2015.

[2] A. Atangana and D. Baleanu, "New fractional derivatives with nonlocal and non-singular kernel: theory and application to heat transfer model," *Thermal Science*, vol. 20, no. 2, pp. 763–769, 2016.

[3] R. Scherer, S. L. Kalla, Y. Tang, and J. Huang, "The Grunwald-Letnikov method for fractional differential equations," *Computers & Mathematcs with Applications*, vol. 62, no. 3, pp. 902–917, 2011.

[4] C. Li, D. Qian, and Y. Q. Chen, "On Riemann-Liouville and Caputo derivatives," *Discrete Dynamics in Nature and Society*, vol. 2011, Article ID 562494, 15 pages, 2011.

[5] V. F. Morales-Delgado, J. F. Gómez-Aguilar, H. Yépez-Martínez, D. Baleanu, R. F. Escobar-Jimenez, and V. H. Olivares-Peregrino, "Laplace homotopy analysis method for solving linear partial differential equations using a fractional derivative with and without kernel singular," *Advances in Difference Equations*, vol. 2016, no. 1, Article ID 164, 2016.

[6] N. A. Sheikh, F. Ali, M. Saqib et al., "Comparison and analysis of the Atangana-Baleanu and Caputo-Fabrizio fractional derivatives for generalized Casson fluid model with heat generation and chemical reaction," *Results in Physics*, vol. 7, pp. 789–800, 2017.

[7] A. Atangana and B. S. T. Alkahtani, "New model of groundwater flowing within a confine aquifer: application of Caputo-Fabrizio derivative," *Arabian Journal of Geosciences*, vol. 9, no. 1, 2016.

[8] D. Kumar, J. Singh, D. Baleanu, and Sushila, "Analysis of regularized long-wave equation associated with a new fractional operator with Mittag-Leffler type kernel," *Physica A*, vol. 492, pp. 155–167, 2018.

[9] J. Singh, D. Kumar, and D. Baleanu, "On the analysis of chemical kinetics system pertaining to a fractional derivative with Mittag-Leffler type kernel," *Chaos*, vol. 27, no. 10, article 103113, 2017.

[10] N. H. Luc, D. Baleanu, L. D. Long, and N. H. Can, "Reconstructing the right-hand side of a fractional subdiffusion equation from the final data," *Journal of Inequalities and Applications*, vol. 2020, no. 1, Article ID 53, 2020.

[11] A. I. el-Mesady, Y. S. Hamed, and A. M. Alsharif, "Jafari transformation for solving a system of ordinary differential equations with medical application," *Fractal and Fractional*, vol. 5, no. 3, p. 130, 2021.

[12] S. Rashid, K. T. Kubra, A. Rauf, Y. M. Chu, and Y. S. Hamed, "New numerical approach for time-fractional partial differential equations arising in physical system involving natural decomposition method," *Physica Scripta*, vol. 96, no. 10, p. 105204, 2021.

[13] S. Farid, R. Nawaz, Z. Shah, S. Islam, and W. Deebani, "New iterative transform method for time and space fractional $(n+1)$-dimensional heat and wave type equations," *Fractals*, vol. 29, no. 3, p. 2150056, 2021.

[14] A. N. Fall, S. N. Ndiaye, and N. Sene, "Black-Scholes option pricing equations described by the Caputo generalized fractional derivative," *Chaos, Solitons & Fractals*, vol. 125, pp. 108–118, 2019.

[15] H. A. Zedan and E. Alaidarous, "Haar wavelet method for the system of integral equations," *Abstract and Applied Analysis*, vol. 2014, Article ID 418909, 9 pages, 2014.

[16] N. Özdemir and M. Yavuz, "Numerical solution of fractional Black–Scholes equation by using the multivariate padé approximation," *Acta physica Polonica*, vol. 132, no. 3-II, pp. 1050–1053, 2017.

[17] O. Abu Arqub, M. al-Smadi, S. Momani, and T. Hayat, "Numerical solutions of fuzzy differential equations using reproducing kernel Hilbert space method," *Soft Computing*, vol. 20, no. 8, pp. 3283–3302, 2016.

[18] N. Ablaoui-Lahmar, O. Belhamitib, and S. M. Bahric, "A new Legendre wavelets decomposition method for solving PDEs," *Malaya Journal of Matematik*, vol. 1, no. 1, pp. 72–81, 2014.

[19] S. Kumar, M. Niwas, and A. M. Wazwaz, "Lie symmetry analysis, exact analytical solutions and dynamics of solitons

for $(2+1)$-dimensional NNV equations," *Physica Scripta*, vol. 95, no. 9, article 095204, 2020.

[20] Z. Cen and A. le, "A robust and accurate finite difference method for a generalized Black-Scholes equation," *Journal of Computational and Applied Mathematics*, vol. 235, no. 13, pp. 3728–3733, 2011.

[21] P. Wilmott, J. Dewynne, and S. Howison, *Option Pricing: Mathematical Models and Computation*, Oxford Financial Press, Oxford, 1993.

[22] C. Vazquez, "An upwind numerical approach for an American and European option pricing model," *Applied Mathematics and Computation*, vol. 97, no. 2-3, pp. 273–286, 1998.

[23] L. Meng and M. Wang, "Comparison of Black–Scholes formula with fractional Black–Scholes formula in the foreign exchange option market with changing volatility," *Asia-Pacific Financial Markets*, vol. 17, no. 2, pp. 99–111, 2010.

[24] Q. Fu, K. Wang, and X. Liu, "The foreign exchange option pricing based on the fractional Black–Scholes model and valuation," *Price Monthly*, vol. 369, pp. 68–70, 2008.

[25] M. B. Matadi and P. L. Zondi, "Invariant solutions of Black–Scholes equation with Ornstein–Uhlenbeck process," *Symmetry*, vol. 13, no. 5, p. 847, 2021.

[26] S. Kumar, D. Kumar, and J. Singh, "Numerical computation of fractional Black–Scholes equation arising in financial market," *Egyptian Journal of Basic and Applied Sciences*, vol. 1, no. 3-4, pp. 177–183, 2014.

[27] M. Yavuz and N. Özdemir, "A different approach to the European option pricing model with new fractional operator," *Mathematical Modelling of Natural Phenomena*, vol. 13, no. 1, p. 12, 2018.

[28] S. Rashid, Z. Hammouch, H. Aydi, A. G. Ahmad, and A. M. Alsharif, "Novel computations of the time-fractional Fisher's model via generalized fractional integral operators by means of the Elzaki transform," *Fractal and Fractional*, vol. 5, no. 3, p. 94, 2021.

[29] S. Rashid, K. T. Kubra, and J. L. G. Guirao, "Construction of an approximate analytical solution for multi-dimensional fractional Zakharov–Kuznetsov equation via Aboodh Adomian decomposition method," *Symmetry*, vol. 13, no. 8, p. 1542, 2021.

[30] H. Jafari, "A new general integral transform for solving integral equations," *Journal of Advanced Research*, vol. 32, pp. 133–138, 2020.

[31] V. Daftardar-Gejji and H. Jafari, "An iterative method for solving nonlinear functional equations," *Journal of Mathematical Analysis and Applications*, vol. 316, no. 2, pp. 753–763, 2006.

[32] I. Ullah, H. Khan, and M. T. Rahim, "Numerical solutions of fifth and sixth order nonlinear boundary value problems by Daftardar Jafari method," *Journal of Computational Engineering*, vol. 2014, Article ID 286039, 8 pages, 2014.

[33] K. Wang and S. Liu, "Application of new iterative transform method and modified fractional homotopy analysis transform method for fractional Fornberg-Whitham equation," *Journal of Nonlinear Sciences and Applications*, vol. 9, no. 5, pp. 2419–2433, 2016.

[34] S. Widatalla and M. Z. Liu, "New iterative method based on Laplace decomposition algorithm," *Journal of Applied Mathematics*, vol. 2013, Article ID 286529, 7 pages, 2013.

[35] L. Debnath and D. Bhatta, *Integral Transforms and Their Applications*, CRC Press, Boca Raton, FL, USA, 2014.

[36] F. Jarad and T. Abdeljawad, "A modified Laplace transform for certain generalized fractional operators," *Results in Nonlinear Analysis*, vol. 1, no. 2, pp. 88–98, 2018.

[37] G. K. Watugala, "Sumudu transform: a new integral transform to solve differential equations and control engineering problems," *International Journal of Mathematical Education in Science and Technology*, vol. 24, no. 1, pp. 35–43, 1993.

[38] K. S. Aboodh, "The new integral transform Aboodh transform," *The Global Journal of Pure and Applied Mathematics*, vol. 9, pp. 35–43, 2013.

[39] S. A. P. Ahmadi, H. Hosseinzadeh, and Y. A. Cherati, "A new integral transform for solving higher order linear ordinary differential equations," *Nonlinear Dynamics and Systems Theory*, vol. 19, no. 2, pp. 243–252, 2019.

[40] S. A. P. Ahmadi, H. Hosseinzadeh, and A. B. Y. Cherati, "A new integral transform for solving higher order linear ordinary Laguerre and Hermite differential equations," *International Journal of Applied and Computational Mathematics*, vol. 5, no. 5, 2019.

[41] T. M. Elzaki, "The new integral transform Elzaki transform," *Global Journal of Pure and Applied Sciences*, vol. 7, no. 1, pp. 57–64, 2011.

[42] Z. H. Khan and W. A. Khan, "N-transform properties and applications," *NUST Journal of Engineering Science*, vol. 1, no. 1, pp. 127–133, 2008.

[43] M. M. Abdelrahim Mahgoub, "The new integral transform Mohand transform," *The Advances in Theoretical and Applied Mathematics*, vol. 12, no. 2, pp. 113–120, 2017.

[44] M. M. Abdelrahim Mahgoub, "The new integral transform Sawi transform," *The Advances in Theoretical and Applied Mathematics*, vol. 14, no. 1, pp. 81–87, 2019.

[45] H. Kamal and A. Sedeeg, "The new integral transform Kamal transform," *The Advances in Theoretical and Applied Mathematics*, vol. 11, no. 4, pp. 451–458, 2016.

[46] H. Kim, "On the form and properties of an integral transform with strength in integral transforms," *Far East Journal of Mathematical Sciences*, vol. 102, no. 11, pp. 2831–2844, 2017.

[47] H. Kim, "The intrinsic structure and properties of Laplace-typed integral transforms," *Mathematical Problems in Engineering*, vol. 2017, Article ID 1762729, 8 pages, 2017.

[48] M. Meddahi, H. Jafari, and M. N. Ncube, "New general integral transform via Atangana–Baleanu derivatives," *Advances in Difference Equations*, vol. 2021, no. 1, Article ID 385, 2021.

[49] A. Atangana and I. Koca, "Chaos in a simple nonlinear system with Atangana-Baleanu derivatives with fractional order," *Chaos Solitons Fractals*, vol. 89, pp. 447–454, 2016.

[50] M. Yavuz and T. Abdeljawad, "Nonlinear regularized long-wave models with a new integral transformation applied to the fractional derivative with power and Mittag-Leffler kernel," *Advances in Difference Equations*, vol. 2020, no. 1, Article ID 367, 2020.

[51] A. Bokhari, "Application of Shehu transform to Atangana–Baleanu derivatives," *The Journal of Mathematics and Computer Science*, vol. 20, no. 2, pp. 101–107, 2020.

[52] M. G. Mittag-Leffler, "Sur la nouvelle fonction Ea(x)," *Comptes Rendus Académie des Sciences*, vol. 2, p. 1003, 1903.

[53] I. L. el-Kalla, "Convergence of the Adomian method applied to a class of nonlinear integral equations," *Applied Mathematics Letters*, vol. 21, no. 4, pp. 372–376, 2008.

Hindawi
Journal of Function Spaces
Volume 2021, Article ID 1111417, 12 pages
https://doi.org/10.1155/2021/1111417

Research Article

A Comparison Study of Numerical Techniques for Solving Ordinary Differential Equations Defined on a Semi-Infinite Domain Using Rational Chebyshev Functions

Mohamed A. Ramadan,[1] **Taha Radwan**,[2,3] **Mahmoud A. Nassar**,[4] **and Mohamed A. Abd El Salam**[4]

[1]*Mathematics & Computer Science Department, Faculty of Science, Menoufia University, Shebin El-Kom, Egypt*
[2]*Department of Mathematics, College of Science and Arts in Ar Rass, Qassim University, Ar Rass, Saudi Arabia*
[3]*Department of Mathematics and Statistics, Faculty of Management Technology and Information Systems, Port Said University, Port Said, Egypt*
[4]*Mathematics Department, Faculty of Science, Al-Azhar University, Nasr City, 11884 Cairo, Egypt*

Correspondence should be addressed to Taha Radwan; t.radwan@qu.edu.sa

Received 5 October 2021; Revised 16 November 2021; Accepted 17 November 2021; Published 7 December 2021

Academic Editor: Youssri Hassan Youssri

A rational Chebyshev (RC) spectral collocation technique is considered in this paper to solve high-order linear ordinary differential equations (ODEs) defined on a semi-infinite domain. Two definitions of the derivative of the RC functions are introduced as operational matrices. Also, a theoretical study carried on the RC functions shows that the RC approximation has an exponential convergence. Due to the two definitions, two schemes are presented for solving the proposed linear ODEs on the semi-infinite interval with the collocation approach. According to the convergence of the RC functions at the infinity, the proposed technique deals with the boundary value problem which is defined on semi-infinite domains easily. The main goal of this paper is to present a comparison study for differential equations defined on semi-infinite intervals using the proposed two schemes. To demonstrate the validity of the comparisons, three numerical examples are provided. The obtained numerical results are compared with the exact solutions of the proposed problems.

1. Introduction

In the spectral methods, the most common basis functions are Chebyshev polynomials (CPs), which play an important role in the interpolation problems. Many researchers considered CPs to solve differential equations in the finite domain $[-1, 1]$ (see [1–8] and [9]), but they often fail in the larger domain, also if the exact solution of the problem was in a rational form. For this reason, the rational Chebyshev (RC) functions are applied in the large domain $[0, l]$ where $l \longrightarrow \infty$, which provide a major success in dealing with differential equations (DEs) defined in the open domain $[0, l]$. Many researchers studied RC functions for treating man different problems of differential, integrodifferential equations (IDEs), partial, and some other physical-engineering problems as in [10, 11] and [12]. Abbasbandy et al. [13] applied the RC collocation method to get numerical solution of the magnetohydrodynamic flow (MHF) of an incompressible viscous fluid (VF) over a stretching sheet problem. Ramadan et al. in [14, 15] and [16], Yalçınbas et al. in [17], and Parand and Razzaghi in [18] are scrupulous in the use of RC functions to express the approximate solution of high-order ordinary differential equations (ODEs) by different spectral approaches. In [19], Parand and Razzaghi introduced RC functions for solving a population growth of a species within a closed system, named as a Volterra model, where the authors converted the Volterra population model first to an equivalent nonlinear ODE; the solution is approximated by the RC functions with the unknown coefficients. The authors of [20, 21] introduced the RC function

approximation with the collocation technique for solving the natural convection of the Darcian fluid (DF) about a vertical full cone embedded in porous media (PM) with a prescribed wall temperature. Ramadan et al. [22, 23] obtained an approximate solution of the applied collocation method based on RC functions to treat high-order linear IDEs with variable coefficients. In [24], the authors applied the RC collocation approach for approximating nonlinear biomathematical problems, namely, the systematic logistic growth, the Lotka-Volterra system (prey-predator model), the simple two-species Lotka-Volterra model, and the prey-predator model with limit cycle (periodic behavior).

All the aforementioned work either relied on the RC functions as a basis defined of an open interval or used it to treat a specific application or used truncated matrices. The truncation in matrices was handled for the first time by us in [15], and it was also an application on open period equations. In this work, a comparison study for solving linear ODEs defined on semi-infinite domains using a spectral collocation method is presented. The equation under investigation is a high-order nonhomogeneous linear variable coefficient ordinary differential equation defined on semi-infinite domain $[0, \infty)$. Two algorithms are considered by the collocation method with the RC functions as basis functions. The matrices of derivative for RC functions introduced with regular definition with truncation and improved one, which lead us to two different schemes. The collocation points that are used here are suggested by us, and they are defined on the interval $[0, \infty)$, which deal with the boundary value problems defend on $[0, \infty)$ or if one of the mixed conditions tends to infinity. So, we suggested new collocation points that are valid for dealing with a problem of this type.

2. Preliminaries

In this section, the definition and some properties of the RC functions are listed; also, the convergence for RC functions will be discussed.

The Chebyshev polynomials $T_n(x)$ are an orthonormal system in the closed interval [-1, 1], where the weight function for $T_n(x)$ is $w_T(x) = 1/\sqrt{1-x^2}$, and they may be generated using the recurrence formulae:

$$T_{n+1}(x) = 2xT_n(x) - T_{n-1}(x), \quad n \geq 1, \tag{1}$$

with the initials

$$T_0(x) = 1, T_1(x) = x. \tag{2}$$

For more details about $T_n(x)$, see Ref. [8].

2.1. The RC Functions. The RC functions are orthonormal on the open interval $[0, \infty)$, defined as

$$R_n(\chi) = T_n\left(\frac{x-1}{x+1}\right), \quad x = \cos\varphi, \varphi \in [0, \pi], \tag{3}$$

and they form an orthonormal set of functions with respect to the weight function $w_R(x) = x^{-1/2}(x+1)^{-1}$, and they can be generated with the aid of the following recurrence formulae:

$$R_{n+1}(x) = 2\left(\frac{x-1}{x+1}\right)R_n(x) - R_{n-1}(x), \quad n \geq 1, \tag{4}$$

with the initials

$$R_0(x) = 1, R_1(x) = \frac{x-1}{x+1}, \tag{5}$$

and the property of the orthogonality is

$$\int_0^\infty R_r(x)R_s(x)w_R(x)dx = \frac{c_s\pi}{2}\delta_{rs}, \tag{6}$$

where $c_0 = 2$, $c_s = 1$ for all $s \geq 1$ and δ_{rs} is the Kronecker delta function.

Let $\Omega = \{x : 0 \leq x < \infty\}$, and we note that $R_n(x)$ is the eigen function of the singular Sturm-Liouville problem of the following form:

$$w_R^{-1}(x)\frac{d}{dx}\left[w_R^{-1}(x)\frac{d}{dx}R_n(x)\right] + n^2R_n(x) = 0, \quad x \in \Omega. \tag{7}$$

2.2. Function Spaces. In this subsection, the order of convergence for RC functions will be discussed; let us begin with assuming that

$$L_w^2(\Omega) = \left\{\xi : \|\xi\|_w = \left(\int_0^\infty |\xi(x)|^2 w_R(x)dx\right)^{1/2} < \infty\right\}, \tag{8}$$

represent the space functions, and the inner product is denoted here as

$$\langle \alpha, \beta \rangle_{w_R}, \tag{9}$$

such that

$$\langle \varphi, \varphi \rangle_w = \left(\|\varphi\|_{w_R}\right)^2. \tag{10}$$

Subsequently, from the property of orthogonality (relation (6)), we get the fact that RC functions form a set of orthonormal basis of $L_w^2(\Omega)$. Also, let us define the normed spaces $H_w^r(\Omega)$ and $H_{w,A}^r(\Omega)$ as

$$H_{w_R}^r(\Omega) = \left\{\xi : \|\xi\|_{r,w_R} = \left(\sum_{k=0}^r \left\|\frac{d^k}{dx^k}\xi\right\|_{w_R}\right)^{1/2} < \infty\right\},$$
$$H_{w_R,\theta}^r(\Omega) = \left\{\xi : \|\xi\|_{r,w_R,\theta} = \left(\sum_{k=0}^r \left\|(x+1)^{r/2+k}\frac{d^k}{dx^k}\xi\right\|_{w_R}\right)^{1/2} < \infty\right\}, \tag{11}$$

where $r \geq 0$ and k is a positive integer constant, and we let θ be the Sturm-Liouville operator in (7), namely, it may be written as

$$\theta\xi = -w_R^{-1}\left(w_R^{-1}\xi'\right)'. \tag{12}$$

Let N be a positive integer such that $N < \infty$, and $\mathfrak{R}_N = \text{span}\{R_0, R_1, \cdots, R_N\}$.

Theorem 1. *For any $r \geq 0$, and c is a generic positive constant independent of any variable, and $\phi \in \mathfrak{R}_N$, then*

$$\|\xi\|_{r,w_R} \leq cN^{2r}\|\xi\|_{w_R}. \tag{13}$$

The proof of Theorem 1 is given in [25].

Since the set of RC functions is orthonormal and a complete set, we assume that $f(x)$ is defined over the space Ω; then, it be may expanded in terms of RC functions as

$$f(x) = \sum_{i=0}^{\infty} a_i R_i(x), \tag{14}$$

where

$$a_i = \frac{\langle f, R_i\rangle_{w_R}}{\left(\|R_i\|_{w_R}\right)^2} = \frac{2}{c_s\pi}\int_0^{\infty} f(x)R_i(x)w_R(x)dx. \tag{15}$$

Infinite series expression (14) represents as a spectral truncated approximation as follows

$$f_N(x) = \sum_{i=0}^{N} a_i R_i(x). \tag{16}$$

The order of convergence for the RC function approximation will be obtained using several orthonormal projections. From (16), it is clear that f_N is the orthogonal projection of f onto $\mathfrak{R}_N$ with respect to the inner product (10). For all of the above, especially Theorem 1, the following theorem is presented and contains the order of convergence of RC functions.

Theorem 2. *For any function f such that $f \in H^r_{w_R,\theta}(\Omega)$, where $r \geq 0$, there exists a positive constant c independent of N such that*

$$\|f_N - f\|_{r,w_R} \leq cN^{-r}\|f\|_{r,w_R,\theta}. \tag{17}$$

The complete proof of Theorem 2 is found in [13] (or see Ref. [25] for more details); this theorem shows that the RC approximation has exponential convergence.

2.3. Operational Matrix. This subsection introduces the form of operational matrix for the RC functions; the derivative of the vector $\mathbf{R}(x) = [R_0(x)R_1(x)R_2(x)\cdots R_N(x)]$ can be expressed by

$$\mathbf{R}'(x) = \frac{d\mathbf{R}(x)}{dx} \approx \mathbf{R}(x)\mathbf{D}^T, \tag{18}$$

where $\mathbf{D}$ is $(N+1)\times(N+1)$ operational differentiation matrix. The elements of $\mathbf{D}$ are found by differentiating (4) and using $R_1(x) = (x-1)/(x+1)$, then

$$R'_{n+1}(x) = 2(R_1(x)\cdot R_n(x))' - R'_{n-1}(x), \tag{19}$$

also using the multiplication relation:

$$R_m(x)\cdot R_n(x) = \frac{1}{2}\left[R_{m+n} + R_{|m-n|}\right]. \tag{20}$$

The approximation sign in (18) made by a truncation to the last column of $\mathbf{D}$ (by consideration that $R'_i(x) = 0$, for $i > N$) to get an invertible square operational matrix $\mathbf{D}$ (see Ref. [14]). The structure of the matrix $\mathbf{D}$ is obtained as a lower-Heisenberg matrix. The matrix $\mathbf{D}$ can be expressed as $\mathbf{D} = \mathbf{D}_1 + \mathbf{D}_2$, where $\mathbf{D}_1$ is a tridiagonal matrix which is obtained from

$$\mathbf{D}_1 = \text{diag.}\left(\frac{7}{4}(i-1), -(i-1), \frac{1}{4}(i-1)\right), \quad i = 1, 2, \cdots, N+1, \tag{21}$$

and the entire elements of matrix $\mathbf{D}_2$ are d_{ij}, obtained from

$$d_{21} = -1, d_{ij} = \begin{cases} 0, & j \geq i-1, \\ k(i-1)c_j, & j < i-1. \end{cases} \tag{22}$$

In addition to $k = (-1)^{i+j+1}$, $c_1 = 1$ and $c_j = 2$ for $j \geq 2$.

Consequently, the kth-order derivative of the row matrix $\mathbf{R}(x)$, which is given in (18), is obtained as

$$\frac{d^k\mathbf{R}(x)}{dx^k} = [\mathbf{R}(x)]^{(k)} \approx \mathbf{R}(x)\left(\mathbf{D}^T\right)^k, \tag{23}$$

And we note here that $\mathbf{R}^{(0)}(x) = \mathbf{R}(x)$, $R'_i(x) = 0$, for $i > N$. Definitions (18) and (23) were introduced for the first time in [18, 19], and many works have used them; see, for example, Refs. [20–22], [23, 24], and [17].

3. The Improved Differentiation of the RC Functions

In the present section, an improved definition of differentiation for the RC functions is introduced. There was a need to find an improvement to definition (23), because in the higher derivatives, when using this definition, a week approximation is obtained. The truncated definition (18) and the kth-order derivative (23) give us a regular truncated differentiation of the RC functions (RRC). Generally, the derivative of the rational or fractional functions increases the order of the denominator (in contrast to polynomials that reduce the order at differentiation), so the truncation

increases as the order of the derivative increases (more than one column in Equation (18)). For example, the fourth-order derivative of the vector $\mathbf{R}(x)$ at $N = 3$, the truncated terms in the row vector $\mathbf{R}(x)$ are (the last four terms) R_4, R_5, R_6, R_7. This will lead to unsatisfied approximating in high-order DEs using the presented RRC definition (18). Therefore, an improved definition of the derivative of RC functions will be proposed next.

First, a vector will be inserted into (18) to treat the truncated terms, which will improve the regular definition. This manner will be called an improved derivative of the RC functions and will be indicated by IRC.

Additionally, the first-order derivative of the row matrix $R(x)$ is

$$\mathbf{R}'(x) = \frac{d\mathbf{R}(x)}{dx} = \mathbf{R}(x)\mathbf{D}^T + \mathbf{Z}(x), \tag{24}$$

where

$$\mathbf{Z}(x) = [0 \quad 0 \quad 0 \quad \cdots \quad 0 \quad d_{N+1,N+1}R_{N+1}(x)]_{1\times(N+1)}. \tag{25}$$

Theorem 3. *The kth derivative of the matrix vector $\mathbf{R}(x)$, in terms of itself, is defined as*

$$[\mathbf{R}(x)]^{(k)} = \mathbf{R}(x)\left(\mathbf{D}^T\right)^k + \sum_{i=0}^{k-1}\mathbf{Z}^{(i)}(x)\left(\mathbf{D}^T\right)^{k-i-1}, \quad k \geq 1, \tag{26}$$

where

$$\mathbf{Z}^{(k)}(x) = \left[0 \quad 0 \quad 0 \quad \cdots \quad 0 \quad d_{N+1,N+2}\mathbf{R}_{N+1}^{(k)}(x)\right]. \tag{27}$$

Proof. Using the assumption (24) as the first derivative, and differentiating (24), then we get

$$\mathbf{R}''(x) = \mathbf{R}'(x)\mathbf{D}^T + \mathbf{Z}'(x), \tag{28}$$

or

$$\begin{aligned}\mathbf{R}''(x) &= \left\{\mathbf{R}(x)\mathbf{D}^T + \mathbf{Z}(x)\right\}\mathbf{D}^T + \mathbf{Z}'(x)\\ &= \mathbf{R}(x)\left(\mathbf{D}^T\right)^2 + \mathbf{Z}(x)\mathbf{D}^T + \mathbf{Z}'(x),\end{aligned} \tag{29}$$

and by induction, we get the kth derivative as relation (26).□ □

As a special case, if $\mathbf{Z}(x) = 0$, it leads us to the regular RC definition in relations (18) and (23). The introduced definition (24) and the kth-order derivative (26) give us an improved differentiation of the RC functions.

4. Problem Statement

In this study, the form of high-order ODEs which represents a linear nonhomogeneous with variable coefficients defined on a semi-infinite domain is

$$\sum_{k=0}^{m} Q_k(x)f^{(k)}(x) = g(x), \quad 0 \leq x < \infty, \tag{30}$$

which forms m^{th}-order ODEs; the previous forms of DEs are subjected to the following conditions:

$$f^{(k)}(\gamma_i) = \lambda_i, \quad 0 \leq \gamma_i < \infty, i = 0, 1, \cdots, m-1, \tag{31}$$

where the $Q_k(x)$ and $g(x)$ are well-defined functions on Ω, and γ_j and λ_i are constants (initial value problem), where γ_j may tend to ∞ (boundary value problems).

Now, we consider that the approximate solution $f_N(x)$ according to (16) for the exact solution $f(x)$ of equation (30) in the vector form as

$$f_N(x) = \sum_{n=0}^{N} a_n R_n(x) = \mathbf{R}(x)\mathbf{A}, \tag{32}$$

$$f_N^{(k)}(x) = \sum_{n=0}^{N} a_n (R_n(x))^{(k)} = \mathbf{R}^{(k)}(x)\mathbf{A}, \tag{33}$$

where

$$\mathbf{A} = [a_0 \ a_1 \ \cdots \ a_N]. \tag{34}$$

5. Fundamental Relation-Based Matrix Forms

In the beginning, we provide the fundamental matrix relation of the solution of (30) by two schemes using the RC collocation approach.

Assuming that the solution $f(x)$ of (30) can be expressed as relation (32), which is a truncated RC series, then $f(x)$ and its kth derivative $f^{(k)}(x)$ are written in the matrix forms (32) and (33) such that $k = 0, 1, \cdots, m$, and $m \leq N$, where $f^{(0)}(x) \equiv f(x)$, $a_0, a_1, \cdots, a_N$ are the RC coefficients to be determined later.

Now, let the collocation points x_s as

$$x_s = \frac{1 + \cos(s\pi/N)}{1 - \cos(s\pi/N)}, \quad s = 0, 1, \cdots, N, \tag{35}$$

and at the end points $(s = 0, s = N)$ $x_0 \longrightarrow \infty$, $x_N = 0$, namely,

$$\begin{aligned}R_n(x) &= 1 \text{ when } x \longrightarrow \infty, \text{for all } n,\\ R_n(x) &= \cos(n\pi) = (-1)^n \text{ when } x \longrightarrow 0, \text{ for all } n.\end{aligned} \tag{36}$$

Permanently, the RC functions are convergent at both end points 0 and ∞; in addition, the presence of infinity in the collocation points $(x_0 \longrightarrow \infty)$ does not cause a failure in the substitution.

Hence, upon substituting these points (35) into (30), one obtains

$$\sum_{k=0}^{m} Q_k(x_s)f^{(k)}(x_s) = g(x_s), \quad s = 0, 1, 2, \cdots, N. \tag{37}$$

The matrix form of the obtained system (37) is written farther as

$$\sum_{k=0}^{m} \mathbf{Q}_k \mathbf{F}^{(k)} = \mathbf{G}, \tag{38}$$

where

$$\mathbf{Q}_k = \begin{bmatrix} Q_k(x_0) & 0 & \cdots & 0 \\ 0 & Q_k(x_1) & \cdots & 0 \\ 0 & 0 & \ddots & \vdots \\ 0 & 0 & \cdots & Q_k(x_N) \end{bmatrix},$$

$$\mathbf{F}^{(k)} = \begin{bmatrix} f^{(k)}(x_0) \\ f^{(k)}(x_1) \\ \vdots \\ f^{(k)}(x_N) \end{bmatrix}, \quad \mathbf{G} = \begin{bmatrix} g(x_0) \\ g(x_1) \\ \vdots \\ g(x_N) \end{bmatrix}. \tag{39}$$

5.1. The RRC Scheme. From (23), we know that the first scheme RRC gives us a derivative of RC functions from the kth order; thus, equation (38) takes the form

$$\mathbf{F}^{(k)} = \mathbf{R}\left(\mathbf{D}^T\right)^k \mathbf{A}, \tag{40}$$

where

$$\mathbf{R} = \begin{bmatrix} \mathbf{R}(x_0) \\ \mathbf{R}(x_1) \\ \mathbf{R}(x_2) \\ \vdots \\ \mathbf{R}(x_N) \end{bmatrix} = \begin{bmatrix} R_0(x_0) & R_1(x_0) & \cdots & R_N(x_0) \\ R_0(x_1) & R_1(x_1) & \cdots & R_N(x_1) \\ R_0(x_2) & R_0(x_2) & \cdots & R_0(x_2) \\ \vdots & \vdots & \ddots & \vdots \\ R_0(x_N) & R_1(x_N) & \cdots & R_N(x_N) \end{bmatrix}. \tag{41}$$

Hence, from (38) and (40), one obtains the fundamental matrix equation for (30) as

$$\sum_{k=0}^{m} \mathbf{Q}_k \mathbf{R}\left(\mathbf{D}^T\right)^k \mathbf{A} = \mathbf{G}. \tag{42}$$

Also, we obtain the matrix forms corresponding to condition (31) as follows: setting $x = \gamma_j$ in (33), we get the fundamental matrix form corresponding to the condition (31):

$$\mathbf{R}(\gamma_i)\left(\mathbf{D}^T\right)^k \mathbf{A} = \lambda_i, \quad 0 \le \gamma_i < \infty, i = 0, 1, \cdots, m-1. \tag{43}$$

5.2. The IRC Scheme. We studied the improved and regular differentiating RC functions in the preceding section. Now, we deduce the fundamental matrix relation by the IRC scheme.

Substituting relation (26) into (40), we get

$$\mathbf{F}^{(k)} = \left\{ \mathbf{R}\left(\mathbf{D}^T\right)^k + \sum_{i=0}^{k-1} \mathbf{Z}^{(i)} \left(\mathbf{D}^T\right)^{k-i-1} \right\} \mathbf{A}, \tag{44}$$

where

$$\mathbf{Z} = \begin{bmatrix} \mathbf{Z}(x_0) \\ \mathbf{Z}(x_1) \\ \vdots \\ \mathbf{Z}(x_N) \end{bmatrix} = \begin{bmatrix} Z_0(x_0) & Z_1(x_0) & \cdots & Z_N(x_0) \\ Z_0(x_1) & Z_1(x_1) & \cdots & Z_N(x_1) \\ \vdots & \vdots & \ddots & \vdots \\ Z_0(x_N) & Z_1(x_N) & \cdots & Z_N(x_N) \end{bmatrix}. \tag{45}$$

Hence, from (38) and (44), the fundamental matrix equation for (30) is obtained as

$$\sum_{k=0}^{m} \mathbf{Q}_k \left\{ \mathbf{R}\left(\mathbf{D}^T\right)^k + \sum_{i=0}^{k-1} \mathbf{Z}^{(i)} \left(\mathbf{D}^T\right)^{k-i-1} \right\} \mathbf{A} = \mathbf{G}. \tag{46}$$

Similarly, the matrix form corresponding to the condition (31) using (26) is obtained as

$$\left\{ \mathbf{R}(\gamma_i)\left(\mathbf{D}^T\right)^k + \sum_{i=0}^{k-1} \mathbf{Z}^{(i)}(\gamma_i) \left(\mathbf{D}^T\right)^{k-i-1} \right\} \mathbf{A} = \lambda_i, \tag{47}$$

for $i = 0, 1, \cdots, m-1$, so that $0 \le \gamma_j < \infty$.

6. Method of Solution

Due to the collocation method, the regular (42) and the improved (46) fundamental matrix equations for the proposed problem (30) correspond to a system of algebraic equations with $(N+1)$ equations for the $(N+1)$ unknown RC coefficients $a_0, a_1, \cdots, a_N$..

One writes matrix equations (42) and (46) compactly as

$$\mathbf{SA} = \mathbf{G}, \tag{48}$$

or in the augmented form as

$$[\mathbf{S}\,;\mathbf{G}]. \tag{49}$$

Equations (43) and (47) obtain the matrix form for the condition (31); also, they are written compactly as

$$\mathbf{H}_i \mathbf{A} = [\lambda_i], \tag{50}$$

so that $\mathbf{S}$ and $\mathbf{H}_i$ for RRC are defined by

$$\begin{aligned} \mathbf{S} &= \left[s_{pq}\right] = \sum_{k=0}^{m} \mathbf{Q}_k \mathbf{R}\left(\mathbf{D}^T\right)^k, \quad p, q = 0, 1, \cdots, N, \\ \mathbf{H}_i &= [\, h_{i0} \quad h_{i1} \quad \cdots \quad h_{\mathrm{iN}} \,] = \mathbf{R}\left(\gamma_j\right)\left(\mathbf{D}^T\right)^k, \end{aligned} \tag{51}$$

while $\mathbf{S}$ and $\mathbf{H}_i$ for IRC are defined by

$$\begin{aligned}\mathbf{S} &= [s_{pq}] = \sum_{k=0}^{m} \mathbf{Q}_k \left\{ \mathbf{R}\left(\mathbf{D}^T\right)^k + \sum_{i=0}^{k-1} \mathbf{Z}^{(i)} \left(\mathbf{D}^T\right)^{k-i-1} \right\},\\ \mathbf{H}_i &= [\, h_{i0} \quad h_{i1} \quad \cdots \quad h_{iN} \,]\\ &= \left\{ \mathbf{R}\left(\gamma_j\right)\left(\mathbf{D}^T\right)^k + \sum_{i=0}^{k-1} \mathbf{Z}^{(i)}\left(\gamma_j\right) \left(\mathbf{D}^T\right)^{k-i-1} \right\}.\end{aligned} \tag{52}$$

Hence, the approximate solution of (30) under the condition (31) may be obtained by exchanging the rows of matrices (50) by the last (or first) m rows of the matrix (49), then getting the required augmented matrix as

$$\left[\tilde{\mathrm{S}}\,;\tilde{\mathbf{G}}\right] = \begin{bmatrix} s_{00} & s_{01} & \cdots & s_{0N} & ; & g(x_0) \\ s_{10} & s_{11} & \cdots & s_{1N} & ; & g(x_1) \\ \cdots & \cdots & \cdots & \cdots & ; & \cdots \\ s_{N-m,0} & s_{N-m,1} & \cdots & s_{N-m,N} & ; & g(x_{N-m}) \\ h_{00} & h_{01} & \cdots & h_{0N} & ; & \lambda_0 \\ h_{10} & h_{11} & \cdots & h_{1N} & ; & \lambda_1 \\ \cdots & \cdots & \cdots & \cdots & ; & \cdots \\ h_{m-1,0} & h_{m-1,1} & \cdots & h_{m-1,N} & ; & \lambda_{m-1} \end{bmatrix}. \tag{53}$$

If rank $\tilde{\mathbf{S}}$ is equal to rank $[\tilde{\mathbf{S}}\,;\tilde{\mathbf{G}}]$, then the algebraic system has a solution, and if the two ranks are equal to $N+1$, then the solution is unique, the inverse matrix method is used here to solve the system, and one may write the matrix equation (49) as

$$\mathbf{A} = \left(\tilde{\mathbf{S}}\right)^{-1} \tilde{\mathbf{G}}. \tag{54}$$

Therefore, the RC coefficients a_n, $n = 0, 1, \cdots, N$ are uniquely determined.

7. Test Examples

In the present section, three numerical test examples are given to explain the applicability of the proposed two techniques. Using own codes written in MATHEMATICA 10.0. package, the numerical results and figures are presented, as shown in the illustrative comparison tables.

The absolute error is given to compare the efficiency of the proposed schemes, given by $e_N = |f^i_{\text{Exact}} - f^i_{\text{Approximate}}|$, and evaluated at selected points for some N. The error norms L_2 and L_∞ calculated in an interval $x \in [0, b]$ are given by

$$L_b^2 = \sqrt{h \sum_{i}^{l} \left(f^i_{\text{Exact}} - f^i_{\text{Approximate}} \right)^2},$$

$$L_b^\infty = \text{Max} \left| f^i_{\text{Exact}} - f^i_{\text{Approximate}} \right|, \tag{55}$$

for the h step size along the interval $x \in [0, b]$. All numeric calculations are carried out on a regular machine Intel(R) Core(TM) i7 CPU, 3.2 GHz.

Example 1. Let us assume the following fourth-order boundary value problem

$$f^{(4)}(x) - \frac{1}{4}(1+x)^{-2} f''(x) + \frac{1}{2}(1+x)^{-4} f(x) = \frac{x^2 - 238x + 713}{(x+1)^6},$$

$$x \in [0, \infty), \tag{56}$$

with $f(0) = 0, f'(1) = 1/2, f''(1) = 1/2, f(x) \longrightarrow 2$ when $x \longrightarrow \infty$.

We have

$$\begin{aligned} m = 4,\ Q_0(x) &= \frac{1}{2(1+x)^4},\ Q_1(x) = 0,\ Q_2(x) = -\frac{1}{4(1+x)^2},\\ Q_3(x) &= 0,\ Q_4(x) = 1,\ g(x) = \frac{x^2 - 238x + 713}{(x+1)^6}. \end{aligned} \tag{57}$$

Thus, for $N = 5$, the numeric collocation points according to (35) are

$$\begin{aligned} x_1 &= \frac{1 + 1/4\left(1+\sqrt{5}\right)}{1 - 1/4\left(1+\sqrt{5}\right)},\\ x_2 &= \frac{1 - 1/4\left(1-\sqrt{5}\right)}{1 + 1/4\left(1-\sqrt{5}\right)},\\ x_3 &= \frac{1 + 1/4\left(1-\sqrt{5}\right)}{1 - 1/4\left(1-\sqrt{5}\right)},\\ x_4 &= \frac{1 - 1/4\left(1+\sqrt{5}\right)}{1 + 1/4\left(1+\sqrt{5}\right)},\\ x_0 &\longrightarrow \infty, x_5 = 0. \end{aligned} \tag{58}$$

The fundamental matrix equation of problem using RRC is

$$\left\{ \mathbf{Q}_0\mathbf{R} + \mathbf{Q}_1\mathbf{R}\mathbf{D}^T + \mathbf{Q}_2\mathbf{R}\left(\mathbf{D}^T\right)^2 + \mathbf{Q}_3\mathbf{R}\left(\mathbf{D}^T\right)^3 + \mathbf{Q}_4\mathbf{R}\left(\mathbf{D}^T\right)^4 \right\}\mathbf{A} = \mathbf{G}, \tag{59}$$

while the fundamental matrix equation of problem using IRC is

$$\begin{aligned}&\Big\{\mathbf{Q}_0\mathbf{R}+\mathbf{Q}_1\left(\mathbf{R}\mathbf{D}^T+\mathbf{Z}\right)+\mathbf{Q}_2\left(\mathbf{R}\left(\mathbf{D}^T\right)^2+\mathbf{Z}\mathbf{D}^T\right)\\&\quad+\mathbf{Z}'+\mathbf{Q}_3\left(\mathbf{R}\left(\mathbf{D}^T\right)^3+\mathbf{Z}\left(\mathbf{D}^T\right)^2+\mathbf{Z}'\mathbf{D}^T+\mathbf{Z}''\right)\\&\quad+\mathbf{Q}_4\left(\mathbf{R}\left(\mathbf{D}^T\right)^4+\mathbf{Z}\left(\mathbf{D}^T\right)^3+\mathbf{Z}'\left(\mathbf{D}^T\right)^2+\mathbf{Z}''\mathbf{D}^T+\mathbf{Z}'''\right)\Big\}\mathbf{A}=\mathbf{G},\end{aligned} \tag{60}$$

where $\mathbf{Q}_0, \mathbf{Q}_2, \mathbf{Q}_4, \mathbf{R}, \mathbf{D}^T, \mathbf{Z}, \mathbf{Z}', \mathbf{Z}''$, and $\mathbf{Z}'''$ are matrices with a given size of 6×6, for this example at $N=5$,

$$\mathbf{Q}_0=\begin{bmatrix}0&0&0&0&0&0\\0&0.0000415747&0&0&0&0\\0&0&0.00712393&0&0&0\\0&0&0&0.0917553&0&0\\0&0&0&0&0.334673&0\\0&0&0&0&0&0.5\end{bmatrix},$$

$$\mathbf{Q}_4=\begin{bmatrix}1&0&0&0&0&0\\0&1&0&0&0&0\\0&0&1&0&0&0\\0&0&0&1&0&0\\0&0&0&0&1&0\\0&0&0&0&0&1\end{bmatrix},$$

$$\mathbf{Q}_2=\begin{bmatrix}0&0&0&0&0&0\\0&-0.00227966&0&0&0&0\\0&0&-0.0298411&0&0&0\\0&0&0&-0.107095&0&0\\0&0&0&0&-0.204534&0\\0&0&0&0&0&-0.25\end{bmatrix},$$

$$\mathbf{D}^T=\begin{bmatrix}0&3/4&-2&3&-4&5\\0&-1&7/2&-6&8&10\\0&1/4&-2&21/4&-8&10\\0&0&1/2&-3&7&-10\\0&0&0&3/4&-4&35/4\\0&0&0&0&1&-5\end{bmatrix},$$

$$\mathbf{R}=\begin{bmatrix}1&1&1&1&1&1\\1&\frac{1}{4}\left(1+\sqrt{5}\right)&\frac{1}{4}\left(-1+\sqrt{5}\right)&\frac{1}{4}\left(1-\sqrt{5}\right)&\frac{1}{4}\left(-1-\sqrt{5}\right)&-1\\1&\frac{1}{4}\left(-1+\sqrt{5}\right)&\frac{1}{4}\left(-1-\sqrt{5}\right)&\frac{1}{4}\left(-1-\sqrt{5}\right)&\frac{1}{4}\left(-1+\sqrt{5}\right)&1\\1&\frac{1}{4}\left(1-\sqrt{5}\right)&\frac{1}{4}\left(-1-\sqrt{5}\right)&\frac{1}{4}\left(1+\sqrt{5}\right)&\frac{1}{4}\left(-1+\sqrt{5}\right)&-1\\1&\frac{1}{4}\left(-1-\sqrt{5}\right)&\frac{1}{4}\left(-1+\sqrt{5}\right)&\frac{1}{4}\left(-1+\sqrt{5}\right)&\frac{1}{4}\left(-1-\sqrt{5}\right)&1\\1&-1&1&-1&1&-1\end{bmatrix},$$

Table 1: Comparing the CPU time used by seconds for RRC and IRC schemes.

N	CPU time used by RRC scheme	CPU time used by IRC scheme
4	0.094	0.155
5	0.11	0.19
6	0.156	0.241

$$\mathbf{Z}=\begin{bmatrix}0&0&0&0&0&\frac{5}{4}\\0&0&0&0&0&\frac{5}{16}\left(-1-\sqrt{5}\right)\\0&0&0&0&0&\frac{5}{16}\left(-1+\sqrt{5}\right)\\0&0&0&0&0&\frac{5}{16}\left(-1+\sqrt{5}\right)\\0&0&0&0&0&\frac{5}{16}\left(-1-\sqrt{5}\right)\\0&0&0&0&0&\frac{5}{4}\end{bmatrix},$$

$$\mathbf{Z}'=\begin{bmatrix}0&0&0&0&0&0\\0&0&0&0&0&\frac{15}{32}\left(-7+3\sqrt{5}\right)\\0&0&0&0&0&\frac{-75}{32}\left(-3+\sqrt{5}\right)\\0&0&0&0&0&\frac{-15}{32}\left(7+3\sqrt{5}\right)\\0&0&0&0&0&\frac{75}{32}\left(3+\sqrt{5}\right)\\0&0&0&0&0&-90\end{bmatrix}0,$$

$$\mathbf{Z}''=\begin{bmatrix}0&0&0&0&0&0\\0&0&0&0&0&\frac{15}{64}\left(-2+\sqrt{5}\right)\\0&0&0&0&0&\frac{75}{64}\left(90-41\sqrt{5}\right)\\0&0&0&0&0&\frac{15}{64}\left(-2-\sqrt{5}\right)\\0&0&0&0&0&\frac{75}{64}\left(90+41\sqrt{5}\right)\\0&0&0&0&0&2280\end{bmatrix}0,$$

$$\mathbf{Z}'''=\begin{bmatrix}0&0&0&0&0&0\\0&0&0&0&0&\frac{15}{128}\left(901-403\sqrt{5}\right)\\0&0&0&0&0&\frac{375}{128}\left(-1237-553\sqrt{5}\right)\\0&0&0&0&0&\frac{15}{128}\left(901+403\sqrt{5}\right)\\0&0&0&0&0&\frac{375}{128}\left(-1237-553\sqrt{5}\right)\\0&0&0&0&0&-40020\end{bmatrix}. \tag{61}$$

Table 2: Comparison between absolute errors with $\lambda = 1$ given by two proposed schemes.

x	RRC scheme		IRC scheme	
	e_{20}	e_{30}	e_{20}	e_{30}
0	1	1	1	1
0.5	2.23497×10^{-7}	1.59521×10^{-9}	4.61847×10^{-8}	3.66704×10^{-9}
1	4.90784×10^{-7}	5.74586×10^{-10}	5.93028×10^{-7}	6.13636×10^{-9}
1.5	4.68739×10^{-9}	2.52918×10^{-9}	2.2526×10^{-8}	1.4928×10^{-9}
2	1.78495×10^{-7}	1.33078×10^{-8}	1.8386×10^{-6}	9.67304×10^{-9}
2.5	1.43122×10^{-6}	1.99709×10^{-8}	1.11684×10^{-7}	9.44468×10^{-9}
3	1.35397×10^{-6}	7.57517×10^{-9}	2.11749×10^{-6}	2.75718×10^{-9}
3.5	2.16835×10^{-6}	3.82668×10^{-8}	1.29148×10^{-6}	1.00546×10^{-8}
5	3.534×10^{-6}	2.72901×10^{-8}	1.27908×10^{-6}	2.26605×10^{-8}
7.5	5.73755×10^{-6}	1.88112×10^{-7}	2.23981×10^{-7}	6.70631×10^{-8}
10	7.31028×10^{-6}	2.76595×10^{-7}	4.59453×10^{-6}	3.03553×10^{-9}

Table 3: Comparison between absolute errors with $\lambda = 2$ given by two proposed schemes.

x	RRC scheme		IRC scheme	
	e_{20}	e_{30}	e_{20}	e_{30}
0	1	1	1	1
0.5	3.31737×10^{-6}	3.91279×10^{-8}	4.85215×10^{-6}	2.86433×10^{-7}
1	1.21648×10^{-5}	2.30618×10^{-7}	6.13597×10^{-6}	9.11931×10^{-8}
1.5	1.68999×10^{-5}	3.20837×10^{-7}	2.99644×10^{-5}	6.97906×10^{-8}
2	2.57922×10^{-5}	3.48555×10^{-7}	2.71531×10^{-5}	8.9908×10^{-7}
2.5	2.07512×10^{-5}	4.35107×10^{-7}	8.88987×10^{-6}	1.01733×10^{-7}
3	3.12895×10^{-5}	6.64248×10^{-7}	4.44485×10^{-5}	3.8419×10^{-7}
3.5	1.99079×10^{-5}	2.69503×10^{-7}	1.5211×10^{-5}	1.08309×10^{-6}
5	1.14161×10^{-6}	1.06864×10^{-6}	2.31729×10^{-5}	6.46631×10^{-7}
7.5	5.4514×10^{-5}	1.43524×10^{-6}	2.57514×10^{-5}	1.97968×10^{-7}
10	2.13571×10^{-4}	2.89479×10^{-6}	4.48328×10^{-5}	2.05962×10^{-6}

Then, we obtain the augmented matrix (49) with respect to RRC as

$$\left[\tilde{\mathbf{S}}\,;\tilde{\mathbf{G}}\right] = \begin{bmatrix} 1 & -1 & 1 & -1 & 1 & -1 & ; & 0 \\ 0 & 0.5 & 0 & -1.5 & 0 & 2.5 & ; & 0.5 \\ 1 & 0.83333 & 0.38888 & -0.18518 & -0.69753 & -0.97736 & ; & 1.22222 \\ 1 & 1 & 1 & 1 & 1 & 1 & ; & 2 \\ 0.33467 & -28.72592 & 405.80168 & -2818.03109 & 12516.65380 & -33329.69198 & ; & 376.69653 \\ 0.5 & -47.5 & 760.03125 & -6080.75 & 30513.0625 & -86383.3125 & ; & 713 \end{bmatrix}. \tag{62}$$

Then, we solve the equation (49) to find the RC coefficients in the matrix form:

$$\mathbf{A} = \left[-0.0124202 \quad 1.00234 \quad 1.01636 \quad -0.00117103 \quad -0.00393679 \quad -0.00117103\right], \tag{63}$$

Table 4: Comparing the L_{10}^{2} and L_{10}^{∞} on interval $x \in [0, 10]$ for $\lambda = 1$.

N	RRC scheme		IRC scheme	
	L_{10}^{2}	L_{10}^{∞}	L_{10}^{2}	L_{10}^{∞}
20	1.70683×10^{-9}	7.31028×10^{-6}	6.74223×10^{-10}	4.59453×10^{-6}
30	2.44349×10^{-12}	2.76595×10^{-7}	1.06979×10^{-15}	9.79285×10^{-8}

Table 5: Comparing the L_{10}^{2} and L_{10}^{∞} on interval $x \in [0, 10]$ for $\lambda = 2$.

N	RRC scheme		IRC scheme	
	L_{10}^{2}	L_{10}^{∞}	L_{10}^{2}	L_{10}^{∞}
20	1.45682×10^{-6}	2.13571×10^{-4}	6.41968×10^{-8}	5.10902×10^{-5}
30	2.67643×10^{-10}	2.89479×10^{-6}	1.35486×10^{-11}	2.05962×10^{-6}

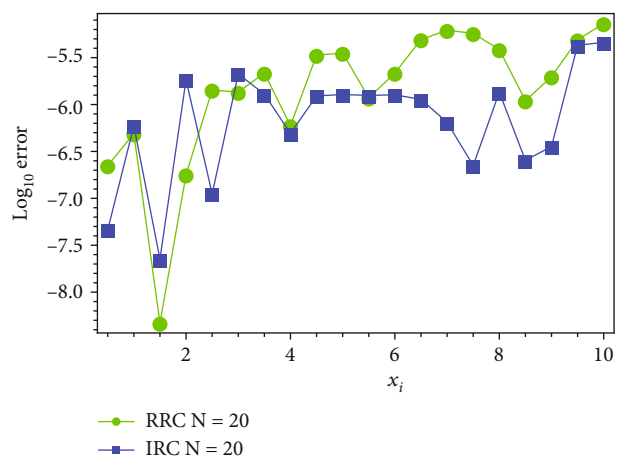

Figure 1: The absolute errors for the proposed two schemes when $N = 20$ with $\lambda = 1$.

Table 6: Comparing the CPU time used for RRC and IRC schemes.

N	RRC scheme		IRC scheme	
	$\lambda = 1$	$\lambda = 2$	$\lambda = 1$	$\lambda = 2$
20	1.173	1.172	1.938	1.985
30	3.89	3.858	4.591	4.61

while the augmented matrix (49) with respect to IRC as

$$\left[\tilde{S}\,;\tilde{\mathbf{G}}\right] = \begin{bmatrix} 1 & -1 & 1 & -1 & 1 & -1 & ; & 0 \\ 0 & 0.5 & 0 & -1.5 & 0 & 2.5 & ; & 0.5 \\ 1 & 0.83333 & 0.38888 & -0.18518 & -0.69753 & -0.97736 & ; & 1.22222 \\ 1 & 1 & 1 & 1 & 1 & 1 & ; & 2 \\ 0.33467 & -28.72592 & 405.42246 & -2799.72562 & 12543.47181 & -40972.42064 & ; & 376.69653 \\ 0.5 & -47.5 & 760.5 & -6159.5 & 33696.5 & -141135.5 & ; & 713 \end{bmatrix}. \tag{64}$$

Table 7: Comparison between absolute errors given by two proposed schemes.

X	RRC scheme		IRC scheme	
	e_{20}	e_{30}	e_{20}	e_{30}
0	1	1	1	
0.1	2.20484×10^{-8}	4.0709×10^{-9}	5.80324×10^{-9}	7.13895×10^{-10}
0.7	8.86658×10^{-9}	6.84228×10^{-8}	1.84652×10^{-8}	6.01463×10^{-8}
2.4	5.81316×10^{-7}	2.90517×10^{-7}	2.83721×10^{-6}	1.27556×10^{-7}
3.8	3.56672×10^{-6}	5.43355×10^{-7}	2.68921×10^{-6}	2.70375×10^{-8}
5	4.19425×10^{-6}	6.64317×10^{-7}	1.59222×10^{-6}	2.63469×10^{-8}
6.7	4.01577×10^{-5}	8.70798×10^{-7}	4.96175×10^{-6}	5.53538×10^{-8}
13.8	1.06869×10^{-4}	9.22562×10^{-7}	1.33586×10^{-5}	7.21039×10^{-7}
14.4	8.5269×10^{-4}	8.87894×10^{-7}	2.31729×10^{-5}	5.63274×10^{-8}
18.6	1.26741×10^{-4}	1.59984×10^{-6}	1.20205×10^{-5}	1.12601×10^{-6}
20	1.87513×10^{-4}	1.10906×10^{-6}	1.20881×10^{-4}	9.73054×10^{-7}

Table 8: Comparing the L_{10}^{2} and L_{10}^{∞} on interval $x \in [0, 10]$ for $\lambda = -1$.

N	RRC scheme		IRC scheme	
	L_{10}^{2}	L_{10}^{∞}	L_{10}^{2}	L_{10}^{∞}
20	1.12301×10^{-6}	8.5269×10^{-4}	4.667×10^{-7}	1.20881×10^{-4}
30	3.28475×10^{-11}	8.16818×10^{-6}	8.92851×10^{-12}	2.83766×10^{-6}

Similarly, we compute the RC coefficients in the matrix form:

$$\mathbf{A} = \begin{bmatrix} 0 & 1 & 1 & 0 & 0 & 0 \end{bmatrix}. \tag{65}$$

Substituting by the RC coefficients of the RRC scheme in Equation (32), we get an approximate solution of this problem, while, if we use the RC coefficients of the IRC scheme in Equation (32), we get the exact solution $2x(x-3)/(x+1)^2$. We note that the RRC scheme gives the exact solution at $N = 6$ while the IRC scheme gives the exact solution at $N = 4$, which shows that the IRC scheme obtains better accuracy than the RRC due to the truncation found in RRC (18). In addition, the CPU time used for the RRC and IRC schemes at different $N$is listed in Table 1. Table 1 shows that the time used for calculating the solution by RRC is less than the time for IRC, because of the added truncated terms in coding. Therefore, the time for getting the exact solution by IRC (better accuracy at $N = 4$) is close to that given by RRC (at $N = 6$). The following examples show the comparison of the two schemes strongly with numeric table's results.

Example 2. Consider Laguerre-eigen problem [26]

$$xf''(x) + (x+1)f'(x) + \lambda f(x) = 0, \quad x \in [0,\infty), \tag{66}$$

Table 9: Comparing the CPU time used by seconds for RRC and IRC schemes $\lambda = -1$.

N	CPU time used by RRC scheme	CPU time used by IRC scheme
20	0.844	0.971
30	2.345	2.657

has the exact eigen solutions

$$\begin{aligned} f(x) &= 1, \quad \lambda = 0, \\ f(x) &= e^{-x}L_n(x), \quad \lambda = n+1, n \geq 0, \end{aligned} \tag{67}$$

where $L_n(x)$ are the well-known Laguerre polynomials of degree n; Equation (66) is a boundary value problem, so the conditions are "natural" at both endpoints where $f(0) = 1$ and $f(x) = 1$ when $x \longrightarrow \infty$. By applying the proposed two schemes as in the previous example, we obtain the solution $f(x) = 1$, which is the exact eigen solution when $\lambda = 0$. For $N = 3$, the RRC scheme gives the exact eigen solution, while the IRC is satisfied with $N = 2$ to find this solution. In Tables 2 and 3, the resulting values for $N = 20$ and 30 using the present two schemes together with the exact values of the solution $f(x) = e^{-x}L_n(x)$, $\lambda = n+1$, $n \geq 0$, are tabulated with different values of λ. The error reduces when the series increased. The numeric values of the error norms L_2 and L_∞ in interval $x \in [0, 10]$ is given in Tables 4 and 5 with different values of λ. Additionally, the absolute errors e_N for the two

schemes when $N = 20$ are plotted in Figure 1. In Table 6, the CPU time used for RRC and IRC schemes at different N shows that IRC needs time more than RRC because of the calculation of the added terms of B.

Example 3. Consider Whittaker's equation eigen problem [26] of the form

$$f''(x) + \left[\frac{-1}{4} + \frac{1}{f(x)} + \frac{\lambda}{f(x)}\right] f(x) = 0, \quad x \in [0,\infty), \tag{68}$$

where λ is the eigen value; it represents a special case of Whittaker's equation. The exact given solution of (68) is $f(x) = e^{-0.5x} L_n^1(x)$, where $\lambda = n, n \geq 0$, is an integer and $L_n^k(x)$ is the well-known associated Laguerre polynomials of kth order and degree n. If $\lambda = -1$, (68) gives a special case or linear Whittaker's equation as

$$4f''(x) - f(x) = 0, \quad x \in [0,\infty). \tag{69}$$

The exact solution is $f(x) = e^{-0.5x}$ with the boundary conditions $f(0) = 1$ and $f(x) = 1$ when $x \longrightarrow \infty$.

By the same procedure, the RC collocation method using the proposed two schemes is applied to solve (69) with the subjected boundary conditions. In Table 7, the numerical result for $N = 20$ and 30 using the proposed schemes is compared with the exact values of $f(x) = e^{-0.5x}$. The computation of L_2 and L_∞ on interval $x \in [0, 10]$ is given in Table 8. In Table 9, the CPU time used for RRC and IRC schemes at different N shows that IRC needs time more than RRC.

8. Conclusion

A rational Chebyshev (RC) spectral collocation technique is considered in this paper to solve high-order ordinary differential equations (ODEs) defined on a semi-infinite domain using the proposed two schemes. Two definitions of the derivative of the RC functions are introduced, namely, the regular and improved definitions. Due to the two definitions, two schemes are presented for solving the proposed ODEs with variable coefficients in the semi-infinite interval. According to the convergence of the RC functions at the infinity, the proposed technique deals with the boundary value problem which is defined on semi-infinite domains easily. Furthermore, an intriguing advantage of this approach is the ability to find the analytical exact solutions if the equation has a solution in a rational function form. To demonstrate the applicability of the proposed approach, three illustrative examples are given. The calculated numerical values and comparisons proved that the improved scheme is better with more calculation than the regular scheme which is based on the truncation in the definition. The method may extend to the case of nonlinear DEs with variable coefficients, which the authors are investigating.

Data Availability

The authors declare that there is no data associated with this research.

Conflicts of Interest

The authors declare that they have no competing interests.

Authors' Contributions

All authors carried out the proofs and conceived of the study. All authors read and approved of the final form of the manuscript.

Acknowledgments

The researchers would like to thank the Deanship of Scientific Research, Qassim University, for funding the publication of this project.

References

[1] P. Agarwal, M. Attary, M. Maghasedi, and P. Kumam, "Solving higher-order boundary and initial value problems via Chebyshev–spectral method: application in elastic foundation," *Symmetry*, vol. 12, no. 6, p. 987, 2020.

[2] A. Akyüz and M. Sezer, "Chebyshev polynomial solutions of systems of high-order linear differential equations with variable coefficients," *Applied Mathematics and Computation*, vol. 144, no. 2-3, pp. 237–247, 2003.

[3] S. H. Aziz, M. Rasheed, and S. Shihab, "New properties of modified second kind Chebyshev polynomials," *Journal of Southwest Jiaotong University*, vol. 55, no. 3, p. 3, 2020.

[4] E. A. Butcher and O. A. Bobrenkov, "On the Chebyshev spectral continuous time approximation for constant and periodic delay differential equations," *Communications in Nonlinear Science and Numerical Simulation*, vol. 16, no. 3, pp. 1541–1554, 2011.

[5] V. N. Mishra, H. R. Marasi, H. Shabanian, and M. Nosraty, "Solution of Voltra-Fredholm integro-differential equations using Chebyshev collocation method," *Global Journal of Technology and Optimization*, vol. 8, no. 1, p. 210, 2017.

[6] A. H. Khater, R. S. Temsah, and M. Hassan, "A Chebyshev spectral collocation method for solving Burgers'-type equations," *Journal of Computational and Applied Mathematics*, vol. 222, no. 2, pp. 333–350, 2008.

[7] S. D. Kim and S. V. Parter, "Preconditioning Chebyshev spectral collocation method for elliptic partial differential equations," *SIAM Journal on Numerical Analysis*, vol. 33, no. 6, pp. 2375–2400, 1996.

[8] J. C. Mason and D. C. Handscomb, *Chebyshev Polynomials*, CRC press, 2002.

[9] M. Sezer and M. Kaynak, "Chebyshev polynomial solutions of linear differential equations," *International Journal of Mathematical Education in Science and Technology*, vol. 27, no. 4, pp. 607–618, 1996.

[10] S. Deniz and M. Sezer, "Rational Chebyshev collocation method for solving nonlinear heat transfer equations," *International Communications in Heat and Mass Transfer*, vol. 114, article 104595, 2020.

[11] P. S. Malachivskyy, Y. V. Pizyur, and R. P. Malachivsky, "Chebyshev approximation by a rational expression for functions of many variables," *Cybernetics and Systems Analysis*, vol. 56, no. 5, pp. 811–819, 2020.

[12] X. Zhang and J. P. Boyd, "Revisiting the Thomas-Fermi equation: accelerating rational Chebyshev series through coordinate transformations," *Applied Numerical Mathematics*, vol. 135, pp. 186–205, 2019.

[13] S. Abbasbandy, H. Roohani Ghehsareh, and I. Hashim, "An approximate solution of the MHD flow over a non-linear stretching sheet by rational Chebyshev collocation method," *UPB Scientific Bulletin*, vol. 74, 2012.

[14] M. A. Ramadan, K. R. Raslan, T. S. El Danaf, and M. A. Abd El Salam, "On the exponential Chebyshev approximation in unbounded domains: a comparison study for solving high-order ordinary differential equations," *International Journal of Pure and Applied Mathematics*, vol. 105, no. 3, pp. 399–413, 2015.

[15] M. A. Ramadan, K. R. Raslan, and M. A. Nassar, "An approximate analytical solution of higher-order linear differential equations with variable coefficients using improved rational Chebyshev collocation method," *Applied and Computational Mathematics*, vol. 3, no. 6, pp. 315–322, 2014.

[16] M. A. Ramadan, K. R. Raslan, and M. A. Nassar, "Numerical solution of system of higher order linear ordinary differential equations with variable coefficients using two proposed schemes for rational Chebyshev functions," *Global Journal of Mathematics*, vol. 3, no. 2, pp. 322–337, 2016.

[17] S. Yalçınbas, N. Özsoy, and M. Sezer, "Approximate solution of higher order linear differential equations by means of a new rational Chebyshev collocation method," *Mathematical and Computational Applications*, vol. 15, no. 1, pp. 45–56, 2010.

[18] K. Parand and M. Razzaghi, "Rational Chebyshev tau method for solving higher-order ordinary differential equations," *International Journal of Computer Mathematics*, vol. 81, no. 1, pp. 73–80, 2004.

[19] K. Parand and M. Razzaghi, "Rational Chebyshev tau method for solving Volterra's population model," *Applied Mathematics and Computation*, vol. 149, no. 3, pp. 893–900, 2004.

[20] K. Parand, Z. Delafkar, and F. Baharifard, "Rational Chebyshev tau method for solving natural convection of Darcian fluid about a vertical full cone embedded in porous media whit a prescribed wall temperature," *World Academy of Science, Engineering and Technology*, vol. 5, no. 8, pp. 1186–1191, 2011.

[21] A. M. Ramadan, K. R. Raslan, and M. A. Nassar, "Solving natural convection of Darcian fluid about a vertical full cone embedded in porous media whit a prescribed wall temperature is introduced using rational," *Applied Mathematics and Information Science*, vol. 14, no. 5, pp. 1–8, 2020.

[22] A. M. Ramadan, K. Raslan, and M. A. E. G. Nassear, "A rational Chebyshev functions approach for Fredholm-Volterra integro-differential equations," *Computational Methods for Differential Equations*, vol. 3, no. 4, pp. 284–297, 2015.

[23] M. A. Ramadan, K. Raslan, A. Hadhoud, and M. Nassar, "Numerical solution of high-order linear integro differential equations with variable coefficients using two proposed schemes for rational Chebyshev functions," *New trends in mathematical sciences*, vol. 4, no. 3, p. 22, 2016.

[24] A. M. Ramadan, D. Baleanu, and M. A.-G. Nassar, "Highly accurate numerical technique for population models via rational Chebyshev collocation method," *Mathematics*, vol. 7, no. 10, p. 913, 2019.

[25] B. Guo, J. Shen, and Z. Wang, "Chebyshev rational spectral and pseudospectral methods on a semi-infinite interval," *International Journal for Numerical Methods in Engineering*, vol. 53, no. 1, pp. 65–84, 2002.

[26] M. A. Ramadan, K. R. Raslan, A. R. Hadhoud, and M. A. Nassar, "Rational Chebyshev functions with new collocation points in semi-infinite domains for solving higher-order linear ordinary differential equations," *Journal of Advances in Mathematics*, vol. 11, no. 7, pp. 5403–5410, 2015.

Hindawi
Journal of Function Spaces
Volume 2021, Article ID 5922853, 13 pages
https://doi.org/10.1155/2021/5922853

Research Article

An Efficient Hybrid Numerical Scheme for Nonlinear Multiterm Caputo Time and Riesz Space Fractional-Order Diffusion Equations with Delay

A. K. Omran,[1,2] **M. A. Zaky**,[3,4] **A. S. Hendy**,[1,5] **and V. G. Pimenov**[1,6]

[1]*Department of Computational Mathematics and Computer Science, Institute of Natural Sciences and Mathematics Ural Federal University, 19 Mira St., Yekaterinburg 620002, Russia*
[2]*Department of Mathematics, Faculty of Science, Al-Azhar University, Assiut 71524, Egypt*
[3]*Department of Mathematics, Nazarbayev University, Nur-Sultan, Kazakhstan*
[4]*Department of Applied Mathematics, Physics Division, National Research Centre, Dokki, Cairo 12622, Egypt*
[5]*Department of Mathematics, Faculty of Science, Benha University, Benha 13511, Egypt*
[6]*Institute of Mathematics and Mechanics, Ural Branch of the Russian Academy of Sciences, 16 Kovalevskoy St., Yekaterinburg 620000, Russia*

Correspondence should be addressed to M. A. Zaky; ma.zaky@yahoo.com and A. S. Hendy; a.s.khendi@urfu.ru

Received 27 October 2021; Revised 17 November 2021; Accepted 19 November 2021; Published 6 December 2021

Academic Editor: Youssri Hassan Youssri

In this paper, we construct and analyze a linearized finite difference/Galerkin–Legendre spectral scheme for the nonlinear multiterm Caputo time fractional-order reaction-diffusion equation with time delay and Riesz space fractional derivatives. The temporal fractional orders in the considered model are taken as $(0 < \beta_0 < \beta_1 < \beta_2 < \cdots < \beta_m < 1)$. The problem is first approximated by the $L1$ difference method on the temporal direction, and then, the Galerkin–Legendre spectral method is applied on the spatial discretization. Armed by an appropriate form of discrete fractional Grönwall inequalities, the stability and convergence of the fully discrete scheme are investigated by discrete energy estimates. We show that the proposed method is stable and has a convergent order of $2 - \beta_m$ in time and an exponential rate of convergence in space. We finally provide some numerical experiments to show the efficacy of the theoretical results.

1. Introduction

Fractional-order partial differential equations have evolved into powerful tools for describing a wide range of anomalous behavior and complex systems in natural science and engineering [1–8]. In addition, time delay occurs frequently in realistic world and it has been considered in numerous mathematical models, e.g., automatic control systems with feedback and population dynamics. Moreover, fractional differential equations with delay have been used widely in a variety of scientific and technical disciplines, including the study of natural phenomena, mathematical modelling, and the studies of porous media [9, 10]. Recently, a two-term time-fractional differential equation that contains specific instances of the fractional diffusion-wave problem (see, for example, [11, 12]) has been investigated in the literature.

In recent years, multiterm time-fractional differential equations have attracted the attention of many researchers. The ability of these equations to describe complex multirate physical phenomena is a motivating force behind their development (see, e.g., [13–15]). They were proposed to improve the modelling accuracy by accurately depicting the anomalous diffusion process [16], accurately modelling various types of viscoelastic damping [17], and accurately reproducing the unsteady flow of a fractional Maxwell fluid [18] and Oldroyd-B fluid [19]. Daftardar-Gejji and Bhalekar [20] considered the multiterm time-fractional diffusion wave equation with constant coefficients. Through the use of a

domain decomposition technique, they were able to derive the linear and nonlinear diffusion-wave equations of the fractional order. Luchko [21] used an appropriate maximum principle and the Fourier technique to study the existence, uniqueness, and a priori estimates for the multiterm time-fractional diffusion equation with variable coefficients. A new analytic technique for solving three types of multiterm time-space fractional advection diffusion equations with nonhomogeneous Dirichlet boundary conditions was proposed by Jiang et al. [22], based on Luchko's theorem and the equivalent relationship between the Laplacian operator and the Riesz fractional derivative. Ding and Jiang [23] used the technique of spectral representation of the fractional Laplacian operator in order to provide the analytical solutions for the multiterm time-space fractional advection-diffusion equations with mixed boundary conditions. For the solution of initial-boundary value problems of multiterm time fractional diffusion equations, Li et al. [24] examined the well-posedness and long-time asymptotic behaviour of the equations. Zaky [25] constructed a Legendre spectral tau algorithm to deal with the multiterm time-fractional diffusion equations. Hendy [26] presented numerical treatment for solving a class of one-dimensional multiterm time-space fractional advection-diffusion equations with a temporal delay of the functional type. Hendy and De Staelen [27] developed a high-order numerical approximation approach for multiterm time convection diffusion wave equations with a nonlinear fixed time delay. To solve a coupled system of nonlinear multiterm time-space fractional diffusion equations over a nonuniform temporal mesh, Hendy and Zaky [28] developed an effective finite difference/spectral approach. Very recently, Zaky et al. [29] presented a discrete fractional Grönwall inequality that is consistent with the $L2-1_\sigma$ to cope with the analysis of multiterm time-fractional partial differential equations. The key advantage of the proposed discrete Grönwall inequality over earlier efforts was that it can be utilised to provide optimal error estimates for multiterm fractional problems with nonlinear delay. Inspired by these inequalities, we can state and prove the convergence and stability estimates for our proposed fully discrete scheme. The discrete versions of Grönwall inequalities are of high concern in the numerical analysis of the numerical schemes for fractional differential equations [30, 31].

Single-term fractional differential equations are often unable to describe some of the changing characteristics of the systems accurately. However, several multiterm fractional differential equations provide us with new tools to solve such problems. The multiterm time-fractional diffusion equation is useful not only for modelling the behaviour of viscoelastic fluids and rheological materials [32] but also for approximating distributed-order differential equations [33]. Hence, studies on the multiterm time-fractional differential equations have become important and useful for different applications. The multiterm time-fractional diffusion equation, whose weight function is taken into the linear combination of the Dirac δ-functions, is an important special case of the time-fractional diffusion equation of distributed order. In this paper, we consider the numerical approximations to the following generalized nonlinear multiterm time-space fractional reaction-diffusion equations with delay:

$$\sum_{r=0}^{m} q_r \frac{\partial^{\beta_r} u}{\partial t^{\beta_r}} = \kappa \frac{\partial^\alpha u}{\partial |x|^\alpha} + f(u(x,t), u(x,t-\tilde{s})) + g(x,t), \quad x \in \Omega, t \in I, \tag{1}$$

endowed with initial-boundary conditions of the form

$$\begin{cases} u(x,t) = \psi(x,t), & x \in \Omega, t \in [-\tilde{s}, 0], \\ u(a,t) = u(b,t) = 0, & t \in I. \end{cases} \tag{2}$$

Here, $\Omega = (a,b) \subset \mathbb{R}$ and $I = (0,T] \subset \mathbb{R}$ are space and time domains, respectively. We denote $\partial^{\beta_r}/\partial t^{\beta_r}$ as the Caputo fractional derivative with the fractional orders $(0 < \beta_0 < \beta_1 < \beta_2 < \cdots < \beta_m < 1)$. The parameters κ, s are positive constants. The parameters q_r are absolutely positive. Also, $1 < \alpha < 2$ is the space fractional order. The left and right Riemann-Liouville fractional derivatives of order $\alpha(n-1 < \alpha < n)$ on the infinite domain [34] are defined as

$$\begin{aligned} {}_{-\infty}D_x^\alpha u(x,t) &= \frac{1}{\Gamma(n-\alpha)} \frac{\partial^n}{\partial x^n} \int_{-\infty}^{x} (x-\tau)^{n-1-\alpha} u(\tau,t) d\tau, \\ {}_xD_\infty^\alpha u(x,t) &= \frac{(-1)^n}{\Gamma(n-\alpha)} \frac{\partial^n}{\partial x^n} \int_{x}^{\infty} (\tau-x)^{n-1-\alpha} u(\tau,t) d\tau, \end{aligned} \tag{3}$$

where $\Gamma(x)$ is the gamma function. Thus, the space fractional derivative in the Riesz form on the space interval Ω can be defined as [35]

$$\begin{aligned} \frac{\partial^\alpha u}{\partial |x|^\alpha} &= -c_\alpha ({}_aD_x^\alpha u(x,t) + {}_xD_b^\alpha u(x,t)), \\ c_\alpha &= \frac{1}{2\cos(\pi\alpha/2)}, 1 < \alpha < 2. \end{aligned} \tag{4}$$

The Caputo derivative $\partial^\beta/\partial t^\beta$ is defined as

$$\frac{\partial^\beta}{\partial t^\beta} u(x,t) = \frac{1}{\Gamma(1-\beta)} \int_0^t (t-r)^{-\beta} \frac{\partial}{\partial r} u(x,r) dr, 0 < \beta < 1. \tag{5}$$

The main aim of this work is to construct and analyze an efficient linearized numerical scheme for the nonlinear multiterm Riesz space and Caputo time fractional reaction-diffusion problem with fixed delay. A hybrid numerical scheme combines the Galerkin–Legendre spectral schemes, and a uniform $L1$-type interpolation technique is designed. The main challenges of the considered work are represented in how to numerically approximate the time Caputo fractional derivative, Riesz space fractional derivatives, and the time delay to produce an easy-to-implement and consistent numerical scheme. Overcoming all of these challenges to yield a hybrid linear numerical scheme is a first target. The

other target is to analyze the convergence and stability. The theoretical analysis of the constructed fully discrete scheme is successfully estimated using appropriate discrete fractional Grönwall inequalities, and the scheme is proven to be unconditionally stable and convergent.

The outline of this paper is as follows. In the next section, we will go over some essential definitions and properties of fractional derivative spaces, fractional Sobolev spaces, and Jacobi polynomials. The steps needed to construct a fully discrete scheme on a uniform mesh are detailed in Section 3. Some technical lemmas from the literature are summarized in Section 4. Furthermore, the stability and the convergence analyses of the fully discrete scheme are studied in Section 5. Finally, numerical experiments are performed in Section 6 to illustrate the convergence analysis of the proposed approach.

2. Preliminaries

We here give some essential fractional derivative spaces [36] and their required features which will be helpful in the coming analysis. After that, the definition of Jacobi polynomials and their basic properties are recalled. We now fix some notations for the sake of clearness:

(i) $(\cdot,\cdot)_{0,\Omega}$ is the inner product on the space $L^2(\Omega)$ with the L^2-norm $\|\cdot\|_{0,\Omega}$

(ii) The maximum norm is defined as $\|\cdot\|_\infty$

(iii) $C_0^\infty(\Omega)$ is the space of smooth functions with compact support in Ω

(iv) $H^r(\Omega)$ and $H_0^r(\Omega)$ are the usual Sobolev spaces with the norm $\|\cdot\|_r$ and seminorm $|\cdot|_r$

(v) $\mathscr{P}_N(\Omega)$ is the space of polynomials defined on the domain Ω with degree at most N

(vi) The approximation space $\mathscr{W}_N^0$ is defined as $\mathscr{W}_N^0 = \mathscr{P}_N(\Omega) \cap H_0^1(\Omega)$

(vii) I_N is the Legendre-Gauss-Lobatto interpolation operator $I_N : C(\bar{\Omega}) \longrightarrow \mathscr{W}_N$ as

$$u(x_k) = I_N u(x_k) \in \mathscr{P}_N, \quad k = 0, 1, \cdots, N. \tag{6}$$

Definition 1. Fractional derivative spaces and their related norms and seminorms are defined as follows [36]:

(i) Left fractional space: let $\eta > 0$. Define the seminorm $|u|_{J_L^\eta(\Omega)} = \|{}_aD_x^\eta u\|_{0,\Omega}$ and the norm $\|u\|_{J_L^\eta(\Omega)} = \left(|u|^2_{J_L^\eta}(\Omega) + \|u\|^2_{0,\Omega}\right)^{1/2}$, and let J_L^η (or $J_{L,0}^\eta$) denote the closure of $C^\infty(\Omega)$ (or $C_0^\infty(\Omega)$) with respect to $\|\cdot\|_{J_L^\eta(\Omega)}$

(ii) Right fractional space: let $\eta > 0$. Define the seminorm $|u|_{J_R^\eta(\Omega)} = \|{}_xD_b^\eta u\|_{0,\Omega}$ and the norm $\|u\|_{J_R^\eta(\Omega)} = \left(|u|^2_{J_R^\eta(\Omega)} + \|u\|^2_{0,\Omega}\right)^{1/2}$, and let J_R^η (or $J_{R,0}^\eta$) denote the closure of $C^\infty(\Omega)$ (or $C_0^\infty(\Omega)$) with respect to $\|\cdot\|_{J_R^\eta(\Omega)}$

(iii) Symmetric fractional space: let $\eta \neq n - (1/2)$, $n \in \mathbb{N}$. Define the seminorm $|u|_{J_s^\eta(\Omega)} = \left|\left({}_aD_x^\eta u, {}_xD_b^\eta u\right)_{0,\Omega}\right|^{1/2}$ and the norm $\|u\|_{J_s^\eta(\Omega)} = \left(|u|^2_{J_s^\eta}(\Omega) + \|u\|^2_{0,\Omega}\right)^{1/2}$, and let J_s^η (or $J_{s,0}^\eta$) denote the closure of $C^\infty(\Omega)$ (or $C_0^\infty(\Omega)$) with respect to $\|\cdot\|_{J_s^\eta(\Omega)}$

(iv) Fractional Sobolev space: let $\eta > 0$. Define the fractional Sobolev space $H^\eta(\Omega)$ as $H^\eta(\Omega) = \{u \in L^2(\Omega) \mid |\omega|^\eta \mathscr{F}(\hat{u}) \in L^2(\mathbb{R})\}$, endowed with the seminorm $|u|_{H^\eta(\Omega)} = \||\omega|^\eta \mathscr{F}(\hat{u})\|_{0,\mathbb{R}}$ and the norm $\|u\|_{H^\eta(\Omega)} = \left(|u|^2_{H^\eta(\Omega)} + \|u\|^2_{0,\Omega}\right)^{1/2}$, where $\mathscr{F}(\hat{u})$ is the Fourier transformation of $\hat{u}$ and $\hat{u}$ is the extension of zero of u outside Ω. Denote by $H^\eta(\Omega)$ (or $H_0^\eta(\Omega)$) the closure of $C^\infty(\Omega)$ (or $C_0^\infty(\Omega)$) with respect to $\|\cdot\|_{H^\eta(\Omega)}$.

Lemma 2 (see [36]). *The spaces $J_L^\eta, J_R^\eta, J_s^\eta$, and H^η are equivalent, with equivalent seminorms and norms if $\eta \neq n - (1/2)$, $n \in \mathbb{N}$.*

Lemma 3 (adjoint property). *Let $1 < \eta < 2$, then for any $u \in H_0^\eta(\Omega)$ and $v \in H_0^{\eta/2}(\Omega)$, we get*

$$\begin{aligned}\left({}_aD_x^\eta u, v\right)_{0,\Omega} &= \left({}_aD_x^{\eta/2} u, {}_xD_b^{\eta/2} v\right)_{0,\Omega}, \left({}_xD_x^\eta u, v\right)_{0,\Omega} \\ &= \left({}_xD_x^{\eta/2} u, {}_aD_b^{\eta/2} v\right)_{0,\Omega}.\end{aligned} \tag{7}$$

Spectral methods are characterized by the expansion of the solution in terms of global and, usually, orthogonal polynomials [37–40]. Now, we present the Jacobi polynomials and some of their basic properties. The vital role in the field of spectral methods arose from the nature of Jacobi weights which are related to the singular kernels of time Caputo fractional derivatives of order $0 < \beta < 1$. Denote $J_i^{\mu,\nu}(x), \mu, \nu > -1$ as the i-th order Jacobi polynomial of index defined on $[-1, 1]$. As all classic orthogonal polynomials, $\{J_i^{\mu,\nu}(x)\}_{i=0}^N$ satisfies the following three-term-recurrence relation:

$$\begin{cases} J_0^{\mu,\nu}(x) = 1, \\ J_1^{\mu,\nu}(x) = \dfrac{1}{2}(2 + \mu + \nu)x + \dfrac{1}{2}(\mu - \nu), \\ J_{i+1}^{\mu,\nu}(x) = \left(A_i^{\mu,\nu} x - B_i^{\mu,\nu}\right) J_i^{\mu,\nu}(x) - C_i^{\mu,\nu} J_{i-1}^{\mu,\nu}(x), \quad \text{if } 1 \le i \le N. \end{cases} \tag{8}$$

The recursion coefficients are given by

$$\begin{cases} A_i^{\mu,\nu} = \dfrac{(2i+\mu+\nu+1)(2i+\mu+\nu+2)}{2(i+1)(i+\mu+\nu+1)}, \\ B_i^{\mu,\nu} = \dfrac{(2i+\mu+\nu+1)(\nu^2-\mu^2)}{2(i+1)(i+\mu+\nu+1)(2i+\mu+\nu)}, \\ C_i^{\mu,\nu} = \dfrac{(2i+\mu+\nu+2)(i+\mu)(i+\nu)}{(i+1)(i+\mu+\nu+1)(2i+\mu+\nu)}. \end{cases} \tag{9}$$

Let $\omega^{\mu,\nu}(x) = (1-x)^{\mu}(1+x)^{\nu}$. Then, one has

$$\int_{-1}^{1} J_i^{\mu,\nu}(x) J_j^{\mu,\nu}(x)\omega^{\mu,\nu}(t)dx = \gamma_i^{\mu,\nu}\delta_{i,j}, \quad \forall i = 0, 1, \cdots, N, \tag{10}$$

where $\delta_{i,j}$ is the Kronecker delta function and

$$\gamma_i^{\mu,\nu} = \frac{2^{(\mu+\nu+1)}\Gamma(i+\mu+1)\Gamma(i+\nu+1)}{(2i+\mu+\nu+1)i!\Gamma(i+\mu+\nu+1)}, \quad \forall i = 0, 1, \cdots, N. \tag{11}$$

In particular, the Legendre polynomial is defined as $L_i(x) = J_i^{0,0}(x)$.

3. The Numerical Scheme

Here, we provide a fully discrete scheme for the problems (1) and (2) based on the $L1$-type approximation for the Caputo time-fractional derivative and the Legendre-Galerkin spectral method in space. To discretize the time-fractional derivatives, we divide the interval $[0, T]$ uniformly with a time step size τ defined by $\tau = \tilde{s}/N_{\tilde{s}}$ such that $N_{\tilde{s}}$ is a positive integer. The uniform partitions given by $t_n = n\tau, \forall -N_{\tilde{s}} \le n \le M$, where $M = \lceil T/\tau \rceil$. The $L1$ interpolation scheme for the time-fractional derivative of order $0 < \beta_r < 1$, $r = 0, 1, 2, \cdots, m$, in the Caputo sense at the time t_n is defined as

$$\begin{aligned} \sum_{r=0}^{m} q_r \left.\frac{\partial^{\beta_r} u}{\partial t^{\beta_r}}\right|_{t=t_n} &= \sum_{r=0}^{m} q_r \int_0^{t_n} u'(x,\eta)\omega_{1-\beta_r}(t_n-\eta)d\eta \\ &= \sum_{r=0}^{m} \frac{q_r}{\Gamma(1-\beta_r)} \sum_{i=1}^{n} \frac{u(x,t_i)-u(x,t_{i-1})}{\tau} \\ &\quad \cdot \int_{t_{i-1}}^{t_i} (t_n-\eta)^{-\beta_r} d\eta + r_\tau^n \\ &= \sum_{r=0}^{m} \frac{q_r}{\Gamma(2-\beta_r)\tau^{\beta_r}} \sum_{i=1}^{n} a_i^{\beta_r} u(x,t_i) \\ &\quad - u(x,t_{i-1}) + r_\tau^n, \end{aligned} \tag{12}$$

where $\omega_{\beta_r}(t) = t^{\beta_r - 1}/\Gamma(\beta_r)$, $t > 0$, and $a_j^{\beta_r} = (j+1)^{1-\beta_r} - j^{1-\beta_r}$, for each $j \ge 0$. If $u \in C^2([0,T]; L^2(\Omega))$, then there exists a constant $C > 0$ such that the truncation error r_τ^n satisfies $\|r_\tau^n\| \le C\tau^{2-\beta_m}$, for each $n = 0, 1, \cdots, M$ (see [41]).

Definition 4. Let $\{u^n\}_{n=0}^{M}$ be a sequence of real functions defined on Ω. We define the multiterm discrete time-fractional difference operator $\sum_{r=0}^{m} q_r D_\tau^{\beta_r}$ by

$$\begin{aligned} \sum_{r=0}^{m} q_r D_\tau^{\beta_r} u^n &= \sum_{r=0}^{m} \frac{q_r}{\Gamma(2-\beta_r)\tau^{\beta_r}} \sum_{i=1}^{n} a_{n-i}^{\beta_r} \delta_t u^i \\ &= \sum_{r=0}^{m} \frac{q_r}{\Gamma(2-\beta_r)\tau^{\beta_r}} \sum_{i=0}^{n} b_{n-i}^{\beta_r} u^i, \quad \forall n = 1, \cdots, M. \end{aligned} \tag{13}$$

In this expression, $\delta_t u^i = u^i - u^{i-1}$, and the constants are defined by $b_0^{\beta_r} = a_0^{\beta_r}, b_n^{\beta_r} = -a_{n-1}^{\beta_r}$, and $b_{n-i}^{\beta_r} = a_{n-i}^{\beta_r} - a_{n-i-1}^{\beta_r}$, for each $i = 1, \cdots, n-1$.

In order to provide a semidiscretized form of (1) at each time t_n, we approximate the time-fractional term through (13). Taylor approximations are used to approximate the nonlinear source function in a linear style. As a consequence, we obtain the discrete-time system:

$$\begin{aligned} \sum_{r=0}^{m} q_r D_\tau^{\beta_r} u^n = \frac{\partial^\alpha u^n}{\partial |x|^\alpha} &+ f\left(2u^{n-1} - u^{n-2}, u^{n-N_{\tilde{s}}}\right) \\ &+ g^n(x), \quad 1 \le n \le M, \forall x \in \Omega, \end{aligned} \tag{14}$$

$$u^n(x) = \psi(x), \quad -N_{\tilde{s}} \le n \le 0, x \in \Omega. \tag{15}$$

We define the following function space to give appropriate base functions such that the boundary conditions are satisfied exactly as clarified in spectral methods for space-fractional differential equations [42, 43].

$$\mathscr{W}_N^0 = \operatorname{span}\{\varphi_n(x) \colon n = 0, 1, \cdots, N-2\}, \tag{16}$$

where for each $\hat{x} \in [-1, 1]$, the function φ_n is given by

$$\varphi_n(x) = L_n(\hat{x}) - L_{n+2}(\hat{x}) = \frac{2n+3}{2(n+1)}\left(1-\hat{x}^2\right) J_n^{1,1}(\hat{x}), \tag{17}$$

and $x = 1/2((b-a)\hat{x} + a + b) \in [a, b]$.

We introduce the parameter $\sigma_r = q_r/\Gamma(2-\beta_r)\tau^{\beta_r}$. Then, the scheme (14) can be rewritten in the following equivalent form:

$$\begin{aligned} \sum_{r=0}^{m} \sigma_r a_0^{\beta_r} u^n - \kappa \frac{\partial^\alpha u^n}{\partial |x|^\alpha} = \sum_{r=0}^{m} \sigma_r a_{n-1}^{\beta_r} u^0 - \sum_{r=0}^{m} \sigma_r \sum_{i=1}^{n-1} b_{n-i}^{\beta_r} u^i \\ + f\left(2u^{n-1} - u^{n-2}, u^{n-N_{\tilde{s}}}\right) \\ + g^n(x), \quad \forall n = 1, \cdots, M. \end{aligned} \tag{18}$$

The fully discrete $L1$-Galerkin spectral scheme consists of the set of approximations $u_N^n \in \mathscr{W}_N^0$, satisfying the system:

$$\begin{cases} \sum_{r=0}^{m} \sigma_r a_0^{\beta_r}(u_N^n, v) - \kappa\left(\frac{\partial^\alpha}{\partial|x|^\alpha} u_N^n, v\right) = \sum_{r=0}^{m} \sigma_r a_{n-1}^{\beta_r}(u_N^0, v) - \sum_{r=0}^{m} \sigma_r \sum_{i=1}^{n-1} b_{n-i}^{\beta_r}(u_N^i, v) + \left(I_N f\left(2u_N^{n-1} - u_N^{n-2}, u_N^{n-N_{\hat{s}}}\right), v\right) + (I_N g^n(x), v), \quad \forall v \in \mathscr{W}_N^0, \forall n = 1, \cdots, M, \\ u_N^n = \pi_N^{1,0}\psi(t_n, x), \quad -N_{\hat{s}} \le n \le 0, \end{cases} \tag{19}$$

where $\pi_N^{1,0}$ is an appropriate projection operator. We expand the approximate solution as

$$u_N^n = \sum_{i=0}^{N-2} \hat{u}_i^n \varphi_i(x). \tag{20}$$

Substituting this expression into (19) and letting $v = \varphi_k$, for each $0 \le k \le N-2$, we obtain the following matrix representation of the uniform L_1-Galerkin spectral scheme:

$$\left(\sum_{r=0}^{m} \sigma_r a_0^{\beta_r} \bar{M} - \kappa c_\alpha\left(S + S^T\right)\right) U^n = K^{n-1} + R^{n-1} + F^n. \tag{21}$$

The notations in this expression are given by the system of identities:

$$\begin{cases} s_{ij} = \int_\Omega {}_aD_x^{\alpha/2}\varphi_i(x)\, {}_xD_b^{\alpha/2}\varphi_j(x)dx, & S = \left(s_{ij}\right)_{i,j=0}^{N-2}, \\ m_{ij} = \int_\Omega \varphi_i(x)\varphi_j(x)dx, & \bar{M} = \left(m_{ij}\right)_{i,j=0}^{N-2}, \\ h_i^{n-1} = \int_\Omega \varphi_i(x) I_N f\left(2u_N^{n-1} - u_N^{n-2}, u_N^{n-N_s}\right)dx, & R^{n-1} = \left(h_0^{n-1}, h_1^{n-1}, \cdots, h_{N-2}^{n-1}\right)^\top, \\ g_i^n = \int_\Omega \varphi_i(x) I_N g^n dx, & F^n = \left(g_0^n, g_1^n, \cdots, g_{N-2}^n\right)^\top, \\ U^n = \left(\hat{u}_0^n, \hat{u}_1^n, \cdots, \hat{u}_{N-2}^n\right)^\top, & K^{n-1} = -\sum_{r=0}^{m} \sigma_r \sum_{j=0}^{n-1} b_{n-j}^{\beta_r} \bar{M} U^j. \end{cases} \tag{22}$$

Lemma 5 (see [42, 43]). *The components of the stiffness matrix S are $s_{ij} = a_i^j - a_i^{j+2} - a_{i+2}^j + a_{i+2}^{j+2}$, for each $i, j = 0, 1, \cdots, N-2$. Here,*

$$\begin{aligned} a_i^j &= \int_\Omega {}_aD_x^{\alpha/2} L_i(\hat{x})\, {}_xD_b^{\alpha/2} L_j(\hat{x})dx \\ &= \left(\frac{b-a}{2}\right)^{1-\alpha} \frac{\Gamma(i+1)\Gamma(j+1)}{\Gamma(i-(\alpha/2)+1)\Gamma(j-(\alpha/2)+1)} \\ &\quad \cdot\cdot \sum_{r=0}^{N} \varpi_r^{-\alpha/2,-\alpha/2} J_i^{\alpha/2,-\alpha/2}\left(x_r^{-\alpha/2,-\alpha/2}\right) J_j^{-\alpha/2,\alpha/2}\left(x_r^{-\alpha/2,-\alpha/2}\right), \end{aligned} \tag{23}$$

and $\{x_r^{-\alpha/2,-\alpha/2}, \varpi_r^{-\alpha/2,-\alpha/2}\}_{i=0}^N$ is the set of Jacobi–Gauss points and weights with respect to the weight function $\omega^{-\alpha/2,-\alpha/2}$. The mass matrix $\bar{M}$ is symmetric, with nonzero components:

$$m_{ij} = m_{ji} = \begin{cases} \frac{b-a}{2j+1} + \frac{b-a}{2j+5}, & \forall i = j, \\ -\frac{b-a}{2j+5}, & \forall i = j+2. \end{cases} \tag{24}$$

4. Technical Lemmas

Several lemmas that will be invoked through our analysis appeared in that section. In the sequel, C and C_u will denote generic positive constants independent of τ, N, and n and may be different under different circumstances. We also fix the following notation $\mathbb{Z}_{[a,b]} = \mathbb{Z} \cap [a, b]$, such that $\mathbb{Z}$ is the set of all integers.

Throughout the coming context, we will use the notation

$$A(u,w)=\kappa c_\alpha\left[\left({}_aD_x^{\alpha/2}u,{}_xD_b^{\alpha/2}w\right)+\left({}_xD_b^{\alpha/2}u,{}_aD_x^{\alpha/2}w\right)\right]. \quad (25)$$

The orthogonal projection operator $\pi_N^{\alpha/2,0}: H_0^{\alpha/2}(\Omega) \longrightarrow \mathscr{W}_N^0$ will be such that

$$A\left(u-\pi_N^{\alpha/2,0}u,w\right)=0, \quad \forall u\in H_0^{\alpha/2}(\Omega), w\in \mathscr{W}_N^0. \quad (26)$$

For convenience of theoretical analysis, we give the following seminorm and norm:

$$|u|_{\alpha/2}:=A(u,u)^{1/2}, \quad (27)$$

$$\|u\|_{\alpha/2}:=\left(\|u\|^2+|u|_{\alpha/2}^2\right)^{1/2}, \quad (28)$$

which are equivalent to the seminorms and norms of $J_L^{\alpha/2}(\Omega)$, $J_R^{\alpha/2}(\Omega)$, $J_S^{\alpha/2}(\Omega)$, and $H^{\alpha/2}(\Omega)$. We recall the following three lemmas from [43].

Lemma 6. *Let α and s be arbitrary real numbers satisfying $0<\alpha<1, \alpha<s, \alpha\neq 1/2$. Then, there exists a positive constant C independent of N such that, for any function $u\in H_0^{\alpha/2}(\Omega)\cap H^s(\Omega)$, the following estimate holds:*

$$\left|u-\pi_N^{\alpha/2,0}u\right|_{\alpha/2}\le CN^{\alpha/2-s}\|u\|_s. \quad (29)$$

Lemma 7. *Suppose that $\Omega=(a,b)$, $u\in H_0^{\alpha/2}(\Omega)$. Then, there exist positive constants $C_1<1$ and C_2 independent of u, such that*

$$C_1\|u\|_{\alpha/2}\le |u|_{\alpha/2}\le \|u\|_{\alpha/2}\le C_2|u|_{H^{\alpha/2}(\Omega)}. \quad (30)$$

The following lemma and remark summarize the properties of the interpolation operator I_N.

Lemma 8 (see [44]). *Let $s\ge 1$. If $u\in H^s(\Omega)$, then there exists a constant $C>0$ independent of N, such that $\|u-I_Nu\|_l\le CN^{l-s}\|u\|_s$, for any $0\le l\le 1$.*

Remark 9. A smooth solution of a fractional differential equation does not mean a smooth source term and vice versa. Therefore, the regularity order s of the solution u is not the same as the regularity order r of the source term g, i.e.,

$$\|I_Ng-g\|\le CN^{-r}\|u\|_r, \quad \forall g\in H^r(\Omega). \quad (31)$$

Lemma 10 (see [45]). *For any function $u(t)$ which is absolutely continuous on $[0,T]$, the following inequality is satisfied:*

$$\left(\frac{\partial^\beta}{\partial t^\beta}u(t),u(t)\right)\ge\frac{1}{2}\frac{\partial^\beta}{\partial t^\beta}\|u(t)\|^2. \quad (32)$$

Lemma 11 (see [46]). *The discrete counterpart to the inequality (32) is given as*

$$\left(D_\tau^\beta u^k,u^k\right)\ge\frac{1}{2}D_\tau^\beta\left\|u^k\right\|^2, \quad (33)$$

such that $D_\tau^\beta u^k$ is the discrete time-fractional difference operator of the L1 type as defined in (13).

Plenty of researchers in recent years are stuck on the study of the continuous fractional Grönwall-type inequalities and their developments. However, the discrete fractional Grönwall-type inequality was far from well investigated, and more recently, the efforts paid in [47–50] tried to fill that gap. In what follows, we present recent discrete fractional-type inequalities. These inequalities play an important role in analyzing stability and convergence of the $L1$-schemes for the multiterm problems with nonlinear delay.

Lemma 12 (discrete fractional Grönwall inequality [29]). *Let $\{\phi^i\}_{i=-N_{\tilde{s}}}^\infty$ and $\{\xi_l\}_{l=0}^\infty$ be nonnegative sequences. Let ε_l, μ_i, $\forall l=0,\cdots,m$, $i\in\mathbb{Z}_{[1,6]}$ and c_0 be positive constants independent of τ. The fractional orders are defined as $0<\beta_0\le\beta_1\le\cdots\le\beta_{m-1}\le\beta_m\le 1$. If $\phi^i\ge 0\forall i\ge 0$, ϕ^0 is known and $\phi^i=0$ if $i<0$,*

$$\begin{aligned}&\sum_{l=0}^m\varepsilon_lD_\tau^{\beta_l}\phi^j\le\mu_1\phi^j+\varepsilon_0\left\|\xi^j\right\|^2\forall j\le N_{\tilde{s}},\\&\sum_{l=0}^m\varepsilon_lD_\tau^{\beta_l}\phi^j\le\mu_1\phi^j+\mu_2\phi^{j-1}+\mu_3\phi^{j-2}+\mu_4\phi^{j-3}+\mu_5\phi^{j-N_{\tilde{s}}-1}\\&\qquad+\mu_6\phi^{j-N_s}+\varepsilon_0\left\|\xi^j\right\|^2,\forall j>N_{\tilde{s}},\end{aligned} \quad (34)$$

where c_0 and $\mu_i(i=1,\cdots,6)$ are positive constants. Then, there exists a positive constant $\tau^*\ge\tau$ such that

$$\phi^n\le 2\left[\frac{c_0t_n^{\beta_m}}{\varepsilon_m\Gamma(1+\beta_m)}\left(\sum_{j=1}^n\left\|\xi^j\right\|^2\tau+\phi^0W\right)\right]E_{\beta_m}\left(\frac{2\mu t_n^{\beta_m}}{\varepsilon_m}\right), \quad (35)$$

where $E_\beta(z)=\sum_{k=0}^\infty z^k/\Gamma(1+k\beta)$ is the Mittag-Leffler function and

$$\begin{aligned}&\sum_{l=0}^m\varepsilon_l\frac{\Delta^{1-\beta_l}}{\Gamma(2-\beta_l)}\sum_{j=1}^k a_{j-1}^{\beta_l}:=W>0,\\&\mu=\mu_1+\frac{\mu_2}{a_0^{\beta_m}-a_1^{\beta_m}}+\frac{\mu_3}{a_1^{\beta_m}-a_2^{\beta_m}}+\frac{\mu_4}{a_2^{\beta_m}-a_3^{\beta_m}}\\&\qquad+\frac{\mu_5}{a_{N_{\tilde{s}}-2}^{\beta_m}-a_{N_{\tilde{s}}-1}^{\beta_m}}+\frac{\mu_6}{a_{N_{\tilde{s}}-1}^{\beta_m}-a_{N_{\tilde{s}}}^{\beta_m}}.\end{aligned} \quad (36)$$

5. Theoretical Analysis

The purpose of this section is to study the efficiency of the fully discrete Galerkin spectral methods for (1) and (2). We start by stability analysis and gives theorem of stability in the first subsection. The second subsection is devoted to the convergence analysis, and the theorem of convergence is given there. For the theoretical analysis requirements, we assume that the function f satisfies the following Lipschitz condition

$$|f(u_1, v_1) - f(u_2, v_2)| \le L(|u_1 - u_2| + |v_1 - v_2|), \tag{37}$$

where L is a positive constant.

5.1. Stability Analysis. The weak formulation of the scheme is as follows: find $\{u_N^k\}_{k=1}^M \in \mathscr{P}_N$, such that

$$\begin{aligned}\left(\sum_{r=0}^{m} q_r D_\tau^{\beta_r} u_N^k, v_N\right) + A\left(u_N^k, v_N\right) &= \left(I_N f\left(2u_N^{k-1} - u_N^{k-2}, u_N^{k-N_{\tilde{s}}}\right), v_N\right) \\ &\quad + \left(I_N g^k, v_N\right), \quad \forall v_N \in \mathscr{P}_N,\end{aligned} \tag{38}$$

with

$$u_N^k = \pi_N^{1,0}\varphi^k, \quad -N_{\tilde{s}} \le k \le 0. \tag{39}$$

It is a linear iterative scheme which means that we need only to get a solution to a system of linear equations at each time level. The well-posedness of that scheme is satisfied by the well-known Lax-Milgram lemma. Assume that $\{\tilde{u}_N^k\}_{k=1}^M$ is the solution of

$$\begin{aligned}\left(\sum_{r=0}^{m} q_r D_\tau^{\beta_r} \tilde{u}_N^k, v_N\right) + A\left(\tilde{u}_N^k, v_N\right) &= \left(I_N f\left(2\tilde{u}_N^{k-1} - \tilde{u}_N^{k-2}, \tilde{u}_N^{k-N_{\tilde{s}}}\right), v_N\right) \\ &\quad + \left(I_N \tilde{g}^k, v_N\right), \quad \forall v_N \in \mathscr{P}_N,\end{aligned} \tag{40}$$

with initial conditions

$$\tilde{u}_N^k = \pi_N^{1,0}\varphi^k, \quad -N_{\tilde{s}} \le k \le 0. \tag{41}$$

Now, we present the theorem of stability in the following context.

Theorem 13. *The fully discrete scheme (38) is unconditionally stable in the sense that for all $\tau > 0$, the following holds:*

$$\left\|u_N^k - \tilde{u}_N^k\right\|^2 \le C \max_{1\le k\le M}\left\|g^k - \tilde{g}^k\right\|^2. \tag{42}$$

Proof. Denote $\eta_N^k = u_N^k - \tilde{u}_N^k$. Subtracting (40) from (38), the following holds:

$$\begin{aligned}\left(\sum_{r=0}^{m} q_r D_\tau^{\beta_r} \eta_N^k, v_N\right) + A\left(\eta_N^k, v_N\right) &= \left(I_N f\left(2u_N^{k-1} - u_N^{k-2}, u_N^{k-N_{\tilde{s}}}\right)\right. \\ &\quad \left. - I_N f\left(2\tilde{u}_N^{k-1} - \tilde{u}_N^{k-2}, \tilde{u}_N^{k-N_{\tilde{s}}}\right), v_N\right) \\ &\quad + \left(I_N g^k - I_N \tilde{g}^k, v_N\right).\end{aligned} \tag{43}$$

According to (37) and using the Hölder inequality and Young's inequality, we derive that

$$\begin{aligned}&\left(I_N f\left(2u_N^{k-1} - u_N^{k-2}, u_N^{k-N_{\tilde{s}}}\right) - I_N f\left(2\tilde{u}_N^{k-1} - \tilde{u}_N^{k-2}, \tilde{u}_N^{k-N_{\tilde{s}}}\right), v_N\right) \\ &\quad \le C L\left(\left\|2\eta_N^{k-1} - \eta_N^{k-2}\right\| + \left\|\eta_N^{k-N_{\tilde{s}}}\right\|\right)\|v_N\| \\ &\quad \le \frac{\varepsilon}{2} CL^2\left\|2\eta_N^{k-1} - \eta_N^{k-2}\right\|^2 + \frac{\varepsilon}{2} CL^2\left\|\eta_N^{k-N_{\tilde{s}}}\right\|^2 + \frac{1}{2\varepsilon}\|v_N\|^2 \\ &\quad \le 4\varepsilon CL^2\left\|\eta_N^{k-1}\right\|^2 + \varepsilon L^2\left\|\eta_N^{k-2}\right\|^2 + \frac{\varepsilon}{2} CL^2\left\|\eta_N^{k-N_{\tilde{s}}}\right\|^2 \\ &\qquad + \frac{1}{2\varepsilon}\|v_N\|^2, \\ &\left(I_N g^k - I_N \tilde{g}^k, v_N\right) \le \frac{\varepsilon}{2} C\left\|g^k - \tilde{g}^k\right\|^2 + \frac{1}{2\varepsilon}\|v_N\|^2.\end{aligned} \tag{44}$$

Then, (43) becomes

$$\begin{aligned}\left(\sum_{r=0}^{m} q_r D_\tau^{\beta_r} \eta_N^k, v_N\right) + A\left(\eta_N^k, v_N\right) &\le \frac{1}{\varepsilon}\|v_N\|^2 + 4\varepsilon CL^2\left\|\eta_N^{k-1}\right\|^2 + \varepsilon L^2\left\|\eta_N^{k-2}\right\|^2 \\ &\quad + \frac{\varepsilon}{2} CL^2\left\|\eta_N^{k-N_{\tilde{s}}}\right\|^2 + \frac{\varepsilon C}{2}\left\|g^k - \tilde{g}^k\right\|^2.\end{aligned} \tag{45}$$

Taking $v_N = \eta_N^k$ and using Lemma 11 and (27), we can deduce that

$$\begin{aligned}\sum_{r=0}^{m} \frac{q_r}{2} D_\tau^{\beta_r}\left\|\eta_N^k\right\|^2 + |\eta|_{\alpha/2}^2 &\le \frac{1}{\varepsilon}\left\|\eta_N^k\right\|^2 + 4\varepsilon CL^2\left\|\eta_N^{k-1}\right\|^2 + \varepsilon L^2\left\|\eta_N^{k-2}\right\|^2 \\ &\quad + \frac{\varepsilon}{2} CL^2\left\|\eta_N^{k-N_{\tilde{s}}}\right\|^2 + \frac{\varepsilon C}{2}\left\|g^k - \tilde{g}^k\right\|^2,\end{aligned} \tag{46}$$

namely,

$$\begin{aligned}\sum_{r=0}^{m} q_r D_\tau^{\beta_r}\left\|\eta_N^k\right\|^2 &\le \frac{2}{\varepsilon}\left\|\eta_N^k\right\|^2 + 8\varepsilon CL^2\left\|\eta_N^{k-1}\right\|^2 + 2\varepsilon L^2\left\|\eta_N^{k-2}\right\|^2 \\ &\quad + \varepsilon CL^2\left\|\eta_N^{k-N_{\tilde{s}}}\right\|^2 + \varepsilon C\left\|g^k - \tilde{g}^k\right\|^2.\end{aligned} \tag{47}$$

By means of Lemma 12 and since $\varepsilon > 0$, there exists a positive constant $\tau^* = \sqrt[\beta_m]{q_m/(2\Gamma(2-\beta_m)2/\varepsilon)}$; when $\tau < \tau^*$, we have

$$\left\|\eta_N^k\right\|^2 \le \frac{2\varepsilon C t_k^{\beta_m}}{q_m \Gamma(1+\beta_m)} E_{\beta_m}\left(2\mu t_k^{\beta_m}/q_m\right) \sum_{k=1}^{M} \left\|g^k - \tilde{g}^k\right\|^2, \quad (48)$$

with $\mu = 2/\varepsilon + (8C\varepsilon L^2/(a_0^{\beta_m} - a_1^{\beta_m})) + (2C\varepsilon L^2/(a_1^{\beta_m} - a_2^{\beta_m})) + (C\varepsilon L^2/(a_{N_s-1}^{\beta_m} - a_{N_s}^{\beta_m}))$. Thus, the scheme is unconditionally stable.□ □

5.2. Convergence Analysis. In this section, we investigate the convergence of the fully discrete scheme (38) using error estimation.

Theorem 14. *Let $\{u^k\}_{k=-N_s}^M$ be the exact solution of equation (1) and $\{u_N^k\}_{k=-N_s}^M$ be the solution of (38). Suppose that ${}_0^C D_t^{\beta_r} u \in L^\infty(0, T; H_0^{\alpha/2}(\Omega) \cap H^s(\Omega))$, $u \in L^\infty(-s, T; H^s(\Omega))$; we have*

$$\left|u^k - u_N^k\right|_{\alpha/2} \le C\left(N^{(\alpha/2)-s} + N^{-r} + \tau^{2-\beta_m}\right), \quad 1 \le k \le M, \quad (49)$$

where C is independent of N and τ.

Proof. Denote $u^k - u_N^k = e_N^k = (u^k - \pi_N^{\alpha/2,0} u^k) + (\pi_N^{\alpha/2,0} u^k - u_N^k) \stackrel{\Delta}{=} \tilde{e}_N^k + \hat{e}_N^k$. The weak formulation of equation (1) is

$$\left(\sum_{r=0}^{m} q_r {}_0^C D_t^{\beta_r} u^k, v_N\right) + A\left(u^k, v_N\right) = \left(f\left(u^k, u^{k-N_{\bar{s}}}\right), v_N\right) + \left(g^k, v_N\right). \quad (50)$$

Subtracting (38) from (50) and owing to the definition of orthogonal projection, the error equation satisfies

$$\left(\sum_{r=0}^{m} q_r D_\tau^{\beta_r} \hat{e}_N^k, v_N\right) + A(\hat{e}_N, v_N) \stackrel{\Delta}{=} R_1^k + R_2^k + R_3^k + R_4^k, \quad (51)$$

where

$$\begin{aligned} R_1^k &= \left(I_N f\left(u^k, u^{k-N_{\bar{s}}}\right) - I_N f\left(2u_N^{k-1} - u_N^{k-2}, u_N^{k-N_{\bar{s}}}\right), v_N\right), \\ R_2^k &= \left(f\left(u^k, u^{k-N_{\bar{s}}}\right) - I_N f\left(u^k, u^{k-N_{\bar{s}}}\right), v_N\right), \\ R_3^k &= \left(\sum_{r=0}^{m} q_r \left(D_\tau^{\beta_r} \pi_N^{\alpha/2,0} u^k - {}_0^C D_t^{\beta_r} u^k\right), v_N\right), \\ R_4^k &= \left(g^k - I_N g^k, v_N\right). \end{aligned} \quad (52)$$

We next estimate the right-hand terms R_1^k, R_2^k, R_3^k, and R_4^k. For the first term R_1^k,

$$\begin{aligned} R_1^k = &\left(I_N f\left(u^k, u^{k-N_{\bar{s}}}\right) - I_N f\left(2u^{k-1} - u^{k-2}, u^{k-N_{\bar{s}}}\right), v_N\right) \\ &+ \left(I_N f\left(2u^{k-1} - u^{k-2}, u^{k-N_{\bar{s}}}\right)\right. \\ &\left. - I_N f\left(2u_N^{k-1} - u_N^{k-2}, u_N^{k-N_{\bar{s}}}\right), v_N\right) \stackrel{\Delta}{=} R_{11}^k + R_{12}^k. \end{aligned} \quad (53)$$

By applying the Taylor expansion, the following holds:

$$\begin{aligned} f\left(u^k, u^{k-N_{\bar{s}}}\right) &= f\left(2u^{k-1} - u^{k-2}, u^{k-N_s}\right) \\ &\quad + \left(u^k - 2u^{k-1} + u^{k-2}\right) f'_1\left(\xi, u^{k-N_{\bar{s}}}\right. \\ &= f\left(2u^{k-1} - u^{k-2}, u^{k-N_{\bar{s}}}\right) + \tilde{c}_u \tau^2. \end{aligned} \quad (54)$$

Furthermore, by means of the Hölder inequality and Young's inequality, we have

$$\begin{aligned} R_{11}^k &\le \left\|I_N f\left(u^k, u^{k-N_{\bar{s}}}\right) - I_N f\left(2u^{k-1} - u^{k-2}, u^{k-N_{\bar{s}}}\right)\right\| \|v_N\| \\ &\le C\left\|f\left(u^k, u^{k-N_{\bar{s}}}\right) - f\left(2u^{k-1} - u^{k-2}, u^{k-N_{\bar{s}}}\right)\right\| \|v_N\| \\ &\le \frac{\varepsilon}{2} \tilde{c}_u \tau^4 + \frac{1}{2\varepsilon} \|v_N\|^2. \end{aligned} \quad (55)$$

According to (37), we can deduce that

$$\begin{aligned} R_{12}^k &\le LC\left(\left\|2e_N^{k-1} - e_N^{k-2}\right\| + \left\|e_N^{k-N_{\bar{s}}}\right\|\right) \|v_N\| \\ &\le LC\left(\left\|2\hat{e}_N^{k-1} - \hat{e}_N^{k-2}\right\| + \left\|\hat{e}_N^{k-N_{\bar{s}}}\right\|\right. \\ &\quad \left. + \left\|2\tilde{e}_N^{k-1} - \tilde{e}_N^{k-2}\right\| + \left\|\tilde{e}_N^{k-N_{\bar{s}}}\right\|\right) \|v_N\| \\ &\le \frac{8\varepsilon}{2} CL^2 \left\|\hat{e}_N^{k-1}\right\|^2 + \frac{2\varepsilon}{2} CL^2 \left\|\hat{e}_N^{k-2}\right\|^2 \\ &\quad + \frac{\varepsilon}{2} L^2 \left\|\hat{e}_N^{k-N_{\bar{s}}}\right\|^2 + \frac{8\varepsilon}{2} CL^2 \left\|\tilde{e}_N^{k-1}\right\|^2 \\ &\quad + \frac{2\varepsilon}{2} CL^2 \left\|\tilde{e}_N^{k-2}\right\|^2 + \frac{\varepsilon}{2} CL^2 \left\|\tilde{e}_N^{k-N_{\bar{s}}}\right\|^2 + \frac{1}{2\varepsilon} \|v_N\|^2. \end{aligned} \quad (56)$$

Moreover, owing to Lemmas 6 and 7, the following holds:

$$\begin{aligned} \left\|\tilde{e}_N^{k-1}\right\|^2 &\le \frac{C}{C_1} N^{\alpha-2s} \left\|u^{k-1}\right\|_s^2, \left\|\tilde{e}_N^{k-2}\right\|^2 \\ &\le \frac{C}{C_1} N^{\alpha-2s} \left\|u^{k-2}\right\|_s^2, \left\|\tilde{e}_N^{k-N_{\bar{s}}}\right\|^2 \\ &\le \frac{C}{C_1} N^{\alpha-2s} \left\|u^{k-N_{\bar{s}}}\right\|_s^2. \end{aligned} \quad (57)$$

Then, (56) becomes

$$R_{12}^k \le 4\varepsilon CL^2\left\|\widehat{e}_N^{k-1}\right\|^2 + \varepsilon CL^2\left\|\widehat{e}_N^{k-2}\right\|^2 + \frac{\varepsilon}{2}CL^2\left\|\widehat{e}_N^{k-N_{\tilde{s}}}\right\|^2 + \frac{C}{C_1}N^{\alpha-2s}\|u\|^2_{L^\infty(-s,T;H^s(\Omega))} + \frac{1}{2\varepsilon}\|\upsilon_N\|^2. \tag{58}$$

Substituting (55) and (58) into (53), we can derive that

$$R_1^k \le \frac{1}{\varepsilon}\|\upsilon_N\|^2 + 4\varepsilon CL^2\left\|\widehat{e}_N^{k-1}\right\|^2 + \varepsilon CL^2\left\|\widehat{e}_N^{k-2}\right\|^2 + \frac{\varepsilon}{2}CL^2\left\|\widehat{e}_N^{k-N_{\tilde{s}}}\right\|^2 + \frac{C}{C_1}N^{\alpha-2s}\|u\|^2_{L^\infty(-s,T;H^s(\Omega))} + \frac{\varepsilon}{2}\tilde{c}_u\tau^4. \tag{59}$$

For the second term R_2^k, by means of the Hölder inequality, the following holds:

$$R_2^k \le \frac{\varepsilon}{2}CN^{-2r}\|u\|^2_{L^\infty(-s,T;H^s(\Omega))} + \frac{1}{2\varepsilon}\|\upsilon_N\|^2. \tag{60}$$

For the third term R_3^k, the following holds:

$$\begin{aligned} R_3^k &= \left(\sum_{r=0}^m q_r\left(D_\tau^{\beta_r}\pi_N^{\alpha/2,0}u^k - {}_0^CD_t^{\beta_r}\pi_N^{\alpha/2,0}u^k\right), \upsilon_N\right) \\ &\quad + \left(\sum_{r=0}^m q_r\left({}_0^CD_t^{\beta_r}\pi_N^{\alpha/2,0}u^k - {}_0^CD_t^{\beta_r}u^k\right), \upsilon_N\right) \\ &= \left(\pi_N^{\alpha/2,0}\sum_{r=0}^m q_r\left(D_\tau^{\beta_r}u^k - {}_0^CD_t^{\beta_r}u^k\right), \upsilon_N\right) \\ &\quad - \left(\sum_{r=0}^m q_r{}_0^CD_t^{\beta_r}\widetilde{e}_N^k, \upsilon_N\right) \triangleq R_{31}^k + R_{32}^k. \end{aligned} \tag{61}$$

Using (12) and the Hölder inequality, the following holds:

$$\begin{aligned} R_{31}^k &\le \frac{\varepsilon}{2}\sum_{r=0}^m q_r\left\|\pi_N^{\alpha/2,0}\left(D_\tau^{\beta_r}u^k - {}_0^CD_t^{\beta_r}u^k\right)\right\|^2 + \frac{1}{2\varepsilon}\|\upsilon_N\|^2 \\ &\le \frac{\varepsilon}{2}C\sum_{r=0}^m q_r\left\|\left(D_\tau^{\beta_r}u^k - {}_0^CD_t^{\beta_r}u^k\right)\right\|^2 + \frac{1}{2\varepsilon}\|\upsilon_N\|^2 \\ &\le \frac{\varepsilon}{2}C_{1,u}\tau^{4-2\beta_m} + \frac{1}{2\varepsilon}\|\upsilon_N\|^2. \end{aligned} \tag{62}$$

Furthermore, according to Lemma 2, we have

$$\begin{aligned} R_{32}^k &\le \frac{\varepsilon}{2}CN^{\alpha-2s}\sum_{r=0}^m q_r\left\|{}_0^CD_t^{\beta_r}u^k\right\|_s^2 + \frac{1}{2\varepsilon}\|\upsilon_N\|^2 \\ &\le \frac{\varepsilon}{2}CN^{\alpha-2s}\sum_{r=0}^m q_r\left\|{}_0^CD_t^{\beta_r}u\right\|^2_{L^\infty(-s,T;H^s(\Omega))} + \frac{1}{2\varepsilon}\|\upsilon_N\|^2. \end{aligned} \tag{63}$$

Thus, (61) becomes

$$R_3^k \le \frac{\varepsilon}{2}CN^{\alpha-2s}\sum_{r=0}^m q_r\left\|{}_0^CD_t^{\beta_r}u\right\|^2_{L^\infty(-s,T;H^s(\Omega))} + \frac{\varepsilon}{2}C_{2,u}\tau^{4-2\beta_m} + \frac{1}{\varepsilon}\|\upsilon_N\|^2. \tag{64}$$

For the fourth term R_4^k, the following holds by invoking Remark 9:

$$R_4^k \le \frac{\varepsilon}{2}CN^{\alpha-2r}\|u\|^2_{L^\infty(-s,T;H^r(\Omega))} + \frac{1}{2\varepsilon}\|\upsilon_N\|^2. \tag{65}$$

Substituting (59), (60), (64), and (65) into (51), we can infer that

$$\begin{aligned} &\left(\sum_{r=0}^m q_rD_\tau^{\beta_r}\widehat{e}_N^k, \upsilon_N\right) + A(\widehat{e}_N, \upsilon_N) \\ &\le \frac{5}{2\varepsilon}\|\upsilon_N\|^2 + 4\varepsilon CL^2\left\|\widehat{e}_N^{k-1}\right\|^2 + \varepsilon CL^2\left\|\widehat{e}_N^{k-2}\right\|^2 \\ &\quad + \frac{\varepsilon}{2}CL^2\left\|\widehat{e}_N^{k-N_{\tilde{s}}}\right\|^2 + \tilde{\mathcal{G}}, \end{aligned} \tag{66}$$

where

$$\begin{aligned} \tilde{\mathcal{G}} &= \varepsilon\tilde{C}N^{\alpha-2s}\left(\sum_{r=0}^m q_r\left\|{}_0^CD_t^{\beta_r}u\right\|^2_{L^\infty(0,T;H^s(\Omega))} + \|u\|^2_{L^\infty(-s,T;H^s(\Omega))}\right) \\ &\quad + \varepsilon\tilde{C}N^{-2r}\|u\|^2_{L^\infty(-s,T;H^r(\Omega))} + \varepsilon\tilde{C}_u\tau^{4-2\beta_m}. \end{aligned} \tag{67}$$

Taking $\upsilon_N = \widehat{e}_N^k$ in (66) and applying Lemma 11, we can conclude that

$$\begin{aligned} &\sum_{r=0}^m \frac{q_r}{2}D_\tau^{\beta_r}\left\|\widehat{e}_N^k\right\|^2 + \left|\widehat{e}_N^k\right|^2_{\alpha/2} \\ &\le \frac{5}{2\varepsilon}\left\|\widehat{e}_N^k\right\|^2 + 4\varepsilon CL^2\left\|\widehat{e}_N^{k-1}\right\|^2 + \varepsilon CL^2\left\|\widehat{e}_N^{k-2}\right\|^2 \\ &\quad + \frac{\varepsilon}{2}CL^2\left\|\widehat{e}_N^{k-N_{\tilde{s}}}\right\|^2 + \tilde{\mathcal{G}}, \end{aligned} \tag{68}$$

namely,

$$\begin{aligned} \sum_{r=0}^m \frac{q_r}{2}D_\tau^{\beta_r}\left\|\widehat{e}_N^k\right\|^2 &\le \frac{5}{\varepsilon}\left\|\widehat{e}_N^k\right\|^2 + 8\varepsilon CL^2\left\|\widehat{e}_N^{k-1}\right\|^2 + 2\varepsilon CL^2\left\|\widehat{e}_N^{k-2}\right\|^2 \\ &\quad + \varepsilon CL^2\left\|\widehat{e}_N^{k-N_{\tilde{s}}}\right\|^2 + \mathcal{G}, \end{aligned} \tag{69}$$

Table 1: The L^2-errors and their convergence orders versus τ and α at $N = 50$ for Example 15.

τ	$\alpha = 1.1$		$\alpha = 1.5$		$\alpha = 1.9$	
	Error	Order	Error	Order	Error	Order
1.5/50	5.057×10^{-5}	—	4.692×10^{-5}	—	4.163×10^{-5}	—
1.5/100	1.927×10^{-5}	1.392	1.989×10^{-5}	1.238	1.783×10^{-5}	1.223
1.5/150	1.094×10^{-5}	1.395	1.192×10^{-5}	1.262	1.086×10^{-5}	1.224
1.5/200	7.327×10^{-6}	1.396	8.283×10^{-6}	1.267	7.592×10^{-6}	1.244
1.5/250	5.365×10^{-6}	1.396	6.226×10^{-6}	1.279	5.732×10^{-6}	1.259
1.5/300	4.159×10^{-6}	1.397	4.933×10^{-6}	1.277	4.560×10^{-6}	1.255
$2-\beta_5$	—	1.333	—	1.333	—	1.333

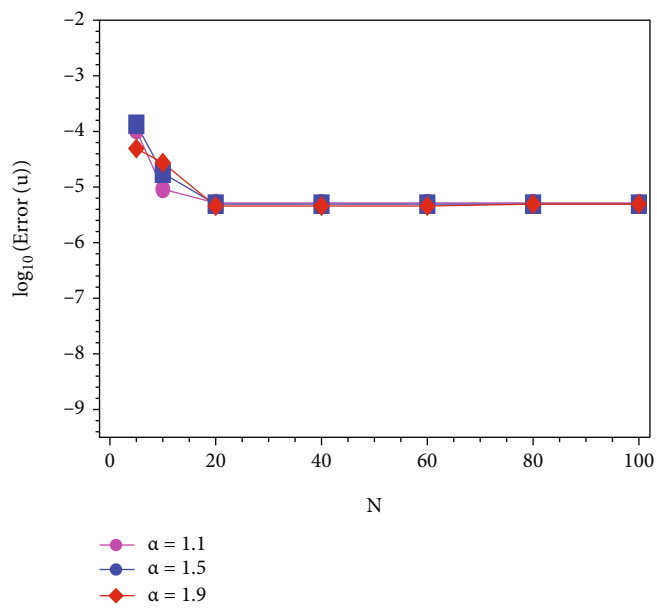

Figure 1: Convergence order in space direction for different values of α at $\tau = 1.5/300$.

with $\mathcal{G} = 2\tilde{\mathcal{G}}$. By means of Lemma 12 and since $\varepsilon > 0$, there exists a positive constant $\tau^* = \sqrt[\beta_m]{q_m/(2\Gamma(2-\beta_m)10/\varepsilon)}$; when $\tau < \tau^*$, we have

$$\left\|\tilde{e}_N^k\right\|^2 \leq \frac{2Gt_k^{\beta_m}}{q_m\Gamma(1+\beta_m)} E_{\beta_m}\left(\frac{2\mu t_k^{\beta_m}}{q_m}\right), \tag{70}$$

with $\mu = 10/\varepsilon + (16\varepsilon CL^2/(a_0^{\beta_m} - a_1^{\beta_m})) + (4C\varepsilon L^2/(a_1^{\beta_m} - a_2^{\beta_m})) + (2C\varepsilon L^2/(a_{N_{\tilde{s}}-1}^{\beta_m} - a_{N_{\tilde{s}}}^{\beta_m}))$. Thus, the scheme is unconditionally convergent. Finally, by means of the triangle inequality and Lemma 6, we complete the proof of (49).□ □

6. Numerical Experiments

Some numerical experiments are performed here to clarify the convergence orders of the considered scheme in time and space. We also show the impact of time- and space-fractional orders on the behaviour of the dynamics for the solution of nonlinear delay reaction diffusion equations. To examine the temporal and spatial convergence orders separately, the orders of convergence in time and space shall be determined from the L^2-error norms defined as

$$\text{Order} = \frac{\ln\left(\|e(N, M_1)\|/\|e(N, M_2)\|\right)}{\ln\left(M_1/M_2\right)}, \tag{71}$$

where $M_1 \neq M_2$.

Example 15. Consider the nonlinear delay reaction-diffusion problem

$$\sum_{r=1}^{Q} \frac{\partial^{\beta_r} u}{\partial t^{\beta_r}}(x,t) = \frac{\partial^{\alpha} u}{\partial |x|^{\alpha}}(x,t) - 2u(x,t) + \frac{u(x,t-1.5)}{1+u^2(x,t-1.5)} + g(x,t), x \in (0,1), t \in (0,1]. \tag{72}$$

We choose the fractional orders $\beta_r = (2Q + r - 5)/3Q$. The source function $g(x,t)$ is given such that problem (72) has the exact solution $t^{\beta_5+1}x^2(1-x)^2$.

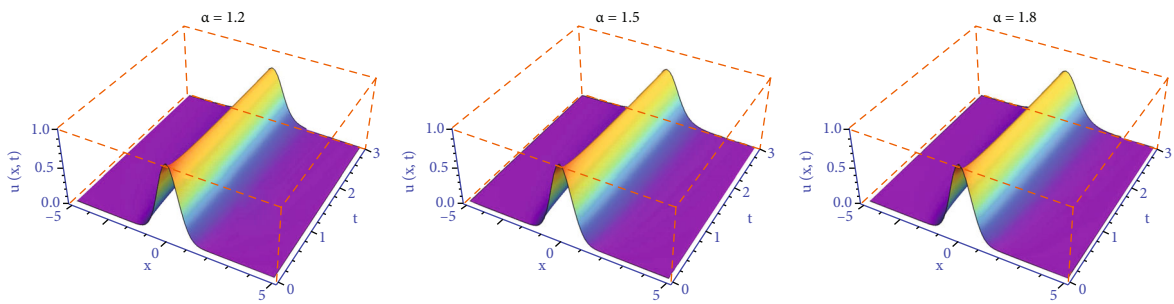

Figure 2: Evaluations of u for different fractional-order parameters α.

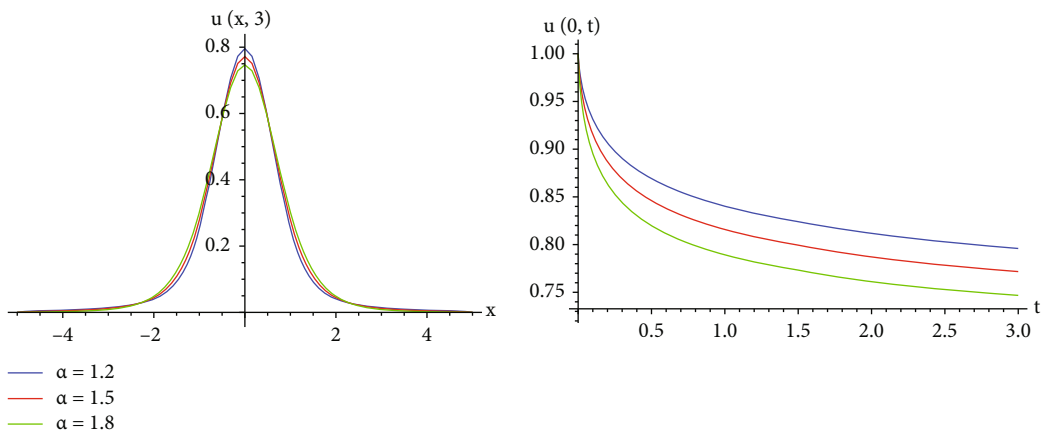

Figure 3: Evaluations of u at $x = 0$ and $t = T$ for different fractional-order parameters α.

In Table 1, we list the L^2-errors and corresponding convergence orders with $\alpha = 1.1, 1.5, 1.9$ and $N = 50$ for $Q = 5$. We can see that these results confirm the expected theoretical order convergence in time. The convergence orders in space are depicted for different values of α and β at $M = 500$ in Figure 1. All the convergence results are in agreement with the theoretical results.

Example 16. We consider the following fractional problem, where the dynamics of the solution is very interesting and the exact solution is unknown:

$$\sum_{r=1}^{8} \frac{\partial^{\beta_r} u}{\partial t^{\beta_r}}(x,t) = \frac{\partial^{\alpha} u}{\partial |x|^{\alpha}}(x,t) + u(x,t)(1-u(x,t)) \cdot (1+u(x,t-1.5)), \quad x \in (a,b), t \in (0,3], \tag{73}$$

with the initial value $u(x,0) = e^{-2x^2}$ and $\beta_r = r/10$.

Figures 2 and 3 show the profiles of the numerical solution with the fractional-order parameters $\alpha = 1.2, 1.5, 1.8$ with $N = 100$ and $\tau = 1.5/500$. We can observe that the fractional-order parameter α affects the shape of the solutions. We can say that the fractional-order parameters can be used in physics to modify the shape of waves without changing the nonlinearity and dispersion effects of the fractional nonlinear problems.

7. Conclusion and Remarks

We have constructed and analyzed a novel explicit finite difference/Galerkin–Legendre spectral scheme for the nonlinear multiterm Riesz space and Caputo time fractional reaction-diffusion equation with delay. The problem was first approximated by the $L1$ difference method on the temporal direction, and then, the Galerkin–Legendre spectral method was applied on the spatial discretization. Using an appropriate form of discrete fractional Grönwall inequality, the stability and the convergence of the fully discrete scheme were investigated. We have proven that the proposed method is stable and has a convergent order $2 - \beta_m$ in time and an exponential rate of convergence in space. High-order difference schemes can be handled to raise the temporal convergence order. This can be done by using the Alikhanov scheme [46], and it can be designed theoretically and numerically easily as shown in our context. Two numerical examples are given to show that the numerical results are consistent with theoretical ones in the case of the smoothness of the solution with respect to time and space.

Data Availability

The data used to support the findings of this study are included within the article.

Conflicts of Interest

The authors declare that they have no competing interests.

Authors' Contributions

A. K. Omran contributed to the conceptualization, writing of the original draft, data curation, figure preparation, and methodology. M. A. Zaky and A.S. Hendy reviewed and edited the manuscript and carried out the experiments, formal analysis, and supervision. V. G. Pimenov contributed to the conceptualization, writing of the original draft, data curation, figure preparation, methodology, and supervision.

Acknowledgments

A. K. Omran is funded by a scholarship under the joint executive program between the Arab Republic of Egypt and Russian Federation. M. A. Zaky wishes to acknowledge the support of the Nazarbayev University Program (091019CRP2120). M. A. Zaky wishes also to acknowledge the partial support of the Science Committee of the Ministry of Education and Science of the Republic of Kazakhstan (Grant "Dynamical Analysis and Synchronization of Complex Neural Networks with Its Applications").

References

[1] M. Abbaszadeh and M. Dehghan, "A class of moving kriging interpolation-based DQ methods to simulate multi-dimensional space Galilei invariant fractional advection-diffusion equation," *Numerical Algorithms*, pp. 1–29, 2021.

[2] M. Abbaszadeh and M. Dehghan, "Fourth-order alternating direction implicit difference scheme to simulate the space-time Riesz tempered fractional diffusion equation," *International Journal of Computer Mathematics*, vol. 98, no. 11, pp. 2137–2155, 2021.

[3] M. Abbaszadeh, H. Pourbashash, and M. Khaksar-e Oshagh, "The local meshless collocation method for solving 2D fractional Klein-Kramers dynamics equation on irregular domains," *International Journal of Numerical Methods for Heat & Fluid Flow*, 2021.

[4] A. S. Hendy and M. A. Zaky, "Combined Galerkin spectral/finite difference method over graded meshes for the generalized nonlinear fractional Schrödinger equation," *Nonlinear Dynamics*, vol. 103, no. 3, pp. 2493–2507, 2021.

[5] A. S. Hendy, M. A. Zaky, R. M. Hafez, and R. H. De Staelen, "The impact of memory effect on space fractional strong quantum couplers with tunable decay behavior and its numerical simulation," *Scientific Reports*, vol. 11, no. 1, article 10275, 2021.

[6] E. Loghman, A. Kamali, F. Bakhtiari-Nejad, M. Abbaszadeh, and M. Amabili, "On the combined shooting-pseudo-arclength method for finding frequency response of nonlinear fractional-order differential equations," *Journal of Sound and Vibration*, vol. 516, article 116521, 2022.

[7] M. A. Zaky and A. S. Hendy, "Convergence analysis of anL1-continuous Galerkin method for nonlinear time-space fractional Schrödinger equations," *International Journal of Computer Mathematics*, vol. 98, no. 7, pp. 1420–1437, 2021.

[8] M. A. Zaky, A. S. Hendy, and J. E. Macías-Díaz, "Semi-implicit Galerkin–Legendre spectral schemes for nonlinear time-space fractional diffusion–reaction equations with smooth and non-smooth solutions," *Journal of Scientific Computing*, vol. 82, no. 1, pp. 1–27, 2020.

[9] M. Benchohra and F. Berhoun, "Impulsive fractional differential equations with state-dependent delay," *Communications in Applied Analysis*, vol. 14, no. 2, p. 213, 2010.

[10] C. Beta, M. Bertram, A. S. Mikhailov, H. H. Rotermund, and G. Ertl, "Controlling turbulence in a surface chemical reaction by time-delay autosynchronization," *Physical Review E*, vol. 67, no. 4, article 046224, 2003.

[11] V. Keyantuo, C. Lizama, and M. Warma, "Asymptotic behavior of fractional order semilinear evolution equations," *Differential and Integral Equations*, vol. 26, no. 7-8, pp. 757–780, 2013.

[12] V. T. Luong, "Decay mild solutions for two-term time fractional differential equations in Banach spaces," *Journal of Fixed Point Theory and Applications*, vol. 18, no. 2, pp. 417–432, 2016.

[13] M. Dehghan and M. Abbaszadeh, "An efficient technique based on finite difference/finite element method for solution of two-dimensional space/multi-time fractional Bloch-Torrey equations," *Applied Numerical Mathematics*, vol. 131, pp. 190–206, 2018.

[14] Z. Liu, F. Liu, and F. Zeng, "An alternating direction implicit spectral method for solving two dimensional multi-term time fractional mixed diffusion and diffusion-wave equations," *Applied Numerical Mathematics*, vol. 136, pp. 139–151, 2019.

[15] K. Van Bockstal, "Existence and uniqueness of a weak solution to a non-autonomous time-fractional diffusion equation (of distributed order)," *Applied Mathematics Letters*, vol. 109, article 106540, 2020.

[16] J. F. Kelly, R. J. McGough, and M. M. Meerschaert, "Analytical time-domain Green's functions for power-law media," *The Journal of the Acoustical Society of America*, vol. 124, no. 5, pp. 2861–2872, 2008.

[17] J. Chen, F. Liu, V. Anh, S. Shen, Q. Liu, and C. Liao, "The analytical solution and numerical solution of the fractional diffusion-wave equation with damping," *Applied Mathematics and Computation*, vol. 219, no. 4, pp. 1737–1748, 2012.

[18] D. Vieru, C. Fetecau, and C. Fetecau, "Flow of a viscoelastic fluid with the fractional Maxwell model between two side walls perpendicular to a plate," *Applied Mathematics and Computation*, vol. 200, no. 1, pp. 459–464, 2008.

[19] L. Feng, F. Liu, I. Turner, and P. Zhuang, "Numerical methods and analysis for simulating the flow of a generalized Oldroyd-B fluid between two infinite parallel rigid plates," *International Journal of Heat and Mass Transfer*, vol. 115, pp. 1309–1320, 2017.

[20] V. Daftardar-Gejji and S. Bhalekar, "Boundary value problems for multi-term fractional differential equations," *Journal of Mathematical Analysis and Applications*, vol. 345, no. 2, pp. 754–765, 2008.

[21] Y. Luchko, "Initial-boundary-value problems for the generalized multi-term time-fractional diffusion equation," *Journal of Mathematical Analysis and Applications*, vol. 374, no. 2, pp. 538–548, 2011.

[22] H. Jiang, F. Liu, I. Turner, and K. Burrage, "Analytical solutions for the multi-term time-fractional diffusion-wave/diffusion equations in a finite domain," *Computers & Mathematics with Applications*, vol. 64, no. 10, pp. 3377–3388, 2012.

[23] X.-L. Ding and Y.-L. Jiang, "Analytical solutions for the multi-term time-space fractional advection-diffusion equations with mixed boundary conditions," *Nonlinear Analysis: Real World Applications*, vol. 14, no. 2, pp. 1026–1033, 2013.

[24] Z. Li, Y. Liu, and M. Yamamoto, "Initial-boundary value problems for multi-term time-fractional diffusion equations with positive constant coefficients," *Applied Mathematics and Computation*, vol. 257, pp. 381–397, 2015.

[25] M. A. Zaky, "A Legendre spectral quadrature tau method for the multi-term time-fractional diffusion equations," *Computational and Applied Mathematics*, vol. 37, no. 3, pp. 3525–3538, 2018.

[26] A. S. Hendy, "Numerical treatment for after-effected multi-term time-space fractional advection–diffusion equations," *Engineering with Computers*, vol. 37, pp. 1–11, 2021.

[27] A. S. Hendy and R. H. De Staelen, "Theoretical analysis (convergence and stability) of a difference approximation for multiterm time fractional convection diffusion-wave equations with delay," *Mathematics*, vol. 8, no. 10, p. 1696, 2020.

[28] A. S. Hendy and M. A. Zaky, "Graded mesh discretization for coupled system of nonlinear multi-term time-space fractional diffusion equations," *Engineering with Computers*, pp. 1–13, 2020.

[29] M. A. Zaky, A. S. Hendy, A. A. Alikhanov, and V. G. Pimenov, "Numerical analysis of multi-term time-fractional nonlinear subdiffusion equations with time delay: what could possibly go wrong?," *Communications in Nonlinear Science and Numerical Simulation*, vol. 96, article 105672, 2021.

[30] A. S. Hendy, M. A. Zaky, and R. H. De Staelen, "A general framework for the numerical analysis of high-order finite difference solvers for nonlinear multi-term time-space fractional partial differential equations with time delay," *Applied Numerical Mathematics*, vol. 169, pp. 108–121, 2021.

[31] A. S. Hendy, M. A. Zaky, and D. Suragan, "Discrete fractional stochastic Gronwall inequalities arising in the numerical analysis of multi-term fractional order stochastic differential equations," *Mathematics and Computers in Simulation*, vol. 193, pp. 269–279, 2022.

[32] C. F. Lorenzo and T. T. Hartley, "Variable order and distributed order fractional operators," *Nonlinear Dynamics*, vol. 29, no. 1-4, pp. 57–98, 2002.

[33] M. Zheng, F. Liu, V. Anh, and I. Turner, "A high-order spectral method for the multi-term time-fractional diffusion equations," *Applied Mathematical Modelling*, vol. 40, no. 7-8, pp. 4970–4985, 2016.

[34] I. Podlubny, *Fractional Differential Equations: An Introduction to Fractional Derivatives, Fractional Differential Equations, to Methods of Their Solution and Some of their Applications*, vol. - volume 198, Elsevier, 1998.

[35] D. Wang, A. Xiao, and W. Yang, "Crank-Nicolson difference scheme for the coupled nonlinear Schrodinger equations with the Riesz space fractional derivative," *Journal of Computational Physics*, vol. 242, pp. 670–681, 2013.

[36] V. J. Ervin and J. P. Roop, "Variational solution of fractional advection dispersion equations on bounded domains in $\mathbb{R}^d$," *Numerical Methods for Partial Differential Equations*, vol. 23, no. 2, pp. 256–281, 2007.

[37] H. Abo-Gabal, M. A. Zaky, A. S. Hendy, and E. H. Doha, "Computational aspects of fractional Romanovski–Bessel functions," *Computational and Applied Mathematics*, vol. 40, no. 4, pp. 1–16, 2021.

[38] I. G. Ameen, M. A. Zaky, and E. H. Doha, "Singularity preserving spectral collocation method for nonlinear systems of fractional differential equations with the right-sided Caputo fractional derivative," *Journal of Computational and Applied Mathematics*, vol. 392, article 113468, 2021.

[39] I. G. Ameen, N. A. Elkot, M. A. Zaky, A. S. Hendy, and E. H. Doha, "A pseudo-spectral scheme for systems of two-point boundary value problems with left and right sided fractional derivatives and related integral equations," *Computer Modeling in Engineering & Sciences*, vol. 128, no. 1, pp. 21–41, 2021.

[40] M. A. Zaky, H. Abo-Gabal, R. M. Hafez, and E. H. Doha, "Computational and theoretical aspects of Romanovski-Bessel polynomials and their applications in spectral approximations," *Numerical Algorithms*, pp. 1–35, 2021.

[41] Y. Lin and C. Xu, "Finite difference/spectral approximations for the time-fractional diffusion equation," *Journal of Computational Physics*, vol. 225, no. 2, pp. 1533–1552, 2007.

[42] J. Shen, "Efficient spectral-Galerkin method I. Direct solvers of second-and fourth-order equations using Legendre polynomials," *SIAM Journal on Scientific Computing*, vol. 15, no. 6, pp. 1489–1505, 1994.

[43] F. Zeng, F. Liu, C. Li, K. Burrage, I. Turner, and V. Anh, "A Crank–Nicolson ADI spectral method for a two-dimensional Riesz space fractional nonlinear reaction-diffusion equation," *SIAM Journal on Numerical Analysis*, vol. 52, no. 6, pp. 2599–2622, 2014.

[44] J. Shen, T. Tang, and L.-L. Wang, *Spectral Methods: Algorithms, Analysis and Applications*, vol. volume 41, Springer Science & Business Media, 2011.

[45] A. A. Alikhanov, "A priori estimates for solutions of boundary value problems for fractional-order equations," *Differential Equations*, vol. 46, no. 5, pp. 660–666, 2010.

[46] A. A. Alikhanov, "A new difference scheme for the time fractional diffusion equation," *Journal of Computational Physics*, vol. 280, pp. 424–438, 2015.

[47] D. Li, H.-L. Liao, W. Sun, J. Wang, and J. Zhang, "Analysis of L1-Galerkin FEMs for time-fractional nonlinear parabolic problems," *Communications in Computational Physics*, vol. 24, no. 1, pp. 86–103, 2018.

[48] L. Li, B. Zhou, X. Chen, and Z. Wang, "Convergence and stability of compact finite difference method for nonlinear time fractional reaction-diffusion equations with delay," *Applied Mathematics and Computation*, vol. 337, pp. 144–152, 2018.

[49] H.-l. Liao, D. Li, and J. Zhang, "Sharp error estimate of the nonuniform L1 formula for linear reaction-subdiffusion equations," *SIAM Journal on Numerical Analysis*, vol. 56, no. 2, pp. 1112–1133, 2018.

[50] H.-l. Liao, W. McLean, and J. Zhang, "A discrete Grönwall inequality with applications to numerical schemes for subdiffusion problems," *SIAM Journal on Numerical Analysis*, vol. 57, no. 1, pp. 218–237, 2019.